Silicon/Boron Exchange Routes to Novel Inorganic-Organic Hybrid Molecules, Oligomers, Polymers and Macrocycles

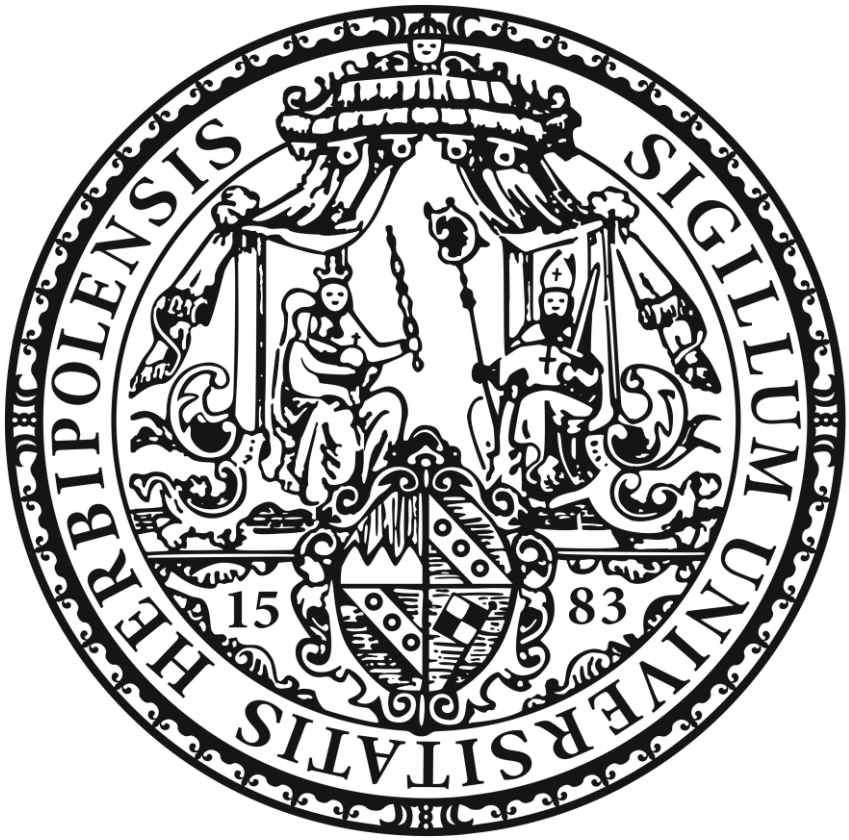

Dissertation zur Erlangung des naturwissenschaftlichen Doktorgrades der Julius-Maximilians-Universität Würzburg

Vorgelegt von

Nicolas Alexander Riensch

Aus Köln

Würzburg 2021

Eingereicht bei der Fakultät für Chemie und Pharmazie am

_____

Gutachter der schriftlichen Arbeit

1. Gutachter	Prof. Dr. Holger Helten
2. Gutachter	PD Dr. Crispin Lichtenberg

Prüfer des öffentlichen Promotionskolloquiums

1. Prüfer	Prof. Dr. Holger Helten
2. Prüfer	PD. Dr. Crispin Lichtenberg
3. Prüfer	_____

Datum des öffentlichen Promotionskolloquiums

_____

Doktorurkunde ausgehändigt am

_____

For those of you that wanna know what this is all about
It's like this:
This is ten percent luck
Twenty percent skill
Fifteen percent concentrated power of will
Five percent pleasure
Fifty percent pain
And a hundred percent reason to remember the name
(Fort Minor, Remember the name, slightly modified)

Acknowledgements

First of all, I would like to thank Prof. Dr. Holger Helten for giving me the opportunity to do my PhD in his research group and for providing such an interesting research topic. Thank you for your trust over the years, the opportunity to attend conferences abroad, for your support, great advice and for inspiring and helpful discussions.

I would also like to thank PD Dr. Crispin Lichtenberg for taking over the second report on my thesis.

Furthermore, I would like to thank the whole Helten group for an excellent working atmosphere, nice Christmas parties, enjoyable lunch times, great evenings and for being friends in and outside the lab. Matthias Maier and Lars Fritze, thank you for taking fun to the next level in our labs. I would like to thank former group members Dr. Artur Lik and Dr. Ozan Ayhan as well as Dr. Thomas Lorenz for welcoming us so warmly several years ago and for their continuous support over the years. I especially want to thank Lars Fritze and Merian Crumbach who kept my company over the years and with whom I have overcome all obstacles. Thank you for your support, a lot of helpful and not always chemistry related discussions, for several activities in and outside the laboratory and for being the great friends you are.

During my PhD time, I had the pleasure to work with some highly motivated students. I would like to thank Laura Bloch, Sven Moos, Julian Günther, Manuel Buckel, Maximilian Fest and Lukas Swoboda for their support and for everything they have done for me during their internships. This particularly meets Maximilian Fest, who did a great job during his internship and master thesis, fighting and succeeding over furylboranes.

I would like to thank my in-house collaboration partners Prof. Dr. Holger Braunschweig and Dr. Ivo Krummenacher. I am grateful for nice discussions and proof-reading of our joint publications.

I would also like to thank Ayse Deniz, Sebastian Kühl, Dr. Alina Adams and Prof. Dr. Andrij Pich from DWI Leibniz Institute of Interactive Materials as well as Lars Müller as former member of our group for a productive cooperation.

Over the years at RWTH Aachen University and JMU Würzburg, a lot of people supported my work with analytical measurements. Therefore, I would like to thank Dr. Klaus Beckerle for GPC measurements, Toni Gossen, Rachida Bohmarat, Dr. Gerhard Fink and Dr. Rüdiger Bertermann for NMR measurements, Brigitte Pütz and Christoph Mahler for MS measurements, Claudia Schleep and Sabine Timmroth for elemental analysis, the Englert group and Lars Fritze for X-ray diffraction experiments. I thank Prof. Dr. Marder for fluorescence spectroscopy access and Sarina Berger and Dr. Florian Rauch for introduction

into UV-vis and fluorescence spectroscopy as well as Dr. Ivo Krummenacher for performing cyclic voltammetry measurements.

A big thank you goes to all my friends who supported me over the last years and during my studies and who know perfectly well who they are and what they did to support me. I want to thank Marcel Lach, whom I know from day 1 at university, for his help during studies, for proofreading my thesis, for a lot of beers and for nice and (not always) successful football games. I owe you a thousand beers for this.

In the end, I can do nothing but thank my parents Martina Spork-Riensch and Reinhard Riensch, my sister Leonie Riensch, my wife Vanessa Riensch and my in-laws for their endless support and love during all the time. You supported me during all the good and bad times, endured my moods, encouraged and pushed me when it was necessary. All this would not have been possible without you and I will never forget this. Vanessa, thank you for being this wonderful, caring and supporting person you are. I am dedicating this thesis to my grandmother Rosemarie Spork. You were the strongest and most inspiring person I have ever known.

List of publications

The publications listed below are partly reproduced in this dissertation with permission from The Royal Society of Chemistry [1-2], from Georg Thieme Verlag KG [3], the Centre National de la Recherche Scientifique (CNRS) and The Royal Society of Chemistry [4] and John Wiley and Sons [5]. Reference [5] is published under a creative common license (CC-BY-NC) and do not require a further permission statement from the publisher.

The table itemizes at which position in this work the paper has been reproduced.

Publication	**Position**
[1] N. A. Riensch, A. Deniz, S. Kühl, L. Müller, A. Adams, A. Pich, H. Helten, *Polym. Chem.* **2017**, *8*, 5264—5268.	Chapter 2.1
[2] N. A. Riensch, L. Fritze, T. Schindler, M. Kremer, H. Helten, *Dalton Trans.* **2018**, *47*, 10399—10403.	Chapter 2.2
[3] L. Fritze, N. A. Riensch, H. Helten, *Synthesis* **2019**, *51*, 399—406.	Chapter 2.3
[4] a) N. A. Riensch, M. Fest, L. Fritze, A. Helbig, I. Krummenacher, H. Braunschweig, H. Helten, *New J. Chem.* **2020,** DOI: 10.1039/D0NJ04297H b) Preliminary results have been included in M. Fest, **2020**, “Synthesis of bifuran-based organoboron building blocks“, master’s thesis, Julius-Maximilians-Universität, Würzburg.	Chapter 2.4
[5] N. A. Riensch, L. Swoboda, A. Lik, I. Krummenacher, H. Braunschweig, H. Helten, *Z. Anorg. Allg. Chem.* **2021**, DOI: 10.1002/zaac.202000476	Chapter 2.5

Further publication:

[6] O. Ayhan, N. A. Riensch, C. Glasmacher, H. Helten*, Chem. Eur. J.* **2018**, *24*, 5883—5894.

Table of Contents

List of Abbreviations

°C	degree celsius
A	Angström
Abs	absorbance
Ag	silver
$Ag[AlOC(CF_3)_3)_4]$	silver tetrakis(perfluoro-*tert*-butoxy)aluminate
AgOTf	silver triflate
$AgNTf_2f$	silver bis(trifluoromethylsulfonyl)imide
AgBr	silver bromide
AgCl	silver chloride
AgX	silver halide
APCI	atmospheric pressure chemical ionization
aq	aqueous
Ar	aromatic ring
arom.	aromatic
ASAP	atmospheric solid analysis probe
ATR	attenuated total reflection
BBr_2	dibromoboryl
BBr_3	tribromoborane
BCl_2	dichloroboryl
BCl_3	trichloroborane
BF_3*OEt	trifluoroborane etherate
$BOMe_3$	trimethyl borate
br	broad
C_6D_6	deuterated benzene
CaH_2	calcium hydride
calcd.	calculated
cat.	catalyst
CD_2Cl_2	deuterated dichloromethane
$CDCl_3$	deuterated chloroform
CH_2Cl_2	dichloromethane
Compd.	Compound
CPMAS	cross polarization magic angle spinning
CTP	catalyst transfer polymerization
Cu	copper powder
CV	cyclo voltammetry
d	doublet

d	days
Da	dalton
DCB	dichlorobenzene
DCM	dichloromethane
DCM-d*2*	deuterated dichloromethane
dd	doublet of doublet
DLS	dynamic light scattering
DMF	dimethylformamide
DP_n	average degree of polymerization
DPMAS	direct polymerization magic angle spinning
DPV	differential pulse voltammetry
DSC	differential scanning calorimetry
e.g.	exempli gratia
$E_{1/2}$	half wave potential
em	emission
elem.	elemental
equiv	equivalents
ESI	electrospray ionization
et al.	and others
Et_2O	diethylether
EtOH	ethanol
eV	electron Volt
ex	excitation
Fc/Fc^+	ferrocen/ferrocenium cation
FESEM	field emission scanning electron microscope
FET	field-effect transistor
^{F}Mes	2,4,6-tris(trifluoro)methylbenzene
Fur	furan
Fur-Li	2-furyllithium
Fur-TMS	2-trimethylsilylfuran
FT-IR	Fourier transform infrared spectroscopy
g	gram
GPC	gel permeation chromatography
h	hour
HCl	hydrochloric acid
HMBC	heteronuclear multiple quantum correlation
HOMO	highest occupied molecular orbital

HR-MS	high resolution mass spectrometry
HSQC	heteronuclear single quantum coherence
HT	head-to-tail
Hz	Hertz
i-Pr	*iso*-propyl
IR spectroscopy	Infrared spectroscopy
J	coupling constant
K	Kelvin
L	liter
LIFDI	liquid injection field desorption ionization
LED	light-emitting diode
LUMO	lowest unoccupied molecular orbital
M	mol per liter
m	multiplet
m.p.	melting point
m/z	mass per charge
max	maximum
mbar	millibar
Me	methyl
Me_3Si-Br	trimethylsilyl bromide
Me_3Si-Cl	trimethylsilyl chloride
Me_3Si-NTf_2	trimethylsilyl bis(trifluoromethylsulfonyl)imide
Me_3Si-OCH_2CF_3	2,2,2-trifluorethoxytrimethyl silane
Me_3Si-OMe	methoxytrimethylsilane
Me_3Si-OTf	trimethylsilyl triflate
MeCN	acetonitrile
MeOH	methanol
Mes	2,4,6-trimethylphenyl
Mes*	2,4,6-tri-*tert*-butylphenyl
Mes*Li	2,4,6-tri-*tert*-butylphenyllithium
mg	milli gram
Mg	magnesium
MHz	Megahertz
min	minute
mL	milliliter
mmol	millimol
M_n	number average molar mass

MS	mass spectrometry
M_v	volume average molar mass
mV	millivolt
M_w	mass average molar mass
M_z	centrifugation average molar mass
NaOMe	sodium methoxide
n-BuLi	*n*-butyllithium
nm	nanometers
NMR	nuclear magnetic resonance
norm.	normalized
o	ortho
o-DCB	ortho-dichlorobenzene
OFET	organic field-effect transistor
OLED	organic light emitting diode
ON	overnight
OPV	organic photovoltaics
p	para
PDI	polydispersity index
PE	petrol ether
Ph	phenyl
Ph-Li	phenyllithium
ppm	parts per million
PVP	polyvinylpyrrolidone
QY	quantum yield
R	organic rest
r.t.	room temperature
RI	refractive index
s	singlet
sept	septet
$SiMe_3$	trimethylsilyl group
SIMS	secondary ion mass spectrometry
T	temperature
TBAF	tetrabutylammonium fluoride
t-BuLi	*tert*-butyllithium
TD-DFT	time-dependent density functional theory
TGA	thermogravimetric analysis
THF	tetrahydrofuran

Thi	thiophene
Thi-BBr_2	2-(dibromoboryl)thiophene
Thi-BCl_2	2-(dichloroboryl)thiophene
Thi-Li	2-thienyllithium
Thi-TMS	2-trimethylsilylthiophene
Tip	2,4,6-isopropylphenyl
TipLi	2,4,6-isopropylphenyllithium
TMEDA	tetramethylendiamin
TMS	trimethylsilyl
TMS-Br	trimethylsilyl bromide
TMS-NTf_2	trimethylsilyl bis(trifluoromethylsulfonyl)imide
TT	tail-to-tail
UV	ultra-violet
V	volt
vis	visible
vs	versus
WCA	weakly coordinating anion
ε	extinction coefficient
λ	wavelength
$\lambda_{abs,max}$	wavelength of absorption maximum
$\lambda_{em,max}$	wavelength of emission maximum
Φ_f	quantum yield
δ	chemical shift

1. Introduction

1.1 Organic Semiconductors

Semiconducting materials can be described as the building blocks of entire modern electronics and computer industry. The demand for new, better, cheaper and more sustainable materials is an important field of material research. Industrially used semiconducting materials are mostly based on inorganic, crystalline solids of group XIV elements, such as silicon and germanium, but also binary and certain ternary compounds, oxides and alloys are used.[1] Replacing those classical inorganic solid-state materials by organic polymers has proven to be an effective way to reduce production costs since organic polymers enable facile processability. Furthermore, the usually soft and lightweight character of such organic compounds increases the flexibility of the obtained systems.[2] For this reason, the development of new semiconducting π-conjugated organic polymers has been extensively studied in the last decades. They have shown promising applicability in modern electronics such as (polymer-based) organic-light-emitting diodes (OLEDs/PLEDs),[3] organic-field-effect transistors (OFETs),[4] organic photovoltaic cells (OPV)[5] and for bioimaging[6] and chemical sensing purposes[7]. To meet the industrial demand for flexible optoelectronic devices, special focus has been on the stability, processability, good solid-state packing, rigidity as well as planarity and high mobility (charge transfer) of the new and improved materials.[3-5] Various classes of organic molecules have been synthesized, characterized and tested with regard to their applicability in industrially used electronic devices. Beside the most commonly used polythiophenes (**i**),[8] other group XVI element-derived chalcogenophene polymers such as polyfurans (**ii**),[9] polyselenophenes (**iii**)[10] and polytellurophenes (**iv**)[10a,11] showed promising potential for electronic devices and have been investigated in this regard (Figure 1).

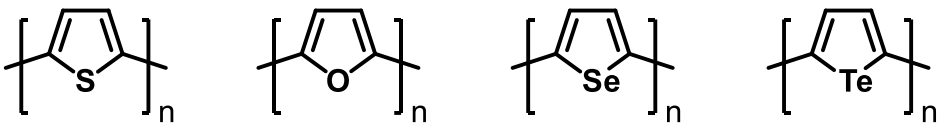

i ii iii iv

Figure 1. Organic polymers derived from chalcogenophenes: polythiophene **i**, polyfuran **ii**, polyselenophene **iii**, polytellurophene **iv**.

Polythiophenes have emerged amongst the most important and most meticulous investigated materials since they offer excellent solution processability, high stability and facile structural modification opportunities.[8] Several synthetic routes have been established for their preparation.[12-20] Unsubstituted 2,5-coupled polythiophene **i** was first synthesized via chemical polymerization of 2,5-dibromothiophene **3a** by Yamamoto and co-workers. It showed high thermal stability and conductivity but lack solubility in common organic solvents.[12a] In order to

enhance the solubility, alkyl groups (e.g. hexyl or dodecyl) were incorporated in the 3-position to obtain new building blocks **3**. Subsequent polymerization thereof afforded poly(3-alkylthiophene)s (P3ATs) **1** with enhance solubility (Scheme 1). Adopting a similar reaction protocol for unsubstituted polythiophene **i**, afforded only randomly coupled 3-alkylthiophenes with different coupling patterns: regioregular head-to-tail (HT), head-to-head (HH) and tail-to-tail (TT) couplings. HT couplings affording regioregular P3ATs (**1a**) are favoured because of the highest degree of coplanarity, which is a prerequisite for effective charge transport (Scheme 1, **1a**).[12c] The latter couplings lead to loss of the π-conjugation as well as decrease in conductivity caused by a twisted structure resulting from steric repulsion between adjacent alkyl groups (Scheme 1, **1b**). Since polythiophenes are an extensively studied class of substances, various strategies for the effective synthesis of exclusively regioregular P3ATs (**1a**) have been investigated and established in the past.[13-20]

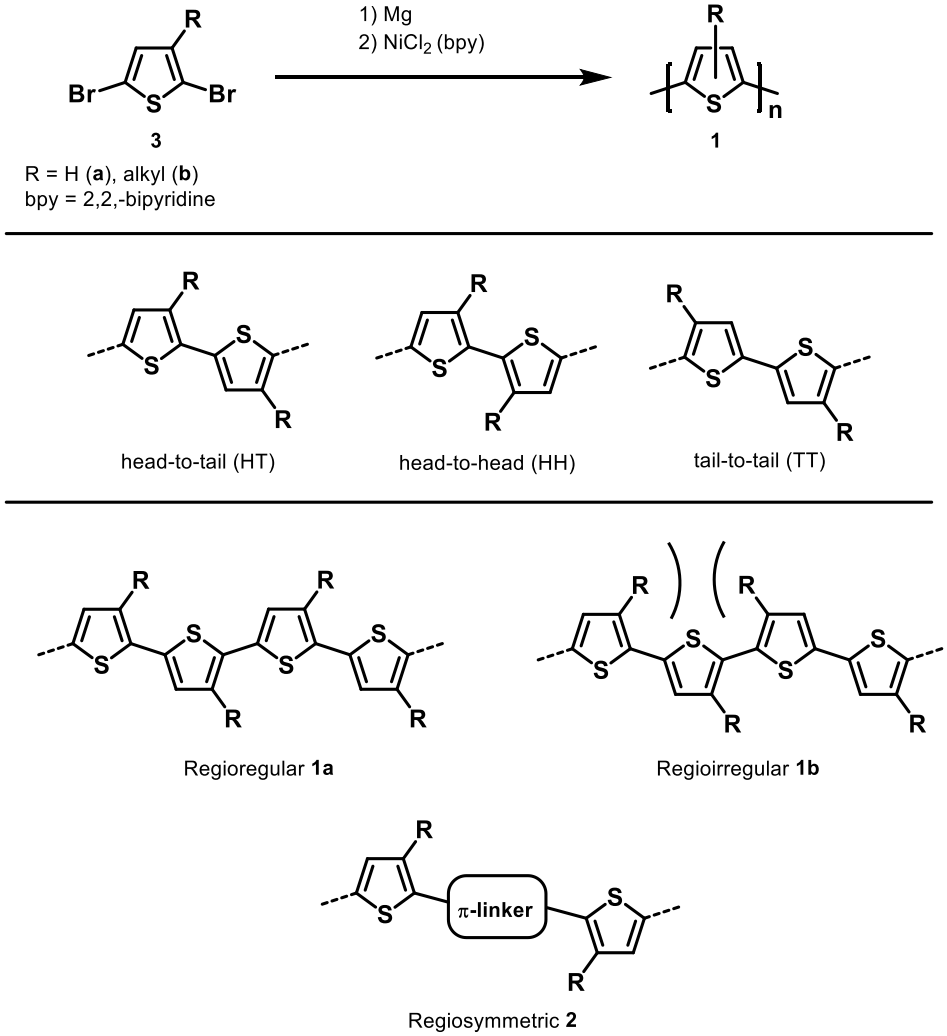

Scheme 1. Top: Polymerization of unsubstituted (**3a**) and substituted 3-alkyl-2,5-dibromothiophene **3b**. Center: Three different possible coupling patterns between 3-alkyl substituted thiophene moieties during polymerization; Bottom: regioregular **1a**, regioirregular **1b** and regiosymmetric **2** coupling products.

In 1992, McCullough reported the synthesis of P3ATs with a degree of 98-100% regioregularity starting from 2-bromo-3-alkythiophene **4** via regiospecific generation of a bifunctional 3-alkylthiophene with bromine in 2 and bromomagnesium in 5 position followed by nickel catalyzed cross-coupling reaction (Scheme 2, reaction I).[13] A similar method was developed by Rieke using “Rieke zinc” to generate an active organozinc monomer which is cross-coupled via Nickel catalysis providing a HT regioregularity of 97-100% (Scheme 2, reaction IIa).[14] Probably the most effective method to obtain P3ATs with a high regioregularity of > 99% is described as Grignard metathesis (GRIM) reaction and is based on a nickel-catalyzed Kumada cross-coupling reaction (Scheme 2, reaction IIb). By this method, average molecular weights (M_n) of 20000-35000 Da with low PDIs of 1.2 – 1.4 are obtained.[15] Studies have discovered that the polymerization proceeds via a catalyst-transfer polycondensation (CTP) mechanism.[16] Further reaction pathways involve Stille and Suzuki-Miyaura C-C cross-coupling reactions with a palladium catalyst, affording a HT regioregularity of >96% and a lower M_n value of 10000 - 16000 Da with a PDI of 1.2 – 1.4.[17,18] The GRIM approach can also be employed for the synthesis of poly(3-alkylselenophene)[10d] and poly(3-alkyltelluorphenes)[22] yielding highly regioregular products. The progress in the selective synthesis of regioregular P3ATs led to the synthesis of a huge amount of new functional polythiophenes. These polymers show enhanced electrical properties due to planarization of the backbone and high crystallinity of the structures and this eventually results in high conductivity.[2c]

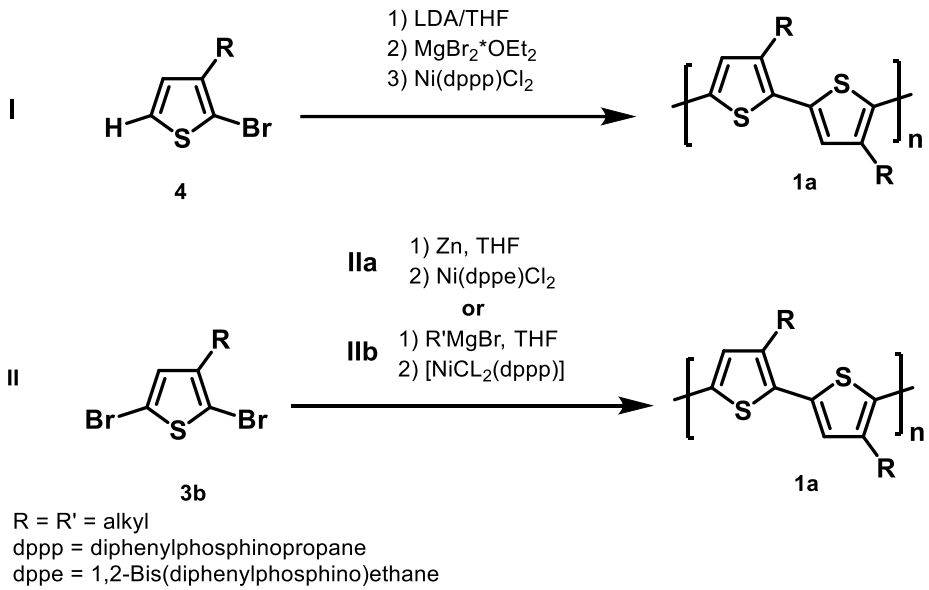

Scheme 2. Synthesis of regioregular P3ATs via different reaction routes.

Furthermore, new studies involve the synthesis of regiosymmetric P3ATs **2** in which a π-linkage is inserted between HH coupled P3ATs to lower the impact of HH couplings. This insertion leads to largely coplanar and highly ordered structures with a reported even higher conductivity.[8a]

The introduction of flexible side chains on the backbone of polythiophenes initially served the purpose of increased solubility and thus better processability. However, it was found that side chain engineering can significantly change the electrical and optical properties of the respective materials. In this context, different kinds of functionalized side chains have been incorporated in the past, ranging from heteroatom-containing groups such as alkoxy **6** and alkylamino groups **7** as well as fluoroalkyl groups **8** (Figure 2).[2c,23] A widely used and well known example is poly-3,4-ethylendioxythiophene (PEDOT, **9**) which is applied, for example, in organic photovoltaics.[24]

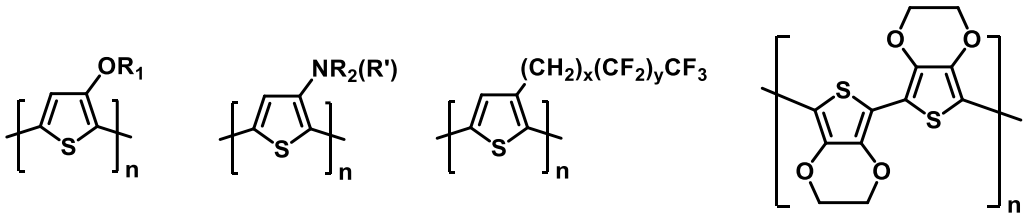

6 **7** **8** **9**

R_1 = alkyl, ethylenglycol
R_2 = H, Me, R' = alkyl
x = 11; y = 3

Figure 2. Side chain modification to afford substituted polythiophenes **6-9**.

A straightforward method to further tune the electronic and optical properties is the copolymerization of thiophene-based electron-rich (donor) buildings blocks with electron-deficient (acceptor) units to create donor-acceptor polymers. In recent years, the synthesis of such polymers composed of an alternating array of both donor and acceptor units has been of special interest since their in-chain donor-acceptor interactions provide a lowering of the band gap and high charge transport ability. Moreover, they are also important light-harvesting systems in solar cells.[4a,25,26]

Varying the chemical structure of both the donor as well as the acceptor unit significantly alters the electronic properties, and it is important to understand the structure-property relationships in order to tailor the desired properties with special regard on the respective energy levels of the HOMO and the LUMO. In recent years, isoindigo (**ID**), diketopyrrolopyrole (**DPP**), thiazolo[5,4-*d*]thiazole (**TzTz**) and benzo[c][1,2,5]thiadiazole (**BTz**) have been extensively studied and used as acceptor units (Figure 3, right part). Frequently used thiophene based donor moities involve e.g. thienothiophene (**TT**), bithiophene (**BT**) or higher homologues such as cyclopentadithiophene (**CPDT**) and benzodithiophene (**BDT**) (Figure 3, left part). From a synthetic point of view, C-C coupling reactions are considered as most ideal candidates for hetero-couplings of aromatic buildings blocks, e.g. via Suzuki-Miyaura or Stille cross-coupling. The properties can also be tuned by varying the sequence of consecutive donor and acceptor units (D-A-D vs D-D-A vs D-A-A). Nevertheless, the side chains play an important role when it

comes to solubility and processability which has to be taken into account when designing new D-A polymers.[26]

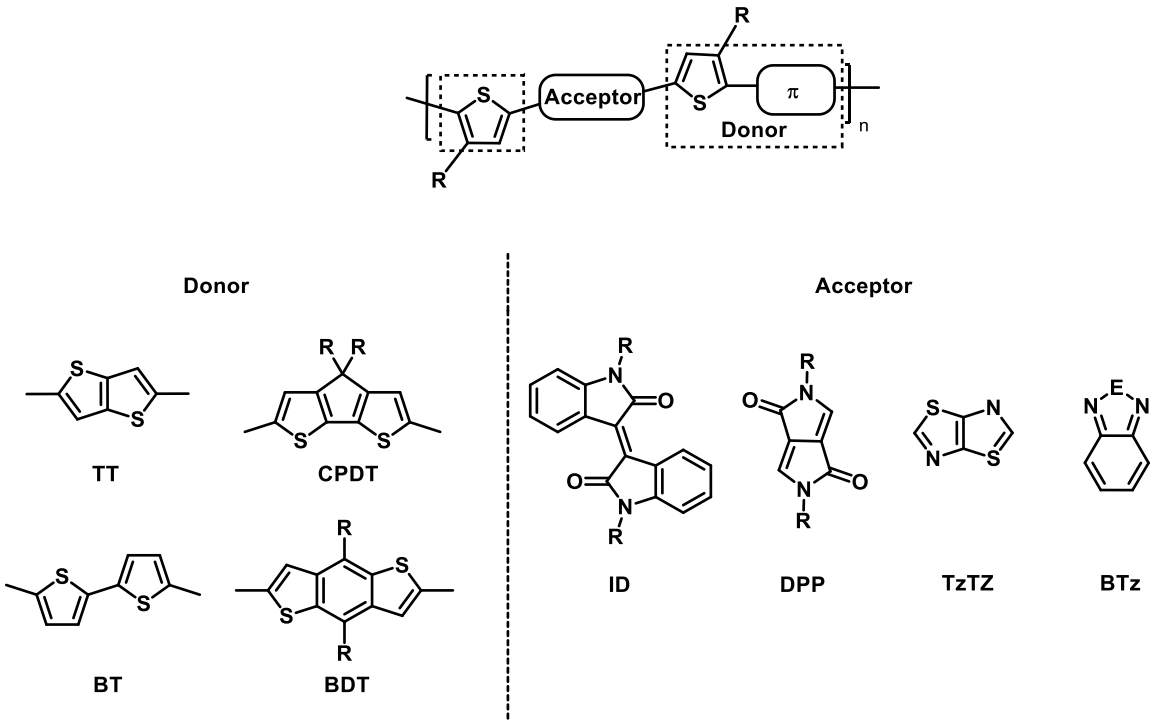

Figure 3. Thiophene based donor-acceptor polymers with frequently used examples for electron-rich (donor, left) and electron-deficient (acceptor, right) units.

Another approach to alter the electronic and optical properties with special focus on the energy levels of the HOMO and the LUMO is substituting the hetero (sulfur) atom. The influence of different heteroatoms in cyclolinear macromolecules **i**-**iv** (cf. Figure 1) plays an important role and was experimentally and computationally studied by different groups.[27]

In comparison to oligothiophenes, oligofurans show significantly improved solubility, which is important for good processability. Furthermore, oligofurans possess an even more rigid, planar structure and shorter inter-ring C-C bond lengths, which points at a less aromatic and more quinoidal structure (Figure 4).[9,28] This observation also agrees well with the pronounced lower aromaticity of furan as compared to thiophene. The smaller size of the oxygen atom compared to its heavier congeners favors planarization. The large coplanar structure in combination with the lower aromaticity of the furan rings strongly favors long-range π-conjugation and charge delocalization.[9]

In general, oligofurans possess enhanced luminescence with strong fluorescence and significantly higher quantum yields (e.g. 78% for trifuran vs 7% for trithiophene).[9a]

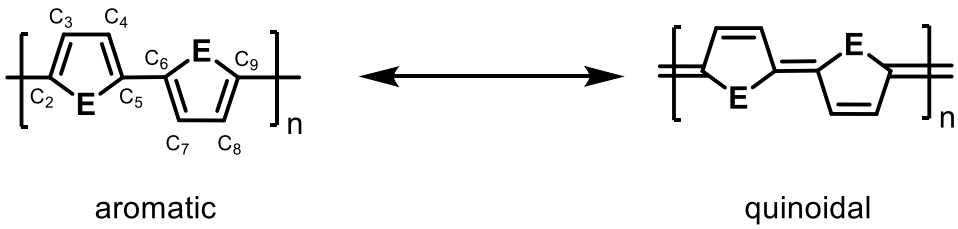

Figure 4. Aromatic and quiniodal resonance form of poly(chalcogene)s **i-iv**.

Although polyfurans show enormous potential as organic polymers for electronic devices, synthetic challenges hampered their use in the past due to their reduced stability in the presence of oxygen and incident light.[9] However, polyfurans will definitively play a more important role in the future since furan rings are biodegradable and can be obtained from entirely renewable resources.[9b,29]

The motivation for the synthesis of both polyselenophenes (**iii**) and polytellurophenes (**iv**) arise from the advantage of the decreasing HOMO-LUMO gap as heavier elements are incorporated within the group XVI heterocycles.[27] This behavior results from a pronounced more quinoid character in the trend S < Se < Te. The decrease in HOMO-LUMO gaps follows the same trend with 2.0 eV (S), 1.9 eV (Se) and 1.5 eV (Te) for polychalcogenes.[11a] Moreover, they also possess enhanced charge transfer by intermolecular Se-Se and Te-Te interactions. As a result, both polyselenophenes (**iii**) and polytellurophenes (**iv**) are considered as attractive candidates for low-band-gap conjugated polymers.[10,11]

The focus of the above described research was on the incorporation of organic polymers (and Se and Te) in semiconducting materials. However, more recently special research interest was on the incorporation of inorganic main group elements into the main chain of such conjugated organic polymers. This approach afforded novel hybrid macromolecules with special features strongly depending on the incorporated element. These macromolecules often show significantly improved properties in comparison to their purely organic relatives.[30] Different types of hybrid macromolecules can be distinguished with regard to the position in which the main-group element is incorporated. If the backbone of the polymers contain both the organic and the inorganic building block, it is called an “inorganic-organic hybrid polymer”, while it is classified as an “organic-inorganic hybrid polymer” if the inorganic building block is located in the side chain and the main chain is purely organic.[2c]

1.2 Cyclolinear Organoboranes

The doping of π-conjugated organic polymers with inorganic main group elements, forming inorganic-organic hybrid polymers, has emerged as promising field in material science. This trend is due to the intriguing properties and often significantly improved features which arise with the integration of such elements into the polymer backbone in comparison to their all organic congeners.[30] The incorporation of tricoordinated boron has been of particular interest since the vacant p-orbital of the trivalent boron can interact with adjacent π-conjugated systems, leading to effective p-π* conjugation, which results in an enhanced electron-accepting ability and often improved photophysical properties (Figure 5).[30,31] Combining inherently electron-deficient borane moieties with electron-rich organic π-conjugated systems has proven to be a versatile method to obtain new donor-acceptor type materials. As a result, π-conjugated organoboranes have aroused tremendous research interest in the last decade. They have been used in several applications for optoelectronic devices such as in polymer-based organic-light emitting diodes (OLEDs), OPVs and OFETs as well as for sensory and bio-imaging purposes.[31-36] The combination with thiophene, as one of the most frequently used organic building blocks, has been of particular interest and provided materials with impressive properties for optoelectronic purposes.[32-34]

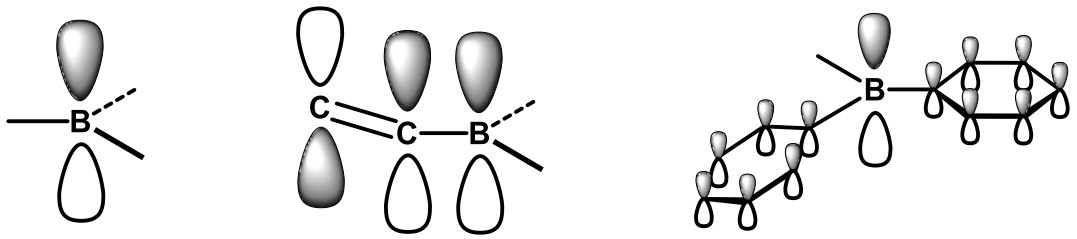

Figure 5. Left: vacant p-orbital of trivalent boron; Center: p-π*-conjugation between boron center and sp^2 carbon atoms; Right: extended π-conjugation over the boron center and adjacent aromatic π-systems.

In the past, the applicability of such organoboranes has been limited due to the intrinsic susceptibility of the boron centers towards small nucleophiles such as water and oxygen. This attack of the nucleophiles would cause a tetrahedral geometry under complete loss of the π-conjugation ability. In order to obtain durable air- and moisture stable materials, effective protection of the vacant orbital of the boron center is necessary.[37-42] In general, three methods are used to protect the boron centers: (A) Embedding of the triarylborane into a rigid, planar structure, thus preventing the formation of a tetrahedral structure via structural constraint (Figure 6, **A**).[37] (B) Attaching a π-donor substituent such as amino groups to electronically saturate the boron centers. However, this might result in a loss of the π-conjugation caused by partial double-bond formation (Figure 6, **B**).[31k] (C) Kinetic stabilization of the boron centers by sterically demanding substituents (Figure 6, **C**).[38]

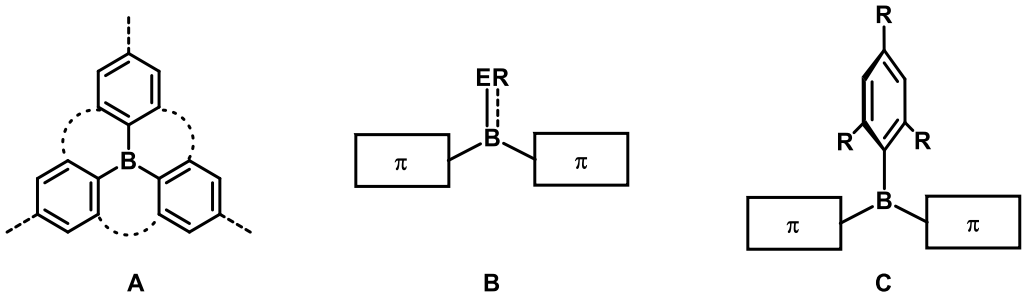

Figure 6. Different types of stabilized triarylboranes: A: stabilization by structural constraint; B: stabilization by electronic effects; C: kinetic stabilization by steric shielding.

Pioneering work on the stability of triarylboranes was performed by Krause and co-workers in the 1930s'.[39] They reported that in comparison to air sensitive triphenylborane (BPh_3), tri-α-naphthylborane showed extended air-stability (signs of oxidation after approx. 14 days).[39c] In 1955, Wittig and co-workers reported the synthesis of tri-(*o*-biphenyl)borane and tri-4-(*N,N*-dimethylamino)phenylborane which indicated extended air-stability as well. These enhanced stabilities were attributed to the surrounding aryl groups which significantly shield the boron atoms in the former case and in the latter to the electronic +*M* effect of the amino substituents.[40] In 1957, the synthesis of the first completely air-stable triarylborane carrying three 2,4,6-trimethylphenylgroups (mesityl, Mes) was reported by Brown and Dodson, and they concluded the correlation of increasing stability with increasing shielding of the boron atoms by the sterical demand of the aryl groups.[38a] Later on, Williams and co-workers found that two mesityl groups connected to the boron centers provide enough steric protection for the conjugated trivalent boron containing π-system.[41]

From this on, the Mes_2B moiety was established as electron-accepting group and was frequently used in combination with electron-donating groups such as oligothiophenes in π-conjugated systems.[42] All studies confirmed that effective shielding of the boron centers is provided by the surrounding formation of a propeller-like structure of the aryl rings.[42] Various functional materials were obtained with interesting properties for non-linear optical, two-photon-absorbing and electron-transporting materials as well as emissive organic solids and emissive materials (Figure 7, a-e).[42-44]

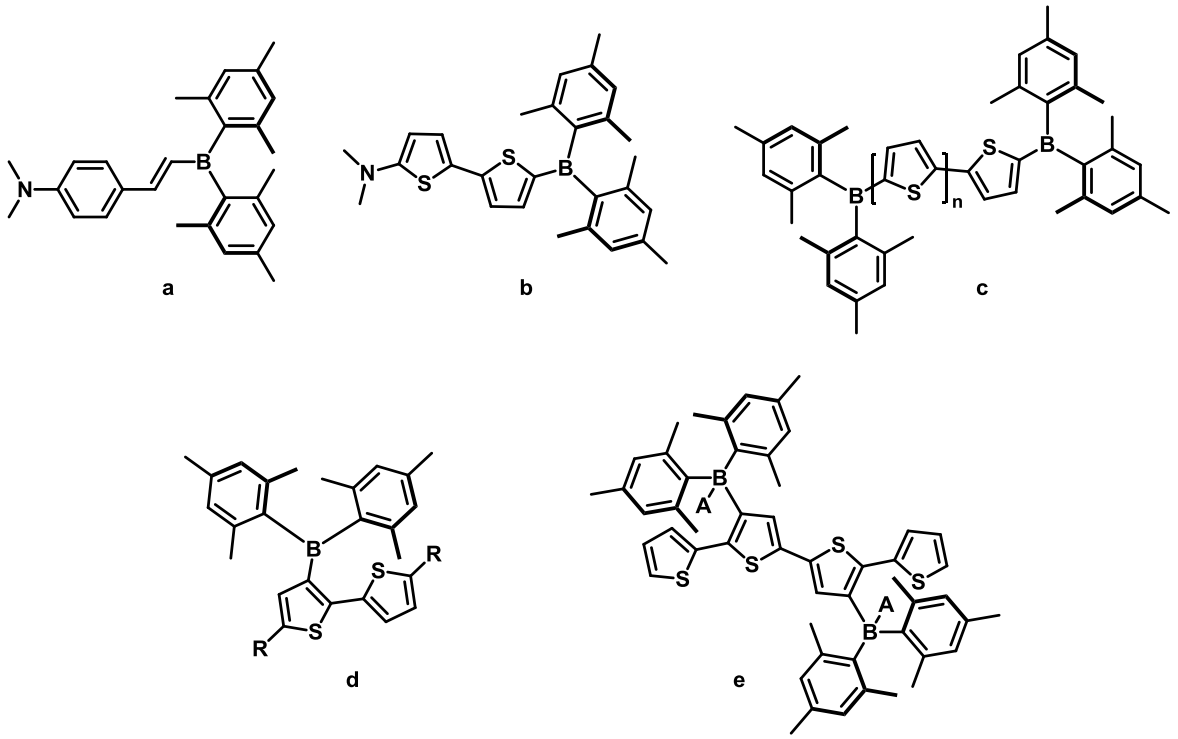

Figure 7. Selected examples for Mes_2B-substituted functional materials and resulting applications as: a) Non-linear optical material; b) Two-photon absorbing material; c) Electron-transporting material; d) Emissive organic solid; e) Turn-on type fluorescence sensor for anions such as F^- or CN^- (adopted from Ref. 44).

The selected examples in figure 7 indicate different classes of materials obtained by effective tuning of the optoelectronic properties as result of incorporation of boron into these systems at the terminal position (**a**-**c**) or in the side chain (**d**-**e**). Changing from monomers to macromolecules, the boron moiety can be either introduced at the terminal position (Figure 8, **D**) to obtain end-group functionalized conjugated polymers, in the side-chain (Figure 8, **E**) to obtain side-chain functionalized boron-doped conjugated polymers or in the main-chain (Figure 8, **F**) to obtain main-chain functionalized boron-doped conjugated polymers (inorganic-organic hybrid polymers). In the latter case, π-conjugated organoborane polymers with tricoordinated boron centers in the main chain participating in the conjugation are obtained.[31o] In every case, effective protection of the boron centers has to be ensured.

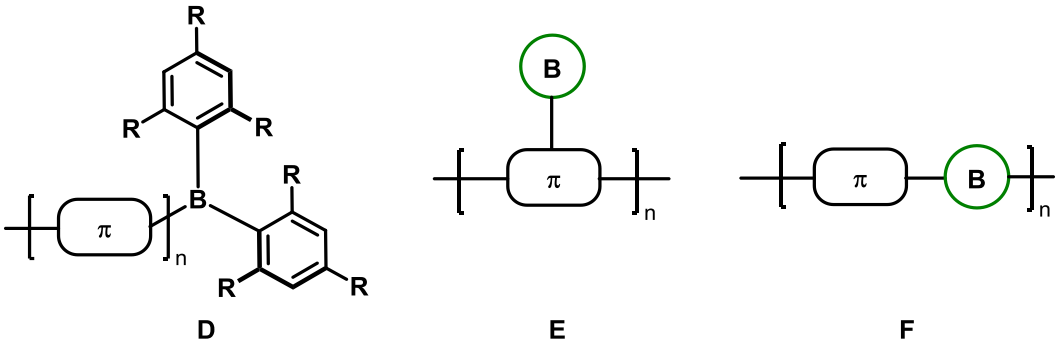

Figure 8. From left to right: Left: end-group functionalized conjugated polymer of type **D**; Center: side-chain functionalized boron-doped conjugated polymer of type **E**; Right: main-chain functionalized boron-doped conjugated polymers (inorganic-organic hybrid polymer) of type **F**.[31o]

In the past, various conjugated organoborane polymers have been synthesized via either B-C or C-C coupling reactions. The first B-C coupling reactions were reported by Chujo and co-workers and were performed following a polyaddition step-growth reaction pathway. These polyaddition reactions include haloboration, phenylboration, haloboration-phenylboration and hydroboration polymerizations (Scheme 3).[45-48] In 1990, Chujo and co-workers reported the synthesis of poly(organoboron halide)s by coupling tribromoborane (BBr_3) and terminal diynes such as **10** in a haloboration reaction. The resulting polymers **11** showed high instability caused by the remaining highly reactive B-Br bonds (Scheme 3, reaction III).[45] The stability of the polymers can be significantly increased when the substituent is changed to triphenylborane (BPh_3) and a phenylboration polymerization reaction is performed to afford polymers **12**. However, the reaction normally requires harsh reaction conditions due to the low reactivity of the triarylborane (Scheme 3, reaction IV).[46] Performing a haloboration-phenylboration polymerization reaction gave access to boron-phenyl substituted polymers **13** and in comparison to the phenylboration polymerization the reaction proceeds at slightly elevated temperatures (100 °C, Scheme 3, reaction V).[47]

In 1998, Chujo and co-workers presented the synthesis of *B*-mesityl substituted polymers **14** via regioselective hydroboration of diethynylarenes **10** with mesitylborane ($MesBH_2$) at ambient temperatures (Scheme 3, reaction VI).[48] Polymers **14** revealed high stability towards air and moisture and were analyzed via gel permeation chromatography which revealed M_n values of 10500 Da and moderate yields (47%) after repeated precipitation.[48c] In 2009, Chujo and co-workers succeeded in the incorporation of the even bulkier 2,4,6-triisopropylphenyl (Tip) group which further enhances the stability by kinetic stabilization of the boron centers as described above.[48d] The hydroboration polymerization approach provided novel access to air- and moisture-stable, readily soluble organoborane polymers.

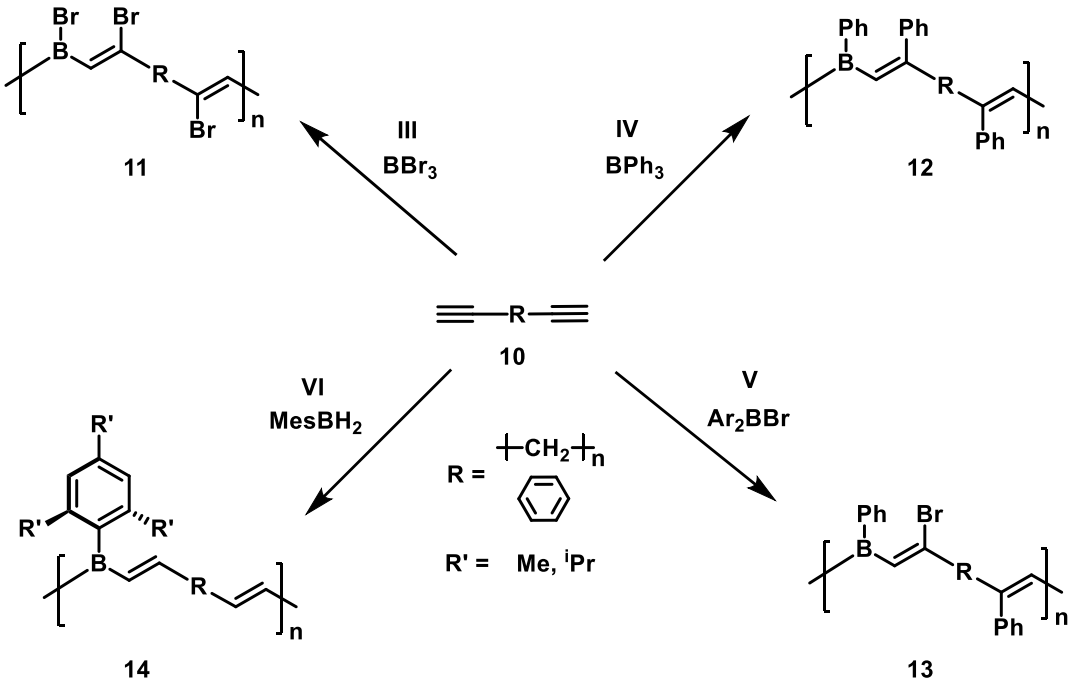

Scheme 3. B-C coupling polyaddition reactions via: (III) haloboration; (IV) phenylboration; (V) haloboration-phenylboration; (VI) hydroboration.

However, this approach is limited to polymers featuring *B*-vinyl linkages. In order to obtain polymers with *B*-aryl or *B*-alkynyl linkages, polycondensation reactions via either C-C or E-C (E = main-group element) coupling reactions have been explored. In general, there are different types of polycondensation strategies to synthesize organoborane polymers as shown in Scheme 4.[2c] C-C coupling type reactions (reactions VII+VIII) are usually transition-metal catalyzed and often proceed via Stille or Suzuki-Miyaura cross-coupling reactions. It can be distinguished between AA/BB type (reactions VII, IX, X) or AB type (reactions VIII, XI) polycondensation reactions. In reaction type VII, an organic building block containing AA-type monomer (can also contain heteroatoms) with leaving groups X is copolymerized with a main-group element containing BB-type monomer with leaving groups Y under formation of the condensation product XY.[2c]

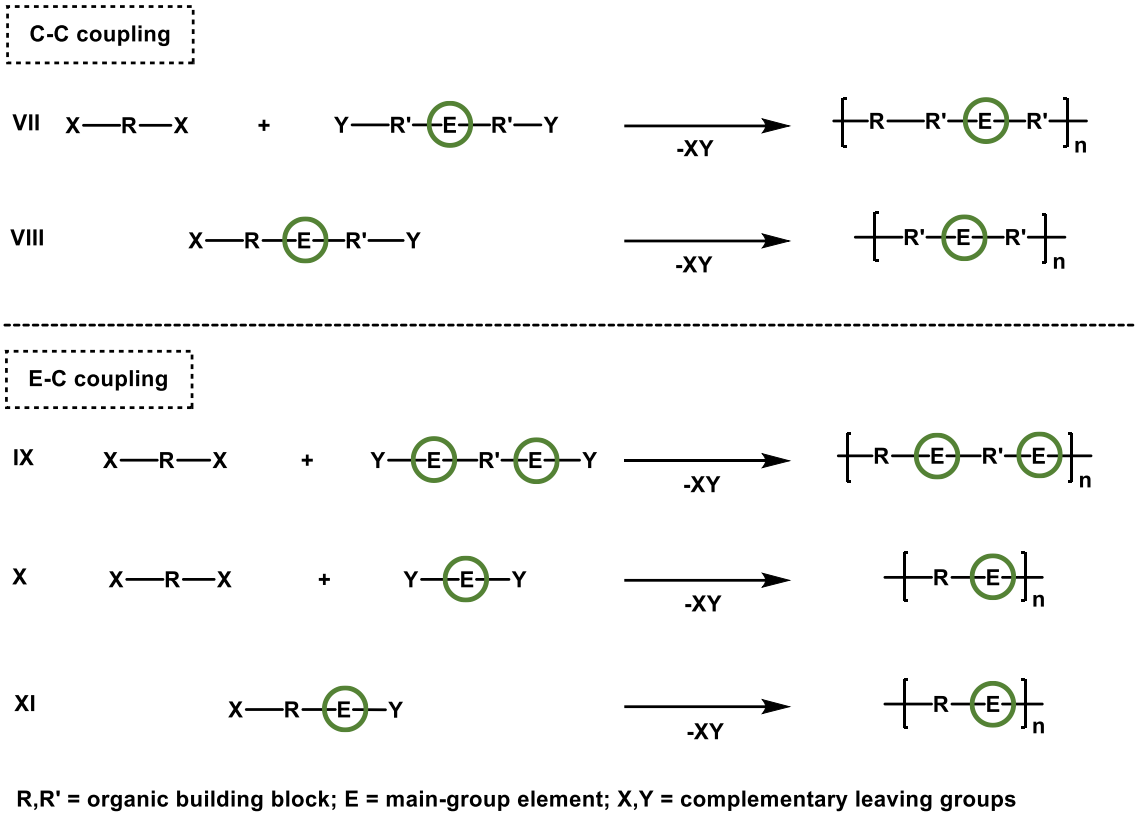

Scheme 4. Different types of polycondensation reactions to give inorganic-organic hybrid polymers: VII), IX), X) AA/BB type polycondensation reactions; VIII), XI) AB type polycondensation reactions.[2c]

For AA/BB type polycondensation reactions, high purity of the starting materials has to be ensured in order to obtain high molecular weight polymers. AB type reaction protocols (reactions VIII and XI) avoid any stoichiometric issues; at every stage of the reaction, the same amount of both complementary functional groups necessary for condensation is available (requirement: absence of any impurities which may destroy one of the two functional groups). This reaction path affords an ideal prerequisite for the formation of high molecular weight polymers. Similar considerations can be made for E-C coupling reactions. The heteroatom-containing coupling partner can either contain two or more (reaction IX) or one heteroatom (reaction X) which also polycondensates with its respective coupling partner under XY formation. Reaction XI proceeds via a related AB-type polycondensation process.[2c]

Of considerable interest was the combination of organoboranes with electron-rich thiophene moieties, resulting in inorganic-organic hybrid polymers with a donor-acceptor structure.[32-34] For C-C coupling reactions, robust dithienylborane building blocks **H** have been extensively explored and used as they are readily available and exhibit excellent stability (Figure 9, top). Effective kinetic stabilization of the boron centers was provided through bulky aryl substituents such as 2,4,6-triisopropylphenyl (Tip), 2,4,6-tri-*tert*-butylphenyl (Mes*, supermesityl) or 2,4,6-tris(trifluoromethyl)phenyl (FMes, fluoromesityl) groups. Furthermore, the steric demand of

these substituents enhances the coplanar structure of the thiophene rings which further enhances π-conjugation.[33]

Marder and Jäkle reported the incorporation of building block **H** into the backbone of conjugated polymers of type **I** by Suzuki-Miyaura cross-coupling reaction between diiodinated building block **15** and diboronated fluorene derivate **16** (Figure 9, reaction XII, bottom left). The obtained polymer **17** showed excellent stability and strong blue luminescence in solution (QY = 31 %) and GPC analysis indicated an average molecular weight of 8400 Da.[31n,33a]

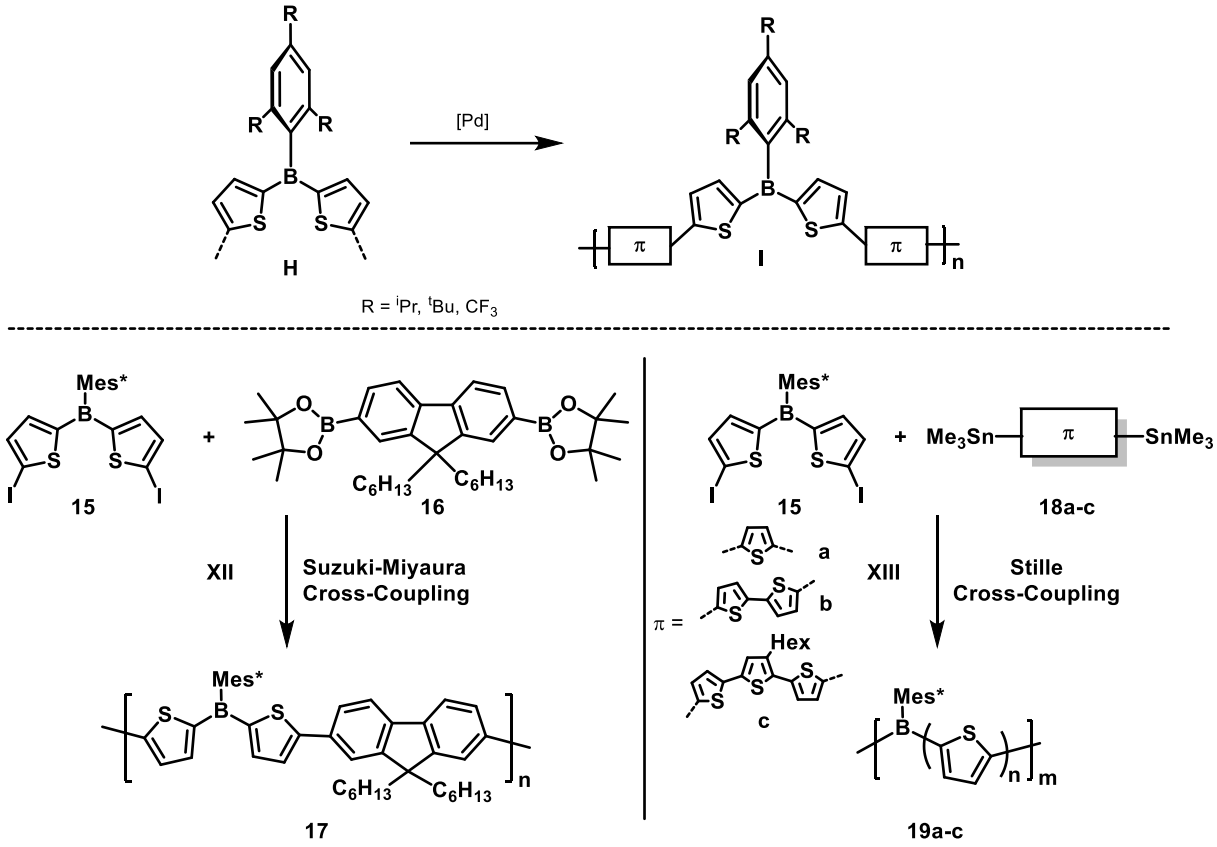

Figure 9. Top: Strategy for the synthesis of air-stable boron-containing inorganic-organic hybrid polymers via palladium catalyzed C-C coupling polycondensation reactions. Bottom left: Suzuki Miyaura cross-coupling reaction (reaction XII). Bottom right: microwave irradiation assisted Stille coupling (reaction XIII).[33a,j]

Jäkle and co-workers also presented the synthesis of a series of cyclolinear poly(oligothiophene borane)s with varying number of thiophene units per repeat unit via microwave irradiation-assisted Stille coupling (Figure 9, reaction XIII, bottom right). In reaction XIII, **15** was reacted with distannylated (oligo)thiophenes **18a-c** with different numbers of thiophene units. The obtained polymers **19a-c** showed high thermal and oxidative stability as well as enhanced optical properties with fluorescence quantum yields up to 38% and a maximum average molecular weight of 11200 Da (for n = 3). For **18c**, solubilizing *n*-hexyl groups had to be attached at the inner thiophene ring of trithiophene to generate polymer **19c**. By varying the length of the thiophene spacer unit which leads to an extension of the π-system,

the emission color could be tuned from blue to deep orange and the band gap was effectively narrowed.[31n,33j] One advantage is the usually high stability of both coupling partners, which gives access to a large number of inorganic-organic polymers being composed of various building blocks.

For B-C polycondensation reactions, organodimetallic reagents such as Grignard reagents **20** or dilithio compounds **21** in combination with boranes with suitable leaving groups such as aryldimethoxyboranes ($ArB(OMe)_2$) can be used for the synthesis of conjugated organoboron polymers with *B*-aryl **22** and *B*-alkynyl linkages **23** (Scheme 5, reactions XIV and XV).[49,50]

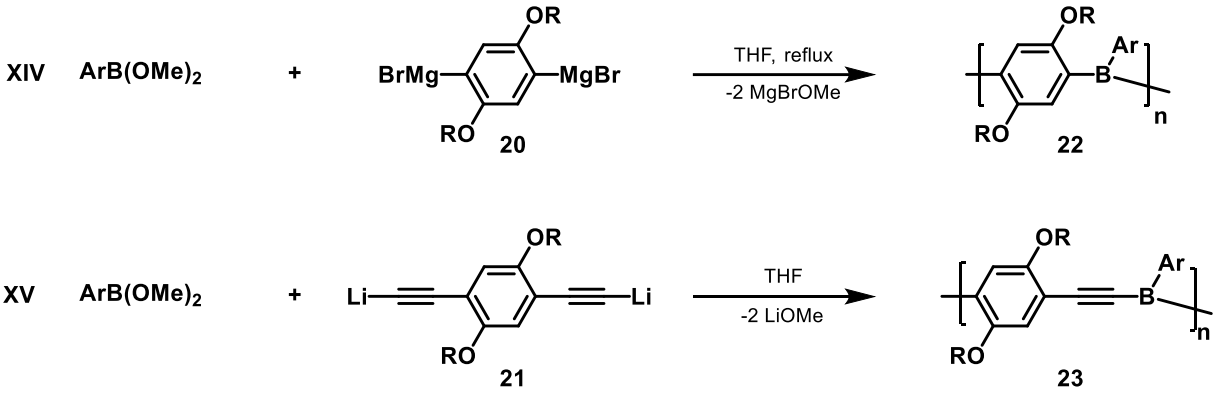

Scheme 5. Synthesis of conjugated organoboron polymers via XIV: Grignard reaction. XV: salt metathesis reaction using dilithio compounds.

Jäkle and co-workers introduced tin/boron exchange polycondensation reaction as a particularly effective method for the synthesis of organoborane polymers.[51] This reaction usually proceeds under mild reactions conditions at room temperature in the absence of coordinating solvents like the above described reactions via organodimetallic reagents. The Sn/B AA/BB type polycondensation reaction proceeds via copolymerization of a distannylated compound, e.g. **24**, and either a aryldihaloborane such as **25** or a bis-haloboryl species such as **28** (Scheme 6, reactions XVI+XVII).[51] For the former case, polymers **26a-c** with different aryl substituents such as pentafluorobenzene or ferrocene units have been prepared by from the respective aryldihaloborane monomers **25a-c**. Polymers **26** obtained via reaction XVI show strong fluorescence, and the emission wavelength can be tuned by the pendant aryl group on the boron. Furthermore, the Lewis acidity of the boron centers is enhanced since the employed aryl substituents are less sterically demanding. This effect leads to enhanced photophysical properties and enables potential applications as sensory materials (**26a,b**). The incorporation of ferrocene units offers interesting opportunities for redox chemistry (**26c**). Nevertheless, these synthesized polymers lack air- and moisture stability.[2c,51a]

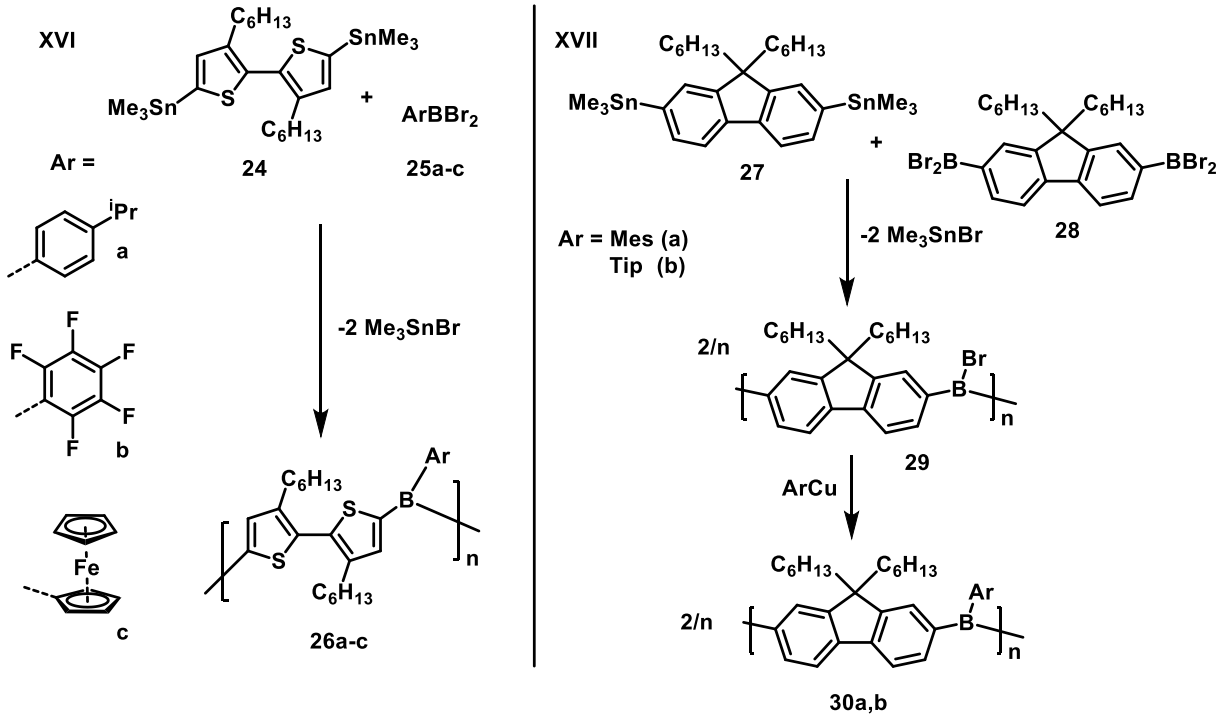

Scheme 6. AA/BB-type tin/boron exchange polycondensation reaction (XVI) via coupling of aryldihaloborane **25a-c** or (XVII) bis-haloboryl species **28** with distannylated coupling partner **24** and **27.**

The copolymerization between the distannylated compound **27** and a bis-haloboryl species **28** afforded the polymer **29**, which has a remaining B-Br bond. In the next step, **29** can be post-modified with bulky substituents, which offers the opportunity to synthesize different polymers **30** from the same precursor. Additionally, the photophysical properties can be fine-tuned by variation of the pendant aryl group.[2c,51b,c] However, the major drawback of this reaction includes the limitation to AA/BB type polycondensation reactions and potential side reactions such as tin-methyl bond cleavage which arise from the high reactivity of the diborylated species. Furthermore, the pronounced high toxicity of the employed organotin compounds limits the potential industrial applicability.[2c]

More recently, Helten and co-workers developed a new B-C coupling method via a silicon/boron exchange condensation reaction.[34] In this method, less toxic organosilicon compounds are used. In comparison to the tin/boron exchange, which readily proceeds at room temperature, the reaction rate for Si/B exchange is significantly lower and thus, a suitable catalyst to promote the reaction is necessary. Helten and co-workers observed that the use of catalytic amounts of electrophilic silyl reagents such as Me_3SiNTf_2 (Tf = SO_2CF_3) effectively accelerate the reaction.[34] The lower reactivity of silicon in comparison to tin renders the synthesis and isolation of AB type monomer **31a** possible, which feature both complementary functional groups necessary for the condensation, $SiMe_3$ and BBr_2 (Scheme 7). This AB type monomer facilitate a more controlled polycondensation, and stoichiometry issues are avoided. AB type monomers **31b** and **34a,b**, however, could not be isolated and had to be used *in-situ*.

Furthermore, compounds **34** feature a solubilizing aryl group, which also provides steric protection of the embedded boron. The Si/B exchange polymerization proceeds under formation of the polymer (precursors) **32** and **35** and the condensation product Me_3SiBr (Scheme 7, reactions XVIII+XIX). The formation of the condensation product can be monitored via ^{1}H-NMR spectroscopy (signal at δ = 0.60 ppm), and it can be easily removed in vacuo after complete reaction. Subsequently, post-modification with TipLi or Mes*Li afforded air- and moisture stable thienyl- and furylborane oligomers **33a,b^{Ar}** and polymers **36a,b^{Ar}**. The obtained poly(furylborane)s **33b^{Mes*}** and **36b^{Mes*}** showed intense blue fluorescence and quantum yields up to 71% and the molecular weight estimated by GPC was up to 3300 Da.[34]

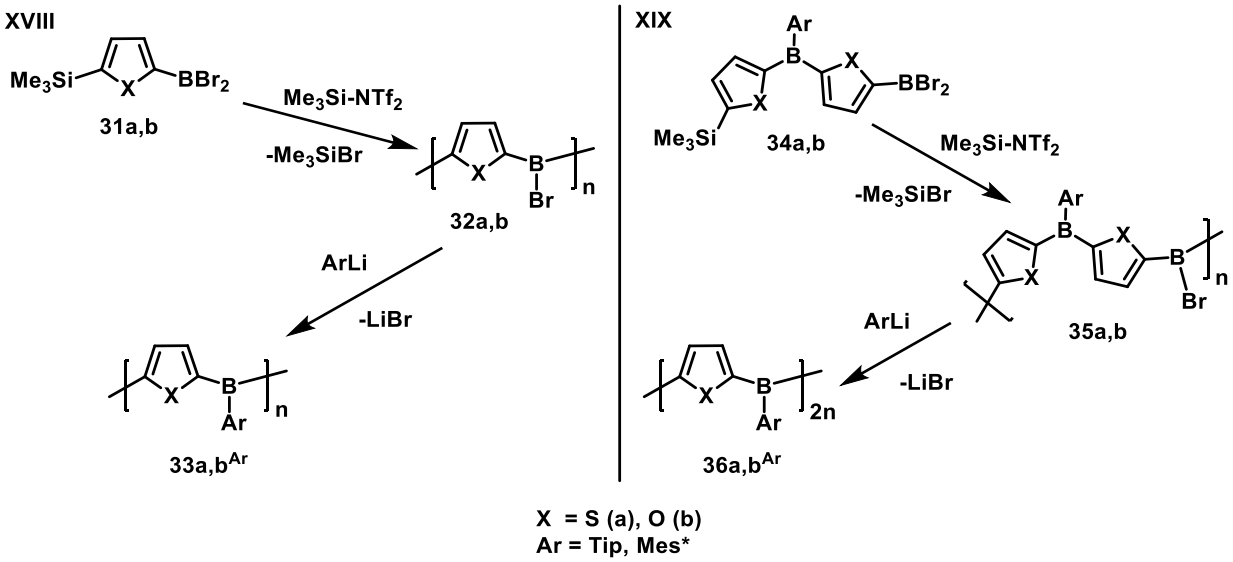

Scheme 7. AB-type silicon/boron exchange polycondensation reaction.

This method has been particular useful for the synthesis of previously scarcely explored cyclolinear furlyborane based materials but has also been applied for the synthesis of a series of cyclolinear thienylborane species as well as mixed compounds. Si/B exchange can also be used for B-N coupling reactions for the synthesis of BCN hybdrid polymers and oligomers.[52]

1.3 Organic Macrocycles

An interesting alternative to linear conjugated oligothiophenes are conjugated macrocycles since they represent the corresponding oligomer chain without the end group functionality, thus excluding perturbing end group effects. Fully conjugated macrocycles with shape-defined length can be formally considered as infinite π-conjugated systems and thus offer unusual and promising optical, electronic and magnetic properties depending on their structural parameters such as conjugation length, ring-size and on the inserted π-systems.[53] Furthermore, they possess a high rigidity and exhibit a shape-persistent inner cavity which can act as host and incorporate small molecules or ions. This host-guest interaction gives rise to potential applications in supramolecular chemistry.[53] Further applications include organic light-emitting diodes, organic field effect transistors and organic solar cells.[8d,53a] In the past, different types of thiophene-based macrocycles have been reported but in most of the cases, *α,β*- or *β,β* linkages led to cross-conjugation and distortion or twisting of the thiophene rings due to interruption of the conjugation. However, in order to obtain a fully conjugated macrocycle, *α*-linkages are of upmost importance which is further supported by theoretical calculations performed by Tol and co-workers on cyclo[12]thiophenes (**C12T**, **J**) and on corresponding charged species **K**, which are formally thiophene substituted annulenes (Figure 10).[8d,54]

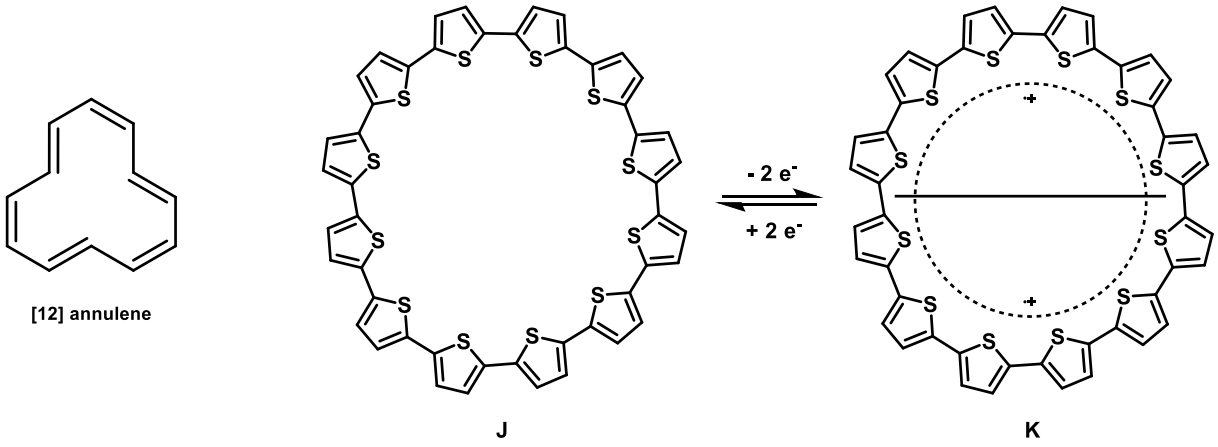

Figure 10. All carbon [12] annulene, neutral cyclo[12]thiophene **J** and charged cyclo[12]thiophene **K**.[54]

The studies indicated an all *syn* confirmation of the thiophene rings as well as a nearly unstrained and coplanar structure.[8d] Upon charging of **J**, first single oxidation led to a radical cation that is delocalized over one part of the circle. A second oxidation step results in the formation of a dicationic radical species **K** in which each of the cation radicals is located on one semicircle. The first synthesis of fully *α*–conjugated cyclothiophenes **C12T**, **C16T** and **C18T** was described by Bäuerle and co-workers in 2000. It was accomplished by copper-mediated oxidative coupling of terminally bis-ethynylated oligothiophenes **37** under pseudo-high dilution conditions (Scheme 8, i). In this commonly used statistical macrocyclization method, oligomerization and macrocyclization reactions are proceeding at the same time to

afford mixtures of macrocycles **38** in low yields. Separation of the compounds was performed by preparative HPLC.[8d,55] Reaction thereof with sulfide afforded the corresponding *α*-conjugated macrocycles **CXT** (Scheme 8, ii).[8d,53] However, **C12T**, **C16T** and **C18T** showed a rather benzoid than annulenoid character with no observable ring current and have to be considered, according to Hückel, as antiaromatic (4n) π annulenes.[8d]

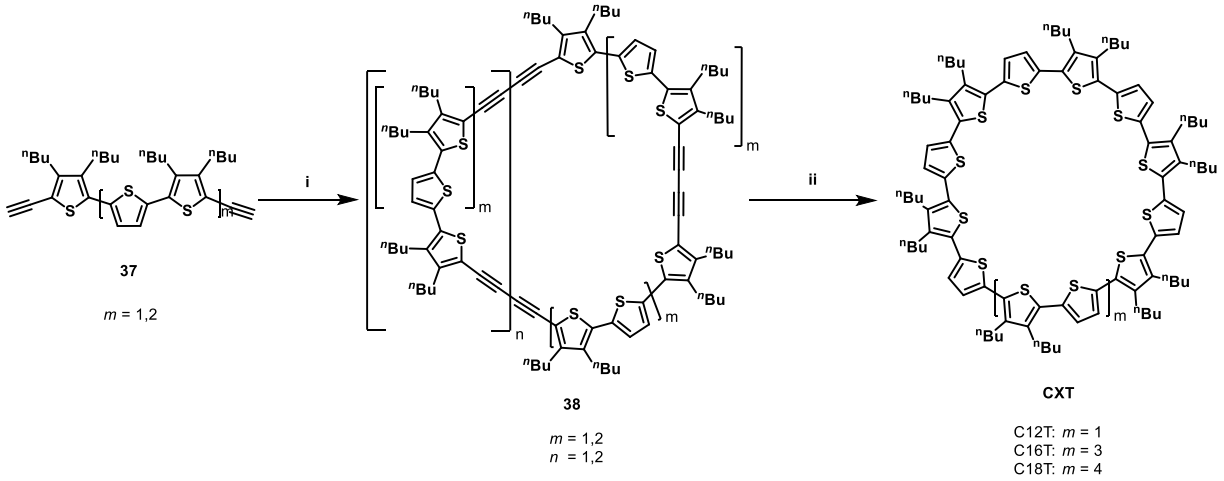

Scheme 8. i) Macrocyclization of thiophenediynes **37** under modified Eglington-Glaser conditions: CuCl, $CuCl_2$, pyridine, RT, 44+48h; ii) Reaction of cyclooligothiophenediacetylenes **38** to fully *α*-conjugated cyclo[*n*]thiophenes (**CXT**): $Na_2S{\cdot}9\ H_2O$, 2-methoxyethanol, *p*-xylene, reflux (4h).[53a,55]

In a different approach, extended oligomers with double functionalization are used to afford only one main product because of intramolecular macrocyclization reaction under high dilution.[8d] Major drawbacks of this approach include the challenging stepwise synthesis of longer starting materials. However, reaction protocols for the synthesis of longer oligothiophenes have been well described in literature and one-step intramolecular cyclization of such a species under pseudo-high dilution afforded two different macrocycles, one obtained by intramolecular reaction and one by an intermolecular reaction, in improved yield.[57] Nevertheless, the overall yield considering the preparation of the precursor in combination with the macrocyclization reaction is comparably low. As a more promising strategy and to avoid low yields and mixtures of cyclic products, template-assisted synthesis of macrocycles has been studied. Bäuerle *et al.* synthesized cyclo[8]thiophene via a platinum intermediate **40** (91% yield) and C-C bond formation through reductive elimination, starting from bis-ethynylated terthiophene **39** in moderate yields. The obtained strained cyclodimeric compound **41** was then converted into **C8T** (Scheme 9).[8d,58] More recently, Bäuerle *et al.* reported the synthesis of highly symmetric extended cyclic structures of **C10T**-**C35T** via multinuclear Pt^{II} complexes.[59] X-ray structural analysis of CXT precursors with different ring sizes revealed that the increasing ring strain with decreasing ring size leads to bending of the butadiyne units and distortion of the thiophene rings.[8d] X-ray structural analysis of **C10T** indicated a nearly circular structure in which the adjacent thiophene rings were twisted by 26-34° to avoid ring strain.[8d,59]

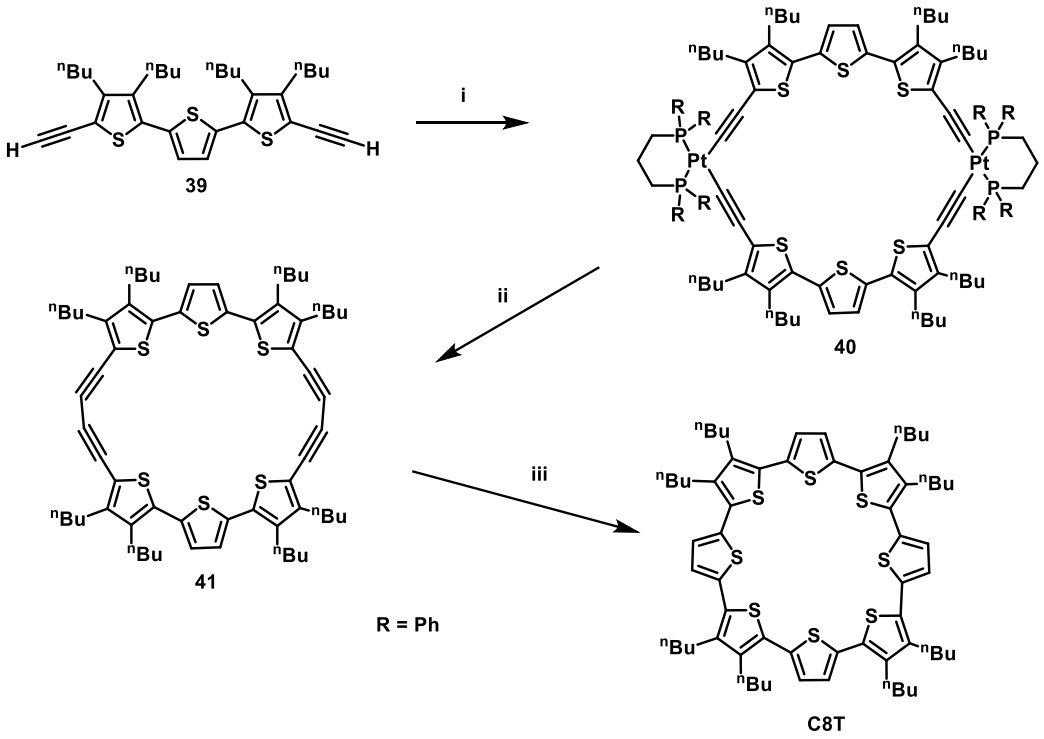

Scheme 9. Template-assisted synthesis of macrocycle **C8T** via platinum-intermediate **40**: i) cis-Pt(dppp)Cl_2, CuI (10 mol%), 2 eq. NEt_3, toluene, rt, 72h; ii) 2 eq. I_2, THF, 60 °C; iii) Na_2S*9 H_2O, xylene, $MeO(CH_2)_2OH$, 140 °C, 24h.[8d,58]

In order to reduce the ring strain induced by all *α*-coupled thiophene rings, different substituents such as vinylene units can be incorporated in the *α*-position. As result, compound **45**, which can be considered as thiophene derivative of [18]annulene (which satisfies Hückel's rule and shows aromatic ring current)[60] with three sulfur bridges and features vinylene units between the thiophene rings was first synthesized by Lewis *et al.*[61] in a multistep procedure in low yields and later on by Cava *et al*. via McMurry coupling of 2,5-thiophenedicarboxyaldehyde **42** in moderate yields (Scheme 10).[62] During the synthesis, a related tetrasulfide macrocycle was also obtained in low yield. X-ray structural analysis of **45** indicated a lack of planarity as well as distortion of the thiophene rings and no significant ring current or additional aromaticity as from the thiophene itself. When the reaction protocol was applied for reductive coupling of higher homologues **43** and **44** tetrathiaporphycene **46** and hexathiahomoporphycene **47** as 4nπ-thiophene analogues of porphycene were obtained (Scheme 10). The former, a 16π macrocycle (**46**), showed no obvious ring current and no planarity and only moderate conjugation as determined by UV-vis spectroscopy and by X-ray structural analysis.[8d,62,63] The latter, a 28π macrocycle (**47**) showed extended conjugation as shown by UV-vis spectroscopy (absorption shifted to higher wavelengths). Furthermore, generating a 26π dicationic species **48** by addition of sulfuric acid was successful and the absorption maximum was shifted from 431 nm to 885 nm, which is in a typical range for porphyrins. Additionally, a strong ring current effect was observed.[8d,62] Different mixed macrocycles being composed of thiophene, furan and

pyrrole moieties have been synthesized as heterocyclic derivatives of [18]annulene and compound **45**. However, none of these compounds indicated planarity, aromaticity as well as incomplete cyclic delocalization.

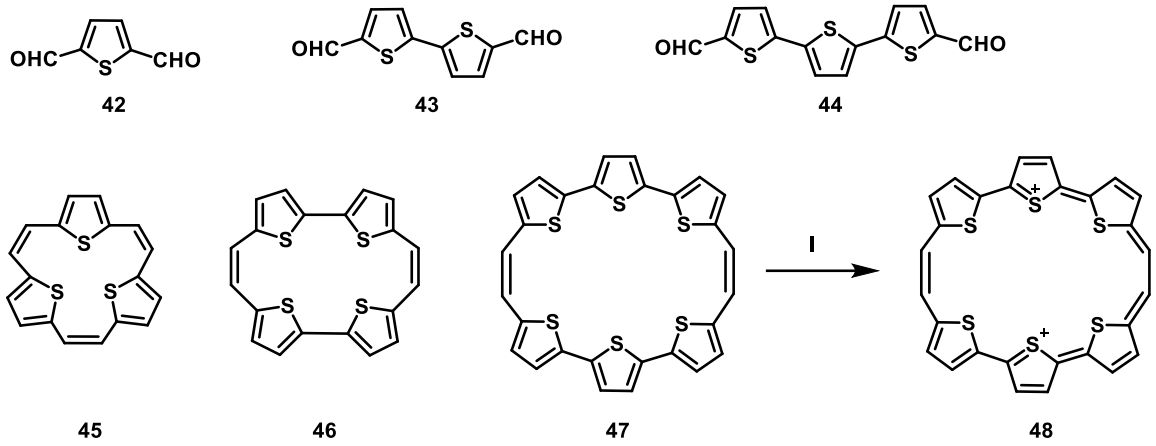

Scheme 10. Synthesis of thiophene based annulenes via McMurray coupling.

These results showed the structural similarity of these thiophene based macrocycles to porphyrins, which are heterocyclic doped variants of fully aromatic [18]annulenes. Porphyrins in general have been extensively studied and are of particular interest since they play a key role in many processes of living organisms such as binding and transport of oxygen or the conversion of light into usable energy. Beside various technological applications therof and related macrocycles, increasing interest in their use as artificial light-harvesting antennae in OPV cells has emerged in recent years.[64] First studies on heteroatom doped variants with this structural motif (X = nitrogen, parent derivative, porphin, **Por**) such as sulfur- **49**, oxygen- **50** and selenium-analogues **51** were first described by Vogel in 1989 (Scheme 11).[65] The dicationic 18π macrocycles **52-54** were obtained by addition of 2,3-dichloro-5,6-dicyano-1,4-benzoquinone (DDQ) to the related neutral 16π macrocyclic forms **49-51**, which have been synthesized starting from furfuryl alcohol (Scheme 11). Interestingly, compound **52** is a violet solid with significant distortion of the thiophene rings up to 23° but still strong absorptions up to 700 nm, resembling dialkylated porphyrin dications. As a result, the limited planarity of the systems did not hamper the electronic delocalization and the aromaticity.[65] Each of the dicationic 18π macrocycles were perfectly stable, colorful solids, while the neutral antiaromatic form (according to Hückel) is instable.

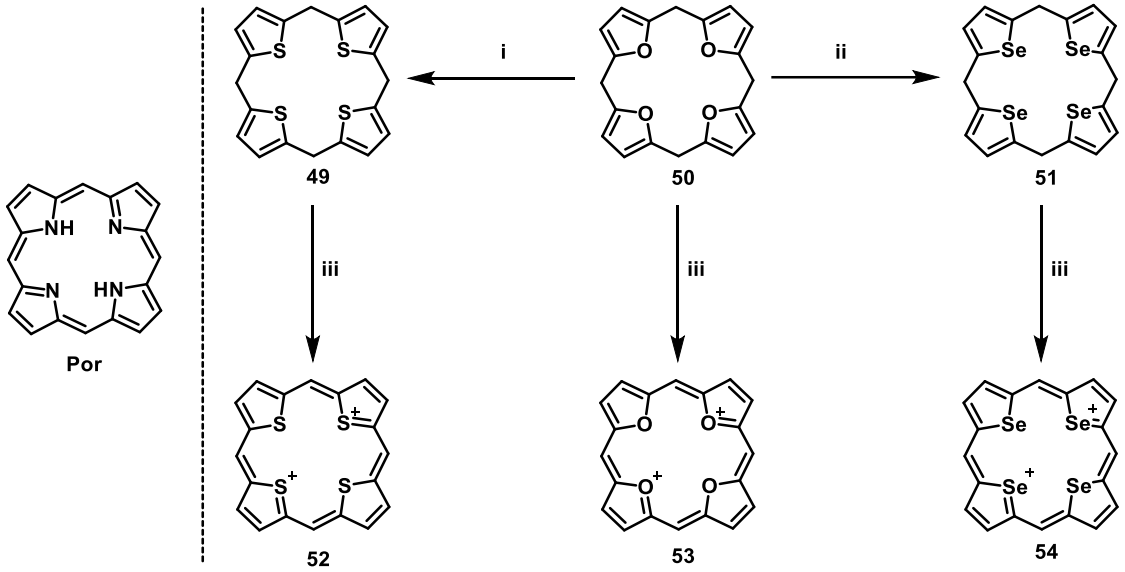

Scheme 11. Syntheses of neutral and charged sulfur- **49,52**, oxygen- **50,53** and selenium **51,54** doped porphyrins: i) H^+, H_2S; ii) H^+, H_2Se; iii) DDQ, $HClO_4^-$.

The first example for an all-thiophene based neutral porphyrinoid structure was described by Cava *et al.* with their synthesis of a 22π macrocycle tetrathia[22]annulene[2,1,2,1] via McMurray coupling of 5,5'-methylenebis-2-thiophenecarboxaldehyde and subsequent addition of DDQ and hydrazine.[8d,66] The aromaticity was confirmed by NMR spectroscopy as a result of deshielding of the protons caused by the aromatic ring current. Furthermore, it was evidenced via UV-Vis spectroscopy and the presence of an absorption maximum at 417 nm. Additional absorptions at higher wavelengths (503-771 nm) can be related to the typical Soret- and Q-bands of porphyrins (cf. Figure 11, UV-Vis spectrum of porphyrin).[66,67]

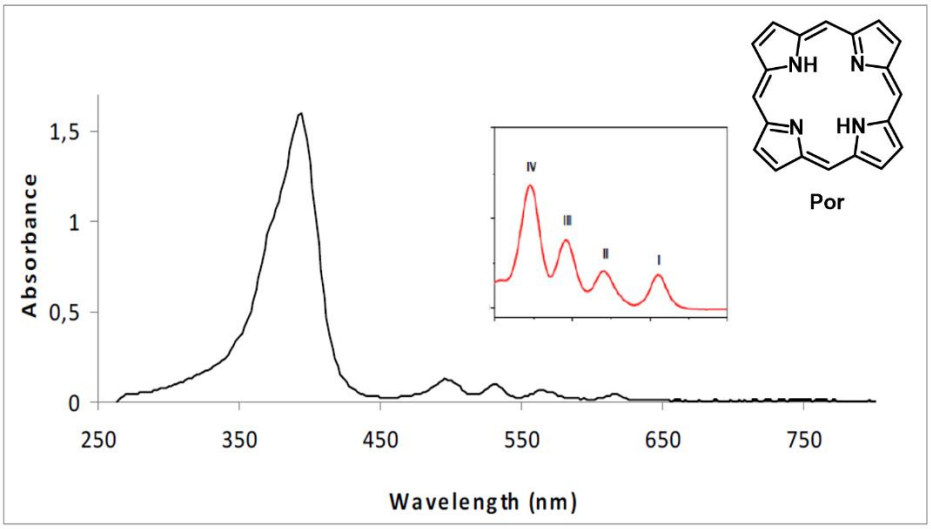

Figure 11. UV-Vis spectrum of standard porphyrin (**Por**, the parent derivative, porphin) with Soret- (approx. 380-420 nm) and Q-bands (approx. 480-600 nm). Insert: Enlargement of Q region between 480-720 nm (taken from Ref. 67).

Different macrocycles with mixed heterocycles incorporated in a porphyrinoid structure have been synthesized.[8d]

1.3.1 Boron-Containing Organic Macrocycles

The incorporation of boron in *meso*-positions of porphyrin was first studied by Siebert and co-workers.[68] In 1998 Corriu, Douglas, Siebert *et al.* synthesized the first boron-bridged tetrathiaporphyrinogen **57** with diisopropylamino groups at boron via reaction of dilithiated species **55** with aminodichloroborane **56** (Scheme 12).[68a]

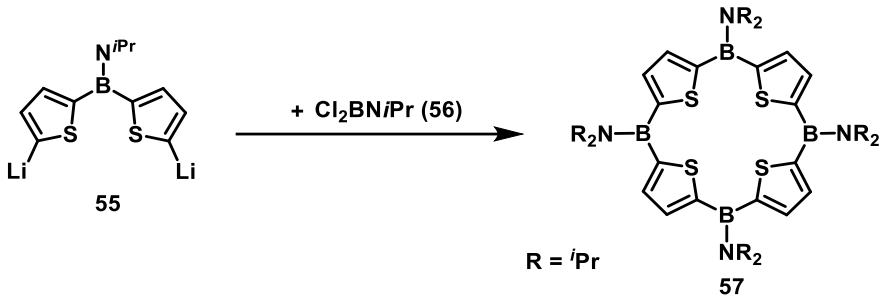

Scheme 12. Synthesis of boron-doped tetrathiaporphyrinogen **57**.

Macrocycle **57** contains a closed cycle of sp^2 hybridized carbon and boron atoms and, thus, could potentially possess macrocyclic π-conjugation, which, however, was not observed. X-ray structure analysis revealed that the four boron atoms are not in the same plane, and the thiophene rings are heavily twisted. The B-C bond lengths for **57** (1.57 Å) are in the range of normal B-C single bonds.[68a] No ring current or communication over the macrocycle between the boron atoms was observed.[68a] Siebert and co-workers also described the synthesis of diboratetrathiaporphyrinogens **61a-d** with different substituents on the boron atoms via reaction of *in-situ* generated dilithiated compound **59** with dialkylamino substituted dichloroboranes **60a-c** or a duryl (2,3,5,6-tetramethylbenzene) substituted dichloroborane **60d** (Scheme 13).

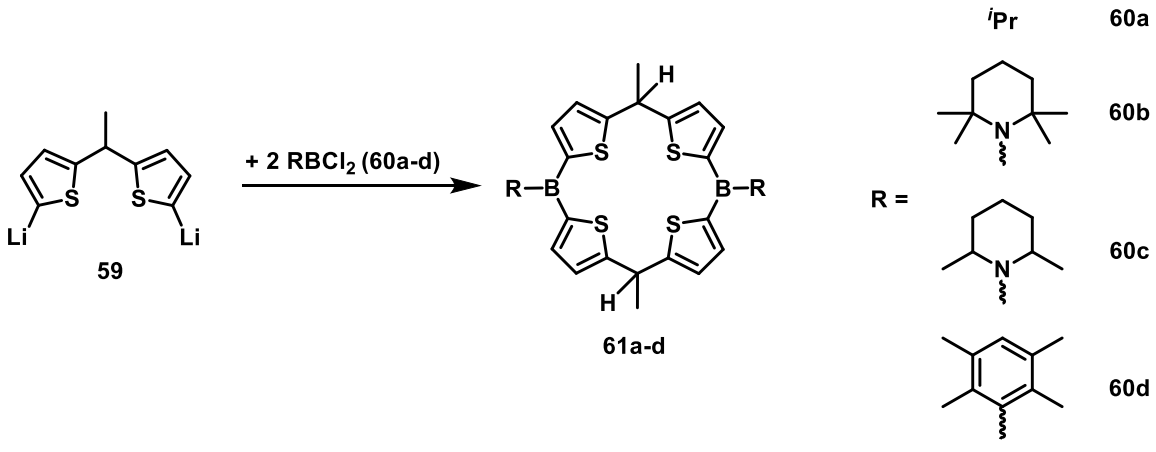

Scheme 13. Synthesis of diboratetraporphyrinogens **61a-d** with different substituents.

Electronic stabilization of the boron atoms by diisopropylamino, tetramethylpiperidyl and dimethylpiperidyl was not sufficient to obtain air- and moisture-stability. Steric protection by the use of a duryl substituent on the boron atom afforded a macrocycle (**60d**) with sterical rather than electronic stabilization.[68c]

In the last decade, Jäkle and co-workers have reported the synthesis of different types of boron-containing conjugated macrocycles **63-67** (Figure 12).[69] In all cases, the reactions were performed under high dilution conditions to avoid the formation of linear oligomeric side products. Macrocycle **63**, a bora-cyclophane, featuring six boron atoms and sterically protected by the bulky Tip substituent, showed complete delocalization of the LUMO over the entire macrocycle, while the HOMO was located on the fluorene building blocks. The electron-deficient nature as result of the incorporated six organoborane moieties offers an ideal prerequisite for anion binding. Characterization via UV-Vis spectroscopy revealed a significant difference to their linear counterpart.[69b] More recently, they reported the synthesis of an even stronger electron-deficient macrocycle **64** with shorter phenylene linkers and FMes groups being attached to the boron atoms, further increasing the electron-acceptor properties.[69c] Additionally, they synthesized an ambipolar phenylene linked B-π-N conjugated macrocycle **65** with three alternating boron and nitrogen atoms sterically protected by bulky substituents. Strong interaction between boron and nitrogen was confirmed by electrochemical measurements and observable solvatochromic effects on the emission was evidenced by an increasing redshift with increasing polarity.[69d] The same effect was observed for macrocycles **66** and **67** with different spacing units but less ring strain.[69e]

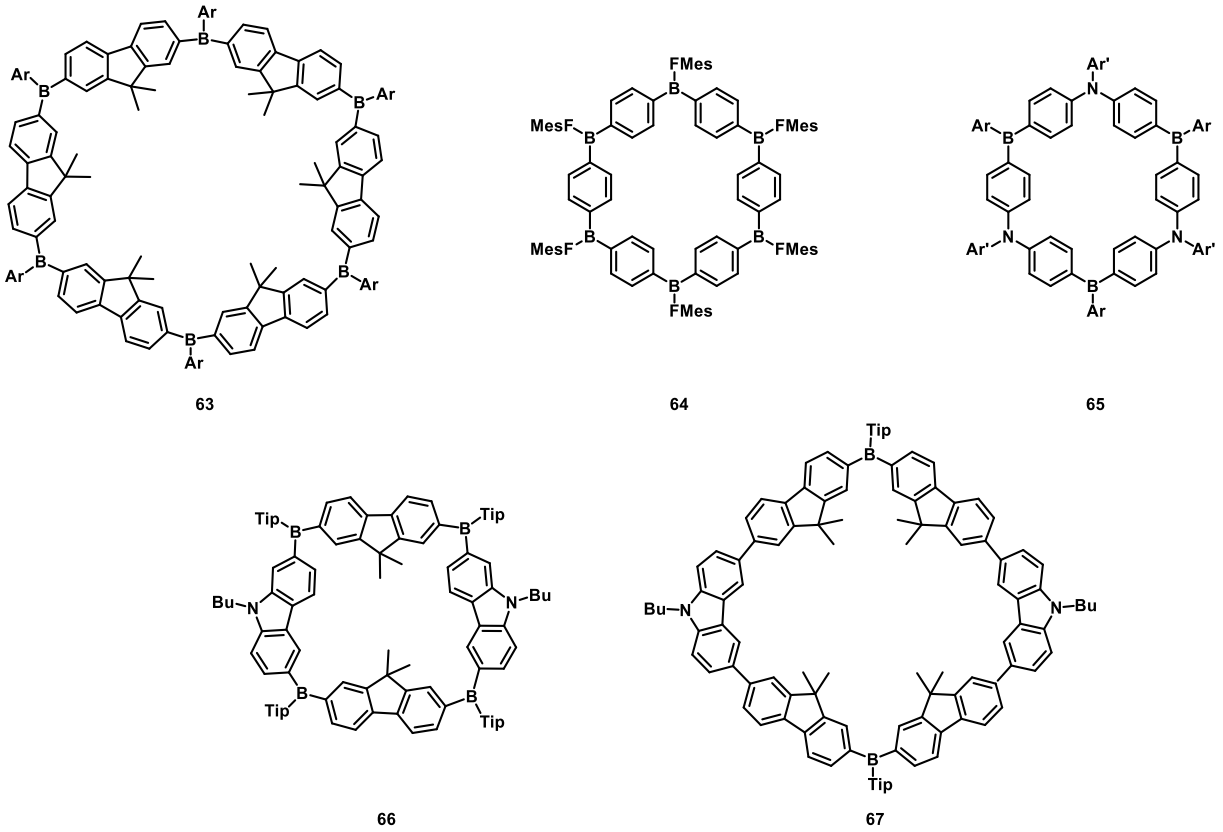

Figure 12. Conjugated organoborane macrocycles **63-67** synthesized by Jäkle and co-workers.

1.4 References

[1] B.G. Yacobi, *Semiconductor Materials: An Introduction to Basic Principles*, Springer 2003 ISBN 0-306-47361-5, pp. 1–3

[2] a) T. M. Swager, *Macromolecules* **2017**, *50*, 4867-4886; b) M. Mooney, A. Nyayachavadi, S. Rondeau-Gagné, *J. Mater. Chem. C*, **2020**, *8*, 14645-14664; c) H. Helten, *"Conjugated Inorganic–Organic Hybrid Polymers"*, in *Encyclopedia of Inorganic and Bioinorganic Chemistry* (Ed.: R. A. Scott), John Wiley, Chichester, **2017.**

[3] A. C. Grimsdale, K. L. Chan, R. E. Martin, P. G. Jokisz, A. B. Holmes, *Chem. Rev.* **2009**, *109*, 897-1091.

[4] a) A. Facchetti, *Chem. Mater.* **2011**, *23*, 733-758; b) C. Wang, H. Dong, W. Hu, Y. Liu, D. Zhu, *Chem. Rev.* **2012**, *112*, 2208-2267; c) J. Mei, Y. Diao, A. L. Appleton, L. Fang, Z. Bao, *J. Am. Chem. Soc.* **2013**, *135*, 6724-6746;

[5] a) Y-J. Cheng, S.-H. Yang, C.-S. Hsu, *Chem. Rev.* **2009**, 109, 5868-5923; b) C. Li, M. Liu, N. G. Pschirer, M. Baumgarten, K. Müllen, *Chem. Rev.* **2010**, *110*, 6817-6855; c) P. M. Beaujuge, J. M. J. Fréchet, *J. Am. Chem. Soc.* **2011**, *133*, 20009-20029.

[6] C. Zhu, L. Liu, Q. Yang, F. Lv, S. Wang, *Chem. Rev.* **2012**, *112*, 4687-4735.

[7] S. W. Thomas III, G. D. Joly, T. M. Swager, *Chem. Rev.* **2007**, *107*, 1339-1386.

[8] a) I. Osaka, R. D. McCullough, *Acc. Chem. Res.* **2008**, *41*, 1202-1214; b) R. D. McCullough, *Adv. Mater.* **1998**, *10*, 93-116; c) T. P. Kaloni, P. K. Giesbrecht, G. Schreckenbach, M. S. Freund, *Chem. Mater.* **2017**, *29*, 10248-10283; d) A. Mishra, C.-Q. Ma, P. Bäuerle, *Chem. Rev.* **2009**, *109*, 1141-1276; e) S. C. Rasmussen, S. J. Evenson, C. B. McCausland, *Chem. Commun.* **2015**, *51*, 4528-4543; f) M. E. Cinar, T. Ozturk, *Chem. Rev.* **2015**, *115*, 3036-3140.

[9] a) O. Gidron, Y. Diskin-Posner, M. Bendikov, *J. Am. Chem. Soc*, **2010**, *132*, 2148-2150; b) O. Gidron, M. Bendikov, *Angew. Chem. Int. Ed.* **2014**, *53*, 2546-2555; c) U. H. F. Bunz, *Angew. Chem. Int. Ed.* **2010**, *49*, 5037-5040; d) C. H. Woo, P. M. Beaujuge, T. W. Holocombe, O. P. Lee, J. M. J. Fréchet, *J. Am. Chem. Soc.* **2010**, *132*, 15547-15549; e) S. Sharma, M. Bendikov, *Chem. Eur. J.* **2013**, *19*, 13127-13139; f) X.-H. Jin, D. Sheberla, L. J. W. Shimon, M. Bendikov, *J. Am. Chem. Soc.* **2014**, *136*, 2592-2601; g) L. Huo, B. Fan, Z. Zhao, X. Sun, D. Wie, M. Yu, Y. Liu, Y. Sun, *Adv. Mater.* **2015**, *27*, 6969-6975; h) H. Cao, P. A. Rupar, *Chem. Eur. J.* **2017**, *23*, 14670-14675; i) A. Islam, Z.-Y. Liu, R.-X. Peng, W.-G. Jiang, T. Lei, W. Li, L. Zhang, R.-J. Yang, Q. Guan, Z.-Y. Ge, *Chinese J. Polym. Sci.* **2017**, *35*, 171-183.

[10] a) G. C. Hoover, D. S. Seferos, *Chem. Sci.* **2019**, *10*, 9182-9188; b) A. Patra, M. Bendikov, *J. Mater. Chem.* **2010**, *20*, 422-433; c) A. Patra, R. Kumar, S. Chand, *Isr. J. Chem.* **2014**, *54*, 621-641; d) M. Heeney, W. Zhang, D. J. Crouch, M. L. Chabinyc, S. Gordeyev, R. Hamilton,

S. J. Higgins, I. McCulloch, P. J. Skabara, D. Sparrowe, S. Tierney, *Chem. Commun.* **2007**, 5061-5063.

[11] a) E. I. Carrera, D. S. Seferos, *Macromolecules* **2015**, *48*, 297-308; b) E. Rivard, *Chem. Lett.* **2015**, *44*, 730-736; c) B. T. Luppi, R. McDonald, M. J. Ferguson, L. Sang, E. Rivard, *Chem. Commun.* **2019**, *55*, 14218-14221.

[12] a) T. Yamamoto, K. Sanechika, A. Yamamoto, *J. Polym. Sci., Polym. Lett. Ed.* **1980**, *18*, 9-12; b) J. W. P. Lin, L. P. Dudek, *J. Polym. Sci., Polym. Lett. Ed.* **1980**, *18*, 2869-2873; c) R. L. Elsenbaumer, K. Y. Jen, R. Oboodi, *Synth. Met.* **1986**, *15*, 169-174.

[13] R. D. McCullough, R. D. Lowe, *J. Chem. Soc. Chem. Commun*. **1992**, *1*, 70-72.

[14] T.-A. Chen and R. D. Rieke, *J. Am. Chem. Soc.* **1992**, *114*, 10087-10089.

[15] R. S. Loewe, S. M. Khersonsky, R. D. McCullough, *Adv. Mater.* **1999**, *11*, 250.

[16] a) R. Miyakoshi, K. Shimono, A. Yokoyama, T. Yokozawa, *J. Am. Chem. Soc.* **2006**, *128*, 16012-16013; b) M. Iovu, E. E. Sheina, R. R. Gil, R. D. McCullough, *Macromolecules* **2005**, *38*, 8649-8656.

[17] A. Iraqi, G. W. Barker, *J. Mater. Chem.* **1998**, *8*, 25-29.

[18] S. Guillerez, G. Bidan, *Synth. Met.* **1998**, *93*, 123-126.

[19] B. S. Ong, Y. Wu, P. Liu, S. Gardner, *J. Am. Chem. Soc.* **2004**, *126*, 3378-3379.

[20] Y.-Y. Lai, T.-C. Tung, W.-W. Liang, Y.-J. Cheng, *Macromolecules* **2015**, *48*, 2978-2988.

[21] J.-R. Pouilot, M. Wakioka, F. Ozawa, Y. Li, M. Leclerc, *Macromol. Chem. Phys.* **2016**, *217*, 1493-1500.

[22] A. A. Jahnke, B. Djukic, T. M. McCormick, E. Buchaca Domingo, C. Hellmann, Y. Lee, D. S. Seferos, *J. Am. Chem. Soc.* **2013**, *135*, 951-954.

[23] T.- Lei, J.-Y. Wang, J. Pei, *Chem. Mater.* **2014**, *26*, 594-603.

[24] S. Kirchmeyer, K. Reuter, *J. Mater. Chem.* **2005**, *15*, 2077-2088.

[25] W. Pisula, K. Müllen, *J. Am. Chem. Soc.* **2015**, *137*, 9503-9505.

[26] a) A. Ajayaghosh, *Chem. Soc. Rev*. **2003**, *32*, 181-191; b) X. Guo, M. Baumgarten, K. Müllen, *Prog. Polym. Sci.* **2013**, *38*, 1832-1908; c) T. Mikie, I. Osaka, *J. Mater. Chem. C.* **2020**, *8*, 14262-14288; d) K. Kawabata, I. Osaka, M. Nakano, N. Takemura, T. Koganezawa, K. Takimiya, *Adv. Electron. Mater.* **2015**, *1*, 1500039; e) H. N. Tsao, D. M. Cho, I. Park, M. R. Hansen, A. Mavrinskiy, D. Y. Yoon, R. Graf, W. Pisula, H. W. Spiess, K. Müllen, *J. Am. Chem. Soc*. **2011**, *133*, 2605-2612; f) K. Takimiya, I. Osaka, M. Nakana, *Chem. Mater.* **2014**, *26*, 587-593.

[27] a) A. Patra, Y. H. Wijsboom, G. Leitus, M. Bendikov, *Chem. Mater.* **2011**, *23*, 896-906; b) S. A. Grefory, A. K. Menon, S. Ye, D. S. Seferos, J. R. Reynolds, S. Yee, *Adv. Energy Mater.* **2018**, *8*, 1802419; c) M. Jeffries-EL, B. M. Kobilka, B. J. Hale, *Macromolecules* **2014**, *47*, 7253-7271.

[28] O. Gidron, N. Varsano, L. J. W. Shimon, G. Leitus, M. Bendikov, *Chem. Commun.* **2013**, *49*, 6256-6258.

[29] A. Gandini, *Green Chem.* **2011**, *13*, 1061-1083.

[30] a) A. M. Priegert, B. W. Raw, S. C. Serin, D. P. Gates, *Chem. Soc. Rev.* **2016**, *45*, 922-953; b) X. He, T. Baumgartner, *RSC Adv.*, **2013**, *3*, 11334-11350; c) F. Vidal, F. Jäkle, *Angew. Chem. Int. Ed.* **2019**, *58*, 5846-5870; *Angew. Chem.* **2019**, *131*, 5904-5929; d) T. Baumgartner, F. Jäkle, *Main Group Strategies towards Functional Hybrid Materials*, Wiley, Chichester, **2018**.

31] a) C. D. Entwistle, T. B. Marder, *Angew. Chem. Int. Ed.* **2002**, *41*, 2927-2931; *Angew. Chem.* **2002**, *114*, 3051-3056; b) C. D. Entwistle, T. B. Marder, *Chem. Mater.* **2004**, *16*, 4574-4585; c) N. Matsumi, Y. Chujo, *Polym. J.* **2008**, *40*, 77-89; d) M. J. D. Bosdet, W. E. Piers, *Can. J. Chem.* **2009**, *87*, 8-29; e) A. Wakamiya and S. Yamaguchi, *Bull. Chem. Soc. Jpn.* **2015**, *88*, 1357-1377; f) A. Lorbach, A. Hübner, M. Wagner, *Dalton Trans.* **2012**, *41*, 6048-6063; g) S. Mukherjee, P. Thilagar, *J. Mater. Chem. C*, **2016**, *4*, 2647-2662; h) Y.-L. Rao, H. Amarne, S. Wang, *Coord. Chem. Rev.* **2012**, *256*, 759-770; i) L. Ji, S. Griesbeck, T. B. Marder, *Chem. Sci.* **2017**, *8*, 846 863; j) S.-Y. Li, Z.-B. Sun, C.-H. Zhao, *Inorg. Chem.* **2017**, *56*, 8705-8717; k) E. von Grotthuss, A. John, T. Kaese, M. Wagner, *Asian J. Org. Chem.* **2018**, *7*, 37-53; l) Z. M. Hudson, S. Wang, *Acc. Chem. Res.* **2009**, *42*, 1584-1596; m) A. G. Crawford, A. D. Dwyer, Z. Liu, A. Steffen, A. Beeby, L.-O. Palsson, D. J. Tozer, T. B. Marder, *J. Am. Chem. Soc.* **2011**, *133*, 13349-13362; n) H. Helten, *Chem. Asian J.* **2019**, *14*, 919-935 ; o) F. Jäkle, *Chem. Rev.* **2010**, *110*, 3985-4022; p) Z. M. Hudson, S. Wang, *Dalton Trans.* **2011**, *40*, 7805-7816; q) Z. Huang, S. Wang, R. D. Dewhurst, N. V. Ignat'ev, M. Finze, H. Braunschweig, *Angew. Chem. Int. Ed.* **2020**, *59*, 8800-8818; *Angew. Chem.* **2020**, *132*, 8882-8900.

[32] a) X.-Y. Wang, F.-D. Zhuang, J.-Y. Wang, J. Pei, *Chem. Commun.* **2015**, *51*, 17532-17535; b) A. Iida, S. Yamaguchi, *J. Am. Chem. Soc.* **2011**, *133*, 6952-6955; c) C.-T. Poon, W. H. Lam, V. W.-W. Yam, *J. Am. Chem. Soc*. **2011**, *133*, 19622-19625; d) H. Braunschweig, A. Damme, J. O. C. Jimenez-Halla, C. Hörl, I. Krummenacher, T. Kupfer, L. Mailänder, K. Radacki, *J. Am. Chem. Soc.* **2012**, *134*, 20169-20177; e) D. R. Levine, M. A. Siegler, J. D. Tovar, *J. Am. Chem. Soc.* **2014**, *136*, 7132-7139; f) S. K. Sarkar, G. R. Kumar, P. Thilagar, *Chem. Commun.* **2016**, *52*, 4175-4178; g) G. R. Kumar, S. K. Sarkar, P. Thilagar, *Chem. Eur. J.* **2016**, *22*, 17215-17225; h) Y. Yan, Z. Sun, C. Li, J. Zhang, L. Lv, X. Liu, X. Liu, *Asian J. Org. Chem.* **2017**, *6*, 496-502; i) Y. Adachi and J. Ohshita, *Organometallics* **2018**, *37*, 869-881; j) J. He, F. Rauch, A. Friedrich, D. Sieh, T: Ribbeck, I. Krummenacher, H. Braunschweig, M. Finze,

T. B. Marder, *Chem. Eur. J.* **2019**, *25*, 13777-13784; k) M. Meier, L. Ji, J. Nitsch, I. Krummenacher, A. Deißenberger, D. Auerhammer, M. Schäfer, T. B. Marder, H. Braunschweig, *Chem. Eur. J.* **2019**, *25*, 4707-4712; l) T. E. Stennett, P. Bissinger, S. Griesbeck, S. Ullrich, I. Krummenacher, M. Auth, A. Sperlich, M. Stolte, K. Radacki, C.-J. Yao, F. Würthner, A. Steffen, T. B. Marder, H. Braunschweig, *Angew. Chem. Int. Ed.* **2019**, *58*, 6449-6454; *Angew. Chem.* **2019**, *131*, 6516-6521; m) S. Griesbeck, M. Ferger, C. Czernetzi, C. Wang, R. Bertermann, A. Friedrich, M. Haehnel, D. Sieh, M. Taki, S. Yamaguchi, T. B. Marder, *Chem. Eur. J.* **2019**, *25*, 7679-7688; n) D. Li, H. Zhang, Y. Wang, *Chem. Soc. Rev.* **2013**, *42*, 8416-8433.

[33] a) X. Yin, J. Chen, R. A. Lalancette, T. B. Marder, F. Jäkle, *Angew. Chem. Int. Ed.* **2014**, *53*, 9761-9765; b) X. Yin, K. Liu, Y. Ren, R. A. Lalancette, Y.-L. Loo, F. Jäkle, Chem. Sci. **2017**, *8*, 5497-5505; c) B. Meng, Y. Ren, J. Liu, F. Jäkle, L. Wang, *Angew. Chem. Int. Ed*, **2018**, *57*, 2183; *Angew. Chem.* **2018**, *130*, 2205-2209; d) Y. Adachi, Y. Ooyama, Y. Ren, X. Yin, F. Jäkle, J. Ohshita, *Polym. Chem.* **2018**, *9*, 291-299; e) Y. Yu, C. Dong, A. F. Alahmadi, B. Meng, J. Liu, F. Jäkle, L. Wang, *J. Mater. Chem. C.* **2019**, *7*, 7427-7432; f) Y. Yu, B. Meng, F. Jäkle, J. Liu, L. Wang, *Chem. – Eur. J.* **2020**, *26*, 873-880; g) C. Reus, F. Guo, A. John, M. Winhold, H.-W. Lerner, F. Jäkle, M. Wagner, *Macromolecules*, **2014**, *47*, 3727-3735; h) Y. Ren, F. Jäkle, *Dalton Trans.* **2016**, *45*, 13996-14007; i) H. Li, A. Sundararaman, K. Venkatasubbaiah, F. Jäkle, *J. Am. Chem. Soc.* **2007**, *129*, 5792-5793; j) X. Yin, F. Guo, R. A. Lalancette, F. Jäkle, *Macromolecules* **2016**, *49*, 537-546;

[34] a) A. Lik, L. Fritze, L. Müller, H. Helten, *J. Am. Chem. Soc.* **2017**, *139*, 5692-5695; b) A. Lik, S. Jenthra, L. Fritze, L. Müller, K.-N. Truong, H. Helten, *Chem. – Eur. J.* **2018**, *24*, 11961-11972.

[35] a) C. R. Wade, A. E. J. Broomsgrove, S: Aldridge, F. P. Gabbai, *Chem. Rev.* **2010**, *110*, 3958-3984. b) H. Zhao, L. A. Leamer, F. P. Gabbai, *Dalton Trans.* **2013**, *42*, 8164-8178.

[36] a) Y. Rong, J. Yu, X. Zhang, W. Sun, F. Ye, I-C. Wu, Y. Zhang, S. Hayden, Y. Zhang, C. Wu, D. T. Chiu, *ACS Macro Lett.* **2014**, *3*, 1051-1054; b) Y. Rong, C. Wu, J. Yu, X. Zhang, F. Ye, M. Zeigler, M. E. Gallina, I-C. Wu, Y. Zhang, Y.-H. Chan, W. Sun, K. Uvdal, D. T. Chiu, *ACS Nano* **2013**, *7*, 376-384.

[37] a) Z. Zhou, A. Wakamiya, T. Kushida, S. Yamaguchi, *J. Am. Chem. Soc.* **2012**, *134*, 4529-4532; b) S. Saito, K. Matsuo, S. Yamaguchi, *J. Am. Chem. Soc.* **2012**, *134*, 9130-9133; c) V. M. Hertz, N. Ando, M. Hirai, M. Bolte, H.-W. Lerner, S. Yamaguchi, M. Wagner, *Organometallics* **2017**, *36*, 2512-2519; d) K. Okada, H. Inokawa, T. Sugawa, M. Oda, *J. Chem. Soc., Chem. Commun.* **1992**, 448-449.

[38] a) H. C. Brown, V. H. Dodson, *J. Am. Chem. Soc.* **1957**, *79*, 2302-2306; b) S. Yamaguchi, S. Akiyama, K. Tamao, *J. Am. Chem. Soc.* **2000**, *122*, 6335-6336. c) C. Reus, S. Weidlich, M. Bolte, H.-W. Lerner, M. Wagner, *J. Am. Chem. Soc.* **2013**, *135*, 12892-12907.

[39] a) E. Krause, *Ber. Dtsch. Chem. Ges.* **1924**, *57*, 216-217; b) E. Krause, H. Polack, *Ber. Dtsch. Chem. Ges.* **1926**, *59*, 777-785; c) E. Krause, P. Nobbe, *Ber. Dtsch. Chem. Ges.* **1930**, *63*, 934-942.

[40] G. Wittig, W. Herwig, *Chem. Ber.* **1955**, *88*, 962-976.

[41] J. C. Doty, B. Babb, P. J. Grisdale, M. Glogowski, J. L. R. Williams, *J. Organomet. Chem.* **1972**, *38*, 229-236.

[42] a) W. Kaim, A. Schulz, *Angew. Chem. Int. Ed.* **1984**, *23*, 615-616; b) J. Fiedler, S. Zalis, A. Klein, F. M. Hornung, W. Kaim, *Inorg. Chem.* **1996**, *35*, 3039-3043; c) Z. Yuan, N. J. Taylor, T. B. Marder, I. D. Williams, S. K. Kurtz, L.-T. Cheng, *J. Chem. Soc., Chem. Commun.* **1990**, 1489-1491; d) M. Lequan, R. M. Lequan, K. C. Ching, *J. Mater. Chem.* **1991**, *1*, 997-999; e) Z. Yuan, N. J. Taylor, R. Ramachandran, T. B. Marder, *Appl. Organomet. Chem.* **1996**, *10*, 305-316; f) Z. Yuan, J. C. Collings, N. J. Taylor, T. B. Marder, C. Jardin, J.-F. Halet, *J. Solid State Chem.* **2000**, *154*, 5-12; g) Z. Yuan, C. D. Entwistle, J. C. Coolings, D. Albesa-Jové, A. S. Batsanov, J. A. K. Howard, N. J. Taylor, H. M. Kaiser, D. E. Kaufmann, S.-Y. Poon, W.-Y. Wong, C. Jardin, S. Fatallah, A. Boucekkine, J.-F. Halet, T. B. Marder, *Chem. Eur. J.* **2006**, *12*, 2758-2771; h) T. Noda and Y. Shirota, *J. Am. Chem. Soc.* **1998**, *120*, 9714-9715; i) W.-L. Jia, D.-R. Bai, T. McCormick, Q.-D. Liu, M. Motala, R.-Y. Wang, C. Seward, Y. Tao, S. Wang, *Chem. Eur. J.* **2004**, *10*, 994-1006; j) J. C. Collings, S.-Y. Poon, C. Le Droumaguet, M. Charlot, C. Katan, L.-O. Palsson, A. Beeby, J. A. Mosely, H. M. Kaiser, D. Kaufmann, W.-Y. Wong, M. Blanchard-Desce, T. B. Marder, *Chem. Eur. J.* **2009**, *15*, 198-208; k) M. Mazzeo, V. Vitale, F. D. Sala, M. Anni, G. Barbarella, L. Favaretto, G. Sotgiu, R. Cingolani, G. Gigli, *Adv. Mater.* **2005**, *17*, 34-39.

[43] a) C.-H. Zhao, A. Wakamiya, Y. Inukai, S. Yamaguchi, *J. Am. Chem. Soc.* **2006**, *128*, 15934-15935; b) C.-H- Zhao, E. Sakuda, A. Wakamiya, S. Yamaguchi, *Chem. Eur. J.* **2009**, *15*, 10603-10612.

[44] A. Wakamiya, in *Main Group Strategies towards Functional Hybrid Materials* (Eds.: T. Baumgartner, F. Jäkle), Wiley, Chichester, **2018**, pp. 1-26.

[45] Y. Chujo, I. Tomita, T. Saegusa, *Macromolecules* **1990**, *23*, 689-692.

[46] N. Matsumi, Y. Chujo, *Polym. Bull.* **1997**, *39*, 295-302.

[47] M. Miyata, N. Matsumi, Y. Chujo, *Polym. Bull.* **1999**, *42*, 505-510.

[48] a) N. Matsumi, K. Naka, Y. Chujo, *J. Am. Chem. Soc.* **1998**, *120*, 5112-5113; b) N. Matsumi, M. Miyata, Y. Chujo, *Macromolecules* **1999**, *32*, 4467-4469; c) Y. Chujo, Y. Sasaki, N. Kinomura, N. Matsumi, *Polymer* **2000**, *41*, 5047-5051; d) A. Nagai, T. Murakami, Y. Nagata, K. Kokado, Y. Chujo, *Macromolecules* **2009**, *42*, 7217-7220.

[49] N. Matsumi, K. Naka, Y. Chujo, *J. Am. Chem. Soc.* **1998**, *120*, 10776-10777.

[50] N. Matsumi, T. Umeyama, Y. Chujo, *Polym. Bull.* **2000**, *44*, 431-436.

[51] a) A. Sundararaman, M. Victor, R. Varughese, F. Jäkle, *J. Am. Chem. Soc*. **2005**, *127*, 13748-13749; b) H. Li, F. Jäkle, *Angew. Chem. Int. Ed.* **2009**, *48*, 2313-2316; *Angew. Chem.* **2009**, *121*, 2349-2353; c) H. Li, F. Jäkle, *Macromol. Rapid Commun.* **2010**, *31*, 915-920.

[52] a) T. Lorenz, A. Lik, F. A. Plamper, H. Helten, *Angew. Chem. Int. Ed.* **2016**, *55*, 7236-7241; *Angew. Chem.* **2016**, *128*, 7352-7357; b) O. Ayhan, T. Eckert, F. A. Plamper, H. Helten, *Angew. Chem. Int. Ed.* **2016**, *55*, 13321-13325; *Angew. Chem.* **2016**, *128*, 13515-13519; c) H. Helten, *Chem. Eur. J.* **2016**, *22*, 12972-12982; d) T. Lorenz, M. Crumbach, T. Eckert, A. Lik, H. Helten, *Angew. Chem. Int. Ed.* **2017**, *56*, 2780-2784; *Angew. Chem.* **2017**, *129*, 2824-2828.

[53] a) M. Iyoda, H. Shimizu, *Chem. Soc. Rev.* **2015**, *44*, 6411-6424; b) M. Iyoda, J. Yamakawa, M. J. Rahman, *Angew. Chem. Int. Ed.* **2011**, *50*, 10522-10553; *Angew. Chem.* **2011**, *123*, 10708-10740.

[54] a) A. J. W. Tol, *Synth. Met.* **1995**, *74*, 95-98.

[55] J. Krömer, I. Rios-Carreras, G. Fuhrmann, C. Musch, M. Wunderlin, T. Debaerdemaeker, E. Mena-Osteritz, P. Bäuerle, *Angew. Chem. Int. Ed.* **2000**, *39*, 3481-3486.

[56] J. Krömer, P. Bäuerle, *Tetrahedron* **2001**, *57*, 3785-3794.

[57] G. Fuhrmann, J. Krömer, P. Bäuerle, *Synth. Met.* **2001**, *119*, 125-126.

[58] G. Fuhrmann, T. Debaerdemaeker, P. Bäuerle, *Chem. Commun.* **2003**, 948-949.

[59] F. Zhang, G. Götz, H. D. F. Winkler, C. A. Schalley, P. Bäuerle*, Angew. Chem. Int. Ed.* **2009**, *48*, 6632-6635; *Angew. Chem.* **2009**, *121*, 6758-6762.

[60] a) F. Sondheimer and R. Wolovsky, *Tetrahedron. Lett.* **1959**, *3*, 3-6; b) F. Sondheimer, R. Wolovsky, Y. Amiel, *J. Am. Chem. Soc.* **1962**, *84*, 274-284.

[61] G. M. Badger, J. A. Elix, G. E. Lewis, *Aust. J. Chem.* **1965**, *18*, 70-89.

[62] Z. Hu, J. L. Atwood, M. P. Cava, *J. Org. Chem.* **1994**, *59*, 8071-8075.

[63] F. Ellinger, A. Gieren, T. Hübner, J. Lex, F. Lucchesini, A. Merz, R. Neidlein, J. Salbeck, *Monatsh. Chem.* **1993**, *124*, 931-943.

[64] a) M. V. Martinez-Diaz, G. de la Torre, T. Torres, *Chem. Commun.* **2010**, *46*, 7090-7108; b) G. Bottari, G. de la Torre, D. M. Guldi, T. Torres, *Chem. Rev.* **2010**, *110*, 6768-6816.

[65] a) E. Vogel, P. Röhrig, M. Sicken, B. Knipp, A. Herrmann, M. Pohl, H. Schmickler, J. Lex, *Angew. Chem. Int. Ed. Engl.* **1989**, *28*, 1651-1655; b) E. Vogel, M. Pohl, A. Herrmann, T. Wiss, C. König, J. Lex, M. Gross, J. P. Gisselbrecht, *Angew. Chem. Int. Ed. Engl.* **1996**, *35*, 1520-1524.

[66] Z. Hu, M. P. Cava, *Tetrahedron Lett.* **1994**, *35*, 3493-3496.

[67] R. Giovanetti, The Use of Spectrophotometry UV-Vis for the Study of Porphyrins. *Macro Nano Spectrosc.* **2012**, *1*, 87-108, DOI: 10.5772/38797.

[68] a) F. H. Carré, R. J.-P- Corriu, T. Deforth, W. E. Douglas, W. S. Siebert, W. Weinmann, *Angew. Chem. Int. Ed.* **1998**, *37*, 652-654; *Angew. Chem.* **1998**, *110*, 654-656; b) T. Köhler, J. Faderl, H. Pritzkow, W. Siebert, *Eur. J. Inorg. Chem.* **2002**, 2942-2946; c) A. Eckert, H. Pritzkow, W. Siebert, *Eur. J. Inorg. Chem.* **2002**, 2064-2068.

[69] a) X. Yin, J. Liu, F. Jäkle, DOI: 10.1002/chem.202003481; b) P. Chen, F. Jäkle, *J. Am. Chem. Soc.* **2011**, *133*, 20142-20145; c) N. Baser-Kirazli, R. A. Lalancette, F. Jäkle, *Angew. Chem. Int. Ed.* **2020**, *59*, 8689-8697; *Angew. Chem.* **2020**, *132*, 8767-8775; d) P. Chen, R. A. Lalancette, F. Jäkle, *Angew. Chem. Int. Ed.* **2012**, *51*, 7994-7998; *Angew. Chem.* **2012**, *124*, 8118-8122; e) P. Chen, X. Yin, N. Baser-Kirazli, F. Jäkle, *Angew. Chem. Int. Ed.* **2015**, *54*, 10768-10772; *Angew. Chem.* **2015**, *127*, 10918-10922.

1.5 Acknowledgement of Collaborators

Some of the work described in this Thesis was performed in collaboration with other researchers. A summary of their contributions is as follows:

Chapter 2.1: **Ayse Deniz** and **Dr. Sebastian Kühl** carried out FESEM analysis of the microspheres and performed DLS and TGA measurements. **Dr. Alina Adams** carried out the solid-state NMR studies. **Lars Müller** performed preliminary tests on the synthesis of cyclomatrix polymers via salt elimination.

Chapter 2.2: **Lars Fritze** contributed equally to this work. **Tobias Schindler** performed cyclic voltammetry measurements. **Marius Kremer** carried out single crystal XRD studies. **Prof. Dr. Holger Helten** carried out all of the time-dependent DFT (TD-DFT) calculations.

Chapter 2.3: **Lars Fritze** contributed equally to this work.

Chapter 2.4: **Maximilian Fest** performed most of the syntheses of the presented compounds. Lars Fritze carried out single crystal XRD studies. **Andreas Helbig** was responsible for time-dependent DFT (TD-DFT) calculations. **Dr. Ivo Krummenacher** performed cyclic voltammetry measurements.

Chapter 2.5: **Lukas Swoboda** and **Dr. Artur Lik** assisted with the experiments. **Dr. Ivo Krummenacher** performed cyclic voltammetry measurements.

2. Results and Discussion

2.1 Borazine-Based Inorganic–Organic Hybrid Cyclomatrix Microspheres by Silicon/Boron Exchange Precipitation Polycondensation

The following section is slightly modified and reproduced from published article[*] with permission from The Royal Society of Chemistry.

Abstract: The synthesis of borazine-based hybrid cyclomatrix polymers has been studied under various conditions. Crosslinked polymers obtained via a novel silicon/boron exchange precipitation polycondensation approach form hybrid cyclomatrix microspheres with a mean diameter of about 900 nm.

Doping of organic compounds with BN units has proven to be a viable strategy to produce novel organic–inorganic hybrid materials with intriguing properties and functions.[1–3] The first examples have just demonstrated the applicability of this approach to polymer chemistry.[3–5] We recently presented the main-chain BN-doped π-conjugated polymers **I** and **II** and the oligo(iminoborane) **III** (Figure 2.1.1). The synthesis of these cyclolinear macromolecules was achieved via a novel silicon/boron exchange polycondensation strategy.[5]

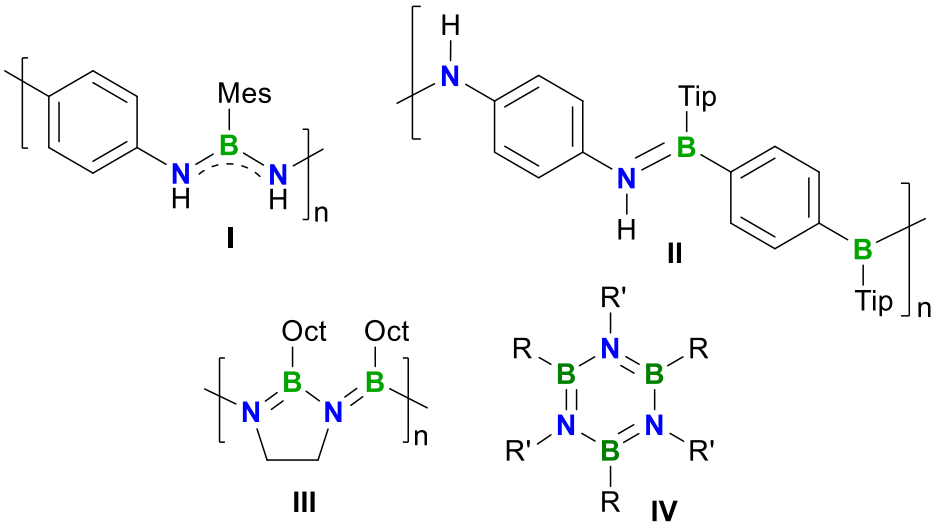

Figure 2.1.1. BN-doped π-conjugated polymers I and II, oligo(iminoborane) III and general structure of borazines IV (Mes = mesityl; Tip = 2,4,6-triisopropylphenyl; Oct = *n*-octyl; R, R' = organic substituents.

Borazines (**IV**), derivatives of the so-called "inorganic benzene", have been mainly used for the fabrication of BN-based ceramics.[6,7] For example, thermolysis of the parent borazine,

[*] N. A. Riensch, A. Deniz, S. Kühl, L. Müller, A. Adams, A. Pich, H. Helten, *Polym. Chem.* **2017**, *8*, 5264—5268.

$(BHNH)_6$, or 2,4,6-triaminoborazines gives highly crosslinked, less well-defined networks of partially fused borazine rings, termed poly(borazylenes), which are suitable precursors to ceramic hexagonal boron nitride (h-BN).[8] Two-dimensional sheets of the UV-emissive h-BN, which is an inorganic graphene analogue, as well as h-BN/graphene hybrids have emerged as promising new materials for electronic applications.[9] Borazine moieties have also been incorporated into the side chains of linear organic and inorganic polymers.[10,11] Recently, borazine-doped star-like polyphenylenes were presented.[12] Furthermore, the synthesis of a series of porous, amorphous borazine-linked polymer networks by condensation of di-, tri- or tetraamines with BCl_3 or from amine–borane adducts was reported, which could be used for gas storage and separation applications.[13]

Precipitation polymerization is a facile method to synthesize polymer particles with spherical morphology in the absence of any added surfactant or sterically stabilizing agent.[14] We and others recently applied this approach to obtain cyclophosphazene-based hybrid cyclomatrix microspheres.[15,16] The formation of cyclomatrix polymers based on the borazine system using this method has not been demonstrated thus far. Herein, we describe the synthesis of such species via different routes. Particularly, the use of our silicon/boron exchange condensation approach under precipitation polymerization conditions leads to smooth microspheres with a diameter of on average 900 nm.

First, we investigated the formation of borazine-based cyclomatrix polymers **3a-c** under common precipitation polycondensation conditions (Scheme 2.1.1). For this, we mixed dilute solutions of *B,B',B''*-trichloro-*N*,*N'*,*N''*-trimethylborazine (**1**)[17] and either of the diamines **2a**, **2b** or **2c** (in 2:3 ratio) in MeCN at ambient temperature in the presence of NEt_3 as an auxiliary base (***Route A***). In each case a finely dispersed white precipitate was immediately formed. After the mixtures had been stirred overnight at room temperature, the insoluble solid products were isolated by filtration to remove the soluble salt-elimination by-product, $[Et_3NH]Cl$, and dried in vacuo prior to analysis via Fourier-transform infrared (FT-IR) and solid state NMR spectroscopy, elemental analysis and field-emission scanning electron microscopy (FESEM).

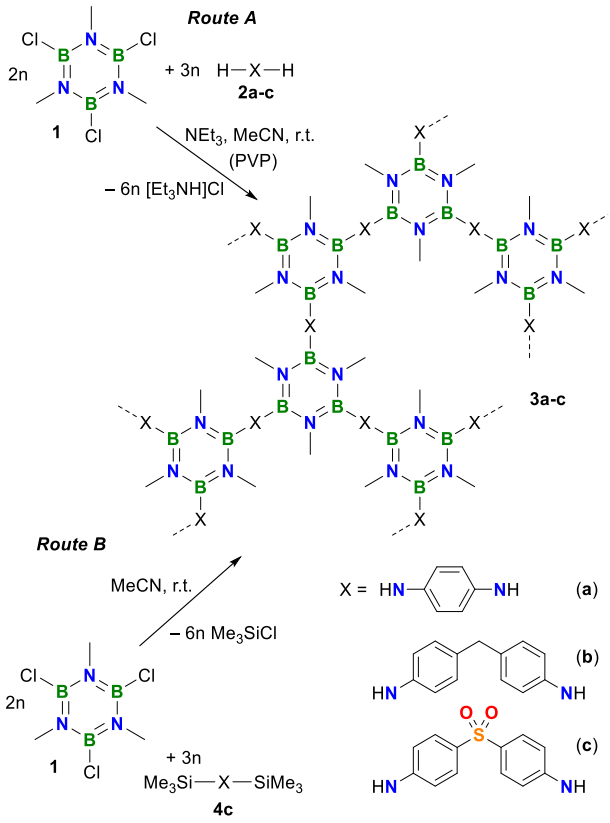

Scheme 2.1.14. Synthesis of borazine-based cyclomatrix hybrid polymers **3a-c** via salt elimination (*Route A*), and synthesis of **3c** via silicon/boron exchange polycondensation (*Route B*)

The products proved to be insoluble in common organic solvents, which evidences their crosslinked nature. For comparison, cyclolinear polymers of type **I–III** (Figure 2.1.1) show good solubility in organic solvents of moderate polarity such as dichloromethane.[5] The formation of the desired cyclomatrix polymers **3a-c** was unambiguously confirmed by FT-IR spectroscopy and ^{13}C and ^{11}B CPMAS. IR absorption bands in the range of 1480 and 1320 cm^{-1} are characteristic for B–N stretching vibrations of borazine rings.[18] The spectrum of the derivative **3c** (Figure 2.1.3a), additionally, shows the characteristic symmetric and antisymmetric stretching vibrations of the O=S=O groups at 1320 and 1140 cm^{-1}, respectively.[19] The ^{13}C CPMAS spectra of all cyclomatrix polymers show, besides the resonances for the organic linker groups, a signal at about 29 ppm, which corresponds to the N$\underline{C}H_3$ group from the borazine moiety built into the polymer network (Figure 2.1.3b and Appendix, Figs. 5.1.29–32). In the ^{11}B CPMAS spectra, the signal from the borazine boron atoms was detected at about 23 ppm for each network polymer (Appendix, Figs. 5.1.34–5.1.36). The carbon contents estimated by elemental analysis were consistently low. This is presumably due to the formation of boron carbide, which often hampers C analysis of boron-containing materials.[20]

Investigation of the morphologies by FESEM revealed that the material obtained from the reaction of **1** with *para*-phenylenediamine (**2a**) showed extended homo-coagulation (Figure

2.1.2a). Similar observations were made also for the product from the reaction with the more flexible diamine **2b** (Appendix, Figure 5.1.2). However, when we carried out the polycondensation of **1** and **2b** in the presence of polyvinyl pyrrolidone (PVP) as a steric stabilizer, i. e., under conventional dispersion polycondensation conditions, spherical polymer particles of **3b** were formed with a mean diameter of d = 184 ± 21 nm (Figure 2.1.2b). Interestingly, the reaction of **1** with 4,4'-diaminodiphenyl sulfone (**2c**) produced smooth cyclomatrix hybrid microspheres even in the absence of any stabilizer or surfactant (Figure 2.1.2c). The particles of **3c**, though partially fused, were of comparable size (d = 183 ± 20 nm) with those of **3b**. This effect highlights the important role of the O=S=O groups in the amine structure providing effective stabilisation of particle nuclei during early stages of the polycondensation process. Also, the average size of the microspheres obtained seemed to be independent of the ratio of borazine to diamine employed in the reaction (Appendix, Figure 5.1.7).

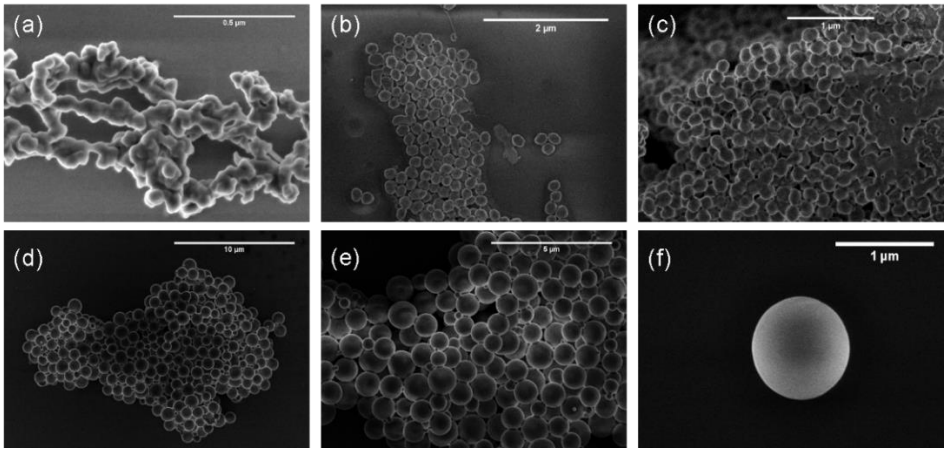

Figure 2.1.2. FESEM micrographs of (a) **3a**, (b) **3b** and (c) **3c** prepared via ***Route A*** (in the case of **3b**, in the presence of PVP), and (d–f) FESEM micrographs of microspheres of **3c** prepared via ***Route B***.

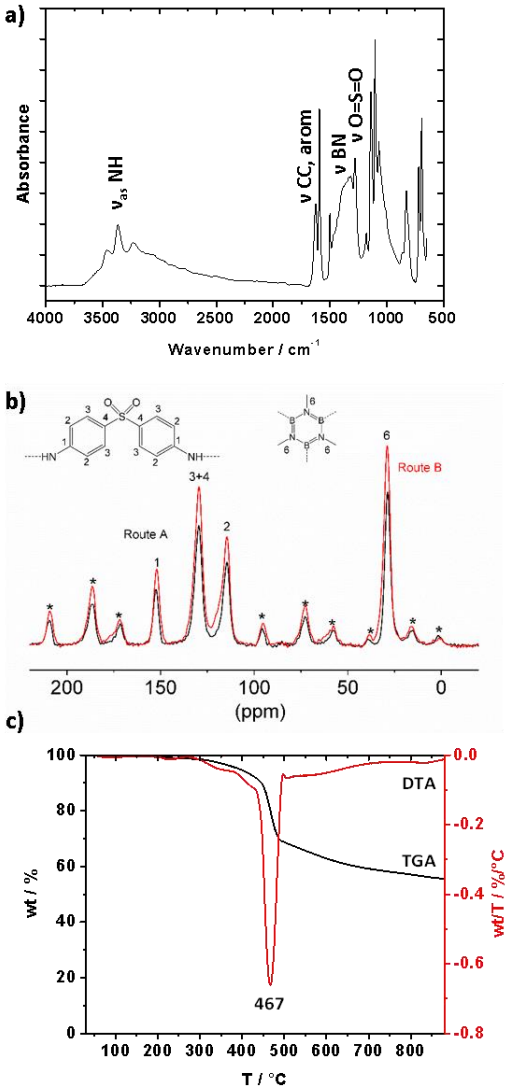

Figure 2.1.3. (a) FT-IR spectrum of **3c**. (b) ^{13}C CPMAS spectra of polymer **3c** obtained via ***Route A*** and ***B***, respectively. The signals marked with an asterisk are spinning sidebands. (c) TGA (black) and DTA curves (red) for **3c** (measured under N2 atmosphere) prepared via ***Route A***.

The new materials showed remarkable thermal stability, as evidenced by thermogravimetric analysis (TGA) with simultaneous monitoring by differential thermal analysis (DTA) (Figure 2.1.3c and Appendix, Figs. 5.1.19–5.1.27). Major mass loss occurred only above ca. 450 °C. The residual mass at 880 °C under N_2 atmosphere amounts to 56 % and in air 25 % (cf. Appendix, Figure 5.1.26).[21] This impressively demonstrates the stabilization imparted by the cyclomatrix architecture. For comparison, the cyclolinear species **III** (Figure 2.1.1) undergoes about 73 % mass loss below 350 °C.[5b]

In the next step of our study we decided to explore the silicon/boron exchange condensation approach under precipitation polycondensation conditions for the synthesis of the derivative **3c**, as a good case in point (Scheme 2.1.1, ***Route B***). The reaction of **1** with **4c** in acetonitrile yielded **3c** by spontaneous condensation of Me_3SiCl at ambient temperature. The formation of

3c was confirmed by FT-IR spectroscopy (Appendix, Fig. 5.1.16), which showed the same characteristic absorption bands as the spectrum of **3c** prepared via ***Route A*** described above. The ^{13}C CPMAS spectra of **3c** obtained via both routes contained the same number of signals with identical signal intensities (Figure 2.1.3b). This demonstrates that the structure of the two samples is indistinguishable by NMR spectroscopy. Notably, for the polymer **3c** prepared via ***Route B***, no signal for residual $SiMe_3$ groups was detected. In acetonitrile, the fully crosslinked material forms a stable colloidal dispersion. FESEM micrographs of the dried product showed that the polymer **3c** had formed microspheres with smooth surface (Figure 2.1.2d–f), which were significantly larger than those obtained via ***Route A***. Besides ca. 25% of smaller particles (d = 331 ± 86 nm), the mean diameter of the bulk microspheres was determined as d = 905 ± 150 nm. The spherical particles proved to be morphologically stable in air for at least six weeks (Appendix, Figure 5.1.12).

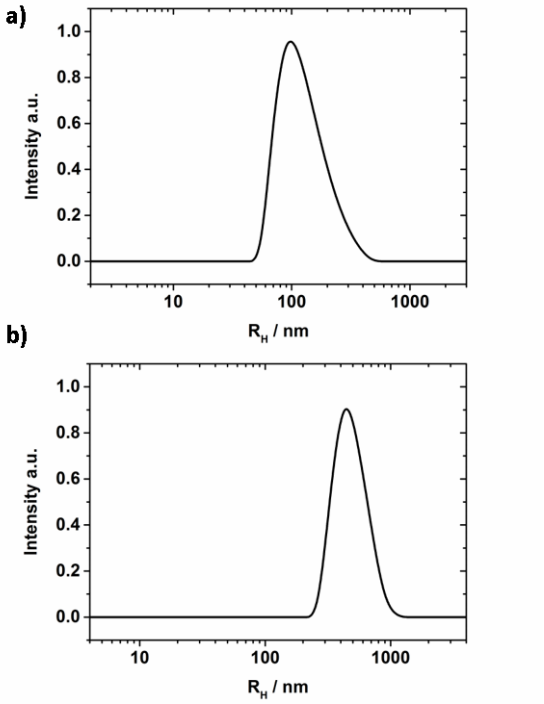

Figure 2.1.4. Intensity weighted size distribution of particles **3c** prepared via ***Route A*** (a) or ***B*** (b), respectively, in acetonitrile by DLS.

The size distributions of particles of **3c** obtained via ***Route A*** and ***B***, respectively, dispersed in acetonitrile were analyzed by dynamic light scattering (DLS). This revealed hydrodynamic radii of R_h = 111 nm (PDI = 0.13, ***Route A***, Figure 2.1.4a) and R_h = 456 nm (PDI = 0.14, ***Route B***, Figure 2.1.4b). These data agree well with the particle sizes measured by FESEM. Therefore, neither aggregation nor significant swelling effects are observed, which is plausible considering the rigid structure of the polymer featuring relatively small linking units. This result further corroborates the assumption that the polymer particles are fully crosslinked.

In order to investigate the effect of the solvent on the product's morphologies, reactions of **1** with **4c** were, additionally, performed in dichloromethane, toluene and in a 1:1 mixture of CH_2Cl_2 and acetonitrile. These reactions, however, yielded less uniform materials. Some smaller and partially fused microspheres were observed by FESEM from reactions in toluene and in the CH_2Cl_2/acetonitrile mixture (Appendix, Figure 5.1.11). Altogether, the best results, so far, with respect to particle formation were obtained when using pure acetonitrile as the solvent.

In conclusion, we have demonstrated the synthesis of borazine-based hybrid cyclomatrix microspheres by precipitation polycondensation for the first time. The formation of larger particles via our novel Si/B exchange precipitation polycondensation approach may be due to the better solubility of the trimethylsilyl group-carrying monomer and the growing oligomers in the reaction medium compared to non-silylated species, thus leading to slower nucleation kinetics in this case and fewer number of nucleation events. Currently, we are investigating the formation mechanism of new borazine-based cyclomatrix hybrid polymers in detail to understand how to tailor their molecular structure and properties. Furthermore, we are exploring the potential of borazine-based cyclomatrix polymers as precursor materials and building blocks for the design of catalyst supports and flame retardant additives.

2.1.1 Experimental section

General procedures. All manipulations were performed under an atmosphere of dry argon using standard Schlenk techniques or in an MBraun glovebox. Tetrahydrofuran, CH_2Cl_2 and toluene were dried and degassed by means of a MBraun SPS-800 solvent purification system. Acetonitrile was dried over P_4O_{10} and subsequently over CaH_2 at reflux and distilled prior to use. 4,4'-Diaminodiphenylmethane, 4,4'-diaminodiphenyl sulfone and *p*-phenylendiamine were purchased from Alfa Aesar and used as received as well. Chlorotrimethylsilane, heptamethyldisilazane and triethylamine were commercially purchased and freshly distilled prior to use. 4,4'-Bis(*N,N'*-trimethylsilyl)amine diphenylsulfone[22] and 2,4,6-trichloro-1,3,5-trimethylborazine[23] were prepared according to methods described in the literature.

ATR spectra were recorded with a 470 Nexus FT-IR of the company *Thermo Nicolet* using a smart splitpea ATR unit with a silicon crystal in single reflection. The samples were scanned over a range of 500–4000 cm^{-1}. Field-emission SEM (FESEM) images were obtained using a *Hitachi-S4800* instrument at an activation voltage of 1.0 kV. The number-average diameter (D_n) and the standard deviation were determined with *ImageJ* software by counting 100−200 individual particles from FESEM micrographs from a non-filtrated sample. Samples for FESEM analysis were prepared by drying dilute particle dispersions on a clean silicon wafer at room temperature (without sputtering). The dried particles were mounted on the object plate with glue. The micrographs were recorded with 1000-, 2000-, 5000-, 10000-, 20000-, 40000-x magnification. TGA-coupled FTIR experiments were carried out on a STA 600 (Perkin Elmer) thermogravimetric analyzer coupled to a FRONTIER (Perkin Elmer) FTIR spectrometer including a TL 8000 (Perkin Elmer) TG-IR-GCMS interface. Samples were measured in a temperature range of 30 to 880 °C at a heating rate of 10 K min^{-1} and a nitrogen flow of 150 mL min^{-1}. Timebase and Pyris software (Perkin Elmer) were used for data processing and analysis. Polydispersity indices (PDI) and hydrodynamic radii of the samples dispersed in acetonitrile were measured on a *Goniometer ALV-GCS3* of the company *ALV*. The measurements were carried out with a constant angle of 90°, a temperature of 20 °C and a time period of 5 x 30 seconds for each measurement. The NMR experiments were conducted at room temperature using an Advance AV700 Bruker NMR spectrometer working at frequencies of 700.23 MHz for ^{1}H, 176.07 MHz for ^{13}C and 224.66 MHz for ^{11}B. All spectra were recorded under MAS (magic angle spinning) conditions using a spinning speed of 10 kHz. The ^{13}C spectra were obtained using ^{1}H-^{13}C cross-polarization with a cross-polarization time of 2 ms and recycle delays ranging from 5 s to 10 s. The direct-polarization method with high-power proton decoupling during acquisition and a recycle delay of 5 s was applied to measure the ^{11}B spectra. The chemical shifts of adamantane and $BF_3{\cdot}OEt_2$ were employed for the external calibration of ^{13}C and respectively ^{11}B spectra.

Synthesis of 3a. *p*-Phenylendiamine (0.0811 g, 0.75 mmol, 1.5 equiv) was dissolved in acetonitrile (85 mL) and triethylamine (3.05 mL) was added. 2,4,6-Trichloro-1,3,5-trimethylborazine (0.1130 g, 0.50 mmol) was dissolved in acetonitrile (25 mL) and the resulting solution was added to the stirred solution of *p*-phenylendiamine, instantly forming a colorless precipitate. The reaction mixture was stirred at room temperature overnight and purified by filtration with membrane filters with a pore size of 100 nm. Then, the product was dried in vacuo (ca. 10^{-2} mbar). Yield: 0.1643 g (59 %); ^{13}C CPMAS (176 MHz): δ = 139.6, 117.7, 26.7 ppm; IR (cm^{-1}): $\tilde{\nu}$ = 1395 (s, ν BN), 1475 (m, ν BN), 1515 (w, ν CC, arom.), 1618 (w, ν CC, arom.), 3000–3500 (w, ν_{as} NH, NH_2) cm^{-1}.

Synthesis of 3b. 4,4'-Diaminodiphenylmethane (0.1487 g, 0.75 mmol, 1.5 equiv) was dissolved in acetonitrile (85 mL) and triethylamine (3.05 mL) was added. 2,4,6-Trichloro-1,3,5-trimethylborazine (0.1130 g, 0.50 mmol) was dissolved in acetonitrile (25 mL) and the resulting solution was added to the stirred solution of 4,4'-diaminodiphenylmethane. The reaction mixture was stirred at room temperature overnight and purified by filtration with membrane filters with a pore size of 100 nm. Then, the product was dried in vacuo (ca. 10^{-2} mbar). Yield: 0.1504 g (54 %); ^{13}C CPMAS (176 MHz): δ = 144.7, 130.0, 116.0, 28.8 ppm; IR (cm^{-1}): $\tilde{\nu}$ = 1406 (s, ν BN), 1475 (m, ν BN), 1513 (w, ν CC, arom.), 1617 (w, ν CC, arom.), 3000–3500 (w, ν_{as} NH, NH_2) cm^{-1}.

Synthesis of 3b with PVP as stabilizing agent. PVP (1.295 g, MW: 55000 g/mol) was dissolved with 4,4'-diaminodiphenylmethane (0.1487 g, 0.75 mmol, 1.5 equiv) in acetonitrile (85 mL). 2,4,6-Trichloro-1,3,5-trimethylborazine (0.1130 g, 0.50 mmol) was dissolved in acetonitrile (25 mL) and the resulting solution was added to the stirred solution of 4,4'-diaminodiphenylmethane. Then, triethylamine (3.05 mL) was added to the stirred solution. The reaction mixture was stirred at room temperature overnight and purified by filtration with membrane filters with a pore size of 100 nm. Then, the product was dried in vacuo (ca. 10^{-2} mbar).

Synthesis of 3c.

Via salt elimination (*Route A*): 4,4'-Diaminodiphenyl sulfone (0.1860 g, 0.75 mmol, 1.5 equiv) was dissolved in acetonitrile (85 mL) and triethylamine (3.05 mL) was added. 2,4,6-Trichloro-1,3,5-trimethylborazine (0.1130 g, 0.50 mmol) was dissolved in acetonitrile (25 mL) and the resulting solution was added to the stirred solution of 4,4'-diaminodiphenyl sulfone. The reaction mixture was stirred at room temperature overnight and purified by filtration with membrane filters with a pore size of 100 nm. Then, the product was dried in vacuo (ca. 10^{-2}

mbar). Yield: 0.1674 g (34 %); ^{13}C CPMAS (176 MHz): δ = 152.5, 129.5, 114.5, 28.7 ppm; IR (cm^{-1}): $\tilde{\nu}$ = 1329 (m, ν BN), 1378 (m, ν BN), 1450 (m, ν BN), 1510 (m, CC, arom.), 1625 (w, CC, arom.), 3000–3500 (w, ν_{as} NH, NH_2) cm^{-1}; elem. anal. calcd. (%):[#] C 51.58, H 4.95, N 17.19, found: C 46.86, H 5.45, N 18.15.

Via silicon/boron exchange (*Route B*): 4,4'-Bis(*N,N'*-trimethylsilyl)amine diphenylsulfone (0.2945 g, 0.75 mmol, 1.5 equiv) was dissolved in acetonitrile (85 mL). 2,4,6-Trichloro-1,3,5-trimethylborazine (0.1130 g, 0.50 mmol) was dissolved in acetonitrile (25 mL) and the resulting solution was added to the stirred solution of 4,4'-diaminodiphenyl sulfone, forming a colorless precipitate during addition. The reaction mixture was stirred at room temperature overnight and purified by filtration with membrane filters with a pore size of 500 nm. Then, the product was dried in vacuo (ca. 10^{-2} mbar). Yield: 0.0955 g (20 %); ^{13}C CPMAS (176 MHz): δ = 152.5, 129.5, 114.5, 28.7 ppm; IR (cm^{-1}): $\tilde{\nu}$ = 1140 (s, ν_s O=S=O), 1320 (m, ν_{as} O=S=O), 1380 (m, ν BN), 1480 (m, ν BN), 1590 (m, ν CC, arom.), 1620 (w, ν CC, arom.), 2950 (w, ν Si-CH_3), 3360 (w, ν_{as} NH) cm^{-1}; elem. anal. calcd. (%):[#] C 51.58, H 4.95, N 17.19, found: C 47.22, H 4.98, N 16.53.

Via silicon/boron exchange (*Route B*) in other solvents: 4,4'-Bis(*N,N'*-trimethylsilyl)amine diphenylsulfone (0.0589 g, 0.150 mmol, 1.5 equiv) was dissolved in CH_2Cl_2, toluene or a mixture of CH_2Cl_2 and acetonitrile (17 mL). 2,4,6-Trichloro-1,3,5-trimethylborazine (0.0227 g, 0.10 mmol) was dissolved in the respective solvent (5 mL) and the resulting solution was added to the stirred solution of 4,4'-diaminodiphenyl sulfone. The reaction mixture was stirred at room temperature overnight and then, the product was dried in vacuo (ca. 10^{-2} mbar). Samples for FESEM analysis were prepared by drying dilute particle dispersions on a clean silicon wafer at room temperature.

[#] Carbon analysis was consistently low, presumably due to the formation of boron carbide, which often hampers C analysis of boron-containing materials.[24,25]

2.1.2 References

[1] (a) Z. Liu and T. B. Marder, *Angew. Chem. Int. Ed.*, 2008, **47**, 242; (b) M. J. Bosdet and W. E. Piers, *Can. J. Chem.*, 2009, **87**, 8; (c) P. G. Campbell, A. J. V. Marwitz and S.-Y. Liu, *Angew. Chem. Int. Ed.*, 2012, **51**, 6074; (d) X.-Y. Wang, J.-Y. Wang and J. Pei, *Chem. Eur. J.*, 2015, **21**, 3528.

[2] (a) B. Neue, J. F. Araneda, W. E. Piers and M. Parvez, *Angew. Chem. Int. Ed.*, 2013, **52**, 9966; (b) H. Braunschweig, K. Geetharani, J. O. C. Jimenez-Halla and M. Schäfer, *Angew. Chem. Int. Ed.*, 2014, **53**, 3500; (c) J. S. A. Ishibashi, J. L. Marshall, A. Mazière, G. J. Lovinger, B. Li, L. N. Zakharov, A. Dargelos, A. Graciaa, A. Chrostowska and S.-Y. Liu, *J. Am. Chem. Soc.*, 2014, **136**, 15414; (d) M. Krieg, F. Reicherter, P. Haiss, M. Ströbele, K. Eichele, M.-J. Treanor, R. Schaub and H. F. Bettinger, *Angew. Chem. Int. Ed.*, 2015, **54**, 8284; (e) X.-Y. Wang, A. Narita, X. Feng and K. Müllen, *J. Am. Chem. Soc.*, 2015, **137**, 7668; (f) S. Wang, D.-T. Yang, J. Lu, H. Shimogawa, S. Gong, X. Wang, S. K. Mellerup, A. Wakamiya, Y.-L. Chang, C. Yang and Z.-H. Lu, *Angew. Chem. Int. Ed.*, 2015, **54**, 15074; (g) X.-Y. Wang, F.-D. Zhuang, X.-C. Wang, X.-Y. Cao, J.-Y. Wang and J. Pei, *Chem. Commun.*, 2015, **51**, 4368; (h) H. Braunschweig, M. A. Celik, F. Hupp, I. Krummenacher and L. Mailänder, *Angew. Chem. Int. Ed.*, 2015, **54**, 6347; (i) X. Wang, F. Zhang, K. S. Schellhammer, P. Machata, F. Ortmann, G. Cuniberti, Y. Fu, J. Hunger, R. Tang, A. A. Popov, R. Berger, K. Müllen and X. Feng, *J. Am. Chem. Soc.*, 2016, **138**, 11606; (j) M. Schäfer, N. A. Beattie, K. Geetharani, J. Schäfer, W. C. Ewing, M. Krahfuß, C. Hörl, R. D. Dewhurst, S. A. Macgregor, C. Lambert and H. Braunschweig, *J. Am. Chem. Soc.*, 2016, **138**, 8212.

[3] H. Helten, *Chem. Eur. J.*, 2016, **22**, 12972.

[4] (a) A. W. Baggett, F. Guo, B. Li, S.-Y. Liu and F. Jäkle, *Angew. Chem. Int. Ed.*, 2015, **54**, 11191; (b) X.-Y. Wang, F.-D. Zhuang, J.-Y. Wang and J. Pei, *Chem. Commun.*, 2015, **51**, 17532.

[5] (a) T. Lorenz, A. Lik, F. A. Plamper and H. Helten, *Angew. Chem. Int. Ed.*, 2016, **55**, 7236; (b) O. Ayhan, T. Eckert, F. A. Plamper and H. Helten, *Angew. Chem. Int. Ed.*, 2016, **55**, 13321; (c) T. Lorenz, M. Crumbach, T. Eckert, A. Lik and H. Helten, *Angew. Chem. Int. Ed.*, 2017, **56**, 2780.

[6] D. Bonifazi, F. Fasano, M. M. Lorenzo-Garcia, D. Marinelli, H. Oubaha and J. Tasseroul, *Chem. Commun.*, 2015, **51**, 15222.

[7] For uses of molecular borazine-based materials for optoelectronic and sensory applications, see: (a) A. Wakamiya, T. Ide and S. Yamaguchi, *J. Am. Chem. Soc.*, 2005, **127**, 14859; (b) I. H. T. Sham, C.-C. Kwok, C.-M. Che and N. Zhu, *Chem. Commun.*, 2005, 3547; (c) M. K. Kesharwani, M. Suresh, A. Das and B. Ganguly, *Tetrahedron Letters*, 2011, **52**, 3636.

[8] (a) P. J. Fazen, E. E. Remsen, J. S. Beck, P. J. Carroll, A. R. McGhie and L. G. Sneddon, *Chem. Mater.*, 1995, **7**, 1942; (b) S. Bernard, C. Salameh and P. Miele, *Dalton Trans.*, 2016, **45**, 861.

[9] (a) Y. Kubota, K. Watanabe, O. Tsuda and T. Taniguchi, *Science*, 2007, **317**, 932; (b) K. Watanabe, T. Taniguchi, T. Niiyama, K. Miya and M. Taniguchi, *Nat. Photonics*, 2009, **3**, 591; (c) L. Ci, L. Song, C. Jin, D. Jariwala, D. Wu, Y. Li, A. Srivastava, Z. F. Wang, K. Storr, L. Balicas, F. Liu and P. M. Ajayan, *Nat. Mater.*, 2010, **9**, 430; (d) C. R. Dean, A. F. Young, I. Meric, C. Lee, L. Wang, S. Sorgenfrei, K. Watanabe, T. Taniguchi, P. Kim, K. L. Shepard and J. Hone, *Nat. Nanotechnol.*, 2010, **5**, 722; (e) M. P. Levendorf, C.-J. Kim, L. Brown, P. Y. Huang, R. W. Havener, D. A. Muller and J. Park, *Nature*, 2012, **488**, 627; (f) C. Huang, C. Chen, M. Zhang, L. Lin, X. Ye, S. Lin, M. Antonietti and X. Wang, *Nat. Commun.*, 2015, **6**, 7698; (g) C. Sánchez-Sánchez, S. Brüller, H. Sachdev, K. Müllen, M. Krieg, H. F. Bettinger, A. Nicolaï, V. Meunier, L. Talirz, R. Fasel and P. Ruffieux, *ACS nano*, 2015, **9**, 9228.

[10] (a) W.-M. Wan, A. W. Baggett, F. Cheng, H. Lin, S.-Y. Liu and F. Jäkle, *Chem. Commun.*, 2016, **52**, 13616; (b) B. Thiedemann, P. J. Gliese, J. Hoffmann, P. G. Lawrence, F. D. Sönnichsen and A. Staubitz, *Chem. Commun.*, 2017, **53**, 7258.

[11] H. R. Allcock, M. F. Welker and M. Parvez, *Chem. Mater.*, 1992, **4**, 296.

[12] D. Marinelli, F. Fasano, B. Najjari, N. Demitri and D. Bonifazi, *J. Am. Chem. Soc.*, 2017, **139**, 5503.

[13] (a) T. E. Reich, K. T. Jackson, S. Li, P. Jena and H. M. El-Kaderi, *J. Mater. Chem.*, 2011, **21**, 10629; (b) K. T. Jackson, M. G. Rabbani, T. E. Reich and H. M. El-Kaderi, *Polym. Chem.*, 2011, **2**, 2775; (c) T. E. Reich, S. Behera, K. T. Jackson, P. Jena and H. M. El-Kaderi, *J. Mater. Chem.*, 2012, **22**, 13524; (d) K. T. Jackson, T. E. Reich and H. M. El-Kaderi, *Chem. Commun.*, 2012, **48**, 8823.

[14] K. Li and H. D. H. Stöver, *J. Polym. Sci. A Polym. Chem.*, 1993, **31**, 3257.

[15] (a) L. Zhu, Y. Zhu, Y. Pan, Y. Huang, X. Huang and X. Tang, *Macromol. React. Eng.*, 2007, **1**, 45; (b) P. Zhang, X. Huang, J. Fu, Y. Huang, Y. Zhu and X. Tang, *Macromol. Chem. Phys.*, 2009, **210**, 792; (c) W. Wei, X. Huang, X. Zhao, P. Zhang and X. Tang, *Chem. Commun.*, 2010, **46**, 487; (d) P. Mohanty and K. Landskron, *New J. Chem.*, 2010, **34**, 215; (e) T. Pan, X. Huang, H. Wei, W. Wei and X. Tang, *Macromol. Chem. Phys.*, 2012, **213**, 1590; (f) Z. Huang, S. Chen, X. Lu and Q. Lu, *Chem. Commun.*, 2015, **51**, 8373.

[16] J. Köhler, S. Kühl, H. Keul, M. Möller and A. Pich, *J. Polym. Sci., Part A: Polym. Chem.*, 2014, **52**, 527.

[17] H. Nöth and H. Sachdev, *Z. Naturforsch. B*, 1997, **52**, 1345.

[18] (a) A. Kaldor and R. F. Porter*, Inor. Chem*., 1971, **10**, 775-785; (b) H. Moutaabbid and M. Moutaabbid, *J. Polym. Eng.*, 2011, **31**, 441-447.

[19] X. Lin, Z. Zhang, L. Chen, F. Zeng, Y. Luo and C. Xu, *J. Organomet. Chem.* 2014, **749**, 251.

[20] (a) V. P. Fadeeva, V. D. Tikhova and O. N. Nikulicheva, *J. Anal. Chem.*, 2008, **63**, 1094; (b) L.-L. Liu, G.-Q. He, Y.-H. Wang and S.-Q. Hu, *RSC Adv.*, 2015, **5**, 101416.

[21] The differences between the TGA curves measured in air and under N_2 atmosphere are presumably due to partial oxidation of the organic groups at elevated temperature in the presence of oxygen.

[22] X. Lin, Z. Zhang, L. Chen, F. Zeng, Y. Luo and C. Xu, J. Organomet. Chem., 2014, **749**, 251.

[23] H. Nöth and H. Sachdev, *Z. Naturforsch. B*, 1997, **52**, 1345.

[24] V. P. Fadeeva, V. D. Tikhova and O. N. Nikulicheva, *J. Anal. Chem.*, 2008, **63**, 1094.

[25] L.-L. Liu, G.-Q. He, Y.-H. Wang and S.-Q. Hu, *RSC Adv.*, 2015, **5**, 101416.

2.2 Difuryl(supermesityl)borane: A Versatile Building Block for Extended π-Conjugated Materials

The following section is slightly modified and reproduced from published article[†] with permission from The Royal Society of Chemistry.

Abstract: Direct functionalization and Pd-catalyzed cross-coupling of difuryl(supermesityl)borane (**1**) led to highly emissive organoborane compounds **3** and **4**. Photophysical and TD-DFT studies reveal an increase of the HOMO levels with higher hetarene content and a stabilization of HOMO and LUMO levels through the B-doping, leading to very robust, air-stable electron-accepting materials.

π-Conjugated organic materials have aroused tremendous research interest in the last decades due to applications in (opto)electronic devices (OLEDs, OFETs, OPVs, etc.) and for sensory and imaging purposes.[1] While thiophene is one of the most popular electron-rich building blocks of organic electronic materials,[2] the use of its lighter congener, furan, as a conceivable alternative for this purpose, has been limited until quite recently.[3] This has been associated with the reduced stability of furan moieties in the presence of oxygen and incident light.[3a,d,h] However, furan rings have some favorable characteristics; significantly, they are biodegradable and can be obtained from entirely renewable resources. Consequentially, the interest in furan-based materials has recently considerably increased.[3] A number of possible ways to stabilize furan against oxygen and light-driven degradation have been identified; one of which being the combination with a strongly electron-withdrawing component. This causes lowering of the HOMO energy and, hence, improved oxidation resistance.[3]

In recent years, triorganoboranes have emerged as potent electron-acceptor building blocks in organic electronics,[4-7] thus, making the development of boron-containing π-conjugated materials a very active field of current research. The incorporation of the vacant p_π orbital on boron into extended π-systems imparts intriguing properties and special features to the resulting materials. Of particular interest has been the combination of borane with thiophene moieties, resulting in valuable donor–acceptor arrays.[4b,6,7] Jäkle and Marder et al. demonstrated the use of very robust dithienylboranes that are kinetically stabilized by bulky 2,4,6-tri-*tert*-butylphenyl (Mes*, supermesityl) or 2,4,6-tris(trifluoromethyl)phenyl (^{F}Mes, fluoromesityl) groups as building blocks for extended π-conjugated materials (Figure 2.2.1).[7a] Jäkle and co-workers subsequently extended the application thereof to combinations with further π systems of

[†] N. A. Riensch, L. Fritze, T. Schindler, M. Kremer, H. Helten, *Dalton Trans.* **2018**, *47*, 10399—10403.

varying electronic demand.[7b-e] One finding from their studies was that the change from mono- to bithiophene moieties attached to boron leads to enhanced luminescence properties of such materials.[7b]

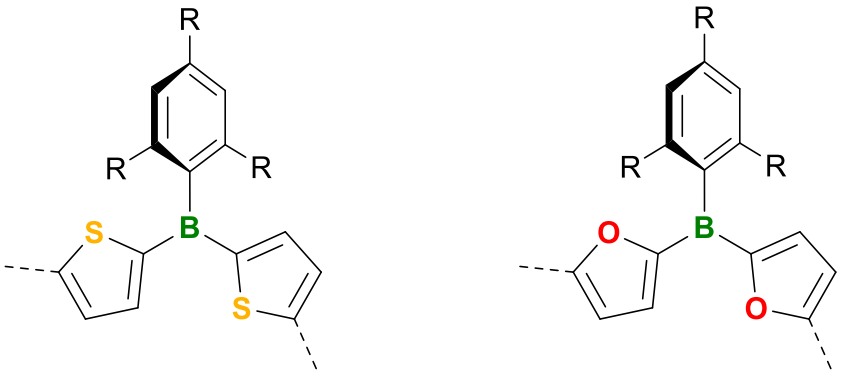

R = ^{i}Pr (i.e., *B*-Tip), ^{t}Bu (i.e., *B*-Mes*), or CF_3 (i.e., *B*-^{F}Mes)

Figure 2.2.1. Kinetically stabilized π-conjugated dithienyl- and difurylborane building blocks.

The combination of borane with furan moieties has only been scarcely explored thus far.[8,9] We recently developed a novel catalytic B–C coupling method, which we applied to access a series of thienylboranes and the first furylborane oligomers and polymers along with some mixed thienyl-/furylborane species.[9,10] We found that *B*-Mes* substituted furylboranes were perfectly stable to air and moisture as well and, moreover, they showed significantly stronger luminescence than their thiophene congeners;[9] in mixed derivatives, emission intensities increased with increasing ratio of furan rings.[9b] Herein, we demonstrate the extension of the conjugated π-system in a difurylborane via direct functionalization and Suzuki–Miyaura cross-coupling. The resulting biaryl-substituted, kinetically stabilized boranes are highly fluorescent, very robust, and exhibit narrowed band gaps. By quantum chemical calculations we elucidate the effect of B-doping in oligo(heteroarene)s.

The reaction of difuryl(supermesityl)borane (**1**)[9a] with 2 equivalents of *t*-BuLi in diethyl ether at −78 °C led to selective dilithiation in the α-position of the furyl groups (Scheme 2.2.1). Subsequent reaction with elemental bromine or iodine afforded the functionalized difurylboranes **2a** and **2b**, respectively, which were isolated in good yields (77 and 80 %). Compounds **2a** and **2b** were then employed in Suzuki–Miyaura cross-coupling reactions with 2-thienyl- or 2-furyl-Bpin (pin = pinacolato), respecttively, to give the biaryl-substituted boranes **3** and **4**, which proved to be perfectly stable in air for at least two weeks.

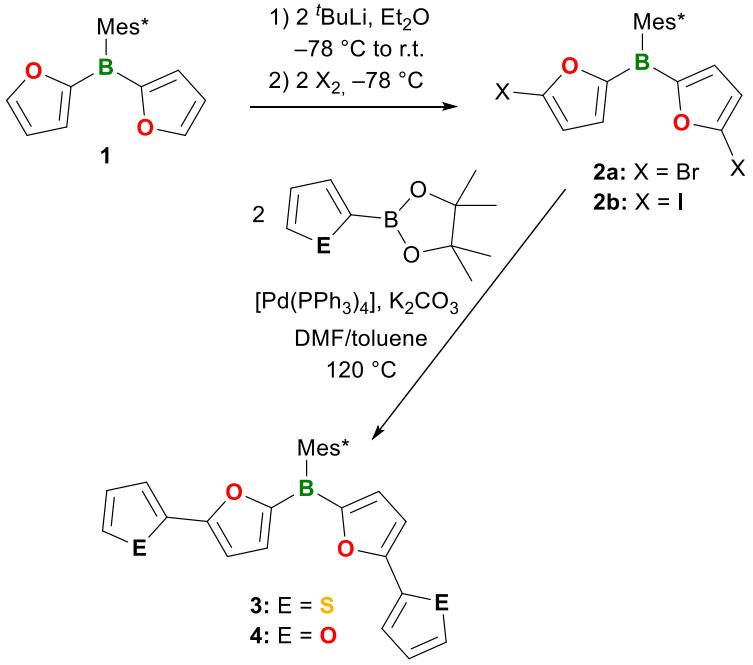

Scheme 2.2.1. Synthesis of π-conjugated organoboranes **3** and **4**.

The constitutions of **2a,b**, **3**, and **4** were unambiguously ascertained by multinuclear NMR spectroscopy and mass spectrometry. The $^{11}B\{^1H\}$ NMR spectra of each compound displayed a resonance at about 46 – 47 ppm, confirming the presence of three-coordinate boron. The ^1H and $^{13}C\{^1H\}$ NMR spectra showed all the expected resonances for the proposed constitution of the products. Noteworthy is that the protons at C^3 of the B-bound furyl groups gave rise to a significantly broadened ^1H signal. This points to hindered rotation about the B–C(furyl) bonds.

The molecular structures of **2a**, **2b**, and **3** in the solid state were additionally determined by single-crystal X-ray diffractometry (Figure 2.2.2). This showed that the boron atoms are trigonal-planar coordinated (sums of the bond angles around boron, $\Sigma(BC_3)$, 359.8 to 360.0°), and the Mes* substituents are nearly perpendicular oriented to the respective BC_3 plane (torsion angles ≥ 84°). The B–C(furyl) bond lengths are in a similar range (1.531–1.543 Å) with those of other furylborane species reported by us previously,[9] but significantly shorter than the B–C(thienyl) bonds in Mes*B(2-thienyl)$_2$ (1.589(6) and 1.568(4) Å).[7a] In each compound, the B-bound furan rings adopt an *anti* arrangement (i.e., with respect to the relative orientation of the O atoms) and form quasiplanar structures which involve also the coordination environments of the boron atoms. The twist angles between the furan ring planes are only 7.1(1)° in **2a**, and 10.1(2), 6.9(2), and 17.1(2)° for the three independent molecules in the asymmetric unit of **2b**. Compound **3** shows a slight rotational disorder about the B1–C1 bond; which, however, does not invert the *anti* conformation of the two furan rings. The furan–furan twist angles are 1.5(1) and 13.6(3)° for the two rotational isomers. The terminal thiophene rings are also largely coplanar with their adjacent furan moieties. The rings that involve the atoms O1 and S1 are *anti*-arranged and have twist angles of 24.7(2) and 25.6(3)° for the two

rotamers. The thiophene moiety involving the S2 atom shows another rotational disorder, which leads to *syn*/*anti*-isomeric conformations at this part of the molecule with twist angles of 5.6(4) and 6.5(5)°. Overall, the largely quasiplanar structures observed in the solid state, form an ideal prerequisite for effective π conjugation over the hetarene rings and the boron centers.

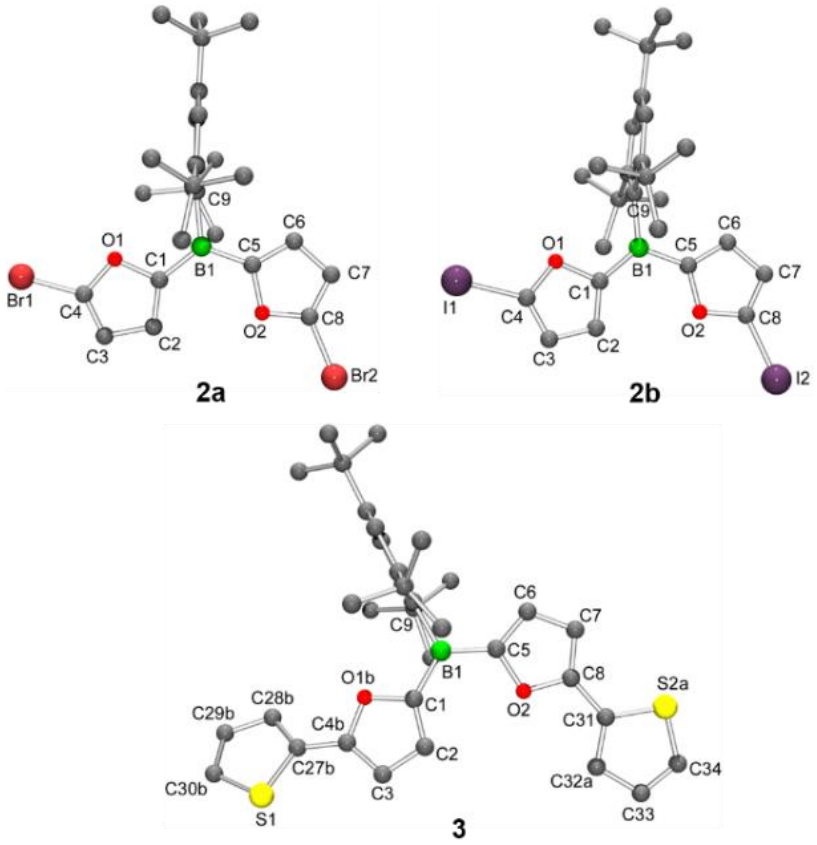

Figure 2.2.2. Molecular structures of **2a**, **2b**, and **3** in the solid-state (H atoms omitted for clarity; for **2b**, only one of three independent molecules of the asymmetric unit with similar structural data is shown; compound **3** shows rotational disorder at the thiophene ring at C31 and the furan–thiophene moiety at C1, only one conformer is shown).

The photophysical characteristics of **2a**, **2b**, **3**, and **4** were investigated by UV–vis and fluorescence spectroscopies. The absorption bands assigned to π–π* transitions in the UV–vis spectra of **2a,b** are slightly redshifted with respect to that of unsubstituted **1** (Fig. 2.2.3, left); the wavelengths of the maxima increase in the order: **1** ($\lambda_{abs,max}$ = 315 nm)[9] < **2a** ($\lambda_{abs,max}$ = 332 nm) < **2b** ($\lambda_{abs,max}$ = 341 nm). The spectra of **3** and **4** display each a strong absorption band at significantly longer wavelength (**3**: $\lambda_{abs,max}$ = 400 nm; **4**: $\lambda_{abs,max}$ = 394 nm) and a weaker band at higher energy (**3**: $\lambda_{abs,max}$ = 329 nm; **4**: $\lambda_{abs,max}$ = 336 nm). While **2a,b** were virtually non-fluorescent, compounds **3** and **4** showed strong blue fluorescence emission with relatively small Stokes shifts (**3**: $\lambda_{em,max}$ = 433 nm, Φ_F = 87 %; **4**: $\lambda_{em,max}$ = 427 nm, Φ_F = 67 %). This points to an effective extension of the conjugated π system through the extra thienyl or furyl groups in **3** and **4**, respectively. Cyclic voltammetry (CV) measurements revealed a reversible

reduction wave for **4** with a half-wave potential of $E_{1/2}$ = −2.53 V (Figure 2.2.3, right) and a quasi-reversible reduction for **3** ($E_{1/2}$ = −2.48 V; see Appendix, Figure 5.2.30). This is somewhat anodic shifted with respect to the reduction wave of **1** ($E_{1/2}$ = −2.83 V).[9b]

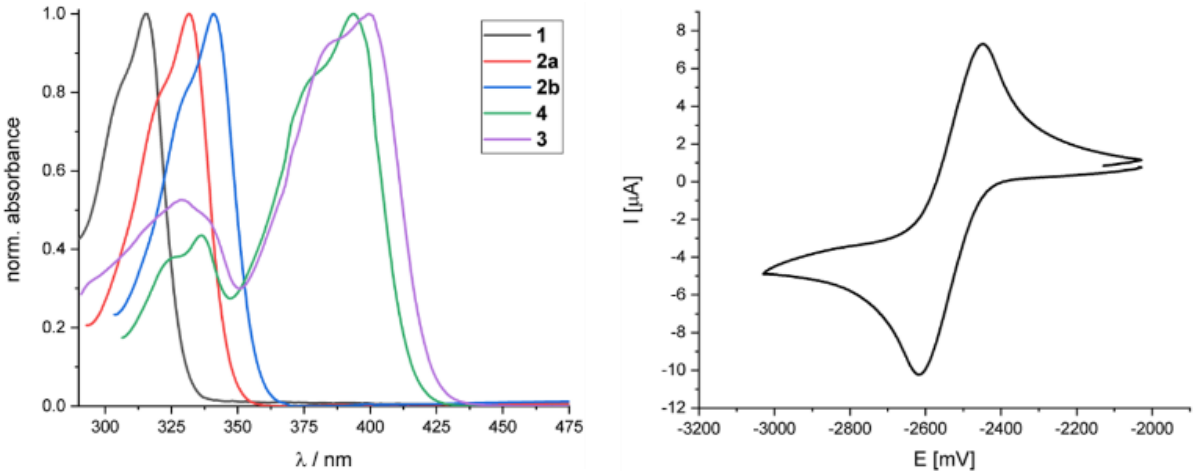

Figure 2.2.3. Left: UV–vis absorption spectra of **1**, **2a**,**b**, **3**, and **4** (in THF). Right: Cyclic voltammogram of **4** ($1 \cdot 10^{-3}$ M in THF; vs Fc^+/Fc; scan rate: 100 mV s^{-1}).

To gain deeper insight into the electronic structures of the new compounds, we carried out a series of time-dependent DFT (TD-DFT) calculations on B3LYP-D3(BJ)/def2-SV(P) level. For computational convenience we slightly truncated the molecules by using mesityl instead of supermesityl substituents (i.e., model systems **1'**,[9b] **2a**,**b'**, **3'**, and **4'**). Our calculations revealed that the maximum absorption band observed in the UV–vis spectra of each compound can be assigned to the excitation from an extended π orbital, fully delocalized over the hetarene rings, to the LUMO, which is an extended π orbital as well but has considerable contribution from the boron atom (Fig. 2.2.4 and experimental section, Figs. 2.2.6-11 and Table 2.2.2). Accordingly, this process is characterized as a π–π* transition associated with some intramolecular charge transfer (ICT) to the boron center.

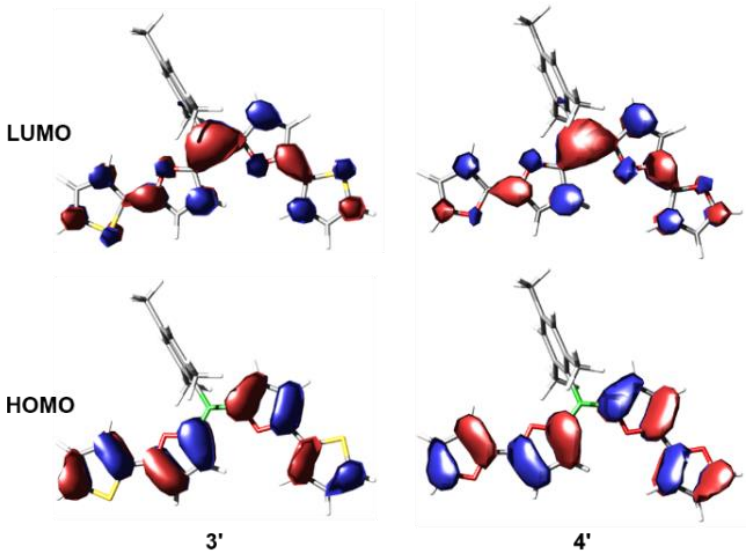

Figure 2.2.4. Calculated frontier orbitals of **3'** and **4'** (isovalue 0.03 a.u.).

The experimentally observed trend of decreasing excitation energies in the order **1** > **2a** > **2b** is well reproduced by the calculations (Figure 2.2.5). The introduction of bromo or iodo substituents leads to a reduced energy gap between the frontier π MOs. According to our calculations, this is due to both an increase in the energy of the occupied π orbital and a decrease in the energy of the LUMO. It should be noted that, in this series, the energetic order of the highest occupied MOs undergoes an inversion. While in **1'**, the π orbital involved in these transitions constitutes the HOMO−2, in **2a'** and **2b'**, it is the HOMO−1. The HOMO (and the HOMO−1 in **1'**) is localized on the mesityl ring, and, hence, the HOMO-to-LUMO transition – as it involves nearly orthogonal π orbitals – is of negligible probability.

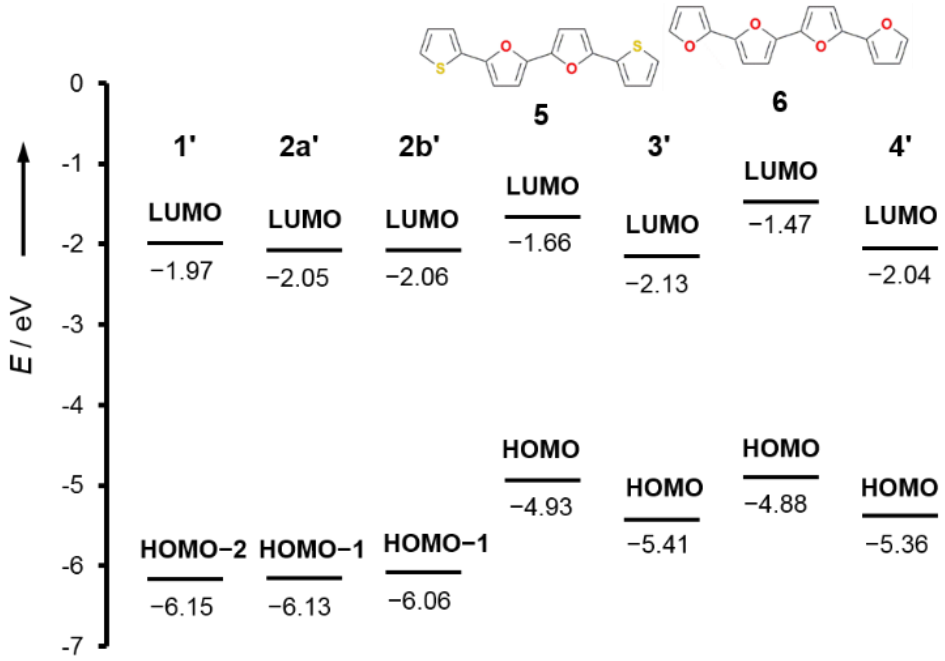

Figure 2.2.5. Calculated frontier π orbital energy levels (B3LYP-D3/def2-SV(P); values in eV).

The major effect of the extension of the conjugated π system when moving to **3'** and **4'**, is that the energy of the highest occupied π orbital, which is in this case the HOMO, is significantly elevated. This is the main reason for the observed dramatic redshift of the π–π* absorption band in these species. The additional minor decrease in the LUMO energy is consistent with the observation of an anodic shift in the electrochemical reduction wave (*vide supra*). Our calculations further revealed that the high-energy band observed in the spectra of **3** and **4** is assigned to a second π–π* transition involving the HOMO and the LUMO+1. The latter has a vertical nodal plane through the boron atom.

With a view to learn more about the effect of the borane group on the electronic structure of the extended π systems in **3** and **4**, we additionally calculated the oligo(hetarene)s **5** and **6** which have the same sequence of hetarene rings as **3** and **4** but lack the borane moiety[11] (see Figure 2.2.5 for their structures). This revealed that the introduction of boron results in significant decrease of both the HOMO and the LUMO energy. The slightly larger influence on the LUMO causes somewhat lower excitation energies for **3'** and **4'** compared to **5** and **6**.

In conclusion, we demonstrated the use of difuryl(supermesityl)borane (**1**) as a valuable building block for extended π-conjugated materials. Facile direct functionalization of **1** and subsequent Suzuki–Miyaura cross-coupling using **2a,b** led to highly fluorescent organoboron hybrid compounds **3** and **4**. The increased hetarene content in these species causes strong elevation of the HOMO levels, resulting in dramatic bathochromic shifts and intensification of the absorption and emission properties. According to our DFT calculations, the B-doping of oligo(heteroarene)s such as **5** and **6** causes significant lowering of both the HOMO and LUMO energy levels. The former effect leads to improved oxidative stability of such materials, while the latter results in enhanced electron-acceptor properties, which is of interest for the development of effective electron-transporting organic materials.[12]

2.2.1 Experimental section

General procedures. All manipulations were performed under an atmosphere of dry argon using standard Schlenk techniques or in an MBraun glove box. Solvents (dichloromethane, *n*-pentane, diethylether, toluene, and tetrahydrofuran) were dried and degassed by means of an MBraun SPS-800 solvent purification system. *N,N'*-Dimethylformamide was dried over $MgSO_4$ and distilled prior to use. Deuterated solvents for NMR spectroscopy were dried and degassed at reflux over Na (C_6D_6) or CaH_2 ($CDCl_3$ and CD_2Cl_2) and freshly distilled prior to use. *n*-Hexane for aqueous work-up, tribromoborane, bromobenzene, thiophene, magnesium turnings, iodine, bromine, and $Pd(PPh_3)_4$ were purchased from commercial sources and used as received. Solutions of *n*-butyllithium (1.6 M and 2.5 M in hexane, respectively) and *tert*-butyllithium (1.7 M in pentane) were purchased from Sigma Aldrich and used as received as well. Furan and 2-isopropoxy-4,4,5,5-tetramethyl-1,3,2-dioxaborolane were commercially purchased and freshly distilled prior to use. Compound **1**,[13a] 2-(4,4,5,5-tetramethyl-(2-thienyl)-1,3,2-dioxaborolane,[13b] and 2-(4,4,5,5-tetramethyl-(2-furyl)-1,3,2-dioxaborolane,[13c] were prepared according to methods described in the literature. NMR spectra were recorded at 25 °C on a Bruker Avance II-400 spectrometer or on a Bruker Avance III HD spectrometer operating at 400 MHz. Chemical shifts were referenced to residual protic impurities in the solvent (^1H) or the deuterio solvent itself (^{13}C) and reported relative to external $SiMe_4$ (^1H, ^{13}C) or $BF_3{\cdot}OEt_2$ (^{11}B) standards. Mass spectra were obtained with the use of a Finnigan MAT95 spectrometer employing electron ionization (EI) using a 70 eV electron impact ionization source. Elemental analysis was performed with a CHN-O-Rapid VarioEL by Heraeus. UV–vis spectra were obtained using a Jasco V-630 spectrophotometer. Fluorescence spectra were obtained with a Jasco FP-6600 spectrofluorometer. Fluorescence quantum yields were determined against perylene as the standard. Melting points (uncorrected) were obtained using a SMP3 melting point apparatus by Stuart in 0.5 mm (o.d.) glass capillaries. Cyclic voltammetry (CV) experiments were carried out on a PGSTAT101 analyzer from Metrohm. The three-electrode system consisted of a Pt disk as working electrode, a Pt wire as counter electrode, and an Ag wire as the reference electrode. The voltammograms were recorded with ca. 10^{-3} M solutions in THF containing $Bu_4N[PF_6]$ (0.1 M) as the supporting electrolyte. The scans were referenced after the addition of a small amount of ferrocene as internal standard. The potentials are reported relative to the ferrocene/ferrocenium couple.

Synthesis of 2a. To a solution of **1** (468.4 mg, 1.20 mmol) in Et_2O (9.0 mL) was added *tert*-butyllithium (1.7 M, 1.45 mL, 2.46 mmol) at −78 °C. Subsequently, the mixture was warmed to room temperature and stirred at for further 3 h. Then, bromine (479.4 mg, 3.00 mmol) was added at −78 °C. The reaction mixture was allowed to warm up to room temperature overnight. All volatiles were removed *in vacuo*, and the brownish crude product was subjected to column

chromatography (AlOx; *n*-hexane) to give **2a** as a colorless solid (m.p. 179.4 °C). Yield: 505.7 mg (0.92 mmol, 77 %); ^{1}H NMR (400 MHz, $CDCl_3$): δ = 7.42 (s, 2H, Mes*-C*H*), 7.30–6.95 (br, 2H, Fur-*H*), 6.44 (d, $^{3}J_{HH}$ = 3.4 Hz, 2H, Fur-*H*), 1.39 (s, 9H, *p*-^{t}Bu-CH_3), 1.19 (s, 18H, *o*-^{t}Bu-CH_3); ^{11}B{^{1}H} NMR (128 MHz, $CDCl_3$): δ = 46.1 (s); ^{13}C{^{1}H} NMR (101 MHz, $CDCl_3$): δ = 166.8 (Fur-*C*-B), 152.7 (Mes*-*C*–*o*-^{t}Bu), 148.9 (Mes*-*C*–*p*-^{t}Bu), 130.7 (Mes*-*C*-B, Fur-*C*H), 129.7 (Fur-*C*Br), 122.1 (Mes*-*C*H), 113.7 (Fur-*C*H), 38.4 (*o*-^{t}Bu-*C*), 34.9 (*p*-^{t}Bu-*C*), 34.4 (*o*-^{t}Bu-*C*H_3), 31.6 (*p*-^{t}Bu-*C*H_3); MS (EI, 70 eV): *m/z* (%) = 548.1 ([M]$^{+}$, 45), 231.2 (C_6H_2-^{i}Pr-(^{t}Bu)$_2$]$^{+}$, 72), 151.1 ([$C_{10}H_4BO$]$^{+\bullet}$, 51), 77.1 ([Ph]$^{+}$, 100); elem. anal. calcd (%) for $C_{26}H_{33}BBr_2O_2$: C 56. 97, H 6.07, found: C 57.26, H 6.08; UV–vis (THF): $\lambda_{abs,max}$ = 332 nm (ε = 26967 L mol^{-1} cm^{-1}); fluorescence (THF): non-emissive.

Synthesis of 2b. To a solution of **1** (780.7 mg, 2.00 mmol) in Et_2O (15 mL) was added *tert*-butyllithium (1.7 M, 2.41 mL, 4.10 mmol) at −78 °C. Subsequently, the mixture was warmed to room temperature and stirred at for further 3 h. Then, a solution of iodine (1.27 g, 5.00 mmol) in THF (2.5 mL) was added at −78 °C. The reaction mixture was allowed to warm up to room temperature overnight. All volatiles were removed *in vacuo*, and the brownish crude product was subjected to column chromatography (silica; *n*-hexane) and sublimation to remove residual iodine to give **2b** as a colorless solid (m.p. 204.5 °C). Yield: 1.03 g (1.60 mmol, 80 %); ^{1}H NMR (400 MHz, $CDCl_3$): δ = 7.41 (s, 2H, Mes*-C*H*), 7.20–6.90 (br, 2H, Fur-*H*), 6.66 (d, $^{3}J_{HH}$ = 3.4 Hz, 2H, Fur-*H*), 1.38 (s, 9H, *p*-^{t}Bu-CH_3), 1.17 (s, 18H, *o*-^{t}Bu-CH_3); ^{11}B{^{1}H} NMR (128 MHz, $CDCl_3$): δ = 45.9 (s); ^{13}C{^{1}H} NMR (101 MHz, $CDCl_3$): δ = 170.5 (Fur-*C*-B), 152.7 (Mes*-*C*–*o*-^{t}Bu), 148.8 (Mes*-*C*–*p*-^{t}Bu), 130.8 (Mes*-*C*-B, Fur-*C*H), 122.3 (Fur-*C*H), 122.0 (Mes*-*C*H), 97.4 (Fur-*C*H), 38.4 (*o*-^{t}Bu-*C*), 34.9 (*p*-^{t}Bu-*C*), 34.4 (*o*-^{t}Bu-*C*H_3), 31.6 (*p*-^{t}Bu-*C*H_3); MS (EI, 70 eV): *m/z* (%) = 642.1 ([M]$^{+}$, 4), 246.3 ([BH_2Mes*]$^{+}$), 69), 232.4 ([C_6H_3-^{i}Pr-(^{t}Bu)$_2$]$^{+}$), 100); elem. anal. calcd (%) for $C_{26}H_{33}BI_2O_2$: C 48.63, H 5.18, found: C 49.89, H 5.25; UV–vis (THF): $\lambda_{abs,max}$ = 341 nm (ε = 31466 L mol^{-1} cm^{-1}); fluorescence (THF): non-emissive.

Synthesis of 3. Compound **2a** (109.6 mg, 0.20 mmol) and 2-(4,4,5,5-tetramethyl-(2-thienyl)-1,3,2-dioxaborolane, (85.1 mg, 0.405 mmol) were charged into a Schlenk flask. Subsequently, dry DMF (3 mL) and toluene (3 ml) were added and the mixture was degassed by freeze-pump-thaw cycles. Then, $Pd(PPh_3)_4$ (15 mol%) followed by K_2CO_3 (164.4 mg, 1.190 mmol) were added under nitrogen. The reaction mixture was heated at 120 °C for 18 hours with vigorous stirring. Then, the mixture was cooled to ambient temperature and diluted with DCM (10 mL). After filtration, all volatiles were removed *in vacuo*, and the product was purified by column chromatography with gradient (hexane:DCM 100:0 -> 80:20). Compound **3** was obtained as a yellow solid (m.p. 184.9 °C). Yield: 62 mg (0.11 mmol, 56 %); ^{1}H NMR (400 MHz, $CDCl_3$): δ = 7.37 (s, 2H, Mes*-C*H*), 7.34 (br d, $^{3}J_{HH}$ = 2.8 Hz, 2H, Thi-*H*), 7.20 (d, $^{3}J_{HH}$ = 5.0 Hz, 2H, Thi-*H*), 6.96–6.94 (dd, $^{3}J_{HH}$ = 3.5 Hz, $^{4}J_{HH}$ = 1.8 Hz, 2H, Thi-*H*), 6.54 (d, $^{3}J_{HH}$ = 3.0 Hz, 2H,

Fur-*H*), 1.34 (s, 9H, *p*-Mes*-C*H*$_3$), 1.17 (s, 18H, *o*-Mes*-C*H*$_3$); ^{11}B{^{1}H} NMR (128 MHz, $CDCl_3$): δ = 47.2 (s); ^{13}C{^{1}H} NMR (101 MHz, $CDCl_3$): δ = 163.7 (Fur-*C*-B), 154.3 (Fur-*C*-C$_{Thi}$), 152.3 (Mes*-*C*–*o*-^{t}Bu), 148.1 (Mes*-*C*–*p*-^{t}Bu), 133.7 (Thi-*C*-C$_{Fur}$), 132.2 (Mes*-*C*-B), 130.1 (Fur-*C*H), 127.7 (Thi-*C*H), 125.3 (Thi-*C*H), 124.0 (Thi-*C*), 121.5 (Mes*-*C*H), 107.0 (Fur-*C*), 38.3 (*o*-^{t}Bu-*C*), 34.3 (*p*-^{t}Bu-*C*), 31.5 (*o*-^{t}Bu-*C*H$_3$), 31.3 (*p*-^{t}Bu-*C*H$_3$); MS (EI, 70 eV): *m/z* (%) = 553.7 ([M]$^+$, 3), 471.7 ([Mes*BFur$_2$Thi]$^+$, 3), 256.9 ([Mes*B]$^+$, 70), 230.9 (C$_6$H$_2$-^{i}Pr-(^{t}Bu)$_2$]$^+$), 100); UV–vis (THF): $\lambda_{abs,max}$ = 329 nm (ε = 60467 L mol^{-1} cm^{-1}), 400 nm (ε = 115763 L mol^{-1} cm^{-1}); fluorescence (THF): $\lambda_{em,max}$ (λ_{ex}=400 nm) = 433 nm (Φ_f = 87.2 %); CV (THF): $E_{1/2}$ = −2.48 V.

Synthesis of 4. Compound **2b** (128.4 mg, 0.20 mmol) and 2-(4,4,5,5-tetramethyl-(2-furyl)-1,3,2-dioxaborolane (78.6 mg, 0.405 mmol) were charged into a Schlenk flask. Subsequently, dry DMF (3 mL) and toluene (3 ml) were added and the mixture was degassed by freeze-pump-thaw cycles. Then, $Pd(PPh_3)_4$ (15 mol%) followed by K_2CO_3 (164.4 mg, 1.190 mmol) were added under nitrogen. The reaction mixture was heated at 120 °C for 18 hours with vigorous stirring. Then, the mixture was cooled to ambient temperature and diluted with DCM (10 mL). After filtration, all volatiles were removed *in vacuo*, and the product was purified by column chromatography with gradient (hexane:DCM 100:0 -> 80:20). Compound **4** was obtained as a brownish solid (m.p. 125 °C). Yield: 34 mg (0.065 mmol, 33 %); ^{1}H NMR (400 MHz, $CDCl_3$): δ = 7.47 (d, $^3J_{HH}$ = 1.7 Hz, 2H, Fur-*H*), 7.43 (s, 2H, Mes*-C*H*), 7.39–7.06 (br, 2H, Fur-*H*), 6.74 (d, $^3J_{HH}$ = 3.4 Hz, 2H, Fur-*H*), 6.70 (d, $^3J_{HH}$ = 3.5 Hz, 2H, Fur-*H)*, 6.50 (dd, $^3J_{HH}$ = 3.5, $^4J_{HH}$ = 1.8 Hz, 2H, Fur-*H*), 1.40 (s, 9H, *p*-Mes*-C*H*$_3$), 1.22 (s, 18H, *o*-Mes*-C*H*$_3$); ^{11}B{^{1}H} NMR (128 MHz, $CDCl_3$): δ = 46.9 (s); ^{13}C{^{1}H} NMR (101 MHz, $CDCl_3$): δ = 164.3 (Fur-*C*-B), 152.9 (Mes*-*C*–*o*-^{t}Bu), 151.7 (Fur-*C*-C$_{Fur}$), 148.8 (Mes*-*C*–*p*-^{t}Bu), 147.2 (Fur-*C*-C$_{Fur}$), 143.1 (Fur-*C*H), 132.8 (Mes*-*C*-B), 130.4 (Fur-*C*H), 122.1 (Mes*-*C*H), 112.2 (Fur-*C*H), 107.7 (Fur-*C*H), 107.6 (Fur-*C*H), 38.8 (*o*-^{t}Bu-*C*), 35.2 (*p*-^{t}Bu-*C*), 34.8 (*o*-^{t}Bu-*C*H$_3$), 31.9 (*p*-^{t}Bu-*C*H$_3$); MS (EI, 70 eV): *m/z* (%) = 521.7 ([M]$^+$, 37), 481.1 ([Ph-*p*-CH$_3$-o-(^{t}Bu)$_2$)$^+$], 63), 230.9 ([C$_6$H$_2$-^{i}Pr-(^{t}Bu)$_2$] $^+$), 100); UV–vis (THF): $\lambda_{abs,max}$ = 336 nm (ε = 45808 L mol^{-1} cm^{-1}), 394 nm (ε = 107771 L mol^{-1} cm^{-1}); fluorescence (THF): $\lambda_{em,max}$ (λ_{ex}= 394 nm) = 427 nm (Φ_f = 67.0 %); CV (THF): $E_{1/2}$ = −2.53 V.

X-ray crystallographic analysis

Suitable single crystals of **2a** (CCDC 1840367) and **2b** (CCDC 1840368) were obtained by slow evaporation of dichloromethane at 4 °C. **3** (CCDC 1843527) was obtained by slow evaporation of hexane at −40 °C. Data were collected on a Bruker SMART APEX CCD detector on a D8 goniometer equipped with an Oxford Cryostream 700 temperature controller at 100(2) K using graphite monochromated Mo-K_α radiation (λ = 0.71073 Å). An absorption correction was carried out semi-empirically using SADABS[14]. The structures were solved with Olex2[15] using Direct Methods (ShelXS[16a]) and refined with the ShelXL[16b] refinement package by full-matrix least squares on F^2. All non-hydrogen atoms were refined anisotropically. In the structure of **3**, atom C4a was refined isotropic to yield a stable structure. The hydrogen atoms were included isotropically and treated as riding. The structure of **2b** displays three independent molecules within the asymmetric unit.

Table 2.2.1. Crystal structure and refinement data for **2a**, **2b** and **3**.

No.	**2a**	**2b**	**3**
Color, habit	colorless plate	colorless block	colorless block
Empirical Formula	$C_{26}H_{33}BBr_2O_2$	$C_{26}H_{33}BI_2O_2$	$C_{34}H_{39}BO_2S_2$
M	548.15	642.17	554.61
Crystal system	triclinic	triclinic	triclinic
Space group	P-1	P-1	P-1
a/Å	9.0914(12)	10.7568(12)	9.299(3)
b/Å	10.6006(14)	17.0259(18)	13.239(5)
c/Å	14.3655(18)	22.758(2)	13.676(5)
α/°	71.643(2)	94.956(2)	97.674(8)
β/°	86.345(2)	94.394(2)	101.180(7)
γ/°	78.848(2)	103.556(2)	107.537(7)
V/Å^3	1289.2(3)	4016.5(7)	1541.5(10)
Z	2	8	2
μ/mm^{-1}	3.163	2.368	0.201
T/K	100	100	100
$\theta_{min,max}$	2.28, 28.66	2.30, 25.32	2.37, 21.82

Completeness	0.90 to θ = 31.2	0.99 to θ = 25.6	0.99 to θ = 26.1
Reflections: total/independent	20064/7513	45558/15014	18294/6097
R_{int}	0.0463	0.0386	0.0794
Final *R*1 and *wR*2	0.0393, 0.0644	0.0351, 0.0464	0.0661, 0.0611
Largest peak, hole/eÅ^{-3}	0.967/−0.715	1.579, −0.719	0.306, −0.401
ρ_{calc}/g cm^{-3}	1.412	1.593	1.195

2.2.2 Computational informations

Computational methods. DFT calculations were carried out with the TURBOMOLE V7.0.1 program package.[17] Optimizations were performed with Becke's three parameter exchange-correlation hybrid functional B3LYP[18] in combination with the valence-double-ζ basis set def2-SV(P).[19] The empirical dispersion correction DFT-D3 by Grimme was used including the three-body term and with Becke-Johnson (BJ) damping.[20] The stationary points were characterized as minima by analytical vibrational frequency calculations.[21] Vertical singlet excitations were calculated by means of time-dependent DFT[22] using the same density functional–basis set combination as specified above.

Table 2.2.2. Results from TD-DFT calculations (π–π* excitation marked in bold).

Compound	No.	λ / nm	Oscillator strength *f*	Orbital contributions	$\|c\|^2$ / %
2a'	1	382.6	0.0108	HOMO → LUMO	99.3
	2	355.5	0.0031	HOMO−2 → LUMO	93.7
	3	**330.6**	**0.5918**	**HOMO−1 → LUMO**	**93.1**
2b'	1	384.3	0.0126	HOMO → LUMO	95.7
	2	356.9	0.0063	HOMO−2 → LUMO	95.1
	3	**339.6**	**0.6164**	**HOMO−1 → LUMO**	**91.1**
5	**1**	**404.8**	**1.2140**	**HOMO → LUMO**	**99.4**
3'	**1**	**418.1**	**0.9106**	**HOMO → LUMO**	**99.4**
	2	397.3	0.0201	HOMO−1 → LUMO	81.0
				HOMO−2 → LUMO	17.3
	3	367.7	0.0015	HOMO−3 → LUMO	97.1
	5	**308.3**	**0.2994**	**HOMO → LUMO+1**	**78.4**
				HOMO−2 → LUMO	**14.9**
6	**1**	**384.6**	**1.2270**	**HOMO → LUMO**	**99.5**
4'	**1**	**410.6**	**0.8855**	**HOMO → LUMO**	**99.4**

	2	390.9	0.0176	HOMO−1 → LUMO	61.6
				HOMO−2 → LUMO	37.2
	3	361.5	0.0014	HOMO−3 → LUMO	98.7
	5	**287.7**	**0.3086**	**HOMO → LUMO+1**	**87.2**
				HOMO−2 → LUMO	**5.8**

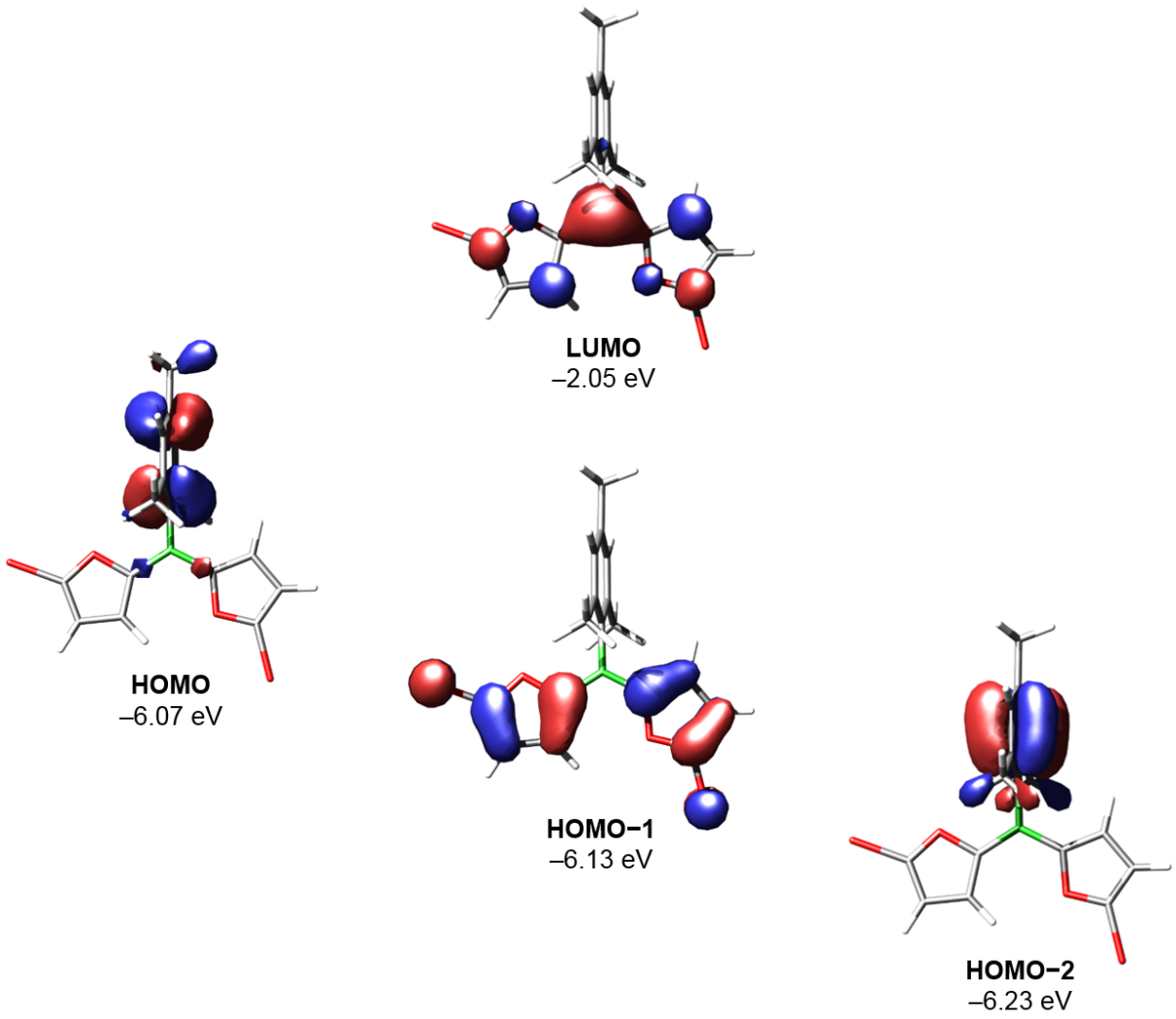

Figure 2.2.6. Calculated frontier orbitals of **2a'** (isovalue 0.04 a.u.).

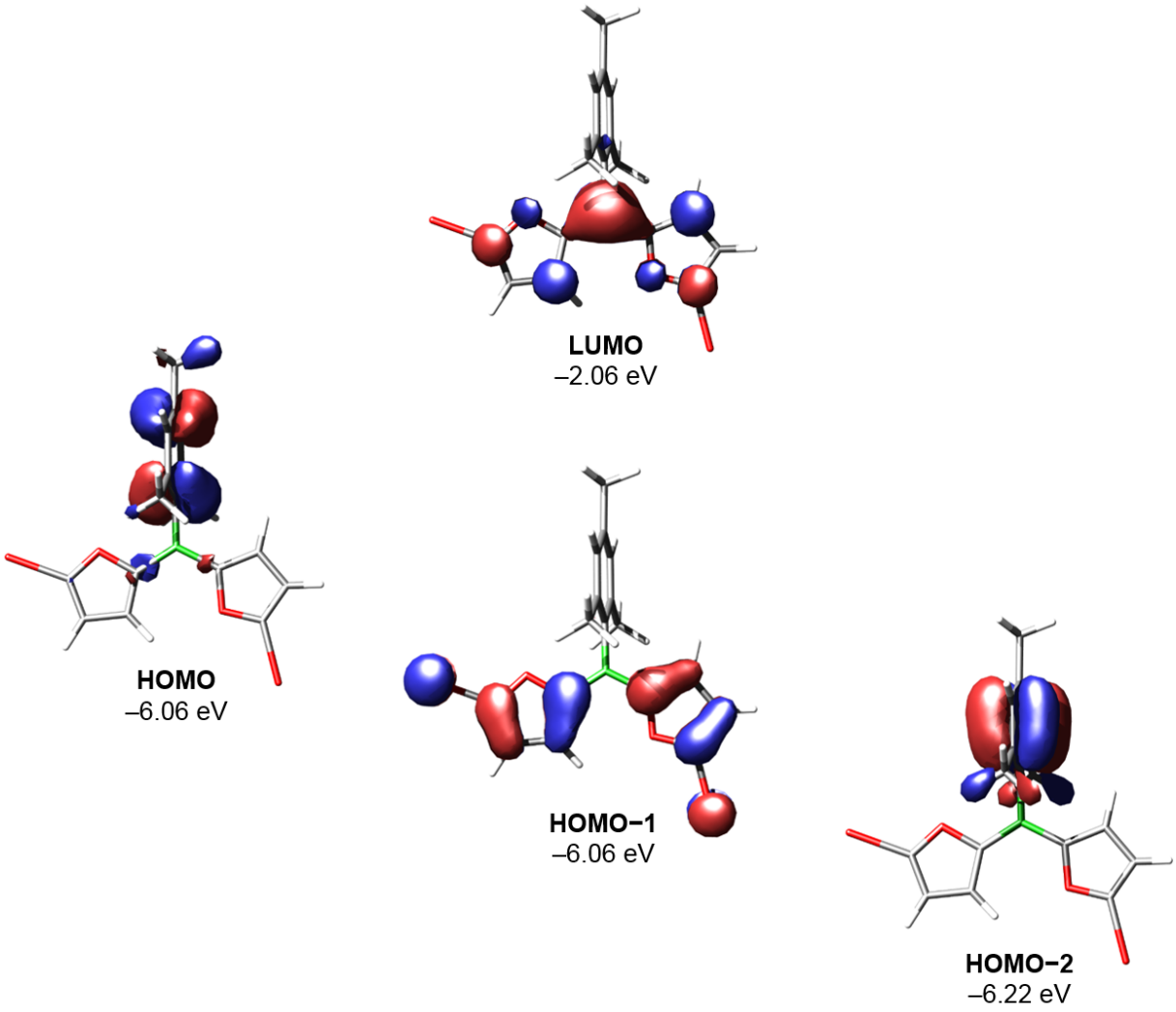

Figure 2.2.7. Calculated frontier orbitals of **2b'** (isovalue 0.04 a.u.).

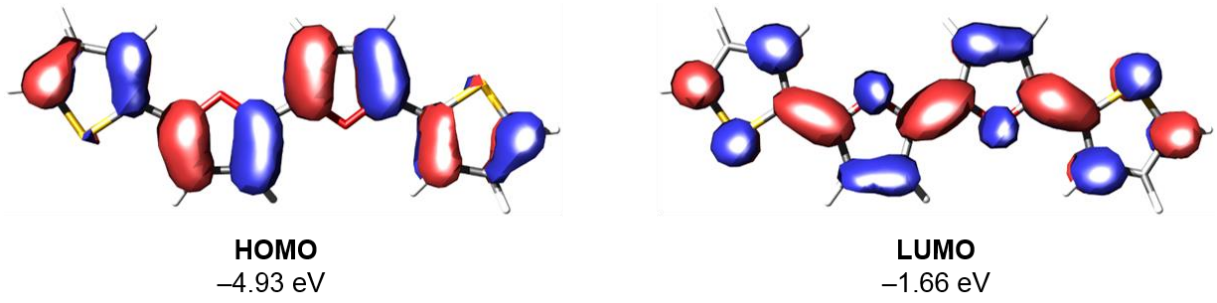

Figure 2.2.8. Calculated frontier orbitals of **5** (isovalue 0.03 a.u.).

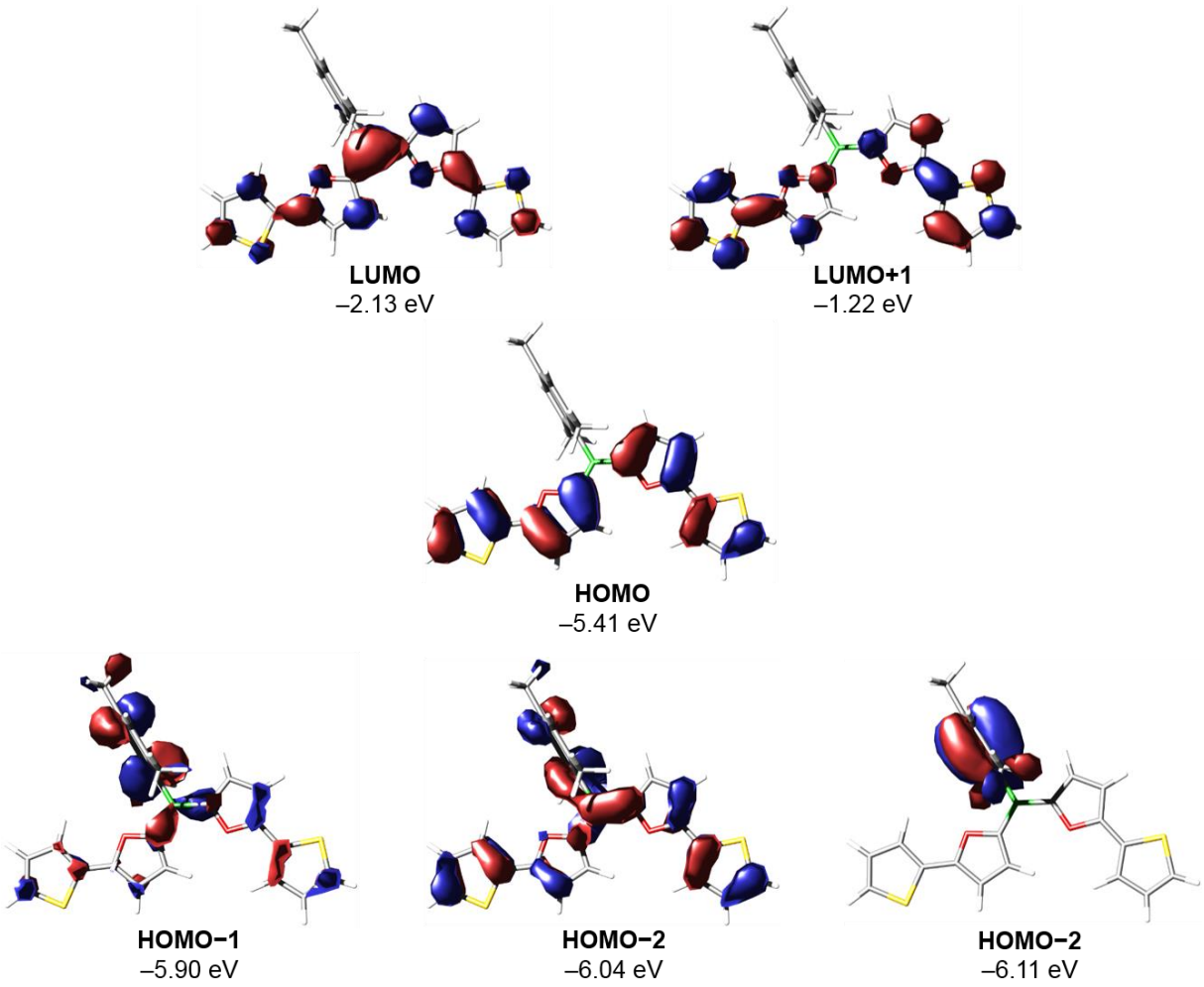

Figure 2.2.9. Calculated frontier orbitals of **3'** (isovalue 0.03 a.u.).

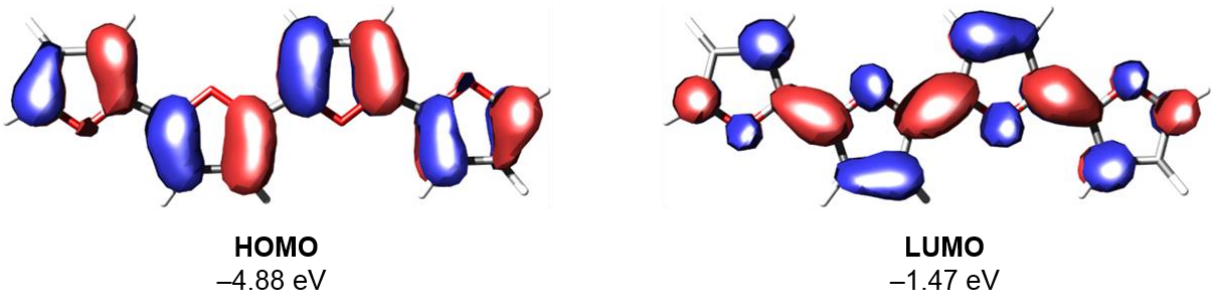

Figure 2.2.10. Calculated frontier orbitals of **6** (isovalue 0.03 a.u.).

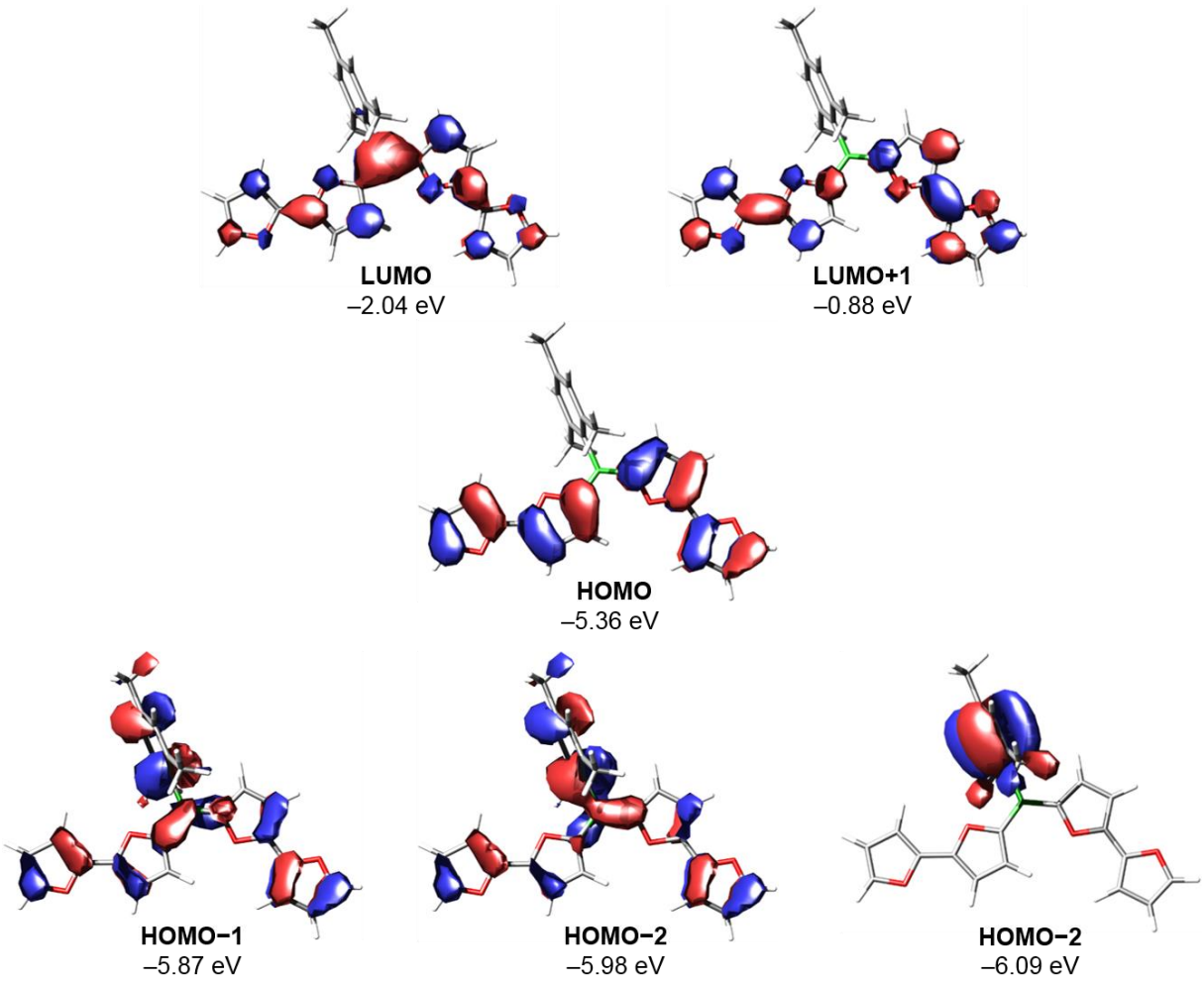

Figure 2.2.11. Calculated frontier orbitals of **4'** (isovalue 0.03 a.u.).

Cartesian coordinates [Å] and total energies [a.u.] of optimized stationary points

2a':

Total energy (B3LYP-D3(BJ)/def2-SV(P)): −5978.533161529

O	0.754565	−0.025894	−2.497581
C	1.476939	−0.023971	−1.306010
C	2.823051	−0.027201	−1.640999
C	2.927392	−0.030531	−3.058272
C	1.624982	−0.028099	−3.506248
B	0.691916	−0.015286	0.007844
C	−0.882491	−0.012943	0.025058
C	−1.593117	1.187375	−0.193562
C	−2.992961	1.182969	−0.152132
C	−3.718005	0.010041	0.091499
C	−3.001702	−1.176979	0.289209

C	−1.601435	−1.204990	0.263484
C	−0.846639	2.468902	−0.488833
C	−5.226049	0.028541	0.164484
C	−0.866737	−2.510975	0.472670
C	1.423792	0.010819	1.357117
C	0.944384	0.073916	2.653996
C	2.058225	0.087907	3.540967
C	3.159917	0.031849	2.719752
O	2.813652	−0.013333	1.429724
Br	4.981254	0.010862	3.119679
H	2.063441	0.133283	4.628001
H	−0.112163	0.107494	2.919882
H	−0.073376	2.675488	0.274274
H	−1.527526	3.336260	−0.522900
H	−0.329021	2.407805	−1.464195
H	−0.257476	−2.491041	1.395040
H	−1.566610	−3.360375	0.548618
H	−0.172574	−2.719917	−0.362683
H	−3.549622	−2.109718	0.465218
H	−3.533586	2.121318	−0.320398
H	3.823817	−0.033135	−3.675020
Br	0.937480	−0.025508	−5.239041
H	3.639722	−0.026828	−0.920873
H	−5.651653	0.835404	−0.457431
H	−5.659491	−0.929424	−0.172731
H	−5.574597	0.197029	1.202303

2b':

Total energy (B3LYP-D3(BJ)/def2-SV(P)): −1426.465505390

O	0.750724	−0.016409	−2.493144
C	1.475551	−0.019124	−1.304459
C	2.820733	−0.022240	−1.642628
C	2.920453	−0.020384	−3.060405
C	1.616924	−0.015507	−3.507757
B	0.692149	−0.014328	0.011060
C	−0.882014	−0.012154	0.027979
C	−1.593195	1.186150	−0.200211
C	−2.993107	1.180696	−0.161878

C	−3.717674	0.008800	0.088240
C	−3.000800	−1.176209	0.295512
C	−1.600486	−1.203206	0.272914
C	−0.847393	2.466751	−0.501206
C	−5.225887	0.026594	0.157852
C	−0.865573	−2.507704	0.490545
C	1.425622	0.007167	1.360115
C	0.946781	0.069468	2.657228
C	2.061720	0.078054	3.542873
C	3.165096	0.019685	2.722534
O	2.814222	−0.022027	1.431754
I	5.197584	−0.010972	3.171693
H	2.063958	0.121338	4.630300
H	−0.109453	0.105681	2.924225
H	−0.078185	2.680135	0.264154
H	−1.529631	3.332652	−0.544573
H	−0.325204	2.399507	−1.473639
H	−0.258080	−2.482768	1.413876
H	−1.565308	−3.356939	0.569539
H	−0.169794	−2.720842	−0.342392
H	−3.548299	−2.108363	0.475840
H	−3.534200	2.117450	−0.337567
H	3.817694	−0.021110	−3.676444
I	0.844744	−0.004573	−5.440362
H	3.639680	−0.025163	−0.925053
H	−5.650915	0.826976	−0.472818
H	−5.657753	−0.935038	−0.170854
H	−5.576736	0.204973	1.193255

5:

Total energy (B3LYP-D3(BJ)/def2-SV(P)): −1561.207217474

C	0.252447	−0.387049	2.568198
C	1.371948	−0.568249	3.353528
C	2.491461	−0.491229	2.475561
C	1.990179	−0.268108	1.208953
O	0.626217	−0.205103	1.269342
H	1.376648	−0.735143	4.428618
H	3.543705	−0.588183	2.739093

C	2.594876	−0.100525	−0.087517
S	4.329195	−0.163997	−0.293125
C	4.187051	0.106231	−1.998045
C	2.875979	0.237759	−2.386492
C	1.963160	0.120489	−1.298856
H	0.878147	0.193656	−1.388165
H	2.571679	0.413457	−3.421032
H	5.084342	0.152253	−2.615717
C	−1.150085	−0.357966	2.857176
C	−2.269255	−0.170495	2.072844
C	−3.388999	−0.251899	2.950120
C	−2.888198	−0.484059	4.215293
O	−1.524274	−0.547794	4.154787
H	−2.273571	0.003647	0.998903
H	−4.441113	−0.152517	2.686971
C	−3.493497	−0.662952	5.509969
S	−5.227861	−0.600390	5.715483
C	−5.086671	−0.888729	7.417510
C	−3.775877	−1.025495	7.805089
C	−2.862484	−0.897292	6.719169
H	−1.777586	−0.972572	6.808111
H	−3.472183	−1.212696	8.837788
H	−5.984260	−0.940463	8.034298

6:

Total energy (B3LYP-D3(BJ)/def2-SV(P)): −915.4046364487

C	0.274378	−0.362287	2.483932
C	1.420791	−0.532174	3.232064
C	2.512648	−0.447732	2.319319
C	1.962673	−0.231292	1.073862
O	0.603240	−0.178619	1.172043
H	1.460227	−0.697366	4.306786
H	3.574764	−0.534274	2.539179
C	2.532241	−0.062463	−0.233184
C	1.981763	0.156345	−1.476360
C	3.082600	0.235351	−2.389339
O	3.890367	−0.121356	−0.332455
C	4.213386	0.059589	−1.639751

H	5.275666	0.036745	−1.873011
H	3.036270	0.401577	−3.464965
H	0.920440	0.247501	−1.698066
C	−1.118806	−0.348657	2.817443
C	−2.265293	−0.179846	2.069165
C	−3.357625	−0.274867	2.980311
C	−2.807771	−0.494987	4.225182
O	−1.447983	−0.539573	4.128204
H	−2.304518	−0.009310	0.995257
H	−4.420004	−0.193603	2.759655
C	−3.377912	−0.676661	5.530254
C	−2.827338	−0.894499	6.773549
C	−3.929103	−0.994219	7.683368
O	−4.736985	−0.637858	5.626466
C	−5.060516	−0.830932	6.931909
H	−6.123600	−0.825272	7.162560
H	−3.882964	−1.165628	8.758184
H	−1.765371	−0.971934	6.997332

3':

Total energy (B3LYP-D3(BJ)/def2-SV(P)): −1935.189219178

C	0.346012	−1.137169	7.912612
C	−1.019654	−1.123680	7.689509
S	−1.895228	−1.384527	9.178766
C	−0.424222	−1.507734	10.079941
C	0.682445	−1.356942	9.278626
C	−1.712788	−0.928816	6.439831
C	−3.057357	−0.879936	6.107570
C	−3.105202	−0.655127	4.708944
C	−1.800968	−0.576525	4.243255
O	−0.961737	−0.749864	5.331936
B	−1.255949	−0.362565	2.826657
C	−2.287316	−0.132462	1.656013
C	−2.878380	1.134923	1.455118
C	−3.789055	1.319140	0.407042
C	−4.141803	0.272383	−0.454190
C	−3.543777	−0.976724	−0.249408
C	−2.622880	−1.191298	0.784518

C	−2.518609	2.295819	2.356196
C	−5.156281	0.481459	−1.553014
C	−1.978486	−2.548797	0.954495
C	0.246955	−0.388227	2.542245
O	0.661441	−0.202050	1.232482
C	2.005021	−0.268141	1.182026
C	2.511930	−0.496179	2.453401
C	1.388789	−0.572217	3.312158
C	2.621810	−0.099505	−0.110301
S	4.354681	−0.173513	−0.314884
C	4.213025	0.107742	−2.015786
C	2.902120	0.250498	−2.405270
C	1.989253	0.132710	−1.319121
H	3.564145	−0.594801	2.717127
H	1.387981	−0.744782	4.386737
H	−2.854811	2.121793	3.394840
H	−1.423904	2.447287	2.398647
H	−2.976182	3.236524	2.005331
H	−6.190189	0.376975	−1.169620
H	−5.032273	−0.256716	−2.364470
H	−5.074712	1.491415	−1.992874
H	−4.233872	2.309531	0.255873
H	−3.798545	−1.807925	−0.916905
H	−0.895791	−2.501848	0.734701
H	−2.079961	−2.920176	1.990967
H	−2.427728	−3.298274	0.280755
H	−3.991299	−0.558509	4.082208
H	−3.893102	−0.992902	6.796774
H	0.903935	0.212874	−1.402343
H	2.600056	0.434690	−3.438879
H	5.110117	0.151990	−2.634100
H	1.072732	−0.990878	7.111748
H	1.706992	−1.401617	9.655134
H	−0.460654	−1.685490	11.155155

4':

Total energy (B3LYP-D3(BJ)/def2-SV(P)): −1289.386741232

O	3.916438	−0.112992	−0.348410

C	2.557358	−0.061474	−0.252090
C	2.007398	0.159538	−1.494990
C	3.108294	0.248259	−2.404909
C	4.239201	0.075374	−1.652458
C	1.975061	−0.234522	1.049511
O	0.634541	−0.183869	1.135732
C	0.265420	−0.371639	2.459946
C	1.433852	−0.539909	3.193093
C	2.530163	−0.453257	2.300426
B	−1.226856	−0.359144	2.795663
C	−2.302265	−0.136843	1.663761
C	−2.894076	1.131390	1.471836
C	−3.846517	1.308302	0.460292
C	−4.240216	0.253277	−0.372662
C	−3.640882	−0.996749	−0.177484
C	−2.679256	−1.204095	0.820219
C	−2.490124	2.300281	2.343105
C	−5.298432	0.454920	−1.430898
C	−2.035894	−2.563046	0.981997
C	−1.720146	−0.575729	4.230747
C	−3.006415	−0.653263	4.744551
C	−2.910484	−0.877311	6.141608
C	−1.555041	−0.925715	6.417957
O	−0.840373	−0.748622	5.288495
C	−0.828783	−1.121142	7.642354
O	−1.559500	−1.302744	8.779033
C	−0.686970	−1.464391	9.804881
C	0.602509	−1.391197	9.351112
C	0.514944	−1.167263	7.940264
H	3.592341	−0.537557	2.521691
H	1.467609	−0.708302	4.267871
H	−2.770831	2.134137	3.399398
H	−1.394942	2.453647	2.326447
H	−2.967335	3.237407	2.009211
H	−6.316014	0.359658	−1.003863
H	−5.211385	−0.292880	−2.238357
H	−5.230816	1.459488	−1.885225
H	−4.292042	2.299344	0.315634

H	−3.927735	−1.834582	−0.823357
H	−0.959354	−2.522235	0.732430
H	−2.110330	−2.926284	2.023710
H	−2.506553	−3.315603	0.326520
H	−3.914073	−0.555729	4.149497
H	−3.713560	−0.991167	6.866926
H	0.944625	0.245860	−1.713199
H	3.063827	0.418887	−3.479884
H	5.301890	0.060065	−1.885207
H	1.331737	−1.053350	7.230162
H	1.507931	−1.485363	9.949348
H	−1.131212	−1.620052	10.785739

2.2.3. References

[1] (a) T. M. Swager, *Macromolecules*, 2017, **50**, 4867; (b) J. Mei, Y. Diao, A. L. Appleton, L. Fang and Z. Bao, *J. Am. Chem Soc.*, 2013, **135**, 6724; (c) S. Allard, M. Forster, B. Souharce, H. Thiem and U. Scherf, *Angew. Chem. Int. Ed.*, 2008, **47**, 4070.

[2] (a) S. C. Rasmussen, S. J. Evenson and C. B. McCausland, *Chem. Commun.*, 2015, **51**, 4528; (b) A. Mishra, C.-Q. Ma and P. Bäuerle, *Chem. Rev.*, 2009, **109**, 1141.

[3] (a) O. Gidron, Y. Diskin-Posner and M. Bendikov, *J. Am. Chem. Soc.*, 2010, **132**, 2148; (b) U. H. F. Bunz, *Angew. Chem. Int. Ed.*, 2010, **49**, 5037; (c) C. H. Woo, P. M. Beaujuge, T. W. Holcombe, O. P. Lee and J. M. J. Fréchet, *J. Am. Chem. Soc.*, 2010, **132**, 15547; (d) O. Gidron and M. Bendikov, *Angew. Chem. Int. Ed.*, 2014, **53**, 2546; (e) A. Luzio, D. Fazzi, F. Nübling, R. Matsidik, A. Straub, H. Komber, E. Giussani, S. E. Watkins, M. Barbatti, W. Thiel, E. Gann, L. Thomsen, C. R. McNeill, M. Caironi and M. Sommer, *Chem. Mater.*, 2014, **26**, 6233; (f) C.-H. Tsai, A. Fortney, Y. Qiu, R. R. Gil, D. Yaron, T. Kowalewski and K. J. T. Noonan, *J. Am. Chem. Soc.*, 2016, **138**, 6798; (g) H. Cao, I. A. Brettell-Adams, F. Qu and P. A. Rupar, *Organometallics*, 2017, **36**, 2565; (h) H. Cao and P. A. Rupar, *Chem. Eur. J.*, 2017, **23**, 14670.

[4] (a) L. Ji, S. Griesbeck and T. B. Marder, *Chem. Sci.*, 2017, **8**, 846; (b) Y. Ren and F. Jäkle, *Dalton Trans.*, 2016, **45**, 13996.

[5] (a) A. John, M. Bolte, H.-W. Lerner and M. Wagner, *Angew. Chem. Int. Ed.*, 2017, **56**, 5588; (b) K. Schickedanz, J. Radtke, M. Bolte, H.-W. Lerner and M. Wagner, *J. Am. Chem. Soc.*, 2017, **139**, 2842; (c) D. L. Crossley, R. J. Kahan, S. Endres, A. J. Warner, R. A. Smith, J. Cid, J. J. Dunsford, J. E. Jones, I. Vitorica-Yrezabal and M. J. Ingleson, *Chem. Sci.*, 2017, **8**, 7969; (d) D. Marinelli, F. Fasano, B. Najjari, N. Demitri and D. Bonifazi, *J. Am. Chem. Soc.*, 2017, **139**, 5503; (e) K. Matsuo, S. Saito and S. Yamaguchi, *Angew. Chem. Int. Ed.*, 2016, **55**, 11984; (f) S. Osumi, S. Saito, C. Dou, K. Matsuo, K. Kume, H. Yoshikawa, K. Awaga and S. Yamaguchi, *Chem. Sci.*, 2016, **7**, 219; (g) S. Wang, D.-T. Yang, J. Lu, H. Shimogawa, S. Gong, X. Wang, S. K. Mellerup, A. Wakamiya, Y.-L. Chang, C. Yang and Z.-H. Lu, *Angew. Chem. Int. Ed.*, 2015, **54**, 15074; (h) X.-Y. Wang, A. Narita, X. Feng and K. Müllen, *J. Am. Chem. Soc.*, 2015, **137**, 7668; (i) L. Ji, R. M. Edkins, A. Lorbach, I. Krummenacher, C. Bruckner, A. Eichhorn, H. Braunschweig, B. Engels, P. J. Low and T. B. Marder, *J. Am. Chem. Soc.*, 2015, **137**, 6750; (j) M. Krieg, F. Reicherter, P. Haiss, M. Ströbele, K. Eichele, M.-J. Treanor, R. Schaub and H. F. Bettinger, *Angew. Chem. Int. Ed.*, 2015, **54**, 8284; (k) A. W. Baggett, F. Guo, B. Li, S.-Y. Liu and F. Jäkle, *Angew. Chem. Int. Ed.*, 2015, **54**, 11191; (l) V. M. Hertz, M. Bolte, H.-W. Lerner and M. Wagner, *Angew. Chem. Int. Ed.*, 2015, **54**, 8800; (m) H. Hirai, K. Nakajima, S. Nakatsuka, K. Shiren, J. Ni, S. Nomura, T. Ikuta and T. Hatakeyama, *Angew. Chem. Int. Ed.*, 2015,

54, 13581; (n) B. Neue, J. F. Araneda, W. E. Piers and M. Parvez, *Angew. Chem. Int. Ed.*, 2013, **52**, 9966; (o) Marwitz, Adam J. V., A. N. Lamm, L. N. Zakharov, M. Vasiliu, D. A. Dixon and S.-Y. Liu, *Chem. Sci.*, 2012, **3**, 825; (p) Y. Kim, H.-S. Huh, M. H. Lee, I. L. Lenov, H. Zhao and F. P. Gabbaï, *Chem. Eur. J.*, 2011, **17**, 2057.

[6] (a) Y. Adachi and J. Ohshita, *Organometallics*, 2018, **37**, 869; (b) H. Shimogawa, O. Yoshikawa, Y. Aramaki, M. Murata, A. Wakamiya and Y. Murata, *Chem. Eur. J.*, 2017, **23**, 3784; (c) S. K. Sarkar, G. R. Kumar and P. Thilagar, *Chem. Commun.*, 2016, **52**, 4175; (d) Z. Zhang, R. M. Edkins, J. Nitsch, K. Fucke, A. Eichhorn, A. Steffen, Y. Wang and T. B. Marder, *Chem. Eur. J.*, 2015, **21**, 177; (e) X.-Y. Wang, F.-D. Zhuang, R.-B. Wang, X.-C. Wang, X.-Y. Cao, J.-Y. Wang and J. Pei, *J. Am. Chem. Soc.*, 2014, **136**, 3764; (f) D. R. Levine, M. A. Siegler and J. D. Tovar, *J. Am. Chem. Soc.*, 2014, **136**, 7132; (g) L. G. Mercier, W. E. Piers, R. W. Harrington and W. Clegg, *Organometallics*, 2013, **32**, 6820; (h) H. Braunschweig, V. Dyakonov, B. Engels, Z. Falk, C. Hörl, J. H. Klein, T. Kramer, H. Kraus, I. Krummenacher, C. Lambert and C. Walter, *Angew. Chem. Int. Ed.*, 2013, **52**, 12852; (i) H. Braunschweig, A. Damme, J. O. C. Jimenez-Halla, C. Hörl, I. Krummenacher, T. Kupfer, L. Mailänder and K. Radacki, *J. Am. Chem. Soc.*, 2012, **134**, 20169; (j) C.-T. Poon, W. H. Lam and V. W.-W. Yam, *J. Am. Chem. Soc.*, 2011, **133**, 19622; (k) A. Iida and S. Yamaguchi, *J. Am. Chem. Soc.*, 2011, **133**, 6952; (l) A. Wakamiya, K. Mori, T. Araki and S. Yamaguchi, *J. Am. Chem. Soc.*, 2009, **131**, 10850; (m) S. Miyasaka, J. Kobayashi and T. Kawashima, *Tetrahedron Lett.*, 2009, **50**, 3467; (n) A. Sundararaman, M. Victor, R. Varughese and F. Jäkle, *J. Am. Chem. Soc.*, 2005, **127**, 13748.

[7] (a) X. Yin, J. Chen, R. A. Lalancette, T. B. Marder and F. Jäkle, *Angew. Chem. Int. Ed.*, 2014, **53**, 9761; (b) X. Yin, F. Guo, R. A. Lalancette and F. Jäkle, *Macromolecules*, 2016, **49**, 537; (c) X. Yin, K. Liu, Y. Ren, R. A. Lalancette, Y.-L. Loo and F. Jäkle, *Chem. Sci.*, 2017, **8**, 5497; (d) B. Meng, Y. Ren, J. Liu, F. Jäkle and L. Wang, *Angew. Chem. Int. Ed.*, 2018, **57**, 2183; (e) Y. Adachi, Y. Ooyama, Y. Ren, X. Yin, F. Jäkle and J. Ohshita, *Polym. Chem.*, 2018, **9**, 291.

[8] (a) B. Wrackmeyer and H. Nöth, *Chem. Ber.*, 1976, **109**, 1075; (b) T. Köhler, J. Faderl, H. Pritzkow and W. Siebert, *Eur. J. Inorg. Chem.*, 2002, 2942; (c) H. Braunschweig, R. D. Dewhurst, C. Hörl, A. K. Phukan, F. Pinzner and S. Ullrich, *Angew. Chem. Int. Ed.*, 2014, **53**, 3241; (d) B. Wrackmeyer, *Z. Naturforsch. B*, 2015, **70**, 421; (e) H. Braunschweig, R. D. Dewhurst and T. Kramer, *Inorg. Chem.*, 2015, **54**, 3619; (f) B. Chen, H. Nie, R. Hu, A. Qin, Z. Zhao and B.-Z. Tang, *Sci. China Chem.*, 2016, **59**, 699.

[9] (a) A. Lik, L. Fritze, L. Müller and H. Helten, *J. Am. Chem. Soc.*, 2017, **139**, 5692; (b) A. Lik, S. Jenthra, L. Fritze, L. Müller, K.-N. Truong and H. Helten*, Chem. Eur. J.*, DOI: 10.1002/chem.201706124.

[10] In this case, we achieved B–C coupling by a catalytic Si/B exchange approach. We also demonstrated B–N coupling via Si/B exchange condensation as a route to BCN hybrid polymers and oligomers; see (a) T. Lorenz, A. Lik, F. A. Plamper and H. Helten, *Angew. Chem. Int. Ed.*, 2016, **55**, 7236; (b) O. Ayhan, T. Eckert, F. A. Plamper and H. Helten, *Angew. Chem. Int. Ed.*, 2016, **55**, 13321; (c) H. Helten, *Chem. Eur. J.*, 2016, **22**, 12972; (d) T. Lorenz, M. Crumbach, T. Eckert, A. Lik and H. Helten, *Angew. Chem. Int. Ed.*, 2017, **56**, 2780; (e) N. A. Riensch, A. Deniz, S. Kühl, L. Müller, A. Adams, A. Pich and H. Helten, *Polym. Chem.*, 2017, **8**, 5264; (f) O. Ayhan, N. A. Riensch, C. Glasmacher and H. Helten, *Chem. Eur. J.*, 2018, **24**, 5883.

[11] This approach was recently applied also by Liu and Jäkle.[7d]

[12] (a) J. Dhar, U. Salzner and S. Patil, *J. Mater. Chem. C*, 2017, **5**, 7404; (b) M. Stolar and T. Baumgartner, *Phys. Chem. Chem. Phys.*, 2013, **15**, 9007.

[13] a) A. Lik, L. Fritze, L. Müller and H. Helten, *J. Am. Chem. Soc*. 2017, **139**, 5692. b) Y. Dienes, S. Durben, T. Karpati, T. Neumann, U. Englert, L. Nyulaszi and T. Baumgartner, *Chem. Eur. J.* 2007, **13**, 7487. c) D. C. Ebner, J. T. Bagdanoff, E. M. Ferreira, R. M. McFadden, D. D. Caspi, R. M. Trend and B. M. Stoltz, *Chem. Eur. J.* 2009, **15**, 12978.

[14] SADABS: Area-Detector Absorption Correction; Siemens Industrial Automation, Inc.: Madison, WI, 1996.

[15] O. V. Dolomanov, L. J. Bourhis, R. J. Gildea, J. A. K. Howard, and H. J. Puschmann, *J. Appl. Cryst.* 2009, **42**, 339.

[16] a) G. M. Sheldrick, *Acta Crystallogr.*, *Sect. A* 2008, **64**, 112; b) G. M. Sheldrick, *Acta Crystallogr.*, *Sect. C* **2015**, *71*, 3.

[17] Turbomole: R. Ahlrichs, M. Bär, M. Häser, H. Horn and C. Kölmel, *Chem. Phys. Lett.* 1989, **162**, 165–169.

[18] a) P. A. M. Dirac, *Proc. R. Soc. London, Ser. A* 1929, **123**, 714–733; b) J. C. Slater, *Phys. Rev.* 1951, **81**, 385–390; c) A. D. Becke, *Phys. Rev. A.* 1988, **38**, 3098–3100; d) C. Lee, W. Yang, R. G. Parr, *Phys. Rev. B* 1988, **37**, 785–789; e) A. D. Becke, *J. Chem. Phys.* 1993, **98**, 5648–5652.

[19] A. Schäfer, H. Horn and R. Ahlrichs*, J. Chem. Phys.* 1992, **97**, 2571–2577.

[20] a) S. Grimme, J. Antony, S. Ehrlich and H. Krieg, *J. Chem. Phys.* 2010, **132**, 154104; b) S. Grimme, S. Ehrlich and L. Goerigk, *J. Comput. Chem.* 2011, **32**, 1456–1465.

[21] P. Deglmann, F. Furche and R. Ahlrichs, *Chem. Phys. Lett.* 2002, **362**, 511–518; b) P. Deglmann and F. Furche, *J. Chem. Phys.* 2002, **117**, 9535–9538.

[22] a) R. Bauernschmitt and R. Ahlrichs, *Chem. Phys. Lett.* 1996, **256**, 454–464; b) R. Bauernschmitt and R. Ahlrichs, *J. Chem. Phys.* 1996, **104**, 9047–9052; c) F. Furche and D. Rappoport, in *Density functional methods for excited states: equilibrium structure and electronic spectra*, ed. M. Olivucci, Elsevier, Amsterdam, 2005.

2.3 Catalytic Si/B Exchange Condensation: A Green B-C Coupling Method That Provides Access to Monodisperse (Het)arylborane "Trimers"[1]

The following section is slightly modified and reproduced from published article[‡] with permission from Georg Thieme Verlag KG.

Abstract: The potential of our metal-free B-C coupling method using catalytic Si/B exchange condensation is demonstrated by the synthesis of a series of monodisperse (het)arylborane oligomers with four (het)arene moieties and three boron centers (i. e., "trimers"). Photophysical and electrochemical investigations evidenced effective π-conjugation over the (het)arene rings and the boron centers.

π-Conjugated organoboranes and organoborane oligomers and polymers have attracted considerable attention in recent years, owing to the intriguing optical and electronic properties such materials can have resulting from the interaction of the vacant p_π orbital of trivalent boron with an adjacent π system (*p*–π conjugation).[2-14] This has enabled applications thereof in organic (opto)electronics, for anion or amine sensing, as well as bio-imaging.[2] For the preparation of organoborane compounds in general, B–C bond forming reactions must be accomplished at one stage, and these are often the crucial steps in the synthesis. The development of efficient B–C coupling processes is therefore a highly active field of current research.[15]

For the synthesis of compounds with recurrent (het)arylborane moieties, i. e. polymers and oligomers, in particular, a number of strategies have been explored.[2] One approach is to assemble the triorganoborane building blocks first and build up the extended structure in a subsequent step via C–C coupling reactions.[8-10] For this, Stille-type cross-coupling reactions were found to be particularly useful,[8] but also Suzuki–Miyaura-,[9] Sonogashira-,[9a] and Yamamoto-type[10] coupling reactions have been successfully applied in some cases. It should be noted that the boron center needs to be kinetically well protected to survive under the cross-coupling conditions applied. An alternative approach makes use of B–C bond formation reactions to construct the extended π-conjugated framework.[7,11,12] With regard to the synthesis of (cyclo)linear polymers and oligomers, this latter method has the advantage that after the B-C coupling process the boron centers may still carry one further leaving group (e. g., Br), which can be replaced by appropriate organic substituents at the post-polymerization stage. This offers the opportunity to generate various materials with tailored properties through "side-group engineering" from a single common precursor.[11b,d,e,12] In this vein, one very efficient B-C coupling polymerization method involves the Sn/B exchange reaction, as demonstrated mainly

‡ L. Fritze, N. A. Riensch, H. Helten, *Synthesis* **2019**, *51*, 399—406.

by Jäkle and colleagues.[8e,11] The major drawback of this method, however, is the use of highly toxic and environmentally harmful organotin compounds (which are also employed in the very popular Stille reaction).

We recently developed a highly efficient and environmentally benign organocatalytic B–C coupling method that uses organosilicon compounds instead (Scheme 2.3.1).[12,14] The uncatalyzed coupling of an aryl(trimethyl)silane with an aryl(dibromo)borane to form a second B–C_{aryl} bond proceeds generally too slowly to be of practical use. However, we found that such reactions can be effectively accelerated by the addition of the electrophilic silyl reagent Me_3SiNTf_2 (Tf = CF_3SO_2) in substoichiometric amounts.[12]

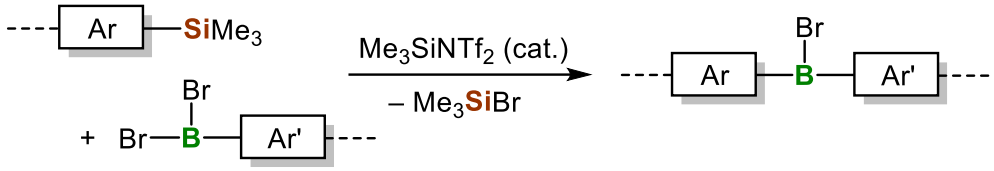

Scheme 2.3.1. General scheme of B-C coupling by catalytic Si/B exchange condensation.

We demonstrated the application of this catalytic approach for the synthesis of a series of (het)arylborane molecules, oligomers, and polymers.[12] While the combination of borane and thiophene moieties has evolved into an attractive and highly valued motif of electronic materials,[4,5] and poly(thienylborane)s had been previously known,[8e,11a] the combination of trivalent boron with furan moieties had been largely unexplored, although the potential of the resulting materials has been recently recognized.[6,16] Our new synthetic method allowed the preparation of the first oligo- and poly(furylborane)s as well as mixed thienyl-/furylborane species.[12] We found that the properties of the obtained materials are effectively tuned by the ratio of the aromatic rings.[12b] With the synthesis of Ph_2BMes^*, we also incorporated benzene rings into a π-extended borane. In the latter case, the Si/B exchange reaction proceeded significantly slower and required increased catalyst loadings, however, it afforded the desired product fully selectively as well.[12] Therefore, the incorporation of benzene rings into longer oligomers has not been further explored as yet.

The longest truly monodisperse hetarylborane oligomers that we prepared so far are one thienylborane trimer and one mixed derivative with a chain composed of three thiophene moieties and one furan ring.[12,17] Herein, we present the synthesis of four new (het)arylborane “trimers”, two of which comprise two furan rings; we also succeeded in the incorporation of benzene moieties into such extended π-conjugated scaffolds.

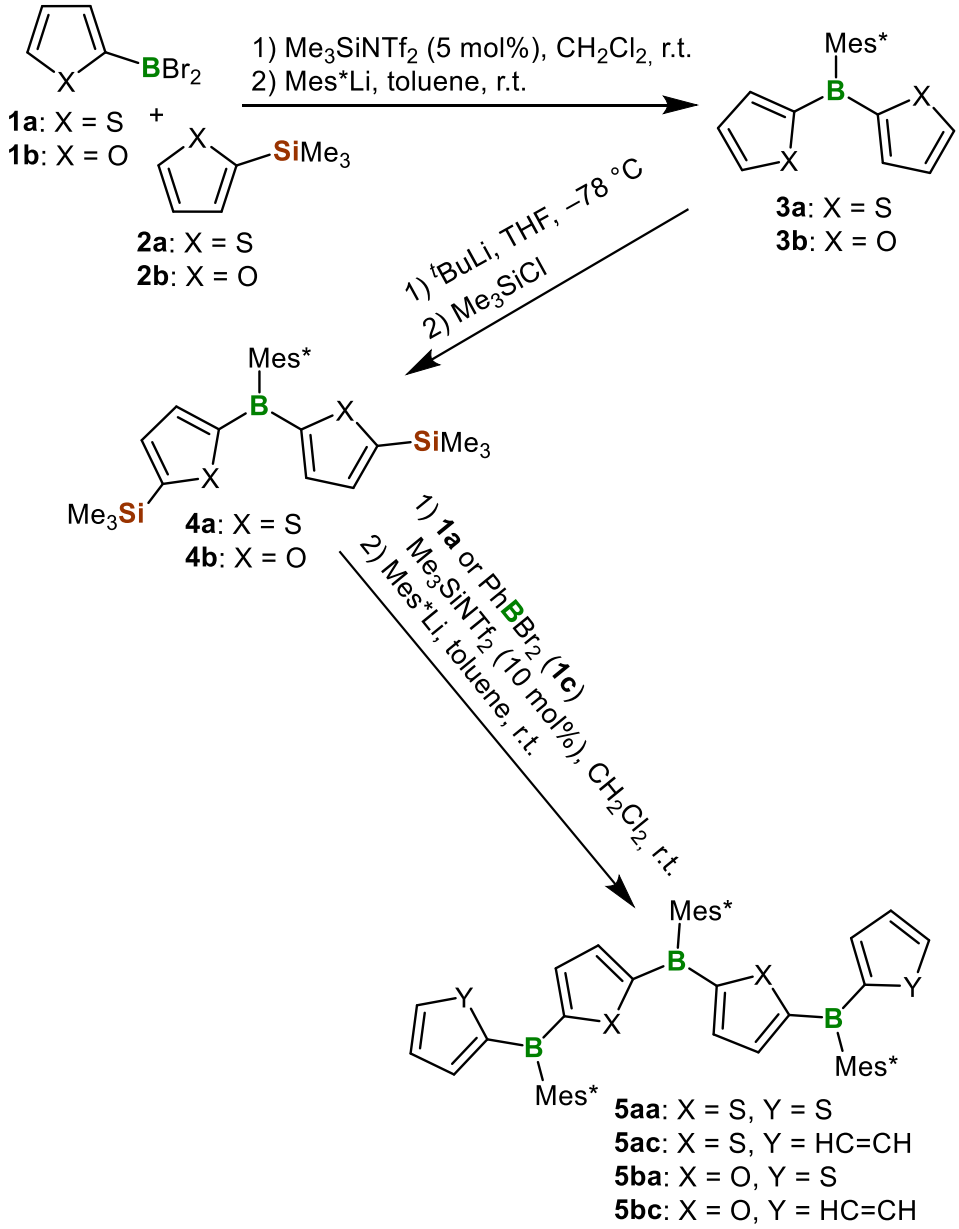

Scheme 2.3.2. Synthesis of cyclolinear (het)arylborane "trimers" **5**.

In the first step of the synthesis, we prepared the dithienyl- and difurylboranes **3a** and **3b** using our catalytic Si/B exchange approach from **1a** and **2a** or **1b**[18] and **2b**, respectively (Scheme 2.3.2). Compound **3b** had been recently reported by us.[12] Here, we used an analogous procedure to synthesize **3a**; the latter of which had been previously reported by Jäkle and Marder, but was in this case prepared via a Sn/B exchange condensation reaction.[9b] We chose 2,4,6-tri-*tert*-butylphenyl (Mes*, supermesityl) as the third, pending substituent on boron, as this group is known to impart effective kinetic stabilization, thus, potentially leading to highly robust materials.[3a,d,8e,9b,12] Compounds **3a,b** were transformed into **4a,b** via dilithiation and subsequent twofold silylation, as we recently described for **4b**.[12a] The syntheses of the (het)arylborane "trimers" **5aa**, **5ac**, **5ba**, and **5bc** were achieved by catalytic silicon/boron exchange reactions between **4a,b** and dibromo(2-thienyl)borane (**1a**) or $PhBBr_2$ (**1c**)[19] in the

presence of 10 mol% of Me_3SiNTf_2 with respect to **4a,b** (i. e., 5 mol% for each site), followed by postmodification with Mes*Li.

Compounds **5aa**, **5ac**, **5ba**, and **5bc** were purified by column chromatography on alumina and isolated in moderate yields (17 – 47 %). Their constitution was unambiguously ascertained by ^{1}H, ^{11}B, and ^{13}C NMR spectroscopy and mass spectrometry; elemental analyses yielded satisfactory results. In their ^{11}B NMR spectra each oligomer gave rise to only one broad peak at about δ = 52 – 63, which is in a typical range for triarylboranes.[3,5,6] The ^{1}H NMR spectra of each compound showed at room temperature significantly broadened signals for the aromatic protons of the (het)arene rings of the oligomer chain. This effect can be ascribed to hindered rotation about the B–$C_{(het)arene}$ bonds, caused by the presence of the bulky Mes* substituents, which is slow on the NMR time scale in that temperature regime.

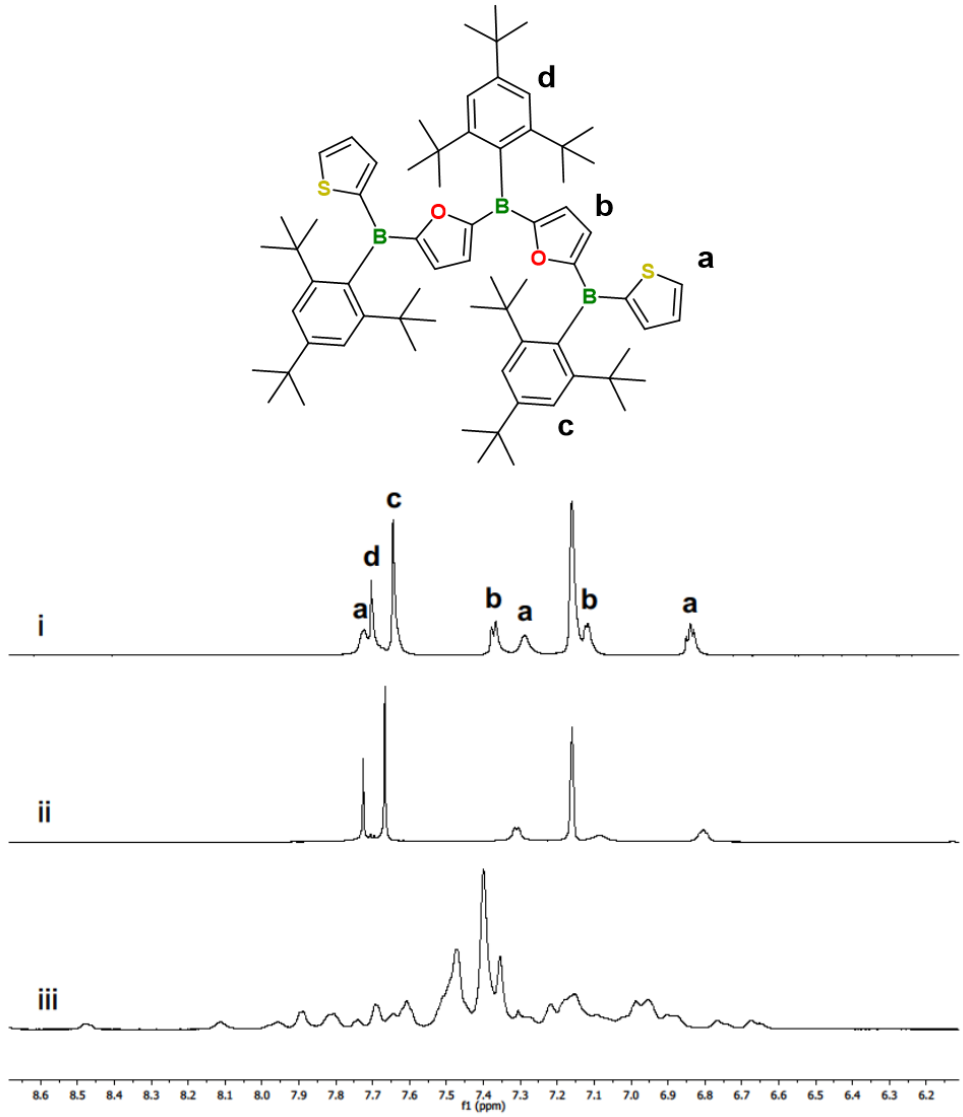

Figure 2.3.1. Aromatic region of the ^{1}H-NMR spectrum of **5ba** (i) at 70 °C (C_6D_6), (ii) at 25 °C (C_6D_6) and (iii) at -80 °C (CD_2Cl_2).

This was confirmed by ^{1}H NMR experiments at variable temperature (VT-NMR) for compound **5ba** as a good case in point. At 25 °C in C_6D_6 only three broad, featureless peaks were observed for all hetarene protons (Figure 2.3.1ii). At elevated temperatures (70 °C, Figure 2.3.1i) free rotation about the B–$C_{hetarene}$ bonds was enhanced, resulting in significant line sharpening associated with separation of the five expected heteroaromatic proton resonances in the correct ratio. At low temperatures (−80 °C, Figure 2.3.1iii, in CD_2Cl_2) the rotational processes were frozen, giving rise to a huge number of peaks in the spectrum. Assuming different relative orientations of the hetarene rings (syn/anti conformers) and, additionally, different relative orientations of the three Mes* groups along the chain, the presence of up to ca. 40 distinct conformers of **5ba** is conceivable.

The UV–vis absorption spectra of the trimers in THF (Figure 2.3.2 and Table 2.3.1) show each an intense band at $\lambda_{abs,max}$ = 371 – 378 nm and a further band at higher energies ($\lambda_{abs,max}$ = 275 – 288 nm). Referring to our previous theoretical investigations, both of them originate from π-π* transitions. The significant bathochromic shifts of the major band of **5** with respect to that of the respective monomers **3a**[9b] and **3b**,[12a] and their silylated derivatives **4a,b**[12] confirms an effective extension of the π-conjugated system through chain elongation in the trimers. This effect is somewhat more pronounced for the thienyl-flanked species **5aa** and **5ba**, pointing to superior conjugation over the thienyl than over the phenyl rings in these systems. As an aside, a comparison of the UV–vis data for **3a,b** and **4a,b** reveals a slight redshift of the π–π* absorption upon silylation at the heterocycles.

Table 2.3.1. Photophysical data of triarylboranes **3**, **4** and trimeric species **5** in THF.

Compd.	$\lambda_{abs,max}$ (nm)	$\lambda_{em,max}$ (nm)
3a[9b]	325	–
3b[12a]	315	400
4a	334	–
4b[12a]	331	–
5aa	377	–
5ac	371	–
5ba	378	404
5bc	371	–

Notable blue fluorescence was only observed for **5ba**. This is consistent with the findings of our previous studies, which revealed enhanced fluorescence intensities with increasing ratio of furan rings in related oligomers and polymers.[12]

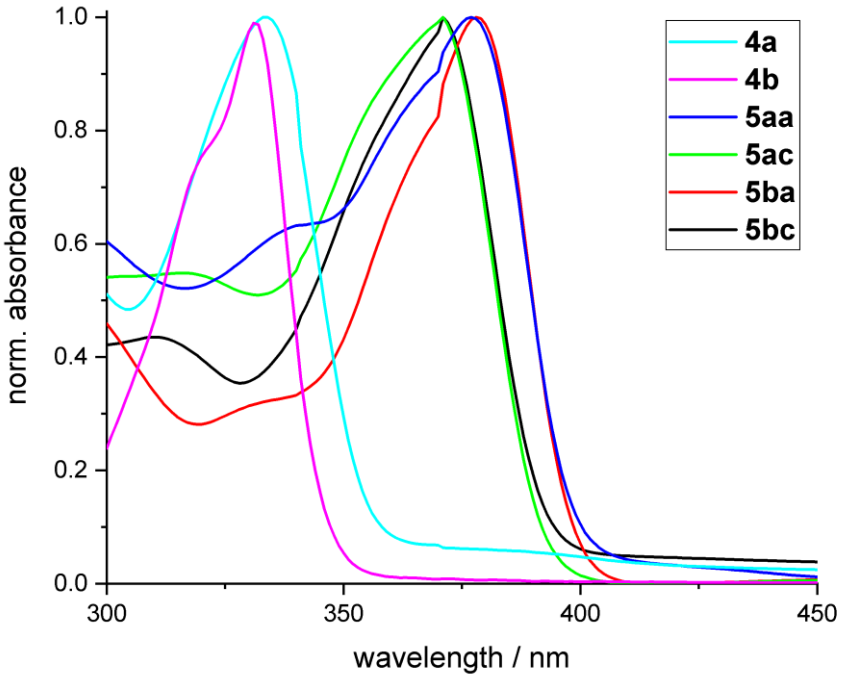

Figure 2.3.2. UV-vis absorption spectra of trimeric species **5** and their precursors **4a** and **4b**[12a] in THF (high-energy bands omitted for clarity).

Cyclic voltammetry (CV) investigations gave for all four trimers two quasi reversible reduction waves, **5aa**: $E_{1/2}$ = −1.96 V, −2.53 V; **5ac**: $E_{1/2}$ = −1.97 V, −2.56 V; **5ba**: $E_{1/2}$ = −2.10 V, −2.75 V; **5bc**: $E_{1/2}$ = −2.11 V, −2.78 V (Figure 2.3.3), consistent with a stepwise reduction of the individual borane moieties in the molecules. A comparison with the corresponding mono-borane **3a** and the dimer analogue by Jäkle and Marder et al.[9b] provides interesting insights. These compounds show one and two reduction waves, respectively, corresponding to the number of boron atoms per molecule. In the trimers **5**, the putative third reduction process is presumably outside the accessible potential range which is limited by the solvent. It is plausible to assume that the two reductions of **5** occur at the outer two boron centers, due to Coulombic repulsion of the negative charges in the generated dianion. Within the series of the thienylboranes, the first reduction wave shifts to less negative potentials with increasing chain length in the order: monomer (**3a**, $E_{1/2}$ = −2.58 V[9b]) < dimer ($E_{1/2}$ = −2.14 V[9b]) < trimer (**5aa**, $E_{1/2}$ = −1.96 V). This demonstrates a decrease of the LUMO energy and, hence, an enhancement of the electron-accepting abilities with chain elongation.

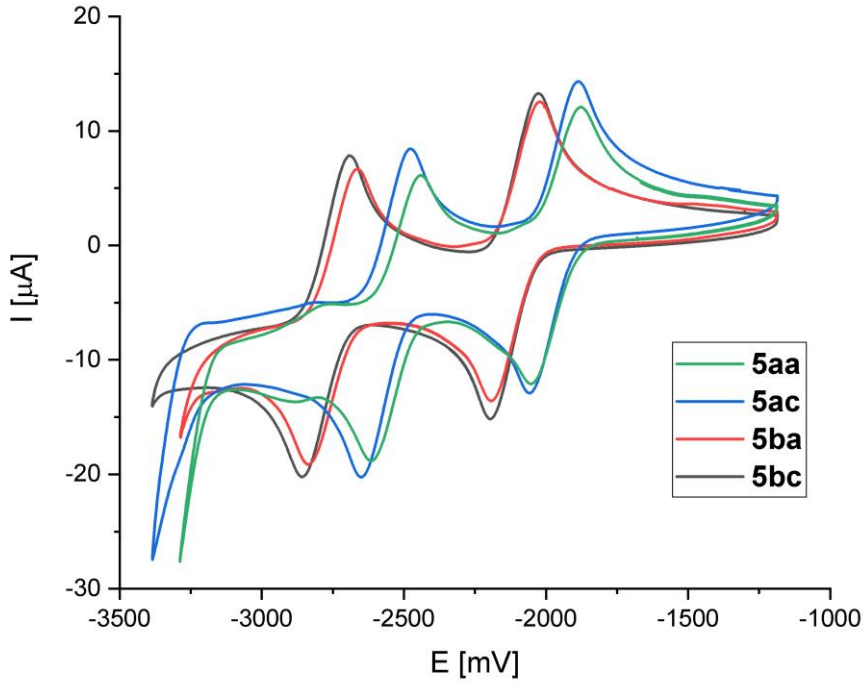

Figure 2.3.3. Cyclic voltammograms of oligomers **5** in THF/0.1 M [*n*-Bu_4N]-[PF_6] (vs. $[Cp_2Fe]^{0/+}$, scan rate: 100 mVs^{-1}).

The large separation between the first and the second reduction waves in **5aa**, **5ac**, **5ba**, and **5bc** evidences strong electronic communication over the heterocycles and the boron center. The slightly smaller separation for **5aa** ($\Delta E_{1/2}$ = 570 mV) compared to that for the corresponding dimer ($\Delta E_{1/2}$ = 700 mV[9b]) is in accordance with the hypothesis that in $\mathbf{5aa^{2-}}$ the two added electrons on average reside in more distant positions. Comparison of the voltammograms for the four different "trimers" reveals that the reduction waves of the derivatives featuring furan rings in their center positions, i. e., **5ba** and **5bc**, are cathodically shifted from those of **5aa** and **5ac**. This correlates with the more electron-rich nature of furan compared to thiophene. It is furthermore noteworthy that the redox waves of **5ba** and **5bc** show a slightly larger spacing ($\Delta E_{1/2}$ = 650 – 670 mV) than those of **5aa** and **5ac** ($\Delta E_{1/2}$ = 570 – 590 mV). This points to a slightly stronger electronic communication within the furylborane derivatives. The nature of the terminal aryl substituent (i. e., thienyl vs. phenyl) has a negligible effect on the reduction potentials of the compounds.

In summary, we have demonstrated the use of our catalytic Si/B exchange condensation method for the synthesis of four new monodisperse oligomers comprising a cyclolinear chain of four (het)arenes and three boron centers, i. e., **5aa**, **5ac**, **5ba**, and **5bc**. We showed that the incorporation of benzene moieties into such (het)arylborane "trimers" is indeed possible, and we succeeded in incorporating two furan rings, thus, leading to materials with enhanced

luminescence properties and strong electronic communication between the boron centers along the chain.

2.3.1 Experimental section

Manipulations involving air and/or moisture sensitive compounds were performed under an atmosphere of dry argon using standard Schlenk techniques or in an MBraun glove box. Solvents (dichloromethane, *n*-pentane, diethylether, toluene, and tetrahydrofuran) were dried and degassed by means of an MBraun SPS-800 solvent purification system. Deuterated solvents for NMR spectroscopy were dried and degassed at reflux over Na (C_6D_6) or CaH_2 ($CDCl_3$ and CD_2Cl_2) and freshly distilled prior to use. Solvents for aqueous work up (*n*-hexane, *n*-pentane, dichloromethane, ethanol, diethylether), sulfuric acid, tribromoborane, bromobenzene, thiophene, 2-bromothiophene, bromine, 2-bromo-1,3,5-triisopropylbenzene, 1,3,5-tri-*tert*-butylbenzene, 1,3,5-tris(trifluoromethyl)benzene, and lithium bis(trifluoromethylsulfonyl)imide were purchased from commercial sources and used as received. Solutions of *n*-butyllithium (1.6 M and 2.5 M in hexane, respectively) and *tert*-butyllithium (1.7 M in pentane) were purchased from Sigma Aldrich and used as received as well. Furan and trimethylsilylchloride were commercially purchased and freshly distilled prior to use. 2,4,6-triisopropylphenyllithium,[20] trimethylsilylbis(trifluoromethylsulfonyl)imide,[21] 2-bromo-1,3,5-tri-*tert*-butylbenzene[22] and 2,4,6-tri-*tert*-butylphenyllithium[9b] were prepared according to methods described in the literature. Compound **3b** was prepared according to a procedure previously described by our group.[12] NMR spectra were recorded at 25 °C on a Bruker Avance II-400 spectrometer or on a Bruker Avance III HD spectrometer operating at 400 MHz. Chemical shifts were referenced to residual protic impurities in the solvent (^{1}H) or the deuterio solvent itself (^{13}C) and reported relative to external $SiMe_4$ (^{1}H, ^{13}C) or $BF_3{\cdot}OEt_2$ (^{11}B) standards. Mass spectra were obtained with the use of a Finnigan MAT95 spectrometer employing electron ionization (EI) or secondary ionization (SIMS) using a 70 eV electron impact ionization source. Elemental analysis was performed with a CHN-O-Rapid VarioEL by Heraeus. UV–vis spectra were obtained using a Jasco V-630 spectrophotometer. Fluorescence spectra were obtained with a Jasco FP-6600 spectrofluorometer. Fluorescence quantum yields were determined against perylene as the standard. Melting points (uncorrected) were obtained using a SMP3 melting point apparatus by Stuart in 0.5 mm (o.d.) glass capillaries. Cyclic voltammetry (CV) experiments were carried out on a BioLogic SP-50 potentiostat. The three-electrode system consisted of a glassy-carbon disk as working electrode, a Pt wire as counter electrode, and an $Ag/AgNO_3$ electrode as the reference electrode. The voltammograms were recorded with ca. 10^{-3} M solutions in THF containing [*n*-Bu_4N][PF_6] (0.1 M) as the supporting electrolyte. The scans were referenced after the

addition of a small amount of ferrocene as internal standard. The potentials are reported relative to the ferrocene/ferrocenium couple.

Bis(thien-2-yl)(2,4,6-tri-tert-butylphenyl)borane (3a)

A solution of **1a** (1.2526 g, 5.0 mmol) in dichloromethane (2.5 mL) was added to a solution of **2a** (781.6 mg, 5.0 mmol) and TMS-NTf_2 (176.8 mg, 0.5 mmol, 10 mol%) in dichloromethane (2.5 mL) at ambient temperatures and the mixture was stirred overnight. Subsequently, the solvent was removed in vacuo, and the solid residue was redispersed in toluene (15 mL). The solution was added dropwise to a suspension of freshly prepared Mes*Li (from Mes*Br, 8 mmol) in toluene (15 mL) at -78 °C and the reaction mixture was allowed to warm up to room temperature overnight. The resulting suspension was diluted with pentane (40 mL) and quenched by the addition of water (50 mL). The organic phase was washed with water (50 mL) and brine (2x 50 mL), dried over $MgSO_4$, and the solvent was removed under reduced pressure. The crude product was further purified via colum chromatography (Al_2O_3) using PE.

Colorless solid; yield: 854 mg (2.0 mmol, 40 %).

The analytical data obtained agree well with those reported for **3a** in the literature.[9b]

Bis(5-trimethylsilyl-thien-2-yl)(2,4,6-tri-tert-butylphenyl)borane (4a)

To a solution of **3a** (1.27 g, 3.0 mmol) dissolved in Et_2O (30.0 mL) was added *t*-butyllithium (3.72 mL, 6.3 mmol) at −78 °C. The resulting mixture was stirred for 3 hours at −78 °C and then allowed to warm up to 0 °C and stirred for 30 minutes. Subsequently, the reaction mixture was cooled to −78 °C again, and trimethylsilylchloride (0.72 g, 6.60 mmol) was added dropwise. The reaction mixture was allowed to warm up to room temperature overnight. After aqueous work-up, all volatiles were removed in vacuo and the resulting greenish residue was further purified by column chromatograph (silica, *n*-hexane). The product was obtained as a colorless solid (500 mg, 0.89 mmol, 37 %).

^{1}H NMR (400 MHz, $CDCl_3$): δ = 7.68 (d, $^3J_{HH}$ = 3.4 Hz, 2 H, Thi-*H*), 7.42 (s, 2 H, Mes*-C*H*), 7.28 (d, $^3J_{HH}$ = 3.4 Hz, 2 H, Thi-*H*), 1.39 (s, 9 H, *p*-*t*Bu-CH_3), 1.14 (s, 18 H, *o*-*t*Bu-CH_3), 0.36 (s, 18 H, *o*-*t*Bu-CH_3); ^{11}B{^{1}H} NMR (128 MHz, $CDCl_3$): δ = 51.5; ^{13}C{^{1}H} NMR (101 MHz, $CDCl_3$): δ = 153.6 (Thi-*C*-B), 151.9 (Thi-*C*-(Si-(*C*H_3)$_3$), 151.5 (Mes*-*C*-*o*-*t*Bu), 148.2 (Mes*-*C*-*p*-*t*Bu), 142.3 (Thi-*C*H), 135.6 (Mes*-*C*-B), 134.9 (Thi-*C*H), 122.5 (Mes*-*C*H), 38.5 (*o*-*t*Bu-*C*(CH_3)$_3$), 34.9 (*o*-*t*Bu-C(*C*H_3)$_3$), 34.6 (*p*-*t*Bu-*C*(*C*H_3)$_3$), 31.4 (*p*-*t*Bu-C(*C*H_3)$_3$), 0.0 (Si-(*C*H_3)$_3$; MS (EI, 70 eV): *m/z* (%) = 566.6 (65) [M]$^+$, 395.5 (65) [$C_{20}H_{24}BS_2Si_2$]$^{\bullet+}$, 231.2 (30) [$C_{17}H_{27}$]$^{\bullet+}$, 147.2 (100) [$C_{11}H_{15}$]$^{\bullet+}$; Anal. Calcd (%) for $C_{32}H_{51}BS_2Si_2$: C 67.80; H 9.07. Found: C 68.20, H 9.04; UV–vis (THF): $\lambda_{abs,max}$ = 281 nm (ε = 16664 L mol^{-1} cm^{-1}), 334 (ε = 20893 L mol^{-1} cm^{-1}).

General procedure for the synthesis of oligomers 5aa and 5ac

To a solution of **4a** (0.48 mmol) in dichloromethane (1 mL) was added TMS-NTf_2 (10 mol%) and the respective diborylated compound **1a** or **1c** (1.0 mmol) in dichloromethane (1 mL) at room temperature. The reaction mixture was stirred for 72 hours. After removal of the solvent in vacuo, the residue was redissolved in toluene (1 mL) and added dropwise to a suspension of freshly prepared Mes*Li (from Mes*Br, 1.6 mmol) in toluene (1 mL) at −78 °C. The mixture was stirred for 7 days at room temperature. Then, the solvent was removed in vacuo and it was extracted with pentane. The organic phase was washed with brine, dried over $MgSO_4$, and the solvent was removed in vacuo. The crude product was purified by column chromatography (AlOx) using PE.

5,5'-Bis[(thien-2-yl)(2,4,6-tri-tert-butylphenyl)boryl]bis(2-thien-5-yl)(2,4,6-tri-tert-butyphenyl)borane (5aa)

yellow powder; yield: 128 mg (0.12 mmol, 23 %); m.p. 154 °C; R_f (PE) = 0.16.

^{1}H NMR (400 MHz, $CDCl_3$): δ = 7.85 (d, $^3J_{HH}$ = 4.7 Hz, 2 H, Thi-*H*), 7.83 – 7.77 (br, 4 H, Thi-*H*), 7.78 – 7.74 (br, 2 H, Thi-*H*), 7.43 (s, 4 H, Mes*-*H*), 7.41 (s, 2 H, Mes*-*H*), 7.22 (dd, J_{HH} = 4.7, 3.5 Hz, 2H, Thi-*H*), 1.39 (s, 18 H, *p*-*t*Bu-CH_3), 1.38 (s, 9 H, *p*-*t*Bu-CH_3), 1.18 (s, 54 H, *o*-*t*Bu-CH_3); ^{11}B{^{1}H} NMR (128 MHz, $CDCl_3$): δ = 55.8 (br); ^{13}C{^{1}H} NMR (101 MHz, $CDCl_3$): δ = 158.4 (Thi-*C*-B), 158.0 (Thi-*C*-B), 152.0 (Mes*-*C*-*o*-*t*Bu), 151.9 (Mes*-*C*-*o*-*t*Bu), 148.8 (Mes*-*C*-*p*-*t*Bu), 148.8 (Mes*-*C*-*p*-*t*Bu), 148.5 (Thi-*C*-B), 142.0 (Thi-*C*H), 141.9 (Thi-*C*H), 141.6 (Thi-*C*H), 136.1 (Thi-*C*H), 135.4 (Mes*-*C*-B), 135.4 (Mes*-*C*-B), 128.7 (Thi-*C*H), 122.7 (Mes*-*C*H), 122.6 (Mes*-*C*H), 38.7 (*o*-*t*Bu-C(CH_3)$_3$), 38.7 (*o*-*t*Bu-*C*(CH_3)$_3$), 35.2 (*o*-*t*Bu-*C*(CH_3)$_3$), 35.1 (*o*-*t*Bu-C(CH_3)$_3$), 34.9 (*p*-*t*Bu-*C*(CH_3)$_3$ and *p*-*t*Bu-C(CH_3)$_3$), 31.6 (*p*-*t*Bu-C(CH_3)$_3$), 31.6 (*p*-*t*Bu-*C*(CH_3)$_3$); MS (SIMS, 70 eV): *m/z* (%) = 1098.7 (3) [M]$^+$, 853.5 (3) [$C_{52}H_{68}B_3S_4$]$^+$, 677.5 (3) [$C_{44}H_{63}B_2S_2$]$^+$, 255.3 (65) [Mes*-B]$^{\bullet+}$, 151.2 (100) [$C_{11}H_8B$]$^{\bullet+}$; Anal. Calcd (%) for $C_{70}H_{97}B_3S_4$: C 76.49, H 8.90, found: C 76.63, H 8.76; UV–vis (THF): $\lambda_{abs,max}$ = 288 nm (ε = 19557 L mol^{-1} cm^{-1}), 377 (ε = 30347 L mol^{-1} cm^{-1}); CV (THF/0.1 M [n-Bu_4N][PF_6], vs. [Cp_2Fe]$^{0/+}$, scan rate: 100 mVs^{-1}): $E_{1/2}$ = −1.96 V, −2.53 V.

5,5'-Bis[phenyl(2,4,6-tri-tert-butylphenyl)boryl]bis(2-thien-5-yl)(2,4,6-tri-tert-butyphenyl)borane (5ac)

colorless powder; yield: 241 mg (0.22 mmol, 47 %); m.p. 139 °C; R_f (PE) = 0.34.

^{1}H NMR (400 MHz, $CDCl_3$): δ = 8.13 (d, $^3J_{HH}$ = 6.9 Hz, 4 H, Ph-*H*), 7.80 – 7.74 (br, 2 H, Thi-*H*), 7.60 (d, $^3J_{HH}$ = 3.6 Hz, 2 H, Thi-*H*), 7.50 – 7.38 (m, 6 H, Ph-*H*), 7.42 (s, 4 H, Mes*-*H*), 7.40 (s, 2 H, Mes*-*H*), 1.38 (s, 18 H, *p*-*t*Bu-CH_3), 1.37 (s, 9 H, *p*-*t*Bu-CH_3), 1.16 (s, 18 H, *o*-*t*Bu-CH_3),

1.12 (s, 36 H, *o*-*t*Bu-CH_3); $^{11}B\{^1H\}$ NMR (128 MHz, $CDCl_3$): δ = 63.4 (br); $^{13}C\{^1H\}$ NMR (101 MHz, $CDCl_3$): δ = 158.1 (br, 2x Thi-*C*-B), 151.9 (Mes*-*C*-*o*-*t*Bu), 151.7 (Mes*-*C*-*o*-*t*Bu), 148.8 (Mes*-*C*-*p*-*t*Bu), 148.8 (Mes*-*C*-*p*-*t*Bu), 143.8 (Ph-*C*-B), 142.8 (Thi-*C*-H), 141.7 (Thi-*C*-H), 138.4 (Ph-*C*H), 136.4 (Mes*-*C*-B), 135.4 (Mes*-*C*-B), 131.2 (Ph-*C*H), 127.8 (Ph-*C*H), 122.6 (Mes*-*C*H), 122.4 (Mes*-*C*H), 38.7 (*o*-*t*Bu-*C*$(CH_3)_3$), 38.5 (*o*-*t*Bu-C(*C*$H_3)_3$), 35.2 (*o*-*t*Bu-*C*$(CH_3)_3$), 35.2 (*o*-*t*Bu-C(*C*$H_3)_3$), 34.9 (*p*-*t*Bu-C(*C*$H_3)_3$), 34.9 (*p*-*t*Bu-*C*$(CH_3)_3$), 31.6 (*p*-*t*Bu-C(*C*$H_3)_3$), 31.6 (*p*-*t*Bu-*C*$(CH_3)_3$); MS (SIMS, 70 eV): *m/z* (%) = 1086.8 (3) $[M]^+$, 841.6 (3) $[C_{56}H_{72}B_3S_2]^+$, 671.6 (3) $[C_{46}H_{65}B_2S]^+$, 255.3 (28) [Mes*-B] $^{\bullet+}$, 151.2 (100) $[C_{11}H_8B]^{\bullet+}$; Anal. Calcd (%) for $C_{74}H_{101}B_3S_2$: C 81.75, H 9.36. Found: C 81.60, H 9.28; UV–vis (THF): $\lambda_{abs,max}$ = 278 nm (ε = 25022 L mol^{-1} cm^{-1}), 316 nm (ε = 21339 L mol^{-1} cm^{-1}), 371 nm (ε = 41004 L mol^{-1} cm^{-1}); CV (THF/0.1 M [n-Bu_4N][PF_6], vs. $[Cp_2Fe]^{0/+}$, scan rate: 100 mVs^{-1}): $E_{1/2}$ = −1.97 V, −2.56 V.

General procedure for the synthesis of oligomers 5ba and 5bc

To a solution of **4b** (256.7 mg, 0.48 mmol) in dichloromethane (1 mL) was added TMS-NTf_2 (10 mol%) and the respective diborylated compound **1a** or **1c** (1.0 mmol) in dichloromethane (1 mL) at room temperature. The reaction mixture was stirred for 72 hours. After removal of the solvent in vacuo, the residue was redissolved in toluene (1 mL) and added dropwise to a suspension of freshly prepared Mes*Li (from Mes*Br, 1.6 mmol) in toluene (1 mL) at room temperature. The reaction was stirred for 7 days at room temperature. Then, the solvent was removed in vacuo and it was extracted with pentane. The organic phase was washed with brine, dried over $MgSO_4$, and the solvent was removed in vacuo. The crude product was purified by column chromatography (AlOx) using PE, followed by a reprecipitation from DCM/EtOH.

5,5'-Bis[(thien-2-yl)(2,4,6-tri-tert-butylphenyl)boryl]bis(2-fur-5-yl)(2,4,6-tri-tert-butyphenyl)borane (5ba)

colorless powder; yield: 94 mg (0.08 mmol, 17 %); m.p. 224 °C; R_f (PE) = 0.29.

^1H NMR (400 MHz, C_6D_6, 70 °C): δ = 7.75 – 7.70 (br, 2 H, Thi-*H*), 7.70 (s, 2 H, Mes*-*H*), 7.65 (s, 4 H, Mes*-*H*), 7.38 (d, $^3J_{HH}$ = 4.7 Hz, 2 H, Thi-*H*), 7.32 – 7.26 (br, 2 H, Fur-*H*), 7.14 – 7.07 (m, 2 H, Fur-*H*), 6.87 – 6.77 (m, 2 H, Thi-*H*), 1.50 (s, 9 H, *p*-*t*Bu-CH_3), 1.41 (s, 18 H, *p*-*t*Bu-CH_3), 1.37 (s, 18 H, *o*-*t*Bu-CH_3), 1.31 (s, 36 H, *o*-*t*Bu-CH_3); $^{11}B\{^1H\}$ NMR (128 MHz, C_6D_6, 70 °C): δ = 51.5 (br); $^{13}C\{^1H\}$ NMR (101 MHz, C_6D_6, 70 °C): δ = 170.6 (br, Fur-*C*-B), 169.2 (br, Fur-*C*-B), 152.8 (Mes*-*C*-*o*-*t*Bu), 152.6 (Mes*-*C*-*o*-*t*Bu), 149.1 (Mes*-*C*-*p*-*t*Bu), 149.1 (Mes*-*C*-*p*-*t*Bu), 147.3 (br, Thi-*C*-B), 142.3 (br, Thi-*C*H), 136.9 (Thi-*C*H), 134.6 (Mes*-*C*-B), 133.5 (Mes*-*C*-B), 128.7 (Thi-*C*H), 128.0 (Fur-*C*H),[23] 127.9 (Fur-*C*H),[23] 122.9 (Mes*-*C*H), 122.3 (Mes*-*C*H), 38.9 (*o*-*t*Bu-C(*C*$H_3)_3$), 38.7 (*o*-*t*Bu-*C*$(CH_3)_3$), 35.2 (*o*-*t*Bu-C(*C*$H_3)_3$), 35.0 (*p*-*t*Bu-C(*C*$H_3)_3$), 34.9

(*o*-*t*Bu-*C*(CH_3)$_3$), 34.7 (*p*-*t*Bu-*C*(CH_3)$_3$), 31.8 (*p*-*t*Bu-*C*(CH_3)$_3$), 31.7 (*p*-*t*Bu-C(*C*H_3)$_3$); MS (EI, 70 eV): *m/z* (%) = 1066.8 (8) $[M]^+$, 255.3 (100) [Mes*-B]$^+$, 231.3 (63) $[C_{17}H_{27}]^{\bullet+}$,199.2 (46) $[C_{14}H_{20}B]^{\bullet+}$, 133.0 (65) $[C_{10}H_{11}]^{\bullet+}$; Anal. Calcd (%) for $C_{70}H_{97}B_3O_2S_2$: C 78.79, H 9.16. Found: C 77.46, H 9.05; UV–vis (THF): $\lambda_{abs,max}$ = 286 nm (ε = 19866 L mol^{-1} cm^{-1}), 378 nm (ε = 39432 L mol^{-1} cm^{-1}); fluorescence (THF): $\lambda_{em,max}$ (λ_{ex} = 378 nm) = 404 nm (Φ_f = 4.3 %); CV (THF/0.1 M [n-Bu_4N][PF_6], vs. [Cp_2Fe]$^{0/+}$, scan rate: 100 mVs^{-1}): $E_{1/2}$ = −2.10 V, −2.75 V.

5,5'-Bis[phenyl(2,4,6-tri-tert-butylphenyl)boryl]bis(2-fur-5-yl)(2,4,6-tri-tert-butyphenyl)borane (5bc)

colorless powder; yield: 181 mg (0.17 mmol, 36 %); m.p. 244 °C; R_f (PE) = 0.21.

^{1}H NMR (400 MHz, $CDCl_3$): δ = 8.25 – 7.90 (br, 4 H, Ph-*H*), 7.49 (s, 2 H, Mes*-*H*), 7.43 (s, 4 H, Mes*-*H*), 7.40 – 7.35 (m, 2 H, Ph-*H*), 7.33 – 7.20 (br, 4 H, Ph-*H*), 7.19 – 7.08 (br, 2 H, Fur-*H*), 7.08 – 6.95 (br, 2 H, Fur-*H*), 1.47 (s, 9 H, *p*-*t*Bu-CH_3), 1.39 (s, 18 H, *o*-*t*Bu-CH_3), 1.15 (s, 18 H, *p*-*t*Bu-CH_3), 1.09 (s, 36 H, *o*-*t*Bu-CH_3); ^{11}B{^{1}H} NMR (128 MHz, C_6D_6): δ = 55.3 (br).; ^{13}C{^{1}H} NMR (101 MHz, $CDCl_3$): δ = 170.2 (br, Fur-*C*-B), 168.9 (br, Fur-*C*-B), 152.3 (Mes*-*C*-*o*-*t*Bu), 151.9 (Mes*-*C*-*o*-*t*Bu), 148.6 (Mes*-*C*-*p*-*t*Bu), 148.5 (Mes*-*C*-*p*-*t*Bu), 143.1 (Ph-*C*-B), 138.4 (br, Ph-*C*H), 135.0 (Mes*-*C*-B), 132.5 (Mes*-*C*-B), 131.2 (Ph-*C*-H), 128.8 (br, Fur-*C*H), 127.7 (Ph-*C*H), 127.6 (br, Fur-*C*H), 122.3 (Mes*-*C*H), 121.9 (Mes*-*C*H), 38.5 (*o*-*t*Bu-C(*C*H_3)$_3$), 38.4 (*o*-*t*Bu-*C*(CH_3)$_3$), 35.0 (*p*-*t*Bu-C(*C*H_3)$_3$), 34.9 (*o*-*t*Bu-C(*C*H_3)$_3$), 34.8 (*p*-*t*Bu-*C*(CH_3)$_3$), 34.6 (*o*-*t*Bu-*C*(CH_3)$_3$), 31.8 (*p*-*t*Bu-*C*(CH_3)$_3$), 31.6 (*p*-*t*Bu-C(*C*H_3)$_3$); MS (EI, 70 eV): *m/z* (%) = 1054.9 (26) $[M]^+$, 732.6 (26) $[C_{50}H_{67}B_3O_2]^{\bullet+}$, 317.3 (27) $[C_{22}H_{31}BO]^{\bullet+}$, 231.3 (100) $[C_6H_2$-^{i}Pr-(^{t}Bu)$_2]^+$; Anal. Calcd (%) for $C_{74}H_{101}B_3O_2$: C 84.24, H 9.65. Found: C 83.53, H 9.68; UV–vis (THF): $\lambda_{abs,max}$ = 275 nm (ε = 50735 L mol^{-1} cm^{-1}), 310 nm (ε = 23040 L mol^{-1} cm^{-1}), 371 nm (ε = 36274 L mol^{-1} cm^{-1}); CV (THF/0.1 M [n-Bu_4N][PF_6], vs. [Cp_2Fe]$^{0/+}$, scan rate: 100 mVs^{-1}): $E_{1/2}$ = −2.11 V, −2.78 V.

2.3.2 References

[1] These authors contributed equally to this work.

[2] Reviews: (a) Wade, C. R.; Broomsgrove, A. E. J.; Aldridge, S.; Gabbai, F. P. *Chem. Rev.* **2010**, *110*, 3958. (b) Jäkle, F. *Chem. Rev.* **2010**, *110*, 3985. (c) Hudson, Z. M.; Wang, S. *Dalton Trans.* **2011**, *40*, 7805. (d) Tanaka, K.; Chujo, Y. *Macromol. Rapid Commun.* **2012**, *33*, 1235. (e) Zhao, H.; Leamer, L. A.; Gabbai, F. P. *Dalton Trans.* **2013**, *42*, 8164. (f) He, X.; Baumgartner, T. *RSC Adv.* **2013**, *3*, 11334. (g) Wakamiya, A.; Yamaguchi, S. *Bull. Chem. Soc. Jpn.* **2015**, *88*, 1357. (h) Ji, L.; Griesbeck, S.; Marder, T. B. *Chem. Sci.* **2017**, *8*, 846. (i) Helten, H. In *Encyclopedia of Inorganic and Bioinorganic Chemistry*, Scott, R. A., Ed., Wiley: Chichester, **2017**, DOI: 10.1002/9781119951438.eibc2496.

[3] Selected examples: (a) Wakamiya, A.; Mishima, K.; Ekawa, K.; Yamaguchi, S. *Chem. Commun.* **2008**, 579. (b) Kim, Y.; Huh, H.-S.; Lee, M. H.; Lenov, I. L.; Zhao, H.; Gabbaï, F. P. *Chem. Eur. J.* **2011**, *17*, 2057. (c) Marwitz, Adam J. V.; Lamm, A. N.; Zakharov, L. N.; Vasiliu, M.; Dixon, D. A.; Liu, S.-Y. *Chem. Sci.* **2012**, *3*, 825. (d) Levine, D. R.; Caruso, A.; Siegler, M. A.; Tovar, J. D. *Chem. Commun.* **2012**, *48*, 6256. (e) Neue, B.; Araneda, J. F.; Piers, W. E.; Parvez, M. *Angew. Chem. Int. Ed.* **2013**, *52*, 9966. (f) Hirai, H.; Nakajima, K.; Nakatsuka, S.; Shiren, K.; Ni, J.; Nomura, S.; Ikuta, T.; Hatakeyama, T. *Angew. Chem. Int. Ed.* **2015**, *54*, 13581. (g) Hertz, V. M.; Bolte, M.; Lerner, H.-W.; Wagner, M. *Angew. Chem. Int. Ed.* **2015**, *54*, 8800. (h) Krieg, M.; Reicherter, F.; Haiss, P.; Ströbele, M.; Eichele, K.; Treanor, M.-J.; Schaub, R.; Bettinger, H. F. *Angew. Chem. Int. Ed.* **2015**, *54*, 8284. (i) Ji, L.; Edkins, R. M.; Lorbach, A.; Krummenacher, I.; Bruckner, C.; Eichhorn, A.; Braunschweig, H.; Engels, B.; Low, P. J.; Marder, T. B. *J. Am. Chem. Soc.* **2015**, *137*, 6750. (j) Wang, X.-Y.; Narita, A.; Feng, X.; Müllen, K. *J. Am. Chem. Soc.* **2015**, *137*, 7668. (k) Wang, S.; Yang, D.-T.; Lu, J.; Shimogawa, H.; Gong, S.; Wang, X.; Mellerup, S. K.; Wakamiya, A.; Chang, Y.-L.; Yang, C. *et al. Angew. Chem. Int. Ed.* **2015**, *54*, 15074. (l) Osumi, S.; Saito, S.; Dou, C.; Matsuo, K.; Kume, K.; Yoshikawa, H.; Awaga, K.; Yamaguchi, S. *Chem. Sci.* **2016**, *7*, 219. (m) Matsuo, K.; Saito, S.; Yamaguchi, S. *Angew. Chem. Int. Ed.* **2016**, *55*, 11984. (n) Crossley, D. L.; Kahan, R. J.; Endres, S.; Warner, A. J.; Smith, R. A.; Cid, J.; Dunsford, J. J.; Jones, J. E.; Vitorica-Yrezabal, I.; Ingleson, M. J. *Chem. Sci.* **2017**, *8*, 7969. (o) Schickedanz, K.; Radtke, J.; Bolte, M.; Lerner, H.-W.; Wagner, M. *J. Am. Chem. Soc.* **2017**, *139*, 2842. (p) John, A.; Bolte, M.; Lerner, H.-W.; Wagner, M. *Angew. Chem. Int. Ed.* **2017**, *56*, 5588.

[4] Ren, Y.; Jäkle, F. *Dalton Trans.* **2016**, *45*, 13996.

[5] For examples of thiophene–borane-based materials, see: (a) Wakamiya, A.; Mori, K.; Araki, T.; Yamaguchi, S. *J. Am. Chem. Soc.* **2009**, *131*, 10850. (b) Iida, A.; Yamaguchi, S. *J. Am. Chem. Soc.* **2011**, *133*, 6952. (c) Poon, C.-T.; Lam, W. H.; Yam, V. W.-W. *J. Am. Chem. Soc.* **2011**, *133*, 19622. (d) Braunschweig, H.; Damme, A.; Jimenez-Halla, J. O. C.; Hörl, C.;

Krummenacher, I.; Kupfer, T.; Mailänder, L.; Radacki, K. *J. Am. Chem. Soc.* **2012**, *134*, 20169. (e) Braunschweig, H.; Dyakonov, V.; Engels, B.; Falk, Z.; Hörl, C.; Klein, J. H.; Kramer, T.; Kraus, H.; Krummenacher, I.; Lambert, C. *et al. Angew. Chem. Int. Ed.* **2013**, *52*, 12852. (f) Mercier, L. G.; Piers, W. E.; Harrington, R. W.; Clegg, W. *Organometallics* **2013**, *32*, 6820. (g) Levine, D. R.; Siegler, M. A.; Tovar, J. D. *J. Am. Chem. Soc.* **2014**, *136*, 7132. (h) Wang, X.-Y.; Zhuang, F.-D.; Wang, R.-B.; Wang, X.-C.; Cao, X.-Y.; Wang, J.-Y.; Pei, J. *J. Am. Chem. Soc.* **2014**, *136*, 3764. (i) Zhang, Z.; Edkins, R. M.; Nitsch, J.; Fucke, K.; Eichhorn, A.; Steffen, A.; Wang, Y.; Marder, T. B. *Chem. Eur. J.* **2015**, *21*, 177. (j) Sarkar, S. K.; Kumar, G. R.; Thilagar, P. *Chem. Commun.* **2016**, *52*, 4175. (k) Shimogawa, H.; Yoshikawa, O.; Aramaki, Y.; Murata, M.; Wakamiya, A.; Murata, Y. *Chem. Eur. J.* **2017**, *23*, 3784. (l) Adachi, Y.; Ohshita, J. *Organometallics* **2018**, *37*, 869.

[6] For furan–borane-based materials, see: (a) Wrackmeyer, B.; Nöth, H. *Chem. Ber.* **1976**, *109*, 1075. (b) Köhler, T.; Faderl, J.; Pritzkow, H.; Siebert, W. *Eur. J. Inorg. Chem.* **2002**, 2942. (c) Braunschweig, H.; Dewhurst, R. D.; Hörl, C.; Phukan, A. K.; Pinzner, F.; Ullrich, S. *Angew. Chem. Int. Ed.* **2014**, *53*, 3241. (d) Braunschweig, H.; Dewhurst, R. D.; Kramer, T. *Inorg. Chem.* **2015**, *54*, 3619. (e) Chen, B.; Nie, H.; Hu, R.; Qin, A.; Zhao, Z.; Tang, B.-Z. *Sci. China Chem.* **2016**, *59*, 699.

[7] (a) Matsumi, N.; Naka, K.; Chujo, Y. *J. Am. Chem. Soc.* **1998**, *120*, 10776. (b) Heilmann, J. B.; Scheibitz, M.; Qin, Y.; Sundararaman, A.; Jäkle, F.; Kretz, T.; Bolte, M.; Lerner, H.-W.; Holthausen, M. C.; Wagner, M. *Angew. Chem. Int. Ed.* **2006**, *45*, 920. (c) Nagai, A.; Murakami, T.; Nagata, Y.; Kokado, K.; Chujo, Y. *Macromolecules* **2009**, *42*, 7217. (d) Lorbach, A.; Bolte, M.; Li, H.; Lerner, H.-W.; Holthausen, M. C.; Jäkle, F.; Wagner, M. *Angew. Chem. Int. Ed.* **2009**, *48*, 4584.

[8] (a) Yamaguchi, I.; Tominaga, T.; Sato, M. *Polym. Int.* **2009**, *58*, 17. (b) Reus, C.; Guo, F.; John, A.; Winhold, M.; Lerner, H.-W.; Jäkle, F.; Wagner, M. *Macromolecules* **2014**, *47*, 3727. (c) Wang, X.-Y.; Zhuang, F.-D.; Wang, J.-Y.; Pei, J. *Chem. Commun.* **2015**, *51*, 17532. (e) Yin, X.; Guo, F.; Lalancette, R. A.; Jäkle, F. *Macromolecules* **2016**, *49*, 537. (f) Yin, X.; Liu, K.; Ren, Y.; Lalancette, R. A.; Loo, Y.-L.; Jäkle, F. *Chem. Sci.* **2017**, *8*, 5497. (g) Adachi, Y.; Ooyama, Y.; Ren, Y.; Yin, X.; Jäkle, F.; Ohshita, J. *Polym. Chem.* **2018**, *9*, 291. (h) Meng, B.; Ren, Y.; Liu, J.; Jäkle, F.; Wang, L. *Angew. Chem. Int. Ed.* **2018**, *57*, 2183.

[9] (a) Zhao, W.; Zhuang, X.; Wu, D.; Zhang, F.; Gehrig, D.; Laquai, F.; Feng, X. *J. Mater. Chem. A* **2013**, *1*, 13878. (b) Yin, X.; Chen, J.; Lalancette, R. A.; Marder, T. B.; Jäkle, F. *Angew. Chem. Int. Ed.* **2014**, *53*, 9761. (c) Baggett, A. W.; Guo, F.; Li, B.; Liu, S.-Y.; Jäkle, F. *Angew. Chem. Int. Ed.* **2015**, *54*, 11191.

[10] (a) Bonifácio, V. D. B.; Morgado, J.; Scherf, U. *J. Polym. Sci., Part A: Polym. Chem.* **2008**, *46*, 2878. (b) Adams, I. A.; Rupar, P. A. *Macromol. Rapid Commun.* **2015**, *36*, 1336.

[11] (a) Sundararaman, A.; Victor, M.; Varughese, R.; Jäkle, F. *J. Am. Chem. Soc.* **2005**, *127*, 13748. (b) Li, H.; Jäkle, F. *Angew. Chem. Int. Ed.* **2009**, *48*, 2313. (c) Chai, J.; Wang, C.; Jia, L.; Pang, Y.; Graham, M.; Cheng, S. Z.D. *Synth. Met.* **2009**, *159*, 1443. (d) Li, H.; Jäkle, F. *Macromol. Rapid Commun.* **2010**, *31*, 915. (e) Chen, P.; Lalancette, R. A.; Jäkle, F. *J. Am. Chem. Soc.* **2011**, *133*, 8802.

[12] (a) Lik, A.; Fritze, L.; Müller, L.; Helten, H. *J. Am. Chem. Soc.* **2017**, *139*, 5692. (b) Lik, A.; Jenthra, S.; Fritze, L.; Müller, L.; Truong, K.-N.; Helten, H. *Chem. Eur. J.* **2018,** *24*, 11961.

[13] Riensch, N. A.; Fritze, L.; Schindler, T.; Kremer, M.; Helten, H. *Dalton Trans.* **2018**, *47*, 10399.

[14] We also demonstrated B–N coupling via Si/B exchange condensation as a route to BCN hybrid polymers and oligomers; see: (a) Lorenz, T.; Lik, A.; Plamper, F. A.; Helten, H. *Angew. Chem. Int. Ed.* **2016**, *55*, 7236. (b) Ayhan, O.; Eckert, T.; Plamper, F. A.; Helten, H. *Angew. Chem. Int. Ed.* **2016**, *55*, 13321. (c) Helten, H. *Chem. Eur. J.* **2016**, *22*, 12972. (d) Lorenz, T.; Crumbach, M.; Eckert, T.; Lik, A.; Helten, H. *Angew. Chem. Int. Ed.* **2017**, *56*, 2780. (e) Riensch, N. A.; Deniz, A.; Kühl, S.; Müller, L.; Adams, A.; Pich, A.; Helten, H. *Polym. Chem.* **2017**, *8*, 5264. (f) Ayhan, O.; Riensch, N. A.; Glasmacher, C.; Helten, H. *Chem. Eur. J.* **2018**, *24*, 5883.

[15] (a) Mkhalid, I. A. I.; Barnard, J. H.; Marder, T. B.; Murphy, J. M.; Hartwig, J. F. *Chem. Rev.* **2010**, *110*, 890. (b) Dudnik, A. S.; Fu, G. C. *J. Am. Chem. Soc.* **2012**, *134*, 10693. (c) Bagutski, V.; Del Grosso, A.; Carrillo, J. A.; Cade, I. A.; Helm, M. D.; Lawson, J. R.; Singleton, P. J.; Solomon, S. A.; Marcelli, T.; Ingleson, M. J. *J. Am. Chem. Soc.* **2013**, *135*, 474. (d) Moon, P. J.; Halperin, H. M.; Lundgren, R. J. *Angew. Chem. Int. Ed.* **2016**, *55*, 1894. (e) Zhao, D.; Xie, Z. *Angew. Chem. Int. Ed.* **2016**, *55*, 3166.

[16] Cao, H.; Rupar, P. A. *Chem. Eur. J.* **2017**, *23*, 14670.

[17] A trimer with three furan rings could only be detected by mass spectrometry.[12b]

[18] Compound **1b** was generated and reacted *in situ*.

[19] Reactions of **1b** with **4a,b** did not yield conclusive results, presumably due to the poor stability of **1b**.

[20] Ruhlandt-Senge, K.; Ellison, J. J.; Wehmschulte, R. J.; Pauer, F.; Power, P. P. *J. Am. Chem. Soc.* **1993**, *115*, 11353.

[21] Mathieu, B.; Ghosez, L. *Tetrahedron* **2002**, *58*, 8219.

[22] Pearson, D. E.; Frazer, M. G.; Frazer, V. S.; Washburn, L. C. *Synthesis* **1976**, *9*, 621.

[23] Determined by HSQC (see Appendix, Figure 5.3.20).

2.4 Bifuran-bridged Bisboranes: Highly Luminescent B-doped Oligohetarenes

The following section is slightly modified and reproduced from published article[§] with permission from the Centre National de la Recherche Scientifique (CNRS) and The Royal Society of Chemistry.

Abstract: A series of bifuran-bridged bis(triarylboranes) have been synthesized via classical metathesis or catalytic silicon/boron exchange reactions, respectively. The products obtained are strongly luminescent, with quantum yields up to 85%, and reversibly twofold reduced via successive one-electron processes.

Thiophene is one of the most extensively explored electron-rich building blocks of π-conjugated materials for organic electronics, optoelectronics and related applications.[1] Recent findings revealed that its heavier analogues, selenophene and tellurophene, exhibit valuable characteristics for such purposes as well.[2] Furan, the lightest five-membered group 16 hetarene, by comparison, has received significantly less attention in that respect.[3] This was attributed to the reduced stability of furan heterocycles in the presence of oxygen and incident light. It is noteworthy, though, that furan rings bear some significant advantages since they are biodegradable and can be obtained from renewable resources. Cyclolinear oligofurans, furthermore, possess highly rigid, planar structures; their planarity is generally even more pronounced than that of their oligothiophene congeners. Combined with a lower degree of aromaticity of the furan ring, this strongly favours conjugation and thus charge delocalization as well as enhanced luminescence. These findings led to considerably increased interest in furan-based electronic materials recently.[3] One possibility to diminish the susceptibility of furan rings towards oxidative degradation is to combine them with strongly electron-withdrawing components. This causes lowering of the HOMO energy, and thus improved oxidation resistance.[3]

Triarylborane moieties have proven to serve as strong electron-acceptor units in organic electronic materials.[4] The doping of π-conjugated systems with trivalent boron atoms has emerged as an effective strategy to produce novel compounds with intriguing properties and functions resulting from the interaction of the π-electrons with the vacant p orbital on boron. This offers unique opportunities in various technology fields, including (opto)electronic, sensory and imaging applications.[4] Here, too, thiophene-based materials are well-established,[5-7] while their furylborane congeners have been only scarcely studied.[8] Jäkle and coworkers have extensively explored dithienylborane building blocks **A**, that are kinetically

[§] N. A. Riensch, M. Fest, L. Fritze, A. Helbig, I. Krummenacher, H. Braunschweig, H. Helten, *New J. Chem.* **2020.**

stabilized by bulky aryl groups as the third *B*-substituent, for conjugated polymers and π-extended molecular compounds (Figure 2.4.1).[6]

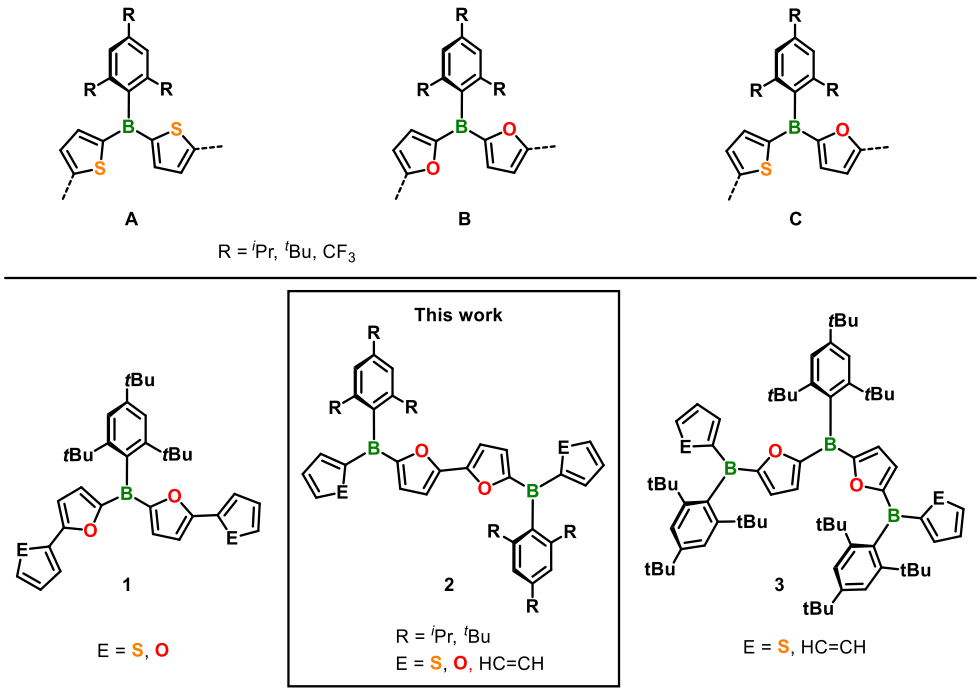

Figure 2.4.1. Top: Kinetically stabilized dithienyl-, difuryl- and mixed furyl(thienyl)borane building blocks **A**–**C**. Bottom: Extended π-conjugated organoboranes **1** and **3** previously presented by us[7c,9] and the bifuran-bridged organoboranes **2** presented herein.

We recently have developed a general, environmentally benign synthesis route to both thienylborane- (**A**) and furylborane-based materials (**B**) as well as mixed species, containing the structural unit **C**, using a novel, highly efficient organocatalytic Si/B exchange procedure.[7,10] This allowed us to access molecules and oligomers such as **1**[9] and **3**[7c] and the first furylborane polymers.[7a,b] Remarkably, all furylborane compounds that we have investigated so far displayed considerably stronger luminescence than their direct thienylborane analogues –without exception– and in mixed derivatives, emission intensities increased with increasing furan content.[7,9] These findings, together with Jäkle's observation that oligo- and poly(oligothiophene boranes) show narrowed band gaps when having more extended oligothiophene-bridges, thus leading to longer absorption and fluorescence emission wavelengths, with maximum quantum yields when the boron centres are bridged by bithiophene units,[6b] motivated us to investigate bifuran-bridged bisboranes **2**. These species, presented herein, are composed of four conjugated arene rings and two boron centres and may be regarded as the missing link between **1** and **3**, having one and three boron centres, respectively. They are highly luminescent and electrochemically stepwise reduced in two reversible processes.

5,5'-Bis(trimethylsilyl)-2,2'-bifuran (**4**)[11] served as starting point for their synthesis (Scheme 2.4.1). Bisborylation thereof with BBr_3 in CH_2Cl_2 afforded **5** in a virtually quantitative reaction. For the synthesis of **2a-c^{Tip}**, we explored *Route A*. Upon addition of 2 equiv. of 2,4,6-

tri*iso*propylphenyl lithium (TipLi) to a solution of **5** in toluene at −78 °C, selective formation of **6** was observed. Subsequently, Me_3SiOMe was added *in situ* to transform **6** into **7**. Compound **7** was then reacted with freshly generated 2-thienyl, 2-furyl and phenyl lithium (**8a-c**), respectively, in diethylether at −78 °C to yield the desired bis(triarylboranes) **2a-c^{Tip}**, which were isolated through re-precipitation.

In the next step, we targeted compounds **2a-c^{Mes*}**, carrying the even bulkier 2,4,6-tri-*tert*-butylphenyl (Mes*, supermesityl) substituents. Previous studies have shown that kinetic stabilization of boron with this group can lead to highly robust organoborane materials with excellent long-term chemical stability, which is of great interest for optoelectronic applications thereof. As we did not succeed in the synthesis of these derivatives via *Route A*, we turned to *Route B*. To this end, compound **4** was reacted with **9a-c** (2 equiv. each) in CH_2Cl_2 at ambient temperature in the presence of catalytic amounts of Me_3SiNTf_2 (Tf = CF_3SO_2; 10 mol%). Subsequently, the Mes* substituents were incorporated through reaction of the intermediates **10a-c** with Mes*Li in toluene. Compounds **2a^{Mes*}** and **2c^{Mes*}** were obtained after column chromatographic workup on alumina in 16 and 7% yield, respectively; the derivative **2b^{Mes*}** could not be isolated; only traces were detected by high-resolution mass spectrometry (HR-MS; see Appendix, Figure 5.4.35).

The constitution of **2a-c^{Tip}**, **2a^{Mes*}** and **2c^{Mes*}** was unambiguously ascertained by ^{1}H, ^{11}B and ^{13}C NMR spectroscopy and MS; elemental analysis yielded satisfactory results. The $^{11}B\{^{1}H\}$ NMR spectra of the compounds show broad resonances between 47 and 60 ppm, confirming the presence of three-coordinate boron. In contrast to **2a-c^{Tip}**, compounds **2a^{Mes*}** and **2c^{Mes*}** showed significant broadening of the ^{1}H signal for the *ortho* protons of the terminal thienyl or phenyl group, respectively, which indicates hindered rotation about the B–$C_{(het)aryl}$ bond caused by the bulky Mes* substituent. We were able to confirm the high stability of **2a^{Mes*}** and **2c^{Mes*}** under ambient conditions, as both compounds showed no sign of decomposition for at least 7 days in moist solution or for several months when stored in air in the solid state (Appendix, Figs. 5.4.26–29).

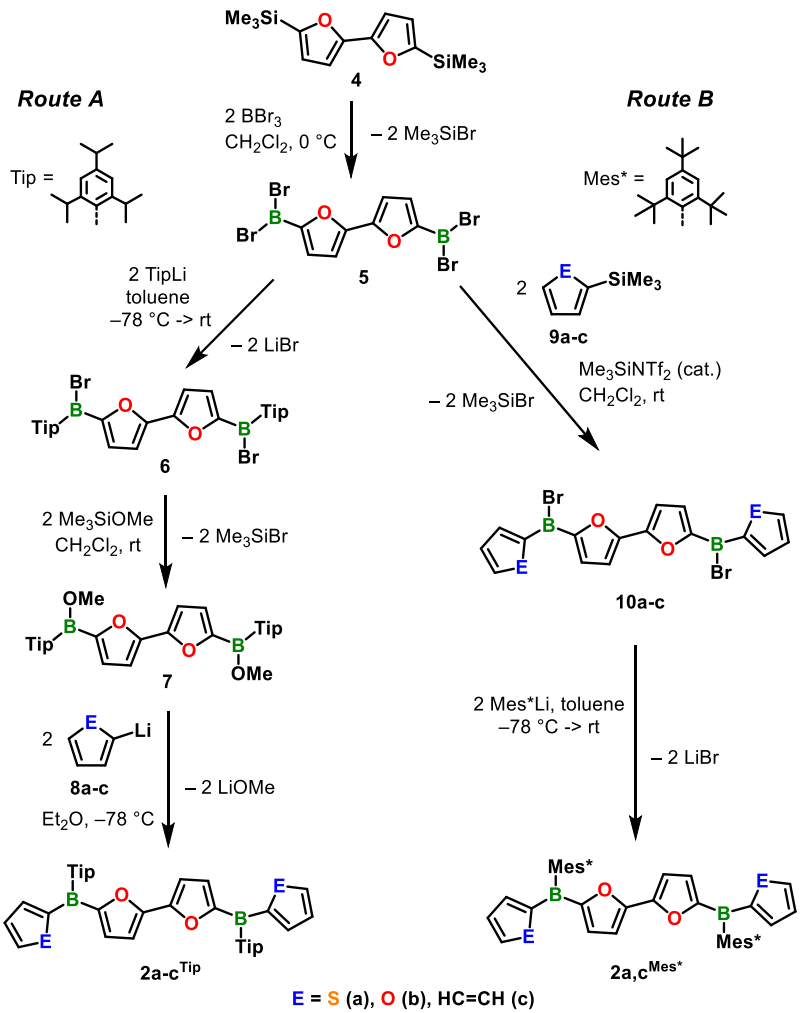

Scheme 2.4.1. Synthesis of bifuran-bridged bisboranes **2** via classical metathesis (*Route A*) or silicon/boron exchange reactions (*Route B*), respectively.

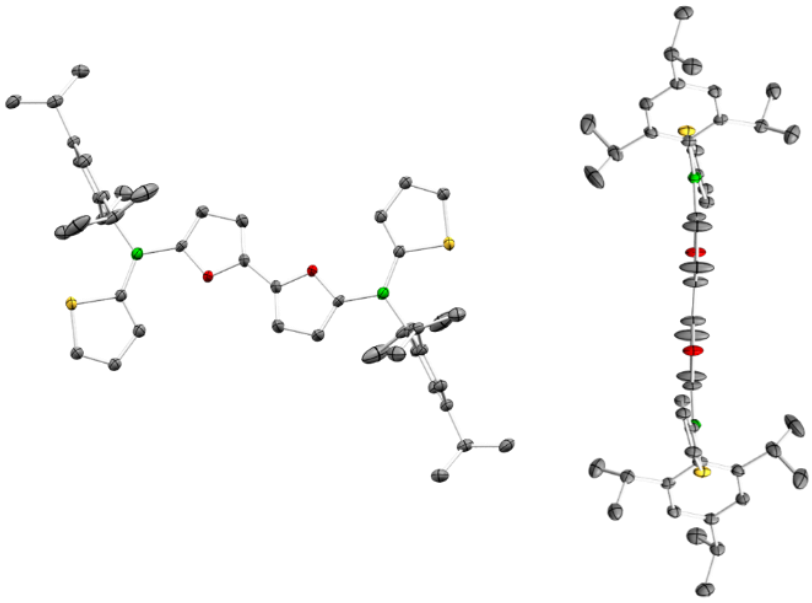

Figure 2.4.2. Molecular structure of **2a**^{Tip} in the solid state (H atoms omitted for clarity) with views perpendicular to (left) and along the extended π plane (right).

The molecular structure of **2a^{Tip}** in the solid state was determined by single-crystal X-ray diffractometry (Fig. 2.4.2). It shows a quasiplanar cyclolinear arrangement comprising the four hetarene rings and the planes of the two trigonal-planar coordinated boron centres ($\sum(BC_3)$ = 360.0°). The furan rings are fully coplanar (twist angle 0.0°) and arranged in *anti* fashion. The rotationally disordered terminal thiophene rings are slightly twisted with respect to their adjacent furan rings by 17.0°. The Tip groups are nearly perpendicular oriented to the respective BC_3 plane with a dihedral angle of 84.0° and point in opposite directions from the "cyclolinear chain". The structure of **2a^{Tip}** is overall similar to that of its all-thiophene analogue by Jäkle et al.[6b]

The UV-vis absorption spectra for **2a-c^{Tip}** and **2a,c^{Mes*}** in THF (Figure 2.4.3a and Table 2.4.1) display each one structured low-energy band with two maxima. Upon excitation at this band, all compounds show intense blue fluorescence with quantum yields between 53 and 85% (Figure 2.4.3b) and very small Stokes shifts (616 – 1029 cm^{-1}). According to our TD-DFT calculations (level: B3LYP-D3(BJ)/def2-SV(P)), performed on mesityl-substituted model systems **2a-c^{Mes}**, this is assigned to a π–π^* transition involving the HOMO and the LUMO of the molecules (Fig. 2.4.3d and experimental section, Figs. 2.4.4 – 2.4.6). Both of those orbitals are characterized as π orbitals extended over all hetarene rings; the participation of the terminal phenyl rings in **2c^{Mes}** is somewhat less pronounced. In each compound the strongest π-contribution comes from the bifuran bridge. The LUMO shows a significant contribution from the boron centre, thus pointing to some degree of charge transfer to boron upon excitation. Compared to the precursor molecule **7**, the absorption and emission wavelengths for **2a-c^{Tip}** are bathochromic shifted by 69 – 86 nm, consistent with extension of the π-conjugated system over the terminal aryl rings. This effect is strongest and virtually identical for both hetaryl-flanked systems **2a^{Tip}** and **2b^{Tip}**. Changing the bulky substituent from Tip to Mes* (cf. **2a^{Tip}** vs. **2a^{Mes*}** and **2c^{Tip}** vs. **2c^{Mes*}**) causes a hypsochromic shift by 9 – 11 nm in the absorption and 6 – 8 nm in the emission, respectively. The influence of the bifuran bridge can be estimated by comparison of the photophysical data for **2a^{Mes*}** with those for its all-thiophene analogue by Jäkle *et al.* ($\lambda_{abs,max}$ = 418 nm, $\lambda_{em,max}$ = 445 nm, ϕ_f = 38%).[6b] With respect to the latter, the absorption and emission maxima for **2a^{Mes*}** are somewhat blue-shifted. Significantly, compound **2a^{Mes*}** gave a higher fluorescence quantum yield (ϕ_f = 53%) and has a slightly smaller Stokes shift. The quantum yield further increases when the terminal thienyl groups are exchanged for furyl (**2b^{Tip}**: ϕ_f = 70%). Interestingly, the strongest luminescence exhibit the phenyl-flanked compounds **2c^{Mes*}** (ϕ_f = 81%) and **2c^{Tip}** (ϕ_f = 85%). Thus, compounds **2a-c^{Tip}** and **2a,c^{Mes*}** are considerably stronger luminescent than trisboranes **3** (see Fig. 2.4.1),[7c] and their absorption maxima are further red-shifted from those of the latter ($\lambda_{abs,max}$ for **3** with E = S, 378 nm and E = HC=CH, 371 nm), despite having a comparable conjugation length. They are

also slightly red-shifted from those of the bihetaryl-substituted boranes **1** ($\lambda_{abs,max}$ for **1** with E = S, 400 nm and with E = O, 394 nm),[9] which are similarly strong fluorescent (ϕ_f for **1** with E = S, 87% and with E = O, 67%). This highlights the positive impact of the bihetaryl units on the optical properties of such compounds.

Cyclic voltammetry (CV) measurements of **2a-c^{Tip}**, **2a,c^{Mes*}** and **7** in THF revealed two electrochemically reversible redox events for each compound, assigned to a stepwise reduction of the two borane moieties (Figure 2.4.3c and Table 2.4.1). The CV waves for **2a-c^{Tip}** and **2a,c^{Mes*}** are significantly anodic shifted with respect to that for the precursor **7**, while this effect is slightly more pronounced for the compounds carrying Tip substituents, **2a-c^{Tip}**. The half-wave potentials for the first reduction event of compounds **2** appear anodic from those of **1** ($E_{1/2}$ for **1** with E = S, −2.48 V and with E = O, −2.53 V)[9] and cathodic from those of **3** ($E_{1/2,1}$ for **3** with E = S, −2.10 V and with E = HC=CH, −2.11 V),[7c] which correlates with the number of electron-accepting boron centres (see Table 2.4.1). The redox splittings of the two reduction events are very similar within the series of the bifuran-bridged bisboranes **2a-c^{Tip}** (340 – 360 mV), **2a,c^{Mes*}** (380 mV) and **7** (320 mV). Again, the influence of bifuran vs. bithiophene bridging the boron centres can be estimated through comparison of **2a^{Mes*}** with its all-thiophene analogue.[6b] The first redox wave for **2a^{Mes*}** appears slightly cathodic from that for the latter ($E_{1/2,1}$ = −2.06 V), in consequence of the more electron-rich nature of furan vs. thiophene.[3e] However, the redox splitting for **2a^{Mes*}** (ΔE = 380 mV) is significantly larger than that for its bithiophene congener (ΔE = 288 mV),[6b] indicative of stronger electronic communication between the boron centres through the bifuran bridge.‡ Compounds **3** also show two reversible reduction waves; therein the redox splittings are even larger (ΔE for **3** with E = S, 650 mV and with E = HC=CH, 670 mV).[7c]

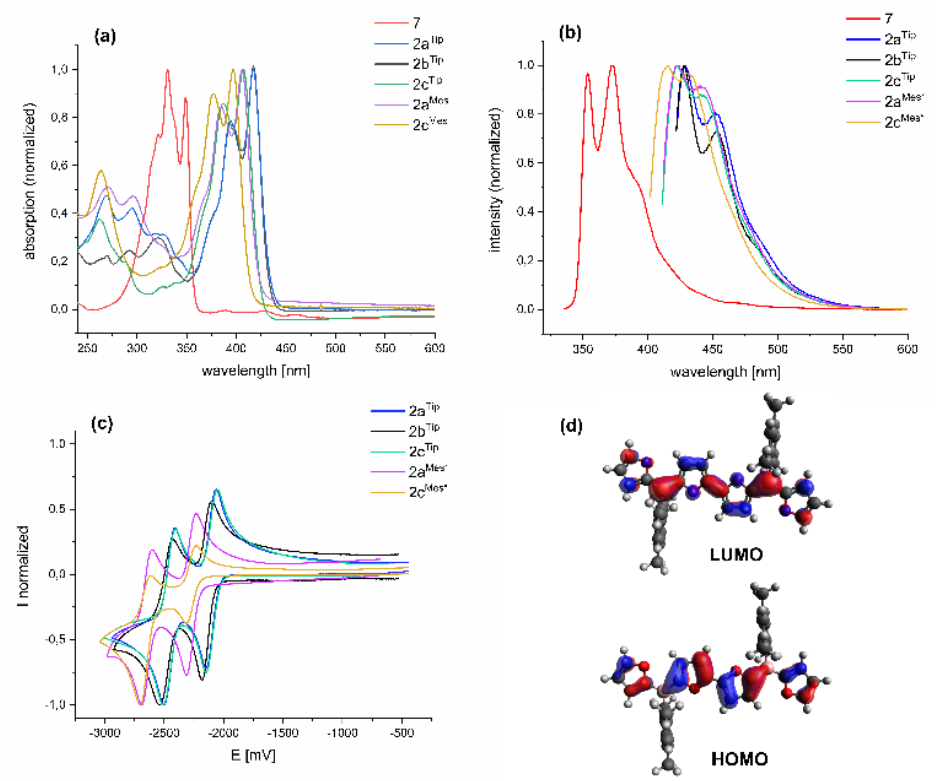

Figure 2.4.3. UV-vis absorption (a) and fluorescence spectra (b) of **7**, **2a-c^{Tip}** and **2a,b^{Mes*}** (in THF), (c) cyclic voltammograms of **2a-c^{Tip}** and **2a,c^{Mes*}** (in THF; vs Fc^+/Fc; scan rate: 250 mV s^{-1}) and (d) calculated frontier orbitals of **2b^{Mes}** (isovalue 0.03 a.u.).

Table 2.4.1. Photophysical and electrochemical data of compounds **7**, **2a-c^{Tip}**, **2a^{Mes*}** and **2c^{Mes*}** (all measurements performed at r.t. in THF).

Compd.	$\lambda_{abs,\,max}$ [nm]	$\lambda_{em,\,max}$ [nm]	φ_f [%]	$E_{1/2,1}$ [V]	$E_{1/2,2}$ [V]
7	331	354	27	−2.72	−3.04
2a^{Tip}	417	429	53	−2.09	−2.44
2b^{Tip}	417	428	70	−2.15	−2.49
2c^{Tip}	407	423	85	−2.09	−2.45
2a^{Mes*}	406	423	53	−2.25	−2.63
2c^{Mes*}	398	415	81	−2.28	−2.66

In conclusion, we have successfully synthesized a series of new boron-doped oligohetarenes, comprised of a cyclolinear chain of four π-conjugated arenes and two boron centres. Apparently, the combination of bifuran with electron-accepting borane moieties leads to

pronouncedly stable and highly luminescent compounds, which in the latter respect, with quantum yields up to 85%, surpass analogous thienylborane-based materials. The two boron centres in the new compounds show strong electronic coupling through the bifuran bridge. Currently, we are exploring the use of this new structural motif as a building block for extended molecular as well as macromolecular conjugated frameworks.

2.4.1 Experimental section

General procedures. All manipulations were performed under an atmosphere of dry argon using standard Schlenk techniques or in an MBraun glove box. Solvents (dichloromethane, *n*-pentane, diethylether, toluene, and tetrahydrofuran) were dried and degassed by means of an MBraun SPS-800 solvent purification system. Methanol was dried over magnesium turnings and freshly distilled prior to use. Deuterated solvents for NMR spectroscopy were dried and degassed at reflux over Na (C_6D_6) or CaH_2 ($CDCl_3$ and CD_2Cl_2) and freshly distilled prior to use. Solvents for aqueous work up (*n*-hexane, *n*-pentane, dichloromethane, ethanol, diethylether), tribromoborane, bromobenzene, thiophene, 2-bromothiophene, bromine, 1,3,5-tri-*tert*-butylbenzene, 2-bromo-1,3,5-triisopropylbenzene and lithium bis(trifluoromethylsulfonyl)imide were purchased from commercial sources and used as received. Solutions of *n*-butyllithium (1.6 M and 2.5 M in hexane, respectively) were purchased from Sigma Aldrich and used as received as well. Trimethylsilylchloride, methoxytrimethylsilane and furan were commercially purchased and freshly distilled prior to use. Copper (II) chloride was commercially purchased and dried at 180 °C for 5 hours prior to use. 2,4,6-triisopropylphenyllithium,[12] trimethylsilylbis(trifluoromethylsulfonyl)imide,[13] 2-bromo-1,3,5-tri-*tert*-butylbenzene,[14] 2,4,6-tri-*tert*-butylphenyllithium,[15] 2,2'-bifuran,[16] and 5,5'-bis(trimethylsilyl)-2,2'-bifuran[17] were prepared according to methods described in the literature. Compounds **9a**, **9b** and **9c** were prepared according to procedures previously described by us.[18] NMR spectra were recorded at 25 °C on a Bruker Avance III HD spectrometer operating at 300 MHz or on a Bruker Avance 500 spectrometer operating at 500 MHz. Chemical shifts were referenced to residual protic impurities in the solvent (^1H) or the deuterated solvent itself (^{13}C) and reported relative to external $SiMe_4$ (^1H, ^{13}C) or $BF_3{\cdot}OEt_2$ (^{11}B) standards. Mass spectra were obtained with the use of a Thermo Scientific Exactive Plus Orbitrap MS system employing either atmospheric sample analysis probe (ASAP), electrospray ionization (ESI) or atmospheric pressure chemical ionization (APCI). Elemental analyses were performed on an Elementar vario MICRO cube elemental analyzer. Cyclic voltammetry experiments were performed using a Gamry Instruments Reference 600 potentiostat. A standard three-electrode cell configuration was employed using a platinum disk working electrode, a platinum wire counter electrode, and a silver wire, separated by a *Vycor* tip, serving as the reference electrode. Tetra-*n*-butylammonium hexafluorophosphate ([*n*-Bu_4N][PF_6]) was employed as the supporting electrolyte. Compensation for resistive losses (*iR* drop) was employed for all measurements. Cyclic voltammetry scans were conducted with a scan rate of 250 mV/s. The scans were referenced after the addition of a small amount of ferrocene as internal standard. The potentials are reported relative to the ferrocene/ferrocenium couple.

Crystals suitable for single-crystal X-ray diffraction were selected, coated in perfluoropolyether oil, and mounted on MiTeGen sample holders. Diffraction data were collected on Bruker X8 Apex II 4-circle diffractometers with CCD area detectors using Mo-Kα radiation. The crystals were cooled using an Oxford Cryostreams low-temperature device. Data were collected at 100 K. The images were processed and corrected for Lorentz-polarization effects and absorption as implemented in the Bruker software packages. The structures were solved using the intrinsic phasing method (SHELXT)[19] and Fourier expansion technique. All non-hydrogen atoms were refined in anisotropic approximation, with hydrogen atoms 'riding' in idealized positions, by full-matrix least squares against F^2 of all data, using SHELXL[20] software and the SHELXLE graphical user interface.[21] Other structural information was extracted using OLEX2 software.[22] UV–vis spectra were obtained using a Jasco V-630 spectrophotometer. Emission spectra were recorded using an Edinburgh Instruments FLSP920 spectrometer equipped with a double monochromator for both excitation and emission, operating in right-angle geometry mode, and all spectra were fully corrected for the spectral response of the instrument. Fluorescence quantum yields were measured using a calibrated integrating sphere from Edinburgh Instruments combined with the FLSP920 spectrometer described above.

Syntheses

Synthesis of 5. To a solution of **4** (0.88 g, 3.1 mmol) in dichloromethane (10 mL) was added tribromoborane (1.94 g, 7.75 mmol) at 0 °C. The reaction mixture was stirred for 2 h. Then, the solvent was removed in vacuo, and a green solid was obtained.

Yield: 1.476 g (3.1 mmol, 100%). ^{1}H NMR (300 MHz, $CDCl_3$): δ = 7.75 (d, $^3J_{HH}$ = 3.7 Hz, 2H, Fur-C*H*), 7.11 (d, $^3J_{HH}$ = 3.7 Hz, 2H, Fur-C*H*) ppm; ^{11}B{^{1}H} NMR (96 MHz, $CDCl_3$): δ = 45.3 (s) ppm. In the following, compound **5** was used without prior isolation.

Synthesis of 7. To a solution of **4** (2.81 g, 10.0 mmol) in dichloromethane (100 ml) was added tribromoborane (10.02 g, 40.0 mmol) at 0 °C. The reaction mixture was stirred for 2 h at 0 °C, then all volatiles were removed in vacuo. The crude residue was re-dissolved in toluene (50 mL) followed by addition of a solution of TipLi (3 equiv.) in toluene at 0 °C. The reaction mixture was allowed to warm up to ambient temperatures and was stirred overnight. The solvent was removed in vacuo, and the resulting solid was extracted with dichloromethane. The obtained compound **6** was used without prior isolation and was then treated with TMS-OMe (3.02 g, 29.0 mmol) at 0 °C. The mixture was stirred overnight at room temperature. After all volatiles were removed in vacuo, an orange solid was obtained as crude product. Precipitation from DCM/MeOH afforded compound **7** as an orange powder.

Overall yield (3 steps): 5.90 g (9.48 mmol, 95%). ^{1}H NMR (500 MHz, $CDCl_3$): δ = 6.99 (s, 4H, Tip-*m*-C*H*), 6.80 (d, $^3J_{HH}$ = 3.5 Hz, 2H, Fur-*H*), 6.75 (d, $^3J_{HH}$ = 3.5 Hz, 2H, Fur-*H*), 3.80 (s, 6H,

O-CH_3), 2.91 (sept, $^3J_{HH}$ = 6.9 Hz, 2H, Tip-*p*-CH(CH_3)$_2$), 2.65 (sept, $^3J_{HH}$ = 6.9 Hz, 2H, Tip-*o*-CH(CH_3)$_2$), 1.29 (d, $^3J_{HH}$ = 6.9 Hz, 12H, Tip-o-CH(CH_3)$_2$), 1.24 (d, $^3J_{HH}$ = 6.7 Hz, 12H, Tip-o-CH(CH_3)$_2$), 1.10 (d, $^3J_{HH}$ = 6.7 Hz, 12H, Tip-*p*-CH(CH_3)$_2$) ppm; ^{11}B{^{1}H} NMR (160 MHz, $CDCl_3$): δ = 42.5 ppm; ^{13}C{^{1}H} NMR (126 MHz, $CDCl_3$): δ = 159.8 (BiFur-*C*-B), 151.0 (BiFur-*C)*, 150.7 (*o*-Tip-*C)*, 149.6 (*p*-Tip-*C)*, 132.1 (Ph-*C*-B), 128.8 (BiFur-*C*H), 120.3 (Ph-*C*H), 108.1 (BiFur-*C*H), 56.1 (B-O*C*H$_3$), 35.2 (*o*-Tip-^{i}Pr-*C*H), 34.5 (*p*-Tip-^{i}Pr-*C*H), 24.8 (Tip-^{i}Pr-*C*H$_3$), 24.6 (Tip-^{i}Pr-*C*H$_3$), 24.2 (Tip-^{i}Pr-*C*H$_3$) ppm; HR-MS (APCI): m/z = 622.4358; calcd. for $C_{40}H_{56}B_2O_4$: 622.4365; elem. anal. calcd. % for $C_{40}H_{56}B_2O_4$: C 77.18, H 9.07; found: C 77.03, H 9.33; UV-Vis (THF): $\lambda_{abs,max}$ = 331 (***ε*** = 40884 L mol^{-1} cm^{-1}), 339 (***ε*** = 32258 L mol^{-1} cm^{-1}), 349 nm (***ε*** = 36431 L mol^{-1} cm^{-1}); fluorescence (THF): $\lambda_{em,max}$ (λ_{ex} = 331 nm) = 354 nm, 372 nm (Φ_f = 27%).

Synthesis of 2a^{Tip}. To a solution of 2-bromothiophene (489 mg, 3.0 mmol) in *n*-hexane (8 mL) was added *n*-butyllithium (2.5 M, 1.16 mL, 2.9 mmol) at room temperature and the reaction mixture was stirred for 3 h. Subsequently, thus generated **8a** was used *in situ* as a colorless suspension and was added to a solution of **7** (621 mg, 1.0 mmol) in THF (5 mL) at 0 °C and the reaction mixture was allowed to warm up to room temperature overnight. After all volatiles were removed in vacuo, the formed solid was extracted with dichloromethane. After all volatiles were removed in vacuo, a brown solid was obtained as crude product. Precipitation from dichloromethane/MeOH afforded **2a^{Tip}** as a yellow solid.

Yield: 400 mg (0.55 mmol, 55%). ^{1}H NMR (500 MHz, $CDCl_3$): δ = 8.14 (d, 2H, $^3J_{HH}$ = 3.3 Hz, Thi-*H*), 7.99 (dd, 2H, $^3J_{HH}$ = 4.6 Hz, $^4J_{HH}$ = 0.9 Hz, Thi-*H*), 7.34 (dd, 2H, $^3J_{HH}$ = 4.6 Hz, $^3J_{HH}$ = 3.6 Hz, Thi-*H*), 7.17 (d, 2H, $^3J_{HH}$ = 3.5 Hz, BiFur-*H*), 7.03 (d, 2H, $^3J_{HH}$ = 3.5 Hz, BiFur-*H*), 7.02 (s, 4H, *m*-Tip-*H*), 2.96 (sept, 2H, $^3J_{HH}$ = 6.9 Hz, *p*-Tip-*i*-Pr-C*H*), 2.57 (sept, 4H, $^3J_{HH}$ = 6.7 Hz, *o*-Tip-*i*-Pr-C*H*), 1.34 (d, 12H, $^3J_{HH}$ = 6.9 Hz, *p*-Tip-*i*-Pr-CH_3), 1.09 (d, 12H, $^3J_{HH}$ = 6.7 Hz, *o*-Tip-*i*-Pr-CH_3), 1.09 (d, 12H, $^3J_{HH}$ = 6.7 Hz, *o*-Tip-*i*-Pr-CH_3) ppm; ^{11}B NMR (160 MHz, $CDCl_3$): δ = 50.0 ppm; ^{13}C{^{1}H} NMR (126 MHz, $CDCl_3$): δ = 165.0 (BiFur-*C*-B), 152.5 (*p*-Tip-*C*-^{i}Pr), 150.2 (*o*-Tip-*C*-^{i}Pr), 148.6 (BiFur-*C*-C), 144.1 (Thi-*C*-B), 143.2 (Thi-*C*H), 138.2 (Thi-*C*H), 136.9 (Tip-*C*-B), 133.1 (BiFur-*C*H), 128.9 (Thi-*C*H), 120.0 (*m*-Tip-*C*H), 110.0 (BiFur-*C*H), 35.2 (*o*-Tip-^{i}Pr-*C*H), 34.3 *(p*-Tip-^{i}Pr-*C*H), 24.4 (*o*-Tip-^{i}Pr-*C*H$_3$), 24.2 *(o*-Tip-^{i}Pr-*C*H$_3$), 24.1 *(p*-Tip-^{i}Pr-*C*H$_3$) ppm; HR-MS (APCI): m/z = 727.3963 [M+H]$^+$; calcd. for $C_{46}H_{56}B_2O_2S_2$: 726.3908; elem. anal. calcd. % for $C_{46}H_{56}B_2O_2S_2$: C 76.03, H 7.77, S 8.82; found: C 75.16, H 7.85, S 8.53; UV-Vis (THF): $\lambda_{abs,max}$ = 375 (***ε*** = 145270 L mol^{-1} cm^{-1}), 394 (***ε*** = 304626 L mol^{-1} cm^{-1}), 417 nm (***ε*** = 390019 L mol^{-1} cm^{-1}); fluorescence (THF): $\lambda_{em,max}$ (λ_{ex} = 417 nm) = 429 nm, 453 nm (Φ_f = 52.8%).

Synthesis of 2b^{Tip}. To a solution of furan (77.1 mg, 1.1 mmol) in THF (1 mL) was added *n*-butyllithium (2.5 M, 0.41 mL, 1.1 mmol) at −78 °C. The mixture was stirred for 0.5 h at room temperature and then for an additional 3 h at 50 °C. After cooling down to ambient temperature, thus generated **8b** was used *in situ* and added to a solution of **7** (200 mg, 0.28 mmol) in THF

(1 mL) at −78 °C and the reaction mixture was allowed to warm up to room temperature overnight. After all volatiles were removed in vacuo, a brown solid was obtained as crude product. Precipitation from dichloromethane/MeOH afforded **2b^{Tip}** as a yellow solid.

Yield: 118 mg (0.17 mmol, 53%). ^{1}H NMR (500 MHz, $CDCl_3$): δ = 7.89 (dd, 2H, $^{3}J_{HH}$ = 1.6 Hz, $^{4}J_{HH}$ = 0.6 Hz, Fur-*H*), 7.68 (s, 2H, Fur-*H*), 7.31 (d, 2H, $^{3}J_{HH}$ = 3.0 Hz, BiFur-*H*), 7.01 (s, 4H, *m*-Tip-*H*), 6.94 (d, 2H, $^{3}J_{HH}$ = 3.6 Hz, BiFur-*H*), 6.62 (dd, 2H, $^{3}J_{HH}$ = 3.5 Hz, $^{3}J_{HH}$ = 1.6 Hz, Fur-*H*), 2.95 (sept, 2H, $^{3}J_{HH}$ = 6.9 Hz, *p*-Tip-*i*-Pr-C*H*, 2.56 (sept, 4H, $^{3}J_{HH}$ = 6.8 Hz, *o*-Tip-*i*-Pr-C*H*), 1.32 (d, 12H, $^{3}J_{HH}$ = 7.0 Hz, *p*-Tip-*i*-Pr-CH_3), 1.09 (d, 24H, $^{3}J_{HH}$ = 6.8 Hz, *o*-Tip-*i*-Pr-CH_3) ppm; ^{11}B NMR (160 MHz, $CDCl_3$): δ = 49.7 ppm; ^{13}C{^{1}H} NMR (126 MHz, $CDCl_3$): δ = 164.5 (BiFur-*C*-B), 163.6 (Fur-*C*-B), 152.6 (BiFur-*C*-*C*), 150.4 (*o*-Tip-*C*-^{i}Pr), 150.3 (Fur-*C*H), 148.5 (*p*-Tip-*C*-^{i}Pr), 135.6 (Tip-*C*-B), 132.9 (BiFur-*C*H), 131.2 (Fur-*C*H), 120.1 (*m*-Tip-*C*H), 112.0 (Fur-*C*H), 109.9 (BiFur-*C*H), 35.5 (*o*-Tip-*i*-Pr-*C*H), 34.4 (*p*-Tip-*i*-Pr-*C*H), 24.4 (*o*-Tip-*i*-Pr-*C*H), 24.3 (*p*-Tip-*i*-Pr-*C*H_3) ppm; HR-MS (APCI): m/z = 695.4425 $[M+H]^+$; calcd. for $C_{46}H_{56}B_2O_4$: 694.4365; elem. anal. calcd. % for $C_{46}H_{56}B_2O_4$: C 79.55, H 8.13; found: C 78.69, H 8.85; UV-Vis (THF): $\lambda_{abs,max}$ = 374 (***ε*** = 138111 L mol^{-1} cm^{-1}), 394 (***ε*** = 286233 L mol^{-1} cm^{-1}), 417 nm (***ε*** = 365475 L mol^{-1} cm^{-1}); fluorescence (THF): $\lambda_{em,max}$ (λ_{ex} = 417 nm) = 428 nm, 453 nm (Φ_f = 69.9%).

Synthesis of 2c^{Tip}. To a solution of 1-bromobenzene (235.5 mg, 1.5 mmol) in THF (2 mL) was added *n*-butyllithium (2.5 M, 0.59 mL, 1.48 mmol) at −78 °C and the reaction mixture was stirred for 2 h at −78 °C. After the reaction mixture had been warmed up to ambient temperatures, thus generated **8c** was used *in situ* and added to a solution of **7** (311.3 mg, 0.5 mmol) in THF (2.5 mL) at −78 °C and the reaction mixture was allowed to warm up to room temperature overnight. After all volatiles were removed in vacuo, the formed solid was extracted with dichloromethane. The solvent was again removed in vacuo and a brown solid was obtained as crude product. Precipitation from dichloromethane/MeOH afforded **2c^{Tip}** as a yellow solid.

Yield: 195 mg (0.27 mmol, 54%). ^{1}H NMR (500 MHz, $CDCl_3$): δ = 8.29 (dd, 4H, $^{3}J_{HH}$ = 6.9 Hz, $^{4}J_{HH}$ = 1.3 Hz, Ph-C*H*), 7.56 (t, 2H, $^{3}J_{HH}$ = 7.3 Hz, Ph-C*H*), 7.49 (t, 4H, $^{3}J_{HH}$ = 7.4 HZ, Ph-C*H*), 7.19 (d, 2H, $^{3}J_{HH}$ = 3.6 Hz, BiFur-C*H*), 7.02 (s, 4H, *m*-Tip-C*H*), 6.98 (d, 2H, $^{3}J_{HH}$ = 3.6 Hz, BiFur-C), 2.96 (sept, 2H, $^{3}J_{HH}$ = 6.9 Hz, *p*-Tip-*i*-Pr-C*H*), 2.49 (sept, 4H, $^{3}J_{HH}$ = 6.7 Hz, *o*-Tip-*i*-Pr-C*H*), 1.34 (d, 12H, $^{3}J_{HH}$ = 6.9 Hz, *p*-Tip-*i*-Pr-CH_3), 1.08 (d, 12H, $^{3}J_{HH}$ = 3.7 Hz, *o*-Tip-*i*-Pr-CH_3), 1.04 (d, 12H, $^{3}J_{HH}$ = 3.7 Hz, *o*-Tip-*i*-Pr-CH_3) ppm; ^{11}B NMR (160 MHz, $CDCl_3$): δ = 58.2 ppm; ^{13}C{^{1}H} NMR (126 MHz, $CDCl_3$): δ = 166.2 (BiFur-*C*-B), 153.0 (*p*-Tip-*C*), 149.9 (*o*-Tip-*C*), 148.6 (BiFur-*C*), 140.6 (Ph-*C*-B), 139.0 (Ph-*C*H), 138.2 (Tip-*C*-B), 134.7 (BiFur-*C*H), 132.6 (Ph-*C*H), 128.0 (Ph-*C*H), 120.1 (*m*-Tip-*C*H), 109.9 (BiFur-*C*H), 35.4 (*o*-Tip-^{i}Pr-*C*H), 34.4 (*p*-Tip-^{i}Pr-*C*H), 24.4 (Tip-^{i}Pr-*C*H_3), 24.3 (Tip-^{i}Pr-*C*H_3), 24.2 (Tip-^{i}Pr-*C*H_3) ppm; HR-MS (APCI): m/z = 715.4845 $[M+H]^+$; calcd. for $C_{50}H_{60}B_2O_2$: 714.4779; UV-vis (THF): $\lambda_{abs,max}$ = 367 (***ε*** = 179408 L mol^{-1} cm^{-}

^{1}), 386 (ε = 349131 L mol^{-1} cm^{-1}), 407 nm (ε = 398403 L mol^{-1} cm^{-1}); fluorescence (THF): $\lambda_{em,max}$ (λ_{ex} = 407 nm) = 423 nm, 443 nm (Φ_f = 85.2%).

Synthesis of 2a^{Mes*}. To a solution of **4** (0.281 g, 1.0 mmol) in dichloromethane (3 mL) was added BBr_3 (0.489 g, 1.95 mmol) at 0 °C and the mixture was stirred for 2.5 h at 0 °C. Then, **9a** (0.329 g, 2.1 mmol) and TMS-NTf_2 (0.035 g, 0.1 mmol) as catalyst were added and the reaction mixture was stirred at room temperature for 3 d. Subsequently, the solvent was removed in vacuo to afford **10a**. The obtained solid was suspended in toluene (3 mL) and Mes*Li (0.631 g, 2.5 mmol) in Et_2O (2 mL) was added at −78 °C. The reaction mixture was stirred for 2 d at room temperature, then all volatiles were removed in vacuo and the crude product was filtrated with dichloromethane, affording the yellow brown crude product after the solvent was removed again in vacuo. Purification by column chromatography (Al_2O_3, *n*-hexane/DCM, 100:4) yielded compound **2a^{Mes*}** as a pale yellow solid.

Yield: 0.132 g (0.16 mmol, 16%). ^{1}H NMR (500 MHz, $CDCl_3$): δ = 7.86 (d, 2H, $^{3}J_{HH}$ = 4.5 Hz, Thi-C*H*), 7.82 (br, 2H, Thi-C*H*), 7.45 (s, 4H, Mes*-C*H*), 7.21 (t, 2H, $^{3}J_{HH}$ = 3.9 Hz, Thi-C*H*), 7.09 (br, 2H, BiFur-C*H*), 6.99 (d, 2H, $^{3}J_{HH}$ = 3.3 Hz, BiFur-C*H*), 1.40 (s, 18H, Mes*-*o*-^{t}Bu-CH_3), 1.21 (s, 36H, Mes*-*p*-^{t}Bu-CH_3) ppm; ^{11}B NMR (160 MHz, $CDCl_3$): δ = 49.2 ppm; ^{13}C{^{1}H} NMR (126 MHz, $CDCl_3$): δ = 166.2 (BiFur-*C*-B), 152.3 (Mes*-*C*-*o*-^{t}Bu) 151.4 (BiFur-*C*-*C*), 148.7 (Mes*-*C*-*p*-^{t}Bu), 147.1 (Thi-*C*), 141.9 (Thi-*C*-H), 136.4 (Thi-*C*H), 133.4 (Mes*-*C*-B), 130.5 (BiFur-*C*H), 128.4 (Thi-*m*-*C*H), 122.6 (Mes*-*C*H), 109.5 (BiFur-*C*H), 38.8 (Mes*-*o*-^{t}Bu-*C*), 35.1 (Mes*-*o*-^{t}Bu-*C*H_3), 34.9 (Mes*-p-^{t}Bu-*C*), 31.6 (Mes*-*p*-^{t}Bu-*C*H_3) ppm; HR-MS (APCI): m/z = 811.4912 [M+H]$^{+}$; calcd. for $C_{52}H_{68}B_2O_2S_2$: 810.4847; elem. anal. calcd. % for $C_{52}H_{68}B_2O_2S_2$: C 77.03, H 8.45, S 7.91; found: C 76.91, H 8.79, S 7.66; UV-Vis (THF): $\lambda_{abs,max}$ = 368 (ε = 195554 L mol^{-1} cm^{-1}), 385 (ε =362094 L mol^{-1} cm^{-1}), 406 nm (ε = 428943 L mol^{-1} cm^{-1}); fluorescence (THF): $\lambda_{em,max}$ (λ_{ex} = 406 nm) = 423 nm, 442 nm (Φ_f = 53.0%).

Attempted synthesis of 2b^{Mes*}. To a solution of **4** (0.281 g, 1.0 mmol) in dichloromethane (3 mL) was added BBr_3 (0.489 g, 1.95 mmol) at 0 °C and the mixture was stirred for 2.5 h at 0 °C. Then, **9b** (0.283 g, 2.0 mmol) and TMS-NTf_2 (0.035 g, 0.1 mmol) as catalyst were added and the reaction mixture was stirred at room temperature for 3 d. Subsequently, the solvent was removed in vacuo, re-dispersed in toluene (3 mL) and Mes*Li (0.631 g, 2.5 mmol) in Et_2O (2 mL) was added at −78 °C. The reaction mixture was stirred for 2 d at room temperature, then all volatiles were removed in vacuo. Analysis via ^{1}H and ^{11}B NMR spectroscopy showed no sign of product formation. However, high-resolution mass spectrometry evidenced the formation of traces of **2b^{Mes*}** (Figure 5.4.35).

Synthesis of 2c^{Mes*}. To a solution of **4** (0.281 g, 1.0 mmol) in dichloromethane (3 mL) was added BBr_3 (0.491 g, 1.96 mmol) at 0 °C and the mixture was stirred for 2.5 h at 0 °C. Then, **9c** (0.300 g, 2.0 mmol) and TMS-NTf_2 (0.035 g, 0.1 mmol) as catalyst were added and the

reaction mixture was stirred at room temperature for 3 d. After the reaction mixture had been stirred for 3 d, the solvent was removed in vacuo to afford crude **10c** and subsequently, Mes*Li (0.631 g, 2.5 mmol) was suspended in toluene and added to the reaction mixture. The mixture was again stirred for 3 d and then treated with water (5 mL), followed by an extraction with dichloromethane. After the solution was dried over $MgSO_4$, the solvent was removed in vacuo and the resulting red solid was subjected to column chromatography (Al_2O_3, *n*-hexane/DCM, 100:0 -> 1:99) with increasing gradient.

Yield: 56 mg (0.07 mmol, 7%). ^{1}H NMR (300 MHz, $CDCl_3$): δ = 8.25 (br s, 4H, Ph-C*H*), 7.47 – 7.38 (m, 10 H, Ph-C*H*/Mes*-C*H*), 7.01 (d, 2H, $^3J_{HH}$ = 3.5 Hz, Fur-*H*), 6.91 (d, 2H, $^3J_{HH}$ = 3.5 Hz, Fur-*H*) ppm; ^{11}B{^{1}H} NMR (160 MHz, $CDCl_3$): δ = 54.6 (s) ppm; ^{13}C{^{1}H} NMR (126 MHz, $CDCl_3$): δ = 166.8 (BiFur-*C*-B), 152.1 (Mes*-*o*-*C*-^{t}Bu), 151.5 (BiFur-*C*-*C*), 148.6 (Mes*-*p*-*C*-^{t}Bu), 143.3 (Ph-*C*-B), 138.5 (Ph-*o*-*C*H), 134.7 (Mes*-*C*-B), 131.7 (BiFur-*C*H), 131.1 (Ph-*p*-*C*H), 127.8 (Ph-*m*-*C*H), 122.4 (Mes*-*C*H), 109.1 (BiFur-*C*H), 38.7 (Mes*-*o*-*C*-CH_3), 35.1 (Mes*-*o*-*C*H_3), 34.9 (Mes*-*p*-*C*-CH_3), 31.6 (Mes*-*p*-*C*H_3) ppm; HR-MS (APCI): m/z = 799.5777 $[M+H]^+$; calcd. for $C_{56}H_{72}B_2O_2$: 798.5718; UV-Vis (THF): $\lambda_{abs,max}$ = 356 (***ε*** = 150591 L mol^{-1} cm^{-1}), 377 (***ε*** = 281330 L mol^{-1} cm^{-1}), 398 nm (***ε*** = 312512 L mol^{-1} cm^{-1}); fluorescence (THF): $\lambda_{em,max}$ (λ_{ex} = 398 nm) = 415 nm, 431 nm (Φ_f = 81.4%).

X-Ray crystallographic analysis

Table 2.4.2. Crystal structure and refinement data for **2a^{Tip}**.

No.	**2a^{Tip}**
CCDC number	2020145
Size / mm	0.437 x 0.318 x 0.159
Empiric Formula	C_{46} H_{56} B_2 O_2 S_2
M / g mol^{-1}	795.58
Crystal system	monoclinic
Space group	P 21/c
a / Å	16.0812(14)
b / Å	9.6707(8)
c / Å	17.1517(15)
α / deg	90
β / deg	117.418(2)
γ / deg	90
V / Å^3	2367.7(4)
Z	2
μ / mm^{-1}	0.151
T / K	100
$\theta_{min,max}$	2.38, 26.49
Completeness	99.9
Reflections: total / independent	4662, 3672
R_{int}	0.1182
Final R1 and wR2	0.0590, 0.1596
Largest peak and hole / e Å^{-3}	0.31, -0.29
ρ_{calc} / g cm^{-3}	1.116

Supporting Computational Information

Computational methods. DFT calculations were carried out with the TURBOMOLE V7.3 program package.[23] Optimizations were performed with Becke's three parameter exchange-correlation hybrid functional B3LYP[24] in combination with the valence-double-ζ basis set def2-SV(P).[25] The empirical dispersion correction DFT-D3 by Grimme was used including the three-body term and with Becke-Johnson (BJ) damping.[26] The stationary points were characterized as minima by analytical vibrational frequency calculations.[27] Vertical singlet

excitations were calculated by means of time-dependent DFT[28] using the same density functional–basis set combination as specified above.

Table 2.4.3. Results from TD-DFT calculations (π–π* excitation marked in bold).

Compound	No.	λ / nm	Oscillator strength *f*	Orbital contributions	$\|c\|^2$ / %
2a^{Mes}	**1**	**422.9**	**0.9345**	**HOMO → LUMO**	**82.8**
				HOMO−2 → LUMO	10.2
	3	402.9	0.3170	HOMO−2 → LUMO	69.3
				HOMO → LUMO	14.9
				HOMO−1 → LUMO	9.4
	15	**276.0**	**0.1488**	**HOMO−5 → LUMO+1**	**76.7**
				HOMO → LUMO+3	17.8
2b^{Mes}	**1**	**417.8**	**1.1764**	**HOMO → LUMO**	**90.1**
	3	399.6	0.1826	HOMO−2 → LUMO	82.5
				HOMO−3 → LUMO+1	8.4
	13	**270.7**	**0.1795**	**HOMO−5 → LUMO+1**	**85.7**
				HOMO → LUMO+2	12.5
2c^{Mes}	1	407.0	0.0689	HOMO−1 → LUMO	85.7
				HOMO−2 → LUMO+1	7.1
	3	**403.4**	**1.0880**	**HOMO → LUMO**	**91.3**
	14	**285.5**	**0.1278**	**HOMO−9 → LUMO**	**90.9**

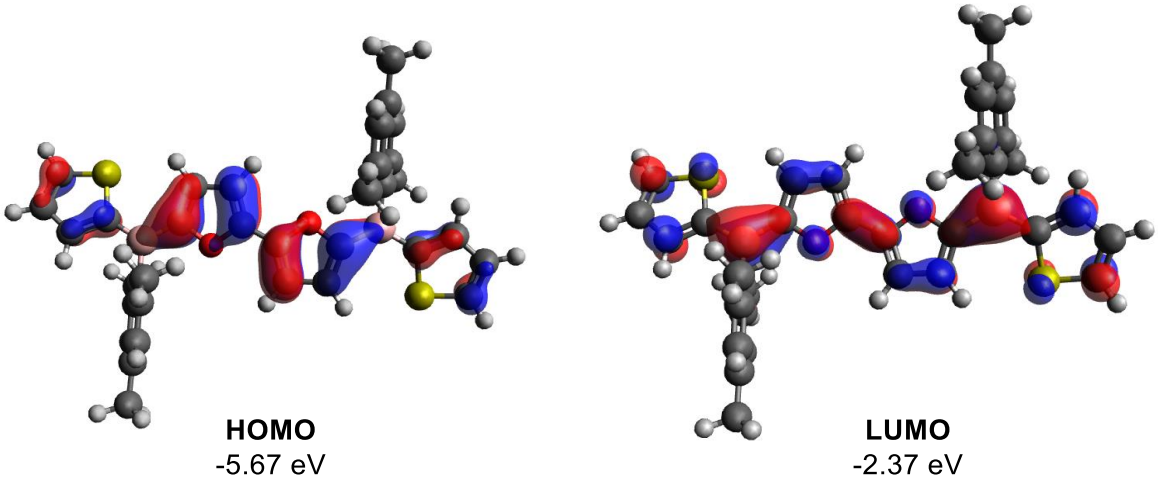

Figure 2.4.4. Calculated frontier orbitals of **2a**^{Mes} (isovalue 0.03 a.u.).

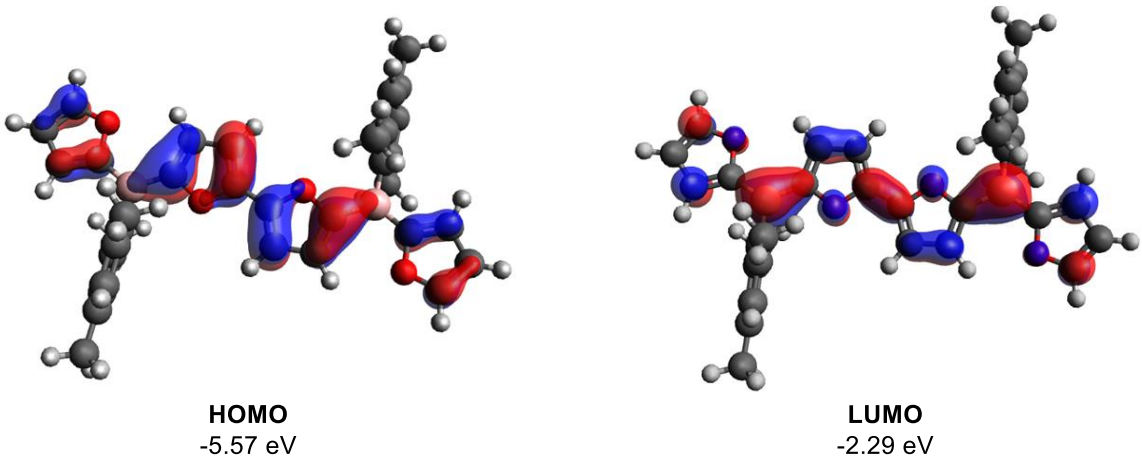

Figure 2.4.5. Calculated frontier orbitals of **2b**^{Mes} (isovalue 0.03 a.u.).

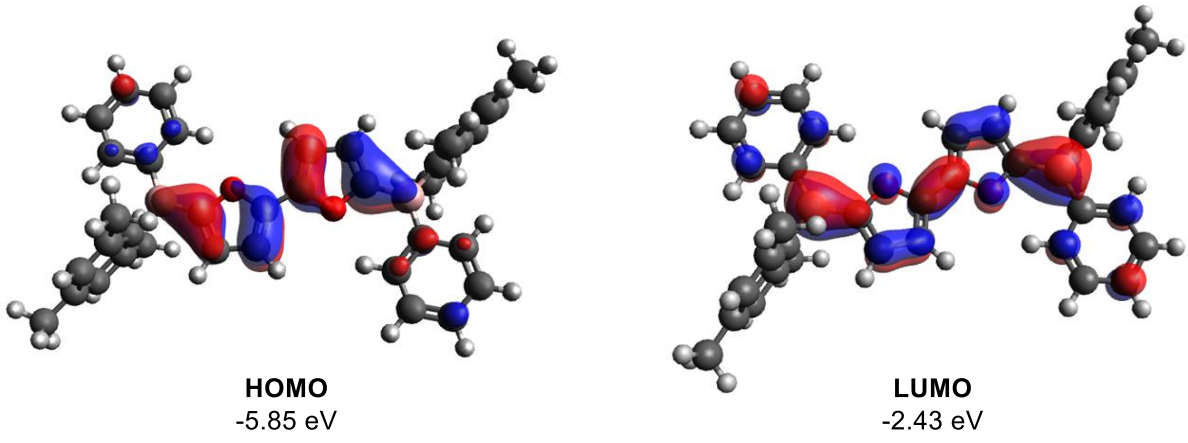

Figure 2.4.6. Calculated frontier orbitals of **2c**^{Mes} (isovalue of 0.03 a.u.).

Cartesian coordinates [Å] and total energies [a.u.] of optimized stationary points

$2a^{Mes}$:

Total energy (B3LYP-D3(BJ)/def2-SV(P)): -2309.169520

C	1.245483	2.539436	3.975807
C	0.515235	1.415241	4.420270
C	1.140092	0.487495	5.282134
C	2.465749	0.696368	5.684378
C	3.194592	1.815573	5.264532
C	2.564615	2.726470	4.407227
B	-0.973834	1.195171	3.951561
C	-2.108693	1.507376	4.948324
C	-1.957501	2.147041	6.174572
C	-3.166419	2.315118	6.900292
C	-4.251723	1.790480	6.229831
S	-3.797873	1.101903	4.720174
C	0.391179	-0.736950	5.760255
C	4.607648	2.048763	5.742740
C	0.613366	3.533429	3.027136
C	-1.231747	0.702199	2.518665
O	-0.121596	0.349314	1.769879
C	-0.525552	-0.016640	0.540711
C	-1.903167	0.085975	0.436060
C	-2.345382	0.544105	1.701158
C	0.481563	-0.426162	-0.396451
C	1.859318	-0.528031	-0.293634
C	2.299838	-0.989387	-1.558312
C	1.185195	-1.148277	-2.374135
O	0.076546	-0.790148	-1.626024
B	0.936011	-1.550036	-3.836874
C	2.049103	-2.093487	-4.756083
S	3.634969	-2.615563	-4.224611
C	4.126590	-3.021980	-5.822240
C	3.129234	-2.776587	-6.742869
C	1.955757	-2.257968	-6.134379
C	-0.511633	-1.374275	-4.435233
C	-1.007269	-0.086502	-4.737290
C	-2.292506	0.055506	-5.276158
C	-3.116884	-1.050765	-5.513880

C	-2.620574	-2.320964	-5.194436
C	-1.334933	-2.498652	-4.668029
C	-0.164236	1.140759	-4.469995
C	-0.843340	-3.891215	-4.337615
C	-4.488867	-0.883776	-6.121715
H	-4.911767	0.111993	-5.900630
H	-4.453804	-0.986813	-7.224074
H	-5.193730	-1.646851	-5.746759
H	-3.255017	-3.199745	-5.357893
H	-2.662994	1.059545	-5.512704
H	-1.655578	-4.633745	-4.417074
H	-0.029719	-4.203988	-5.017180
H	-0.436574	-3.944721	-3.310795
H	0.860003	1.029448	-4.870504
H	-0.608442	2.042440	-4.924891
H	-0.067103	1.325162	-3.383965
H	5.120837	-3.431733	-6.009003
H	3.236818	-2.968626	-7.813155
H	3.330846	-1.174426	-1.856742
H	2.452278	-0.289879	0.587474
H	-3.374502	0.754323	1.989451
H	-2.493938	-0.140557	-0.449573
H	-3.237879	2.796277	7.878730
H	-5.292337	1.769099	6.558410
H	2.944373	-0.037742	6.342733
H	1.251703	4.422556	2.889058
H	-0.371681	3.877043	3.392506
H	0.447235	3.080636	2.031894
H	3.118593	3.606374	4.060169
H	5.119163	1.097806	5.973531
H	4.622289	2.660344	6.666015
H	5.207426	2.586392	4.987262
H	-0.430287	-0.464325	6.447536
H	1.059551	-1.436068	6.291133
H	-0.069583	-1.284316	4.917217
H	-0.978622	2.483787	6.525440
H	1.044091	-2.000047	-6.679360

2b^{Mes}:

Total energy (B3LYP-D3(BJ)/def2-SV(P)): -1663.367040

C	-1.438237	-2.892049	-4.781548
C	-0.755434	-1.682495	-4.530488
C	-1.420360	-0.457206	-4.760687
C	-2.732652	-0.459512	-5.248344
C	-3.418931	-1.652980	-5.509185
C	-2.754995	-2.859977	-5.261672
B	0.725741	-1.692580	-3.992465
C	1.862629	-1.937006	-4.994186
O	3.187729	-1.990434	-4.595332
C	3.949143	-2.202532	-5.680373
C	3.175784	-2.293237	-6.811864
C	1.833441	-2.122024	-6.366396
C	-0.722453	0.851573	-4.466030
C	-4.823866	-1.632044	-6.062496
C	-0.762005	-4.220058	-4.520291
C	1.016625	-1.446237	-2.508897
C	2.169738	-1.390479	-1.734020
C	1.787363	-1.115373	-0.398882
C	0.405141	-1.013975	-0.421756
O	-0.058858	-1.210864	-1.668929
C	-0.554447	-0.745959	0.610957
O	-0.089007	-0.541853	1.856432
C	-1.163105	-0.297434	2.695577
C	-2.317334	-0.359893	1.922874
C	-1.936855	-0.646654	0.589605
B	-0.867640	-0.026776	4.174027
C	-1.997920	0.274757	5.167635
C	-1.956030	0.589853	6.515566
C	-3.295387	0.787568	6.959012
C	-4.079954	0.580751	5.850702
O	-3.327797	0.277049	4.781123
C	0.615622	-0.036305	4.706308
C	1.454143	1.080564	4.495811
C	2.768956	1.063584	4.978035
C	3.287428	-0.043093	5.661993
C	2.451021	-1.150295	5.850342

C	1.128591	-1.161680	5.387702
C	0.940262	2.283666	3.737281
C	0.262369	-2.383087	5.604598
C	4.696917	-0.031928	6.203781
H	-5.427593	-0.828391	-5.604076
H	-4.821626	-1.452250	-7.155402
H	-5.342029	-2.591065	-5.888713
H	-3.278096	-3.805625	-5.443966
H	-3.236379	0.497679	-5.426283
H	-1.463926	-5.061973	-4.645461
H	0.088715	-4.383515	-5.207146
H	-0.355066	-4.269438	-3.493092
H	0.265781	0.905426	-4.959134
H	-1.318265	1.715061	-4.807562
H	-0.547759	0.969795	-3.380377
H	5.023316	-2.268522	-5.509734
H	3.528822	-2.460472	-7.828828
H	3.177399	-1.537222	-2.117962
H	2.418477	-1.000752	0.480488
H	-3.324457	-0.209623	2.306907
H	-2.569248	-0.768515	-0.287863
H	-3.639251	1.047486	7.959524
H	-5.156774	0.616481	5.687918
H	2.840775	-2.032982	6.370129
H	1.662852	3.117185	3.760762
H	-0.014678	2.651040	4.155949
H	0.751012	2.030656	2.677544
H	3.408608	1.937875	4.811742
H	4.727308	0.378810	7.232047
H	5.364184	0.592745	5.584217
H	5.122385	-1.049954	6.247110
H	-0.588466	-2.162387	6.275013
H	0.837620	-3.212362	6.050381
H	-0.168800	-2.744936	4.652589
H	-1.042194	0.665751	7.104397
H	0.926150	-2.128273	-6.969880

$2c^{Mes}$:

Total energy (B3LYP-D3(BJ)/def2-SV(P)): -1667.767930

C	-2.955018	1.460027	-11.076149
C	-3.774925	0.532985	-10.396535
C	-4.963396	0.085772	-11.014001
C	-5.313255	0.569086	-12.281425
C	-4.512222	1.494247	-12.962835
C	-3.332548	1.924720	-12.342899
B	-3.359807	-0.004121	-8.969711
C	-2.455118	-1.268586	-8.846589
C	-1.992019	-1.787637	-7.614973
C	-1.179696	-2.921053	-7.563574
C	-0.808013	-3.572014	-8.745929
C	-1.251280	-3.082021	-9.979398
C	-2.060797	-1.946295	-10.023579
C	-5.847037	-0.920706	-10.311588
C	-4.923197	2.031816	-14.312847
C	-1.671143	1.942151	-10.438563
C	-3.910077	0.808721	-7.784666
O	-3.669551	0.481226	-6.460984
C	-4.288095	1.382586	-5.672382
C	-4.948033	2.323316	-6.445029
C	-4.702802	1.949641	-7.789273
C	-4.164179	1.219100	-4.251013
C	-3.506424	0.276403	-3.478902
C	-3.752408	0.648755	-2.134463
C	-4.542992	1.791181	-2.138401
O	-4.781640	2.120791	-3.461930
B	-5.093707	2.602282	-0.952314
C	-4.688678	2.055708	0.473859
C	-5.510331	1.120015	1.138880
C	-5.137486	0.640507	2.401727
C	-3.963000	1.067402	3.033181
C	-3.156035	1.995806	2.362798
C	-3.501287	2.494070	1.100187
C	-6.786415	0.636788	0.486658
C	-3.592086	0.568394	4.409397
C	-2.609331	3.500069	0.407722
C	-5.990126	3.872784	-1.073649

C	-6.432811	4.408431	-2.305691
C	-7.237917	5.547042	-2.355627
C	-7.623247	6.186322	-1.171257
C	-7.200297	5.679822	0.062678
C	-6.397197	4.539489	0.105283
H	-6.214102	-0.529209	-9.344844
H	-5.294613	-1.852484	-10.087655
H	-6.725126	-1.187914	-10.923791
H	-0.993002	1.098111	-10.212792
H	-1.866773	2.457806	-9.479771
H	-1.130044	2.644322	-11.095130
H	-2.685609	2.640818	-12.862388
H	-4.046471	2.326603	-14.915920
H	-5.564284	2.929002	-14.208406
H	-5.499345	1.285404	-14.887548
H	-2.275149	-1.289726	-6.686054
H	-0.832320	-3.302248	-6.597884
H	-0.171292	-4.461940	-8.705386
H	-0.962421	-3.587356	-10.906439
H	-2.402412	-1.565377	-10.990917
H	-5.058601	2.447663	-8.690593
H	-5.527973	3.164458	-6.069982
H	-2.928133	-0.565647	-3.854454
H	-3.398682	0.148676	-1.233453
H	-2.236045	3.110833	-0.557591
H	-3.157537	4.434068	0.182803
H	-1.735182	3.762783	1.027450
H	-7.461112	1.480575	0.250051
H	-6.579332	0.118087	-0.468094
H	-7.336064	-0.063022	1.138622
H	-5.782461	-0.087442	2.906989
H	-4.038091	-0.420230	4.616064
H	-2.497403	0.482186	4.527386
H	-3.950415	1.260656	5.196189
H	-2.230486	2.342348	2.836669
H	-6.070923	4.146057	1.072895
H	-7.499710	6.176097	0.991271
H	-8.254530	7.080163	-1.210629

H	-7.569004	5.941416	-3.321744
H	-6.138994	3.919674	-3.236161
H	-6.235996	0.210203	-12.751466

2.4.2 References

‡ Half-wave potential splittings are, however, not always reliable indicators of the extent of the electronic coupling in mixed valence species: see, e.g.: R. F. Winter, Organometallics, 2014, 4517.

[1] (a) I. Osaka and R. D. McCullough, *Acc. Chem. Res.*, 2008, **41**, 1202; (b) A. Mishra, C.-Q. Ma and P. Bäuerle, *Chem. Rev*., 2009, **109**, 1141; (c) Y. Olivier, D. Niedzialek, V. Lemaur, W. Pisula, K. Müllen, U. Koldemir, J. R. Reynolds, R. Lazzaroni, J. Cornil and D. Beljonne, *Adv. Mater.*, 2014, **26**, 2119; (d) J. Qian, X. Li, D. J. Lunn, J. Gwyther, Z. M. Hudson, E. Kynaston, P. A. Rupar, M. A. Winnik and I. Manners, *J. Am. Chem. Soc.*, 2014, **136**, 4121.

[2] (a) E. I. Carrera and D. S. Seferos, *Macromolecules*, 2015, **48**, 297; (b) E. Rivard, *Chem. Lett.*, 2015, **44**, 730; (c) E. L. Kynaston, A. Nazemi, L. R. MacFarlane, G. R. Whittell, C. F. J. Faul and I. Manners, *Macromolecules*, 2018, **51**, 1002; (d) G. C. Hoover and D. S. Seferos, *Chem. Sci.*, 2019, **10**, 9182; (e) B. T. Luppi, R. McDonald, M. J. Ferguson, L. Sang and E. Rivard, *Chem. Commun.*, 2019, **55**, 14218.

[3] Examples: (a) O. Gidron, Y. Diskin-Posner and M. Bendikov, *J. Am. Chem. Soc.*, 2010, **132**, 2148; (b) U. H. F. Bunz, *Angew. Chem., Int. Ed.*, 2010, **49**, 5037; (c) T. M. Swager and B. Esser, *Synfacts*, 2010, **5**, 0536; (d) C. H. Woo, P. M. Beaujuge, T. W. Holcombe, O. P. Lee and J. M. J. Fréchet, *J. Am. Chem. Soc.*, 2010, **132**, 15547; (e) S. Sharma and M. Bendikov, *Chem. Eur. J.*, 2013, **19**, 13127; (f) X.-H. Jin, D. Sheberla, L. J. W. Shimon and M. Bendikov, *J. Am. Chem. Soc.*, 2014, **136**, 2592; (g) A. Luzio, D. Fazzi, F. Nübling, R. Matsidik, A. Straub, H. Komber, E. Giussani, S. E. Watkins, M. Barbatti, W. Thiel, E. Gann, L. Thomsen, C. R. McNeill, M. Caironi and M. Sommer, *Chem. Mater.*, 2014, **26**, 6233; (h) L. Huo, T. Liu, B. Fan, Z. Zhao, X. Sun, D. Wei, M. Yu, Y. Liu and Y. Sun, *Adv. Mater.*, 2015, **27**, 6969; (i) H. Cao, I. A. Brettell-Adams, F. Qu and P. A. Rupar, *Organometallics*, 2017, **36**, 2565; (j) H. Cao and P. A. Rupar, *Chem. – Eur. J.*, 2017, **23**, 14670.

[4] Reviews: (a) C. D. Entwistle and T. B. Marder, *Angew. Chem., Int. Ed.*, 2002, **41**, 2927; (b) C. R. Wade, A. E. J. Broomsgrove, S. Aldridge and F. P. Gabbaï, *Chem. Rev.*, 2010, **110**, 3958; (c) F. Jäkle, *Chem. Rev.*, 2010, **110**, 3985; (d) H. Helten, *Chem. Eur. J.*, 2016, **22**, 12972; (e) L. Ji, S. Griesbeck and T. B. Marder, *Chem. Sci.*, 2017, **8**, 846; (f) E. von Grotthuss, A. John, T. Kaese and M. Wagner, *Asian J. Org. Chem.*, 2018, **7**, 37; (g) F. Vidal and F. Jäkle, *Angew. Chem., Int. Ed.*, 2019, **58**, 5846; (h) H. Helten, *Chem. – Asian J.*, 2019, **14**, 919; (i) Z. Huang, S. Wang, R. D. Dewhurst, N. V. Ignat'ev, M. Finze and H. Braunschweig, *Angew. Chem. Int. Ed.*, 2020, **59**, 8800.

[5] (a) Y. Ren and F. Jäkle, *Dalton Trans*., 2016, **45**, 13996, and references therein; examples: (b) A. Wakamiya, K. Mori, T. Araki and S. Yamaguchi, *J. Am. Chem. Soc.*, 2009, **131**, 10850;

(c) A. Iida and S. Yamaguchi, *J. Am. Chem. Soc.*, 2011, **133**, 6952; (d) C.-T. Poon, W. H. Lam and V. W.-W. Yam, *J. Am. Chem. Soc.*, 2011, **133**, 19622; (e) H. Braunschweig, A. Damme, Jimenez-Halla, J Oscar C, C. Hörl, I. Krummenacher, T. Kupfer, L. Mailänder and K. Radacki, *J. Am. Chem. Soc.*, 2012, **134**, 20169; (f) L. G. Mercier, W. E. Piers, R. W. Harrington and W. Clegg, *Organometallics*, 2013, **32**, 6820; (g) D. R. Levine, M. A. Siegler and J. D. Tovar, *J. Am. Chem. Soc.*, 2014, **136**, 7132; (h) X.-Y. Wang, F.-D. Zhuang, R.-B. Wang, X.-C. Wang, X.-Y. Cao, J.-Y. Wang and J. Pei, *J. Am. Chem. Soc.*, 2014, **136**, 3764; (i) S. K. Sarkar, G. R. Kumar and P. Thilagar, *Chem. Commun.*, 2016, **52**, 4175; (j) G. R. Kumar, S. K. Sarkar and P. Thilagar, *Chem. Eur. J.*, 2016, **22**, 17215; (k) Y. Yan, Z. Sun, C. Li, J. Zhang, L. Lv, X. Liu and X. Liu, *Asian J. Org. Chem.*, 2017, **6**, 496; (l) R. E. Messersmith, S. Yadav, M. A. Siegler, H. Ottosson and J. D. Tovar, *J. Org. Chem.*, 2017, **82**, 13440; (m) Y. Adachi and J. Ohshita, *Organometallics*, 2018, **37**, 869; (n) K. Mitsudo, K. Shigemori, H. Mandai, A. Wakamiya and S. Suga, *Org. Lett.*, 2018, **20**, 7336; (o) M. Meier, L. Ji, J. Nitsch, I. Krummenacher, A. Deißenberger, D. Auerhammer, M. Schäfer, T. B. Marder and H. Braunschweig, *Chem. Eur. J.*, 2019, **25**, 4707; (p) T. E. Stennett, P. Bissinger, S. Griesbeck, S. Ullrich, I. Krummenacher, M. Auth, A. Sperlich, M. Stolte, K. Radacki, C.-J. Yao, F. Würthner, A. Steffen, T. B. Marder and H. Braunschweig, *Angew. Chem. Int. Ed.*, 2019, **58**, 6449; (q) S. Griesbeck, M. Ferger, C. Czernetzi, C. Wang, R. Bertermann, A. Friedrich, M. Haehnel, D. Sieh, M. Taki, S. Yamaguchi and T. B. Marder, *Chem. Eur. J.*, 2019, **25**, 7679; (r) J. He, F. Rauch, A. Friedrich, D. Sieh, T. Ribbeck, I. Krummenacher, H. Braunschweig, M. Finze and T. B. Marder, *Chem. Eur. J.*, 2019, **25**, 13777.

[6] (a) X. Yin, J. Chen., R. A. Lalancette, T. B. Marder and F. Jäkle, *Angew. Chem. Int. Ed.*, 2014, **53**, 9761; (b) X. Yin, F. Guo, R. A. Lalancette and F. Jäkle, *Macromolecules*, 2016, **49**, 537; (c) X. Yin, K. Liu, Y. Ren, R. A. Lalancette, Y.-L. Loo and F. Jäkle, *Chem. Sci.*, 2017, **8**, 5497; (d) B. Meng, Y. Ren, J. Liu, F. Jäkle and L. Wan, *Angew. Chem., Int. Ed.*, 2018, **57**, 2183; (e) Y. Adachi, Y. Ooyama, Y. Ren, X. Yin, F. Jäkle and J. Ohshita, *Polym. Chem.*, 2018, **9**, 291; (f) Y. Yu, C. Dong, A. F. Alahmadi, B. Meng, J. Liu, F. Jäkle and L. Wang, *J. Mater. Chem. C*, 2019, **7**, 7427; (g) Y. Yu, B. Meng, F. Jäkle, J. Liu and L. Wang, *Chem. Eur. J.*, 2020, **26**, 873.

[7] (a) A. Lik, L. Fritze, L. Müller and H. Helten, *J. Am. Chem. Soc.*, 2017, **139**, 5692; (b) A. Lik, S. Jenthra, L. Fritze, L. Müller, K.-N. Truong and H. Helten, *Chem. – Eur. J.*, 2018, **24**, 11961; (c) L. Fritze, N. A. Riensch and H. Helten, *Synthesis*, 2019, **51**, 399.

[8] (a) T. Köhler, J. Faderl, H. Pritzkow and W. Siebert, *Eur. J. Inorg. Chem.*, 2002, 2942; (b) H. Braunschweig, R. D. Dewhurst, C. Hörl, A. K. Phukan, F. Pinzner and S. Ullrich, *Angew. Chem., Int. Ed.*, 2014, **53**, 3241; (c) H. Braunschweig, R. D. Dewhurst and T. Kramer, *Inorg. Chem.*, 2015, **54**, 3619; (d) B. Chen, H. Nie, R. Hu, A. Qin, Z. Zhao and B.-Z. Tang, *Sci. China:*

Chem., 2016, **59**, 699. (e) R. Shishido, I. Sasaki, T. Seki, T. Ishiyama and H. Ito, *Chem. Eur. J.*, 2019, **25**, 12924,

[9] N. A. Riensch, L. Fritze, T. Schindler, M. Kremer and H. Helten, *Dalton Trans.*, 2018, **47**, 10399.

[10] For B–N coupling by Si/B exchange, see: (a) T. Lorenz, A. Lik, F. A. Plamper and H. Helten, *Angew. Chem. Int. Ed.*, 2016, **55**, 7236; (b) O. Ayhan, T. Eckert, F. A. Plamper and H. Helten, *Angew. Chem. Int. Ed.*, 2016, **55**, 13321; (c) T. Lorenz, M. Crumbach, T. Eckert, A. Lik and H. Helten, *Angew. Chem. Int. Ed.*, 2017, **56**, 2780; (d) N. A. Riensch, A. Deniz, S. Kühl, L. Müller, A. Adams, A. Pich and H. Helten, *Polym. Chem.*, 2017, **8**, 5264; (e) O. Ayhan, N. A. Riensch, C. Glasmacher and H. Helten, *Chem. Eur. J.*, 2018, **24**, 5883; (f) F. Brosge, T. Lorenz, H. Helten and C. Bolm, *Chem. Eur. J.*, 2019, **25**, 12708.

[11] W. Chen, S. Y. Tan, Y. Zhao and Q. Zhang, *Org. Chem. Front.* 2014, **1**, 391.

[12] K. Ruhlandt-Senge, J. J. Ellison, R. J. Wehmschulte, F. Pauer, P. P. Power, *J. Am.*

Chem. Soc. **1993**, *115*, 11353–11357.

[13] B. Mathieu, L. Ghosez, *Tetrahedron* **2002**, *58*, 8219–8226.

[14] D. E. Pearson, M. G. Frazer, V. S. Frazer, L. C. Washburn, *Synthesis* **1976**, *9*, 621–623.

[15] X. Yin, J. Chen, R. A. Lalancette, T. B. Marder, F. Jäkle, *Angew. Chem. Int. Ed.* **2014**,

53, 9761–9765; *Angew. Chem.* **2014**, *126*, 9919–9923.

[16] J. Zhang, P. Ye, L. He, T. Yuan, Q. Liu, *Heterocycles* **2015**, *91*, 2190–2196.

[17] W. Chen, S. Y. Tan, Y. Zhao, Q. Zhang, *Org. Chem. Front.* **2014**, *1*, 391-394.

[18] A. Lik, L. Fritze, L. Müller, H. Helten, *J. Am. Chem. Soc.* **2017**, *139*, 5692–5695.

[19] G. M. Sheldrick, *Acta Crystallogr. A* **2015**, *71*, 3–8.

[20] Sheldrick, *Acta Crystallogr. A* **2008**, *64*, 112–122.

[21] C. B. Hubschle, G. M. Sheldrick, B. Dittrich, *J. Appl. Crystallogr.* **2011**, *44*, 1281–1284.

[22] O. V. Dolomanov, L. J. Bourhis, R. J. Gildea, J. A. K. Howard, H. Puschmann, *J.*

Appl. Crystallogr. **2009**, *42*, 339–341.

[23] Turbomole: R. Ahlrichs, M. Bär, M. Häser, H. Horn, C. Kölmel, *Chem. Phys. Lett.* **1989**, *162*, 165–169.

[24] a) P. A. M. Dirac, *Proc. R. Soc. London, Ser. A* **1929**, *123*, 714–733; b) J. C. Slater, *Phys. Rev.* **1951**, *81*, 385–390; c) A. D. Becke, *Phys. Rev. A.* **1988**, *38*, 3098–3100; d) C. Lee, W.

Yang, R. G. Parr, *Phys. Rev. B* **1988**, *37*, 785–789; e) A. D. Becke, *J. Chem. Phys.* **1993**, *98*, 5648–5652.

[25] A. Schäfer, H. Horn, R. Ahlrichs, *J. Chem. Phys.* **1992**, *97*, 2571–2577.

[26] a) S. Grimme, J. Antony, S. Ehrlich, H. Krieg, *J. Chem. Phys.* **2010**, *132*, 154104; b) S. Grimme, S. Ehrlich, L. Goerigk, *J. Comput. Chem.* **2011**, *32*, 1456–1465.

[27] P. Deglmann, F. Furche, R. Ahlrichs, *Chem. Phys. Lett.* **2002**, *362*, 511–518; b) P. Deglmann, F. Furche, *J. Chem. Phys.* **2002**, *117*, 9535–9538.

[28] a) R. Bauernschmitt, R. Ahlrichs, *Chem. Phys. Lett.* **1996**, *256*, 454–464; b) R. Bauernschmitt, R. Ahlrichs, *J. Chem. Phys.* **1996**, *104*, 9047–9052; c) F. Furche, D. Rappoport, in Density functional methods for excited states: equilibrium structure and electronic spectra, ed. M. Olivucci, Elsevier, Amsterdam, **2005**.

2.5 Conjugated Bis(triarylboranes) with Disconnected Conjugation

The following section is slightly modified and reproduced from published article[**] with permission from John Wiley and Sons under a creative common license (CC-BY-NC).

Abstract: A series of methylene-bridged bis(triarylboranes) has been synthesized via two complementary routes using metal-free catalytic Si/B exchange condensation under mild conditions. The title compounds comprise two borane moieties that show effective internal p-conjugation involving the respective boron centers and the hetaryl groups attached to them. Conjugation between both borane units, however, is disrupted by the aliphatic linker. Cyclic voltammetry revealed minimal electronic communication between the boron centers, as evidenced by two closely spaced reduction processes. The UV-vis spectra showed bathochromic shifted absorption bands compared to related monoboranes, which is attributed to the methylene bridge. A further red-shift results upon introduction of methyl or $SiMe_3$ groups at the terminal thiophene rings.

π-Conjugated triarylboranes currently attract enormous attention due to intriguing features that result from the interaction of the vacant p orbital on boron with the adjacent π systems (p–π conjugation).[1] This has enabled the application of triarylborane-based materials in various areas such as optoelectronics, sensors, and biological imaging.[1] The combination of trivalent boron with thiophene moieties is of special interest in that respect.[2-5] Jäkle and co-workers extensively explored dithienylboranes, **A** (Figure 2.5.1), which feature a bulky aryl group as the third *B*-substituent to ensure resistance towards hydrolysis and oxidation and provide improved thermal stability, as electron-accepting building blocks for π-conjugated polymers and molecular materials, respectively.[4] In the course of our studies on conjugated organoborane polymers and oligomers, we accomplished to develop a highly efficient, environmentally benign B–C bond formation method using a novel organocatalytic Si/B exchange condensation procedure.[5] This allowed us to access various molecular and macromolecular materials comprising dithienylborane units (**A**) as well as difurylborane (**B**) or mixed diarylborane building blocks (**C–E**). By the combination of boron with furan rings, we particularly broadened the scope of conjugated organoborane materials, as this has been only scarcely studied previously.[6]

Monodisperse oligoboranes such as **1** served us as molecular model systems for respective hetarylborane polymers but they are also valuable compounds in their own right. Recently, we reported a series of bifuran-bridged bisboranes **2**. These compounds may be regarded as complementary to **1**, in a sense, as both species feature four conjugated arene and two borane

[**] N. A. Riensch, L. Swoboda, A. Lik, I. Krummenacher, H. Braunschweig, H. Helten*, Z. Anorg. Allg. Chem.* **2021,** *647*, 421-424.

moieties that are in the former case linked by an electron-accepting (i.e., a third borane) unit and in the latter case by an electron-donating (bifuran) bridge.

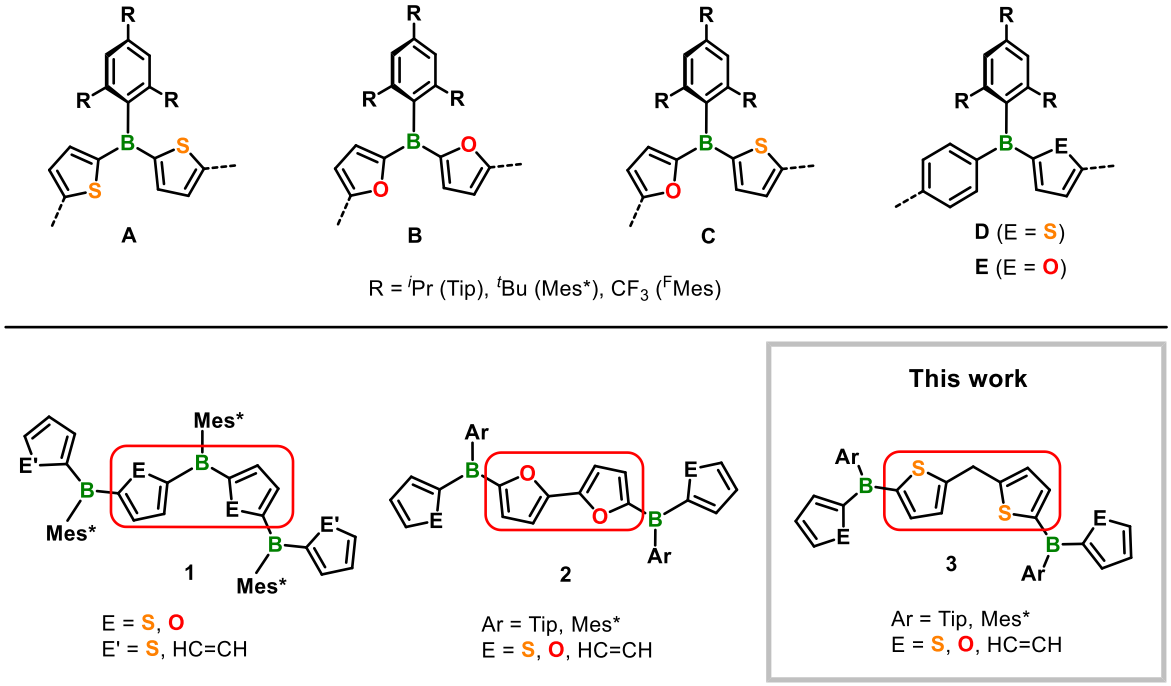

Figure 2.5.1. Kinetically stabilized diarylborane building blocks **A–E**, tris[(het)arylboranes)] **1** and bifuran-bridged bisboranes **2** previously reported by us, and dithienylmethane-bridged bisboranes **3** presented herein.

Bis(triarylboranes) of type **3** comprise a chain of four arene rings as well, but the p conjugation over the chain is disrupted through a methylene-bridge. Herein, we describe the synthesis and characterization of a series of such compounds and compare their photophysical and electrochemical properties with those of **1** and **2** and related monoboranes.

We accomplished the synthesis of bisboranes **3a-e**$^{\mathbf{Tip}}$ and **3a-c**$^{\mathbf{Mes*}}$ using our catalytic Si/B exchange approach via either of two alternative routes, *I* and *II* (Scheme 2.5.1). Compounds **3a-c**$^{\mathbf{Tip}}$ and **3a-c**$^{\mathbf{Mes*}}$ were accessed by the reaction of bis(trimethylsilyl)dithienylmethane **4** with two equivalents of freshly prepared dibromoboryl arenes **6a-c** in CH_2Cl_2 at ambient temperature in the presence of catalytic amounts of Me_3SiNTf_2 (Tf = CF_3SO_2; 10 mol%; *Route I*). The bulky aryl substituents were subsequently incorporated via reaction of the intermediates **8a-c** with TipLi or Mes*Li in toluene, respectively. The fully air- and moisture-stable compounds **3a-c**$^{\mathbf{Tip}}$ and **3a-c**$^{\mathbf{Mes*}}$ were obtained after purification by column chromatography on silica in moderate yields.

We prepared **3a,b**$^{\mathbf{Tip}}$ additionally via *Route II*, and we also targeted compounds **3d,e**$^{\mathbf{Tip}}$ in the same way. To this end, bis(dibromoboryl)dithienylmethane **5** was obtained in nearly quantitative yield by bisborylation of **4** with BBr_3 and subsequent recrystallization. Our catalytic Si/B exchange procedure using Me_3SiNTf_2 was then applied to **5** in combination with **7a,b,d,e**, respectively. Substitution of the B–Br bonds in the latter using TipLi yielded the desired

products **3a,b,d,e^{Tip}**, which were isolated upon column chromatography. Since we have prepared **3a,b^{Tip}** via both synthesis routes, we were then able to compare both approaches. This revealed that *Route I* is to be preferred in these cases, as it afforded the desired products in slightly better yields. On the other hand, *Route II* offers the opportunity of facile variation of the silylated coupling partner. Note that reactants **7a-e** are fully air-stable and can be easily purified by distillation.

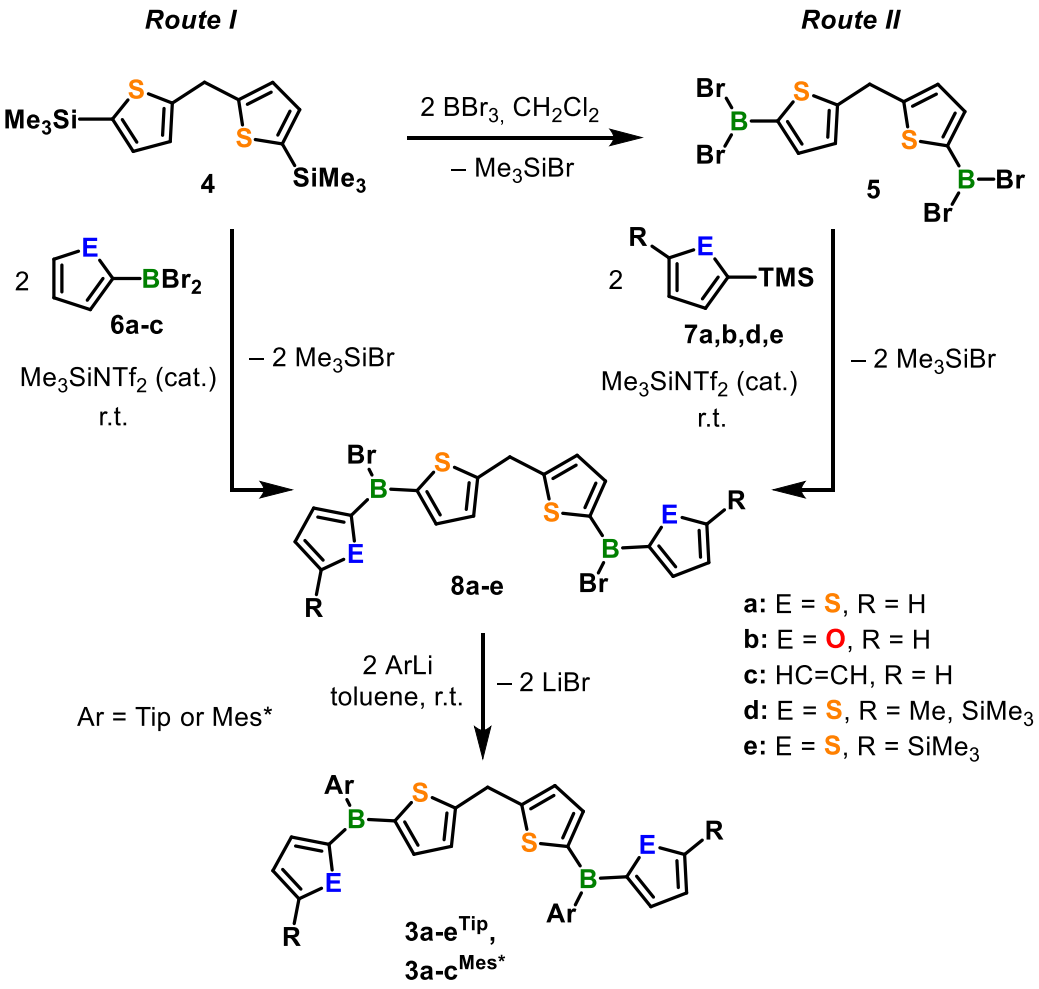

Scheme 2.5.1. Synthesis of methylene-bridged bisboranes **3**.

The constitution of **3a-e^{Tip}** and **3a-c^{Mes*}** was unambiguously ascertained by multinuclear NMR spectroscopy. High-resolution mass spectrometry and elemental analysis yielded satisfactory results. ^{11}B NMR spectroscopy confirmed the presence of three-coordinate boron. The spectra showed broad signals at about 50–51 (**3b^{Ar}**), 56–57 (**3a^{Ar}**, **3d,e^{Tip}**), 60 (**3c^{Mes*}**) and 64 ppm (**3c^{Tip}**), following the order of decreasing electron-releasing character of the (het)arenes attached to the boron center (furyl > thienyl > phenyl), which is also consistent with results we reported previously.[5] In the ^{1}H NMR spectra of the Mes*-featuring derivatives, **3a-c^{Mes*}**, the signals of the aromatic protons adjacent to the boron atom in the terminal thienyl, furyl or phenyl groups appeared significantly broadened. We previously observed this effect for related

compounds such as **1**[5b,c] and **2**[5e] with Ar = Mes* as well. It can be understood as a result of hindered rotation about the B–$C_{(het)aryl}$ bond caused by the bulky Mes* substituent.

The UV-vis absorption spectra for **3a-e^{Tip}** and **3a-c^{Mes*}** in THF each display one structured band at $\lambda_{abs,max}$ = 325–350 nm (Figure 2.5.2 and Table 2.5.1). This is, as expected, at shorter wavelength compared to the π–π* absorption bands of oligoboranes **1** ($\lambda_{abs,max}$ = 371–378 nm)[5b,c] and **2** ($\lambda_{abs,max}$ = 398–417 nm),[5e] which have conjugatively interconnected boron centers. Comparison of the synthesized derivatives of **3** reveals that substitution of Tip by Mes* leads to a marginal hypsochromic shift. The nature of the conjugated (het)aryl substituents has a stronger impact. Alike in **1**[5b,c] and **2**,[5e] the wavelength of the absorption maximum for **3** increases in the order: phenyl << furyl < thienyl. This proves effective π-conjugation within the isolated B(hetaryl)$_2$ or B(aryl)hetaryl moieties, respectively. Interestingly, the absorption bands of bisboranes **3** are bathochromic shifted compared to those of their respective monoborane congeners (**3a^{Tip}** *vs.* TipBThi$_2$:[5a,b] Δλ = 18 nm; **3a^{Mes*}** *vs.* Mes*BThi$_2$:[4a] Δλ = 13 nm; **3b^{Mes*}** *vs.* Mes*B(Fur)Thi:[5b] Δλ = 13 nm). This appears to be an effect of the aliphatic methylene bridge. An additional methyl or a silyl group at the terminal thiophene ring causes a further red-shift by Δλ = 7 nm (**3d^{Tip}** and **3e^{Tip}** *vs.* **3a^{Tip}**). Both effects can be explained by an increase in the HOMO energy caused by electron-rich substituents such as alkyl or $SiMe_3$ groups, which thereby reduces the HOMO-LUMO gap. All compounds **3** are virtually non-fluorescent.

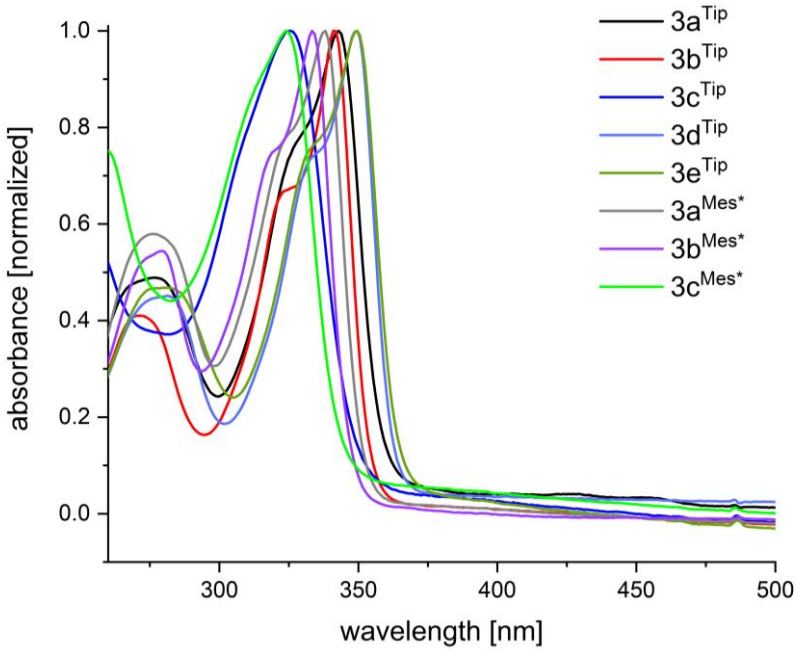

Figure 2.5.2. UV-Vis absorption spectra for **3a-e^{Tip}** and **3a-c^{Mes*}** in THF.

Table 2.5.1. Photophysical and electrochemical data for **3a-e^{Tip}**, **3a-c^{Mes*}**, and related monoboranes (all measurements in THF at r.t.).

Compd.	$\lambda_{abs,\,max}$ [nm]	$E_{1/2,1}$ [V]	$E_{1/2,2}$ [V]
TipBThi$_2$[5a,b]	325	–	–
Mes*BThi$_2$[4]	325	–	–
Mes*B(Fur)Thi[5b]	320	–	–
3a^{Tip}	343	−2.45[a]	[b]
3b^{Tip}	341	−2.54[a]	[b]
3c^{Tip}	326	−2.49[a]	[b]
3d^{Tip}	350	−2.35[a]	[b]
3e^{Tip}	350	−2.40[a]	[b]
3a^{Mes*}	338	−2.55[c]	−2.62[c]
3b^{Mes*}	333	−2.64[c]	−2.75[c]
3c^{Mes*}	325	−2.60[c]	−2.69[c]

[a] From cyclic voltammetry. [b] Not resolved. [c] Determined by differential pulse voltammetry.

The redox behavior of compounds **3a-e^{Tip}** and **3a-c^{Mes*}** was characterized by cyclic and pulse voltammetry in THF (Figure 2.5.3) using tetrabutylammonium hexafluorophosphate as the supporting electrolyte. For each compound, the voltammograms indicate only partially reversible reduction processes as they feature a return oxidation peak at around −1.1 V. In the case of the Mes*-substituted bisboranes, the overlapping first and second reduction waves in the cyclic voltammogram could be resolved by square wave or differential pulse voltammetry, revealing relatively small separations of 70–100 mV (see Appendix, Figs 5.5.59–67). The corresponding pulse voltammograms for the Tip-substituted bisboranes displayed a more complicated behavior, precluding a clear determination of their peak potential separations. However, they can be estimated to be smaller than ca. 150 mV. Therefore, the electrochemical data indicates only a small degree of negative charge distribution or “electronic communication” between the two boron atoms in these bisboranes.

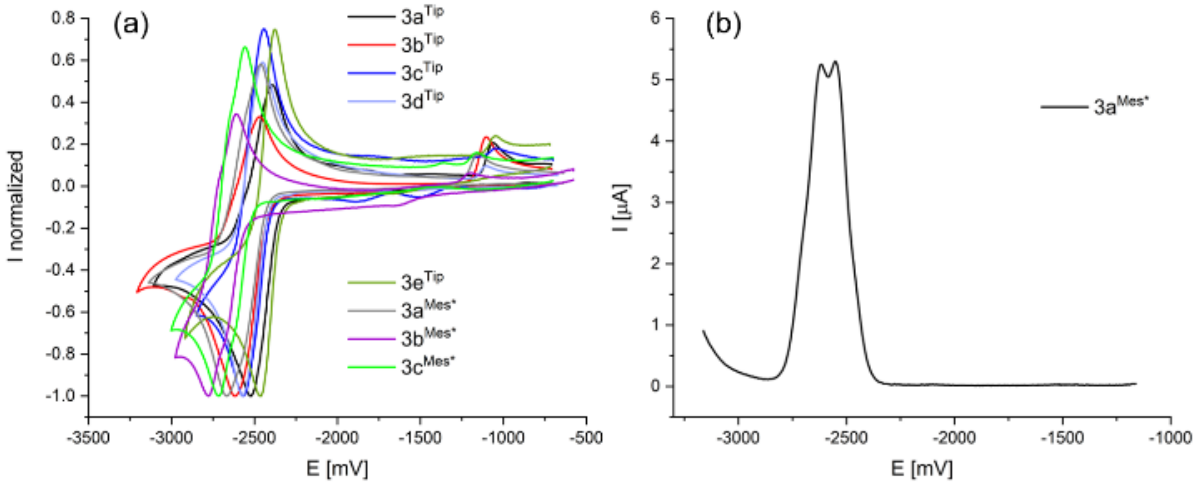

Figure 2.5.3. (a) Cyclic voltammograms for **3a-e^{Tip}** and **3a-c^{Mes}** and (b) differential pulse voltammogram for **3a^{Mes*}** (in THF at r.t; vs. Fc^+/Fc).

In conclusion, we have successfully synthesized a series of new cyclolinear bis(triarylboranes) comprised of four hetarenes and two boron centers connected by a methylene–bridge. While both borane entities are internally effectively conjugated, π-conjugation along the hetarylborane chain and, thus, communication between the boron centers is disrupted by the aliphatic linker unit. Currently, we are exploring the use of these methylene-linked bisboranes as novel building blocks for the construction of extended π-conjugated scaffolds.

2.5.1 Experimental section

General procedures. All manipulations were performed under an atmosphere of dry argon using standard Schlenk techniques or in an MBraun glove box. Solvents (dichloromethane, *n*-pentane, diethylether, toluene, and tetrahydrofuran) were dried and degassed by means of an MBraun SPS-800 solvent purification system. Methanol was dried over magnesium turnings and freshly distilled prior to use. Deuterated solvents for NMR spectroscopy were dried and degassed at reflux over Na (C_6D_6) or CaH_2 ($CDCl_3$ and CD_2Cl_2) and freshly distilled prior to use. Solvents for aqueous work up (*n*-hexane, *n*-pentane, dichloromethane, ethanol, diethylether), dimethoxymethane, sulfuric acid, glacial acid, tribromoborane, bromobenzene, thiophene, 2-bromothiophene, bromine, 1,3,5-tri-*tert*-butylbenzene, 2-bromo-1,3,5-triisopropylbenzene and lithium bis(trifluoromethylsulfonyl)imide were purchased from commercial sources and used as received. Solutions of *n*-butyllithium (1.6 M and 2.5 M in hexane, respectively) were purchased from Sigma Aldrich and used as received as well. Trimethylsilylchloride and furan were commercially purchased and freshly distilled prior to use. Sodium bicarbonate was commercially purchased and used as received. 2,4,6-triisopropylphenyllithium,[7] trimethylsilylbis(trifluoromethylsulfonyl)imide,[8] 2-bromo-1,3,5-tri-*tert*-butylbenzene,[9] 2,4,6-tri-*tert*-butylphenyllithium[10] and 5,5'-bisdibrom-(2,2'-dithienyl)-methane[11] were prepared according to methods described in the literature. Compounds **6a**, **6b** **6c** and **7e** were prepared according to procedures previously described by us.[12] NMR spectra were recorded at 25 °C on a Bruker Avance III HD spectrometer operating at 300 MHz or on a Bruker Avance 500 spectrometer operating at 500 MHz. Chemical shifts were referenced to residual protic impurities in the solvent (^{1}H) or the deuterated solvent itself (^{13}C) and reported relative to external $SiMe_4$ (^{1}H, ^{13}C) or $BF_3{\cdot}OEt_2$ (^{11}B) standards. Mass spectra were obtained with the use of a Thermo Scientific Exactive Plus Orbitrap MS system employing either atmospheric sample analysis probe (ASAP), electrospray ionization (ESI) or atmospheric pressure chemical ionization (APCI). Elemental analyses were performed on an Elementar vario MICRO cube elemental analyzer. Cyclic voltammetry experiments were performed using a Gamry Instruments Reference 600 potentiostat. A standard three-electrode cell configuration was employed using a platinum disk working electrode, a platinum wire counter electrode, and a silver wire, separated by a *Vycor* tip, serving as the reference electrode. Tetra-*n*-butylammonium hexafluorophosphate ([*n*-Bu_4N][PF_6]) was employed as the supporting electrolyte. Compensation for resistive losses (*iR* drop) was employed for all measurements. Cyclic voltammetry scans were conducted with a scan rate of 250 mV/s. The scans were referenced after the addition of a small amount of ferrocene as internal standard. The potentials are reported relative to the ferrocene/ferrocenium couple.

Syntheses

Synthesis of 4. To a solution of 5,5´-dibromodithienylmethane (10.14 g, 30 mmol) in toluene (100 mL) was added *n*-BuLi (1.6 M in hexane, 60 mmol) dropwise at room temperature for 15 min. Upon addition a slightly yellow precipitate was formed. After complete addition the reaction mixture was stirred for another 2 h. Subsequently, trimethylsilylchloride (60 mmol) was added and the reaction mixture was stirred overnight. After filtration and extraction of the solid residue with hexane the solvent was removed under reduced pressure and the crude product was further purified by distillation (bath temperature: 175 °C, head temperature: 140 °C) to obtain a colorless liquid.

Yield: 8.5 g (26.25 mmol, 87%). ^{1}H NMR (300 MHz, $CDCl_3$) δ = 7.09 (d, *J* = 3.3 Hz, 2H, Thi-C*H*), 6.95 (d, *J* = 3.3 Hz, 2H, Thi-C*H*), 4.40 (s, 2H, Thi-C-CH_2), 0.30 (s, 18H, Si(CH_3)$_3$).

Synthesis of 5. To a solution of **4** (5.65 g, 17.4 mmol) in dichloromethane (40 mL) was added triboromoborane (9.154 g, 36.5mmol) at 0 °C. The reaction mixture was stirred for 2 h and subsequently, all volatiles were removed in vacuo. The resulting solid was recrystallized from pentane/ DCM (6:1) at -37 °C to obtain the title compound as reddish/purple solid.

Yield: 8.767 g (17.00 mmol, 98%). ^{1}H NMR (400 MHz, CD_2Cl_2): δ = 7.96 (d, *J* = 3.8 Hz, 2H, Thi-C*H*), 7.21 (d, *J* = 3.8 Hz, 2H, Thi-C*H*), 4.46 (s, 2H, Thi-C-CH_2); ^{11}B NMR (128 MHz, CD_2Cl_2): δ = 47.0 (s); ^{13}C NMR (101 MHz, CD_2Cl_2): δ = 159.6 (s, Thi-*C*-CH$_2$), 145.2 (s, Thi-*C*H), 130.3 (s, Thi-*C*H), 32.2 (s, Thi-C-*C*H$_2$). HR-MS (APCI): m/z = 799.5777 $[M+H]^+$; calcd. for $C_9H_6B_2Br_4S_2$: 515.6831.

General procedure for the synthesis of bisboranes 3a-c^{Tip} and 3a-c^{Mes*} via *Route I*. To a solution of **4** (0.325 g, 1 mmol) in dichloromethane (4 mL), freshly prepared **6a-c** (2 mmol) and TMS-NTf_2 (0.071 g, 0.2 mmol) were added and the reaction mixture was stirred at room temperature for 2 d. Subsequently, the solvent was removed in vacuo to afford crude **8a-c.** The obtained oily solid was suspended in toluene (3.0 mL) and a solution of TipLi (0.462 g, 2.2 mmol) or a suspension of Mes*Li (0.555 g, 2.2 mmol) in toluene (3.0 mL) was added at room temperature, respectively. The reaction mixture was stirred for 2 d at room temperature followed by quenching with water. After aqueous work-up, all volatiles were removed in vacuo to afford crude **3**. Purification by column chromatography (silica, PE -> PE/DCM, 96:4) afforded compound **3** in high purity.

3a^{Tip}. Yield: 0.332 g (0.43 mmol, 43%). ^{1}H NMR (500 MHz, $CDCl_3$): δ = 7.88 (dd, *J* = 4.7, 0.9 Hz, 2H, Thi$_{term}$-C*H*), 7.78 (dd, *J* = 3.6, 0.9 Hz, 2H, Thi$_{term}$-C*H*), 7.68 (d, *J* = 3.6 Hz, 2H, Thi-C*H*), 7.27 – 7.24 (m, 2H, Thi$_{term}$-C*H*), 7.07 (d, *J* = 3.6 Hz, 2H, Thi-C*H*), 6.98 (s, 4H, Tip-C*H*), 4.52 (s,

2H, Thi-C-C*H*$_2$), 2.95 – 2.92 (m, 2H, Tip-*p*-*i*Pr-C*H*), 2.51 – 2.48 (m, 4H, Tip-*o*-*i*Pr-C*H*), 1.32 (d, *J* = 6.9 Hz, 12H, Tip-*p*-*i*PrC*H*$_3$), 1.04 (dd, *J* = 6.7, 5.4 Hz, 24H, Tip-*p*-*i*PrC*H*$_3$); ^{11}B NMR (160 MHz, $CDCl_3$): δ = 56.9 (s). ^{13}C{^{1}H} NMR (126 MHz, $CDCl_3$): δ = 155.1 (s, Thi-*C*-CH$_2$), 149.8 (s, Tip-*o*-*C*$_{ar}$), 148.6 (s, Tip-*p*-*C*$_{ar}$), 145.2 (s, Thi$_{term}$-*C*-B), 144.7 (s, Thi-*C*-B), 142.8 (s, Thi-*C*H), 142.0 (s, Thi$_{term}$-*C*H), 139.2 (s, Tip-*C*-B), 137.1 (s, Thi$_{term}$-*C*H), 129.0 (s, Thi$_{term}$-*C*H), 128.3 (s, Thi-*C*H), 120.1 (s, Tip-*m*-*C*$_{ar}$), 35.3 (s, Tip-*o*-*i*Pr-*C*H), 34.4 (s, Tip-*p*-*i*Pr-*C*H), 31.2 (s, Thi-C-*C*H$_2$), 24.5 – 24.3 (m, Tip-*i*Pr-*C*H$_3$); HR-MS (APCI): m/z = 771.3552 [M-H]$^+$; calcd. for $C_{47}H_{58}B_2S_4$: 772.3607; elem. anal. calcd. % for $C_{47}H_{58}B_2S_4$: C 73.04, H 7.56; found: C 73.03, H 7.86; UV-Vis (THF): $\lambda_{abs,max}$ = 275 nm (21352 L mol^{-1} cm^{-1}), 327 nm (35430 L mol^{-1} cm^{-1}), 343 nm (***ε*** = 43800 L mol^{-1} cm^{-1}).

3b^{Tip}. Yield: 0.175 g (0.24 mmol, 24%); ^{1}H NMR (500 MHz, $CDCl_3$): δ = 7.89 – 7.88 (d, *J* = 1.1, 1.6 Hz, 2H, Thi-C*H*), 7.82 (d, *J* = 3.6 Hz, 2H, Fur-C*H*), 7.09 (d, *J* = 3.0 Hz, 2H, Fur-C*H*), 7.07 d, *J* = 3.6 Hz, 2H, Thi-C*H*), 6.98 (s, 4H, Tip-C*H*), 6.51 (dd, *J* = 3.4, 1.6 Hz, 2H, Fur-C*H*), 4.53 (s, 2H, Thi-C-C*H*$_2$), 2.95 – 2.92 (m, 2H, Tip-*p*-*i*Pr-C*H*), 2.52 – 2.49 (m, 4H, Tip-*o*-*i*Pr-C*H*), 1.31 (d, *J* = 6.9 Hz, 12H, Tip-*p*-*i*PrC*H*$_3$), 1.05 (d, *J* = 2.5 Hz, 24H, Tip-*o*-*i*PrC*H*$_3$); ^{11}B NMR (160 MHz, $CDCl_3$): δ = 51.4 (s). ^{13}C NMR (126 MHz, $CDCl_3$): δ = 164.5 (s, Fur-*C*-B), 155.7 (Fur-CH), 150.2 (s, Thi-*C*H), 143.6 (s, Thi-C-*C*H$_2$, Fur-CH), 150.2 (s, Thi-*C*H), 149.8 (s, Tip-*o*-*C*$_{ar}$), 148.5 (s, Tip-*p*-*C*$_{ar}$), 143.6 (s, Fur-*C*H), 137.3 (s, Tip-*C*-B), 131.2 (s, Fur-*C*H), 128.2 (s, Thi-C*H*), 120.0 (s, Tip-*m*-*C*$_{ar}$), 111.7 (s, Fur-*C*H), 35.2 (s, Tip-*o*-*i*Pr-*C*H), 34.2 (s, Tip-*p*-*i*Pr-*C*H), 31.6 (Thi-C-*C*H$_2$), 24.5 (s, Tip-*p*-*i*Pr-*C*H$_3$), 24.3 (s, Tip-*o*-*i*Pr-*C*H$_3$) ppm; HR-MS (APCI): m/z = 739.4006 [M-H]$^+$; calcd. for $C_{47}H_{58}B_2O_2S_2$: 740.4064; elem. anal. calcd. % for $C_{47}H_{58}B_2O_2S_2$: C 76.21, H 7.89; found: C 76.02, H 8.21; UV-Vis (THF): $\lambda_{abs,max}$ = 272 nm (***ε*** = 22678 L mol^{-1} cm^{-1}), 322 nm (***ε*** = 37877 L mol^{-1} cm^{-1}), 341 nm (***ε*** = 56900 L mol^{-1} cm^{-1}).

3c^{Tip}. Yield: 0.199 g (0.262 mmol, 37%); ^{1}H NMR (500 MHz, $CDCl_3$): δ = 7.91 – 7.90 (m, 4H, Ph-*o*-C*H*), 7.59 (d, *J* = 3.6 Hz, 2H, Thi-C*H*), 7.51 – 7.40 (m, 6H, Ph-C*H*), 7.09 (d, *J* = 3.6 Hz, 2H, Thi-C*H*), 6.98 (s, 4H, Tip-C*H*), 4.52 (s, 2H, Thi-C-C*H*$_2$), 2.93 (sept, ^{3}*J* = 7.0 Hz, 2H, Tip-*p*-*i*Pr-C*H*), 2.44 (sept, ^{3}*J* = 6.7 Hz, 4H, Tip-*p*-*i*Pr-C*H*), 1.31 (d, *J* = 6.9 Hz, 12H, Tip-*p*-*i*PrC*H*$_3$), 1.02 (d, *J* = 6.7 Hz, 12H, Tip-*o*-*i*PrC*H*$_3$), 0.98 (d, ^{3}*J* = 6.7 Hz, 12 H, Tip-*o*-*i*PrC*H*$_3$); ^{11}B NMR (160 MHz, $CDCl_3$): δ = 63.5 (s). ^{13}C NMR (126 MHz, $CDCl_3$): δ = 155.7 (s, Thi-*C*-CH$_2$), 149.3 (s, Tip-*o*-*C*$_{ar}$), 148.6 (s, Tip-*p*-*C*$_{ar}$), 145.4 (s, Thi-*C*-B), 143.3 (s, Thi-*C*H), 142.1 (s, Ph-*C*-B), 140.0 (s, Tip-*C*-B), 137.4 (s, Ph-*o*-*C*H), 131.8 (s, Ph-*p*-*C*H), 128.2 (s, Thi-*C*H), 127.9 (s, Ph-*m*-*C*H), 120.1 (s, Tip-*m*-*C*$_{ar}$), 35.5 (s, Tip-*o*-*i*Pr-*C*H), 34.3 (s, Tip-*p*-*i*Pr-*C*H), 31.6 (s, Thi-C-*C*H$_2$), 24.4 – 24.2 (m, Tip-*i*Pr-*C*H$_3$); HR-MS (APCI): m/z = 759.4407 [M-H]$^+$; calcd. for $C_{51}H_{62}B_2S_2$: 760.4479; elem. anal. calcd. % for $C_{51}H_{62}B_2S_2$: C 80.52, H 8.21; found: C 80.40, H 8.62; UV-Vis (THF): $\lambda_{abs,max}$ = 257 nm (22501 L mol^{-1} cm^{-1}), 307 nm (***ε*** = 32725 L mol^{-1} cm^{-1}), 326 nm (***ε*** = 44500 L mol^{-1} cm^{-1}).

3a^{Mes*}. Yield: 0.298 g (0.348 mmol, 35%): ^{1}H NMR (500 MHz, $CDCl_3$): δ = 7.79 (dd, *J* = 4.7, 1.0 Hz, 2H, Thi_{term}-*H*), 7.67 (d, *J* = 2.7 Hz, 2H, Thi_{term}-*H*), 7.58 (br s, 2H,Thi-*H*), 7.41 (s, 4H, Mes*-H_{ar}), 7.17 (dd, *J* = 4.7, 3.5 Hz, 2H, Thi_{term}-*H*), 6.97 (d, *J* = 3.5 Hz, 2H Thi-*H*), 4.50 (s, 2H, Thi-C-CH_2), 1.38 (s, 18H, Mes*-*p*-*t*BuCH_3), 1.16 (s, 36H, Mes*-*o*-*t*BuCH_3); ^{11}B NMR (160 MHz, $CDCl_3$): δ = 56.0 (s); ^{13}C NMR (126 MHz, $CDCl_3$): δ = 153.5 (s, Thi-*C*-CH_2), 151.8 (s, Mes*-*o*-C_{ar}), 148.6 (s, Mes*-*p*-C_{ar}), 148.2 (s, Thi_{term}-*C*-B), 147.7 (s, Thi-*C*-B), 141.6 (s, Thi-*C*H), 141.2 (s, Thi-*C*H), 135.4 (s, Thi_{term}-*C*-S), 135.2 (s, Mes*-*C*-B), 128.5 (s, Thi_{term}-*C*H), 127.7 (s, Thi-*C*H), 122.7 (s, Mes*-*m*-C_{ar}), 38.8 (s, Mes*-*o*-*t*-Bu-*C*$(CH_3)_3$), 35.0 (s, Mes*-*p*-*t*-Bu-*C*$(CH_3)_3$), 34.8 (s, Mes*-*o*-*t*-Bu-C(*C*$H_3)_3$), 31.6 (s, Mes*-*p*-*t*Bu- C(*C*$H_3)_3$), 31.4 (s, Thi-C-*C*H_2); HR-MS (APCI): m/z = 855.4476 $[M-H]^+$; calcd. for $C_{53}H_{70}B_2S_4$: 856.4546; elem. anal. calcd. % for $C_{53}H_{70}B_2S_4$: C 74.28; H 8.23; found: C 74.51, H 8.60; UV-Vis (THF): $\lambda_{abs,max}$ = 276 nm (***ε*** = 26164 L mol^{-1} cm^{-1}), 323 nm (***ε*** = 34909 L mol^{-1} cm^{-1}), 338 nm (***ε*** = 45300 L mol^{-1} cm^{-1}).

3b^{Mes*}. Yield: 0.091 g (0.11 mmol, 11%); ^{1}H NMR (500 MHz, $CDCl_3$): δ = 7.79 (dd, *J* = 1.6, 0.6 Hz, 2H, Thi-C*H*), 7.52 (br. s, 2H, Thi-C*H*), 7.40 (s, 4H, Mes*-C*H*), 7.10 (d, *J* = 2.1 Hz, 2H, Fur-C*H*), 6.94 (d, *J* = 3.4 Hz, 2H, Fur-C*H*), 6.49 (dd, *J* = 3.4, 1.6 Hz, 2H, Fur-C*H*), 4.48 (s, 2H, Thi-C-CH_2), 1.37 (s, 18H, Mes*-*p*-C-CH_3), 1.15 (s, 36H, Mes*-*o*-C-CH_3); ^{11}B NMR (160 MHz, $CDCl_3$): δ = 50.9 (s); ^{13}C NMR (126 MHz, $CDCl_3$): δ = 165.3 (s, Thi-*C*-B), 153.9 (s, Thi-*C*-CH_2), 152.0 (s, Mes*-*o*-C_{ar}), 148.5 (s, Mes*-*p*-C_{ar}), 147.9 (s, Fur-*C*H), 146.3 (s, Fur-*C*-B), 142.1 (s, Mes*-*m*-C-CH_3), 133.7 (s, Mes*-*C*-B), 127.6 (s, Thi-*C*H), 127.5 (s, Thi-*C*H), 122.4 (s, Fur-*C*H), 111.6 (s, Fur-*C*H), 38.6 (s, Mes*-*o*-*t*-Bu-*C*$(CH_3)_3$), 34.8 (d, *J* = 12.6 Hz, Mes*-*p*-*t*-Bu-*C*$(CH_3)_3$)/ Mes*-*o*-*t*-Bu-C(*C*$H_3)_3$), 31.6 (s, Mes*-*p*-*t*Bu-C(*C*$H_3)_3$), 31.2 (s, Thi-C-*C*H_2); HR-MS (APCI): m/z = 825.5068 $[M+H]^+$; calcd. for $C_{53}H_{70}B_2O_2S_2$: 824.5003; elem. anal. calcd. % for $C_{53}H_{70}B_2O_2S_2$: C 77.17; H 8.55; found: C: 77.16, H 8.78; UV-Vis (THF): $\lambda_{abs,max}$ = 280 nm (***ε*** = 23035 L mol^{-1} cm^{-1}), 319 nm (***ε*** = 31088 L mol^{-1} cm^{-1}), 333 nm (***ε*** = 43700 L mol^{-1} cm^{-1}).

3c^{Mes*}. Yield: 0.199 g (0.24 mmol, 34%); ^{1}H NMR (500 MHz, $CDCl_3$): δ = 8.06 (d, *J* = 6.4 Hz, 4H, Ph-*o*-C*H*), 7.47 (d, *J* = 3.4 Hz, 2H, Thi-C*H*), 7.43 (s, 4H, Mes*-C*H*), 7.42 – 7.36 (m, 6H, Ph-*m/p*-C*H*), 6.98 (d, *J* = 3.6 Hz, 2H, Thi-C*H*), 4.51 (s, 2H, Thi-C-CH_2), 1.39 (s, 18H, Mes*-*p*-C-CH_3), 1.13 (s, 36H, Mes*-*o*-C-CH_3); ^{11}B NMR (160 MHz, $CDCl_3$): δ = 60.2 (s). ^{13}C NMR (126 MHz, $CDCl_3$): δ = 153.8 (s, Thi-*C*-CH_2), 151.6 (s, Mes*-*o*-*C*), 148.5 (s, Mes*-*p*-*C*), 147.5 (s, Thi-*C*-B), 143.8 (s, Ph-*C*-B), 142.3 (s, Thi-*C*H), 138.1 (s, Ph-*o*-*C*H), 136.3 (s, Mes*-*C*-B), 130.8 (s, Ph-*p*-*C*H), 127.7 (s, Ph-*m*-*C*H), 127.4 (s, Thi-*C*H), 122.4 (s, Mes*-*m*-*C*H), 38.6 (s, Mes*-*o*-*t*-Bu-*C*$(CH_3)_3$), 35.1 (s, Mes*-*p*-*t*-Bu-*C*$(CH_3)_3$), 34.9 (s, Mes*-*o*-*t*-Bu-C(*C*$H_3)_3$), 31.6 (s, Mes*-*p*-*t*-Bu-C(*C*$H_3)_3$), 31.3 (s, Thi-C-*C*H_2); elem. anal. calcd. % for $C_{57}H_{74}B_2S_2$: C 81.02, H 8.83; found: C 80.88, H 9.06; UV-Vis (THF): $\lambda_{abs,max}$ = 260 nm (***ε*** = 13935 L mol^{-1} cm^{-1}), 308 nm (***ε*** = 47893 L mol^{-1} cm^{-1}), 325 nm (***ε*** = 57500 L mol^{-1} cm^{-1}).

General procedure for the synthesis of bisboranes 3a,b,d,e^{Tip} via *Route II*. To a solution of **5** (0.2598 g, 0.5 mmol) in dichloromethane (2 mL), **7a,b,d,e** (1 mmol) and TMS-NTf_2 (0.035 g, 0.1 mmol) were added and the reaction mixture was stirred at room temperature for 2 d. Subsequently, the solvent was removed in vacuo to afford crude **8a,b,d,e.** The obtained oily solid was suspended in toluene (1.5 mL) and a solution of TipLi (0.231 g, 1.1 mmol) or a suspension of Mes*Li (0.278 g, 1.1 mmol) in toluene (1.5 mL) was added at room temperature, respectively. The reaction mixture was stirred for 2 d at room temperature, then the reaction mixture was quenched with water. After aqueous work-up, all volatiles were removed in vacuo to afford crude **3**. Purification by column chromatography (silica, PE -> PE/DCM, 96:4) yielded compound **3** in high purity.

3a^{Tip}. Yield: 0.1198 g (0.155 mmol, 31%).

3b^{Tip}. Yield: 0.0383 g (0.052 mmol, 12%).

3d^{Tip}. Yield: 0.1058 g (0.132 mmol, 26%); ^{1}H NMR (500 MHz, $CDCl_3$): δ = 7.61 (t, *J* = 4.4 Hz, 2H, Thi_{term}-C*H*), 7.58 (d, *J* = 3.5 Hz, 2H, Thi-C*H*), 7.04 (d, *J* = 3.6 Hz, 2H, Thi_{term}-C*H*), 6.97 (s, 4H, Tip-C*H*), 6.92 (dd, *J* = 3.5, 1.0 Hz, 2H, Thi-C*H*), 4.50 (s, 2H, Thi-C-CH_2), 2.94 – 2.90 (m, 2H, Tip-*p*-*i*Pr-C*H*), 2.59 (s, 6H, Thi-CH_3), 2.55 – 2.48 (m, 4H, Tip-*o*-*i*Pr-C*H*), 1.31 (d, *J* = 6.9 Hz, 12H, Tip-*o*-*i*PrCH_3), 1.04 (dd, *J* = 6.7, 3.8 Hz, 24H, Tip-*p*-*i*PrCH_3); ^{11}B NMR (160 MHz, $CDCl_3$): δ = 56.1 (s); ^{13}C NMR (126 MHz, $CDCl_3$): δ = 154.6 (s, Thi-*C*-CH_2), 153.2 (s, Tip-*o*-C_{ar}), 149.8 (s, Tip-*p*-C_{ar}), 148.4 (s, Tip-*m*-C_{ar}), 144.8 (s, Thi_{term}-*C*-B), 143.7 (s, Thi-*C*-B), 143.2 (s, Thi_{term}-*C*H), 142.4 (s, Thi_{term}-*C*H), 139.3 (s, Tip-*C*-B), 128.1 (d, *J* = 2.8 Hz, Thi-*C*H), 120.0 (s, Tip-*C*H), 35.2 (s, Tip-*o*-*i*Pr-*C*H), 34.3 (s, Tip-*p*-*i*Pr-*C*H), 31.5 (s, Thi-C-*C*H_2), 24.4 – 24.3 (m, Tip-*i*Pr-*C*H_3), 16.1 (s, Thi-*C*H_3); HR-MS (APCI): m/z = 800.3920 $[M-H]^+$; calcd. for $C_{49}H_{62}B_2S_4$: 799.3857; elem. anal. calcd. % for $C_{49}H_{62}B_2S_4$: C 73.49; H 7.80; found: C 73.33, H 7.88; UV-Vis (THF): $\lambda_{abs,max}$ = 280 nm (***ε*** = 36073 L mol^{-1} cm^{-1}), 332 nm (***ε*** = 61271 L mol^{-1} cm^{-1}), 350 nm (***ε*** = 82500 L mol^{-1} cm^{-1}).

3e^{Tip}. Yield: 0.0965 g (0.105 mmol, 21%); ^{1}H NMR (500 MHz, $CDCl_3$): δ = 7.77 (d, *J* = 3.4 Hz, 2H, Thi_{term}-C*H*), 7.69 (d, *J* = 3.6 Hz, 2H, Thi-C*H*), 7.37 (d, *J* = 3.4 Hz, 2H, Thi_{term}-C*H*), 7.06 (d, *J* = 3.6 Hz, 2H, Thi-C*H*), 6.99 (s, 4H, Tip-C*H*), 4.52 (s, 2H, (s, 2H, Thi-C-CH_2), 2.96 – 2.92 (m, 2H, Tip-*p*-*i*Pr-C*H*), 2.53 – 2.49 (m, 4H, Tip-*o*-*i*Pr-C*H*), 1.33 (d, *J* = 6.9 Hz, 12H, Tip-*p*-*i*PrCH_3), 1.04 (dd, *J* = 6.7, 0.8 Hz, 24H, Tip-*p*-*i*PrCH_3), 0.36 (s, 18H, Si-(CH_3)$_3$); ^{11}B NMR (160 MHz, $CDCl_3$): δ = 56.2 (s); ^{13}C NMR (126 MHz, $CDCl_3$): δ = 155.0 (s, Thi-*C*-CH_2), 154.1 (s, Tip-*o*-C_{ar}), 150.3 (s, Thi_{term}-*C*-B), 149.8 (s, Tip-*p*-C_{ar}), 148.5 (s, Tip-*m*-C_{ar}), 145.0 (s, Thi-*C*-B), 142.9 (d, *J* = 9.2 Hz, Thi_{term}-*C*-B), 139.4 (s, Tip-*C*-B), 135.5 (s, Thi-*C*H), 128.2 (s, Thi-*C*H), 120.1 (s, Tip-C*H*), 35.3 (s, Tip-*o*-*i*Pr-*C*H), 34.3 (s, Tip-*p*-*i*Pr-*C*H), 31.5 (s, Thi-C-*C*H_2) 24.4 – 24.3 (m, Tip-*i*Pr-*C*H_3), 0.1 (s, Si-(*C*H_3)$_3$); ^{29}Si NMR (99 MHz, $CDCl_3$): δ = -6.2 (s). HR-MS (APCI): m/z =

915.4353 $[M-H]^+$; calcd. for $C_{53}H_{74}B_2S_4Si_2$: 916.4398; elem. anal. calcd. % for $C_{53}H_{74}B_2S_4Si_2$: C 69.40; H 8.13; found: C 69.07, H 8.40; UV-Vis (THF): $\lambda_{abs,max}$ = 280 nm (ε = 22983 L mol^{-1} cm^{-1}), 332 nm (ε = 38715 L mol^{-1} cm^{-1}), 350 nm (ε = 50900 L mol^{-1} cm^{-1}).

2.5.2 References

[1] a) C. D. Entwistle, T. B. Marder, *Angew. Chem. Int. Ed.* **2002**, *41*, 2927–2931; *Angew. Chem.* **2002**, *114*, 3051–3056; b) C. R. Wade, A. E. J. Broomsgrove, S. Aldridge, F. P. Gabbaï, *Chem. Rev.* **2010**, *110*, 3958–3984; c) F. Jäkle, *Chem. Rev.* **2010**, *110*, 3985–4022; d) Z. M. Hudson, S. Wang, *Dalton Trans.* **2011**, *40*, 7805–7816; e) H. Zhao, L. A. Leamer, F. P. Gabbaï, *Dalton Trans.* **2013**, *42*, 8164–8178; f) A. Wakamiya, S. Yamaguchi, *Bull. Chem. Soc. Jpn.* **2015**, *88*, 1357–1377; g) H. Helten, *Chem. Eur. J.* **2016**, *22*, 12972–12982; h) S. Mukherjee, P. Thilagar, *J. Mater. Chem. C* **2016**, *4*, 2647–2662; i) L. Ji, S. Griesbeck, T. B. Marder, *Chem. Sci.* **2017**, *8*, 846–863; j) S.-Y. Li, Z.-B. Sun, C.-H. Zhao, *Inorg. Chem.* **2017**, *56*, 8705–8717; k) E. von Grotthuss, A. John, T. Kaese, M. Wagner, *Asian J. Org. Chem.* **2018**, *7*, 37–53; l) H. Helten, *Chem. Asian J.* **2019**, *14*, 919–935; m) Z. Huang, S. Wang, R. D. Dewhurst, N. V. Ignat'ev, M. Finze, H. Braunschweig, *Angew. Chem. Int. Ed.* **2020**, *59*, 8800–8818; *Angew. Chem.* **2020**, *132*, 8882–8900.

[2] Y. Ren, F. Jäkle*, Dalton Trans.* **2016**, *45*, 13996–14007.

[3] Selected examples: a) A. Wakamiya, K. Mori, T. Araki, S. Yamaguchi, *J. Am. Chem. Soc.* **2009**, *131*, 10850–10851; b) A. Iida, S. Yamaguchi, *J. Am. Chem. Soc.* **2011**, *133*, 6952–6955; c) C.-T. Poon, W. H. Lam, V. W.-W. Yam, *J. Am. Chem. Soc*. **2011**, *133*, 19622–19625; d) H. Braunschweig, A. Damme, J. O. C. Jimenez-Halla, C. Hörl, I. Krummenacher, T. Kupfer, L. Mailänder, K. Radacki, *J. Am. Chem. Soc.* **2012**, *134*, 20169–20177; e) L. G. Mercier, W. E. Piers, R. W. Harrington, W. Clegg, *Organometallics* **2013**, *32*, 6820–6826; f) D. R. Levine, M. A. Siegler, J. D. Tovar, *J. Am. Chem. Soc.* **2014**, *136*, 7132–7139; g) X.-.Y. Wang, F.-D. Zhuang, J.-Y. Wang, J. Pei, *Chem. Commun.* **2015**, *51*, 17532–17535; h) S. K. Sarkar, G. R. Kumar, P. Thilagar, *Chem. Commun.* **2016**, *52*, 4175–4178; i) G. R. Kumar, S. K. Sarkar, P. Thilagar, *Chem. Eur. J.* **2016**, *22*, 17215–17225; j) Y. Yan, Z. Sun, C. Li, J. Zhang, L. Lv, X. Liu, X. Liu, *Asian J. Org. Chem.* **2017**, *6*, 496–502; k) R. E. Messersmith, S. Yadav, M. A. Siegler, H. Ottosson, J. D. Tovar, *J. Org. Chem.* **2017**, *82*, 13440–13448; l) Y. Cao, X. Wang, X. Shi, S. M. Clee, P. L. McGeer, M. O. Wolf, C. Orvig, *Angew. Chem. Int. Ed.* **2017**, *56*, 15603–15606; *Angew. Chem.* **2017**, *129*, 15809–15812; m) Y. Adachi, J. Ohshita, *Organometallics* **2018**, *37*, 869–881; n) K. Mitsudo, K. Shigemori, H. Mandai, A. Wakamiya, S. Suga, *Org. Lett.* **2018**, *20*, 7336–7340; o) M. Ito, E. Ito, M. Hirai, S. Yamaguchi, *J. Org. Chem.* **2018**, *83*, 8449–8456; p) T. E. Stennett, P. Bissinger, S. Griesbeck, S. Ullrich, I. Krummenacher, M. Auth, A. Sperlich, M. Stolte, K. Radacki, C.-j. Yao, F. Würthner, A. Steffen, T. B. Marder, H. Braunschweig, *Angew. Chem. Int. Ed.* **2019**, *58*, 6449–6454; *Angew. Chem.* **2019**, *131*, 6516–

6521; q) W. Zhang, D. Yu, Z. Wang, B. Zhang, L. Xu, G. Li, N. Yan, E. Rivard, G. He, *Org. Lett.* **2019**, *21*, 109–113; r) Y. Adachi, F. Arai, F. Jäkle, *Chem. Commun.* **2020**, *56*, 5119–5122.

[4] a) X. Yin, J. Chen, R. A. Lalancette, T. B. Marder, F. Jäkle, *Angew. Chem. Int. Ed.* **2014**, *53*, 9761–9765; *Angew. Chem.* **2014**, *126*, 9919–9923; b) X. Yin, F. Guo, R. A. Lalancette, F. Jäkle, *Macromolecules* **2016**, *49*, 537–546; c) X. Yin, K. Liu, Y. Ren, R. A. Lalancette, Y.-L. Loo, F. Jäkle, *Chem. Sci.* **2017**, 8, 5497–5505; d) B. Meng, Y. Ren, J. Liu, F. Jäkle, L. Wan, *Angew. Chem. Int. Ed*, **2018**, *57*, 2183–2187; *Angew. Chem.* **2018**, *130*, 2205–2209; e) Y. Adachi, Y. Ooyama, Y. Ren, X. Yin, F. Jäkle, J. Ohshita, *Polym. Chem.* **2018**, *9*, 291–299; f) Y. Yu, C. Dong, A. F. Alahmadi, B. Meng, J. Liu, F. Jäkle, L. Wang, *J. Mater. Chem. C* **2019**, *7*, 7427–7432; g) T. A. Welsh, A. Laventure, A. F. Alahmadi, G. Zhang, T. Baumgartner, Y. Zou, F. Jäkle, G. C. Welch, *ACS Appl. Energy Mater.* **2019**, *2*, 1229–1240; h) Y. Yu, B. Meng, F. Jäkle, J. Liu, L. Wang, *Chem. Eur. J.* **2020**, *26*, 873–880.

[5] a) A. Lik, L. Fritze, L. Müller, H. Helten, *J. Am. Chem. Soc.* **2017**, *139*, 5692–5695; b) A. Lik, S. Jenthra, L. Fritze, L. Müller, K.-N. Truong, H. Helten, *Chem. Eur. J.* **2018**, *24*, 11961–11972; c) L. Fritze, N. A. Riensch, H. Helten, *Synthesis* **2019**, *51*, 399–406; d) N. A. Riensch, L. Fritze, T. Schindler, M. Kremer, H. Helten, *Dalton Trans.* **2018**, *47*, 10399–10403; e) N. A. Riensch, M. Fest, L. Fritze, A. Helbig, I. Krummenacher, H. Braunschweig, H. Helten, *New. J. Chem.* **2020**, DOI: 10.1039/D0NJ04297H.

[6] a) T. Köhler, J. Faderl, H. Pritzkow, W. Siebert, *Eur. J. Inorg. Chem.* **2002**, 2942–2946; b) H. Braunschweig, A. Damme, Jimenez-Halla, J Oscar C, C. Hörl, I. Krummenacher, T. Kupfer, L. Mailänder, K. Radacki, *J. Am. Chem. Soc.* **2012**, *134*, 20169–20177; c) H. Braunschweig, R. D. Dewhurst, C. Hörl, A. K. Phukan, F. Pinzner, S. Ullrich, *Angew. Chem. Int. Ed.* **2014**, *53*, 3241–3244; *Angew. Chem.* **2014**, *126*, 3305–3308; d) H. Braunschweig, R. D. Dewhurst, T. Kramer, *Inorg. Chem.* **2015**, *54*, 3619–3623; e) B. Chen, H. Nie, R. Hu, A. Qin, Z. Zhao, B.-Z. Tang, *Sci. China Chem.* **2016**, *59*, 699–706.

[7] K. Ruhlandt-Senge, J. J. Ellison, R. J. Wehmschulte, F. Pauer, P. P. Power, *J. Am. Chem. Soc.* **1993**, *115*, 11353–11357.

[8] B. Mathieu, L. Ghosez, *Tetrahedron* **2002**, *58*, 8219–8226.

[9] D. E. Pearson, M. G. Frazer, V. S. Frazer, L. C: Washburn, *Synthesis* **1976**, *9*, 621–623.

[10] X. Yin, J. Chen, R. A. Lalancette, T. B. Marder, F. Jäkle, *Angew. Chem. Int. Ed.* **2014**, *53*, 9761–9765; *Angew. Chem.* **2014**, *126*, 9919–9923.

[11] Z. Hu, J. L. Atwood, M.P. Cava, *J. Org. Chem.* **1994**, *59*, 8071–8075.

[12] A. Lik, L. Fritze, L. Müller, H. Helten, *J. Am. Chem. Soc.* **2017**, *139*, 5692–5695.

2.6 Catalytic Silicon/Boron Exchange Involving Aryldichloroboranes

In recent years, π-conjugated organoboranes have been of particular interest in material science. The incorporation of the vacant p-orbital of boron into the main chain of organic polymers, thus forming inorganic-organic hybrid polymers with p-π conjugation, has proven to be a versatile strategy to alter the optical and electronic properties of conjugated macromolecular materials.[1,2] These properties are often significantly enhanced as compared to their purely organic congeners and enable applications for organic (opto)electronics, bio-imaging and for sensing purposes.[2-6] In the past, the combination of electron-deficient trivalent borane moieties with electron rich building blocks such as thiophene has been extensively studied.[4-6] The synthesis of extended organoboranes of such type can be performed e.g. via C-C or B-C coupling reactions. A sophisticated method to obtain organoboranes featuring a B-C_{aryl} linkage was reported by Jäkle using distannyl compounds in combination with diboryl species. This method can also be used for the synthesis of oligomers and polymers via tin/boron exchange polycondensation under mild reaction conditions.[7] However, major drawbacks of this reaction procedure are the pronounced high toxicity of the used organotin compounds as well as the limitation to an AA//BB type polycondensation reaction caused by the high reactivity of both the Me_3Sn- and BBr_2-group, which can also lead to tin-methyl cleavage as side reaction. As an alternative, our group recently reported Si/B exchange condensation reactions as a highly efficient, environmentally benign B-C bond formation method (Scheme 2.6.1).[6] The lower reactivity of silylated compounds **1** (Si/B exchange) in comparison to stannylated compounds (Sn/B exchange) in combination with the borylated coupling partner **2** resulted in the need for a suitable catalyst to effectively accelerate the reaction. We observed that the electrophilic silyl species Me_3Si-OTf and especially Me_3Si-NTf_2 served for that purpose. For thiophene-based systems, in the absence of a catalyst, incomplete conversion to **3a** was observed even after 12 days. The use of Me_3Si-OTf (TMS-OTf, catalyst **A**, 5 mol%) effectively accelerated the reaction to a conversion of 95% after 5 days. However, the use of the stronger electrophilic reagent Me_3Si-NTf_2 (TMS-NTf_2, catalyst **B**, 5 mol%) proved to be even more efficient and complete consumption of 2-trimethylsilylthiophene (**1a**) and 2-(dibromoboryl)thiophene (**2a**) was observed after 72 minutes.[6a]

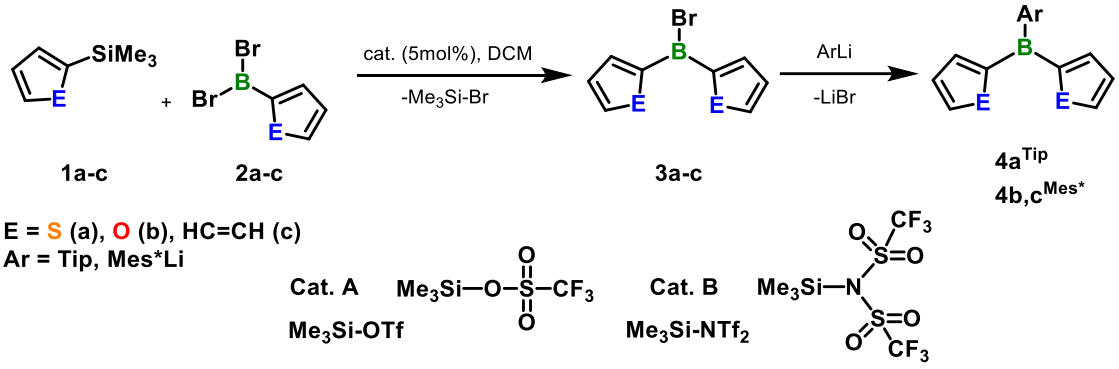

Scheme 2.6.1. Synthesis of **4a-c** via catalytic Si/B exchange.

The reaction progress can be monitored via ^{1}H-NMR spectroscopy and evaluated by the formation of trimethylsilylbromide (Me_3Si-Br, TMS-Br) as condensation product (chemical shift: 0.60 ppm) which can be easily removed in vacuo. For furan-based compounds, full and selective conversion of **1b** and **2b** to **3b** was observed within 2 hours. For the less reactive phenyl species **1c** and **2c**, higher catalyst loadings (25 mol%) and increased substrate concentrations (4 M instead of 1 M) led to 95% conversion within 3 days. In order to obtain air- and moisture stable compounds, the coupling products **3a-c** were further reacted with bulky substituents such as 2,4,6-triisopropylphenyllithium (TipLi) or 2,4,6-tri-*tert*-butylphenyllithium (supermesityl, Mes*Li) to obtain effective kinetic stabilization and protection of the boron centers of **4a-c** from nucleophilic attacks.[6]

Furthermore, we applied this reaction strategy to synthesize furyl- and thienylborane oligomers and polymers via careful monoborylation of disilylated compounds **5a,b** to bifunctional monomers **6a,b** (Scheme 2.6.2, *Route I*). Subsequent catalytic polycondensation reaction thereof afforded oligomers **7a,b** which precipitated from the reaction mixture. After post-modification with bulky substituents, oligomers **8** were obtained in low (**8b^{Mes*}**, 13%) to moderate yields (**8a^{Tip}**, 35%) with an average molecular weight of 1600 Da (estimated via gel permations chromatography, GPC) corresponding to a degree of polymerization of 4 (**8a^{Tip}**) and 5 (**8b^{Mes*}**), respectively.[6]

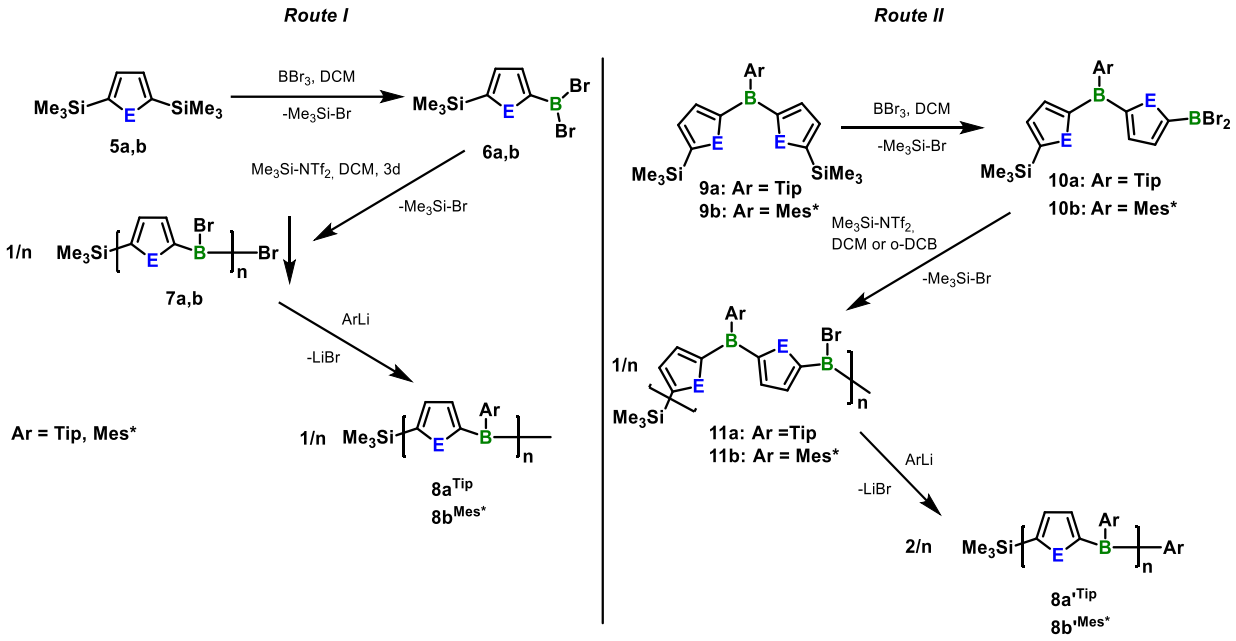

Scheme 2.6.2. Synthesis of oligomers **8a^{Tip}** and **8b^{Mes*}** (*Route I*) and polymers **8a'^{Tip}** and **8b'^{Mes*}** (*Route II*).

The molecular weight could be increased when changing from dichloromethane to more polar *o*-dichlorobenzene (*o*-DCB). With regard to the solubilizing effect of the Tip or Mes* group, we additionally performed the reaction starting from **9a,b** (Scheme 2.6.2, *Route II*). After synthesis of the bifunctional compounds **10a,b** via careful addition of BBr_3 and addition of the catalyst, the forming polymer chain **11a,b** should therefore show increased solubility since it contains one of the bulky groups at every second boron atom. Indeed, the obtained polymeric compounds **8a'^{Tip},8b'^{Mes*}** revealed an increased average molecular weight (3260 Da).[6]

A plausible different reason for the limited molecular weight is the high reactivity of the B-Br bond leading to potential side reactions and decomposition pathways. The latter is even more pronounced for organoboranes in combination with furan moieties. Whereas **2a,c** can be readily synthesized, purified via distillation and stored at low temperatures, **2b** decomposes in solution and upon concentration in vacuo and thus, has to be used *in situ*. Furthermore, bifunctional compounds **6a,b** as well as **10a,b** tend to react with themselves, even in the absence of the catalyst and thus, the level of control is limited especially for **10a** and furan-based materials **6b** and **10b** since they need to be used *in situ*. In general, the use of more stable aryldichloroboranes (vs. aryldibromoboranes) should lead to a higher level of control and should facilitate large-scale use of these compounds. For these reasons, the less reactive 2-dichloroboryl species **12a,b** in combination with **1a,b** were tested as coupling reagents (Scheme 2.6.3).

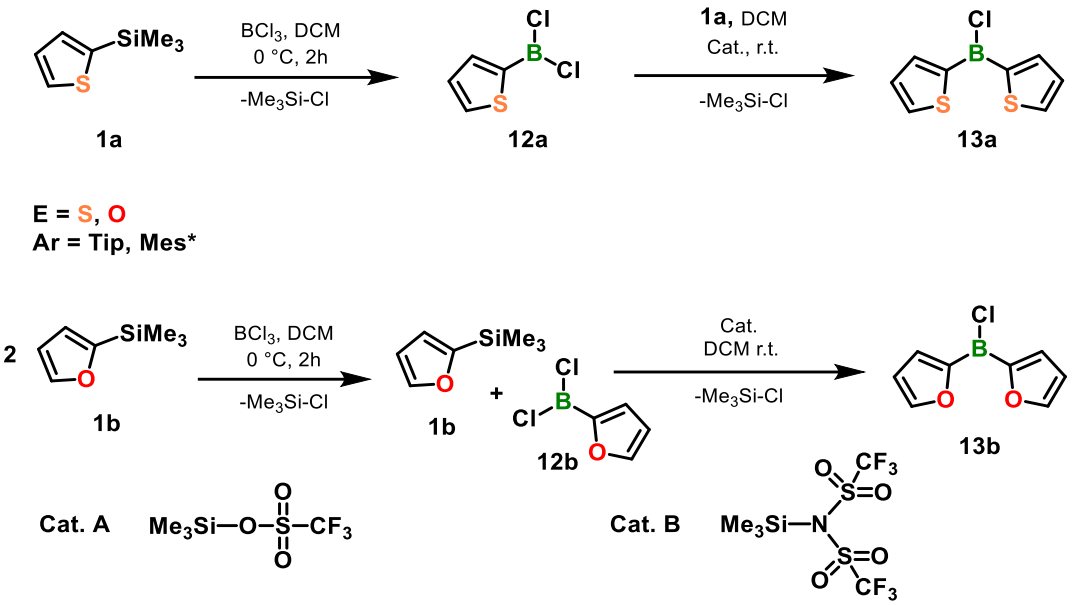

Scheme 2.6.3. Synthesis of dichloroboryl species **12a,b** and subsequent catalytic Si/B exchange reaction to **13a,b**.

Dichloroborylthiophene (**12a**) was obtained by the addition of a slight excess of a solution of trichloroborane (BCl_3, 1M) in dichloromethane to **1a** at 0 °C. After stirring for 2 hours, analysis via NMR spectroscopy indicated complete conversion, and after distillation, **12a** was obtained in an almost quantitative yield. Combining **1a** and **12a** in the absence of a catalyst led to only 5% conversion to chloro-bis(thien-2-yl)borane (**13a**) after 13 d, evidenced by the formation of Me_3Si-Cl (Appendix, Figure 5.6.1). Again, we tried to accelerate the reaction and added substoichiometric amounts of catalysts **A** (10 mol%) and **B** (10 mol%). The reaction progress was monitored via ^{1}H-NMR spectroscopy by means of the formation of the condensation product Me_3Si-Cl that gives a sharp signal at 0.45 ppm. After addition of the catalysts, evidence for the formation of only a small amount of Me_3Si-Cl was observed by ^{1}H-NMR spectroscopy within the first hour. In the case for catalyst **A**, we expected significant slower reaction rates as compared to catalyst **B** (based on observations for B-Br systems)[6] and thus increased the catalyst loading in the former case to 20 mol%. However, after 8 d, only 60 % conversion to **13a** was observed (Appendix, Figure 5.6.2). In the case for catalyst **B**, after 24 h, almost complete conversion to **13a**, evidenced by signals at 8.23 ppm (C_3-*H*), 8.00 ppm (C_5-*H*) and 7.38 ppm (C_4-*H*), was observed with only small residues of starting materials **1a** and **12a** left (Figure 2.6.1). Furthermore, a distinct signal at 7.16 ppm points to formed thiophene (**Thi**), probably as result of desilylation of **1a**. An additional signal at 0.44 ppm can be related to the formation of a C-H activation product **13a'** (Scheme 2.6.4.).

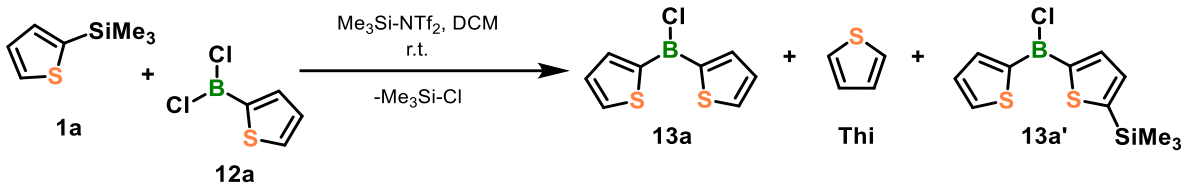

Scheme 2.6.4. Product distribution after catalytic Si/B exchange reaction of **1a** and **12a** after 24 h.

Previous studies on aryldibromoborane-based systems investigated by Dr. Artur Lik[6,8] suggested the formation of a reactive species **2a'** through the reaction of borylated compound **2a** with the catalyst Me_3Si-NTf_2 and according to our observations, this can also be transferred to aryldichloroborane systems under formation of **12a'** (Scheme 2.6.5, top). Subsequent electrophilic attack of **12a'** at the thienyl ring can then either occur at C2-position (*Si/B exchange pathway,* Scheme 2.6.5, center right) or at C5-position (*C-H activation pathway*, Scheme 2.6.5, center left) to form zwitterionic intermediates **I-1** and **I-II**. Elimination of H-NTf_2 yielded the observed species **13a'** (C-H activation product). Elimination of Me_3Si-NTf_2 from **I-II** afforded compound **13a**.

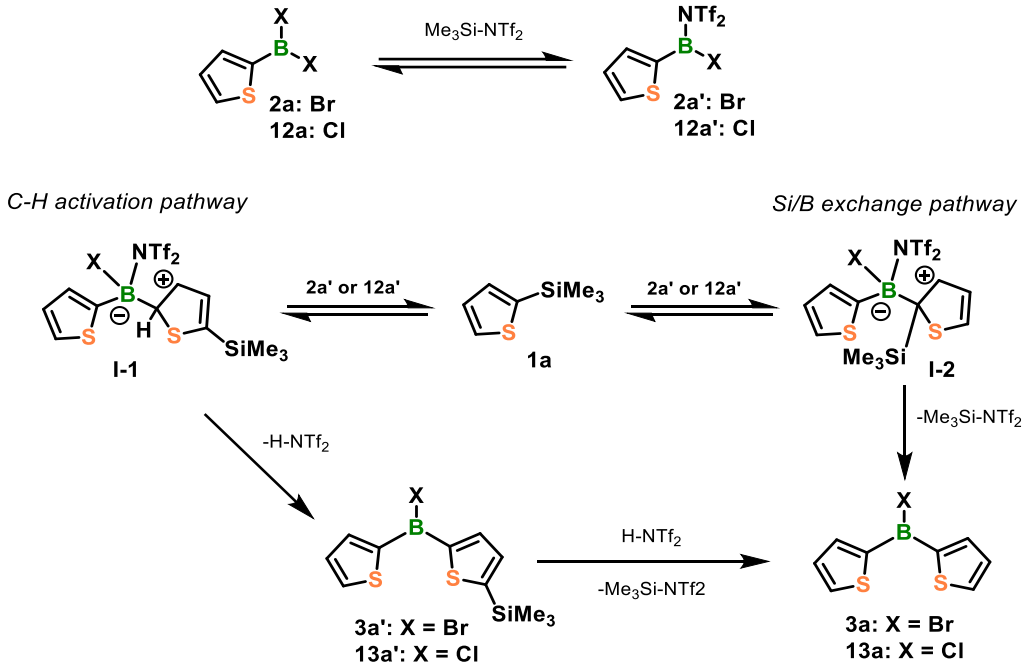

Scheme 2.6.5. Reaction between silylated compound **1a** and *in situ* formed catalytically active species **2a'**,**12a'** via *C-H activation pathway* (left) or *Si/B exchange pathway* (right) to yield compounds **3a**,**13a**.

1a was completely consumed after less than 48 hours. Interestingly, the amount of **13a'** decreases and the amount of desired compound **13a** increases slowly over time (a small amount of **13a'** was still present after 5 d). A plausible reason for this is the reaction of **13a'** with formed H-NTf_2 during the C-H activation pathway (Scheme 2.6.5, bottom). The presence of H-NTf_2 would also explain the small amount of formed thiophene.

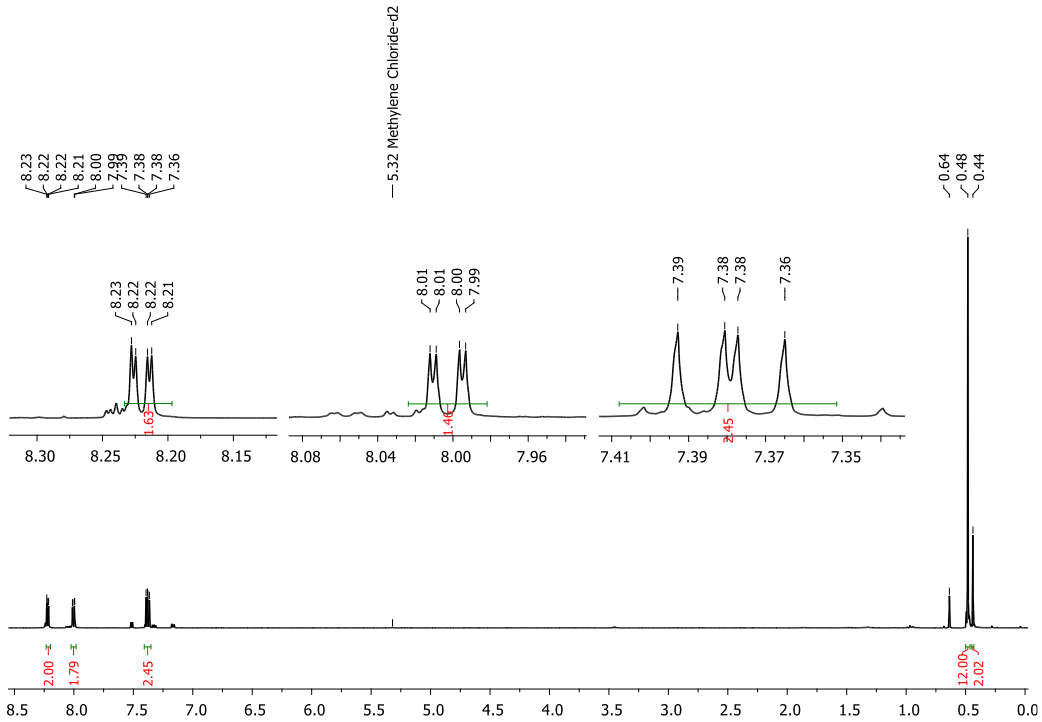

Figure 2.6.1. ^{1}H NMR spectrum of the reaction between **1a** and **12a** in the presence of catalyst **B** (10 mol%) after 48 h.

The formation of **13a'** was proven by an independent synthesis thereof via combining 2,5-bis(trimethylsilyl)thiophene (**5a**) and **12a** in the presence of catalytic amounts of catalyst **B** (10 mol%) in DCM (Scheme 2.6.6) and comparing the signals in the recorded ^{1}H NMR spectrum (Appendix, Figure 5.6.5). Full conversion to **13a'** was obtained within 24 hours.

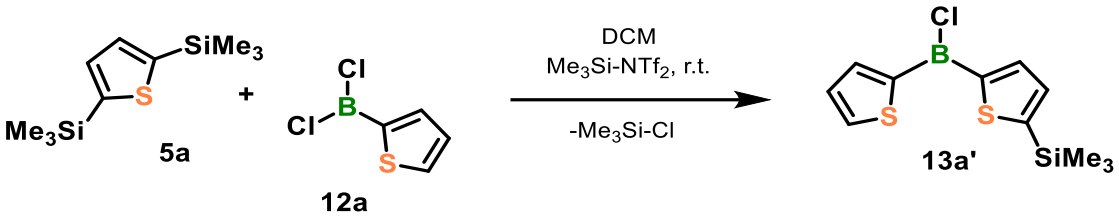

Scheme 2.6.6. Synthesis of **13a'**.

We additionally carried out an analogous reaction with furan based starting materials **1b** and **12b**. The reaction of **1b** with a solution of BCl_3 (1M in DCM) added at 0 °C afforded **12b** in a clean and selective reaction. The latter was stable in solution for several hours and showed no sign of decomposition in DCM. Upon concentration in vacuo, a black solid was formed, which was not soluble in common organic solvents, eventually resulting in complete decomposition of the compound. In an optimized reaction procedure, we reacted two equivalents of **1b** with one equivalent BCl_3 (1M in DCM) to generate an equimolar ratio of **1b** and **12b** *in situ* (Scheme 2.6.7; for ^{1}H NMR of in situ prepared **12b** see Appendix, Figure 5.6.8). After addition of catalyst **A** (20 mol%), complete conversion to chloro-bis(fur-2-yl)borane (**13b**) was observed within 48

hours (Appendix, Figure 5.6.9). The use of catalyst **B** (10 mol%) led to a complete conversion to **13b** with respective ^{1}H NMR signals at 7.88 ppm (C_3-*H*), 7.75 ppm (C_5-*H*) and 6.62 ppm (C_4-*H*) within 19 hours (Figure 2.6.2). The faster reaction time for furan vs. thiophene based systems confirms the expected higher reactivity of the Si/B exchange reaction for more electron rich systems. However, small furan signals at 6.4 ppm and 7.45 ppm (approx. less than 5%) point to an occurring desilylation reaction of **1b,** which probably originates as side reaction during the synthesis of **12b** (probably as a result of small HCl impurities in the BCl_3 solution). When the reaction is carried out with higher catalyst loading (20 mol%), complete consumption of **1b** was observed within 3 h. In this case, a small signal at 0.42 ppm again points to the formation of a C-H activation product **13b'**, which was completely consumed within 24 h.

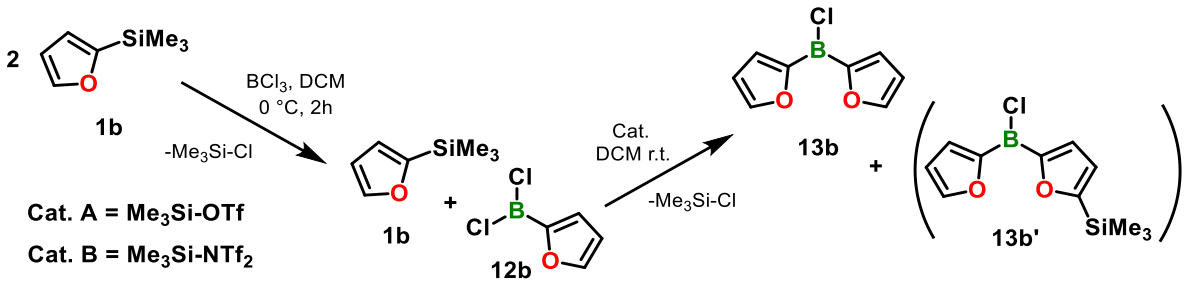

Scheme 2.6.7. In situ generation of a mixture of **1b** and **12b** and subsequent catalytic Si/B exchange reaction.

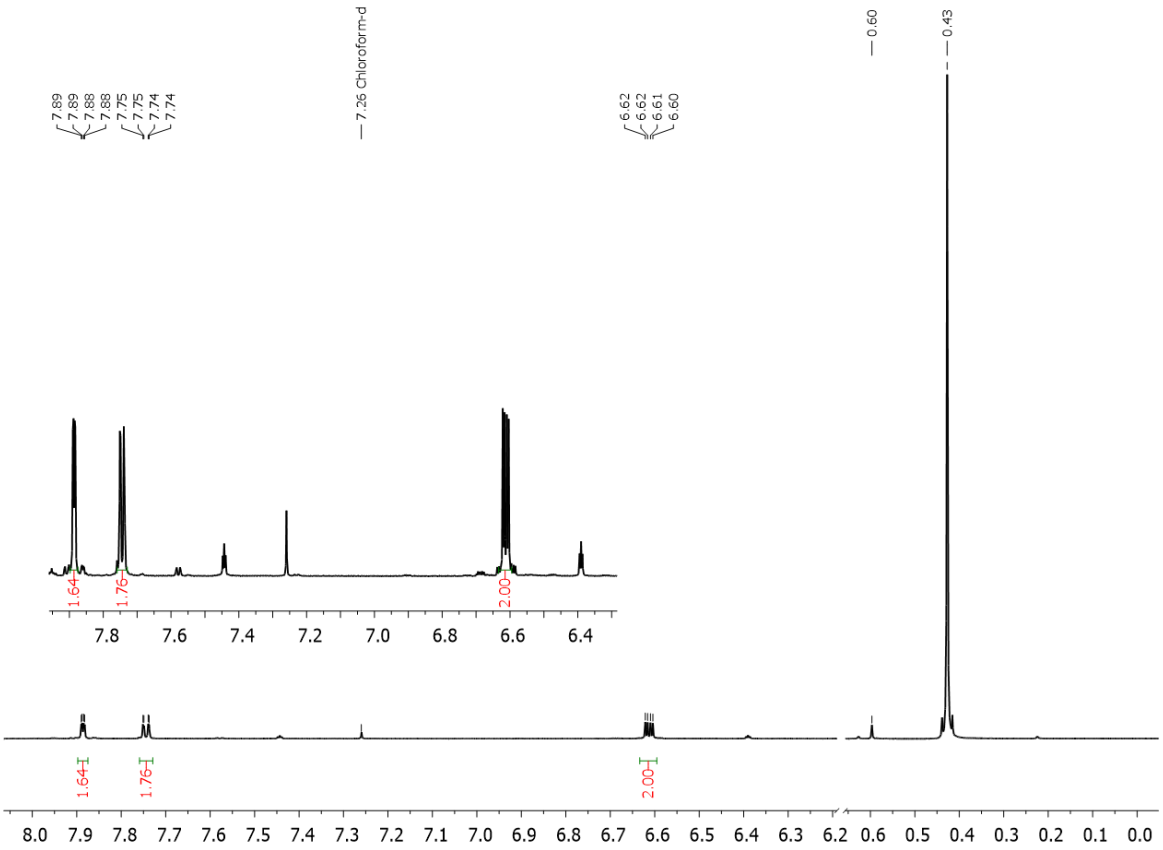

Figure 2.6.2. Synthesis of chloro-bis(fur-2-yl)borane (**13b**) via catalytic Si/B exchange.

We then attempted the reaction for phenyl species **1c** and 1**2c** with catalyst **B** (20 mol%) at ambient temperature (Scheme 2.6.8).

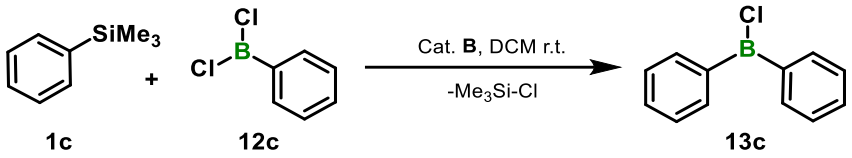

Scheme 2.6.8. Synthesis of **13c.**

These phenyl species are less activated compared to the thiophene and furan based compounds, and indeed, condensation proceeded significantly slower. Despite a clean and selective reaction to **13c**, conversion was only up to 60 % after 7 days (Appendix, Figure 5.6.12).

Based upon these results, $Me_3Si\text{-}NTf_2$ (cat. **B**) seems to be a suitable catalyst for the Si/B exchange for both thiophene and furan based systems with BCl_2 groups. Nevertheless, the reaction rate is significantly lower in comparison to the more reactive B-Br based systems (72 min for **1a**/**2a** vs. approx. 48 h for **1a**/**12a**; < 2 h for **1b**/**2b** vs approx. 19 h for **1b**/**12b**). In general, the B-Cl bond is more stable than the B-Br bond. This leads on the one hand to a higher stability of the respective boryl species but on the other hand to a significantly slower reaction rate. In order to accelerate the condensation reaction, we considered silver based catalysts as interesting candidates since the silver(I) cation has a high affinity to the chloride anion (or a halide in general). Furthermore, silver salts in combination with weakly coordinating anions (WCA)[9] for halide abstraction are easily accessible.[9,10] We performed our studies with different catalysts (Figure 2.6.3), including silvertriflate (AgOTf, cat. **C**), silver triflimide ($AgNTF_2$, cat. **D**) as well as silver tetrakis(perfluoro-*tert*-butoxy)aluminate ($Ag[AlOC(CF_3)_3)_4]$, cat. **E**). We additionally used $Me_3Si\text{-}F\text{-}Al(OC(CF_3)_3)$ (cat. **F**) as alternative which may react as a silylium species while forming a more weakly coordinating anion compared to that in catalysts **A** and **B**. Catalyst **F** was synthesized and provided by Krossing and co-workers.[10c] They also presented detailed studies on structure and reactivity of poly- and perfluorinated alkoxy ligands.[10]

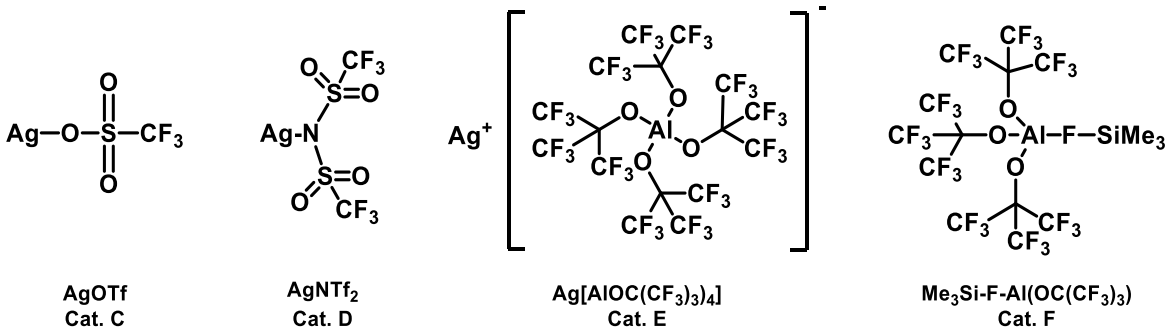

Figure 2.6.3. Different catalysts used for Si/B exchange reactions.

Based on the high affinity of the silver cation to halides, we considered that the silver cation will react with **12a** to form silver chloride, probably a borinium cation[11] **12a'** and the respective anion **Y**$^-$, thus initiating the reaction (Scheme 2.6.9). Silver cations are prone to light-induced decomposition and therefore, we performed the reactions under light exclusion. Depending on the size and electronic effects, the anion can be either bound to the boron atom to afford **12a''** which can be considered as masked borinium cation or not bound to afford **12a'**.[11] The latter case is more pronounced for the weaker coordinating anions of catalysts **E** and **F**.

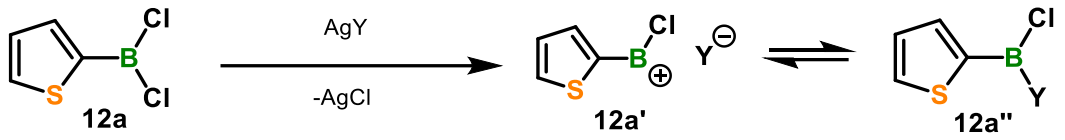

Y = OTf, NTf_2, $Al(OC(CF_3)_3)_4$

Scheme 2.6.9. Reaction of **12a** with silver-based catalysts **C-E**.

The above described results confirm that catalysts **A** and **B** are able to catalyze the Si/B exchange reaction of aryldichloroboranes, but significantly slower compared to aryldibromoboranes. The next step is to evaluate the reactivity of the four new catalysts with special focus on the use of silver cations instead of the silyl species (Cat. **C**, **D** vs. Cat. **A**, **B**), the use of weaker coordinating anions in combination with silver cations (Cat. **E** vs. Cat. **C**, **D**) and the use of an electrophilic silyl compound forming a weaker coordinating anion (Cat. **F** vs. Cat. **A**, **B**). We performed the reaction between **1a** and **12a** under our standard reaction conditions (1M in DCM) with substoichiometric amounts of catalysts **C-F** (5 mol%). The reactions with catalysts **C-E** were performed under light exclusion. Catalyst **C** only showed poor solubility in both dichloromethane and benzene and almost no conversion was observed even after several days, evidenced by the formation of only a small amount of Me_3Si-Cl. Interestingly, the formation of TMS-OTf (0.55 ppm) was observed by ^{1}H-NMR spectroscopy which probably forms as catalytically active species after formation of silver chloride (Appendix, Figure 5.6.14). On the other hand, catalyst **D** showed enhanced solubility and the condensation reaction (cf. Scheme 2.6.4) proceeded fast and was complete within 5 h, as evidenced by almost complete consumption of **1a** observed via ^{1}H NMR spectroscopy (Figure 2.6.4).

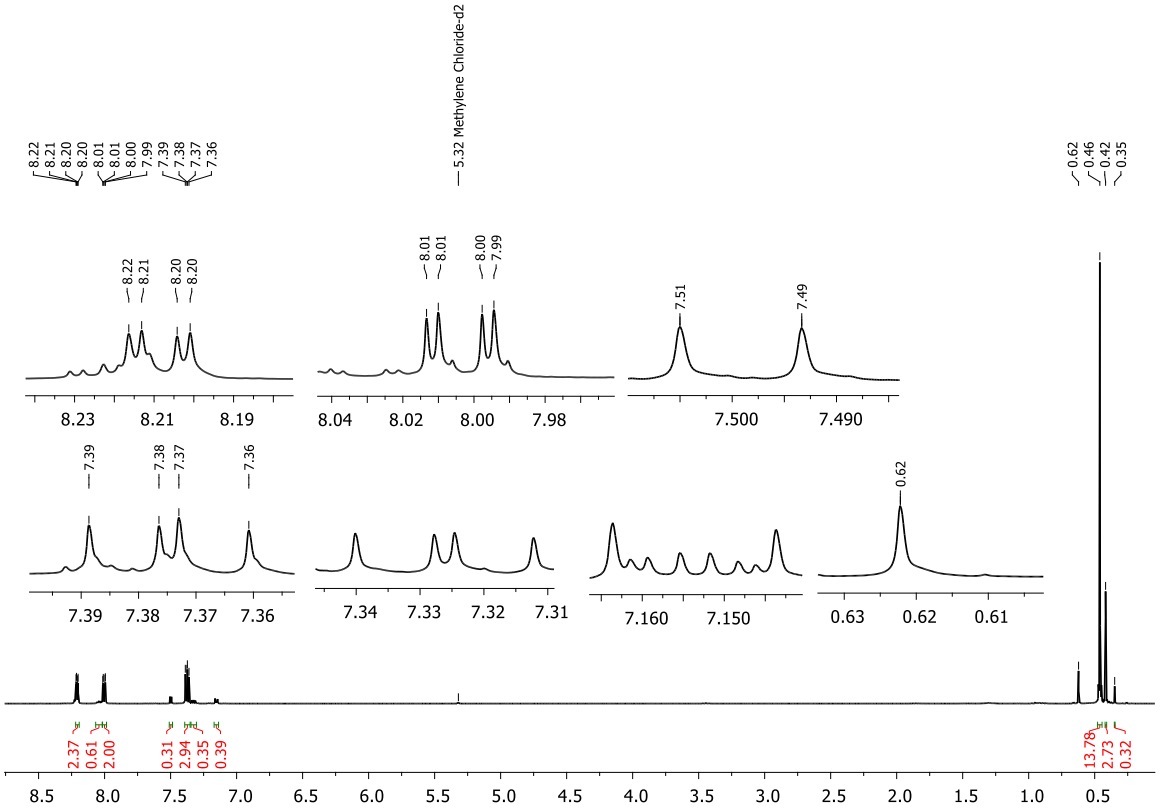

Figure 2.6.4. ^{1}H NMR spectrum of a mixture of **1a** and **12a** in the presence of catalyst **D** (5 mol%) after 5 h.

^{1}H NMR spectroscopy evidenced the formation of TMS-NTf_2 (0.62 ppm). This observation additionally points to our suggested chloride abstraction from **12a** by the silver cation. Subsequently, the anion needs a Me_3Si cation source to form the catalytically active species Me_3Si-NTf_2, which is probably achieved by the reaction with **1a** under formation of the product **13a** (Scheme 2.6.10, also see Scheme 2.6.5). Furthermore, a small signal for thiophene (7.16 ppm) and the C-H activation product (0.42 ppm) was observed. Interestingly, according to the conversion of the starting materials (5 h vs 24 h for cat. **B**), the reaction proceeds even faster as compared to the reaction with pure Me_3Si-NTf_2 (cat. **B**), which can be considered as catalytically active species, although in the case for catalyst **D**, this species is formed *in situ*. Usually, if Ag-NTf_2 is considered as precatalyst, a certain period of activation time should cause an induction period as compared to pure Me_3Si-NTf_2 (unless the activation of the precatalysts is very fast, which seems to be the case). A possible reason for the faster reaction rate might be that some kind of silver-sulfur interaction take place.

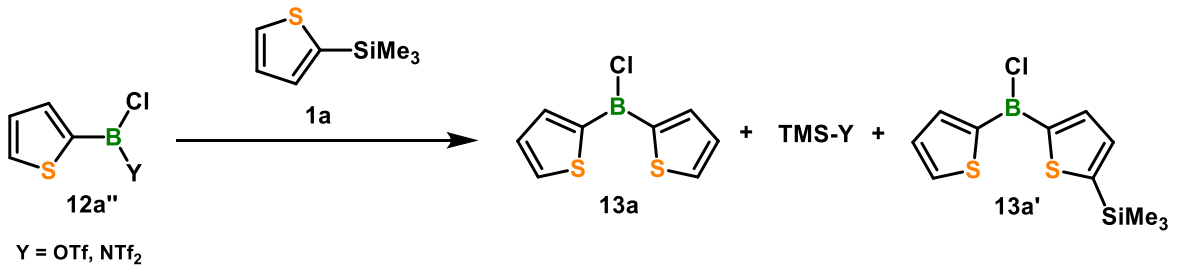

Scheme 2.6.10. Reaction of **12a''** with **1a** under formation of the catalytically active species TMS-Y.

Catalyst **E** showed excellent solubility in dichloromethane and after the catalyst (5 mol%) was added to the mixture of **1a** and **12a**, precipitation of a solid, probably silver chloride was observed immediately. Analysis via ^{1}H NMR spectroscopy revealed a complete consumption of the starting materials within less than 10 minutes, impressively demonstrating the high reactivity of the catalyst. However, the aromatic region of the recorded ^{1}H NMR spectrum revealed the formation of by-products (Figure 2.6.5).

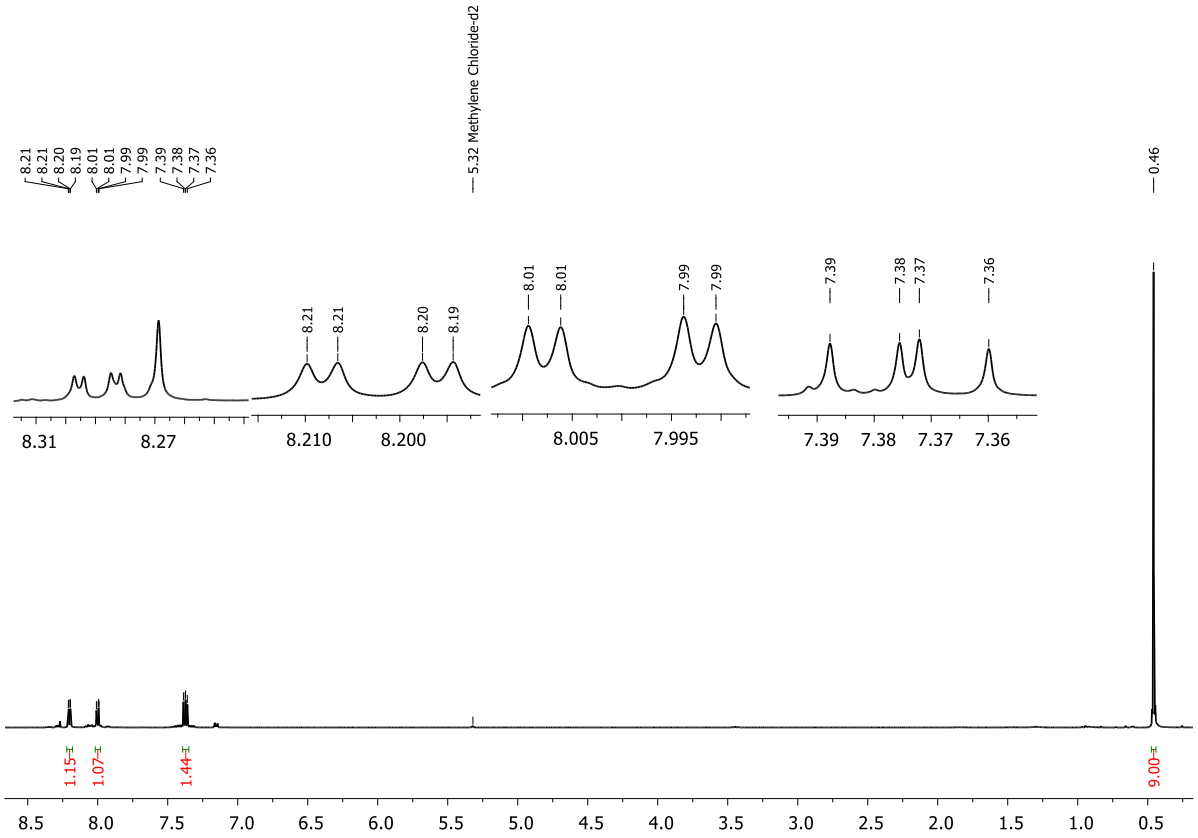

Figure 2.6.5. ^{1}H NMR spectrum of a mixture of **1a** and **12a** in the presence of catalyst **E** (5 mol%).

Evaluation of the signals suggested desilylation as well as C-H activation with subsequent fast condensation to give **13a''** as occurring side reactions (Scheme 2.6.11, top). This observation is evidenced by the characteristic signal for formed thiophene (multiplet at 7.16 ppm, approx. 15%) as well as a sharp signal for the protons of the central thiophene ring of **13a''** (8.27 ppm). Nevertheless, overall integration of the signals confirmed **13a** as major product. The formation

of **13a''** as side product was evidenced by concerted synthesis thereof via **5a** and two equivalents of **12a** in dichloromethane (Scheme 2.6.11, bottom, cf. Appendix Figure 5.6.17).

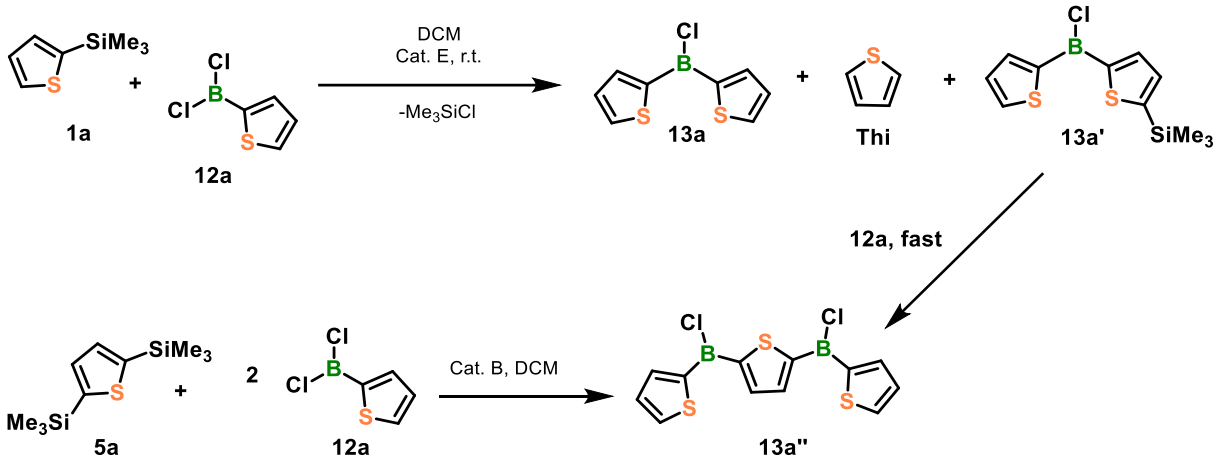

Scheme 2.6.11. Top: Catalytic Si/B exchange reaction between **1a** and **12a** and observed product distribution after 1 h 40. Bottom: Synthesis of 13a'' via catalytic Si/B exchange reaction between **5a** and 2 equivalents **12a**.

In order to avoid the fast follow-up reaction to **13a''**, the reaction was repeated at 0 °C and -78 °C, respectively. Indeed, by comparing the recorded ^{1}H NMR spectra at room temperature, 0 °C and -78 °C, effective suppressing of **13a''** formation can be observed for the reactions at both lower temperatures. Nevertheless, the formation of the C-H activation product **13a'** was observed both at 0 °C and -78 °C (Appendix, Figure 5.6.18). For comparison, catalyst **E** (5 mol%) was also added to a mixture of **1a** and **2a** (Thi-BBr_2). As expected, the reaction was also complete after less than 10 minutes. Analogous side products as described above were observed by ^{1}H NMR spectroscopy (Appendix, Figure 5.6.19).

To prevent any possible C-H activation pathway, the starting materials were derivatized with a methyl group in 5-position. Therefore, **1a^{Me}** was synthesized by lithiation of 2-methylthiophene and subsequent addition of Me_3Si-Cl. Borylation thereof with a solution of BCl_3 in dichloromethane afforded **12a^{Me}** in high yield (Appendix, Figs. 5.6.21-22). Compounds **1a^{Me}** and **12a^{Me}** were then reacted under standard reaction conditions in the presence of catalyst **E** (5 mol%) under light exclusion (Scheme 2.6.12).

Scheme 2.6.12. Synthesis of **13a^{Me}** via catalytic Si/B exchange of **1a^{Me}** and **12a^{Me}**.

Full and selective conversion to **13a^{Me}** was obtained within minutes. The recorded ^{1}H NMR spectrum showed complete consumption of the starting materials as well as no sign of desilylation or C-H activation (Figure 2.6.6). In the aliphatic region, only one signal for TMS-Cl

(0.43 ppm) evidenced a clean and selective reaction to **13a^{Me}**. The two signals in the aromatic region at 7.94 ppm and 6.98 ppm are assigned to the thiophene protons and the singlet at 2.62 ppm to the methyl protons.

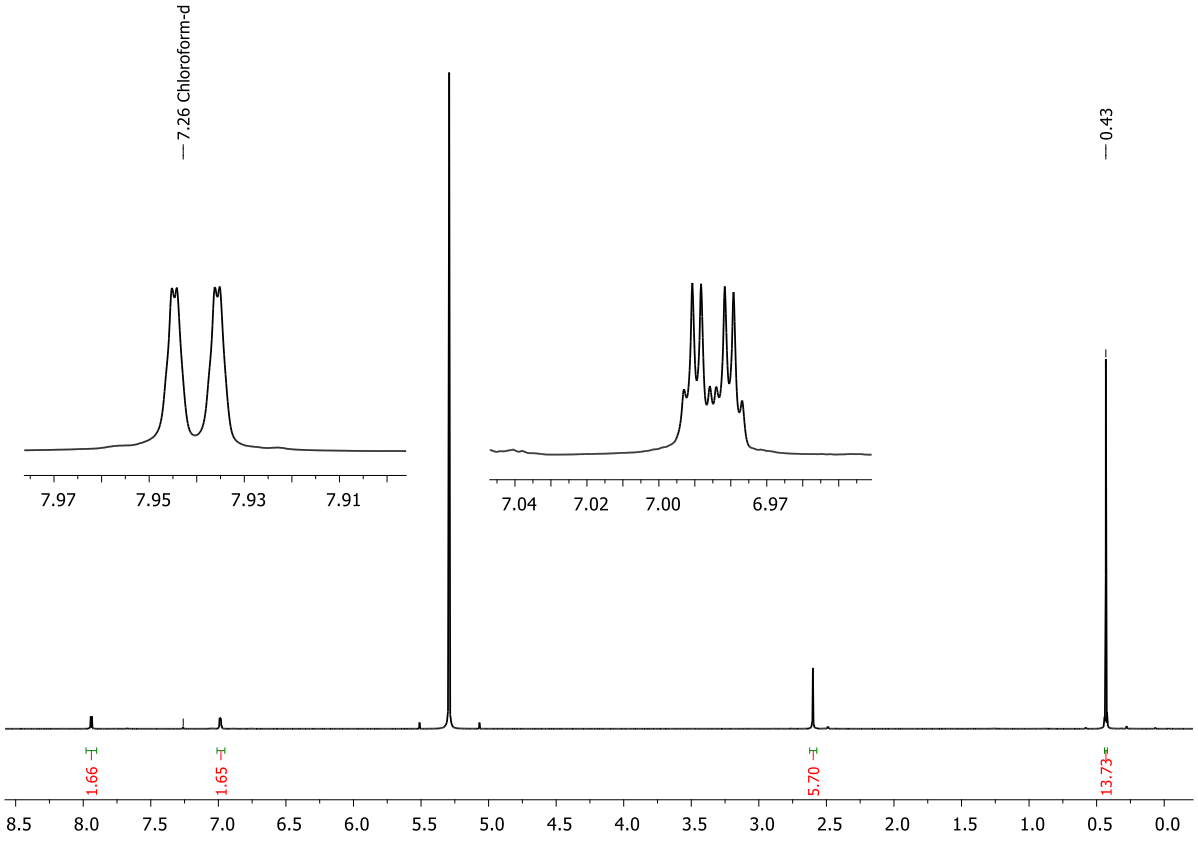

Figure 2.6.6. ^{1}H NMR spectrum of a mixture of **1a^{Me}** and **12a^{Me}** in the presence of catalyst **E** (5 mol%).

Similar results were obtained when catalyst **F** (5 mol%) was used. Again, full consumption of the starting materials was observed within minutes and **13a** was formed as major product beside thiophene and **13a''**. Evaluation of the signals in the recorded ^{1}H NMR spectrum indicated a smaller amount of side products (Appendix, Figure 5.6.25). The same was true for the reaction between **1a** and **2a** (Appendix, Figure 5.6.27). The reaction with methyl-derivatized compounds afforded a clean and selective conversion to **13a^{Me}**. As described for catalyst **E**, C-H activation was effectively suppressed (Appendix, Figure 5.6.29).

The obtained results gave some interesting insights. First, the use of a silver cation instead of the electrophilic silyl species featuring the same anion led to a faster reaction rate in the former case (Cat. **D** > Cat. **B**). However, for cat. **D**, precipitation confirmed the formation of silver chloride and the recorded ^{1}H NMR spectrum indicated the formation of $Me_3Si\text{-}NTf_2$. These observations led to the assumption that in both cases, $Me_3Si\text{-}NTf_2$ probably reacts as the catalytically active species. Usually, the *in situ* formation of the catalytically active species should lead to a slower reaction rate due to an induction period (in this case, $Ag\text{-}NTf_2$ is acting as precatalyst). A potential explanation for this might be derived from the hard and soft acid

and bases concept by Pearson (HSAB theory),[12] suggesting a strong affinity of silver (soft acid) to the sulfur (soft base). Maybe the precipitated silver chloride plays a role in mediating the catalytic process. The use of catalysts **E** and **F**, both featuring weaker coordinating anions (vs. Cat. **B**, **D**) led to significantly faster reaction rates. These observations mean that both weaker coordinating anions strongly accelerate the catalytic Si/B reaction independently from the chosen cation. However, in the case of cat. **E**, the amount of side products was larger as for cat. **F**, pointing to at least some influence of the respective cation. The reactivity of the catalysts featuring the Me_3Si cation increase in the order A << B << F, which means that the more electrophilic and more weakly coordinating, the faster the reaction rate. To get a better understanding of the interaction between the catalyst and both starting materials, single **1a** and single **12a** were combined with both catalysts. Interestingly, when catalyst **E** (5 mol%) was added to a solution of **1a** in DCM, desilylation occurred and a considerable amount of thiophene (15%) was obtained (Appendix, Figure 5.6.31). No thiophene formation was observed when catalyst **F** and **1a** were mixed. These observations confirm some influence of the silver cation in combination with thiophene based systems. When cat. **E** was added to **12a**, precipitation occurred immediately. Furthermore, a small new signal arises in the ^{11}B NMR spectrum (46.3 ppm) while the ^{1}H NMR spectrum remained virtually unchanged (Appendix, Figure 5.6.32). The reaction of catalyst **F** with **12a** led to the formation of TMS-Cl (Appendix, Figure 5.6.35).

Concerning the above-mentioned high affinity of silver cations to sulfur based on the HSAB theory, we additionally investigated furan based systems. The interaction between silver (soft acid) and oxygen (hard base) should be less pronounced. Furthermore, previous results in our group concerning the catalytic Si/B exchange for aryldibromoboranes indicated a faster reaction for more electron-rich furylboranes.[6] First, we compared again the influence of the silver cation (Cat. **D**) with the electrophilic silyl species (Cat. **B**). The reaction of **1b** with **12b** with catalyst **D** afforded a clean and selective reaction to the desired condensation product **13b** within 1.5 h (Scheme 2.6.13). Again, the reaction rate is significantly faster as compared to the reaction with cat. **B** (approx. 19 h), suggesting some influence of the precipitated silver chloride or of potential silver-oxygen interactions. The latter effect should be less pronounced according to HSAB theory as compared to silver-sulfur interactions.

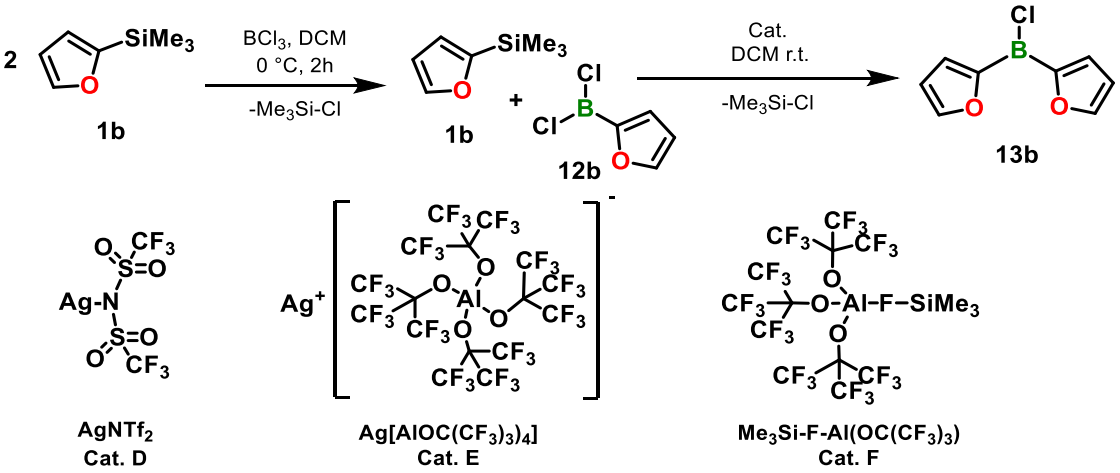

Scheme 2.6.13. Catalytic Si/B exchange reaction to afford **13b**.

We then employed catalyst **E** and to our delight, the reaction proved to be highly efficient and selective. Full conversion to **13b** was obtained within less than 20 minutes, and no evidence for desilylation was observed by ^{1}H NMR spectroscopy (Figure 2.6.7).

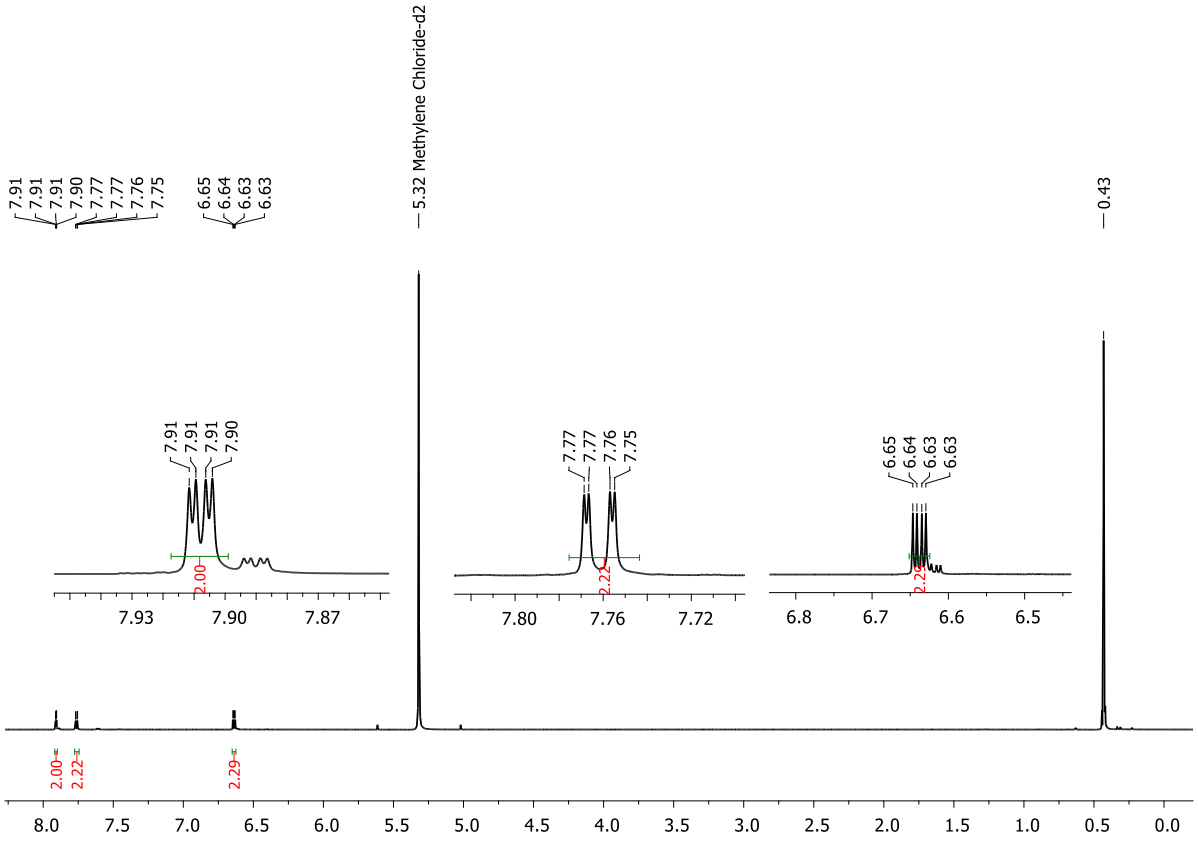

Figure 2.6.7. ^{1}H NMR spectrum of a mixture of **1b** and **12b** in the presence of catalyst **E** (5 mol%).

Interestingly, combining catalyst **E** with only **1b** indicated no evidence for desilylation as pronounced (and observed) for **1a** (Appendix, Figure 5.6.33), which might also be explained with the HSAB concept. Additionally, the reaction was carried out with methylated starting materials **1b^{Me}** and **12b^{Me}** (Scheme 2.6.14). The synthesis of **1b^{Me}** was carried out according

to literature.[13] The *in situ* generation of **12b^{Me}** was performed by reacting two equivalents of **1b^{Me}** with a solution of BCl_3 in dichloromethane at 0 °C to obtain a 1:1 mixture of both coupling reagents (Appendix, Figure 5.6.40). After addition of catalyst **E** (5mol%), complete consumption of the starting materials was observed within 10 minutes. As expected, no side products were observed in the recorded ^{1}H NMR spectrum (Appendix, Figure 5.6.42).

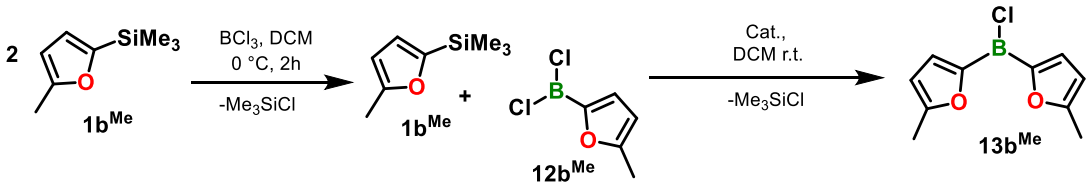

Scheme 2.6.14. *In situ* generation of a mixture of **1b^{Me}** and **12b^{Me}** and subsequent catalytic Si/B exchange.

The same results and observations were obtained when catalyst **F** was used. Again, complete consumption of the starting materials was observed within less than 1 hour (Appendix, Figs 5.6.44-46). Interestingly, the use of an excess of **1b** or **1b^{Me}** in combination with **12b**/**12b^{Me}** led to trifurylborane formation to a small extent as evidenced by ^{11}B-NMR spectroscopy (δ = 34.0 ppm for Fur_3B, 33.0 ppm for $MeFur_3B$) and comparing to chemical shifts reported by *Nöth et al*.[14] This was not observed when an excess of **1a** was added to **12a**. In this case, a multitude of signals were observed in the recorded ^{1}H NMR spectrum and they could not be assigned to the desired trithienylborane. Furthermore, the reaction was performed with **1b** and 2-(dibromoboryl)furan (**2b**) in the presence of catalyst **E**. The reaction proceeded extremely fast and after less than 7 minutes, full conversion to **3b** was observed (Appendix, Figure 5.6.47).

In general, the combination of furan moieties with borane has been scarcely explored in the past due to the high reactivity of the resulting species and synthetic challenges. In the above described reactions, the use of dichloroboryl species instead of dibromoboryl species strongly simplifies the use of such compounds since they can be generated and stored in solution for at least several hours or used *in-situ*. Furthermore, **12b^{Me}** can be purified by distillation and stored neat at low temperatures. The employed catalysts **D-F** are highly efficient and, in comparison to thiophene based systems, yielded highly selective reactions. As a result, the combination of dichlorofurylboranes with silver-based catalysts seems to be highly advisable.

Previous results have shown that the reactivity of less activated phenyl species was comparably low and therefore, we performed the reaction of **1c** and **12c** with the more active catalyst **E** (5 mol%). Monitoring the reaction progress via ^{1}H-NMR spectroscopy revealed proceeding desilylation processes occurring over time, which can be evaluated by the formation of benzene (sharp signal at 7.38 ppm). The condensation product **13c** was only obtained to a small extent and the recorded ^{1}H-NMR spectrum after 72 hours showed only

36% conversion of the boryl species although **1c** was completely consumed (Appendix, Figure 5.6.49). Increasing the catalyst loadings to 15 mol% led to a slightly increased degree of conversion, but still desilylation significantly occurs. Rising the temperature to 70 °C with a catalyst loading of 20 mol% to favor the condensation reaction rather than desilylation led to complete decomposition and a black solid was formed. The related ^{1}H NMR spectrum indicated benzene formation (Appendix, Figure 5.6.51).

In order to extend the number of accessible compounds and the opportunity to tune the electronic properties through the hetarene ratio, we additionally performed Si/B exchange reactions to obtain mixed thienyl-/furyl-/ phenylborane species. Therefore, we performed reactions with all possible combinations of **1a-c** and **12a-c**. In the absence of a catalyst, no condensation reaction was evidenced by ^{1}H-NMR spectroscopy after 18 hours which enables a high level of control. In the following, substoichiometric amounts of catalysts **B**, **E** and **F** were added to the reaction mixtures to accelerate the condensation reaction (Scheme 2.6.15).

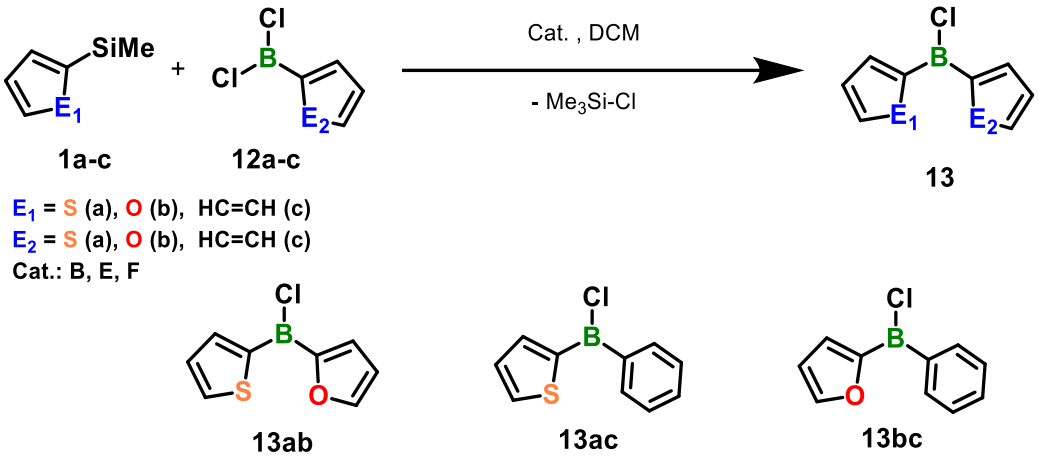

Scheme 2.6.15. Synthesis of mixed chloro-(het)arylboranes **13**.

Major differences can be seen depending on the position of the Ar-$SiMe_3$ and Ar-BCl_2 functionalities at the respective (het)arene. The use of catalyst **B** (10 mol%) for the reaction mixtures of **1a/12b**, **1a/12c, 10b/12c** and **1b/12a** led to a clean and selective reaction to **13ab**, **13ac**, **13bc** and **13ba** within 24 hours (see Appendix, Figs 5.6.53-60). Interestingly, the reaction between the less electron rich phenyl species **12c** and **1a/1b** proceeds extremely fast within 24 hours, while the reaction between **1c** and **12a** to afford **13ca** was not complete even after three days (Appendix, Figure 5.6.61). The same trend was observed for the combination of **1b/12c** vs. **1c/12b**. The reaction of **1b** with **12c** was complete within less than 24 hours while the latter only had a conversion of approx. 50% after 3 days (Appendix, Figure 5.6.62). The combination of **1b** and **12a** or **1a** and **12b** afforded chloro-(2-thienyl-2-furyl)borane **13ba** within less than 24 hours and analysis via ^{1}H-NMR spectroscopy indicated some minor formation of a C-H activation side product. Based on these observations, an ideal combination of **1** and **12**

is suggested when the silylated compound is more electron rich (Fur > Thi > Ph) and the borylated compound is less electron rich (Ph > Thi > Fur). The combination of **1c** with both **12a**/**12b** is not appropriate. The $^{11}B\{^{1}H\}$ NMR resonances of compounds **13** are between 41.7 ppm and 62.8 ppm (Table 2.6.1). For mixed compounds the ^{11}B resonances can be estimated, which means that the resonance of **13ab** appears at a chemical shift of δ = 44.7 ppm, which is in between these of **13a** (δ = 48.7 ppm) and **13b** (δ = 41.7 ppm). In the recorded $^{11}B\{^{1}H\}$ NMR spectra, a minor amount of residual borylated species was often observed, which caused a sharp signal.

Table 2.6.1. Observed $^{11}B\{^{1}H\}$ NMR shifts of compounds **12** and **13**.

Cmpd.	**12a**	**12b**	**12c**	**13a**	**13b**	**13c**	**13ab**	**13ac**	**13bc**
δ [ppm]	48.7	45.0	55.4	48.7	41.7	62.8	44.7	55.4	51.0

In comparison to catalyst **B**, the use of catalyst **E** and **F** significantly accelerates the reaction and complete conversion to **13ab**, **13ba**, **13ac** and **13bc** was observed within less than 4 hours. However, significant desilylation was obtained if **1c** was used in combination with **12a,b**. After 24 hours, complete consumption of **1c** was observed by ^{1}H-NMR spectroscopy and a sharp signal arised at 7.38 ppm, which can be assigned to forming benzene. Therefore, to obtain compounds **13ac** and **13bc** with catalysts E and F, the Si/B exchange reaction should be performed with coupling partners **1a,b** and **12c**.

In order to obtain air- and moisture stable compounds, bulky substituents were introduced as third substituent. For dithienylborane **13a**, Tip provides enough steric protection, while for furan- and benzene-based systems and mixed species, Mes* was used as even bulkier substituent (Scheme 2.6.16).

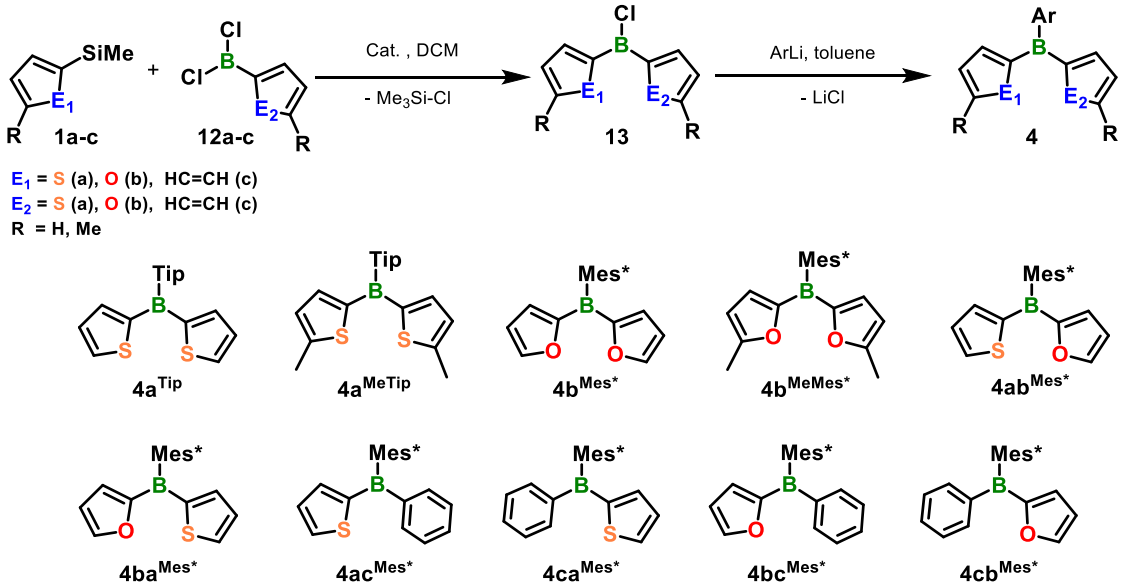

Scheme 2.6.16. Si/B exchange reaction with subsequent arylation to afford triarylboranes **4**.

After purification of the compounds via column chromatography, the triarylboranes **4** were obtained in moderate to good yields (16-56%) as colorless, crystalline solids. For thiophene based systems, the yield for reactions in which catalysts **E** and **F** have been used, is comparably lower, probably as a result of the above discussed side reactions. In comparison to their Br-substituted relatives, the yield can be slightly increased by performing the arylation reaction in a mixture of toluene and diethylether. Furthermore, for the synthesis of Tip-substituted compounds, the reaction of **13a** and **13a^{Me}** with Grignard reagent TipMgBr (instead of TipLi) gave satisfying yields. The observed ^{1}H and ^{11}B{^{1}H} NMR chemical shifts for triarylboranes **4a^{Tip}**, **4b^{Mes*}**, **4ab^{Mes*}** (and thus **4ba^{Mes*}**) agree well with the data obtained previously in our group.[6] The ^{11}B{^{1}H} NMR resonances of triarylboranes **4** appear at chemical shift in between δ = 46.2 and 56.3 ppm (Table 2.6.2).

Table 2.6.2. Observed ^{11}B{^{1}H} NMR shifts of triarylboranes **4**.

Cmpd.	**4a^{Tip}**	**4a^{MeTip}**	**4b^{Mes*}**	**4b^{MeMes*}**	**4ab^{Mes*}**	**4ac^{Mes*}**	**4bc^{Mes*}**
δ [ppm]	56.1	54.5	47.7	46.2	50.2	56.3	44.7

The constitution of **4a^{MeTip}**, **4b^{MeMes*}**, **4ac^{Mes*}**and **4bc^{Mes*}** was unambiguously ascertained by ^{1}H, ^{11}B and ^{13}C NMR spectroscopy, mass spectrometry and elemental analysis (Appendix, Figs. 5.6.63-71). Crystals suitable for single-crystal X-ray analysis for compounds **4a^{MeTip}**, **4b^{MeMes*}** and **4bc^{Mes*}** were obtained by slow crystallization in pentane (Figure 2.6.8). For **4a^{MeTip}** and **4b^{MeMes*}**, however, the quality of the obtained X-ray data was too poor to allow the discussion of structural parameters. The solid-state structure of compound **4bc^{Mes*}** was determined by single-crystal X-ray diffraction. The boron center is trigonal-planar coordinated

(sums of bond angles around the boron atom: 360 °) and the pendent Mes* group is nearly perpendicular orientated to the BC_3 plane (88 °). The (het)aryl rings are slightly twisted out of plane with an interplanar angle of 14.6°.

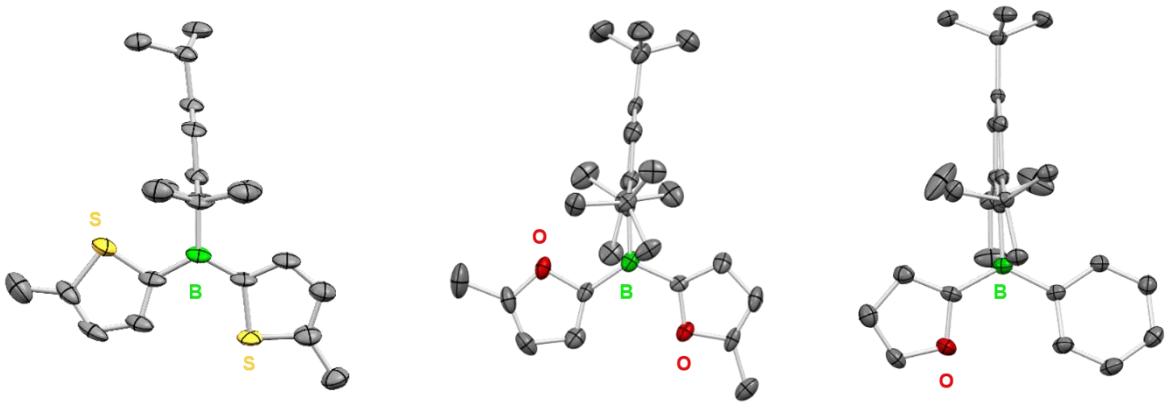

Figure 2.6.8. Molecular structure of **4a**^{MeTip} (left), **4b**^{MeMes*} (center) and **4bc**^{Mes*} (right) in the solid state (H-Atoms omitted for clarity).

After evaluating that catalysts **B**, **E** and **F** show good results for the Si/B exchange of various Ar-BCl_2 compounds, we attempted polycondensation reactions using bifunctional species **15a,b** to avoid any stoichiometric issues (Scheme 2.6.17).

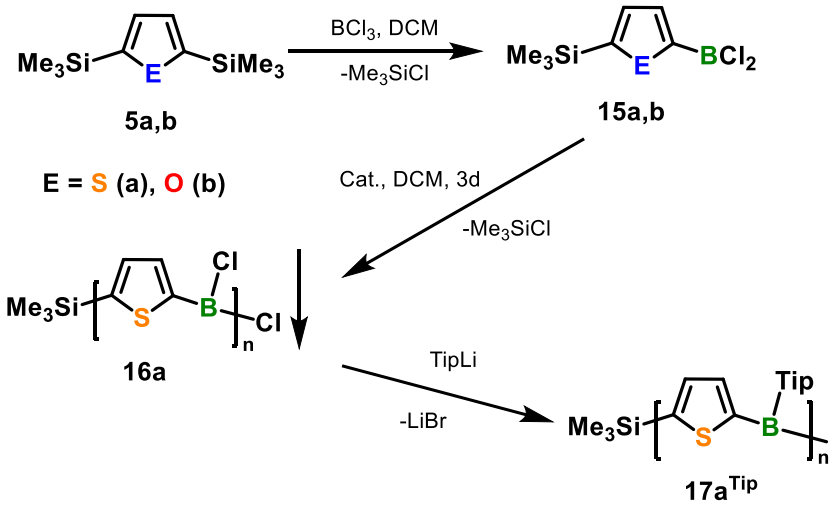

Scheme 2.6.17. Synthesis of oligomers **17a**^{Tip} via catalytic Si/B exchange polycondensation reaction.

In order to synthesize **15a**, 5 equivalents of a BCl_3 solution (1M in DCM) were added to neat **5a** in one portion at 0°C (reaction protocol adapted and slightly modified from Braunschweig and co-workers).[15] After stirring for a short period of time (45 minutes), all volatiles were removed in vacuo, and crude **15a** was further purified by short-distance distillation to afford **15a** as a colorless liquid in good yield (74 %). On the other hand, **15b** was obtained by careful addition of a BCl_3 solution (1 equiv., 1M in DCM) to **5b** in DCM. After stirring for 1 h and removal of all volatiles, **15b** was selectively obtained and can be further purified by short-distance

distillation to obtain **15b** as a colorless liquid in good yields (71%). Both compounds show no evidence for a proceeding condensation reaction when stored at ambient temperatures for several days. This stability enables a high level of control since the compounds can be, in comparison to their BBr_2-relatives, purified and stored for a long time. After addition of catalyst **B**, polycondensation reaction was performed in DCM at ambient temperature. Again, precipitation was observed which points to the proceeding polycondensation reaction and after the reaction mixture had been stirred for 3 days, addition of aryl lithium reagent afforded **17a^{Tip}** in moderate yields. The obtained oligomers were perfectly air and moisture stable and the data obtained from ^{1}H NMR spectroscopy agree well with the data obtained previously for **17a^{Tip}** in our group.[6a] Analysis of **17a^{Tip}** via GPC indicated the formation of oligomeric species with an average molecular weight of 2316 Da which corresponds to 6 repeating units on average. As result, by using compound **15a** instead of **5a**, we were able to increase the molecular weight by 769 Da. Nevertheless, at some point, precipitation occurred which means that a critical molecular weight has been reached. This precipitation probably is the reason for the still limited molecular weight.

It is obvious that the success of the polymerization reaction can be determined on the one hand by the proceeding polycondensation reaction itself, and on the other hand by the successful and effective arylation/post-modification reaction in order to obtain air and moisture stable compounds. The primary idea was that the high reactivity of the Ar-BBr_2 species might lead to several side reactions and thus to decomposition, limiting the accessible maximum molecular weight. However, another possibility is an incomplete post-modification reaction in which high molecular weight macromolecules are formed during the polycondensation process, but then chain cleavage occurrs as a result of decomposition, either within the oligomer chain or at the end of the chain (Scheme 2.6.18).

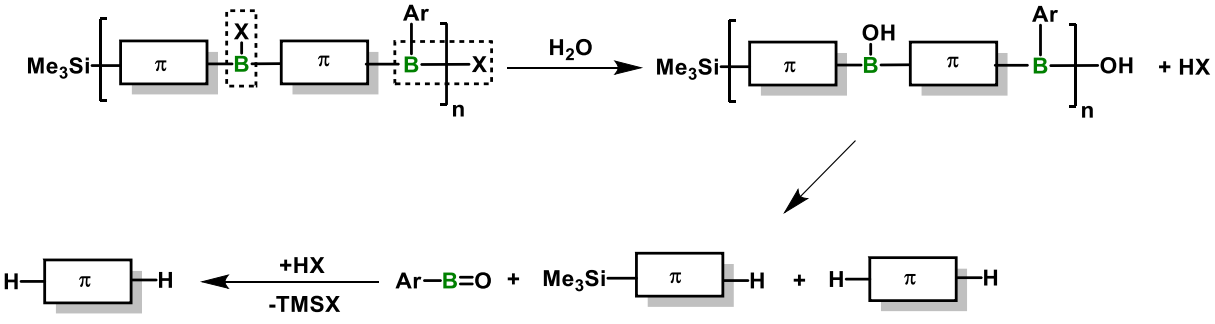

Scheme 2.6.18. Decomposition pathways as result of incomplete arylation within the oligomer chain or at the chain end causing chain cleavage.

In this case, the remaining halide **X** (Cl, Br) would react with water to form a hydrolized species (Ar_2BOH) and the respective acid **HX**. In the next step, elimination could lead to chain cleavage with formation of an oxoarylborane (Ar-B=O) and the respective chain fragment. Furthermore, the previously formed acid could then cause a cleavage of the remaining silyl group.To get

more insight into the general arylation behaviour, this study will concentrate on 2nd and 3rd substitution of thienyl- and furylboranes.

After the Si/B exchange reaction, compounds **3** and **13** and oligomers **7** and **16** all feature remaining and highly reactive halide functionalites (Figure 2.6.9). Those are divided into two different chemical surroundings with $\mathbf{X_1}$ flanked by two hetaryl rings (Ar_2BX) and $\mathbf{X_2}$ and $\mathbf{X_3}$ with only one connected hetaryl ring ($ArBX_2$).

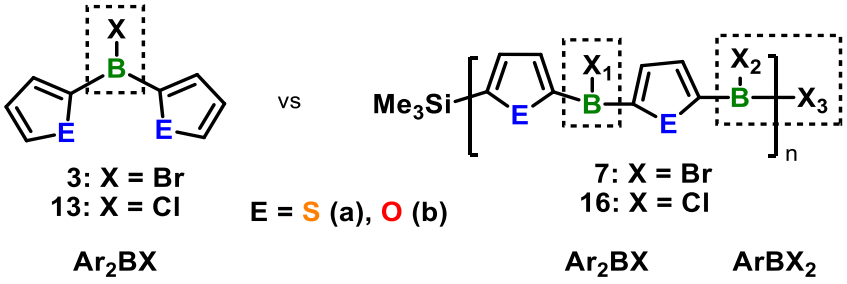

Figure 2.6.9. Chemical surroundings of compounds **3**,**13** and oligomers **7**,**16** before arylation.

The structural motif of both the monomer precursor **3, 13** (Ar_2BX) and the polymer precursor **7, 16** ($ArBX_2$) can be transferred to several starting materials and intermediates for the synthesis of organoboron compounds. Previous results in our group have shown that **3** readily reacts with aryllithium reagents in toluene. The same is true for compounds **13** and the yield can be slightly increased by using diethylether/toluene mixture.

However, it is not clear whether both remaining halides in an $ArBX_2$ type compound can be replaced by two bulky substituents concerning both steric and electronic reasons. Therefore, we reacted Het-BBr_2 **2a** and Het-BCl_2 **12a** compounds with two equivalents of TipLi (Scheme 2.6.19, I) to give **18a^{Tip}**. After addition of the aryllithium reagent, the solution turned dark immediately and analysis via ^{1}H- and ^{11}B{^{1}H}-NMR showed no evidence for the formation of **18a^{Tip}**. In fact, the ^{1}H-NMR spectra indicated the formation of a large amount of Ar-H while the ^{11}B{^{1}H} spectra point at adduct formation (δ = -11.1 ppm, see Appendix, Figure 5.6.79). In the case for the addition of 2 equivalents of Mes*, a broad signal in ^{11}B-NMR spectroscopy evidenced the formation of a monoarylated compound beside a sharp signal in the adduct region (δ = -12.4 ppm). Attempts to break up the adduct with different reagents such as TMS-Cl or $NaOCH_2CF_3$ failed.

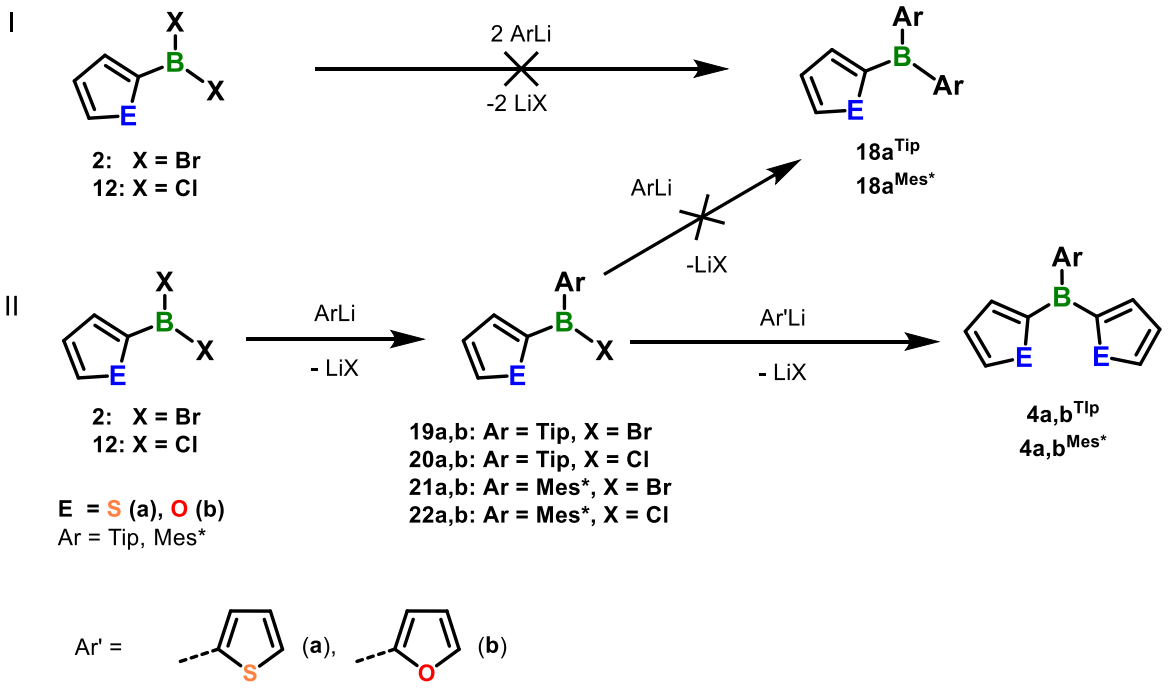

Scheme 2.6.19. (I): Attempted diarylation of $ArBX_2$ type species; (II) stepwise monoarylation and follow-up 3rd substitution.

A different opportunity is the stepwise introduction of two aryl substituents. This method allows us to flexibly introduce different aryl groups as third substituent after successful monoarylation with either TipLi or Mes*Li (Scheme 2.6.19, II). Starting from $HetBX_2$ (**2**, **12**), we added one equivalent of a solution of TipLi or a suspension of Mes*Li to afford compounds **19**-**22**. The reaction mixtures were stirred overnight and in each case precipitation occurred which evidenced the formation of LiX. After filtration and removal of all volatiles in vacuo, we obtained compounds **19-22** in low to good yields (10-55%) with comparably lower yields for Mes*- substituted systems, especially for furylboranes. Crystallization in pentane afforded compounds **19a**, **20a** and **22a** as slightly colored crystals. Compounds **19b**, **20b**, **21a,b** and **22b** were obtained as slightly colored solids. Compounds **19-22** were fully characterized by NMR spectroscopy (Appendix, Figs 5.6.81-98). We first attempted to obtain diarylated compounds **18** by adding one equivalent of TipLi or Mes*Li to the monoarylated compounds **19**-**22**, respectively. Again, an immediate color change was observed and the recorded $^{11}B\{^1H\}$-NMR spectra only indicated adduct formation. As alternative, we then added a freshly prepared suspension of 2-thienyllithium (ThiLi) or 2-furyllithium (Fur-Li) to obtain the symmetric triarylboranes **4**.

The reaction of the Tip-substituted compounds **19a,20a** and **19b** with Thi-Li and Fur-Li afforded the desired symmetric triarylboranes in moderate (**4b**^{Tip}, 40 %) to excellent yields (**4a**^{Tip}, 83-92%). However, when the same reaction was carried out with Mes*-substituted compounds **21a**-**22a**, no reaction occurred even after several days or after heating to 40 °C or 70 °C, respectively. As a good case in point, we reacted **19b** with **1b** in the presence of catalyst **B** to

obtain, in ideal circumstances, triarylborane **4b**^{Tip}. The reaction was monitored by ^{1}H-NMR spectroscopy and as expected, no formation of the condensation product was observed. The solid state structures of **19a**, **20a** and **22a** were determined by single-crystal X-ray diffraction (Figure 2.6.10.).

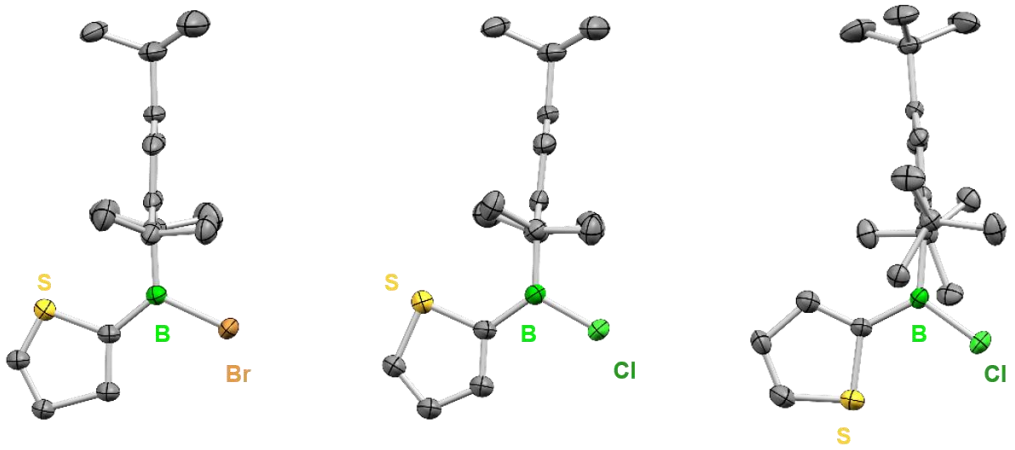

Figure 2.6.10. Molecular structure of **19a** (left), **20a** (center) and **22a** (right) in the solid state (H-Atoms omitted for clarity).

Additionally, we synthesized methoxy and trifluorethoxy derivatized compounds **23a,b** and **24a,b** to be able to use ether solvents to increase the reactivity of the lithiated species (Scheme 2.6.20). The reaction of **19a,b** with methoxytrimethylsilane (Me_3Si-OMe) or 2,2,2-trifluorethoxytrimethylsilane (Me_3Si-OCH_2CF_3) in DCM at room temperature afforded **23a,b** and **24a,b** (27-91%), respectively. Again, the addition of Me_3Si-OMe or Me_3Si-OCH_2CF_3 to Mes*-substituted compounds **21a** and **22a** led to no reaction even after heating and stirring for several days (Scheme 2.6.20, bottom). As observed for the attempted third substitution with FurLi and ThiLi, once again, no third substitution can be carried out probably due to the larger steric demand of Mes*. The reaction of Tip-substituted compound **23** and **24** with ThiLi or FurLi in a mixture of toluene/diethylether afforded triarylboranes **4**.

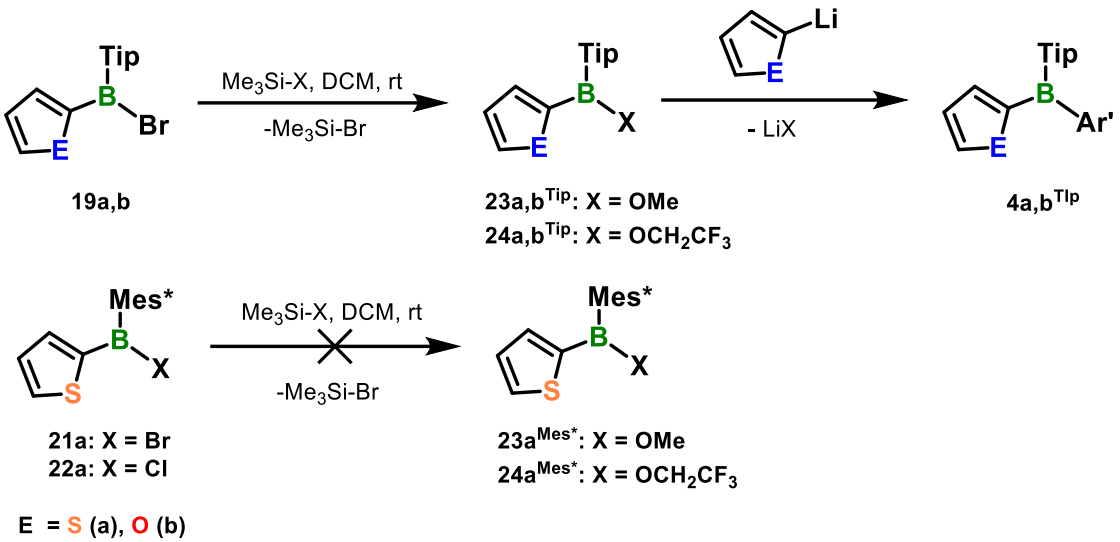

Scheme 2.6.20. Top: Synthesis of compounds **23a,b^{Tip}** and **24a,b^{Tip}** and follow-up 3rd substitution. Bottom: Attempted synthesis of compounds **23a^{Mes*}** and **24a^{Mes*}**.

The experiments described above show that it is unlikely that both halides in an $ArBX_2$ system will be replaced in a concerted reaction with two equivalents of TipLi or Mes*Li. A stepwise reaction via addition of one equivalent aryllithium with subsequent introduction of ThiLi or FurLi led to triarylboranes only in the case when Tip rather than Mes* is used as substituent. In order to obtain Mes* substituted compounds, the only opportunity in our case is to perform a Si/B exchange reaction to afford an Ar_2BX species with subsequent addition of Mes*Li (cf. Scheme 2.6.16)

To investigate more realistic polycondensation-like conditions, we synthesized compounds **25** which already feature an electron deficient boron center as well as a solubilizing aryl group via Si/B exchange reaction and subsequent arylation (Scheme 2.6.21). After careful addition of tribromoborane (BBr_3), we obtained compounds **26** in an almost quantitative yield. Starting from this point, we can use catalytic Si/B exchange reaction with silylated compound **1a** to afford **27a** *(Route A)*. Subsequent addition of TipLi afforded triarylborane **28a** in moderate yield (37%). Alternatively, monoarylation reaction by addition of TipLi afforded **29a** (*Route B*), which is then reacted with a freshly prepared solution of ThiLi to give triarylborane **28a** in improved yields (59%). Furthermore, we succeeded in derivatization of **29a** with Me_3Si-OMe and Me_3Si-OCH_2CF_3 to afford compounds **30a**, **31a**. Addition of ThiLi in a mixture of toluene/diethylether afforded triarylborane **28a**. The addition of two equivalents of TipLi to compound **26a** also did not lead to the formation of a triarylborane featuring two Tip groups ($ThiBTip_2$). The same is true when TipLi (1 equiv.) was added to **29a**.

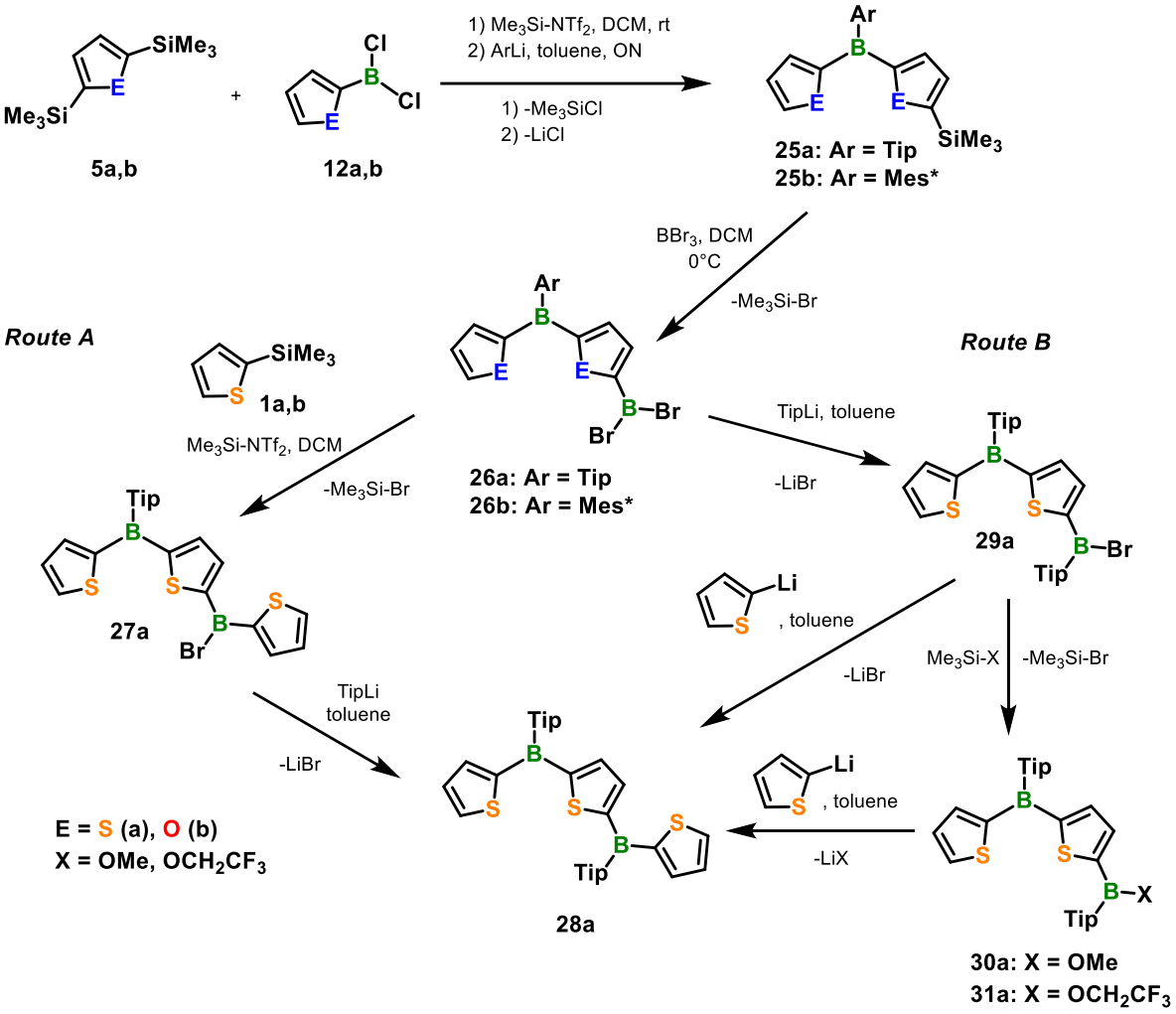

Scheme 2.6.21. Complementary routes to bis-triarylborane **28a** via A: Si/B exchange and salt-metathesis or B: monoarylation and subsequent salt-metathesis.

Compounds **25**-**27a** and **29a-31a** were fully characterized by NMR spectroscopy and mass spectrometry (see Appendix, Figs. 5.6.112-133). The solid state structures of **25a,b** were determined by single-crystal X-ray diffraction (Figure 2.6.11). Both boron centers are trigonal-planar coordinated (sums of bond angles around the boron atom: 360 ° for **25a** and 359.9 ° for **25b**) and the pendent aryl groups are nearly perpendicular orientated to the BC_3 plane (87.7 ° for Tip-substituted **25a** and 89.2 ° for Mes*-substituted **25b**). The furan rings in **25b** adopt an *anti*-arrangement and are slightly twisted out of plane (20.2 °). In comparison, the thiophene rings adopt a *syn*-arrangement and show slight rotational disorder. The two thiophene rings have a twist angle of 13.3 °, which is proportionally smaller (as compared to **25b**), but the value is averaged over the disordered thiophene rings.

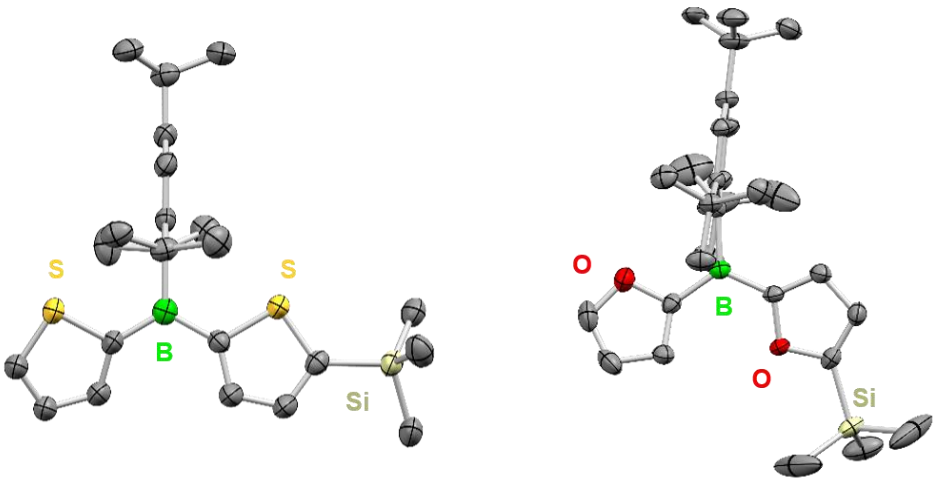

Figure 2.6.11. Molecular structure of **25a** (left) and **25b** (right) in the solid state (H-Atoms omitted for clarity).

Based on the obtained results, it is unlikely that the concomitant 2nd and 3rd substitution with TipLi or Mes*Li led to oligomers featuring two bulky aryl groups as final end groups. It is more plausible that chain cleavage or decomposition will lead to triarylborane being composed of two thienyl- or furyl units and one sterically demanding substituent. The results from both the "simple" model systems and the more polymerization-like model systems clearly indicate a successful 2nd and 3rd substitution via either *Route A* or *Route B* for Tip-substituted compounds. In the case for Mes* substituted compounds, only *Route A* will probably afford 2nd and 3rd substitution. These approaches are applied to polycondensation reactions and three different reaction routes were tested (Scheme 2.6.22). After catalyst **B** had been added to either **6a** or **15a** and oligomers **7a** or **16a** were obtained, reaction *Routes A* and *B* can be used to obtain compounds **32a** and **33a**. The former is obtained via Si/B exchange reaction and addition of **1a**. In this case, it is important that the Si/B exchange does not lead to any 3rd substitution, which was not observed for catalyst **B** in previous experiments.

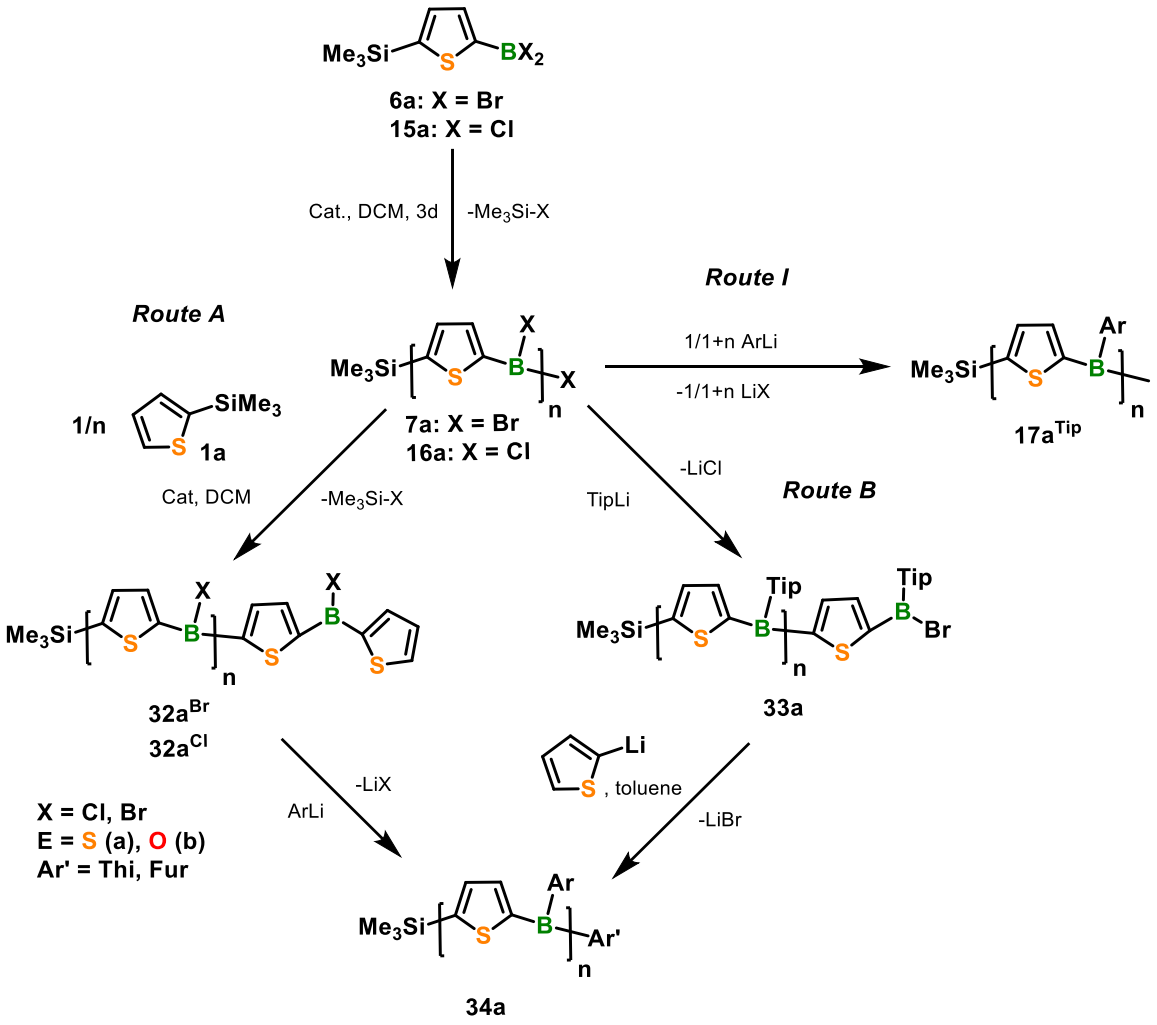

Scheme 2.6.22. Complementary routes to oligomers **17a**^{Tip} and **34a** via Route *I*: addition of an excess of ArLi; A: Si/B exchange- and follow-up salt-metathesis reaction or B: monoarylation- and subsequent salt-metathesis reaction.

After addition of TipLi, all remaining halides in the polymer chain as well as the halide in the end group should be substituted to afford **34a**. In compound **33a**, all Ar_2BX type halides in the polymer chain as well as one halide at the end group are substituted with an aryl group in the first step. Since we know that Mes* provides too much steric bulk for subsequent 3rd substitution and the fact that Tip-substituted oligo(furyl)boranes lack air- and moisture stability, we concentrated on thienylboranes. After addition of a freshly prepared suspension of ThiLi in toluene to **33a**, we obtained oligomer **34a** in low yields. In both cases, purification was difficult due to inadequate precipitation, which had to be repeated several times. However, the obtained average molecular weight (M_n) estimated by GPC is increased by 595 g/mol for *Route A* (2145 g/mol vs. 1550 g/mol[6a]). Performing the arylation in a mixture of toluene/diethylether led to a slightly increased M_n value (2280 g/mol). This corresponds to a chain length of 6, on average (Appendix, Figs. 5.6.151-152). In the case for *Route B*, predominantly low molecular weight compounds were obtained, probably due to the higher

reactivity of ThiLi which may cause chain cleavage. Performing the Si/B exchange polycondensation reaction for **6a** in DCM at elevated temperatures (40 °C) and subsequent arylation via *Route I*, almost no influence on the obtained M_n (1734 g/mol vs. 1550 g/mol, Appendix, Figure 5.6.148) was observed. The polycondensation reaction for **7a** was additionally performed in *ortho*-dichlorobenzene at 70°C and in this approach, an increased M_n of 2119 g/mol (569 g/mol more than previously reported for oligomer **17a**$^{\mathbf{Tip}}$)$^{\mathbf{6}}$ was obtained by GPC analysis.

In conclusion, the catalytic Si/B exchange approach to obtain conjugated organoborane molecules and oligomers was successfully extended to aryl-BCl_2 species, which provide a significantly higher level of control due to better stability. Six different catalysts were tested with the best results for catalyst **B**, **D**, **E** and **F**. For thienylborane systems, catalyst **B** afforded the cleanest reactions, but the reaction rate was significantly lower as compared to the other catalysts as well as for the BBr_2 species with the same catalyst. For furylboranes, even the metal-free catalysts **A** (48 h vs > 8 d) and **B** (19 h vs. 48 h) show increased reaction rates in comparison to thienyl-based systems. To our delight, catalysts **D**, **E** and **F** showed remarkable selectivity and reactivity for the scarcely explored furylboranes. For catalyst **E** and **F**, complete and selective conversion was observed within less than 1 hour. This impressively demonstrates the effective rate acceleration through the combination of the silver cation and the weaker coordinating anion. Furthermore, we studied the synthesis and reactivity of thienyl- and furylboranes with regard to arylation protocols. We found that both *Routes A* and *B* afforded compound **28a** in good yields. Transferring these approaches to polycondensation reactions, in the case for *Route A*, we were able to significantly increase the molecular weight of the polymer products.

As the formation of B-C bonds is of particular interest for the synthesis of organoboron compounds, we believe that the extension of the Si/B exchange to aryl-BCl_2 based systems and especially the high selectivity of the presented catalysts will add a significant contribution to various fields of organoboron chemistry.

2.6.1. Experimental section

General procedures. All manipulations were performed under an atmosphere of dry argon using standard Schlenk techniques or in an MBraun glove box. Solvents (dichloromethane, *n*-pentane, diethylether, toluene, and tetrahydrofuran) were dried and degassed by means of an MBraun SPS-800 solvent purification system. Methanol was dried over magnesium turnings and freshly distilled prior to use. Deuterated solvents for NMR spectroscopy were dried and degassed at reflux over Na (C_6D_6) or CaH_2 ($CDCl_3$ and CD_2Cl_2) and freshly distilled prior to use. Solvents for aqueous work up (*n*-hexane, *n*-pentane, dichloromethane, ethanol, diethylether), tribromoborane, bromobenzene, 2-methylthiophene, 2-methylfuran, thiophene, 2-bromothiophene, bromine, 1,3,5-tri-*tert*-butylbenzene, 2-bromo-1,3,5-triisopropylbenzene, silver trifluoromethanesulfonate, silver bis(trifluoromethane sulfonide, silver tetrakis/perfluoro-^{t}butoxy)aluminate and lithium bis(trifluoromethylsulfonyl)imide were purchased from commercial sources and used as received. Solutions of *n*-butyllithium (1.6 M and 2.5 M in hexane, respectively), *t*-butyllithium (1.7 M in pentane) and trichloroborane (1 M in DCM and hexane) were purchased from Sigma Aldrich and used as received as well. Trimethylsilylchloride, methoxytrimethylsilane, 2,2,2-trifluoroethoxytrimethysilane and furan were commercially purchased and freshly distilled prior to use. 2,4,6-triisopropylphenyllithium,[16] trimethylsilylbis(trifluoromethylsulfonyl)imide,[17] 2-bromo-1,3,5-tri-*tert*-butylbenzene,[18] 2,4,6-tri-*tert*-butylphenyllithium[5a], **12c**[19] and **12b^{Me}**[13] were prepared according to methods described in the literature. Compounds **1a-c**, **2a,b** and **5a,b** were prepared according to procedures previously described by us.[6] NMR spectra were recorded at 25 °C on a Bruker Avance III HD spectrometer operating at 300 MHz, on a Bruker Avance II-400 spectrometer operating at 400 MHz, on a Bruker Avance III HD spectrometer operating at 400 MHz or on a Bruker Avance 500 spectrometer operating at 500 MHz. Chemical shifts were referenced to residual protic impurities in the solvent (^{1}H) or the deuterated solvent itself (^{13}C) and reported relative to external $SiMe_4$ (^{1}H, ^{13}C) or $BF_3{\cdot}OEt_2$ (^{11}B) standards. Mass spectra were obtained with the use of a Thermo Scientific Exactive Plus Orbitrap MS system employing either atmospheric sample analysis probe (ASAP), electrospray ionization (ESI) or atmospheric pressure chemical ionization (APCI). Elemental analyses were performed on an Elementar vario MICRO cube elemental analyzer. Crystals suitable for single-crystal X-ray diffraction were selected, coated in perfluoropolyether oil, and mounted on MiTeGen sample holders. Diffraction data were collected on Bruker X8 Apex II 4-circle diffractometers with CCD area detectors using Mo-Kα radiation. The crystals were cooled using an Oxford Cryostreams low-temperature device. Data were collected at 100 K. The images were processed and corrected for Lorentz-polarization effects and absorption as implemented in the Bruker software packages. The structures were solved using the intrinsic phasing method (SHELXT)[20] and Fourier expansion technique. All non-hydrogen atoms were refined in anisotropic

approximation, with hydrogen atoms 'riding' in idealized positions, by full-matrix least squares against F^2 of all data, using SHELXL[21] software and the SHELXLE graphical user interface.[22] Other structural information was extracted using OLEX2 software.[23]

Syntheses

Combining 1a and 12a in the absence of a catalyst. To a solution of **1a** (0.078 g, 0.5 mmol) in deuterated dichloromethane (CD_2Cl_2, 0.25 mL) was added a solution **12a** (0.082 g, 0.5 mmol) in CD_2Cl_2 and the reaction was stirred for several days. Monitoring the reaction via ^{1}H-NMR spectroscopy indicated only 5% consumption of the starting materials after 13d.

^{1}H NMR (300 MHz, CD_2Cl_2): δ = 8.08 (dd, *J* = 3.7, 1.0 Hz, 1H, **12a**-*H*), 8.04 (dd, *J* = 4.7, 1.0 Hz, 1H, **12a**-*H*), 7.64 (dd, *J* = 4.6, 0.9 Hz, 1H, **1a**-*H*), 7.35 – 7.32 (m, 2H, **1a**+**12a**-*H*), 7.24 (dd, *J* = 4.6, 3.3 Hz, 1H, **1a**-*H*), 0.40 (s, 9H, 1a-Si(C*H*$_3$)$_3$).

The small peaks at 8.25 ppm, 8.01 ppm and 7.41-7.39 ppm can be related to small extent of condensation reaction (5 mol%), which is further evidenced by TMS-Cl formation (0.50 ppm, ca. 5%).

General procedure for catalytic Si/B exchange of 1 and 12 with the respective catalysts.

To a solution of silylated compound **1** (0.5 mmol) and borylated compound **12** (0.5 mmol) in dichloromethane (0.5 mL) was added the respective catalyst (5-20 mol%) at ambient temperature, and the mixture was stirred over a certain period of time. The reaction progress was monitored by ^{1}H and ^{11}B{^{1}H} NMR spectroscopy. Reactions utilizing catalysts C, D and E were carried out in the absence of light.

Synthesis of 13a via catalysts A-F. To a solution of **1a** (0.078 g, 0.5 mmol) and **12a** (0.082 g, 0.5 mmol) in CD_2Cl_2 (0.50 mL) was added TMS-OTf (Cat. **A**, 0.022 g, 0.1 mmol, 20 mol%), TMS-NTf_2 (Cat. **B**, 0.019 g, 0.05 mmol, 10 mol%), AgOTf (Cat. **C**, 0.006 g, 0.025 mmol, 5 mol%), $AgNTf_2$ (Cat. **D**, 0.010 g, 0.025 mmol, 5 mol%), $Ag[AlOC(CF_3)_3)_4$ (Cat. **E**, 0.027 g, 0.025 mmol, 5 mol%) or Me_3Si-F-$Al(OC(CF_3)_3$ (Cat. **F**, 0.021 g, 0.025 mmol, 5 mol%) at ambient temperature, and the mixtures were stirred for at least 24 hours. Complete consumption of the starting materials was observed within 48 h (Cat. **B**), within 5 h (Cat. **D**), after 10 minutes (Cat. **E**) and after 20 minutes (Cat. **F**).

^{1}H NMR (300 MHz, CD_2Cl_2): δ = 8.22 (dd, *J* = 3.7, 1.0 Hz, 2H, Thi-*H*), 8.00 (dd, *J* = 4.7, 1.0 Hz, 2H, Thi-*H*), 7.38 (dd, *J* = 4.7, 3.7 Hz, 2H, Thi-*H*); ^{11}B NMR (96 MHz, CD_2Cl_2): δ = 48.7 (s).

Synthesis of 13b via catalysts A, B, D-F. To a solution of **1b** (0.070 g, 0.5 mmol) in dichloromethane (0.25 mL) was added a solution of trichloroborane in dichloromethane (1M, 0.25 mmol, 0.25 mL) at 0°C and the reaction mixture was stirred for 2 h without maintaining the temperature. After the reaction was complete (monitoring by ^{1}H-NMR spectroscopy: **12b**:

^{1}H NMR (400 MHz, $CDCl_3$): δ = 7.86 (s, 1H, Fur-*H*), 7.58 (d, *J* = 3.5 Hz, 1H, Fur-*H*), 6.60 (dd, *J* = 3.5, 1.4 Hz, 1H, Fur-*H*)), catalyst **A** (20 mol%, 0.011 g, 0.050 mmol, 20 mol%), catalyst **B** (0.010 g, 0.025 mmol, 10 mol%), catalyst **D** (5 mol%, 0.010 g, 0.125 mmol), catalyst **E** (5 mol%, 0.013 g, 0.125 mmol, 5 mol%) or catalyst **F** (5 mol%, 0.011 g, 0.0125 mmol) were added and the reaction mixture was stirred overmnight. Complete consumption of the starting materials was observed within 48 h (Cat. **A**), 19 h (Cat. **B**), 1.5 h (Cat. **D**) and less than 10 minutes (Cat. **E**+**F**).

13b: ^{1}H NMR (300 MHz, CD_2Cl_2): δ = 7.89 (dd, *J* = 1.6, 0.6 Hz, 2H, Fur-*H*), 7.74 (dd, *J* = 3.5, 0.6 Hz, 2H, Fur-*H*), 6.61 (dd, *J* = 3.5, 1.6 Hz, 2H, Fur-*H*); ^{11}B NMR (96 MHz, $CDCl_3$): δ = 41.7 (s).

Attempted synthesis of 13c via catalysts B, E, F.

To a solution of **1c** (0.075 g, 0.5 mmol) and **12c** (0.079 g, 0.5 mmol) in CD_2Cl_2 (0.50 mL) was added cat. **B** (0.044 g, 0.1 mmol, 20 mol%), cat. **E** (0.027 g, 0.25 mmol, 5 mol%) or cat. **F** (0.022 g, 0.025 mmol, 5 mol%) at ambient temperature, and the mixture was stirred for several days. Monitoring of the reaction progress by ^{1}H and ^{11}B{^{1}H} NMR spectroscopy indicated only 50% conversion after 7 days in the case for catalyst **B** and several side reactions for catalysts **E** and **F** as discussed in the main part

Synthesis of 13a'. To a solution of **5a** (0.114 g, 0.5 mmol) and **12a** (0.082 g, 0.5 mmol) in $CDCl_3$ (0.5 mL) was added catalyst **B** (0.017 g, 0.045 mmol, 9 mol%). The reaction mixture was stirred for 3 days and the reaction progress was monitored by ^{1}H and ^{11}B{^{1}H} NMR spectroscopy.

^{1}H NMR (300 MHz, $CDCl_3$): δ = 8.21 (d, *J* = 3.6 Hz, 2H, Thi-*H*), 7.94 (dd, *J* = 4.7, 1.0 Hz, 1H, Thi-*H*), 7.47 (d, *J* = 3.5 Hz, 1H, Thi-*H*), 7.37 – 7.32 (m, 1H, Thi-*H*), 0.42 (s, 9H, -Si(C*H*$_3$)$_3$).

Synthesis of 13a''. To a solution of **5a** (0.114 g, 0.5 mmol) and **12a** (0.165 g, 1.0 mmol) in $CDCl_3$ (0.5 mL) was added catalyst **B** (0.017 g, 9 mol%). The reaction mixture was stirred for 13 days and the reaction progress was monitored by ^{1}H and ^{11}B{^{1}H} NMR spectroscopy.

^{1}H NMR (300 MHz, $CDCl_3$): δ = 8.28 (dd, *J* = 3.7, 1.0 Hz, 2H, Thi-*H*), 8.24 (s, 2H, Thi-*H*), 8.03 (dd, *J* = 4.7, 1.0 Hz, 2H, Thi-*H*), 7.39 (dd, *J* = 4.7, 3.7 Hz, 2H, Thi-*H*); ^{11}B NMR (96 MHz, $CDCl_3$): δ = 48.7 (s).

Synthesis of 13a^{Me}.To a solution of **1a^{Me}** (0.339 g, 2.0 mmol) in dichloromethane (1.00 mL) was added a solution of trichloroborane in dichloromethane (1M, 1.0 mmol, 1.0 mL) at 0°C and the reaction mixture was stirred for 2 h without maintaining the temperature. After the reaction was complete (monitoring by ^{1}H-NMR spectroscopy: **12a^{Me}**: ^{1}H NMR (300 MHz, $CDCl_3$): δ = 7.84 (d, *J* = 3.7 Hz, 2H, Thi-*H*), 6.98 (dd, *J* = 3.7, 0.9 Hz, 2H, Thi-*H*), 2.61 (s, 6H,Thi-C*H*$_3$), ^{11}B NMR (96 MHz, $CDCl_3$): δ = 47.8 (s)), catalysts **E** (5 mol%) or **F** (5 mol%) were added and

the reaction mixture was stirred overnight. Analysis via ^{1}H-NMR spectroscopy indicated complete conversion to **13^{Me}** within less than 1 hour.

13a^{Me}: ^{1}H NMR (400 MHz, $CDCl_3$): δ = 7.96 – 7.92 (m, 2H, Thi-*H*), 6.98 (dd, *J* = 3.6, 1.0 Hz, 2H, Thi-*H*), 2.62 – 2.57 (s, 6H, Thi-C*H*$_3$); ^{11}B NMR (128 MHz, $CDCl_3$): δ = 46.7 (s).

Synthesis of 13b^{Me}. To a solution of **1b^{Me}** (0.309 g, 2.0 mmol) in dichloromethane (1.00 mL) was added a solution of trichloroborane in dichloromethane (1M, 1.0 mmol, 1.0 mL) at 0°C and the reaction mixture was stirred for 2h without maintaining the temperature. After the reaction was complete (monitoring by ^{1}H-NMR spectroscopy: **13b^{Me}**: ^{1}H NMR (300 MHz, $CDCl_3$): δ = 7.50 (d, *J* = 3.4 Hz, 2H, Fur-*H*), 6.23 (d, *J* = 2.9 Hz, 2H, Fur-*H*), 2.44 (s, 6H, Fur-C*H*$_3$); ^{11}B NMR (96 MHz, $CDCl_3$): δ = 44.7 (s)), catalysts **E** (5 mol%) or **F** (5 mol%) were added and the reaction mixture was stirred overnight. Analysis via ^{1}H-NMR spectroscopy indicated complete conversion to **13b^{Me}** within less than 1 hour.

13b^{Me}: ^{1}H NMR (400 MHz, CD_2Cl_2): δ = 7.66 (d, *J* = 3.4 Hz, 2H, Fur-*H*), 6.26 (dd, *J* = 3.4, 0.8 Hz, 2H, Fur-*H*), 2.47 (s, 6H, Fur-C*H*$_3$); ^{11}B NMR (128 MHz, CD_2Cl_2): δ = 40.0 (s).

Synthesis of 13ba. To a solution of **1b** (0.070 g, 0.5 mmol) and **12a** (0.082 g, 0.5 mmol) in CD_2Cl_2 (0.50 mL) was added cat. **B** (0.019 g, 0.05 mmol, 10 mol%) at ambient temperature, and the mixture was stirred overnight. Complete consumption of the starting materials was observed within 24 hours.

13ba: ^{1}H NMR (300 MHz, CD_2Cl_2): δ = 8.35 (dd, ^{3}J = 3.7 Hz, ^{4}J =0.9 Hz, 1H, Thi-*H*), 8.02 (dd, ^{3}J = 4.7 Hz, ^{4}J =1.0 Hz, 1H, Thi-*H*), 7.95 (dd, ^{3}J = 1.5 Hz, ^{4}J = 0.5 Hz, 1H, Fur-*H*), 7.68 (dd, ^{3}J = 3.5 Hz, ^{4}J = 0.5 Hz, 1H, Fur-*H*), 7.37 (dd, ^{3}J = 4.7, 3.7 Hz, 1H, Thi-*H*), 6.65 (dd, ^{3}J = 3.5, 1.6 Hz, 1H, Fur-*H*); ^{11}B NMR (96 MHz, CD_2Cl_2): δ = 44.7 (s).

Synthesis of 13ac. To a solution of **1a** (0.078 g, 0.5 mmol) and **12c** (0.079 g, 0.5 mmol) in CD_2Cl_2 (0.50 mL) was added cat. **B** (0.019 g, 0.05 mmol, 10 mol%) at ambient temperature, and the mixture was stirred overnight. Complete consumption of the starting materials was observed within 24 hours.

13ac: ^{1}H NMR (300 MHz, CD_2Cl_2): δ = 8.20 – 8.14 (m, 2H, Ph-*H*), 8.12 (dd, ^{3}J = 3.7 Hz, ^{4}J = 0.9 Hz, 1H, Thi-*H*), 8.05 (dd, ^{3}J = 4.7 Hz, ^{4}J = 0.9 Hz, 1H, Thi-*H*), 7.70 – 7.60 (m, 1H, Ph-*H*), 7.60 – 7.50 (m, 2H, Ph-*H*), 7.40 (dd, ^{3}J = 4.7, 3.7 Hz, 1H, Thi-*H*); ^{11}B NMR (96 MHz, CD_2Cl_2): δ = 55.4 (s).

Synthesis of 13bc. To a solution of **1b** (0.070 g, 0.5 mmol) and **12c** (0.079 g, 0.5 mmol) in CD_2Cl_2 (0.50 mL) was added cat. **B** (0.019 g, 0.05 mmol, 10 mol%) at ambient temperature, and the mixture was stirred overnight. Complete consumption of the starting materials was observed within 24 hours.

13bc: ^{1}H NMR (300 MHz, CD_2Cl_2): δ = 8.39 (dd, *J* = 8.2, 1.4 Hz, 2H, Ph-*H*), 7.98 (dd, ^{3}J = 1.5 Hz, ^{4}J = 0.5 Hz, 1H, Fur-*H*), 7.74 (dd, ^{3}J = 3.5 Hz, ^{4}J = 0.5 Hz, 1H, Fur-*H*), 7.67 – 7.59 (m, 1H, Ph-*H*), 7.58 – 7.50 (m, 2H, Ph-*H*), 6.68 (dd, ^{3}J = 3.6 Hz, 1.6 Hz, 1H, Fur-*H*); ^{11}B NMR (96 MHz, CD_2Cl_2): δ = 51.0 (s).

General procedure for the synthesis of air- and moisture stable triarylboranes 4.

To a solution of **1a** (0.078 g, 0.5 mmol) and **12a** (0.082 g, 0.5 mmol) in CD_2Cl_2 (0.50 mL) was added the respective catalyst (5-10 mol%) at ambient temperature, and the mixture was stirred for at least 24 hours. The resulting solution was evaporated to dryness to yield crude **13**, which was then redissolved in toluene (0.50 mL). Then, a solution of TipLi (0.55 mmol) or a suspension of Mes*Li (0.55 mmol) in toluene (1.00 mL) was added at ambient temperature. The reaction mixture was stirred overnight. The resulting suspension was diluted with *n*-pentane and quenched by the addition of water. After aqueous work-up, all volatiles were removed in vacuo and crude compound **4** was subjected to column chromatography (silica, PE).

4a^{MeTip}: ^{1}H NMR (400 MHz, $CDCl_3$): δ = 7.58 (d, *J* = 3.5 Hz, 2H, Thi-*H*), 6.99 (s, 2H, Tip-*H*), 6.94 – 6.90 (m, 2H, Thi-*H*), 2.94 (dt, *J* = 13.8, 6.9 Hz, 1H, *p*-^{i}Pr-*H*), 2.60 (s, 6H, Thi-CH_3), 2.55 (dd, *J* = 13.4, 6.7 Hz, 2H, *o*-^{i}Pr-*H*), 1.32 (d, *J* = 6.9 Hz, 6H, *p*-^{i}Pr-CH_3), 1.06 (d, *J* = 6.7 Hz, 12H, *o*-^{i}Pr-CH_3); ^{11}B NMR (128 MHz, $CDCl_3$): δ = 54.5 (s); ^{13}C NMR (101 MHz, $CDCl_3$): δ = 152.8 (s, Thi-*C*-CH_3), 149.8 (s, Tip-*C*-*o*-^{i}Pr), 148.4 (s, Tip-*C*-*p*-^{i}Pr), 143.9 (br. s, Thi-*C*-B), 143.0 (s, Thi-*C*H) 139.5 (br. s, Tip-*C*-B), 128.1 (s, Thi-*C*H), 120.0 (s, Tip-*C*H), 35.2 (s, *o*-^{i}Pr-*C*H), 34.4 (s, *p*-^{i}Pr-*C*H), 24.4 (s, *o*-^{i}Pr-*C*H_3), 24.3 (s, *p*-^{i}Pr-*C*H_3), 16.0 (s, Thi-C-*C*H_3).

4b^{MeMes*}: ^{1}H NMR (500 MHz, $CDCl_3$): δ = 7.40 (s, 2H, Mes*-*H*), 7.05 (br. s, 1H, Fur-*H*), 6.09 (d, *J* = 2.5 Hz, 2H, Fur-*H*), 2.40 (s, 6H, Fur-CH_3), 1.37 (s, 9H, *p*-^{t}Bu-CH_3), 1.18 (s, 18H, *o*-^{t}Bu-CH_3); ^{11}B NMR (160 MHz, $CDCl_3$): δ = 46.2 (s); ^{13}C NMR (126 MHz, $CDCl_3$): δ = 163.5 (br. s, Fur-*C*-B), 158.5 (s, Fur-*C*-CH_3), 152.3 (s, Mes*-*C*-*o*-^{t}Bu), 148.1 (s, Mes*-*C*-*p*-^{t}Bu), 133.4 (s, Mes*-*C*-B), 129.7 (s, Fur-C*H*), 121.8 (s, Mes*-*C*H), 108.3 (s, Fur-*C*H), 38.5 (s, *o*-^{t}Bu-*C*H_3), 34.9 (s, *p*-^{t}Bu-*C*H_3), 34.3 (s, *o*-^{t}Bu-*C*H_3), 31.6 (s, *p*-^{t}Bu-*C*H_3), 14.4 (s, Fur-C-*C*H_3); HR-MS (APCI): m/z = 419.3102; calcd. for $C_{28}H_{39}BO_2$: 418.3043.

4bc^{Mes*}: ^{1}H NMR (500 MHz, $CDCl_3$): δ = 8.10 (s, 2H, Ph-*H*), 7.84 (dd, *J* = 1.6, 0.6 Hz, 1H, Fur-*H*), 7.46 – 7.35 (m, 5H, Ph-*H*+Mes*-*H*), 7.04 (d, *J* = 3.3 Hz, 1H, Fur-*H*), 6.51 (dd, *J* = 3.4, 1.6 Hz, 1H, Fur-*H*), 1.39 (s, 9H, *p*-^{t}Bu-CH_3), 1.11 (s, 18H, *o*-^{t}Bu-CH_3); ^{11}B NMR (160 MHz, $CDCl_3$): δ = 56.3 (s); ^{13}C NMR (126 MHz, $CDCl_3$): δ = 165.7 (br. s, Fur-*C*-B), 151.8 (s, Mes*-*C*-*o*-^{t}Bu), 148.5 (s, Mes*-*C*-*p*-^{t}Bu), 148.1 (s, Fur-*C*H), 143.2 (br. s, Ph-*C*-B), 138.3 (br. s, Ph-*C*H), 134.9 (br. s, Mes*-*C*-B), 131.1 (s, Ph-*C*H), 129.0 (s, Fur-*C*H), 127.7 (s, Ph-*C*H), 122.2 (s, Mes*-*C*H), 111.4 (s, Fur-*C*H), 38.4 (s, *o*-^{t}Bu-*C*H_3), 34.9 (s, *p*-^{t}Bu-*C*H_3), 34.7 (s, *o*-^{t}Bu-*C*H_3), 31.6 (s, *p*-^{t}Bu-*C*H_3).

Synthesis of 15b. To a solution of **5b** (0.6887 g, 3.24 mmol) in dichloromethane (1 mL) was added a solution of trichloroborane (3.18 mmol, 1 M in DCM) at 0°C. The reaction mixture was stirred for 1 h and then, all volatiles were removed in vacuo and the resulting crude liquid was further purified by short distance distillation to afford **15b** as slightly yellowish liquid.

^{1}H NMR (300 MHz, $CDCl_3$): δ = 7.54 (d, *J* = 3.5 Hz, 1H, Fur-*H*), 6.75 (d, *J* = 3.5 Hz, 1H, Fur-*H*), 0.33 (s, 9H, -Si(C*H*$_3$)$_3$); ^{11}B NMR (96 MHz, CD_2Cl_2): δ = 45.8 (s); ^{13}C NMR (75 MHz, $CDCl_3$): δ = 173.1 (s), 131.4 (s, Fur-*C*H), 121.5 (s, Fur-*C*H), -1.8 (s, -Si(*C*H$_3$)$_3$); ^{29}Si NMR (60 MHz, $CDCl_3$): δ = -8.7 (s).

Synthesis of oligomer 17a^{Tip}. To a solution **15a** (0.148 g, 0.6 mmol) in DCM (0.6 mL) was added Me_3Si-NTf_2 (0.021 g, 0.060 mmol, 10 mol%) and the reaction mixture was stirred at ambient temperature for 7 d. Then, the solvent was removed in vacuo and the residue was redissolved in toluene (0.9 ml). Subsequently, a solution of TipLi (0.158 g, 0.750 mmol) in toluene (0.9 ml) was added and the reaction mixture was stirred for additional 3 d. After removal of all volatiles in vacuo, the residue was dissolved in pentane and extracted with brine (3x). The combined organic phases were dried over $MgSO_4$ and the solvent was removed *in vacuo*. The crude product was dissolved in pentane and precipitated in ethanol to afford **17a^{Tip}** as an off-white solid (0.055 gg, 26%). The data obtained for ^{1}H and ^{11}B-NMR spectroscopy are in good accordance with data previously reported in our group.[6a]

General procedure for the synthesis of monoarylated compounds 19-22. To a solution of **12** (1.0 equiv.) in toluene (1.5 mL/mmol) was added a solution of TipLi (1.1 equiv.) or a suspension of Mes*Li (1.1 equiv.) in toluene (1.5 mL/mmol) at ambient temperature and the reaction mixture was stirred overnight. The resulting suspension was filtrated, and all volatiles were removed in vacuo. The crude compound was further purified by addition of pentane and crystallization at low temperatures. Compounds **19a** (orange), **20a** (orange) and **22a** (colorless) were obtained as crystals. Compounds **20b**, **21b**, **21a** and **22b** were obtained as colored solids.

19a. Yield: 44 %. ^{1}H NMR (400 MHz, $CDCl_3$): δ = 8.03 (dd, *J* = 4.6, 0.9 Hz, 1H, Thi-*H*), 7.91 (d, *J* = 3.5 Hz, 1H, Thi-*H*), 7.32 (dd, *J* = 4.6, 3.7 Hz, 1H, Thi-*H*), 7.03 (s, 2H, Tip-*H*), 2.95 (s, 1H, *p*-^{i}Pr-*H*), 2.73 – 2.61 (m, 2H, *o*-^{i}Pr-*H*), 1.32 (d, *J* = 6.9 Hz, 6H, *p*-^{i}Pr-C*H*$_3$), 1.27 (d, *J* = 6.7 Hz, 6H, *o*-^{i}Pr-C*H*$_3$), 1.15 (d, *J* = 6.7 Hz, 6H, *o*-^{i}Pr-C*H*$_3$); ^{11}B NMR (128 MHz, $CDCl_3$): δ = 61.5 (s).

19b. Yield: 55 %. ^{1}H NMR (300 MHz, $CDCl_3$): δ = 7.93 (dd, *J* = 1.6, 0.6 Hz, 1H, Fur-*H*), 7.52 (d, *J* = 2.9 Hz, 1H, Fur-*H*), 7.06 (s, 2H, Tip-*H*), 6.62 (dd, *J* = 3.5, 1.6 Hz, 1H, Fur-*H*), 3.04 – 2.89 (m, 1H, *p*-^{i}Pr-*H*), 2.75 – 2.61 (m, 2H, *o*-^{i}Pr-*H*), 1.34 (d, *J* = 6.9 Hz, 6H, *p*-^{i}Pr-C*H*$_3$), 1.30 (d, *J* = 6.7 Hz, 6H, *o*-^{i}Pr-C*H*$_3$), 1.18 (d, *J* = 6.7 Hz, 6H, *o*-^{i}Pr-C*H*$_3$); ^{11}B NMR (128 MHz, $CDCl_3$): δ = 59.2 (s).

20a. Yield: 57 %. ^{1}H NMR (400 MHz, $CDCl_3$): δ = 7.97 (dd, *J* = 4.6, 0.8 Hz, 1H, Thi-*H*), 7.87 (d, *J* = 3.3 Hz, 1H, Thi-*H*), 7.29 (dd, *J* = 4.5, 3.7 Hz, 1H, Thi-*H*), 7.05 (s, 2H, Tip-*H*), 3.02 – 2.89 (m, 1H, *p*-^{i}Pr-*H*), 2.73 – 2.61 (m, 2H, *o*-^{i}Pr-*H*), 1.33 (d, *J* = 6.9 Hz, 6H, *p*-^{i}Pr-C*H*$_3$), 1.28 (d, *J* = 6.7 Hz, 6H, *o*-^{i}Pr-C*H*$_3$), 1.17 (d, *J* = 6.7 Hz, 6H, *o*-^{i}Pr-C*H*$_3$); ^{11}B NMR (128 MHz, $CDCl_3$): δ = 59.6 (s); ^{13}C NMR (101 MHz, $CDCl_3$): δ = 150.1 (s, Tip-*C*-*o*-^{i}Pr), 149.7 (s, Tip-*C*-*o*-^{i}Pr), 144.3 (br. s, Thi-*C*-B), 142.6 (s, Thi-C*H*), 139.6 (s, Thi-*C*H), 135.7 (s, Tip-*C*-B), 129.6 (s, Thi-*C*H), 120.6 (s, Tip-*C*H), 35.7 (s, *o*-^{i}Pr-*C*H), 34.5 (s, *p*-^{i}Pr-*C*H), 24.9 (s, *o*-^{i}Pr-*C*H$_3$), 24.2 (s, *o*-^{i}Pr-*C*H$_3$), 24.1 (*p*-^{i}Pr-*C*H$_3$). MS (ESI): m/z = 332.2; calcd. for $C_{19}H_{26}BClS$: 332.1.

20b. Yield: 22 %. ^{1}H NMR (500 MHz, $CDCl_3$): δ = 7.85 (dd, *J* = 1.6, 0.6 Hz, 1H, Fur-*H*), 7.39 (s, 1H, Fur-*H*), 7.00 (s, 2H, Tip-*H*), 6.57 (dd, *J* = 3.5, 1.6 Hz, 1H, Fur-*H*), 2.96 – 2.87 (m, 1H, *p*-^{i}Pr-*H*), 2.66 – 2.57 (m, 2H, *o*-^{i}Pr-*H*), 1.28 (d, *J* = 6.9 Hz, 6H, *p*-^{i}Pr-C*H*$_3$), 1.24 (d, *J* = 6.7 Hz, 6H, *o*-^{i}Pr-C*H*$_3$), 1.13 (d, *J* = 6.7 Hz, 6H, *o*-^{i}Pr-C*H*$_3$); ^{11}B NMR (160 MHz, $CDCl_3$): δ = 57.0 (s); ^{13}C NMR (126 MHz, $CDCl_3$): δ = 161.6 (br. s, Fur-*C*-B), 151.4 (s, Fur-*C*H), 150.1 (s, Tip-*C*-*p*-^{i}Pr), 149.9 (s, Tip-*C*-*o*-^{i}Pr), 131.3 (s, Fur-*C*H), 122.2 (br. s, Tip-*C*-B), 120.6 (s, Tip-*C*H), 112.4 (s, Fur-*C*H), 35.6 (s, *o*-^{i}Pr-*C*H), 34.5 (s, *p*-^{i}Pr-*C*H), 24.7 (s, *o*-^{i}Pr-*C*H$_3$), 24.2 (s, *o*-^{i}Pr-*C*H$_3$), 24.1 (s, *p*-^{i}Pr-*C*H$_3$).

21a^{Mes*}: Yield: 28 %. ^{1}H NMR (500 MHz, $CDCl_3$): δ = 7.89 (d, *J* = 4.5 Hz, 1H, Thi-*H*), 7.44 (s, 2H, Mes*-*H*), 7.22 – 7.18 (m, 1H, Thi-*H*), 1.36 (s, 9H, *p*-^{t}Bu-C*H*$_3$), 1.35 (s, 18H, *o*-^{t}Bu-C*H*$_3$); ^{11}B NMR (160 MHz, $CDCl_3$): δ = 57.0 (s); ^{13}C NMR (126 MHz, $CDCl_3$): δ = 152.3 (s, Mes*-*C*-*o*-^{t}Bu), 150.3 (s, Mes*-*C*-*p*-^{t}Bu), 149.3 (s, Thi-*C*H), 141.8 (br. s, Thi-*C*-B), 138.5 (s, Thi-*C*H), 133.0 (br. s, Mes*-*C*-B), 129.3 (s, Thi-*C*H), 122.6 (s, Mes*-*C*H), 38.7 (s, *o*-^{t}Bu-*C*H$_3$), 35.0 (s, *p*-^{t}Bu-*C*H$_3$), 34.8 (s, *o*-^{t}Bu-*C*H$_3$), 31.5 (s, *p*-^{t}Bu-*C*H$_3$); HR-MS (LIFDI): m/z = 420.1465; calcd. for $C_{22}H_{32}BBrS$: 418.1501.

22a^{Mes*}: Yield: 23%. ^{1}H NMR (500 MHz, $CDCl_3$): δ = 7.83 (d, *J* = 4.3 Hz, 1H, Thi-*H*), 7.44 (s, 2H, Mes*-*H*), 7.16 (s, 1H, Thi-*H*), 1.36 (s, 9H, *p*-^{t}Bu-C*H*$_3$), 1.34 (s, 18H, *o*-^{t}Bu-C*H*$_3$); ^{11}B NMR (160 MHz, $CDCl_3$): δ = 59.3 (s); ^{13}C NMR (126 MHz, $CDCl_3$): δ = 152.6 (s, Mes*-*C*-*o*-^{t}Bu), 150.2 (s, Mes*-*C*-*p*-^{t}Bu), 148.2 (br. s, Thi-*C*H), 141.9 (s, Thi-*C*-B), 137.5 (s, Thi-*C*H), 131.7 (s, Mes*-*C*-B), 129.1 (s, Thi-*C*H), 122.3 (s, Mes*-*C*H), 38.5 (s, *o*-^{t}Bu-*C*H$_3$), 35.0 (s, *p*-^{t}Bu-*C*H$_3$), 34.5 (s, *o*-^{t}Bu-*C*H$_3$), 31.5 (s, *p*-^{t}Bu-*C*H$_3$); HR-MS (LIFDI): m/z = 374.1991; calcd. for $C_{22}H_{32}BClS$: 374.2006.

22b^{Mes*}: Yield: 10%. ^{1}H NMR (500 MHz, $CDCl_3$): δ = 7.74 (s, 1H, Fur-*H*), 7.44 (s, 2H, Mes*-*H*), 6.56 – 6.49 (m, 1H, Fur-*H*), 1.35 (s, 9H, *p*-^{t}Bu-C*H*$_3$), 1.33 (s, 18H, *o*-^{t}Bu-C*H*$_3$); ^{11}B NMR (160 MHz, $CDCl_3$): δ = 56.1 (s); HR-MS (LIFDI): m/z = 358.2222; calcd. for $C_{22}H_{32}BClO$: 358.2235.

General procedure for the synthesis of monoarylated compounds 23^{Tip} and 24^{Tip}. To a solution of **19a,b** (1.0 equiv.) in DCM (1 M) was added TMS-OMe (3 equiv.) or TMS-OCH_2CF_3 (3 equiv.) at ambient temperatures and the resulting solution was stirred overnight. All volatiles were removed in vacuo and the crude compound was further purified by addition of pentane and crystallization at low temperatures. Compounds **23** and **24** were obtained as colored solids.

23a^{Tip}. Yield: 63 %. ^{1}H NMR (400 MHz, $CDCl_3$): δ = 7.66 (dd, *J* = 4.7, 0.7 Hz, 1H, Thi-*H*), 7.35 (dd, *J* = 3.5, 0.7 Hz, 1H, Thi-*H*), 7.12 (dd, *J* = 4.6, 3.5 Hz, 1H, Thi-*H*), 7.01 (s, 2H, Tip-*H*), 3.76 (s, 3H, -OC*H*$_3$), 2.98 – 2.86 (m, 1H, *p*-^{i}Pr-*H*), 2.69 – 2.54 (m, 2H, *o*-^{i}Pr-*H*), 1.30 (d, *J* = 6.9 Hz, 6H, *p*-^{i}Pr-C*H*$_3$), 1.24 (d, *J* = 6.9 Hz, 6H, *o*-^{i}Pr-C*H*$_3$), 1.08 (d, *J* = 6.7 Hz, 6H, *o*-^{i}Pr-C*H*$_3$); ^{11}B NMR (126 MHz, $CDCl_3$): δ = 45.2 (s); MS (ESI): m/z = 328.1; calcd. for $C_{20}H_{29}BOS$: 328.2.

23b^{Tip}. Yield: 56 %. ^{1}H NMR (500 MHz, $CDCl_3$): δ = 7.67 (dd, *J* = 1.5, 0.5 Hz, 1H, Fur-*H*), 6.99 (s, 2H, Tip-*H*), 6.80 (d, *J* = 3.3 Hz, 1H, Fur-*H*), 6.39 (dd, *J* = 3.3, 1.6 Hz, 1H, Fur-*H*), 3.78 (s, 3H, -OC*H*$_3$), 2.96 – 2.86 (m, 1H, *p*-^{i}Pr-*H*), 2.66 – 2.57 (m, 2H, *o*-^{i}Pr-*H*), 1.29 (d, *J* = 6.9 Hz, 6H, *p*-^{i}Pr-C*H*$_3$), 1.24 (d, *J* = 6.8 Hz, 6H, *o*-^{i}Pr-C*H*$_3$), 1.09 (d, *J* = 6.7 Hz, 6H, *o*-^{i}Pr-C*H*$_3$); ^{11}B NMR (160 MHz, $CDCl_3$): δ = 42.7 (s); ^{13}C NMR (126 MHz, $CDCl_3$): δ = 159.8 (s, Fur-*C*-B), 150.6 (s, Tip-*C*-*o*-^{i}Pr), 149.6 (s, Tip-*C*-*p*-^{i}Pr), 147.6 (s, Fur-C*H*), 131.9 (s, Tip-*C*-B), 126.3 (s, Fur-C*H*), 120.3 (s, Tip-C*H*), 110.7 (s, Fur-*H*), 55.7 (s, -O*C*H$_3$), 35.2 (s, *o*-^{i}Pr-*C*H), 34.4 (s, *p*-^{i}Pr-*C*H), 24.8 (s, *o*-^{i}Pr-*C*H$_3$), 24.6 (s, *o*-^{i}Pr-*C*H$_3$), 24.2 (s, *p*-^{i}Pr-*C*H$_3$); HR-MS (APCI): m/z = 313.2326; calcd. for $C_{20}H_{29}BO_2$: 312.2261.

24a^{Tip}. Yield: 27 %. ^{1}H NMR (500 MHz, $CDCl_3$): δ = 7.73 (dd, *J* = 4.7, 1.0 Hz, 1H, Thi-*H*), 7.48 (dd, *J* = 3.5, 1.0 Hz, 1H, Thi-*H*), 7.16 (dd, *J* = 4.7, 3.5 Hz, 1H, Thi-*H*), 7.02 (s, 2H, Tip-*H*), 4.24 (d, *J* = 8.5 Hz, 2H, -OC*H*$_2$CF$_3$), 2.97 – 2.87 (m, 1H, *p*-^{i}Pr-*H*), 2.62 – 2.50 (m, 2H, *o*-^{i}Pr-*H*), 1.29 (d, *J* = 6.9 Hz, 6H, *p*-^{i}Pr-C*H*$_3$), 1.22 (d, *J* = 6.7 Hz, 6H, *o*-^{i}Pr-C*H*$_3$), 1.07 (d, *J* = 6.6 Hz, 6H, *o*-^{i}Pr-C*H*$_3$); ^{11}B NMR (160 MHz, $CDCl_3$): δ = 45.8 (s); ^{13}C NMR (126 MHz, $CDCl_3$): δ = 150.7 (s, s, Tip-*C*-*o*-^{i}Pr), 150.4 (s, Tip-*C*-*p*-^{i}Pr), 140.4 (Thi-*C*-B), 140.1 (s, Thi-*C*H), 134.6 (s, Thi-*C*H), 131.0 (br. s, Tip-C-*B*), 128.5 (s, Thi-*C*H), 120.8 (s, Tip-*C*H), 66.1-65.2 (q, -O*C*H$_2$CF$_3$), 35.4 (s, *o*-^{i}Pr-*C*H), 34.5 (s, *p*-^{i}Pr-*C*H), 25.0 (s, *o*-^{i}Pr-*C*H$_3$), 24.5 (s, *o*-^{i}Pr-*C*H$_3$), 24.2 (s, *p*-^{i}Pr-*C*H$_3$); ^{19}F NMR (471 MHz, $CDCl_3$): δ = -75.3 (s); HR-MS (APCI): m/z = 396.2 $[M-H]^+$; calcd. for $C_{21}H_{28}BF_3OS$: 397.2.

24b^{Tip}: Yield: 91 %. ^{1}H NMR (500 MHz, $CDCl_3$): δ = 7.71 (dd, *J* = 1.6, 0.6 Hz, 1H, Fur-*H*), 7.01 (s, 2H, Tip-*H*), 6.97 (dd, *J* = 3.4, 0.6 Hz, 1H, Fur-*H*), 6.43 (dd, *J* = 3.4, 1.6 Hz, 1H, Fur-*H*), 4.32 (d, *J* = 8.5 Hz, 2H, -OC*H*$_2$CF$_3$), 2.91 (d, *J* = 6.9 Hz, 1H, *p*-^{i}Pr-*H*), 2.62 – 2.46 (m, 2H, *o*-^{i}Pr-*H*), 1.29 (d, *J* = 6.9 Hz, 6H, *p*-^{i}Pr-C*H*$_3$), 1.23 (d, *J* = 6.6 Hz, 6H, *o*-^{i}Pr-C*H*$_3$), 1.09 (d, *J* = 6.5 Hz, 6H, *o*-^{i}Pr-C*H*$_3$); ^{11}B NMR (160 MHz, $CDCl_3$): δ = 43.9 (s); ^{13}C NMR (126 MHz, $CDCl_3$): δ = 158.6 (s, Fur-*C*-B), 150.8 (s, Tip-*C*-*o*-^{i}Pr), 150.3 (s, Tip-*C*-*p*-^{i}Pr), 148.5 (s, Fur-C*H*), 130.6 (s, Tip-*C*-

B), 127.7 (s, Fur-*C*H), 120.7 (s, Tip-C*H*), 110.9 (s, Fur-*C*H), 66.0-65.2 (q, O*C*H$_2$CF$_3$), 35.4 (s, *o*-^{i}Pr-*C*H), 34.5 (s, *p*-^{i}Pr-*C*H), 25.0 (s, *o*-^{i}Pr-*C*H$_3$), 24.3 (s, *o*-^{i}Pr-*C*H$_3$), 24.1 (s, *p*-^{i}Pr-*C*H$_3$); ^{19}F NMR (471 MHz, $CDCl_3$) δ -75.27 (t, *J* = 8.5 Hz).

General procedure for the syntheses of triarylboranes 4a,b^{Tip} from monoarylated compounds 19-24. A solution of compounds **19-24** (0.5 mmol) in toluene (0.5 mL) was added to a suspension of ThiLi (0.045 g, 0.5 mmol) in toluene (0.5 mL) at ambient temperature. The reaction mixture was stirred overnight and then quenched by the addition of water. After aqueous work-up and removal of all volatiles, the crude triarylborane **4** was obtained in high purity. The recorded ^{1}H- and ^{11}B{^{1}H} spectra were compared to the data previously obtained in our group.[6]

4a^{Tip} via **19a**. Yield: 93 %.

4a^{Tip} via **20a**. Yield: 64 %.

4a^{Tip} via **23a**. Yield: 93 %.

4b^{Tip} via **19b**. Yield: 40 %.

Synthesis of 25a. To a solution of **5a** (0.114 g, 0.5 mmol) and **12a** (0.082 g, 0.5 mmol) in $CDCl_3$ (0.5 mL) was added catalyst **B** (0.017 g, 0.045 mmol, 9 mol%). The reaction mixture was stirred for 3 days and the reaction progress was monitored by ^{1}H and ^{11}B{^{1}H} NMR spectroscopy. Then, all volatiles were removed in vacuo and the crude solid was redissolved in toluene (1.5 mL). A solution of TipLi (0,126 g, 0.6 mmol) in toluene (1.5 mL) was added at ambient temperature and the reaction was stirred overnight. The reaction mixture was washed with brine (3 x 5.0 ml), dried over $MgSO_4$ and all volatiles were removed in vacuo. The crude product was purified by column chromatography (PE) and **25a** was obtained as colorless solid. The synthesis can also be carried out via the reaction of **1a** (1.143 g, 5.0 mmol) with **2a** (1.269 g, 5.0 mmol) in the presence of catalyst **B** (0.177 g, 0.5 mmol, 10 mol%).

25a: Yield: 1.320 g (2.90 mmol, 58%). ^{1}H NMR (400 MHz, $CDCl_3$): δ = 7.91 (dd, *J* = 4.7, 0.9 Hz, 1H, Thi-*H*), 7.86 (dd, *J* = 3.6, 0.9 Hz, 1H, Thi-*H*), 7.83 (d, *J* = 3.4 Hz, 1H, Thi-*H*), 7.40 (d, *J* = 3.4 Hz, 1H, Thi-*H*), 7.29 (dd, *J* = 4.7, 3.6 Hz, 1H, Thi-*H*), 7.01 (s, 2H, Tip-*H*), 3.03 – 2.91 (m, 1H, *p*-^{i}Pr-*H*), 2.59 – 2.45 (m, 2H, *o*-^{i}Pr-*H*), 1.34 (d, *J* = 6.9 Hz, 6H, *p*-^{i}Pr-C*H*$_3$), 1.05 (dd, *J* = 6.7, 3.0 Hz, 12H, *o*-^{i}Pr-C*H*$_3$), 0.38 (s, 9H, -Si(C*H*$_3$)$_3$); ^{11}B NMR (126 MHz, $CDCl_3$): δ = 55.5 (s); ^{13}C NMR (101 MHz, $CDCl_3$): δ = 154.4 (s, Thi-*C*-Si), 150.4 (s, Thi-*C*-B), 149.8 (s, Tip-*C*-*o*-^{i}Pr), 148.6 (s, Tip-*C*-*p*-^{i}Pr), 145.7 (s, Thi-*C*-B), 143.2 (s, Thi-*C*H), 142.3 (s, Thi-*C*H), 139.6 (s, Tip-*C*-B), 137.4 (s, Thi-*C*H), 135.6 (s, Thi-*C*H), 129.0 (s, Thi-*C*H), 120.1 (s, Tip-*C*H), 35.4 (s, *o*-^{i}Pr-*C*H), 34.4 (s, *p*-^{i}Pr-*C*H), 24.5 – 24.2 (m, *o/p*-^{i}Pr-*C*H$_3$), 0.1 (s, Si(*C*H$_3$)$_3$); ^{29}Si NMR (79 MHz, $CDCl_3$): δ = -6.1 (s); MS (ESI): m/z = 452.2; calcd. for $C_{26}H_{37}BS_2Si$: 452.2.

Synthesis of 25b. A solution of **1b** (0.60 g, 4.0 mmol) in DCM (2 mL) was cooled to 0 °C and treated with a solution of BCl_3 in DCM (1.95 mmol, 1M, 1.95 ml). After the reaction mixture was stirred for 2 h at 0 °C, **12b** (0.429 g, 2.0 mmol) and $Me_3Si\text{-}NTf_2$ (0.070 gg, 0.2 mmol), 10 mol%) were added. The reaction mixture was allowed to warm up to ambient temperature overnight. Subsequently, after removal of all volatiles in vacuo, a solution of Mes*Li (0.505 g, 2 mmol) in Et_2O (6.0 ml) was added at ambient temperature and the resulting suspension was stirred overnight. The reaction mixture was washed with brine (3 x 5.0 ml), dried over $MgSO_4$ and all volatiles were removed under reduced pressure. The crude product was purified by column chromatography (PE) and **25b** was obtained as colorless solid.

25b: Yield: 0.183 g (0.36 mmol, 21%). ^{1}H NMR (500 MHz, $CDCl_3$): δ = 7.75 (dd, *J* = 1.6, 0.6 Hz, 1H, Fur-*H*), 7.42 (s, 2H, Mes*-*H*), 7.35 (s, 1H, Fur-*H*), 7.16 (s, 1H, Fur-*H*), 6.70 (d, *J* = 3.3 Hz, 1H, Fur-*H*), 6.53 (dd, *J* = 3.4, 1.6 Hz, 1H, Fur-*H*), 1.39 (s, 9H, *p*-^{t}Bu-CH_3), 1.16 (s, 18H, *o*-^{t}Bu-CH_3), 0.30 (s, 9H, -Si(CH_3)$_3$); ^{11}B NMR (126 MHz, $CDCl_3$): δ = 47.5 (s); ^{13}C NMR (126 MHz, $CDCl_3$): δ = 168.1 (s, Fur-*C*-Si), 166.9 (s, Fur-*C*-B), 152.2 (s, Mes*-*C*-*o*-^{t}Bu), 148.3 (s, Mes*-*C*-*p*-^{t}Bu), 147.8 (s, Fur-*C*H), 133.0 (s, Mes*-*C*-B), 128.0 (s, Fur-*C*H), 127.4 (s, Fur-*C*H), 121.8 (s, Mes*-*C*H), 120.9 (s, Fur-*C*H), 111.6 (s, Fur-*C*H), 38.3 (s, *o*-^{t}Bu-*C*H$_3$), 34.4 (s, *p*-^{t}Bu-*C*H$_3$), 34.2 (s, *o*-^{t}Bu-*C*H$_3$), 31.6 (s, *p*-^{t}Bu-*C*H$_3$), -1.4 (s); ^{29}Si NMR (99 MHz, $CDCl_3$): δ = -10.2 (s); HR-MS (APCI): m/z = 463.3191 [M+H$^+$]; calcd. for $C_{29}H_{43}BO_2Si$: 462.3125.

Synthesis of 26a. A solution of **25a** (2.226 g, 5.0 mmol) in DCM (10 mL) was cooled to 0 °C and BBr_3 (1.466 g, 6.25 mmol) was added. The reaction was stirred at 0 °C for 3 h and then allowed to warm up to ambient temperatures. All volatiles were removed *in vacuo* to give a dark, viscous oil. The crude product was dissolved in hexane and filtered. The solvent was removed in vacuo to afford the desired product as a brown, highly viscous oil in approx. 95% purity by ^{1}H-NMR.

26a: Yield: 2.048 g (3.7 mmol, 74%). ^{1}H NMR (300 MHz, $CDCl_3$): δ = 8.21 (d, *J* = 3.7 Hz, 1H, Thi-*H*), 8.04 (dd, *J* = 5.8, 4.2 Hz, 2H, Thi-*H*), 7.99 (d, *J* = 3.7 Hz, 1H, Thi-*H*), 7.39 (dd, *J* = 4.7, 3.6 Hz, 1H, Thi-*H*), 7.14 (s, 2H, Tip-*H*), 3.13 – 3.01 (m, 1H, *p*-^{i}Pr-*H*), 2.65 – 2.49 (m, 2H, *o*-^{i}Pr-*H*), 1.43 (d, *J* = 6.9 Hz, 6H, *p*-^{i}Pr-CH_3), 1.17 (d, *J* = 6.7 Hz, 12H, *o*-^{i}Pr-CH_3); ^{11}B NMR (126 MHz, $CDCl_3$): 50.3 (s).

Synthesis of 29a. A solution of **26a** (1,65 g, 3.00 mmol) in toluene (9 mL) was cooled to −78 °C and a solution of TipLi (0.694 mg, 3.30 mmol) in toluene (4 mL) was added. The reaction was allowed to slowly warm up to ambient temperature and stirred for 3 d. The reaction mixture was filtered followed by removal of all volatiles in vacuo. For further purification of the product, the solid was washed with pentane twice, then dried in vacuo and precipitated in cold toluene (-30 °C). After filtration, the compound was obtained as an off white solid.

29a: Yield: 1.149 g (1.68 mmol, 56%). ^{1}H NMR (500 MHz, $CDCl_3$): δ = 8.00 (d, *J* = 3.7 Hz, 1H, Thi-*H*), 7.98 (dd, *J* = 4.7, 0.9 Hz, 1H, Thi-*H*), 7.90 – 7.88 (m, 2H, Thi-*H*), 7.32 (dd, *J* = 4.7, 3.6 Hz, 1H, Thi-*H*), 6.99 (s, 2H, Tip-*H*), 6.99 (s, 2H, Tip-*H*), 2.93 (dd, *J* = 6.9, 2.6 Hz, 2H, *p*-^{i}Pr-C*H*), 2.68 – 2.60 (m, 2H, *o*-^{i}Pr-C*H*), 2.48 – 2.41 (m, 2H, *o*-^{i}Pr-C*H*), 1.30 (dd, *J* = 9.9, 6.9 Hz, 12H), 1.25 (d, *J* = 6.7 Hz, 6H), 1.11 (d, *J* = 6.7 Hz, 6H), 1.02 (dd, *J* = 13.6, 6.7 Hz, 12H); ^{11}B NMR (160 MHz, $CDCl_3$): 59.6 (s); ^{13}C NMR (126 MHz, $CDCl_3$): δ = 159.5 (br. s, Thi-*C*-B), 155.0 (br. s, Thi-*C*-B), 150.3 (s, Tip-*C*-*o*-^{i}Pr), 149.7 (s, Tip-*C*-*o/p*-^{i}Pr), 149.1 (s, Tip-*C*-*o/p*-^{i}Pr), 145.3 (br. s, Thi-*C*-B), 143.3 (s, Thi-*C*H), 143.2 (s, Thi-*C*H), 142.0 (s, Thi-*C*H), 138.9 (Thi-*C*H), 138.8 (br. s, Tip-*C*-B), 137.4, 136.8 (Tip-*C*-B), 129.4 (s, Thi-*C*H), 120.8 (s, Tip-*C*H), 120.3 (s, Tip-*C*H), 35.8 (s, *o*-^{i}Pr-*C*H), 35.7 (*p*-^{i}Pr-*C*H), 34.5 (*o*-^{i}Pr-*C*H), 34.4 (*p*-^{i}Pr-*C*H), 24.5, 24.3, 24.3, 24.2, 24.1, 24.1; HR-MS (APCI): m/z = 672.2802 [M-H^{+}]; calcd. for $C_{38}H_{51}B_2BrS_2$: 675.2835.

Synthesis of 30a. To a solution of **29a** (0.032 g, 0.048 mmol) in CDCl3 (0.5 mL, in a Young-NMR-tube), Me_3Si-OMe (0.030 g, 0.285 mmol) was added at ambient temperature. After stirring for 2 h, ^{1}H-NMR spectroscopy indicated the complete conversion of **29a**. All volatiles were removed in vacuo to give an off-white solid.

30a: Yield: ^{1}H NMR (500 MHz, $CDCl_3$): δ = 7.91 (dd, *J* = 4.7, 0.9 Hz, 1H, Thi-*H*), 7.88 (dd, *J* = 3.6, 0.9 Hz, 1H, Thi-*H*), 7.75 (d, *J* = 3.5 Hz, 1H, Thi-*H*), 7.45 (d, *J* = 3.5 Hz, 1H, Thi-*H*), 7.28 (dd, *J* = 4.7, 3.6 Hz, 1H, Thi-*H*), 7.01 (s, 2H, Tip-*H*), 6.98 (s, 2H, Tip-*H*), 3.78 (s, 3H, -OCH_3), 2.98 – 2.88 (m, 2H, *p*-^{i}Pr-C*H*), 2.65 – 2.58 (m, 2H, *o*-^{i}Pr-C*H*), 2.53 – 2.44 (m, 2H, *o*-^{i}Pr-C*H*), 1.30 (t, *J* = 7.0 Hz, 12H), 1.27 – 1.22 (m, 6H), 1.07 (d, *J* = 6.1 Hz, 6H), 1.03 (d, *J* = 6.7 Hz, 6H), 1.00 (d, *J* = 6.7 Hz, 6H), ^{11}B NMR (160 MHz, $CDCl_3$): 58.6 (s, Ar_3*B*), 45.3 (s, Ar*B*OMe); ^{13}C NMR (126 MHz, $CDCl_3$): δ = 152.4 (br. s, Thi-*C*-B), 150.3 (br. s, Thi-*C*-B), 149.7 (s, Tip-*C*-*o*-^{i}Pr), 149.6 (s, Tip-*C*-*o/p*-^{i}Pr), 148.6 (s, Tip-*C*-*o/p*-^{i}Pr), 145.6 (br. s, Thi-*C*-B), 142.4 (s, Thi-*C*H), 142.3 (s, Thi-*C*H), 139.6 (s, Thi-*C*H), 137.7 (s, Thi-*C*H), 132.8 (br. s, Tip-*C*-B), 129.1 (s, Thi-*C*H), 120.4 (s, Tip-*C*H), 120.1 (s, Tip-*C*H), 56.2 (s, B-O*C*H_3), 35.4 (d, *J* = 14.8 Hz), 34.4 (d, *J* = 10.5 Hz), 24.7 (s), 24.3 (dd, *J* = 8.6, 6.6 Hz); HR-MS (APCI): m/z = 624.3802; calcd. for $C_{39}H_{54}B_2BS_2$: 624.3780.

Synthesis of 31a. **29a** (0.041 g, 0.061 mmol) was dissolved in $CDCl_3$ (0.5 mL) and Me_3Si-OCH_2CF_3 (0.060 g, 0.384 mmol) was added at ambient temperature. After 2 h, all volatiles were removed in vacuo affording an off-white solid in high purity.

31a: Yield: 0.020 g (0.028 mmol, 46%). ^{1}H NMR (500 MHz, $CDCl_3$): δ = 7.94 (dd, *J* = 4.7, 0.9 Hz, 1H, Thi-*H*), 7.90 (dd, *J* = 3.6, 0.9 Hz, 1H, Thi-*H*), 7.77 (d, *J* = 3.6 Hz, 1H, Thi-*H*), 7.63 (d, *J* = 3.6 Hz, 1H, Thi-*H*), 7.31 (dd, *J* = 4.7, 3.6 Hz, 1H, Thi-*H*), 7.04 (s, 2H, Tip-*H*), 7.00 (s, 2H, Tip-*H*), 4.29 (q, *J* = 8.5 Hz, 2H, -O*C*H_2CF_3), 2.95 (dd, *J* = 12.4, 6.9 Hz, 2H, *p*-^{i}Pr-C*H*), 2.64 – 2.54 (m, 2H, *o*-^{i}Pr-C*H*), 2.53 – 2.46 (m, 2H, *o*-^{i}Pr-C*H*), 1.32 (dd, *J* = 6.9, 6.1 Hz, 12H), 1.25 (s, 6H), 1.09 (s, 6H), 1.05 (d, *J* = 6.7 Hz, 6H), 1.01 (d, *J* = 6.7 Hz, 6H); ^{11}B NMR (160 MHz, $CDCl_3$):

57.3 (s, Ar_3B), 46.3 (s, Ar_2BOR); ^{13}C NMR (126 MHz, $CDCl_3$): δ = 153.8 (br. s, Thi-*C*-B), 151.6 (br. s, Thi-*C*-B), 150.6 (Tip-*C*-*o*/*p*-^{i}Pr), 150.5 (Tip-*C*-*o*/*p*-^{i}Pr), 149.7 (Tip-*C*-*o*/*p*-^{i}Pr), 148.8 (Tip-*C*-*o*/*p*-^{i}Pr), 145.6 (br. s, Thi-*C*-B), 142.6 (Thi-*C*H), 142.3 (Thi-*C*H), 140.2 (s, Thi-*C*H), 139.3 (br. s, Tip-*C*-B), 138.1 (Thi-*C*H), 131.0 (br. s, Tip-*C*-B), 129.2 (s, Thi-*C*H), 127.1, 124.9, 122.7, 122.2, 120.9 (s, Tip-*C*H), 120.2 (s,Tip-*C*H), 66.2-65.3 (q, OCH_2CF_3), 35.6, 35.6, 34.5, 34.4, 24.3, 24.3, 24.3, 24. 3, 24.1; ^{19}F NMR (471 MHz, $CDCl_3$) δ -75.1 (t, *J* = 8.5 Hz); HR-MS (APCI): m/z = 692.3676 [M-H$^+$]; calcd. for $C_{40}H_{53}B_2F_3OS_2$: 693.3726.

Synthesis of 28a via 27a. To a solution of **26a** (0.275 g, 0.50 mmol) in DCM (0.5 mL), **1a** (0.082 g, 0.53 mmol) and Me_3Si-NTf_2 (0.018 g, 0.05 mmol, 10 mol%) were added and the resulting mixture was stirred for 48 h. The reaction progress was monitored and after complete conversion (^{1}H NMR (300 MHz, $CDCl_3$): δ = 8.28 – 8.24 (m, 2H, Thi-*H*), 8.04 (dd, *J* = 4.7, 1.0 Hz, 1H, Thi-*H*), 8.00 (d, *J* = 3.7 Hz, 1H, Thi-*H*), 7.97 (dd, *J* = 3.6, 0.9 Hz, 1H, Thi-*H*), 7.92 (d, *J* = 3.7 Hz, 1H, Thi-*H*), 7.36 (ddd, *J* = 10.5, 4.7, 3.7 Hz, 2H, Thi-*H*), 7.05 (s, 2H, Tip-*H*), 3.03 – 2.91 (m, 1H, *p*-i^{Pr}-C*H*), 2.59 – 2.43 (m, 2H, *o*-i^{Pr}-C*H*), 1.35 (d, *J* = 6.9 Hz, 6H, *p*-i^{Pr}-CH_3), 1.08 (dd, *J* = 6.7, 2.6 Hz, 12H, *o*-i^{Pr}-CH_3); ^{11}B NMR (96 MHz, $CDCl_3$): δ = 52.6 (s)), all volatiles were removed in vacuo and the resulting crude solid was redissolved in toluene (2.0 mL). The solution was cooled to –78 °C and a solution of TipLi (0.115 g, 0.55 mmol) in toluene (1.5 mL) was added. After stirring for 24 h, the reaction was quenched by the addition of *n*-pentane and all volatiles were removed in vacuo. After aqueous work-up and repeated washing with methanol, a yellow solid was obtained. Yield: 0.127 g (0.19 mmol, 38%). The data obtained for ^{1}H and ^{11}B-NMR spectroscopy are in good accordance with data previously reported in our group.[6b]

Synthesis of 28a via 29a.

a) In toluene: To a suspension of 1-thienyllithium (0.023 g, 0.26 mmol) in toluene (0.5 mL), a solution of **29a** (0.084 g, 0.125 mmol) in toluene (1 mL) was added at −78 °C. The reaction was allowed to slowly warm up to ambient temperature and was stirred for 48 h. The reaction was quenched by the addition of isopropanol and pentane. All volatiles were removed in vacuo and the resulting solid was extracted with pentane and brine solution. After aqueous work-up, all volatiles were removed in vacuo to afford the **28a** as yellow oil.

b) In toluene/Et_2O: The reaction can also be carried out via combining Thi-Li (0.023 g, 0.26 mmol) in Et_2O (0.5 mL) with a suspension of **29a** (0.168 g, 0. 25 mmol) in toluene (0.5 mL). After stirring overnight, removal off all volatiles in vacuo, aqueous work-up and purification by column chromatography (PE; silica), **28a** was obtained as colorless solid.

Yield: 0.055 g (0.081 mmol, 36%). The data obtained for ^{1}H and ^{11}B-NMR spectroscopy are in good accordance with data previously reported in our group.[6b]

Synthesis of 28a via 30a. An in *situ* prepared solution of **30a** (starting from **29a**: 0.1684 g, 0.25 mmol) in Et_2O or THF (0.5 mmol) was added to a solution of Thi-Li (0.023 g, 0.26 mmol) in Et_2O (0.5 mL) at ambient temperatures. After removal of all volatiles in vacuo, a slightly yellow solid was obtained in high purity.

Synthesis of oligomer 34a via 32a (*Route A*). To a solution of **5a** (0.326 g, 1.0 mmol) in DCM (1.0 mL) was added $Me_3Si\text{-}NTf_2$ (0.035 g, 0.1 mmol, 10mol%) and the reaction mixture was stirred for 3 d. After stirring for 24 h, precipitation occurred. The solvent was removed in vacuo and the residue was redissolved in DCM (2 ml). Subsequently, **1a** (0.058 g, 0.5 mmol) and $Me_3Si\text{-}NTf_2$ (0.017 g, 0.05 mmol) were added and the reaction mixture was stirred for additional 2 d. The solvent was removed in vacuo, the residue dissolved in toluene (2.0 ml) and a solution of TipLi (0.210 g, 1.0 mmol) in toluene (1.0 ml) was added and the reaction mixture was stirred for 3 d. The solvent was removed in vacuo and after aqueous work-up and repeated precipitation in a mixture of pentane and ethanol, **34a** was obtained as an off-white solid.

Yield: (0.066 g, 18%). ^{1}H NMR (300 MHz, $CDCl_3$): δ = 7.90 (m, 13H), 6.97 (m, 13H), 2.91 (m, 9H), 2.48 (m, 15H), 1.29 (m, 57H), 1.00 (m, 105H), 0.34 (s, 9H) ppm. The data obtained for ^{1}H and ^{11}B-NMR spectroscopy are in good accordance with data previously reported in our group.[6a]

Synthesis of oligomer 34a via 33a (*Route B*). To a solution of **5a** 0.326 g, 1.0 mmol) in DCM (1.0 mL) was added $Me_3Si\text{-}NTf_2$ (0.035 g, 0.1 mmol, 10mol%) and the reaction mixture was stirred for 3 d. After stirring for 24 h, precipitation occurred. The solvent was removed in vacuo and the residue was redissolved in toluene (3.0 ml). Subsequently, a solution of TipLi (0.210 g, 1.0 mmol) in toluene (3.0 mL) was added and the reaction mixture was stirred for additional 3 d. The solvent was removed in vacuo, the residue redissolved in toluene (3 ml) and the resulting suspension was treated with a solution of ThiLi (0.045 g, 0.50 mmol) in Et_2O (1.5 ml) and stirred for 3 d. The solvent was removed in vacuo and after aqueous work-up and repeated precipitation in a mixure of pentane and ethanol, **34a** was obtained as an off-white solid.

Yield: (0.078 g, 21%). The data obtained for ^{1}H and ^{11}B-NMR spectroscopy are in good accordance with data previously reported in our group.[6a]

X-Ray structural analysis

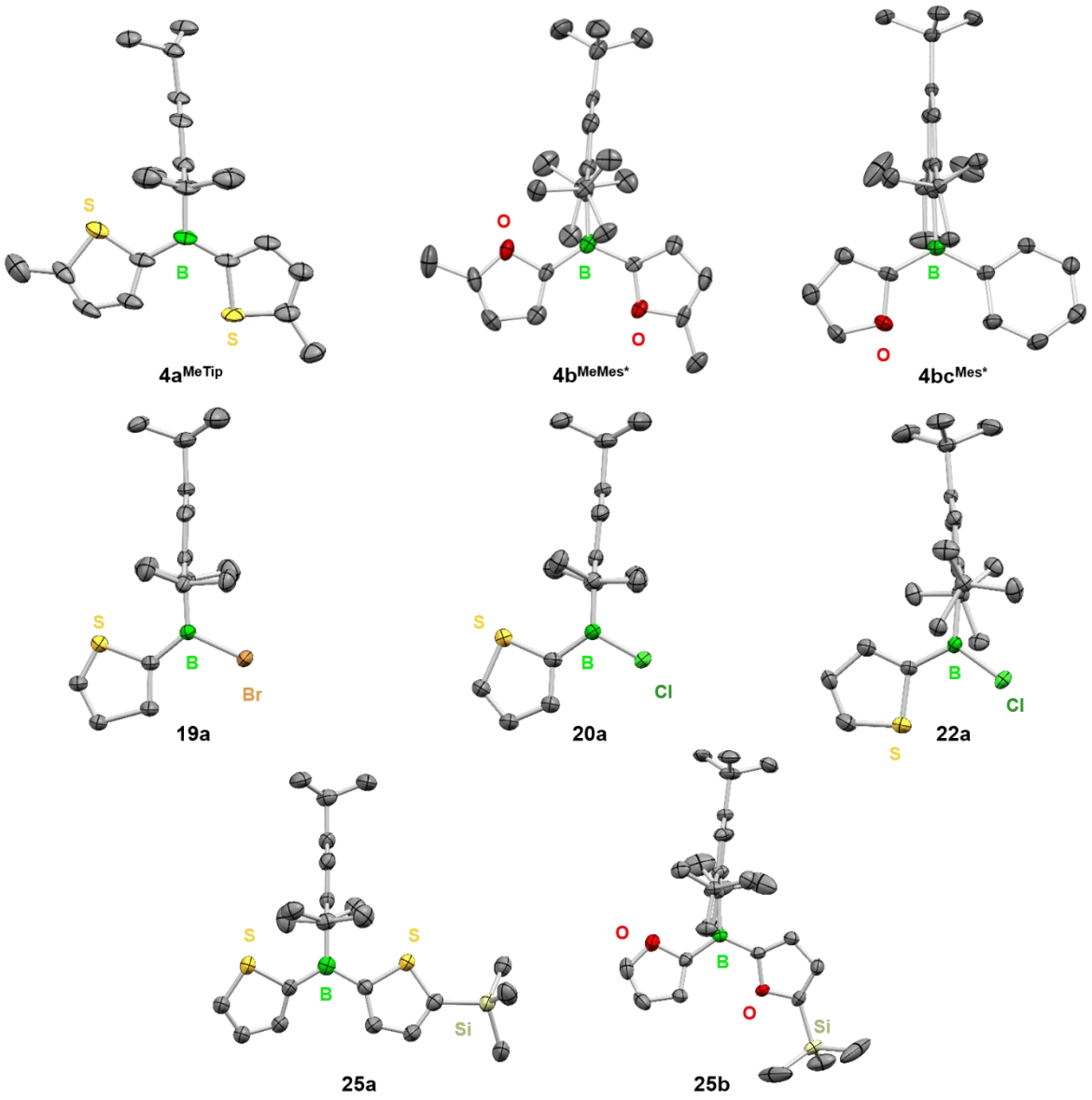

Figure 2.6.12. From top left to bottom right: Molecular structure of **4a**^{MeTip}, **4b**^{MeMes*}, **4bc**^{Mes*}, **19a, 20a, 22a, 25a** and **25b** in the solid state (H-Atoms omitted for clarity).

Table 2.6.3. Crystal structure and refinement data for **19a**, **20a**, **22a**.

No.	**19a**	**22a**	**20a**
Size / mm	0.28 x 0.26 x 0.25	0.22 x 0.14 x 0.14	0.32 x 0.29 x 0.23
Empiric Formula	C19 H26 B Br S	C22 H32 B Cl S	C19 H26 B Cl S
M	377.18	374.79	332.72
Crystal system	monoclinic	monoclinic	monoclinic
Space group	P 1 21/n 1	P 1 21/c 1	P 1 21/n 1
a/Å	9.0955(5)	10.2631(6)	9.126(2)
b/Å	15.9687(8)	18.3945(10)	16.008(4)
c/Å	13.1652(7)	11.7484(6)	12.939(3)
α/°	90	90	90
β/°	93.9160(10)	102.2730(10)	94.148(4)
γ/°	90	90	90
V/Å^3	1907.69(17)	2167.2(2)	1885.2(7)
Z	4	4	4
μ/mm^{-1}	2.259	0.275	0.308
T/K	100	100	100
$\theta_{min,max}$	2.55, 29.39	2.21, 26.06	2.54, 20.52
Completeness	94.6	96.7	96.7
Reflections: total/independent	5747, 4656	6482, 5025	5634, 3861
R_{int}	0.0377	0.0526	0.0727
Final R1 and wR2	0.0384, 0.1081	0.0449, 0.1215	0.0512, 0.1345
Largest peak, hole/eÅ^{-3}	1.909, -0.683	0.635, -0.207	0.792, -0.384
ρ_{calc}/g cm^{-3}	1.313	1.149	1.172

Table 2.6.4. Crystal structure and refinement data for **25a** and **25b**.

No.	**25a**	**25b**
Size / mm	0.18 x 0.14 x 0.14	0.42 x 0.36 x 0.32
Empiric Formula	C26 H37 B S2 Si	C29 H43 B O2 Si
M	452.57	462.53
Crystal system	monoclinic	monoclinic
Space group	P 1 21/c 1	P 1 21/n 1
a/Å	17.213(5)	13.210(7)
b/Å	9.564(3)	9.473(6)
c/Å	17.650(5)	22.594(17)
α/°	90	90
β/°	116.026(6)	91.39(2)
γ/°	90	90
V/Å^3	2610.9(13)	2827(3)
Z	4	4
μ/mm^{-1}	0.261	0.105
T/K	100	100
$\theta_{min,max}$	2.49, 17.75	2.33, 26.80
Completeness	99.3	100.0
Reflections: total/independent	4783, 2773	5560, 4710
R_{int}	0.0875	0.0606
Final R1 and wR2	0.0644, 0.1568	0.0543, 0.1386
Largest peak, hole/eÅ^{-3}	0.319, -0.348	0.572, -0.512
ρ_{calc}/g cm^{-3}	1.151	1.087

2.6.2. References

[1] a) A. M. Priegert, B. W. Raw, S. C. Serin, D. P. Gates, *Chem. Soc. Rev.* **2016**, *45*, 922-953; b) X. He, T. Baumgartner, *RSC Adv.*, **2013**, *3*, 11334-11350; c) F. Vidal, F. Jäkle, *Angew. Chem. Int. Ed.* **2019**, *58*, 5846-5870; *Angew. Chem.* **2019**, *131*, 5904-5929; d) T. Baumgartner, F. Jäkle, *Main Group Strategies towards Functional Hybrid Materials*, Wiley, Chichester, **2018**.

[2] a) C. D. Entwistle, T. B. Marder, *Angew. Chem. Int. Ed.* **2002**, *41*, 2927-2931; *Angew. Chem.* **2002**, *114*, 3051-3056; b) C. D. Entwistle, T. B. Marder, *Chem. Mater.* **2004**, *16*, 4574-4585; c) F. Jäkle, *Chem. Rev.* **2010**, *110*, 3985-4022.

[3] a) C. R. Wade, A. E. J. Broomsgrove, S. Aldridge, F. P. Gabbai, *Chem. Rev.* **2010**, *110*, 3958-3984 ; b) H. Helten, *Chem. – Asian J.* **2019**, *14*, 919-935; c) H. Helten, *Chem. Eur. J.* **2016**, *22*, 12972-; d) H. Zhao, L. A. Leamer, F. P. Gabbai, *Dalton Trans.* **2013**, *42*, 8164-8178; e) L. Ji, S. Griesbeck, T. B. Marder, *Chem. Sci.* **2017**, *8*, 846-863; f) A. Wakamiya and S. Yamaguchi, *Bull. Chem. Soc. Jpn.* **2015**, *88*, 1357-1377; g) Z. Huang, S. Wang, R. D. Dewhurst, N. V. Ignat'ev, M. Finze, H. Braunschweig, *Angew. Chem. Int. Ed.* **2020**, *59*, 8800-8818; *Angew. Chem.* **2020**, *132*, 8882-8900.

[4] a) X.-Y. Wang, F.-D. Zhuang, J.-Y. Wang, J. Pei, *Chem. Commun.* **2015**, *51*, 17532-17535; b) A. Iida, S. Yamaguchi, *J. Am. Chem. Soc.* **2011**, *133*, 6952-6955; c) C.-T. Poon, W. H. Lam, V. W.-W. Yam, *J. Am. Chem. Soc*. **2011**, *133*, 19622-19625; d) H. Braunschweig, A. Damme, J. O. C. Jimenez-Halla, C. Hörl, I. Krummenacher, T. Kupfer, L. Mailänder, K. Radacki, *J. Am. Chem. Soc.* **2012**, *134*, 20169-20177; e) D. R. Levine, M. A. Siegler, J. D. Tovar, *J. Am. Chem. Soc.* **2014**, *136*, 7132-7139; f) S. K. Sarkar, G. R. Kumar, P. Thilagar, *Chem. Commun.* **2016**, *52*, 4175-4178; g) G. R. Kumar, S. K. Sarkar, P. Thilagar, *Chem. Eur. J.* **2016**, *22*, 17215-17225; h) Y. Yan, Z. Sun, C. Li, J. Zhang, L. Lv, X. Liu, X. Liu, *Asian J. Org. Chem.* **2017**, *6*, 496-502; i) Y. Adachi and J. Ohshita, *Organometallics* **2018**, *37*, 869-881; j) J. He, F. Rauch, A. Friedrich, D. Sieh, T: Ribbeck, I. Krummenacher, H. Braunschweig, M. Finze, T. B. Marder, *Chem. Eur. J.* **2019**, *25*, 13777-13784; k) M. Meier, L. Ji, J. Nitsch, I. Krummenacher, A. Deißenberger, D. Auerhammer, M. Schäfer, T. B. Marder, H. Braunschweig, *Chem. Eur. J.* **2019**, *25*, 4707-4712; l) T. E. Stennett, P. Bissinger, S. Griesbeck, S. Ullrich, I. Krummenacher, M. Auth, A. Sperlich, M. Stolte, K. Radacki, C.-J. Yao, F. Würthner, A. Steffen, T. B. Marder, H. Braunschweig, *Angew. Chem. Int. Ed.* **2019**, *58*, 6449-6454; *Angew. Chem.* **2019**, *131*, 6516-6521; m) S. Griesbeck, M. Ferger, C. Czernetzi, C. Wang, R. Bertermann, A. Friedrich, M. Haehnel, D. Sieh, M. Taki, S. Yamaguchi, T. B. Marder, *Chem. Eur. J.* **2019**, *25*, 7679-7688; n) D. Li, H. Zhang, Y. Wang, *Chem. Soc. Rev.* **2013**, *42*, 8416-8433.

[5] a) X. Yin, J. Chen, R. A. Lalancette, T. B. Marder, F. Jäkle, *Angew. Chem. Int. Ed.* **2014**, *53*, 9761-9765; b) X. Yin, K. Liu, Y. Ren, R. A. Lalancette, Y.-L. Loo, F. Jäkle, Chem. Sci. **2017**, *8*, 5497-5505; c) B. Meng, Y. Ren, J. Liu, F. Jäkle, L. Wang, *Angew. Chem. Int. Ed*, **2018**, *57*,

2183; *Angew. Chem.* **2018**, *130*, 2205-2209; d) Y. Adachi, Y. Ooyama, Y. Ren, X. Yin, F. Jäkle, J. Ohshita, *Polym. Chem.* **2018**, *9*, 291-299; e) Y. Yu, C. Dong, A. F. Alahmadi, B. Meng, J. Liu, F. Jäkle, L. Wang, *J. Mater. Chem. C.* **2019**, *7*, 7427-7432; f) Y. Yu, B. Meng, F. Jäkle, J. Liu, L. Wang, *Chem. – Eur. J.* **2020**, *26*, 873-880; g) C. Reus, F. Guo, A. John, M. Winhold, H.-W. Lerner, F. Jäkle, M. Wagner, *Macromolecules*, **2014**, *47*, 3727-3735; h) Y. Ren, F. Jäkle, *Dalton Trans.* **2016**, *45*, 13996-14007; i) H. Li, A. Sundararaman, K. Venkatasubbaiah, F. Jäkle, *J. Am. Chem. Soc.* **2007**, *129*, 5792-5793; j) X. Yin, F. Guo, R. A. Lalancette, F. Jäkle, *Macromolecules* **2016**, *49*, 537-546;

[6] a) A. Lik, L. Fritze, L. Müller, H. Helten, *J. Am. Chem. Soc.* **2017**, *139*, 5692-5695; b) A. Lik, S. Jenthra, L. Fritze, L. Müller, K.-N. Truong, H. Helten, *Chem. – Eur. J.* **2018**, *24*, 11961-11972.

[7] a) A. Sundararaman, M. Victor, R. Varughese, F. Jäkle, *J. Am. Chem. Soc*. **2005**, *127*, 13748-13749; b) H. Li, F. Jäkle, *Angew. Chem. Int. Ed.* **2009**, *48*, 2313-2316; *Angew. Chem.* **2009**, *121*, 2349-2353; c) H. Li, F. Jäkle, *Macromol. Rapid Commun.* **2010**, *31*, 915-920.

[8] A. Lik Dissertation: Thienyl- and Furylborane Oligomers, Polymers, and Macrocycles – Development of a Catalytic Si/B Exchange Reaction As a Novel B-C Bond Formation Method (2017).

[9] a) S. H. Strauss, *Chem. Rev.* **1993**, *93*, 927-942; b) T. A. Engesser, M. R. Lichtenthaler, M. Schleep, I. Krossing, *Chem. Soc. Rev.* **2016**, *45*, 789-899; c) I. M. Riddlestone, A. Kraft, J. Schaefer, I. Krossing, *Angew. Chem. Int. Ed.* **2018**, *57*, 13982-14024; *Angew. Chem.* **2018**, *130*, 14178-14221.

[10] a) I. Krossing, *Chem. Eur. J.* **2001**, 490-502; b) I. Krossing, H. Brands, R. Feuerhake, S. Koenig, *J. Fluorine Chem.* **2001**, *112*, 83-90; c) A. Martens, P. Weis, M. C. Krummer, M. Kreuzer, A. Meierhöfer, S. C. Meier, J. Bohnenberger, H. Scherer, I. Riddlestone, I. Krossing, *Chem. Sci.* **2018**, *9*, 7058-7068.

[11] For a review on Borinium, Borenium, and Boronium Ions see: W. E. Piers, S. C. Bourke, K. D. Conroy, *Angew. Chem. Int. Ed.* **2005**, *44*, 5016-5036.

[12] R. G. Pearson, *J. Am. Chem. Soc.* **1963**, *85*, 22, 3533-3539.

[13] Y. Sawama, S. Asai, T. Kawajiri, Y. Monguchi, H. Sajiki, *Chem. Eur. J.* **2015**, *21*, 2222-2229.

[14] B. Wrackmeyer, H. Nöth, *Chem. Ber.* **1976**, *109*, 1075-1088.

[15] H. Braunschweig, A. Damme, J. O. C. Jimenez-Halla, C. Hoerl, I. Krummenacher, T. Kupfer, L. Maila, *J. Am. Chem. Soc.* **2012**, *134*, 20169-20177.

[16] K. Ruhlandt-Senge, J. J. Ellison, R. J. Wehmschulte, F. Pauer, P. P. Power, *J. Am. Chem. Soc.* **1993**, *115*, 11353–11357.

[17] B. Mathieu, L. Ghosez, Tetrahedron **2002**, *58*, 8219–8226.

[18] D. E. Pearson, M. G. Frazer, V. S. Frazer, L. C: Washburn, *Synthesis* **1976**, *9*, 621–623.

[19] W. Haubold, J. Herdtle, W. Gollinger, W. Einholz, *J. Organomet. Chem*. **1986**, *315*, 1-8.

[20] G. M. Sheldrick, *Acta Crystallogr. A* **2015**, *71*, 3-8.

[21] Sheldrick, *Acta Crystallogr. A* **2008**, *64*, 112-122.

[22] C. B. Hubschle, G. M. Sheldrick, B. Dittrich, *J. Appl. Crystallogr.* **2011**, *44*, 1281-1284.

[23] O. V. Dolomanov, L. J. Bourhis, R. J. Gildea, J. A. K. Howard, H. Puschmann, *J. Appl. Crystallogr.* **2009**, *42*, 339-341.

2.7 Synthetic Routes to Tetrabora- and Diboraporphyrinogens

Porphyrins are an essential class of naturally occurring macrocyclic compounds. Their structural motif consists of an aromatic macrocycle of four pyrrole rings linked by four methine bridges. They play a key role in many essential processes, e.g. the metabolism of living organisms and the conversion of light into usable energy. The parent compound is called porphin; substituted derivatives thereof are called porphyrins. Metal complexes of porphyrins such as the iron-containing porphyrines found as heme (of haemoglobin) and the magnesium-containing reduced porphyrine chlorophyll occur naturally and are of particular importance in biological systems (Figure 2.7.1).[1]

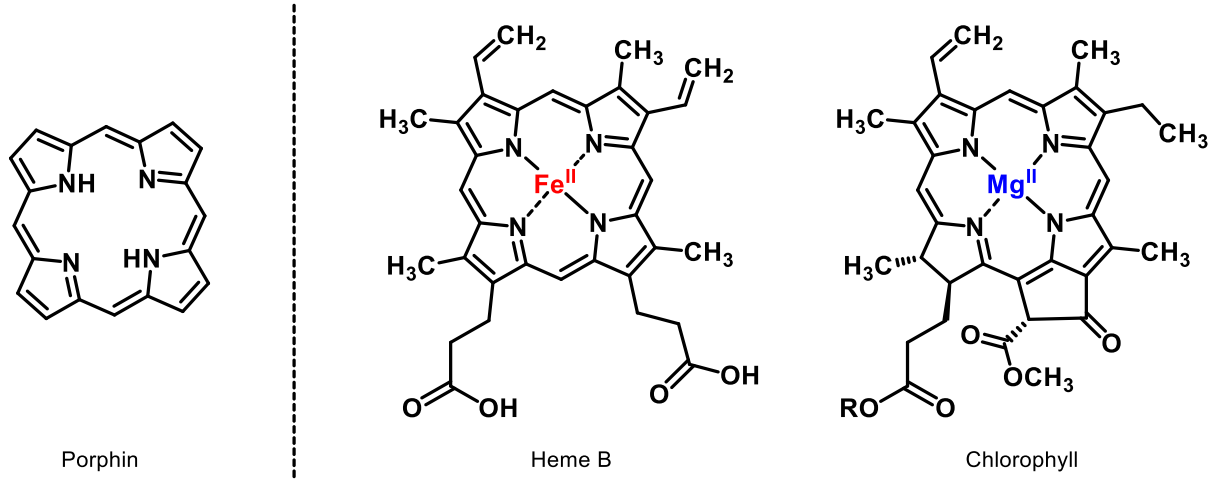

Porphin | Heme B | Chlorophyll

Figure 2.7.1. Structural motif of porphyrin (porphin, the parent derivative) and naturally occurring metal complexes heme B and chlorophyll derived from porphyrins.

Porphyrins and related macrocycles have potential use in mimicking enzymes, molecular electronic devices, catalytic reactions, and conversion of solar energy and have therefore attracted considerable attention in recent years. Special interest was in the use of such species as artificial light-harvesting antennae in organic photovoltaic (OPV) cells.[1] However, the use of such cells is still limited due to insufficient power efficiency, probably resulting from poor light-harvesting abilities as well as poor charge carriage and unbalanced charge transport of the employed dyes.[2] In order to improve material properties, research is conducted in the field of developing new organic, inorganic and hybrid materials. In this context, π-conjugated organic materials have been of particular interest in the past, and the doping of purely organic backbones with inorganic elements, such as boron, leading to inorganic-organic hybrid materials, has proven to be an effective tool in the generation of new materials with special features and often significantly improved properties.[3-5] In this regard, π-conjugated organoboranes and organoborane polymers have emerged as important classes of such inorganic-organic hybrid materials.[4,5] The combination of the vacant p_π orbital of the boron with an adjacent organic π system leads to intriguing optical and electronic properties as a result of

effective p-π* conjugation. The obtained materials show promising applicability for (opto)electronic devices as well as for sensory or imaging applications.[4-5] Towards the creation of inorganic-organic hybrid macrocycles containing boron, Jäkle and co-workers have presented the synthesis of different types of boron-doped conjugated macrocycles with two, three, four or six boron centers and different linking units.[6] The electron-deficient nature of the incorporated boron centers provide an ideal prerequisite for anion binding which can be used for sensing applications.[6]

2.7.1. Tetraboraporphyrinogens

The incorporation of boron in *meso*-positions of porphyrin-related frameworks was first reported by Siebert and co-workers in 1998. They synthesized the first fully boron doped tetrathiaporphyrinogen **A** with diisopropylamino groups at the boron centers (Figure 2.7.2).[7] In this macrocycle, no evidence for macrocyclic π-conjugation was observed despite featuring a closed cycle of sp^2 hybridized carbon and boron atoms. X-ray structure analysis revealed a twist of the thiophene rings out of the plane that includes the four boron atoms.[7,8] A plausible reason might be the significant double bond character of the B=N bond from the stabilizing amino groups, as demonstrated by resonance structure **B**, which effectively prevents any macrocyclic π-electron delocalization over the boron atoms as well as any ring current.[7] Our idea was to attach sterically demanding, non-π-donating substituents such as Tip or Mes* at the boron centers to ensure a stabilizing effect while maintaining macrocyclic π-conjugation to obtain macrocycles of type **C** (Figure 2.7.2).

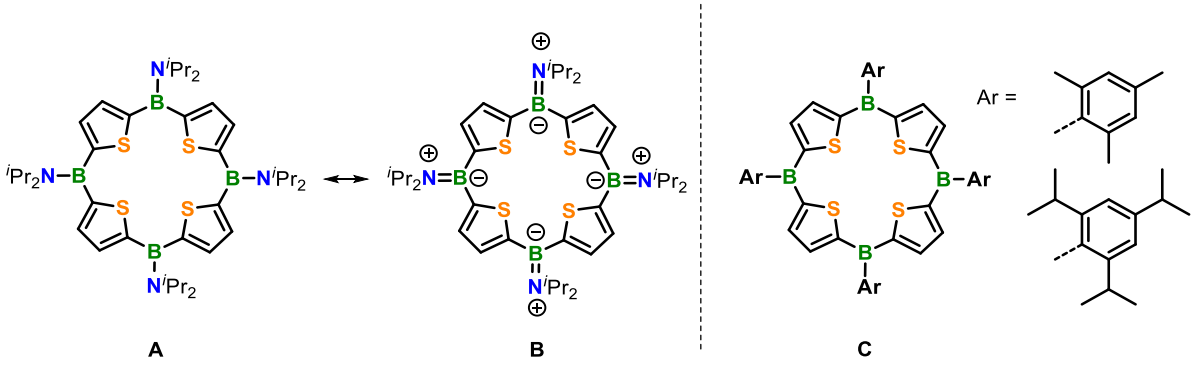

Figure 2.7.2. Two resonance forms of boron-doped tetrathiaporphyrinogens **A**, **B** with amino groups as substituents and targeted macrocycle **C** featuring bulky substituents.

In this work, we present the synthesis of the first fully π-conjugated boron-doped tetrathiaporphyrinogen. Previous work from our group aimed at the synthesis of such a macrocycle with mesityl groups being attached to the boron centers (Scheme 2.7.1).[9] These results to confirmed the successful synthesis of **7a** by secondary ion-mass spectrometry (SIMS) but also confirmed decomposition upon aqueous work-up and subjection to column chromatography. Therefore, with a view to provide sufficient kinetic stabilization of the boron

centers, in subsequent studies, we concentrated on the incorporation of Tip as exocyclic substituent on the boron to obtain macrocycle **7b**.

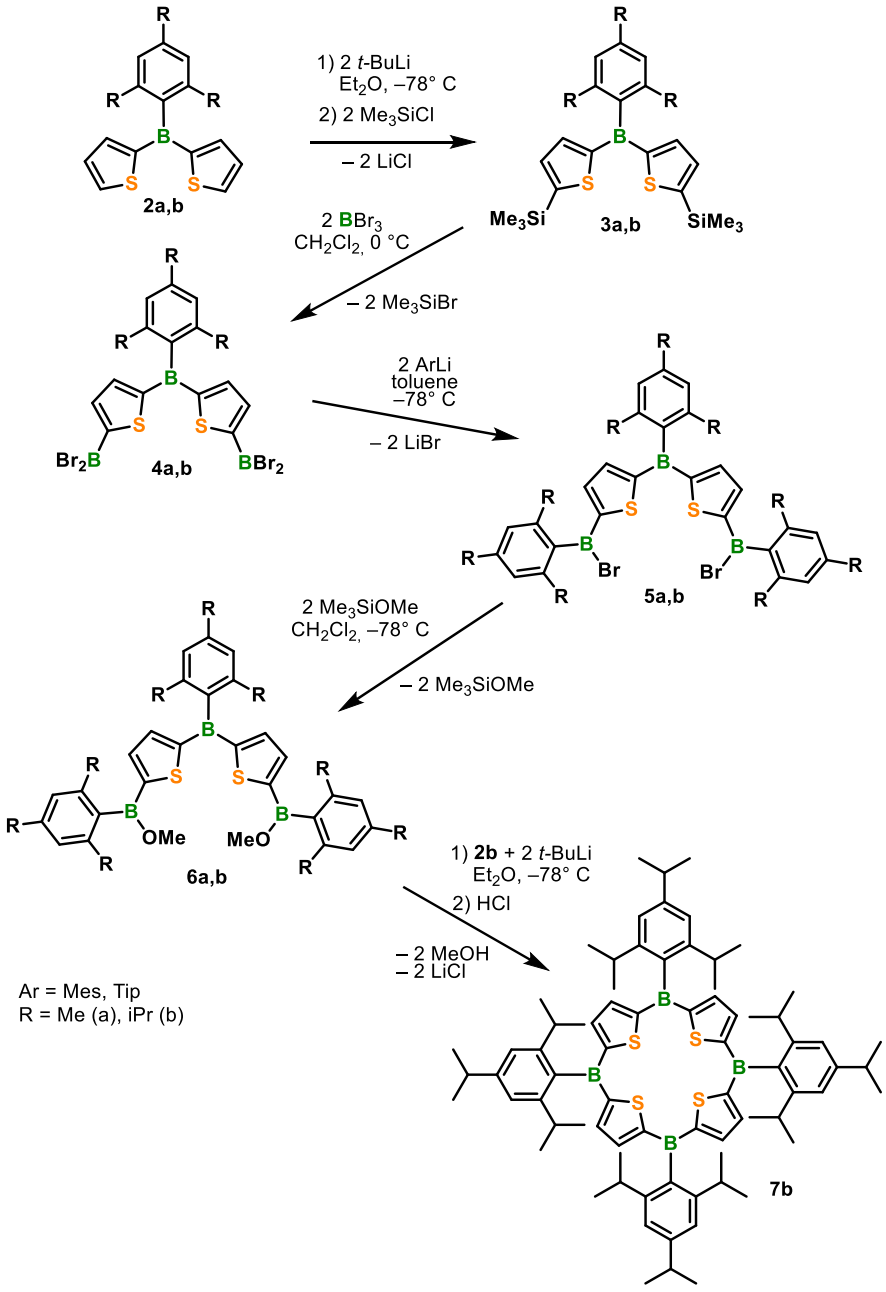

Scheme 2.7.1. Synthesis of boron-bridged tetrathiaporphyrinogen precursors **6a,b** and macrocycle **7b.**

The synthesis of Mes- (a) and Tip- (b) substituted compounds **2a,b-7b** was developed and carried out by Dr. Artur Lik and was part of his dissertation.[9] Selective dilithiation of **2b**, followed by addition of Me_3Si-Cl afforded **3b** in good yield (84%). Bisborylation of **3b** by twofold silicon/boron exchange with BBr_3 afforded **4b** in an almost quantitative reaction (97%). Further reaction with 2 equivalents of TipLi selectively yielded the twofold monoarylated compound **5b**. We were not able to remove residual TipH impurities or crystallize the compound due to the high reactivity of the B-Br bond and the limitation to non-ether solvents. Our attempts to access the desired macrocycle **7b** by direct reaction of **5b** with dilithiated **2b** were unsuccessful.[9] In

this work, we found that the addition of an excess of Me_3Si-OMe in dichloromethane at low temperature selectively transforms the B-Br bond into a B-OMe bond affording **6b** in higher yields as compared to the previously used addition of sodium methoxide. Furthermore, the forming Me_3Si-Br can be easily removed in vacuo. We accomplished to purify and isolate **6b** by precipitation it in a mixture of dichloromethane and methanol. This enabled us, despite of lower reactivity of the B-OMe bond, to increase the reactivity of the lithiated species **2b** by employing ether solvents such as diethyl ether and THF. Macrocycle **7b** was obtained from the reaction of **6b** with dilithiated **2b** in diethyl ether at –78 °C. Addition of HCl in the last step led to immediate precipitation, which was beneficial for the separation of byproducts. In an optimized reaction protocol, we carried out the work-up under inert conditions since previous experiments indicated slowly proceeding partial decomposition in moist solution (on a large time scale). After precipitating the product with a mixture of DCM/methanol, a yellow solid was obtained which was repeatedly washed with hexane to remove potential linear by-products. The solubility of these linear side products in hexane was reported in previous studies.[10] The ^{1}H-NMR spectrum of the product showed two broad singlets at 6.95 ppm (Tip-*H*) and 7.90 ppm (Thi-*H*). In the latter the thiophene protons overlap due to the identical chemical environment through the ring structure (Figure 2.7.3). As in the case of linear thienylborane oligomers and polymers of similar constitution, no ^{11}B NMR signal could be detected (Appendix, Figure 5.7.4).

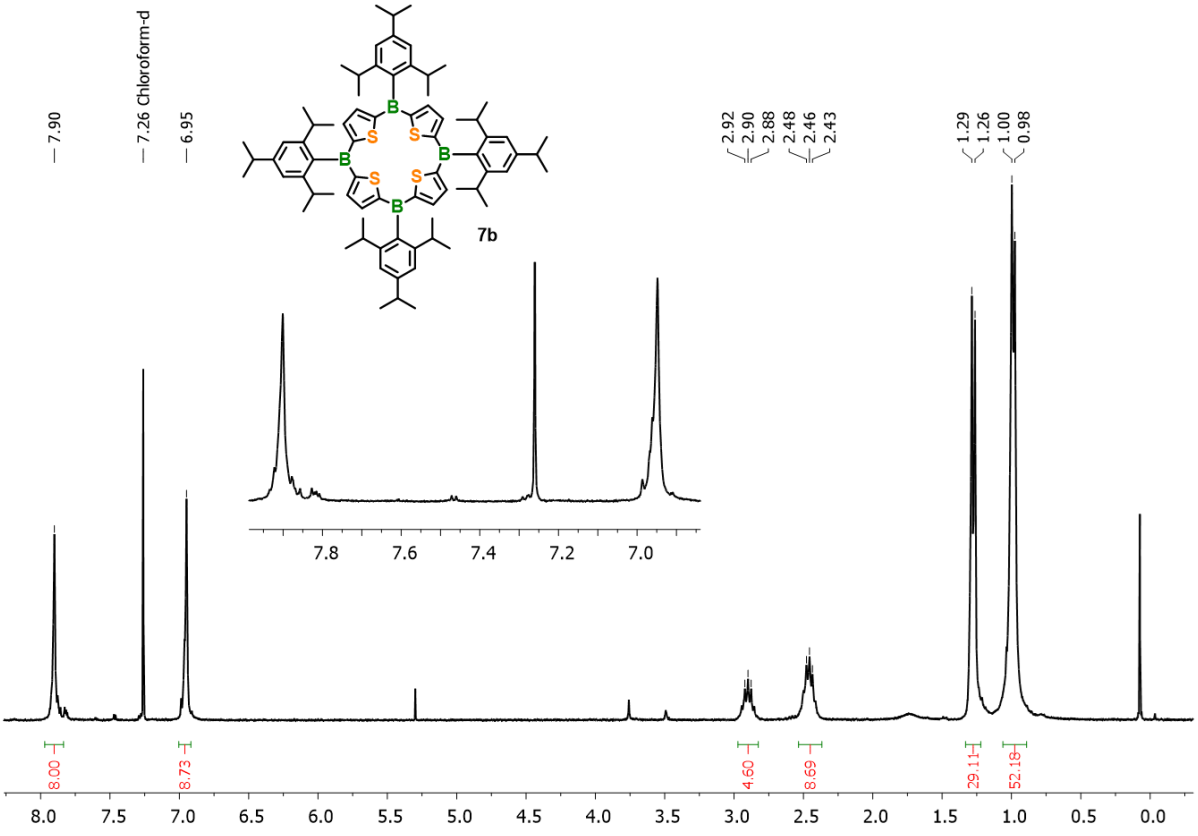

Figure 2.7.3. ^{1}H-NMR spectrum of macrocycle **7b** after repeated washing with hexane.

Secondary-ion mass spectrometry (SIMS) and liquid injection field desorption ionisation (LIFDI) mass spectrometry indicated the presence of the desired macrocycle. The latter was recorded in the range up to m/z = 4000 g/mol and evidenced the presence of macrocycles with different ring sizes from 4 to 10, with **7b** as the predominant product (Figure 2.7.4, MW of repeating unit: 296.177). A plausible reason for the formation of rings with different sizes is the reaction of a mono- or dilithiated species with unlithiated species **2b**, which might be present as result of incomplete lithiation or may have formed due to small extent of decomposition during the lithiation procedure. Since the lithiated species is extremely sensitive towards higher temperatures, a plausible reason for partial decomposition is the addition of a new batch Et_2O to decrease the concentration for the macrocyclization reaction. Despite the added E_2O was cooled to -78 °C and added by means of a transfer canula, this procedure might slightly rise the temperature which could cause the decomposition.

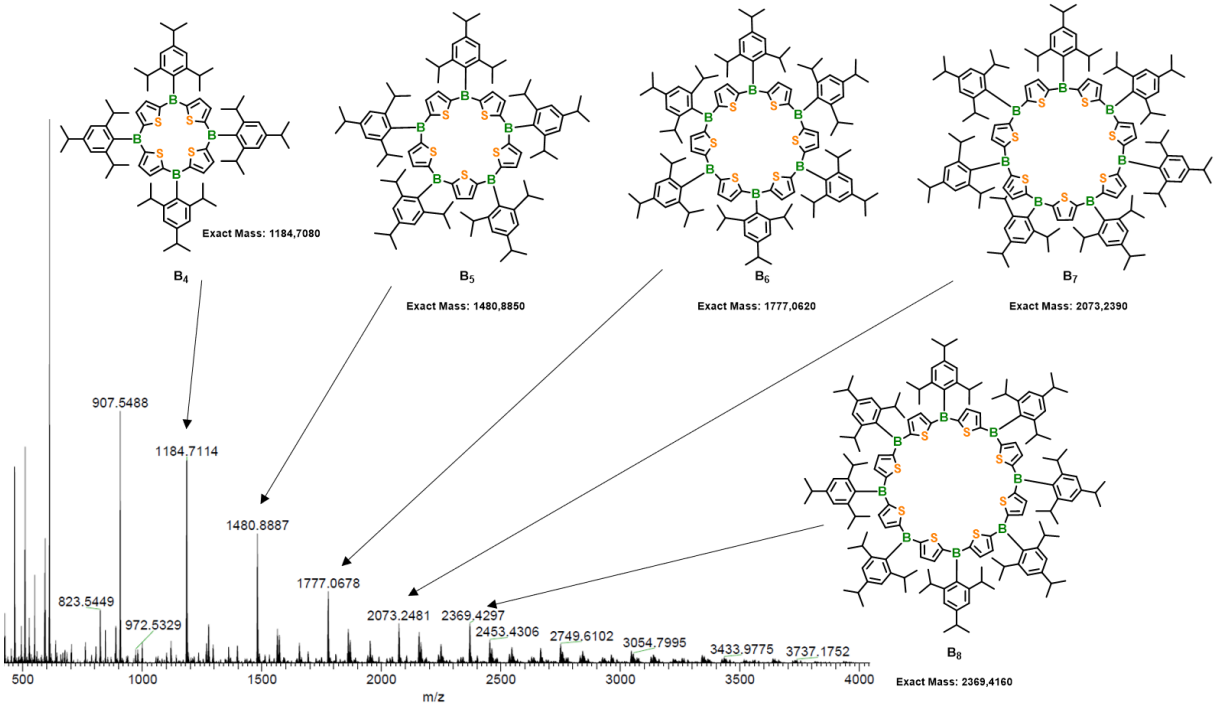

Figure 2.7.4. HR-MS distribution of macrocycle **7b**.

Analysis of **7b** via gel permeation chromatography (GPC) indicated an estimated average molecular weight (M_n) of approx. 7600 Da, which is 6 times higher as expected. This higher molecular weight is probably due to an overestimation by the GPC method due to calibration with polystyrene as result of different separation behavior for cyclic structures on the GPC column (Appendix, Figure 5.7.92). The presence of high-molecular-weight linear polymers can be excluded through careful washing with hexane as executed during work-up. Attempts to separate and isolate the macrocycles with different ring sizes via preparative gel permeation chromatography were not successful. All conducted crystallization attempts in various solvents

and solvent mixtures failed, probably because of the presence of a mixture of different ring sizes.

The optical properties of **6b** and **7b** have been investigated and described by Dr. Artur Lik in previous experiments in our group.[9] These data clearly point to π-conjugation across the boron centers within the macrocycle. The measurements were repeated under inert conditions to exclude the effect of potential decomposition products. An absorption band ($\lambda_{abs,\,max}$ = 420 nm) with a shoulder at approximately 396 nm and a long tail in the visible region was observed (Figure 2.7.5, black), which is in good accordance with the data obtained from non-inert measurements. The bands obtained are reminiscent of the Soret and Q-bands of porphyrins and can therefore be considered as further evidence of a porphyrinoid structure (Figure 2.7.5, inlet).[11] Additionally, the absorption maximum is bathochromic shifted by 95 nm compared to **2b** ($\lambda_{abs,\,max}$ = 325 nm).[10a] The bathochromic shift of **7b** is even more pronounced as for a corresponding tris(het)arylborane ("trimer", $\lambda_{abs,\,max}$ = 412 nm)[10b] and oligomers **O** ($\lambda_{abs,\,max}$ = 409 nm).[10] Furthermore, compound **7b** showed intense teal fluorescence (Figure 2.7.5, dashed, $\lambda_{em,\,max}$ = 505 nm). We additionally performed cyclic voltammetry measurements in THF and DCM and compared the results to linear oligomers **O**[10a] and trimeric species **T**[10b] (Figure 2.7.6).

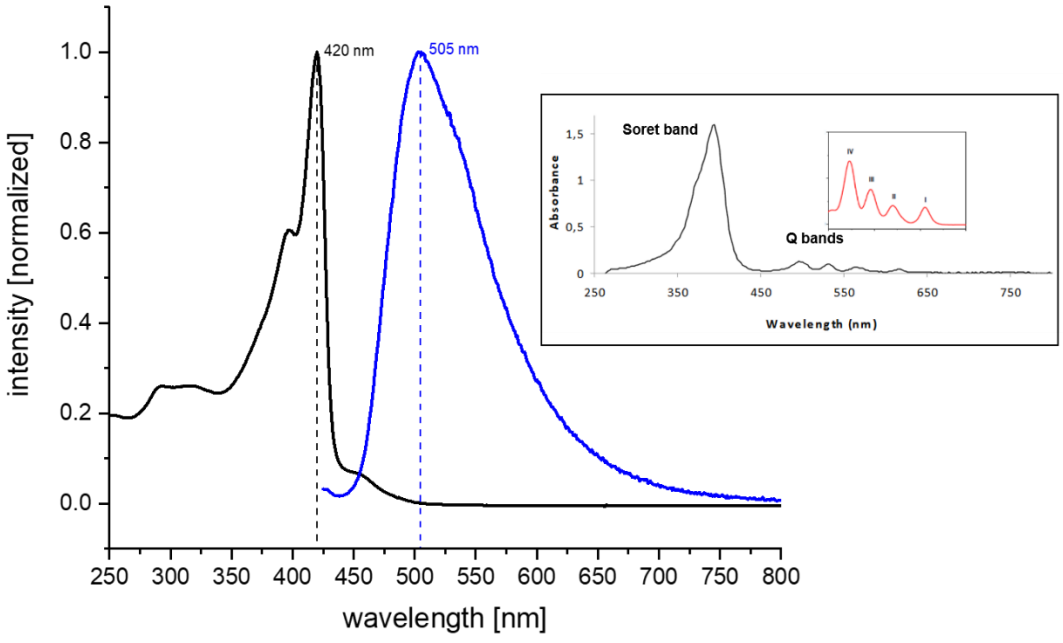

Figure 2.7.5. UV-vis absorption spectrum of **7b** (black) and fluorescence spectrum of **7b** (dashed) in THF (excited at 420 nm). Inlet: UV-vis absorption spectrum of porphyrin.[11]

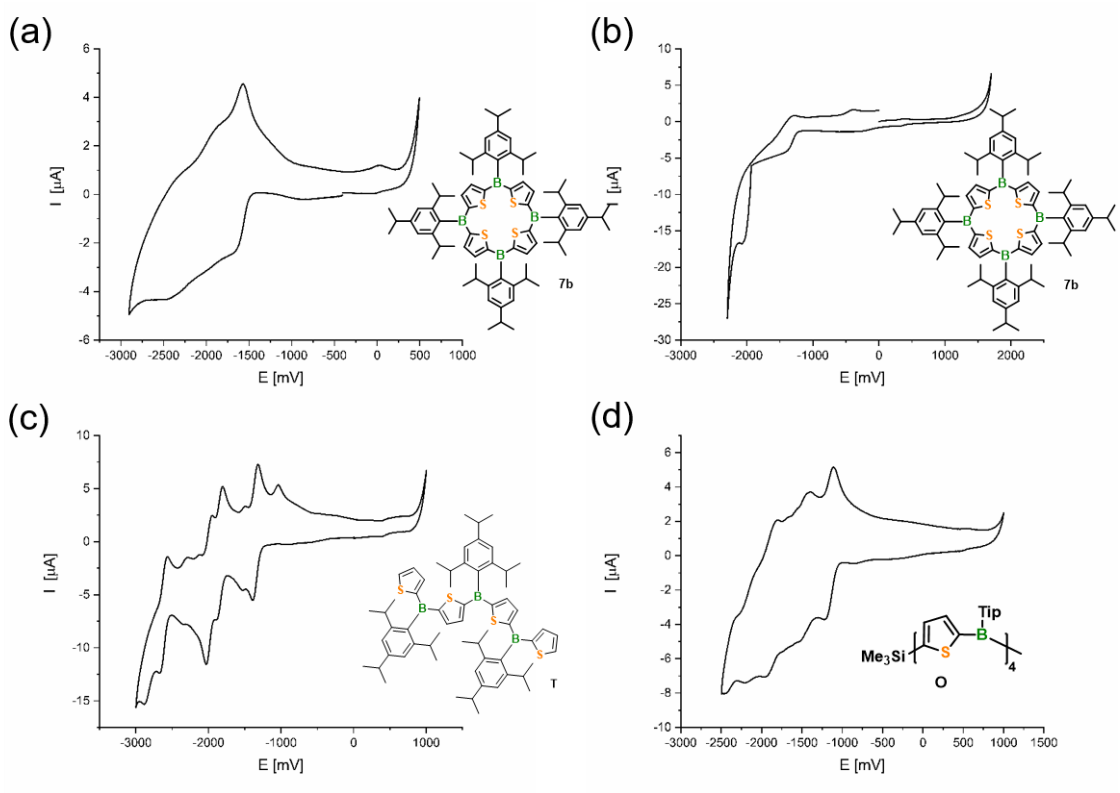

Figure 2.7.6. Cyclic voltammograms for **7b** (a) in THF, (b) in DCM, (c) tris(het)arylborane **T** in THF and (d) linear oligomer **O** in THF.

The cyclic voltammogram of **7b** in THF revealed a broad range of irreversible reduction events between -1.5 and -3.0 V (Figure 2.7.6, a). In DCM, no oxidation event was observed, which could have been expected due to the presence of the four electron rich thiophene rings (Figure 2.7.6, b). Compared to **7b**, "trimeric" species **T** and oligomeric species **O** show multiple reduction events again, but the onset energies are slightly anodically shifted (approx. -1.2 V for **T** and -1.0 V for **O** vs. -1.5 V for **7b**, Figure 2.7.6, c,d). Furthermore, the voltammogram for **7b** is significantly broadened.

With a view to isolate and crystallize the B_4 macrocycle **7b**, the next step was to find a way to prevent the formation of rings of different sizes. Therefore, we chose a different reaction route which involves the synthesis of asymmetric "trimeric species" **14a** in a multi-step synthesis featuring one silyl and one stannyl functionality in either of the terminal positions (Scheme 2.7.2). Our idea was that after addition of a trihaloborane, selective tin/boron exchange should occur as result of significantly higher reactivity of the stannyl group in comparison to the silyl group. Subsequent macrocyclization under high-dilution conditions via intramolecular Si/B exchange should afford the B_4 macrocycle **7b** only. Therefore, we first synthesized compound **11a** as described in chapter 2.6. starting from monosilylated triarylborane **8a**. After borylation, monoarylation and subsequent conversion of the B-Br into a B-OMe functionality by means of Me_3Si-OMe, we obtained compound **11a**. The addition of

monolithiated species **12a** in diethylether at -78 °C afforded monosilylated compound **13a** with an overall yield of 62%. Attempted lithiation thereof with *n*-BuLi or *t*-BuLi and *N,N,N',N'*-tetramethylethylenediamine (TMEDA) as additive were not successful. The use of a freshly prepared solution of lithium diisopropylamide (LDA) as lithiation agent, followed by the addition of a solution of trimethylstannylchloride (Me_3Sn-Cl, 1M in THF) at -78 °C led to clean conversion to asymmetric compound **14a** in high yield (78%).

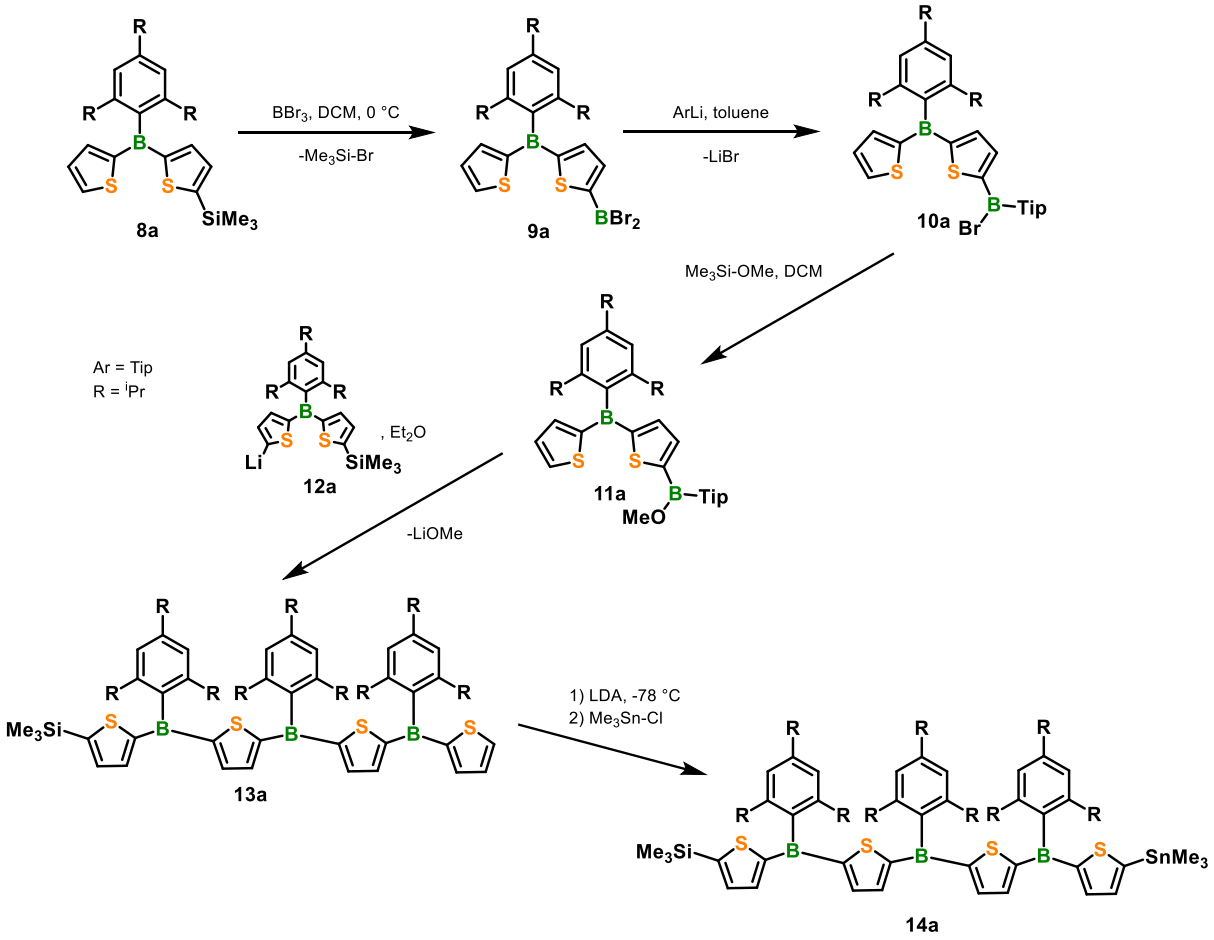

Scheme 2.7.2. Multi-step synthesis of asymmetric compound **14a.**

Careful addition of a trihaloborane to **14a** should lead to selective tin/boron exchange. To get a better understanding of the reactivity of the asymmetric compound, test reactions were performed with the smaller asymmetric compound **15a** (Scheme 2.7.3). After lithiation of **8a** to afford **12a**, compound **15a** was obtained upon addition of a solution of Me_3Sn-Cl (1M in THF) at -78 °C. Crystals suitable for X-ray analysis were obtained by slow evaporation of hexane at room temperature (Figure 2.7.7). In the molecular structure of **15a** in the solid state, the Tip group is orientated nearly perpendicular to the respective BC_3 plane (dihedral angle: 84.0°). The thiophene rings are almost coplanar adopting *syn* conformation (interplanar angle between both rings: 6.9°). The constitution of compounds **8a, 13a** and **14a** was unambiguously ascertained by multinuclear NMR spectroscopy and HR-MS (APCI, Appendix, Figs 5.7.72-73).

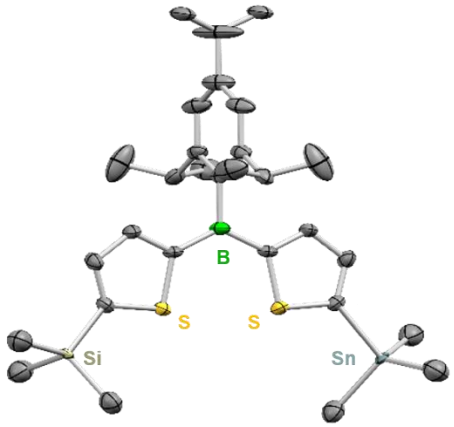

Figure 2.7.7. Molecular structure of **15a** in the solid state (H-Atoms omitted for clarity).

Careful addition of BBr_3 to a solution of **15a** in DCM afforded no clean reaction to compound **16a**. The recorded ^{1}H-NMR spectrum revealed the formation of both Me_3Sn-Br as main- and Me_3Si-Br as side condensation products (Scheme 2.7.3, upper part). It is conceivable that after successful tin/boron exchange, the high reactivity of the B-Br bond can lead to further condensation reaction with the Me_3Si groups to afford extended linear compounds (which would yield the observed Me_3Si-Br, Scheme 2.7.3, bottom part).

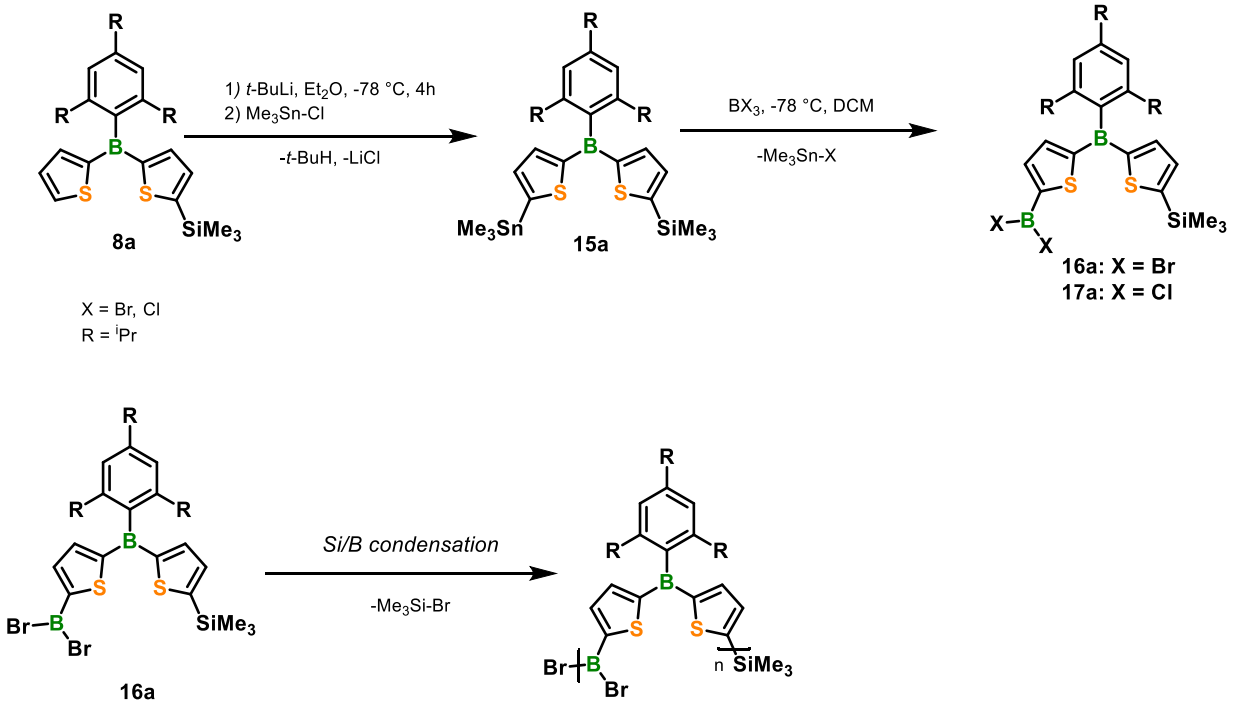

Scheme 2.7.3. Top: Selective monoborylation of **15a** to afford compounds **16a** and **17a**. Bottom: Si/B exchange condensation as potential side reaction.

Interestingly, after addition of exact one equivalent of BCl_3 (1 M in DCM) to **15a**, no signal for Me_3Si-Cl were observed in the ^{1}H-NMR spectrum which is consistent with the results described

in chapter 2.6; In the absence of a catalyst, no proceeding Si/B exchange with aryl-BCl_2 compounds was observed. Nevertheless, no selective conversion to **17a** was observed, as indicated by several signals for by-products in the aromatic region in the recorded ^{1}H-NMR spectrum (Appendix, Figure 5.7.20). Addition of a solution of **15a** in DCM to a solution of BCl_3 (1M in DCM) led by comparison to a cleaner reaction, but still some impurities were present.

The addition of a solution of **14a** to either BBr_3 or BCl_3 at -78 °C under high dilution led to a selective Sn/B exchange reaction with no signs of Me_3Si-X formation within 30 minutes (Scheme 2.7.4). Hypothetically, under pseudo high-dilution conditions a ring-closing reaction should proceed to form macrocycles **20a,21a**.

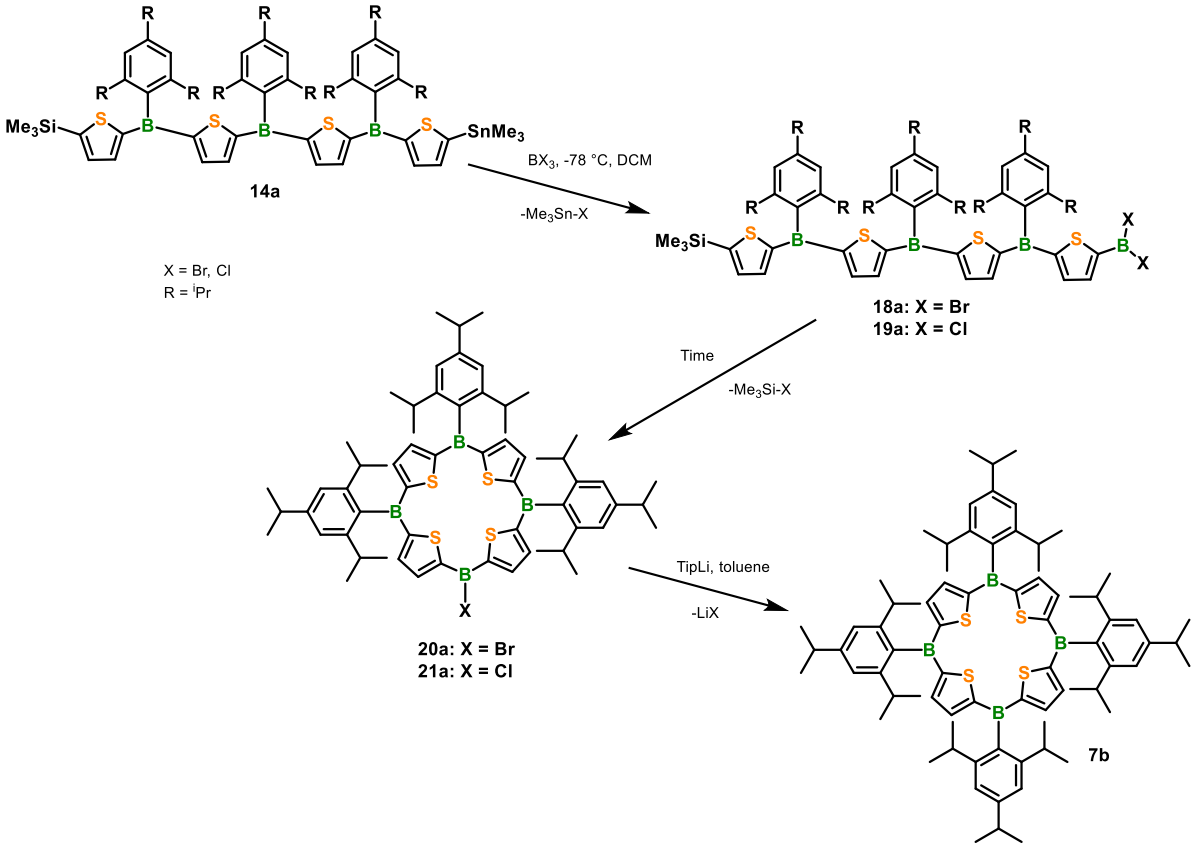

Scheme 2.7.4. Selective Sn/B exchange and subsequent macrocyclization attempt under pseudo high-dilution to afford **20a,21a.**

The reaction progress after addition of BCl_3 to **14a** was studied in detail by recording ^{1}H-NMR spectra after 30 minutes (Figure 2.7.8, b), 25 h (Figure 2.7.8, c), after addition of trimethylsilyltriflimide (Me_3Si-NTf_2, 10 mol%, Figure 2.7.8, d) as catalyst, after 25 h after the catalyst had been added (Figure 2.7.8, e) and after another batch of catalyst was added (40 mol%) and the reaction mixture had been stirred for 5 days in total (Figure 2.7.8, f). In Figure 2.7.8 the aliphatic region of the recorded spectra is compared to that of **14a** (Figure 27.8, a; see Appendix, Figure 5.7.26 for full spectrum).

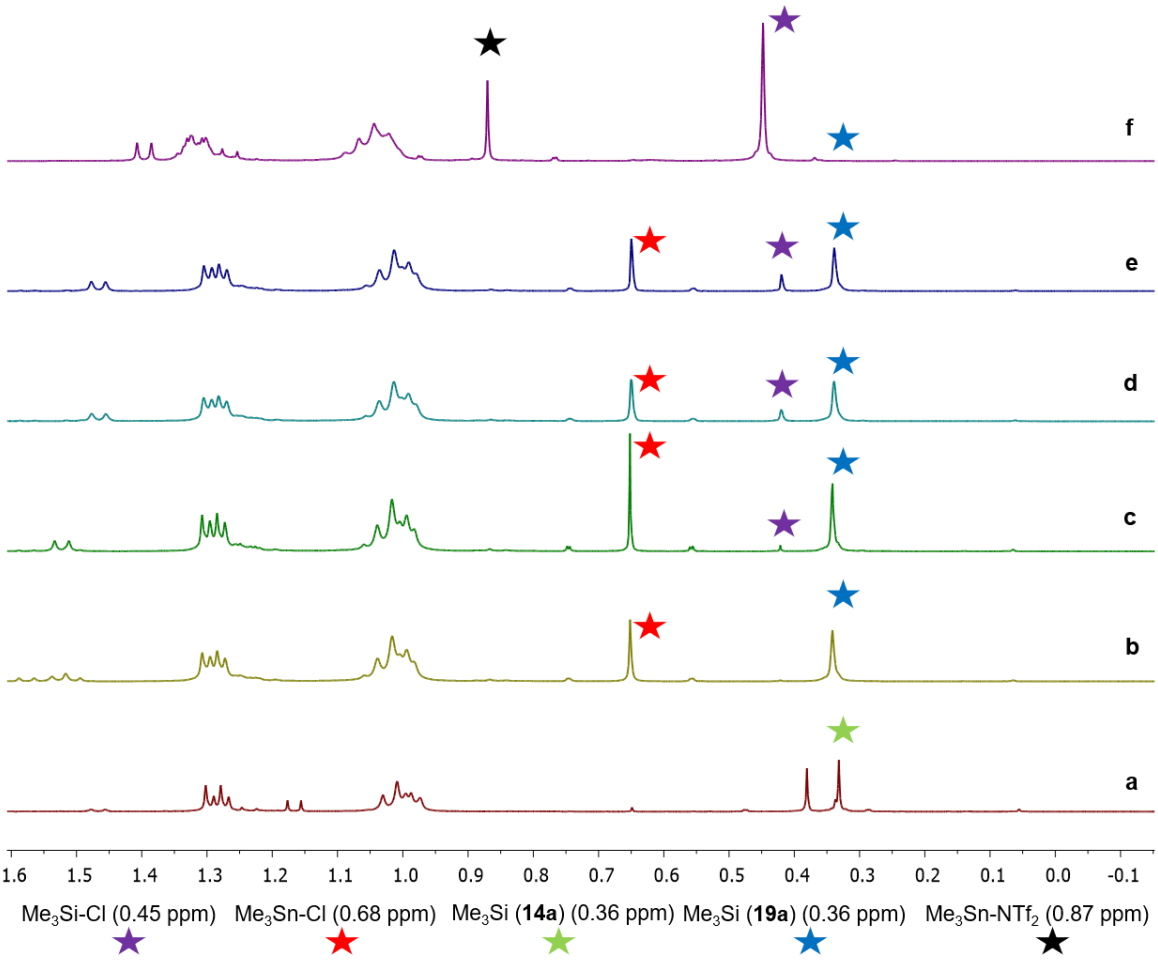

Figure 2.7.8. ^{1}H NMR spectra recorded during the attempted synthesis of **21a**. (a) ^{1}H NMR spectrum of compound **14a**, (b) after addition of BCl_3 solution and stirring for 30 minutes, (c) after stirring for 25h, (d) after addition of catalytic amount of Me_3Si-NTf_2 (10 mol%), (e) after stirring for 25 h after the catalyst had been added, (f) after addition of another 40 mol% cat and stirring for total 5 days. Stars: Chemical shifts of silylated (purple) and stannylated (red) condensation products, silyl group of **14a** (green) and **19a** (blue) and forming Me_3Sn-NTf_2 (black).

The addition of a solution of **14a** in DCM to a solution of BCl_3 at -78 °C led to selective Sn/B exchange within 30 minutes as evidenced by the formation of Me_3Sn-Cl (0.68 ppm) as condensation product (red star). The TMS group of formed **19a** remained unchanged (blue star). After stirring for 25 h, only a small amount of Me_3Si-Cl (0.45 ppm, purple star) was observed (Figure 2.7.8, c). The addition of Me_3Si-NTf_2 (10 mol%) to accelerate the Si/B exchange and stirring for 1 h (d) and 25 h (e) only led to insignificant changes. After another batch of catalyst was added (40 mol %) and the reaction mixture was stirred for additional 3 d, another signal arose at 0.87 ppm, which is assigned to formed Me_3Sn-NTf_2 (black star).[12] Interestingly, the TMS-group of **14a** was completely consumed, indicating a clean reaction with only formed Me_3Si-Cl (purple star) and Me_3Sn-NTf_2 (black star) after 5 days of total reaction time (Figure 2.7.8, f). The appearance of these signals point to a successful conversion to **21a** since no residual TMS-group is left which would be the case for linear by-products. Performing

the same reaction protocol and monitoring the reaction progress for **18a** led to significant differences. First, after addition of BBr_3 and stirring for 25 h, a second TMS-species was observed in the recorded ^{1}H-NMR spectrum (0.37 ppm, cf. Appendix, Figure 5.7.22). The Me_3Sn group was completely converted to Me_3Sn-Br (0.78 ppm). The second TMS signal might point to occurring Si/B exchange as follow-up reaction (formation of Me_3Si-Br was observed to a minor amount). After the reaction mixture was stirred for 5 days in total and two batches of catalyst (10 and 40 mol%) had been added, no formation of Me_3Sn-NTf_2 was observed as seen for B-Cl species, and the TMS-group of **19a** was still present (Appendix, Figure 5.7.24). However, some Si/B exchange condensation has occurred as evidenced by the formation of Me_3Si-Br (0.62 ppm, partially overlapping with the signal of the catalyst: 0.60 ppm). Then, all volatiles were removed in vacuo and the crude solid was redissolved in toluene. TipLi in toluene was added at -78 °C and the reaction mixture was stirred for another 3 days. Since the reaction progress for *in situ* generated **21a** seemed promising, we performed analysis via mass spectrometry, but unfortunately only the molecular ion peak for **13a** was observed., A possible reason for this, besides occurring decomposition during the analytical process, might be a protodeboration reaction as a result of small impurities of water to afford **13a** and boric acid as side reactions in one of the reaction steps. Another plausible reason is the elimination of the BX_2 species due to tin-methyl bond cleavage. Overall, the synthesis of macrocycle **7b** via asymmetric “trimer” **14a** seems to be prone to decomposition and side reactions. However, this reaction protocol seems promising and screening different reaction parameters such as concentration, solvents (e.g., toluene instead of DCM), temperature and time are planned for further attempts.

In order to further enhance the acceptor character of the obtained materials, we attempted to introduce electron withdrawing ^{F}Mes groups as substituent at the boron centers (Scheme 2.7.5). ^{F}Mes-substituted triarylborane **2c** was obtained by catalytic silicon/boron exchange of trimethylsilylthiophene with 2-dibromoborylthiophene in the presence of a substoichiometric amount of Me_3Si-NTf_2 (5 mol%) and subsequent derivatization with freshly prepared ^{F}MesLi.[13] Selective dilithiation thereof followed by reaction with 2 equivalents of Me_3Si-Cl afforded **3c**. Bisborylation of **3c** was performed in dichloromethane via twofold silicon/boron exchange with BBr_3 and yielded **4c** in a virtually quantitative reaction. Upon treatment of **4c** with 2 equivalents of freshly prepared ^{F}MesLi, selective monoarylation occurred at each boryl group to afford **5c** in moderate yield. Addition of a slight excess of Me_3Si-OMe at ambient temperature transformed the B-Br bond into a B-OMe bond. **6c** was precipitated in a mixture of dichloromethane and methanol, filtered, and crystals suitable for X-ray analysis were obtained by slow crystallization in a 1:1 mixture of dichloromethane and methanol (Figure 2.7.9). The constitution of compounds **3c** and **6c** was unambiguously ascertained by multinuclear NMR spectroscopy. Mass spectrometry of **3c**, **5c** and **6c** yielded the respective molecular ion peaks

(HR-MS, see Appendix, Figs. 5.7.75-77). Compounds **4c** and **5c** were analyzed by ^{1}H- and ^{11}B NMR spectroscopy and were used *in situ* without further purification.

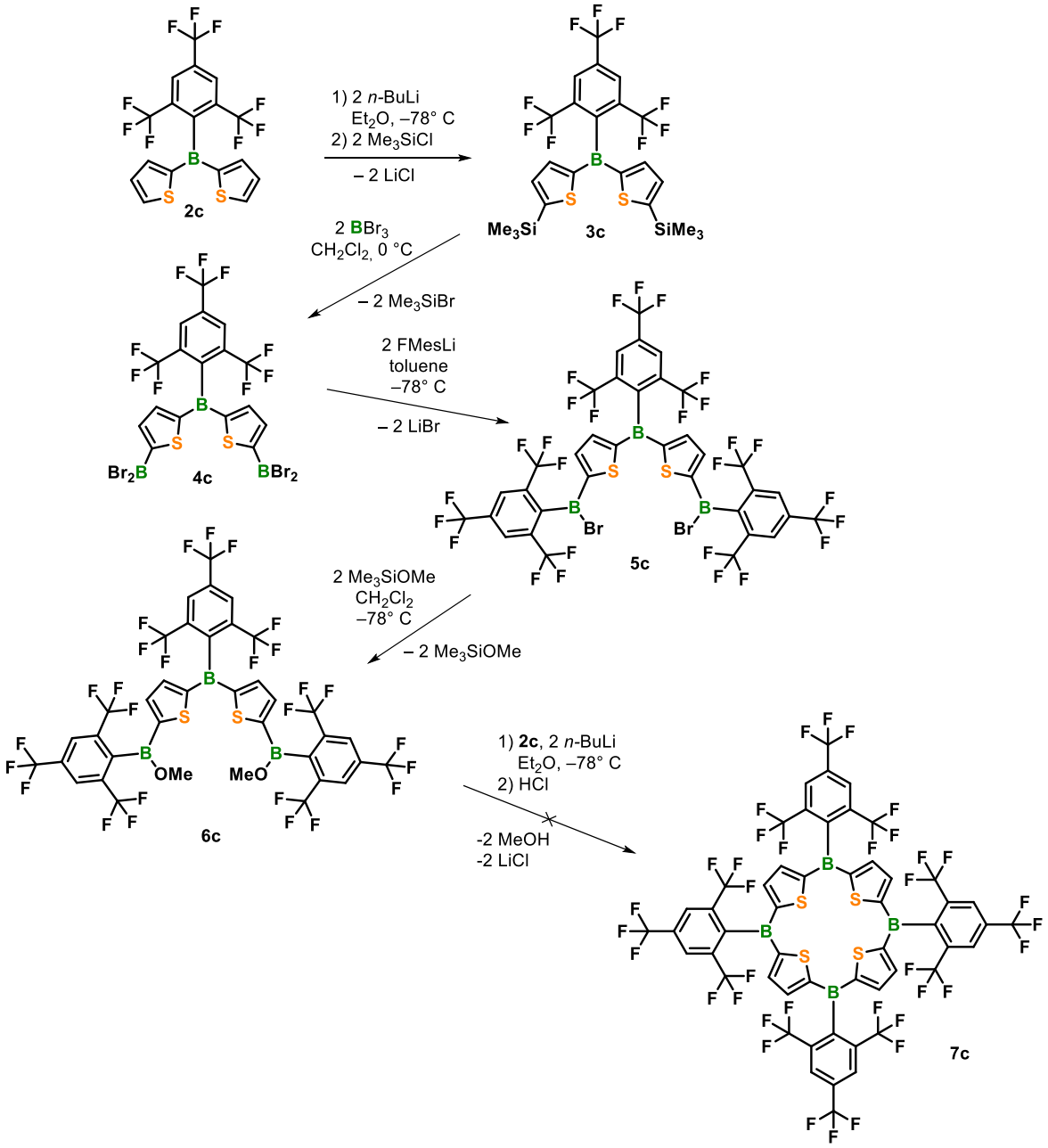

Scheme 2.7.5. Synthesis of boron-bridged tetrathiaporphyrinogen ring precursor **6c** and attempted macrocyclization reaction to afford **7c**.

We then reacted **6c** with dilithiated compound **2c** in diethyl ether at -78 °C under the same conditions as employed for the synthesis of **7b**. After work-up, analysis via ^{1}H-NMR spectroscopy and HR-MS showed no sign of formation of **7c**. Probably the influence of the electron withdrawing ^{F}Mes leads to a stabilization of the negative charge of the lithiated species and thus to lower reactivity thereof. Heating the reaction mixture to 50 °C showed no beneficial effect. Therefore, the reaction was carried out in a mixture of diethyl ether and THF to increase the reactivity of the lithiated species. Unfortunately, even after stirring the mixture for 10 d and

subsequent heating while occasionally monitoring the reaction progression via ^{1}H NMR spectroscopy, no evidence for the formation of **7c** was observed. The same result was observed when TMEDA was used as additive during the lithiation process and for the subsequent macrocyclization attempt.

Crystals suitable for single-crystal X-ray analysis for both ring precursors **6b,c** were obtained from a saturated DCM/methanol mixture (Figure 2.7.9). For **6b**, however, the quality of the obtained X-ray data was too poor to allow the discussion of structural parameters. The solid-state structure of ring-precursor **6c** was determined by single-crystal X-ray diffraction. The boron centers are trigonal-planar coordinated (sums of bond angles around the boron atoms: 360° for the outer boron atoms, 359.8° for the inner boron atom). The thiophene rings are twisted out of the plane with an interplanar angle of 31°. The ^{F}Mes group is nearly perpendicular orientated to the BC_3 plane (84°), thus preventing π-interaction of the vacant p orbital of the boron with this aromatic system.

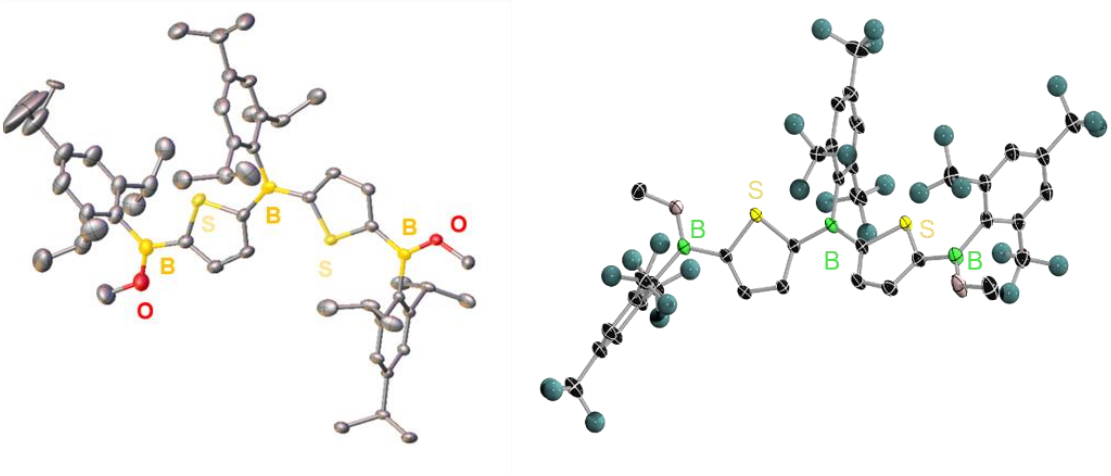

Figure 2.7.9. Molecular structure of **6b** (left) and **7c** (right) in the solid state (H-Atoms omitted for clarity).

As the ring-closing reaction was not successful, a similar synthetic approach via generation of an asymmetric trimer as described for the Tip-substituted compounds was chosen (Scheme 2.7.6). Monosilylated compound **8b** was obtained after Si/B exchange reaction of 2,5-bis(trimethylsilylthiophene) with 2-(dibromoboryl)thiophene in the presence of catalytic amounts of Me_3Si-NTf_2 (10 mol%). After removal of all volatiles in vacuo, the crude product was redissolved in toluene and added to a suspension of freshly prepared ^{F}MesLi in toluene. After stirring for 2 days, **8b** was obtained in good yield and purified by column chromatography (PE pure). Careful monoborylation with BBr_3 in DCM at low temperature afforded **9b** and reaction thereof with ^{F}MesLi yielded compound **10b**. The BBr species was converted into a BOMe species through addition of a slight excess of Me_3Si-OMe to yield **11b**. Compound **8b** was analyzed by multinuclear NMR spectroscopy and HR-MS (APCI, Appendix, Figure 5.7.78)

while **9b**, **10b** and **11b** were analyzed by ^{1}H- and ^{11}B NMR spectroscopy and the former two were used without further purification. Compound **11b** can be purified by washing with a mixture of DCM/methanol to remove residual ^{F}MesH and other minor by-products.

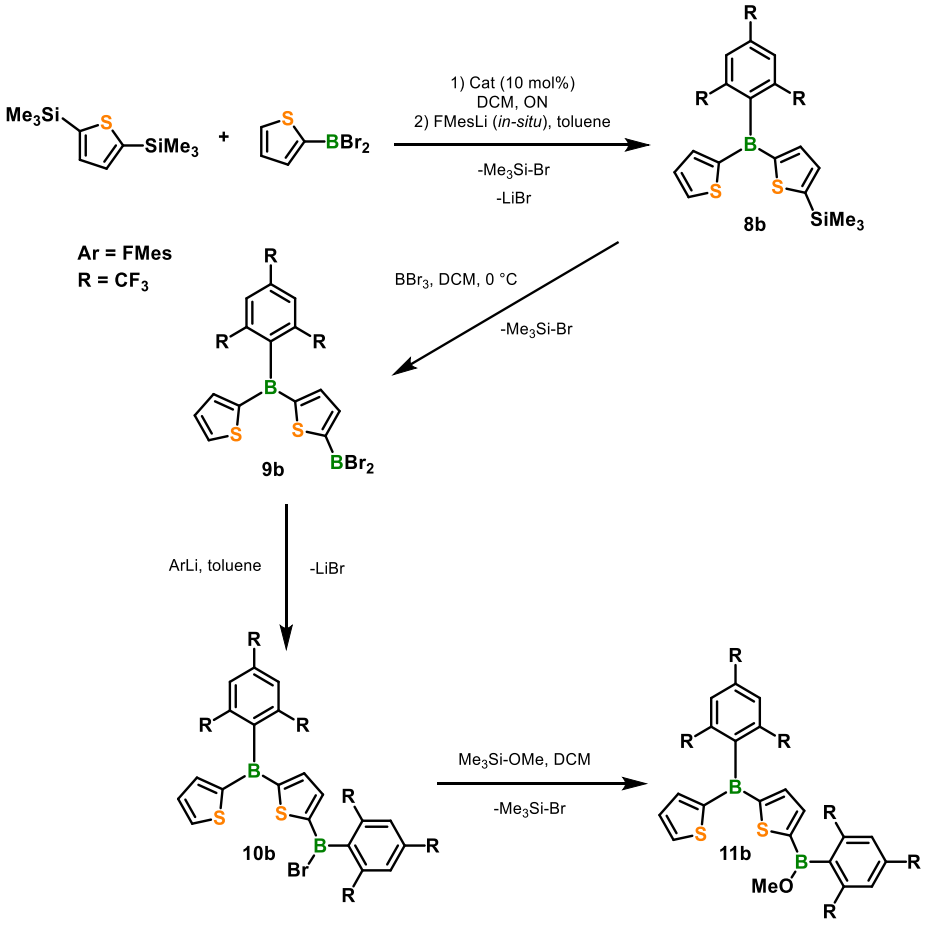

Scheme 2.7.6. Synthesis of monoarylated compound **11b**.

The employed lithiation conditions to selectively obtain monolithiated species **12b** were previously tested by quenching with Me_3Si-Cl to obtain the disilylated compound **3c** in high yields (92%) (Scheme 2.7.7, top right). Furthermore, we succeeded in the synthesis of asymmetric compound **22** (Scheme 2.7.7, bottom right).

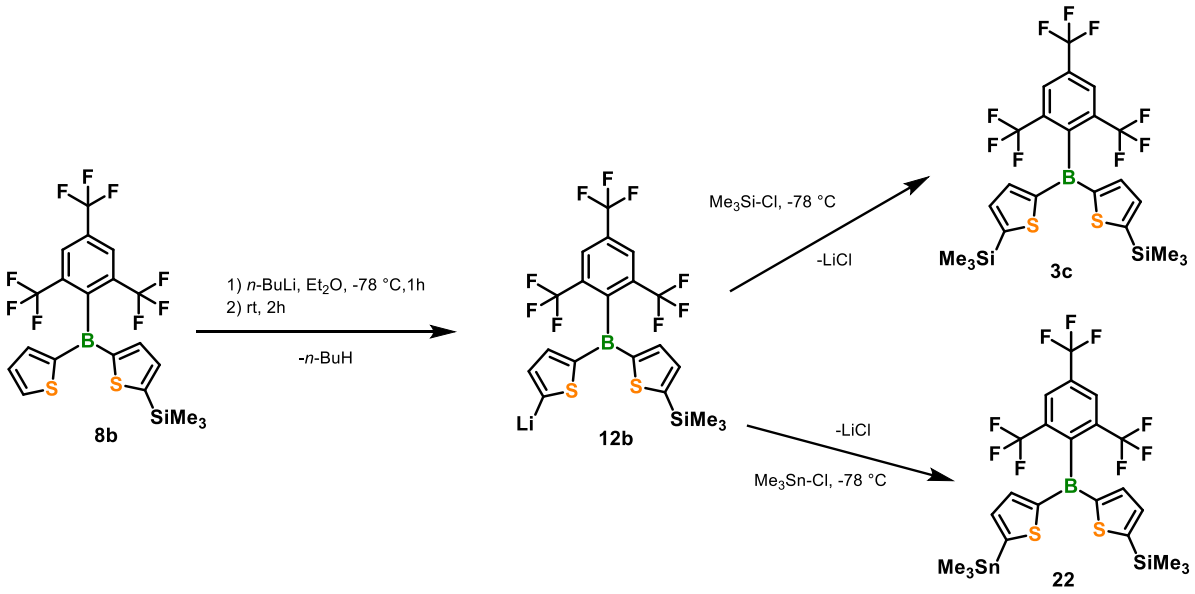

Scheme 2.7.7. Selective monolithiation to afford compound **12b** and subsequent silylation (top) and stannylation (bottom) reaction.

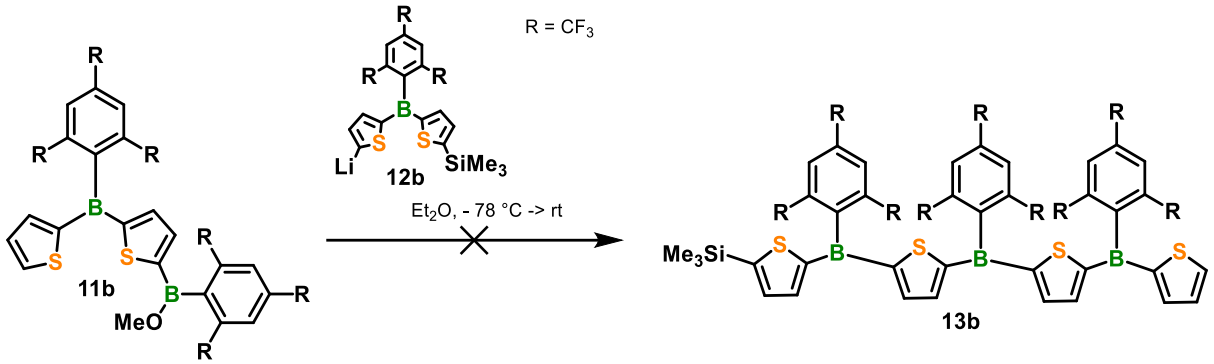

Scheme 2.7.8. Attempted synthesis of monosilylated compound **13b**.

We then attempted to react purified compound **11b** with *in situ* prepared monolithiated species **12b** in Et_2O (Scheme 2.7.8). Unfortunately, analysis via ^{1}H- and ^{11}B-NMR spectroscopy indicated no conversion to compound **13b**, and after column chromatography, only recovery of **11b** was observed. Again, the reaction of a lithiated species featuring ^{F}Mes groups with a BOMe species was not successful (as compared to the reaction between **6c** and dilithiated species **2c**). Future attempts will include the generation of more reactive B-OR^{F} species such as **11c** and **11d** (Figure 2.7.10).

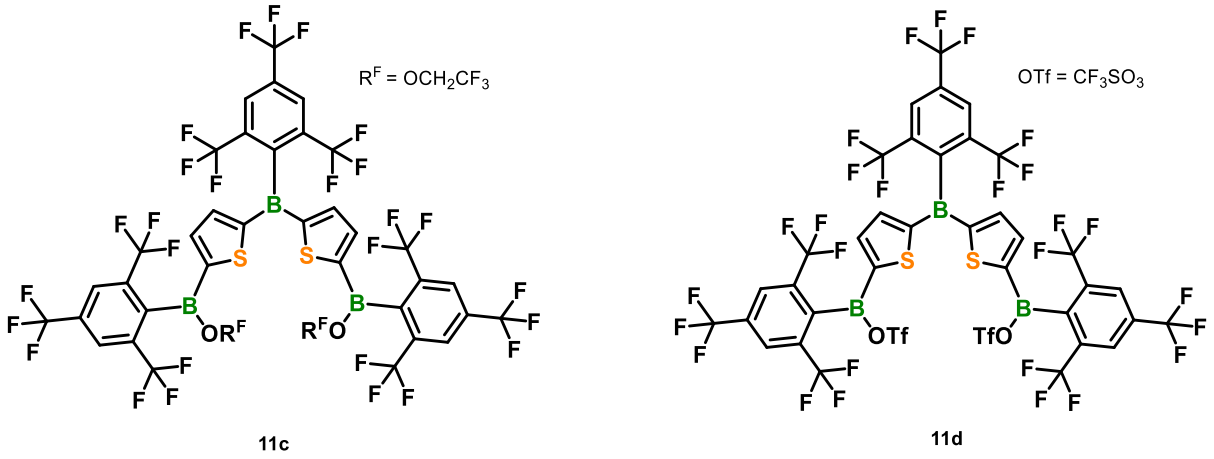

Figure 2.7.10. Compounds **11c** and **11d** featuring more reactive leaving groups.

In conclusion, we succeeded in the synthesis of conjugated boron-doped porphyrinogens with different ring sizes in which the boron centers are kinetically stabilized by bulky Tip groups. We obtained analytical evidence for a porphyrinoid structure and future investigations will cover its coordination behavior as well as applicability for organic electronic applications as well as reduction studies. Furthermore, we developed a promising new reaction pathway to obtain **7b** selectively, but optimization of the reaction parameters has to be performed. Unfortunately, so far, both reaction routes did not work for the ^{F}Mes based systems. For this reason, a different strategy for the introduction of ^{F}Mes groups in a macrocyclic structure has to be found. Since the synthesis of compound **2c** is achieved via Si/B exchange and subsequent introduction of the bulky ^{F}Mes group, possible future plans will involve this kind of reaction protocol. It is conceivable to react **3c** with **4c** under high dilution conditions followed by the incorporation of the ^{F}Mes group (Scheme 2.7.9). Another possibility could be the use of stannylated compound **23**.

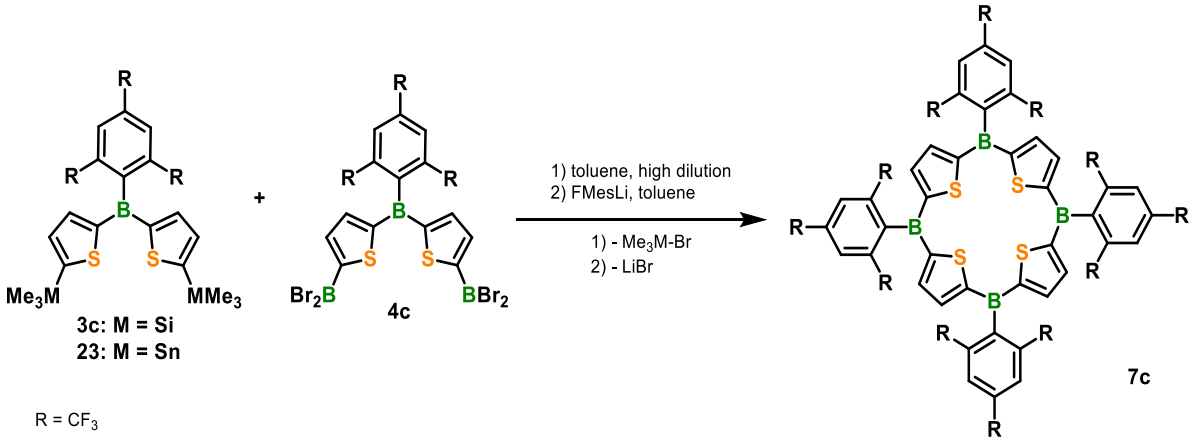

Scheme 2.7.9. Synthesis of **3c** or **23** with **4c** under high dilution conditions and subsequent arylation to obtain **7c**.

2.7.2. Diboraporphyrinogens

The integration of boron in two of the four *meso*-positions of porphyrin-related frameworks leads to the class of diboraporphyrinogens and was first studied by Siebert and co-workers.[7c] They synthesized diboraporphyrinogens of type **D** via reaction of dilithiated compound **24** with $RBCl_2$ species **25a-d** (Figure 2.7.11). In order to obtain air- and moisture-stable compounds, electronic stabilization of the boron centers through electronic saturation by means of diisopropylamino (**25a**), tetramethylpiperidyl (**25b**) or dimethylpiperidyl (**25c**) groups was attempted but provided not sufficient stabilization. The incorporation of sterically demanding duryl-substituents (**25d**) on the boron atom led to enhanced stability, which is of particular interest for further approaches. In general, in most of the reported boron-containing macrocycles a much lower Lewis acidity of the boron centers is obtained as a result of π-overlap with exocyclic alkoxy or amino groups or tetracoordination.[7,14] For this reason, we concentrated on the incorporation of sterically demanding aryl substituents which should provide effective kinetic stabilization while at the same time maintaining the Lewis acidity of the boron centers. We considered 2,4,6-triisopropylphenyl- (Tip) and 2,4,6-tri-*tert*-butylphenyl groups (Mes*) as most promising candidates for macrocycles of type **E**.

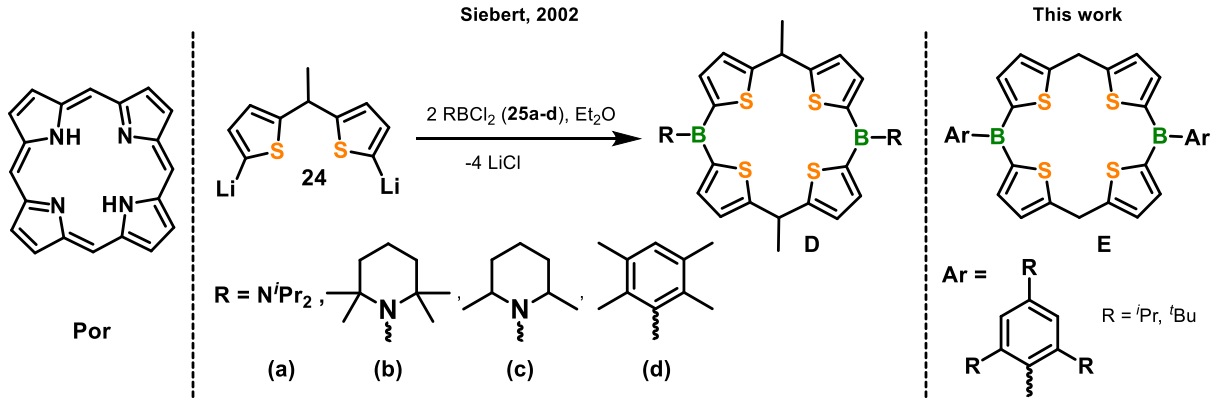

Figure 2.7.11. Structural motif of porphyrins (Por, porphin, the parent derivative, left), diboraporphyrinogen **D** with amino and aryl substituents on the boron center and targeted compound **E** featuring bulky aryl substituents.

As starting point for our synthetic approach served disilylated compound **28** which can be obtained from twofold lithiation of either 2,2'-dithienylmethane (**26a**) or 5,5'-bisdibromo-5,5'-dithienylmethane (**26b**) in Et_2O with *n*-BuLi and subsequent addition of Me_3Si-Cl at -78 °C (Scheme 2.7.10). Twofold silicon/boron exchange reaction with a solution of trihaloborane (BCl_3 or BBr_3) in DCM yielded compounds **29a,b** as colored solids in high yields (approx. 95%). Subsequent addition of a solution of TipLi in toluene at lower temperatures led to selective monoarylation at both boron centers to give **30a,b**. The reaction pathway via **29a** led to a somewhat cleaner reaction with a slightly increased yield and was therefore used more frequently. The addition of a slight excess of methoxytrimethylsilane (Me_3Si-OMe) afforded compound **31a**, which could be purified by precipitation in a mixture of DCM and methanol to

remove residual TipH impurities. The introduced methoxy group leads to electronic saturation of the boron atoms (+M effect) and thus, the reactivity in comparison to compounds **30a,b** is significantly reduced. On the other hand, the absence of B-Cl or B-Br bonds in **31a** allows the use of ether solvents such as diethyl ether or THF. Furthermore, the addition of an excess of 2,2,2-trifluoroethoxytrimethysilane (Me_3Si-OCH_2CF_3) to **30a** or **30b** led to compound **31b,** which should show increased reactivity because of the electron-withdrawing effect of the CF_3 groups. The addition of Me_3Si-OCH_2CF_3 to **30b** afforded compound **31b** within several hours, while the lower reactivity of the B-Cl bond in comparison to B-Br bond causes a longer reaction time. Both the excess of added Me_3Si-OR and formed Me_3Si-X can be easily removed in vacuo. The characterization of compounds **26b**, **28** and **29b** was presented in chapter 2.5. Compounds **29a**, **30** and **31** were characterized by multinuclear NMR-spectroscopy and mass spectrometry. Crystals suitable for X-ray analysis for **29a** were obtained by Dr. Artur Lik by crystallization in a mixture of pentane/toluene (2:1) at low temperatures. For **31a,** crystals suitable for X-ray analysis were obtained by slow crystallization in a mixture of DCM/methanol (Figure 2.7.12).

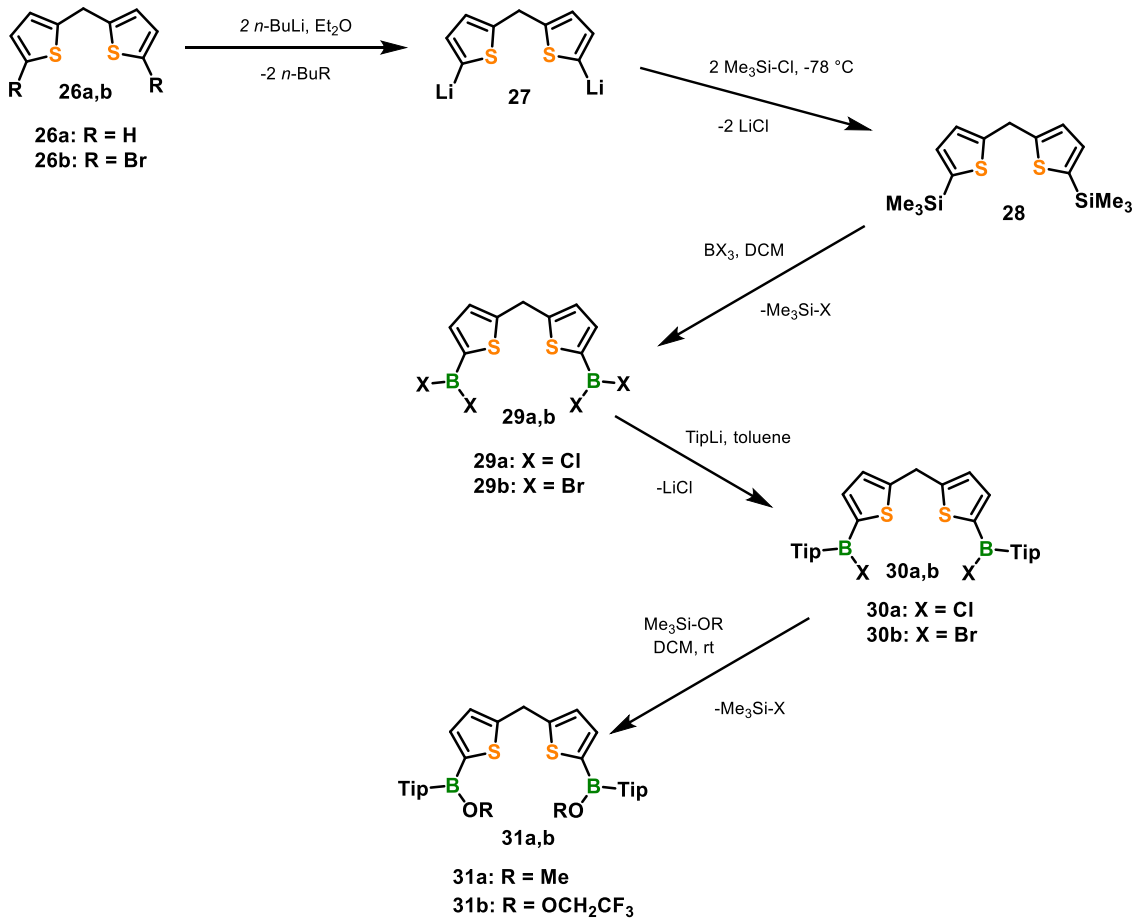

Scheme 2.7.10. Synthesis of compounds **30** and **31**.

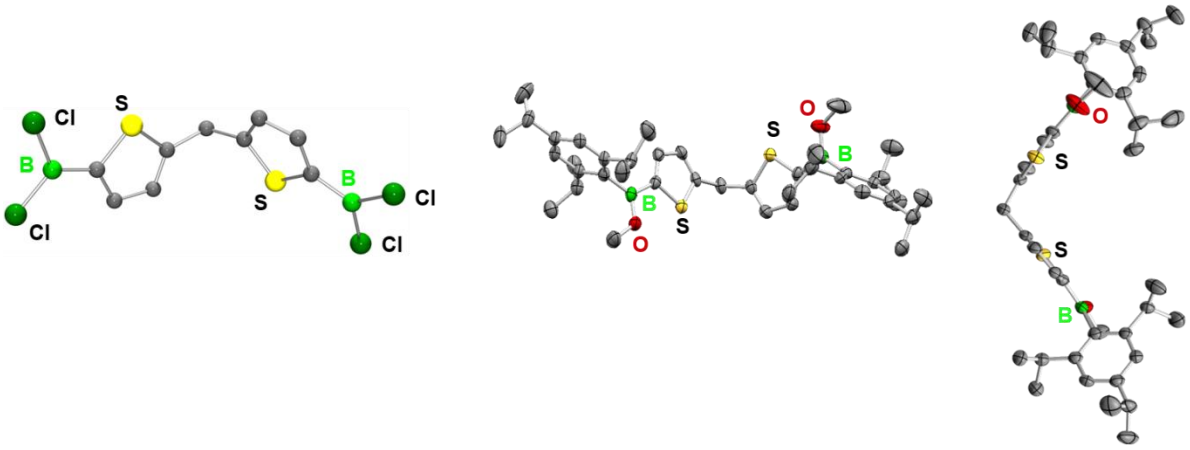

Figure 2.7.12. Solid-state structures of **29a** and **30a** (H-atoms omitted for clarity).

The reactivity of ring precursor **31b** towards a lithiated species was tested in a model reaction in which **31b** was reacted with two equivalents of freshly prepared 2-thienyllithium (Thi-Li) in Et_2O at -78 °C (Scheme 2.7.11, top). Interestingly, the addition of only a small amount of lithiated species led to an immediate intense dark blue coloration of the reaction mixture. The coloration might be an evidence for deprotonation at the methylene bridge to obtain a π-conjugated anionic species. Under inert conditions, the coloration was stable but contact with air or moist solution caused immediate quenching of the color. After quenching with water and aqueous work-up, analysis via ^{1}H-NMR spectroscopy confirmed the formation of **32**. Full characterization of **32** and related compounds was described in chapter 2.5. To perform the ring-closing reaction and obtain diboraporphyrinogen **33**, the ring precursors **30** and **31** were reacted with dilithiated compound **27** under pseudo high-dilution conditions (Scheme 2.7.11, bottom).

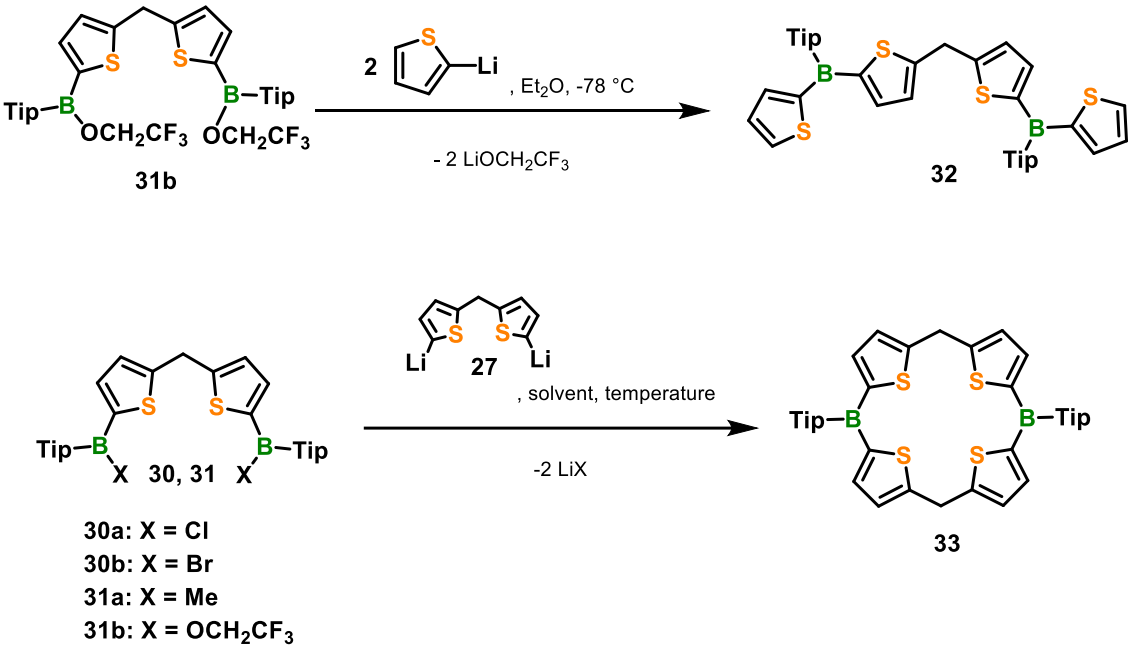

30a: X = Cl
30b: X = Br
31a: X = Me
31b: X = OCH_2CF_3

Scheme 2.7.11. Top: Model reaction to obtain compound **32**. Bottom: Attempted synthesis of diboraporphyrinogene **33**.

In a standard reaction procedure, the freshly prepared lithiated species **27** was cooled down to –78°C and a solution of **30** or **31** in the respective solvent was added at -78 °C under high-dilution (0.01 M-0.1 M). ^{1}H and ^{11}B-NMR monitoring of reactions in which **30a** was combined with a small amount of Et_2O indicated a certain tolerance towards ether solvents at least on a small time scale (within 24 h, see Appendix, Figs. 5.7.59-61), however, the preferred solvent was toluene to avoid any possible ether cleavage. The reactivity can be slightly increased by varying the solvent in which the lithiated species was generated in the order toluene > Et_2O > THF. The lithiation can be performed in each of these solvents and lithiated compound **27** showed sufficient stability. The use of compounds **30,31** allows free choice of the solvent, but as result of decreased reactivity in comparison to B-Cl or B-Br bonds, the reaction was preferably performed in ether solvents. Again, after a few drops of lithiated species had been added to the solution of **30a,b**, a color change to dark blue occurred. The reaction of both **30a,b** (in toluene) with **27** (in toluene, Et_2O and THF) led to no conversion to the desired compound, and analysis via NMR spectroscopy showed no evidence for a reaction with the lithiated species at all (also excluding the formation of linear products), even in concentrated solutions (1 M). The same results were obtained for **31a,b** (in Et_2O and THF) which were reacted with **27** (in Et_2O and THF). No conversion to the desired macrocycle was observed. In comparison to the successful model reaction to compound **32**, one difference is the methylene bridge in 2-position as electron pushing group. Therefore, a further model reaction was performed in which **31a,b** were reacted with two equivalents of lithiated 2-methylthiophene in diethylether or THF to obtain **32-Me** (Scheme 2.7.12). Unfortunately, the reaction was not successful and no evidence for the formation of **32-Me** was observed in both ^{1}H- and ^{11}B-

spectroscopy as well as in HR-MS. Side reactions caused by the reaction of formed *n*-butane with the lithiated species or the methylene bridge (the latter was not observed in any previous experiments) were tried to avoid by using *tert*-butyllithium as lithiation agent. However, the change of the lithiation agent did not lead to a successful reaction to **32-Me**.

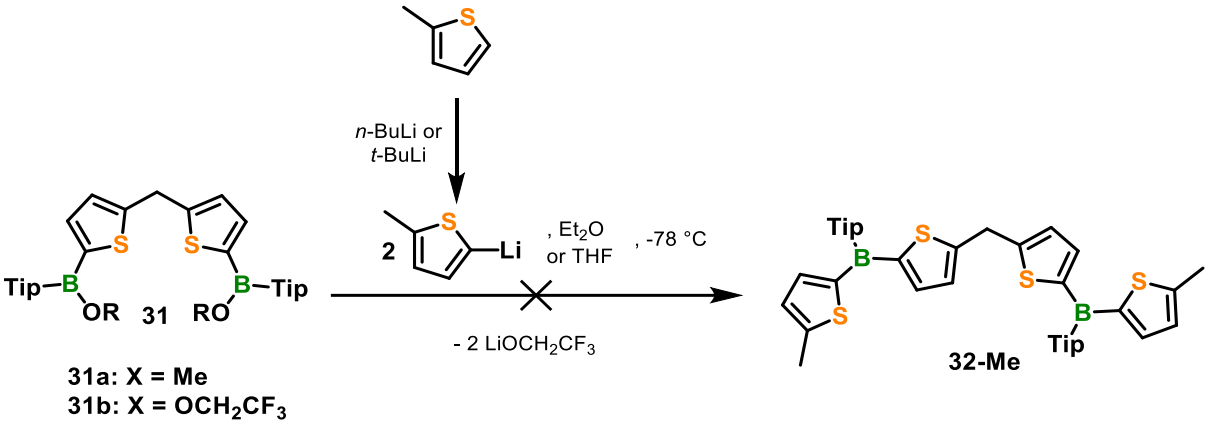

Scheme 2.7.12. Attempted synthesis of **32-Me.**

Further research in this field may involve the reaction of disilylated **28** or distannylated compounds **33** in combination with compounds **29a,b** under high dilution to obtain macrocycles **34** (Scheme 2.7.13). This pathway allows the subsequent incorporation of sterically demanding substituents which leads to different accessible diboraporphyrinogens within the same reaction sequence. By doing this, variation of the aryl substituent can result in potential increase in acceptor properties (use of ^{F}Mes) or extended stability (use of Mes*) of macrocycles of type E.

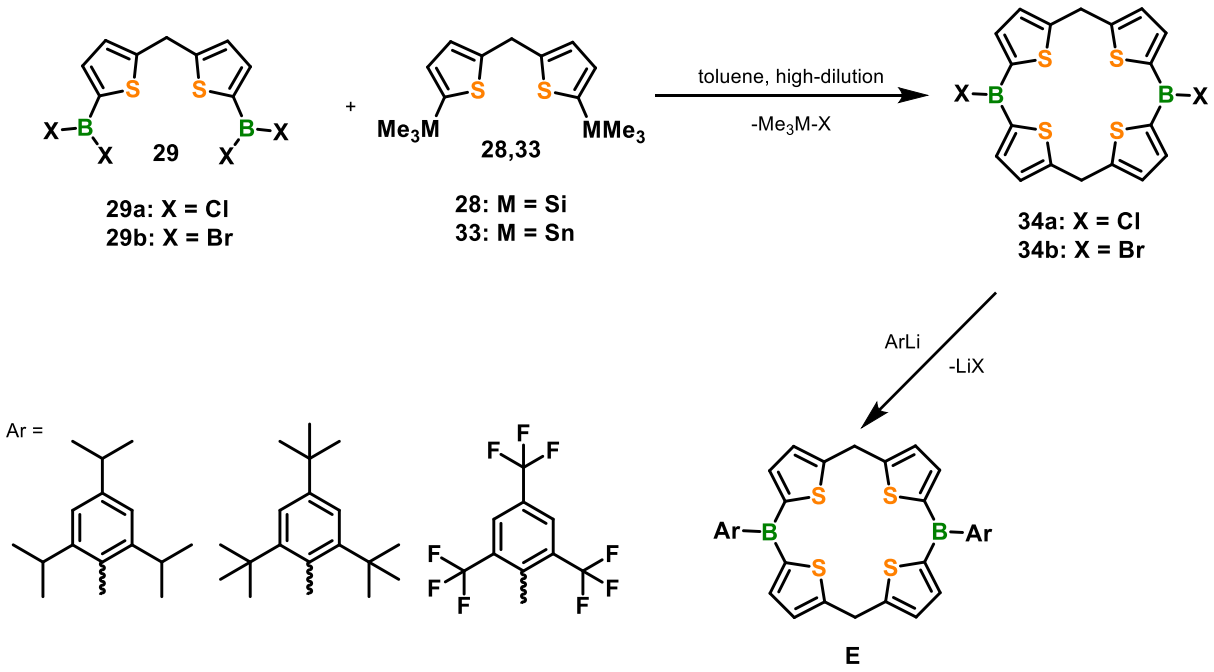

Scheme 2.7.13. Reaction of **29** with **28** or **33** under high dilution conditions and subsequent arylation to obtain diboraporphyrinogens of type **E** with different accessible aryl substituents.

2.7.3. Experimental section

General procedures. All manipulations were performed under an atmosphere of dry argon using standard Schlenk techniques or in an MBraun glove box. Solvents (dichloromethane, *n*-pentane, diethylether, toluene, and tetrahydrofuran) were dried and degassed by means of an MBraun SPS-800 solvent purification system. Methanol was dried over magnesium turnings and freshly distilled prior to use. THF and diethylether for ring-closing reactions were dried and degassed at reflux over sodium and freshly distilled prior to use. Deuterated solvents for NMR spectroscopy were dried and degassed at reflux over sodium (C_6D_6) or CaH_2 ($CDCl_3$ and CD_2Cl_2) and freshly distilled prior to use. Solvents for aqueous work up (*n*-hexane, *n*-pentane, dichloromethane, methanol, ethanol, diethylether), sodium hypochlorite, thiophene, tribromoborane, 2-bromothiophene, sulfuric acid, glacial acid, dimethoxymethane 2-bromo-1,3,5-triisopropylbenzene, 1,3,5-tris(trifluoromethyl)benzene and lithium bis(trifluoromethylsulfonyl)imide were purchased from commercial sources and used as received. Solutions of *n*-butyllithium (1.6 M and 2.5 M in hexane, respectively), *t*-butyllithium (1.7 M in pentane), trimethylstannyl chloride (1M in THF) and hydrogenchloride (2 M in diethyl ether) were purchased from Sigma Aldrich and used as received as well. Trimethylsilylchloride, methoxytrimethylsilane and 2,2,2-trifluoroethoxytrimethysilane were commercially purchased and freshly distilled prior to use. 2,4,6-triisopropylphenyllithium,[15] trimethylsilylbis(trifluoromethylsulfonyl)imide[16], 1,3,5-tris(trifluoromethyl)phenyllithium[13] and 5,5'-dibromo-2,2'-dithienylmethane[17] were prepared according to methods described in the literature. Compounds **2b**, **3b**, **4b, 5b, 6b, O, T** and 2-thienyllithium were prepared according to procedures previously described by us.[9,10] NMR spectra were recorded at 25 °C on a Bruker Avance III HD spectrometer operating at 300 MHz or on a Bruker Avance 500 spectrometer operating at 500 MHz. Chemical shifts were referenced to residual protic impurities in the solvent (^{1}H) or the deuterated solvent itself (^{13}C) and reported relative to external $SiMe_4$ (^{1}H, ^{13}C) or $BF_3{\cdot}OEt_2$ (^{11}B) standards. Mass spectra were obtained with the use of a Thermo Scientific Exactive Plus Orbitrap MS system employing either atmospheric sample analysis probe (ASAP), electrospray ionization (ESI), atmospheric pressure chemical ionization (APCI) or liquid injection field desorption ionisation (LIFDI). Elemental analyses were performed on an Elementar vario MICRO cube elemental analyzer. Cyclic voltammetry experiments were performed using a Gamry Instruments Reference 600 potentiostat. A standard three-electrode cell configuration was employed using a platinum disk working electrode, a platinum wire counter electrode, and a silver wire, separated by a *Vycor* tip, serving as the reference electrode. Tetra-*n*-butylammonium hexafluorophosphate ([*n*-Bu_4N][PF_6]) was employed as the supporting electrolyte. Compensation for resistive losses (*iR* drop) was employed for all measurements. Cyclic voltammetry scans were conducted with a scan rate of 250 mV/s. The

scans were referenced after the addition of a small amount of ferrocene as internal standard. The potentials are reported relative to the ferrocene/ferrocenium couple. Crystals suitable for single-crystal X-ray diffraction were selected, coated in perfluoropolyether oil, and mounted on MiTeGen sample holders. Diffraction data were collected on Bruker X8 Apex II 4-circle diffractometers with CCD area detectors using Mo-Kα radiation. The crystals were cooled using an Oxford Cryostreams low-temperature device. Data were collected at 100 K. The images were processed and corrected for Lorentz-polarization effects and absorption as implemented in the Bruker software packages. The structures were solved using the intrinsic phasing method (SHELXT)[18] and Fourier expansion technique. All non-hydrogen atoms were refined in anisotropic approximation, with hydrogen atoms 'riding' in idealized positions, by full-matrix least squares against F^2 of all data, using SHELXL[19] software and the SHELXLE graphical user interface.[20] Other structural information was extracted using OLEX2 software.[21] UV–vis spectra were obtained using a Jasco V-630 spectrophotometer. Emission spectra were recorded using an Edinburgh Instruments FLSP920 spectrometer equipped with a double monochromator for both excitation and emission, operating in right-angle geometry mode, and all spectra were fully corrected for the spectral response of the instrument. Fluorescence quantum yields were measured using a calibrated integrating sphere from Edinburgh Instruments combined with the FLSP920 spectrometer described above.

Syntheses

Synthesis of 6b. To a solution of **5b** (12.082 g, 12.5 mmol) in DCM (55 mL) was added Me_3Si-OMe (3.257 g, 31.25 mmol) at ambient temperature and the reaction mixture was stirred for 2 h. All volatiles were removed in vacuo and the resulting crude brown solid was redissolved in DCM (30 mL). Addition of methanol (40 mL) led to precipitation and after filtration and removal of all volatiles in vacuo, a colorless solid was obtained. Crystals suitable for X-ray analysis were obtained through slow crystallization in a mixture of DCM/methanol. The data obtained for ^{13}C NMR spectroscopy are in good accordance with the data described by Dr. Artur Lik.[9]

Yield: 6.733 g (7.75 mmol, 62%). ^1H NMR (400 MHz, $CDCl_3$): δ = 7.78 (d, *J* = 3.5 Hz, 2H, Thi-*H*), 7.44 (d, *J* = 3.5 Hz, 2H, Thi-*H*), 6.99 (s, 4H, Tip-*H*), 6.94 (s, 2H, Tip-*H*), 3.77 (s, 6H, O-C*H*$_3$), 2.99 – 2.84 (m, 4H, *p*-^{i}Pr-*H*), 2.66 – 2.54 (m, 4H, *o*-^{i}Pr-*H*), 2.51 – 2.41 (m, 2H, *o*-^{i}Pr-*H*), 1.29 (d, 3*J* = 6.9 Hz, 18H, *p*-^{i}Pr-C*H*$_3$), 1.23 (d, *J* = 6.2 Hz, 12H, *o*-^{i}Pr- C*H*$_3$), 1.05 (d, *J* = 6.0 Hz, 12H, *o*-^{i}Pr- C*H*$_3$), 0.98 (d, *J* = 6.7 Hz, 12H, *o*-^{i}Pr- C*H*$_3$). ^{11}B NMR (128 MHz, $CDCl_3$): δ = 45.8 (Ar-*B*OMe), Ar$_3$*B*: not detectable.

Synthesis of 7b. A solution of **2b** (0.380 g, 1.0 mmol) in Et_2O (7.5 mL) was cooled to -78 °C and then, a solution of *t*-BuLi (2.1 mmol, 1.24 mL) was added dropwise and the resulting

suspension was stirred for 4 h at this temperature. Subsequently, Et_2O (12.5 mL) was cooled to -78 °C and added to the lithiated species followed by the addition of a cold (-78 °C) solution of **6b** (0.869 g, 1.0 mmol) in Et_2O (10.0 mL). The reaction mixture was allowed to slowly warm up to ambient temperature. The addition of a solution of HCl (2 M in Et_2O, 1.1 mL) led to immediate precipitation, which was helpful for work-up. After removal of all volatiles in vacuo, the orange colored solid was redispersed in pentane (25 mL) and filtered. Then, methanol (25 mL) was added which led to precipitation. After filtration, the resulting solid was repeatedly washed with *n*-hexane to remove remaining linear side products.

Yield: 0.040 g (3.2 %). ^{1}H NMR (300 MHz, $CDCl_3$): δ = 7.90 (s, 8H, Thi-*H*), 6.95 (s, 8H, Tip-*H*), 2.97 – 2.83 (m, 4H, *p*-^{i}Pr-*H*), 2.53 – 2.37 (m, 8H, *o*-^{i}Pr-*H*), 1.27 (d, *J* = 6.9 Hz, 24H, *p*-^{i}Pr-C*H*$_3$), 0.99 (d, *J* = 6.5 Hz, 48H, *o*-^{i}Pr-C*H*$_3$). The obtained data for ^{11}B and ^{13}C NMR spectroscopy are in good accordance with previous results.[9]

Synthesis of 13a. A solution of **8a** (1.36 g, 3.00 mmol) in Et_2O (30 mL) was cooled down to -78 °C and a solution of *t*-BuLi in pentane (3.60 mmol, 2.25 mL) was added dropwise. The reaction mixture was stirred at this temperature for 4.5 h. Then **11a** (1.87 g, 3.00 mmol) in Et_2O (10 mL) was added and the solution was allowed to warm up to ambient temperature overnight. After aqueous workup and removal of all volatiles in vacuo, the crude product was subjected to column chromatography (silica, PE/DCM 100:0 -> 90:10) to give a yellow solid.

Yield: 1.96 g (62%). ^{1}H NMR (500 MHz, $CDCl_3$): δ = 7.95 (dd, *J* = 4.7, 0.9 Hz, 1H, Thi-*H*), 7.92 – 7.87 (m, 5H, Thi-*H*), 7.85 (d, *J* = 3.6 Hz, 1H, Thi-*H*), 7.42 (d, *J* = 3.4 Hz, 1H, Thi-*H*), 7.31 (dd, *J* = 4.7, 3.6 Hz, 1H, Thi-*H*), 7.00 (s, 2H, Tip-*H*), 6.99 (s, 2H, Tip-*H*), 6.99 (s, 2H, Tip-*H*), 2.94 (dd, *J* = 8.4, 5.0 Hz, 3H, *p*-^{i}Pr-*H*), 2.51 (ddd, *J* = 8.9, 5.3, 2.8 Hz, 6H, *o*-^{i}Pr-*H*), 1.32 (dd, *J* = 4.0, 2.9 Hz, 18H, *p*-^{i}Pr-C*H*$_3$), 1.06 – 1.01 (m, 36H, *o*-^{i}Pr-C*H*$_3$), 0.37 (s, 9H, Si-(C*H*$_3$)$_3$); ^{11}B NMR (160 MHz, $CDCl_3$): δ = 56.9 (s); ^{13}C NMR (126 MHz, $CDCl_3$): δ = 157.5 (br. s, Thi-*C*-B), 156.9 (br. s, Thi-*C*-B), 156.1 (br. s, Thi-*C*-B), 156.0 (br. s, Thi-*C*-B), 155.6 (s, Thi-*C*-Si), 150.7 (br. s), 149.7 (s, Tip-*C*-*o*-^{i}Pr), 149.6 (s, Tip-*C*-*o*-^{i}Pr), 149.6 (s, Tip-*C*-*o*-^{i}Pr), 148.9 (s, Tip-*C*-*p*-^{i}Pr), 148.8 (s, Tip-*C*-*p*-^{i}Pr), 148.7 (s, Tip-*C*-*o*-^{i}Pr), 145.4, 143.5 (s, Thi-*C*H), 142.8 (s, Thi-*C*H), 142.6 (s, Thi-*C*H), 142.3 (s, Thi-*C*H), 142.0 (s, Thi-*C*H), 139.4 (br. s, Tip-*C*-B), 139.1 (br. s, Tip-*C*-B), 139.0 (br. s, Tip-*C*-B), 138.3 (s, Thi-*C*H), 135.7 (s), 129.3 (s), 120.2 (3xs, Tip-*C*H), 35.7 (d, *J* = 15.5 Hz), 34.4 (d, *J* = 2.2 Hz), 24.3 (d, *J* = 8.9 Hz), 0.1 (s, Thi-C-Si(*C*H$_3$)$_3$); ^{29}Si NMR (99 MHz, $CDCl_3$): δ = -6.0 (s); HR-MS (APCI): m/z = 1044.5739; calcd. for $C_{64}H_{87}B_3S_4Si$: 1044.5753.

Synthesis of 14a. To a solution of **13a** (0.523 g, 0.5 mmol) in THF (1 mL) was added a freshly prepared solution of LDA (0.889 mmol, 0.5 mL) dropwise at -78 °C. The reaction mixture was stirred for 3.5 h maintaining the temperature. Then, a solution of Me_3Sn-Cl in THF (0.5 mmol, 0.5 mL) was added dropwise. Immediately, the formation of a lightly red color was observed. The solution was allowed to slowly warm up to ambient temperature overnight. Then, the

brownish mixture was quenched by the addition of an aqueous NaOCl solution and more water. After aqueous workup and removal of all volatiles in vacuo, a green colored solid was obtained.

Yield: 0.474 g (78%, 0.39 mmol). ^{1}H NMR (300 MHz, $CDCl_3$): δ = 7.97 (d, *J* = 3.4 Hz, 1H, Thi-*H*), 7.93 – 7.86 (m, 5H, Thi-*H*), 7.41 (dd, *J* = 5.0, 3.4 Hz, 2H, Thi-*H*), 7.00 (s, 4H, Tip-*H*), 6.99 (s, 2H, Tip-*H*), 3.03 – 2.85 (m, 3H, *p*-^{i}Pr-*H*), 2.65 – 2.43 (m, 6H, *o*-^{i}Pr-*H*), 1.32 (dd, *J* = 6.9, 3.6 Hz, 18H, *p*-^{i}Pr-CH_3), 1.09 – 0.99 (m, 38H, *o*-^{i}Pr-CH_3), 0.42 (s, 9H, Sn-(CH_3)$_3$), 0.37 (s, 9H, Si-(CH_3)$_3$); ^{11}B NMR (96 MHz, $CDCl_3$): no signal detected; ^{13}C NMR (75 MHz, $CDCl_3$): δ =; ^{29}Si NMR (60 MHz, $CDCl_3$): δ = -6.0 (s); ^{119}Sn NMR (112 MHz, $CDCl_3$): δ = -26.2 (s); HR-MS (APCI): m/z = 1208.5421; calcd. for $C_{67}H_{95}B_3S_4SiSn$: 1208.5387.

Synthesis of 15a. To a solution of **8a** (0.113 g, 0.25 mmol) in Et_2O (2.5 mL) was added a solution of *t*-BuLi in pentane (0.3 mmol, 0.188 mL) dropwise at -78 °C. The reaction mixture was stirred for 4 h maintaining the temperature and then, a solution of $SnMe_3$-Cl in THF (0.275 mmol, 0. 275 ml) was added dropwise. The reaction mixture was allowed to warm up to ambient temperature overnight followed by quenching by the addition of an aqueous NaOCl solution and more water. After aqueous workup and removal of all volatiles in vacuo, the crude product can be further purified by crystallization in hexane to afford crystals.

Yield: 0.105 g (68%, 0.17 mmol). ^{1}H NMR (500 MHz, $CDCl_3$): δ = 7.87 (d, *J* = 3.4 Hz, 1H, Thi-*H*), 7.81 (d, *J* = 3.4 Hz, 1H, Thi-*H*), 7.37 (d, *J* = 3.4 Hz, 1H, Thi-*H*), 7.36 (d, *J* = 3.4 Hz, 1H, Thi-*H*), 6.99 (s, 2H, Tip-*H*), 3.01 – 2.90 (m, 1H, *p*-^{i}Pr-*H*), 2.57 – 2.44 (m, 2H, *o*-^{i}Pr-*H*), 1.33 (d, *J* = 6.9 Hz, 6H, *p*-^{i}Pr-CH_3), 1.03 (d, *J* = 6.7 Hz, 12H, *o*-^{i}Pr-CH_3), 0.41 (s, 9H, -Sn(CH_3)$_3$), 0.36 (s, 9H, -Si(CH_3)$_3$); ^{11}B NMR (160 MHz, $CDCl_3$): δ = 56.1 (s); ^{13}C NMR (126 MHz, $CDCl_3$): δ = 154.0 (s, Thi-*C*-Si), 152.9 (s, Thi-*C*-Sn), 151.4 (br. s, Thi-*C*-B), 150.9 (br. s, Thi-*C*-B), 149.7 (s, Tip-*C*-*o*-^{i}Pr), 148.3 (s, Tip-*C*-*p*-^{i}Pr), 143.0 (s, Thi-*C*H), 142.9 (s,Thi-*C*H), 139.9 (br. s, Tip-*C*-B), 136.8 (s, Thi-*C*H), 135.5 (s, Thi-*C*H), 120.0 (s, Tip-*C*H), 35.3 (s, *o*-^{i}Pr-*C*H), 34.3 (s, *p*-^{i}Pr-*C*H), 24.6 – 24.2 (m, o+p-^{i}Pr-*C*H_3), 0.1 (s, Thi-C-Si(*C*H_3)$_3$), -8.0 (s, Thi-C-Sn(*C*H_3)$_3$); ^{29}Si NMR (99 MHz, $CDCl_3$): δ = -6.2 (s); ^{119}Sn NMR (187 MHz, $CDCl_3$): δ = -26.8 (s).

Synthesis of 16a. A solution of **15a** (0.154 g, 0.25 mmol) was dissolved in DCM (0.5 mL) and added to a solution of BBr_3 (0.061 g, 0.245 mmol) in DCM (0.6 mL) at 0 °C. After stirring for 30 minutes, the reaction progress was monitored by ^{1}H- and ^{11}B NMR spectroscopy.

Synthesis of 17a. A solution of **15a** (0.135 g, 0.22 mmol) was dissolved in DCM (0.9 mL) and added to a solution of BCl_3 in DCM (1M, 0.217 mmol, 0.217 mL) at 0 °C. After stirring for 30 minutes, the reaction progress was monitored by ^{1}H- and ^{11}B NMR spectroscopy.

Attempted synthesis of macrocycle 20a via 18a. A solution of **14a** (0.060 g, 0.05 mmol) in $CDCl_3$ (0.50 mL) was added dropwise to a solution of BBr_3 (0.0123 g, 0.049 mmol) in $CDCl_3$ (0.25 mL) at -78 °C. The cooling was removed and the reaction progress was monitored by

^{1}H- and ^{11}B NMR spectroscopy. After stirring for 25h, Me_3Si-NTf_2 (10 mol%) was added and the reaction mixture was stirred for 1 d while monitoring the reaction progress. After stirring overnight, another batch of catalyst (40 mol%) was added and the reaction mixture was stirred for 3 days.

Attempted synthesis of macrocycle 21a via 19a. A solution of **14a** (0.060 g, 0.05 mmol) in $CDCl_3$ (0.50 mL) was added dropwise to a solution of BCl_3 in DCM (1M, 0.049 mmol) at -78 °C. The cooling was removed, and the progress was monitored by ^{1}H- and ^{11}B NMR spectroscopy. After stirring for 25h, Me_3Si-NTf_2 (10 mol%) was added and the reaction mixture was stirred for 1 d while monitoring the reaction progress. After stirring overnight, another batch of catalyst (40 mol%) was added and the reaction mixture was stirred for 3 days.

Synthesis of 2c. To a solution of 2-trimethylsilylthiophene (12.51 g, 80 mmol) in DCM (50 mL) was added BBr_3 (9.82 g, 39.2 mmol) at 0 °C and the reaction mixture was stirred for 2.5 h without maintaining the temperature. Then, Me_3Si-NTf_2 (1.41 g, 3.7 mmol) was added in substoichiometric amount (5 mol%) and the resulting reaction mixture was stirred for another 2 h. Subsequently, all volatiles were removed in vacuo and the crude solid was redispersed in toluene (40 mL). This solution was added to a freshly prepared suspension of ^{F}MesLi (starting from 60 mmol of ^{F}MesH)[13] in toluene (40 mL) at 0 °C. The reaction mixture was stirred for 2 days and quenched by the addition of water. After aqueous work-up, crude **2c** was further purified by column chromatography (silica; PE) to afford **2c** as colorless solid.

Yield: 12.05 g (26.3 mmol, 67%). The obtained NMR spectroscopy data are in good accordance with data obtained from literature.[13]

Synthesis of 3c. To a solution of **2c** (8.247 g, 18 mmol) in diethylether (130 mL) was added *n*-BuLi (23.63 mL, 37.8 mmol) dropwise at -78°C. The reaction mixture was stirred for 1 h at this temperature and 2 h at ambient temperature. Afterwards, the reaction mixture was cooled to -78°C and Me_3Si-Cl (4.302 g, 39.6 mmol) was added. The reaction mixture was slowly warmed to ambient temperatures and stirred overnight. The resulting suspension was diluted with *n*-pentane and quenched by adding water. The organic phase was washed with water and brine, dried over $MgSO_4$ and the solvent was removed in vacuo. The crude product was further purified using column chromatography (silica; PE).

Yield: 10.23 g (16.98 mmol, 94%); ^{1}H NMR (500 MHz, $CDCl_3$): δ = 8.16 (s, 2H, ^{F}Mes-*H*), 7.60 (d, *J* = 3.5 Hz, 2H, Thi-*H*), 7.37 (d, *J* = 3.5 Hz, 2H, Thi-*H*), 0.38 (s, 18H, -Si(CH_3)$_3$); ^{11}B NMR (160 MHz, $CDCl_3$): δ = 50.5 (s); ^{13}C NMR (126 MHz, $CDCl_3$): δ = 155.7 – 155.5 (m, Thi-*C*-Si), 147.0 (br. s, Thi-*C*-B), 145.5 (br. s, ^{F}Mes-C-B), 144.0 (d, *J* = 6.7 Hz, Thi-*C*H), 142.6 (d, *J* = 6.7 Hz, Thi-*C*H), 136.3 (d, *J* = 6.2 Hz, Thi-*C*H), 135.0 (d, *J* = 6.3 Hz, ^{F}Mes-C-*C*F_3), 134.5 (s, ^{F}Mes-C-*C*F_3), 131.7 (s, ^{F}Mes-C-*C*F_3), 126.8 (d, *J* = 6.1 Hz, ^{F}Mes-*C*-CF_3), 125.5 (d, *J* = 6.1 Hz, ^{F}Mes-*C*H), 123.7 (d, *J* = 5.0 Hz, ^{F}Mes-*C*-CF_3), 123.1 (t, *J* = 4.5 Hz, ^{F}Mes-*C*-CF_3), 1.4-(-1.42) (q, Thi-

C-Si(*C*H)$_3$, 0.5 (s), -0.5 (s), -1.42 (s).; ^{19}F NMR (471 MHz, $CDCl_3$): δ = -56.2 (s), -63.0 (s); ^{29}Si NMR (99 MHz, $CDCl_3$): δ = -5.7 (s); HR-MS (APCI): m/z = 602.0794; calcd. for $C_{23}H_{24}BF_9S_2Si_2$: 602.0807.

Synthesis of 4c. To a solution of **3c** (7.32 g, 12.14 mmol) in dichloromethane (20 mL) was added BBr_3 (8.51 g, 33.99 mmol) dropwise at 0°C. The solution was stirred for 2 h without maintaining the temperature. After removal of all volatiles in vacuo, the yellow residue was washed with dichloromethane (2x 20 mL) and the solvent was removed in vacuo to yield **4c** as a grey solid.

Yield: 8.403 g (10.5 mmol, 86%); ^{1}H NMR (400 MHz, $CDCl_3$): δ = 8.20 (s, 2H, ^{F}Mes-*H*), 8.13 (d, *J* = 3.8 Hz, 2H, Thi-*H*), 7.79 (d, *J* = 3.8 Hz, 2H, Thi-*H*); ^{11}B NMR (128 MHz, $CDCl_3$): δ = 49.9 (s); ^{19}F NMR (377 MHz, $CDCl_3$): δ = -55.8 (s), -63.2 (s).

Synthesis of 5c. A solution of **4c** (6.08 g, 7.62 mmol) in toluene (50 mL) was added dropwise to a freshly prepared suspension of ^{F}MesLi[13] (starting from 6.879 g, 24.4 mmol ^{F}MesH) in toluene (125 mL) at -78 °C. The reaction mixture was stirred overnight. Subsequently, the reaction mixture was filtrated, washed with *n*-pentane (2x 5 mL) and the solvent was removed in vacuo yielding a brown solid. The crude compound was used without further purification.

^{1}H NMR (500 MHz, $CDCl_3$): δ = 8.16 (s, 2H, ^{F}Mes-*H*), 8.15 (s, 4H, ^{F}Mes-*H*), 7.77 (s, 4H, Thi-*H*); ^{11}B NMR (160 MHz, $CDCl_3$): δ = 60.2 (s).

Synthesis of 6c. The above synthesized compound **5c** was dissolved in DCM (40 mL). Me_3Si-OMe (1.512 g, 14.5 mmol) was added at ambient temperatures and after stirring for 30 minutes, all volatiles were removed in vacuo. The resulting solid was redissolved in a mixture of dichloromethane (3 mL) and methanol (9 mL). After 48h, colorless crystals suitable for X-ray analysis were obtained. Filtration afforded **6c** as colorless solid.

Yield: 2.17 g (1.97 mmol, 25%); ^{1}H NMR (500 MHz, $CDCl_3$): δ = 8.16 (s, 4H, ^{F}Mes-*H*), 8.12 (s, 2H, ^{F}Mes-*H*), 7.59 (d, *J* = 3.7 Hz, 2H, Thi-*H*), 7.21 (d, *J* = 3.7 Hz, 2H, Thi-*H*), 3.75 (s, 6H, O-C*H*$_3$); ^{11}B NMR (160 MHz, $CDCl_3$): δ = 41.4 (s, Ar_2B), Ar_3B not detectable; ^{13}C NMR (126 MHz, $CDCl_3$): δ = 150.6 (br. s, Thi-*C*-B), 148.9 (br. s, Thi-*C*-B), 144.5 (br. s, ^{F}Mes-*C*-B), 142.6 (s, Thi-*C*H), 139.2 (s, Thi-*C*H), 138.2 (br. s, ^{F}Mes-*C*-B), 135.0-134.5 (q, ^{F}Mes-C-*C*F_3), 134.7-133.9 (q, ^{F}Mes-C-*C*F_3), 133.2-132.3 (q, ^{F}Mes-C-*C*F_3), 132.2-131.5 (q, ^{F}Mes-C-*C*F_3), 126.2 (br. s, ^{F}Mes-*C*H), 126.0 (br. s, ^{F}Mes-*C*H), 124.5 (q, ^{F}Mes-*C*-CF_3), 124.3 (q, ^{F}Mes-*C*-CF_3), 122.3 (q, ^{F}Mes-*C*-CF_3), 122.1 (q, ^{F}Mes-*C*-CF_3), 56.7 (Thi-C-*C*H_3) ; ^{19}F NMR (471 MHz, $CDCl_3$): δ = -56.3 (s), -59.4 (s), -63.1 (s), -63.3 (s); HR-MS (APCI): m/z = 1102.0374; calcd. for $C_{37}H_{16}B_3F_{27}O_2S_2$: 1102.0440.

Attempted synthesis of 7c. A solution of **2c** (0.2291 g, 0.5 mmol) in Et_2O (3.75 mL) was cooled to -78 °C and then, a solution of *n*-BuLi (1.05 mmol, 0.66 mL) was added dropwise and

the resulting suspension was stirred for 1 h at this temperature and for 2 h at ambient temperature. Subsequently, Et_2O (12.5 mL) was cooled to -78 °C and added to the lithiated species at -78 °C followed by the addition of a cold (-78 °C) solution of **6b** (0.551 g, 0.5 mmol) in Et_2O (5.0 mL). The reaction mixture was allowed to slowly warm up to ambient temperature. After quenching with water and aqueous work-up, no evidence for the successful formation of **7c** was obtained via ^{1}H-NMR spectroscopy or HR-MS. The same is true when THF is used instead of Et_2O, when longer reaction times are used, with TMEDA as deaggregation agent to increase the reactivity of the lithiated species or when elaborate temperatures (40 °C, 70 °C) are used.

Synthesis of 8b. A solution of 2,5-bis(trimethylsilyl)thiophene (2.49 g, 10.8 mmol) was added to a solution of 2-bromothiophene (2.73 g, 10.8 mmol) in DCM (5 mL). Then, Me_3Si-NTf_2 (0.200 g, 0.53 mmol, 5 mol%) was added and the reaction mixture was stirred overnight. After removal of all volatiles in vacuo, the resulting solid was redissolved in toluene (15 mL) and added to a solution of freshly prepared ^{F}MesLi (3.42 g, 11.9 mmol) in toluene (15 mL). The reaction mixture was stirred overnight and quenched by the addition of water. After aqueous work-up, the crude compound was further purified by column chromatography (silica: PE) to afford **8b** as colorless viscous liquid.

Yield: 3.38 g (6.91 mmol, 64%). ^{1}H-NMR (300 MHz, $CDCl_3$): δ = 8.16 (s, 2H, ^{F}Mes-*H*), 7.97 (d, $^3J_{HH}$ = 4.7, 1H, Thi-*H*), 7.60 (dd, $^3J_{HH}$ = 3.7 Hz, $^4J_{HH}$ = 0.8 Hz, 1H, Thi-*H*), 7.58 (d, $^3J_{HH}$ = 3.5, 1H, Thi-*H*), 7.38 (d, $^3J_{HH}$ = 3.5, 1H, Thi-*H*), 7.28 (dd, $^3J_{HH}$ = 4.6 Hz, $^3J_{HH}$ = 3.6 Hz, 1H, Thi-*H*), 0.38 (s, 9H, -Si(CH_3)$_3$) ppm. ^{11}B{^{1}H}-NMR (96 MHz, $CDCl_3$): δ = 51.5 ppm.

Synthesis of 9b. To a solution of **8b** (0.121 g, 0.23 mmol) in toluene (0.5 mL) was added BBr_3 (0.063 g, 0.252 mmol) dropwise at – 78 °C. The reaction mixture was allowed to warm up to ambient temperature overnight. Then, all volatiles were removed in vacuo, affording **9b** as brownish oil. The compound was used without further purification.

^{1}H-NMR (300 MHz, $CDCl_3$): δ = 8.18 (s, 2H, ^{F}Mes-*H*), 8.09 (m, 2H, Thi-*H*), 7.71 – 7.66 (m, 2H, Thi-*H*) 7.33 (dd, $^3J_{HH}$ = 4.7 Hz, $^3J_{HH}$ = 3.7 Hz, 1H, Thi-*H*) ppm. ^{11}B{^{1}H}-NMR (96 MHz, $CDCl_3$): δ = 49.8 ppm.

Synthesis of 10b. A solution of **9b** (starting from 1.06 g, 2.0 mmol **8b**) in toluene (2 mL) was added to a freshly prepared solution of ^{F}MesLi (0.720 g, 2.50 mmol) in toluene (4 mL) at ambient temperatures. The resulting yellow suspension was stirred overnight and subsequent filtration and removal of all volatiles in vacuo afforded an orange oil as crude **10b** which was confirmed by ^{11}B NMR spectroscopy. Compound **10b** was used without further purification.

^{11}B{^{1}H}-NMR (96 MHz, $CDCl_3$): δ = 52.7 (br).

Synthesis of 11b. Crude compound **10b** was dissolved in DCM (4 mL) and Me_3Si-OMe (0.417 g, 4.0 mmol) was added at ambient temperatures. The reaction mixture was stirred overnight and then, all volatiles were removed in vacuo. The resulting yellow-brownish oil was attempted to crystallize in a mixture of DCM/methanol, which led to a slightly purified compound.

^{1}H NMR (300 MHz, $CDCl_3$): δ = 8.17 (s, 2H, ^{F}Mes-*H*), 8.14 (s, 2H, ^{F}Mes-*H*), 7.99 (d, *J* = 4.6 Hz, 1H, Thi-*H*), 7.62 (dd, ^3J = 3.6, ^4J = 0.9 Hz, 1H, Thi-*H*), 7.56 (d, *J* = 3.6 Hz, 1H, Thi-*H*), 7.28 (dd, ^3J = 4.6, 3.7 Hz, 1H, Thi-*H*), 7.22 (d, *J* = 3.6 Hz, 1H, Thi-*H*), 3.76 (s, 3H, -OCH_3); ^{11}B NMR (96 MHz, $CDCl_3$): δ = 51.9 (s, Ar_3B), 42.6 (s, Ar_2B-OMe).

Synthesis of 22 via 12b. To a solution of **8b** (0.133 g, 0.25 mmol) in Et_2O (2.5 mL) was added *n*-BuLi in hexane (0.263 mmol, 0.164 mL) at -78 °C. The reaction mixture was stirred for 1 h at this temperature and for another 2 h at ambient temperature. Then, a solution of Me_3Sn-Cl in THF (0.25 mmol, 0.25 mL) was added dropwise at -78 °C. The reaction mixture was allowed to warm up to ambient temperature overnight and was quenched by adding a NaClO solution. After aqueous work-up, all volatiles were removed in vacuo affording a viscous orange oil. Purification via crystallization or column chromatography (cleavage of Me_3Sn groups) was not successful so far.

Yield: 0.111 g (0.16 mmol, 62%). ^{1}H NMR (300 MHz, $CDCl_3$): δ = 8.16 (s, 2H, ^{F}Mes-*H*), 7.65 (d, *J* = 3.4 Hz, 1H, Thi-*H*), 7.60 (d, *J* = 3.5 Hz, 1H, Thi-*H*), 7.37 (dd, *J* = 4.3, 3.5 Hz, 2H, Thi-*H*), 0.44 (s, 9H, -Sn(CH_3)$_3$), 0.38 (s, 9H, -Si(CH_3)$_3$); ^{11}B NMR (96 MHz, $CDCl_3$): δ = 54.6 (s).

Attempted synthesis of 13b. To a solution of **8b** (0.530 g, 1.0 mmol) in Et_2O (2.0 mL) was added *n*-BuLi (1.05 mmol, 0.66 mL) dropwise at -78 °C. The reaction mixture was stirred for 1 h at this temperature and additional 3 h at ambient temperatures. Subsequently, a solution of **11b** (0.780 g, 1.0 mmol) in Et_2O (2 mL) was cooled to -78 °C and added to the reaction mixture at -78 °C. After stirring overnight, the reaction mixture was quenched by the addition of water and pentane. Aqueous work-up followed by removal of all volatiles in vacuo and purification by column chromatography led to the recovery of compound **8b** as major product.

Synthesis of 29a. To a solution of BCl_3 (1M, 52 mmol) in DCM (52 mL) was added bis(trimethylsilyl)dithienylmethane (**28**) (8.35 g, 25.80 mmol) dropwise at 0 °C. The resulting reaction mixture was stirred for 2 h in the ice bath without maintaining the temperature. After removal of all volatiles in vacuo the reddish residue was further purified by recrystallization from pentane/toluene (2:1) to yield **29a** as slightly pink-colored needles.

Yield: 8.7 g (25.60 mmol, quantitative); ^{1}H NMR (400 MHz, $CDCl_3$): δ = 7.88 (d, *J* = 3.7 Hz, 2H, Thi-*H*), 7.13 – 7.08 (m, 2H, Thi-*H*), 4.49 (s, 2H, -CH_2); ^{11}B NMR (128 MHz, $CDCl_3$): δ = 48.4 (s); ^{13}C NMR (101 MHz, $CDCl_3$): δ = 157.3 (s, Thi-*C*), 143.7 (s, Thi-*C*H), 138.8 (br. s, Thi-*C*-B),

129.2 (s, Thi-*C*H), 31.4 (s, -*C*H_2); HR-MS (LIDFI): m/z = 339.8851; calcd. for $C_9H_6B_2Cl_4S_2$: 341.8806.

Synthesis of 29b. To a solution of BBr_3 (9.154 g, 36.54 mmol) in DCM (40 mL) was added bis(trimethylsilyl)dithienylmethane **28** (5.648 g, 17.40 mmol) dropwise at 0 °C. The resulting orange solution was stirred for 2 h in the ice bath without maintaining the temperature. After removal of all volatile compounds the reddish residue is further purified by recrystallization from pentane DCM (6:1) to yield **29b** as a slightly purple colored solid. The obtained analytical data are in good accordance with the data obtained and described in chapter 2.5.

Synthesis of 30a. To a solution of **29a** (1.311 g, 3.8 mmol) in toluene (6 mL) was added a solution of TipLi (1.758 g, 8.36 mmol) in toluene (8 mL) dropwise at -78 °C. The reaction mixture was slowly allowed to warm up to ambient temperatures and stirred overnight. Then, the suspension was filtrated and washed twice with pentane (2x 10 mL). All volatiles were removed in vacuo affording a reddish solid.

Yield: 2.447 g (3.62 mmol, 95 %). ^{1}H NMR (300 MHz, $CDCl_3$): δ = 7.70 (d, *J* = 3.6 Hz, 2H, Thi-*H*), 7.08 (d, *J* = 3.7 Hz, 2H, Thi-*H*), 7.01 (s, 4H, Tip-*H*), 4.49 (s, 2H, -CH_2), 3.01 – 2.85 (m, 2H, *p*-^{i}Pr-C*H*), 2.63 (dq, *J* = 13.4, 6.7 Hz, 4H, *o*-^{i}Pr-C*H*), 1.30 (d, *J* = 6.9 Hz, 12H, *p*-^{i}Pr-CH_3), 1.25 (d, *J* = 6.7 Hz, 12H, *o*-^{i}Pr-CH_3), 1.14 (d, *J* = 6.7 Hz, 12H, *o*-^{i}Pr-CH_3); ^{11}B NMR (96 MHz, $CDCl_3$): δ = 61.5 (s); ^{13}C NMR (75 MHz, $CDCl_3$): δ = 156.7 (s, Thi-*C*-CH_2), 150.0 (s, Tip-*C*-*o*-^{i}Pr), 149.6 (s, Tip-*C*-*p*-^{i}Pr), 143.6 (br. s, Thi-*C*-B), 142.9 (s, Thi-*C*H), 135.3 (br. s, Tip-*C*-B), 128.8 (s, Thi-*C*H), 120.4 (s, Tip-*C*H), 35.5 (s, *o*-^{i}Pr-*C*H), 34.4 (s, *p*-^{i}Pr-*C*H), 31.6 (s, -*C*H_2), 24.7 (s, *o*-^{i}Pr-*C*H_3), 24.0 (d, *J* = 4.6 Hz, *o*+*p*-^{i}Pr-*C*H_3).

Synthesis of 30b. 29b (6.970 g, 13.42 mmol) was suspended in pentane (135 mL) and cooled down to -78 °C. TipLi (5.785 g, 27.51 mmol) was dissolved in a mixture of pentane/toluene (65/65 mL) and added dropwise to the stirring suspension. The reaction mixture was stirred overnight. After complete reaction time, filtration and washing with toluene (2x 30 mL) afforded a yellow liquid. A highly viscous oil was obtained after removal of all volatiles in vacuo. The residue was purified by repeated solvation in pentane and subsequent removal of the solvent to yield the title compound as a yellow to orange solid.

Yield: 4.370 g (5.70 mmol, 71 %); ^{1}H NMR (400 MHz, $CDCl_3$): δ = 7.73 (d, *J* = 3.2 Hz, 2H, Thi-*H*), 7.10 (d, *J* = 3.7 Hz, 2H, Thi-*H*), 6.98 (s, 4H, Tip-*H*), 4.44 (s, 2H, -CH_2), 2.96 – 2.86 (m, 2H, *p*-^{i}Pr-C*H*), 2.63 (hept, *J* = 6.8 Hz, 4H, *o*-^{i}Pr-C*H*), 1.28 (d, *J* = 6.9 Hz, 12H, *p*-^{i}Pr-CH_3), 1.23 (d, *J* = 6.7 Hz, 12H, *o*-^{i}Pr-CH_3), 1.11 (d, *J* = 6.7 Hz, 12H, *o*-^{i}Pr-CH_3); ^{11}B NMR (128 MHz, $CDCl_3$) δ 62.8 (s).

Synthesis of 31a. A solution of **30b** (1.533 g, 2.0 mmol) in DCM (8 mL) was added dropwise to a suspension of sodium methoxide (0.119 g, 2.2 mmol) in DCM (8 mL) at -78 °C. The mixture

was stirred overnight. Afterwards, the resulting mixture was filtrated and washed two times with toluene (2x4 mL). A highly viscous yellow solid was obtained after removal of the solvent in vacuo (ca. 10^{-2} mbar). The residue was purified by repeated washing with methanol followed by filtration to remove TipH. The reaction can also be performed with Me_3Si-OMe which lead to significantly higher yields (approx. 95%) and more facile work-up conditions (cf. synthesis of **31b**)

Yield: 2.460 g (3.68 mmol, 46 %); ^{1}H NMR (500 MHz, $CDCl_3$): δ = 7.16 (d, *J* = 3.5 Hz, 2H, Thi-*H*), 6.99 (s, 4H, Tip-*H*), 6.88 (d, *J* = 3.5 Hz, 2H, Thi-*H*), 4.40 (s, 2H, -C*H*$_2$), 3.72 (s, 6H, -OC*H*$_3$), 2.96 – 2.86 (m, 2H, *p*-^{i}Pr-C*H*), 2.66 – 2.57 (m, 4H, *o*-^{i}Pr-C*H*), 1.29 (d, *J* = 6.9 Hz, 12H, *p*-^{i}Pr-C*H*$_3$), 1.22 (s, 12H, *o*-^{i}Pr-C*H*$_3$), 1.08 (d, *J* = 6.7 Hz, 12H, *o*-^{i}Pr-C*H*$_3$); ^{11}B NMR (160 MHz, $CDCl_3$): δ = 44.5 (s); ^{13}C NMR (126 MHz, $CDCl_3$): δ = 151.0 (s, Thi-*C*-CH$_2$), 150.4 (s, Tip-*C*-*o*-^{i}Pr), 149.4 (s, Tip-*C*-*p*-^{i}Pr), 141.1 (br. s, Thi-*C*-B), 139.4 (s, Thi-*C*H), 132.8 (br. s, Tip-*C*-B), 127.3 (s, Thi-*C*H), 120.3 (s, Tip-*C*H), 55.9 (s, Thi-C-*C*H$_3$), 35.2 (s, *o*-^{i}Pr-*C*H), 34.4 (s, *p*-^{i}Pr-*C*H), 31.3 (s, -*C*H$_2$), 24.8 (d, *J* = 16.4 Hz, *o*-^{i}Pr-*C*H$_3$), 24.2 (s, *p*-^{i}Pr-*C*H$_3$); HR-MS (LIDFI): m/z = 668.4056; calcd. for $C_{41}H_{58}B_2O_2S_2$: 668.4064.

Synthesis of 31b. 30a (1.136 g, 1.44 mmol) was dissolved in DCM (2.0 mL) and Me_3Si-OCH_2CF_3 (1.221 g, 4.22 mmol) was added in one portion at ambient temperature. The reaction mixture was stirred for 2 days. Afterwards, all volatiles were removed in vacuo and redissolved in pentane and precipitated at -40 °C. After filtration and washing with pentane (2x 5 mL), all volatiles were removed in vacuo. A slightly pink colored viscous solid was obtained.

Yield: 1.16 g (1.44 mmol, 86 %). ^{1}H NMR (300 MHz, $CDCl_3$): δ = 7.33 (d, *J* = 3.5 Hz, 2H), 7.03 (d, *J* = 4.9 Hz, 4H), 6.95 (d, *J* = 3.5 Hz, 2H), 4.44 (s, 1H), 4.23 (q, *J* = 8.5 Hz, 4H), 2.94 (dt, *J* = 13.8, 6.9 Hz, 2H), 2.59 (dt, *J* = 13.4, 6.7 Hz, 4H), 1.31 (d, *J* = 6.9 Hz, 12H), 1.24 (d, *J* = 6.8 Hz, 12H), 1.10 (d, *J* = 6.6 Hz, 12H); ^{11}B NMR (96 MHz, $CDCl_3$): δ = 46.4 (s); ^{13}C NMR (75 MHz, $CDCl_3$): δ = 152.4 (s, Thi-*C*-CH$_2$), 150.7 (s, Tip-*C*-*o*-^{i}Pr), 150.3 (s, Tip-*C*-*p*-^{i}Pr), 140.5 (s, Thi-*C*H), 139.7 (br. s, Thi-*C*-B), 131.0 (br. s, Tip-*C*-B), 127.5 (s, Thi-*C*H), 120.7 (s, Tip-*C*H), 65.6 (q, -O*C*H$_2$CF$_3$), 35.4 (s, *o*-^{i}Pr-*C*H), 34.5 (s, *p*-^{i}Pr-*C*H), 31.3 (s, -*C*H$_2$), 25.1 (s, *o*-^{i}Pr-*C*H$_3$), 24.5 (s, *o*-^{i}Pr-*C*H$_3$), 24.1 (s, *p*-^{i}Pr-*C*H$_3$); ^{19}F NMR (377 MHz, $CDCl_3$): δ = -75.30 (s); HR-MS (LIDFI): m/z = 804.3801; calcd. for $C_{43}H5_6B_2F_6O_2S_2$: 804.3812.

X-Ray structural analysis

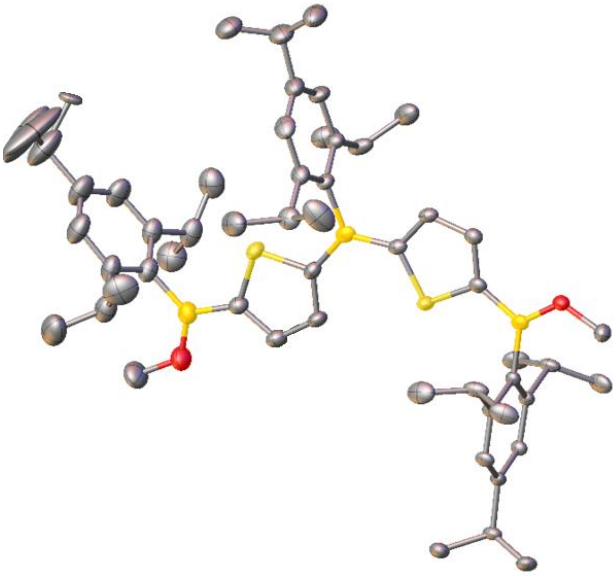

Figure 2.7.13. Molecular structure of **6b** in the solid state (H atoms omitted for clarity).

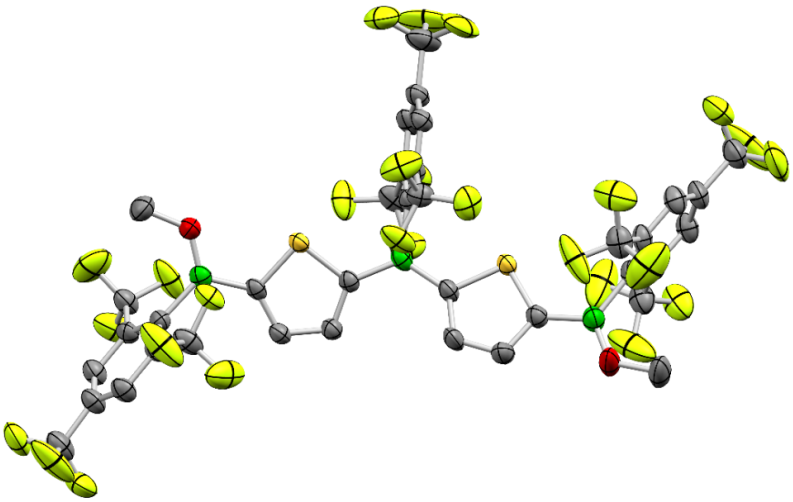

Figure 2.7.14. Molecular structure of **6c** in the solid state (H atoms omitted for clarity).

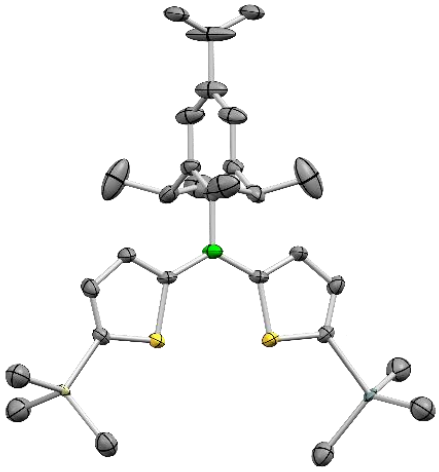

Figure 2.7.15. Molecular structure of **15a** in the solid state (H atoms omitted for clarity).

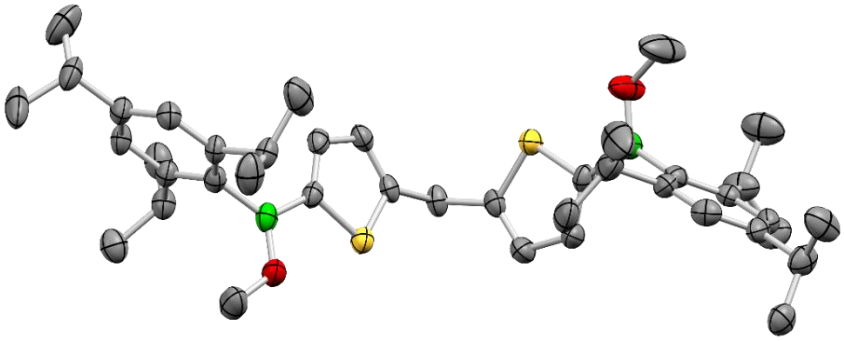

Figure 2.7.16. Molecular structure of **31a** in the solid state (H-atoms omitted for clarity).

Table 2.7.1. Crystal structure and refinement data for **6c** and **15a**.

No.	**6c**	**15a**
Size / mm	0.19 x 0.13 x 0.07	
Empiric Formula	C37 H16 B3 F27 O2 S2	C28.93 H44.90 B S2 Si Sn
M	1102.05	614.48
Crystal system	triclinic	orthorhombic
Space group	P -1	P b c n
a/Å	8.1784(4)	10.639(8)
b/Å	15.3133(7)	15.666(7)
c/Å	17.3813(9)	18.720(7)
α/°	94.522(2)	90
β/°	94.934(2)	90
γ/°	101.974(2)	90
V/Å^3	2111.08(18)	3120(3)
Z	2	4
μ/mm^{-1}	0.282	1.007
T/K	100	100
$\theta_{min,max}$	2.36, 26.02	2.176, 26.737
Completeness	99.9	99.8
Reflections: total/independent	8312, 6149	3306, 3180
R_{int}	0.0646	0.0543
Final R1 and wR2	0.0520, 0.1363	0.0732, 0.1830
Largest peak, hole/eÅ^{-3}	0.867, -0.580	0.558, -1.407
ρ_{calc}/g cm^{-3}	1.734	1.308

Table 2.7.2. Crystal structure and refinement data for **31a**.

No.	**31a**
Size / mm	0.39 x 0.36 x 0.22
Empiric Formula	C41 H58 B2 O2 S2
M	668.61
Crystal system	monoclinic
Space group	P 1 21/c 1
a/Å	9.5661(5)
b/Å	17.7525(10)
c/Å	23.5420(11)
α/°	90
β/°	100.204(3)
γ/°	90
V/Å^3	3934.7(4)
Z	4
μ/mm^{-1}	0.168
T/K	100
$\theta_{min,max}$	1.758, 27.169
Completeness	98.2
Reflections: total/independent	8589, 5372
R_{int}	0.1218
Final R1 and wR2	0.0630, 0.1719
Largest peak, hole/eÅ^{-3}	0.537, -0.383
ρ_{calc}/g cm^{-3}	1.129

2.7.4. References

[1] a) M. V. Martinez-Diaz, G. de la Torre, T. Torres, *Chem. Commun.* **2010**, *46*, 7090-7108; b) G. Bottari, G. de la Torre, D. M. Guldi, T. Torres, *Chem. Rev.* **2010**, *110*, 6768-6816; c) E. Sitte, M. O. Senge, *Eur. J. Org. Chem.* **2020**, 3171-3191.

[2] Y.-J. Cheng, S.-H. Yang, C.-S. Hu, *Chem. Rev.* **2009**, *109*, 5868-5923.

[3] For examples for thiophene-based macrocycles see: a) M. Iyoda, H. Shimizu, *Chem. Soc. Rev.* **2015**, *44*, 6411-6424; b) M. Iyoda, J. Yamakawa, M. J. Rahman, *Angew. Chem. Int. Ed.* **2011**, *50*, 10522-10553; *Angew. Chem.* **2011**, *123*, 10708-10740; c) A. Mishra, C.-Q. Ma, P. Bäuerle, *Chem. Rev.* **2009**, *109*, 1141-1276.

[4] a) A. M. Priegert, B. W. Raw, S. C. Serin, D. P. Gates, *Chem. Soc. Rev.* **2016**, *45*, 922; b) X. He, T. Baumgartner, *RSC Adv.*, **2013**, *3*, 11334-11350; c) F. Vidal, F. Jäkle, *Angew. Chem. Int. Ed.* **2019**, *58*, 5846-5870; *Angew. Chem.* **2019**, *131*, 5904-5929; d) T. Baumgartner, F. Jäkle, *Main Group Strategies towards Functional Hybrid Materials*, Wiley, Chichester, **2018**.

[5] a) C. D. Entwistle, T. B. Marder, *Angew. Chem. Int. Ed.* **2002**, *41*, 2927-2931; *Angew. Chem.* **2002**, *114*, 3051-3056; b) C. D. Entwistle, T. B. Marder, *Chem. Mater.* **2004**, *16*, 4574-4585; c) N. Matsumi, Y. Chujo, *Polym. J.* **2008**, *40*, 77-89; d) M. J. D. Bosdet, W. E. Piers, *Can. J. Chem.* **2009**, *87*, 8-29; e) A. Wakamiya, S. Yamaguchi, *Bull. Chem. Soc. Jpn.* **2015**, *88*, 1357-1377; f) A. Lorbach, A. Hübner, M. Wagner, *Dalton Trans.* **2012**, *41*, 6048-6063; g) S. Mukherjee, P. Thilagar, *J. Mater. Chem. C*, **2016**, *4*, 2647-2662; h) Y.-L. Rao, H. Amarne, S. Wang, *Coord. Chem. Rev.* **2012**, *256*, 759-770; i) L. Ji, S. Griesbeck, T. B. Marder, *Chem. Sci.* **2017**, *8*, 846 863; j) S.-Y. Li, Z.-B. Sun, C.-H. Zhao, *Inorg. Chem.* **2017**, *56*, 8705-8717; k) E. von Grotthuss, A. John, T. Kaese, M. Wagner, *Asian J. Org. Chem.* **2018**, *7*, 37-53; l) Z. M. Hudson, S. Wang, *Acc. Chem. Res.* **2009**, *42*, 1584-1596; m) A. G. Crawford, A. D. Dwyer, Z. Liu, A. Steffen, A. Beeby, L.-O. Palsson, D. J. Tozer, T. B. Marder, *J. Am. Chem. Soc.* **2011**, *133*, 13349-13362; n) H. Helten, *Chem. Asian J.* **2019**, *14*, 919-935 ; o) F. Jäkle, *Chem. Rev.* **2010**, *110*, 3985-4022; p) Z. M. Hudson, S. Wang, *Dalton Trans.* **2011**, *40*, 7805-7816; q) Z. Huang, S. Wang, R. D. Dewhurst, N. V. Ignat'ev, M. Finze, H. Braunschweig, *Angew. Chem. Int. Ed.* **2020**, *59*, 8800-8818; *Angew. Chem.* **2020**, *132*, 8882-8900.

[6] a) X. Yin, J. Liu, F. Jäkle, *Chem. Eur. J.* **2020**, *26*, 1-15: DOI: 10.1002/chem.202003481; b) P. Chen, F. Jäkle, *J. Am. Chem. Soc.* **2011**, *133*, 20142-20145; c) N. Baser-Kirazli, R. A. Lalancette, F. Jäkle, *Angew. Chem. Int. Ed.* **2020**, *59*, 8689-8697; *Angew. Chem.* **2020**, *132*, 8767-8775; d) P. Chen, R. A. Lalancette, F. Jäkle, *Angew. Chem. Int. Ed.* **2012**, *51*, 7994-7998; *Angew. Chem.* **2012**, *124*, 8118-8122; e) P. Chen, X. Yin, N. Baser-Kirazli, F. Jäkle, *Angew. Chem. Int. Ed.* **2015**, *54*, 10768-10772; *Angew. Chem.* **2015**, *127*, 10918-10922.

[7] a) F. H. Carré, R. J.-P- Corriu, T. Deforth, W. E. Douglas, W. S. Siebert, W. Weinmann, *Angew. Chem. Int. Ed.* **1998**, *37*, 652-654; *Angew. Chem.* **1998**, *110*, 654-656; b) T. Köhler, J. Faderl, H. Pritzkow, W. Siebert, *Eur. J. Inorg. Chem.* **2002**, 2942-2946; c) A. Eckert, H. Pritzkow, W. Siebert, *Eur. J. Inorg. Chem.* **2002**, 2064-2068.

[8] M. O. Senge, *Angew. Chem. Int. Ed.* **1998**, *37*, 1071-1072.

[9] A. Lik Dissertation: Thienyl- and Furylborane Oligomers, Polymers, and Macrocycles – Development of a Catalytic Si/B Exchange Reaction As a Novel B-C Bond Formation Method (2017).

[10] a) A. Lik, L. Fritze, L. Müller, H. Helten, *J. Am. Chem. Soc.* **2017**, *139*, 5692-5695; b) A. Lik, S. Jenthra, L. Fritze, L. Müller, K.-N. Truong, H. Helten, *Chem. – Eur. J.* **2018**, *24*, 11961-11972.

[11] R. Giovanetti, The Use of Spectrophotometry UV-Vis for the Study of Porphyrins. *Macro Nano Spectrosc.* **2012**, 1, 87-108, DOI: 10.5772/38797.

[12] A. Vij, Y. Y. Zheng, R. L. Kirchmeier, J. M. Shreeve, *Inorg. Chem*. **1994**, *33*, 3281-3288.

[13] X. Yin, J. Chen, R. A. Lalancette, T. B. Marder, F. Jäkle, *Angew. Chem. Int. Ed.* **2014**, *53*, 9761-9765.

[14] P. Chen, F. Jäkle, *J. Am. Chem. Soc.* **2011**, *133*, 20142-20145 and references therein.

[15] K. Ruhlandt-Senge, J. J. Ellison, R. J. Wehmschulte, F. Pauer, P. P. Power, *J. Am. Chem. Soc.* **1993**, *115*, 11353–11357.

[16] B. Mathieu, L. Ghosez, Tetrahedron **2002**, *58*, 8219–8226.

[17] Z. Hu, J. L. Atwood, M. P. Cava, *J. Org. Chem.* **1994**, *59*, 8071-8075.

[18] G. M. Sheldrick, *Acta Crystallogr. A* **2015**, *71*, 3-8.

[19] Sheldrick, *Acta Crystallogr. A* **2008**, *64*, 112-122.

[20] C. B. Hubschle, G. M. Sheldrick, B. Dittrich, *J. Appl. Crystallogr.* **2011**, *44*, 1281-1284.

[21] O. V. Dolomanov, L. J. Bourhis, R. J. Gildea, J. A. K. Howard, H. Puschmann, *J. Appl. Crystallogr.* **2009**, *42*, 339-341.

3. Conclusion

This work has demonstrated the potential of Si/B exchange reactions as a facile and highly effective B-C bond formation method for the synthesis of organoboron molecules, oligomers, polymers and macrocycles. This approach made it possible to synthesize a variety of novel inorganic-organic hybrid materials with special features and fascinating properties.

In the first chapter, it is described that silicon/boron exchange precipitation condensation in acetonitrile gave access to borazine-based hybrid cyclomatrix polymeric microspheres **3c** (Figure 3.1, left: ***Route B***). In comparison to common precipitation polycondensation conditions proceeding via salt elimination (Figure 3.1, left: ***Route A***), microspheres with a smoother surface and significantly larger mean diameters were obtained (Figure 3.1, top: 905 ± 105 nm vs 183 ± 20 nm). Potential reasons for this effect might be occurring slower nucleation kinetics and fewer numbers of nucleation events induced by the enlarged solubility of the trimethylsilyl group-carrying monomer and the growing oligomers in the reaction medium. The successful synthesis of the cyclomatrix polymers was confirmed by FT-IR spectroscopy and solid-state NMR spectroscopy (Figure 3.1, bottom right: ^{13}C and ^{11}B CPMAS). Thermogravimetric analysis indicated remarkable thermal stability with a residual mass at 880 °C under N_2 atmosphere up to 56%, which makes the obtained cyclomatrix polymers potential precursors for flame retardant additives.

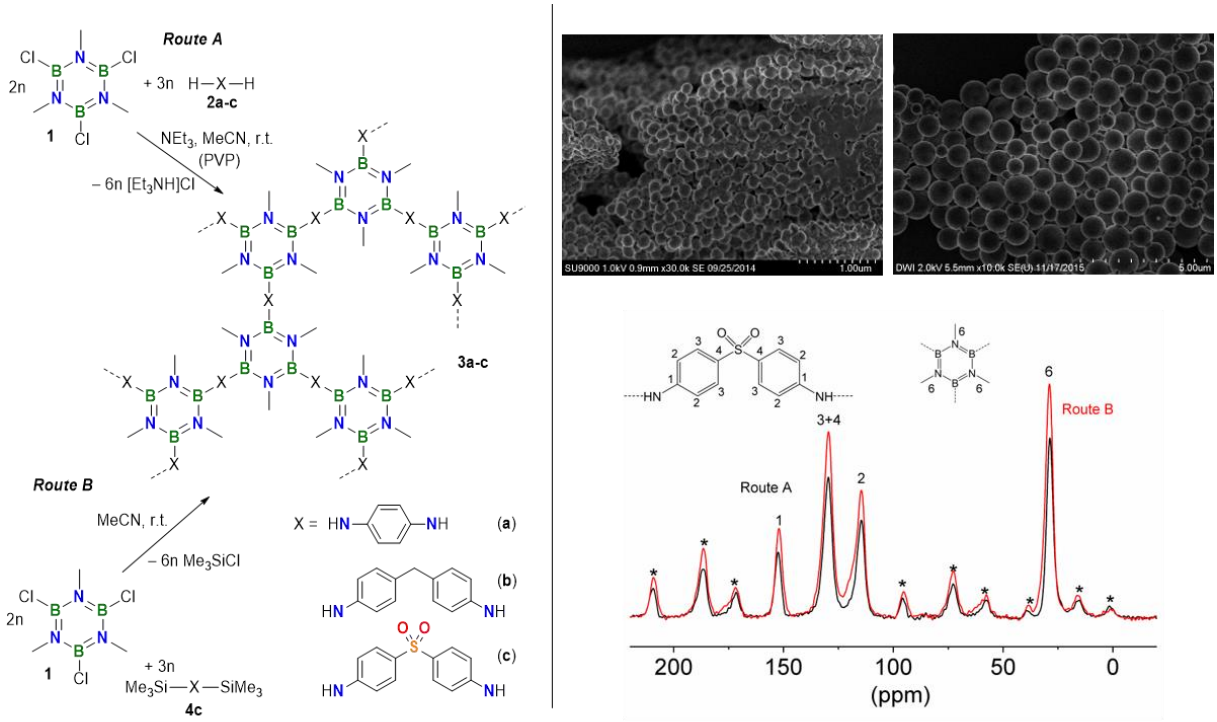

Figure 3.1. Left: Synthesis of cyclomatrix polymers **3a-c** via salt elimination (***Route A***) and synthesis of **3c** via Si/B exchange polycondensation (***Route B***). Top right: FESEM micrographs of **3c** via ***Route A*** (left) and via ***Route B*** (right). Bottom right: ^{13}C CPMAS spectra of **3c** via ***Route A*** and ***B*** respectively.

In chapter 2.2-2.4, different synthetic strategies were investigated that provide access to novel organoborane molecules featuring furylborane units in the main chain. In chapter 2.2, the use of Suzuki-Miyaura cross-coupling for the reaction between dibrominated or diiodinated difuryl(supermesityl)borane (**5**) and the respective coupling partner **6** afforded π-extended organoboranes **7** (Figure 3.2, top). In chapter 2.3 and 2.4, it was demonstrated that catalytic Si/B exchange is a highly efficient and flexible method to obtain extended organoboranes **13-15** via reaction of disilylated compounds **8a-10a** or diborylated compound **8b** with the respective coupling reagent **11** or **12** (Figure 3.2, center). Furthermore, in chapter 2.4, salt metathesis reactions between compound **16** and lithiated species **17a,b** are described (Figure 3.2, bottom).

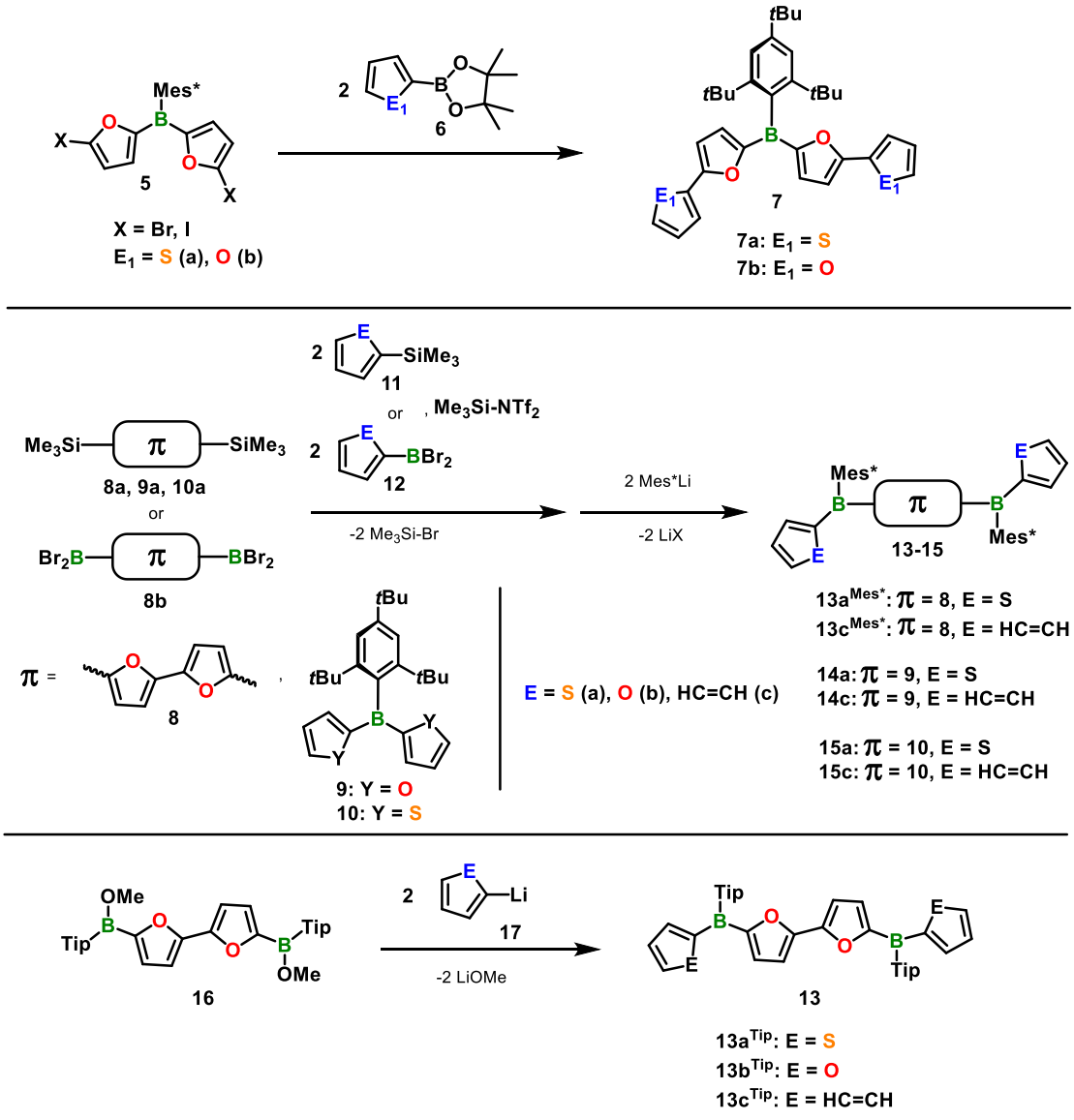

Figure 3.2. Synthetic routes to extended π-conjugated organoboranes. Top: Suzuki-Miyaura cross.coupling reaction to afford organoboranes **7**. Center: Catalytic Si/B exchange reaction to afford Tip- and Mes*-substituted bifuran-bridged bisboranes **13** and tris(het)arylboranes **14,15.** Bottom: Salt elimination reaction to afford bifuran-bridged bisboranes **13^{Tip}**.

The investigations have shown that the use of the salt elimination reaction pathway is limited to Tip-substituted compounds, while the Si/B exchange reaction pathway offers the possibility to both introduce Tip or Mes* as sterically demanding substituents. The focus was on the synthesis of different triarylboranes **7** and **13-15** being composed of four conjugated arene rings and 1,2 or 3 boron centers, respectively. Furthermore, kinetically stabilized furylboranes were established as highly robust and versatile building blocks for π-conjugated materials, leading to enhanced luminescence properties in comparison to the more frequently used thienylboranes. By increasing the amount of boron atoms, varying the linking unit in these systems, and choosing different (het)arenes, facile tuning of the electronic and acceptor properties was possible. Thiophene, furan and benzene units as terminal substituents were successfully incorporated. The obtained compounds can be regarded as π-extended organoboranes **7**, bifuran-bridged bisboranes **13** and tris(het)arylboranes **14**, **15** (Figure 3.3, top). The obtained organoboranes were perfectly air- and moisture stable. X-ray analysis of compounds **7a** and **13a**^{Tip} revealed an anti-arrangement of the hetarene rings, as well as largely coplanar structures with the terminal thiophene rings in both cases (Figure 3.3, bottom).

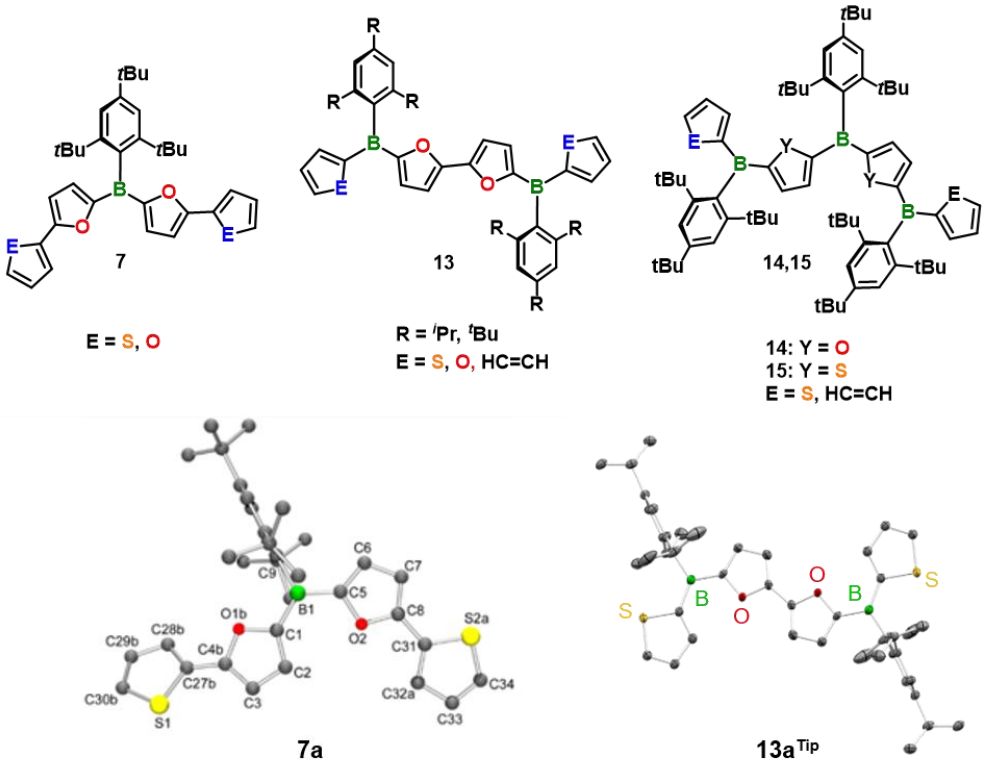

Figure 3.3. Top: Extended π-conjugated organoboranes **7,** bifuran-bridged bisboranes **13** and tris(het)arylboranes **14,15.** Bottom: Molecular structure of thienyl-flanked compounds **7a** and **13a**^{Tip} in the solid state (H-atoms omitted for clarity).

Optical and cyclic voltammetry measurements revealed strong luminescence properties as well as strong electronic communication between the boron centers along the π-conjugated chain. UV-vis and fluorescence spectroscopic analysis of all compounds indicated a

bathochromic shift when compared to kinetically stabilized diarylborane building blocks (Mes*BFur$_2$ or Mes*BThi$_2$) which can be explained by effective extension of the π-system. The wavelength of the absorption maximum increases in the order: phenyl << thienyl < furyl, although there is only a small difference between the latter two. In general, stronger luminescence properties were obtained for furylborane compounds as compared to their direct thienylborane relatives. Highly luminescent compounds **7** and **13** were obtained with quantum yields up to 89 %, which further highlights the effective role of chain extension by a bihetaryl unit. Cyclic voltammetry measurements indicated electrochemically reversible redox events according to the number of boron atoms for **7** and **13**, with the exception that a potential third redox process for compounds **14** and **15** is outside the accessible potential range, which is probably limited by the solvent. With increasing boron content, the electron acceptor properties are enhanced as demonstrated by anodically shifted redox events.

Chapter 2.5 describes the synthesis of a series of dithienylmethane-bridged bisboranes **18** via catalytic Si/B exchange, which are composed of four hetarene rings and two boron atoms as well, but in this case, conjugation between both boron centers is interrupted by the aliphatic linker (Figure 3.4). The redox behaviour was characterized by cyclic and pulse voltammetry in THF. For Mes* substituted compounds, the differential pulse voltammogram indicated two reduction waves with relatively small separations between 70-100 mV (Figure 3.4, right). This clearly points to a low degree of electronic communication between the boron atoms caused by the interruption of the π-system. UV-vis spectroscopy indicated a bathochromic shift when compared to aryldithienylborane building blocks (e.g. 325 nm for ArBTh$_2$ vs. 343 nm for **18a^{Tip}** and 338 nm for **18a^{Mes*}**). This effect can be attributed to the aliphatic methylene bridge. Consistently, the introduction of additional electron pushing methyl or silyl groups (**18d,e^{Tip}**) leads to a further red shift which can be explained by an increase in the HOMO energy, thus reducing the HOMO-LUMO gap.

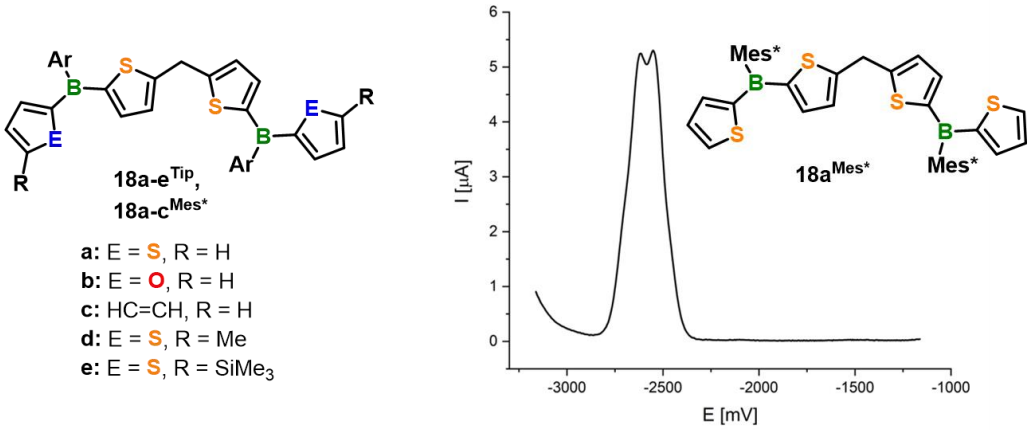

Figure 3.4. Left: Methylene-bridged bisboranes **18** obtained via catalytic Si/B exchange reaction. Right: differential pulse voltammogram for **18a^{Mes*}.**

In chapter 2.6, a catalyst screening was performed to extend the applicability of the Si/B exchange reaction from hetaryl-BBr_2 species to less reactive hetaryl-BCl_2 species as the substrates. For the reaction between Si/B exchange coupling partners **19** and **20**, six different catalysts were employed (Figure 3.5). The investigations have shown that the state-of-the-art catalyst Me_3Si-NTf_2 (cat. **B**, 10 mol%) successfully accelerates the reaction between **19a** and **20a**, but almost complete conversion to **21a** was only observed after 24 hours (vs. 72 minutes for Thi-BBr_2). In the absence of a catalyst, only 5% conversion was observed even after 13 days. For the reaction between **19b** and **20b**, complete conversion was observed within 19 hours, which points to a generally faster reaction, probably due to the more electron-rich system of furan. This trend is also observed for catalysts **A**, **C**-**F**.

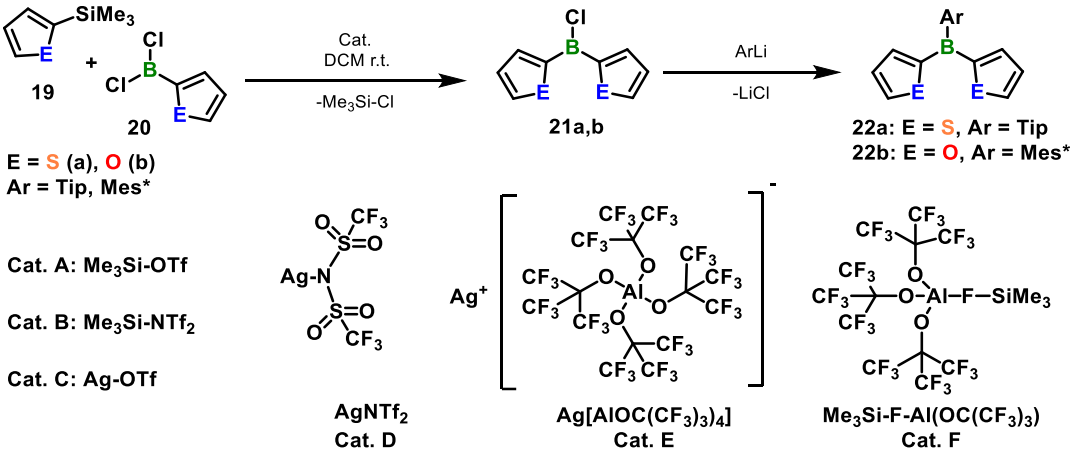

Figure 3.5. General scheme for Si/B exchange of compounds **19** and **20** using different catalysts **A**-**F** and subsequent arylation to afford triarylboranes **22.**

The use of silver-based catalyst **D** (5 mol%) further accelerates the Si/B exchange reaction and complete conversion of the starting materials to afford **21a** was observed within 5 hours. The use of catalysts **E** and **F**, which feature either the silver cation (cat. **E**) or an electrophilic silyl species (cat. **F**) in combination with a weaker coordinating anion leads to an impressive acceleration of the reaction. For both catalysts, complete conversion of the starting materials **19** and **20** was observed within less than 1 hour. Interestingly, it was demonstrated that the reaction with furyl-based starting materials was more selective and no evidence for any C-H activation side reaction was observed as it was the case for thiophene-based systems. In general, catalytic Si/B exchange for furyl-BCl_2 seems to be of particular interest since: a) combinations of boron with furan moieties are only scarcely explored and often only low yields were obtained; b) synthesis and storage of furyl-BCl_2 species is possible which enables a high level of control; c) the Si/B exchange is comparably faster, thus allowing the use of cheap and metal-free catalysts **A** and **B** to perform the model reaction within 24 h and 19 h. Air- and moisture stable triarylboranes **22** were obtained after addition of a solution of TipLi or a suspension of Mes*Li. The Si/B exchange reaction can also be applied to synthesize mixed

thienyl (a)/furyl (b)/phenyl (c) systems and also methyl substituted compounds **22**^{MeAr} (Figure 3.6, left). Starting from disilylated compound **23**, bifunctional compounds **24** can be synthesized via careful monoborylation using BX_3. Compounds **24a,b** can be purified and isolated and used for AB polycondensation reactions, avoiding any stoichiometric issues (Figure 3.6, right). Following this route, oligomer **26a**^{Tip} with an average molecular weight (M_n) of 2316 Da was synthesized, which corresponds to 6 repeating units (2 more repeating units as compared to Br-systems). In general, the use of more stable aryldichloroboranes (vs. aryldibromoboranes) should facilitate large-scale use of these compounds.

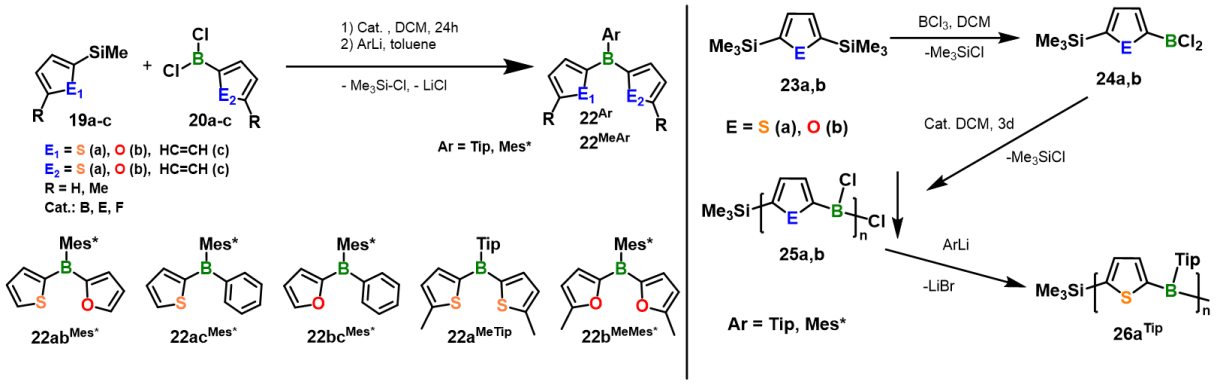

Figure 3.6. Left: Catalytic Si/B exchange reaction to afford symmetric, mixed and methylated triarylboranes **22.** Right: Catalytic Si/B exchange polycondensation reaction to afford oligomers **26**^{aTip}**.**

In chapter 2.7, synthetic routes to tetrabora- and diboraporphyrinogens were investigated. The syntheses of these macrocycles were attempted in a multi-step reaction procedure in which the final macrocyclization reaction was attempted under pseudo-high dilution conditions. In all cases, the methoxy-substituted ring-precursors **27**, **28** and **29** were successfully synthesized (Figure 3.7). The final macrocyclization reaction was successful for the synthesis of tetraboraporphyrinogen **30** (B_4), although analysis via HR-MS indicated the formation of higher homologues with different ring sizes (B_5-B_{10}) of the macrocycles as well (Figure 3.8). Beside ^{1}H-NMR spectroscopy, further evidence for the presence of a porphyrinoid structure was observed in UV-vis and fluorescence spectroscopy, which revealed a bathochromic shift in comparison to model compounds and linear oligomers as well as absorption bands reminiscent of Soret and Q bands observable in standard porphyrins.

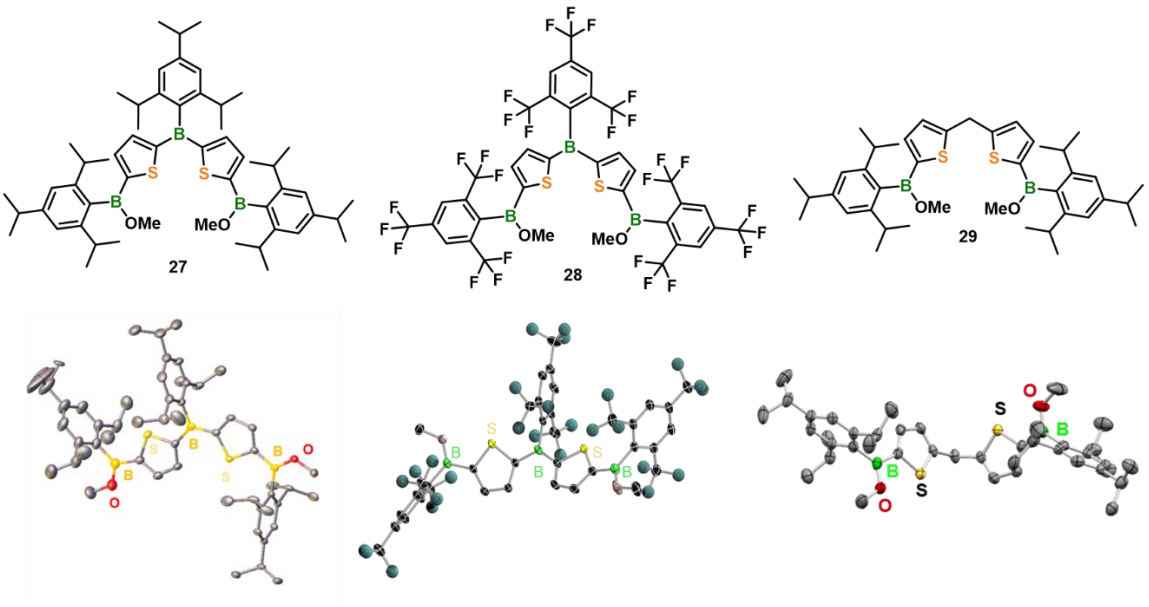

Figure 3.7. Ring precursors **27-29** and their molecular structure in the solid-state (H-Atoms omitted for clarity).

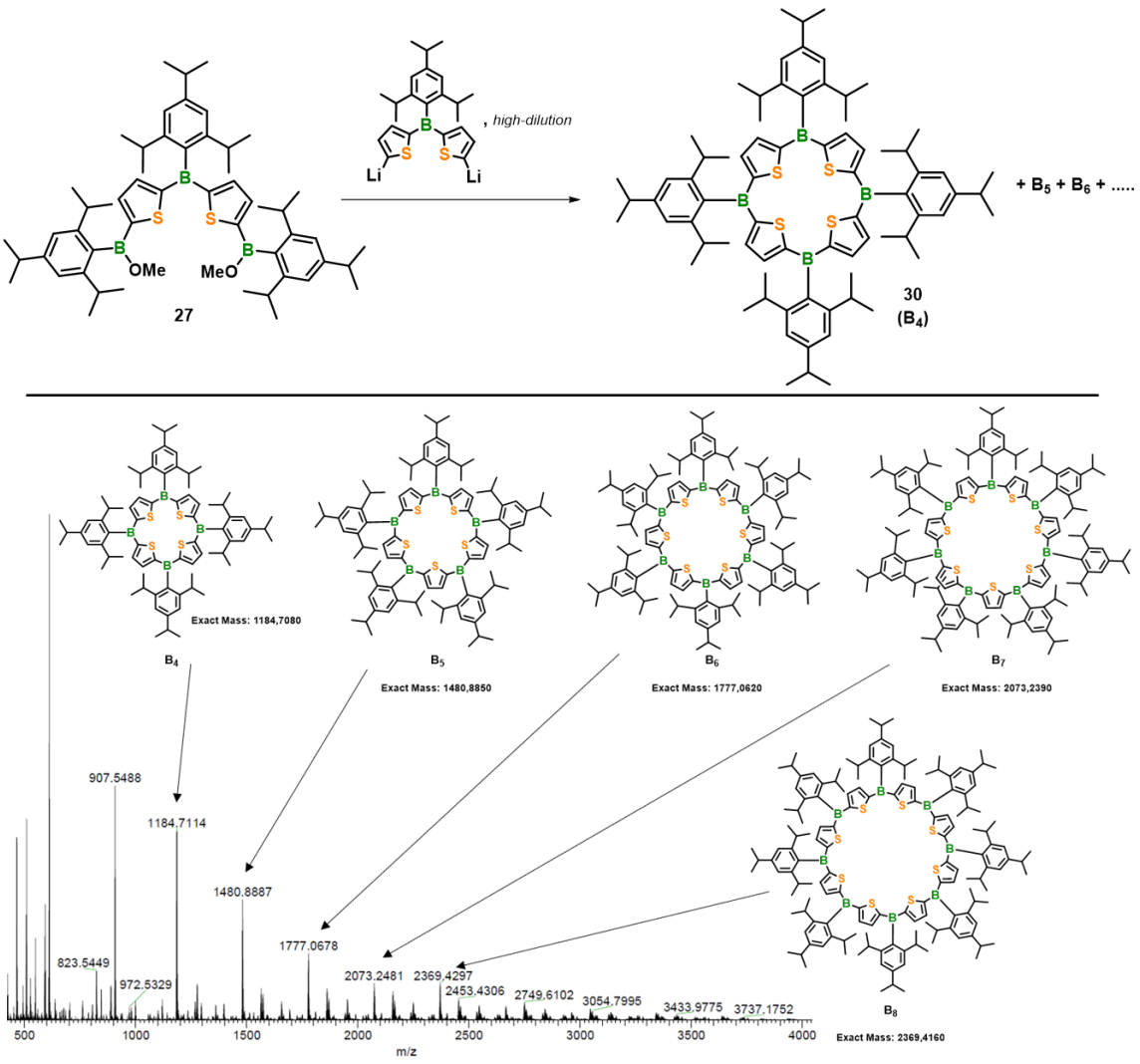

Figure 3.8. Top: Macrocyclization reaction under high-dilution conditions. Bottom: LIFDI mass spectrum of purified compound **30** (**B4**) indicating the presence of higher homologues (B_5-B_8).

During the synthesis of thienyl- or furylborane molecules (Chapter 2.2-2.5), oligomers (Chapter 2.6) or macrocycles (Chapter 2.7), at some point, substituting the reactive boron-halide functionalities by sterically demanding substituents or additional thiophene or furan rings is necessary to obtain air- and moisture-stable compounds and to prevent decomposition. Therefore, the general reactivity of thienyl- and furylboranes towards 2nd and 3rd substitution was investigated. The structural motif of those compounds can be divided into two different chemical surroundings with X_1 flanked by two hetaryl rings (Ar_2BX) and X_2, X_3 with only one connected hetaryl ring ($ArBX_2$). In Ar_2BX species, the two aryl rings can either consist of two hetarene rings (thiophene or furyl) or one hetaryl ring and one aryl substituent (Figure 3.9).

Thienyl- or furyl-based model compounds **20** and **31** as well as dithienyl- and difurylchloroboranes **21** and extended compounds **32-34** were synthesized featuring different chemical surroundings, halides and (het)aryl substituents on the boron atoms (Figure 3.9). To obtain kinetically stabilized triarylboranes, the incorporation of the aryl substituents can be done within one step (Figure 3.10, *Route I*) or stepwise (Figure 3.10, *Route II* and *III*).

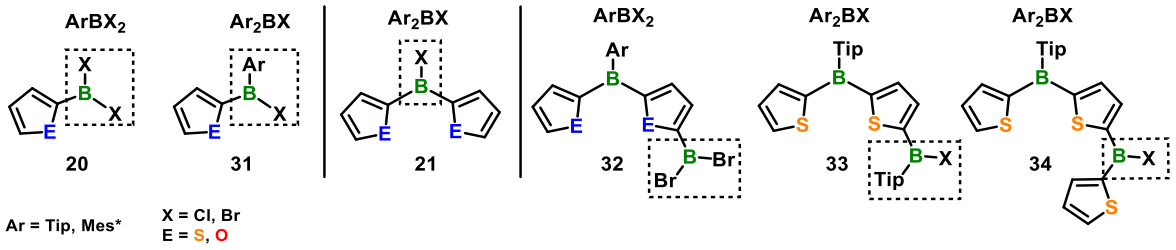

Figure 3.9. Chemical surroundings of investigated $ArBX_2$ and Ar_2BX thienyl- and furylboranes.

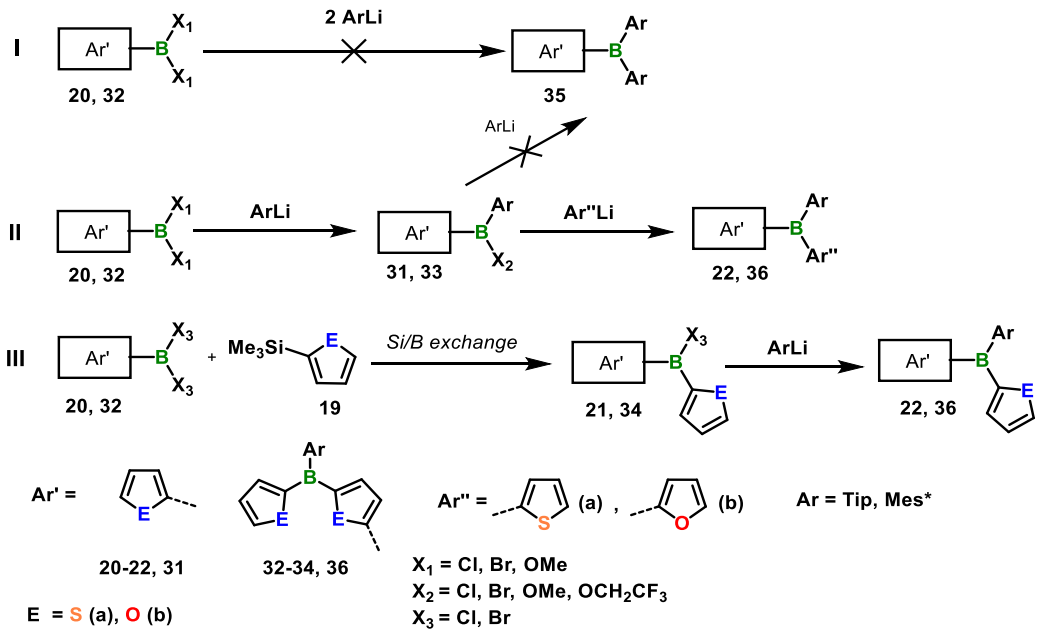

Figure 3.10. Synthetic strategies to obtain triarylboranes starting from $ArBX_2$ species. *I*: Concerted diarylation; *II*: Stepwise reaction via monoarylated compounds **31,33** and subsequent addition of ThiLi or FurLi. *III*: Stepwise reaction via catalytic Si/B exchange to afford compounds **21,34** and subsequent addition of aryllithium reagent.

In general, the investigations have shown that it is unlikely that both halides in an $ArBX_2$ system will be replaced by two equivalents of TipLi or Mes*Li (Route *I*) or in a stepwise procedure (*Route II*, addition of another equivalent ArLi). A stepwise reaction via addition of one equivalent of ArLi and subsequent addition of ThiLi or FurLi led to triarylboranes only in the case when Tip rather than Mes* is used as Ar (Route *II*). In order to obtain Mes*- substituted compounds, the only possibility appears to be performing a Si/B exchange reaction to afford an Ar_2BX species with subsequent addition of Mes*Li (Route *III*). Route *III* also allows access to Tip-substituted systems and has proven to be particularly flexible.

These results should provide valuable information for the general management and substitution behaviour of organoboranes when it comes to 2nd and 3rd substitution with bulky or (het)aryl substituents and can be applied e.g. for polycondensation reactions.

4. Zusammenfassung

Diese Arbeit zeigt, dass die Silizium/Bor Austauschreaktion eine einfache und hocheffektive Methode zur Bildung von B-C Bindungen für die Synthese von Bororganischen Molekülen, Oligomeren und Makrozyklen ist. Dieser Ansatz ermöglichte die Synthese einer Vielzahl von neuartigen anorganisch-organischen Hybridmaterialien mit besonderen Merkmalen und Eigenschaften.

Im ersten Kapitel wird beschrieben, dass die Silizium/Bor-Austausch-Fällungsreaktion in Acetonitril den Zugang zu Borazin-basierten hybriden Cyclomatrix-Polymer-Partikeln **3c** ermöglichte (Abbildung 4.1, links: ***Route B***). Im Vergleich zu üblichen Fällungspolykondensationsbedingungen, die über eine Salzeliminierung ablaufen (Abbildung 4.1, links: ***Route A***), konnten Partikel mit einer glatteren Oberfläche und deutlich größeren mittleren Durchmessern erhalten werden (Abbildung 4.1, oben: 905 ± 105 nm vs. 183 ± 20 nm). Mögliche Gründe für diesen Effekt könnte eine langsamer ablaufende Nukleationskinetik und eine geringere Anzahl von Nukleationsereignissen sein, die durch eine erhöhte Löslichkeit des Trimethylsilylgruppen-tragenden Monomers und der wachsenden Oligomere im Reaktionsmedium hervorgerufen werden. Die erfolgreiche Synthese der Cyclomatrix-Polymere wurde durch FT-IR Spektroskopie und Festkörper-NMR Spektroskopie bestätigt (Abbildung 4.1, unten rechts: ^{13}C und ^{11}B CPMAS). Die thermogravimetrische Analyse zeigte eine bemerkenswerte thermische Stabilität mit einer Restmasse von bis zu 56% bei 880 °C unter N_2-Atmosphäre, was die erhaltenen Cyclomatrix Polymere zu potenziellen Vorstufen für flammhemmende Additive macht.

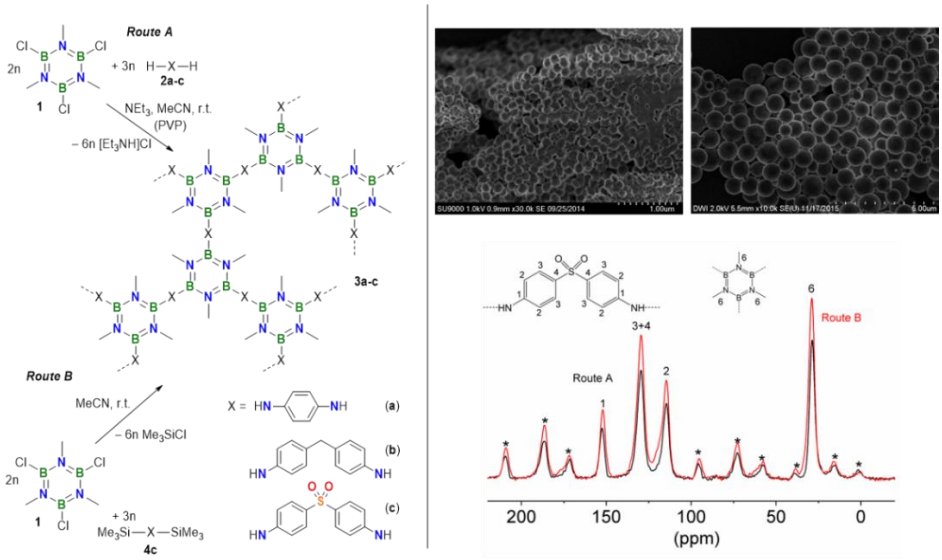

Abbildung 4.1. Links: Synthese der Cyclomatrix Polymere **3a-c** über Salzeliminierung (***Route A***) und Synthese von **3c** über Si/B Austausch-Polykondensation (***Route B***). Oben rechts: FESEM-Mikroskopische Aufnahmen von **3c** über ***Route A*** (links) and über ***Route B*** (rechts). Unten rechts: ^{13}C CPMAS Spektrum von **3c** über ***Route A*** bzw. ***B***.

In den Kapiteln 2.2-2.4 wurden verschiedene Synthesestrategien, die den Zugang zu neuartigen Bororganischen Molekülen mit Furylboraneinheiten in der Hauptkette ermöglichen sollen, untersucht. In Kapitel 2.2 konnten durch Anwendung der Suzuki-Miyaura-Kreuzkupplung für die Reaktion zwischen dibromierten oder diiodiertem Difuryl(supermesityl)boran (**5**) und dem jeweiligen Kupplungspartner **6** π-verlängerte Organoborane **7** erhalten werden (Abbildung 4.2, oben). In Kapitel 2.3 und 2.4 wurde gezeigt, dass der katalytische Si/B Austausch eine hocheffiziente und flexible Methode ist, um ausgedehnte Organoborane **13-15** durch die Reaktion von disilylierten Verbindungen **8a-10a** oder einer diborylierten Verbindung **8b** mit dem jeweiligen Kupplungsreagenz **11** oder **12** zu erhalten (Abbildung 4.2, Mitte). Außerdem wurden in Kapitel 2.4 Salzmetathesereaktionen zwischen Verbindung **16** und lithiierten Spezies **17a,b** durchgeführt (Abbildung 4.2, unten).

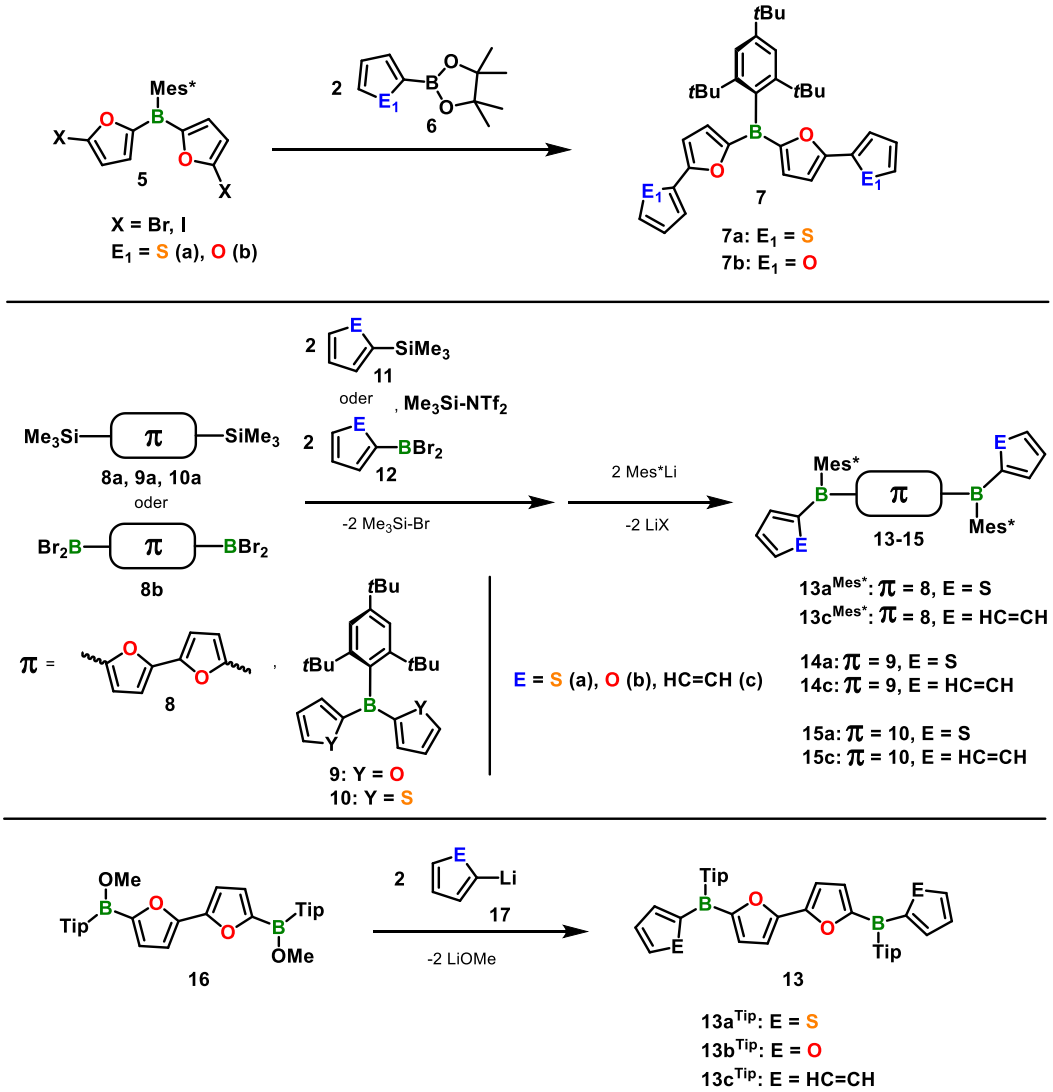

Abbildung 4.2. Synthetische Routen zu erweiterten π–konjugierten Organoboranen. Oben: Suzuki-Miyaura-Kreuzkupplungsreaktion zu Organoboranen **7**. Mitte: Katalytischer Si/B Austausch zur Bildung von Tip- und Mes*-substituierten bifuranverbrückten Bisboranen **13** und Tris(het)arylboranen **14,15**. Unten: Salzeliminierungsreaktion zu den bifuranverbrückten Bisboranen **13^{Tip}.**

Die Untersuchungen haben gezeigt, dass die Anwendung des Reaktionsweges über Salzeliminierungen auf Tip-substituierte Verbindungen beschränkt ist, während der Reaktionsweg über den Si/B-Austausch die Möglichkeit bietet, sowohl Tip als auch Mes* als sterisch anspruchsvolle Substituenten einzuführen. Der Fokus lag dabei auf der Synthese verschiedener Triarylborane **7** und **13-15**, die aus vier konjugierten Arenringen und 1,2 bzw. 3 Bor-Zentren aufgebaut sind. Darüber hinaus wurden kinetisch stabilisierte Furylborane als sehr robuste und vielseitige Bausteine für π-konjugierte Materialien etabliert, die zu verbesserten Lumineszenz-Eigenschaften im Vergleich zu den häufiger verwendeten Thienylboranen führen. Durch die Erhöhung der Anzahl an Boratomen, die Variation der Verknüpfungseinheit in diesen Systemen und die Wahl verschiedener (Het)arene war ein einfaches Tuning der elektronischen und der Akzeptor Eigenschaften möglich. Thiophen-, Furan- und Benzol-Einheiten konnten als terminale Substituenten eingebaut werden. Die dargestellten Verbindungen können als π-verlängerte Organoborane **7**, bifuranverbrückte Bisborane **13** und Tris(het)arylborane **14**, **15** betrachtet werden (Abbildung 4.3, oben). Die erhaltenen Organoborane waren perfekt Luft- und Feuchtigkeitsstabil. Die Röntgenstrukturanalyse der Verbindungen **7a** und **13a**^{Tip} zeigte eine Anti-Anordnung der Hetarene Ringe sowie in beiden Fällen weitgehend koplanare Strukturen mit den terminalen Thiophenringen (Abbildung 4.3, unten).

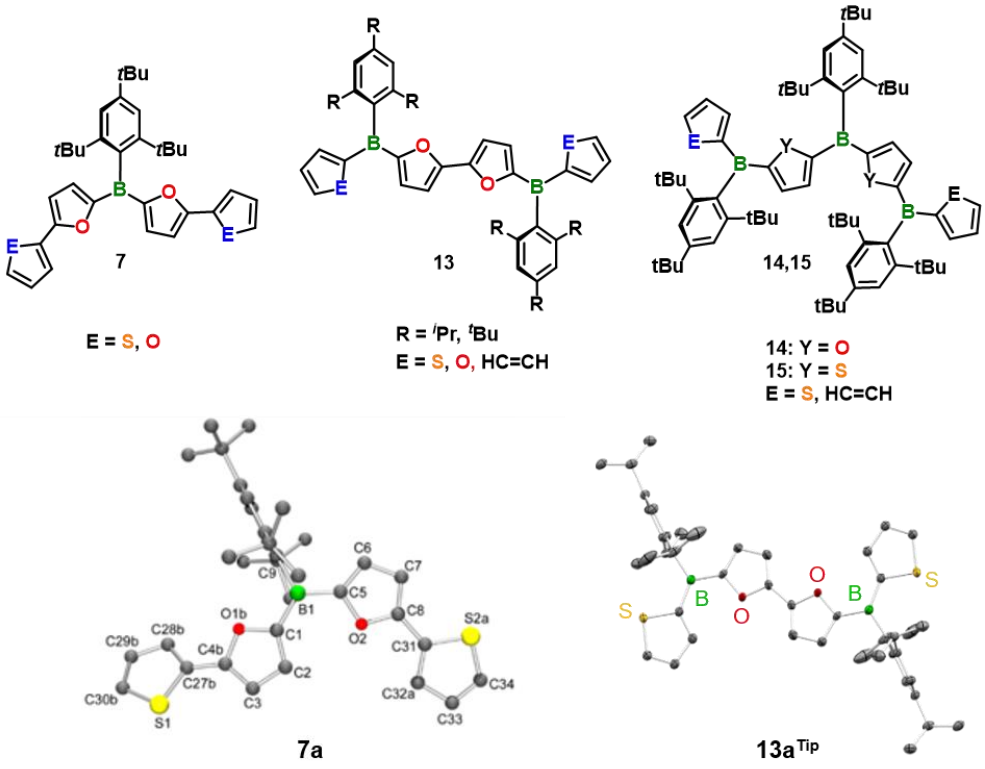

Abbildung 4.3. Oben: Erweiterte π-konjugierte Organoborane **7**, bifuranverbrückte Bisborane **13** und Tris(het)arylborane **14,15**. Unten: Molekularstruktur der Thienyl-flankierten Verbindungen **7a** und **13a**^{Tip} im Festkörper (H-Atome zur Verdeutlichung weggelassen).

Optische und Cyclovoltammetrie-Messungen zeigten starke Lumineszenz-Eigenschaften sowie eine starke elektronische Kommunikation zwischen den Bor-Zentren entlang der π-konjugierten Kette. Die UV-Vis und fluoreszenzspektroskopische Analyse aller Verbindungen zeigte eine bathochrome Verschiebung im Vergleich zu kinetisch stabilisierten Diarylboran-Bausteinen (Mes*$BFur_2$ oder Mes*$BThi_2$), welche durch eine effektive Verlängerung des π-Systems erklärt werden kann. Die Wellenlänge des Absorptionsmaximums steigt in der Reihenfolge: Phenyl << Thienyl < Furyl, wobei zwischen den beiden letzteren nur ein geringer Unterschied besteht. Im Allgemeinen wurden stärkere Lumineszenz-Eigenschaften für Furylboranverbindungen im Vergleich zu ihren direkten Thienylboran-Verwandten erhalten. Die stark lumineszierenden Verbindungen **7** und **13** konnten mit Quantenausbeuten von bis zu 89 % erhalten werden, was die effektive Rolle der Kettenverlängerung durch eine Bihetaryl-Einheit weiter untermauert. Cyclovoltammetrie-Messungen zeigten elektrochemisch reversible Redoxvorgänge entsprechend der Anzahl der Boratome für **7** und **13** an, mit der Ausnahme, dass ein möglicher dritter Redoxvorgang für die Verbindungen **14** und **15** außerhalb des zugänglichen Potenzialbereichs liegt, welcher wahrscheinlich durch das Lösungsmittel begrenzt ist. Mit zunehmendem Bor-Gehalt werden die Elektronenakzeptor Eigenschaften verbessert, was sich in anodisch verschobenen Redoxereignissen widerspiegelt.

In Kapitel 2.5 wird die Synthese einer Reihe von Dithienylmethanverbrückten Bisboranen **18** über den katalytischen Si/B-Austausch beschrieben, die ebenfalls aus vier Hetarenringen und zwei Boratomen aufgebaut sind, aber in diesem Fall ist die Konjugation zwischen den beiden Borzentren durch den aliphatischen Linker unterbrochen (Abbildung 4.4). Das Redoxverhalten wurde mittels Cyclo- und Pulsvoltammetrie in THF charakterisiert. Für Mes*-substituierte Verbindungen zeigte das Differentialpulsvoltammogramm zwei Reduktionswellen mit relativ kleinen Abständen zwischen 70-100 mV (Abbildung 4.4, rechts). Dies weist eindeutig auf einen geringen Grad an elektronischer Kommunikation zwischen den Boratomen hin, der durch die Unterbrechung des π-Systems verursacht wurde. Die UV-Vis Spektroskopie zeigte eine bathochrome Verschiebung im Vergleich zu Aryldithienylboran-Bausteinen (z.B. 325 nm für $ArBTh_2$ vs. 343 nm für **18a^{Tip}** und 338 nm für **18a^{Mes*}**). Dieser Effekt kann auf die aliphatische Methylenbrücke zurückgeführt werden. Folgerichtig führt der Einbau zusätzlicher elektronenschiebender Methyl- oder Silylgruppen (**18d,e^{Tip}**) zu einer weiteren Rotverschiebung, was durch eine Erhöhung der HOMO-Energie und damit eine Verringerung der HOMO-LUMO-Lücke erklärt werden kann.

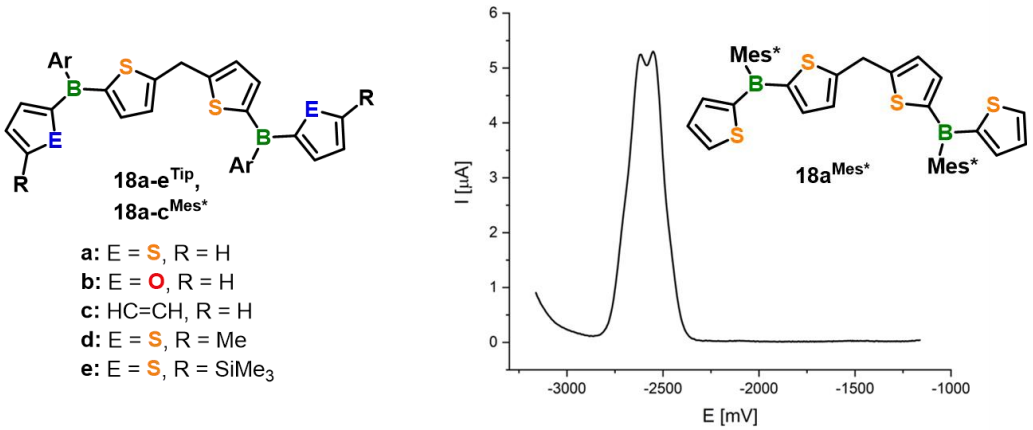

Abbildung 4.4. Links: Methylenverbrückte Bisborane **18**, erhalten durch katalytische Si/B-Austauschreaktion. Rechts: Differential-Puls-Voltammogramm für **18a^{Mes*}**.

In Kapitel 2.6 wurde ein Katalysatorscreening durchgeführt, um die Anwendbarkeit der Si/B Austauschreaktion von Hetaryl-BBr_2 auf weniger reaktive Hetaryl-BCl_2-Spezies als Substrate zu erweitern. Für die Reaktion zwischen den Si/B-Austausch-Kupplungspartnern **19** und **20** wurden sechs verschiedene Katalysatoren eingesetzt (Abbildung 4.5). Die Untersuchungen haben gezeigt, dass der geläufigste Katalysator Me_3Si-NTf_2 (Kat. **B**, 10 mol%) die Reaktion zwischen **19a** und **20a** erfolgreich beschleunigt, aber eine fast vollständige Umsetzung zu **21a** erst nach 24 Stunden (vs. 72 Minuten für Thi-BBr_2) beobachtet wurde. In Abwesenheit eines Katalysators wurde selbst nach 13 Tagen nur ein Umsatz von 5% erhalten. Für die Reaktion zwischen **19b** und **20b** konnte eine vollständige Umsetzung innerhalb von 19 Stunden beobachtet werden, was auf eine allgemein schnellere Reaktion hinweist, wahrscheinlich aufgrund des elektronenreicheren Systems von Furan. Dieser Trend wird auch für die Katalysatoren **A**, **C**-**F** beobachtet.

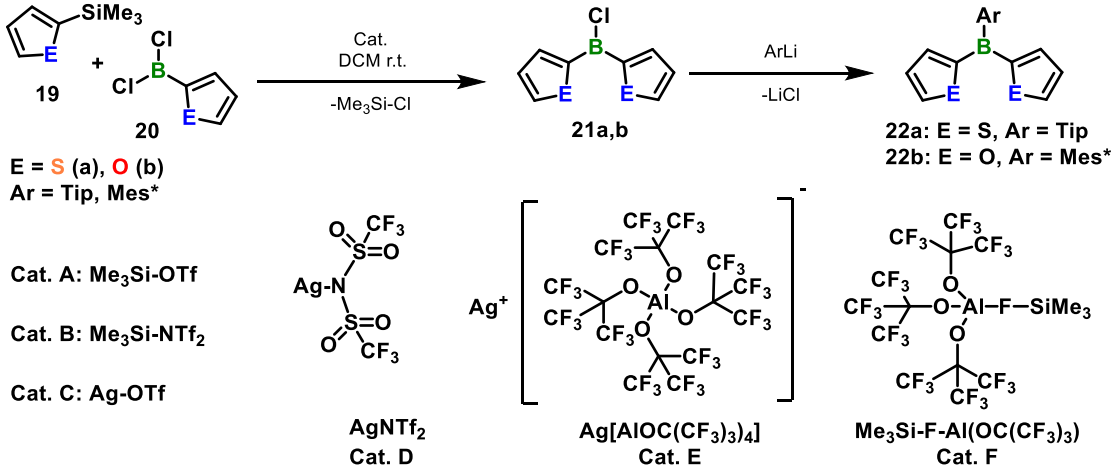

Abbildung 4.5. Allgemeines Schema für den Si/B-Austausch der Verbindungen **19** und **20** unter Verwendung verschiedener Katalysatoren **A**-**F** und anschließender Arylierung zur Bildung von Triarylboranen **22**.

Die Verwendung des Silber-basierten Katalysator **D** (5 mol%) beschleunigte die Si/B-Austauschreaktion weiter und die vollständige Umsetzung der Ausgangsmaterialien zu **21a** wurde innerhalb von 5 Stunden beobachtet. Die Verwendung der Katalysatoren **E** und **F**, die entweder ein Silberkation (Kat. **E**) oder eine elektrophile Silylspezies (Kat. **F**) in Kombination mit einem schwächer koordinierenden Anion aufweisen, führte zu einer beeindruckenden Beschleunigung der Reaktion. Für beide Katalysatoren wurde eine vollständige Umsetzung der Ausgangsmaterialien **19** und **20** innerhalb von weniger als 1 Stunde beobachtet. Interessanterweise wurde gezeigt, dass die Reaktion mit Furan-basierten Ausgangsmaterialien selektiver war und kein Hinweis auf eine C-H-Aktivierungsnebenreaktion beobachtet wurde, so wie es bei Thiophen-basierten Systemen der Fall war. Generell scheint der katalytische Si/B Austausch für Furyl-BCl_2 von besonderem Interesse zu sein, da: a) Kombinationen von Boranen mit Furan-Resten nur wenig erforscht sind und oft nur geringe Ausbeuten erzielt wurden; b) die Synthese und Lagerung von Furyl-BCl_2 Spezies möglich ist, was ein hohes Maß an Kontrolle ermöglicht; c) der Si/B Austausch vergleichsweise schneller ist und somit die Verwendung von billigen und metallfreien Katalysatoren **A** und **B** erlaubt, um die Modellreaktion innerhalb von 24 Stunden und 19 Stunden durchzuführen. luft- und feuchtigkeitsstabile Triarylborane **22** konnten nach Zugabe einer Lösung von TipLi oder einer Suspension von Mes*Li erhalten werden. Die Si/B Austauschreaktion kann auch zur Synthese von gemischten Thienyl- (a)/ Furyl- (b)/ Phenyl (c) Systemen und auch von methylsubstituierten Verbindungen $\mathbf{22}^{\mathbf{MeAr}}$ eingesetzt werden (Abbildung 4.6, links). Ausgehend von der disilylierten Verbindung **23** können bifunktionelle Verbindungen **24** durch vorsichtige Monoborylierung mit BX_3 synthetisiert werden. Die Verbindungen **24a,b** können aufgereinigt und isoliert werden und anschließend für AB-Polykondensationsreaktionen verwendet werden, wobei jegliche stöchiometrische Probleme vermieden werden (Abbildung 4.6, rechts). Auf diesem Weg wurde das Oligomer $\mathbf{26a}^{\mathbf{Tip}}$ mit einem durchschnittlichen Molekulargewicht (M_n) von 2316 Da synthetisiert, was einer Anzahl an Wiederholungseinheiten von 6 entspricht (2 Wiederholungseinheiten mehr als im Vergleich zum Br-System). Generell sollte die Verwendung von stabileren Aryldichloroboranen (im Vergleich zu Aryldibromoboranen) den großtechnischen Einsatz dieser Verbindungen erleichtern.

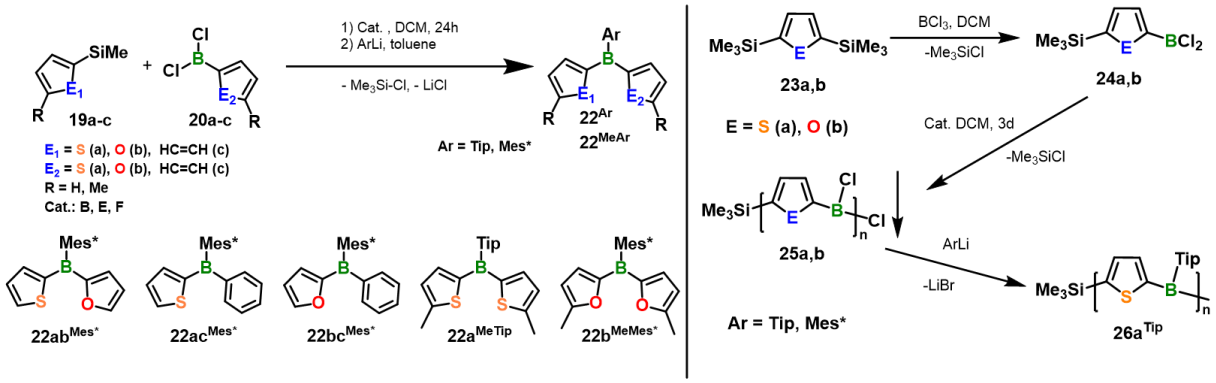

Abbildung 4.6. Links: Katalytische Si/B-Austauschreaktion zur Herstellung von symmetrischen, gemischten und methylierten Triarylboranen **22.** Rechts: Katalytische Si/B-Austauschpolykondensationsreaktion zur Herstellung von Oligomeren **26a^{Tip}.**

In Kapitel 2.7 wurden Synthesewege zu Tetrabora- und Diboraporphyrinogenen untersucht. Die Synthesen dieser Makrozyklen wurden in einem mehrstufigen Reaktionsverfahren durchgeführt, bei dem die abschließende Makrozyklisierungsreaktion unter Pseudo-Hochverdünnungsbedingungen durchgeführt wurde. In allen Fällen wurden die Methoxy-substituierten Ringvorstufen **27**, **28** und **29** erfolgreich synthetisiert (Abbildung 4.7). Die abschließende Makrozyklisierungsreaktion war für die Synthese vom Tetraboraporphyrinogen **30** (B_4) erfolgreich, obwohl die Analyse mittels HR-MS auch die Bildung höherer Homologe mit unterschiedlichen Ringgrößen (B_5-B_{10}) der Makrozyklen anzeigt (Abbildung 4.8). Neben der ^{1}H-NMR Spektroskopie wurden weitere Hinweise auf das Vorliegen einer porphyrinoiden Struktur in der UV-Vis und Fluoreszenzspektroskopie beobachtet, die eine bathochrome Verschiebung im Vergleich zu Modellverbindungen und linearen Oligomeren sowie Absorptionsbanden, die an Soret- und Q-Banden erinnern und in Standard-Porphyringen zu beobachten sind, zeigen.

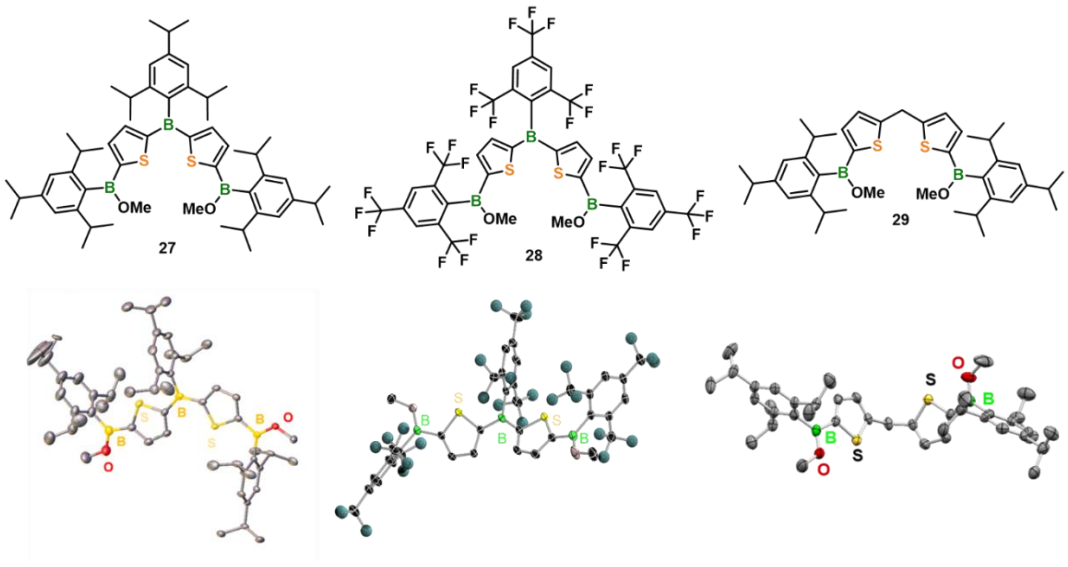

Abbildung 4.7. Ringvorstufen **27-29** und ihre molekulare Struktur im Festkörper (H-Atome zur Verdeutlichung weggelassen).

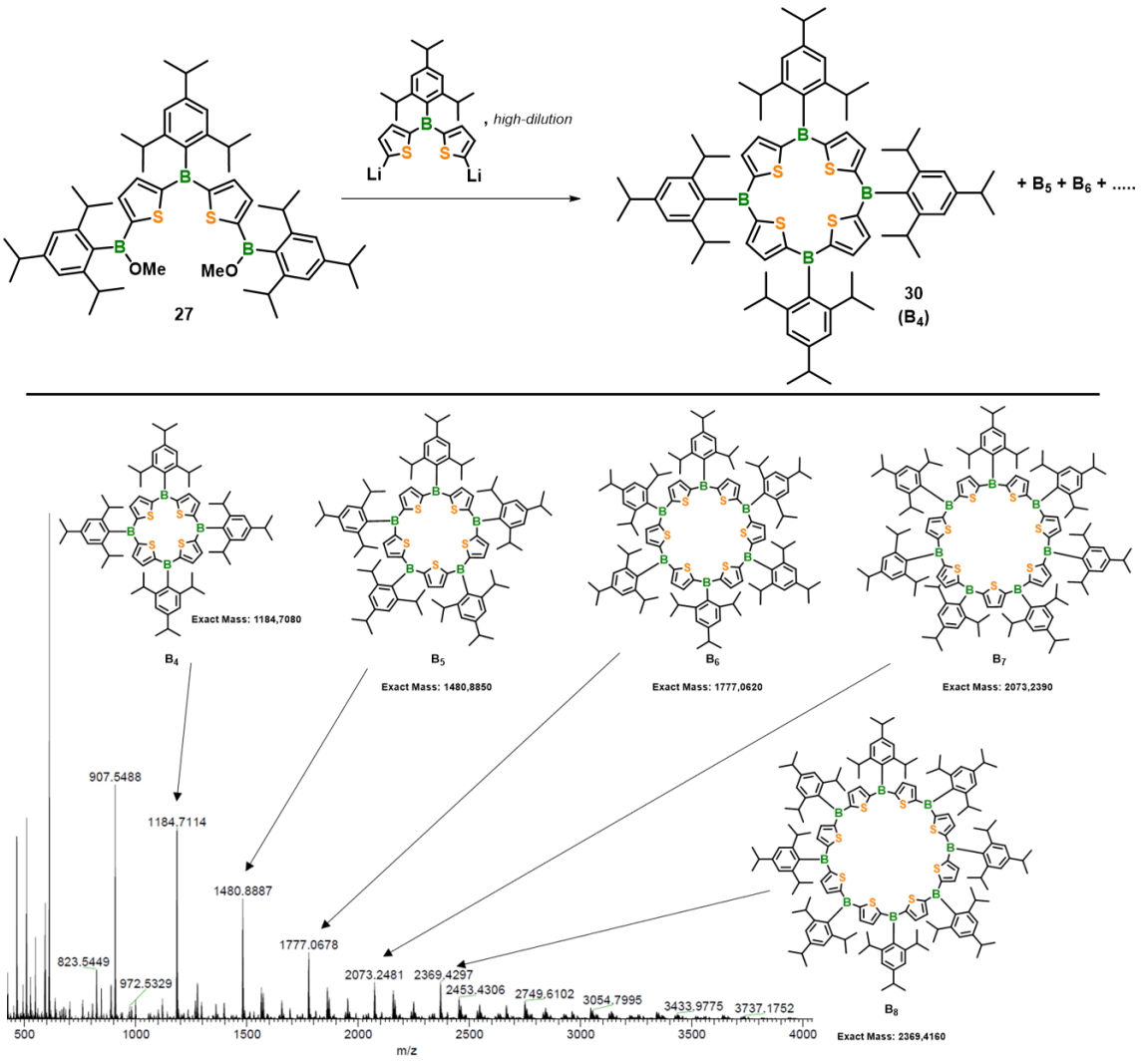

Abbildung 4.8. Top: Makrozyklisierungsreaktion unter Hochverdünnungsbedingungen. Unten: LIFDI-Massenspektrum der aufgereinigten Verbindung **30 (B_4)**, welches die Anwesenheit höherer Homologe (B_5-B_8) zeigt.

Bei der Synthese von Thienyl- oder Furylboranmolekülen (Kapitel 2.2-2.5), Oligomeren (Kapitel 2.6) oder Makrozyklen (Kapitel 2.7) ist es an einem bestimmten Punkt notwendig, die reaktiven Borhalogenid-Funktionalitäten durch sterisch anspruchsvolle Substituenten oder zusätzliche Thiophen- oder Furanringe zu ersetzen, um luft- und feuchtigkeitsstabile Verbindungen zu erhalten und einer Zersetzung vorzubeugen. Daher wurde die allgemeine Reaktivität von Thienyl- und Furylboranen gegenüber der Zweit- und Drittsubstitution untersucht. Das strukturelle Motiv dieser Verbindungen lässt sich in zwei unterschiedliche chemische Umgebungen unterteilen, wobei X_1 von zwei Hetarylringen flankiert werden kann (Ar_2BX) und X_2, X_3 nur einen verbundenen Hetarylring aufweisen ($ArBX_2$). Bei Ar_2BX Arten können die beiden Arylringe entweder aus zwei Hetarenringen (Thiophen oder Furan) oder aus einem Hetarenring und einem Arylsubstituenten bestehen (Abbildung 4.9).

Thienyl- oder Furyl-basierte Modellverbindungen **20** und **31** sowie Dithienyl- und Difurylchlorborane **21** und ausgedehnte Verbindungen **32-34** wurden mit unterschiedlicher chemischer Umgebung, Halogenen und (Het)arylsubstituenten an den Boratomen synthetisiert (Abbildung 4.9). Um kinetisch stabilisierte Triarylborane zu erhalten, kann der Einbau der Arylsubstituenten in einem Schritt (Abbildung 4.10, *Route I*) oder schrittweise (Abbildung 4.10, *Route II* und *III*) erfolgen.

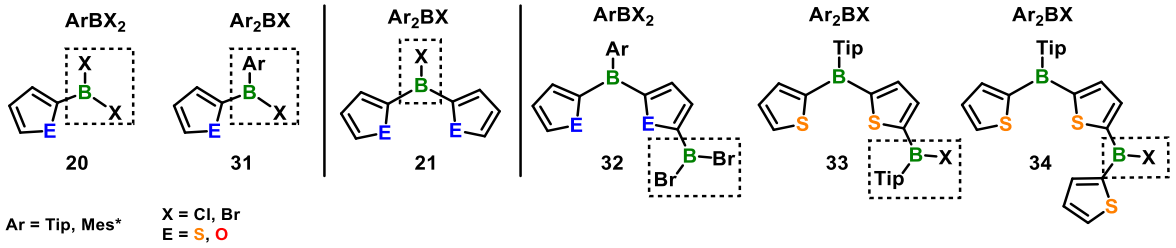

Abbildung 4.9. Chemische Umgebung der untersuchten $ArBX_2$ and Ar_2BX Thienyl- und Furylborane.

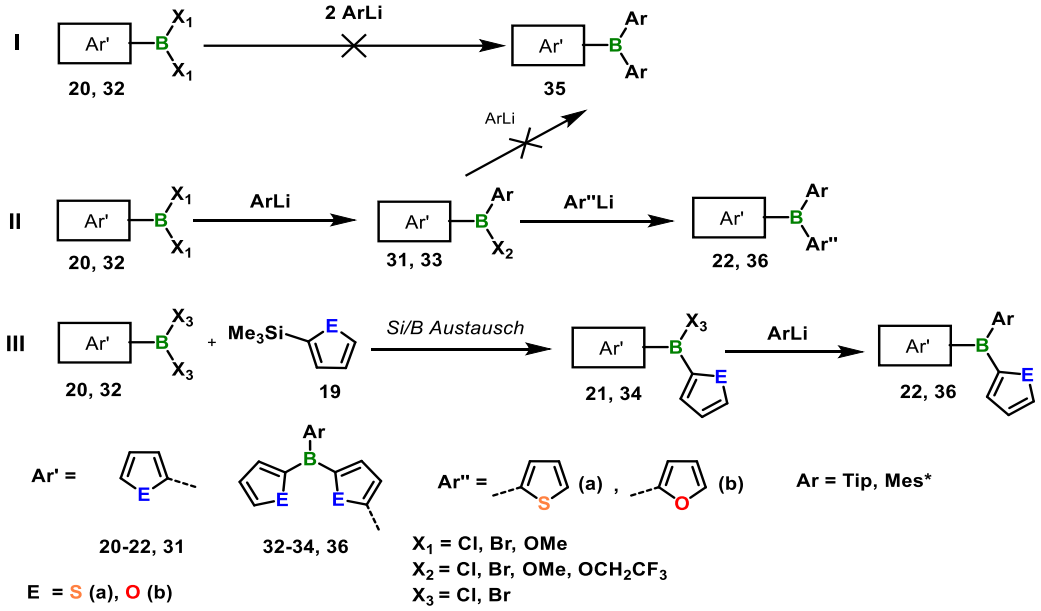

Abbildung 4.10. Synthesestrategien zur Darstellung von Triarylboranen ausgehend von $ArBX_2$ Spezien. I: Konzertierte Diarylierung. II: Schrittweise Reaktion über monoarylierte Verbindung **31,33** und anschließende Addition von ThiLi oder FurLi. III: Schrittweise Reaktion über katalytischen Si/B-Austausch zu den Verbindungen **21,34** und anschließender Zugabe von Aryllithium-Reagenzien.

Generell haben die Untersuchungen gezeigt, dass es unwahrscheinlich ist, dass beide Halogene in einem $ArBX_2$ System durch zwei Äquivalente TipLi oder Mes*Li (*Route I*) oder in einem schrittweisen Verfahren (*Route II*, Zugabe eines weiteren Äquivalents ArLi) substituiert werden. Eine schrittweise Reaktion über die Zugabe von einem Äquivalent ArLi und anschließender Zugabe von ThiLi oder FurLi führt nur dann zu Triarylboranen, wenn Tip statt Mes* als Arylrest verwendet wird (*Route II*). Um Mes*-substituierte Verbindungen zu erhalten, scheint die einzige Möglichkeit die Durchführung einer Si/B Austauschreaktion zu sein, um

eine Ar_2BX-Spezies zu erhalten, die dann mit Mes*Li weiter umgesetzt werden kann (*Route III*). *Route III* ermöglicht auch den Zugang zu Tip-substituierten System und hat sich als besonders flexibel herausgestellt.

Diese Ergebnisse sollen wertvolle Information für die allgemeine Handhabung und das Substitutionsverhalten von Organoboranen liefern, wenn es um die Zweit- und Drittsubstitution mit sterisch anspruchsvollen oder (Het)aryl-Substituenten geht. Die Ergebnisse können dann z.B. für Polykondensationsreaktionen angewendet werden.

5. Appendix

5.1 Borazine-based Inorganic–Organic Hybrid Cyclomatrix Microspheres by Silicon/Boron Exchange Precipitation Polycondensation

Field-Emission Scanning Electron Microscopy (FESEM)

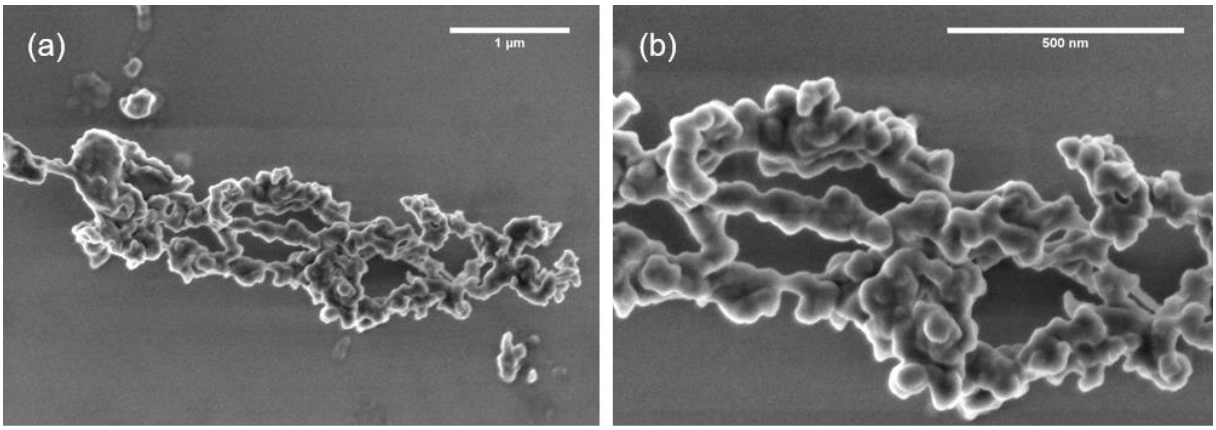

Figure 5.1.1. FESEM micrographs of **3a**.

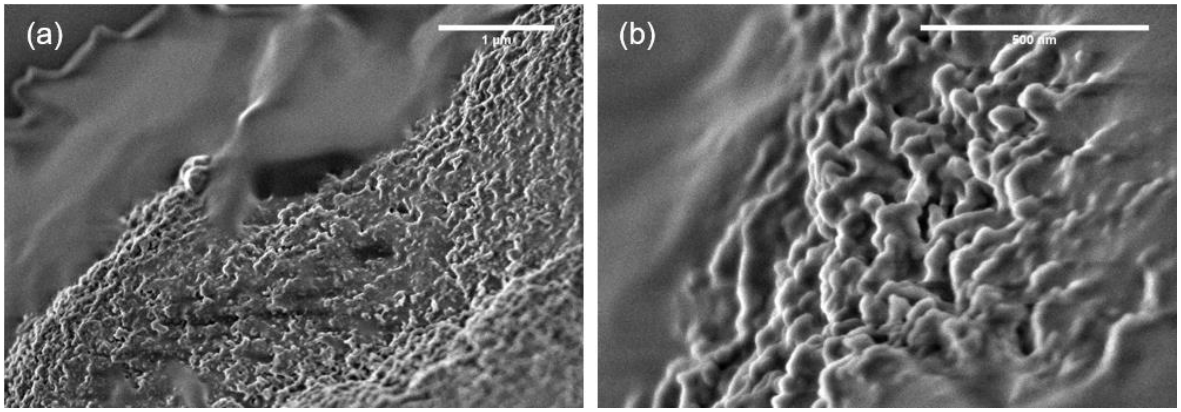

Figure 5.1.2. FESEM micrographs of **3b**.

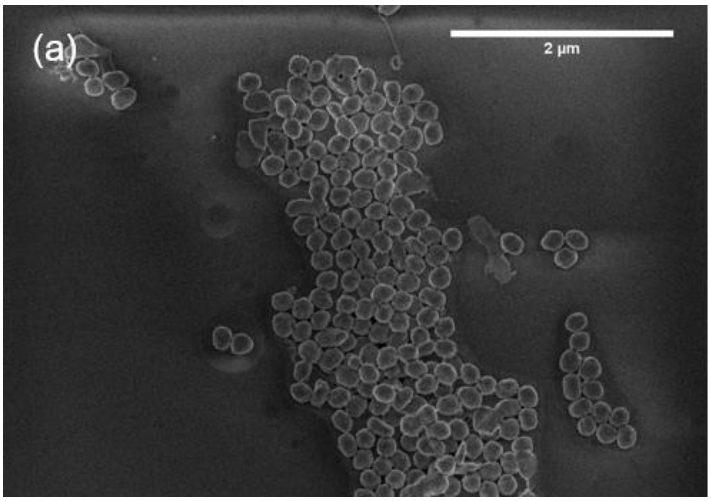

Figure 5.1.3. FESEM micrograph of microspheres of **3b** obtained from a reaction using PVP as a stabilizing agent.

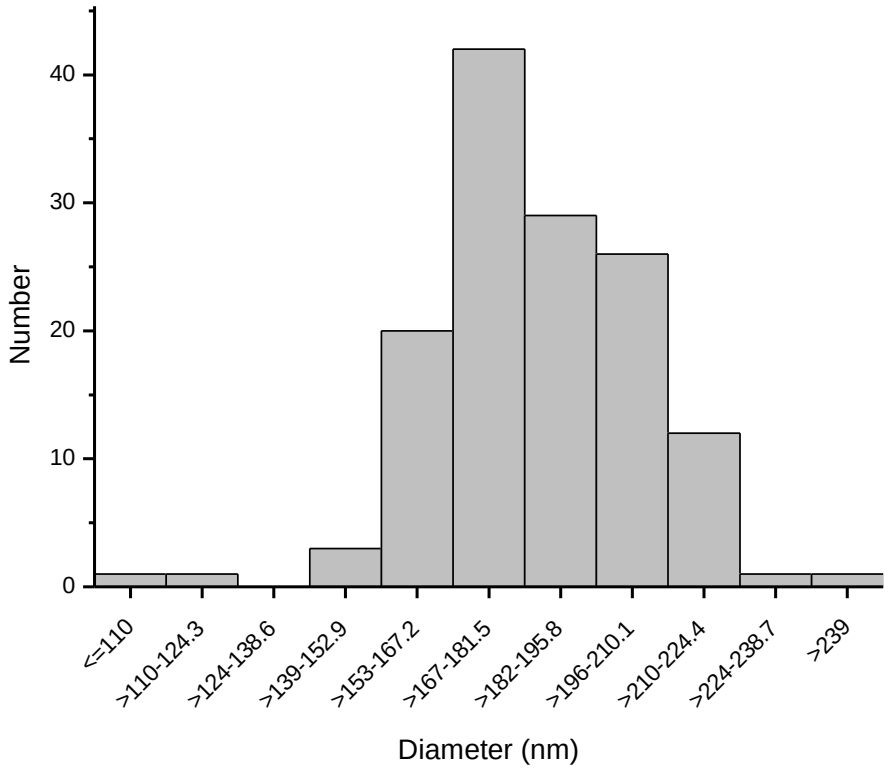

Figure 5.1.4. Histogram of **3b** microspheres obtained from a reaction using PVP as a stabilizing agent. Mean particle diameter: 184 nm ± 21 nm.

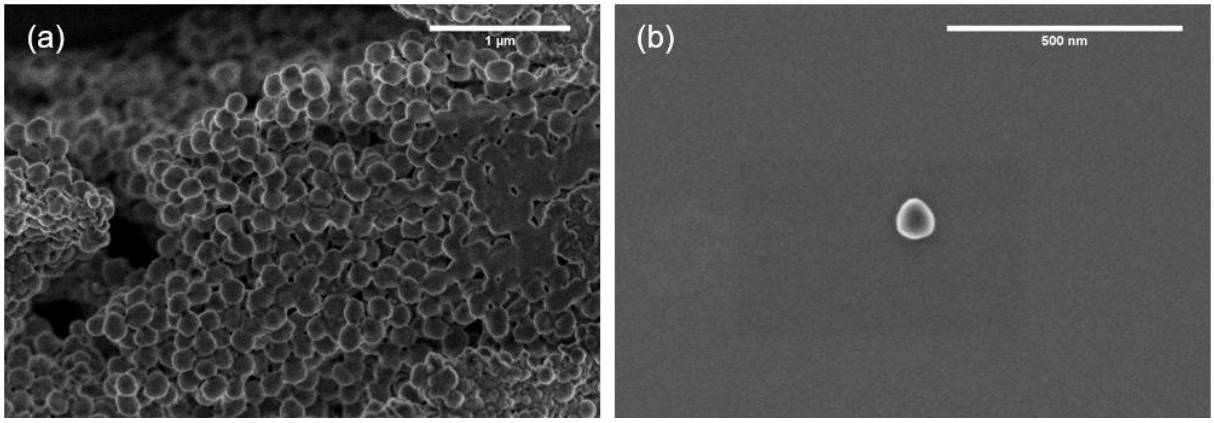

Figure 5.1.5. FESEM micrographs of **3c** microspheres obtained from a reaction via ***Route A***.

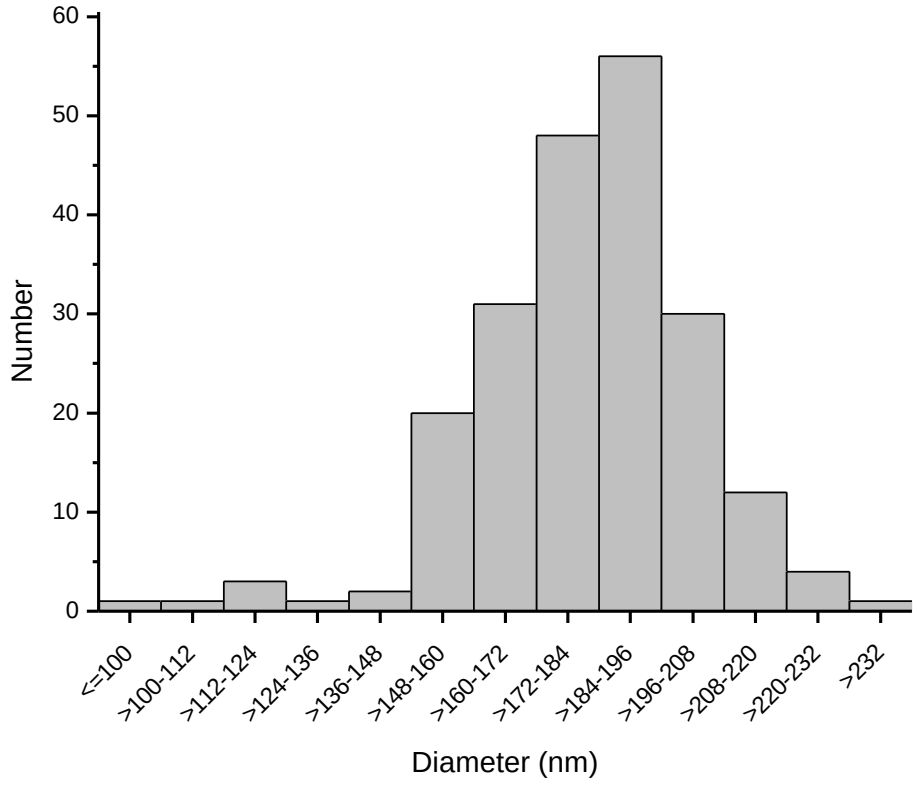

Figure 5.1.6. Histogram of **3c** microspheres obtained from a reaction via ***Route A***. Mean particle diameter: 183 nm ± 20 nm.

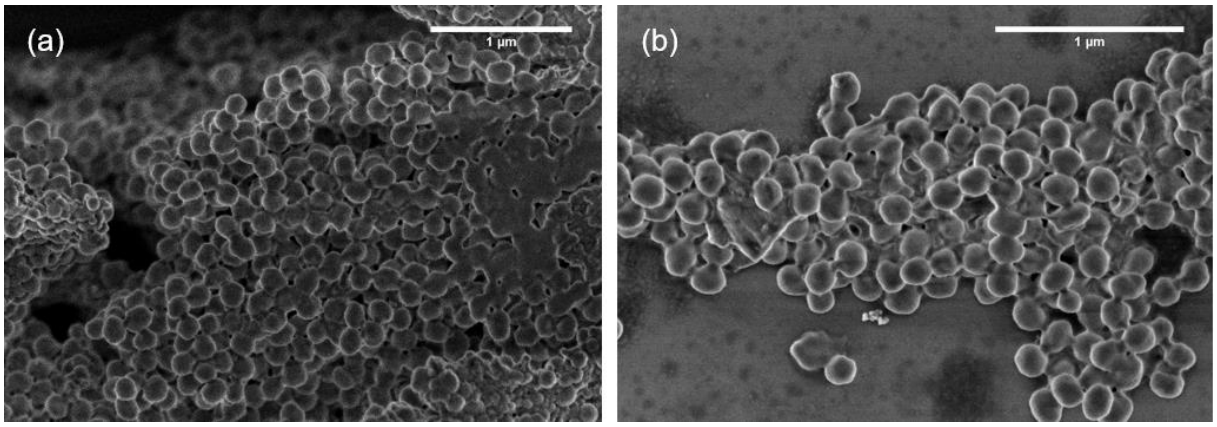

Figure 5.1.7. FESEM micrographs of **3c** microspheres obtained from a reaction via ***Route A*** with increased diamine concentration: a) 12.5 mmol L^{-1}, b) 21.0 mmol L^{-1}.

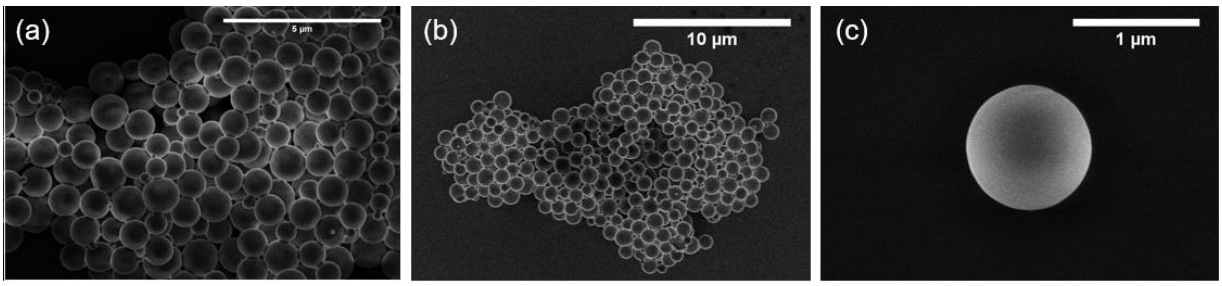

Figure 5.1.8. FESEM micrographs of **3c** microspheres obtained from a reaction via ***Route B***.

Figure 5.1.9. Images of particle formation of **3c** recorded during addition of a solution of **1** to a solution of **4c** in acetonitrile (***Route B***). From left (1) to right (3): (1) before addition, (2) after addition of 10 mL of a total volume of 25 mL, (3) after addition of 15 mL of a total volume of 25 mL.

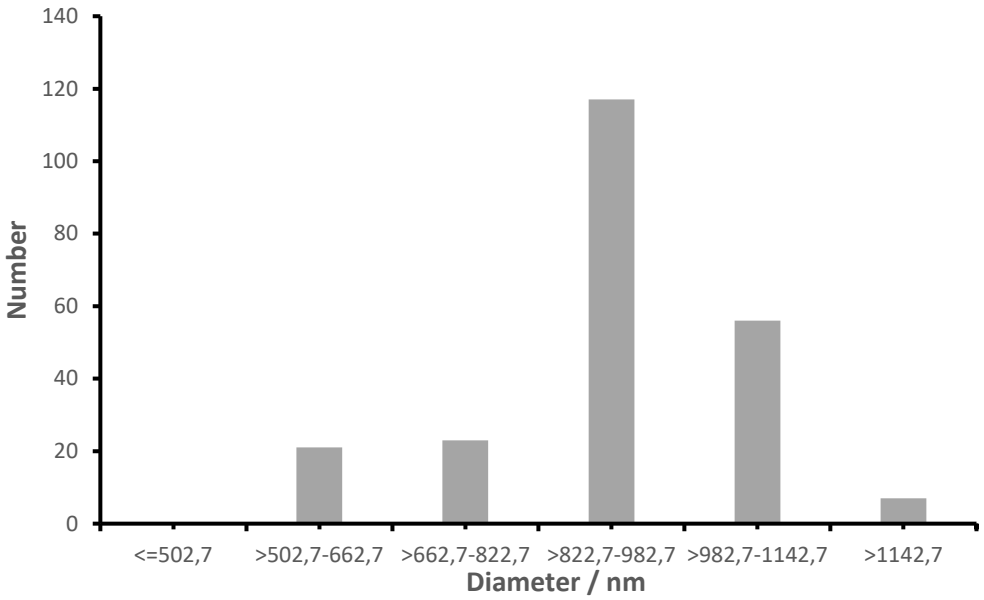

Figure 5.1.10. Histogram of **3c** microspheres obtained from a reaction via ***Route B***. Mean particle diameter: 905 nm ± 150 nm. A minor amount of smaller microspheres (<500 nm) is present, while the larger microspheres (>500 nm) are predominating. Considering all microspheres, the overall mean particle diameter is 761 nm ± 283 nm.

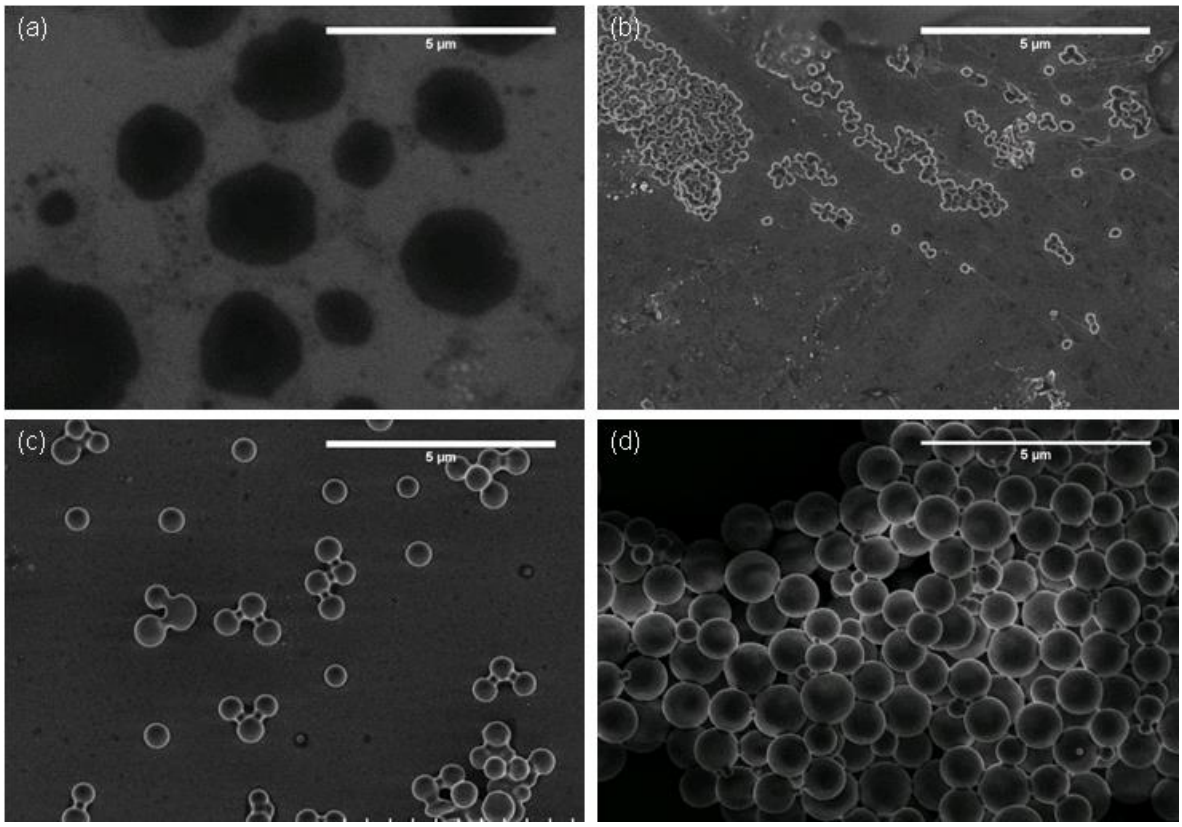

Figure 5.1.11. FESEM micrographs of **3c** obtained from reactions via ***Route B*** in different solvents: a) CH_2Cl_2, b) toluene, c) CH_2Cl_2/acetonitrile (% v/v, 50:50), d) acetonitrile.

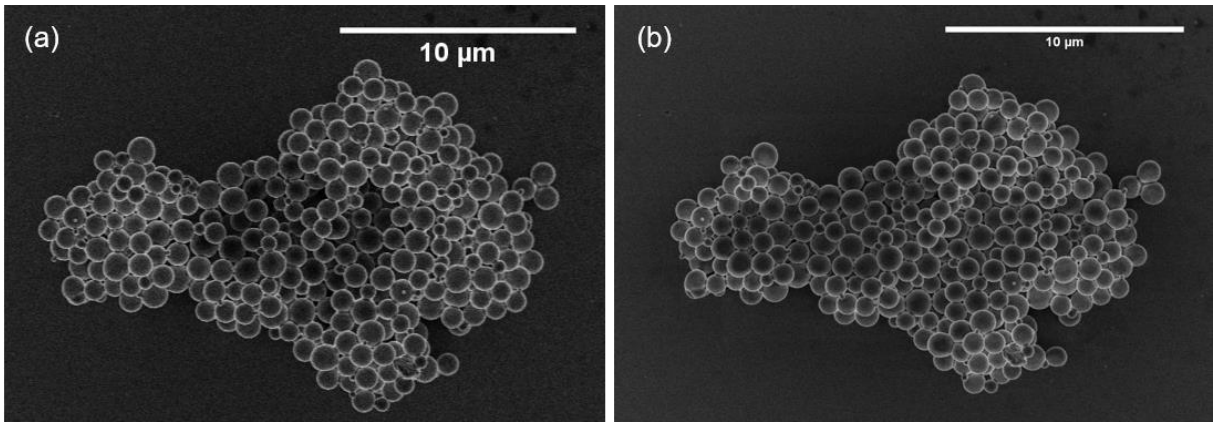

Figure 5.1.12. FESEM micrographs of **3c** microspheres obtained from a reaction via ***Route B***, a) immediately upon synthesis, b) after six weeks in air.

Fourier Transformation Infrared Spectroscopy (FTIR)

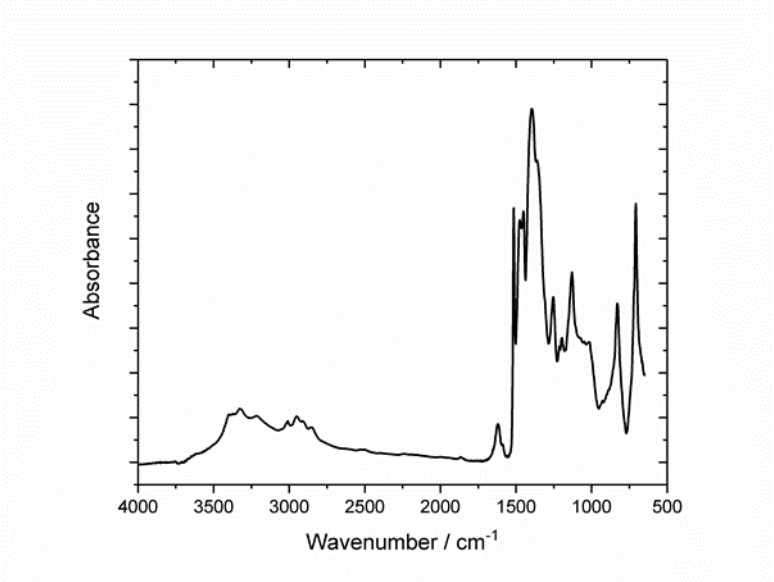

Figure 5.1.13. FTIR spectrum of **3a**.

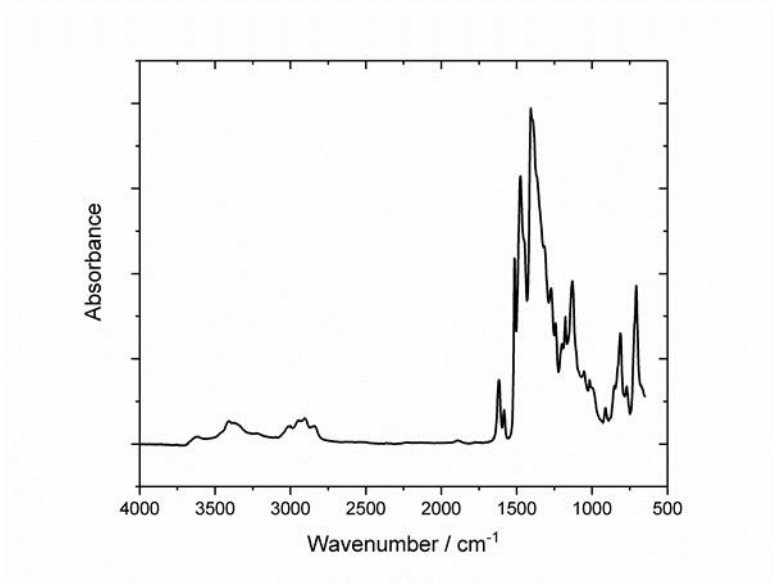

Figure 5.1.14. FTIR spectrum of **3b**.

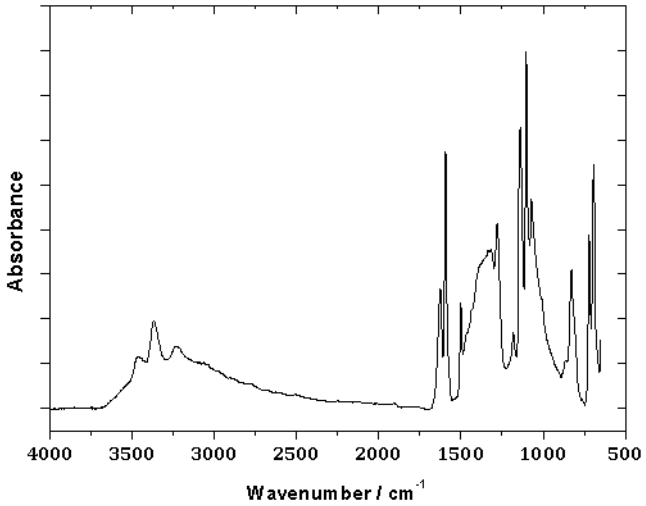

Figure 5.1.15. FTIR spectrum of **3c** obtained from a reaction via ***Route A***.

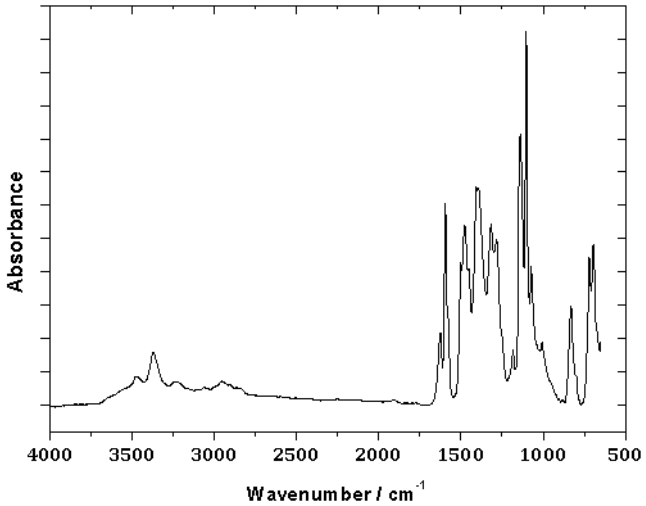

Figure 5.1.16. FTIR spectrum of **3c** obtained from a reaction via ***Route B***.

Dynamic Light Scattering (DLS)

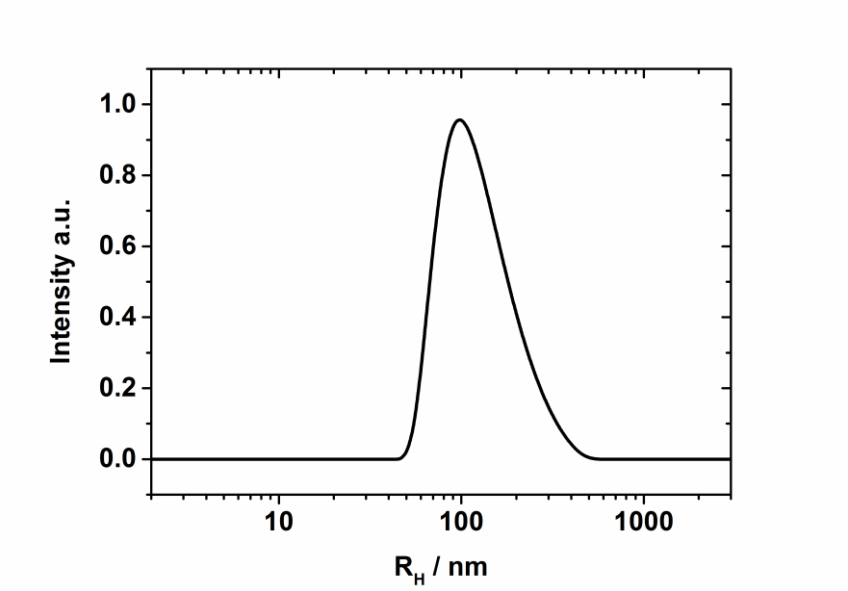

Figure 5.1.17. Intensity weighted size distribution of particles of **3c** dispersed in acetonitrile from DLS obtained from a reaction via ***Route A***.

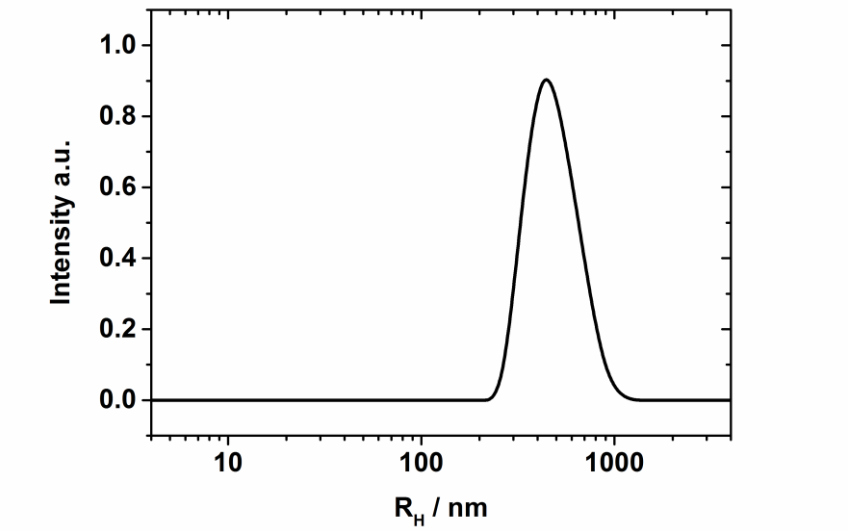

Figure 5.1.18. Intensity weighted size distribution of particles of **3c** dispersed in acetonitrile from DLS obtained from a reaction via ***Route B***.

Thermogravimetric Analysis (TGA)

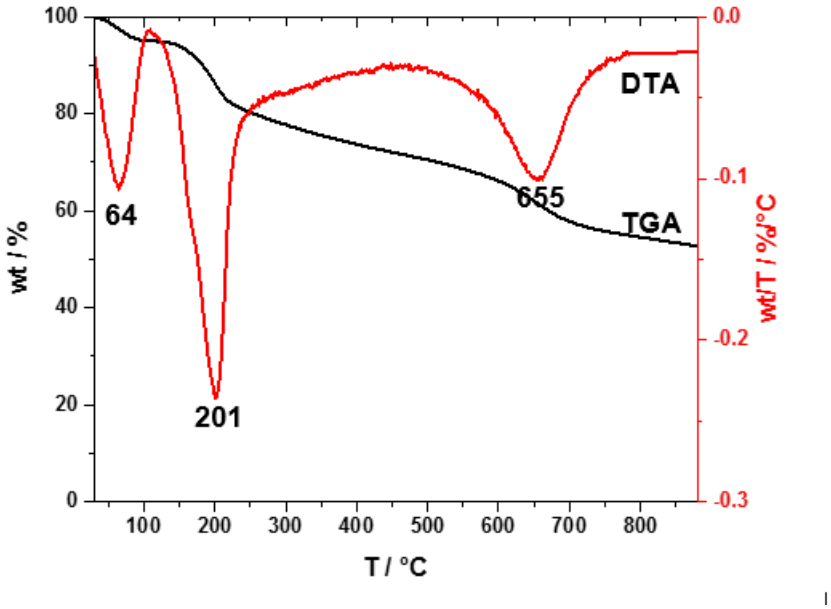

Figure 5.1.19. TGA (black) and DTA (red) curves of **3a** up to 880 °C in N_2 atmosphere.

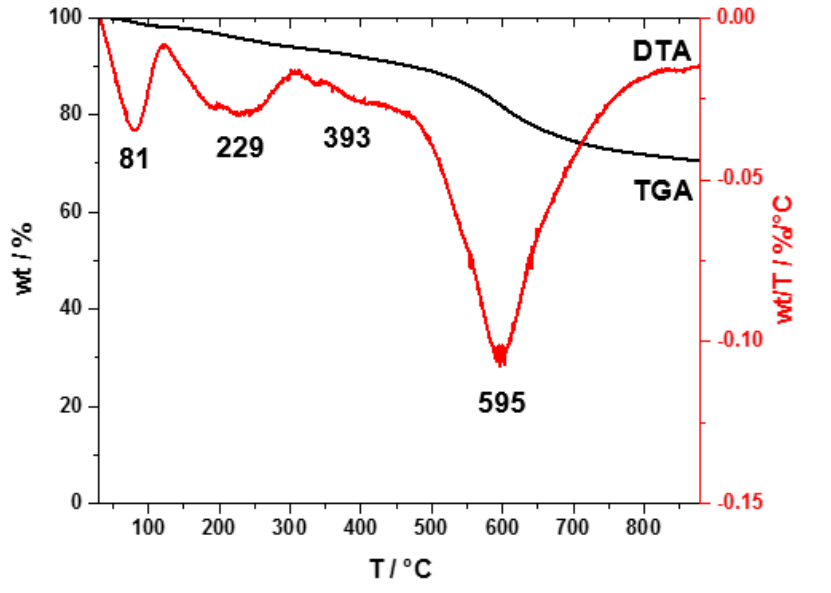

Figure 5.1.20. TGA (black) and DTA (red) curves of **3b** up to 880 °C in N_2 atmosphere.

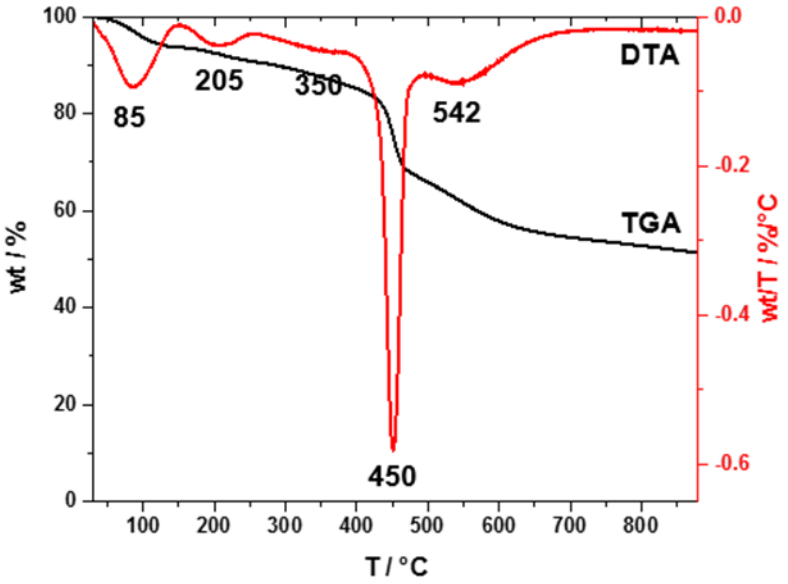

Figure 5.1.21. TGA (black) and DTA (red) curves of **3c** microspheres obtained from a reaction via ***Route A*** up to 880 °C in N_2 atmosphere.

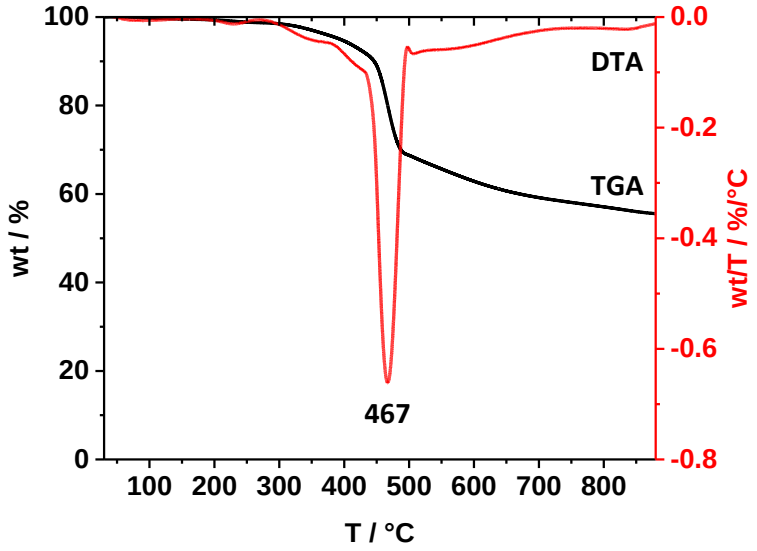

Figure 5.1.22. TGA (black) and DTA (red) curves of **3c** microspheres obtained from a reaction via ***Route A*** up to 880 °C in N_2 atmosphere after pretreatment in vacuo at 160 °C for 16 h.

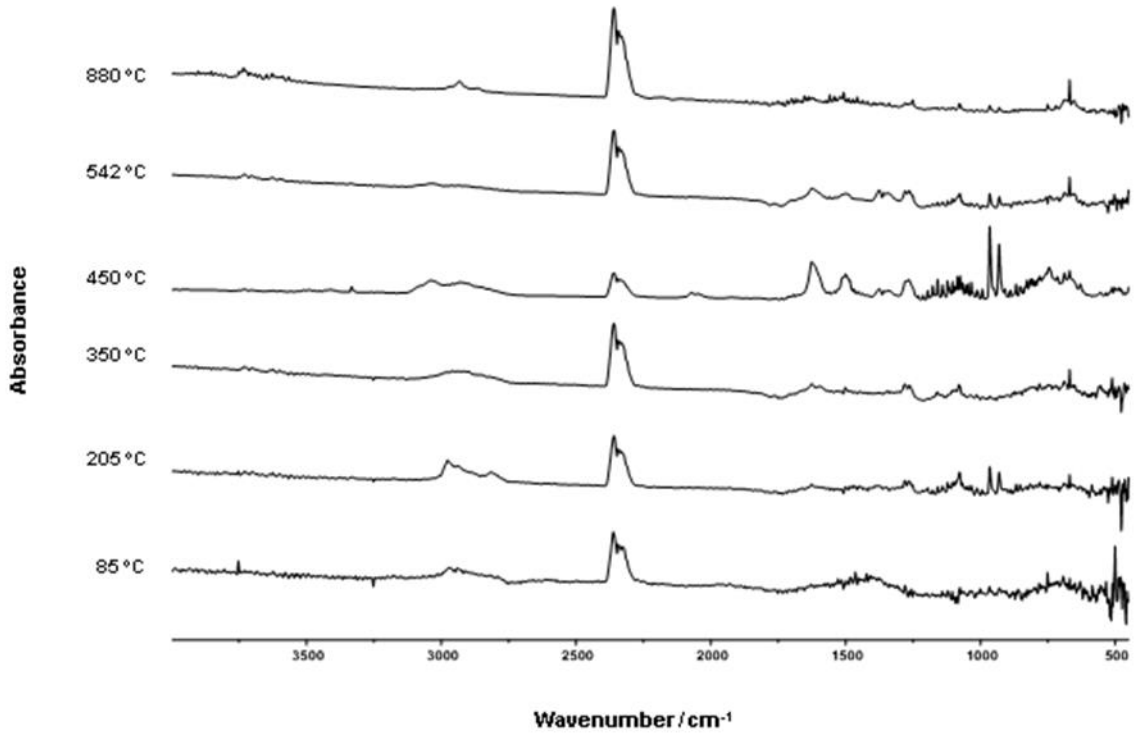

Figure 5.1.23. FTIR spectra of **3c** microspheres obtained from a reaction via ***Route A*** from TGA-coupled-FTIR analysis in N_2 atmosphere.

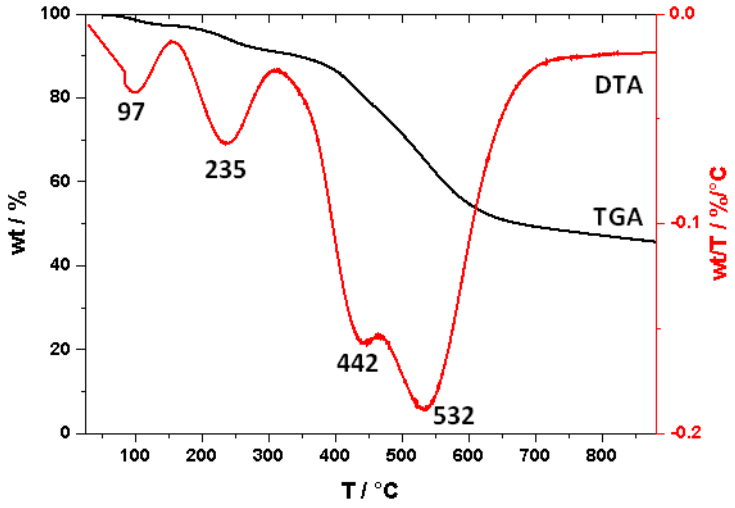

Figure 5.1.24. TGA (black) and DTA (red) curves of **3c** microspheres obtained from a reaction via ***Route B*** up to 880 °C in N_2 atmosphere.

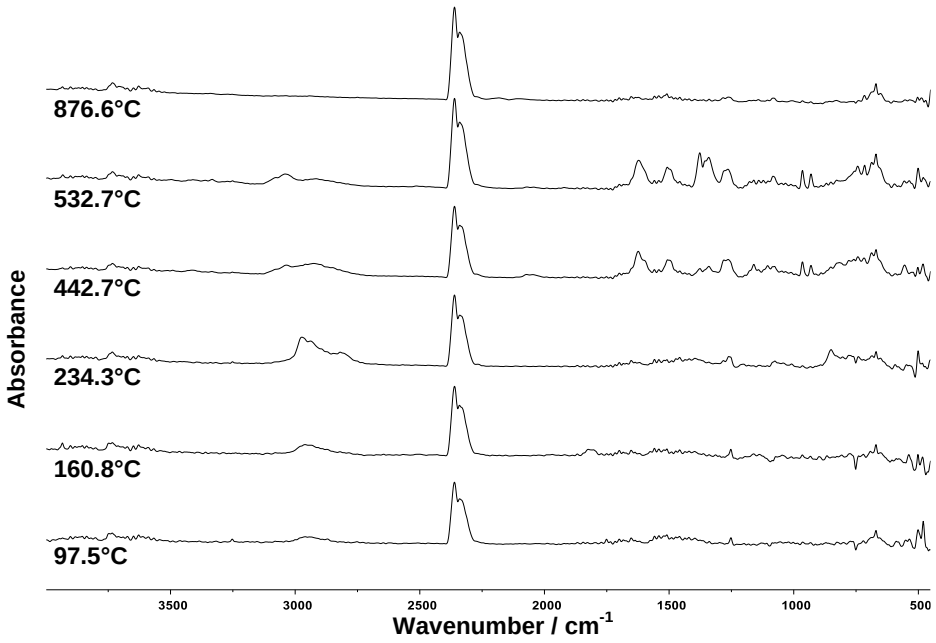

Figure 5.1.25. FTIR spectra of **3c** microspheres obtained from a reaction via ***Route B*** from TGA-coupled-FTIR analysis in N_2 atmosphere.

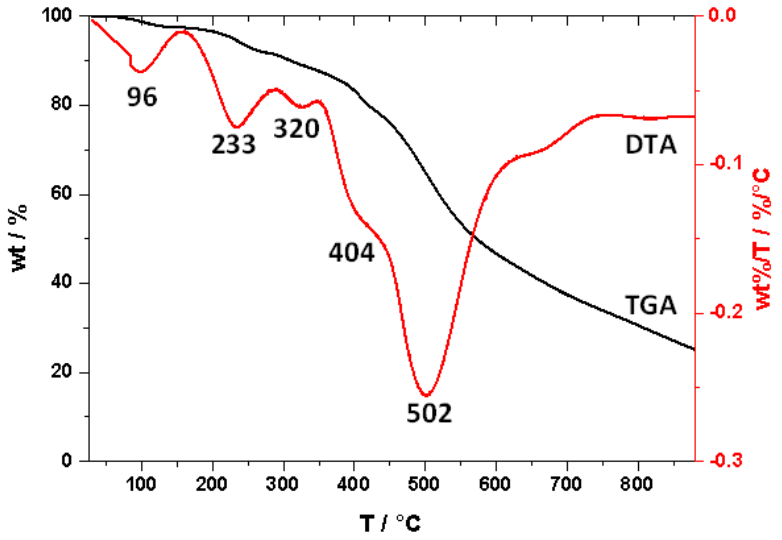

Figure 5.1.26. TGA (black) and DTA (red) curves of **3c** microspheres obtained from a reaction via ***Route B*** up to 880 °C in synthetic air.

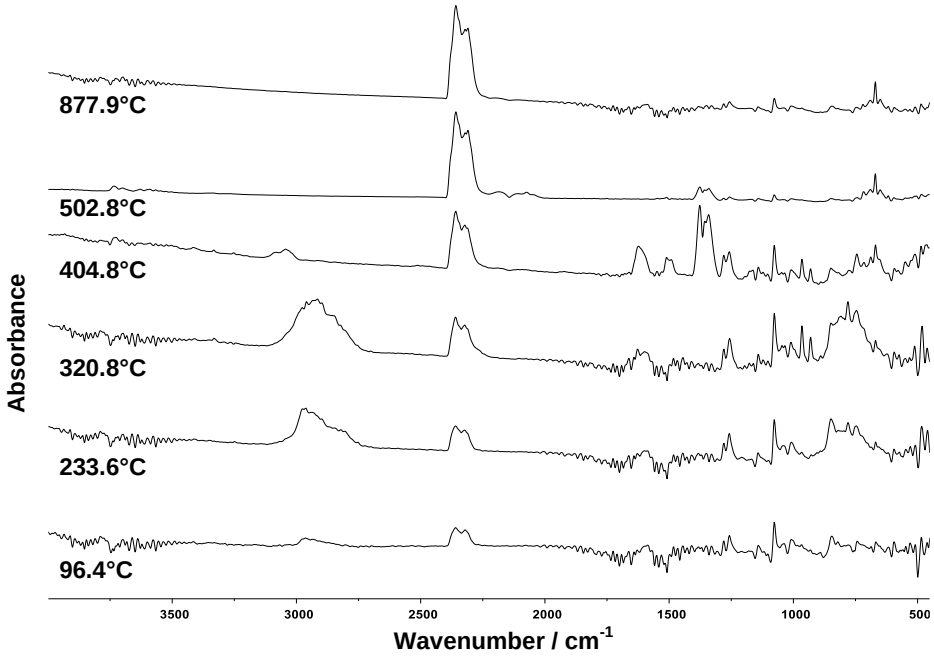

Figure 5.1.27. FTIR spectra of **3c** microspheres obtained from a reaction via ***Route B*** from TGA-coupled-FTIR analysis in synthetic air.

NMR Spectra

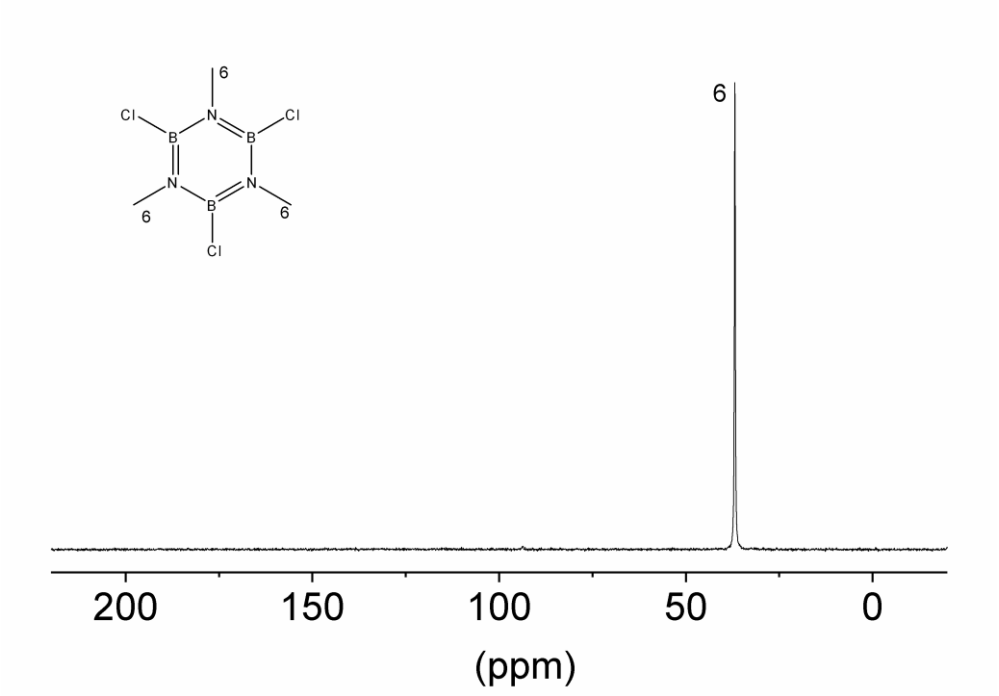

Figure 5.1.28. ^{13}C CPMAS spectrum of **1**.

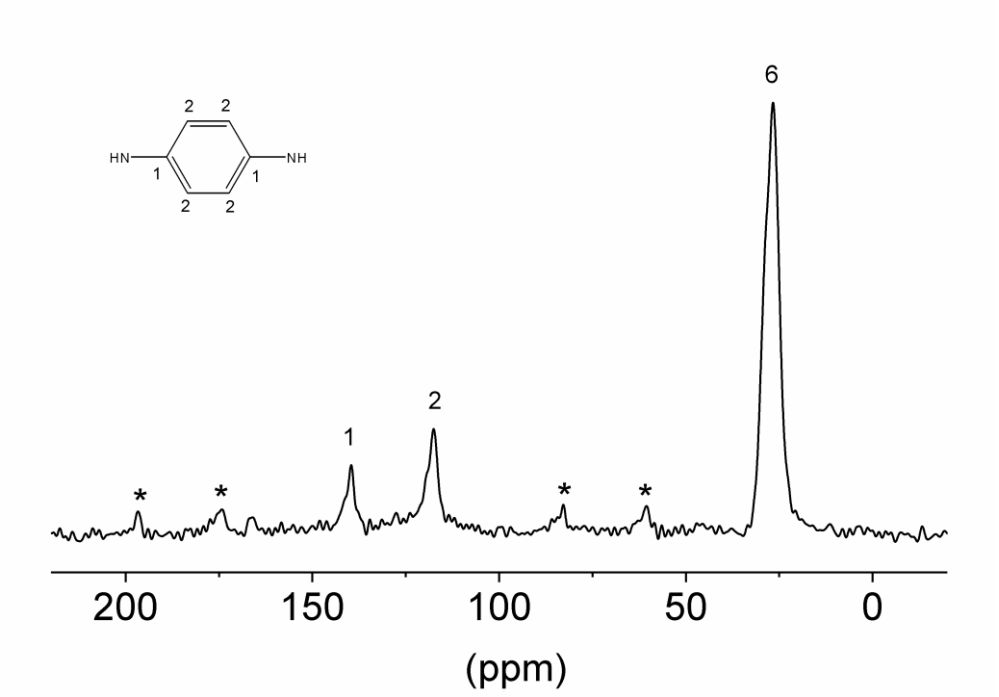

Figure 5.1.29. ^{13}C CPMAS spectrum of **3a**. The signals marked with asteriks are spinning sidebands. The signal labeled with 6 represents the N$\underline{C}H_3$ signal from the borazine ring in **3a**.

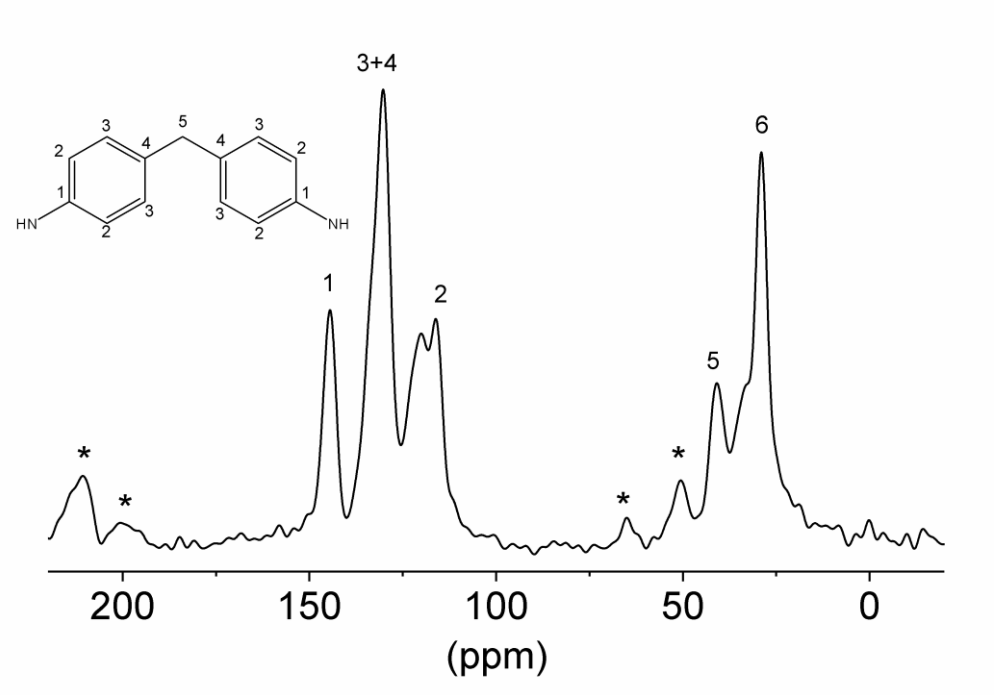

Figure 5.1.30. ^{13}C CPMAS spectrum of **3b**. The signals marked with asteriks are spinning sidebands. The signal labeled with 6 represents the N<u>C</u>H$_3$ signal from the borazine ring in **3b**.

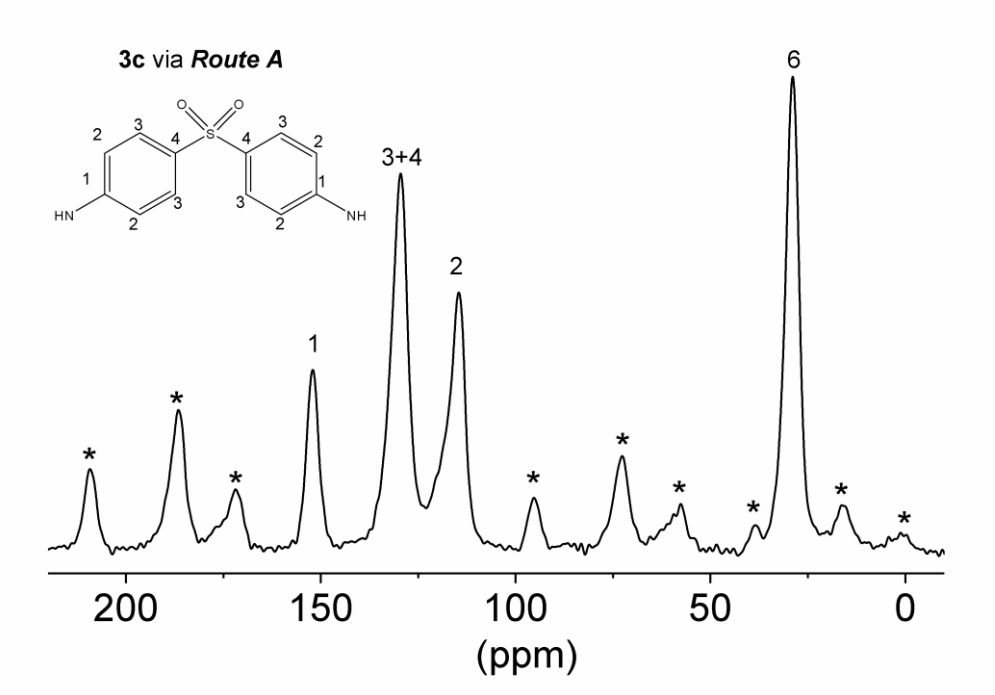

Figure 5.1.31. ^{13}C CPMAS spectrum of **3c** via ***Route A***. The signals marked with asteriks are spinning sidebands. The signal labeled with 6 represents the N<u>C</u>H$_3$ signal from the borazine ring in **3c**.

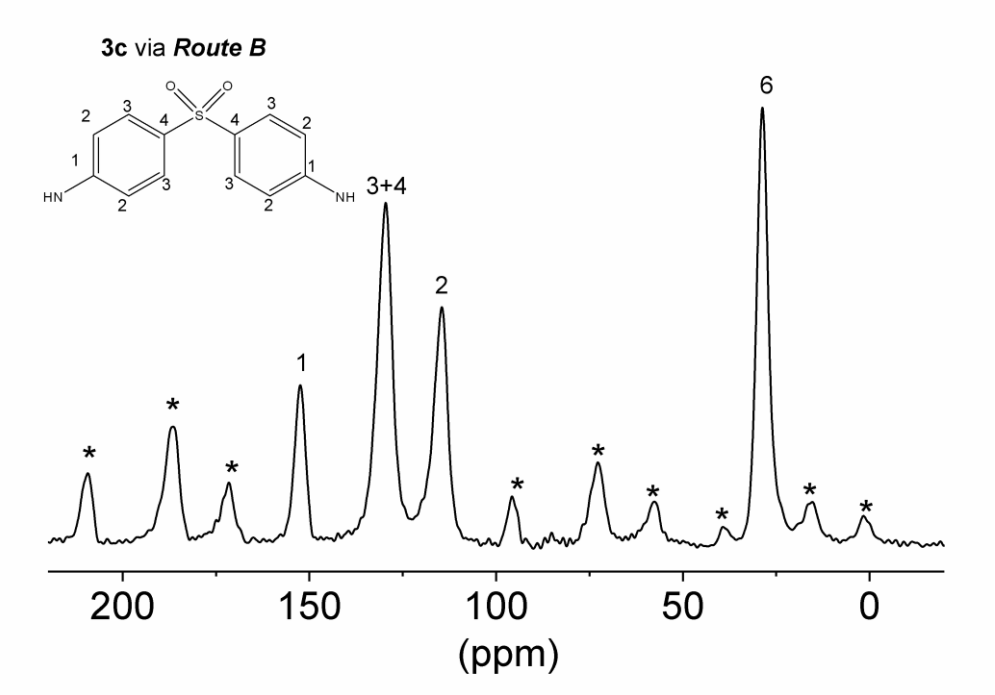

Figure 5.1.32. ^{13}C CPMAS spectrum of **3c** via ***Route B***. The signals marked with asteriks are spinning sidebands. The signal labeled with 6 represents the N<u>C</u>H$_3$ signal from the borazine ring in **3c**.

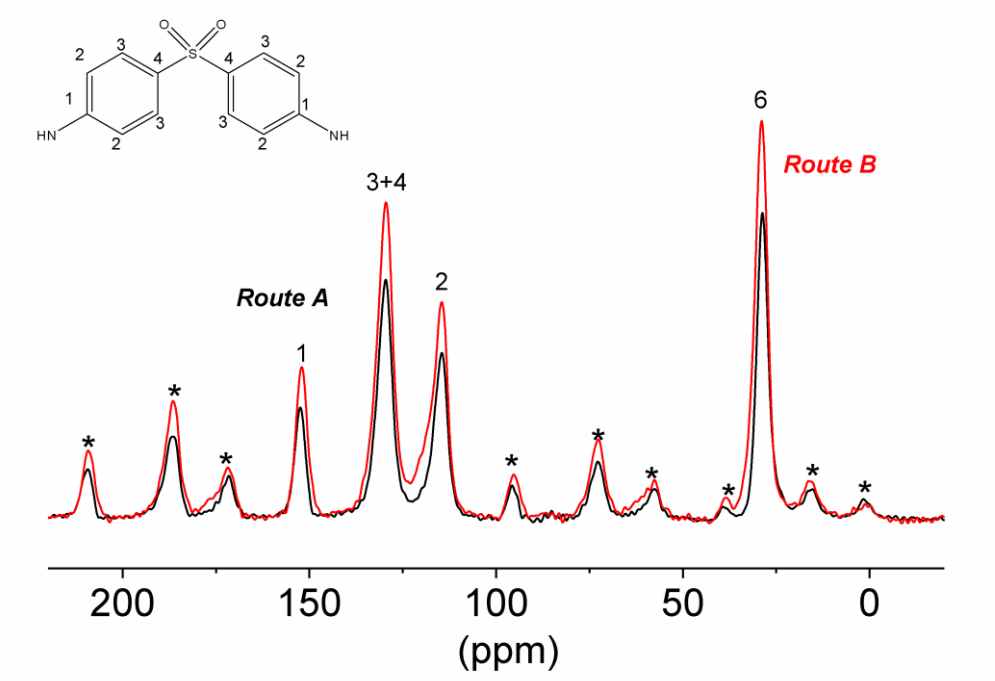

Figure 5.1.33. ^{13}C CPMAS spectra of the polymers **3c** via ***Route A*** and ***B***. The intensities of all signals of polymer **3c** via both routes are equal but in the present figure higher due to multiplication by the same factor for better view. The signals marked with asteriks are spinning sidebands. The signal labeled with 6 represents the N<u>C</u>H$_3$ signal from the borazine ring in **3c**.

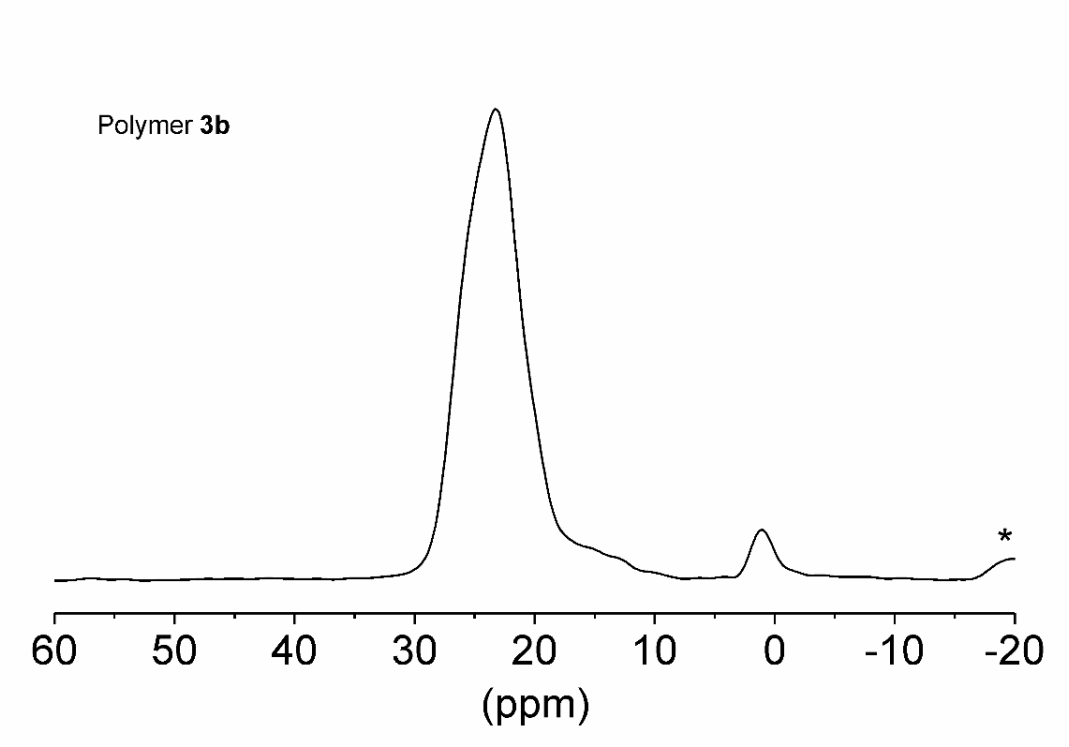

Figure 5.1.34. ^{11}B DPMAS spectrum of **3b**. The signals marked with asteriks are spinning sidebands.

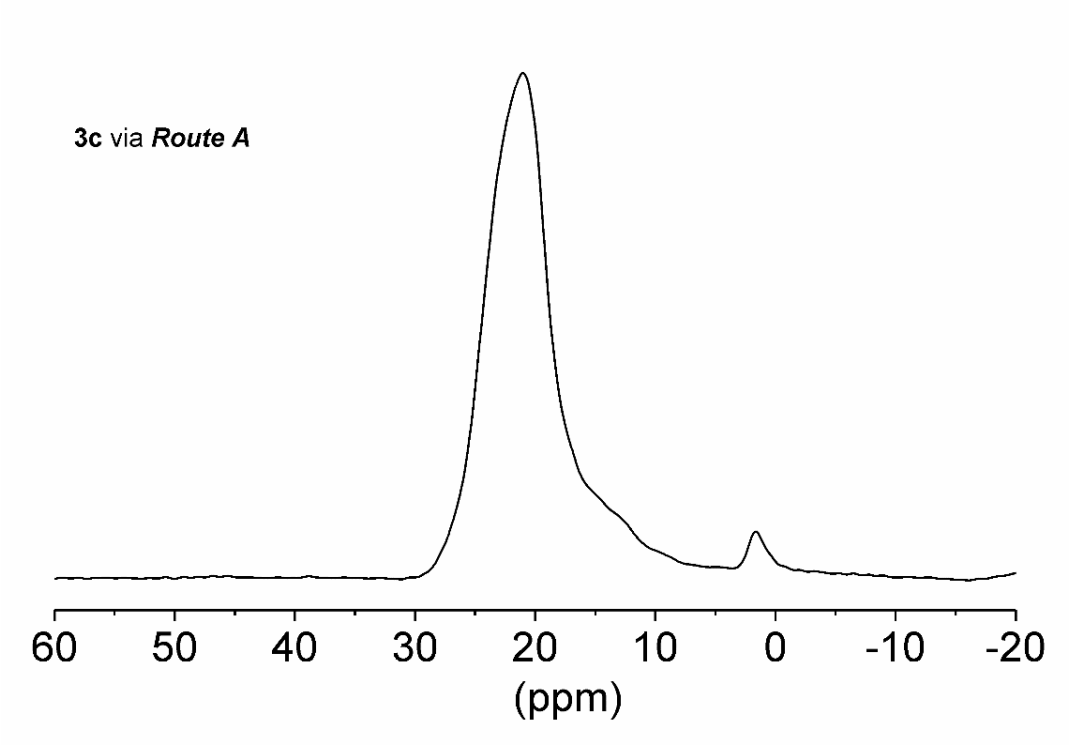

Figure 5.1.35. ^{11}B DPMAS spectrum of **3c** via ***Route A***. The signals marked with asteriks are spinning sidebands.

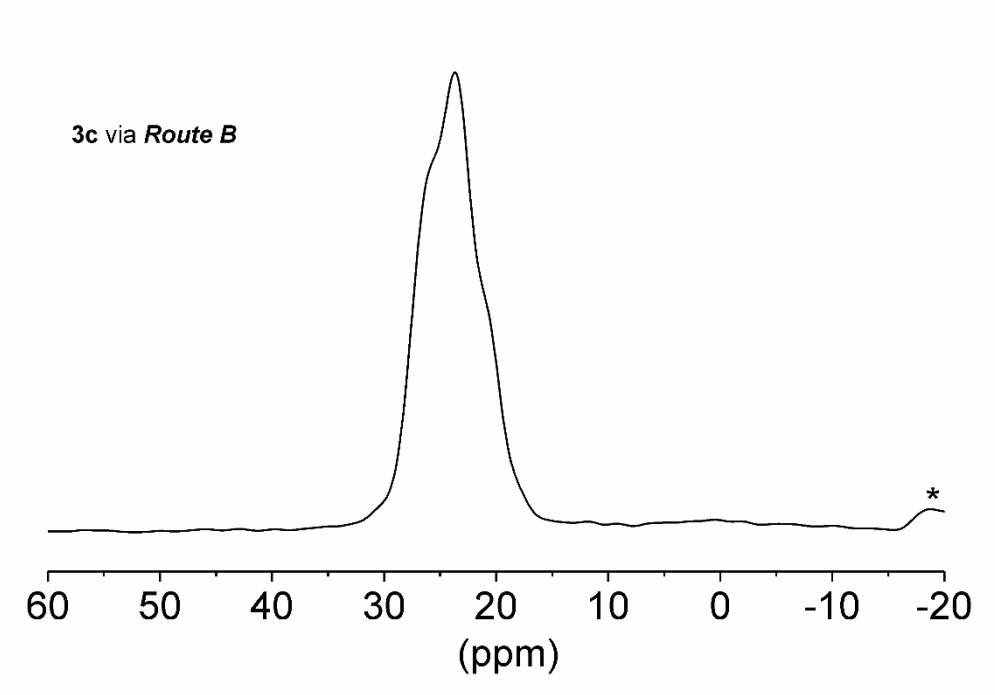

Figure 5.1.36. ^{11}B DPMAS spectrum of **3c** via ***Route B***. The signals marked with asteriks are spinning sidebands.

5.2 Difuryl(supermesityl)borane: A Versatile Building Block for Extended π-Conjugated Materials

NMR spectra

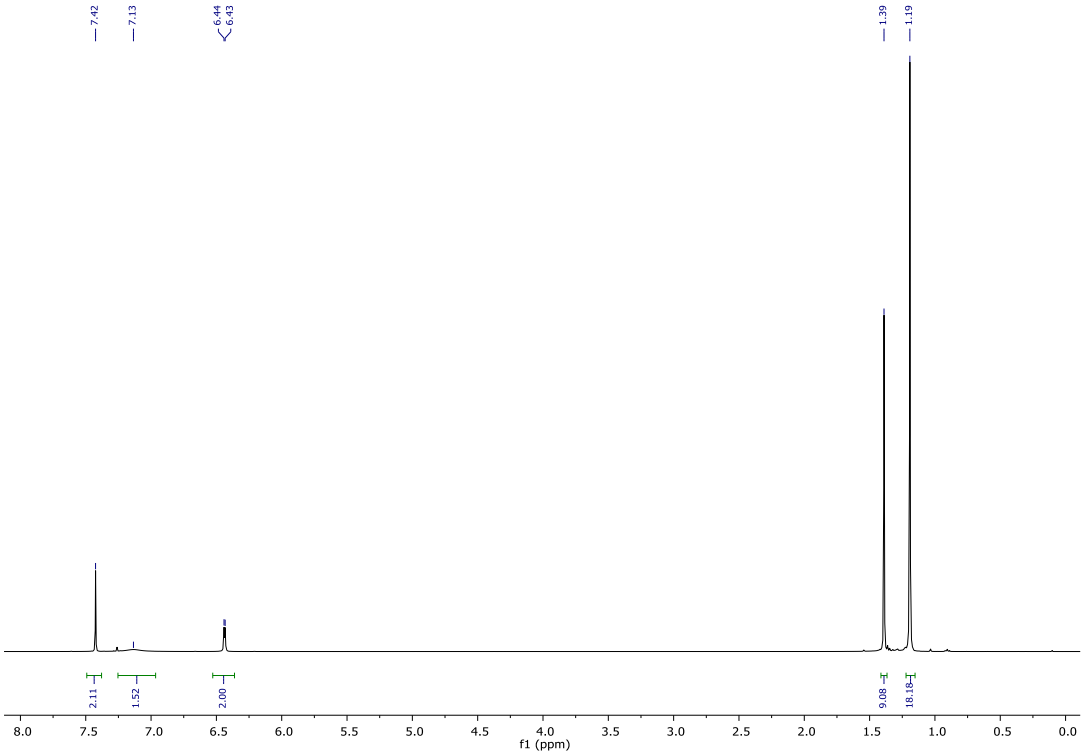

Figure 5.2.1. ^{1}H NMR spectrum of **2a** (in $CDCl_3$, 400 MHz).

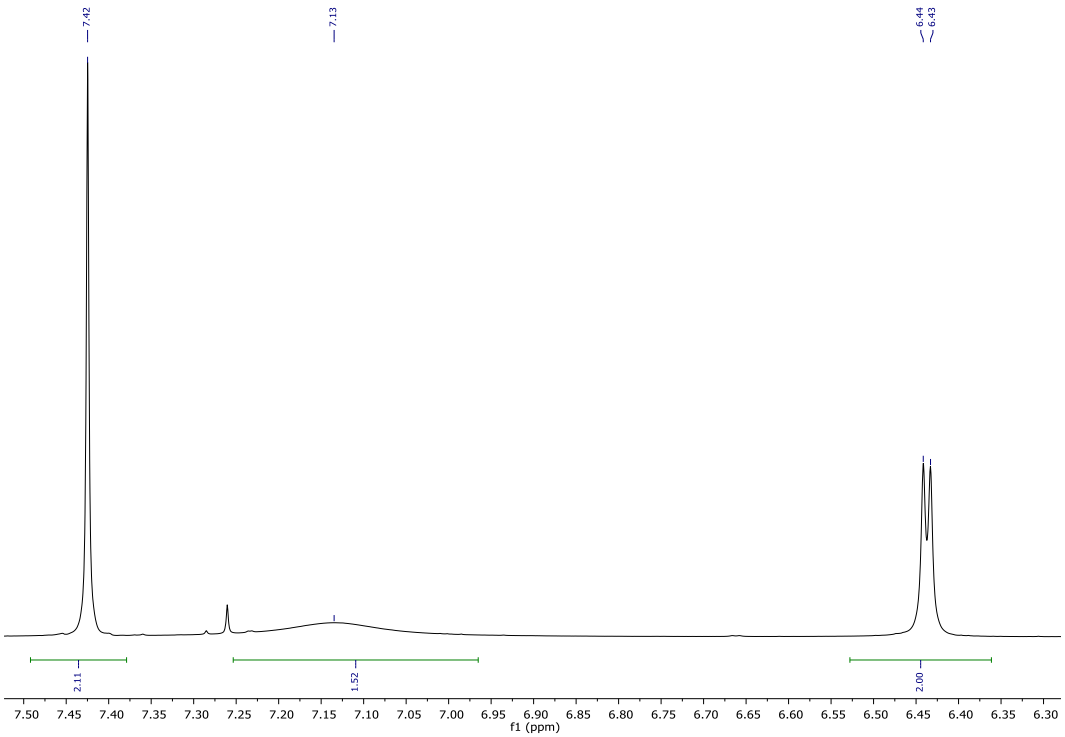

Figure 5.2.2. Detail (aromatic region) of the ^{1}H NMR spectrum of **2a** (in $CDCl_3$, 400 MHz).

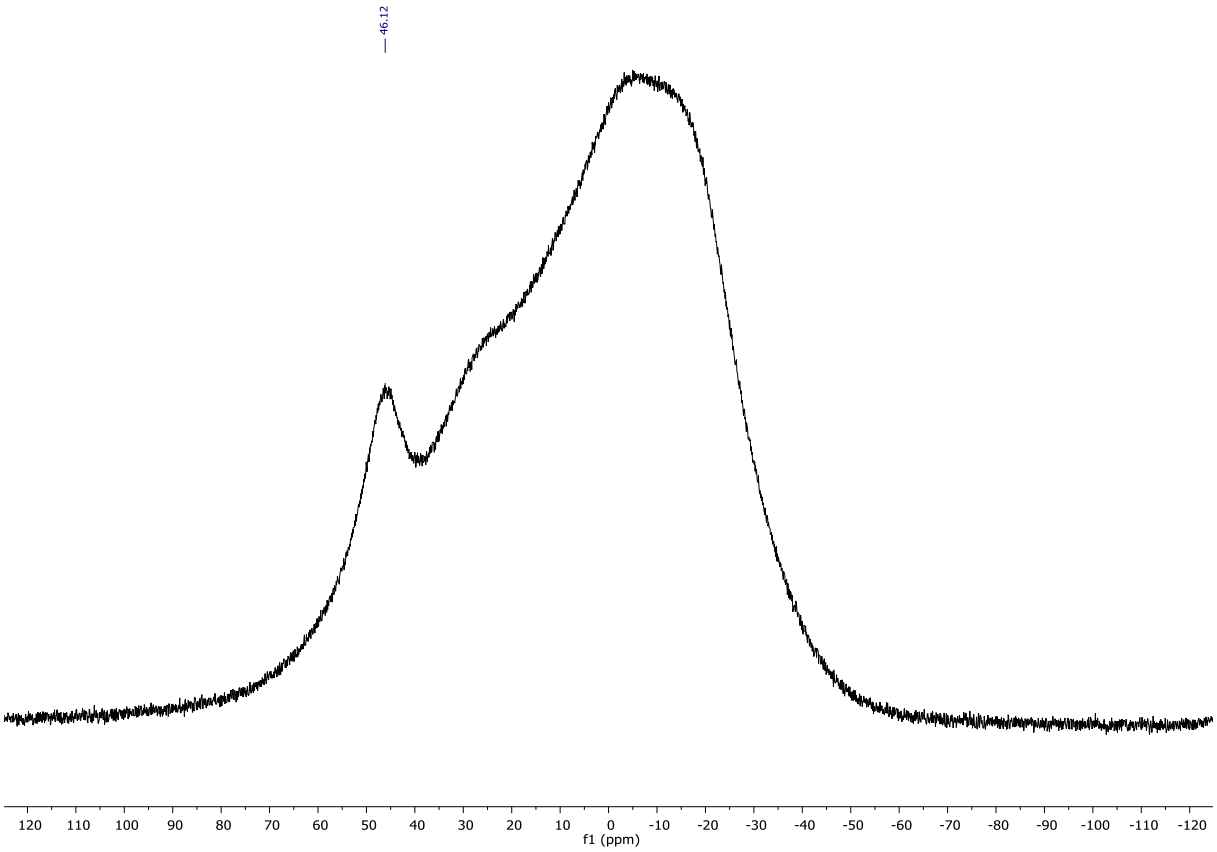

Figure 5.2.3. $^{11}B\{^{1}H\}$ NMR spectrum of **2a** (in $CDCl_3$, 128 MHz).

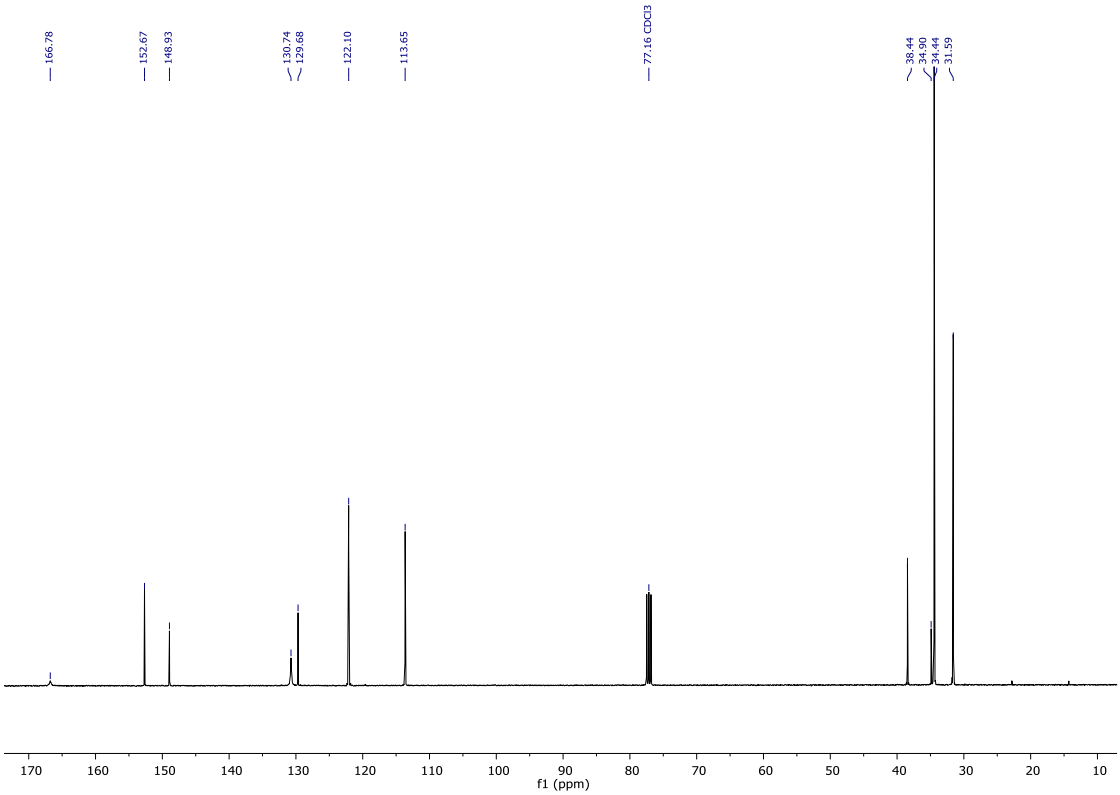

Figure 5.2.4. ^{13}C NMR spectrum of **2a** (in $CDCl_3$, 101 MHz).

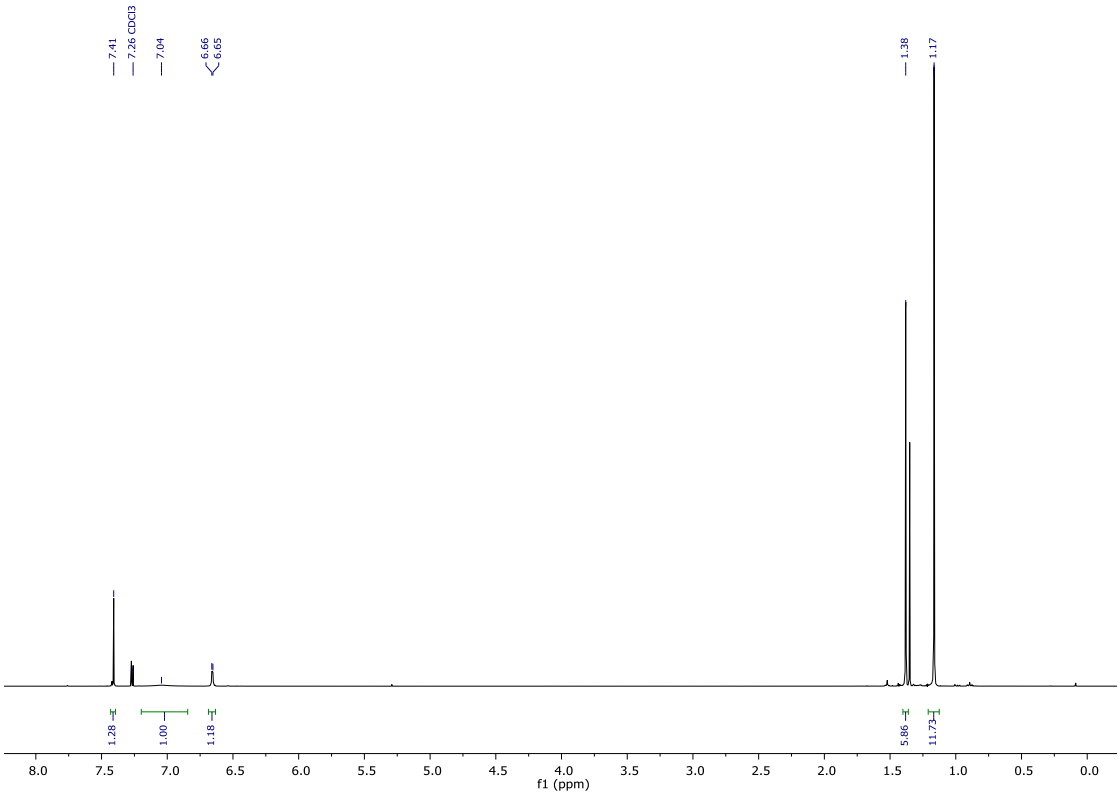

Figure 5.2.5. ^{1}H NMR spectrum of **2b** (in $CDCl_3$, 400 MHz).

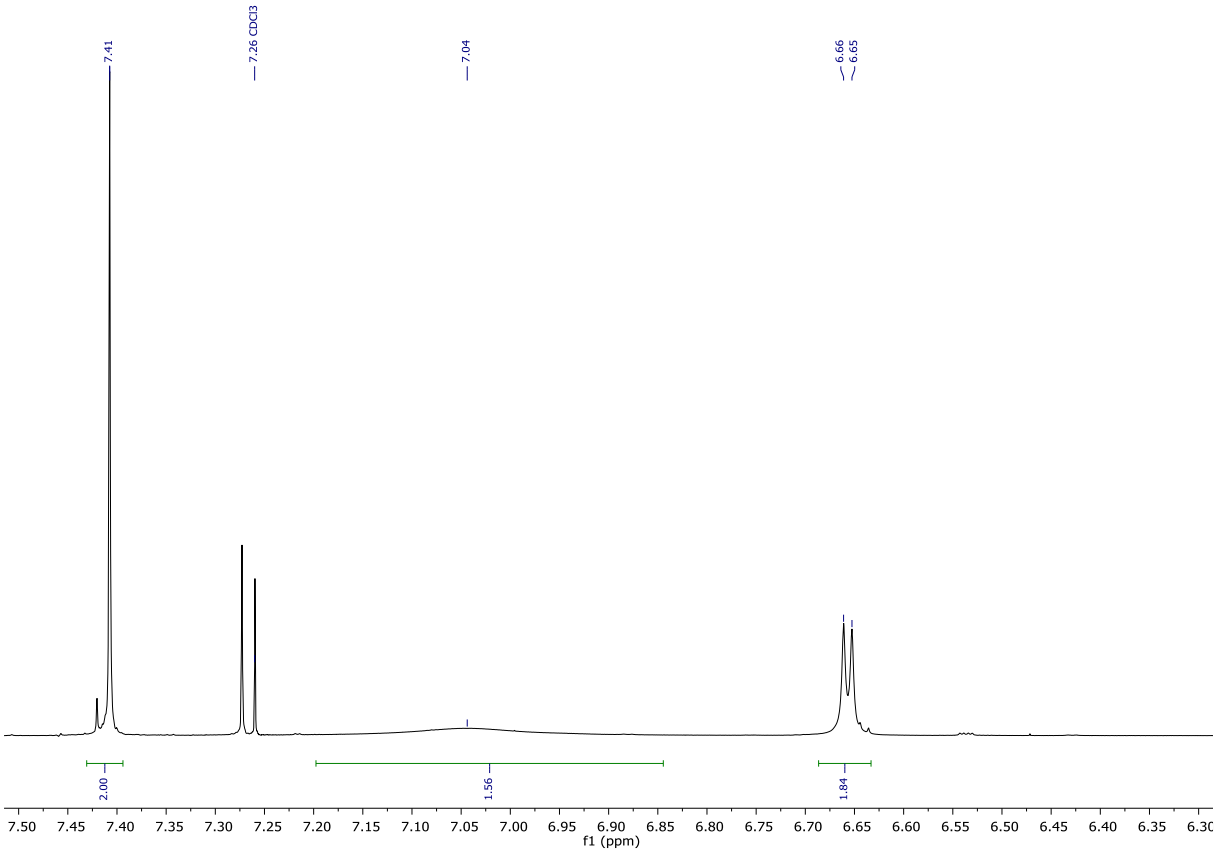

Figure 5.2.6. Detail (aromatic region) of the ^{1}H NMR spectrum of **2b** (in $CDCl_3$, 400 MHz).

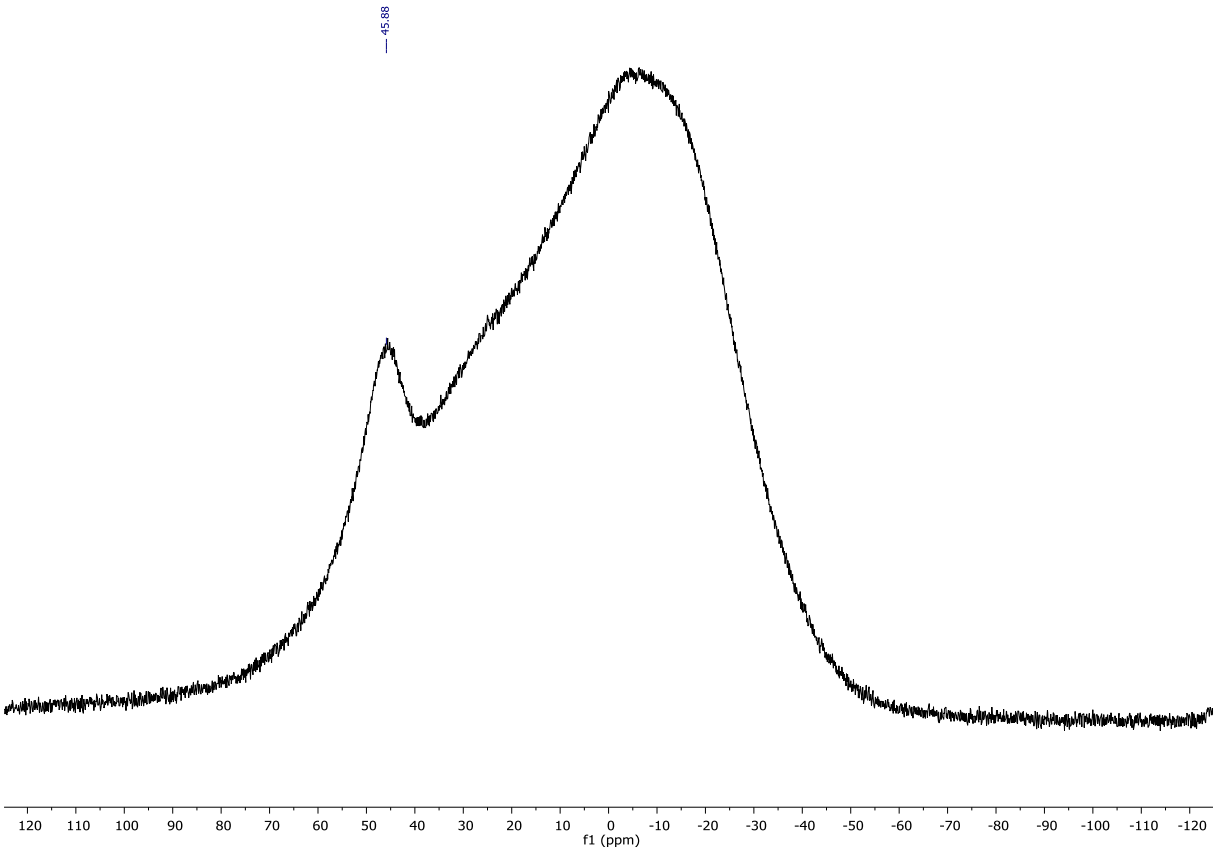

Figure 5.2.7. $^{11}B\{^{1}H\}$ NMR spectrum of **2b** (in $CDCl_3$, 128 MHz).

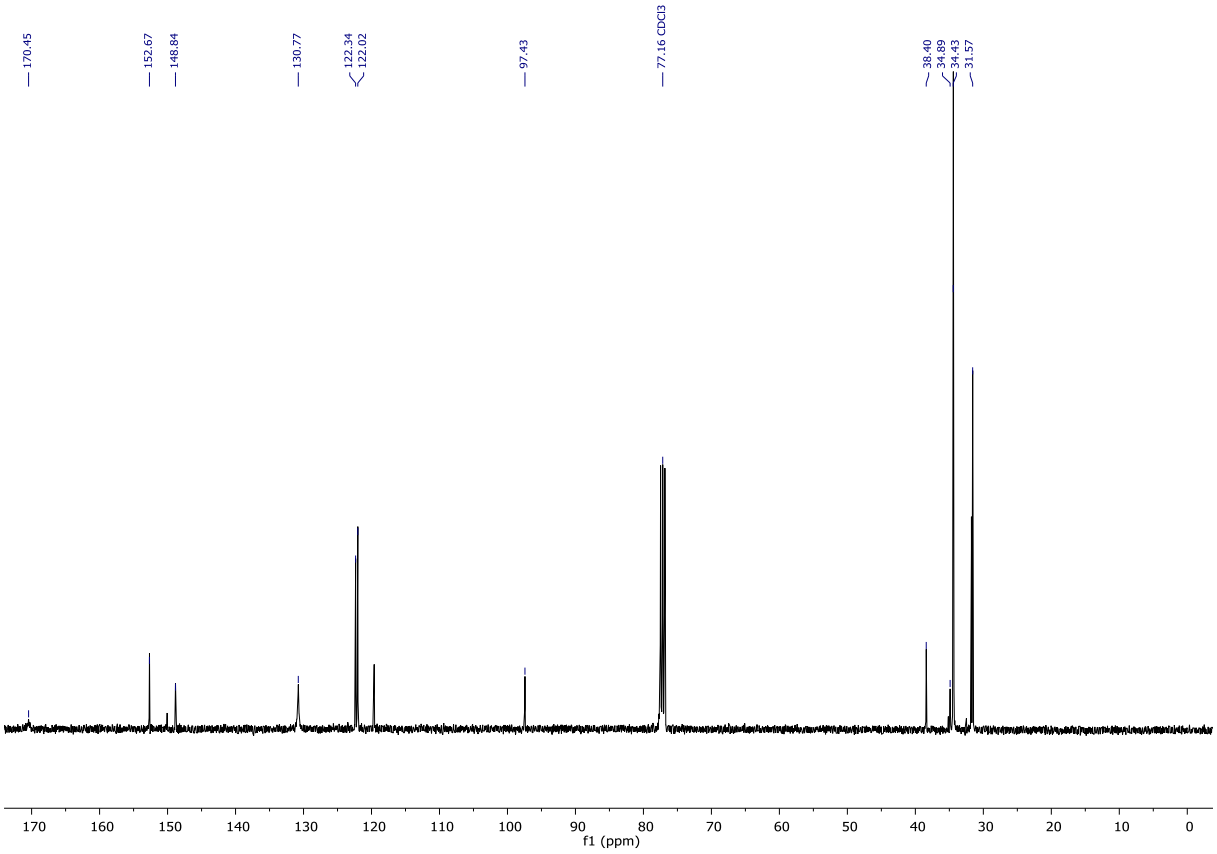

Figure 5.2.8. ^{13}C NMR spectrum of **2b** (in $CDCl_3$, 101 MHz).

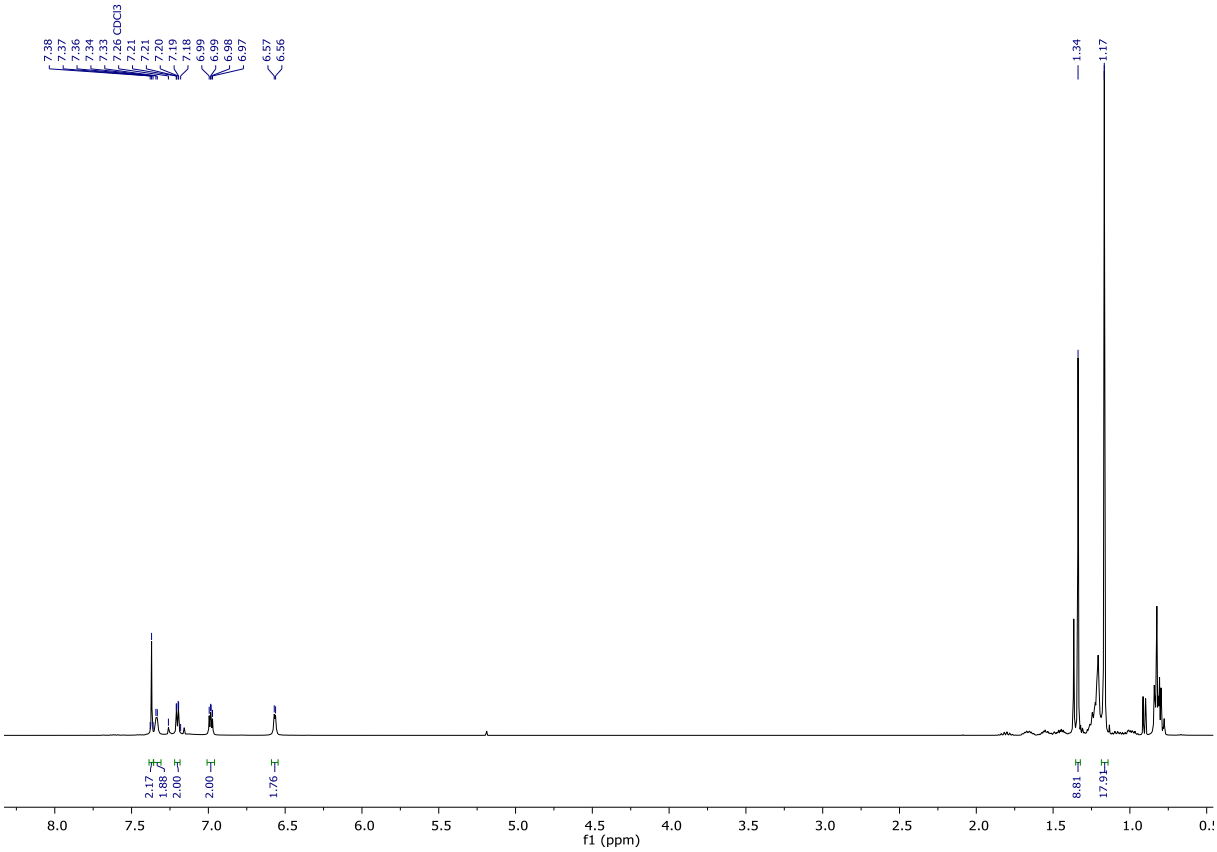

Figure 5.2.9. ^{1}H NMR spectrum of **3** (in $CDCl_3$, 400 MHz).

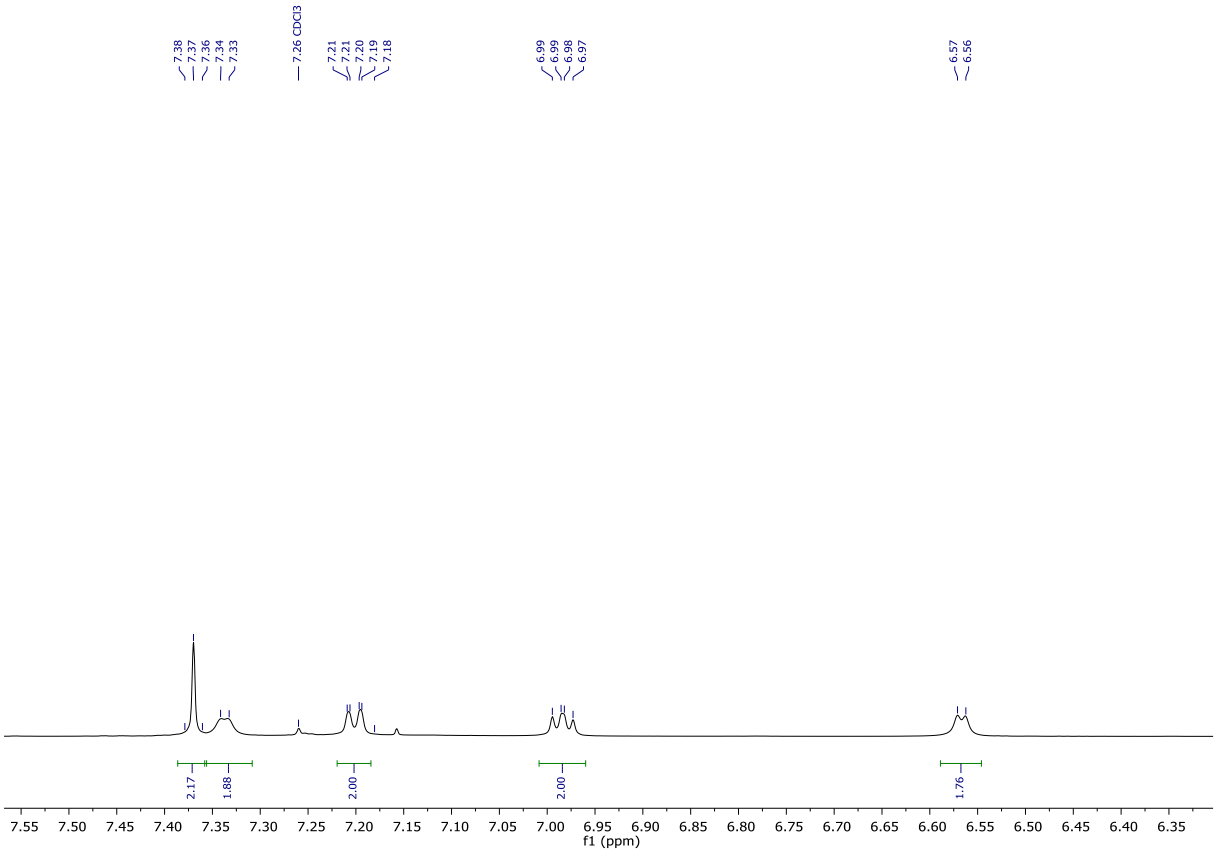

Figure 5.2.10. Detail (aromatic region) of the ^{1}H NMR spectrum of **3** (in $CDCl_3$, 400 MHz).

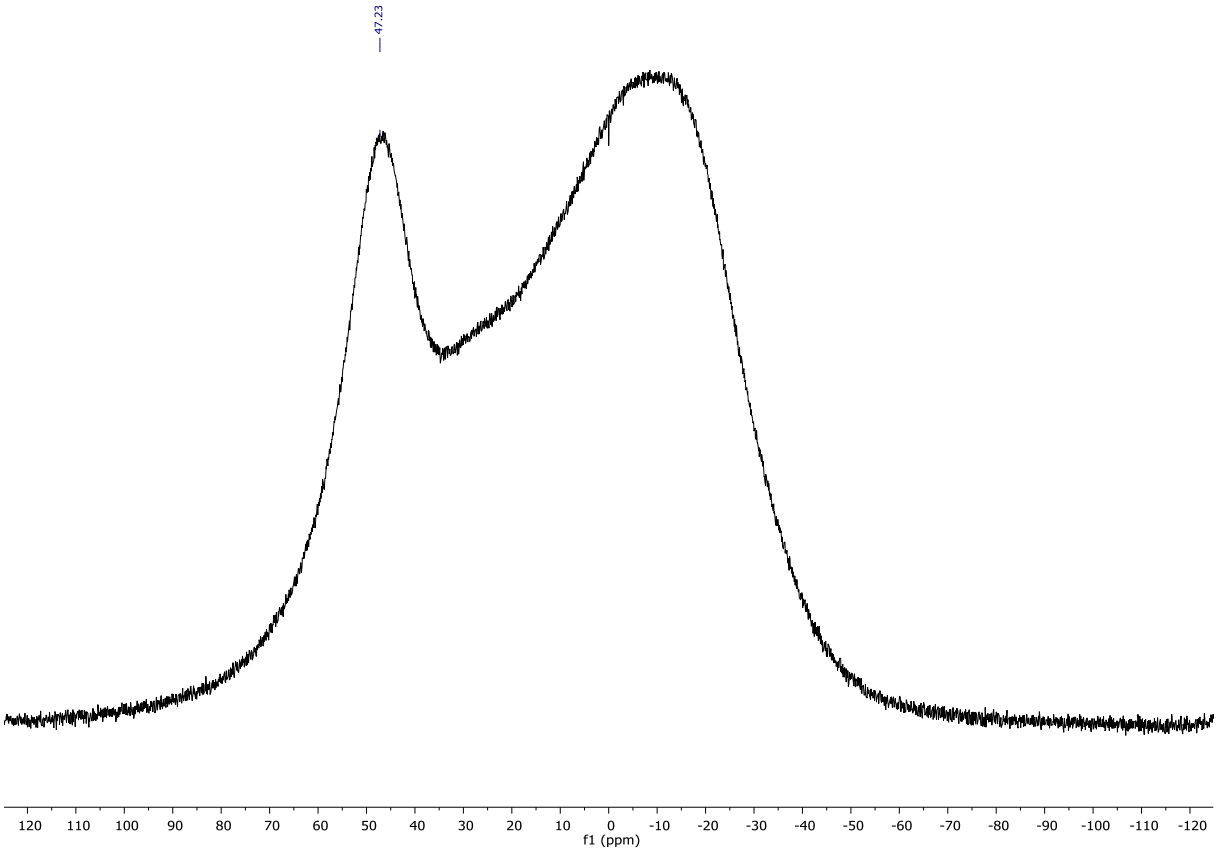

Figure 5.2.11. $^{11}B\{^{1}H\}$ NMR spectrum of **3** (in $CDCl_3$, 128 MHz).

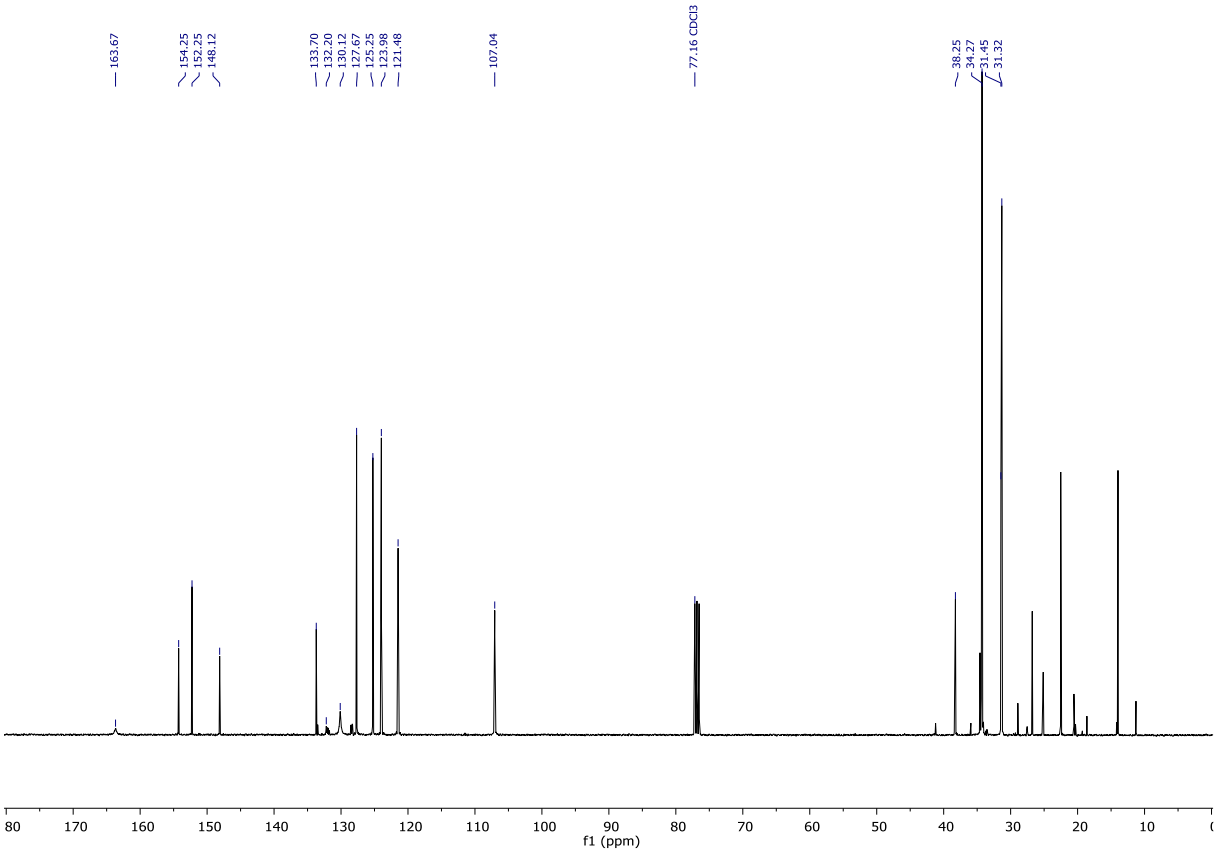

Figure 5.2.12. ^{13}C NMR spectrum of **3** (in $CDCl_3$, 101 MHz).

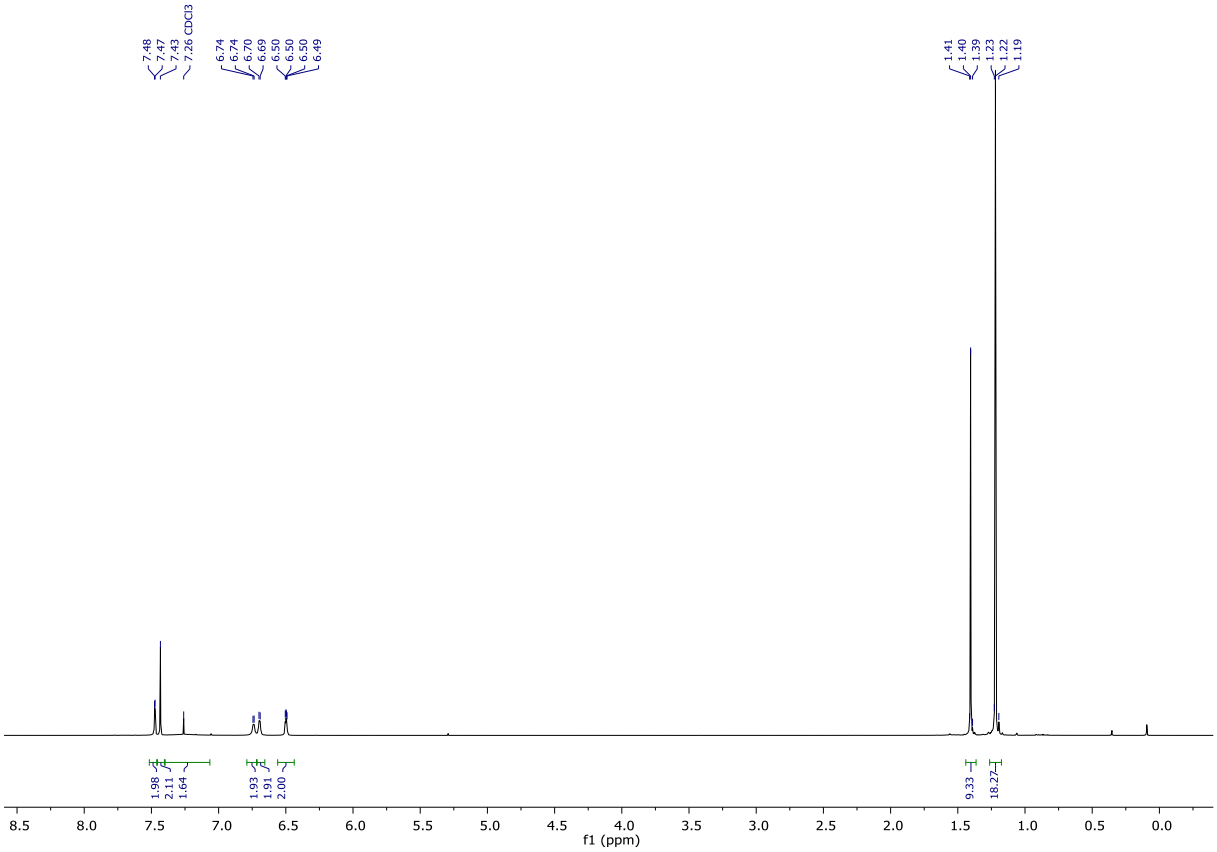

Figure 5.2.13. ^{1}H NMR spectrum of **4** (in $CDCl_3$, 400 MHz).

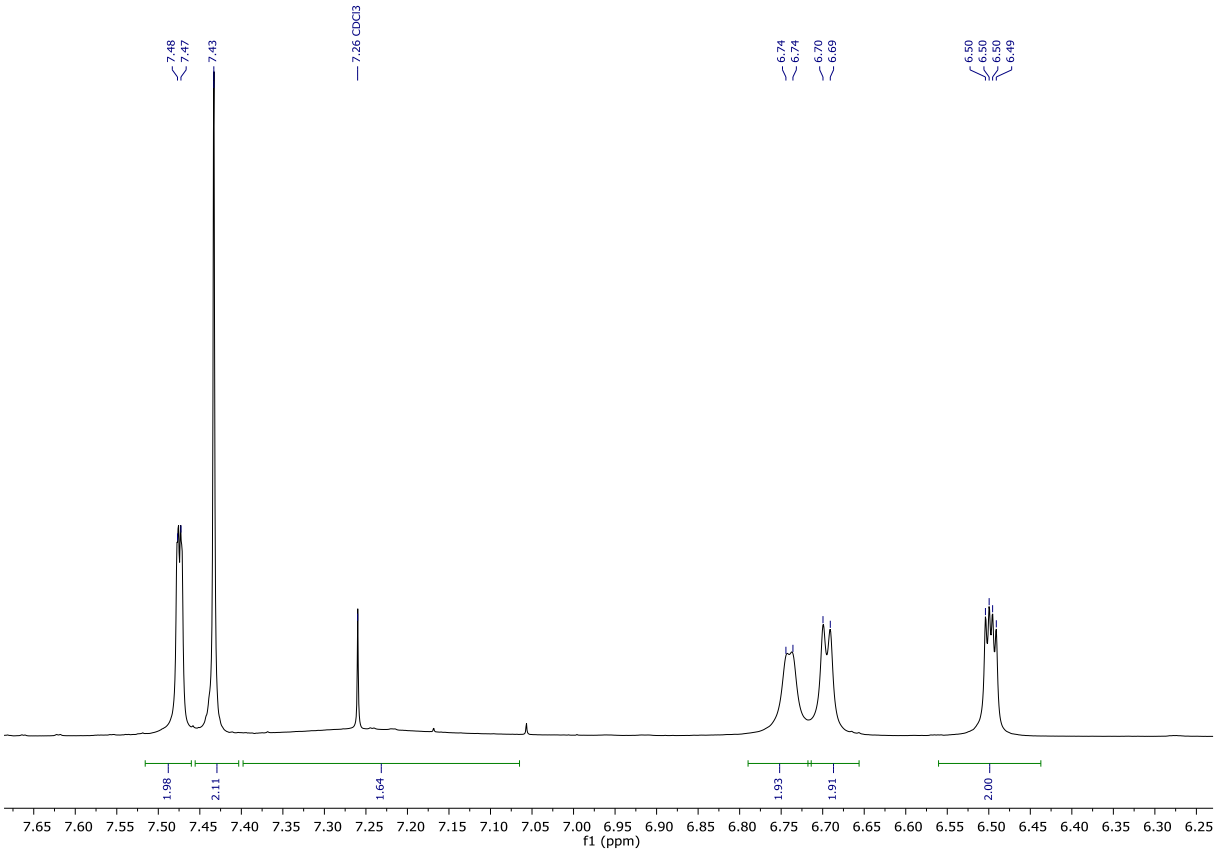

Figure 5.2.14. Detail (aromatic region) of the ^{1}H NMR spectrum of **4** (in $CDCl_3$, 400 MHz).

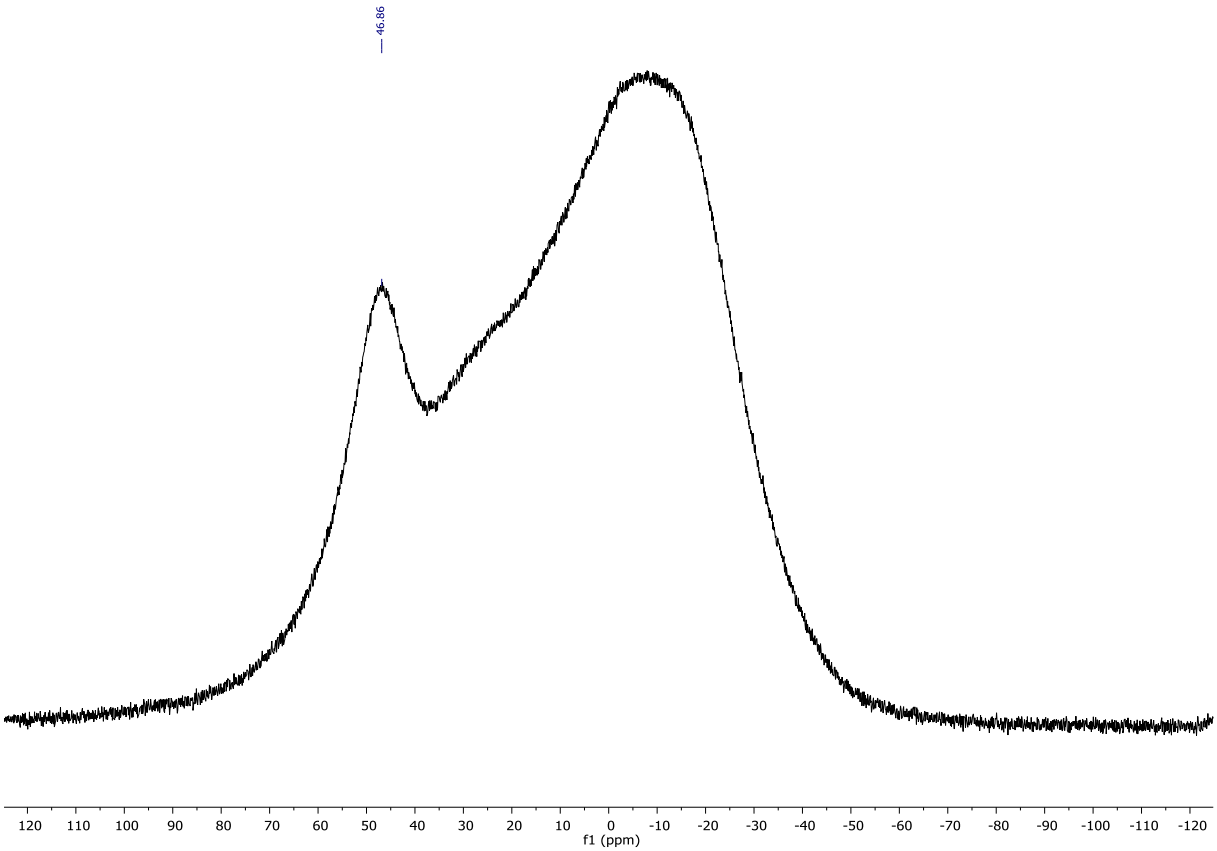

Figure 5.2.15. $^{11}B\{^{1}H\}$ NMR spectrum of **4** (in $CDCl_3$, 128 MHz).

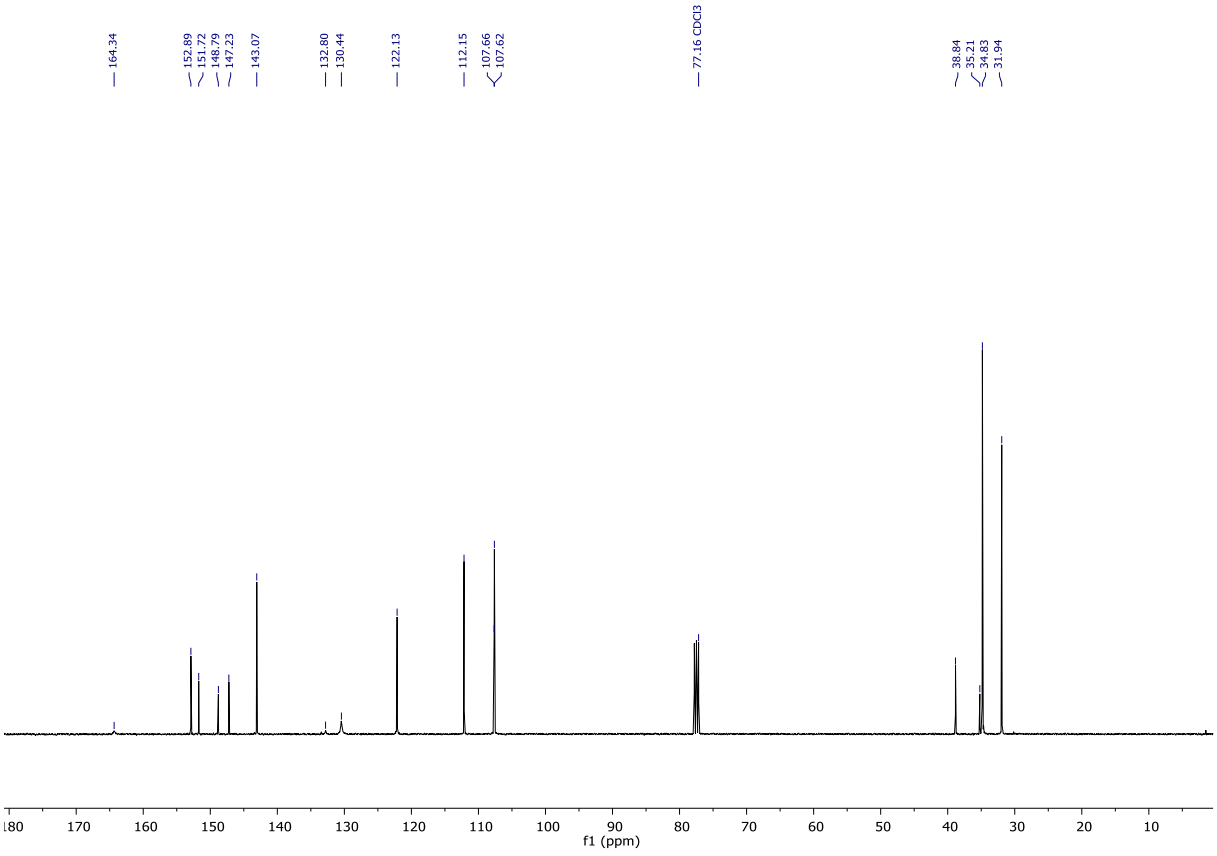

Figure 5.2.16. ^{13}C NMR spectrum of **4** (in $CDCl_3$, 101 MHz).

UV–vis Spectra

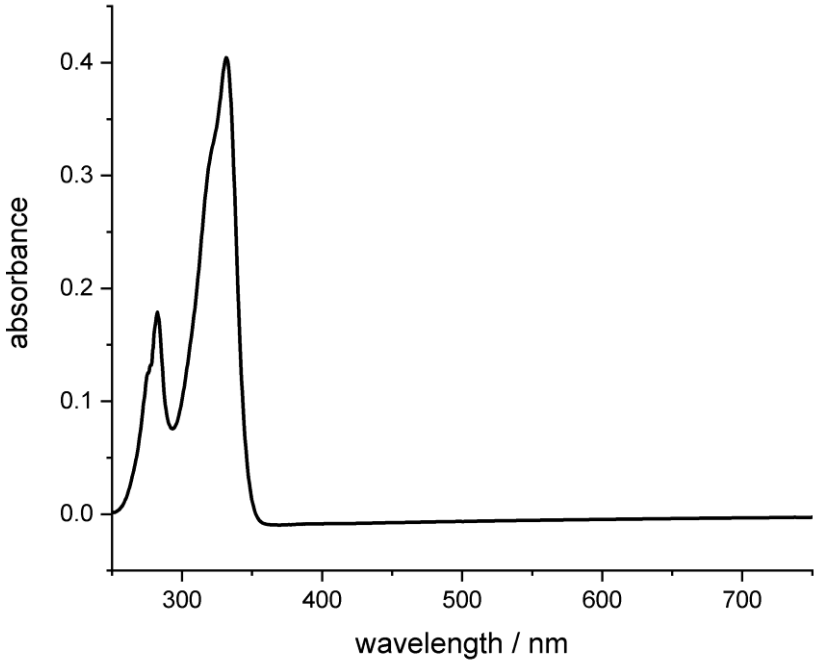

Figure 5.2.17. UV–vis spectrum of **2a** (in THF).

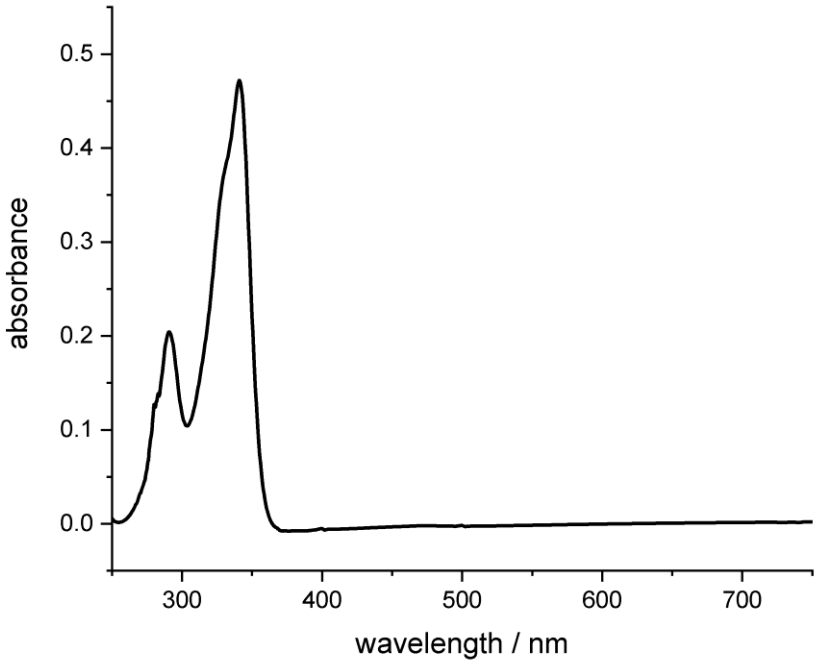

Figure 5.2.18. UV–vis spectrum of **2b** (in THF).

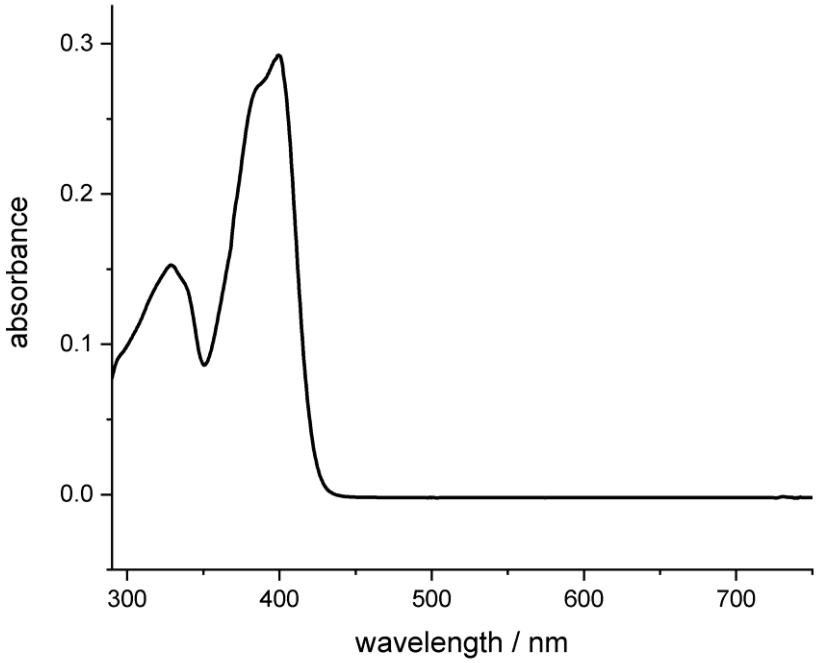

Figure 5.2.19. UV–vis spectrum of **3** (in THF).

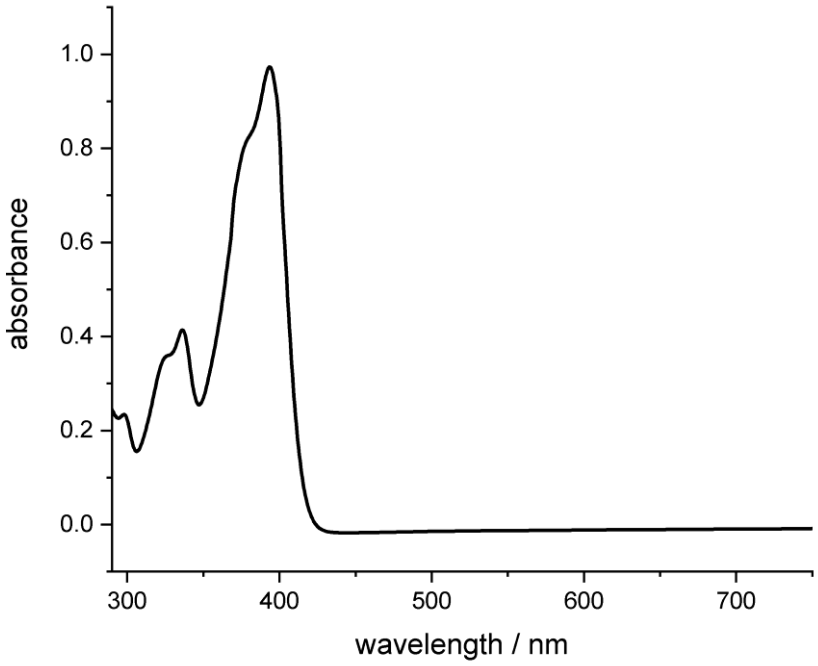

Figure 5.2.20. UV–vis spectrum of **4** (in THF).

Fluorescence spectra

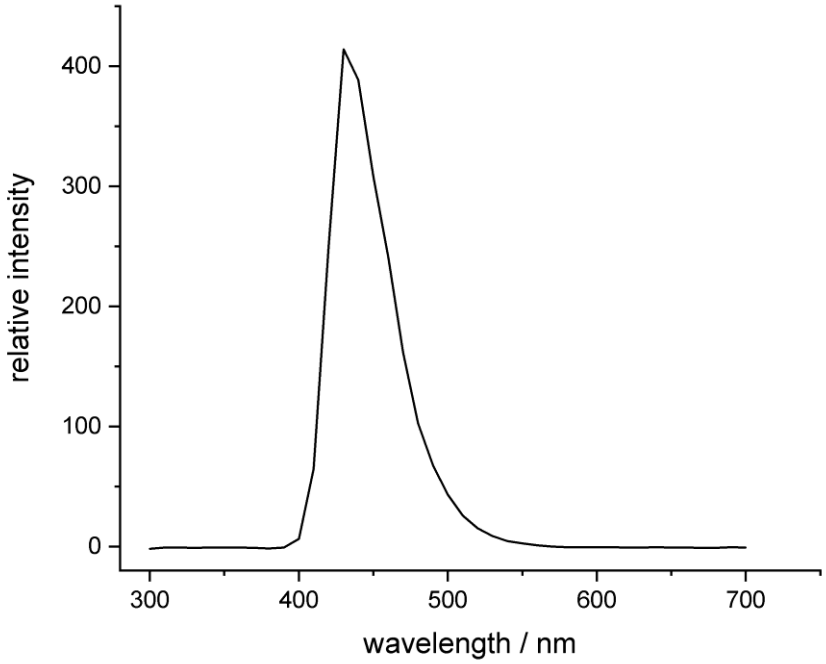

Figure 5.2.21. Fluorescence spectrum of **3** (in THF, λ_{ex} = 400 nm).

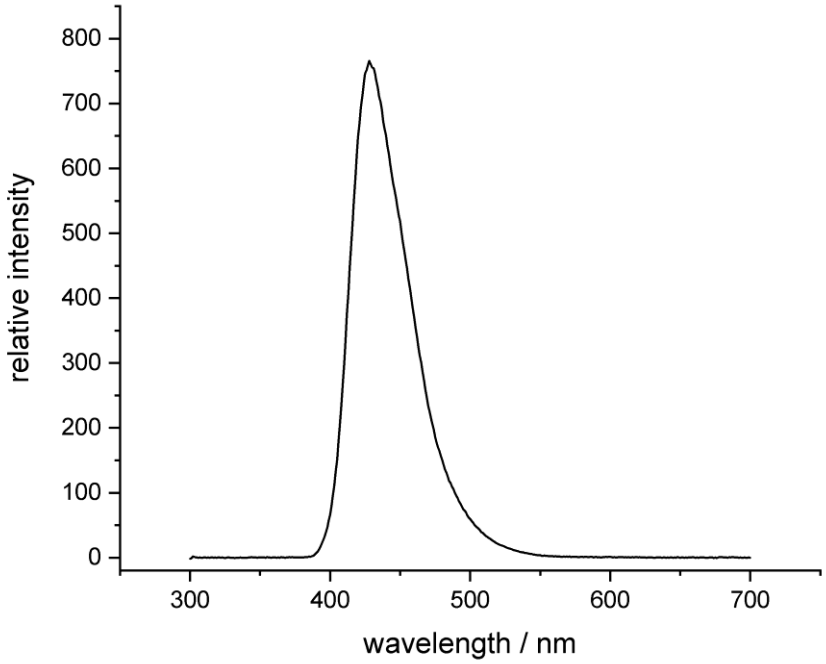

Figure 5.2.22. Fluorescence spectrum of **4** (in THF, λ_{ex} = 394 nm).

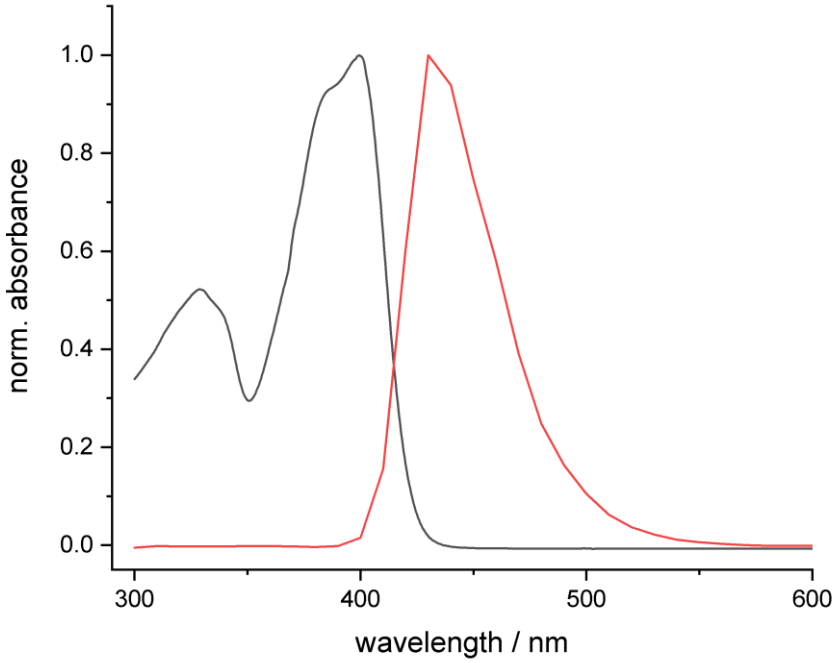

Figure 5.2.23. UV–vis (black) and fluorescence (red) spectra of **3** (in THF).

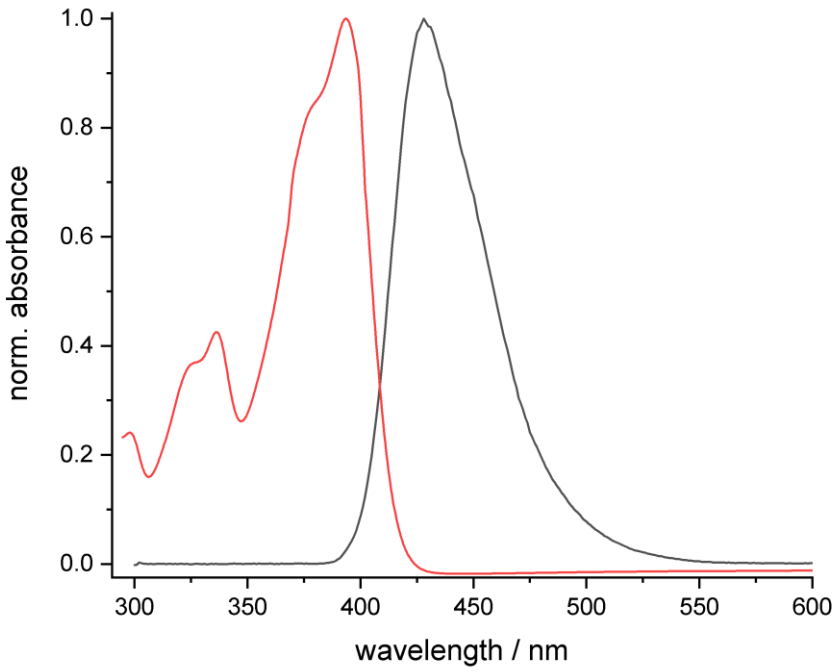

Figure 5.2.24. UV–vis (red) and fluorescence (black) spectra of **4** (in THF).

Mass spectra

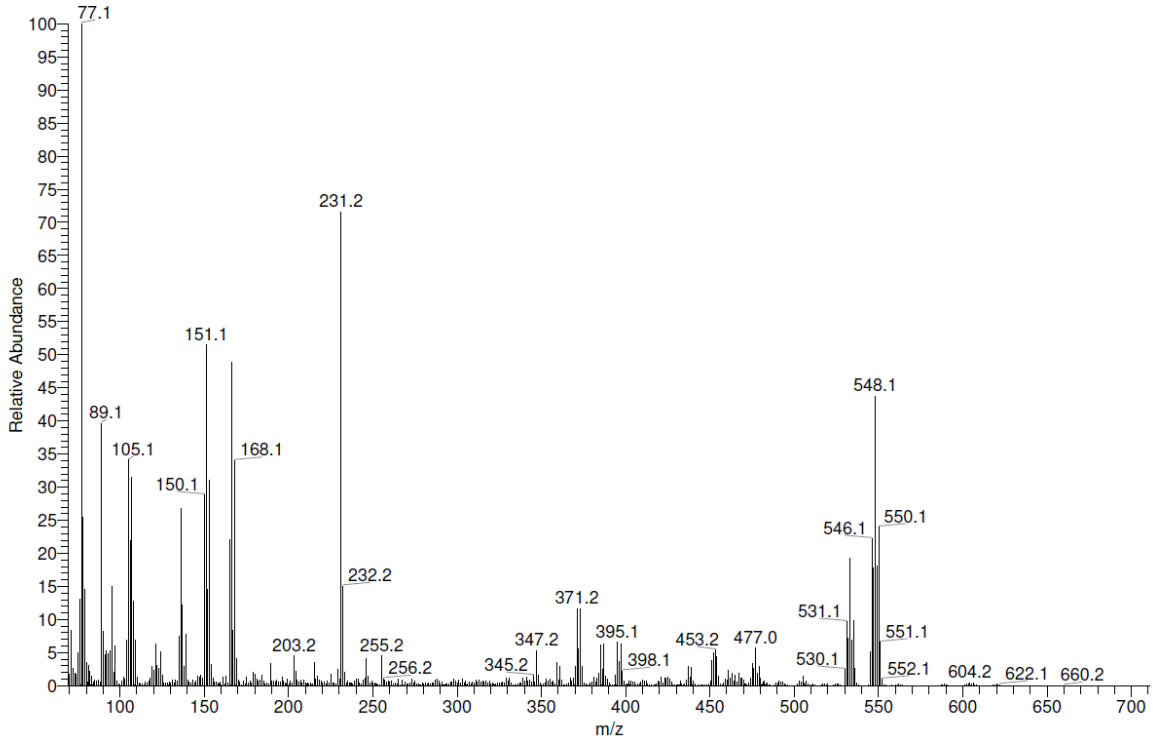

Figure 5.2.25. EI mass spectrum of **2a**.

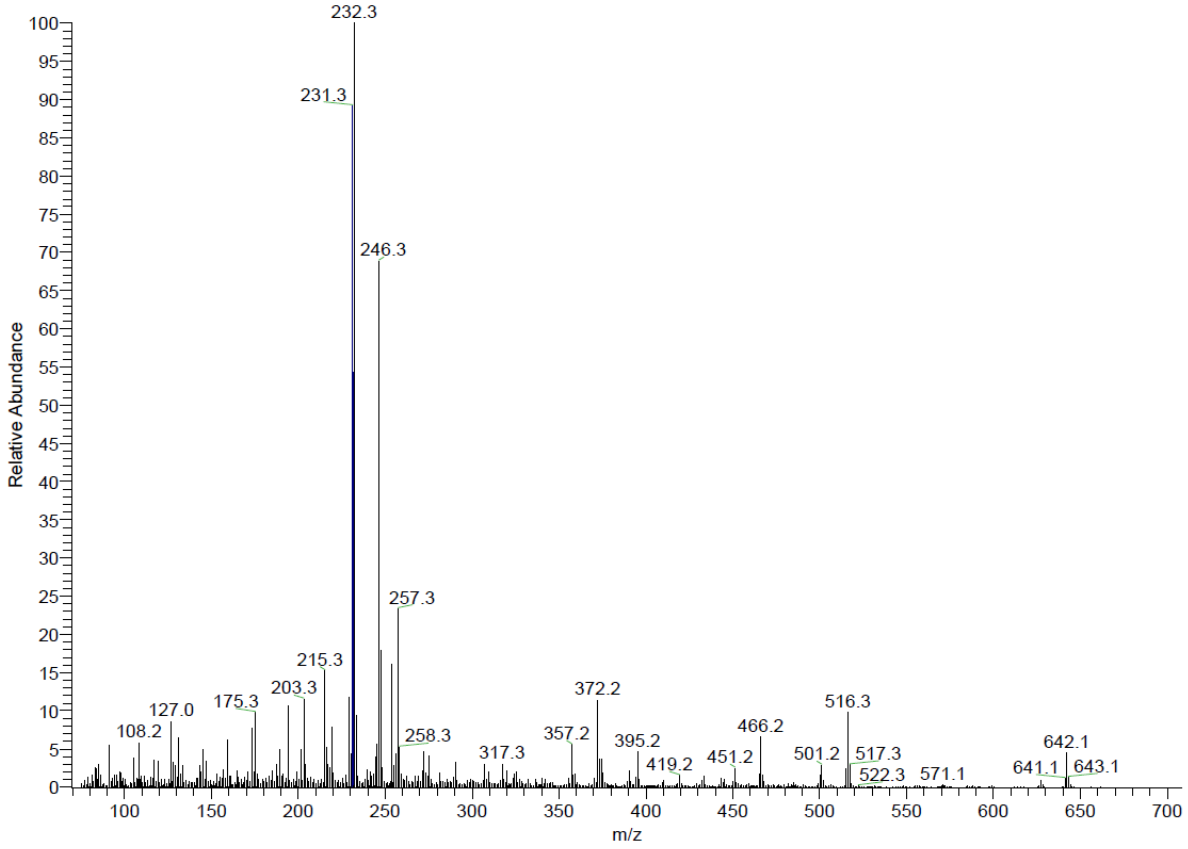

Figure 5.2.26. EI mass spectrum of **2b**.

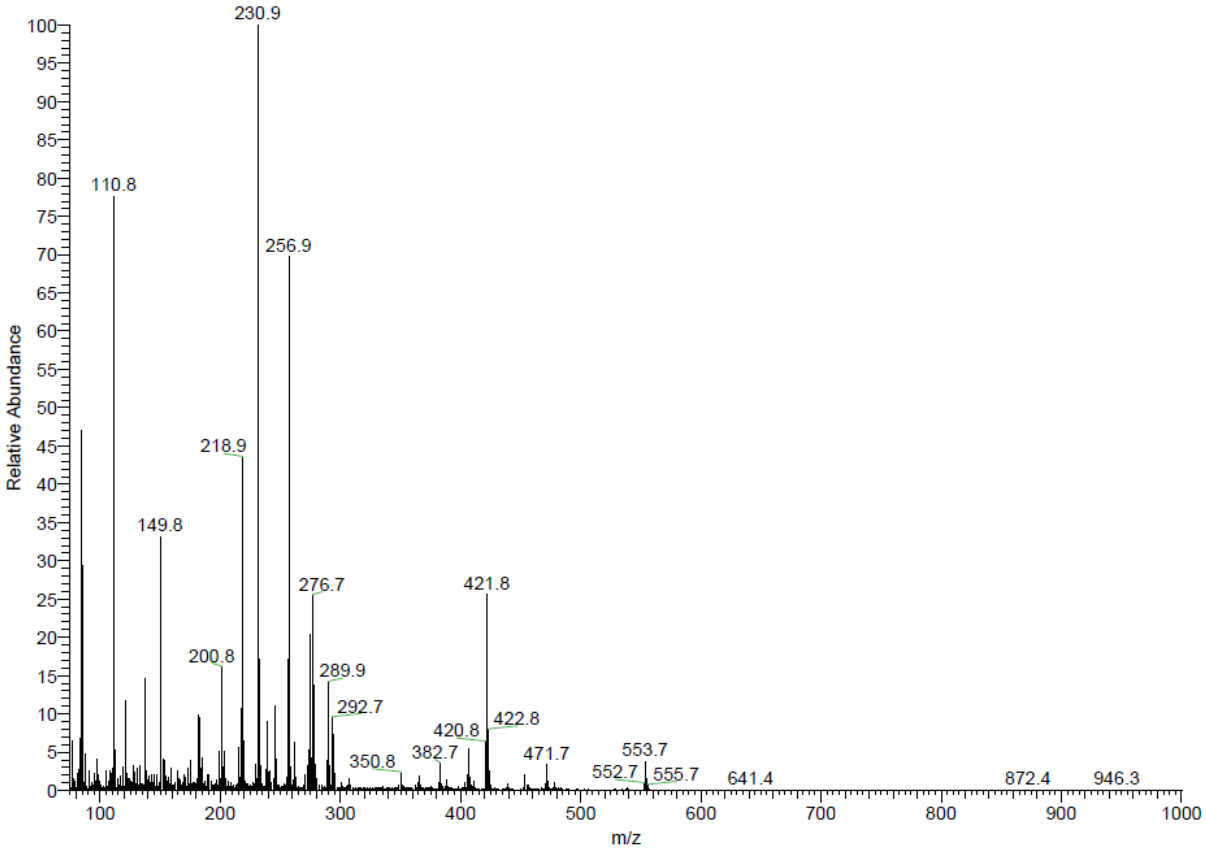

Figure 5.2.27. EI mass spectrum of **3**.

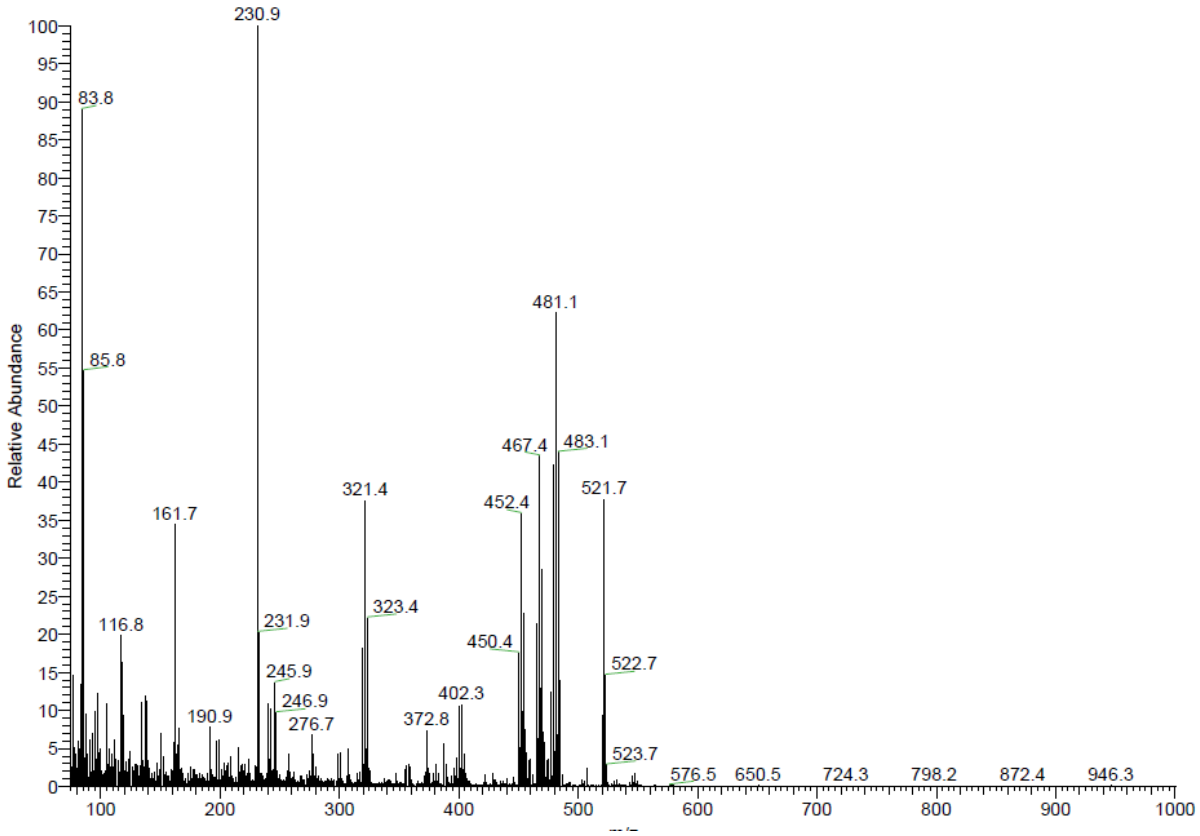

Figure 5.2.28. EI mass spectrum of **4**.

Cyclic Voltammetry

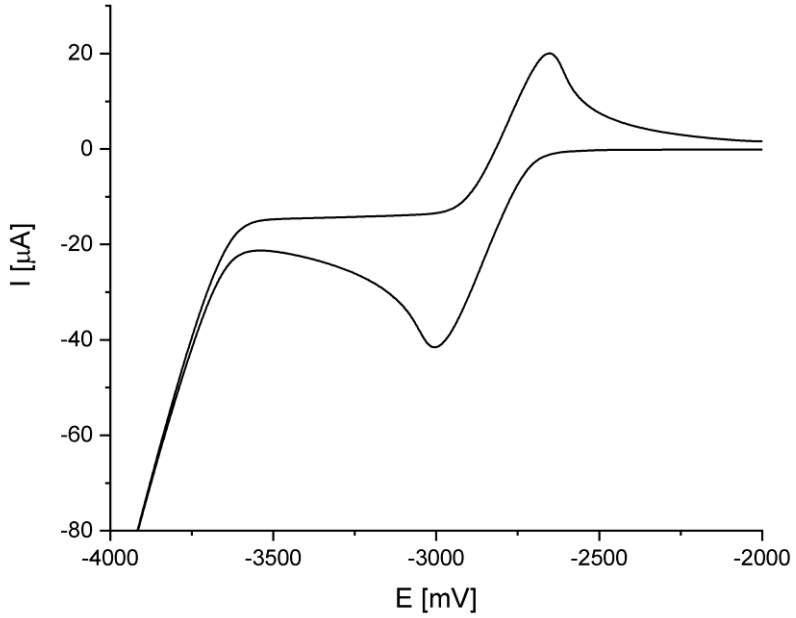

Figure 5.2.29. Cyclic voltammogram of **1** in THF ($1 \cdot 10^{-3}$ M), recorded vs the ferrocene/ferrocenium couple as internal standard (scan rate: 100 mV s^{-1}).

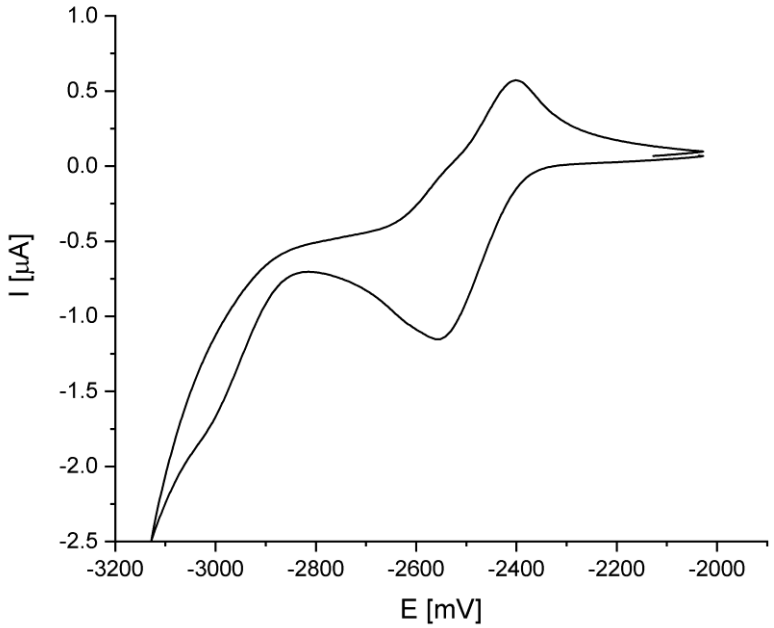

Figure 5.2.30. Cyclic voltammogram of **3** in THF ($1 \cdot 10^{-3}$ M), recorded vs the ferrocene/ferrocenium couple as internal standard (scan rate: 100 mV s^{-1}).

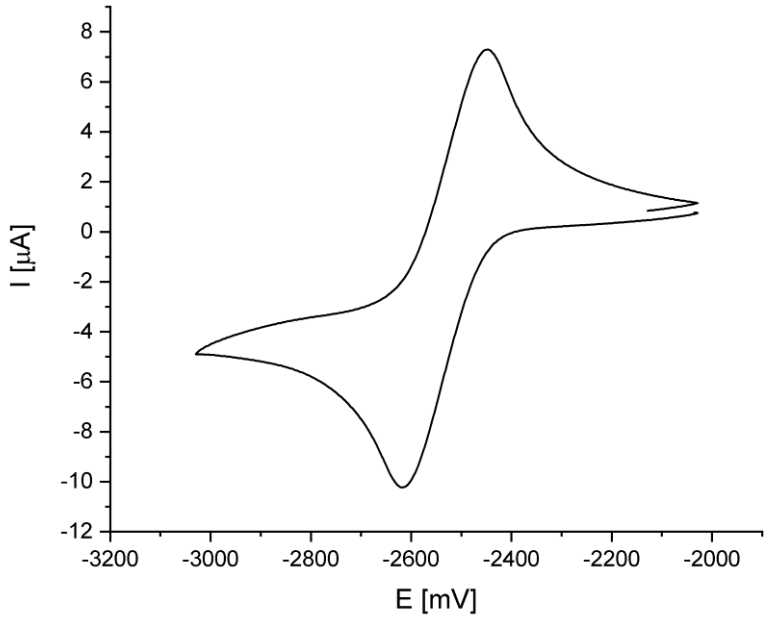

Figure 5.2.31. Cyclic voltammogram of **4** in THF ($1 \cdot 10^{-3}$ M), recorded vs the ferrocene/ferrocenium couple as internal standard (scan rate: 100 mV s^{-1}).

5.3 Catalytic Si/B Exchange Condensation: A Green B-C Coupling Method That Provides Access to Monodisperse (Het)arylborane “Trimers“

NMR spectra

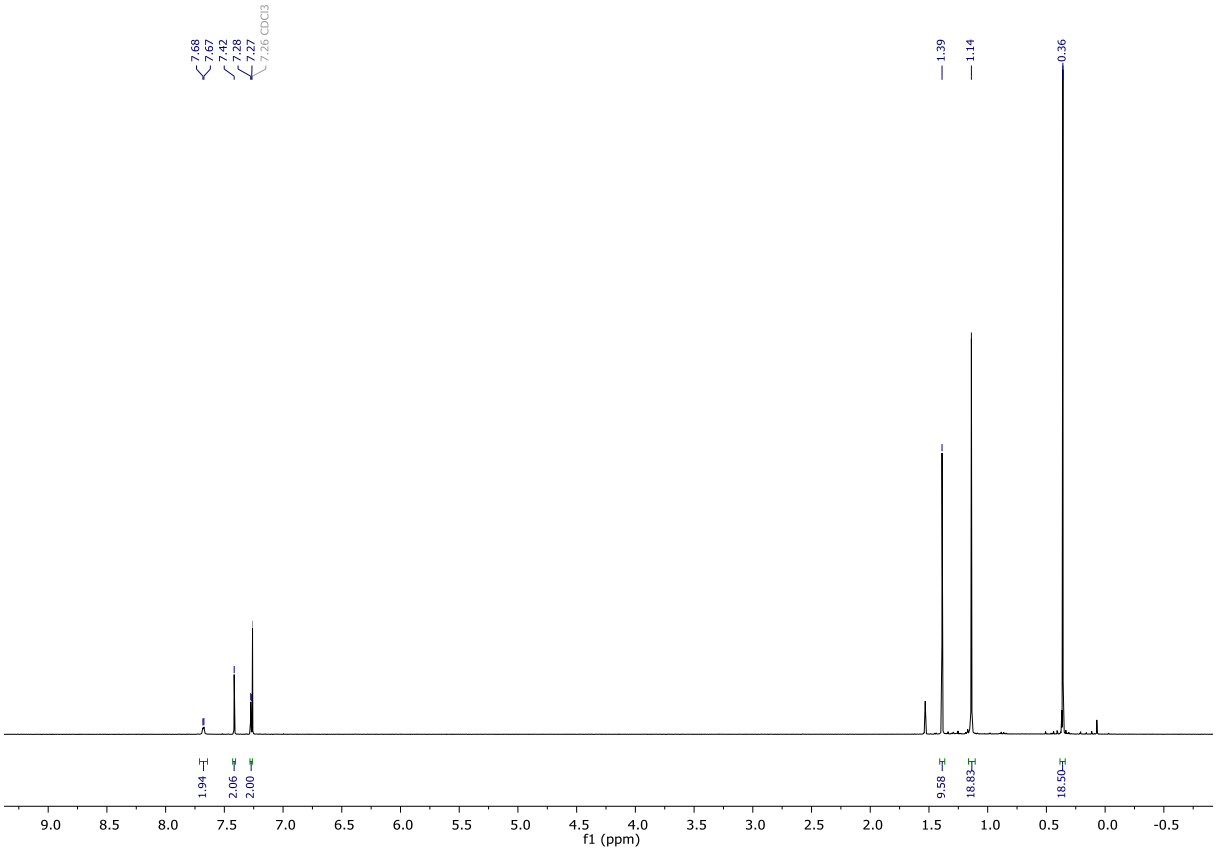

Figure 5.3.1. ^{1}H NMR spectrum of **4a** (in $CDCl_3$, 400 MHz).

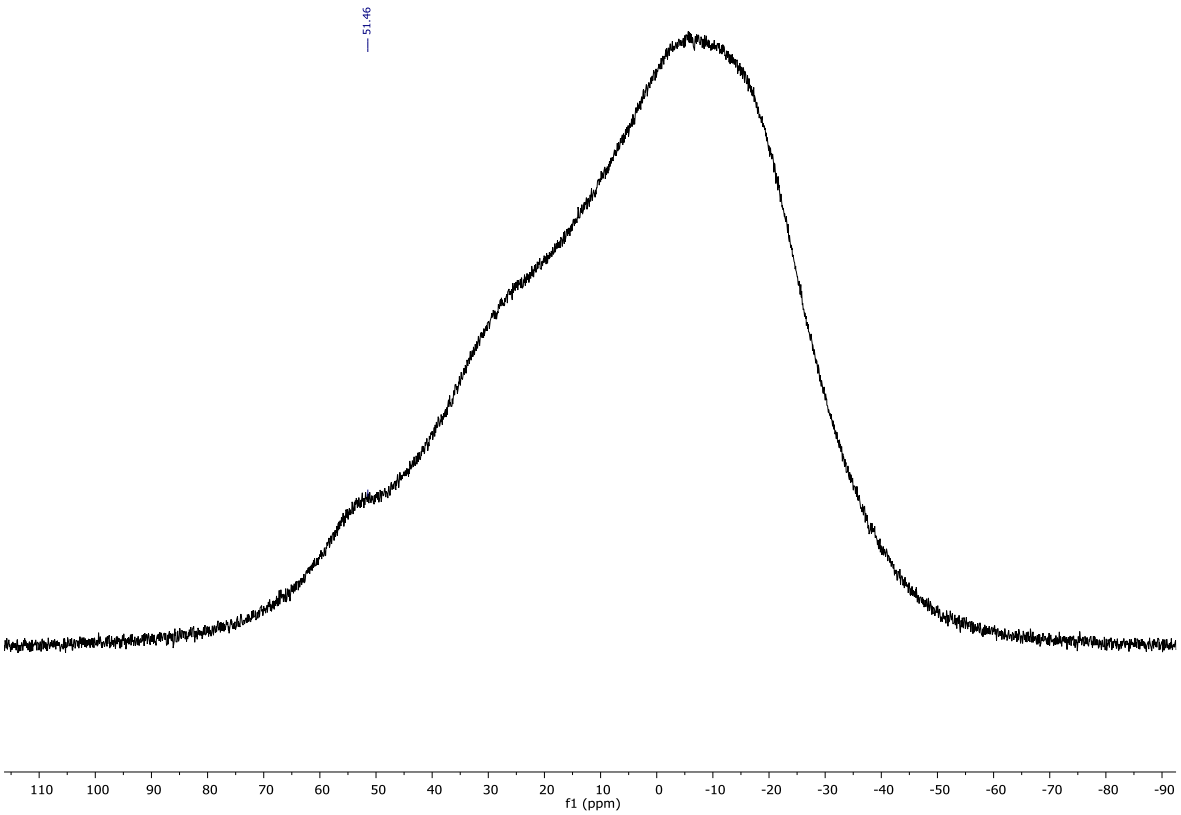

Figure 5.3.2. $^{11}B\{^{1}H\}$ NMR spectrum of **4a** (in $CDCl_3$, 128 MHz).

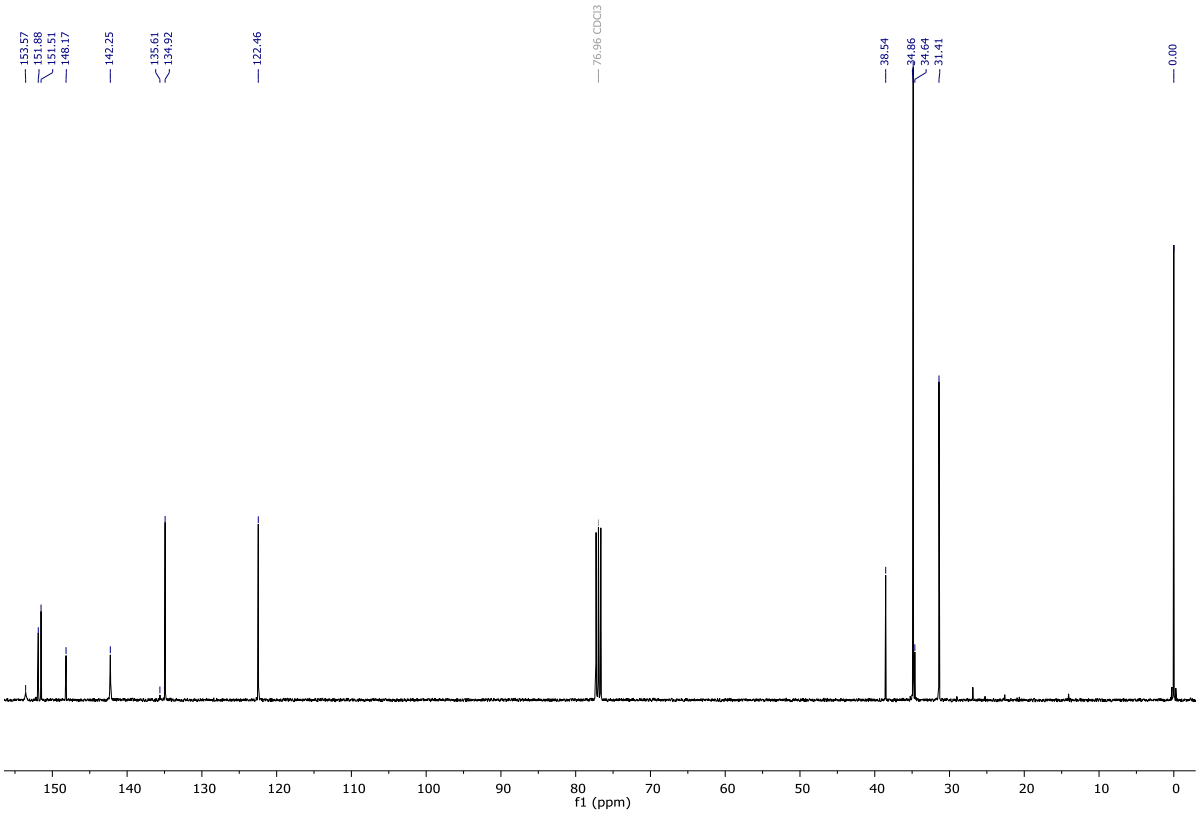

Figure 5.3.3. ^{13}C NMR spectrum of **4a** (in $CDCl_3$, 101 MHz).

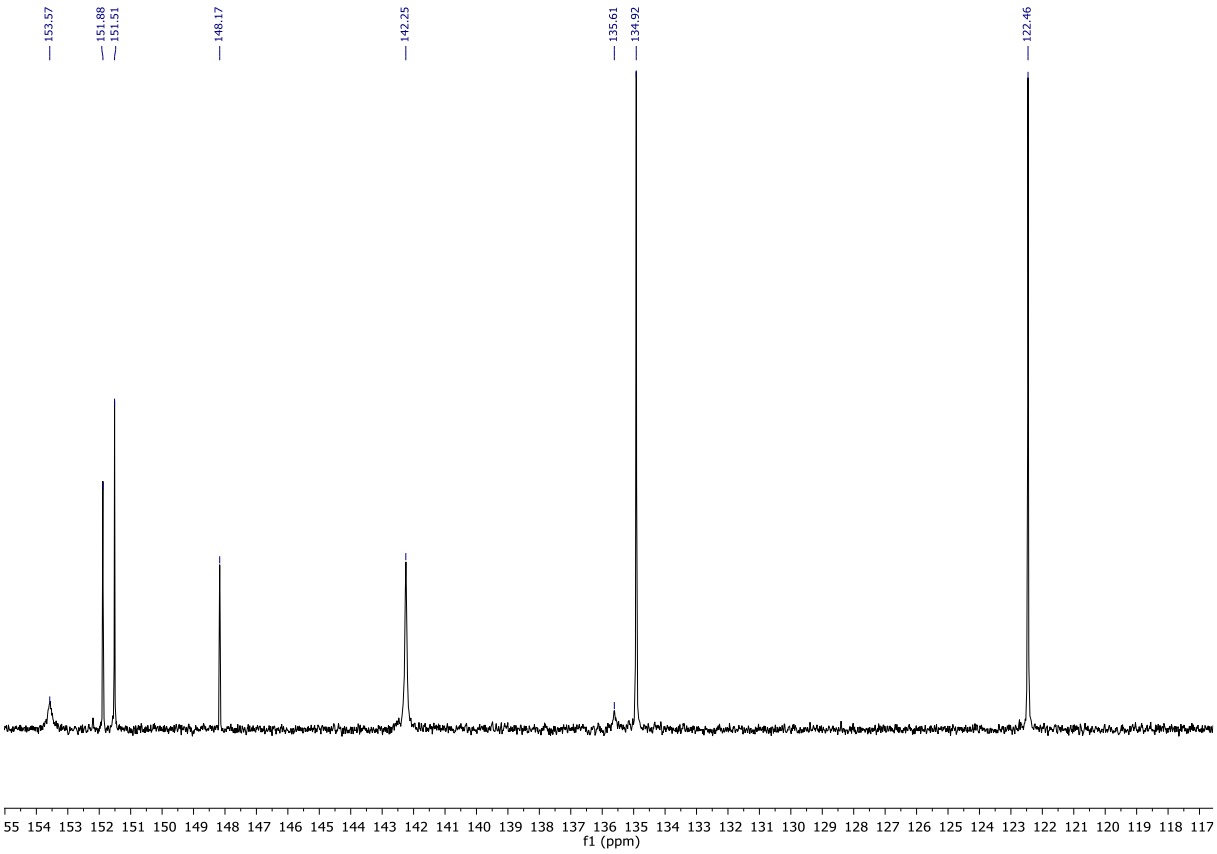

Figure 5.3.4. Detail (aromatic region) of the ^{13}C NMR spectrum of **4a** (in $CDCl_3$, 101 MHz).

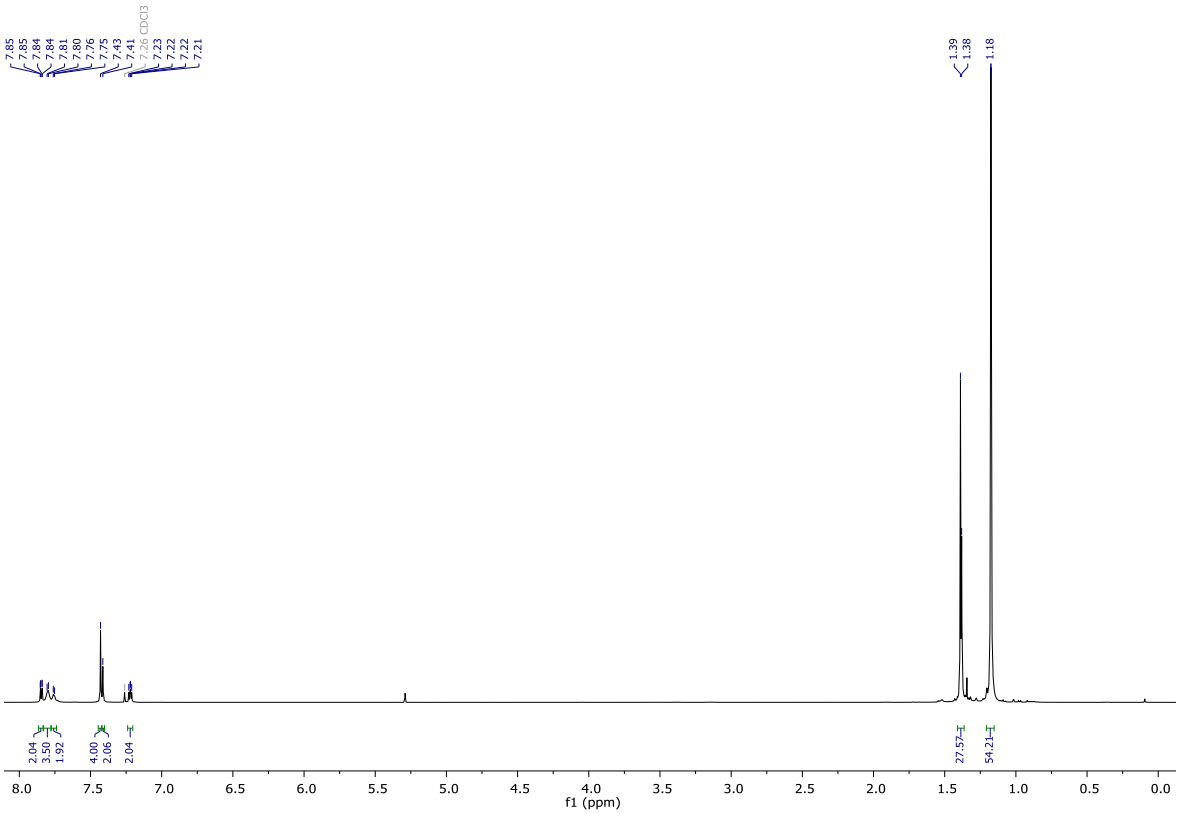

Figure 5.3.5. ^{1}H NMR spectrum of **5aa** (in $CDCl_3$, 400 MHz).

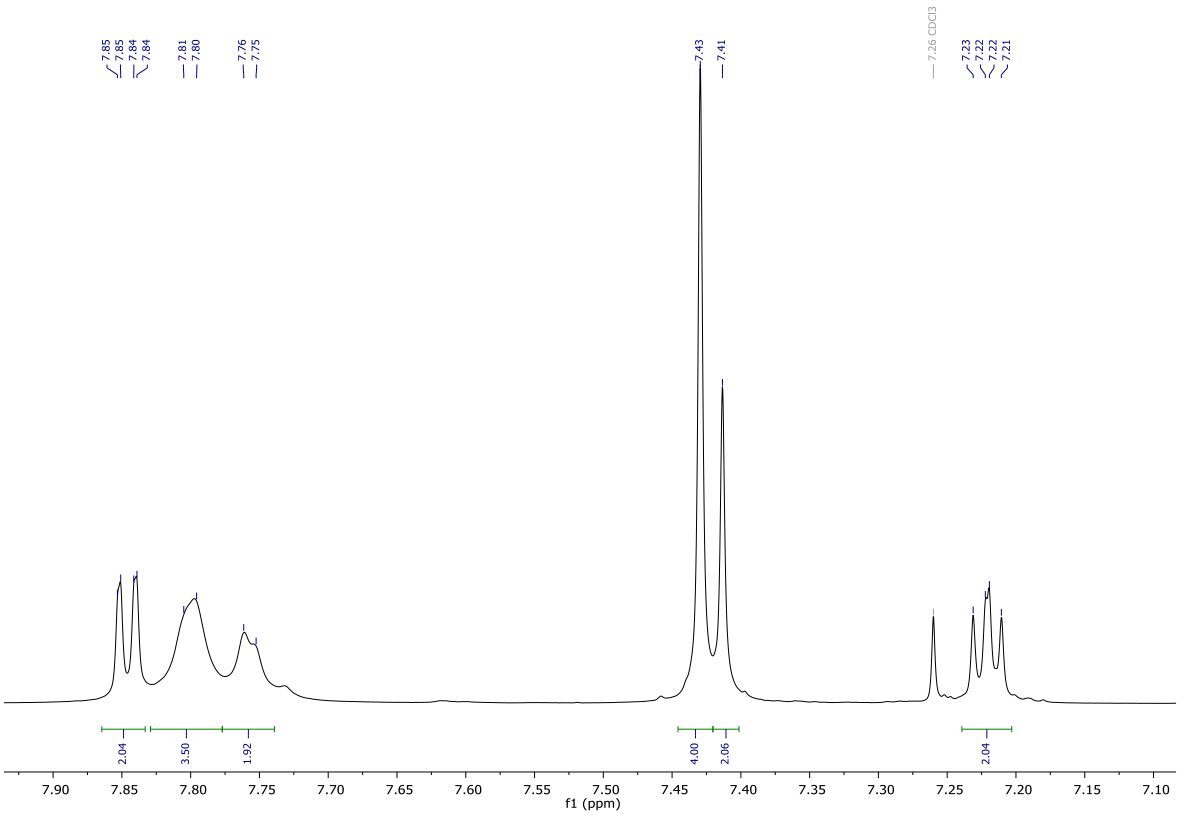

Figure 5.3.6. Detail (aromatic region) of the ^{1}H NMR spectrum of **5aa** (in $CDCl_3$, 400 MHz).

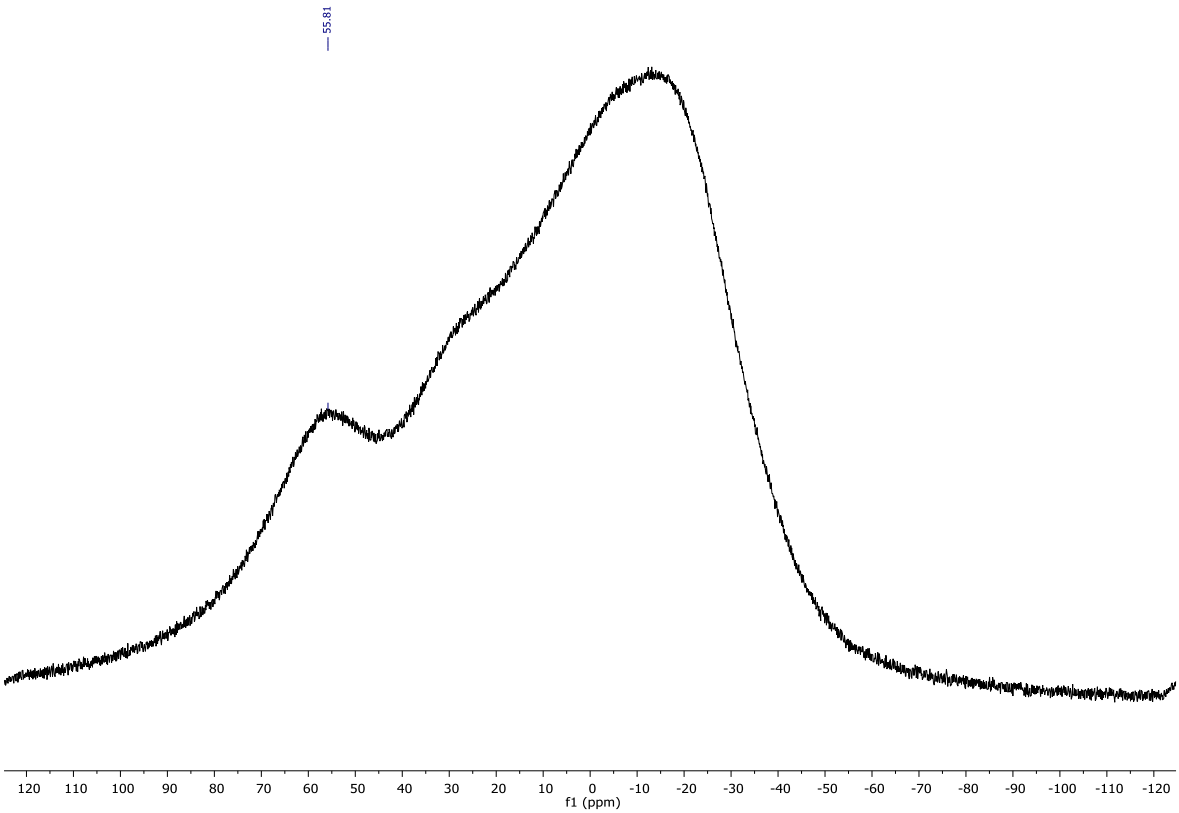

Figure 5.3.7. $^{11}B\{^{1}H\}$ NMR spectrum of **5aa** (in $CDCl_3$, 128 MHz).

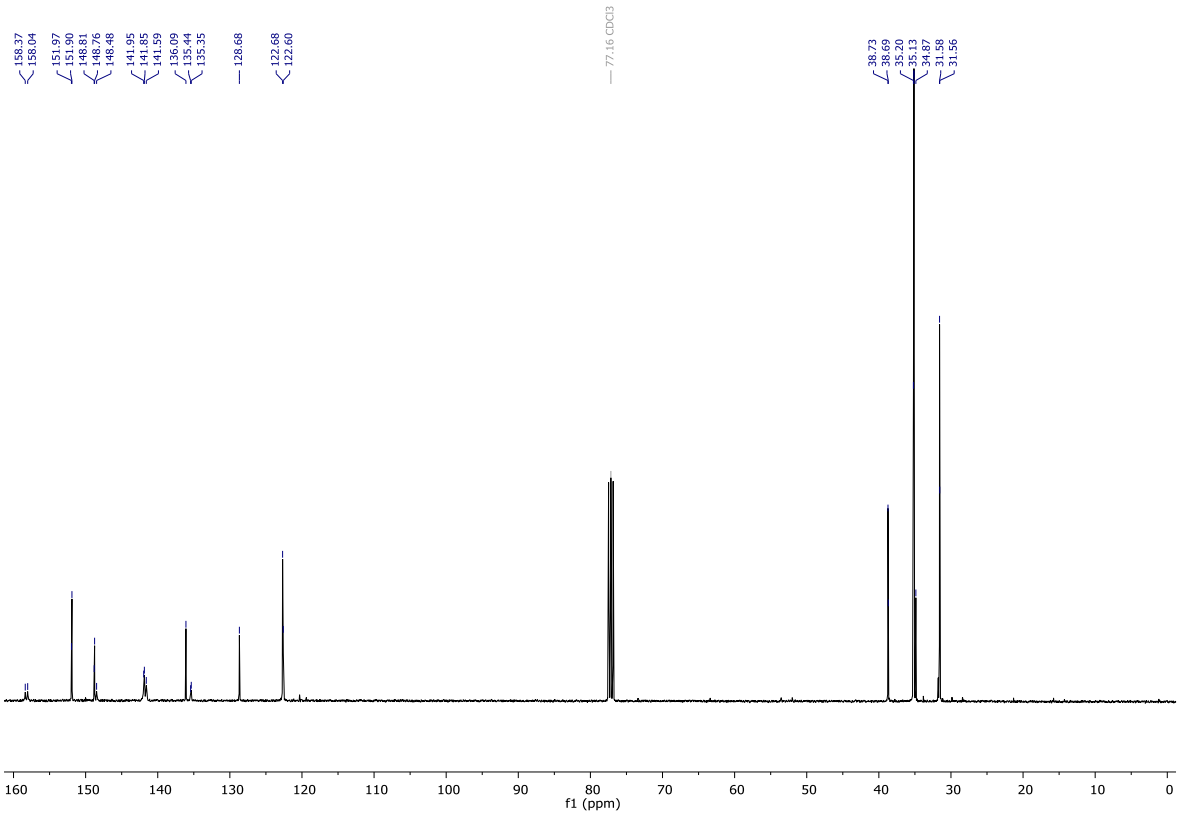

Figure 5.3.8. ^{13}C NMR spectrum of **5aa** (in $CDCl_3$, 101 MHz).

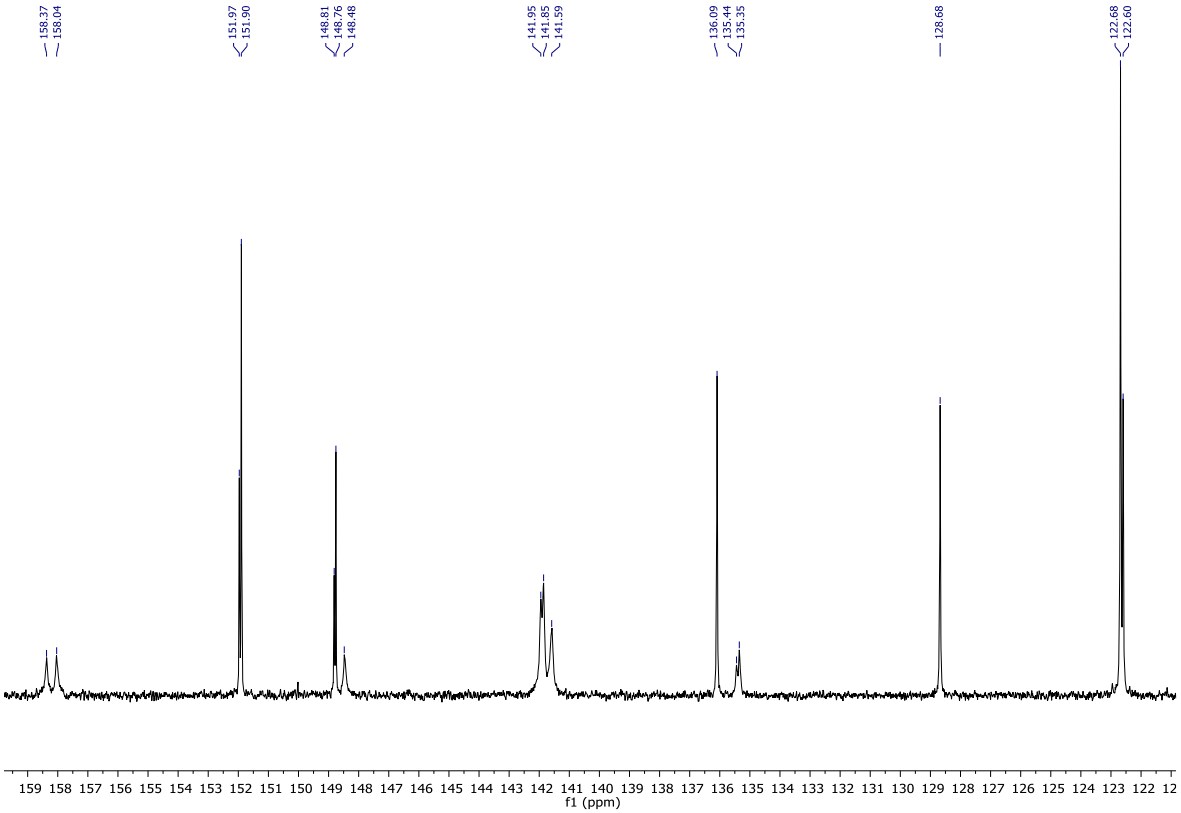

Figure 5.3.9. Detail (aromatic region) of the ^{13}C NMR spectrum of **5aa** (in $CDCl_3$, 101 MHz).

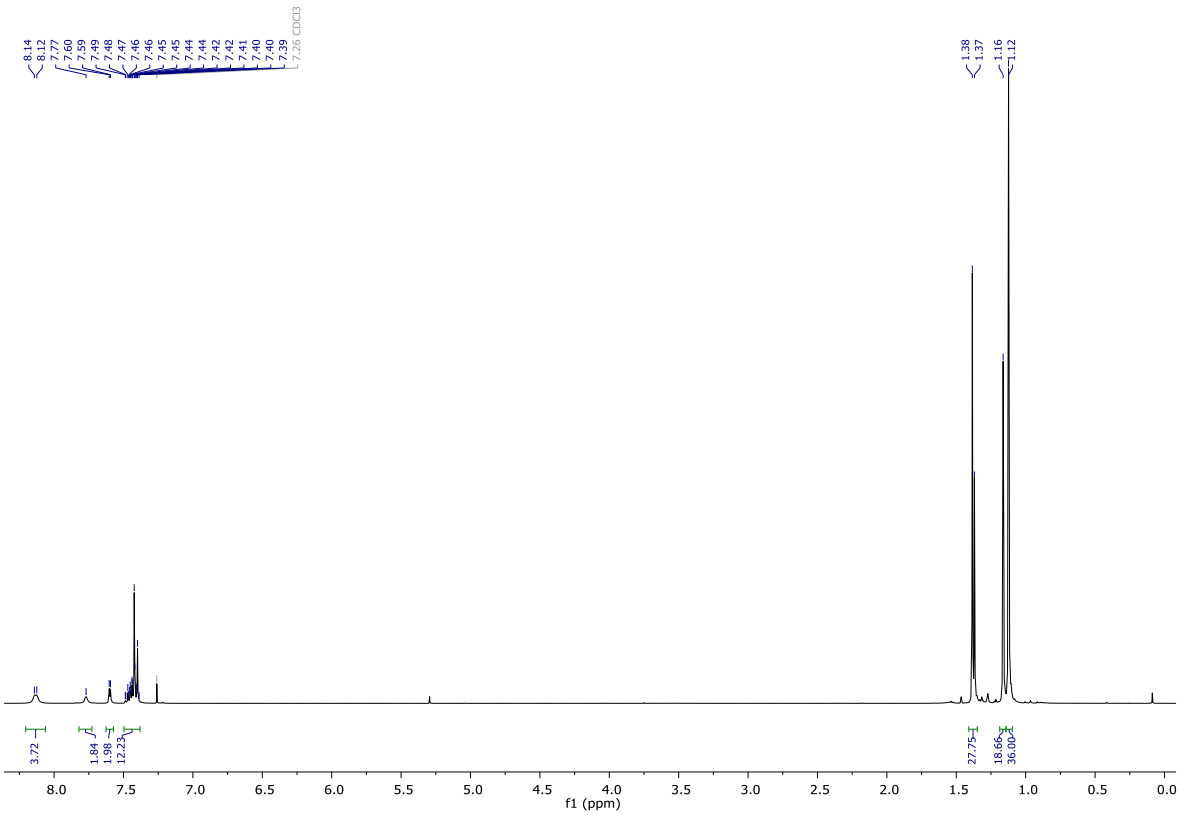

Figure 5.3.10. ^{1}H NMR spectrum of **5ac** (in $CDCl_3$, 400 MHz).

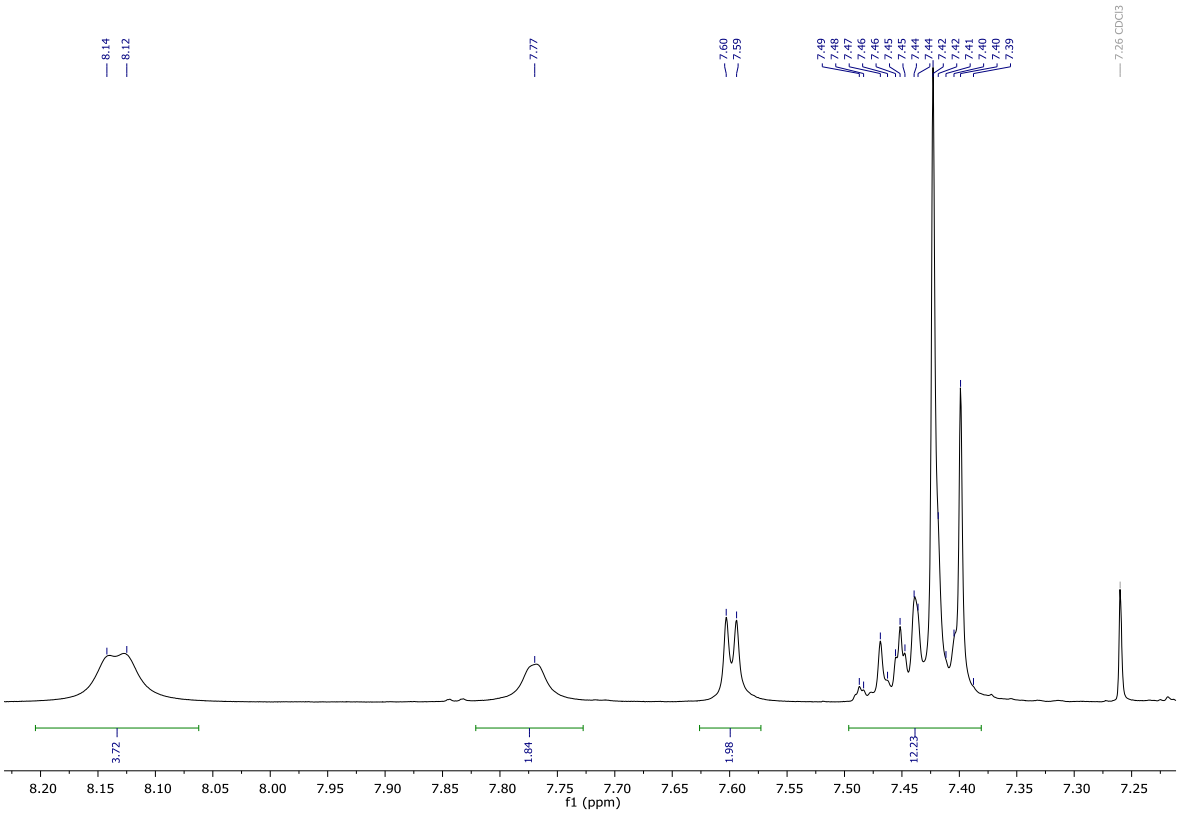

Figure 5.3.11. Detail (aromatic region) of the ^{1}H NMR spectrum of **5ac** (in $CDCl_3$, 400 MHz).

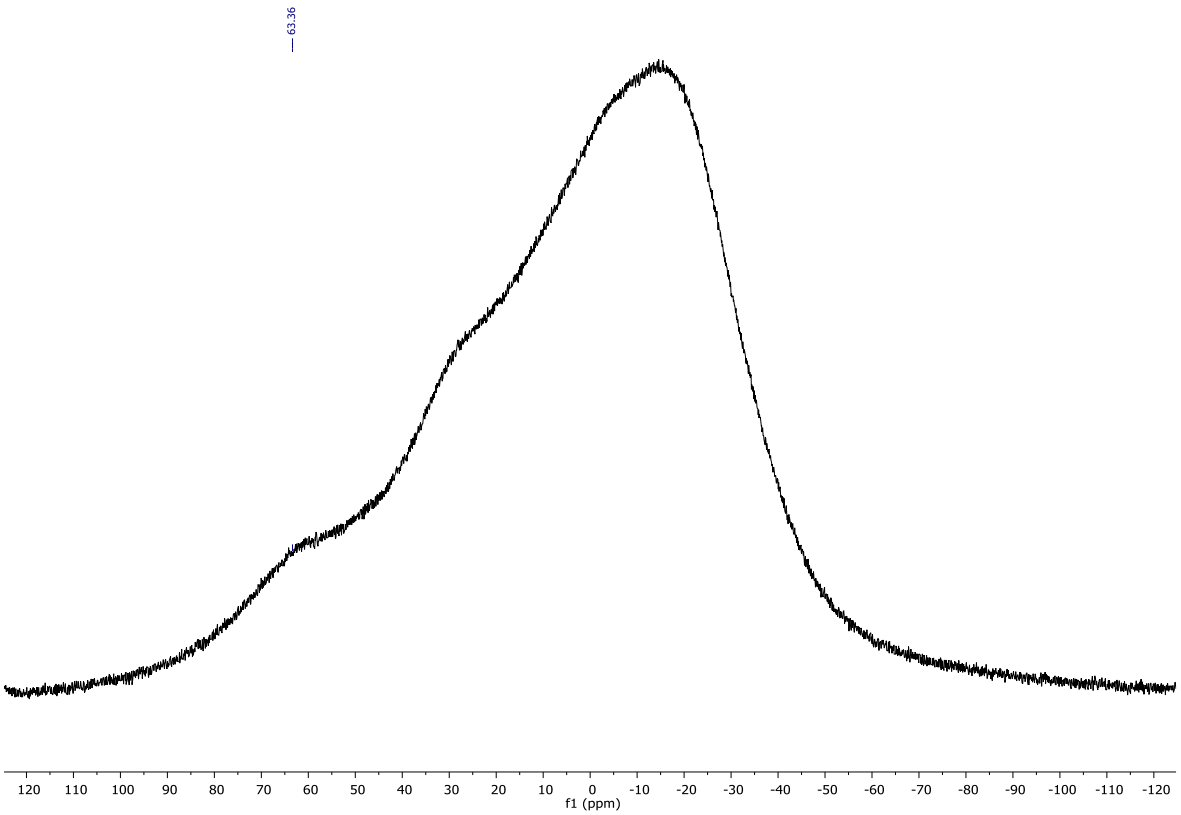

Figure 5.3.12. $^{11}B\{^{1}H\}$ NMR spectrum of **5ac** (in $CDCl_3$, 128 MHz).

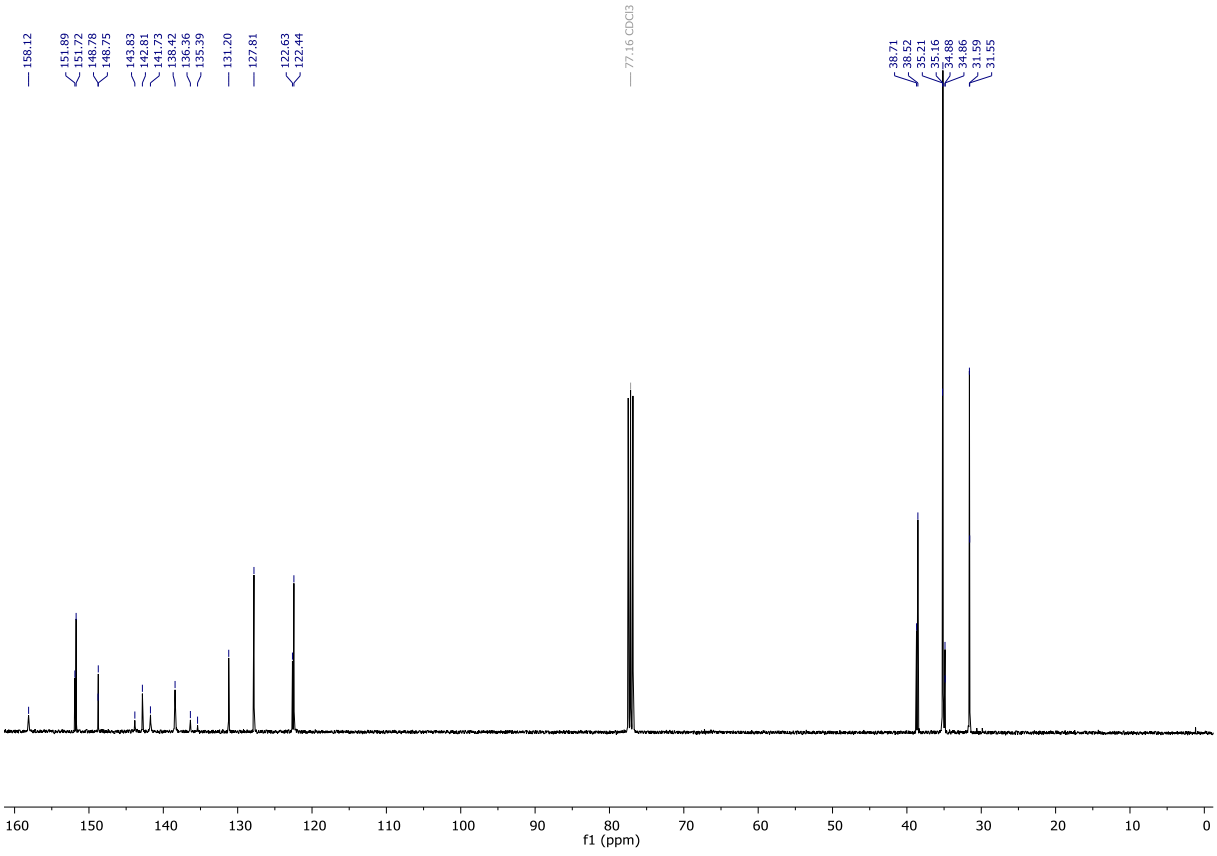

Figure 5.3.13. ^{13}C NMR spectrum of **5ac** (in $CDCl_3$, 101 MHz).

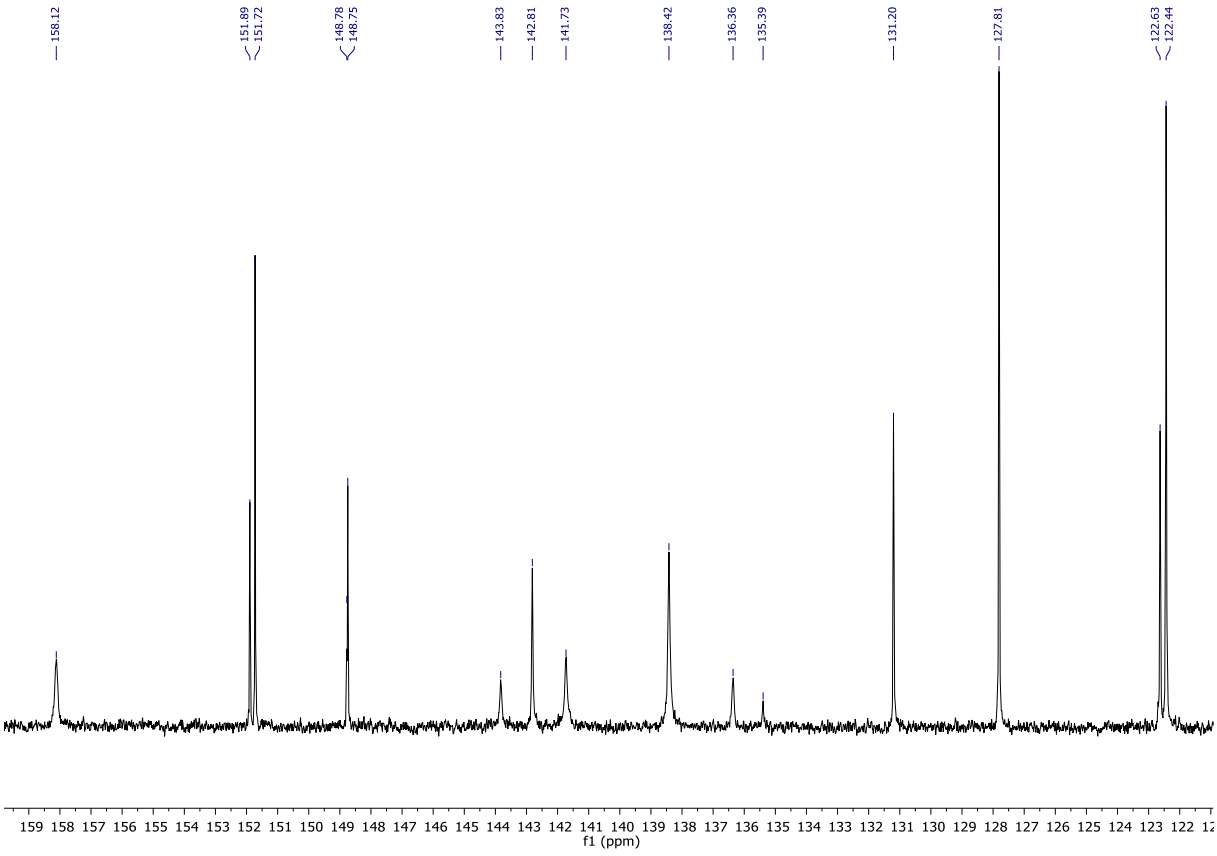

Figure 5.3.14. Detail (aromatic region) of the ^{13}C NMR spectrum of **5ac** (in $CDCl_3$, 101 MHz).

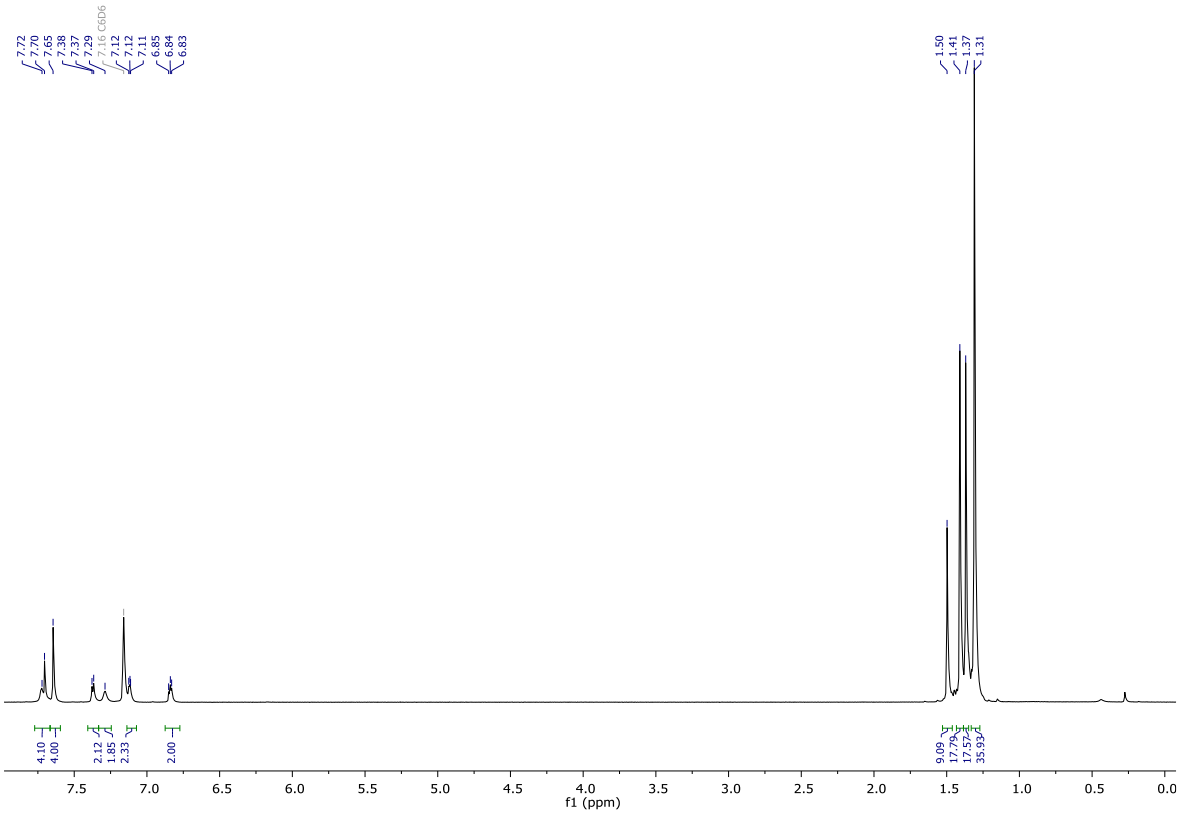

Figure 5.3.15. ^{1}H NMR spectrum of **5ba** (in C_6D_6, at 70°C, 400 MHz).

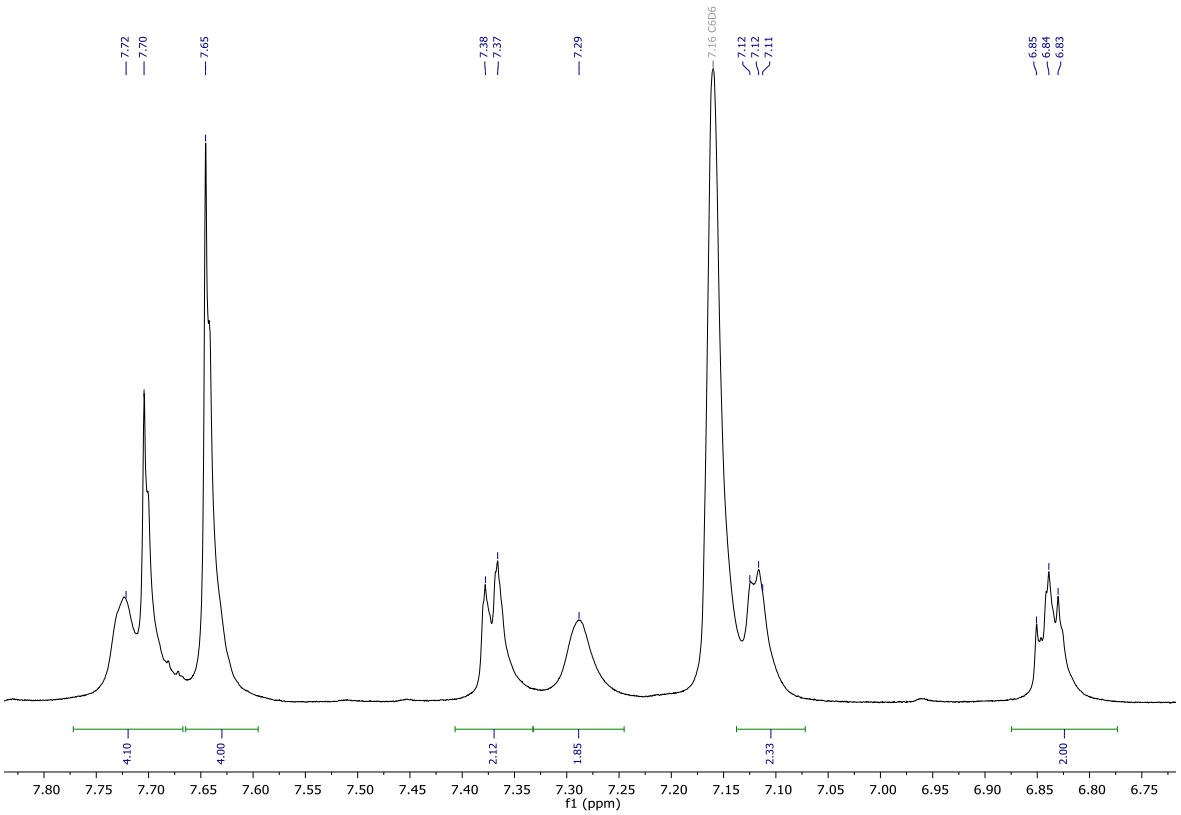

Figure 5.3.16. Detail (aromatic region) of the ^{1}H NMR spectrum of **5ba** (in C_6D_6, at 70°C, 400 MHz).

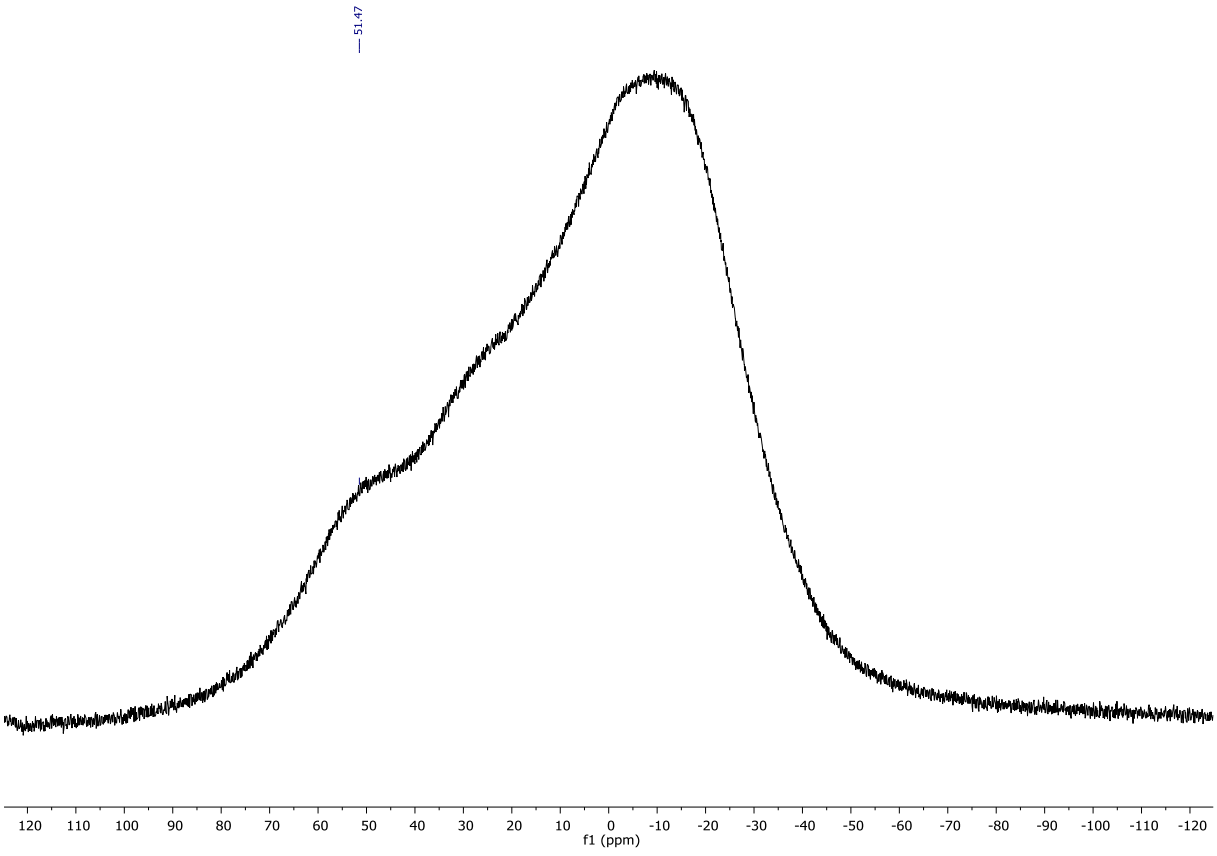

Figure 5.3.17. $^{11}B\{^{1}H\}$ NMR spectrum of **5ba** (in C_6D_6, at 70°C, 128 MHz).

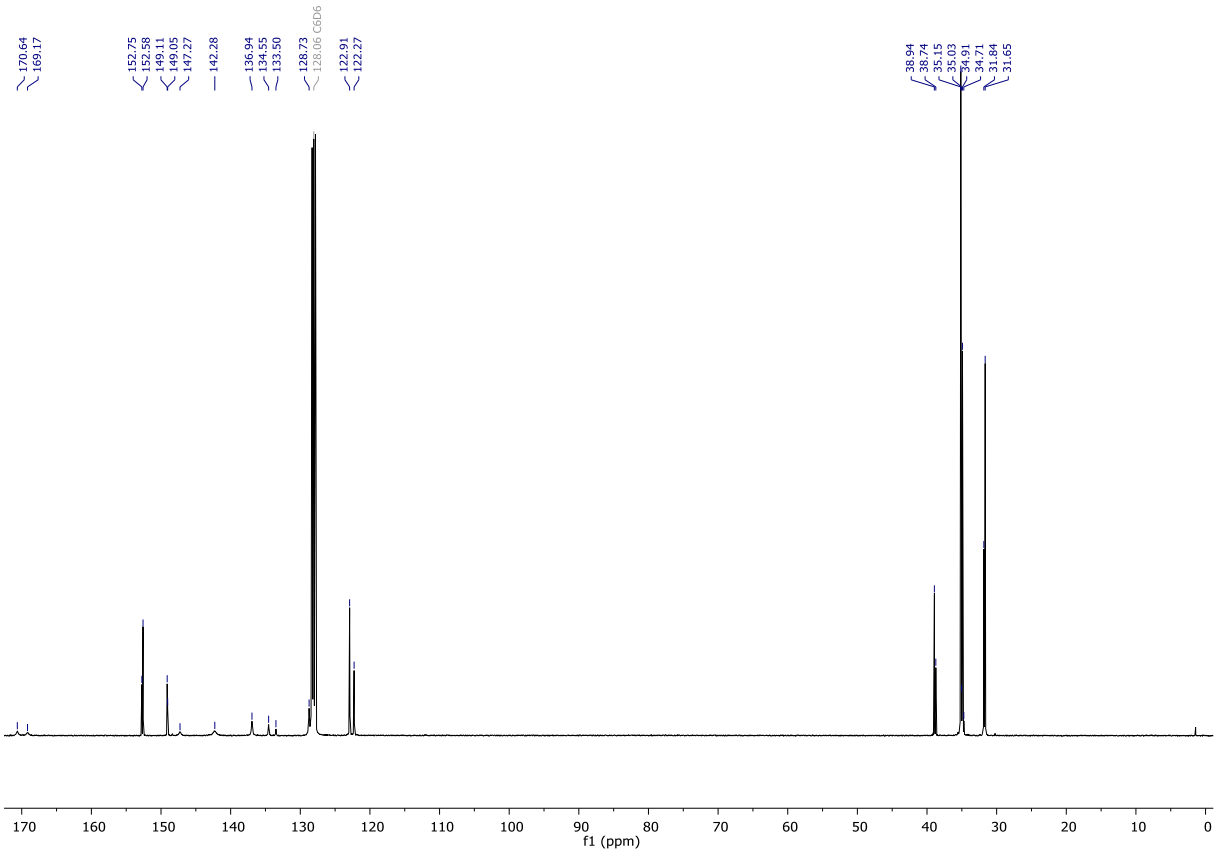

Figure 5.3.18. ^{13}C NMR spectrum of **5ba** (in C_6D_6, at 70°C, 101 MHz).

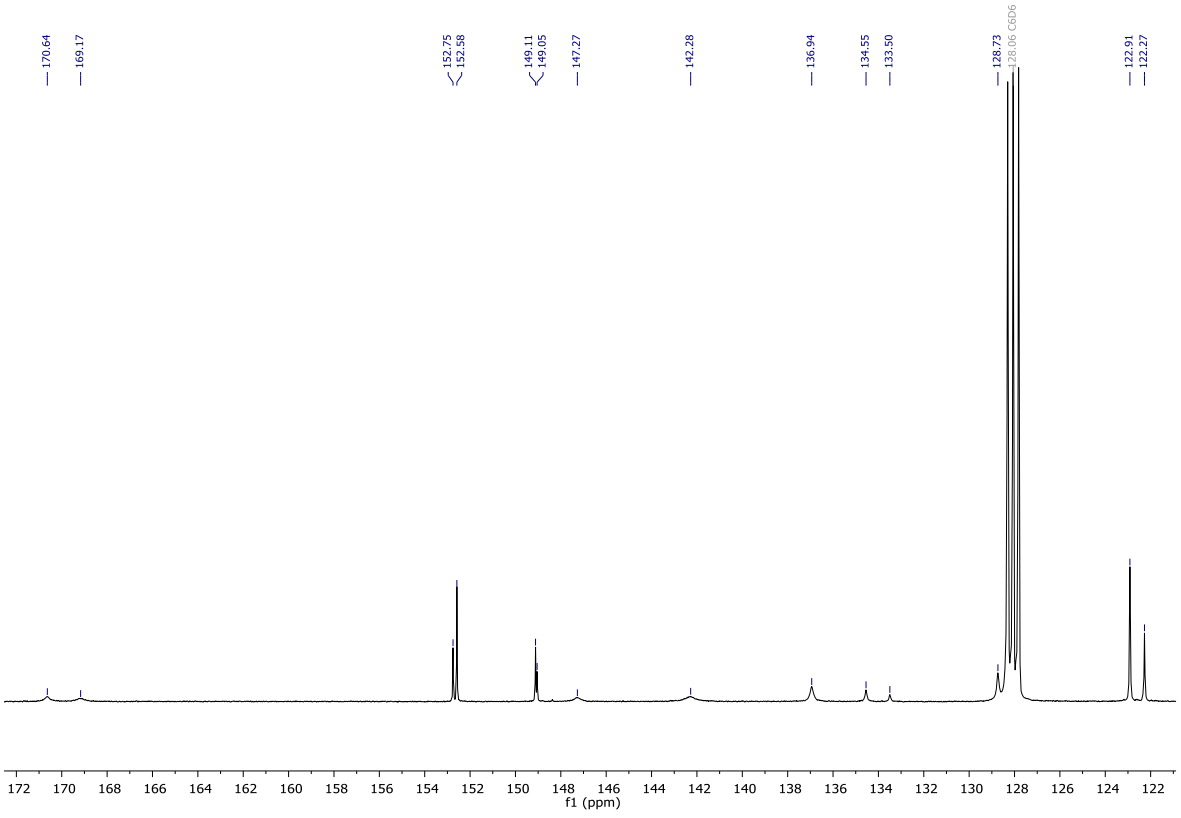

Figure 5.3.19. Detail (aromatic region) of the ^{13}C NMR spectrum of **5ba** (in C_6D_6, at 70°C, 101 MHz).

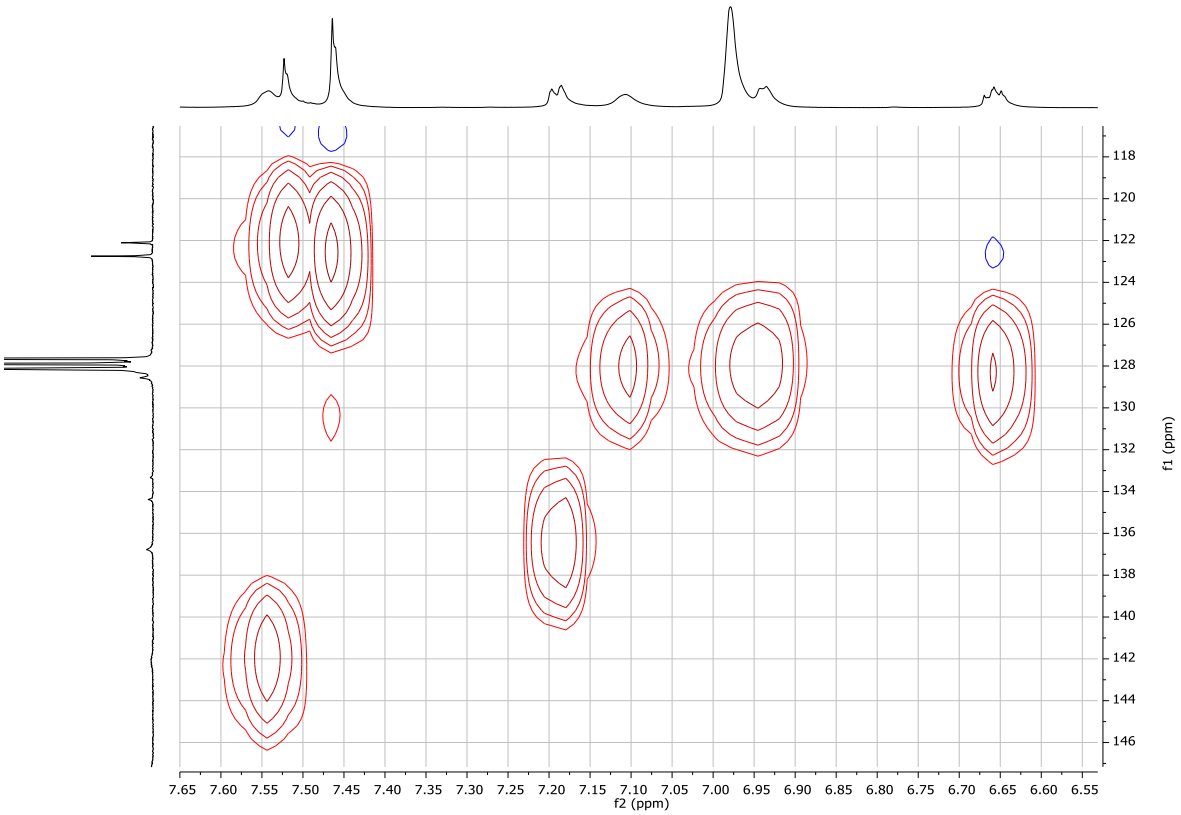

Figure 5.3.20. Detail of HSQC spectrum of **5ba** (in C_6D_6, at 70°C, 101 MHz).

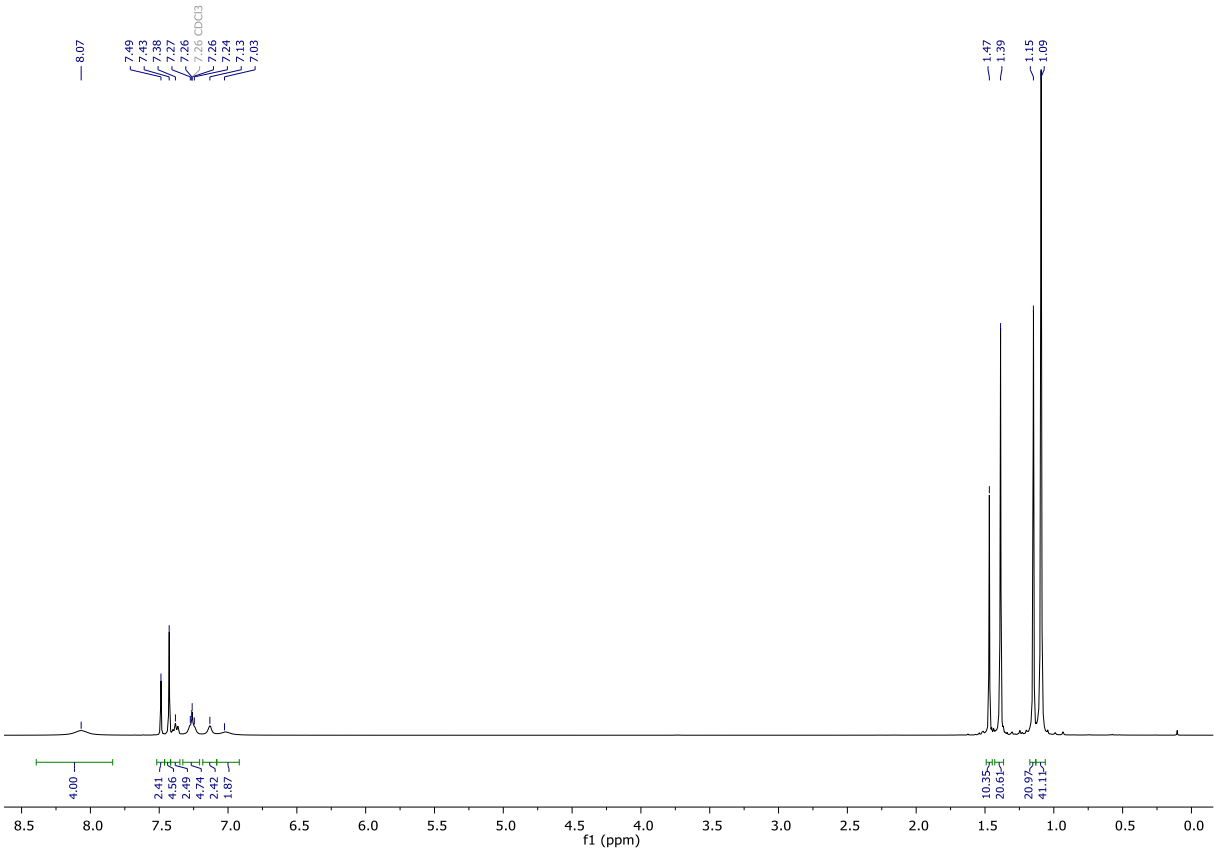

Figure 5.3.21. ^{1}H NMR spectrum of **5bc** (in $CDCl_3$, 400 MHz).

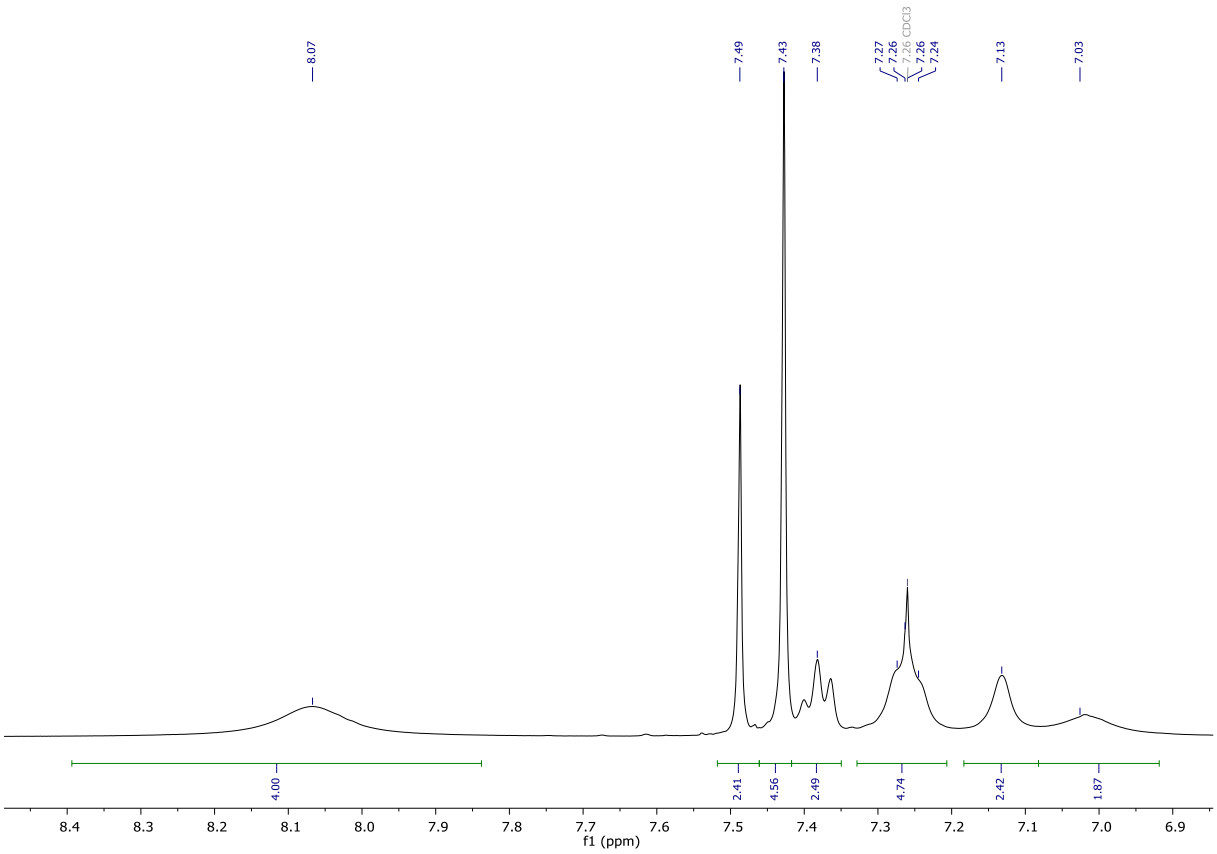

Figure 5.3.22. Detail (aromatic region) of the ^{1}H NMR spectrum of **5bc** (in $CDCl_3$, 400 MHz).

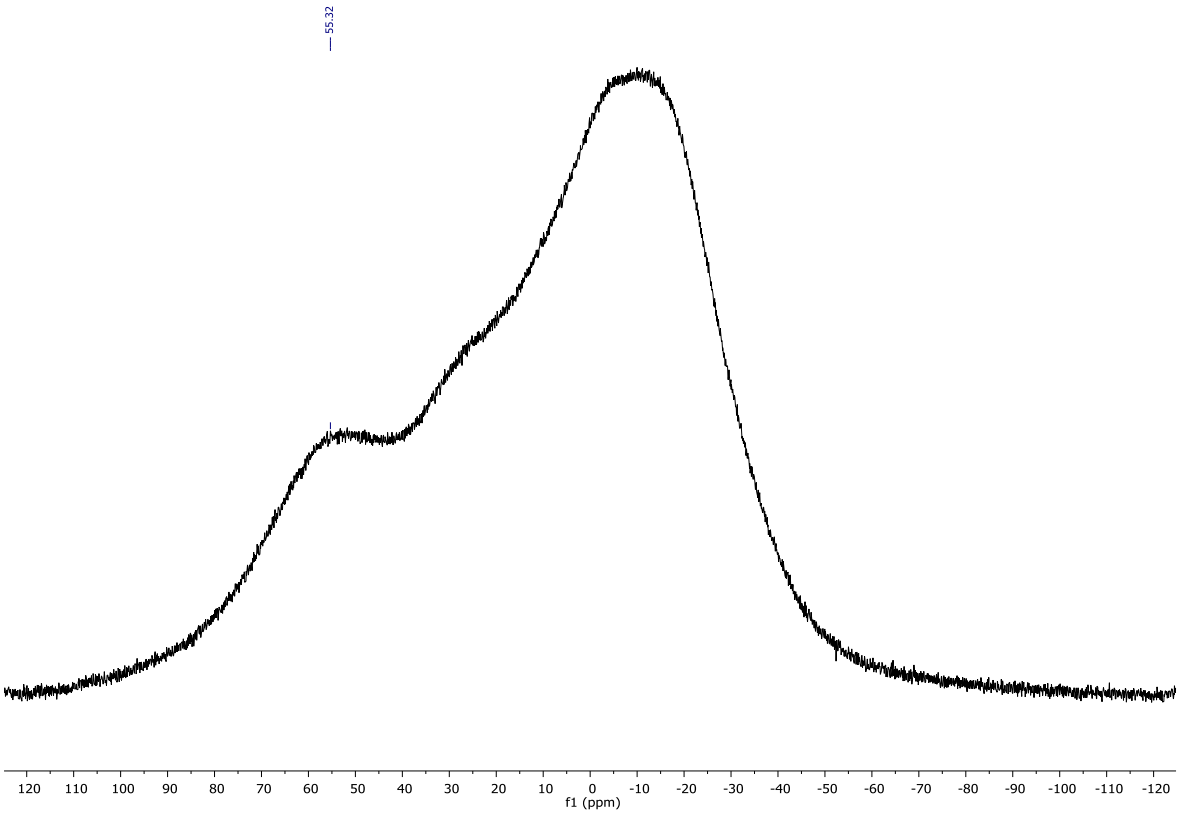

Figure 5.3.23. $^{11}B\{^{1}H\}$ NMR spectrum of **5bc** (in $CDCl_3$, 128 MHz).

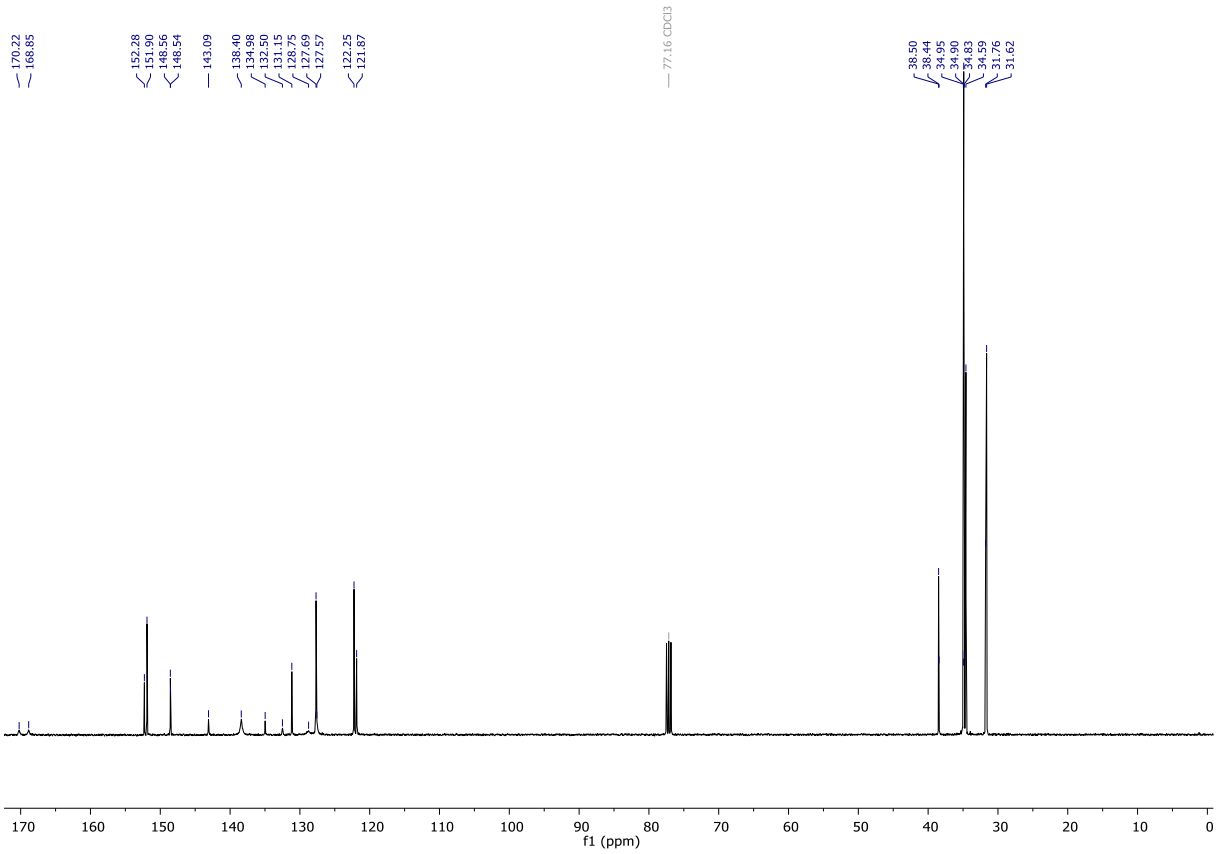

Figure 5.3.24. ^{13}C NMR spectrum of **5bc** (in $CDCl_3$, 101 MHz)

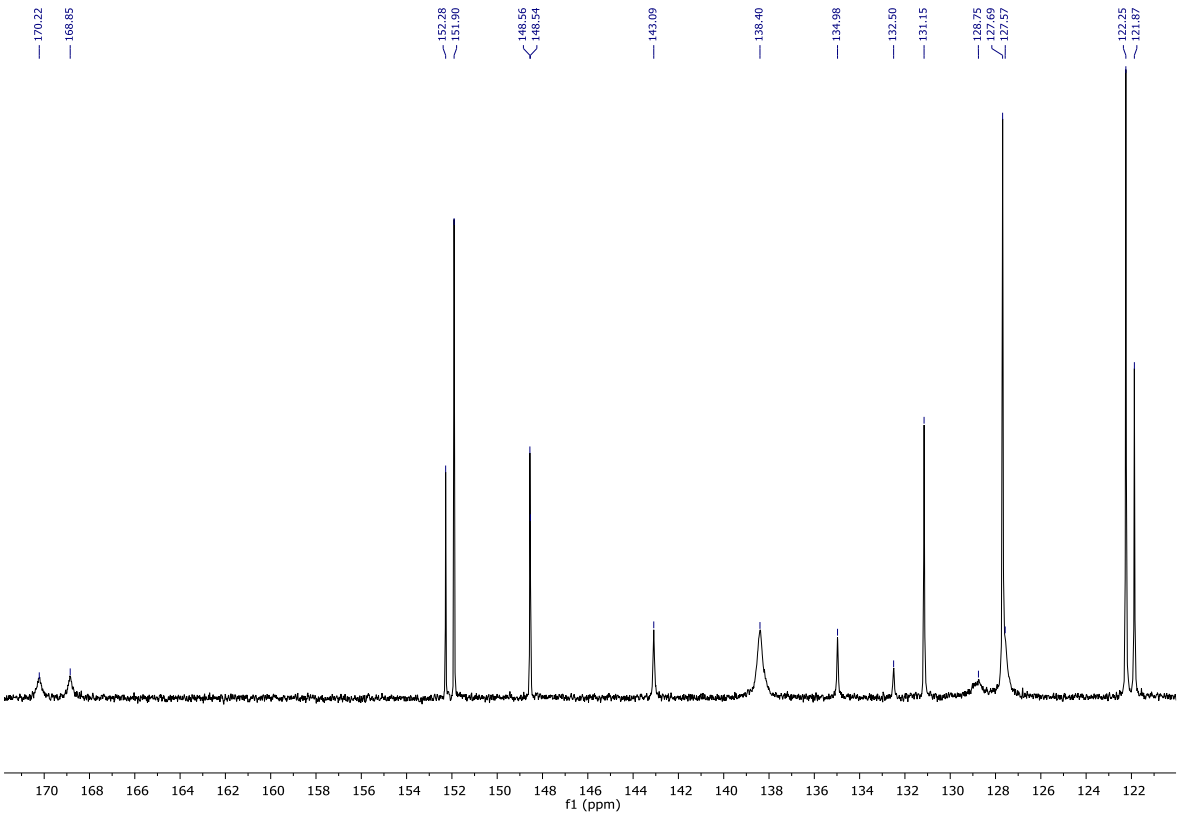

Figure 5.3.25. Detail (aromatic region) of the ^{13}C NMR spectrum of **5bc** (in $CDCl_3$, 101 MHz).

UV–vis spectra

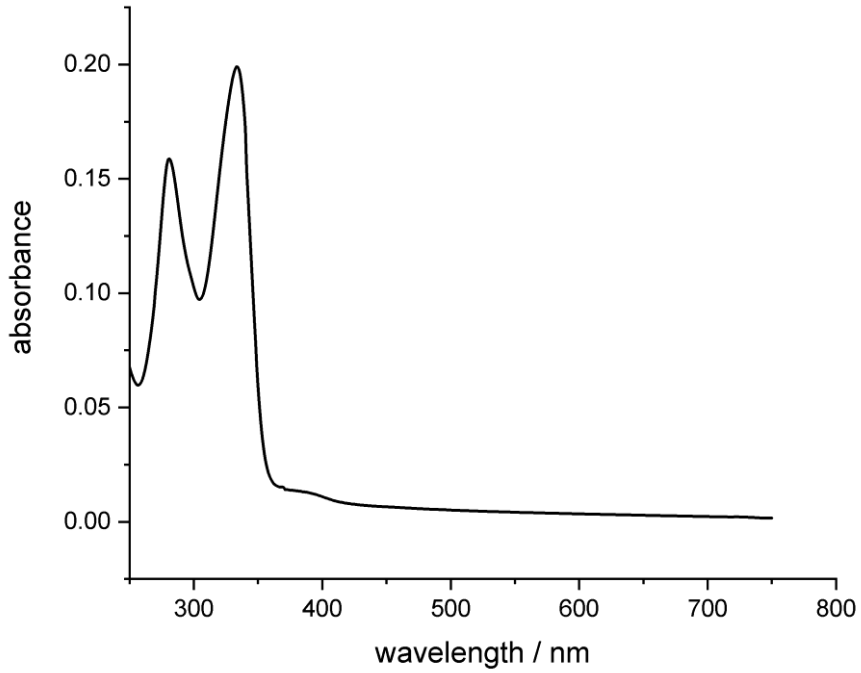

Figure 5.3.26. UV–vis spectrum of **4a** (in THF).

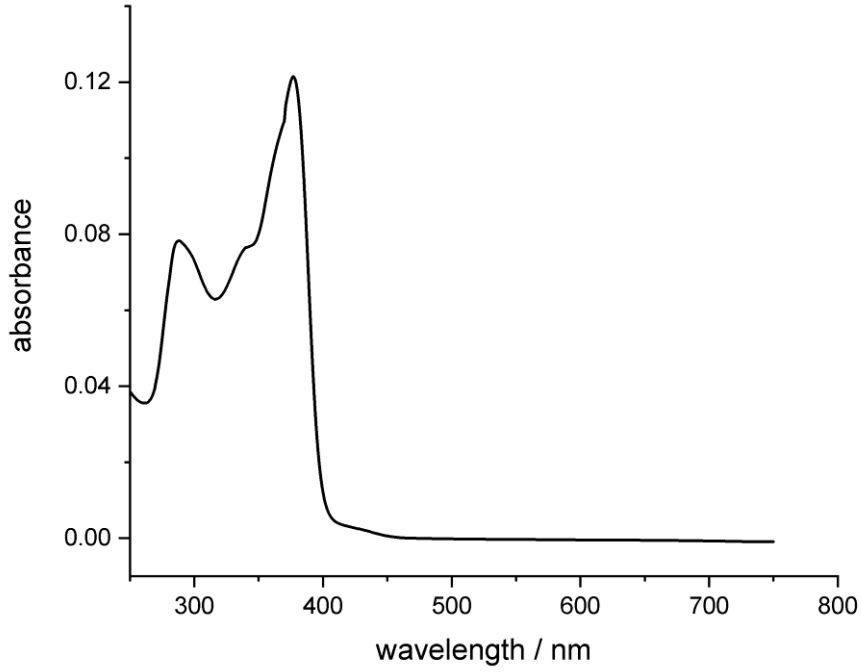

Figure 5.3.27. UV–vis spectrum of **5aa** (in THF).

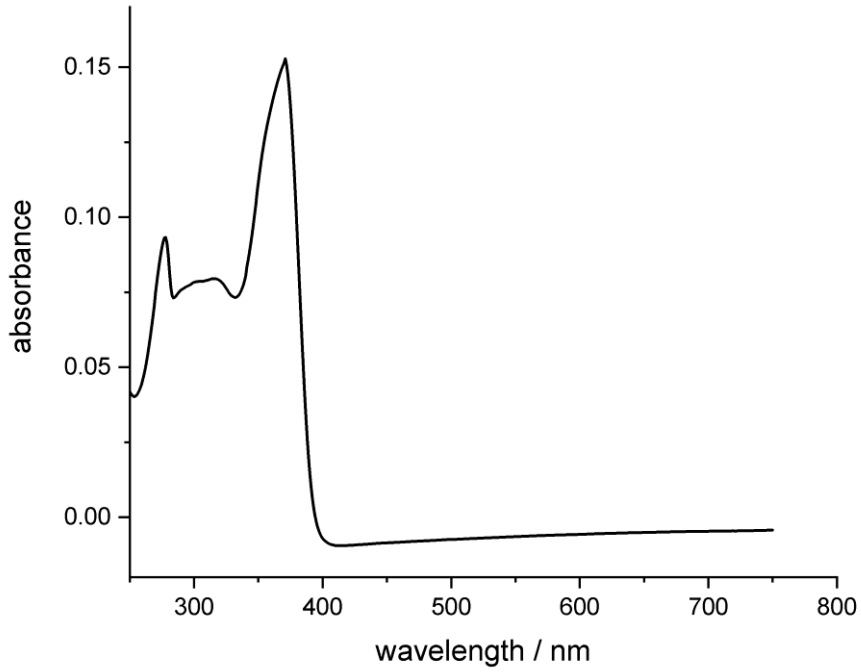

Figure 5.3.28. UV–vis spectrum of **5ac** (in THF).

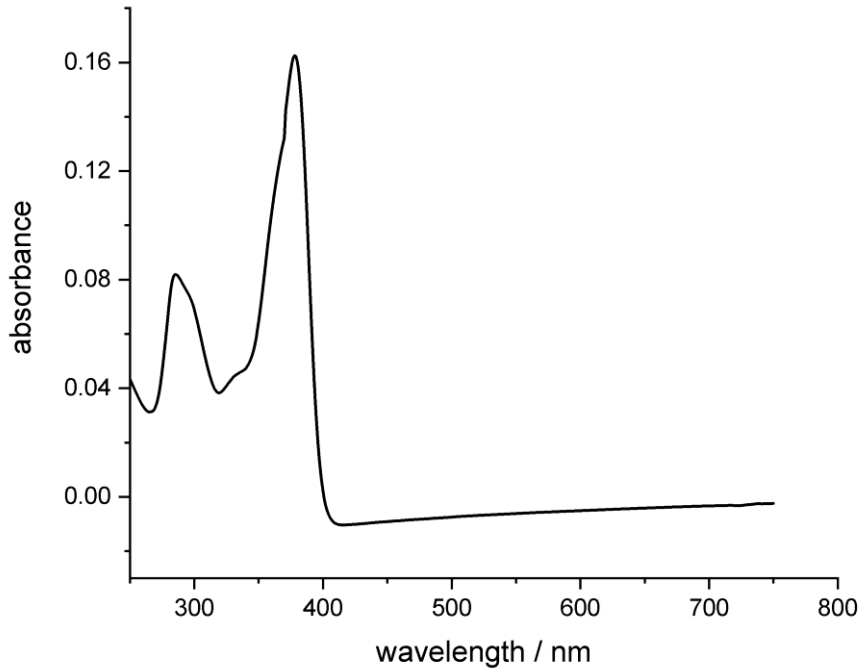

Figure 5.3.29. UV–vis spectrum of **5ba** (in THF).

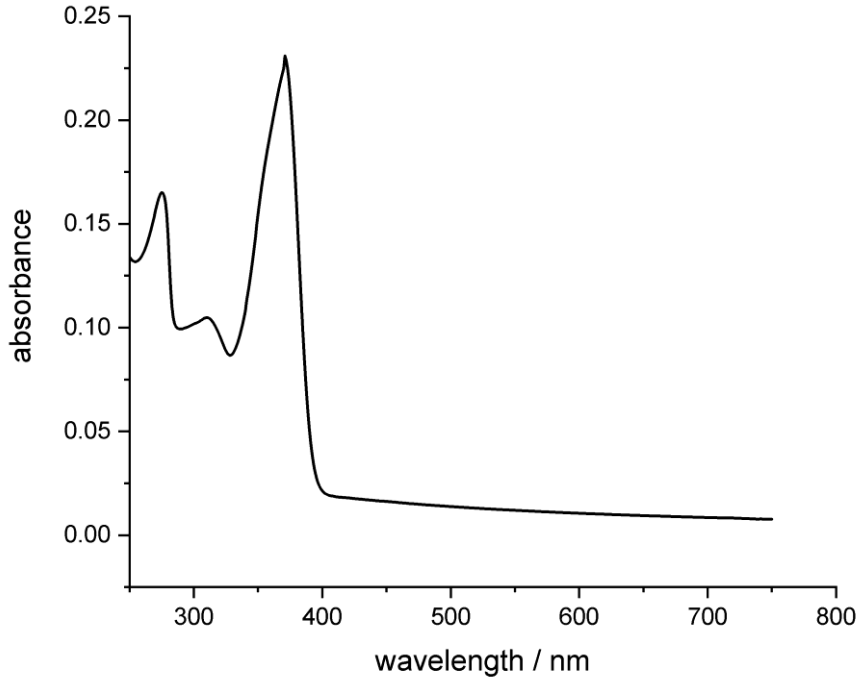

Figure 5.3.30. UV–vis spectrum of **5bc** (in THF).

Fluorescence spectra

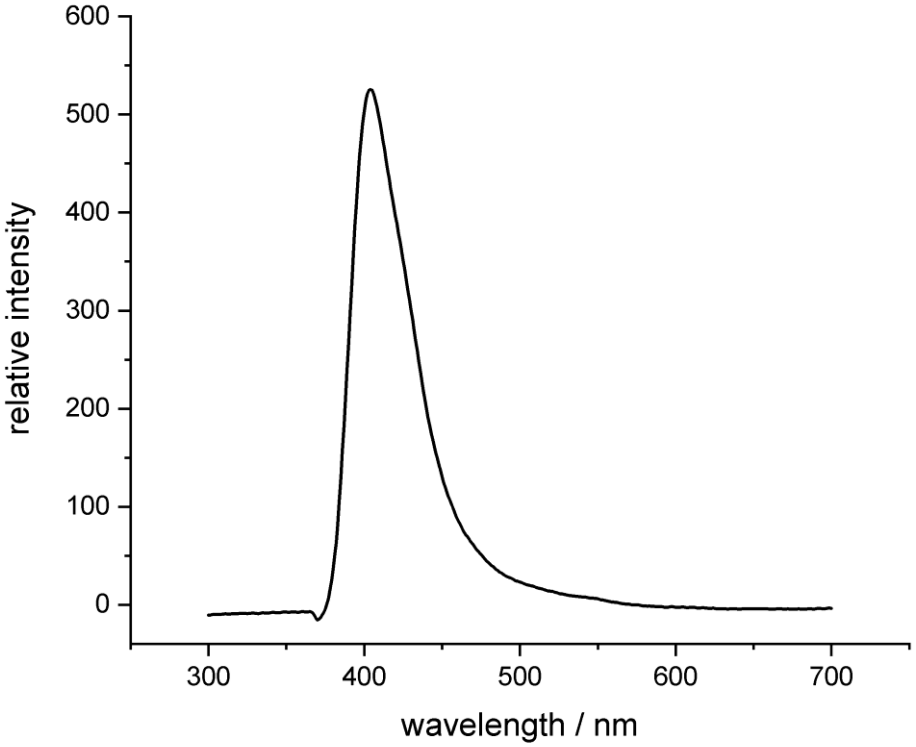

Figure 5.3.31. Fluorescence spectrum of **5ba** (in THF, λ_{ex} = 378 nm).

Mass spectra

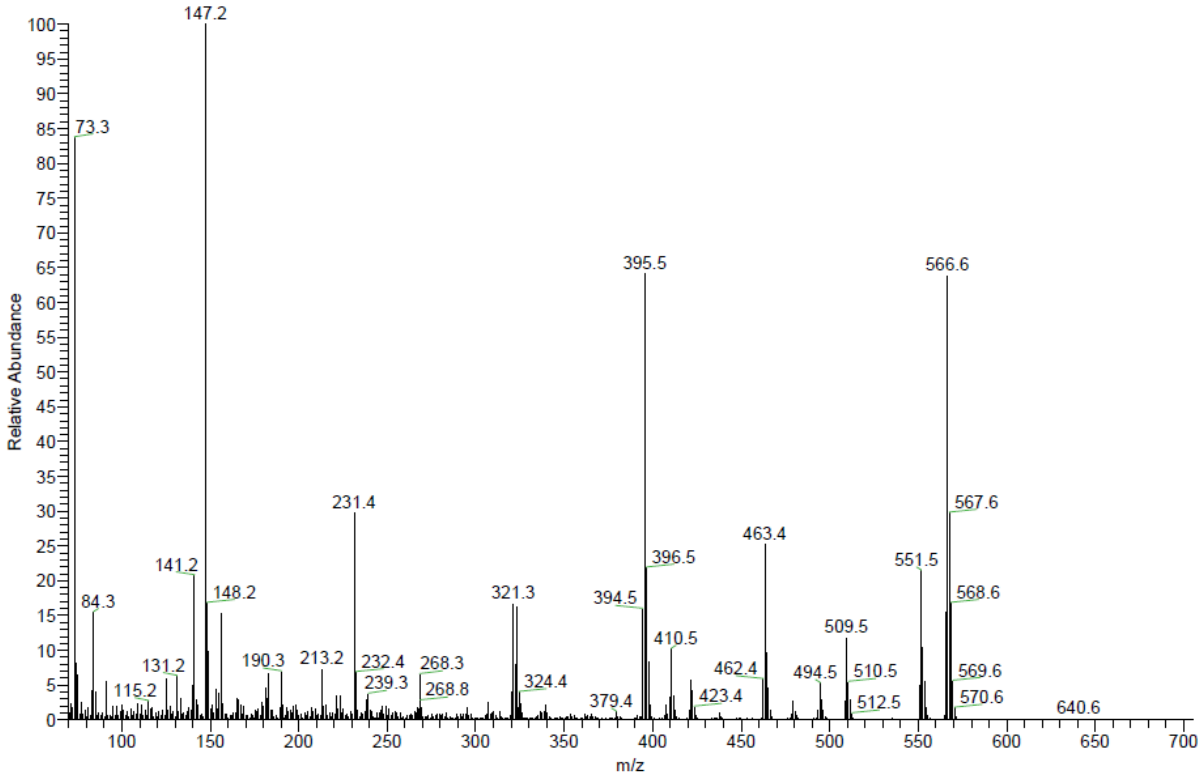

Figure 5.3.32. EI mass spectrum of **4a**.

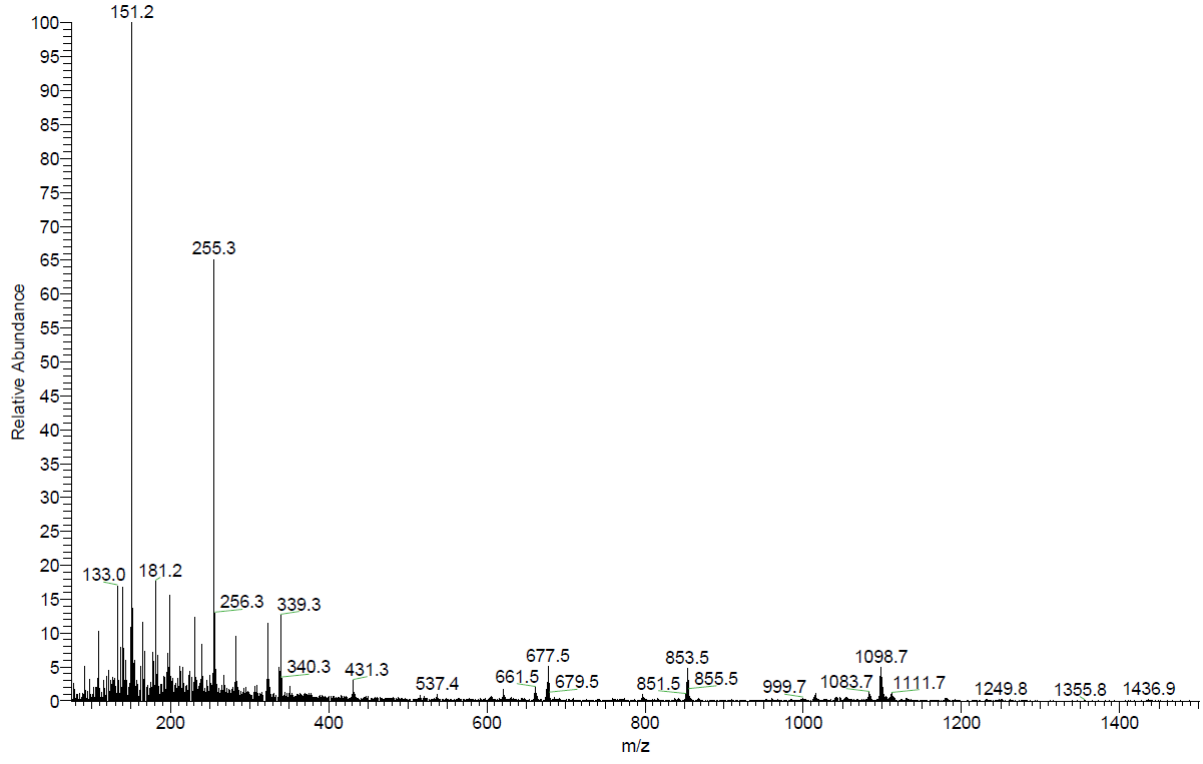

Figure 5.3.33. SIMS mass spectrum of **5aa**.

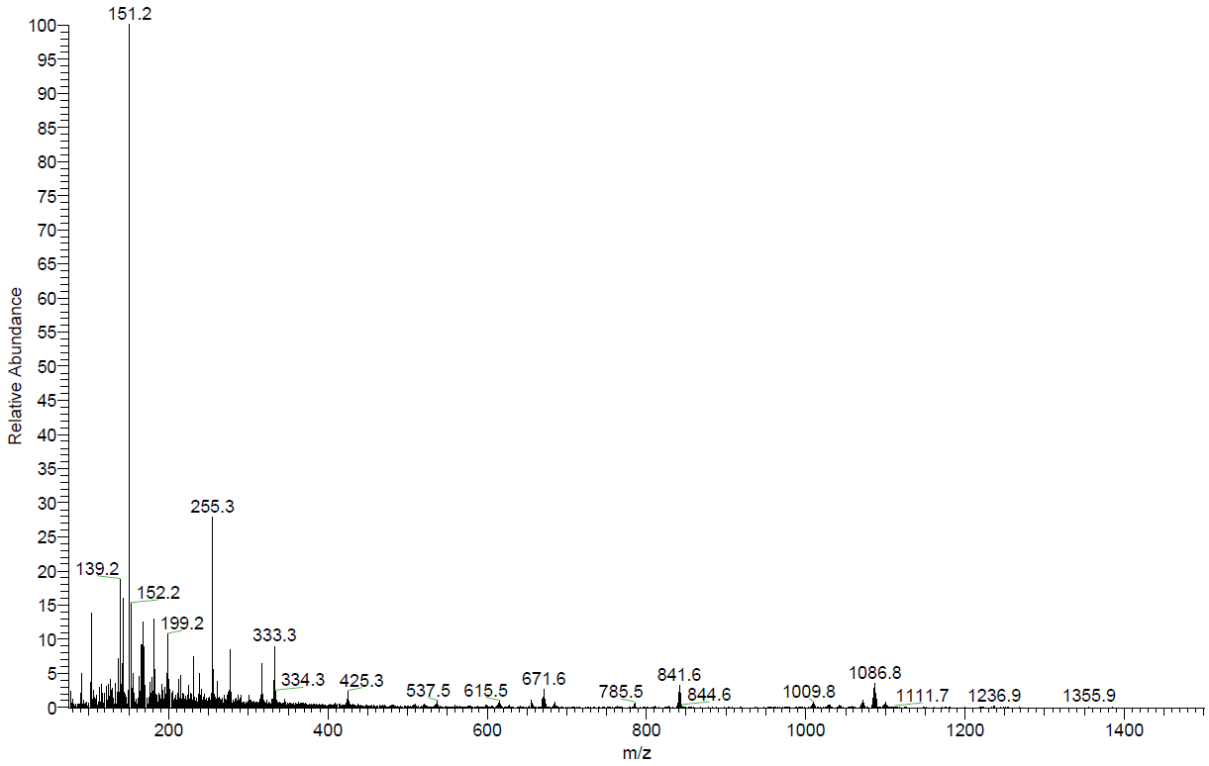

Figure 5.3.34. SIMS mass spectrum of **5ac**.

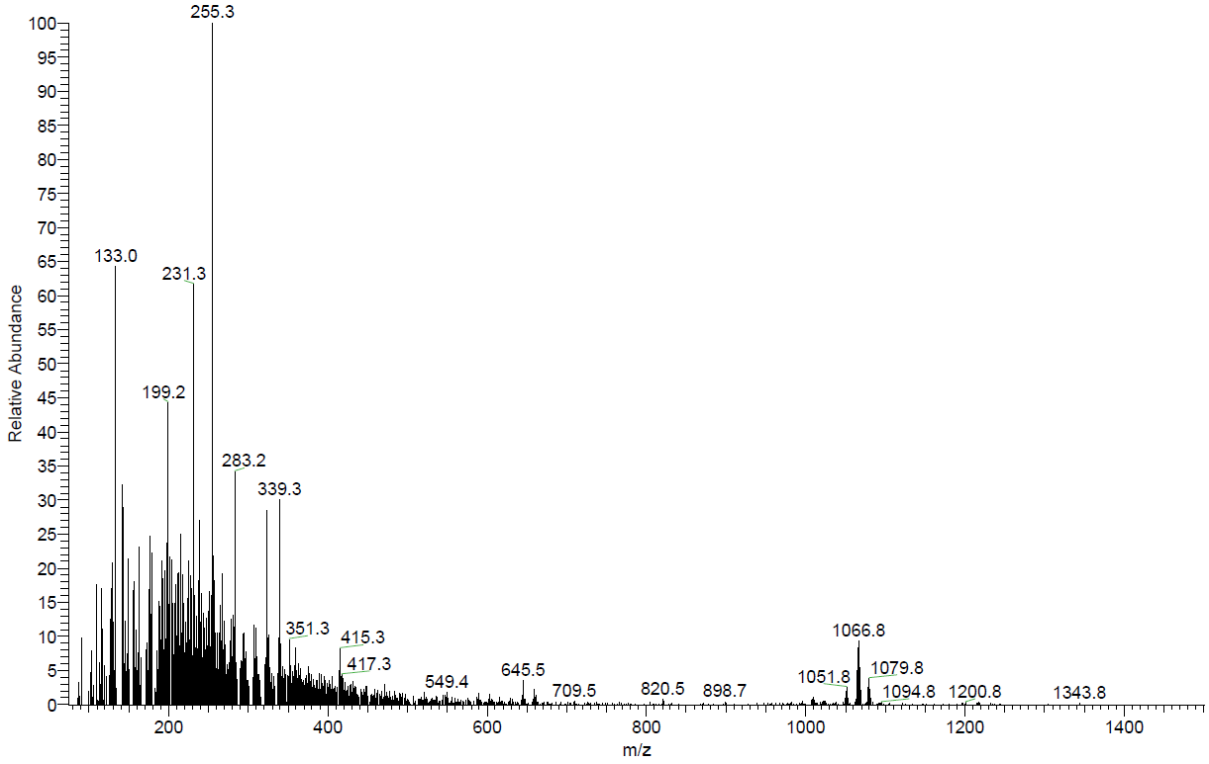

Figure 5.3.35. SIMS mass spectrum of **5ba**.

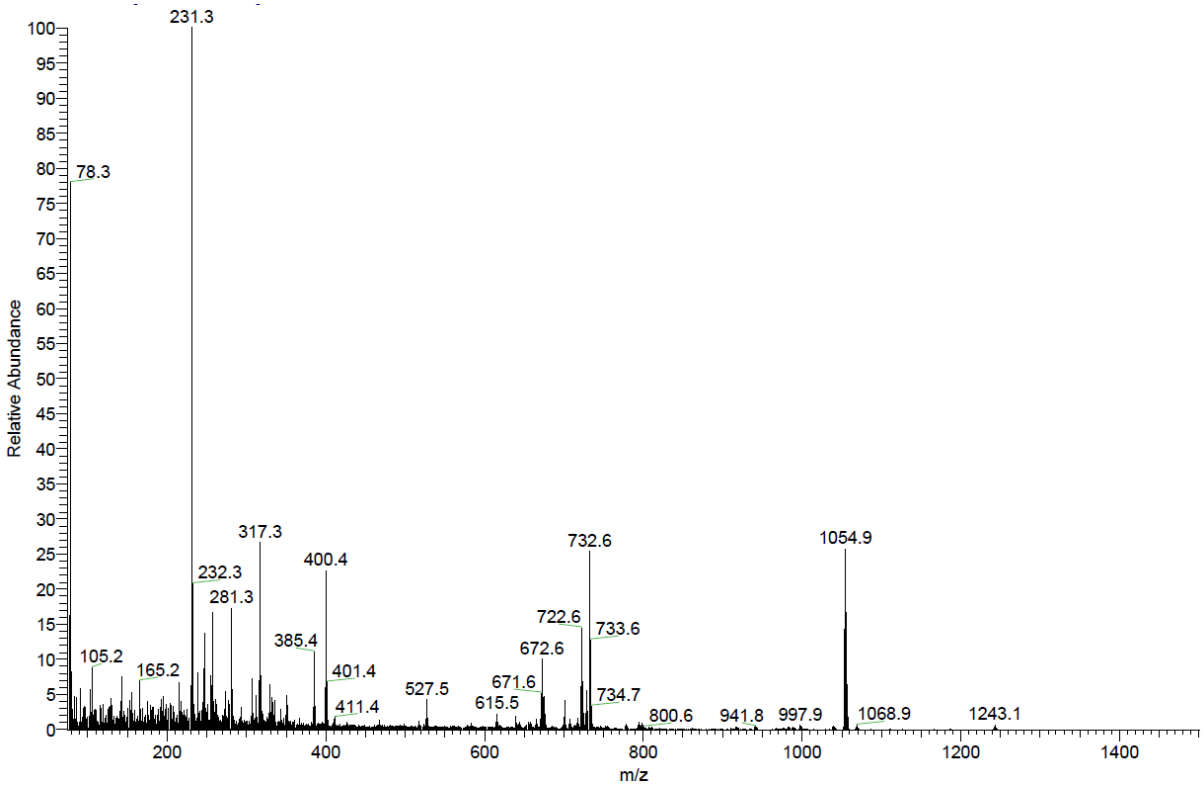

Figure 5.3.36. EI mass spectrum of **5bc**.

Cyclic Voltammetry

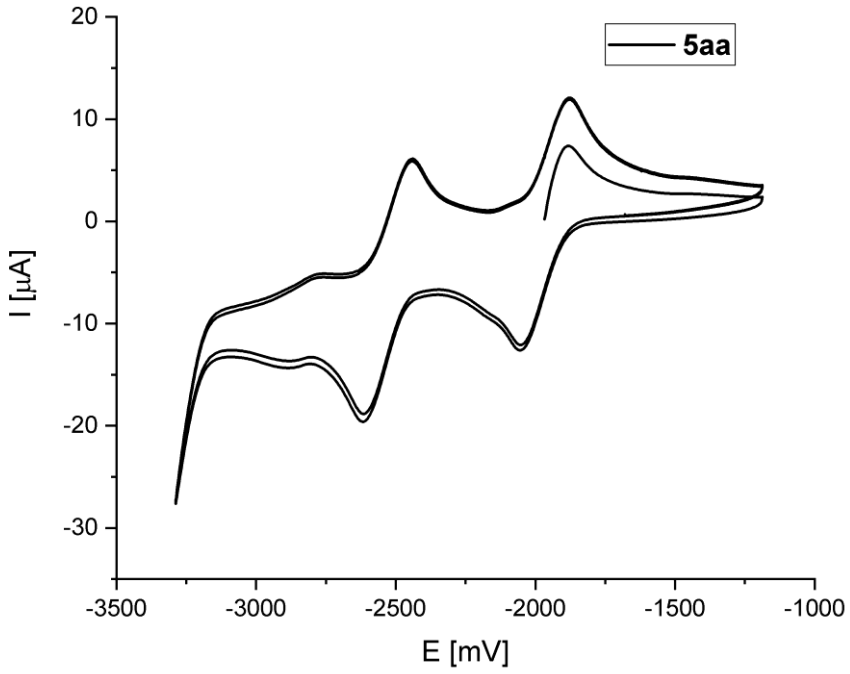

Figure 5.3.37. Cyclic voltammogram of **5aa** in THF ($1 \cdot 10^{-3}$ M), recorded vs the ferrocene/ferrocenium couple as internal standard (scan rate: 100 mV s^{-1}).

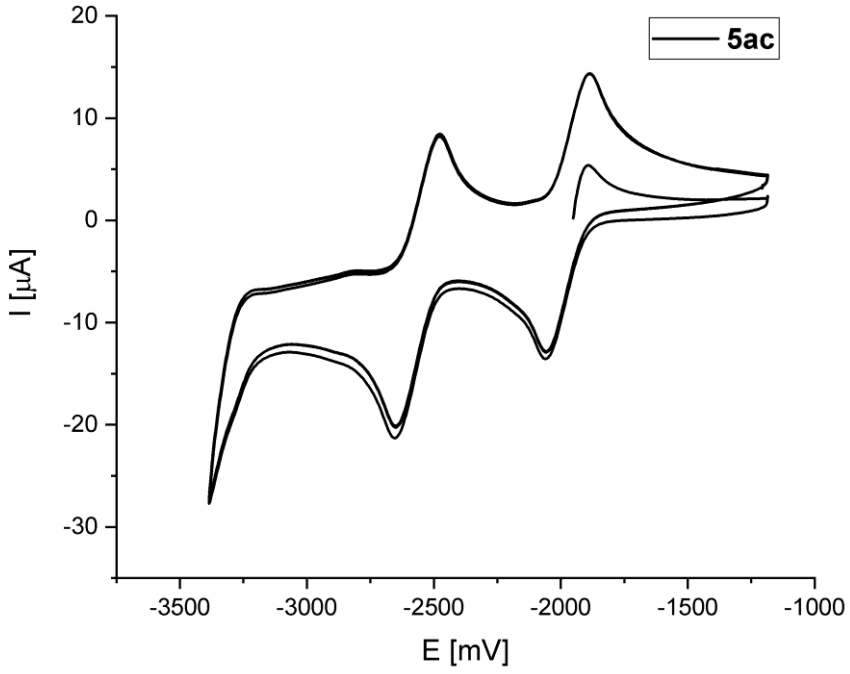

Figure 5.3.38. Cyclic voltammogram of **5ac** in THF ($1 \cdot 10^{-3}$ M), recorded vs the ferrocene/ferrocenium couple as internal standard (scan rate: 100 mV s^{-1}).

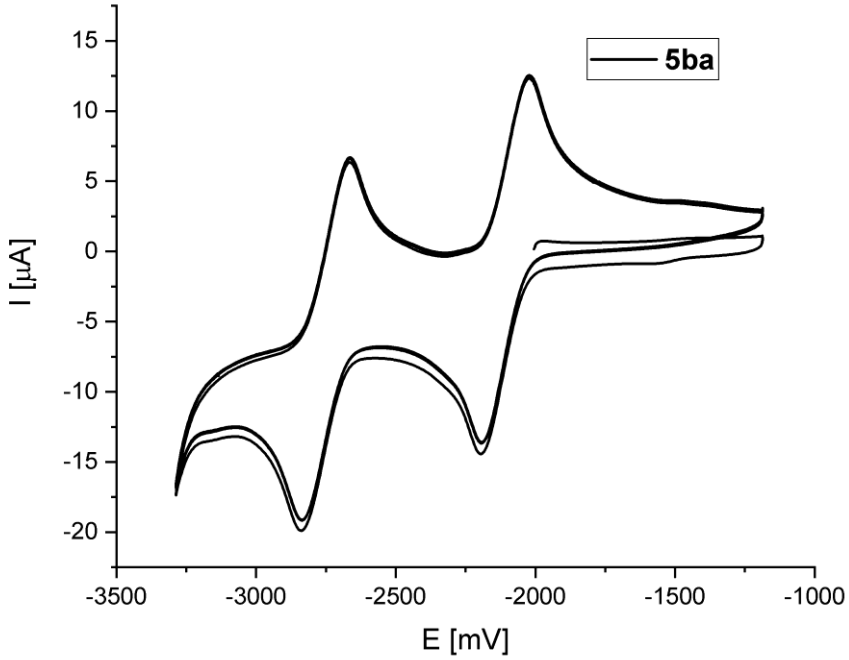

Figure 5.3.39. Cyclic voltammogram of **5ba** in THF ($1 \cdot 10^{-3}$ M), recorded vs the ferrocene/ferrocenium couple as internal standard (scan rate: 100 mV s^{-1}).

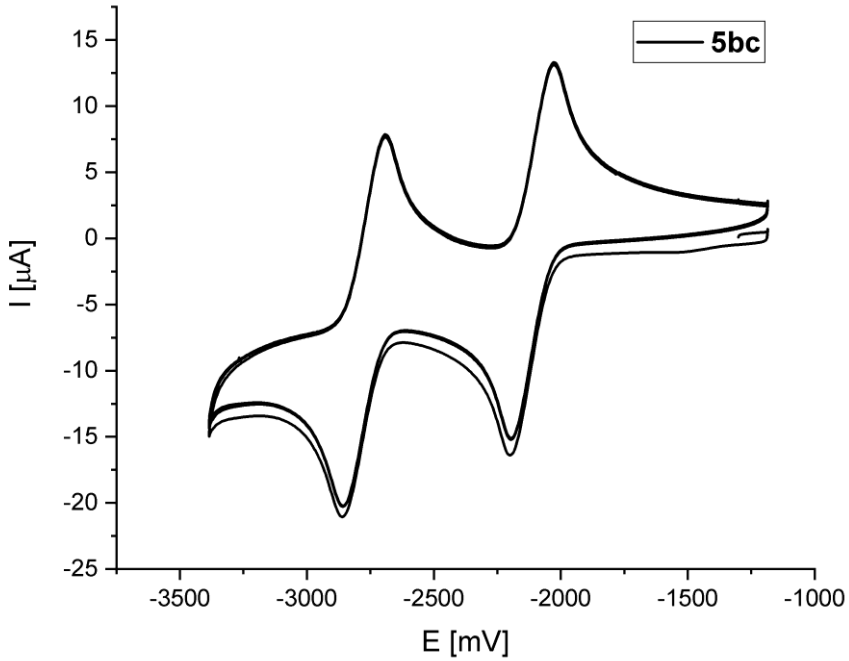

Figure 5.3.40. Cyclic voltammogram of **5bc** in THF ($1 \cdot 10^{-3}$ M), recorded vs the ferrocene/ferrocenium couple as internal standard (scan rate: 100 mV s^{-1}).

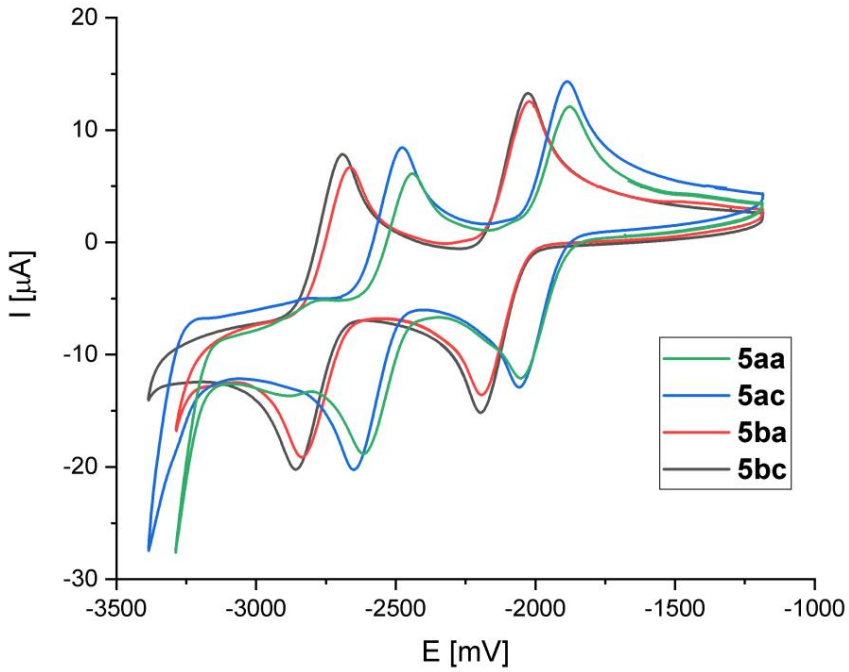

Figure 5.3.41. Comparison of the cyclic voltammograms of **5** in THF ($1 \cdot 10^{-3}$ M), recorded vs the ferrocene/ferrocenium couple as internal standard (scan rate: 100 mV s^{-1}).

5.4 Bifuran-bridged Bisboranes: Highly Luminescent B-doped Oligohetarenes

NMR spectra

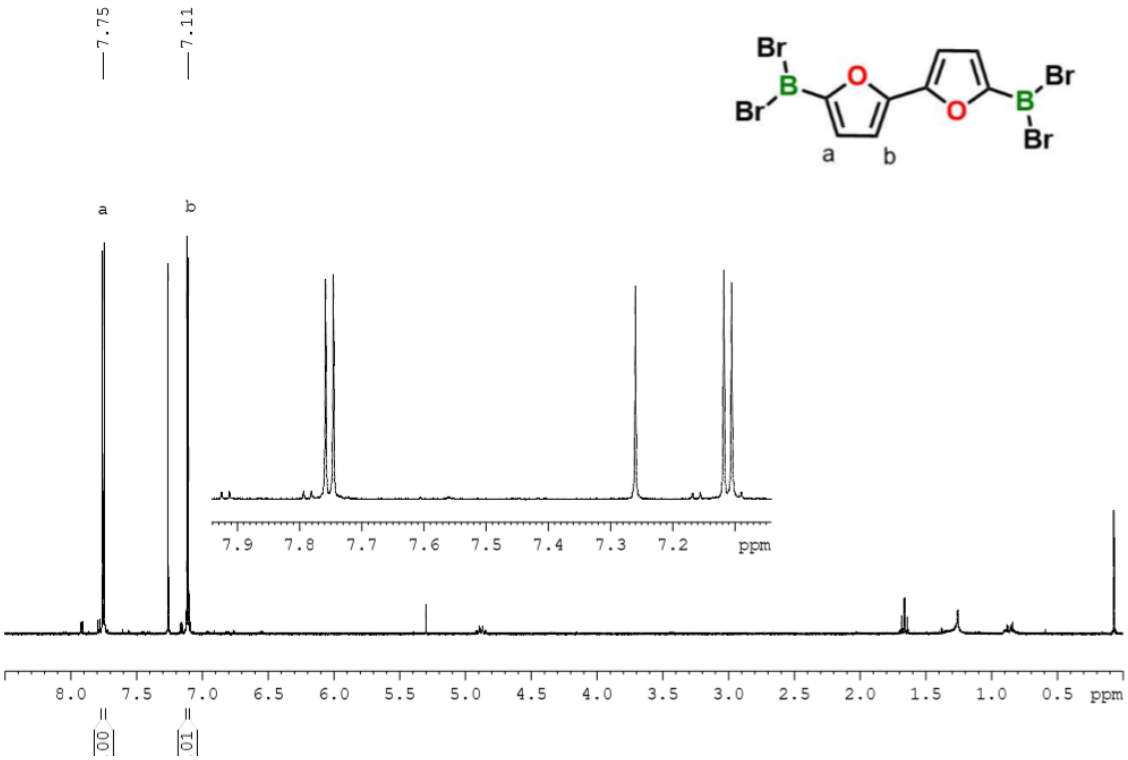

Figure 5.4.1. ^{1}H NMR spectrum of **5** (300 MHz, in $CDCl_3$).

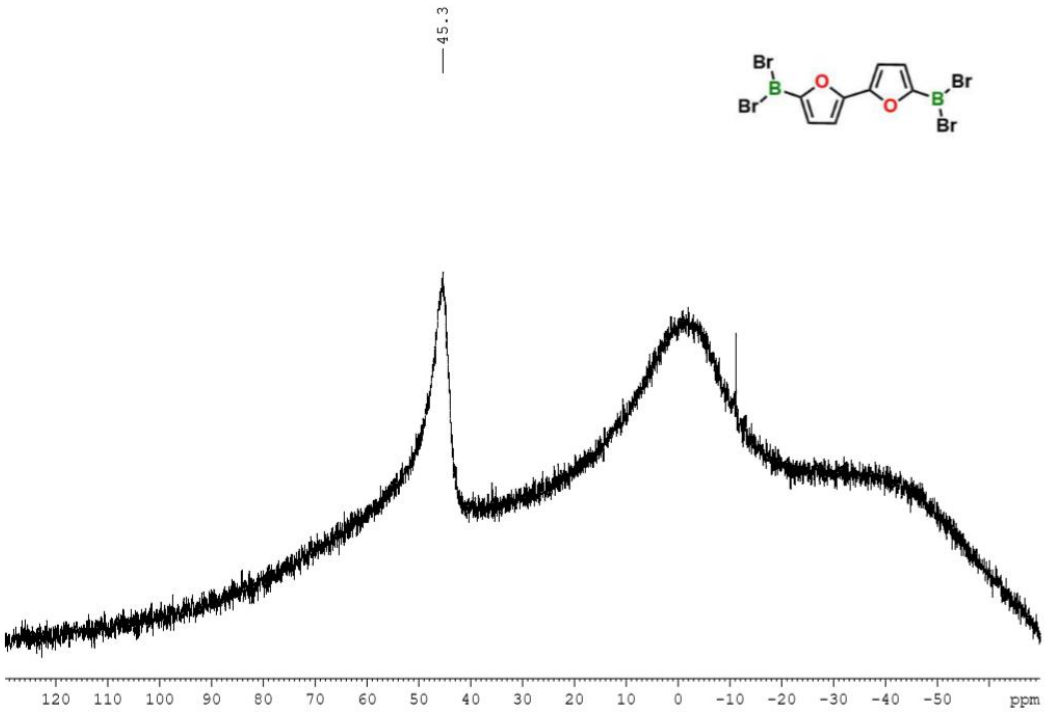

Figure 5.4.2. $^{11}B\{^{1}H\}$ NMR spectrum of **5** (96 MHz, in $CDCl_3$).

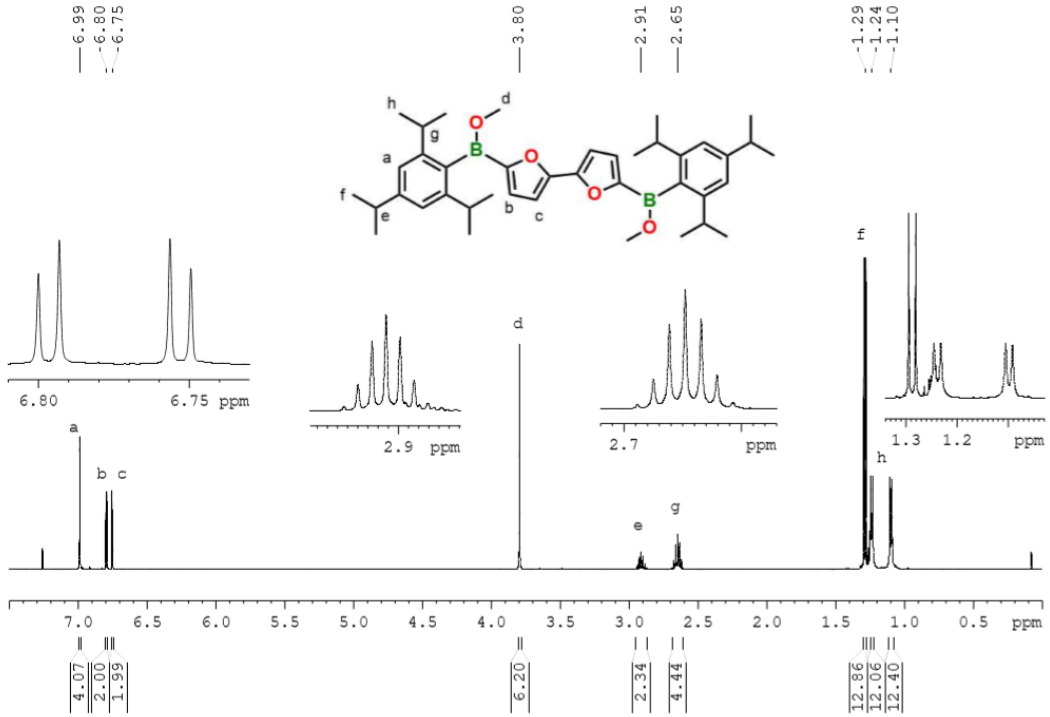

Figure 5.4.3. ^{1}H NMR spectrum of **7** (500 MHz, in $CDCl_3$).

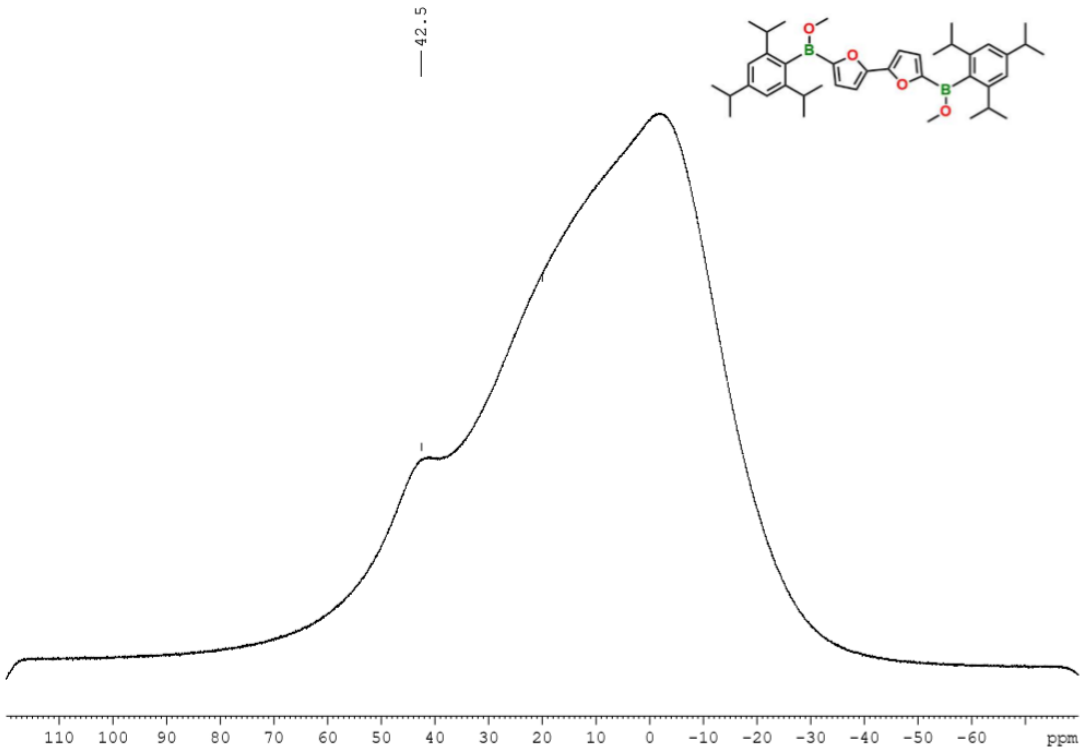

Figure 5.4.4. $^{11}B\{^{1}H\}$ NMR spectrum of **7** (160 MHz, in $CDCl_3$).

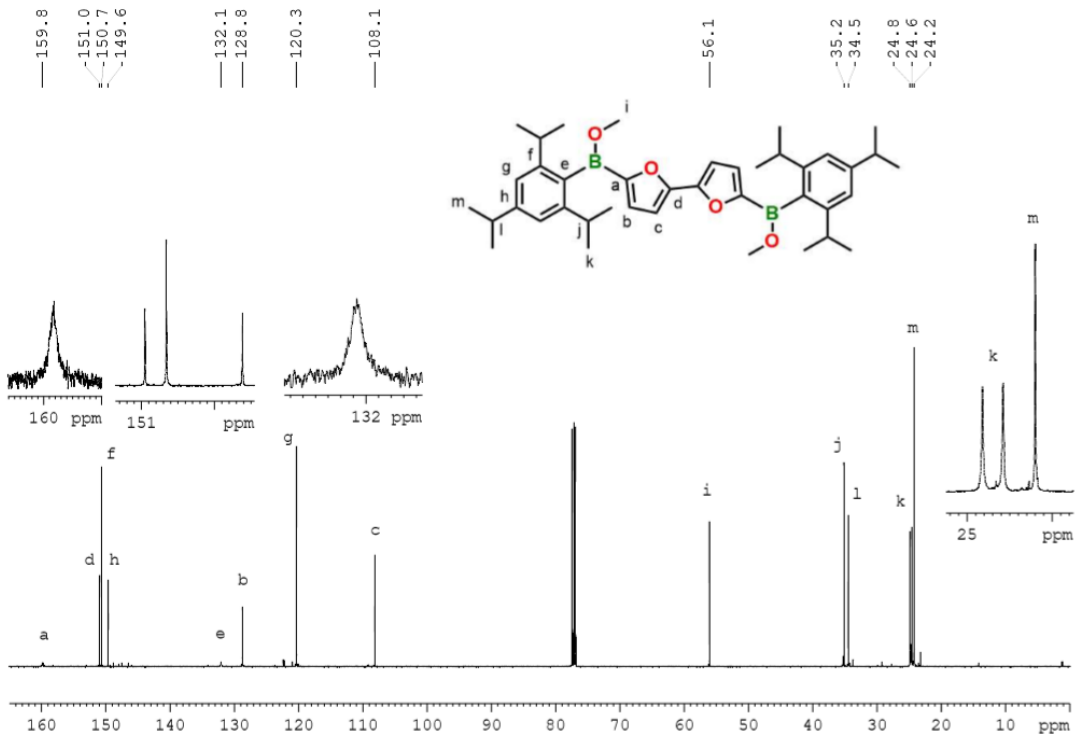

Figure 5.4.5. $^{13}C\{^{1}H\}$ NMR spectrum of **7** (126 MHz, in $CDCl_3$).

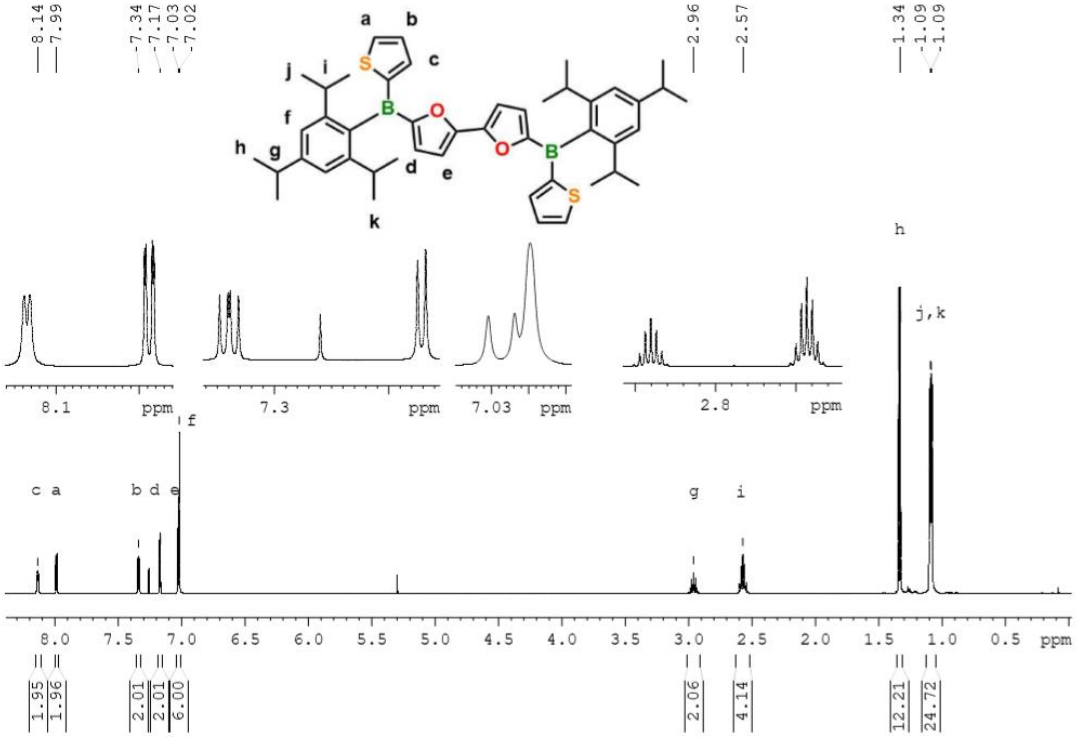

Figure 5.4.6. ^{1}H NMR spectrum of **2a^{Tip}** (500 MHz, in $CDCl_3$).

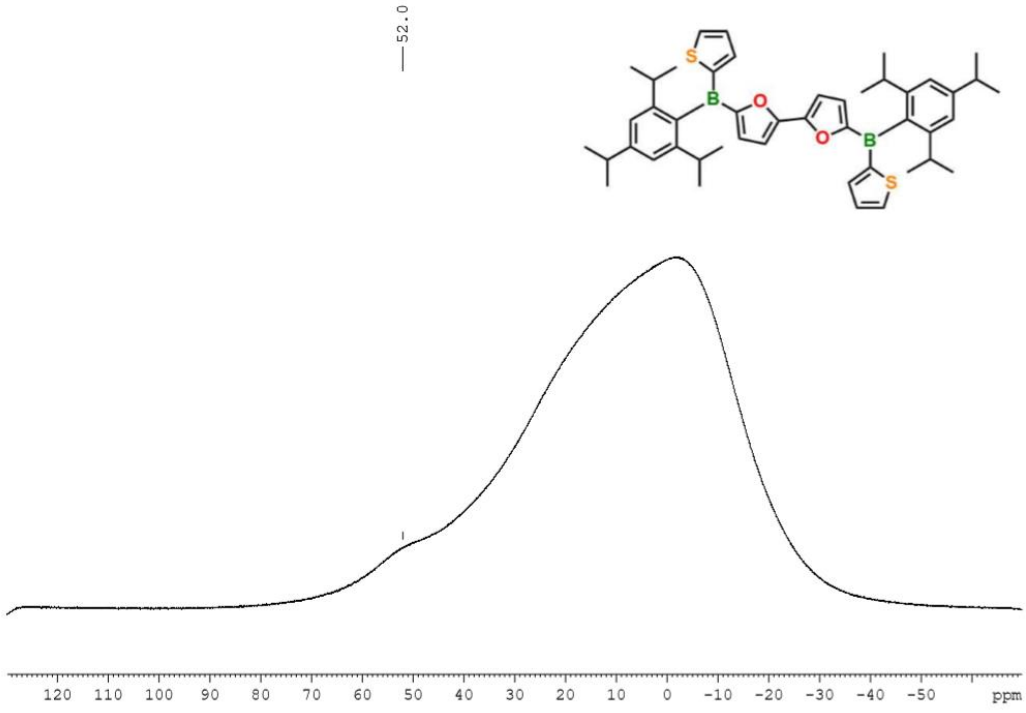

Figure 5.4.7. $^{11}B\{^{1}H\}$ NMR spectrum of **2a^{Tip}** (160 MHz, in $CDCl_3$).

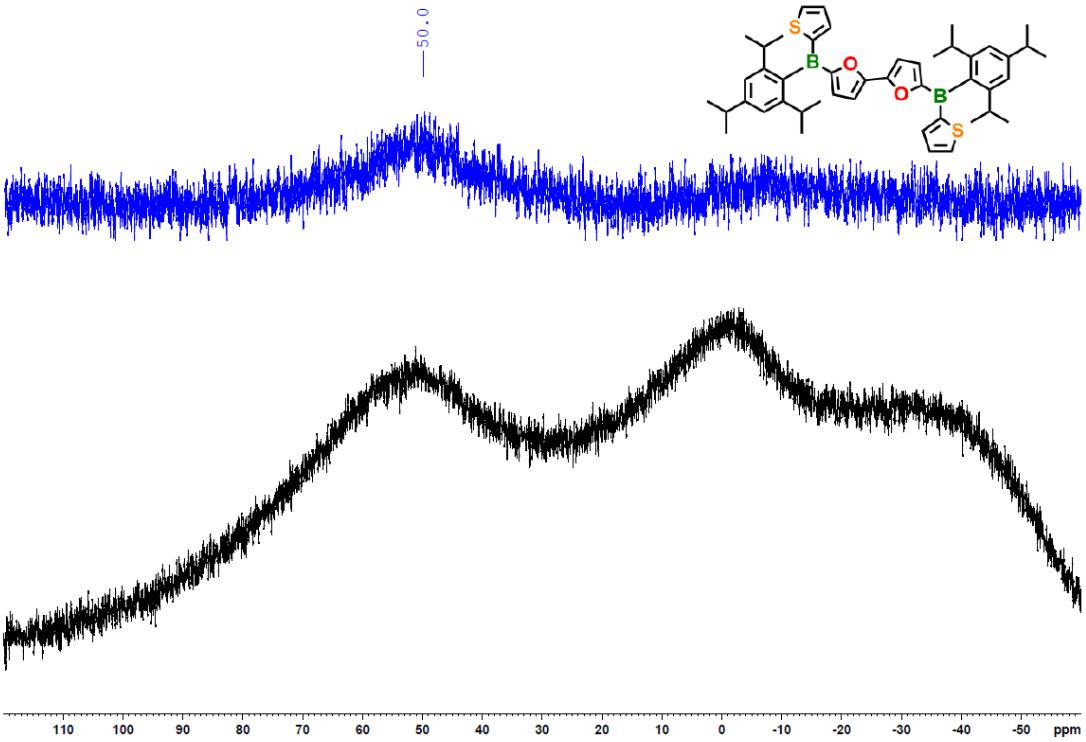

Figure 5.4.8. $^{11}B\{^1H\}$ NMR spectrum of **2a^{Tip}** (96 MHz, in $CDCl_3$) before (black) and after (blue) background substraction.

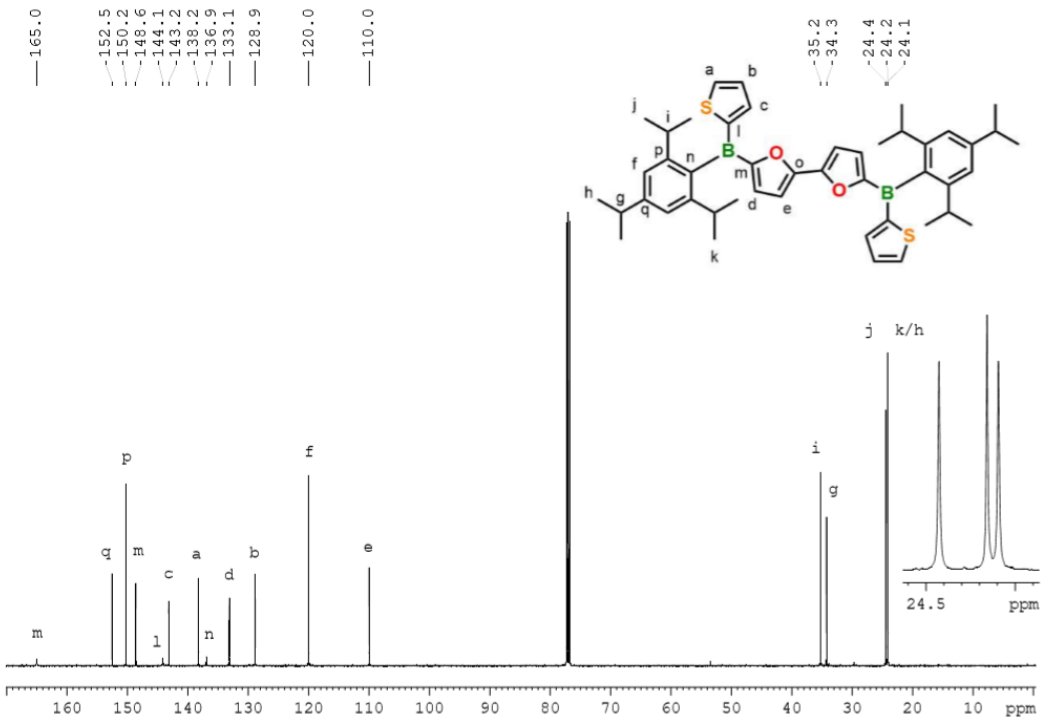

Figure 5.4.9. $^{13}C\{^1H\}$ NMR spectrum of **2a^{Tip}** (126 MHz, in $CDCl_3$).

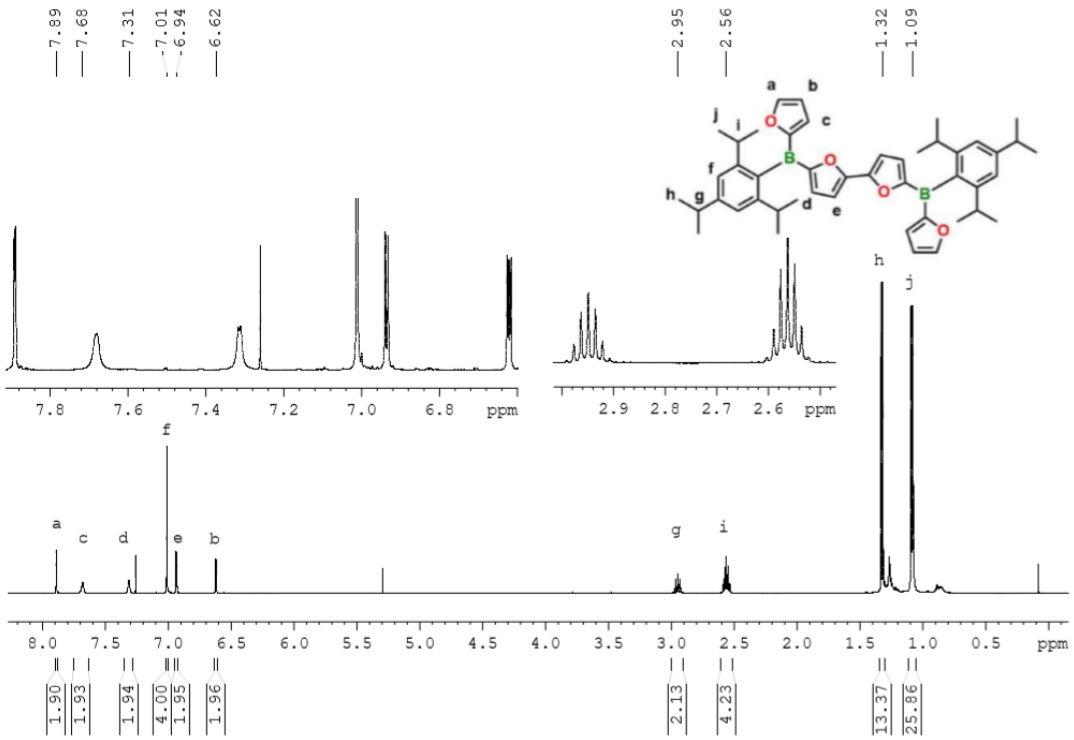

Figure 5.4.10. ^{1}H NMR spectrum of **2b^{Tip}** (500 MHz, in $CDCl_3$).

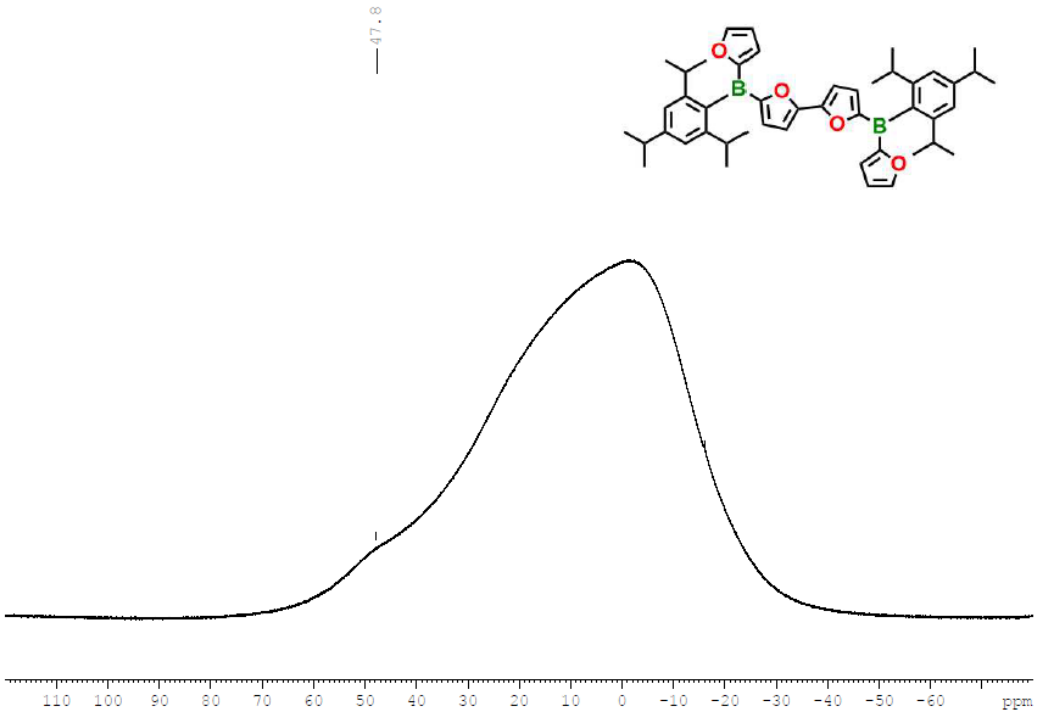

Figure 5.4.11. $^{11}B\{^{1}H\}$ NMR spectrum of **2b^{Tip}** (160 MHz, in $CDCl_3$).

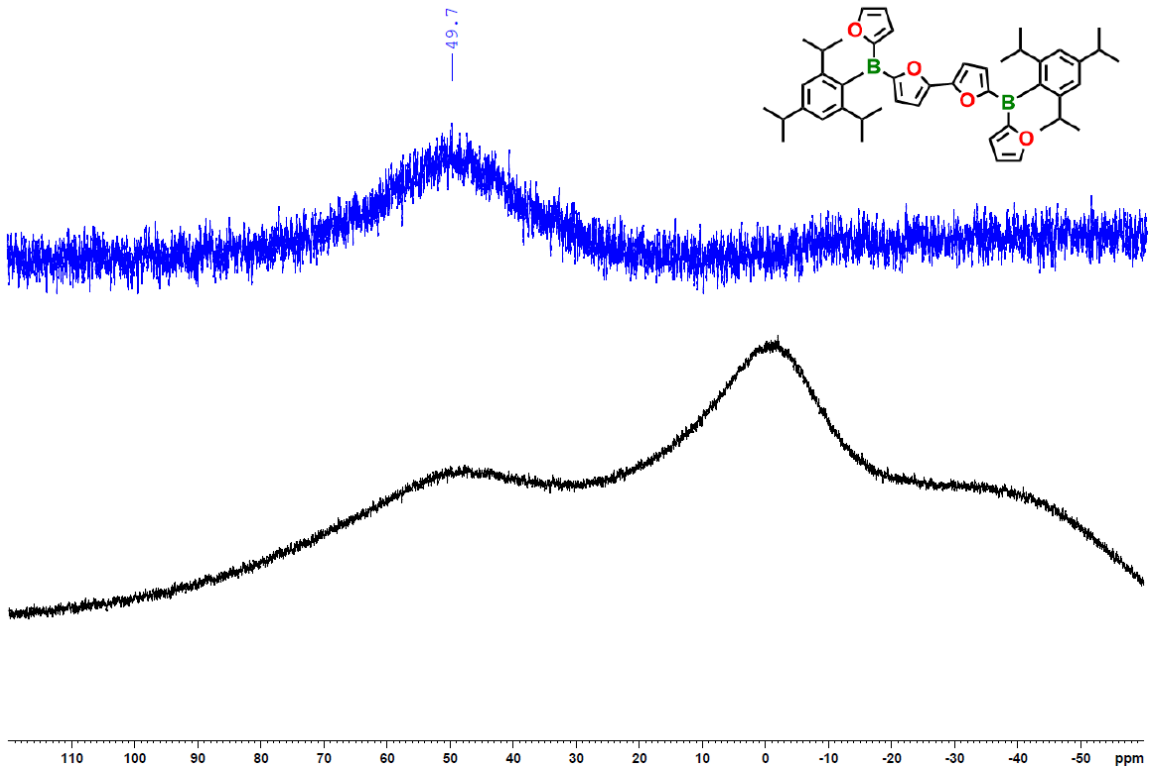

Figure 5.4.12. $^{11}B\{^1H\}$ NMR spectrum of **2b^{Tip}** (96 MHz, in $CDCl_3$) before (black) and after (blue) background substraction.

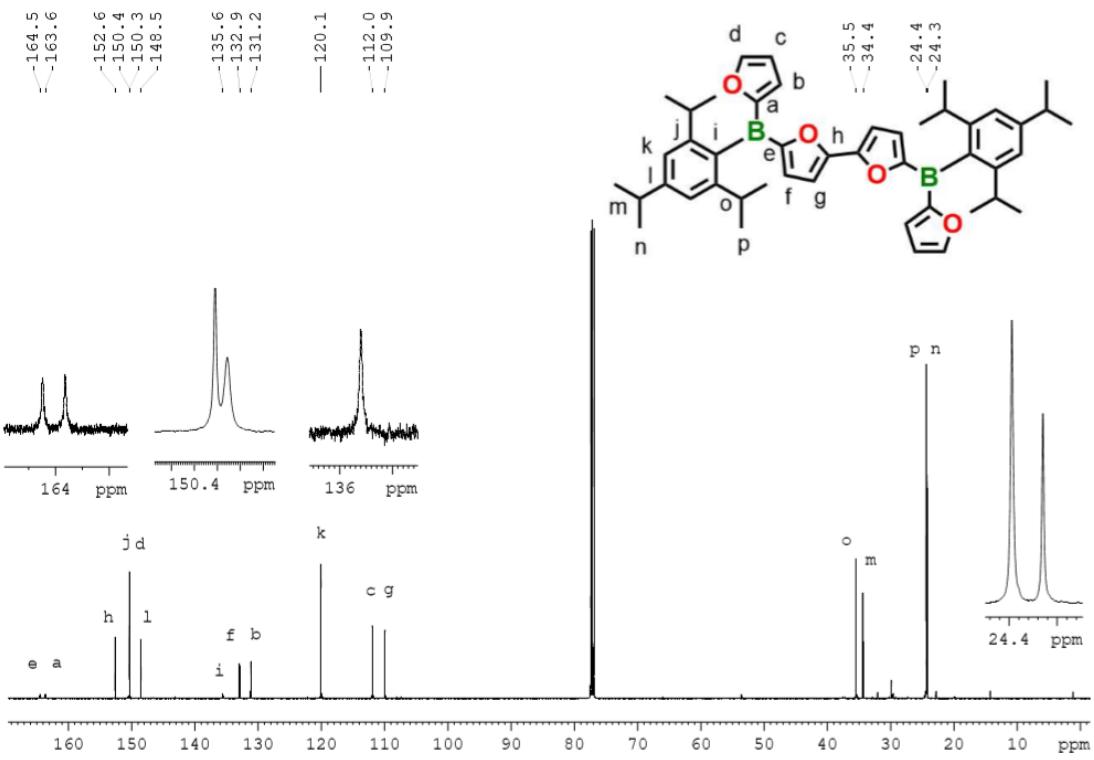

Figure 5.4.13. $^{13}C\{^1H\}$ NMR spectrum of **2b^{Tip}** (126 MHz, in $CDCl_3$).

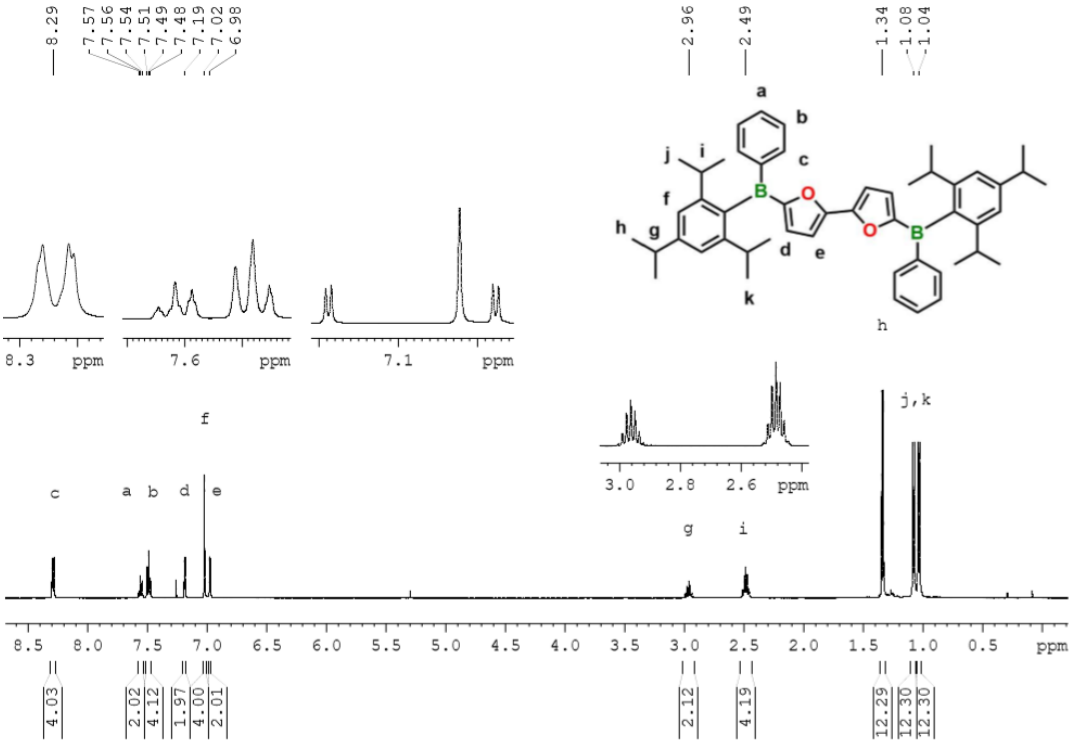

Figure 5.4.14. ^{1}H NMR spectrum of **2c^{Tip}** (500 MHz, in $CDCl_3$).

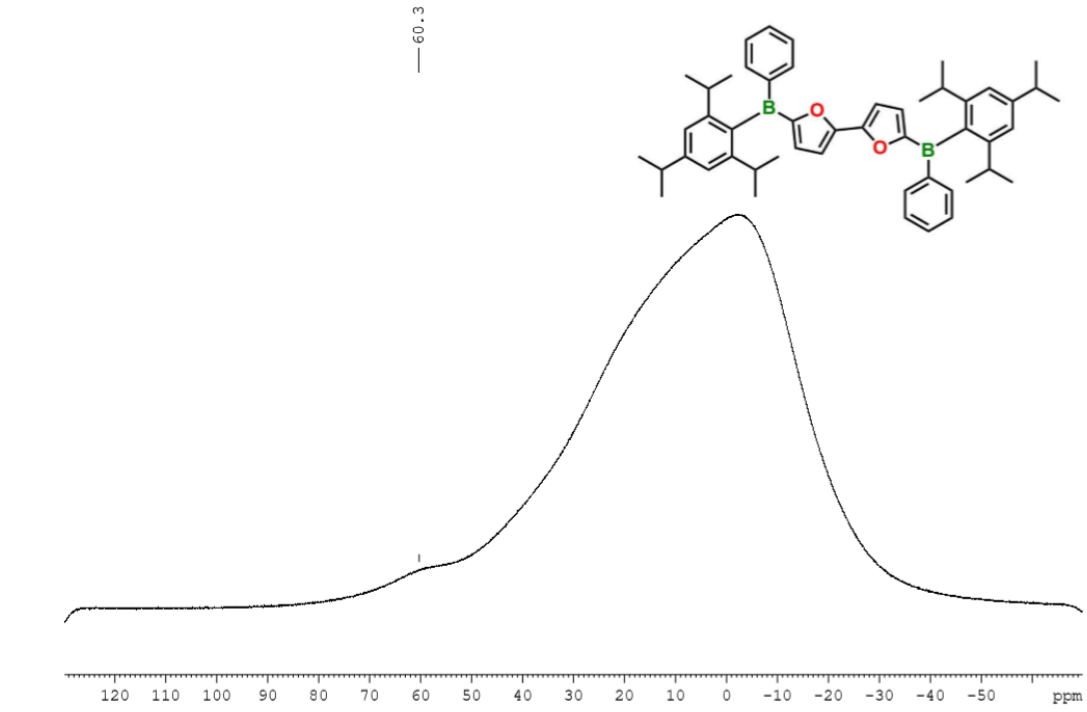

Figure 5.4.15. $^{11}B\{^{1}H\}$ NMR spectrum of **2c^{Tip}** (160 MHz, in $CDCl_3$).

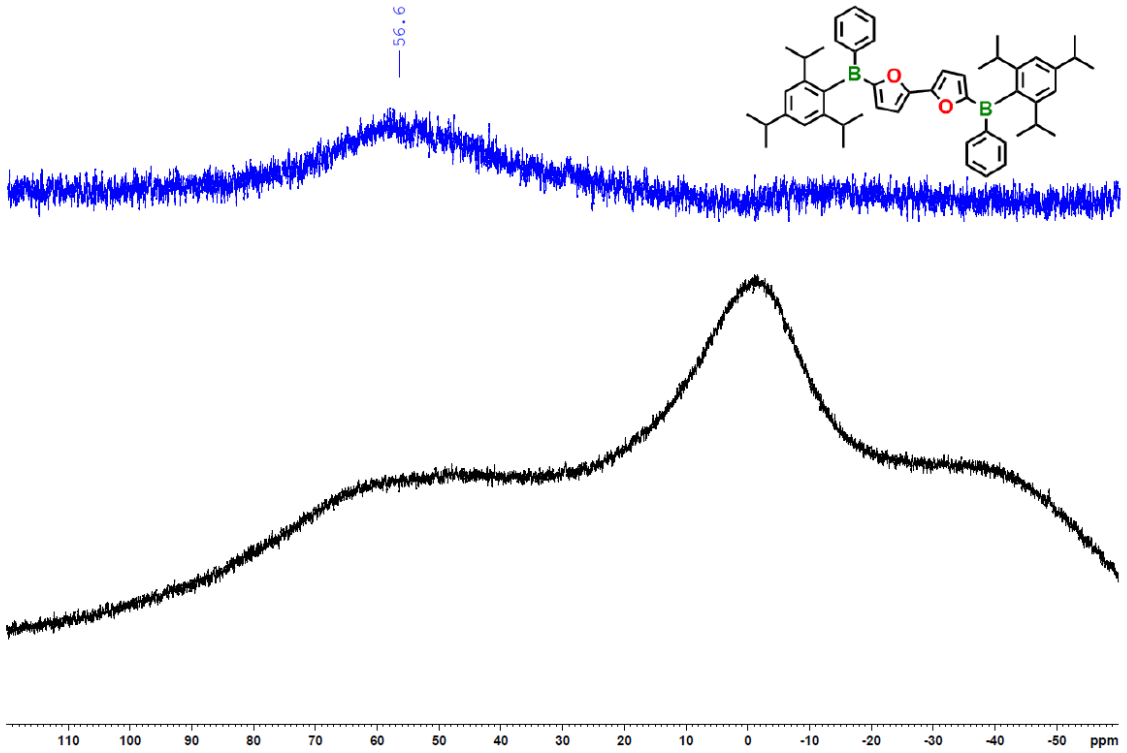

Figure 5.4.16. $^{11}B\{^1H\}$ NMR spectrum of **2c^{Tip}** (96 MHz, in $CDCl_3$) before (black) and after (blue) background substraction.

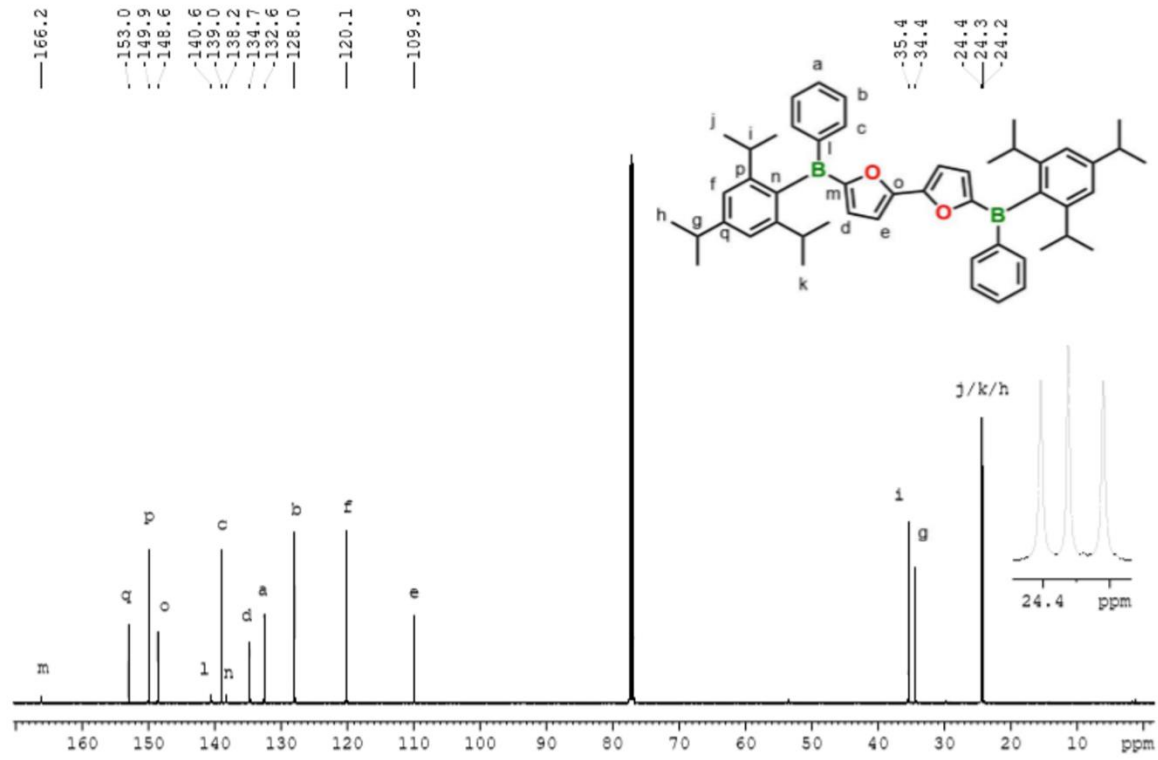

Figure 5.4.17. $^{13}C\{^1H\}$ NMR spectrum of **2c^{Tip}** (126 MHz, in $CDCl_3$).

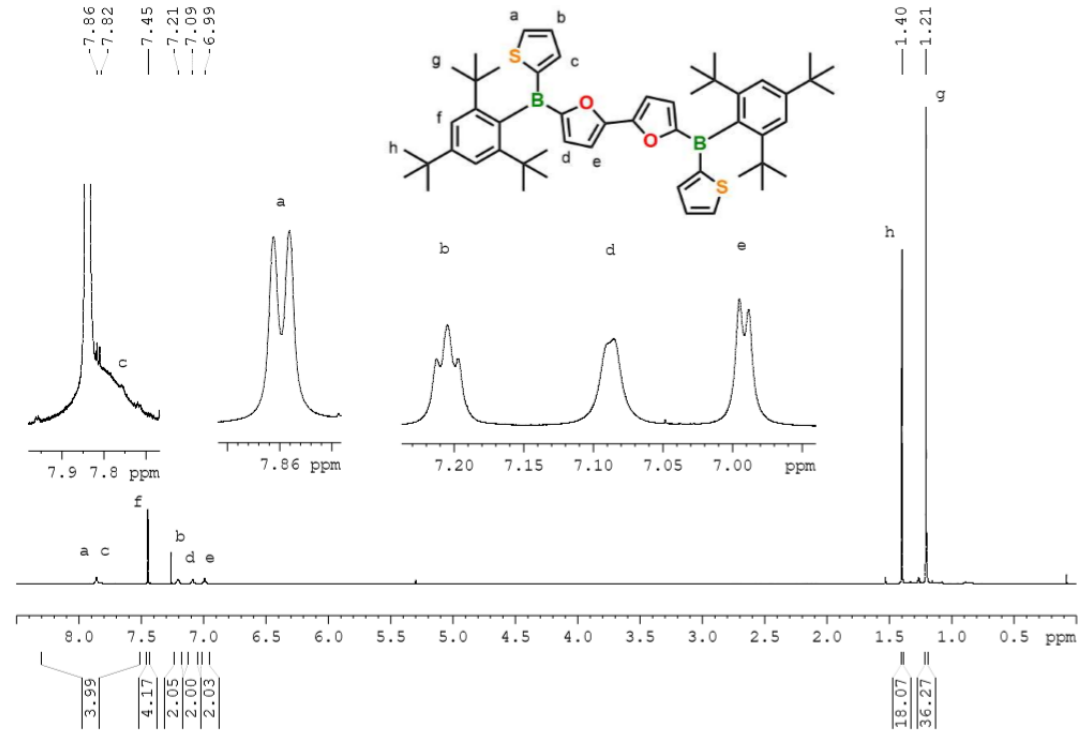

Figure 5.4.18. ^{1}H NMR spectrum of **2a^{Mes*}** (500 MHz, in $CDCl_3$).

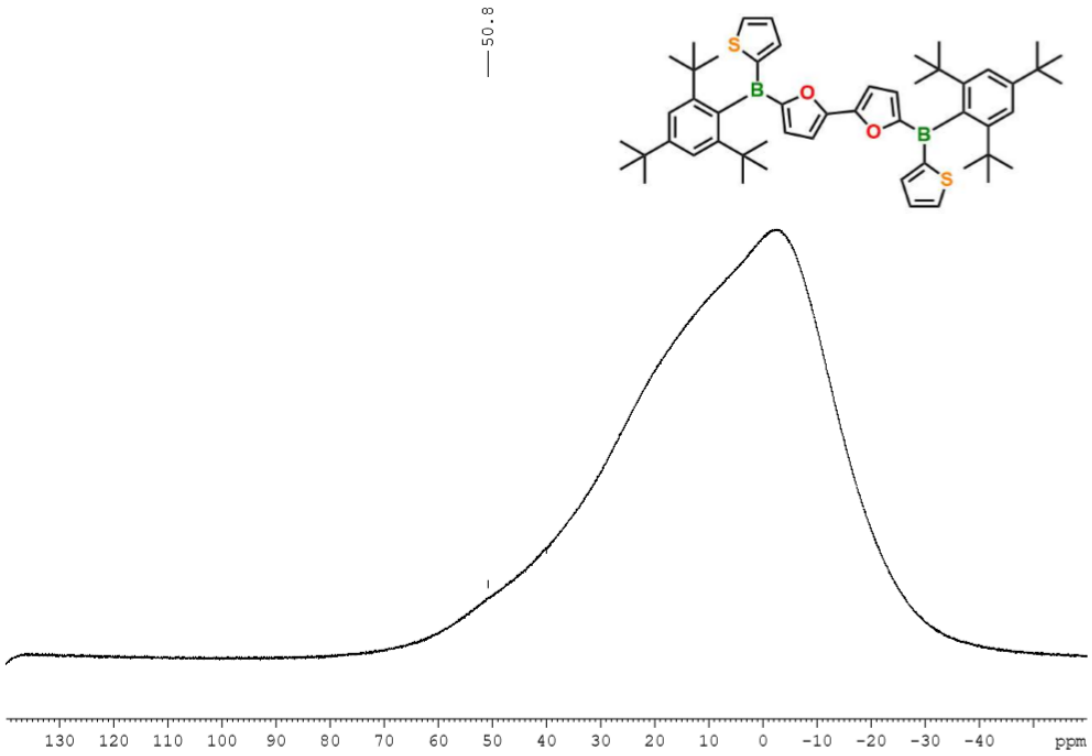

Figure 5.4.19. $^{11}B\{^{1}H\}$ NMR spectrum of **2a^{Mes*}** (160 MHz, in $CDCl_3$).

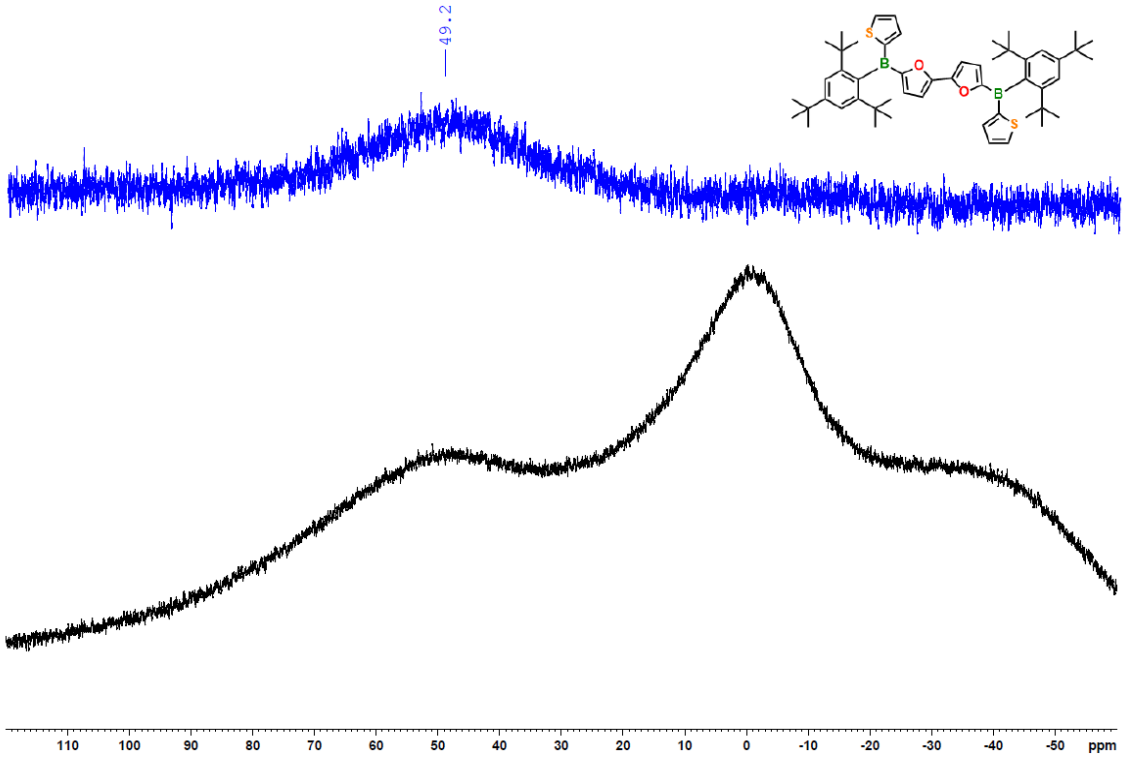

Figure 5.4.20. $^{11}B\{^1H\}$ NMR spectrum of **2a^{Mes*}** (96 MHz, in $CDCl_3$) before (black) and after (blue) background substraction**.**

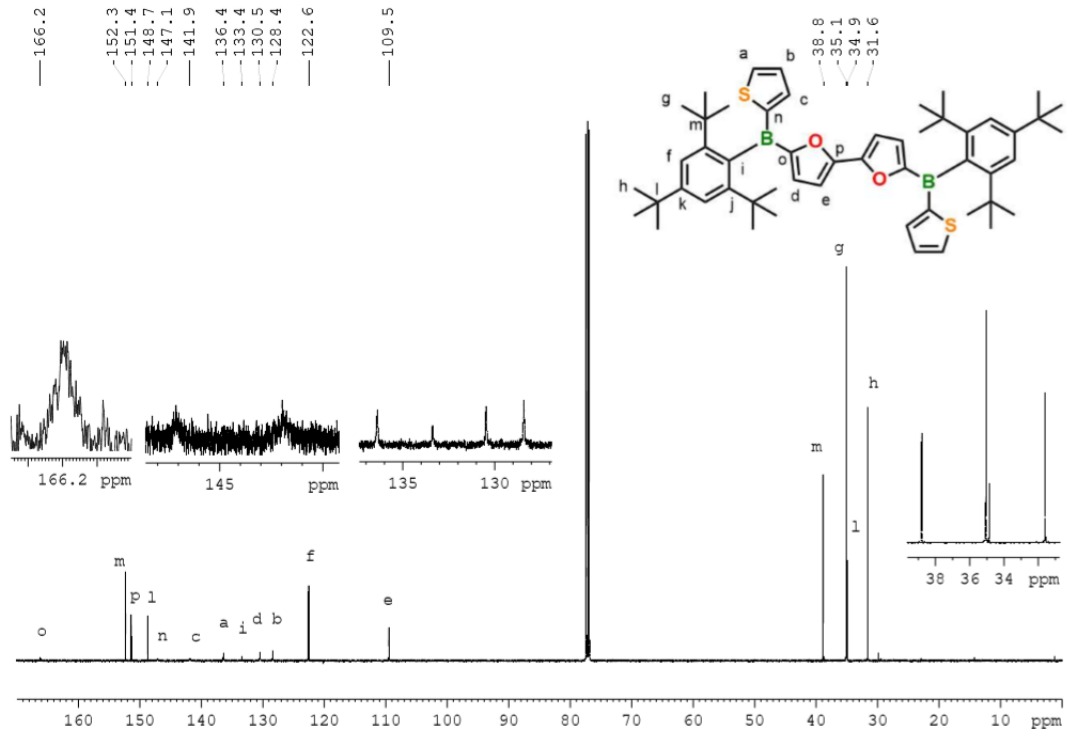

Figure 5.4.21. $^{13}C\{^1H\}$ NMR spectrum of **2a^{Mes*}** (126 MHz, in $CDCl_3$).

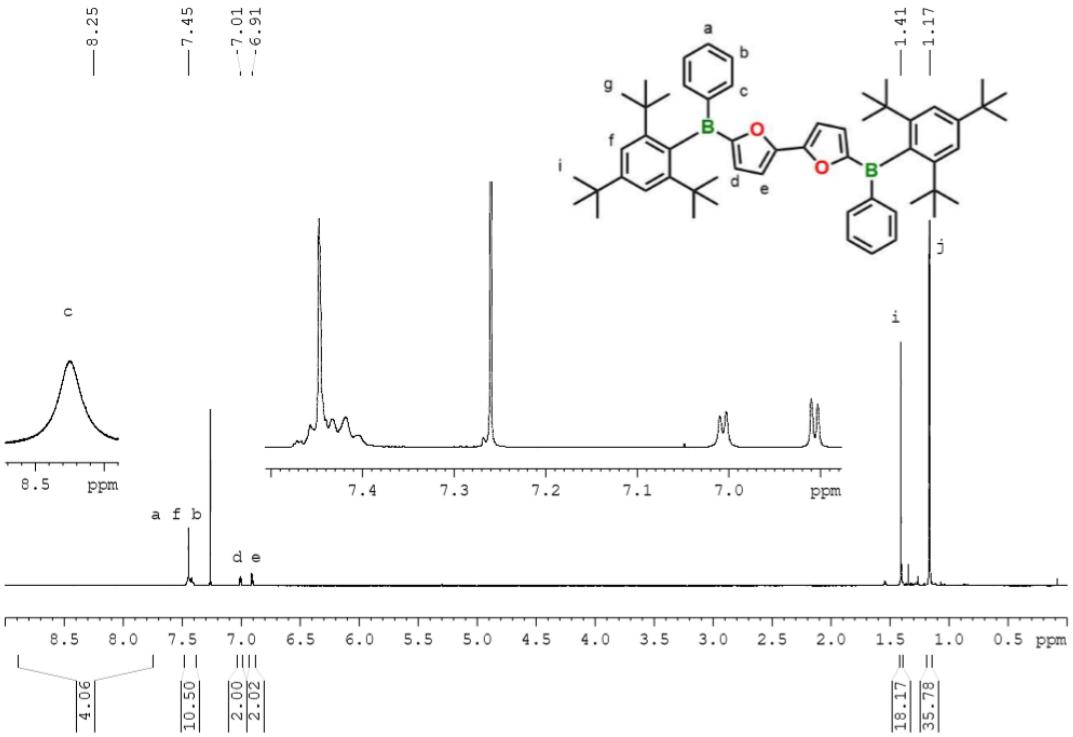

Figure 5.4.22. ^{1}H NMR spectrum of **2c^{Mes*}** (500 MHz, in $CDCl_3$).

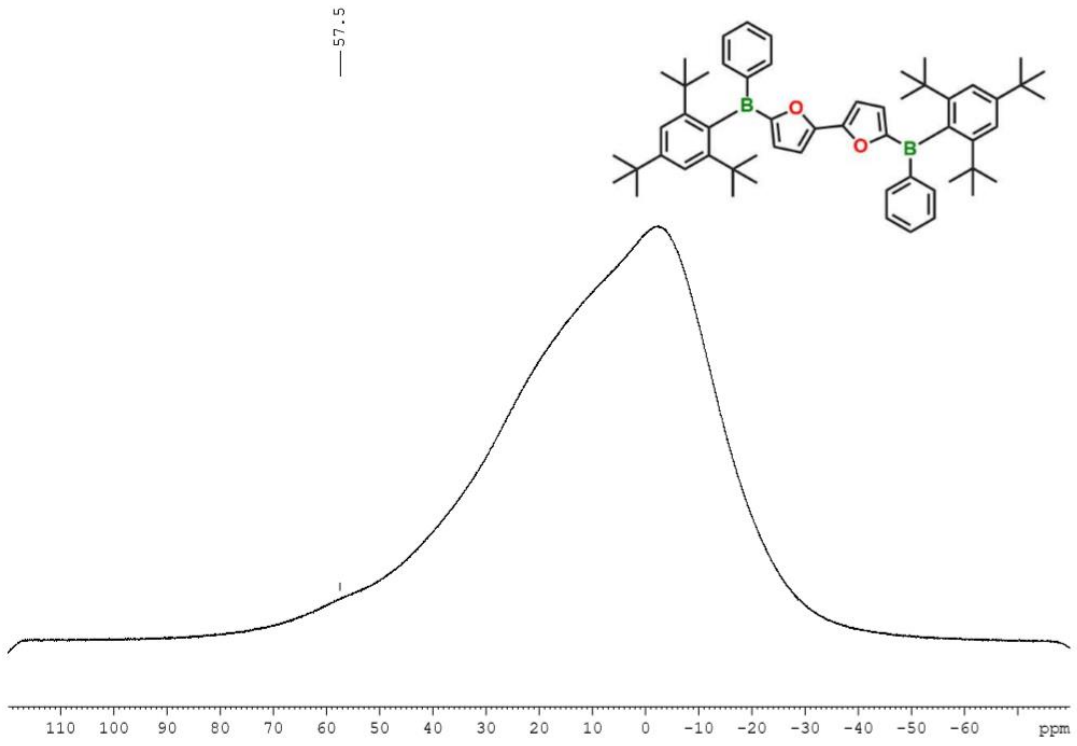

Figure 5.4.23. $^{11}B\{^{1}H\}$ NMR spectrum of **2c^{Mes*}** (160 MHz, in $CDCl_3$).

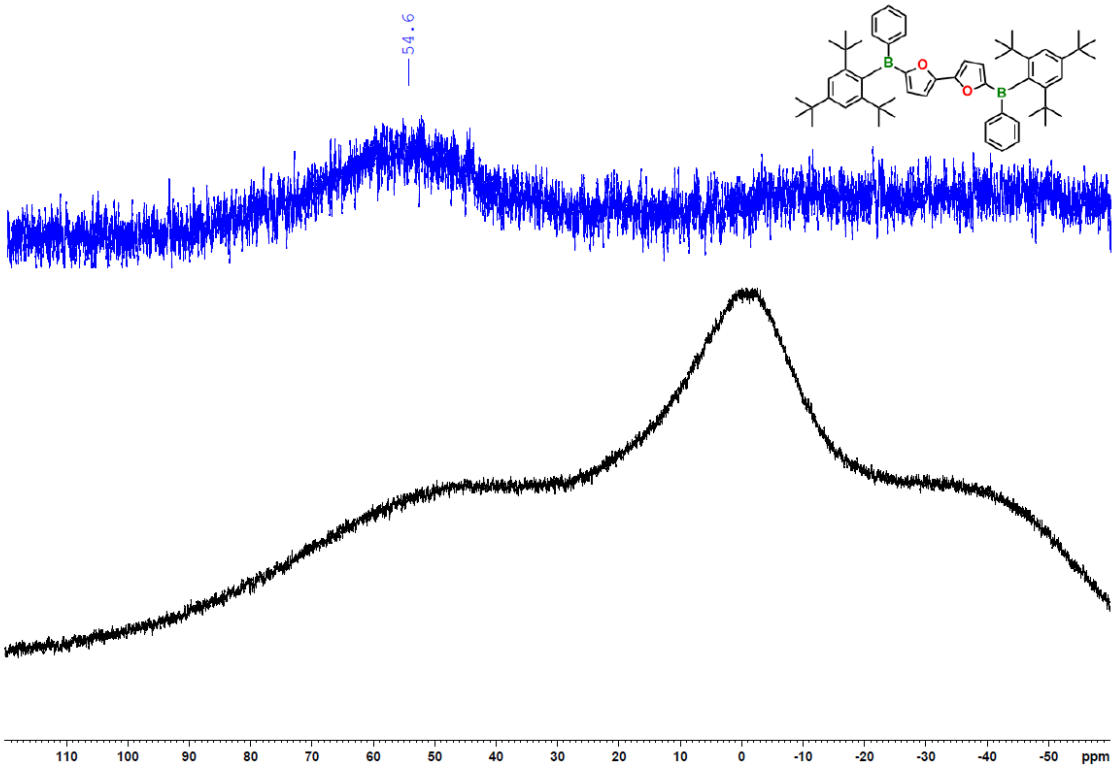

Figure 5.4.24. $^{11}B\{^1H\}$ NMR spectrum of **2c^{Mes*}** (96 MHz, in $CDCl_3$) before (black) and after (blue) background substraction.

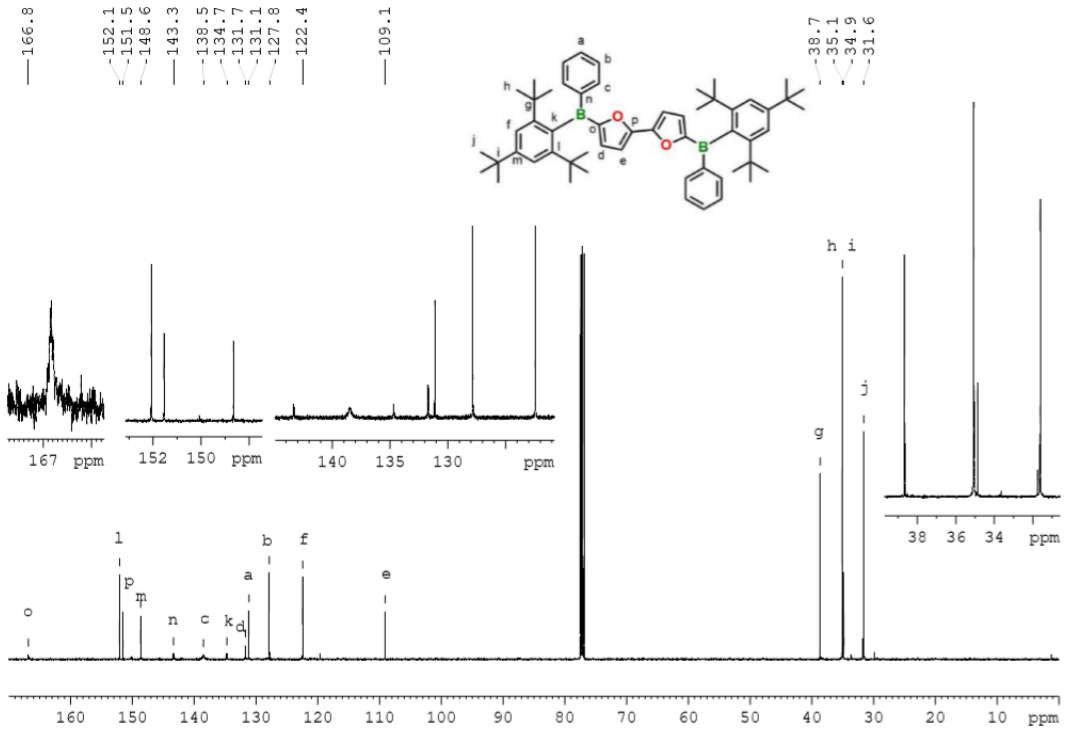

Figure 5.4.25. $^{13}C\{^1H\}$ NMR spectrum of **2c^{Mes*}** (126 MHz, in $CDCl_3$).

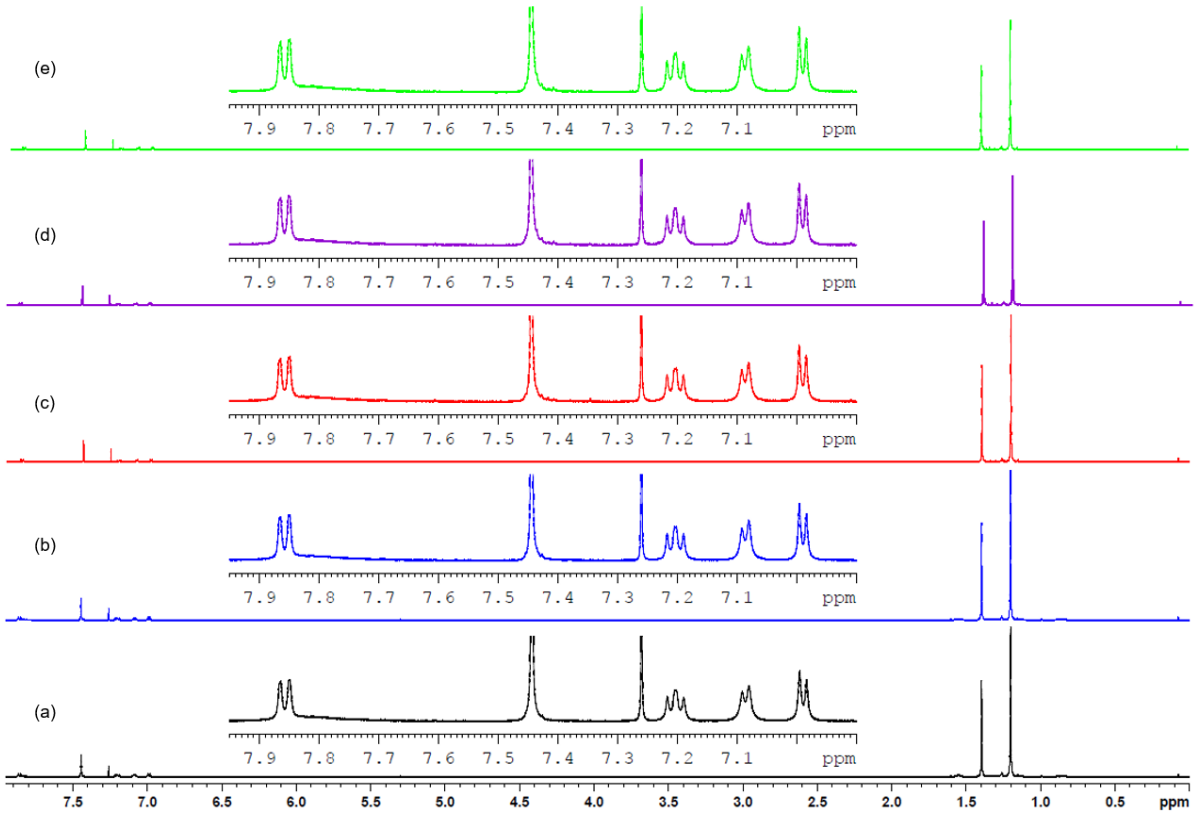

Figure 5.4.26. Stability tests of **2a**^{Mes*} determined by ^{1}H NMR spectroscopy (300 MHz) after storage in moist solution ($CDCl_3$) in air, a) after 1 h, b) after 1 d, c) after 3 d, d) after 5 d, e) after 7 d.

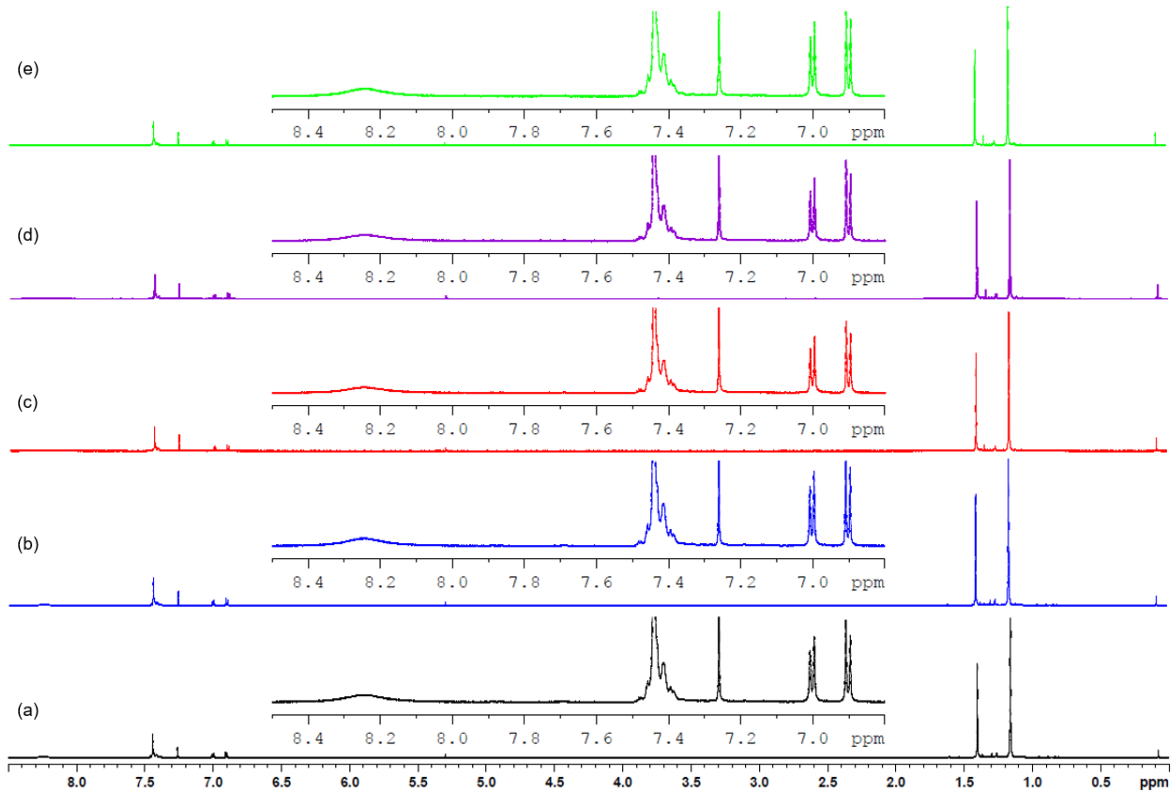

Figure 5.4.27. Stability tests of **2c**^{Mes*} determined by ^{1}H NMR spectroscopy (300 MHz) after storage in moist solution ($CDCl_3$) in air, a) after 1 h, b) after 1 d, c) after 3 d, d) after 5 d, e) after 7 d.

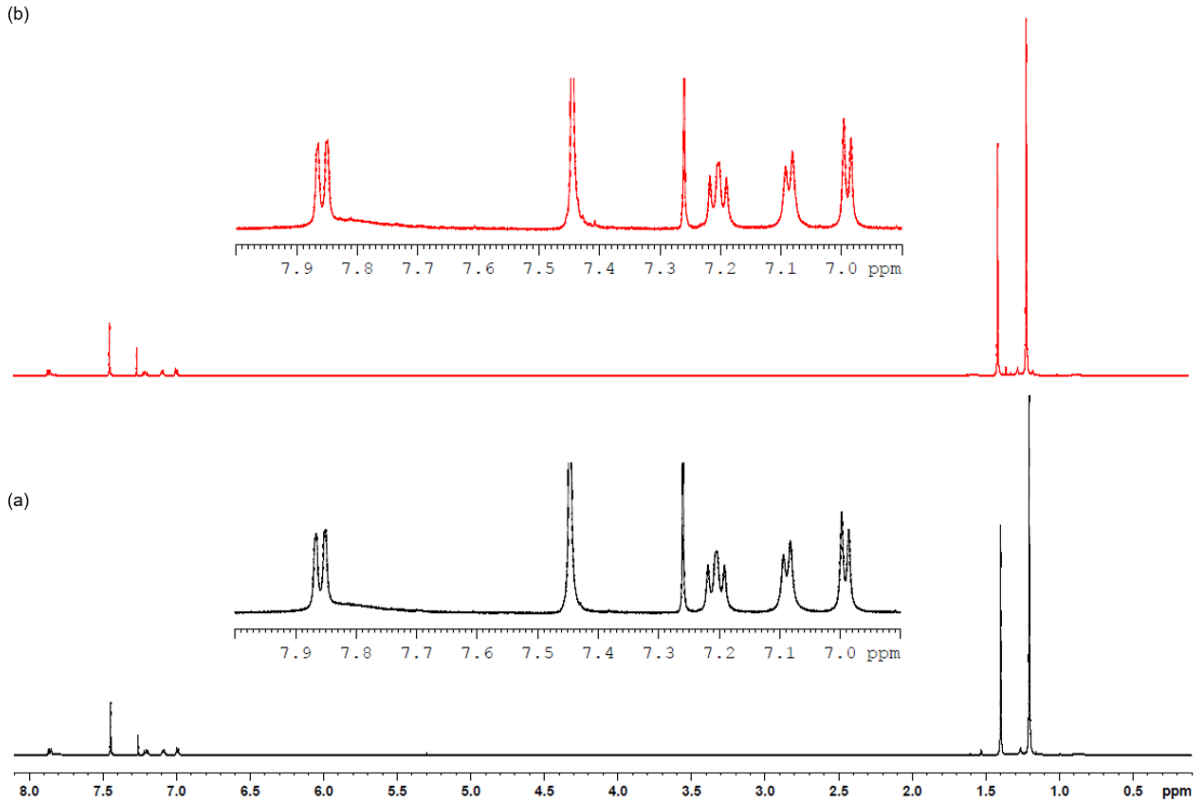

Figure 5.4.28. Stability tests of **2a**^{Mes*} determined by ^{1}H NMR spectroscopy (300 MHz), a) after aqueous work-up, b) after storage as a solid in air for 2 months.

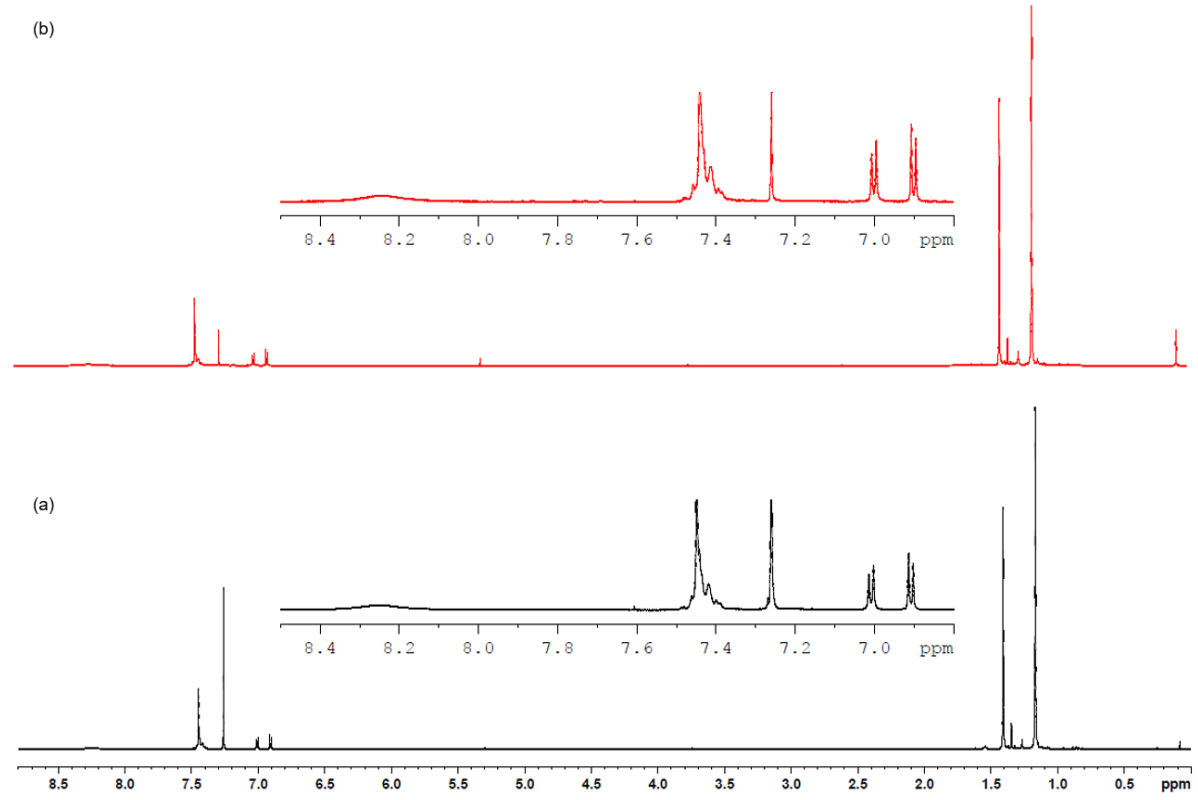

Figure 5.4.29. Stability tests of **2c**^{Mes*} determined by ^{1}H NMR spectroscopy (300 MHz), a) after aqueous work-up, b) after storage as a solid under air for 9 months.

Mass spectra

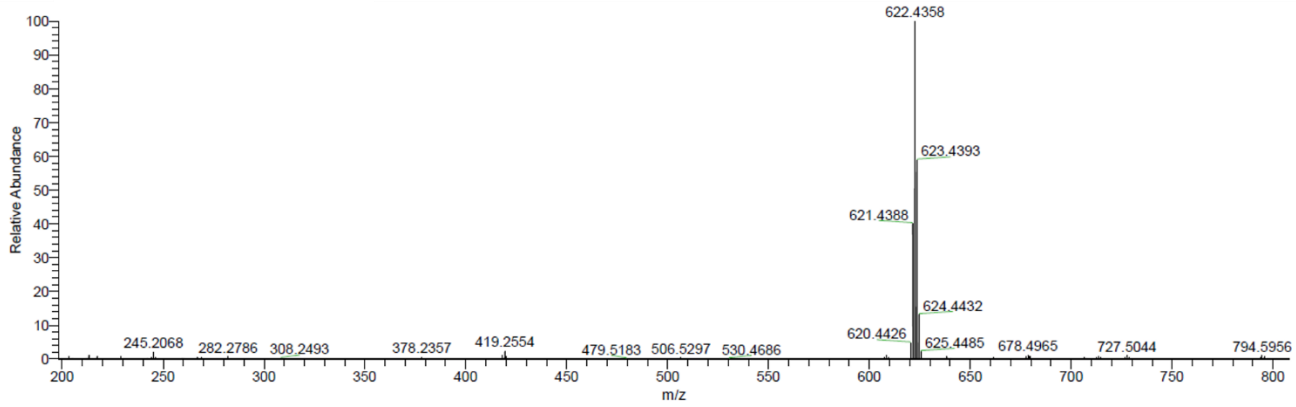

Figure 5.4.30. APCI mass spectrum of **7**.

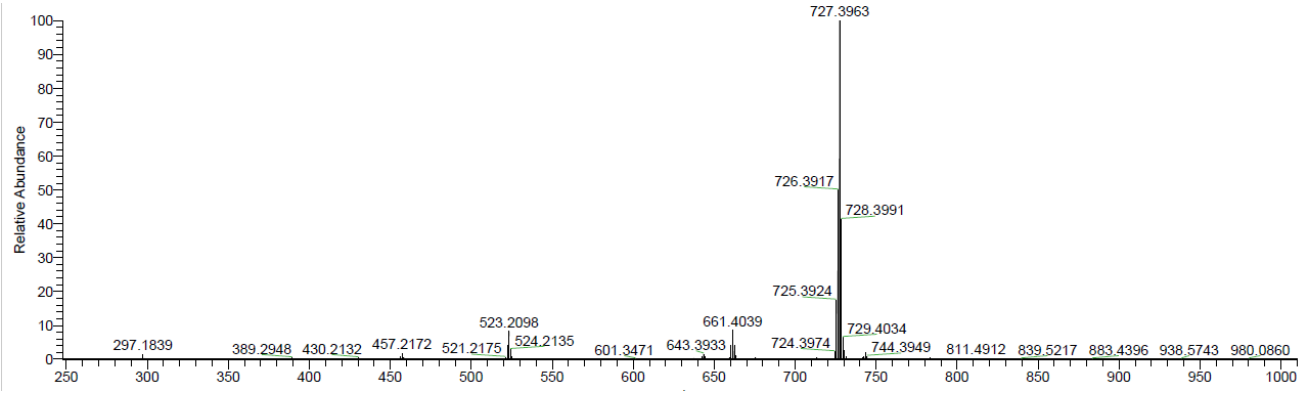

Figure 5.4.31. APCI mass spectrum of **2a^{Tip}**.

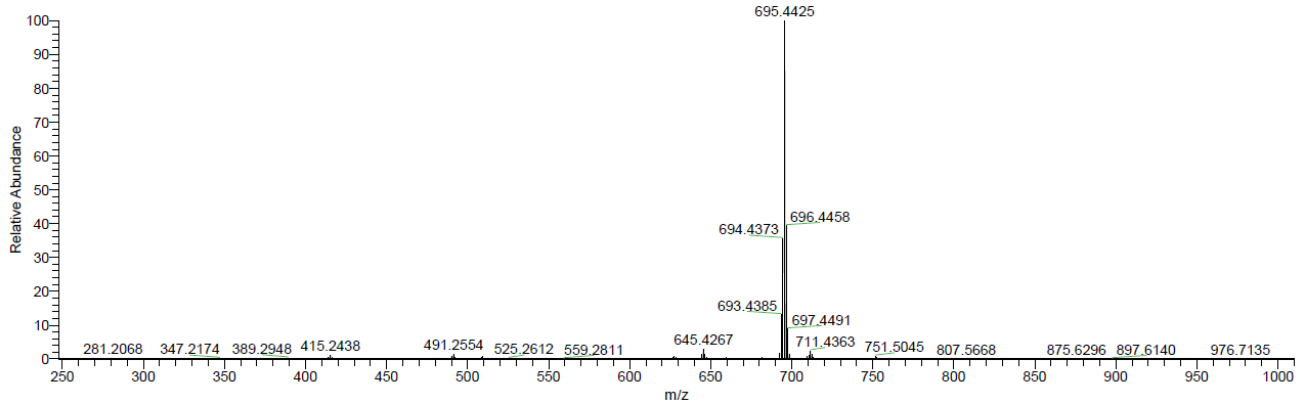

Figure 5.4.32. APCI mass spectrum of **2b^{Tip}**.

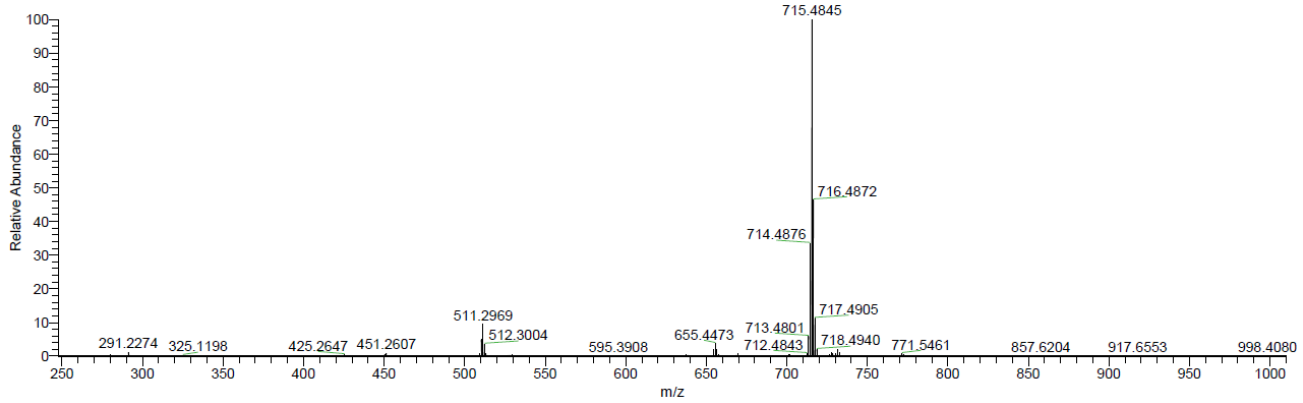

Figure 5.4.33. APCI mass spectrum of **2c^{Tip}**.

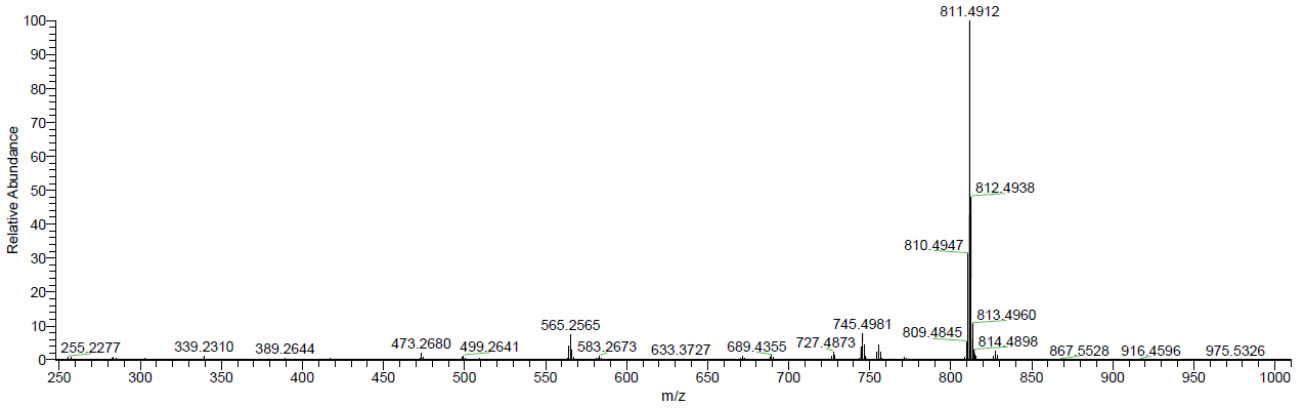

Figure 5.4.34. APCI mass spectrum of **2a^{Mes*}**.

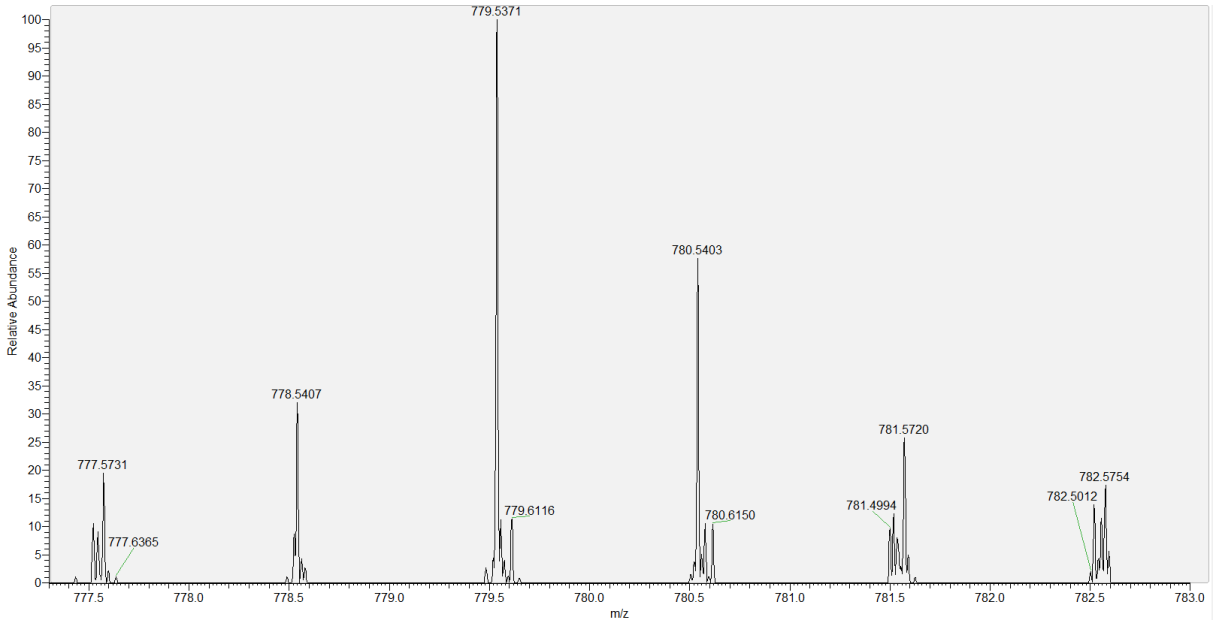

Figure 5.4.35. APCI mass spectrum of **2b^{Mes*}** traces.

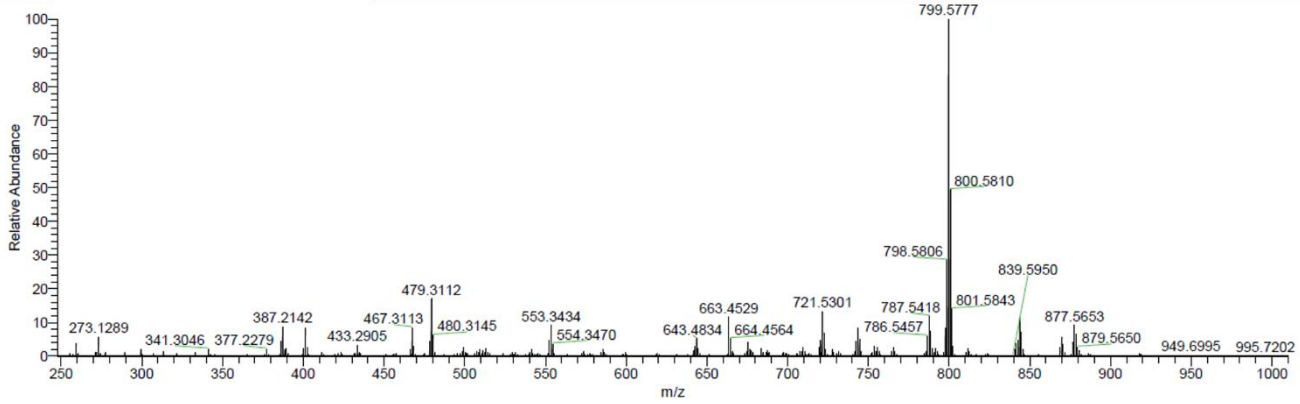

Figure 5.4.36. APCI mass spectrum of **2c^{Mes*}**.

UV/Vis spectra

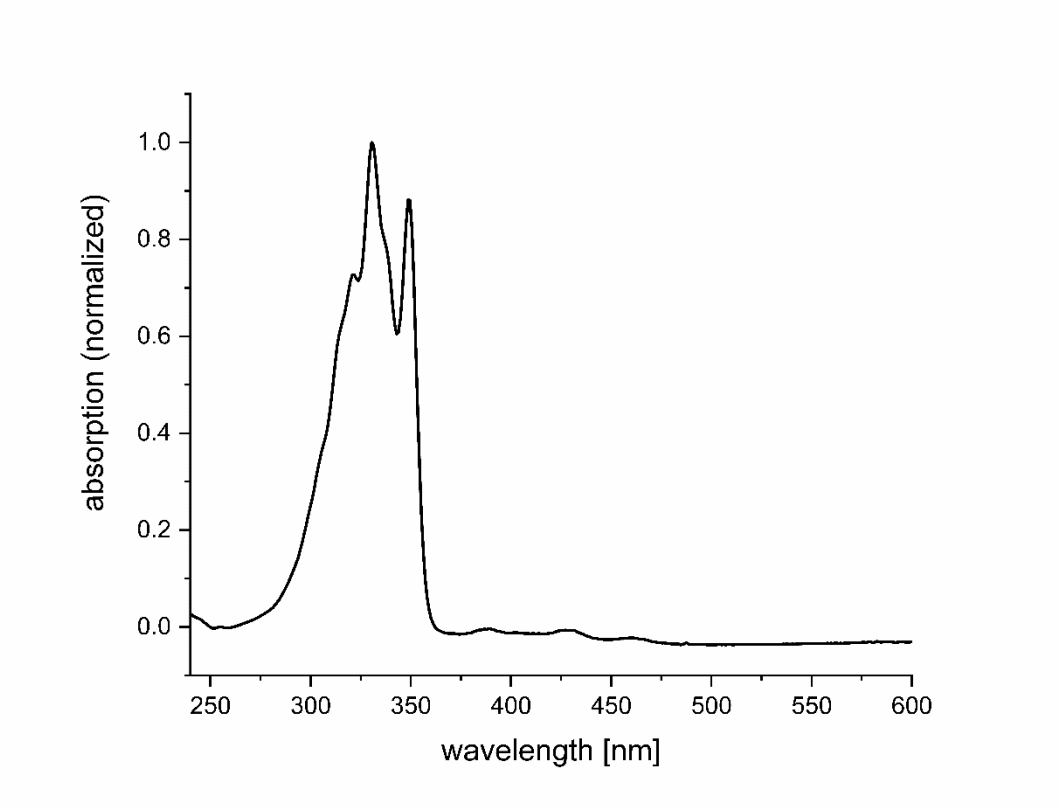

Figure 5.4.37. UV-Vis spectrum of **7** (in THF).

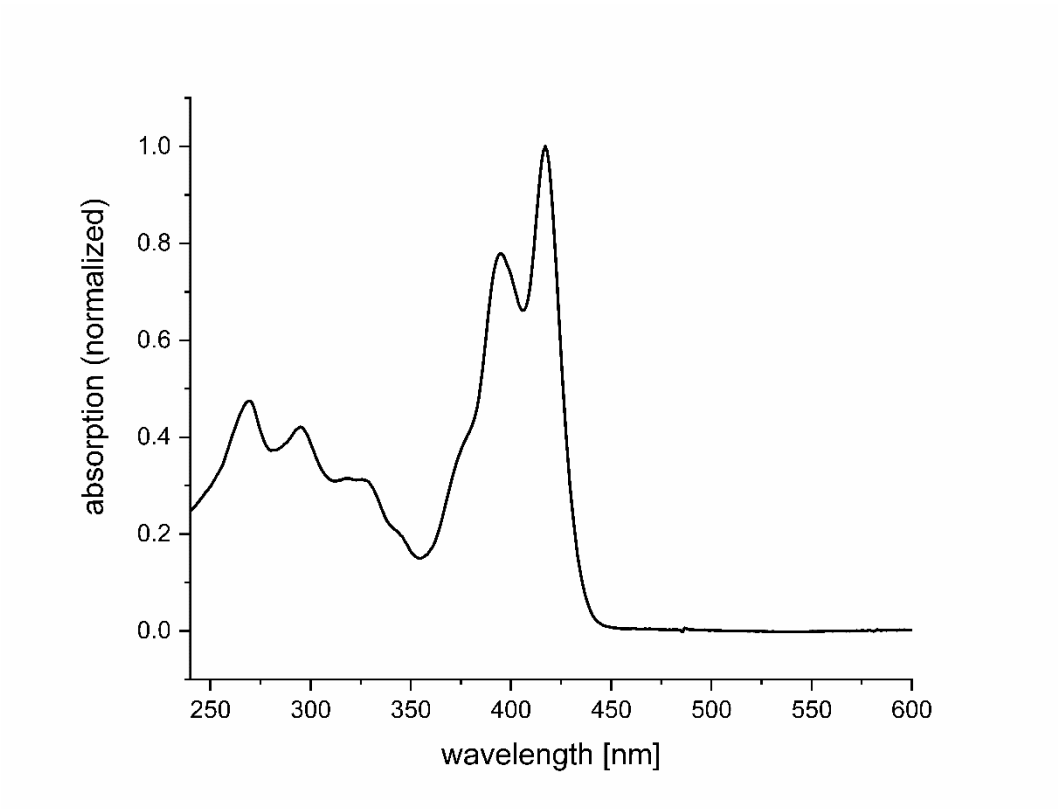

Figure 5.4.38. UV-Vis spectrum of **2a^{Tip}** (in THF).

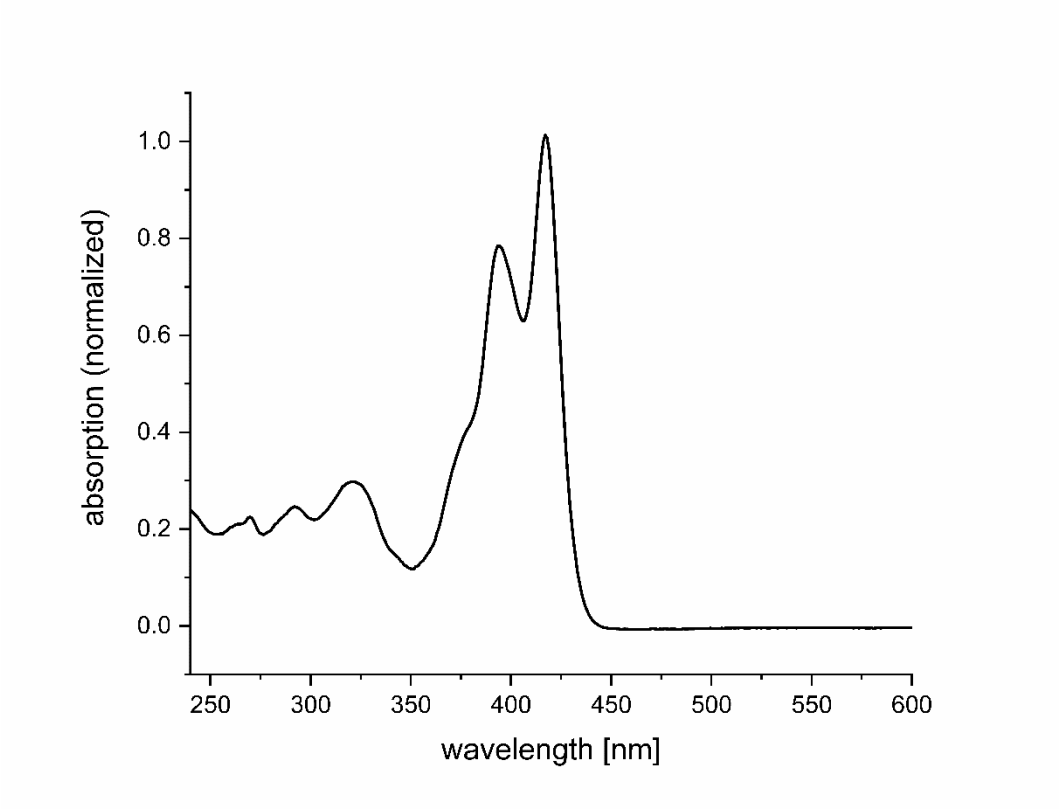

Figure 5.4.39. UV-Vis spectrum of **2b^{Tip}** (in THF).

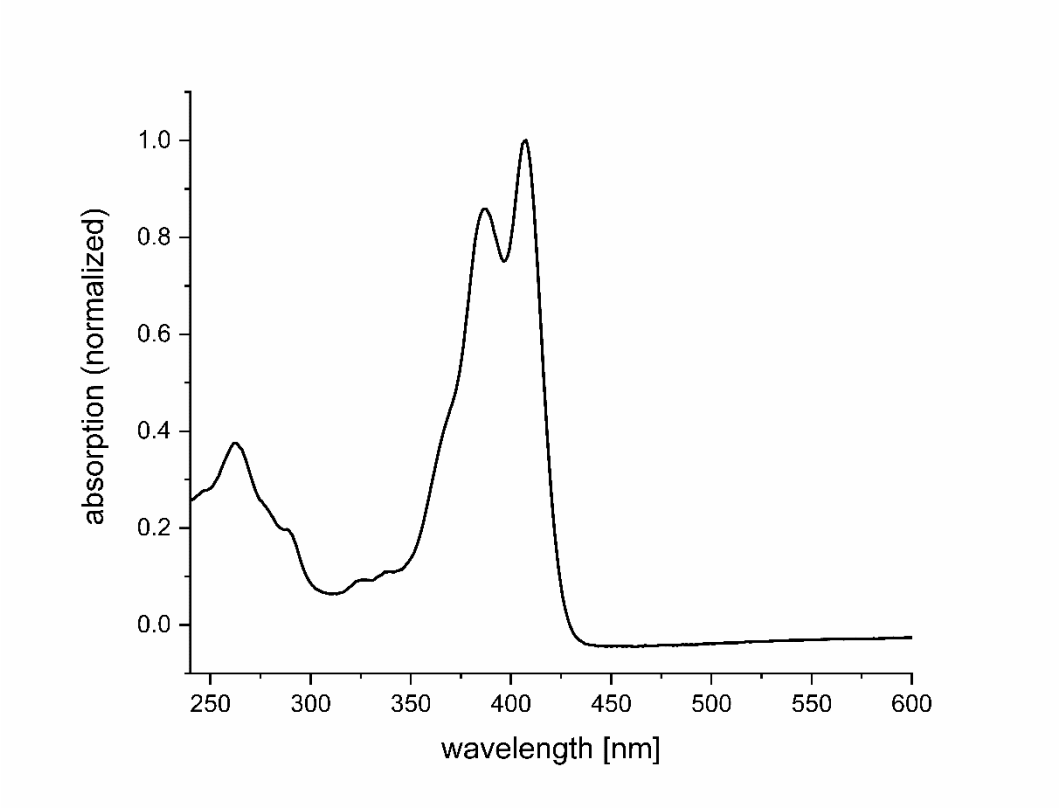

Figure 5.4.40. UV-Vis spectrum of **2c^{Tip}** (in THF).

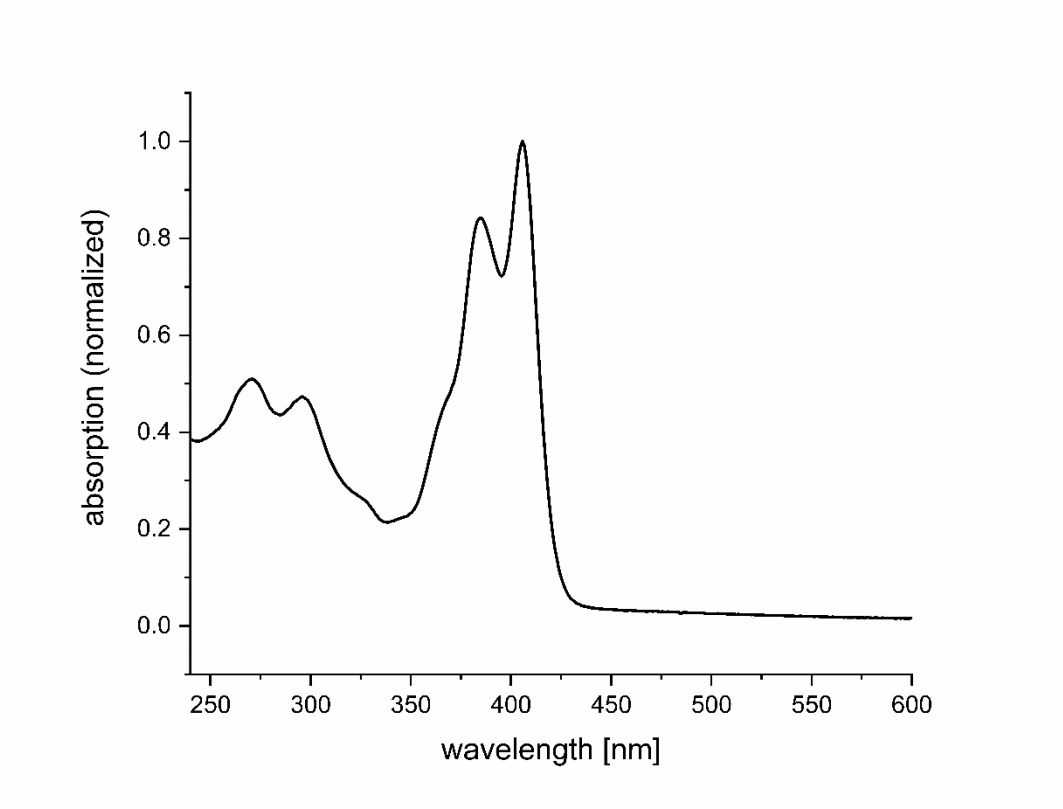

Figure 5.4.41. UV-Vis spectrum of **2a**^{Mes*} (in THF).

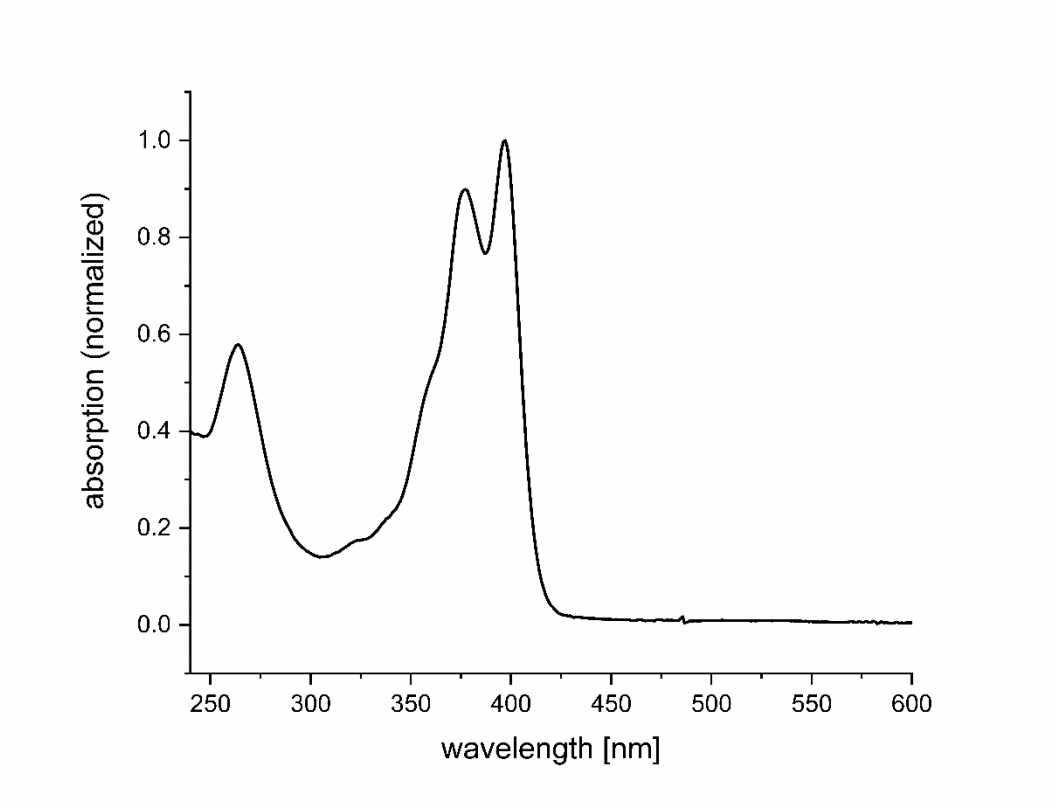

Figure 5.4.42. UV-Vis spectrum of **2c**^{Mes*} (in THF).

Fluorescence spectra

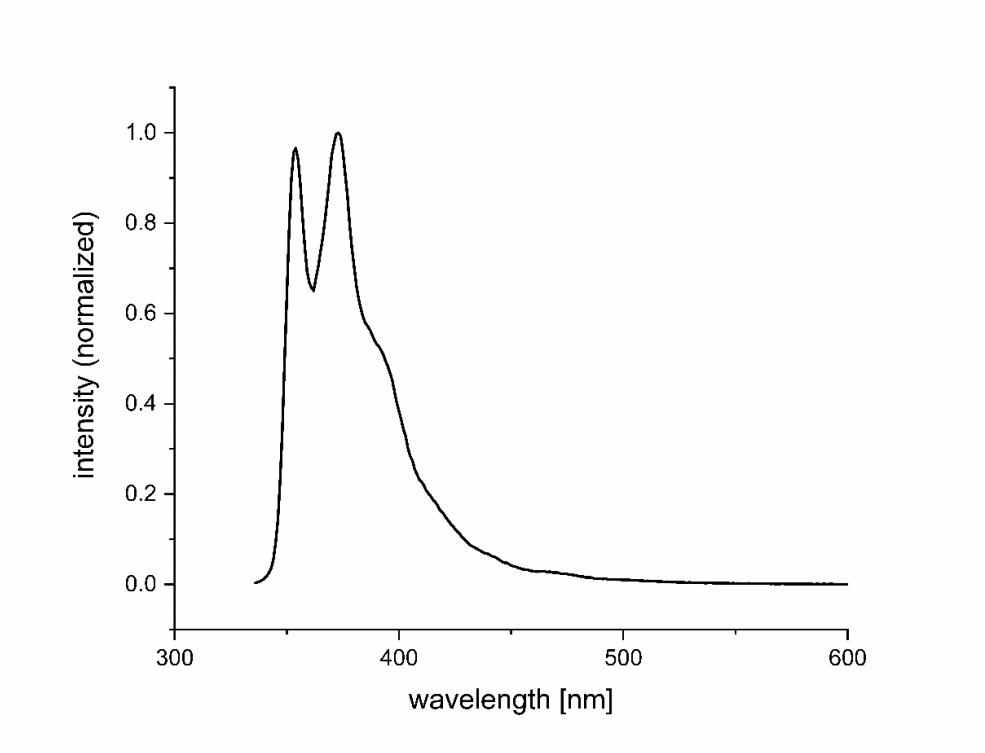

Figure 5.4.43. Fluorescence spectrum of **7** (in THF, $\lambda_{ex} = 331$ nm).

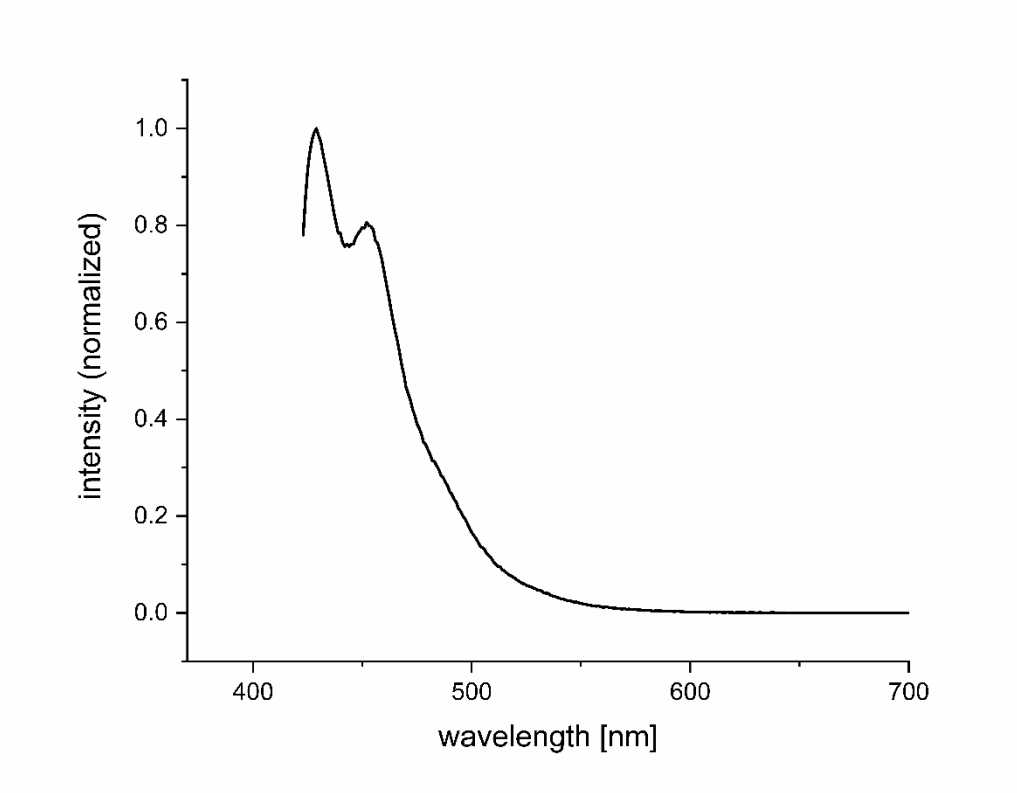

Figure 5.4.44. Fluorescence spectrum of **2a**^{Tip} (in THF, $\lambda_{ex} = 417$ nm).

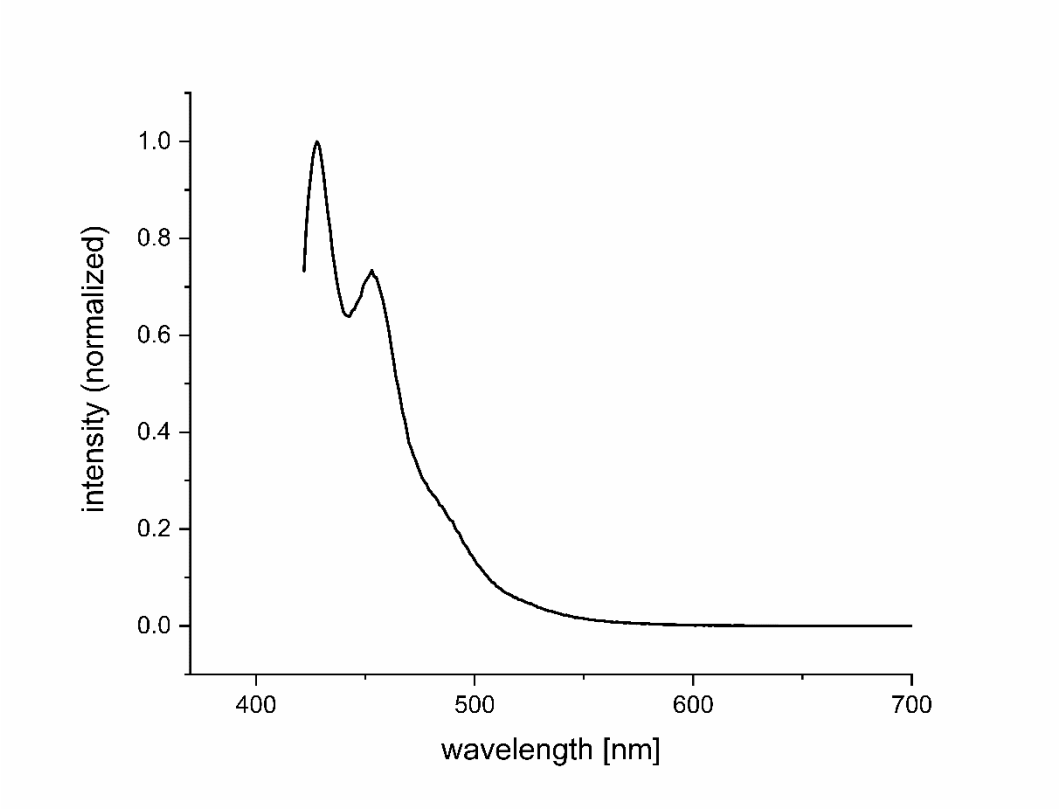

Figure 5.4.45. Fluorescence spectrum of **2b^{Tip}** (in THF, λ_{ex} = 417 nm).

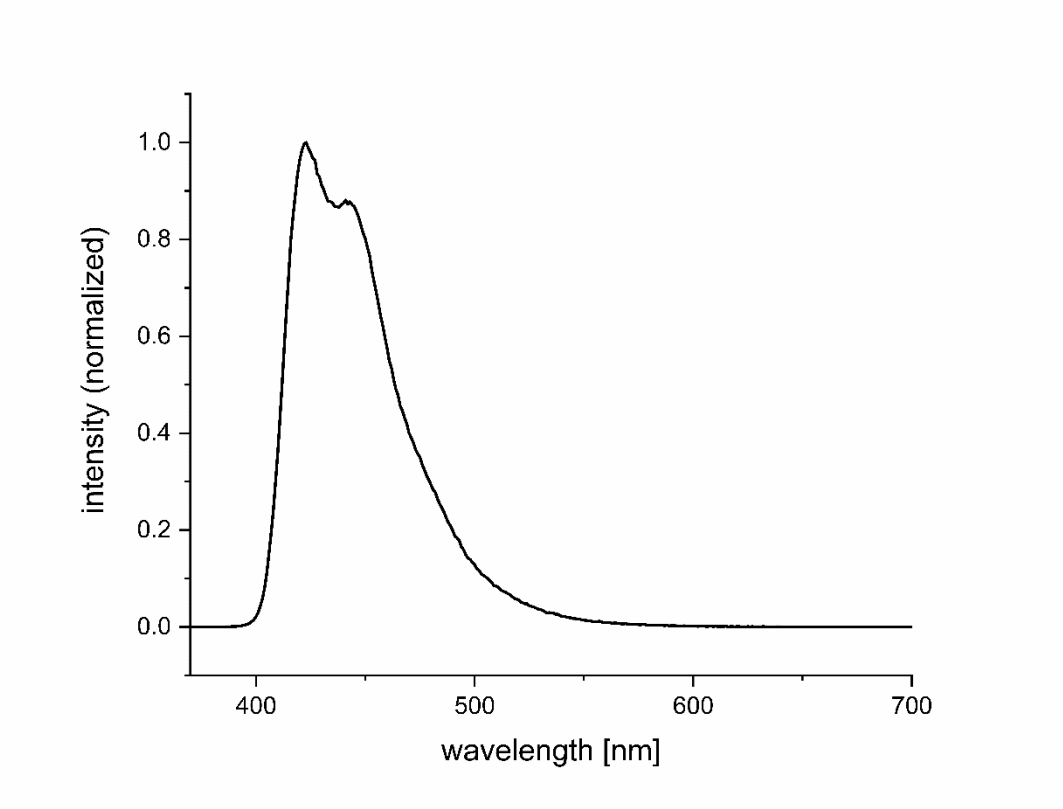

Figure 5.4.46. Fluorescence spectrum of **2c^{Tip}** (in THF, λ_{ex} = 407 nm).

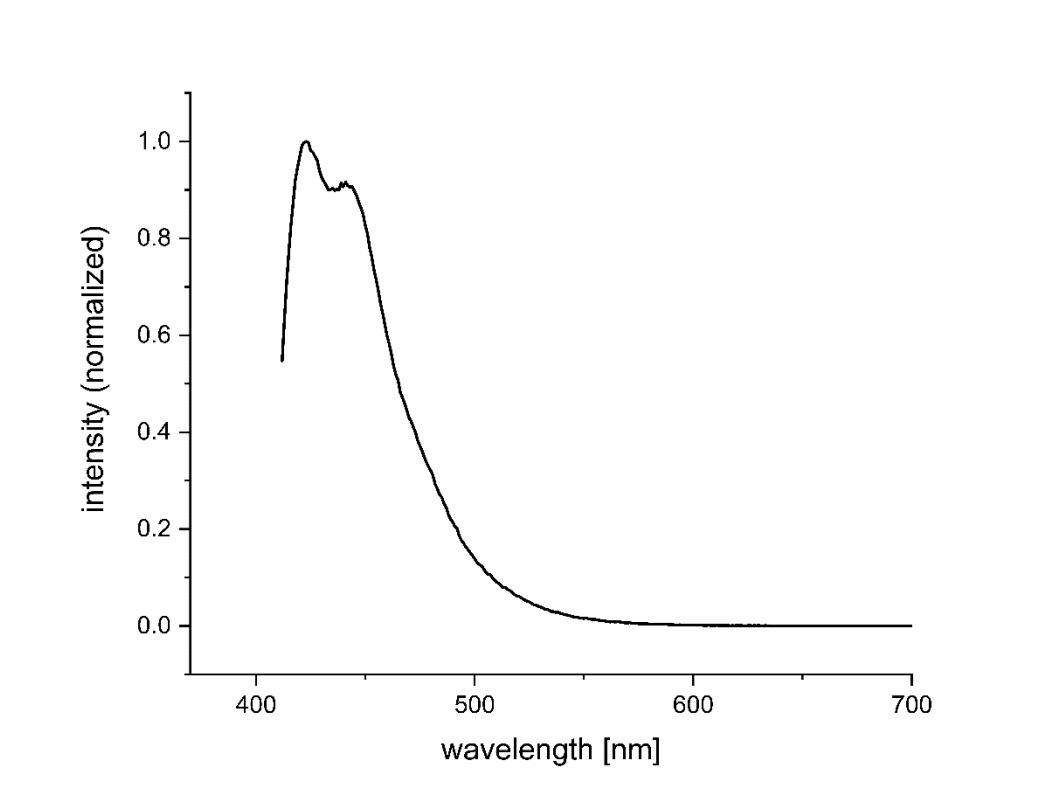

Figure 5.4.47. Fluorescence spectrum of **2a**^{Mes*} (in THF, λ_{ex} = 406 nm).

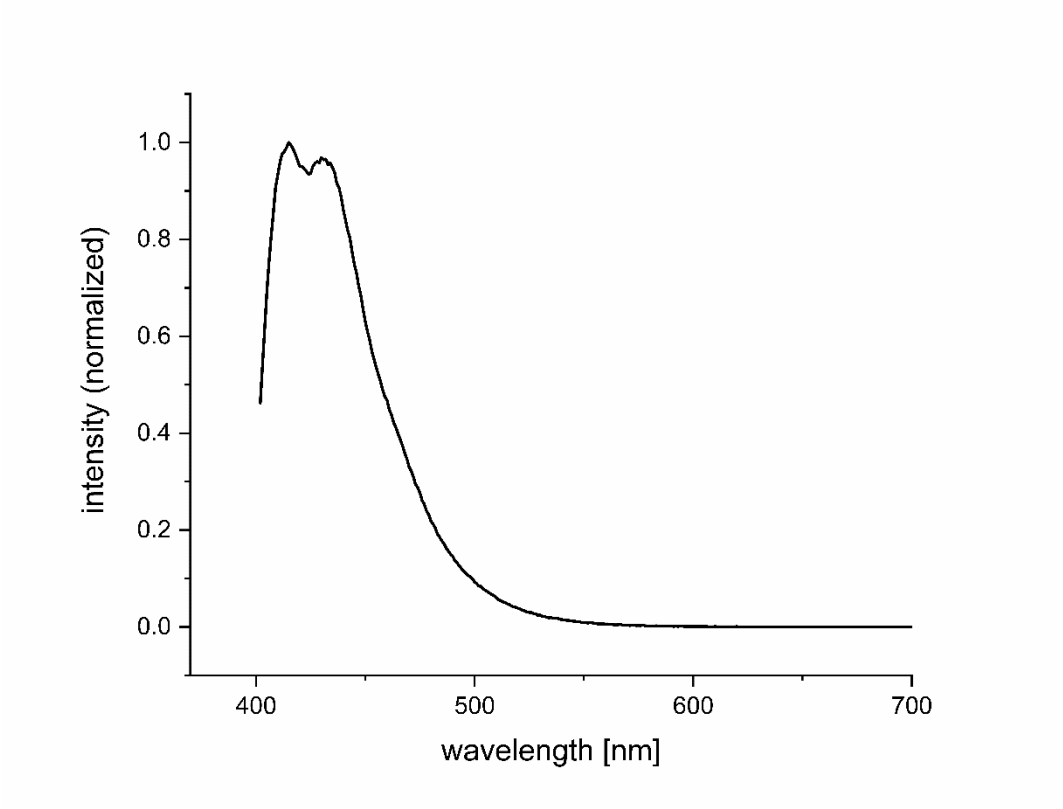

Figure 5.4.48. Fluorescence spectrum of **2c**^{Mes*} (in THF, λ_{ex} = 398 nm).

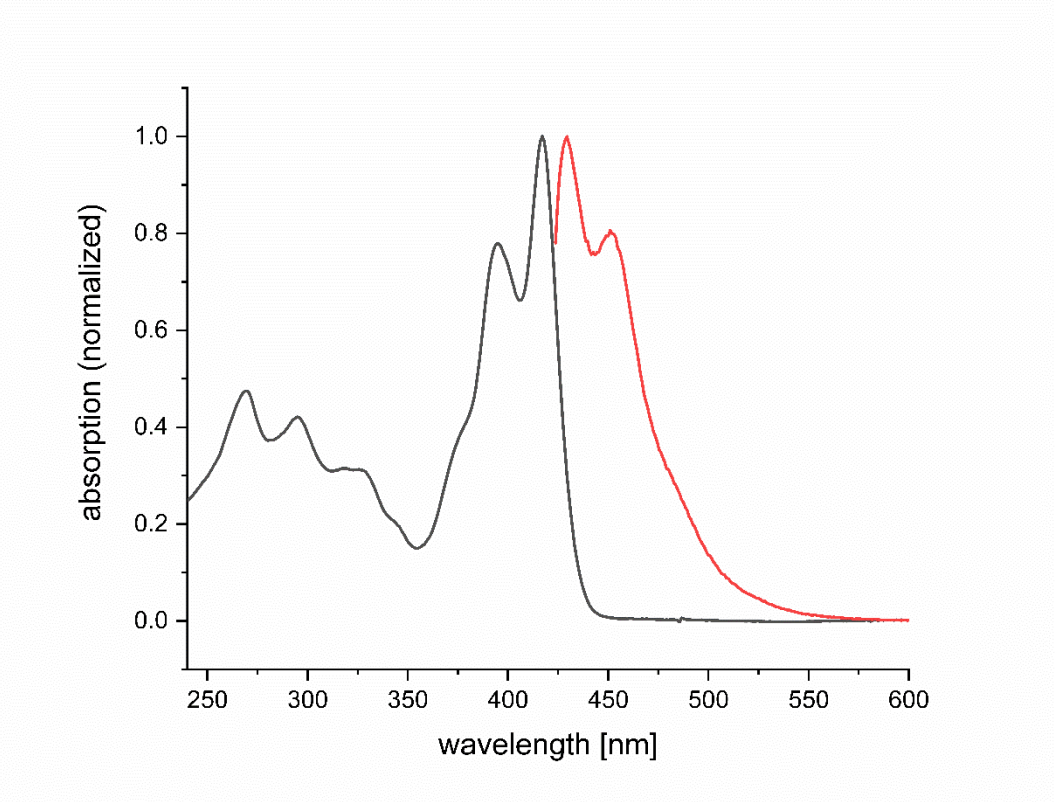

Figure 5.4.49. UV-Vis (black) and fluorescence spectrum (red) of **2a**^{Tip}.

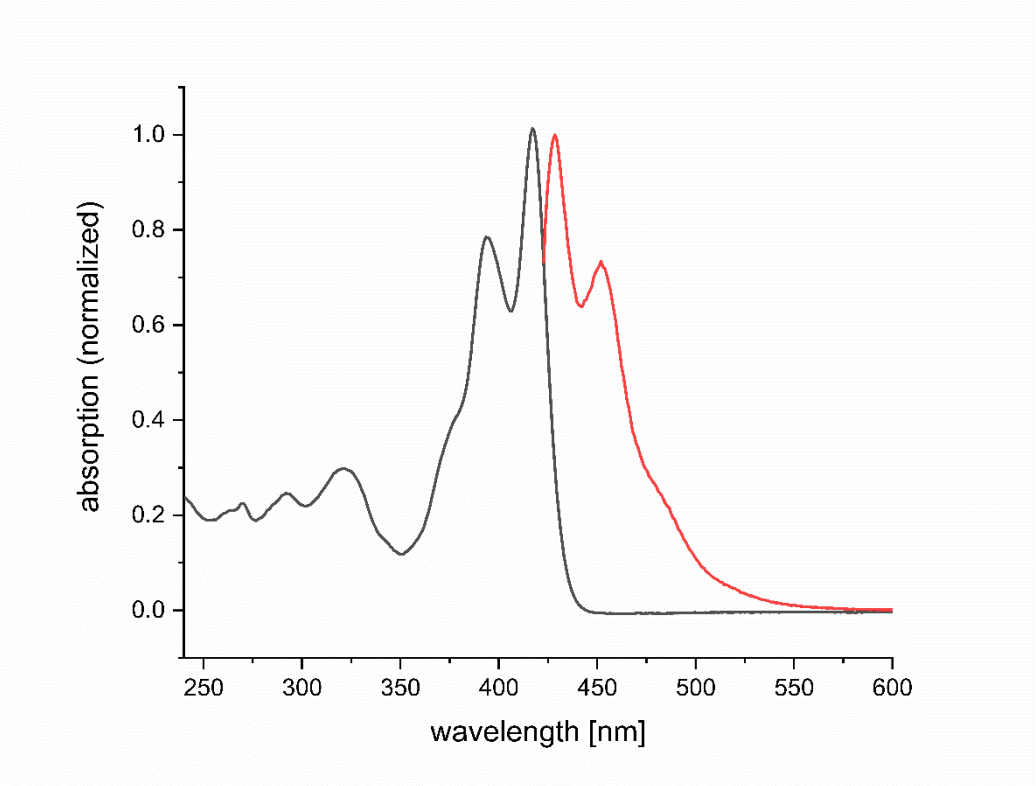

Figure 5.4.50. UV-Vis (black) and fluorescence spectrum (red) of **2b**^{Tip}.

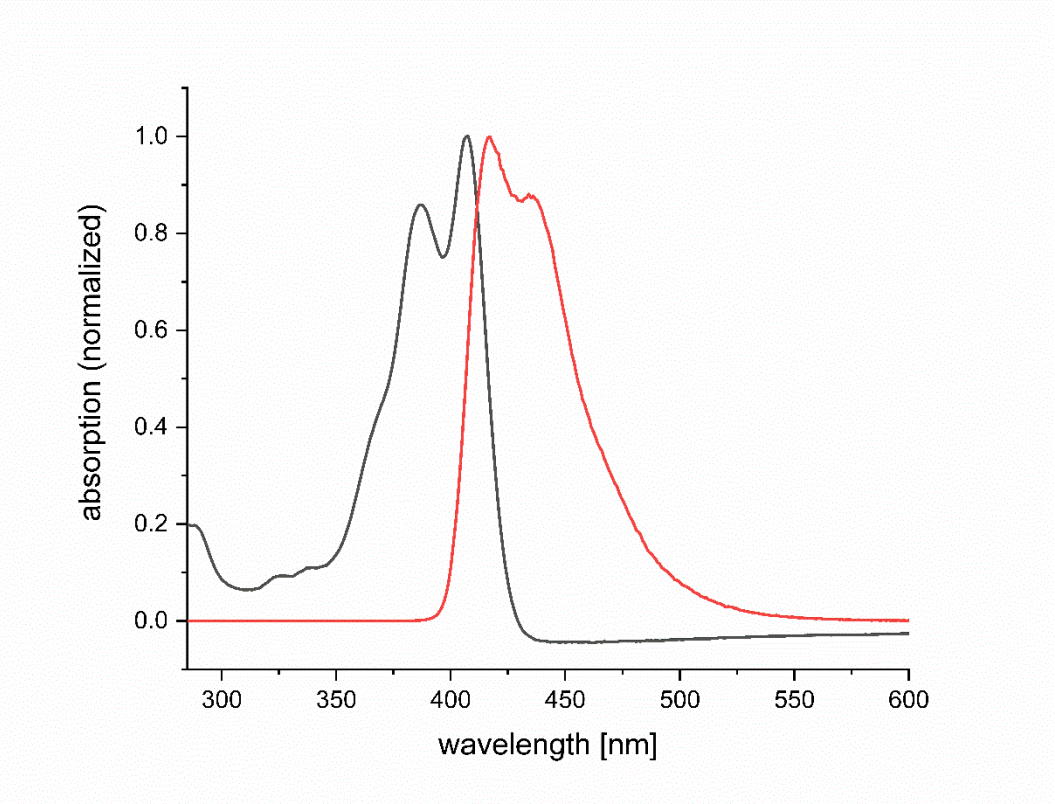

Figure 5.4.51. UV-Vis (black) and fluorescence spectrum (red) of **2c^{Tip}**.

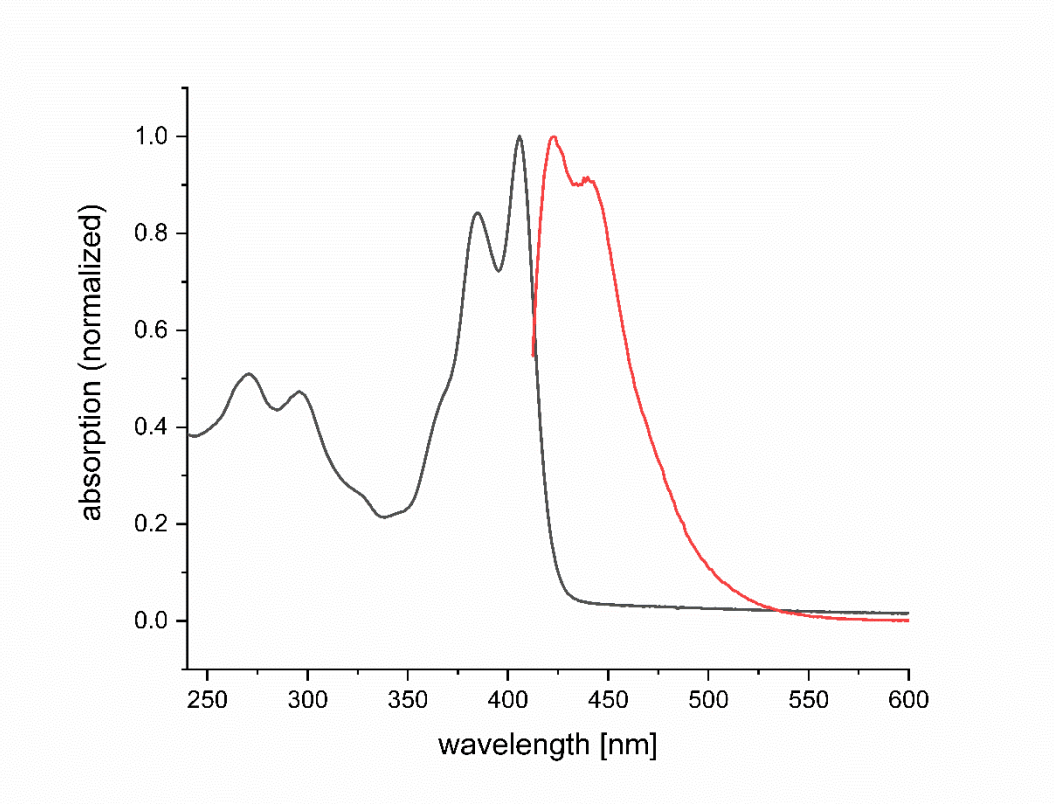

Figure 5.4.52. UV-Vis (black) and fluorescence spectrum (red) of **2a^{Mes*}**.

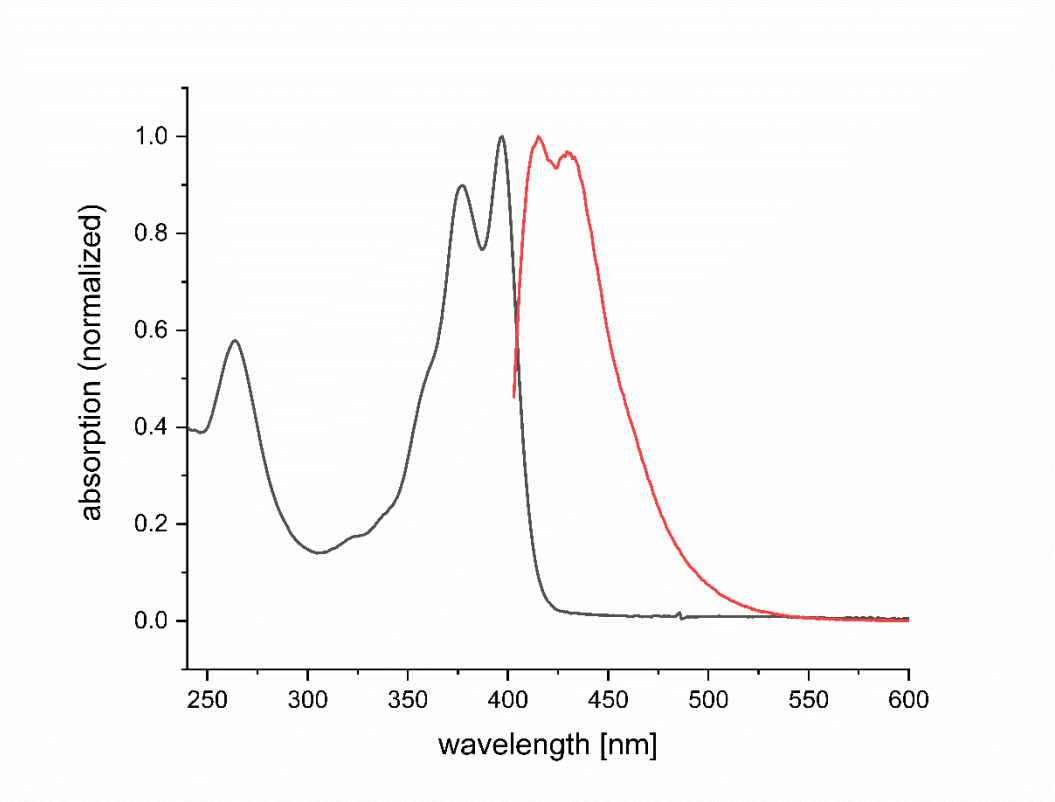

Figure 5.4.53. UV-Vis (black) and fluorescence spectrum (red) of **2c**^{Mes*}.

Cyclic Voltammetry

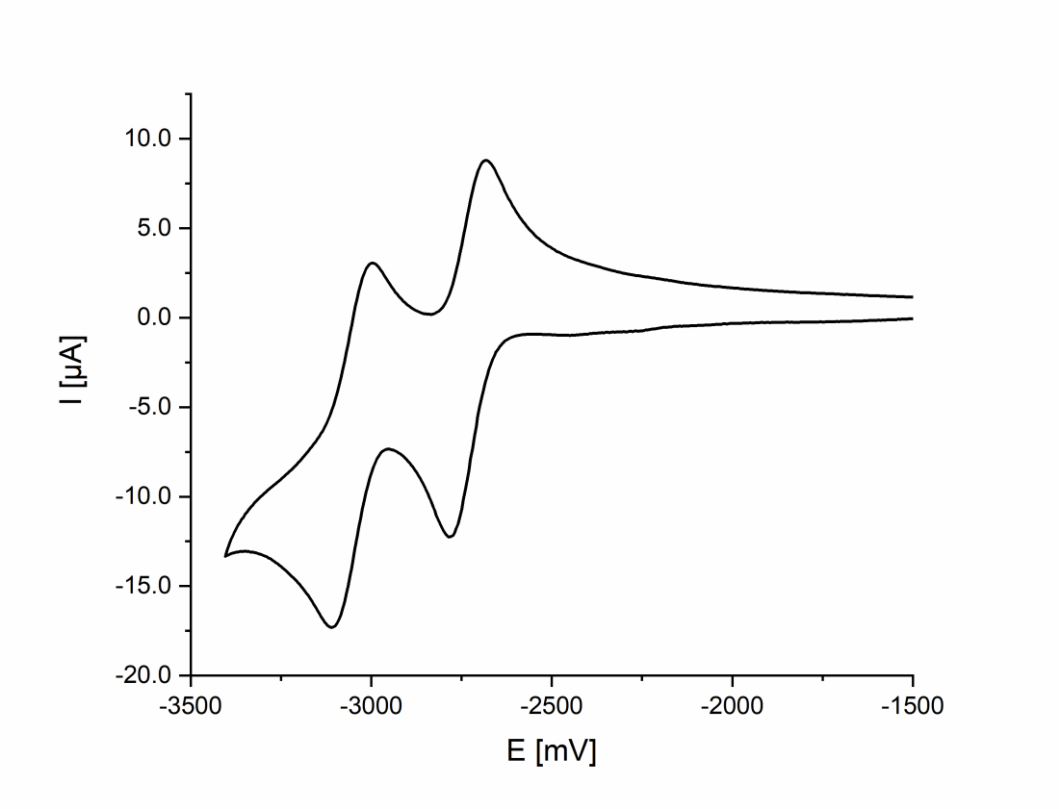

Figure 5.4.54. Cyclic voltammogram of **7** (in THF).

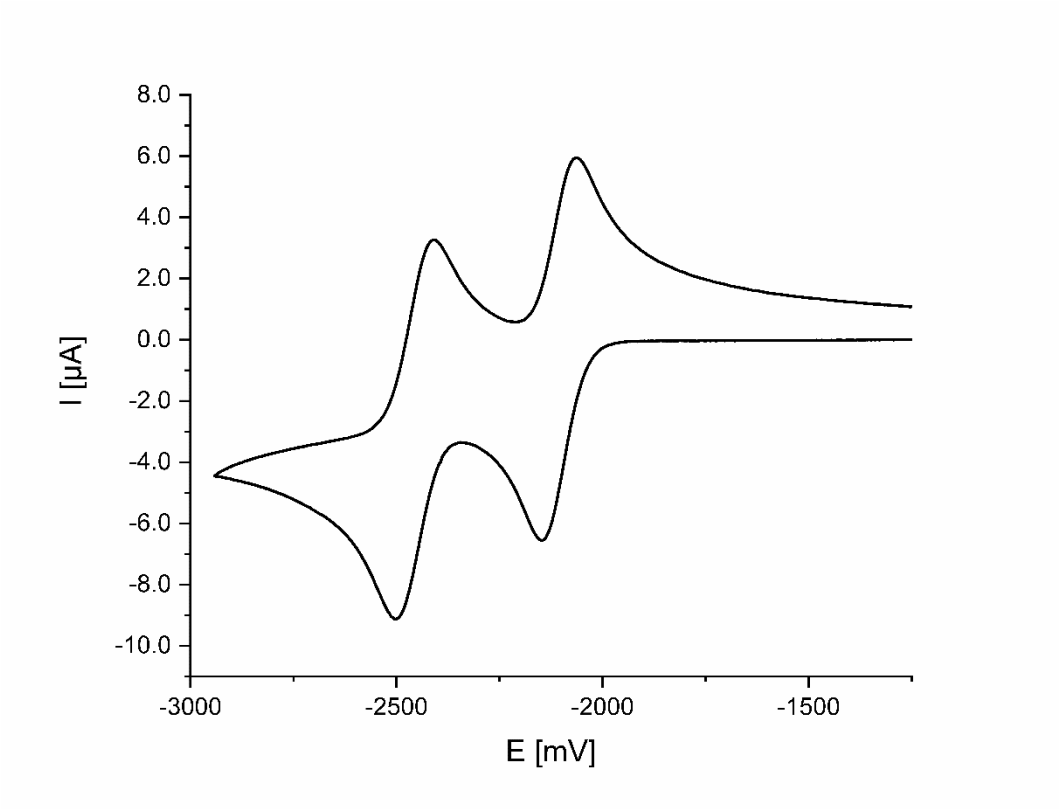

Figure 5.4.55. Cyclic voltammogram of **2a^{Tip}** (in THF).

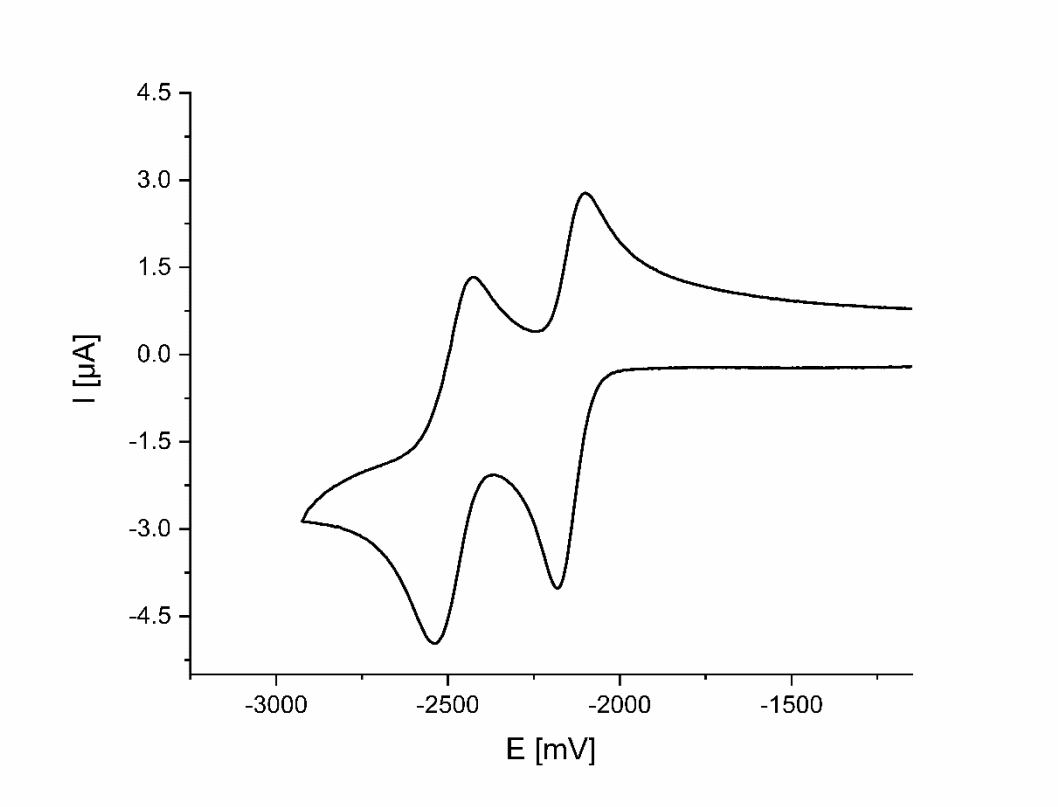

Figure 5.4.56. Cyclic voltammogram of **2b^{Tip}** (in THF).

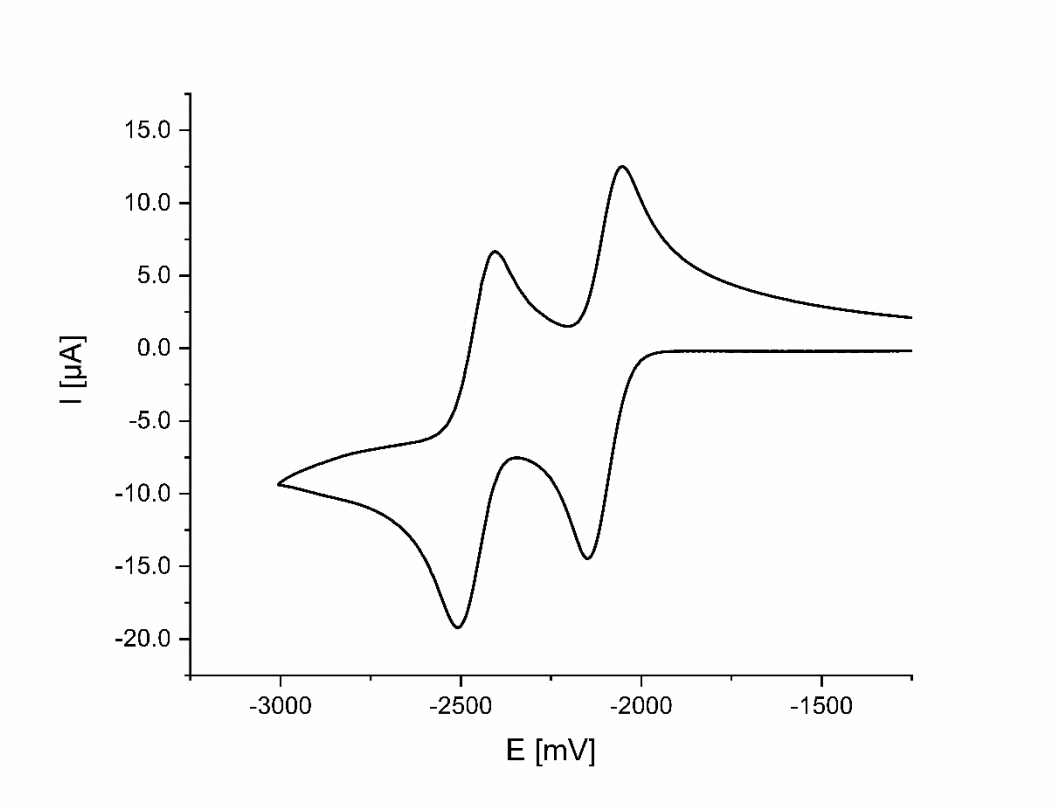

Figure 5.4.57. Cyclic voltammogram of **2c^{Tip}** (in THF).

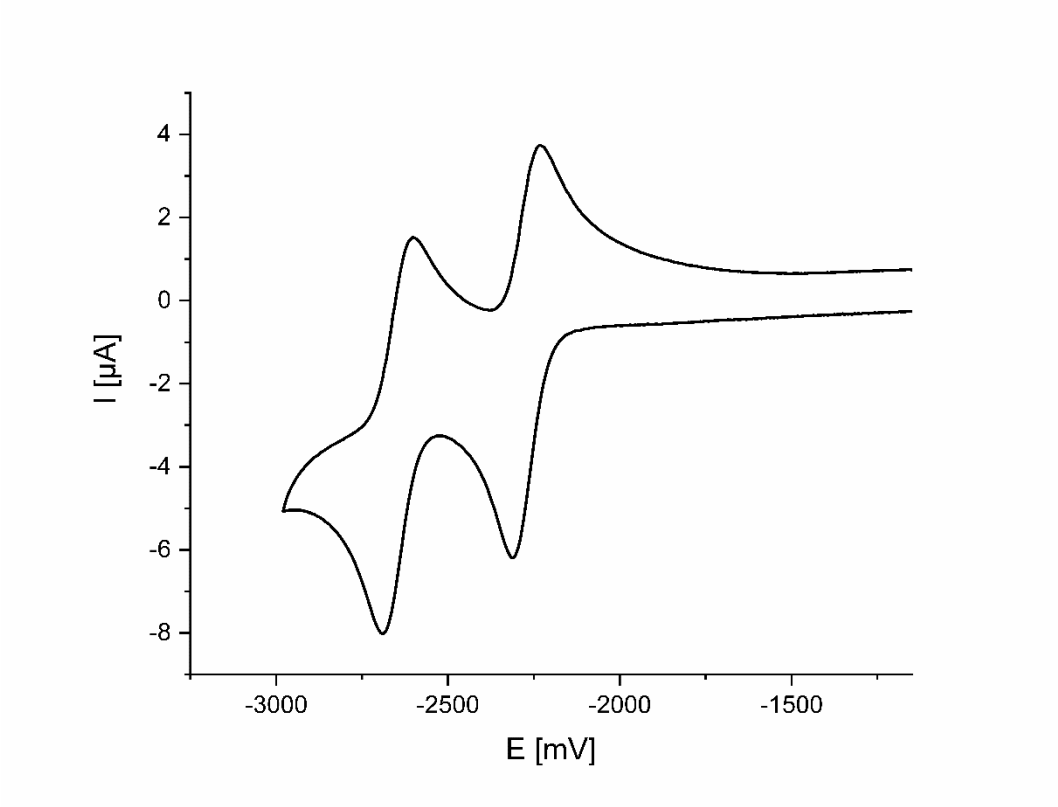

Figure 5.4.58. Cyclic voltammogram of **2a**^{Mes*} (in THF).

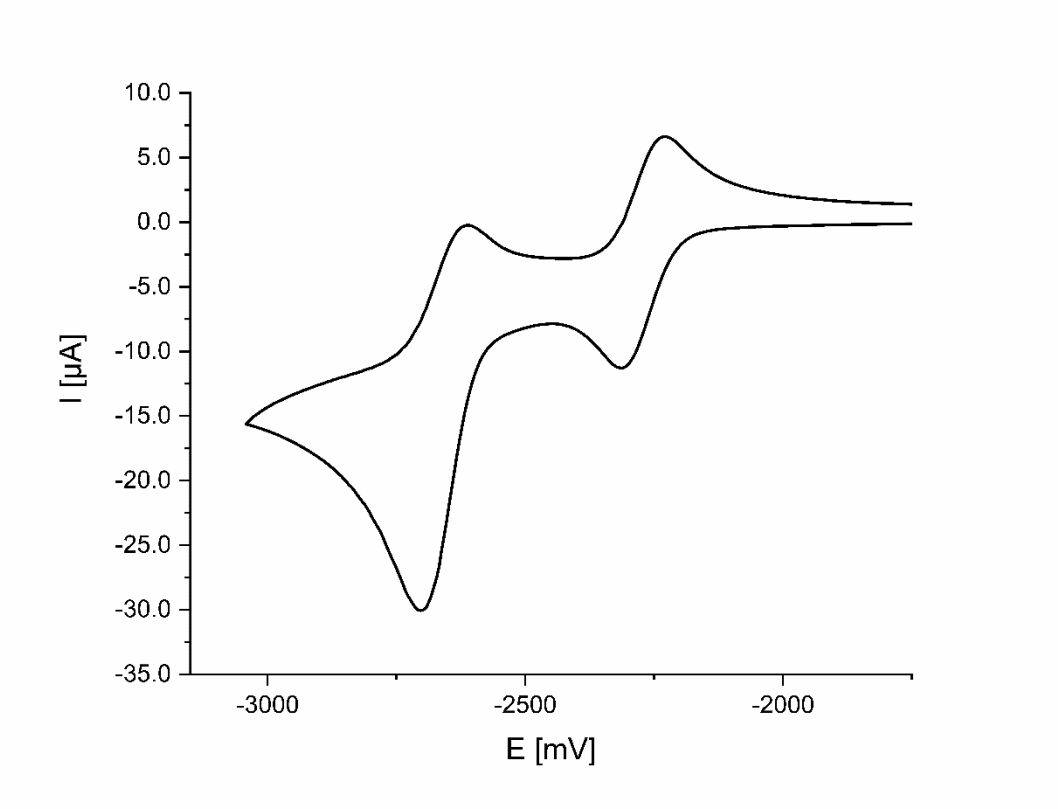

Figure 5.4.59. Cyclic voltammogram of **2c**^{Mes*} (in THF).

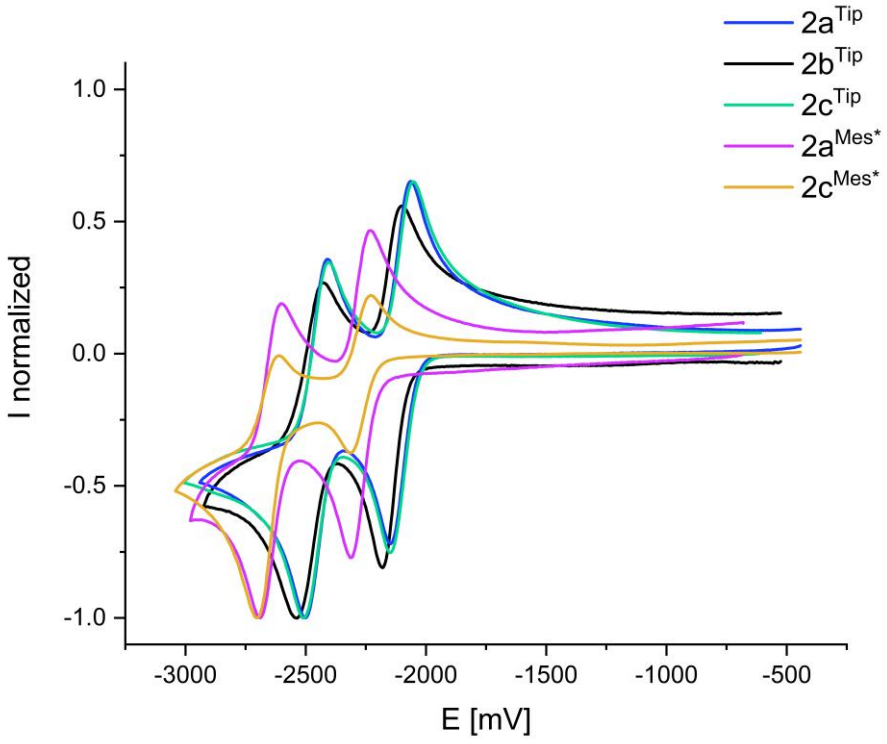

Figure 5.4.60. Overlay of cyclic voltammograms of **2a^{Tip}**, **2b^{Tip}**, **2c^{Tip}**, **2a^{Mes*}** and **2c^{Mes*}** (in THF).

5.5 Conjugated Bis(triarylboranes) with Disconnected Conjugation

NMR spectra

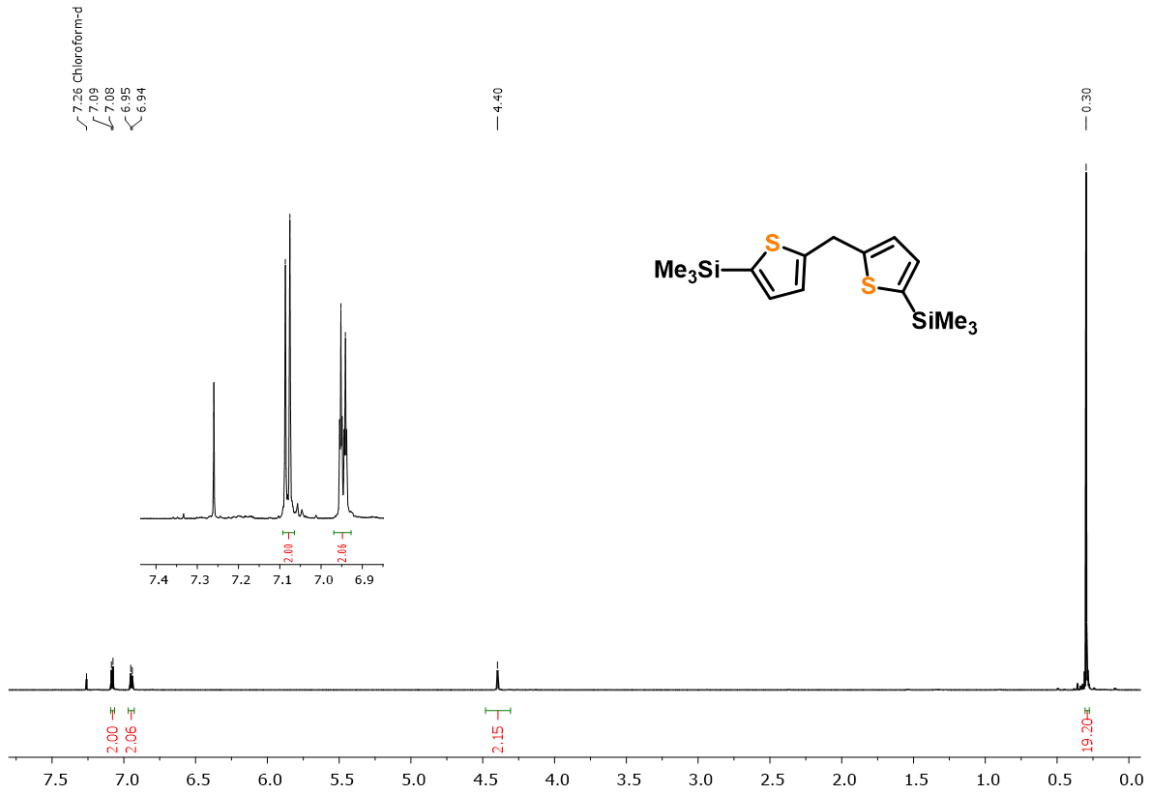

Figure 5.5.1. ^{1}H NMR spectrum of **4** (300 MHz, in $CDCl_3$).

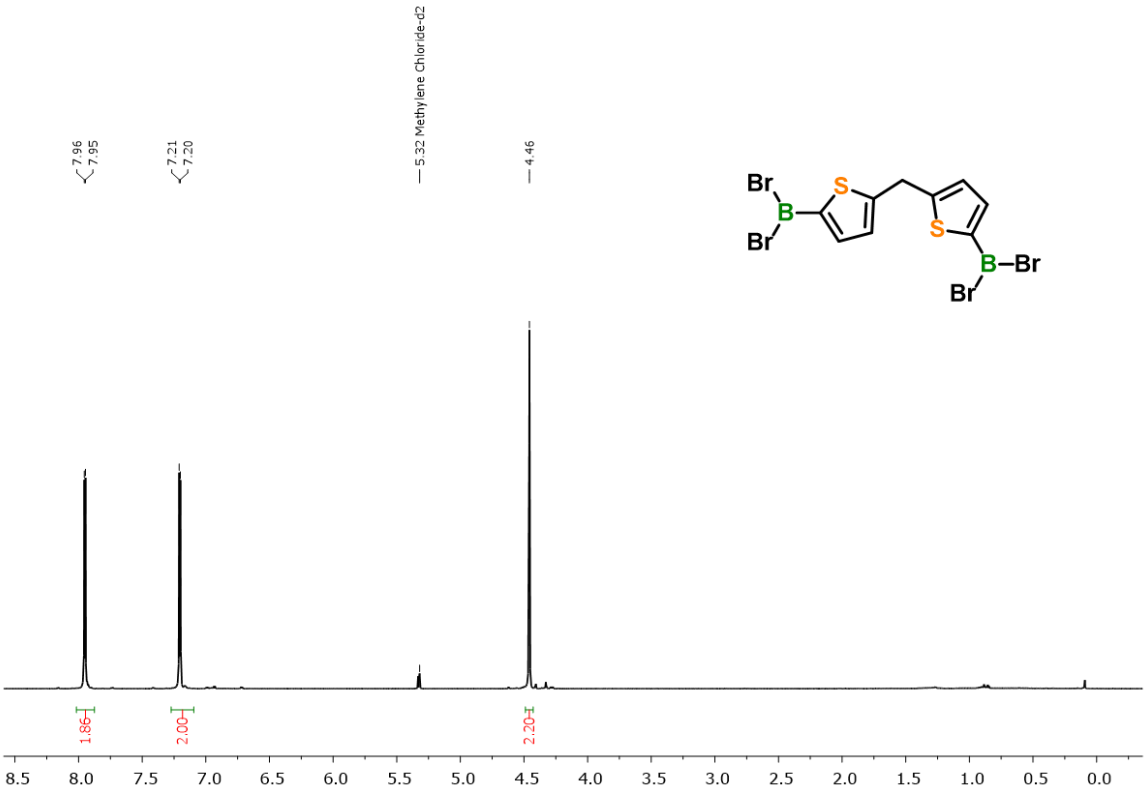

Figure 5.5.2. ^{1}H NMR spectrum of **5** (400 MHz, in CD_2Cl_2).

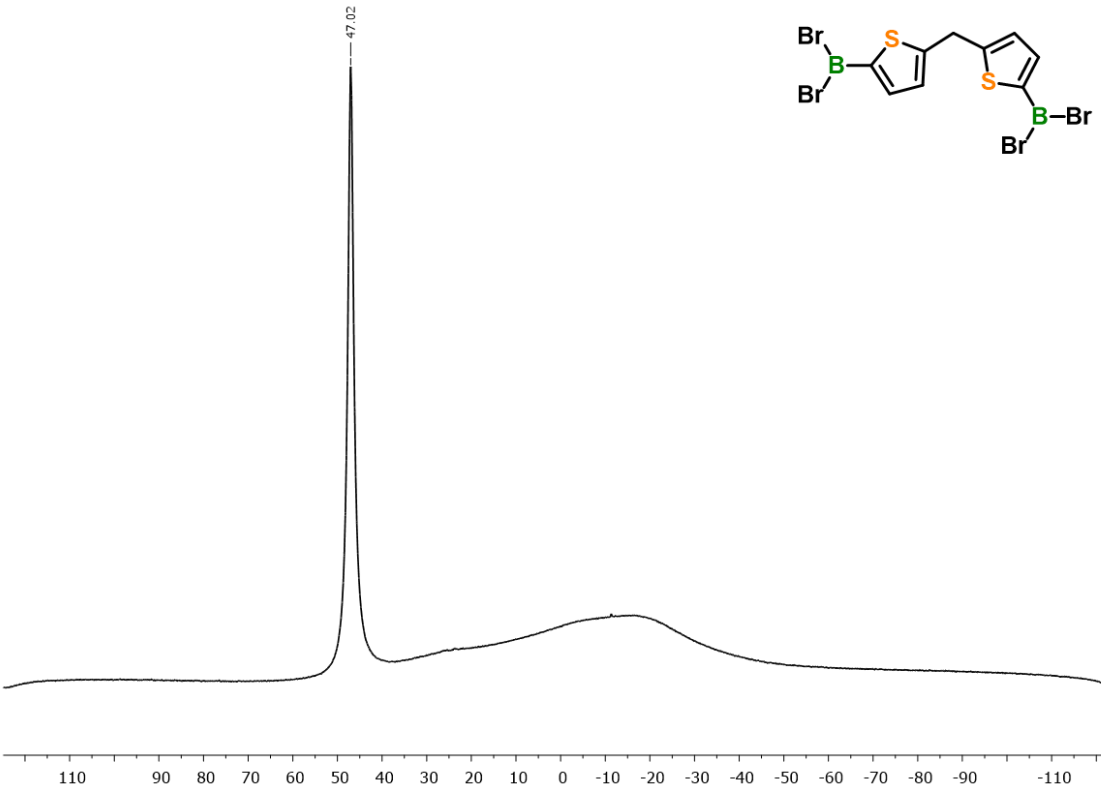

Figure 5.5.3. $^{11}B\{^{1}H\}$ NMR spectrum of **5** (128 MHz, in CD_2Cl_2).

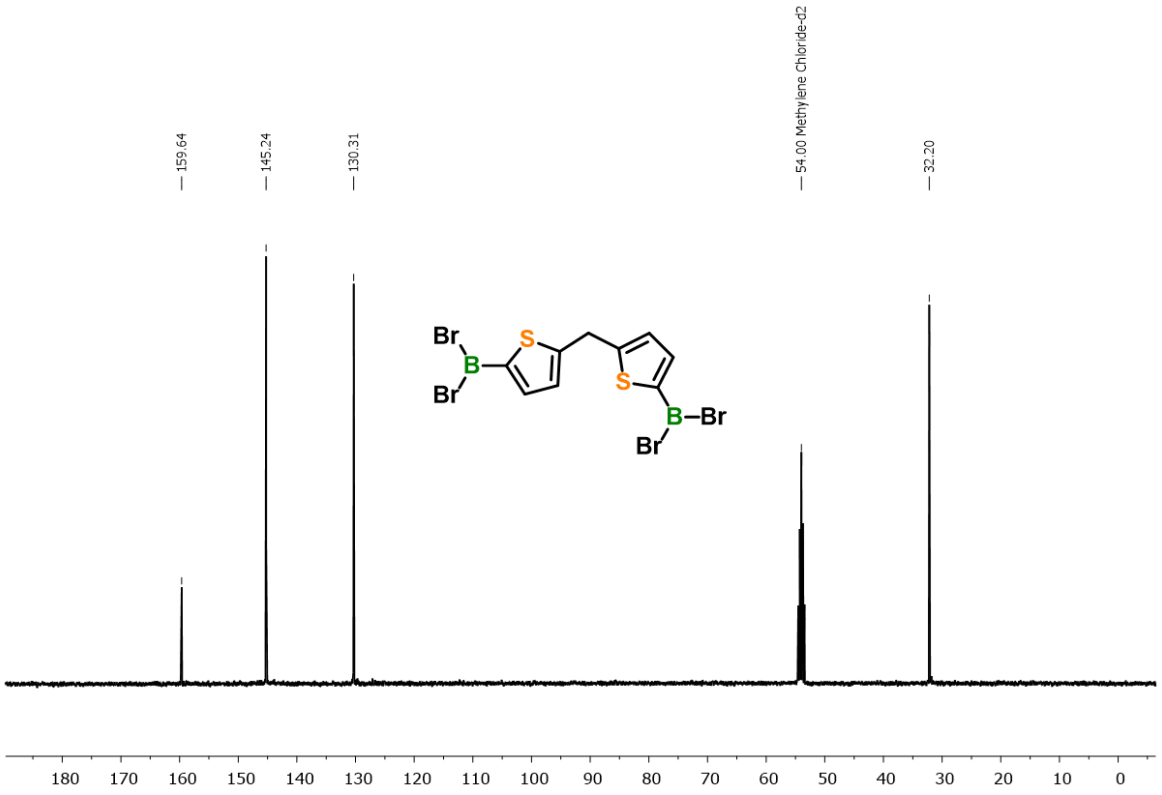

Figure 5.5.4. $^{13}C\{^{1}H\}$ NMR spectrum of **5** (101 MHz, in CD_2Cl_2).

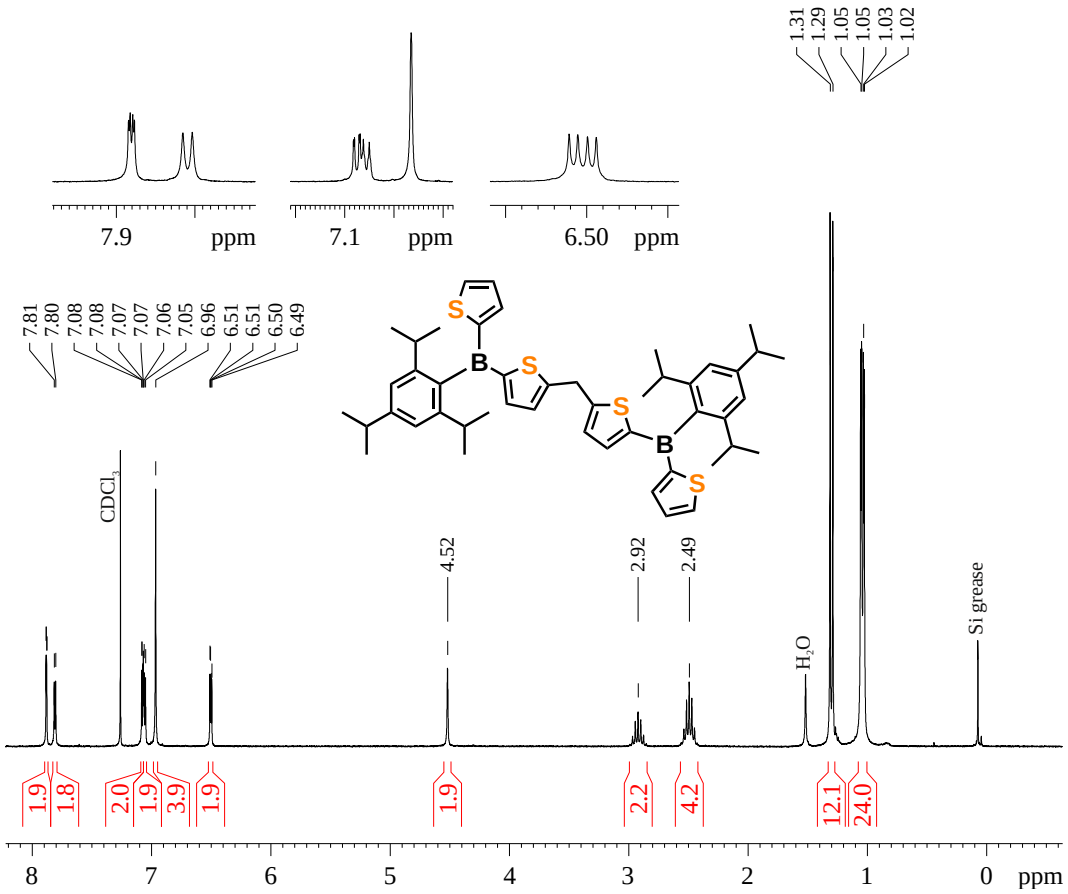

Figure 5.5.5. ^{1}H NMR spectrum of **3a^{Tip}** (500 MHz, in $CDCl_3$).

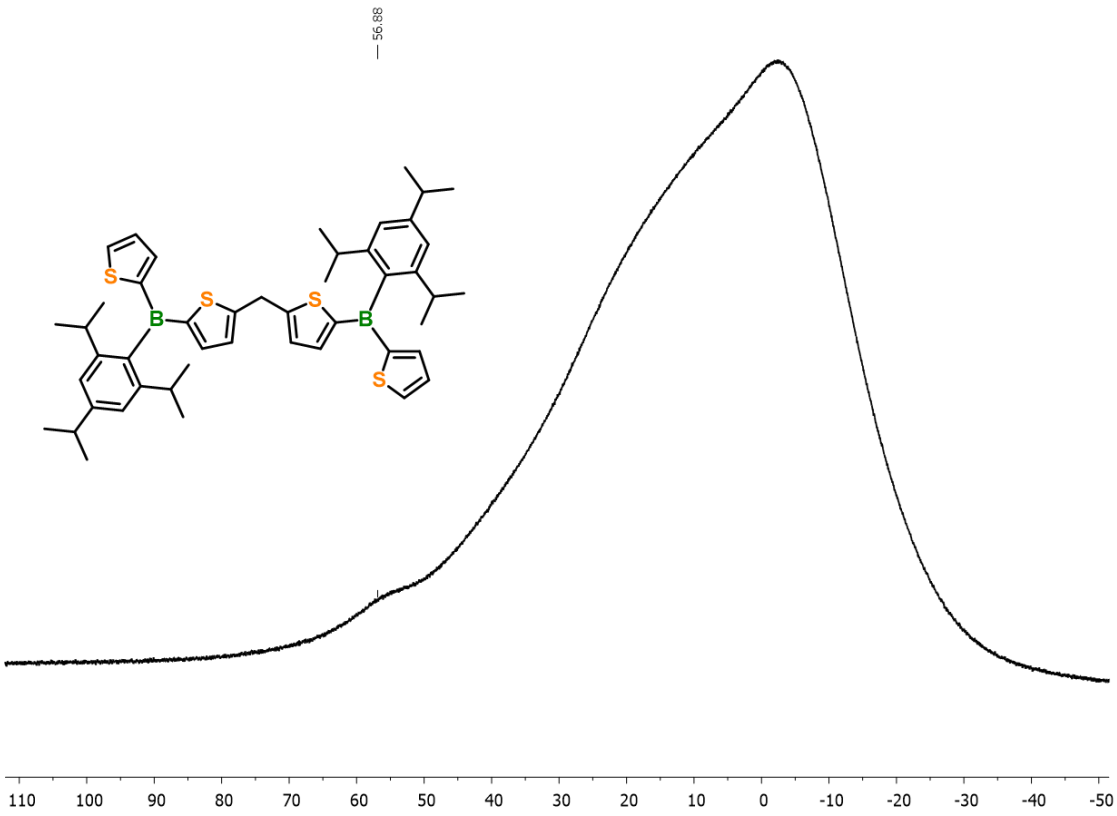

Figure 5.5.6. $^{11}B\{^{1}H\}$ NMR spectrum of **3a^{Tip}** (160 MHz, in $CDCl_3$).

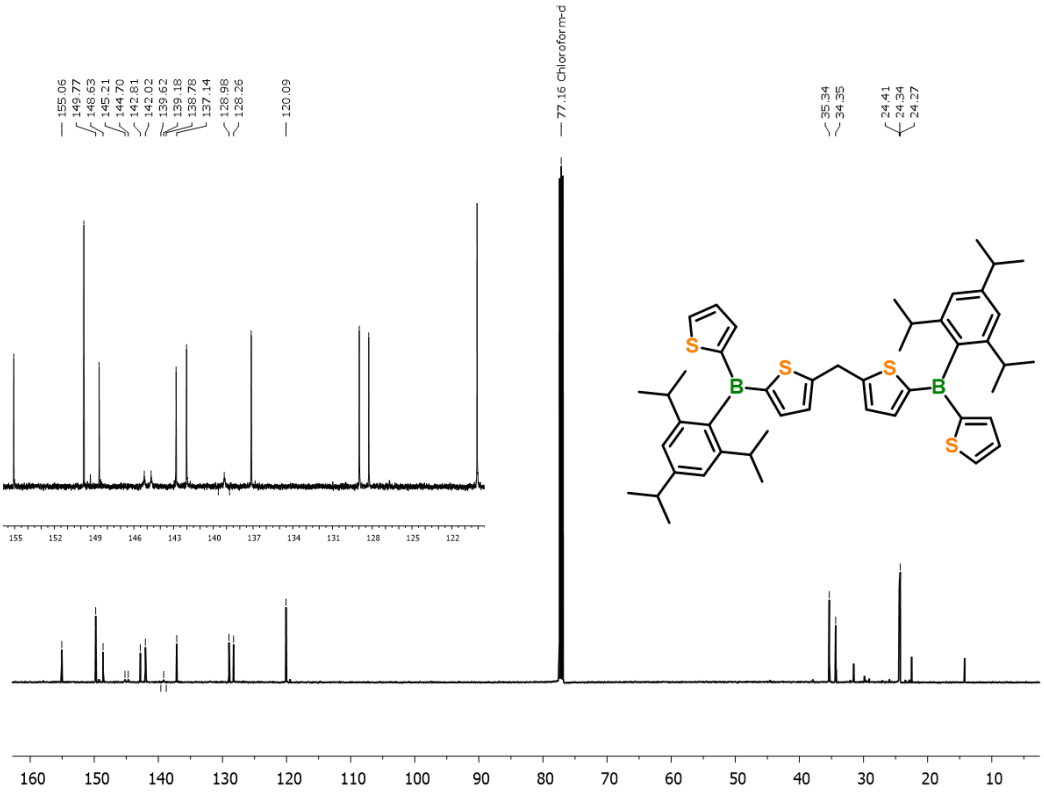

Figure 5.5.7. $^{13}C\{^{1}H\}$ NMR spectrum of **3a^{Tip}** (101 MHz, in $CDCl_3$).

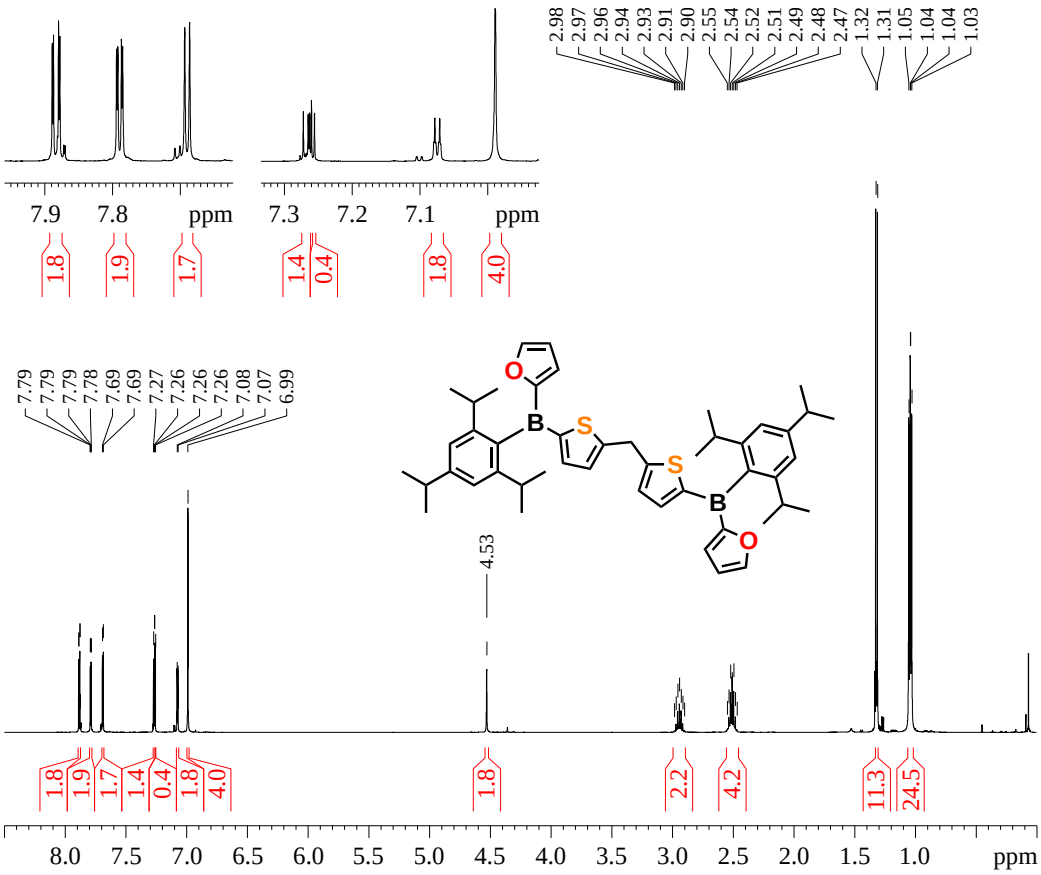

Figure 5.5.8. ^{1}H NMR spectrum of **3b^{Tip}** (500 MHz, in $CDCl_3$).

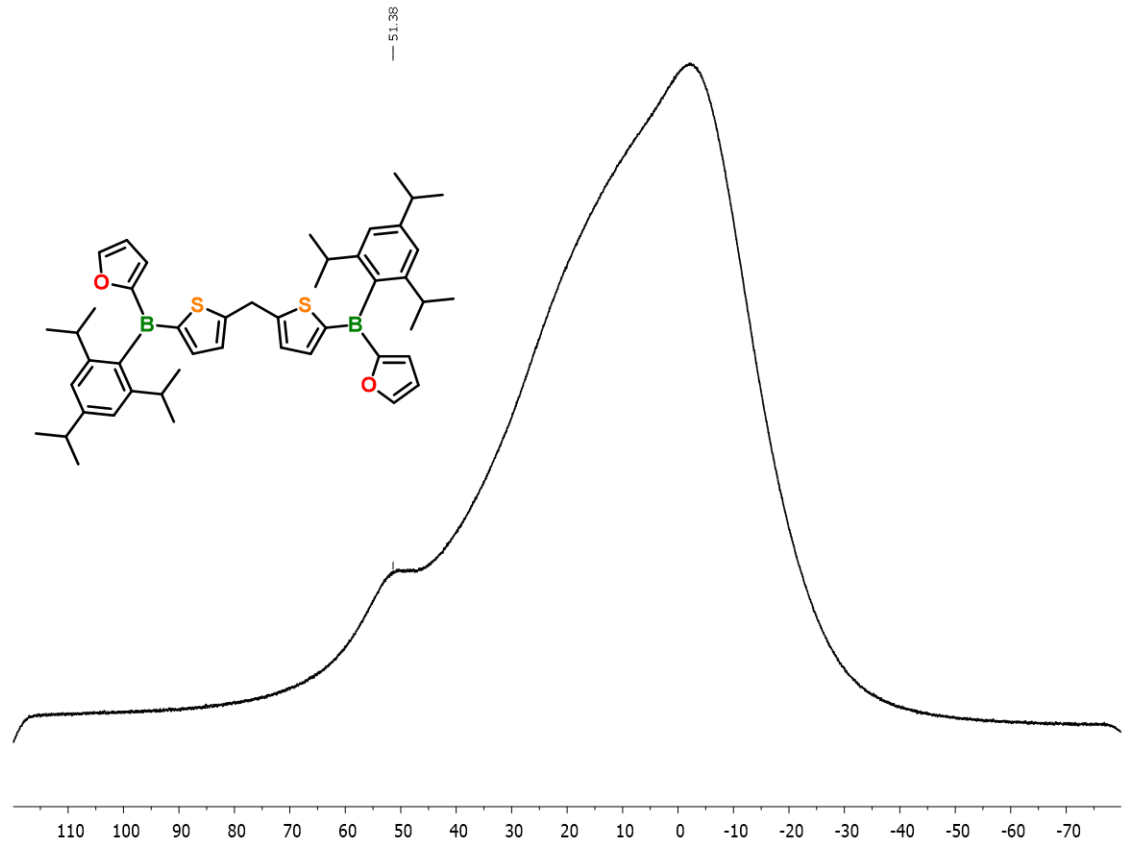

Figure 5.5.9. ^{11}B{^{1}H} NMR spectrum of **3b^{Tip}** (160 MHz, in $CDCl_3$).

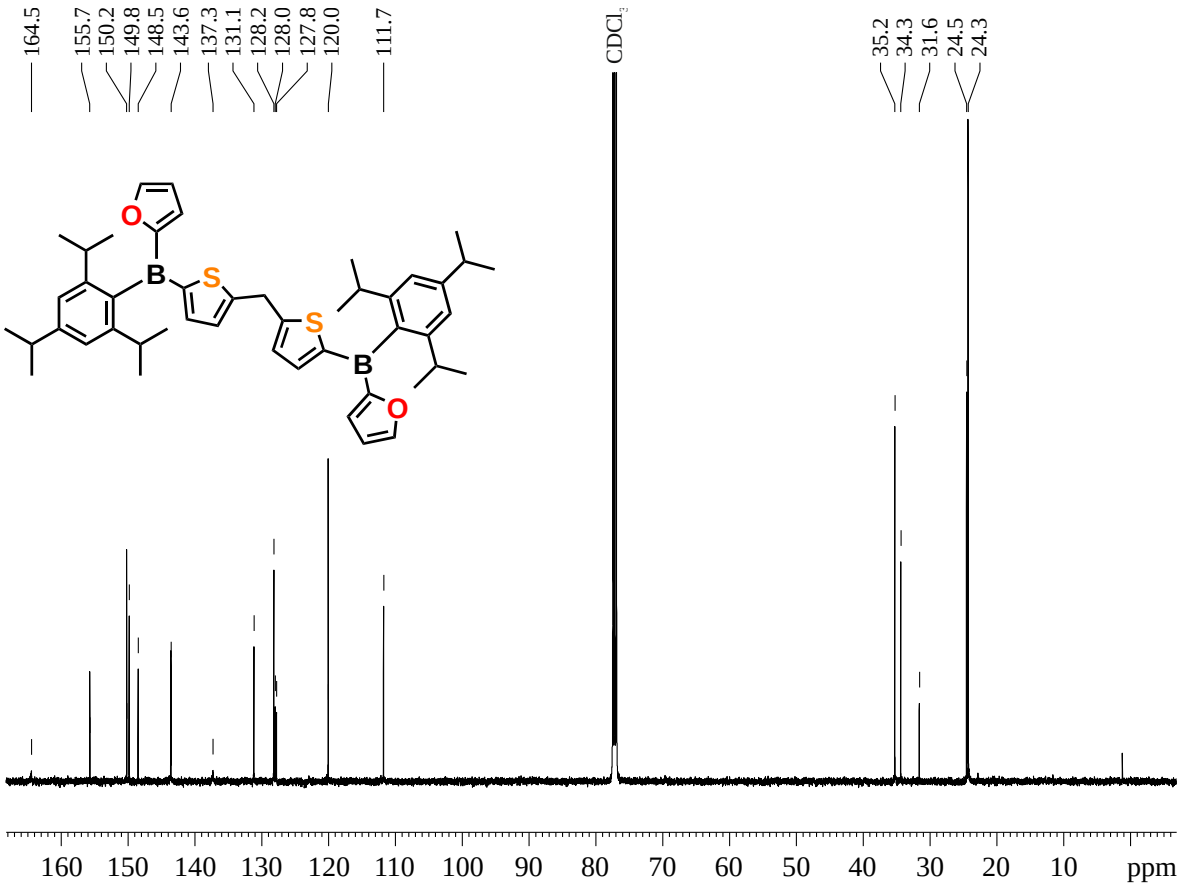

Figure 5.5.10. $^{13}C\{^{1}H\}$ NMR spectrum of **3b^{Tip}** (101 MHz, in $CDCl_3$).

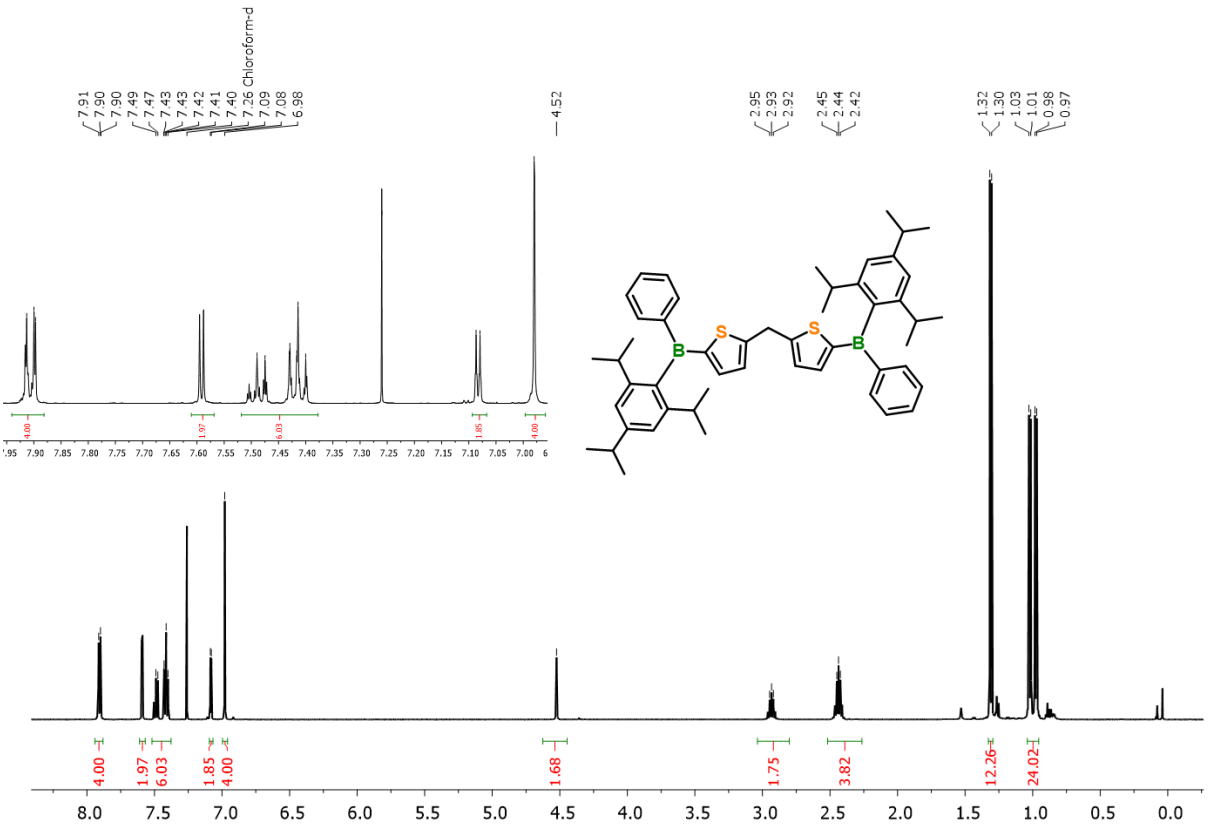

Figure 5.5.11. ^{1}H NMR spectrum of **3c^{Tip}** (500 MHz, in $CDCl_3$).

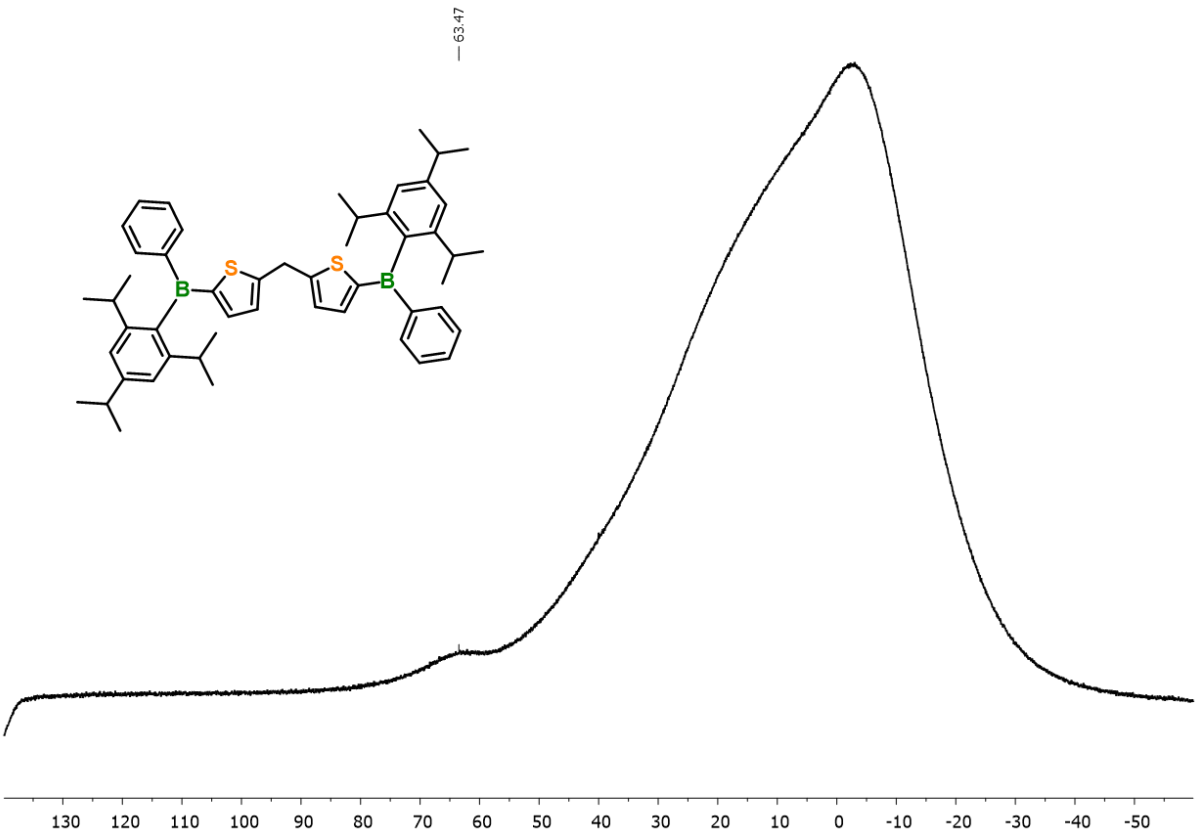

Figure 5.5.12. $^{11}B\{^{1}H\}$ NMR spectrum of **3c^{Tip}** (160 MHz, in $CDCl_3$).

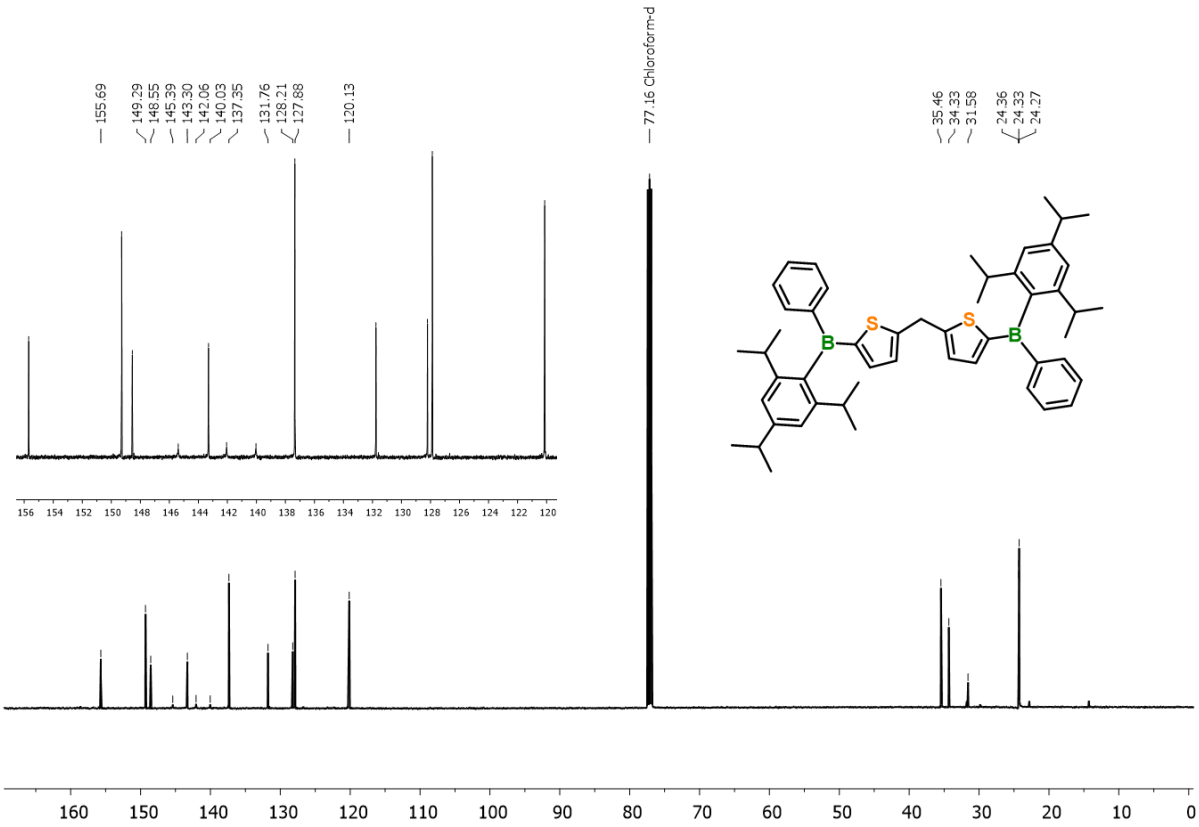

Figure 5.5.13. $^{13}C\{^{1}H\}$ NMR spectrum of **3c^{Tip}** (101 MHz, in $CDCl_3$).

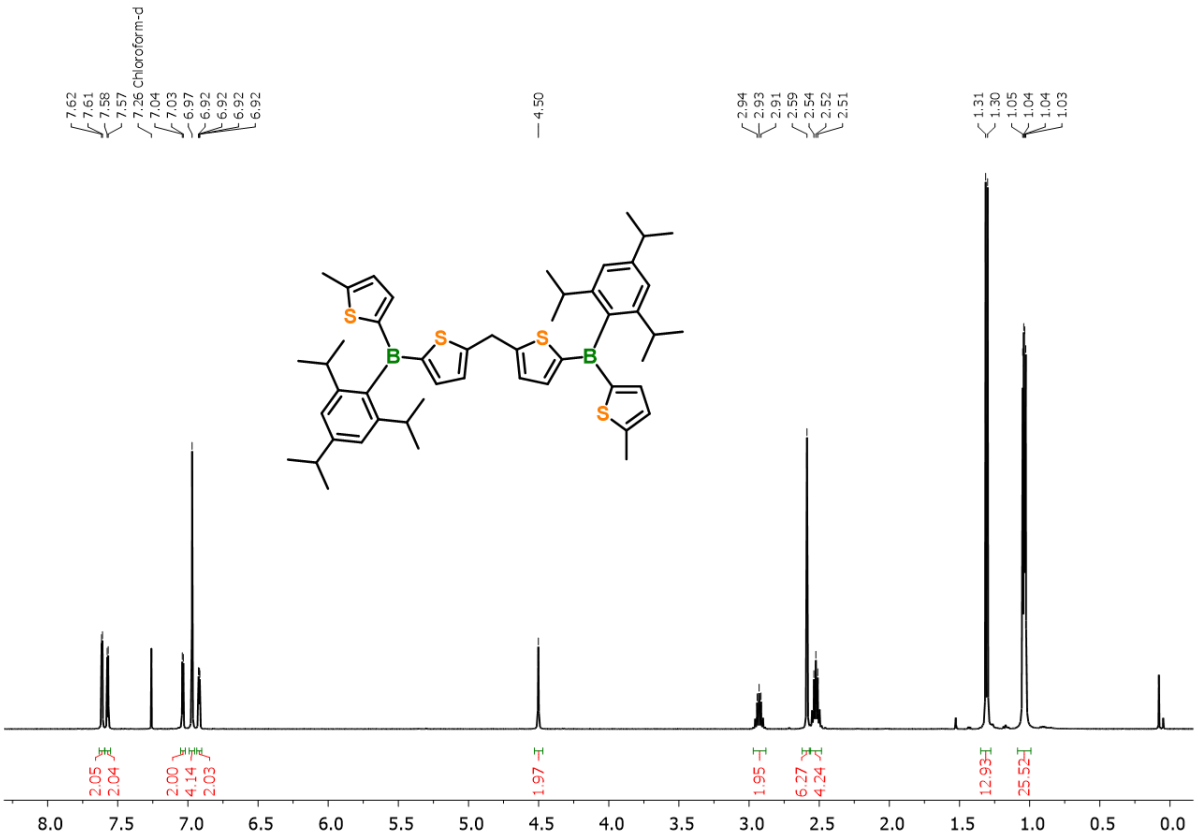

Figure 5.5.14. ^{1}H NMR spectrum of **3d^{Tip}** (500 MHz, in $CDCl_3$).

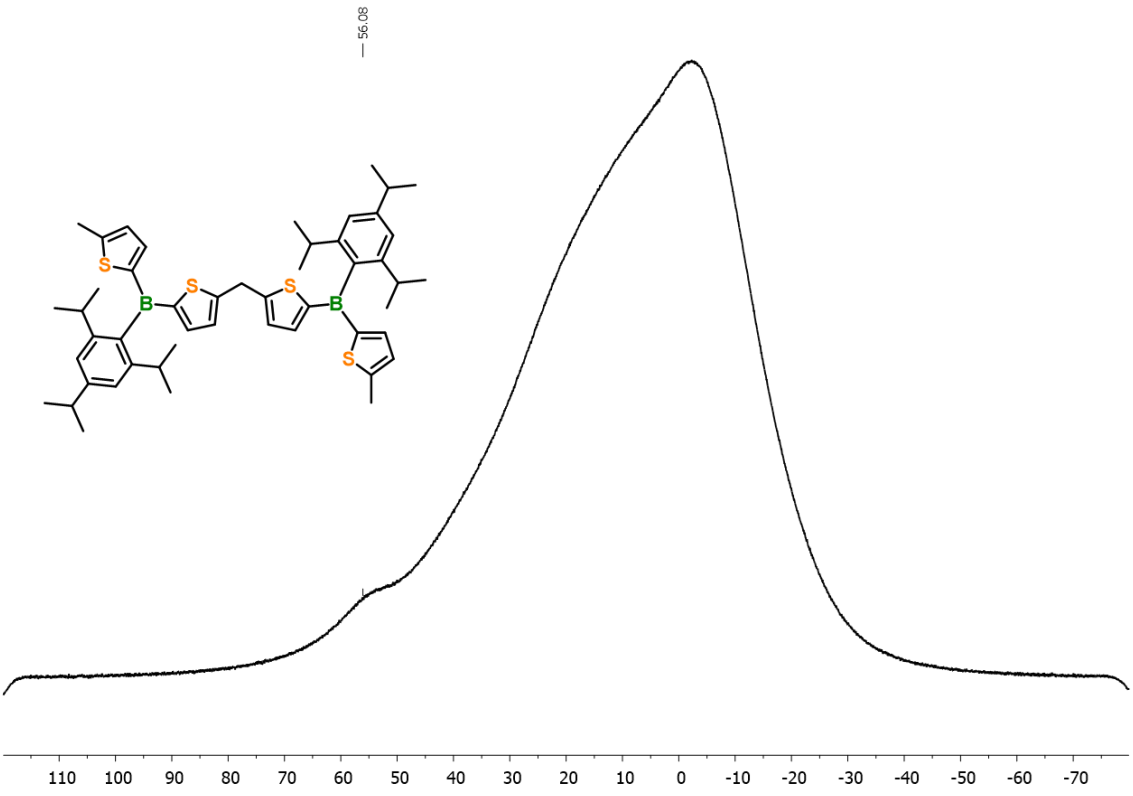

Figure 5.5.15. $^{11}B\{^{1}H\}$ NMR spectrum of **3d^{Tip}** (160 MHz, in $CDCl_3$).

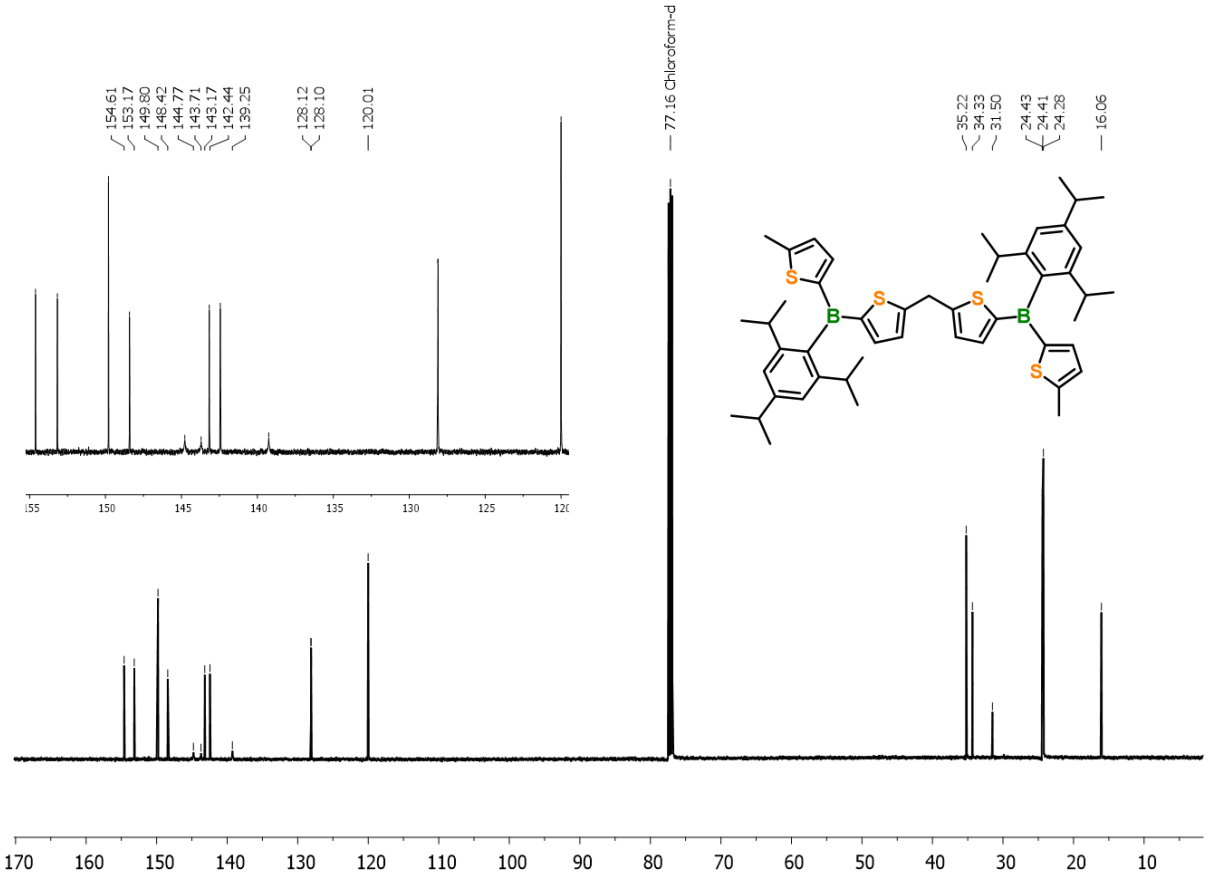

Figure 5.5.16. $^{13}C\{^{1}H\}$ NMR spectrum of **3d^{Tip}** (101 MHz, in $CDCl_3$).

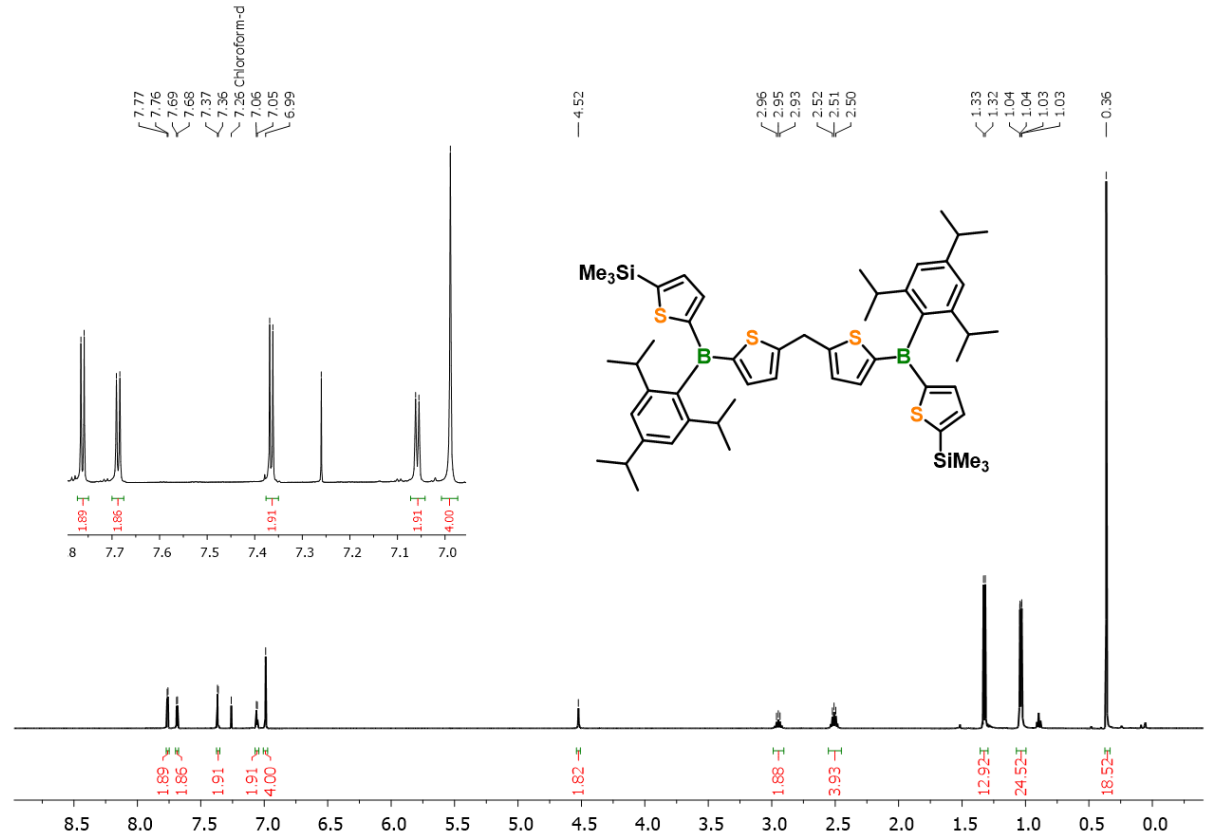

Figure 5.5.17. ^{1}H NMR spectrum of **3e^{Tip}** (500 MHz, in $CDCl_3$).

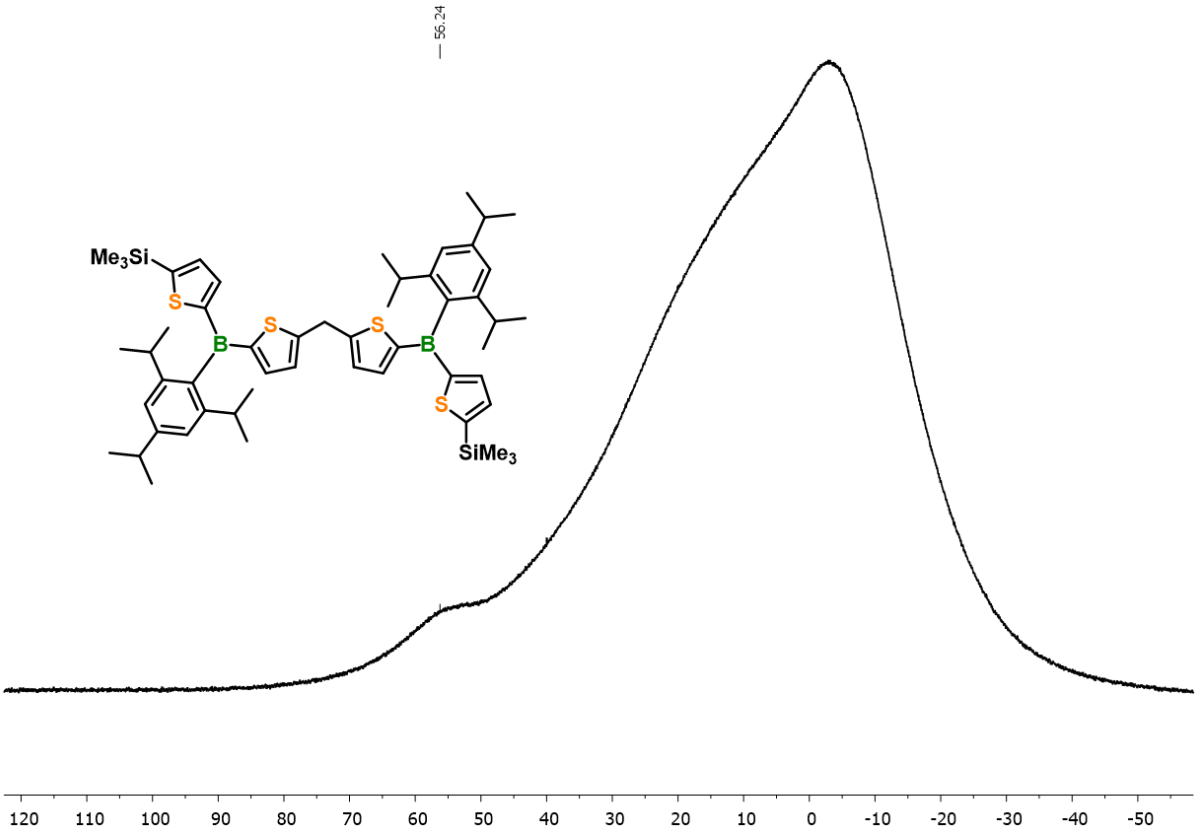

Figure 5.5.18. $^{11}B\{^{1}H\}$ NMR spectrum of **3e^{Tip}** (160 MHz, in $CDCl_3$).

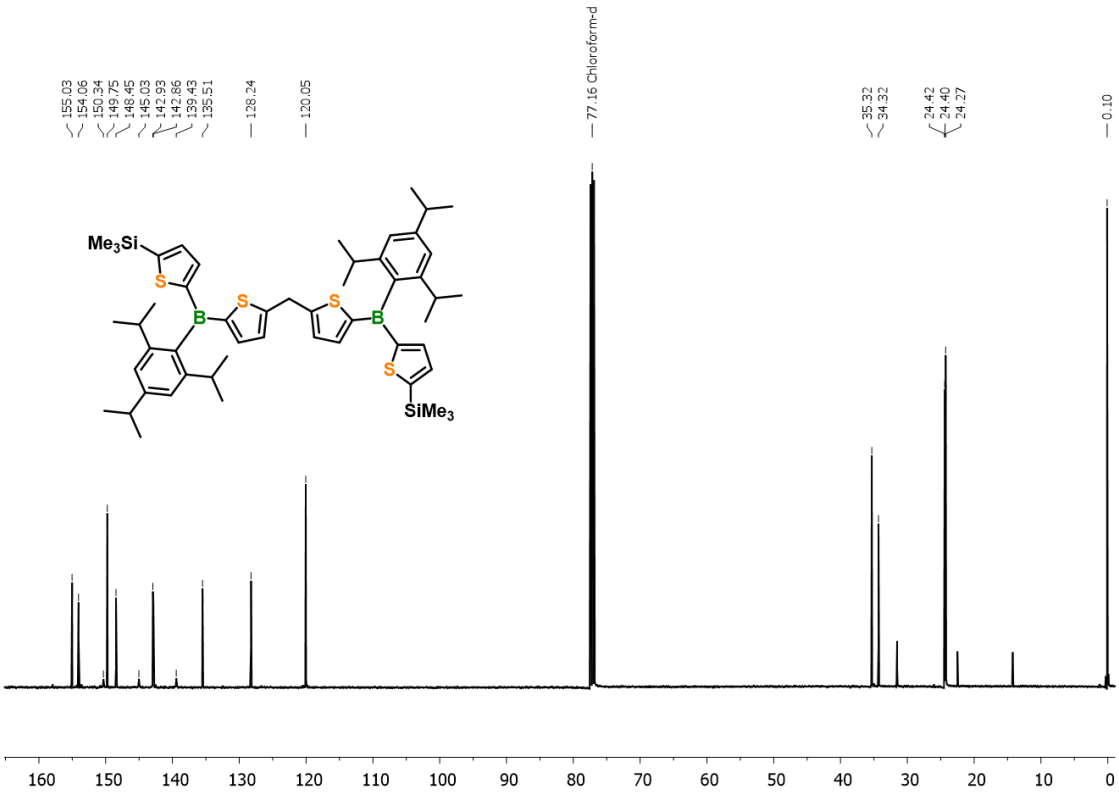

Figure 5.5.19. $^{13}C\{^{1}H\}$ NMR spectrum of **3e^{Tip}** (101 MHz, in $CDCl_3$).

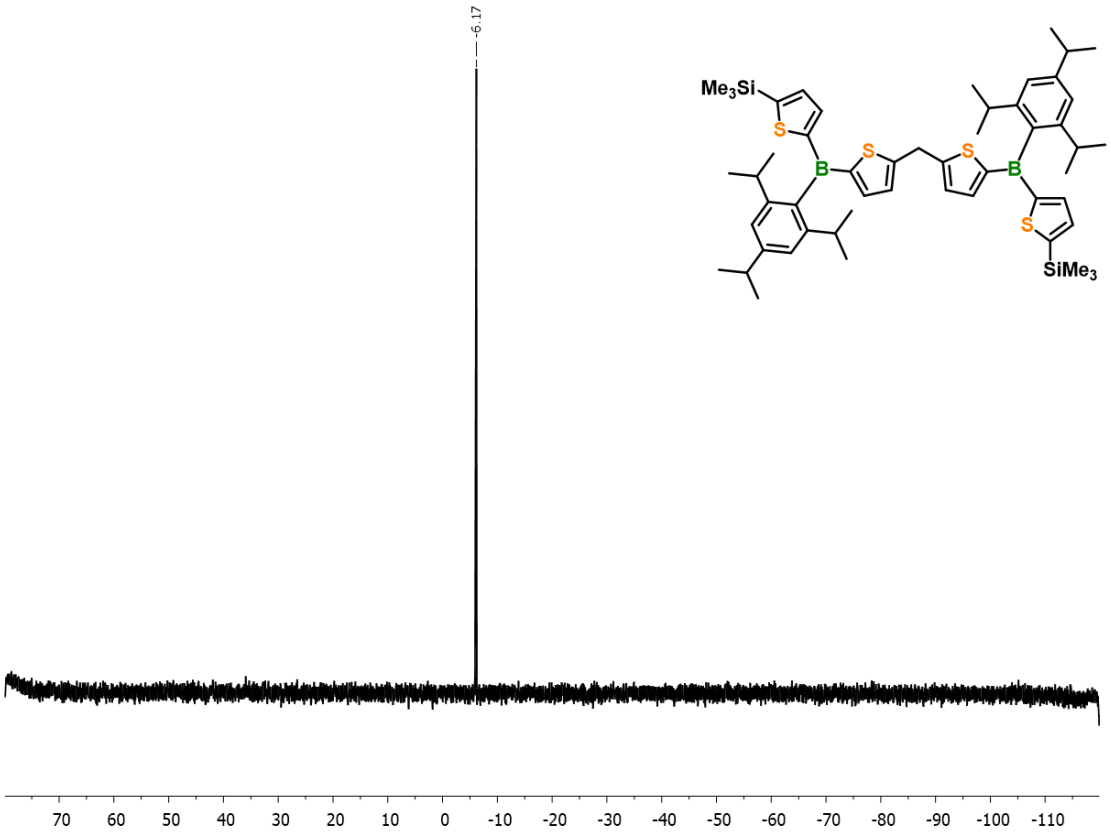

Figure 5.5.20. ^{29}Si NMR spectrum of **3e^{Tip}** (99 Mhz, in $CDCl_3$).

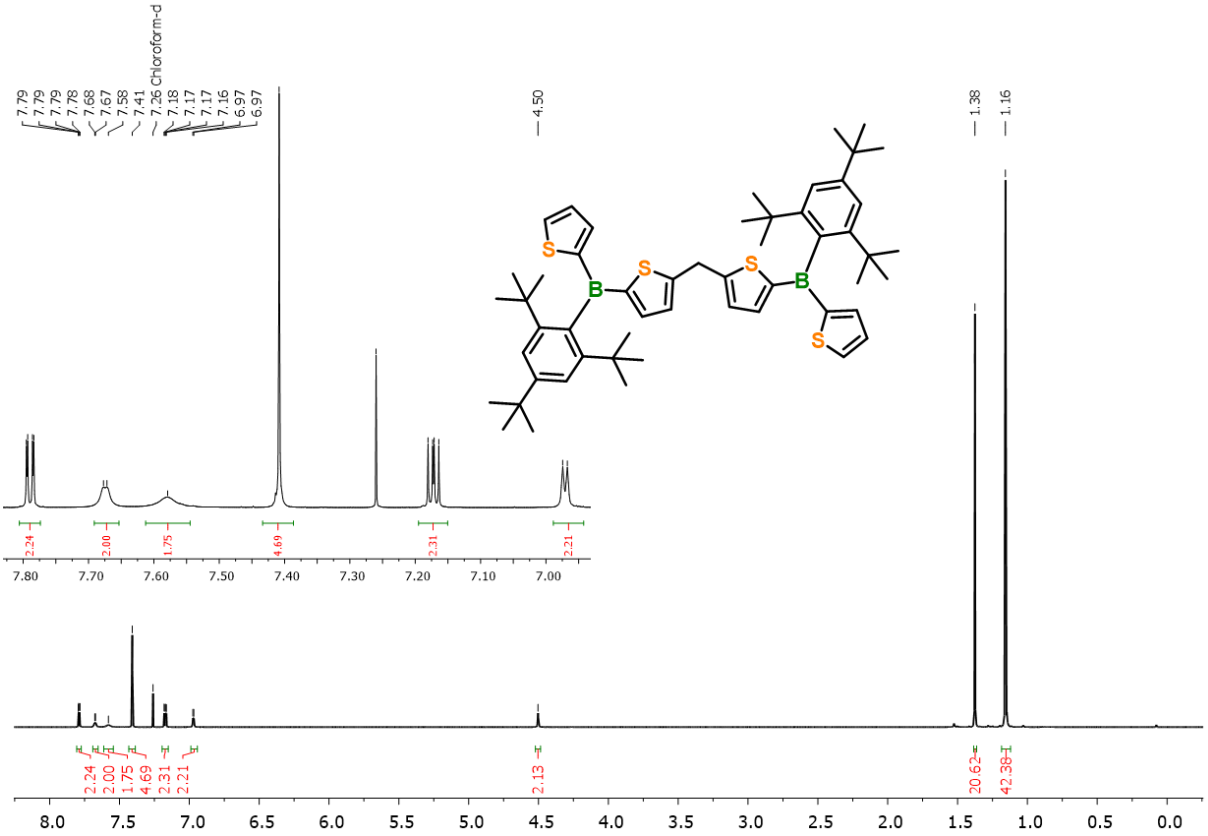

Figure 5.5.21. ^{1}H NMR spectrum of **3a^{Mes*}** (500 MHz, in $CDCl_3$).

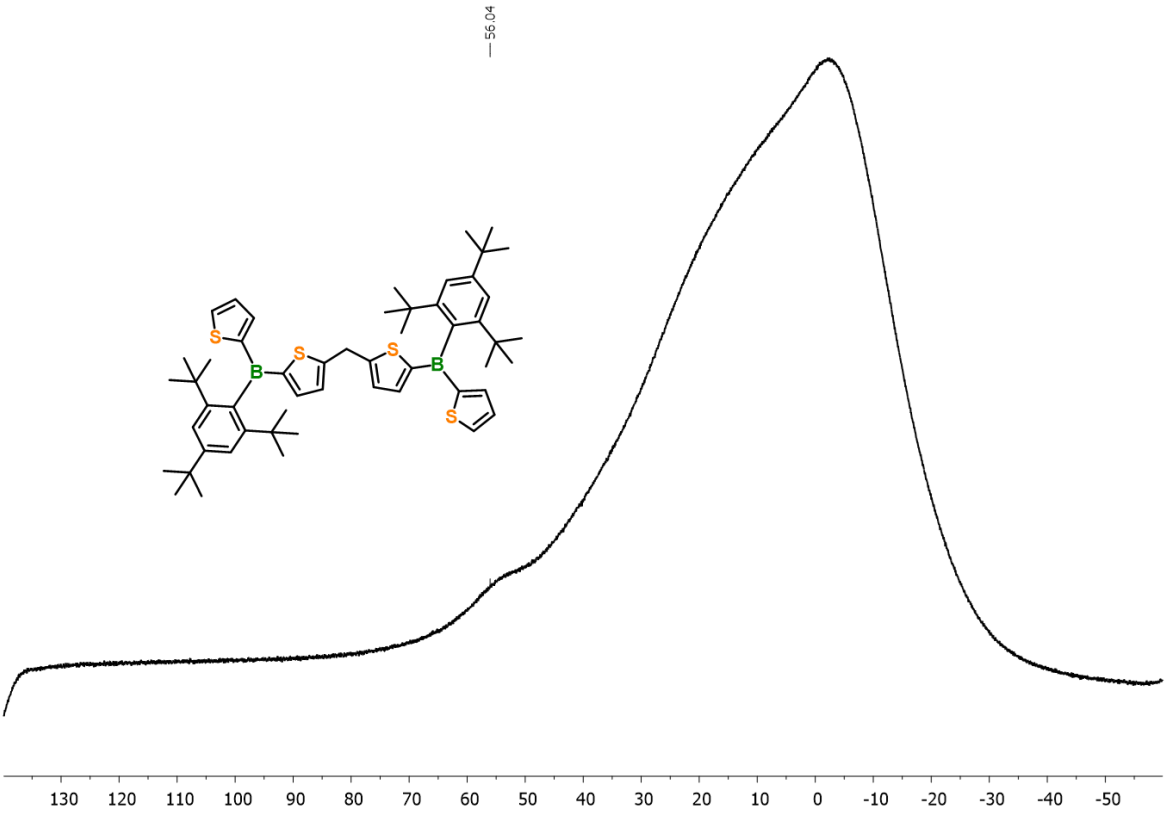

Figure 5.5.22. $^{11}B\{^{1}H\}$ NMR spectrum of **3a^{Mes*}** (160 MHz, in $CDCl_3$).

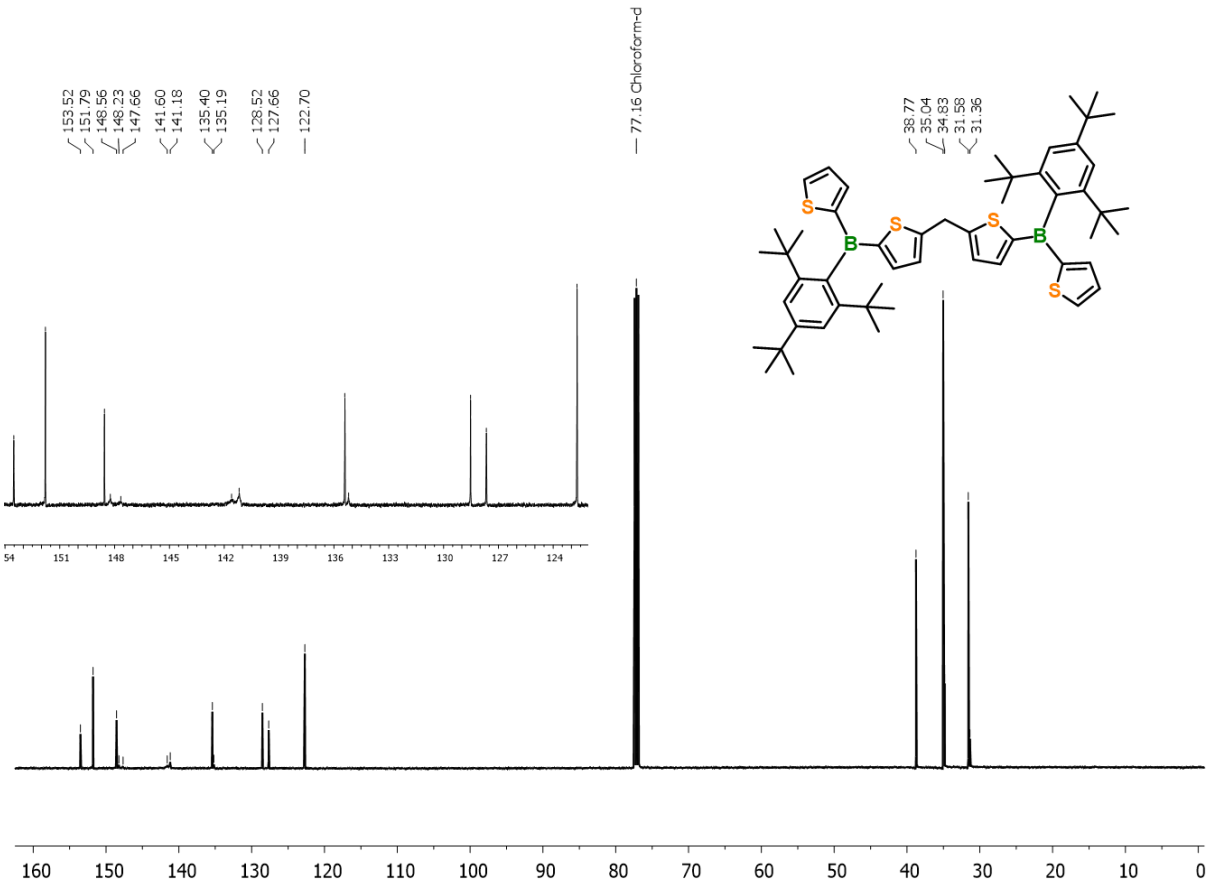

Figure 5.5.23. $^{13}C\{^{1}H\}$ NMR spectrum of **3a^{Mes*}** (101 MHz, in $CDCl_3$).

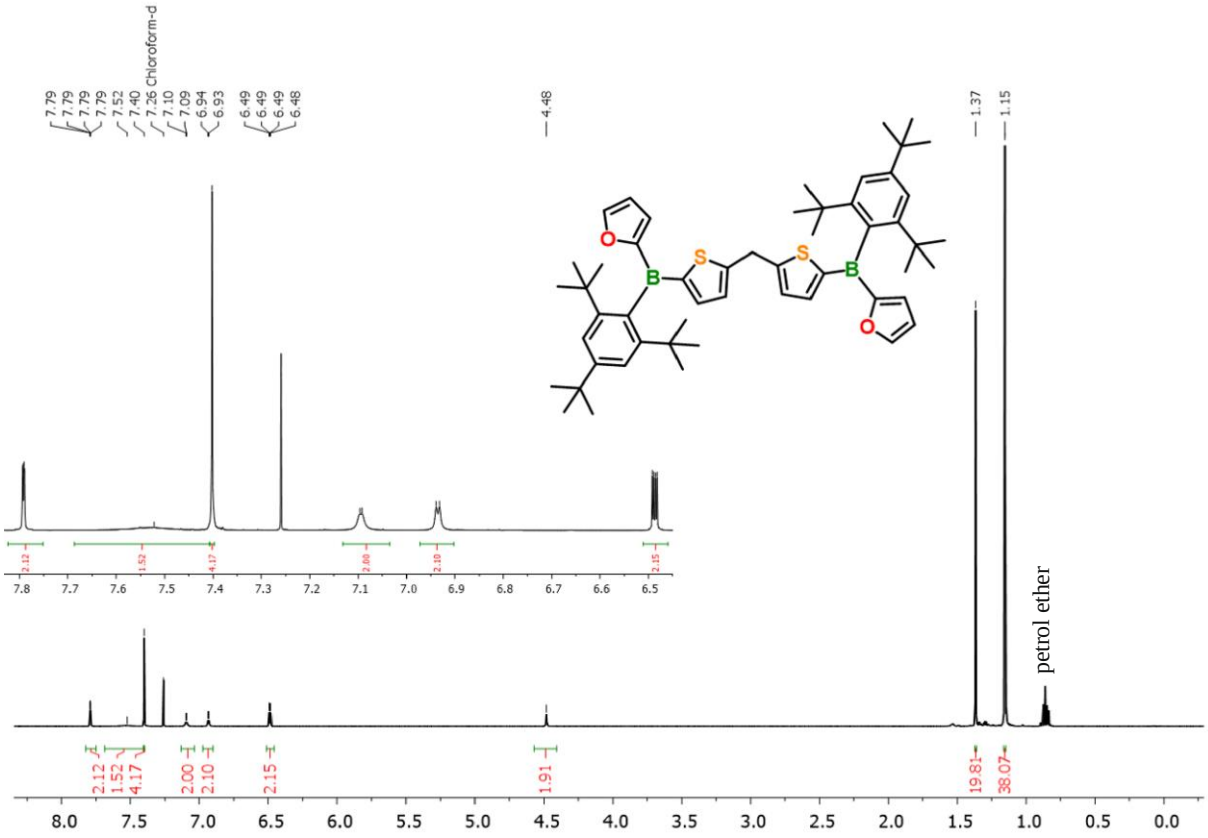

Figure 5.5.24. ^{1}H NMR spectrum of **3b^{Mes*}** (500 MHz, in $CDCl_3$).

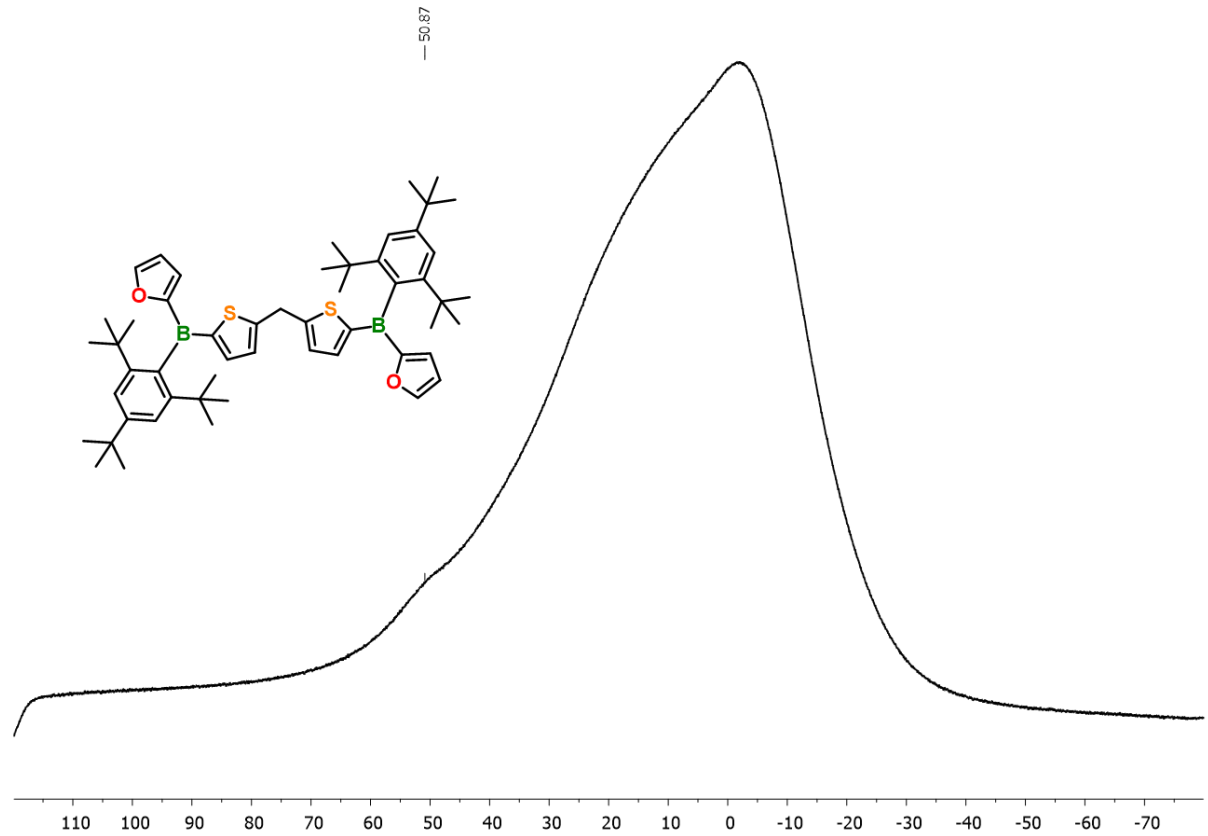

Figure 5.5.25. ^{11}B{^{1}H} NMR spectrum of **3b^{Mes*}** (160 MHz, in $CDCl_3$).

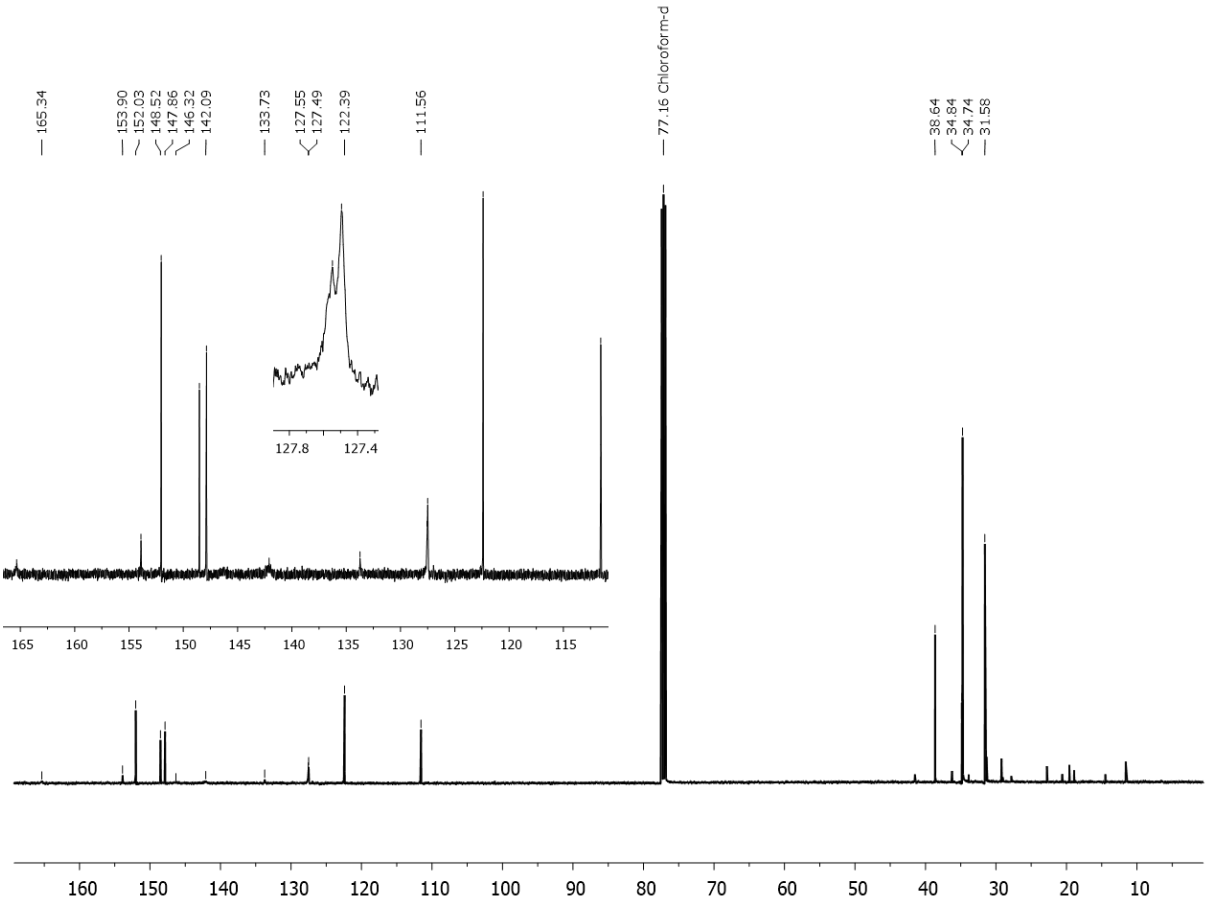

Figure 5.5.26. $^{13}C\{^{1}H\}$ NMR spectrum of **3b**^{Mes*} (101 MHz, in $CDCl_3$).

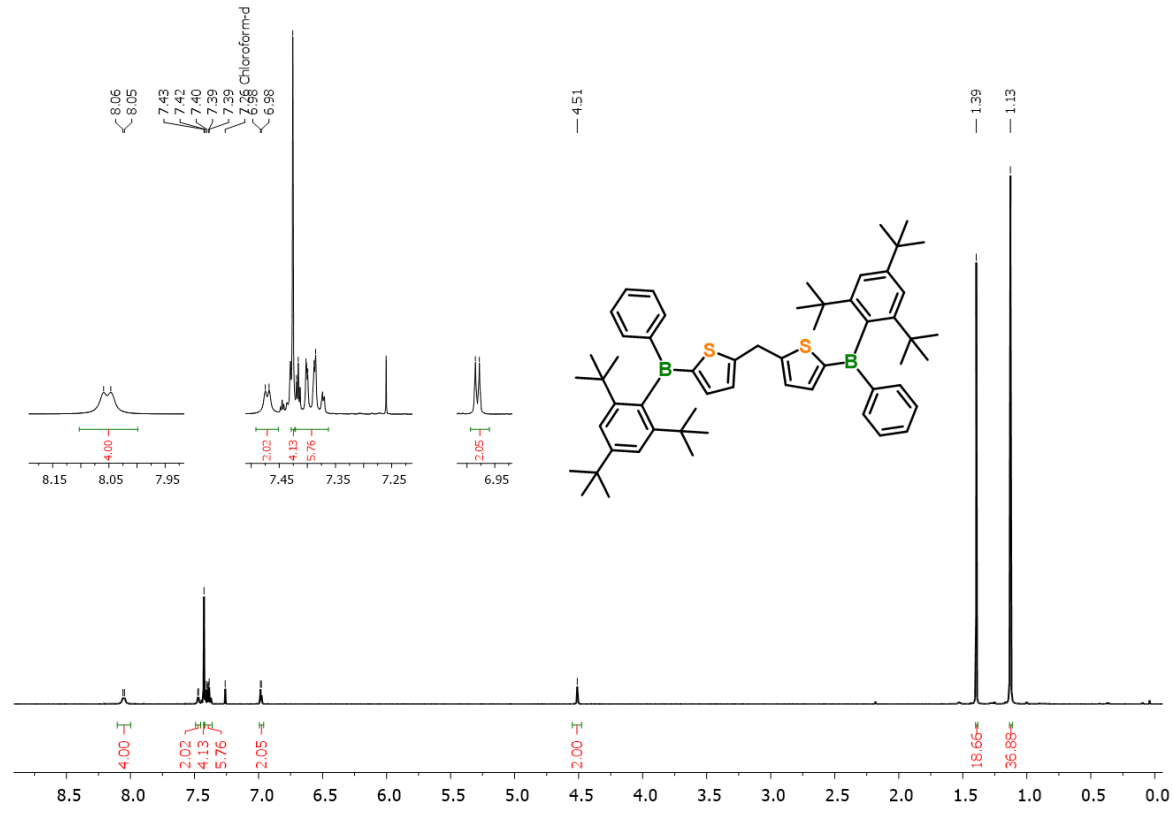

Figure 5.5.27. ^{1}H NMR spectrum of **3c**^{Mes*} (500 MHz, in $CDCl_3$).

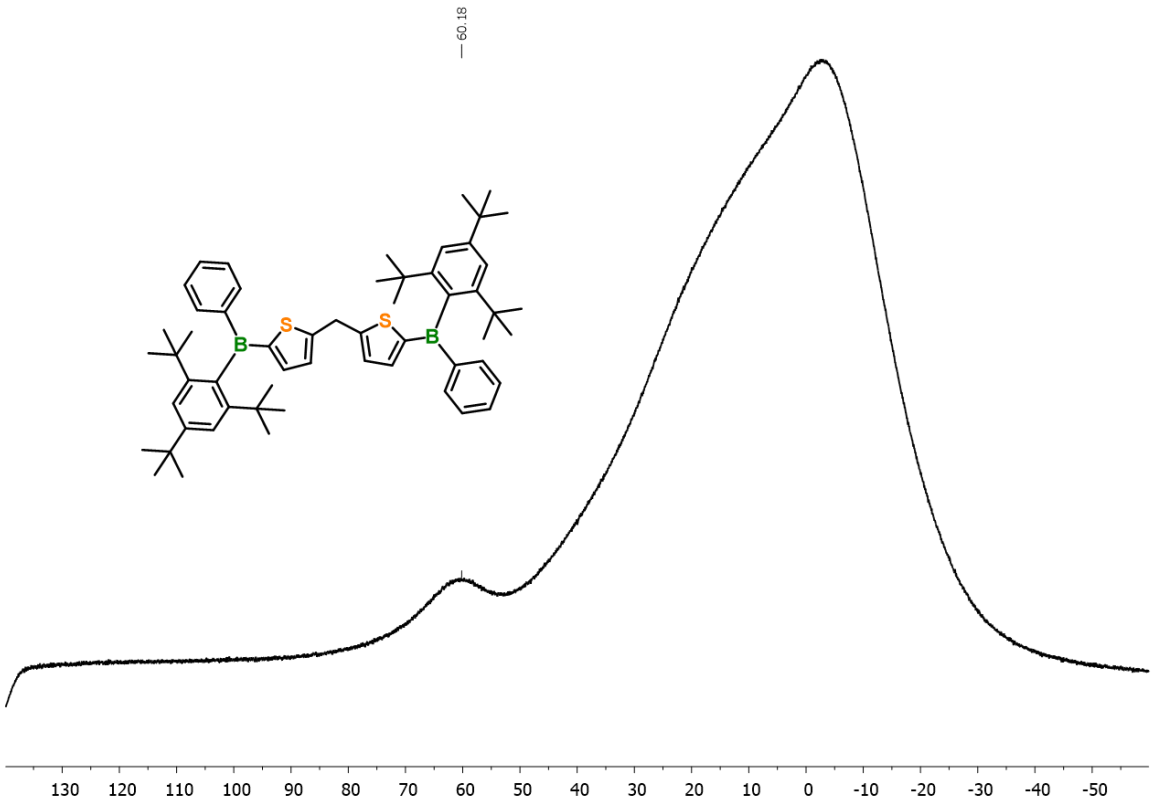

Figure 5.5.28. $^{11}B\{^{1}H\}$ NMR spectrum of **3c^{Mes*}** (160 MHz, in $CDCl_3$).

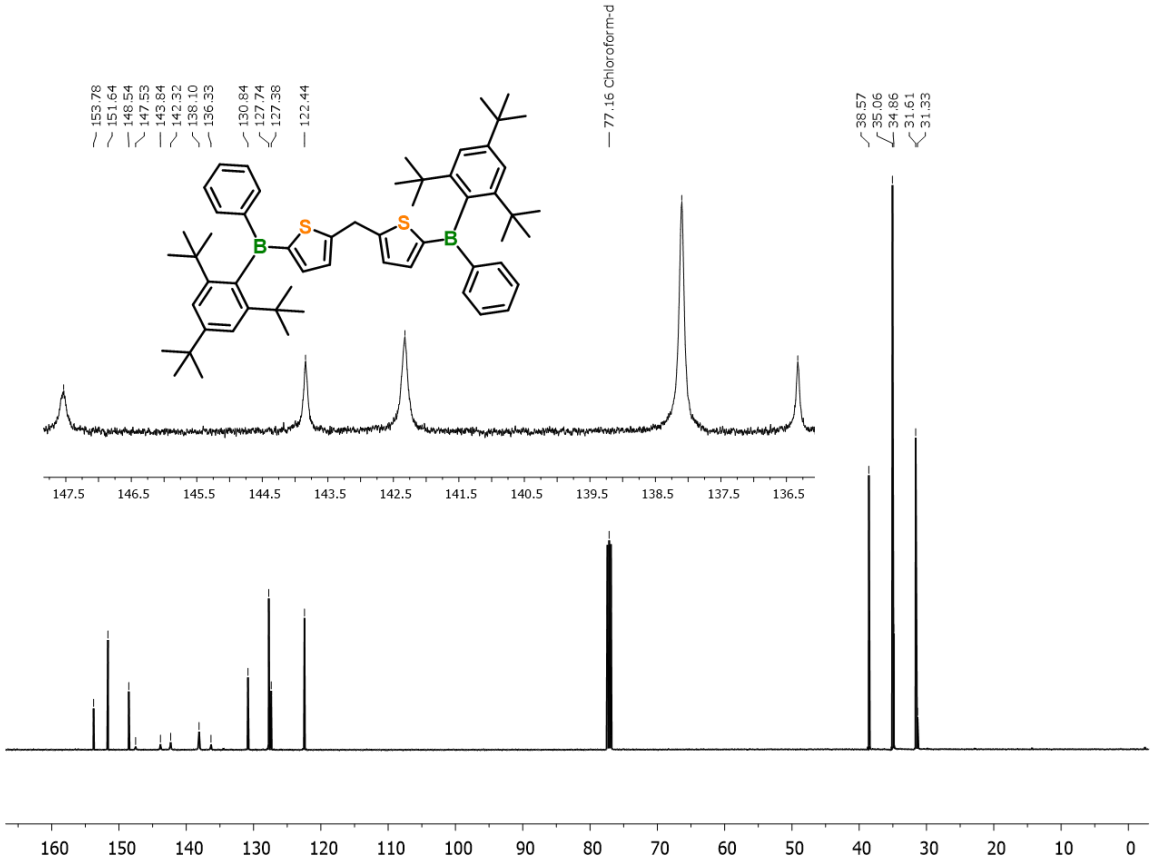

Figure 5.5.29. $^{13}C\{^{1}H\}$ NMR spectrum of **3c^{Mes*}** (101 MHz, in $CDCl_3$).

UV-vis spectra

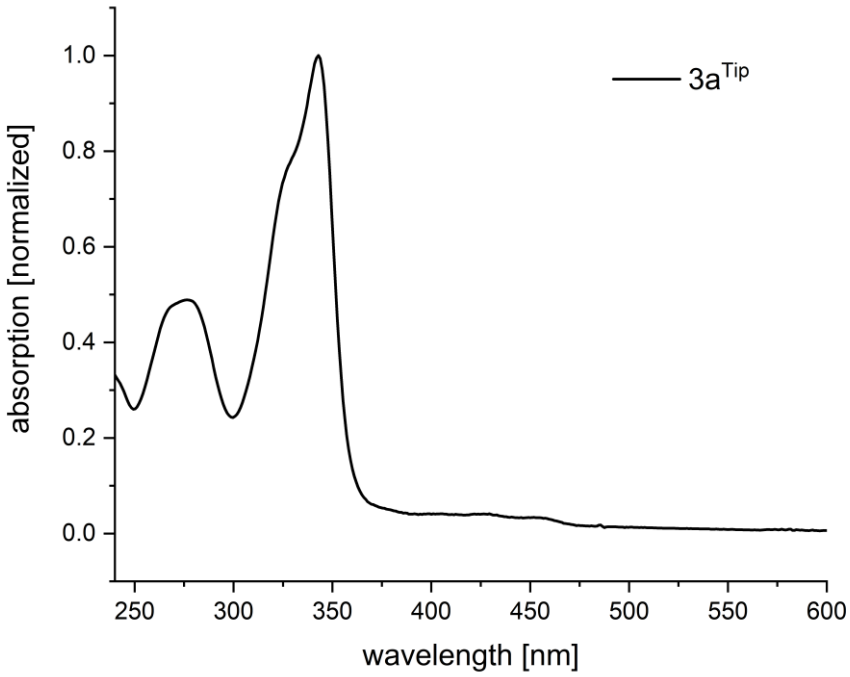

Figure 5.5.30. UV-Vis spectrum of **3a^{Tip}** (in THF).

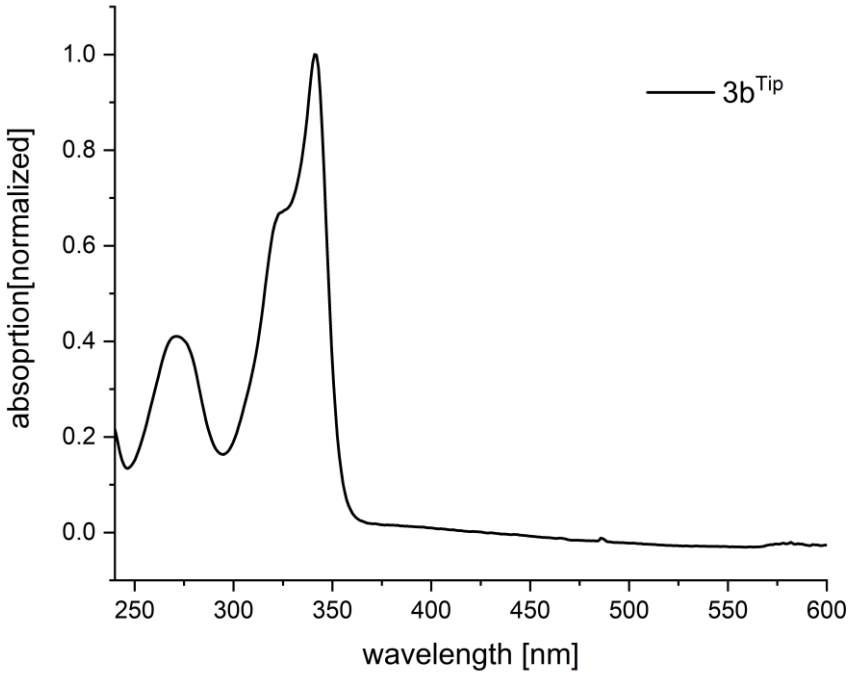

Figure 5.5.31. UV-Vis spectrum of **3b^{Tip}** (in THF).

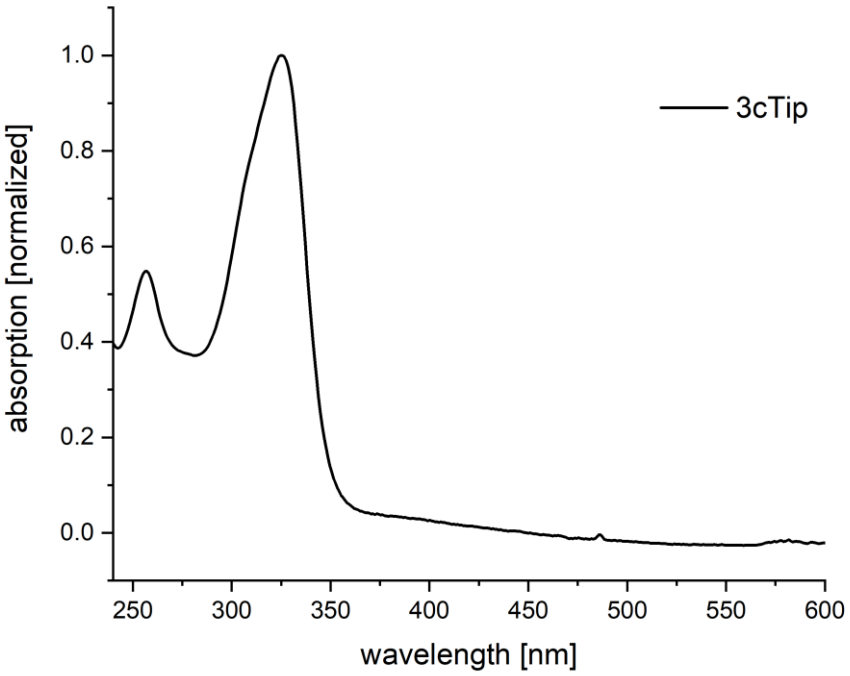

Figure 5.5.32. UV-Vis spectrum of **3c^{Tip}** (in THF).

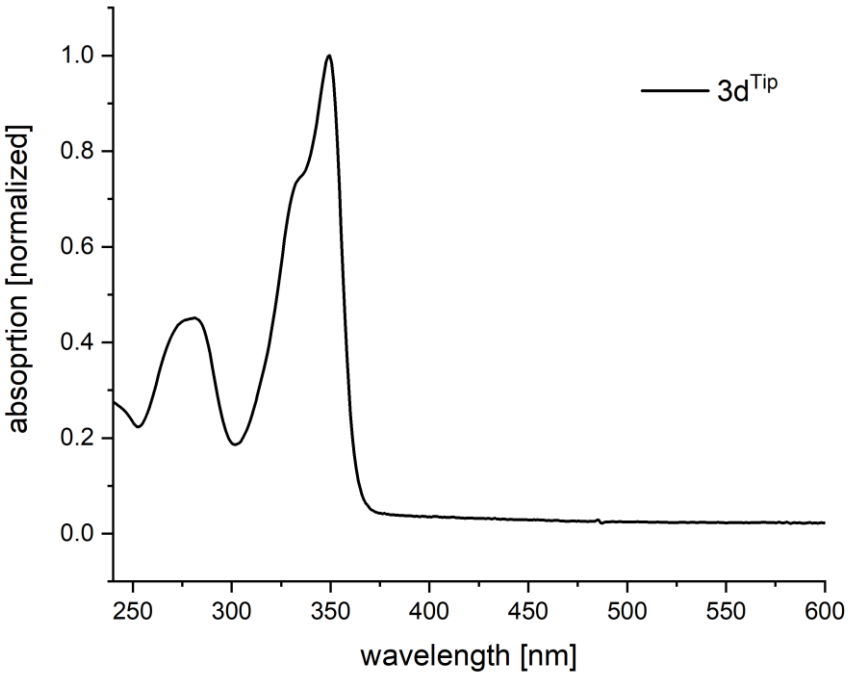

Figure 5.5.33. UV-Vis spectrum of **3d^{Tip}** (in THF).

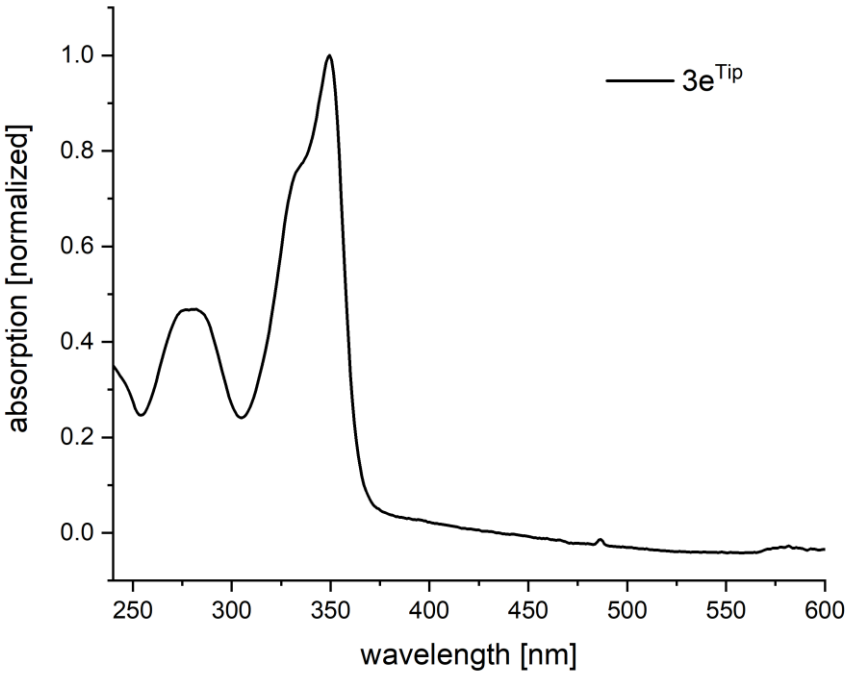

Figure 5.5.34. UV-Vis spectrum of **3e^{Tip}** (in THF).

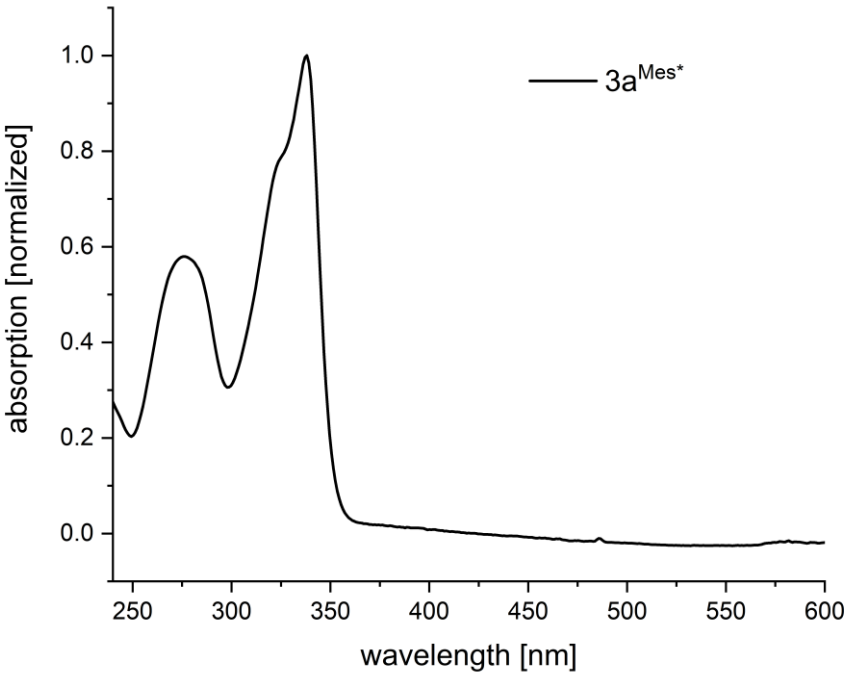

Figure 5.5.35. UV-Vis spectrum of **3a^{Mes*}** (in THF).

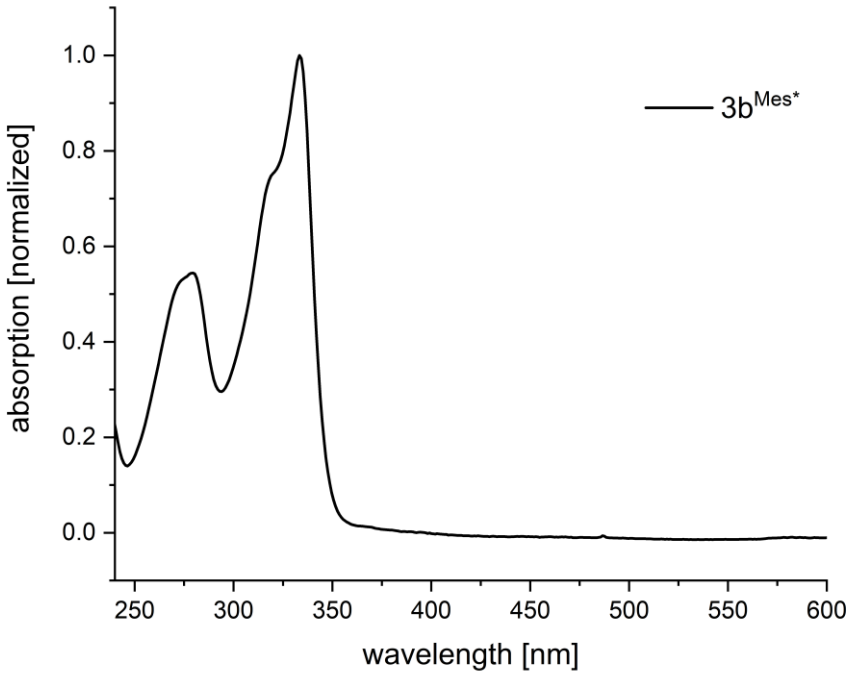

Figure 5.5.36. UV-Vis spectrum of **3b^{Mes*}** (in THF).

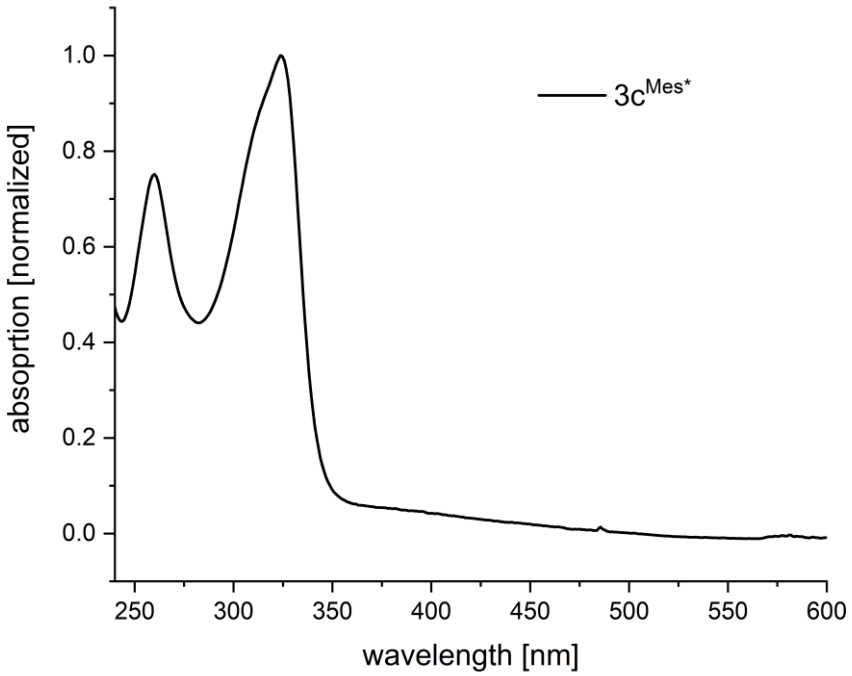

Figure 5.5.37. UV-Vis spectrum of **3c^{Mes*}** (in THF).

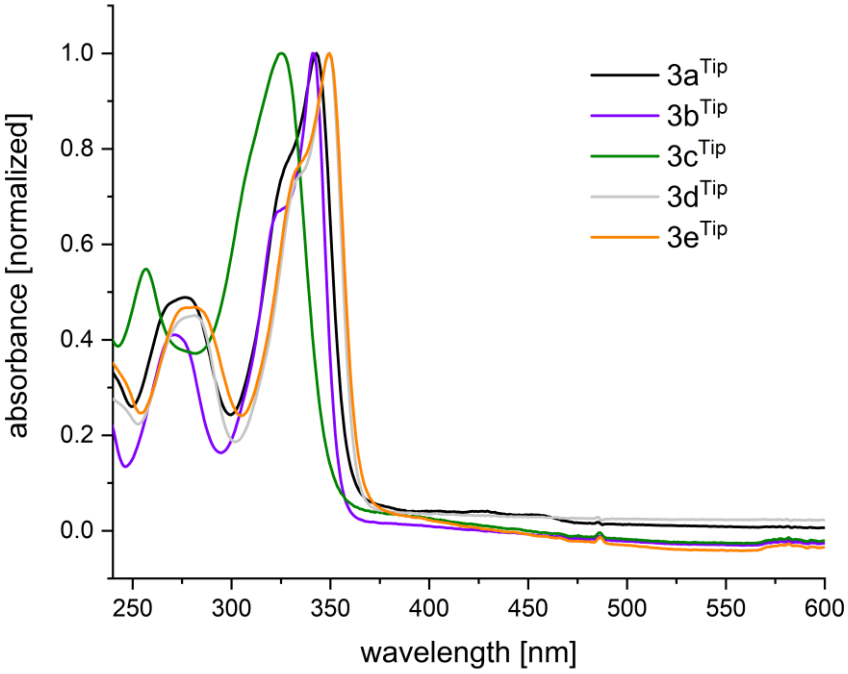

Figure 5.5.38. Overlay of UV-Vis spectra of **3a-e^{Tip}** (in THF).

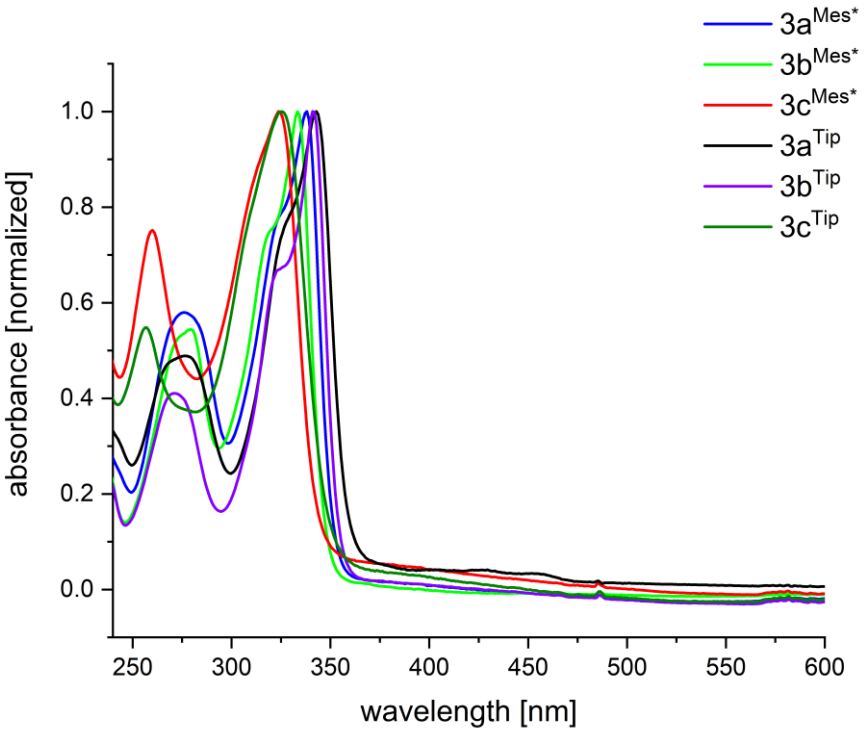

Figure 5.5.39. Overlay of UV-Vis spectra of **3a-c^{Tip}** and **3a-c^{Mes*}** (in THF).

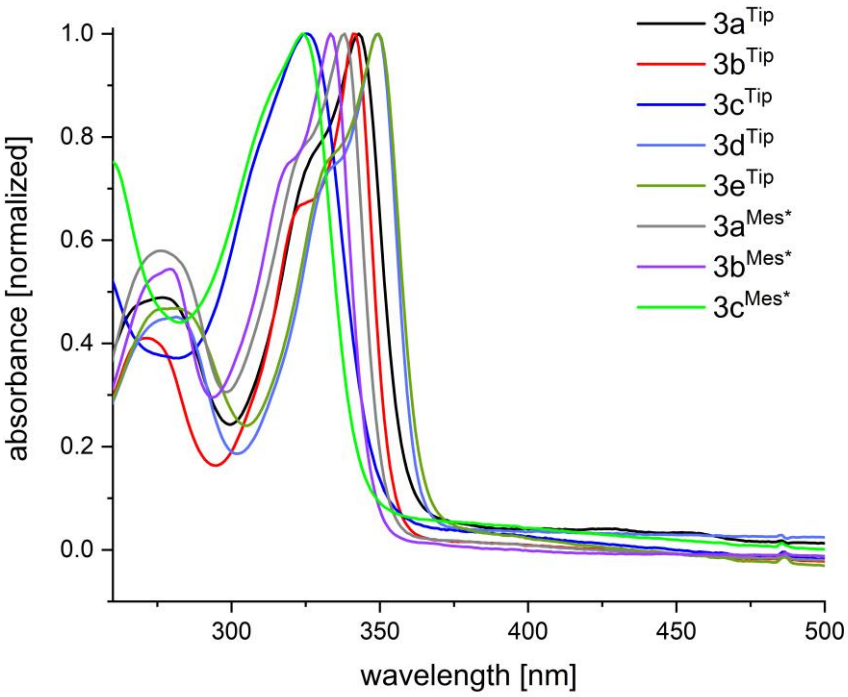

Figure 5.5.40. Overlay of UV-Vis spectra of **3a-e^{Tip}** and **3a-c^{Mes*}** (in THF).

Mass spectra

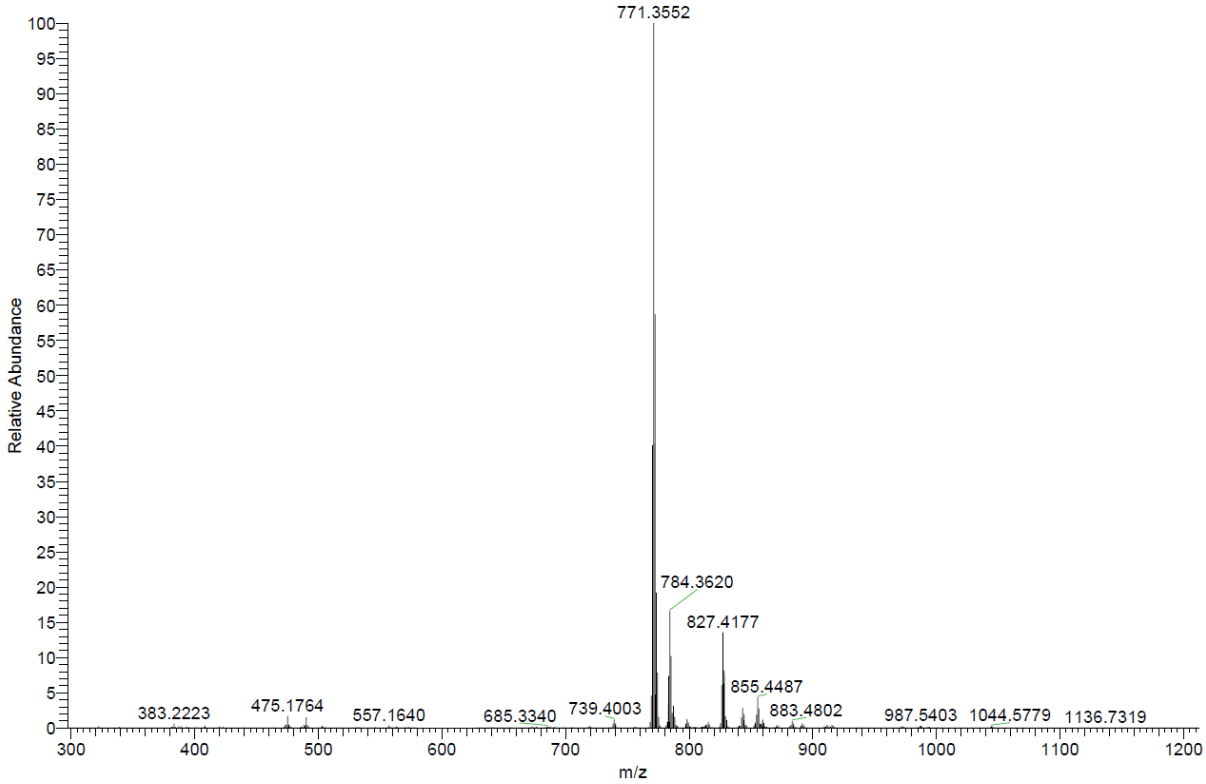

Figure 5.5.41. APCI mass spectrum of **3a**^{Tip}.

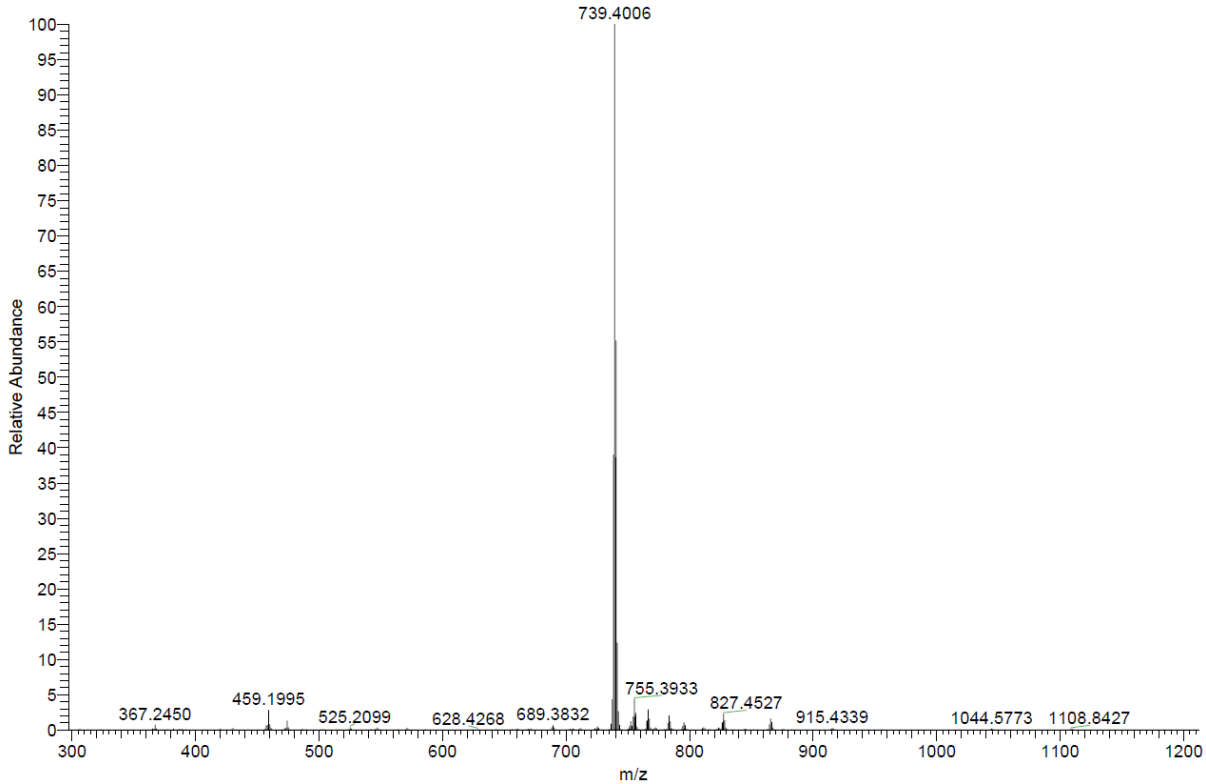

Figure 5.5.42. APCI mass spectrum of **3b**^{Tip}.

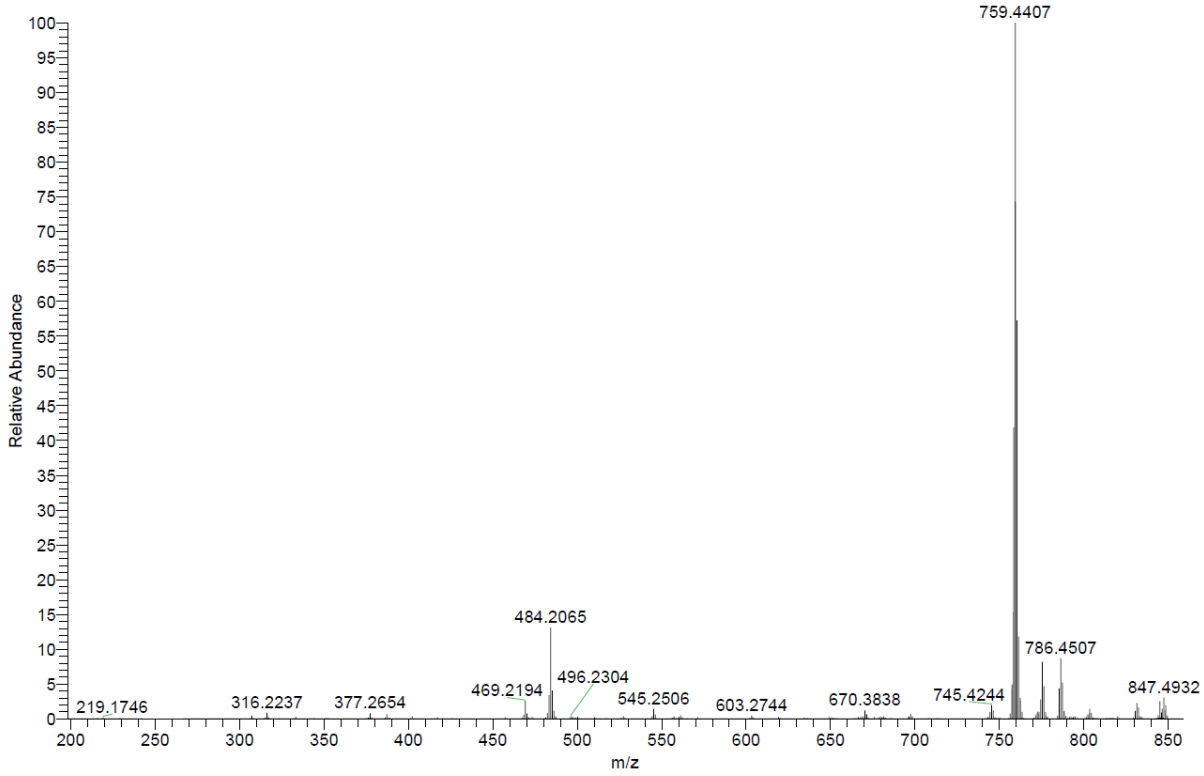

Figure 5.5.43. APCI mass spectrum of **3c**^{Tip}.

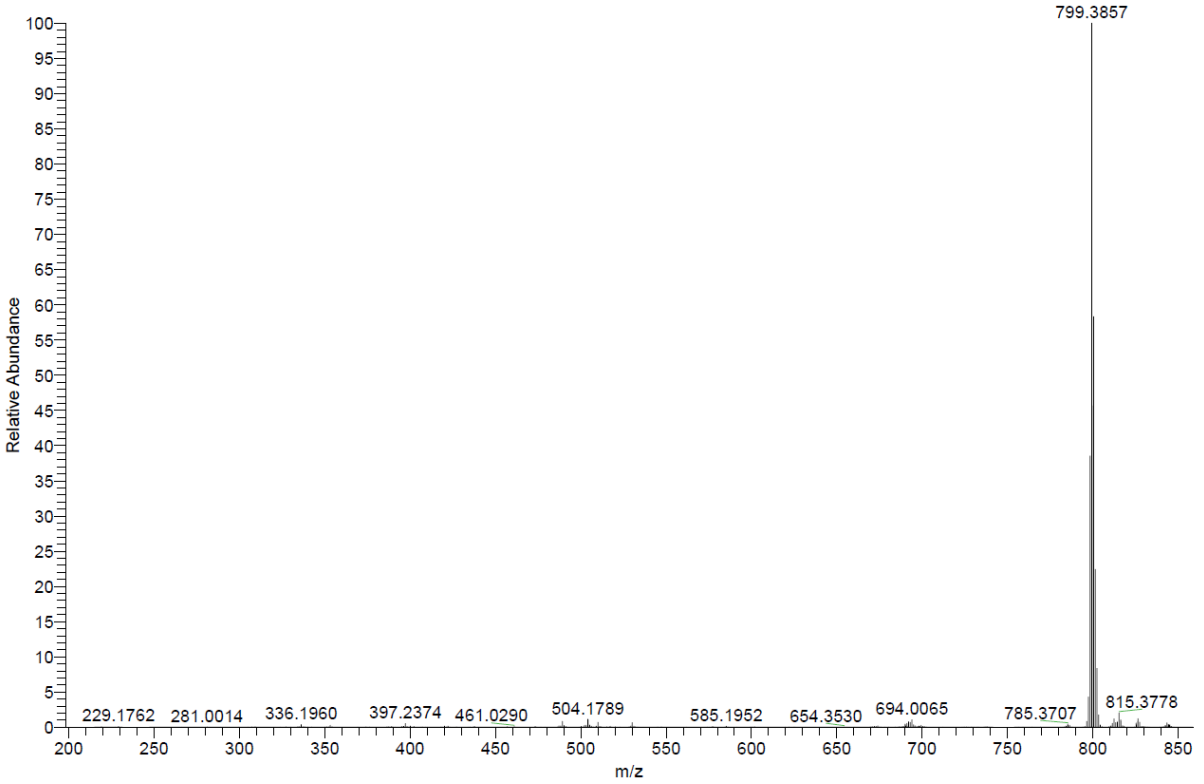

Figure 5.5.44. APCI mass spectrum of **3d**^{Tip}.

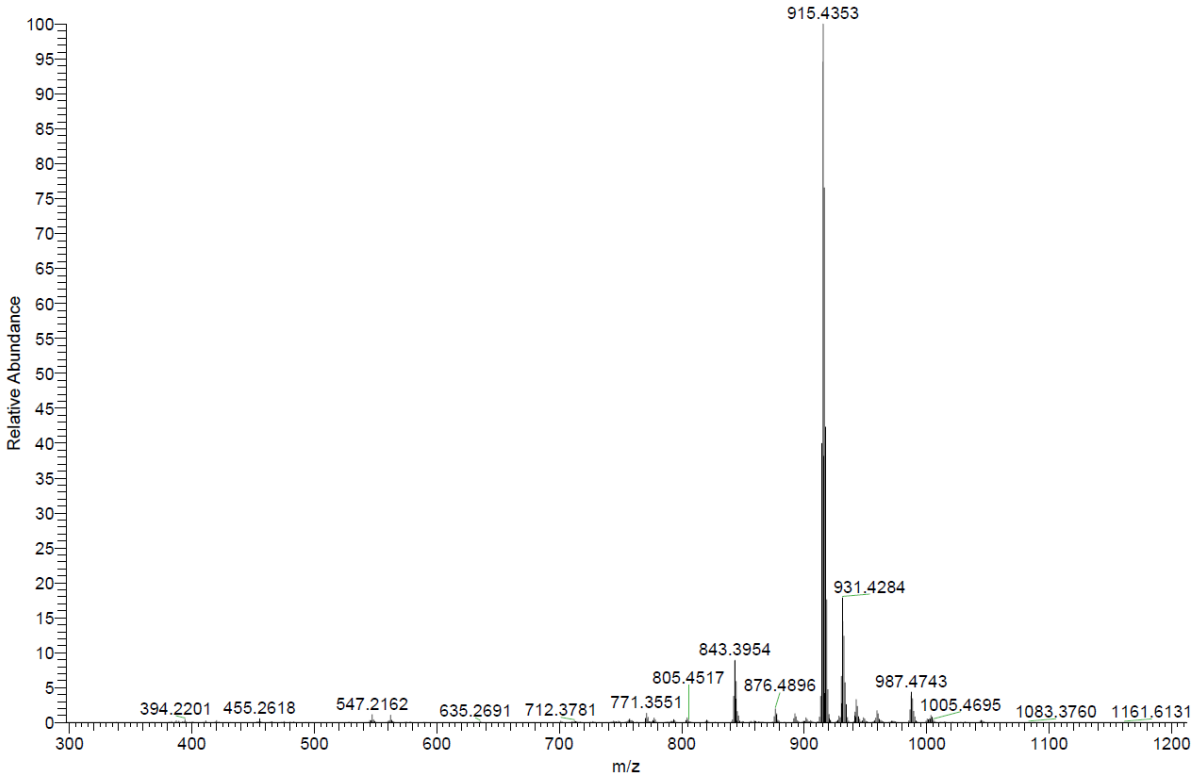

Figure 5.5.45. APCI mass spectrum of **3e^{Tip}**.

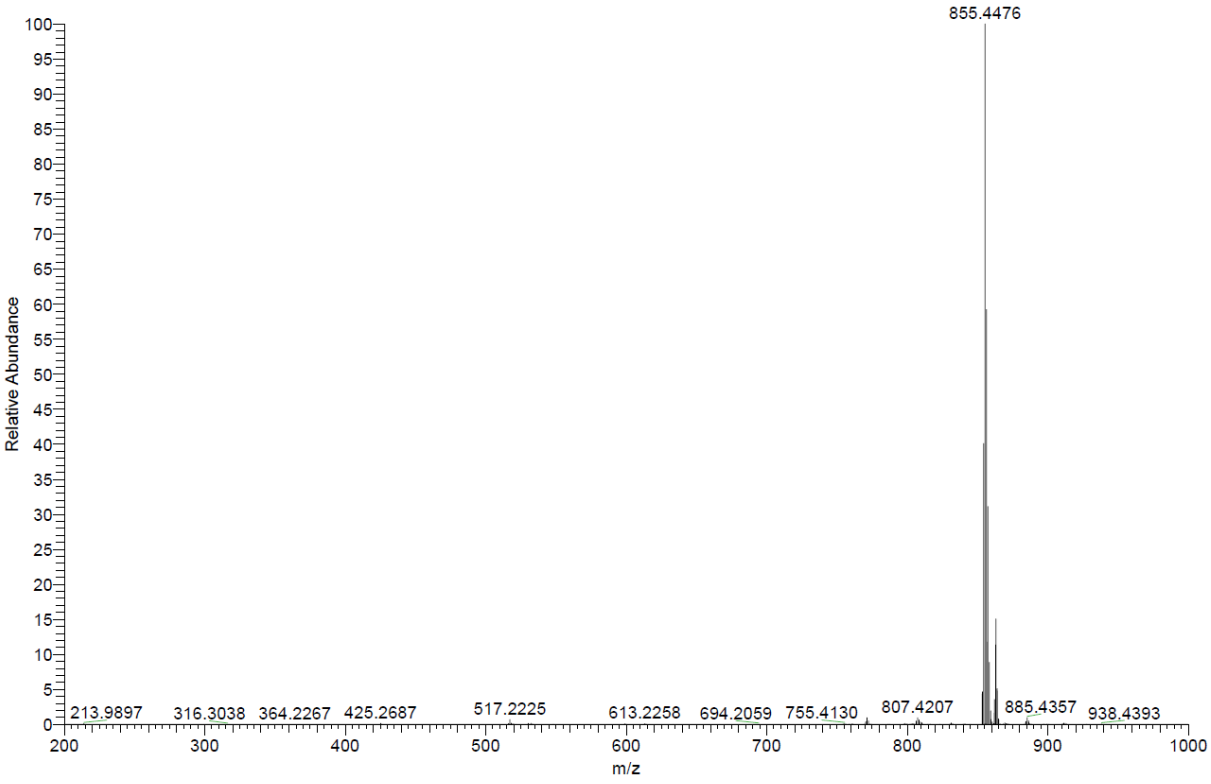

Figure 5.5.46. APCI mass spectrum of **3a^{Mes*}**.

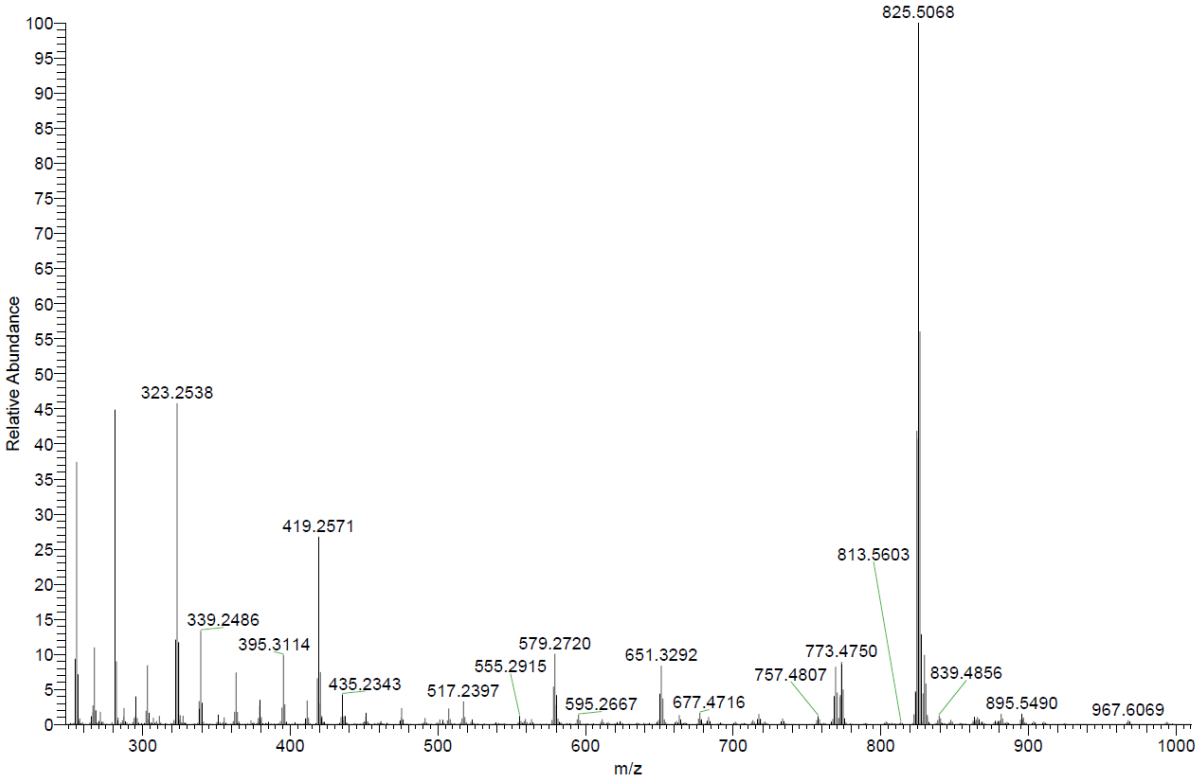

Figure 5.5.47. APCI mass spectrum of **3b**$^{\mathbf{Mes*}}$.

Cyclic Voltammetry

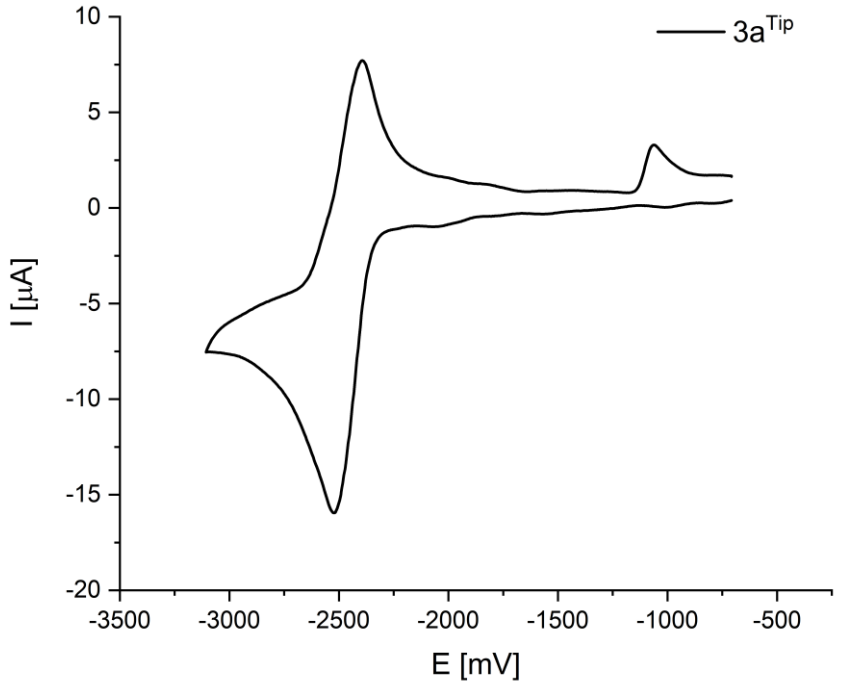

Figure 5.5.48. Cyclic voltammogram of **3a^{Tip}** (in THF).

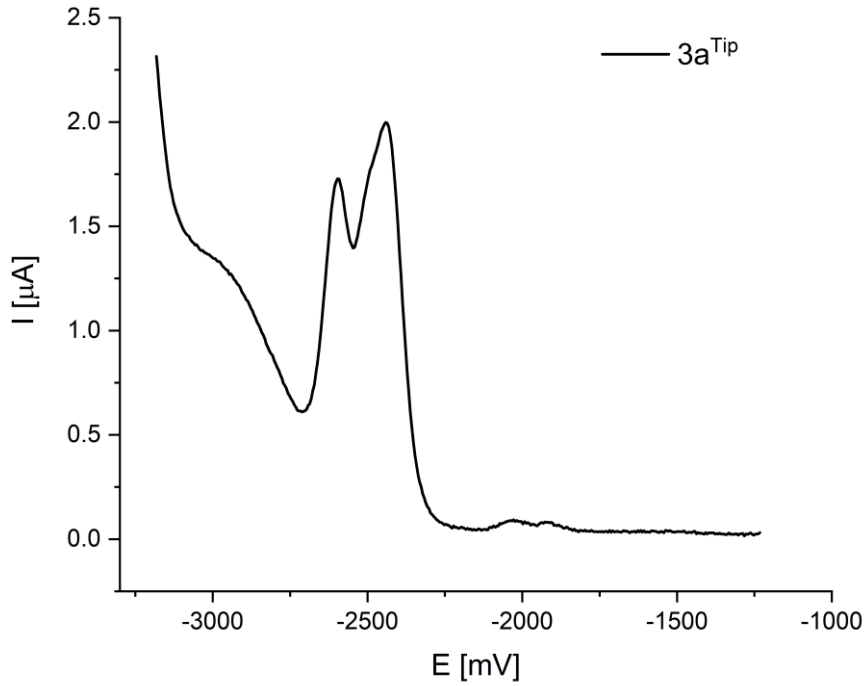

Figure 5.5.49. Differential pulse voltammogram of **3a^{Tip}** (in THF).

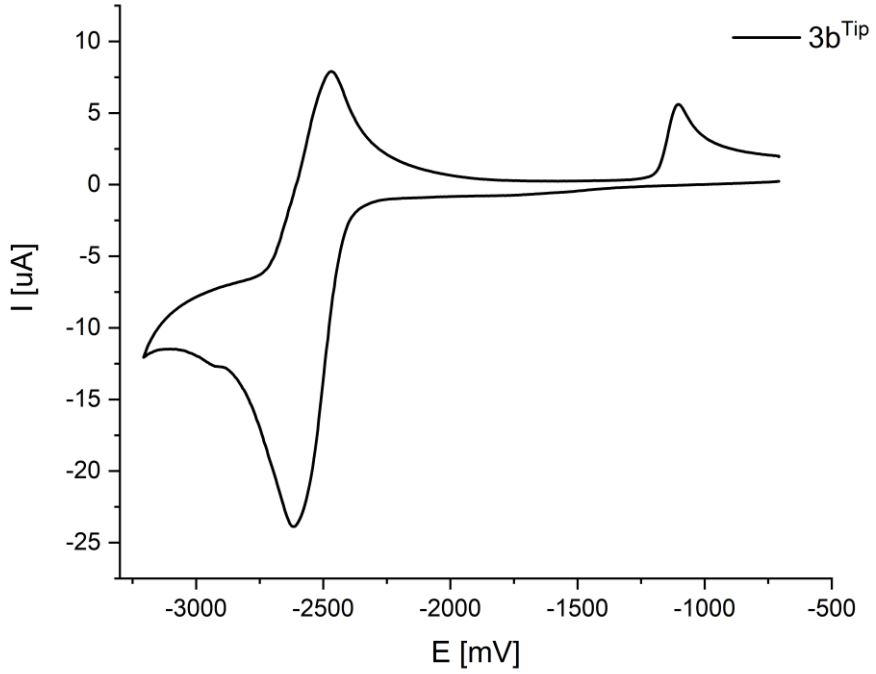

Figure 5.5.50. Cyclic voltammogram of **3b^{Tip}** (in THF).

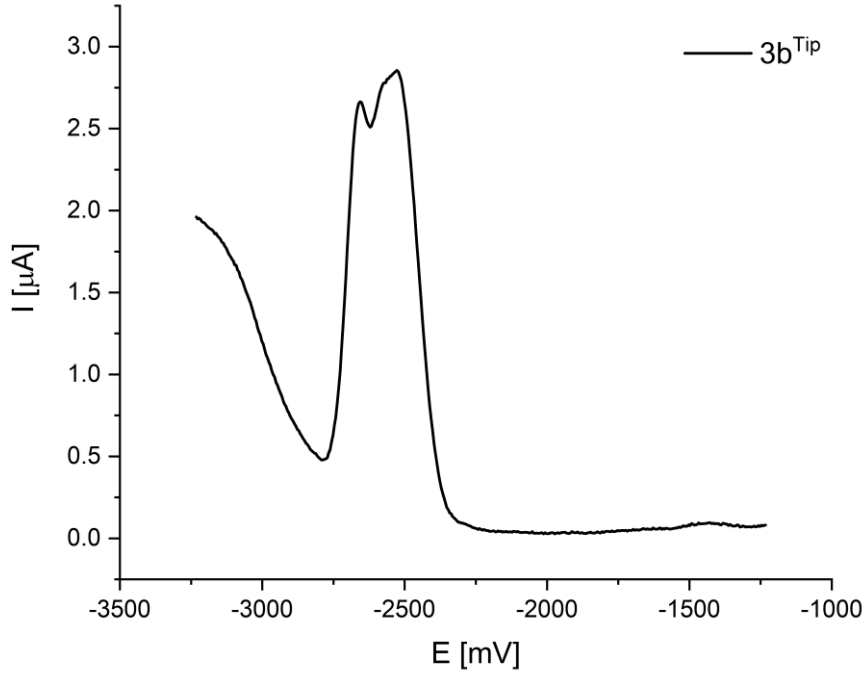

Figure 5.5.51. Differential pulse voltammogram of **3b^{Tip}** (in THF).

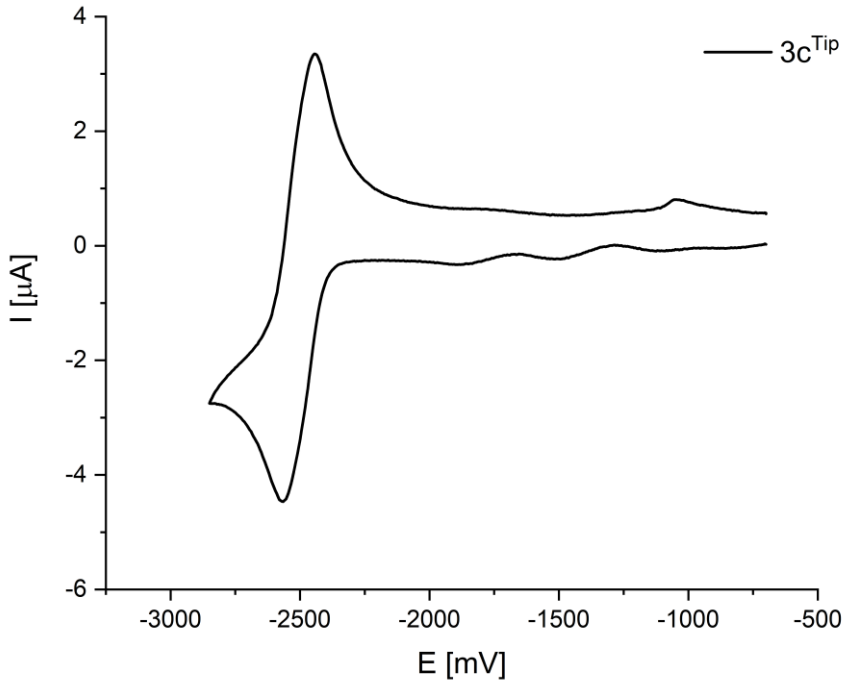

Figure 5.5.52. Cyclic voltammogram of **3c^{Tip}** (in THF).

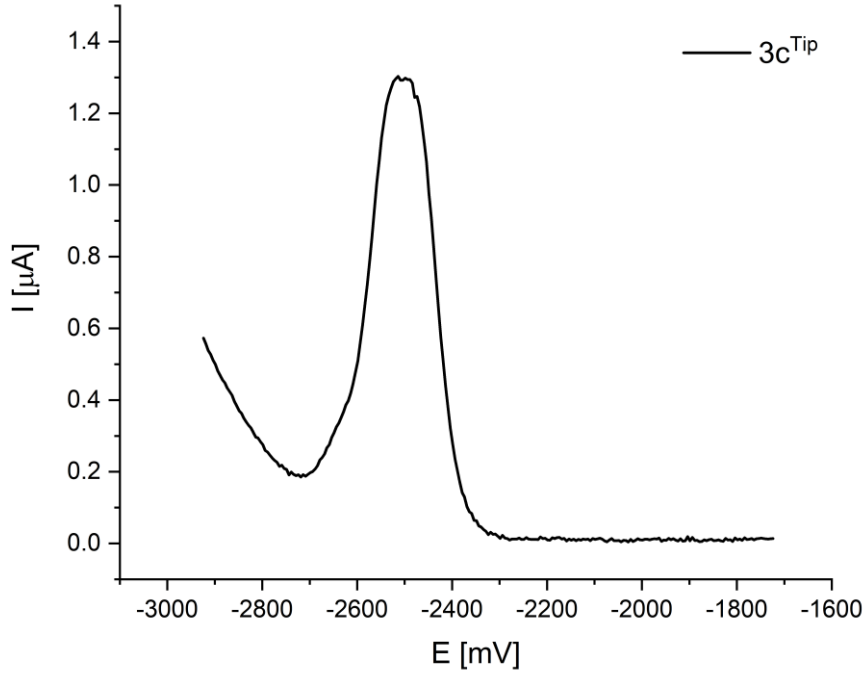

Figure 5.5.53. Differential pulse voltammogram of **3c^{Tip}** (in THF).

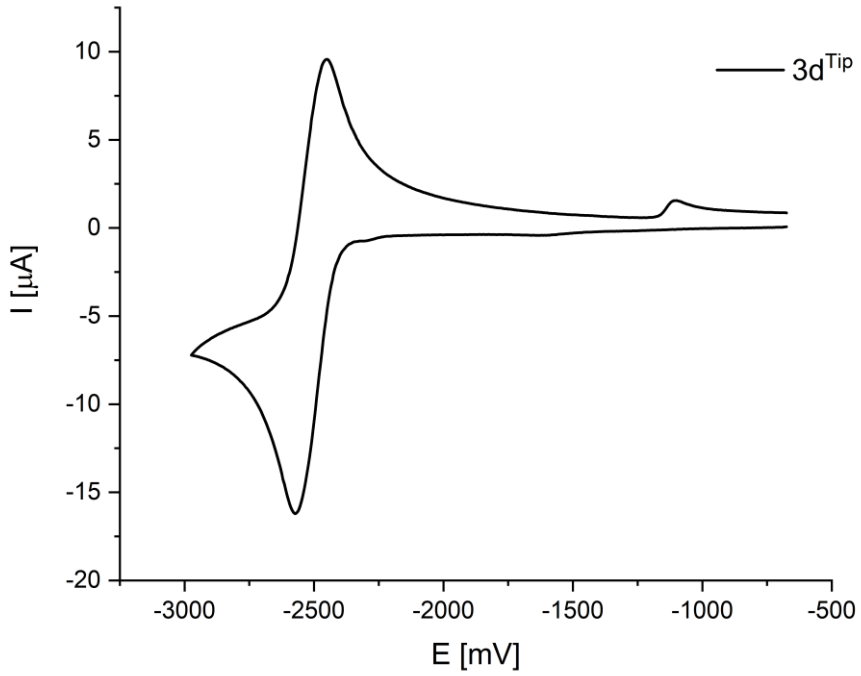

Figure 5.5.54. Cyclic voltammogram of **3d^{Tip}** (in THF).

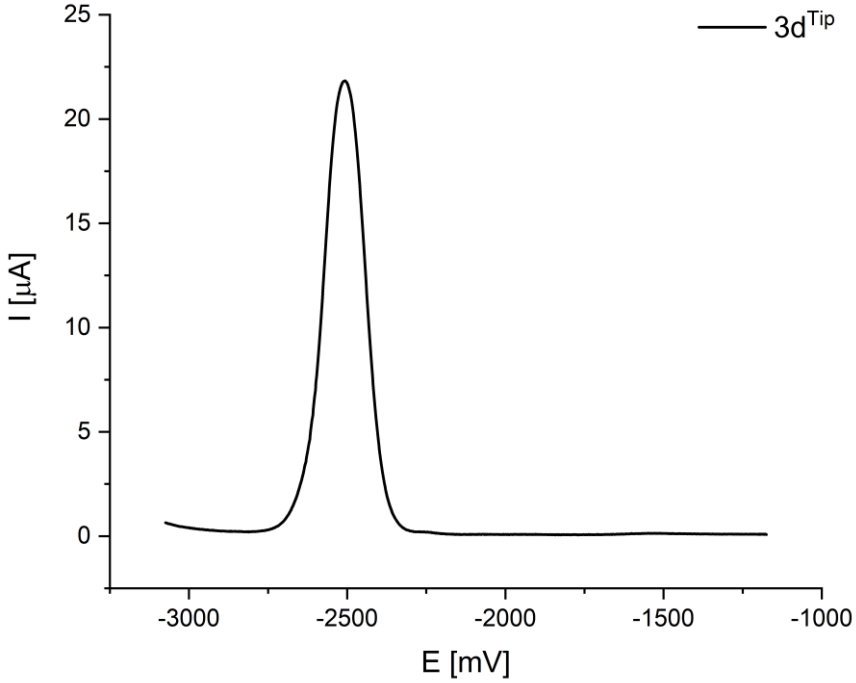

Figure 5.5.55. Square wave voltammogram of **3d^{Tip}** (in THF).

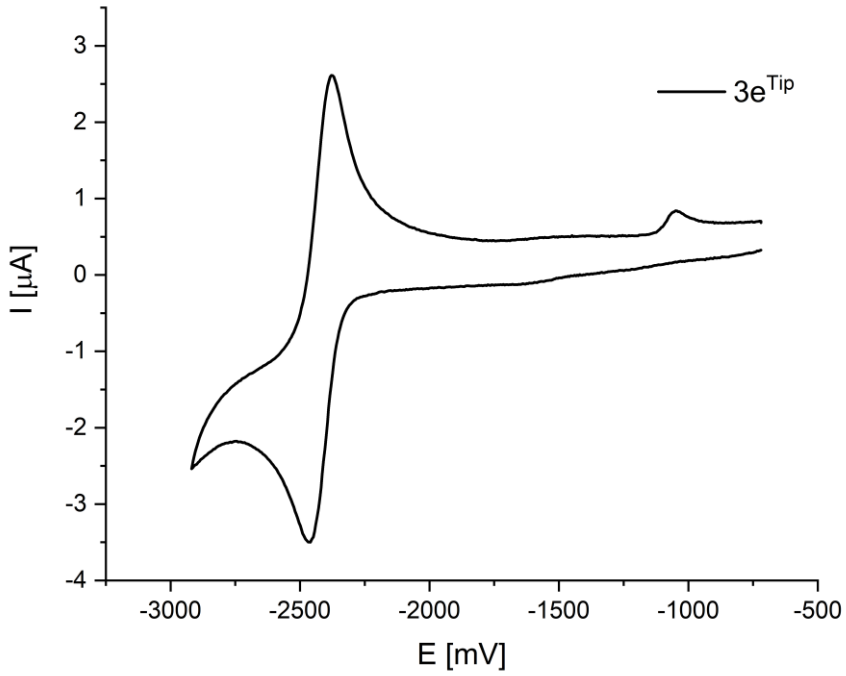

Figure 5.5.56. Cyclic voltammogram of **3e^{Tip}** (in THF).

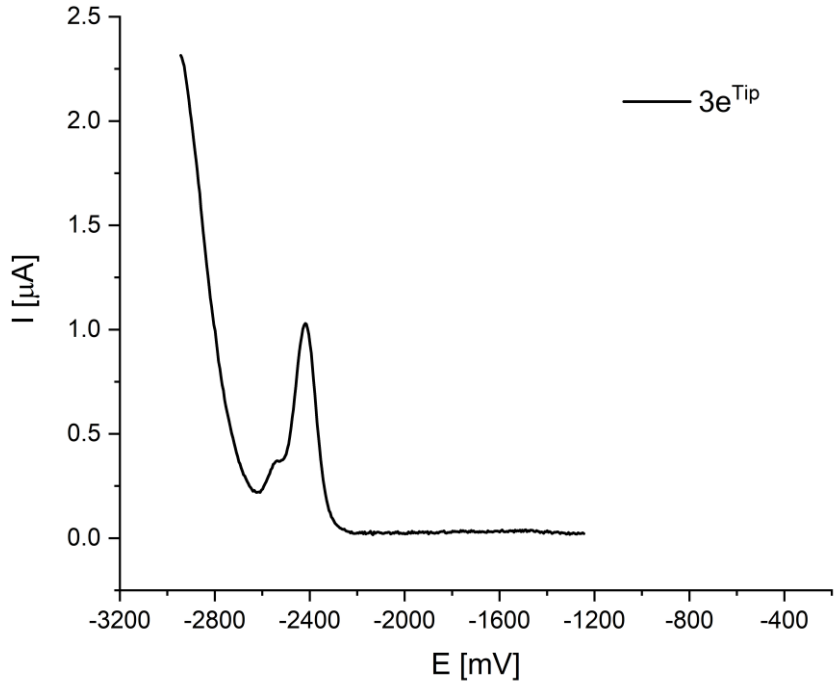

Figure 5.5.57. Differential pulse voltammogram of **3e^{Tip}** (in THF).

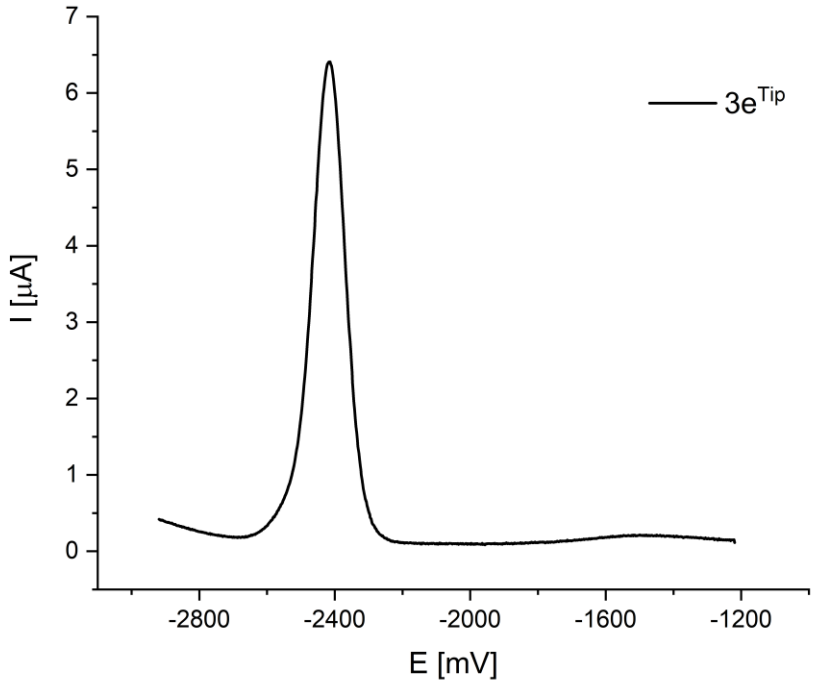

.

Figure 5.5.58. Square wave voltammogram of **3e^{Tip}** (in THF).

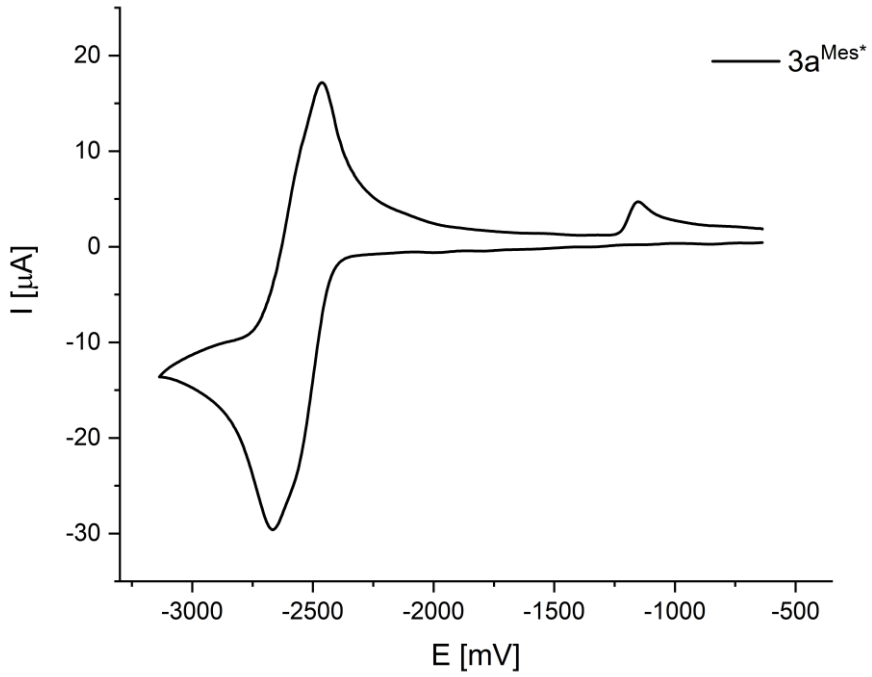

Figure 5.5.59. Cyclic voltammogram of **3a^{Mes*}** (in THF).

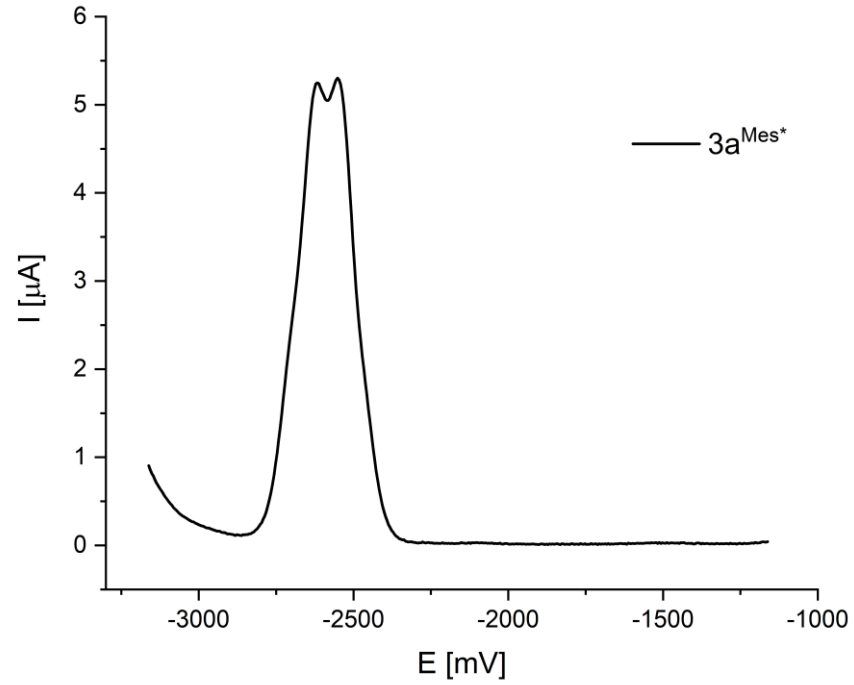

Figure 5.5.60. Differential pulse voltammogram of **3a^{Mes*}** (in THF).

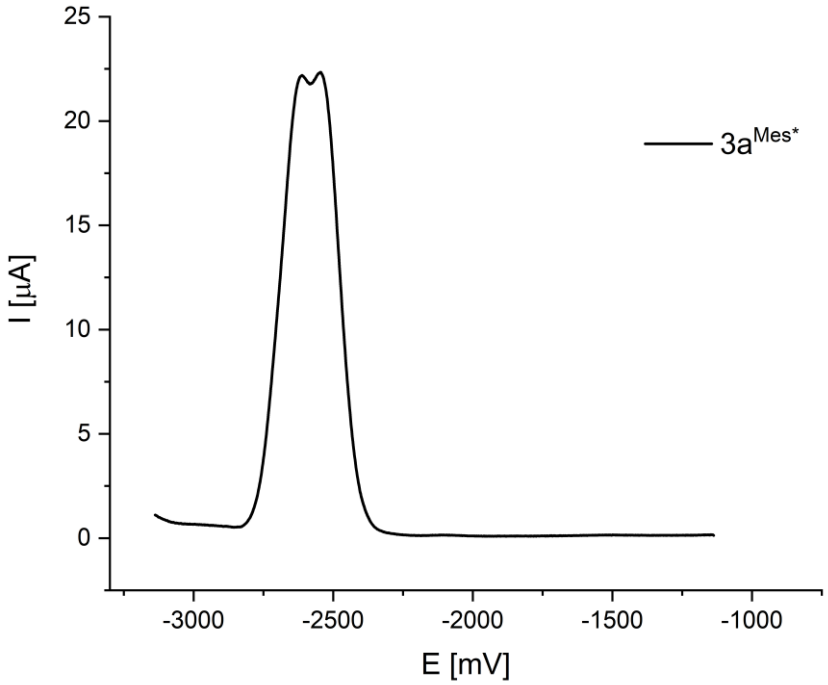

Figure 5.5.61. Square wave voltammogram of **3a^{Mes*}** (in THF).

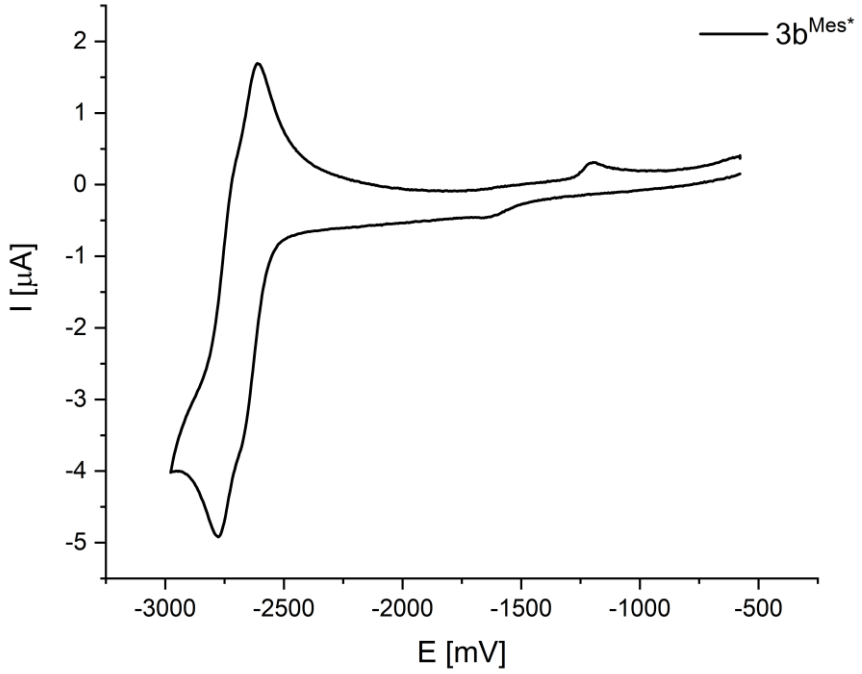

Figure 5.5.62. Cyclic voltammogram of **3b^{Mes*}** (in THF).

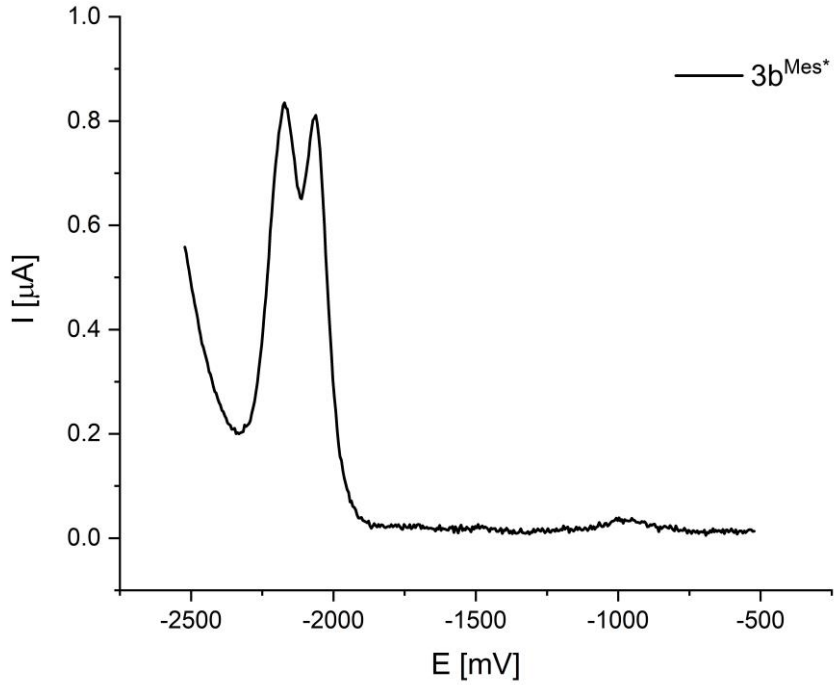

Figure 5.5.63. Differential pulse voltammogram of **3b^{Mes*}** (in THF).

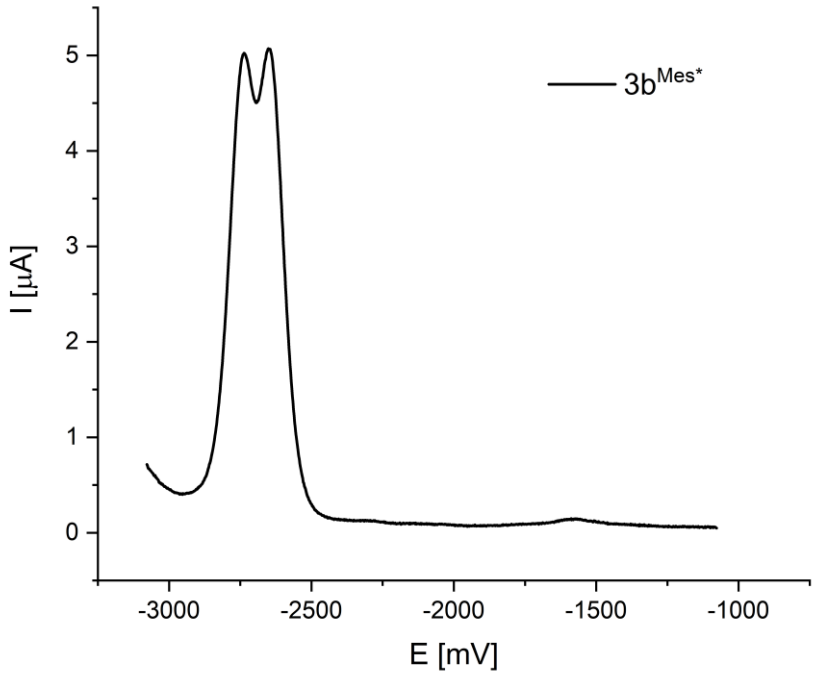

Figure 5.5.64. Square wave voltammogram of **3b^{Mes*}** (in THF).

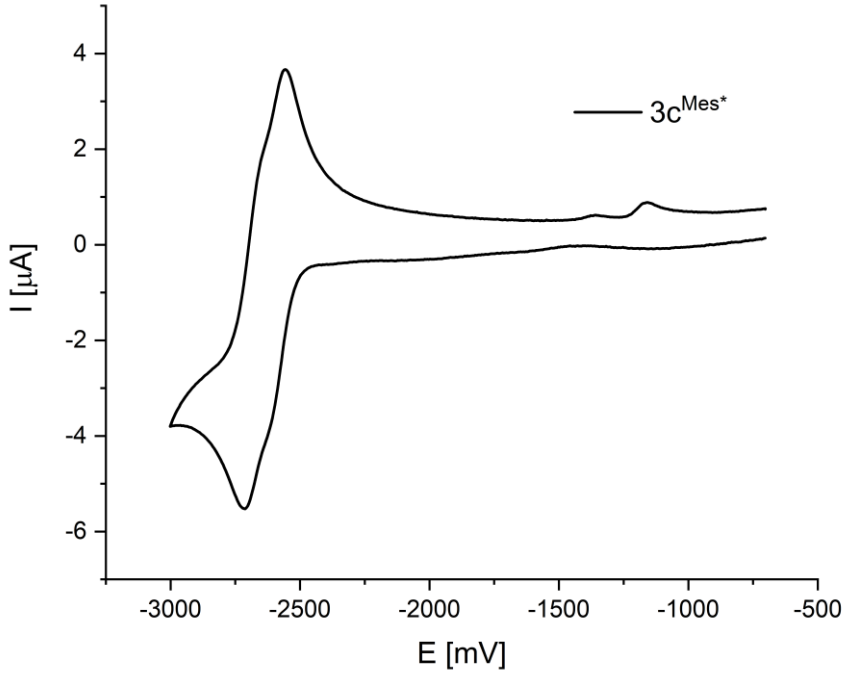

Figure 5.5.65. Cyclic voltammogram of **3c^{Mes*}** (in THF).

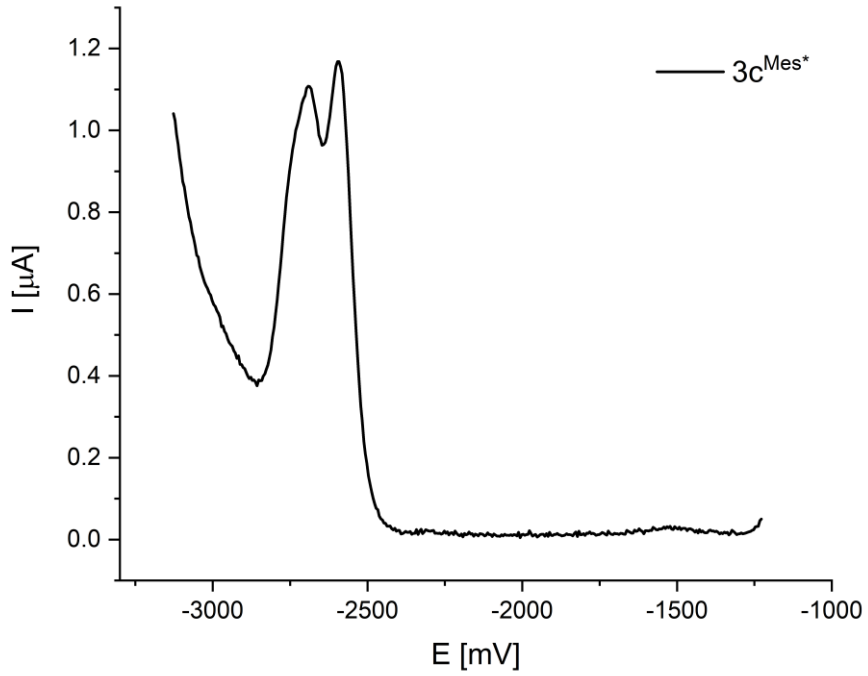

Figure 5.5.66. Differential pulse voltammogram of **3c^{Mes*}** (in THF).

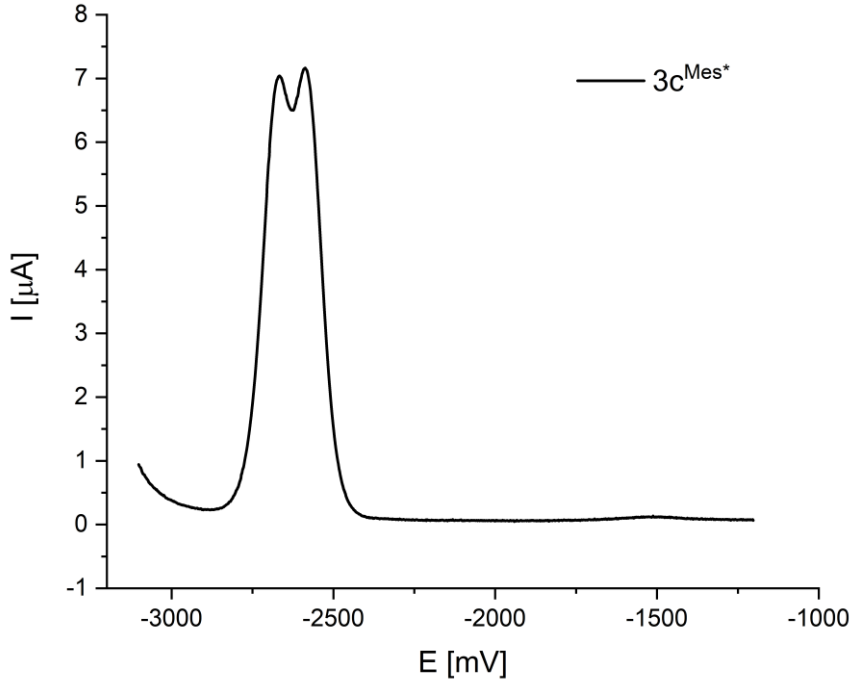

Figure 5.5.67. Square wave voltammogram of **3c^{Mes*}**(in THF).

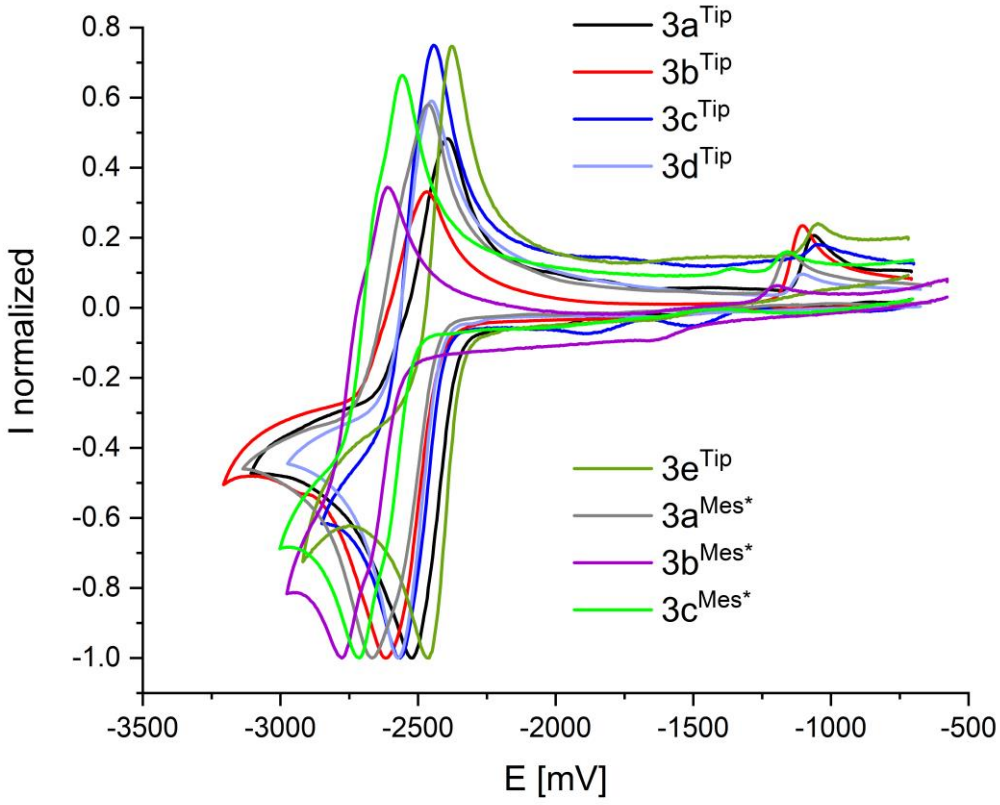

Figure 5.5.68. Overlay of cyclic voltammograms of **3a-e^{Tip}** and **3a-c^{Mes*}**(in THF).

5.6 Catalytic Silicon/Boron Exchange Involving Aryldichloroboranes

NMR-spectra

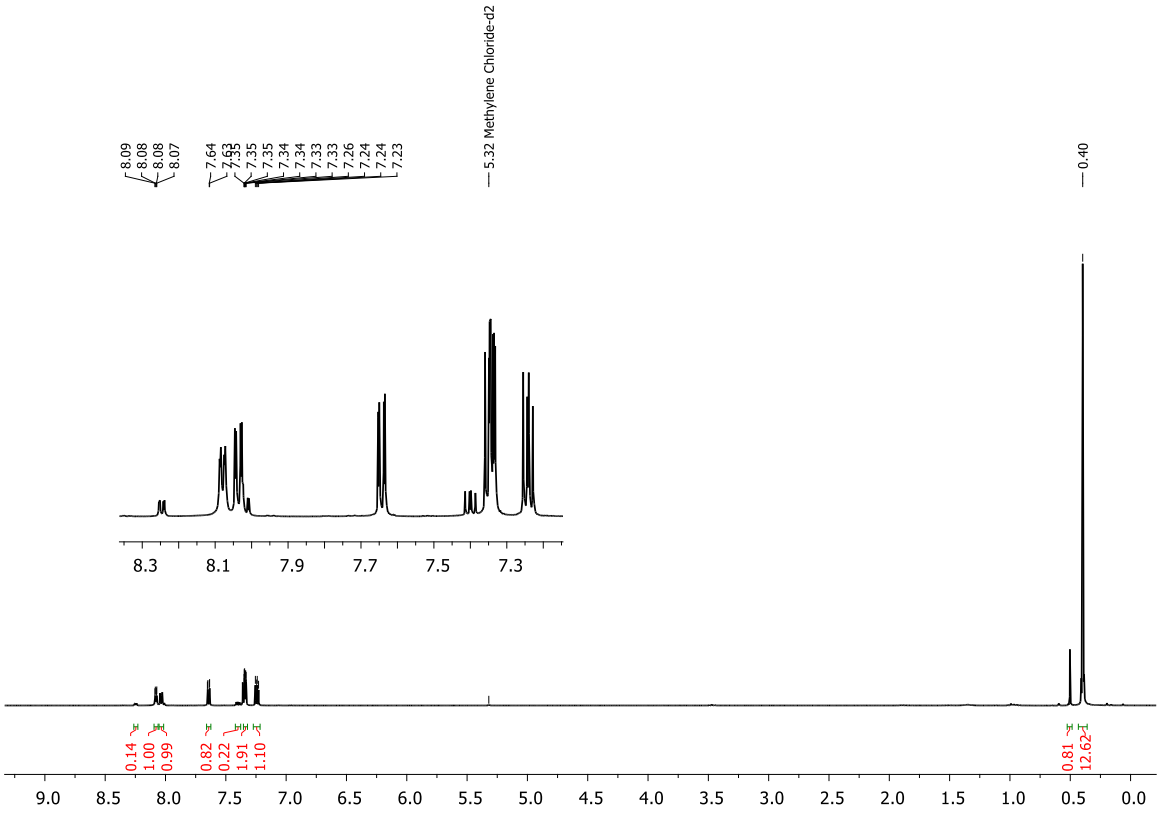

Figure 5.6.1. ^{1}H NMR spectrum of a mixture of **1a** and **12a** in the absence of a catalyst after 13 d (CD_2Cl_2, 300 MHz).

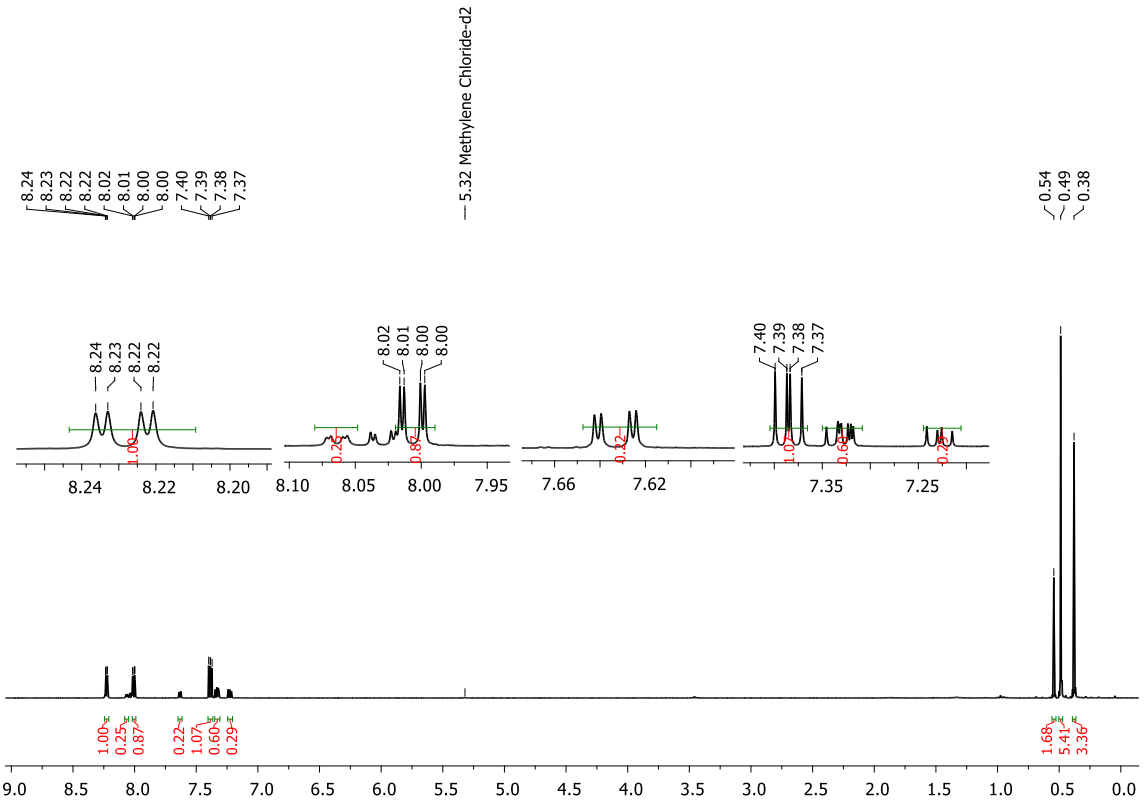

Figure 5.6.2. ^{1}H NMR spectrum of a mixture of **1a** and **12a** in the presence of catalyst **A** after 8 d (CD_2Cl_2, 300 MHz).

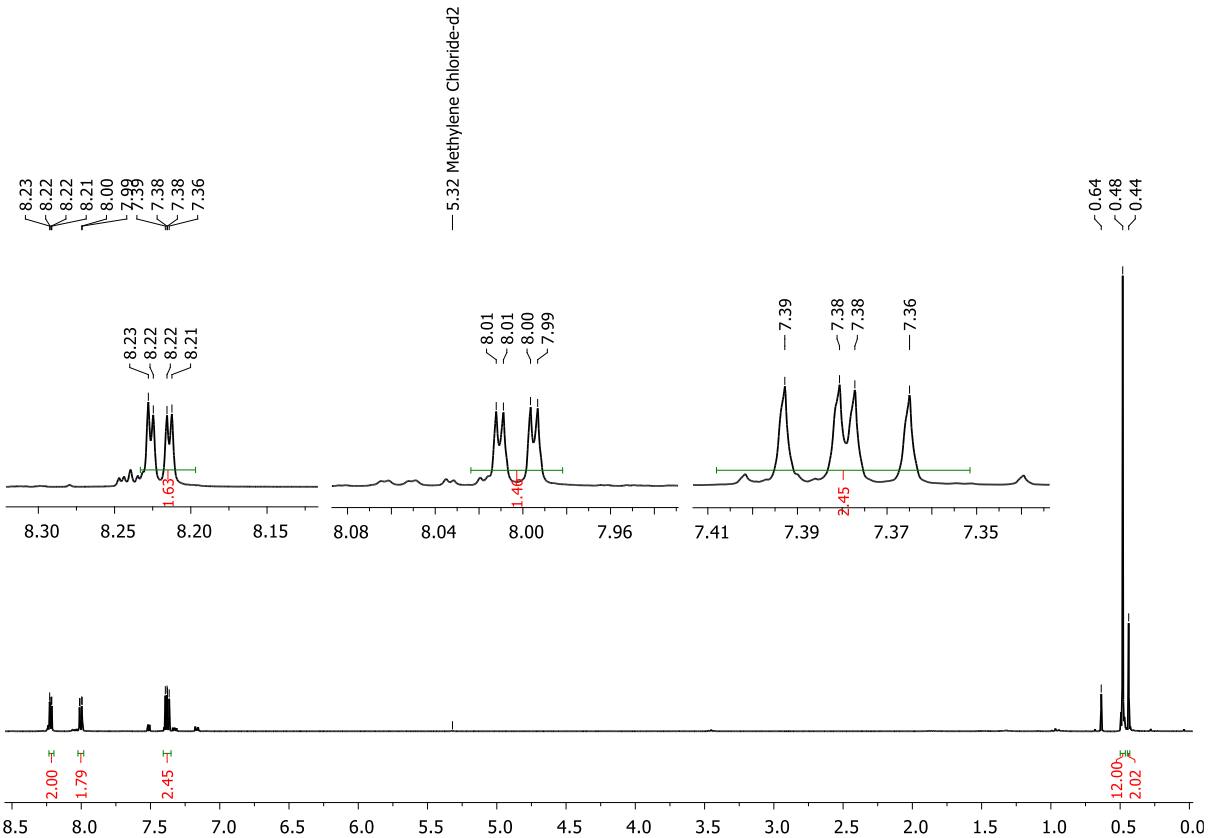

Figure 5.6.3. ^{1}H NMR spectrum of a mixture of **1a** and **12a** in the presence of catalyst **B** after 2 d (CD_2Cl_2, 300 MHz).

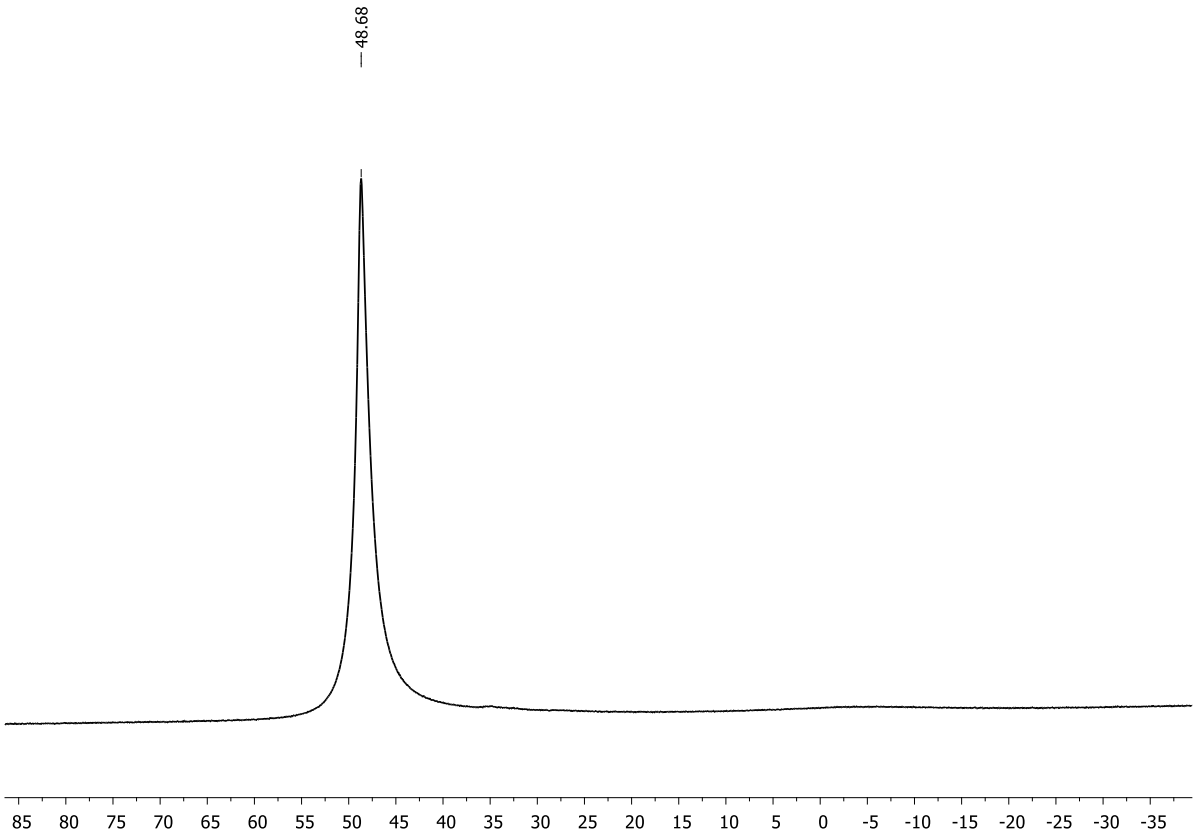

Figure 5.6.4. $^{11}B\{^{1}H\}$ NMR spectrum of a mixture of **1a** and **12a** in the presence of catalyst **B** after 2 d (CD_2Cl_2, 96 MHz).

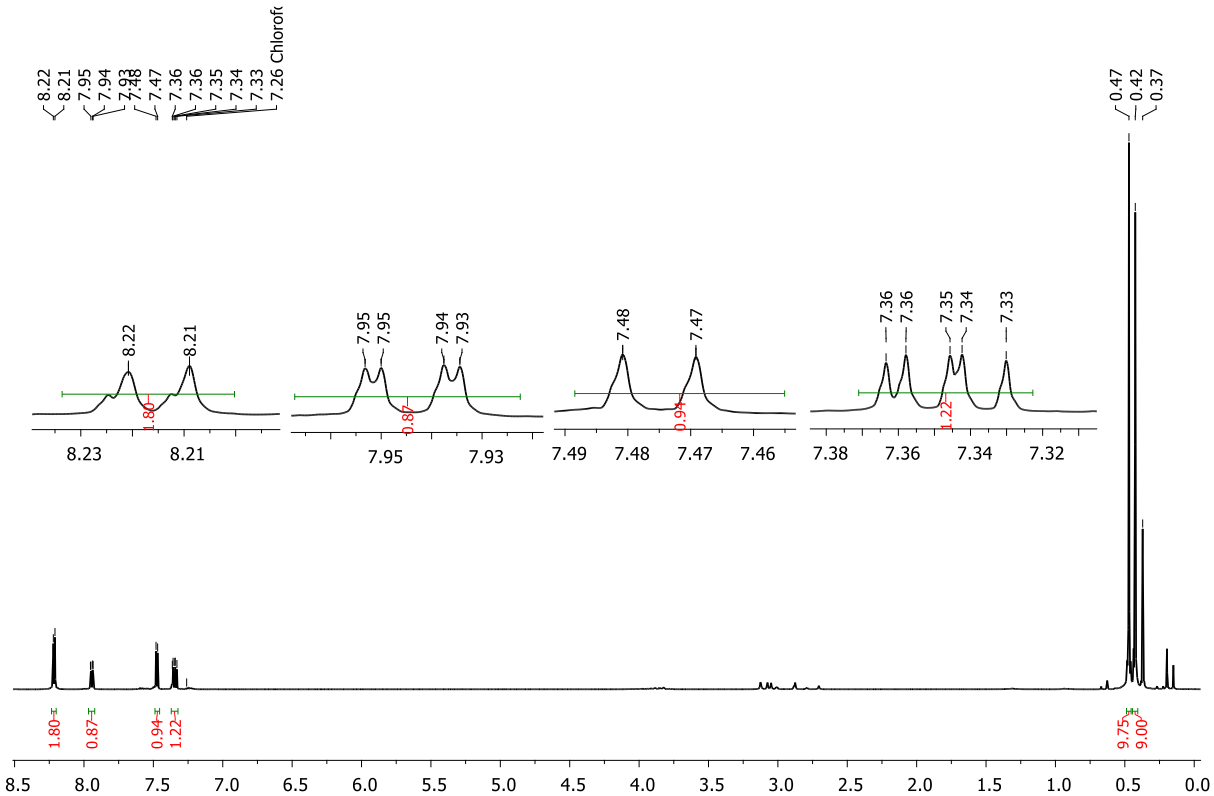

Figure 5.6.5. ^{1}H NMR spectrum of a mixture of **5a** and **12a** in the presence of catalyst **B** after 24 h ($CDCl_3$, 300 MHz).

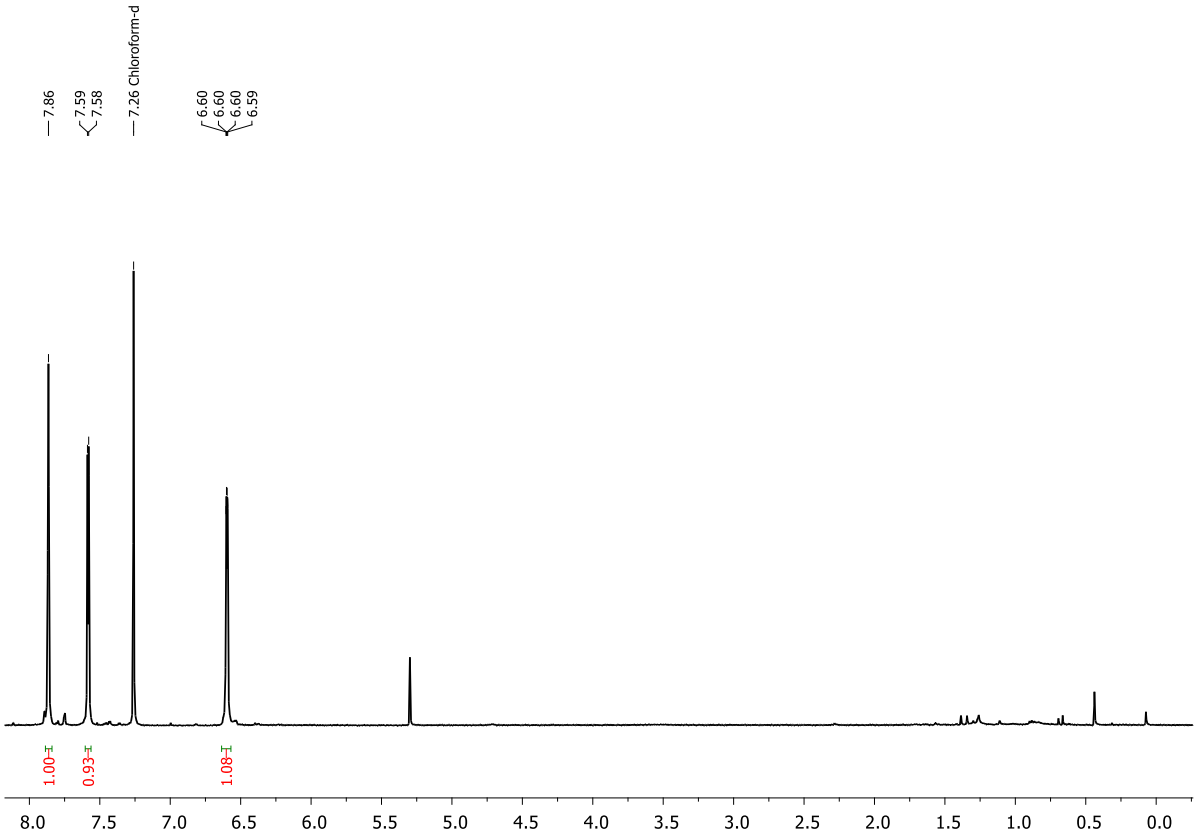

Figure 5.6.6. ^{1}H NMR spectrum of **12b** ($CDCl_3$, 300 MHz).

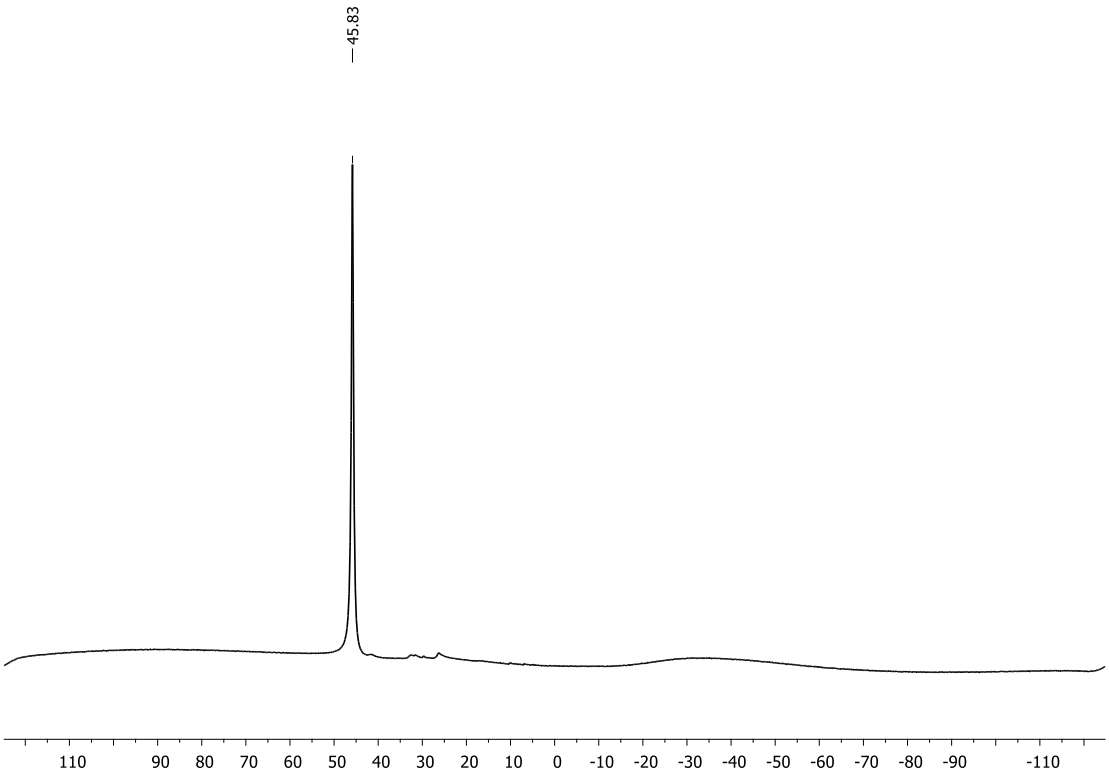

Figure 5.6.7. $^{11}B\{^{1}H\}$ NMR spectrum of **12b** ($CDCl_3$, 96 MHz).

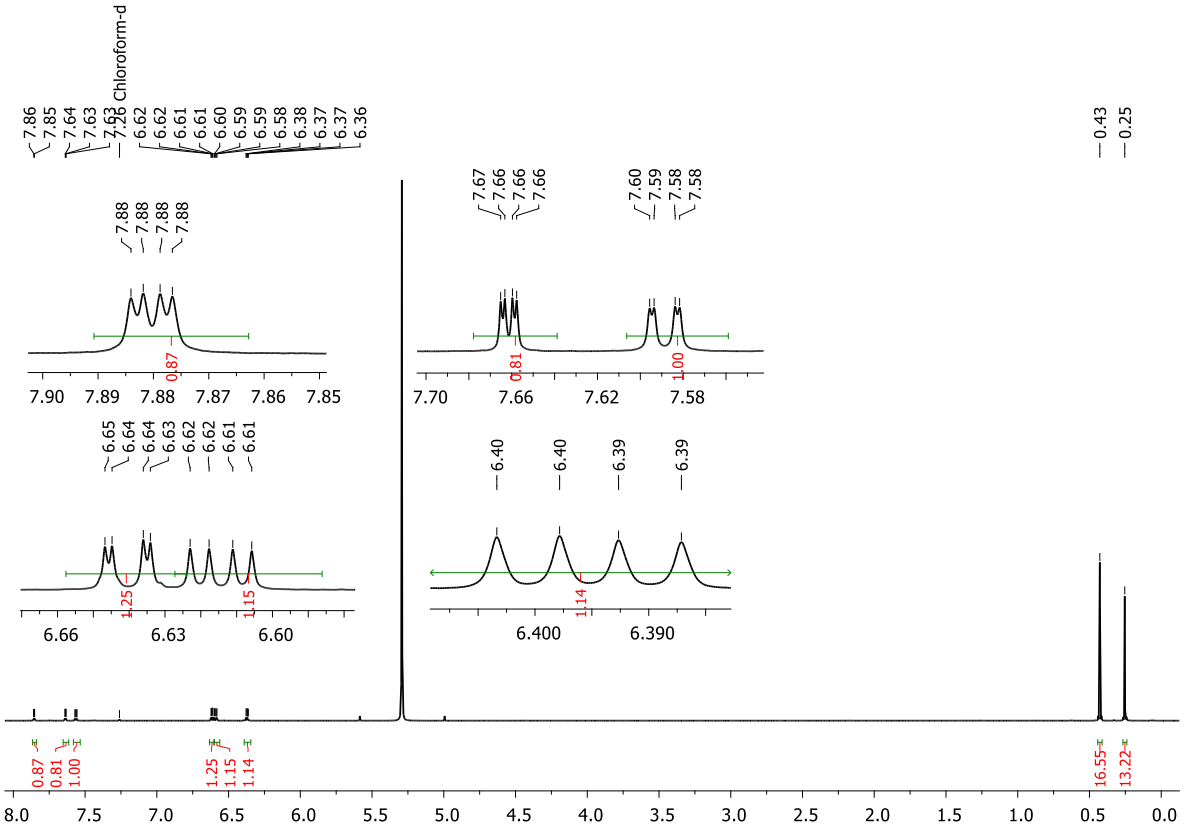

Figure 5.6.8. ^{1}H NMR spectrum of a mixture of **1b** and *in-situ* generated **12b** ($CDCl_3$, 300 MHz).

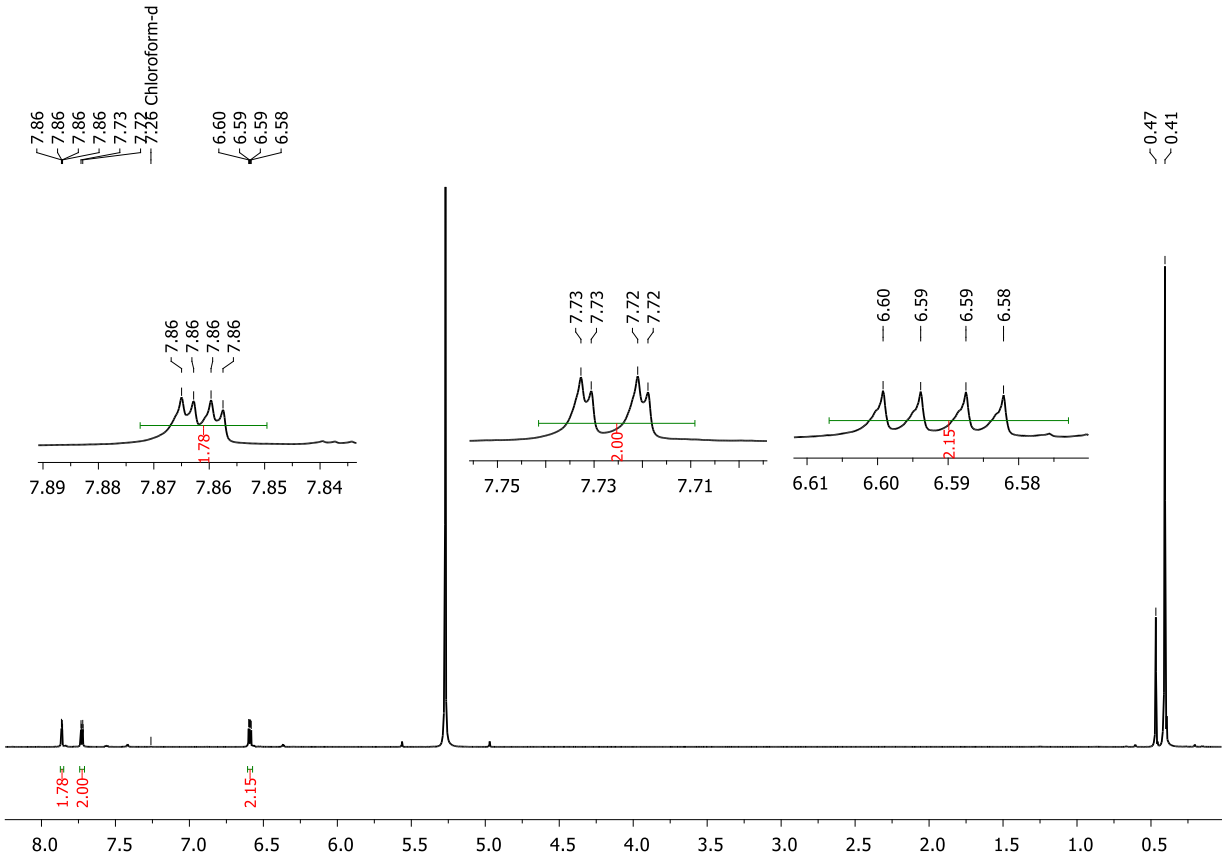

Figure 5.6.9. ^{1}H NMR spectrum of a mixture of **1b** and **12b** in the presence of catalyst **A** (20 mol%) after 48 h ($CDCl_3$, 300 MHz).

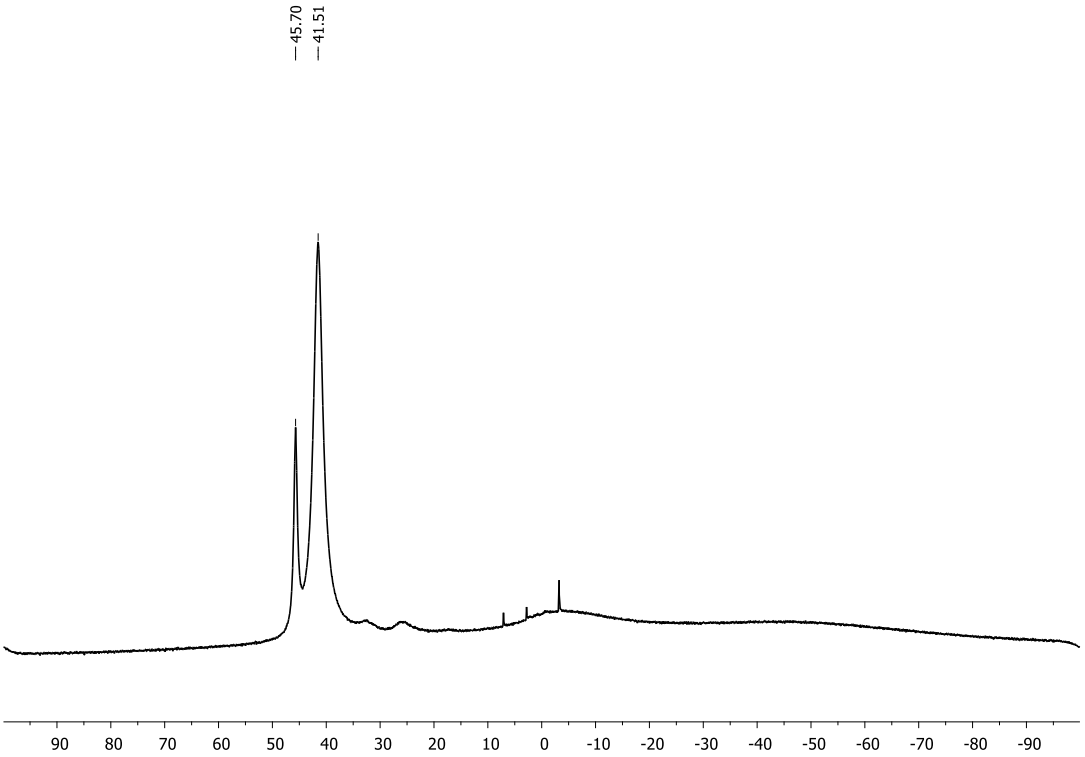

Figure 5.6.10. $^{11}B\{^{1}H\}$ NMR spectrum of a mixture of **1b** and **12b** in the presence of catalyst **A** (20 mol%) after 48 h ($CDCl_3$, 96 MHz).

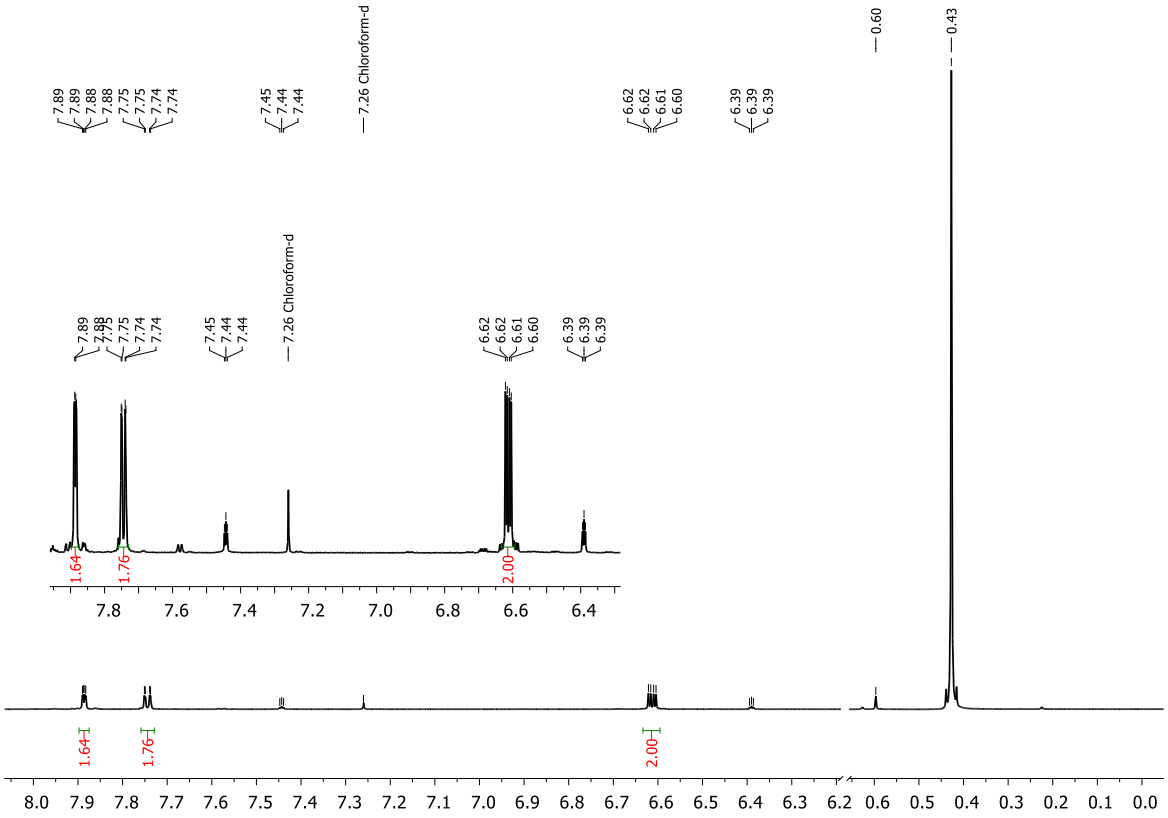

Figure 5.6.11. ^{1}H NMR spectrum of a mixture of **1b** and **12b** in the presence of catalyst **B** (10 mol%) after 19 h ($CDCl_3$, 300 MHz).

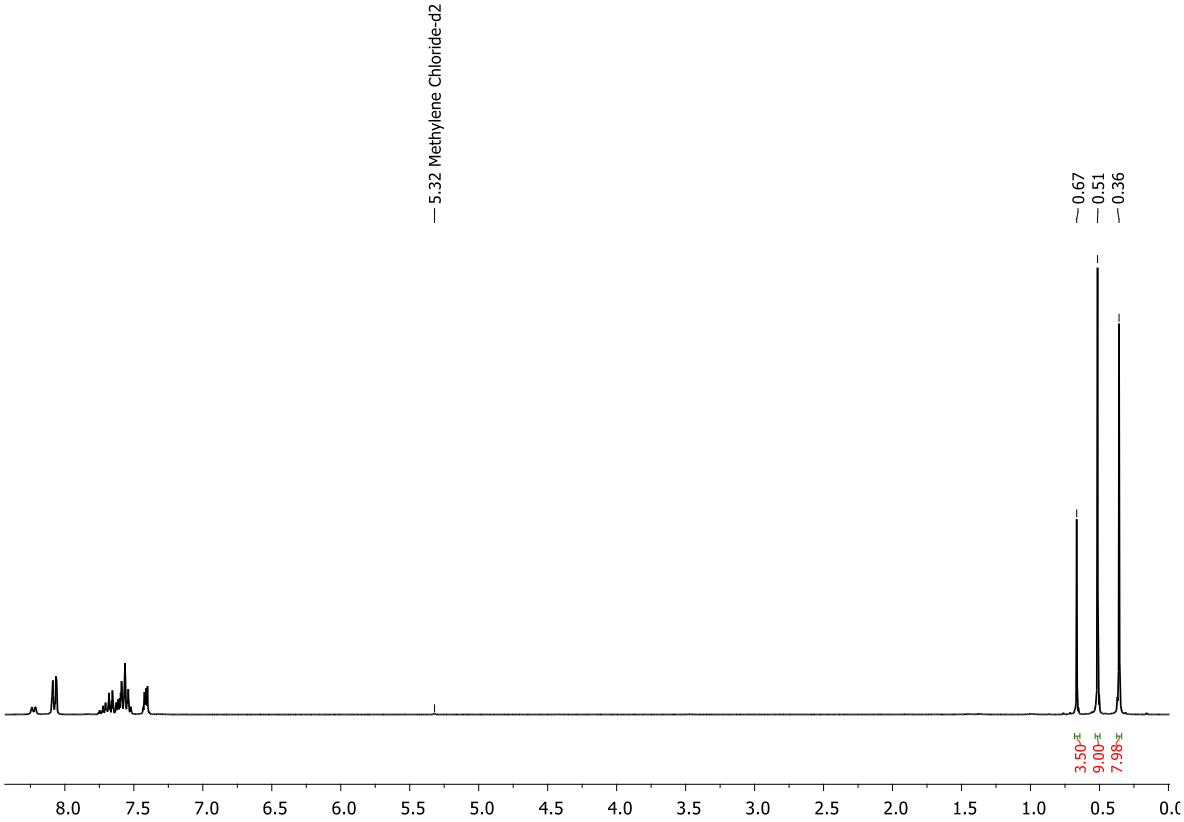

Figure 5.6.12. ^{1}H NMR spectrum of a mixture of **1c** and **12c** in the presence of catalyst **B** (20 mol%) after 7 d (CD_2Cl_2, 300 MHz).

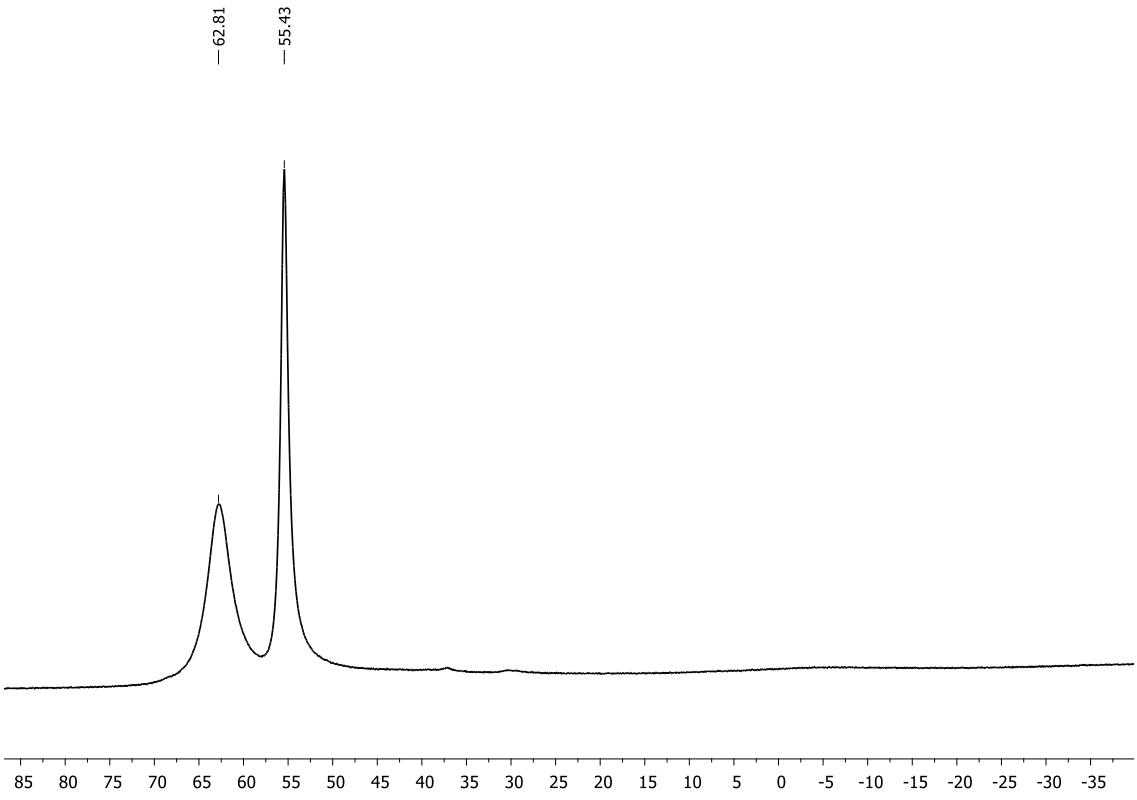

Figure 5.6.13. ^{11}B{^{1}H} NMR spectrum of a mixture of **1c** and **12c** in the presence of catalyst **B** (20 mol%) after 7 d (CD_2Cl_2, 96 MHz).

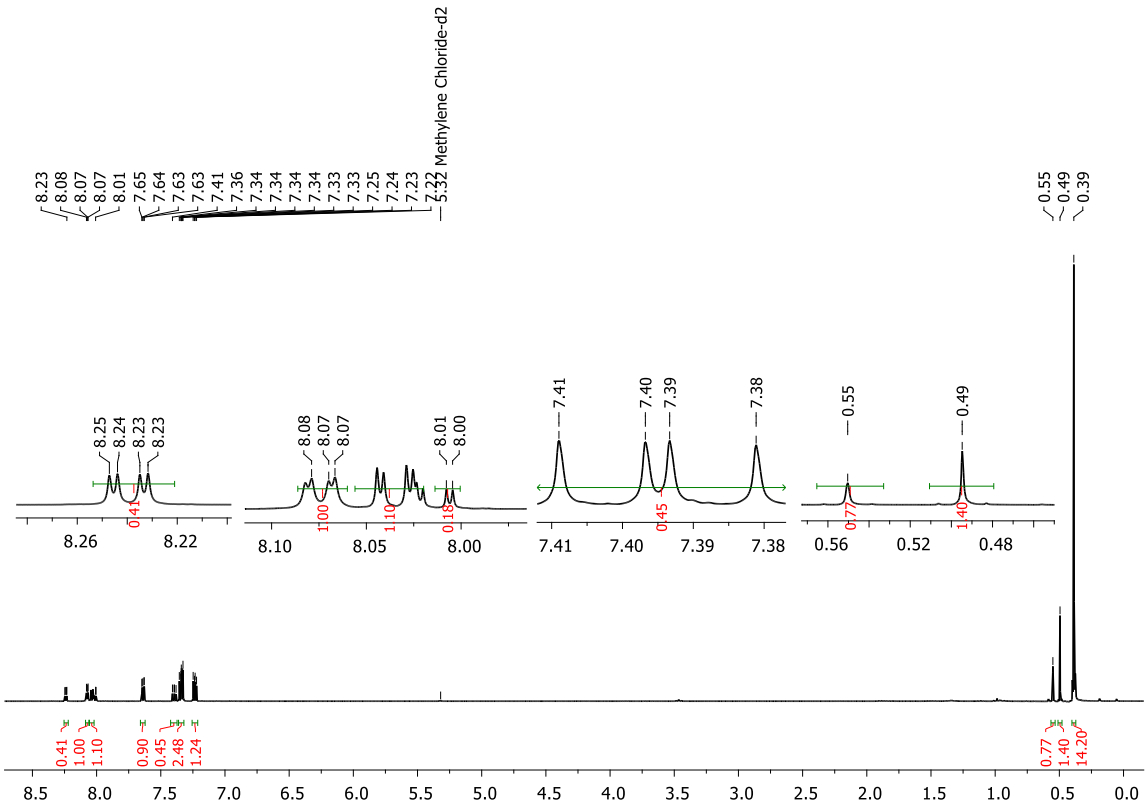

Figure 5.6.14. ^{1}H NMR spectrum of a mixture of **1a** and **12a** in the presence of catalyst **C** (5 mol%) after 2 d (CD_2Cl_2, 300 MHz).

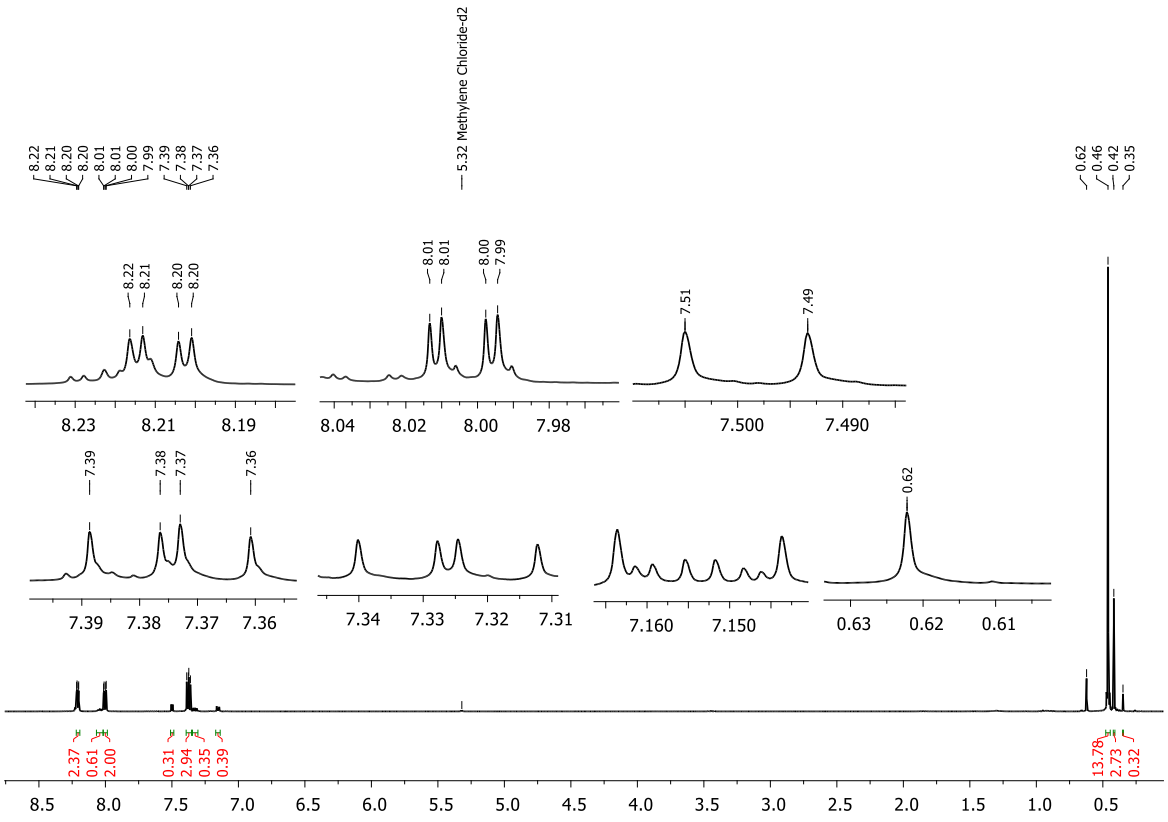

Figure 5.6.15. ^{1}H NMR spectrum of a mixture of **1a** and **12a** in the presence of catalyst **D** (5 mol%) after 5 h (CD_2Cl_2, 300 MHz).

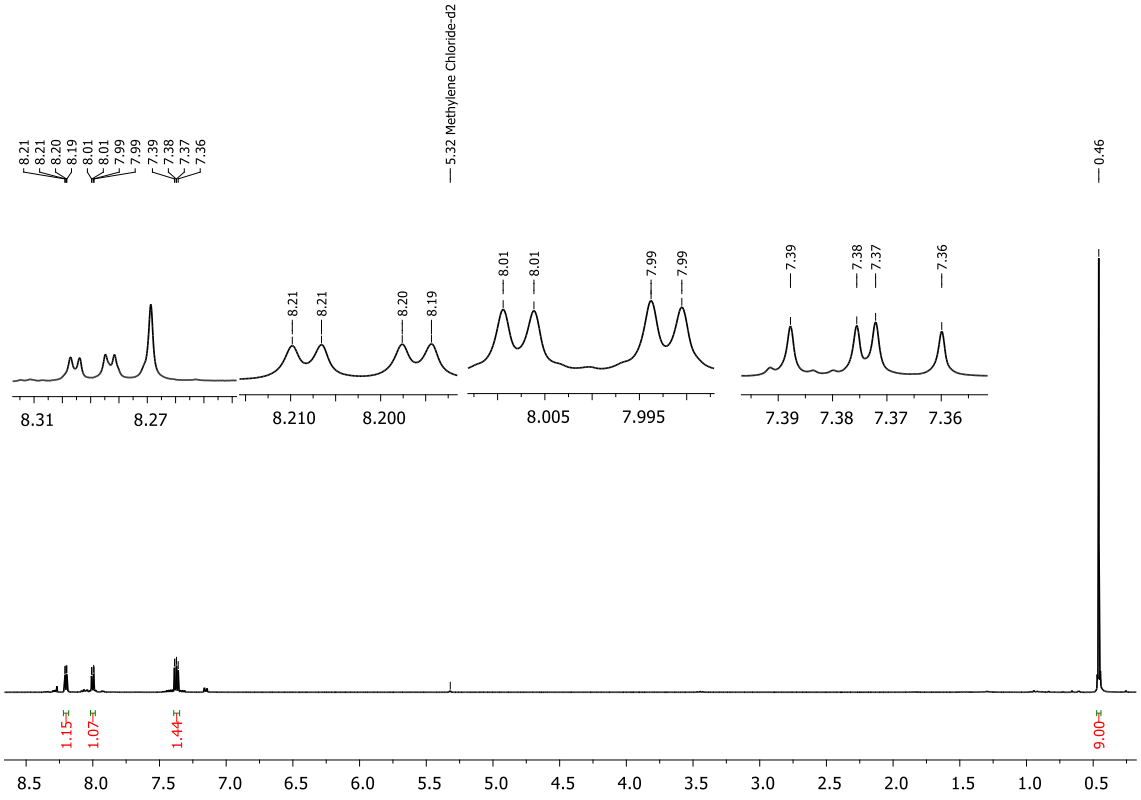

Figure 5.6.16. ^{1}H NMR spectrum of a mixture of **1a** and **12a** in the presence of catalyst **E** (5 mol%) after 1h 40 (CD_2Cl_2, 300 MHz).

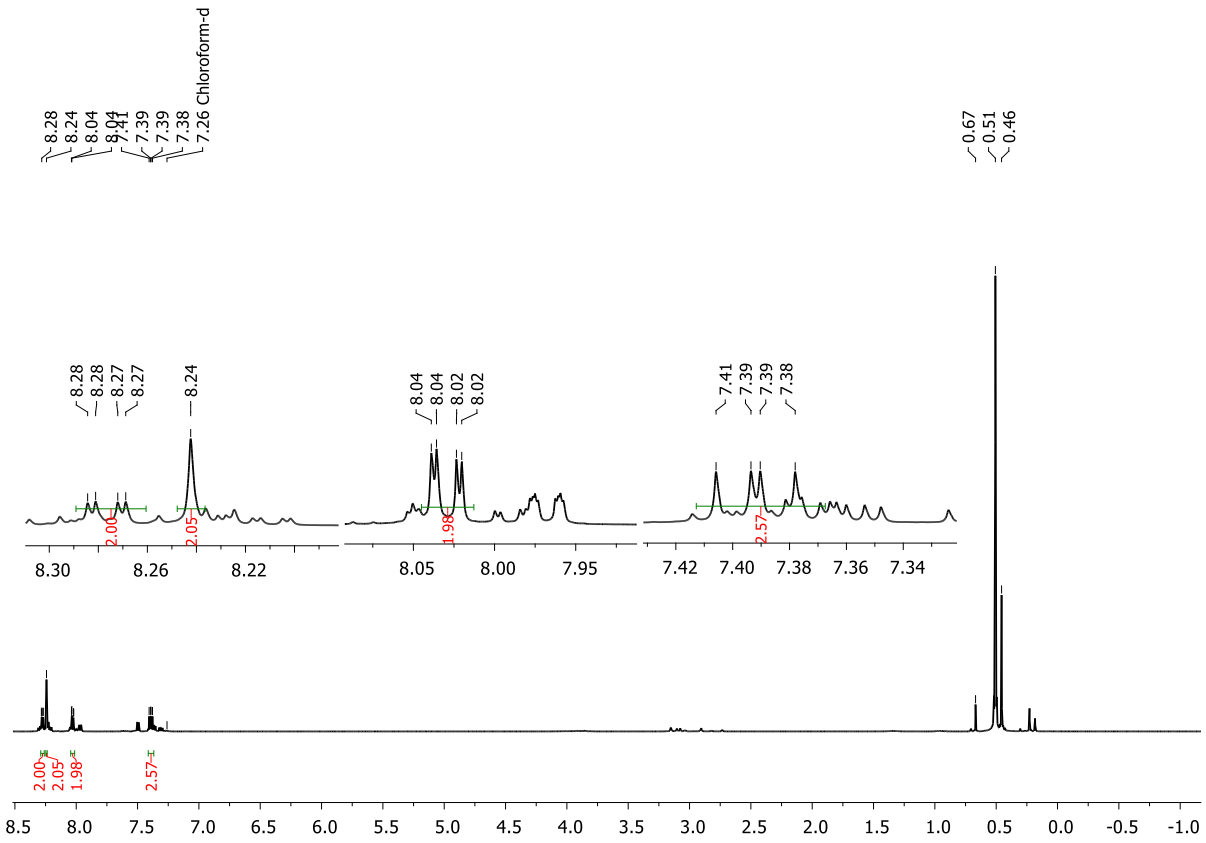

Figure 5.6.17. ^{1}H NMR spectrum of a mixture of **5a** and two equivalents of **12a** in the presence of catalyst **B** (10 mol%) after 13 d ($CDCl_3$, 300 MHz).

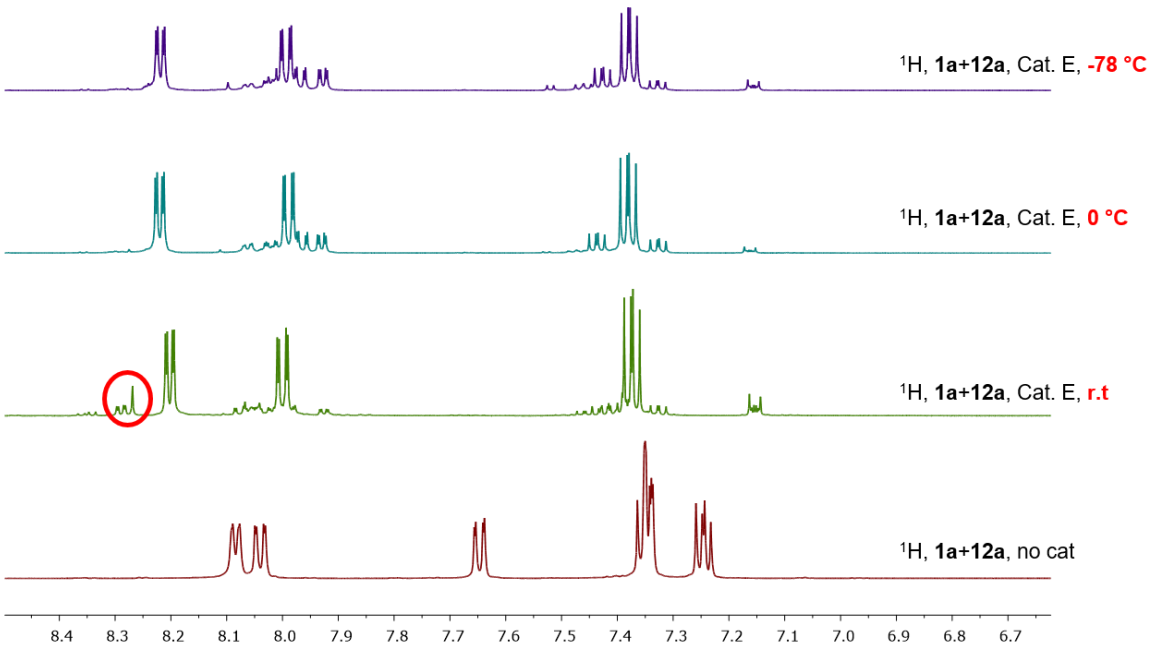

Figure 5.6.18. ^{1}H NMR spectrum of a mixture of **1a** and **12a** in the absence (red) and in the presence of catalyst **E** (5 mol%) after 24 h at different temperatures (CD_2Cl_2, 300 MHz).

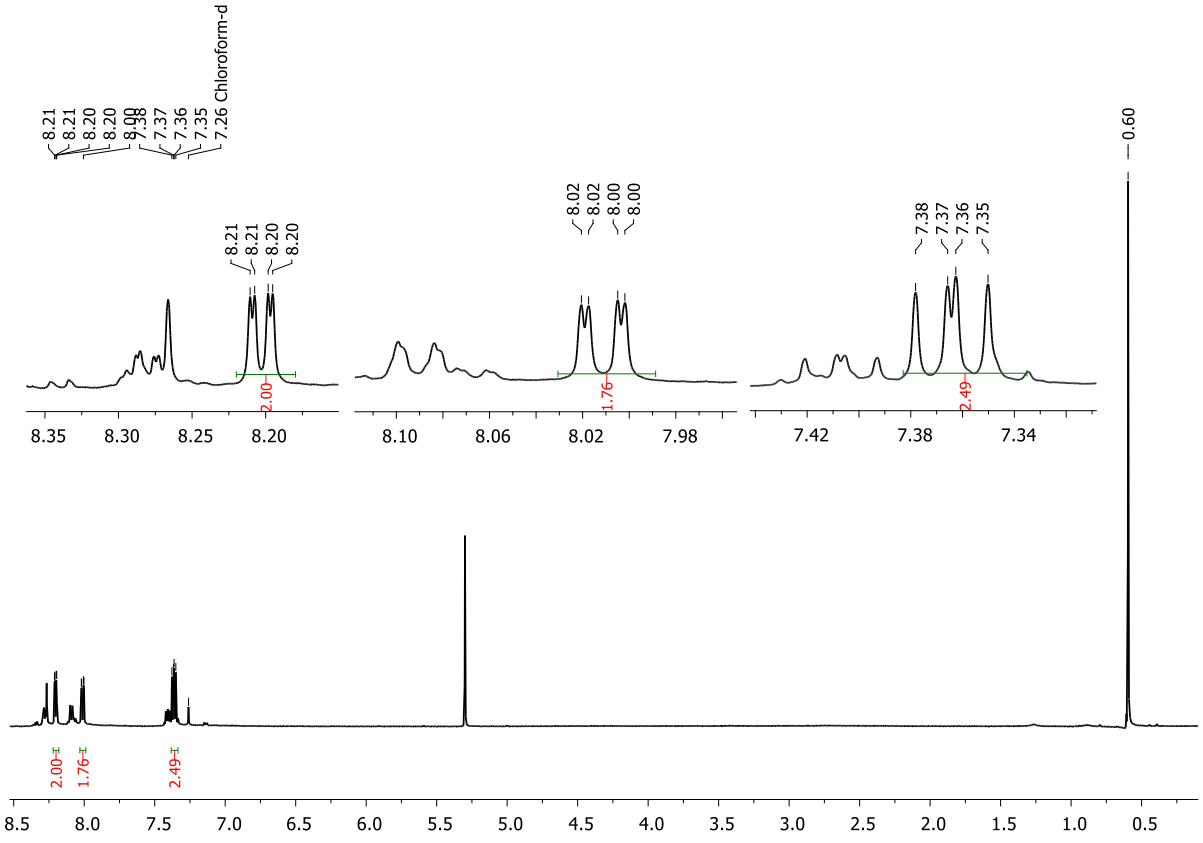

Figure 5.6.19. ^{1}H NMR spectrum of a mixture of **1a** and **2a** in the presence of catalyst **E** (5 mol%) after 4 h ($CDCl_3$, 300 MHz).

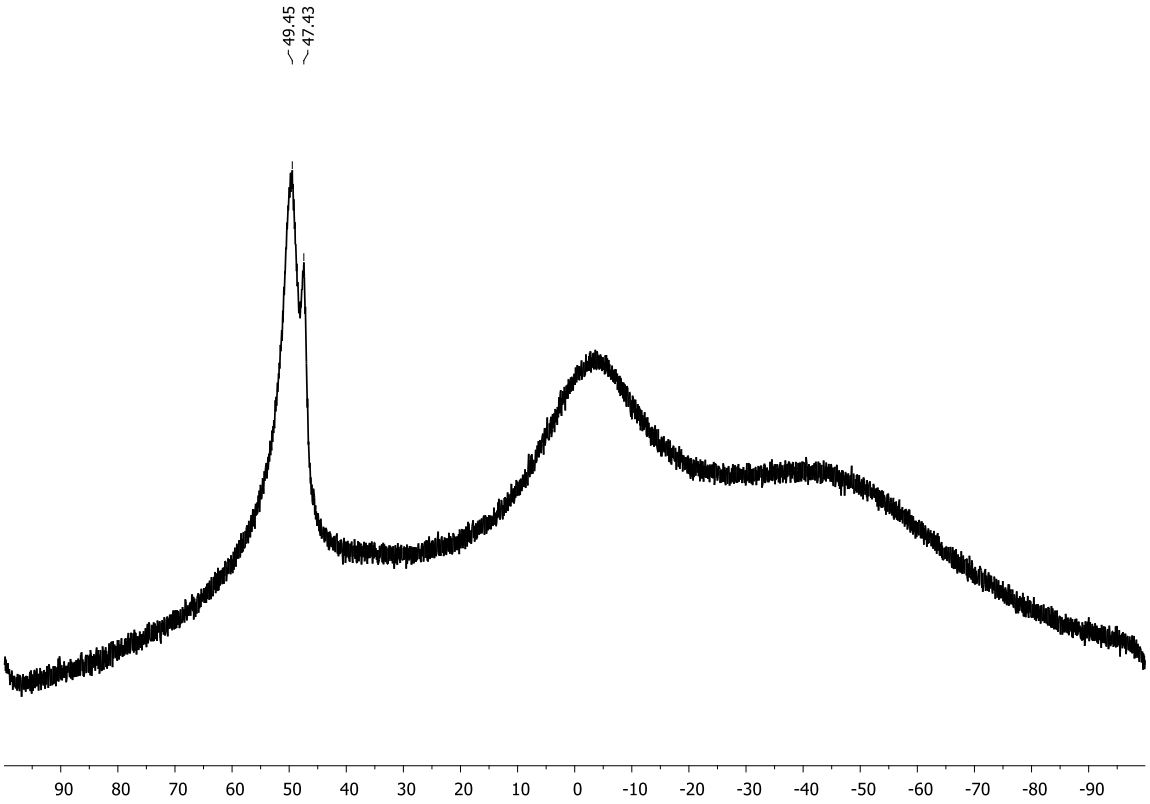

Figure 5.6.20. $^{11}B\{^{1}H\}$ NMR spectrum of a mixture of **1a** and **2a** in the presence of catalyst **E** (5 mol%) after 4 h ($CDCl_3$, 96 MHz).

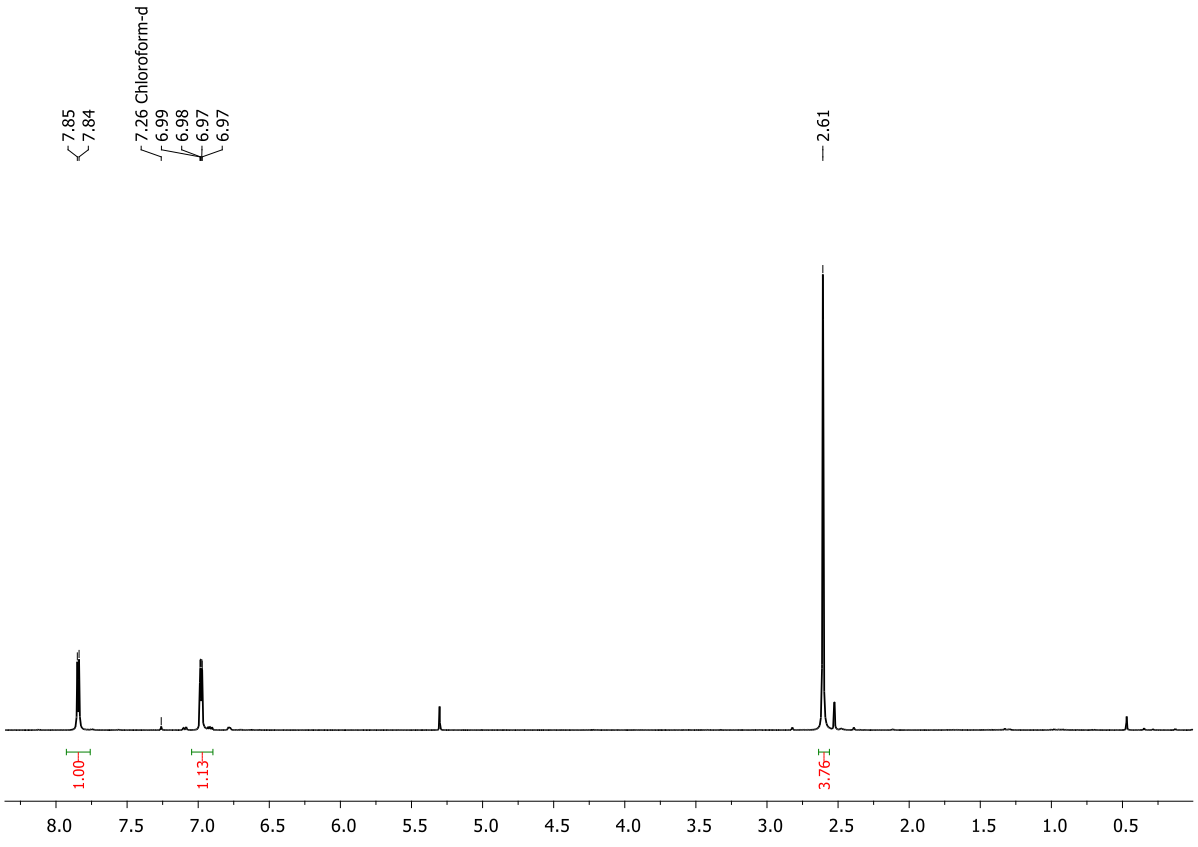

Figure 5.6.21. ^{1}H NMR spectrum of **12a^{Me}** ($CDCl_3$, 300 MHz).

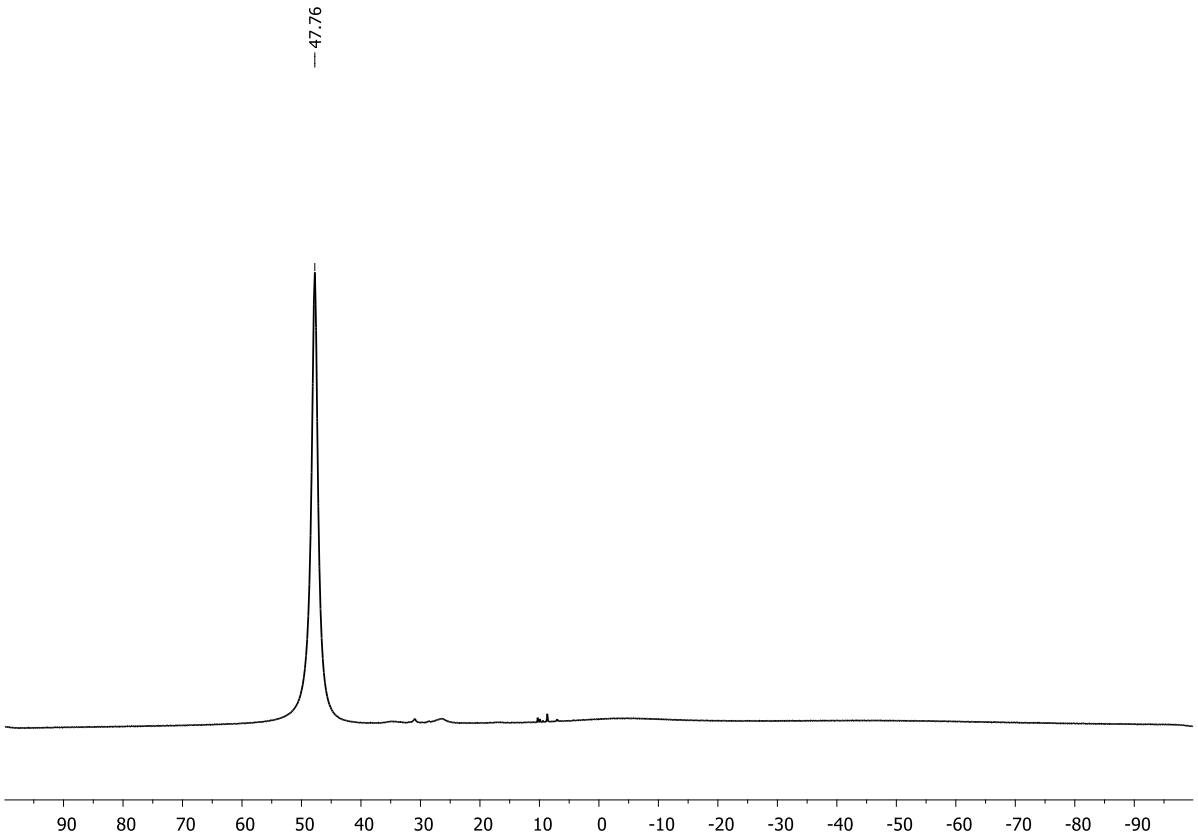

Figure 5.6.22. $^{11}B\{^{1}H\}$ NMR spectrum of **12a^{Me}** ($CDCl_3$, 96 MHz).

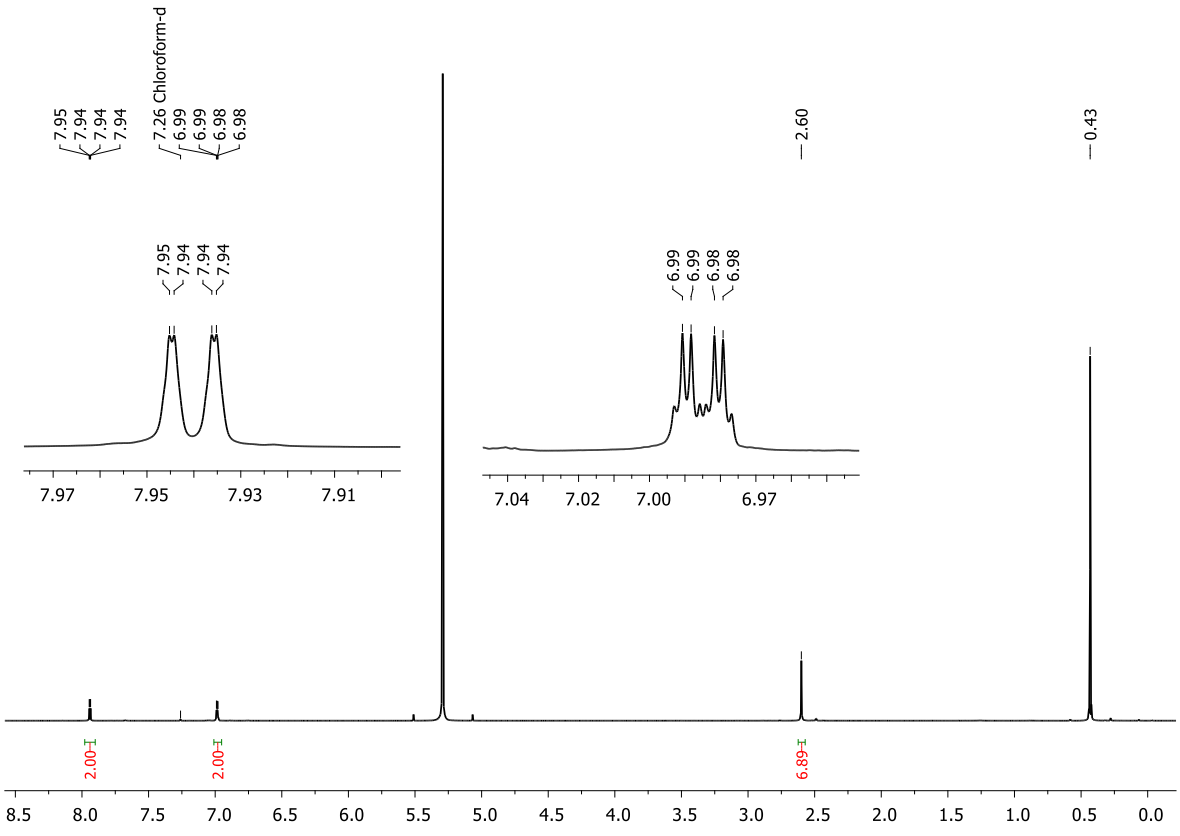

Figure 5.6.23. ^{1}H NMR spectrum of a mixture of **1a^{Me}** and **12a^{Me}** in the presence of catalyst **E** (5 mol%) after 4 h ($CDCl_3$, 300 MHz).

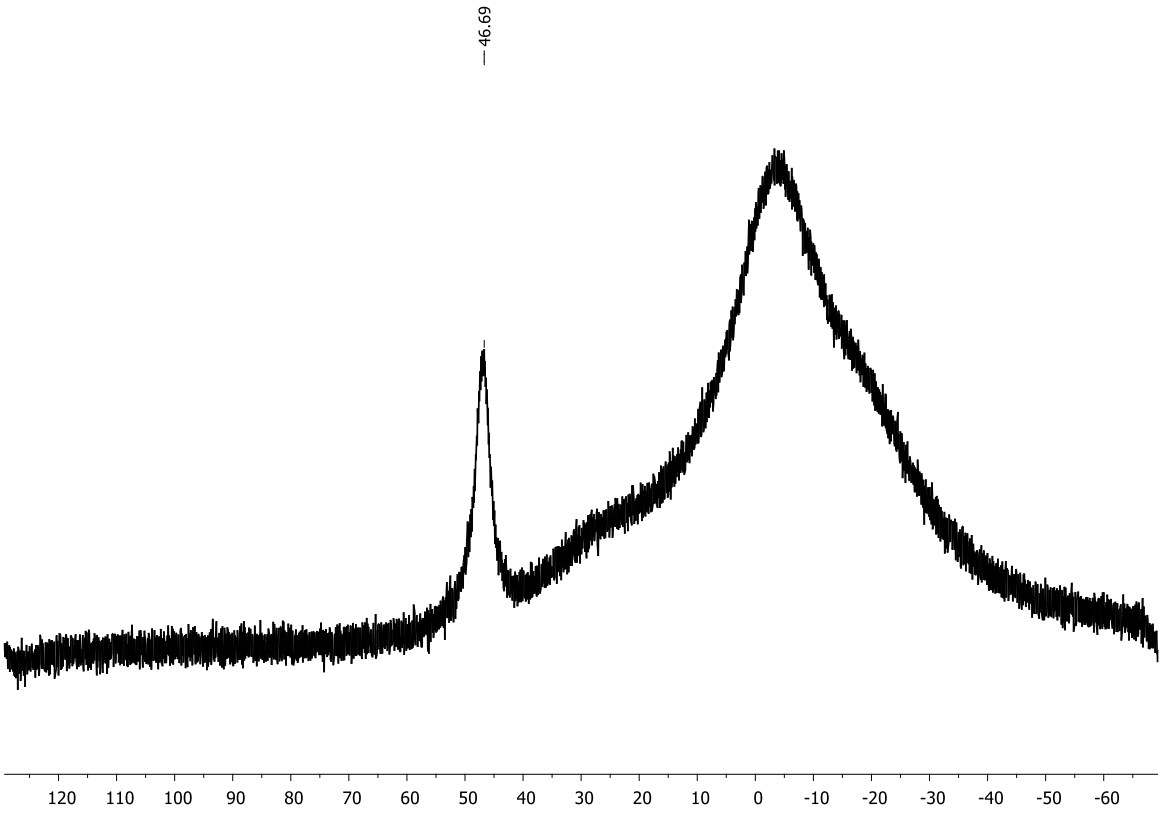

Figure 5.6.24. $^{11}B\{^{1}H$ NMR} spectrum of a mixture of **1a^{Me}** and **12a^{Me}** in the presence of catalyst **E** (5m ol%) after 4 h ($CDCl_3$, 96 MHz).

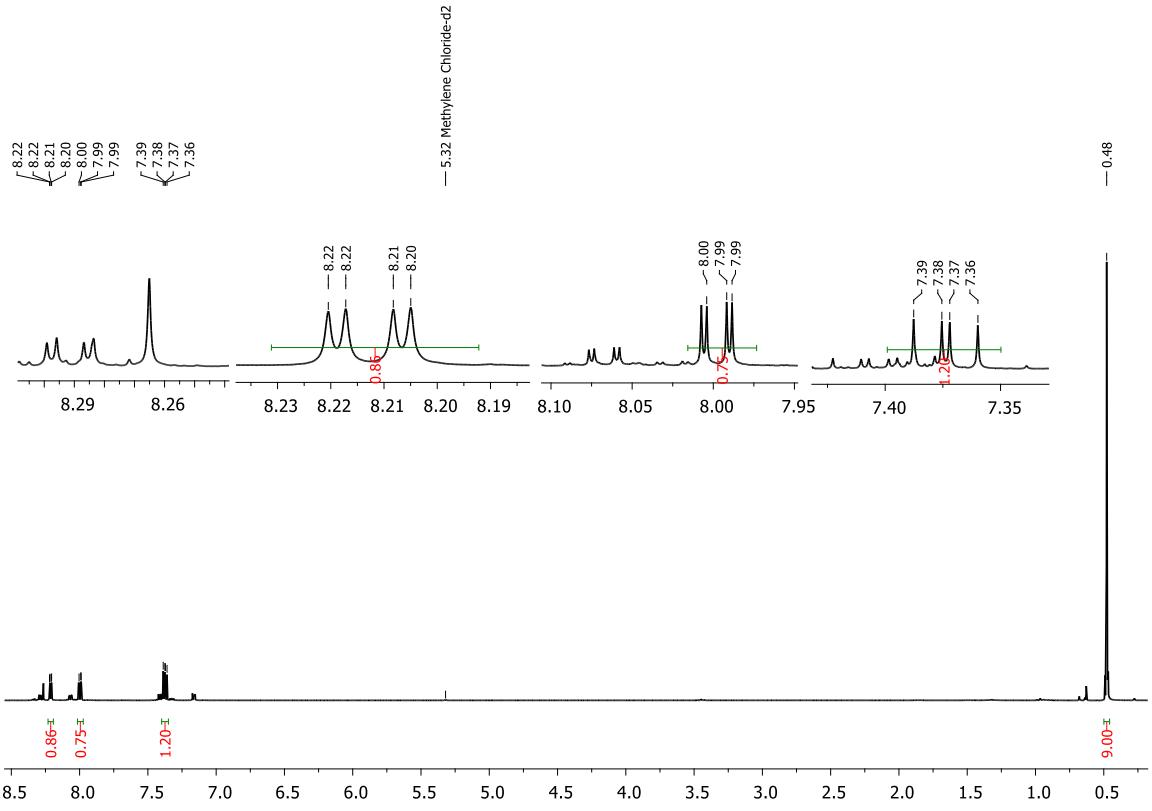

Figure 5.6.25. ^{1}H NMR spectrum of a mixture of **1a** and **12a** in the presence of catalyst **F** (5 mol%) after 1 h 40 (CD_2Cl_2, 300 MHz).

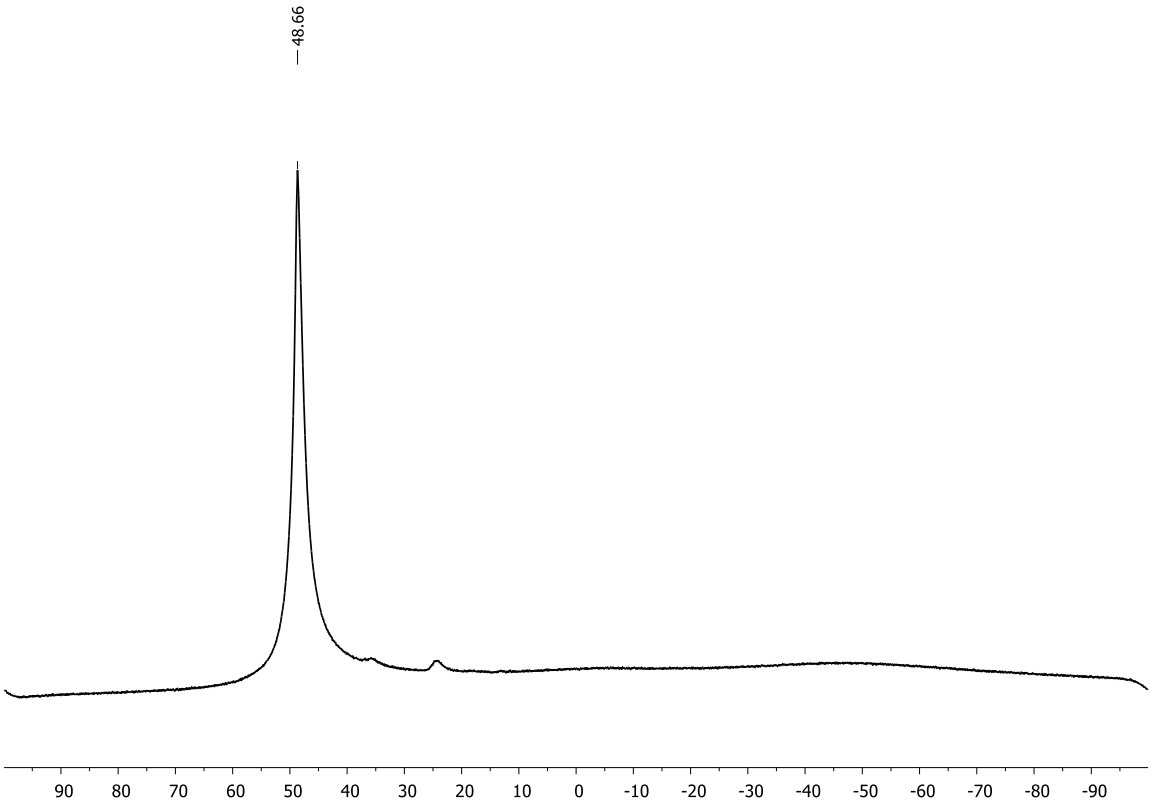

Figure 5.6.26. $^{11}B\{^{1}H\}$ NMR spectrum of a mixture of **1a** and **12a** in the presence of catalyst **F** (5 mol%) after 1 h 40 (CD_2Cl_2, 96 MHz).

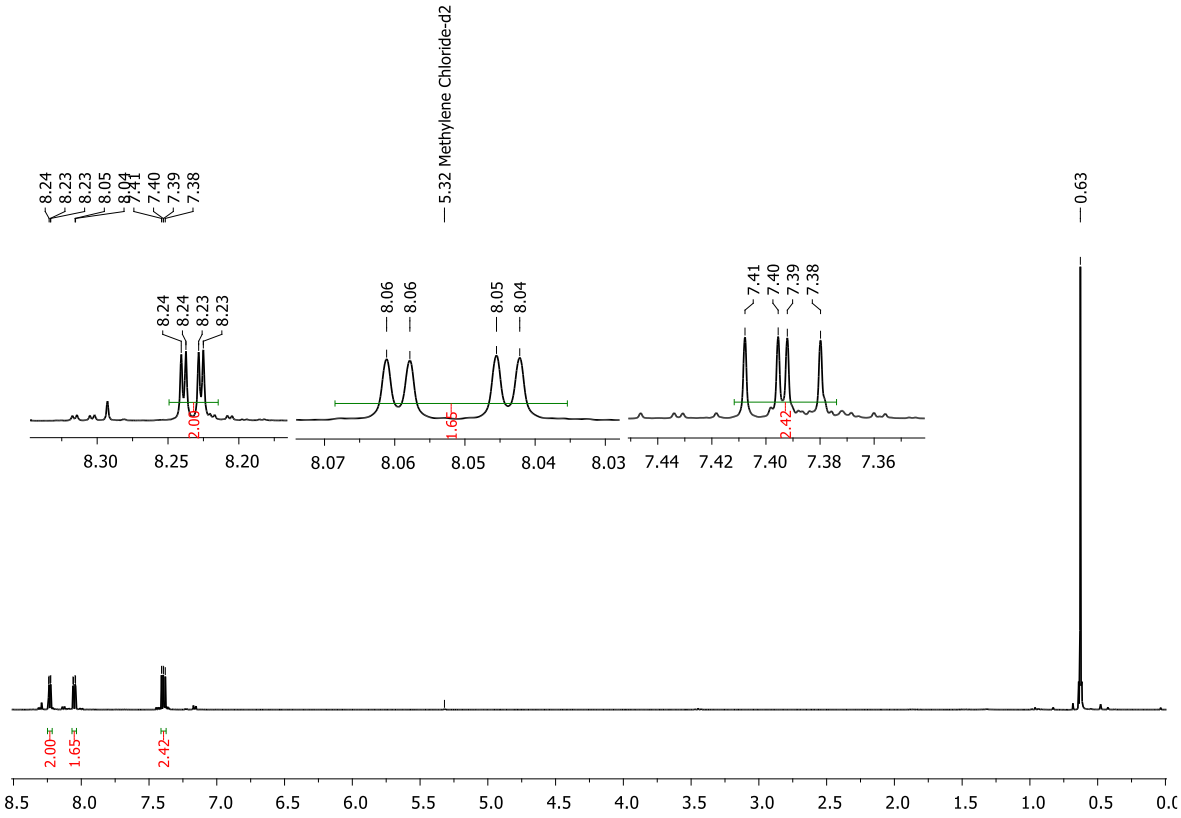

Figure 5.6.27. ^{1}H NMR spectrum of a mixture of **1a** and **2a** in the presence of catalyst **F** (5 mol%) after 3 h (CD_2Cl_2, 300 MHz).

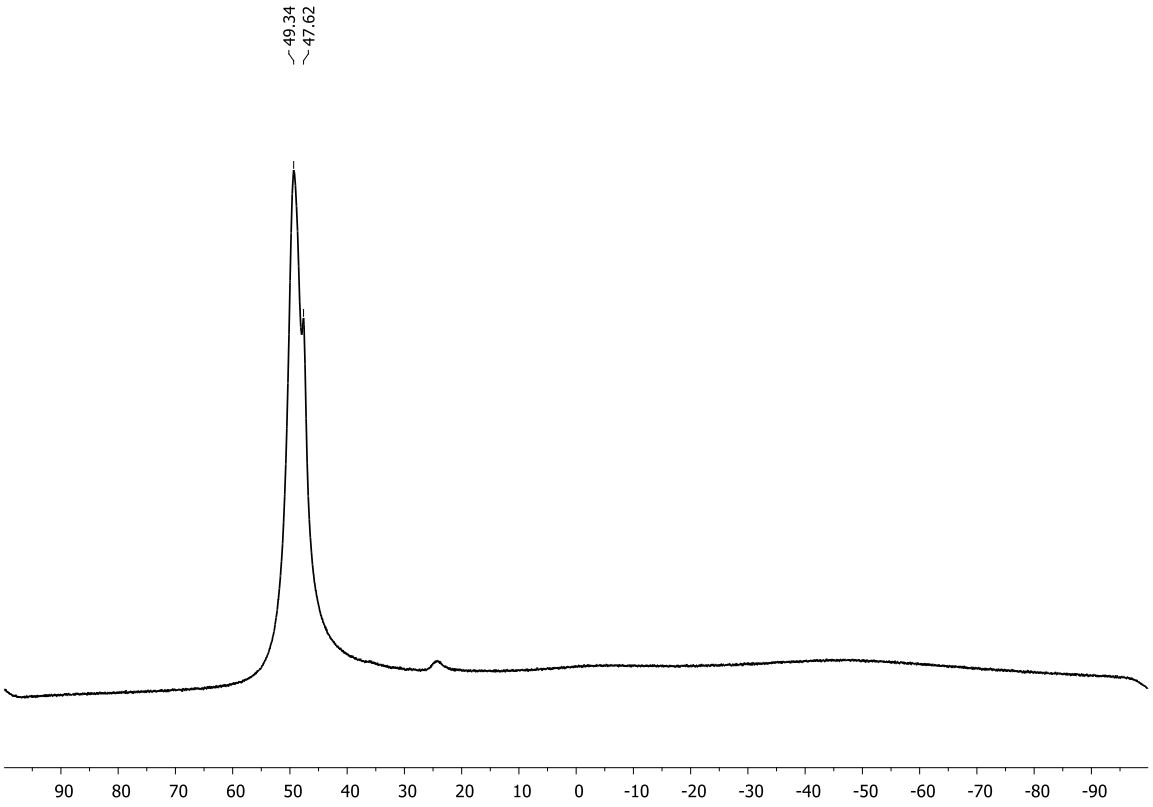

Figure 5.6.28. $^{11}B\{^{1}H\}$ NMR spectrum of a mixture of **1a** and **2a** in the presence of catalyst **F** (5 mol%) after 3 h (CD_2Cl_2, 96 MHz).

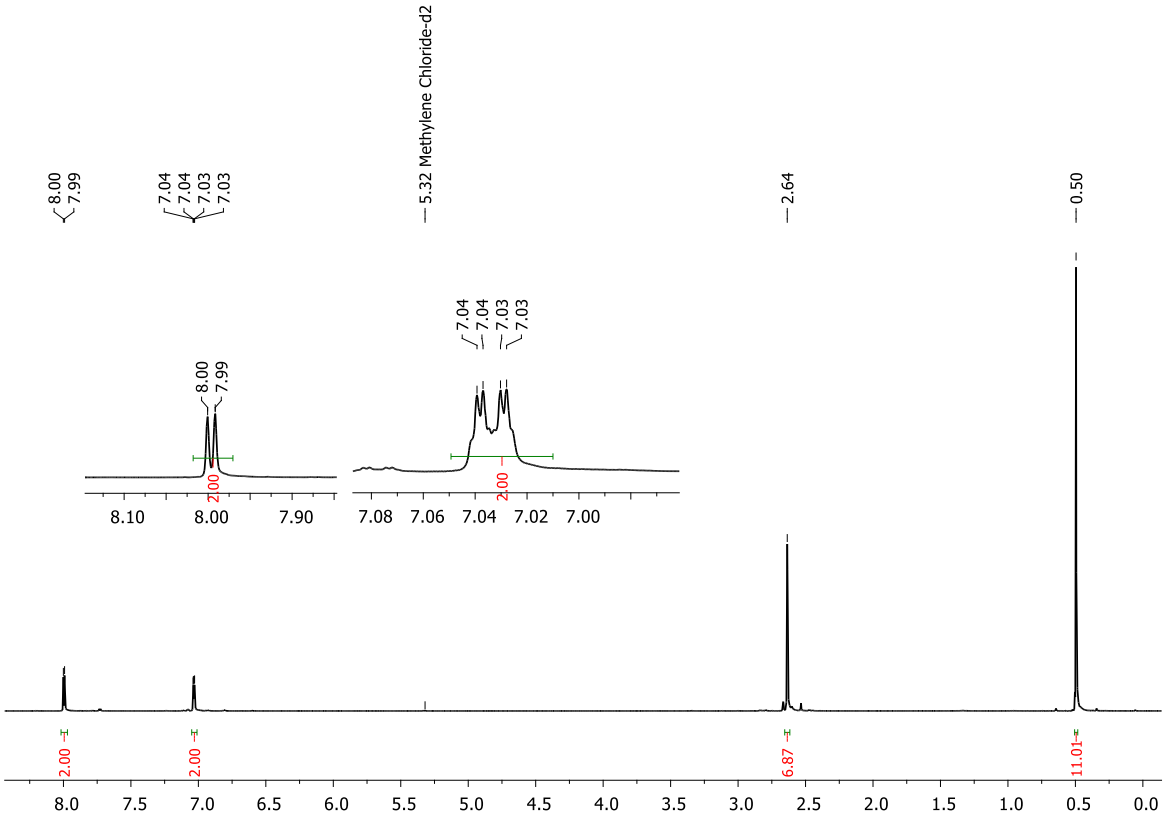

Figure 5.6.29. ^{1}H NMR spectrum of a mixture of **1a^{Me}** and **12a^{Me}** in the presence of catalyst **F** (5mol%) after 4 h (CD_2Cl_2, 300 MHz).

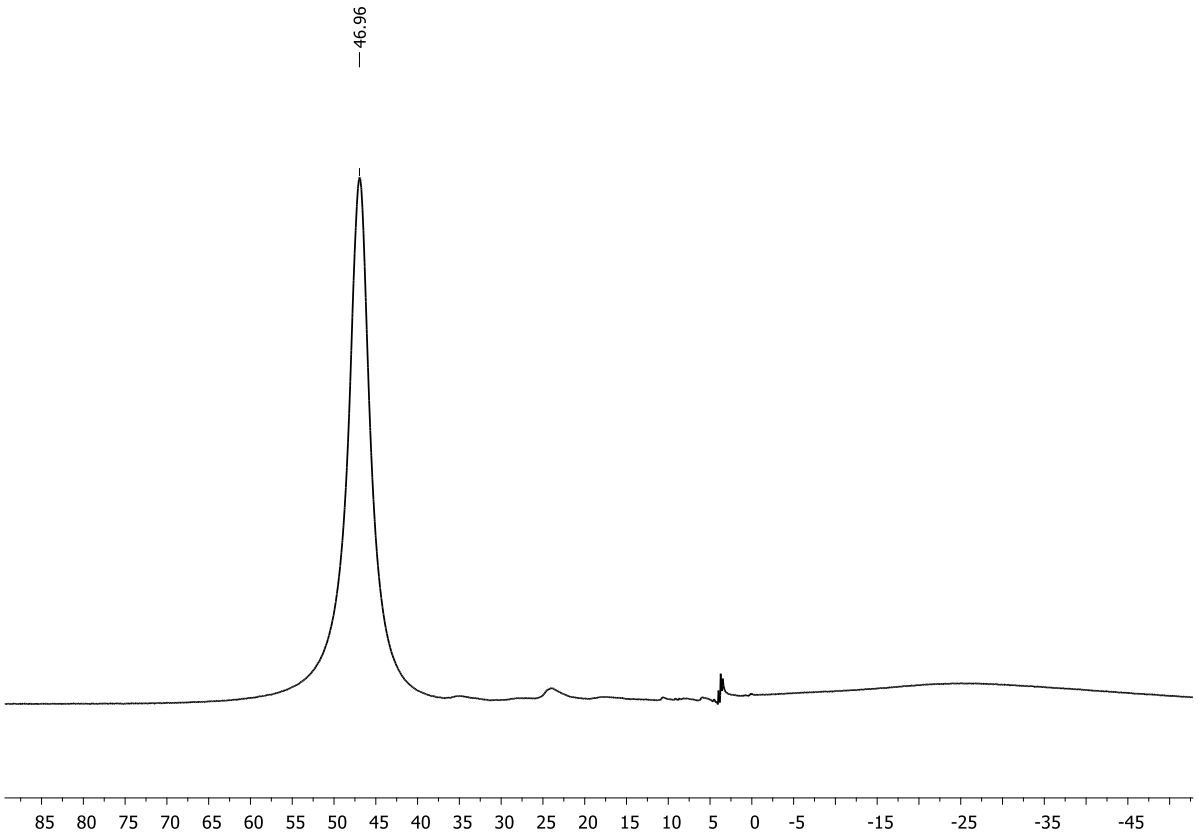

Figure 5.6.30. $^{11}B\{^{1}H\}$ NMR spectrum of a mixture of **1a^{Me}** and **12a^{Me}** in the presence of catalyst **F** (5 mol%) after 4 h (CD_2Cl_2, 96 MHz).

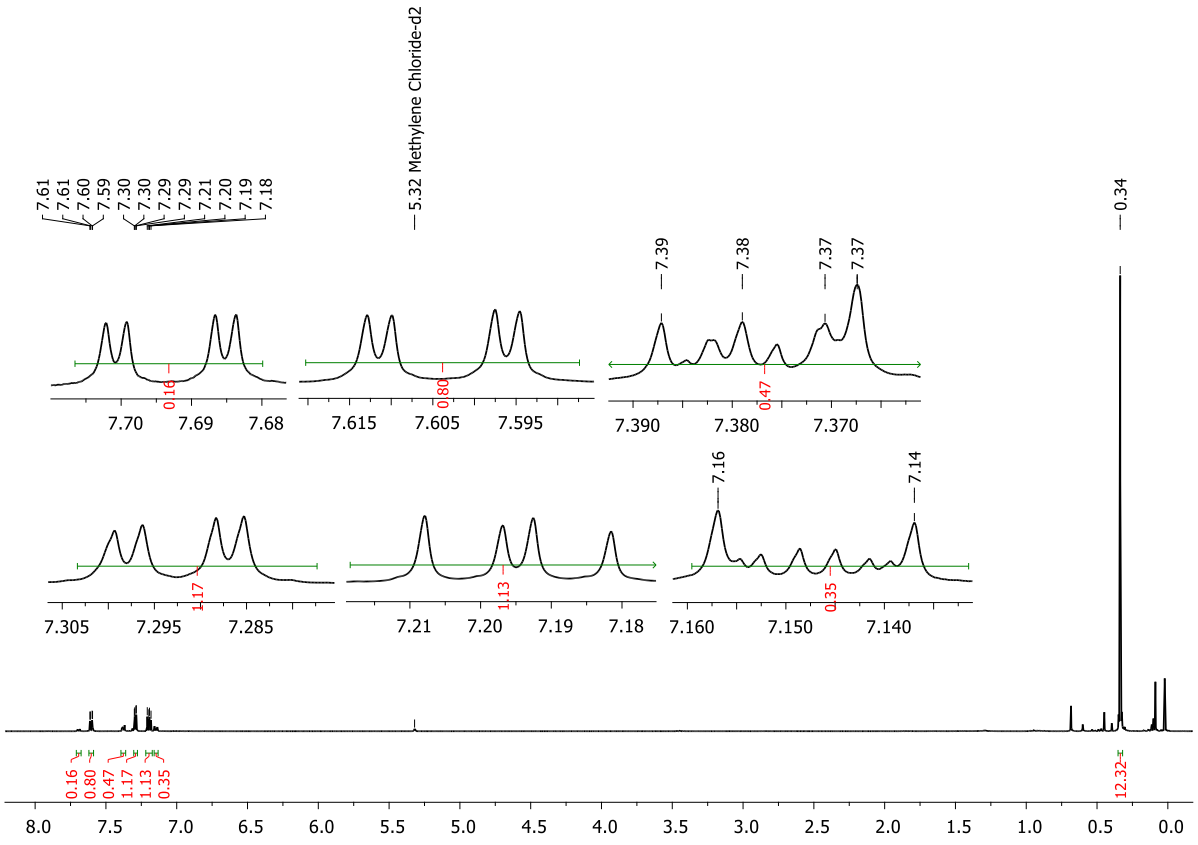

Figure 5.6.31. ^{1}H NMR spectrum of a mixture of **1a** and catalyst **E** (5 mol%) (CD_2Cl_2, 300 MHz).

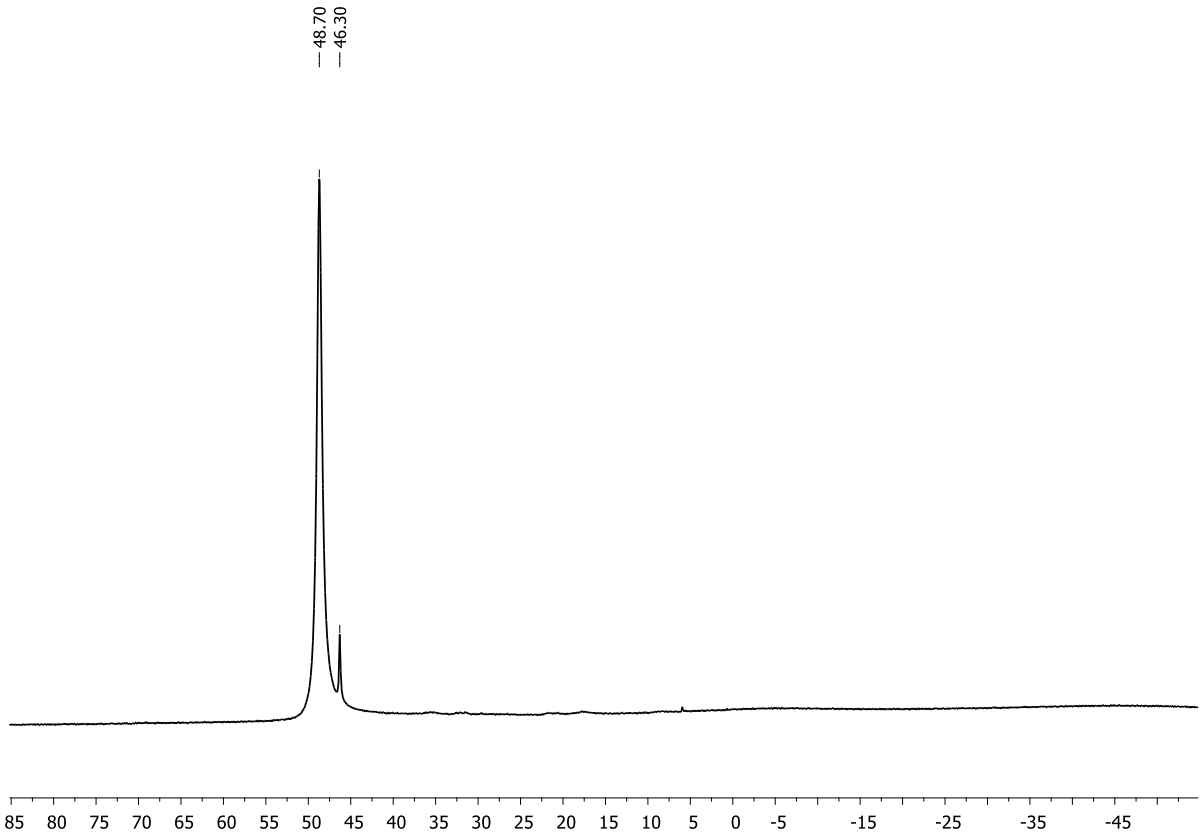

Figure 5.6.32. $^{11}B\{^{1}H\}$ NMR spectrum of a mixture of **12a** and catalyst **E** (5 mol%) (CD_2Cl_2, 96 MHz).

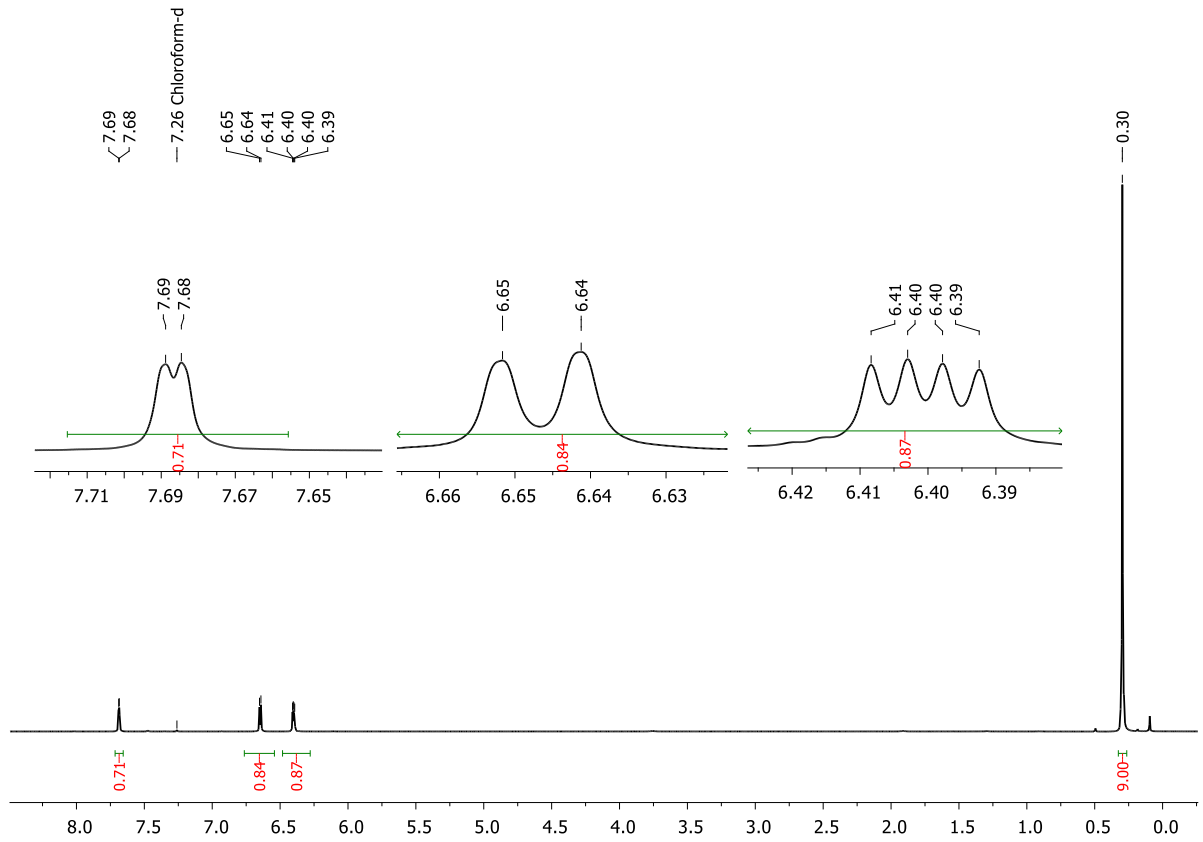

Figure 5.6.33. ^{1}H NMR spectrum of a mixture of **1b** and catalyst **E** (5 mol%) (CD_2Cl_2, 300 MHz).

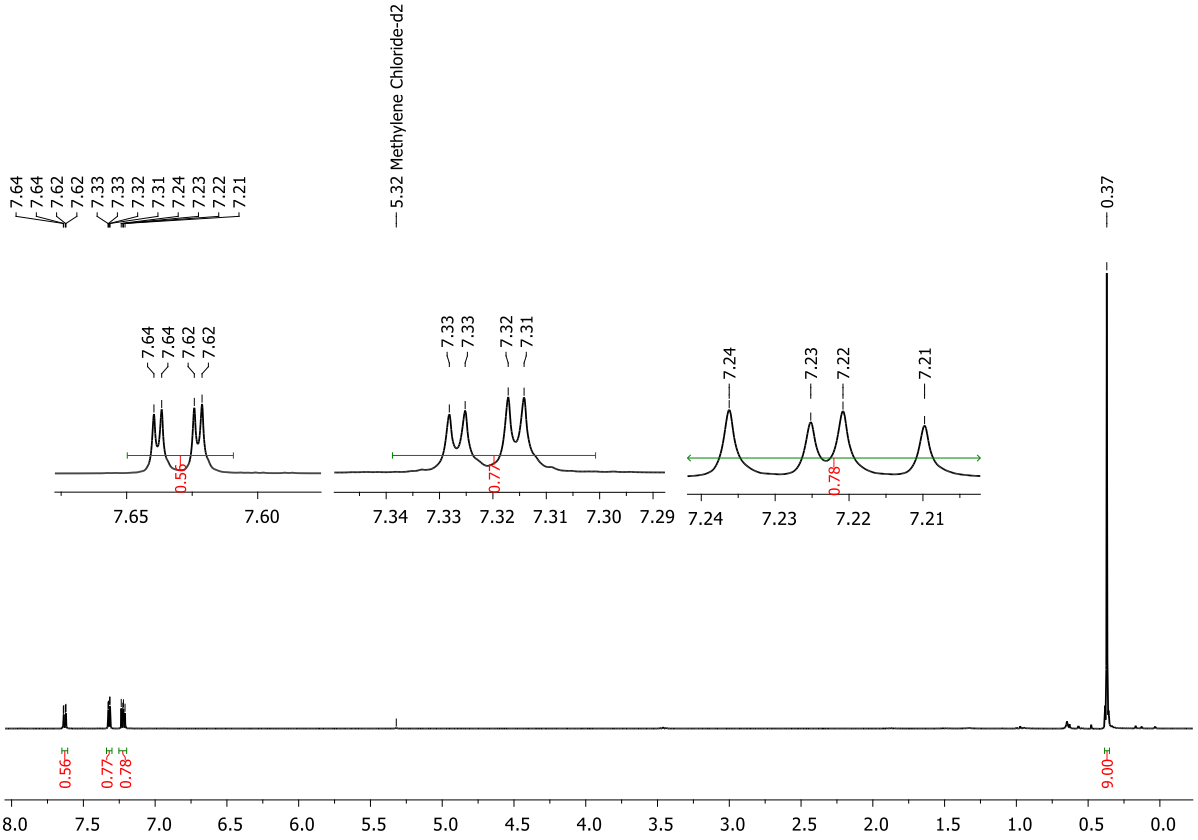

Figure 5.6.34. ^{1}H NMR spectrum of a mixture of **1a** and catalyst **F** (5 mol%) (CD_2Cl_2, 300 MHz).

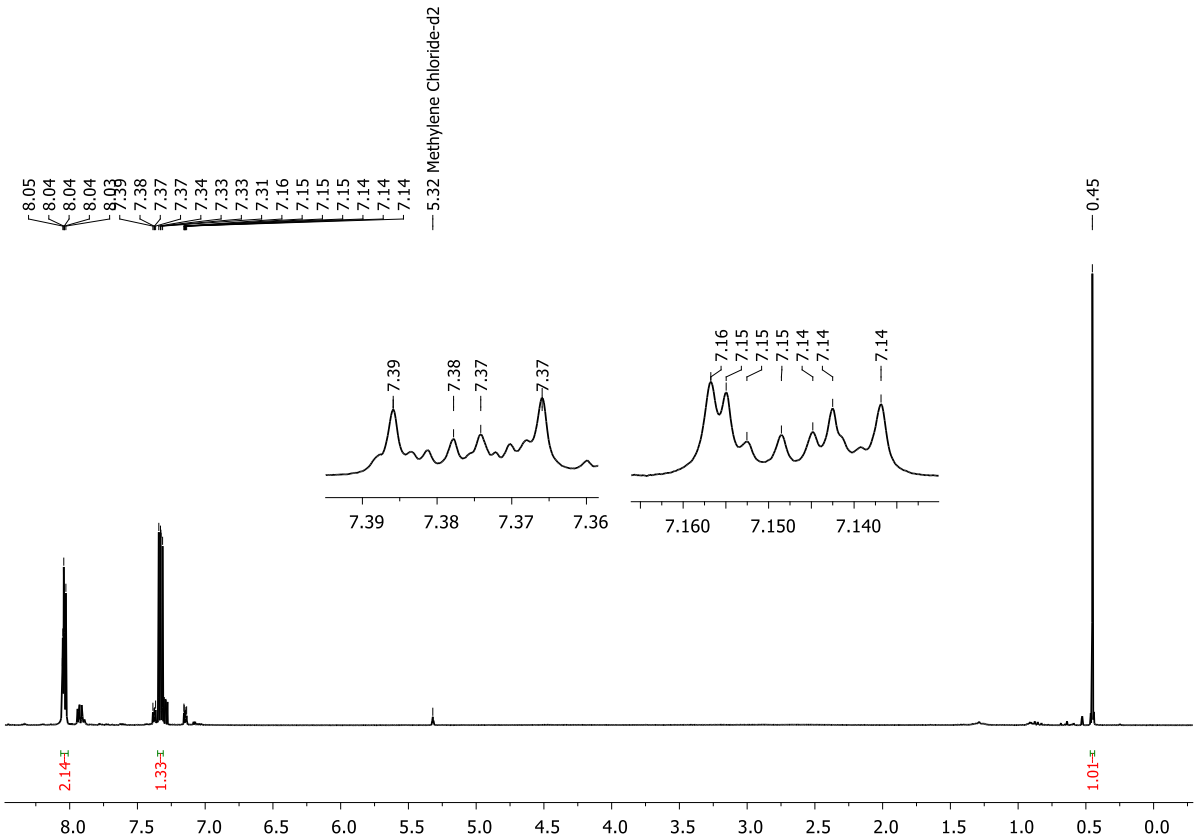

Figure 5.6.35. ^{1}H NMR spectrum of a mixture of **12a** and catalyst **F** (5 mol%) (CD_2Cl_2, 300 MHz).

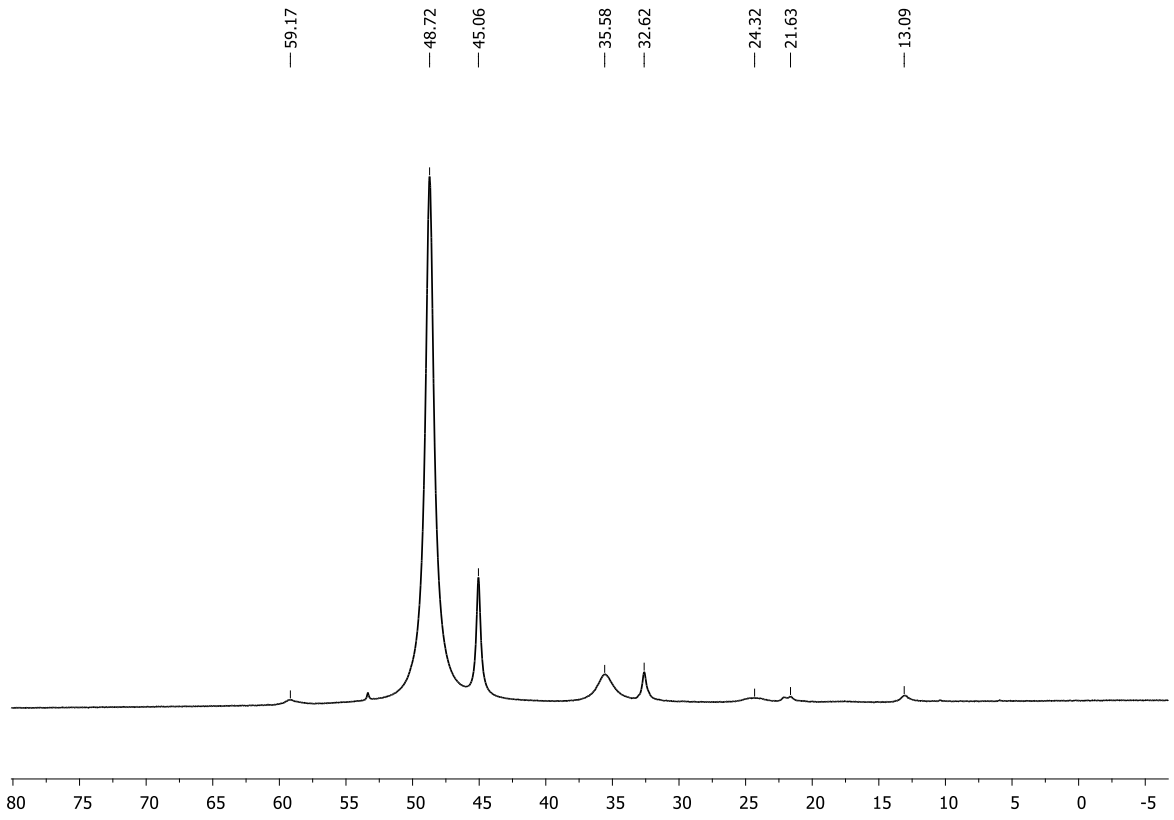

Figure 5.6.36. $^{11}B\{^{1}H\}$ NMR spectrum of a mixture of **12a** and catalyst **F** (5 mol%) (CD_2Cl_2, 96 MHz).

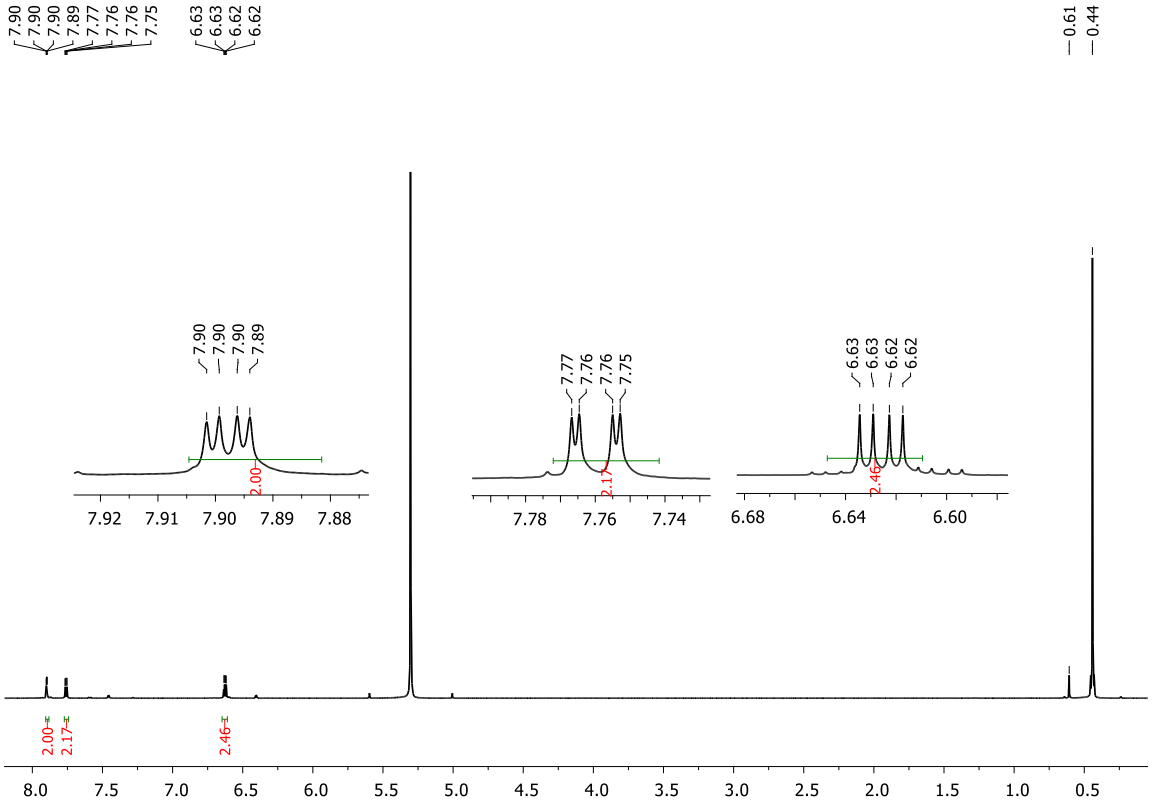

Figure 5.6.37. ^{1}H NMR spectrum of a mixture of **1b** and **12b** in the presence of catalyst **D** (5 mol%) after 1 d (CD_2Cl_2, 300 MHz).

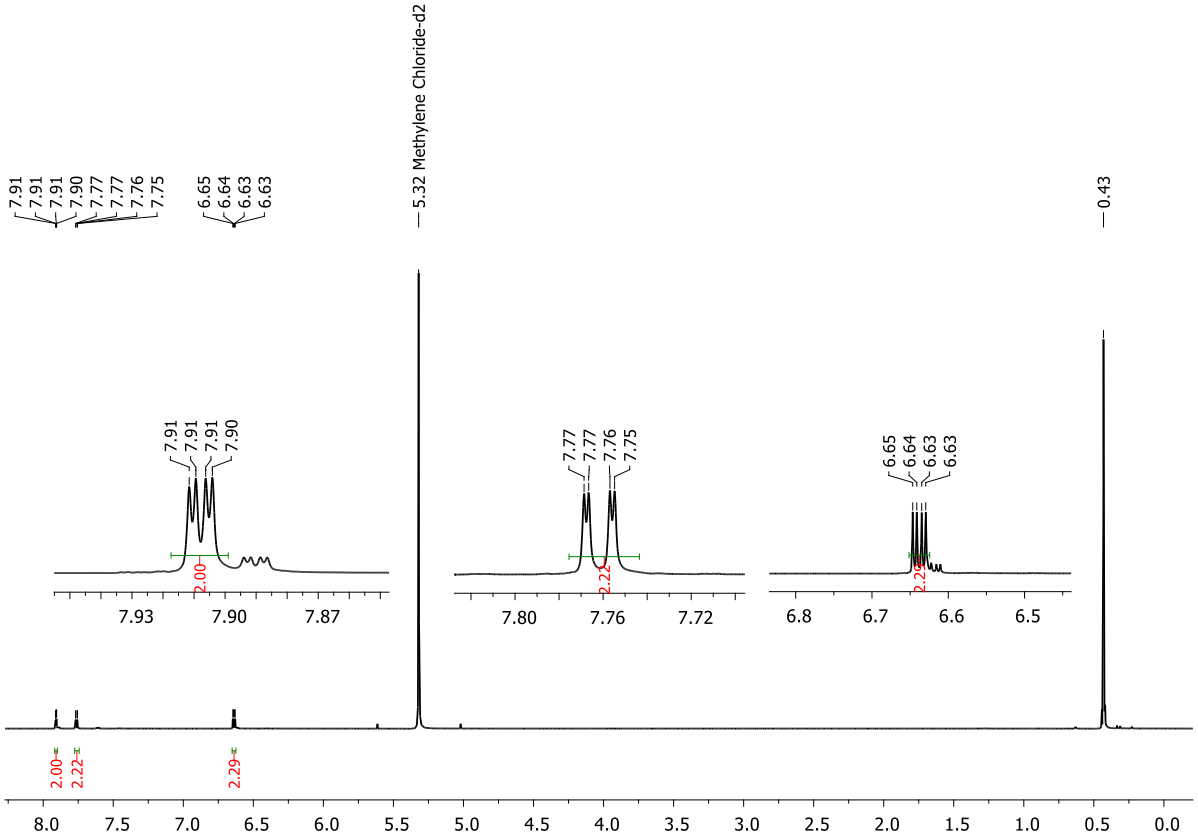

Figure 5.6.38. ^{1}H NMR spectrum of a mixture of **1b** and **12b** in the presence of catalyst **E** (5mol%) (CD_2Cl_2, 300 MHz).

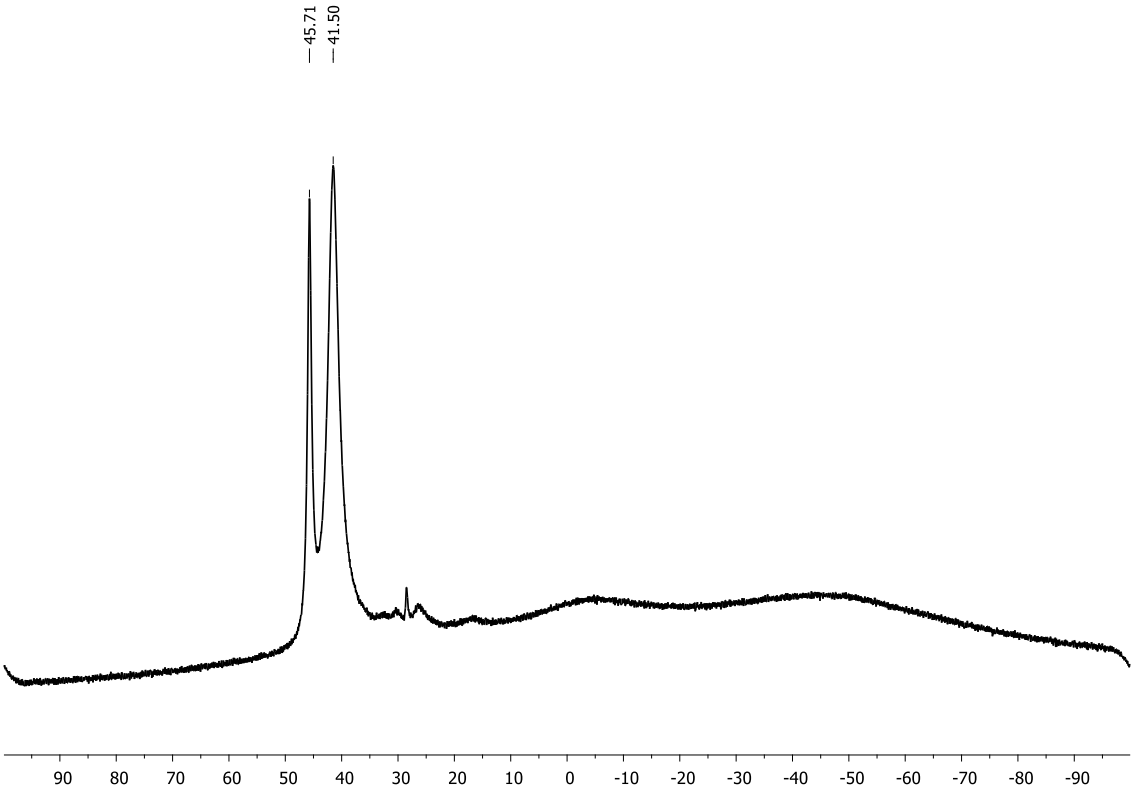

Figure 5.6.39. $^{11}B\{^{1}H\}$ NMR spectrum of a mixture of **1b** and **12b** in the presence of catalyst **E** (5mol%) (CD_2Cl_2, 96 MHz).

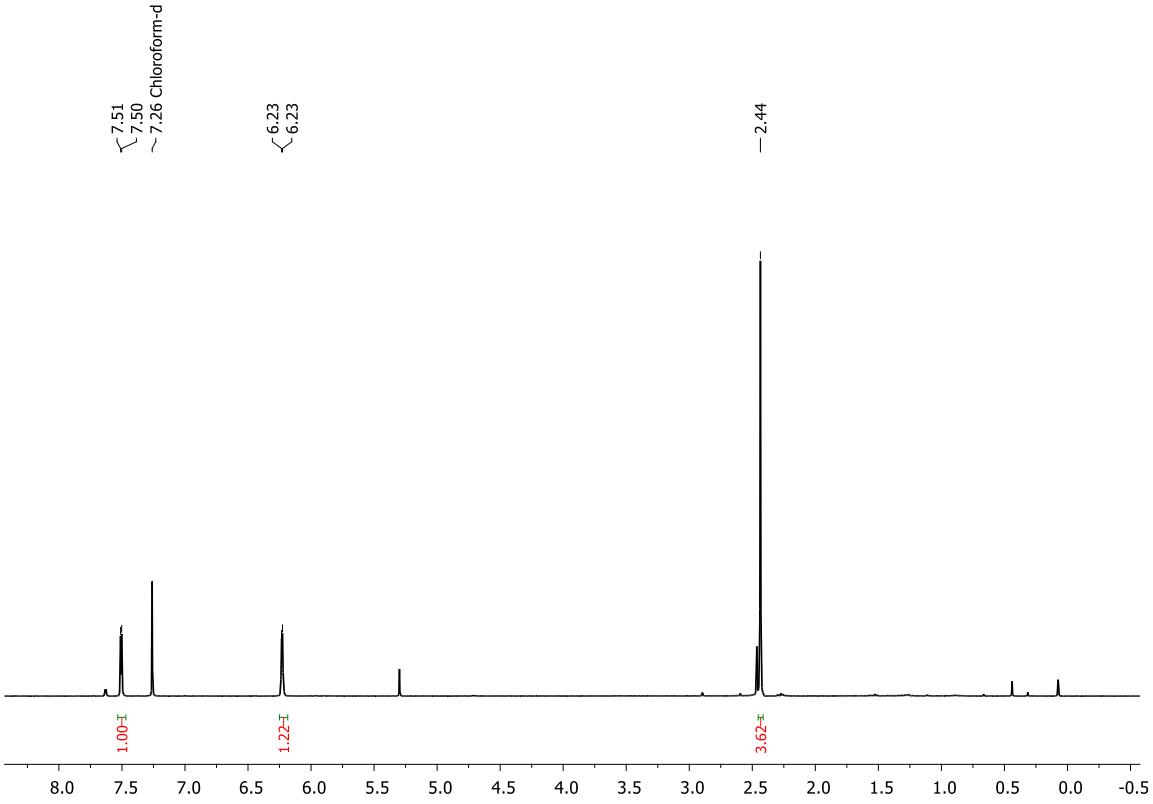

Figure 5.6.40. ^{1}H NMR spectrum of a mixture of **12b^{Me}** ($CDCl_3$, 300 MHz).

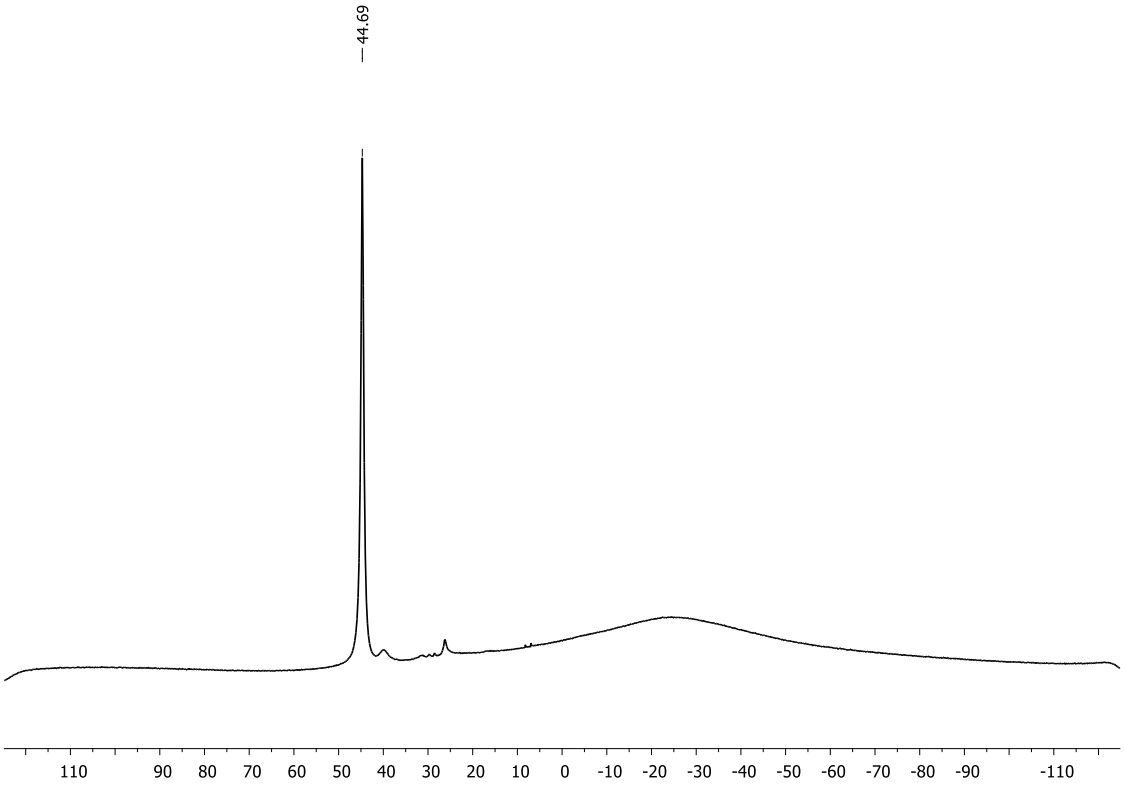

Figure 5.6.41. ^{11}B{^{1}H} NMR spectrum of **12b^{Me}** ($CDCl_3$, 96 MHz).

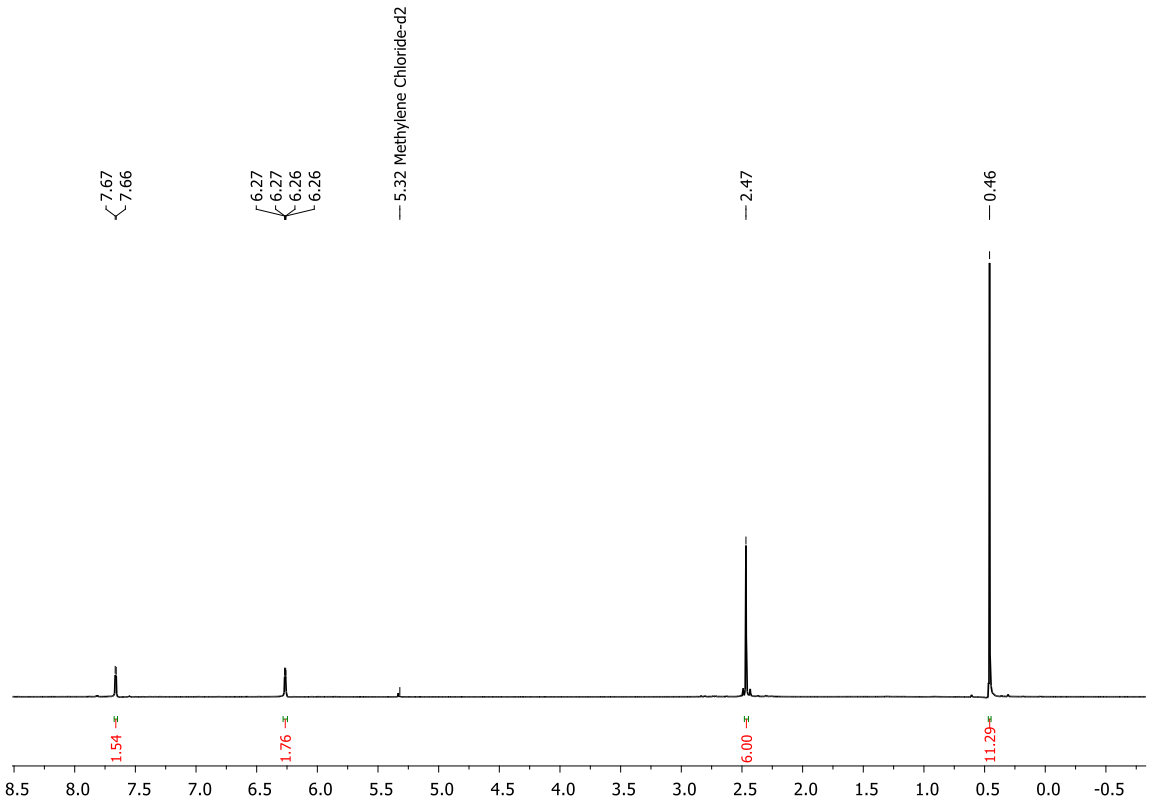

Figure 5.6.42. ^{1}H NMR spectrum of a mixture of **1b^{Me}** and **12b^{Me}** in the presence of catalyst **E** (5mol%) (CD_2Cl_2, 300 MHz).

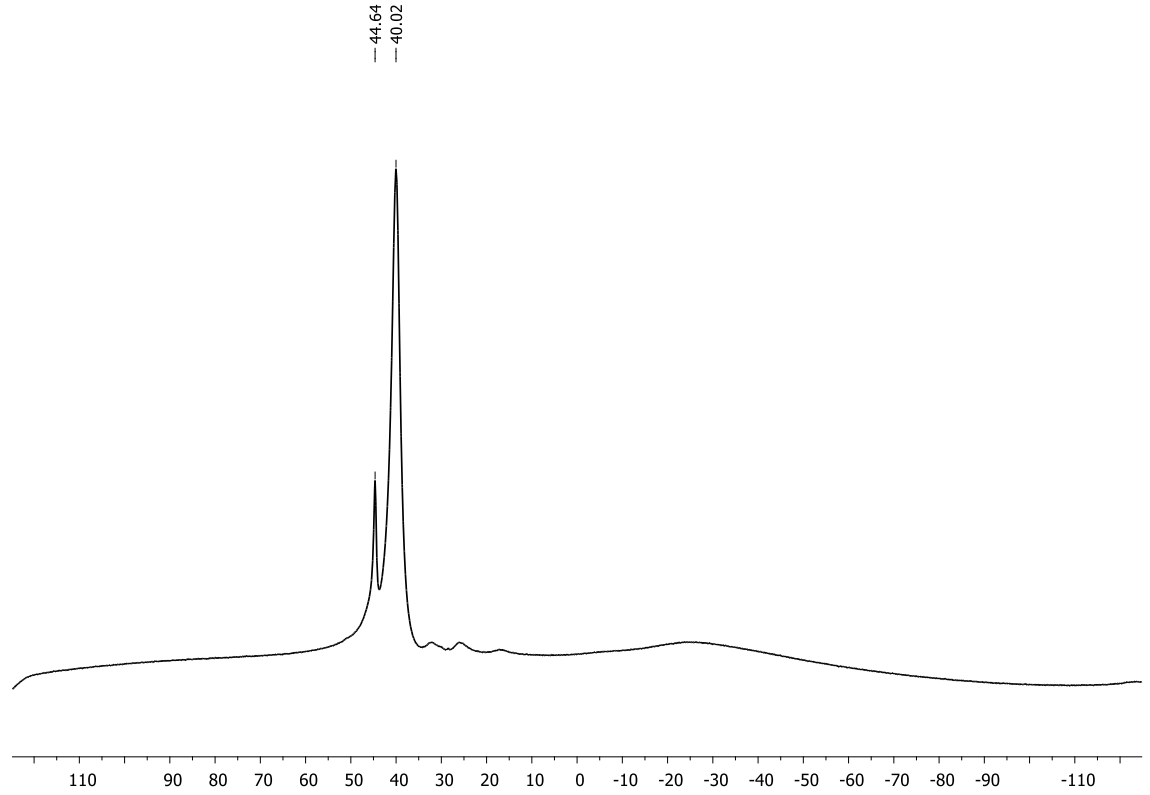

Figure 5.6.43. ^{11}B{^{1}H} NMR spectrum of a mixture of **1b^{Me}** and **12b^{Me}** in the presence of catalyst **E** (5mol%) (CD_2Cl_2, 96 MHz).

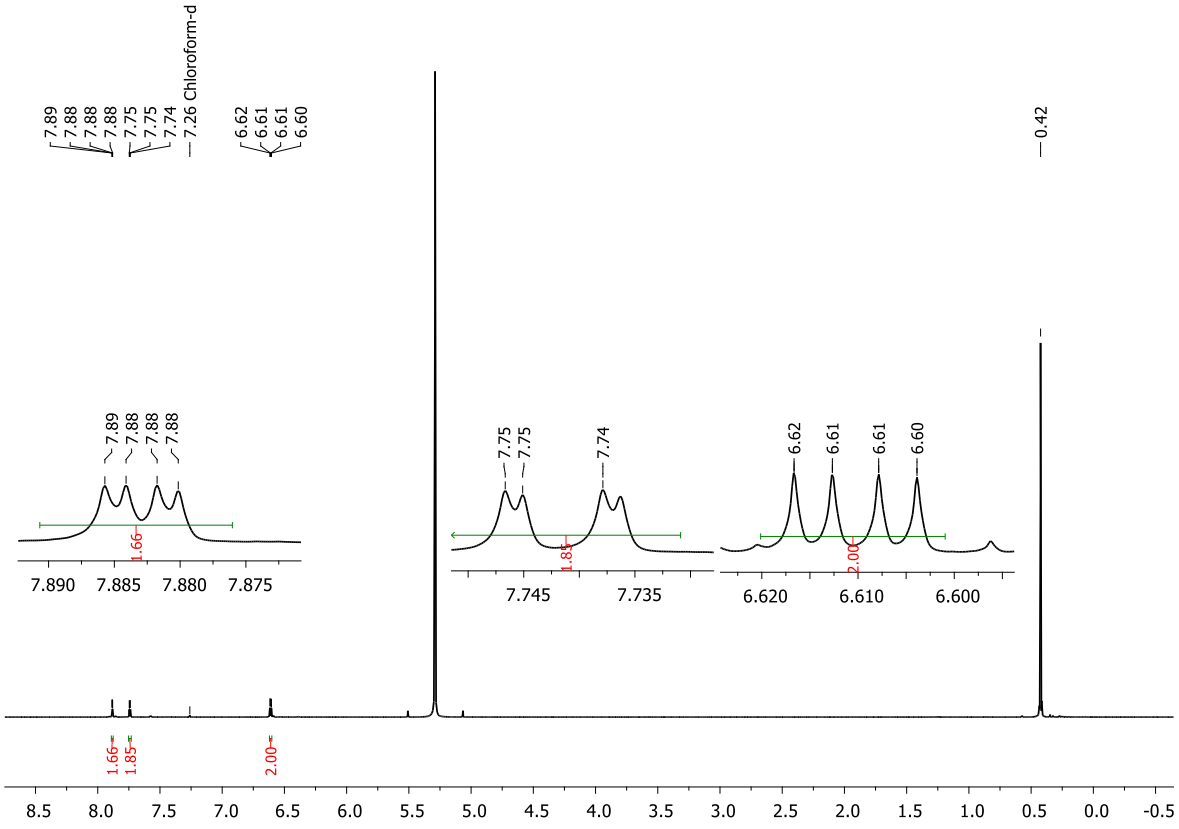

Figure 5.6.44. ^{1}H NMR spectrum of a mixture of **1b** and **12b** in the presence of catalyst **F** (5 mol%) ($CDCl_3$, 300 MHz).

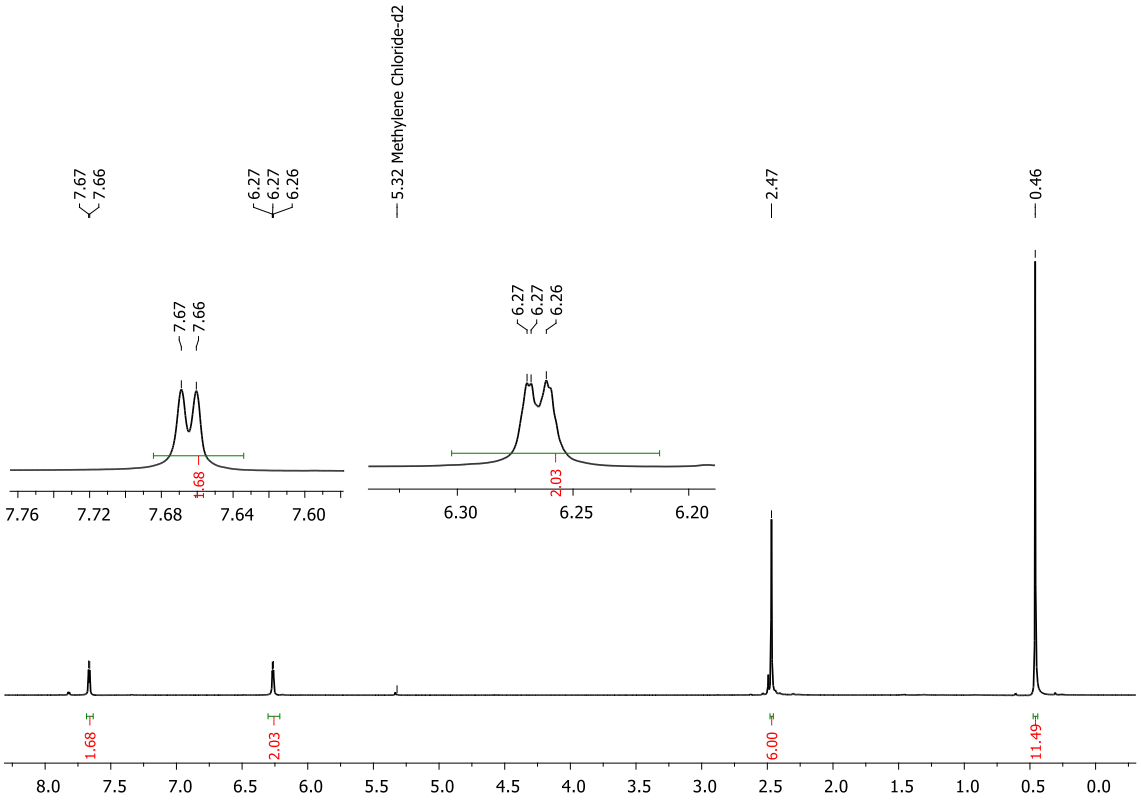

Figure 5.6.45. ^{1}H NMR spectrum of a mixture of **1b^{Me}** and **12b^{Me}** in the presence of catalyst **F** (5 mol%) (CD_2Cl_2, 300 MHz).

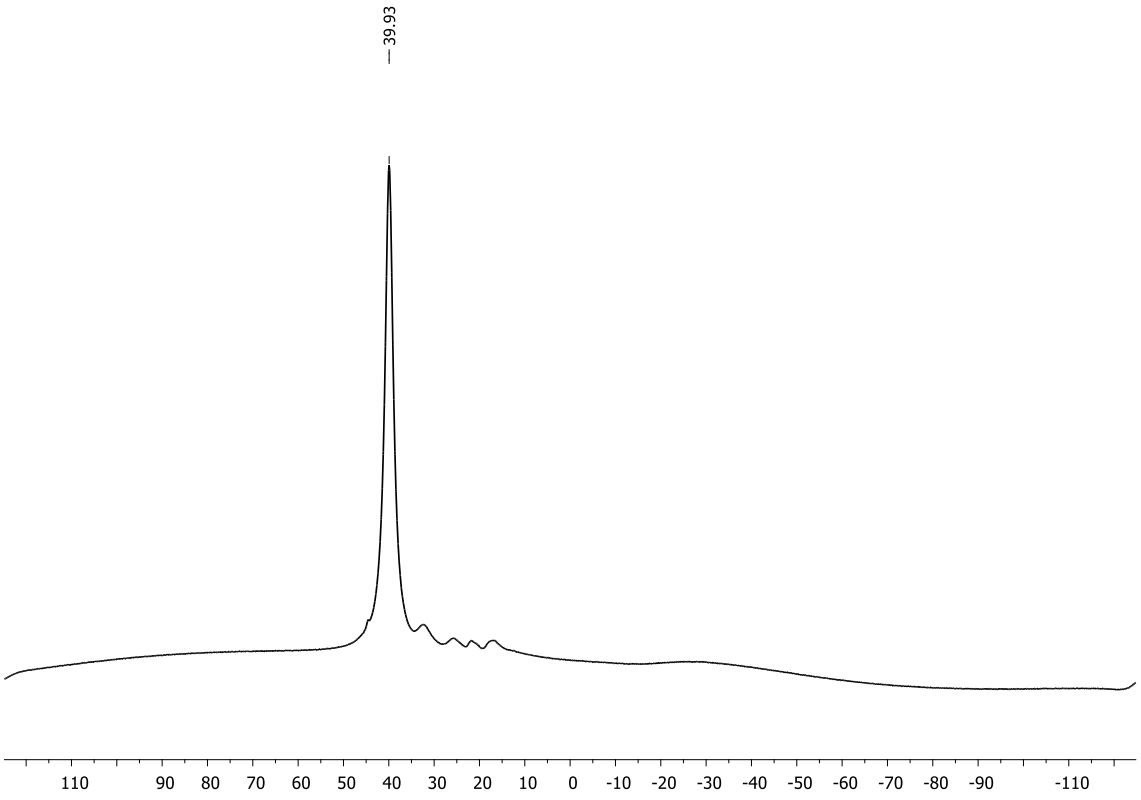

Figure 5.6.46. $^{11}B\{^{1}H\}$ NMR spectrum of a mixture of **1b^{Me}** and **12b^{Me}** in the presence of catalyst **F** (5 mol%) (CD_2Cl_2, 96 MHz).

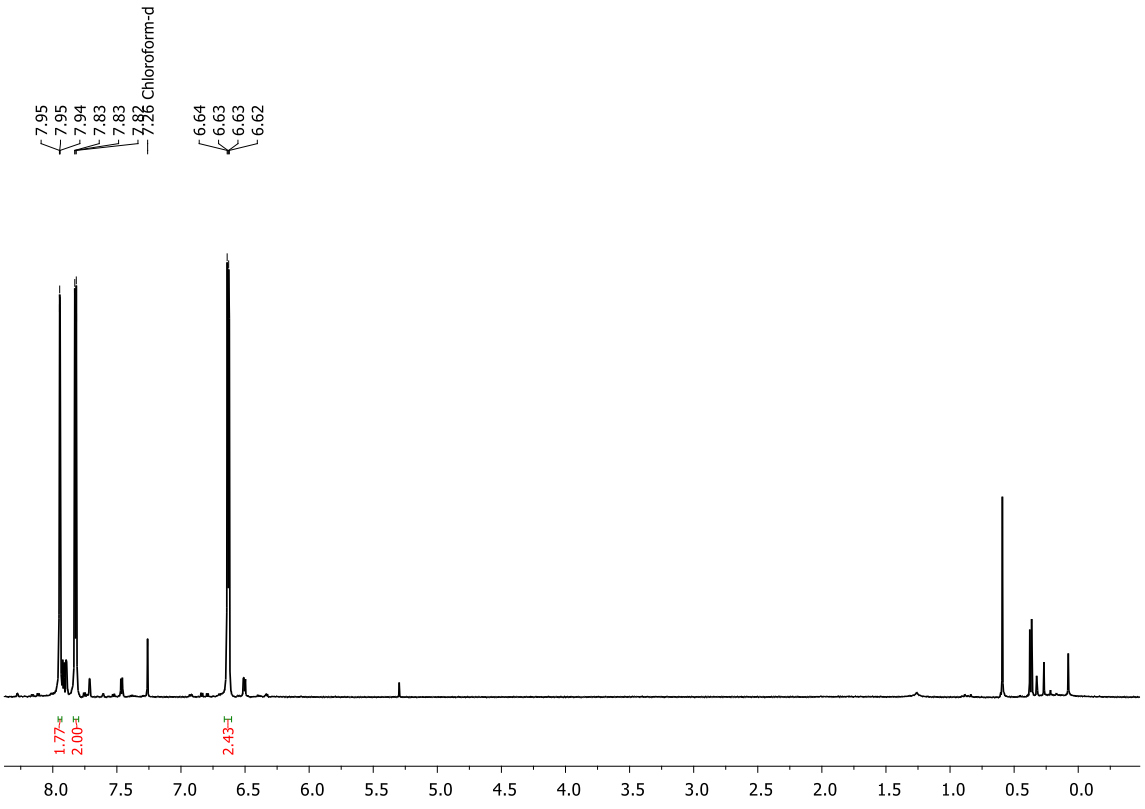

Figure 5.6.47. ^{1}H NMR spectrum of a mixture of **1b** and **2b** in the presence of catalyst **E** (5 mol%) and applying HV ($CDCl_3$, 300 MHz).

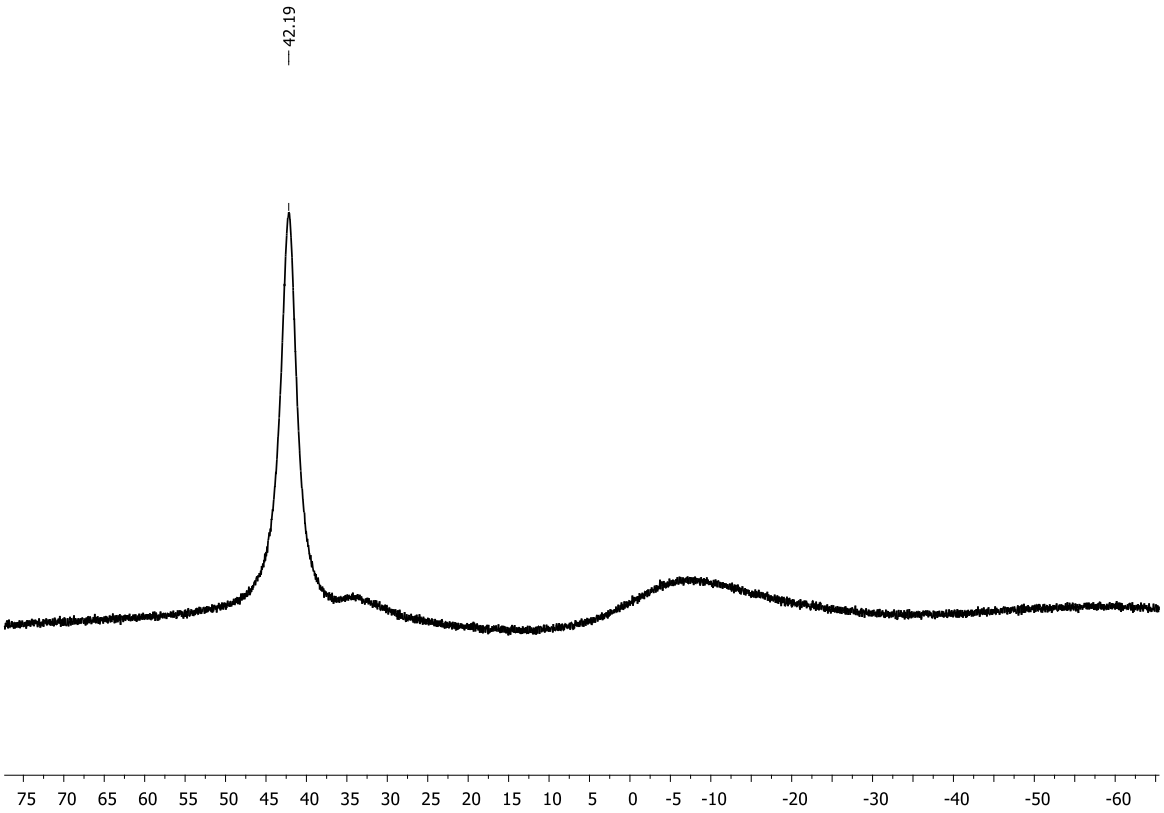

Figure 5.6.48. $^{11}B\{^{1}H\}$ NMR spectrum of a mixture of **1b** and **2b** in the presence of catalyst **E** (5 mol%) and applying HV ($CDCl_3$, 96 MHz).

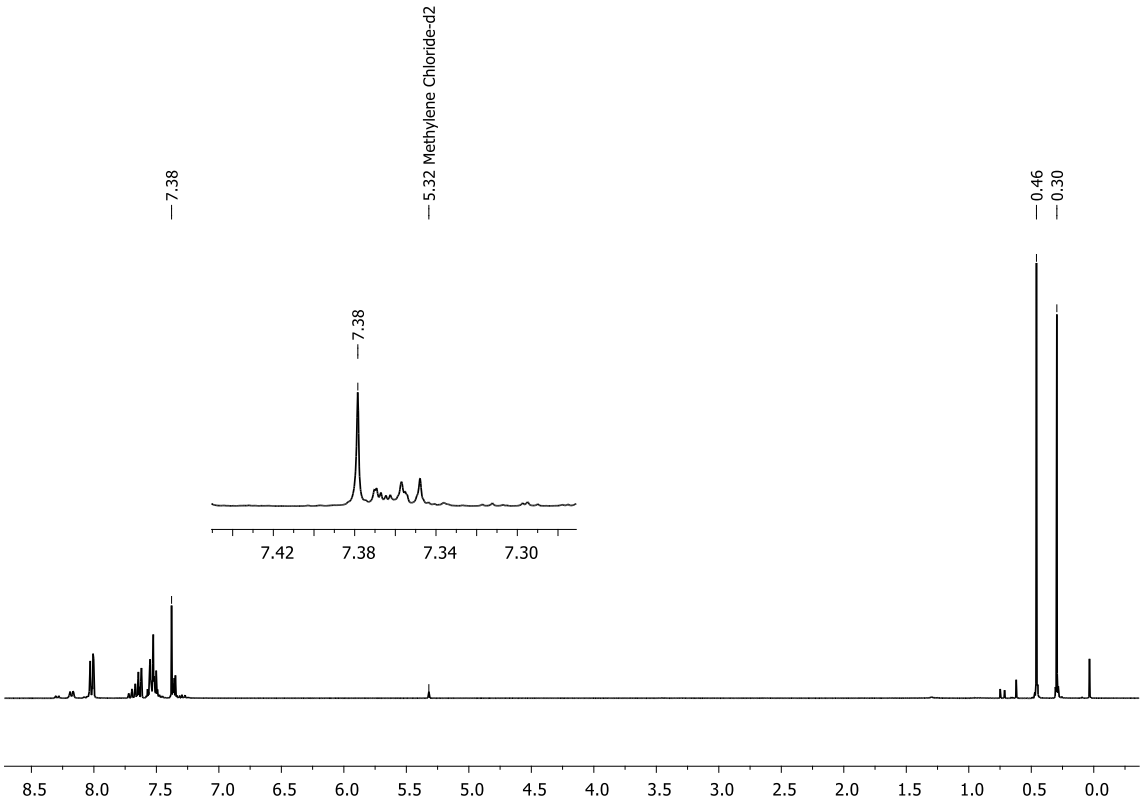

Figure 5.6.49. ^{1}H NMR spectrum of a mixture of **1c** and **12c** in the presence of catalyst **E** (5 mol%) after 3 d (CD_2Cl_2, 300 MHz).

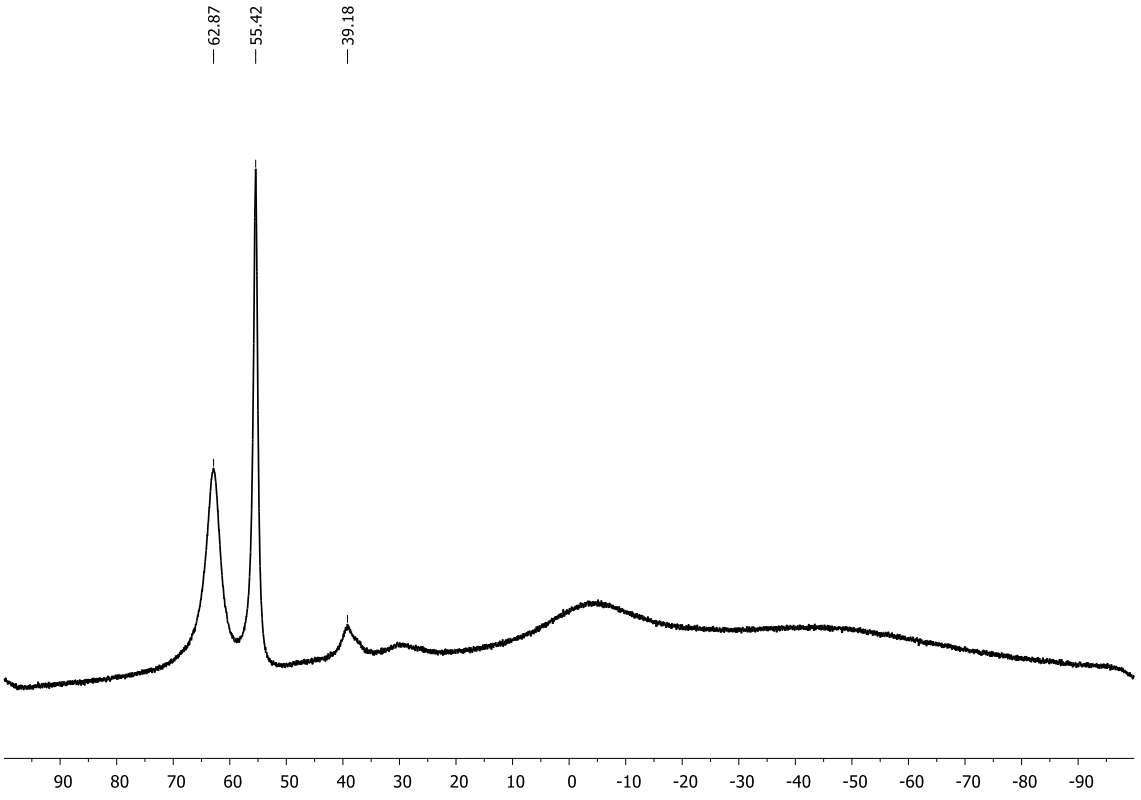

Figure 5.6.50. $^{11}B\{^{1}H\}$ NMR spectrum of a mixture of **1c** and **12c** in the presence of catalyst **E** (5mol%) after 3 d (CD_2Cl_2, 96 MHz).

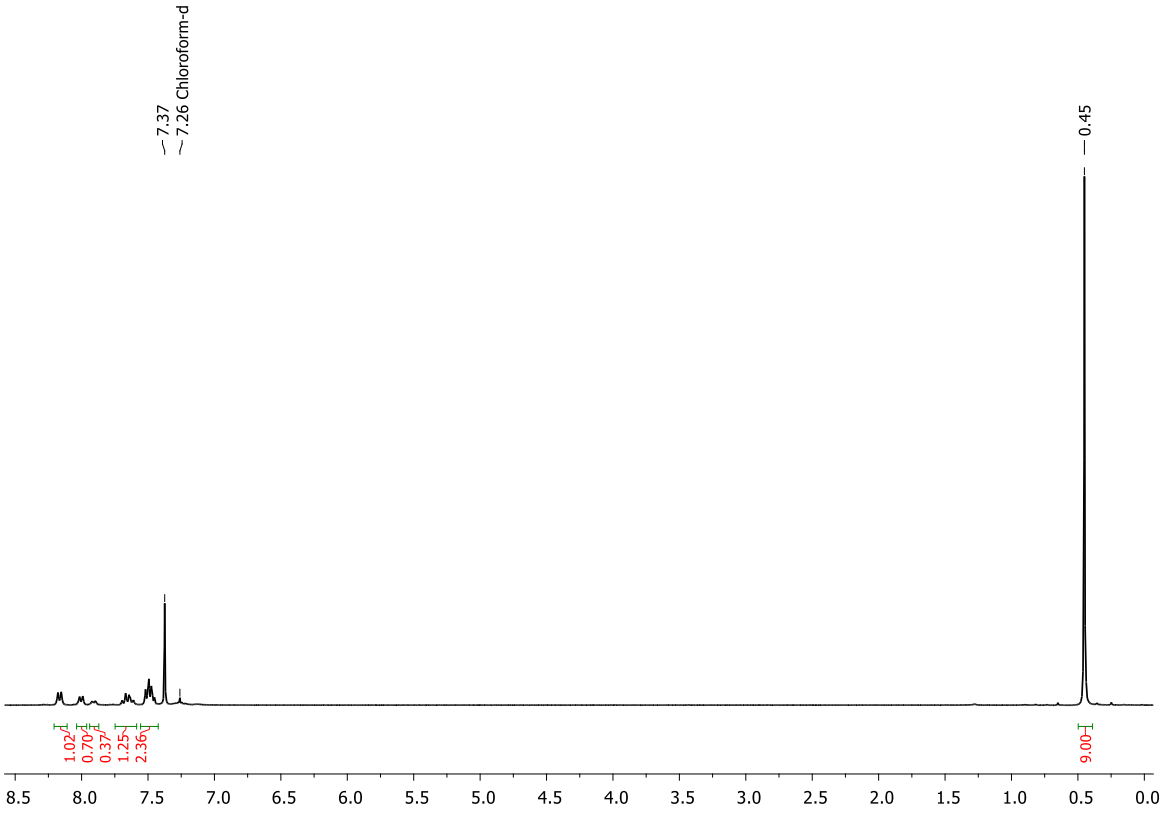

Figure 5.6.51. ^{1}H NMR spectrum of a mixture of **1c** and **12c** in the presence of catalyst **E** (20 mol%) and heating to 70 °C ($CDCl_3$, 300 MHz).

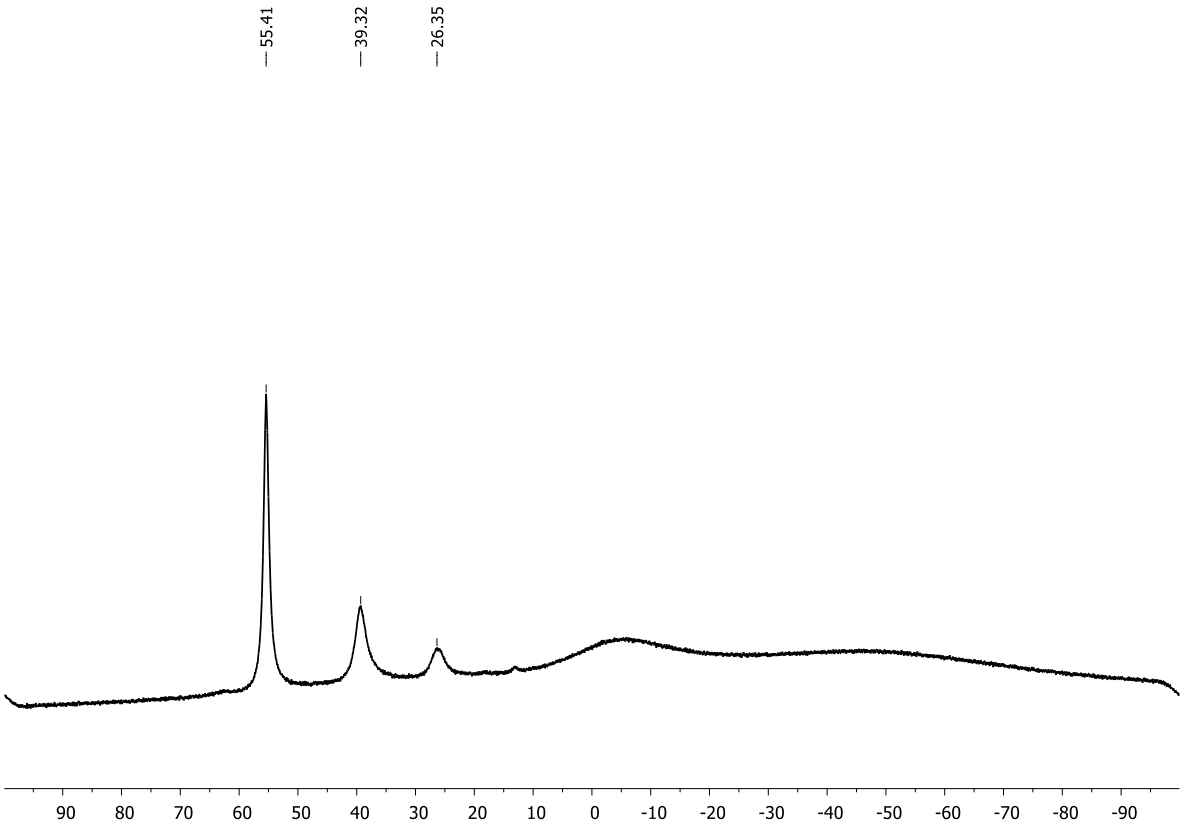

Figure 5.6.52. $^{11}B\{^{1}H\}$ NMR spectrum of a mixture of **1c** and **12c** in the presence of catalyst **E** (20 mol%) and heating to 70 °C ($CDCl_3$, 96 MHz).

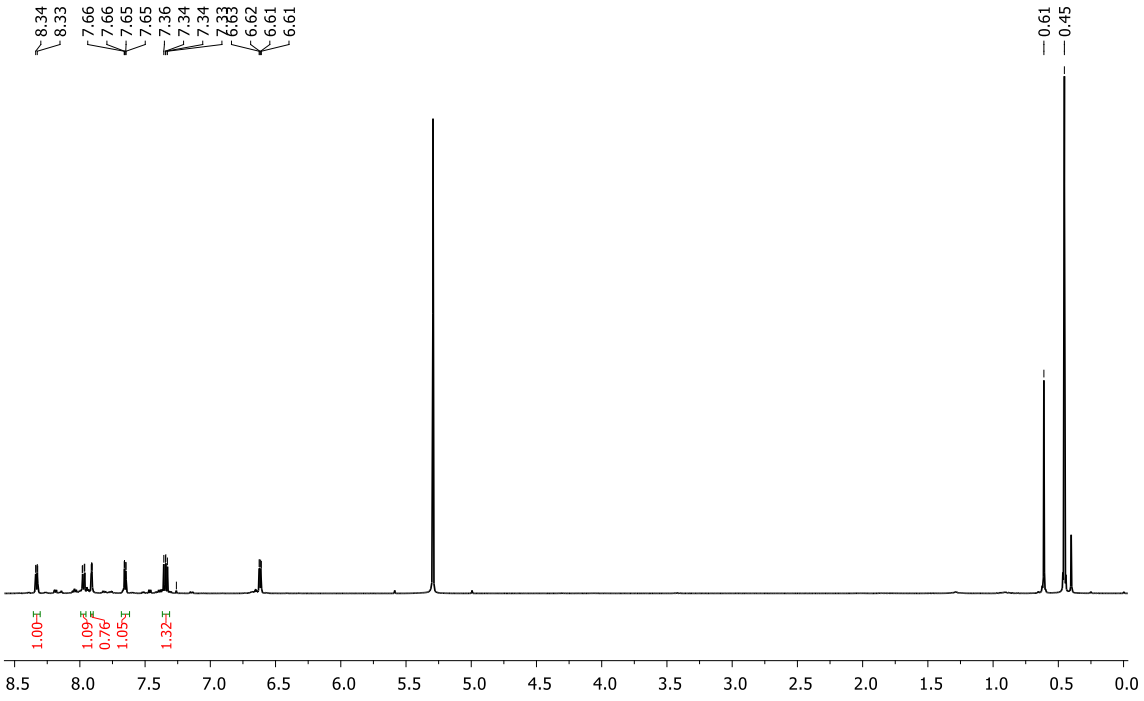

Figure 5.6.53. ^{1}H NMR spectrum of a mixture of **1a** and **12b** in the presence of catalyst **B** (10 mol%) after 19 h ($CDCl_3$, 300 MHz).

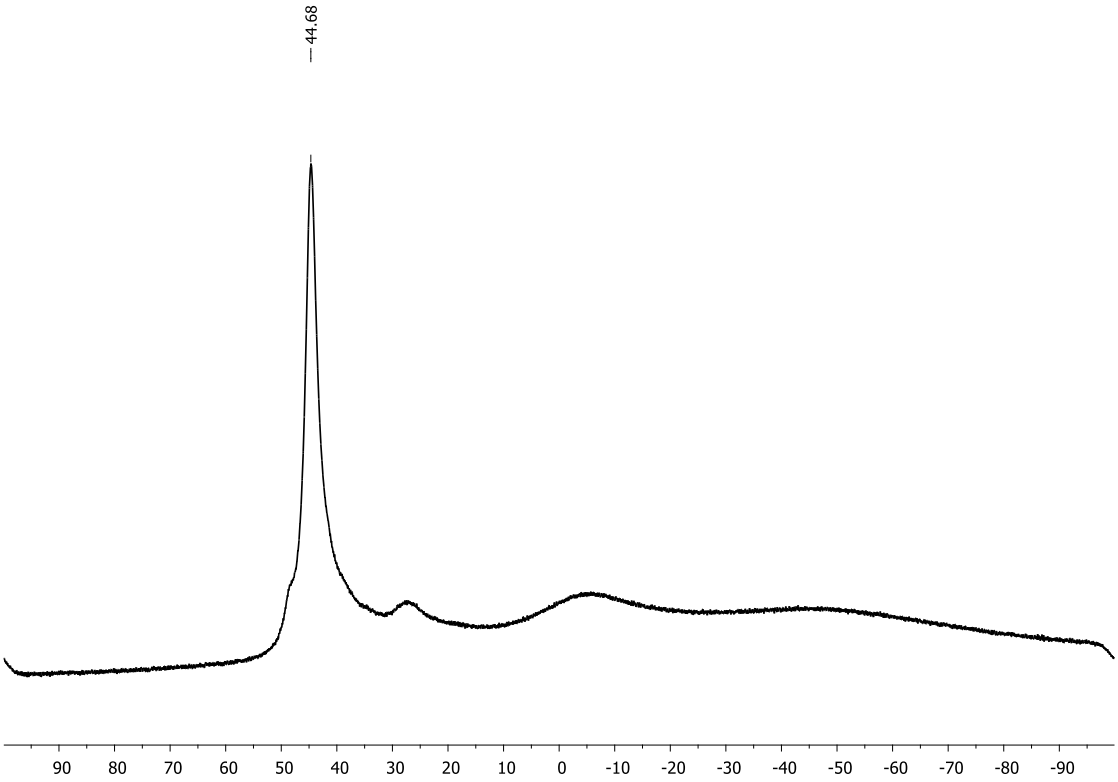

Figure 5.6.54. $^{11}B\{^{1}H\}$ NMR spectrum of a mixture of **1a** and **12b** in the presence of catalyst **B** (10 mol%) after 19 h ($CDCl_3$, 96 MHz).

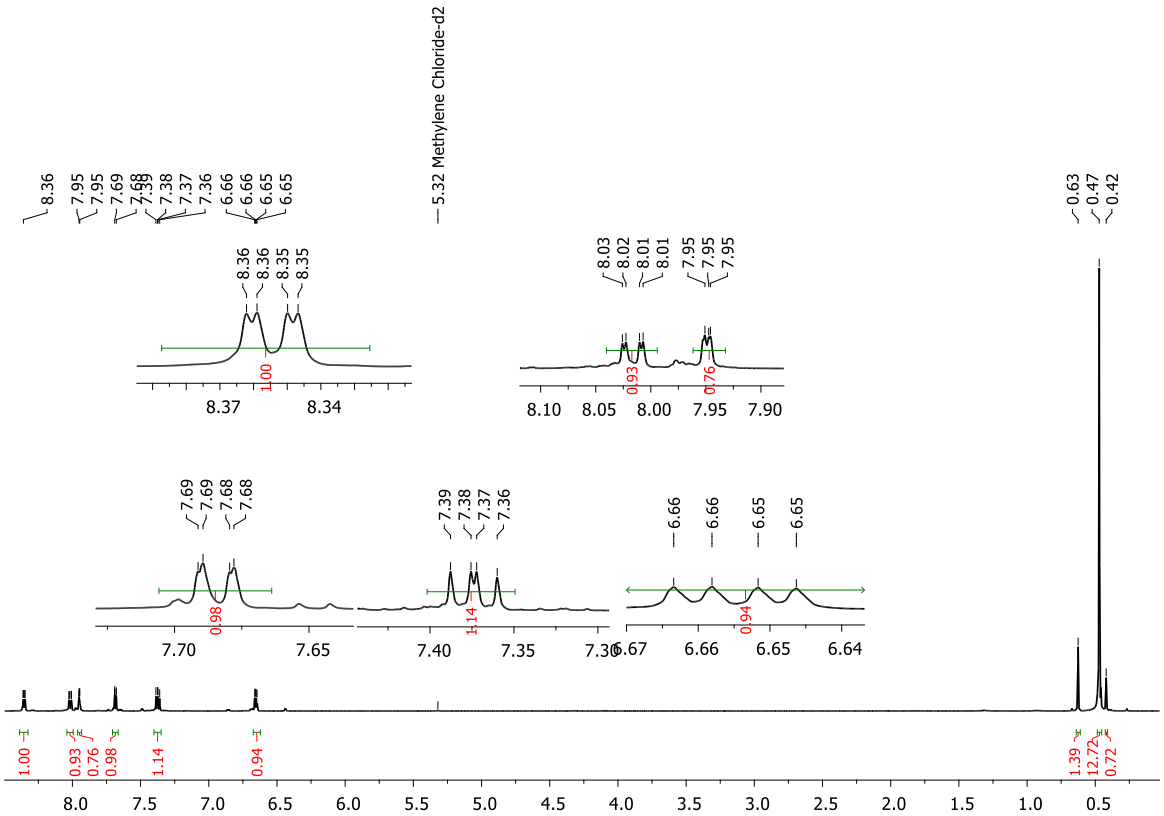

Figure 5.6.55. ^{1}H NMR spectrum of a mixture of **1b** and **12a** in the presence of catalyst **B** (10 mol%) after 24 h (CD_2Cl_2, 300 MHz).

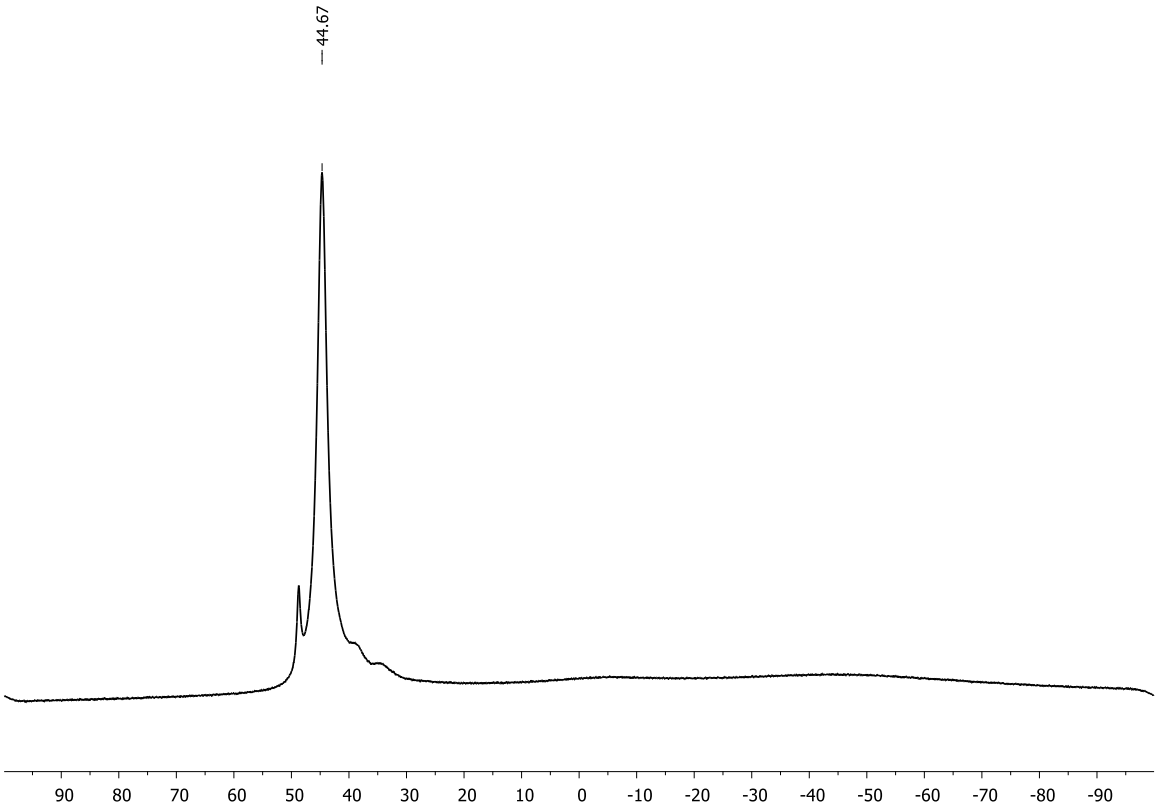

Figure 5.6.56. $^{11}B\{^{1}H\}$ NMR spectrum of a mixture of **1b** and **12a** in the presence of catalyst **B** (10 mol%) after 24 h (CD_2Cl_2, 96 MHz).

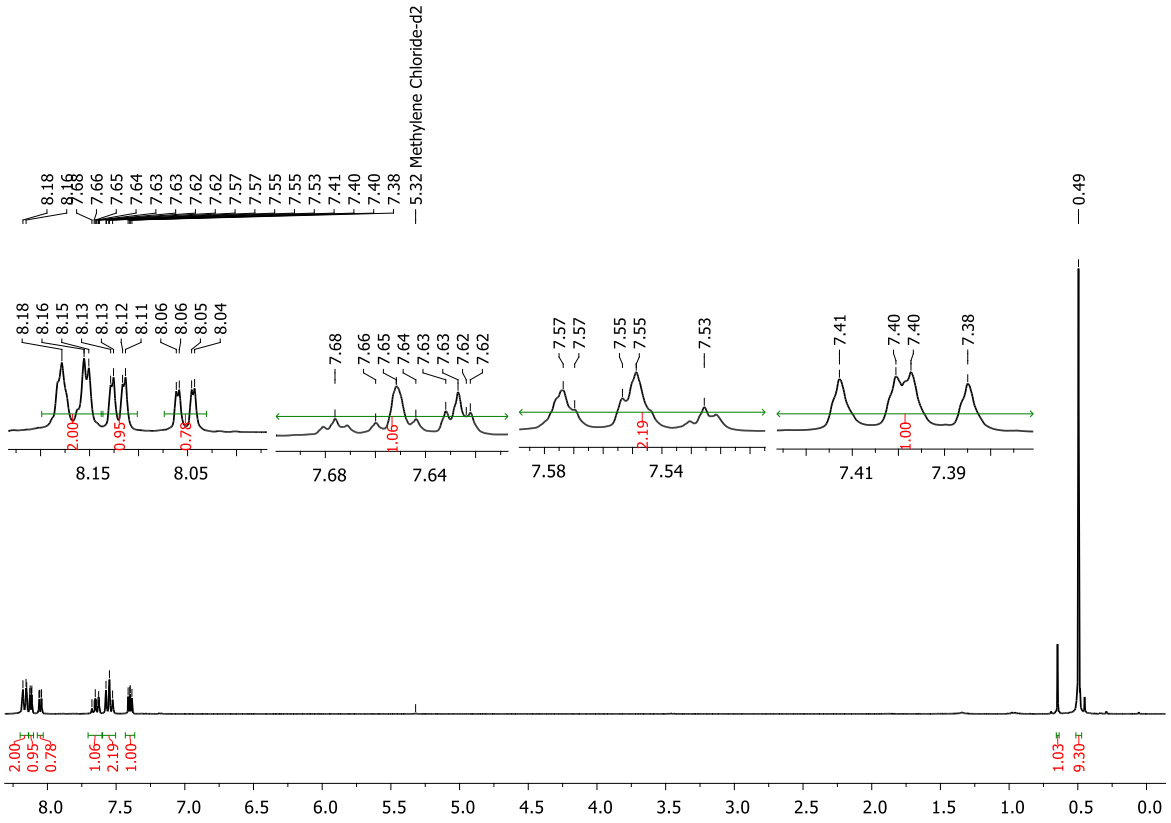

Figure 5.6.57. ^{1}H NMR spectrum of a mixture of **1a** and **12c** in the presence of catalyst **B** (10 mol%) after 24 h (CD_2Cl_2, 300 MHz).

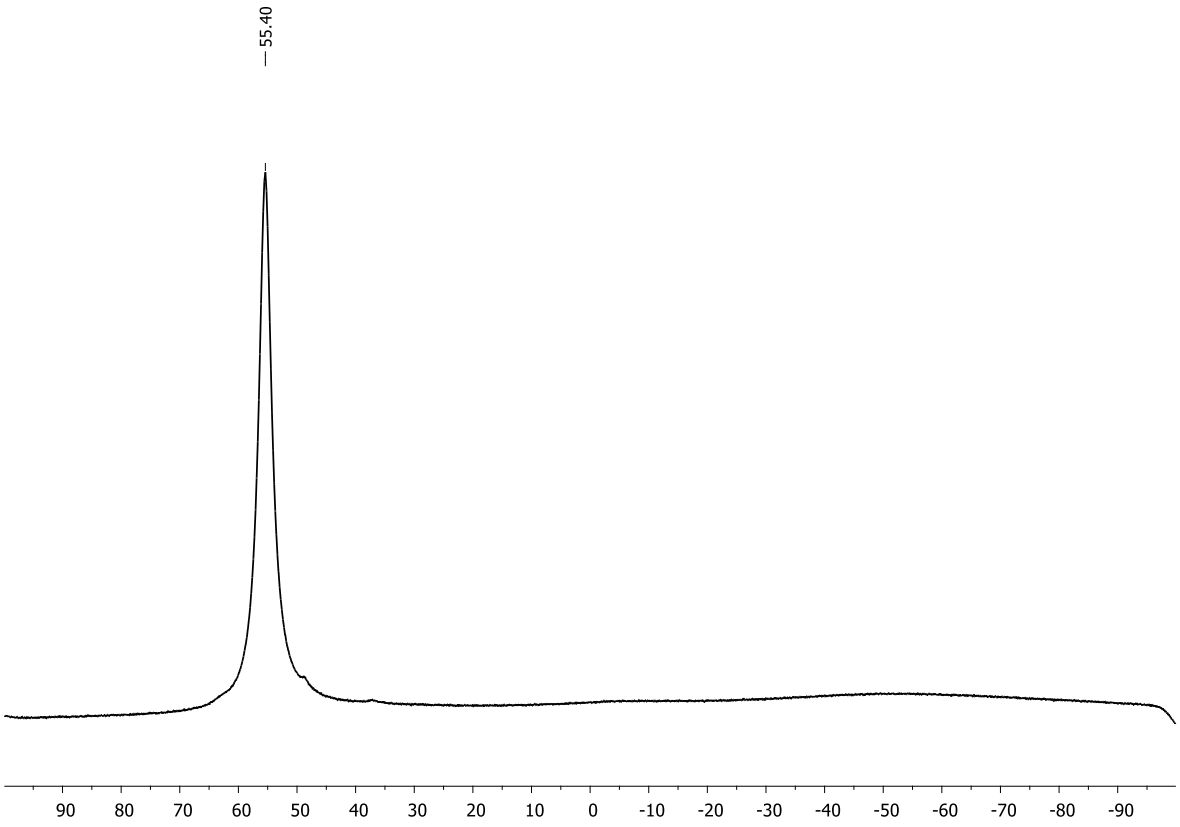

Figure 5.6.58. $^{11}B\{^{1}H\}$ NMR spectrum of a mixture of **1a** and **12c** in the presence of catalyst **B** (10 mol%) after 24 h (CD_2Cl_2, 96 MHz).

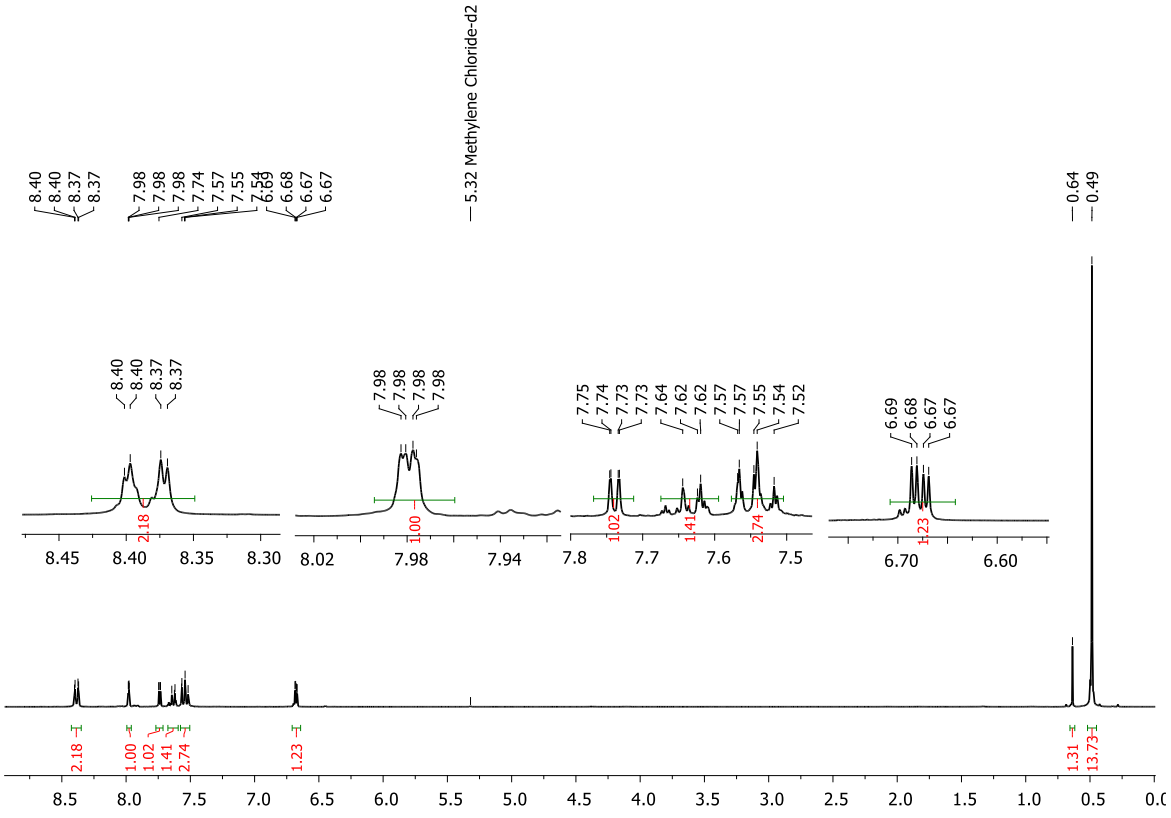

Figure 5.6.59. ^{1}H NMR spectrum of a mixture of **1b** and **12c** in the presence of catalyst **B** (10 mol%) after 24 h (CD_2Cl_2, 300 MHz).

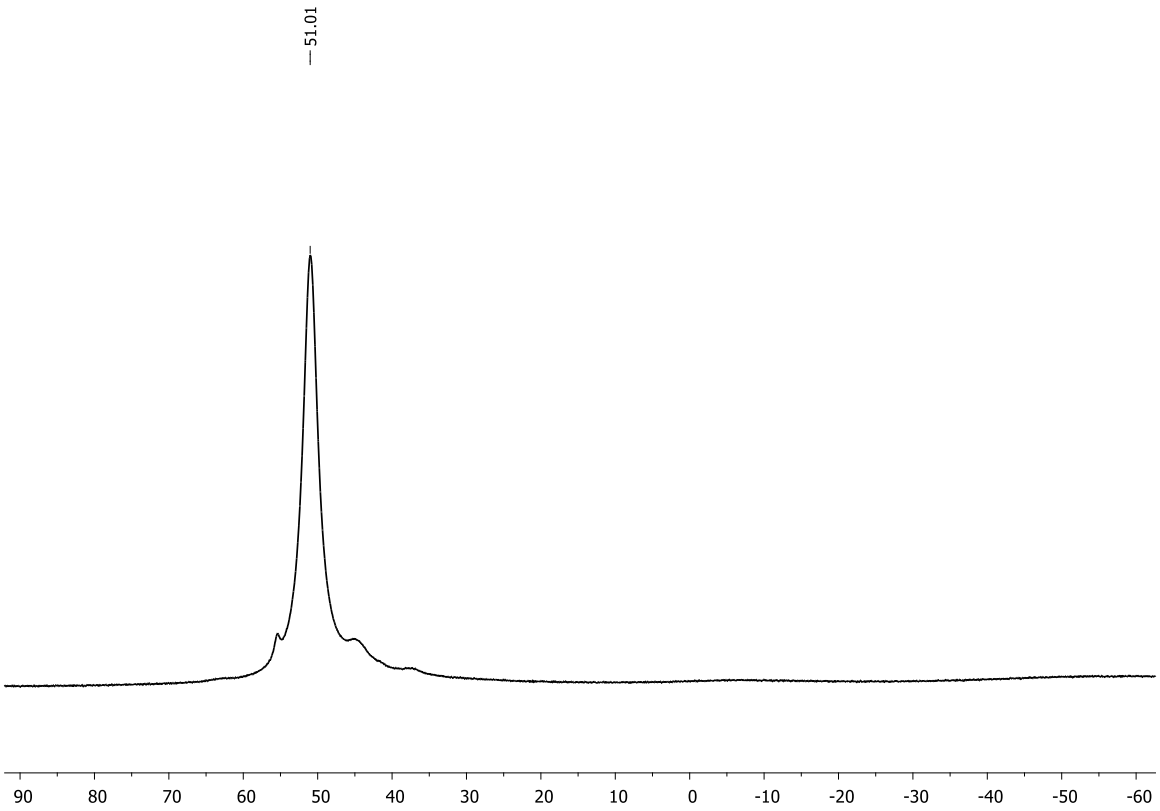

Figure 5.6.60. $^{11}B\{^{1}H\}$ NMR spectrum of a mixture of **1b** and **12c** in the presence of catalyst **B** (10 mol%) after 24 h (CD_2Cl_2, 96 MHz).

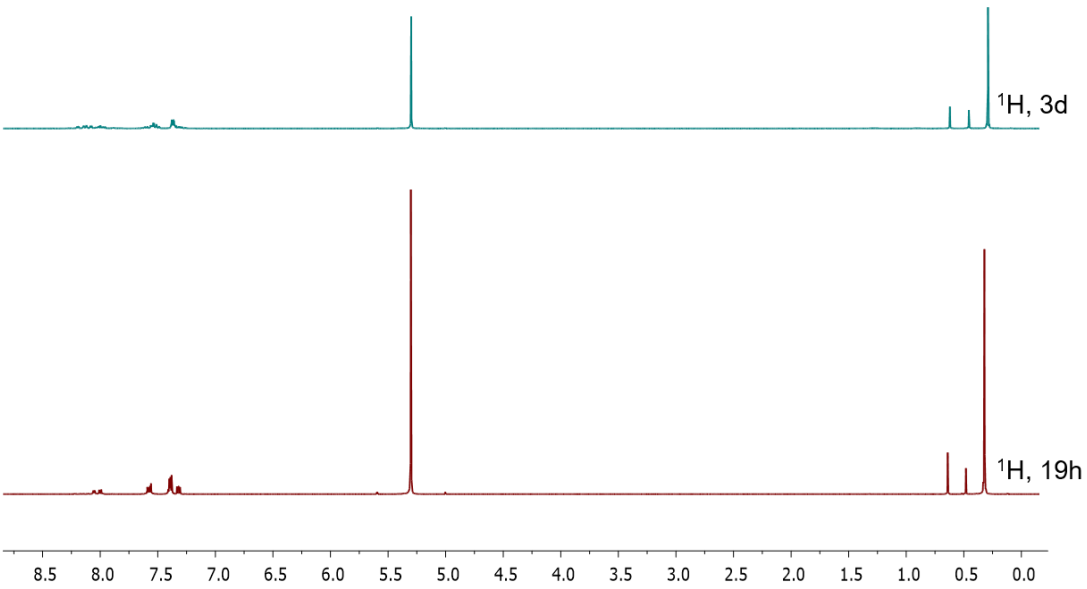

Figure 5.6.61. ^{1}H NMR spectrum of a mixture of **1c** and **12a** in the presence of catalyst **B** (10 mol%) after 19 h (red) and 3 d (teal) ($CDCl_3$, 300 MHz).

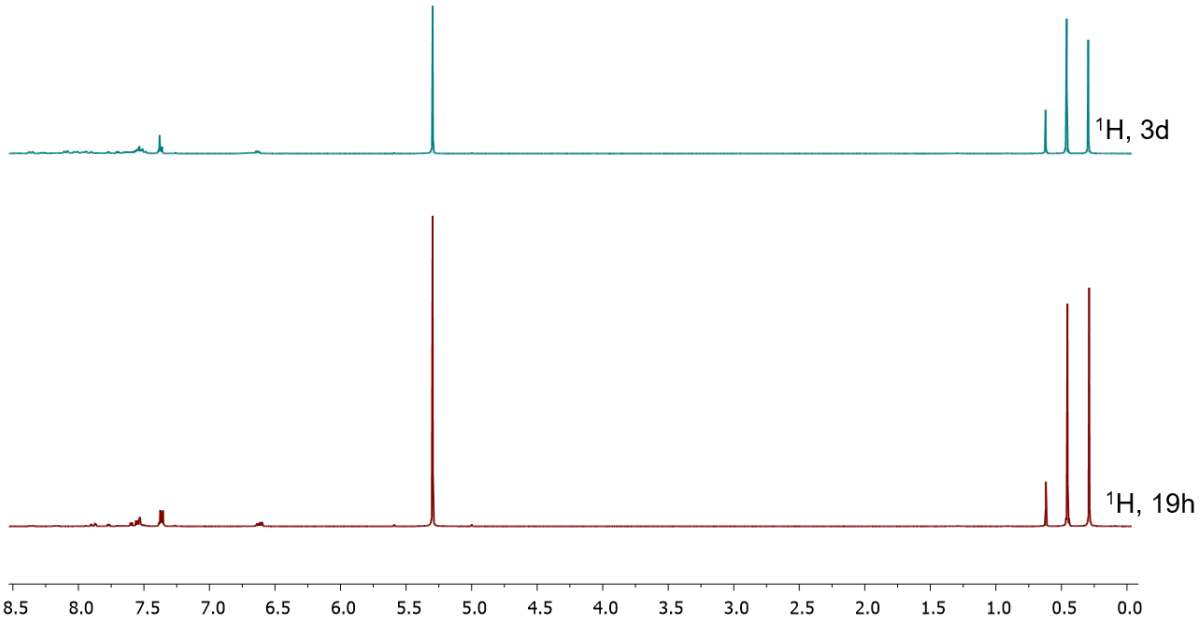

Figure 5.6.62. ^{1}H NMR spectrum of a mixture of **1c** and **12b** in the presence of catalyst **B** (10 mol%) after 19 h (red) and 3 d (teal) ($CDCl_3$, 300 MHz).

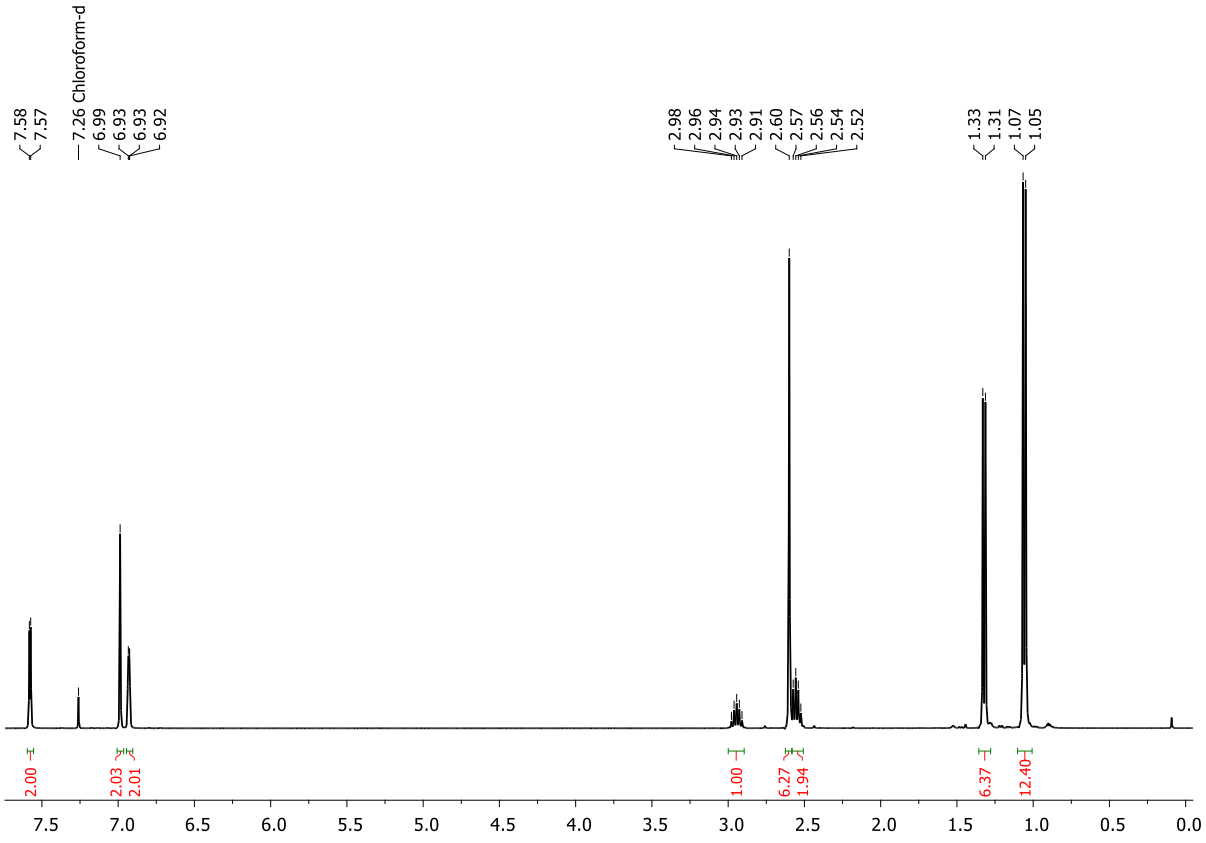

Figure 5.6.63. ^{1}H NMR spectrum of **4a^{MeTip}** (400 MHz, in $CDCl_3$).

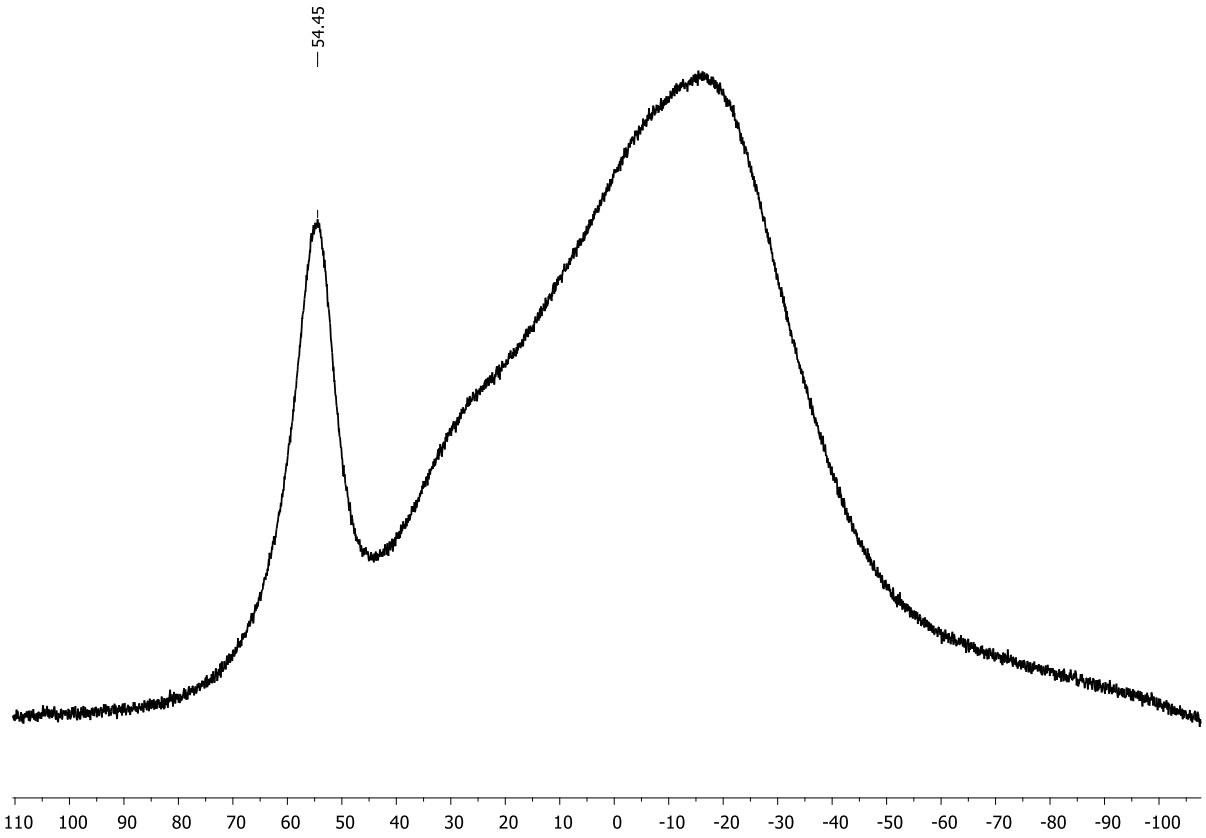

Figure 5.6.64. $^{11}B\{^{1}H\}$ NMR spectrum of **4a^{MeTip}** (126 MHz, in $CDCl_3$).

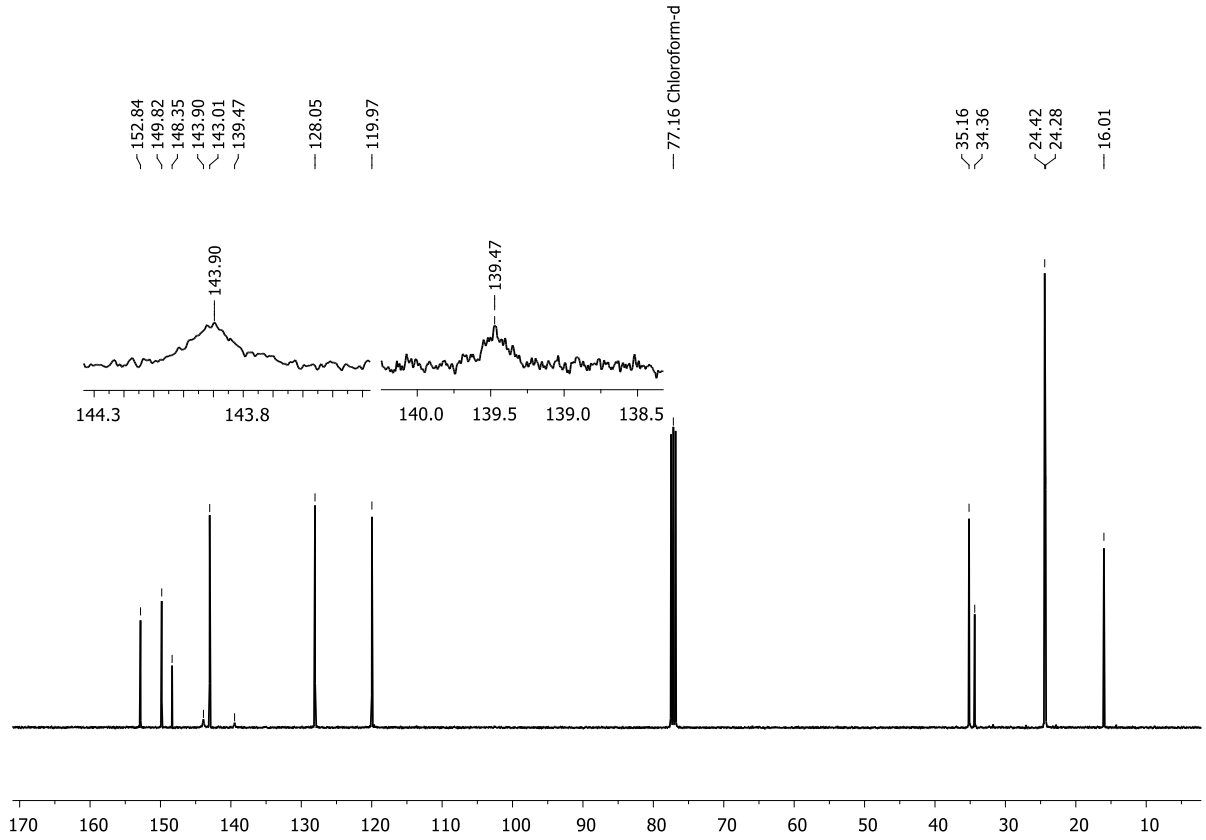

Figure 5.6.65. $^{13}C\{^{1}H\}$ NMR spectrum of **4a^{MeTip}** (101 MHz, in $CDCl_3$).

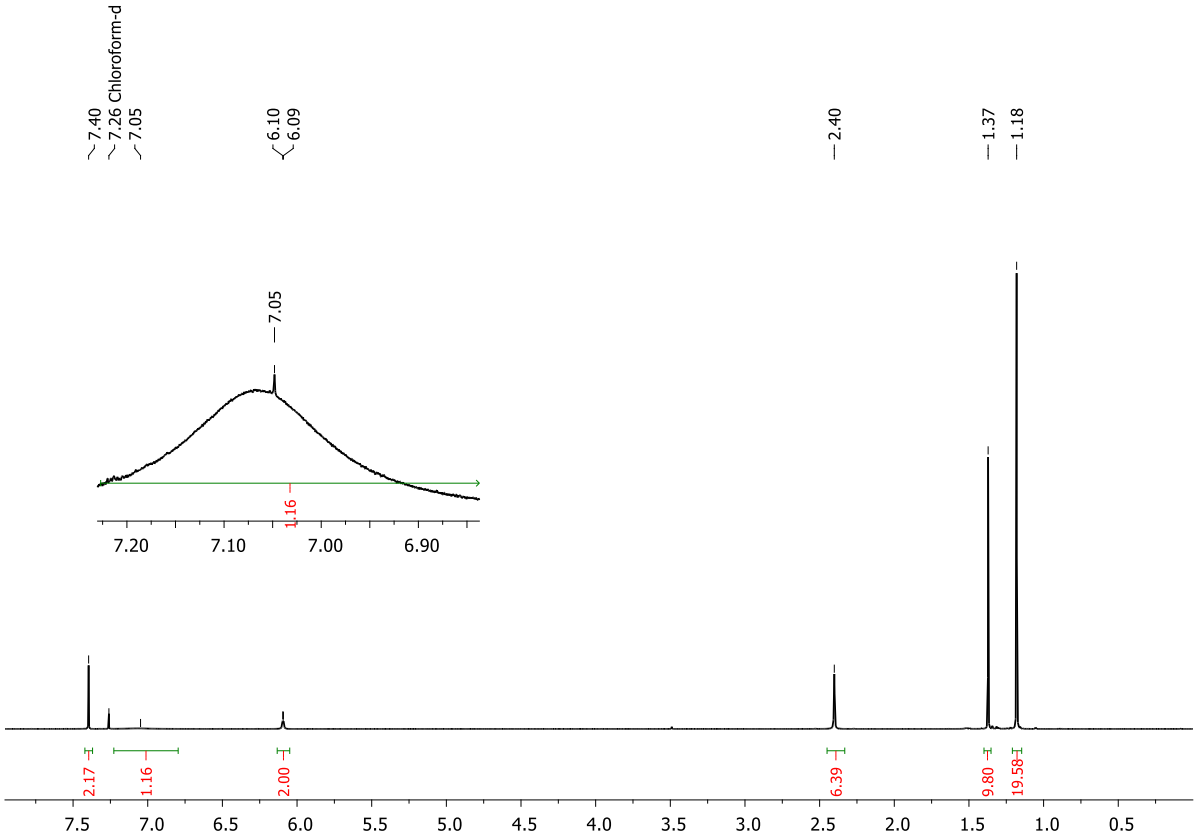

Figure 5.6.66. ^{1}H NMR spectrum of **4b^{MeMes*}** (500 MHz, in $CDCl_3$).

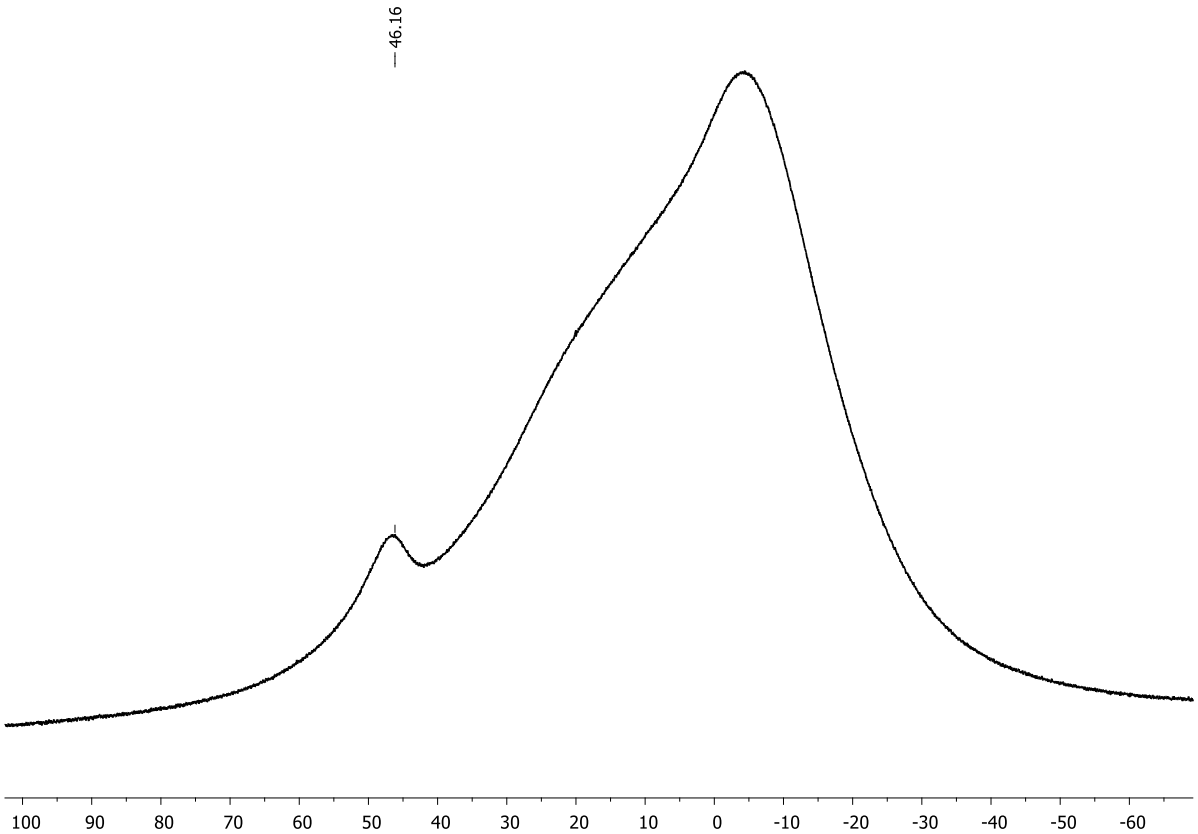

Figure 5.6.67. ^{11}B{^{1}H} NMR spectrum of **4b^{MeMes*}** (160 MHz, in $CDCl_3$).

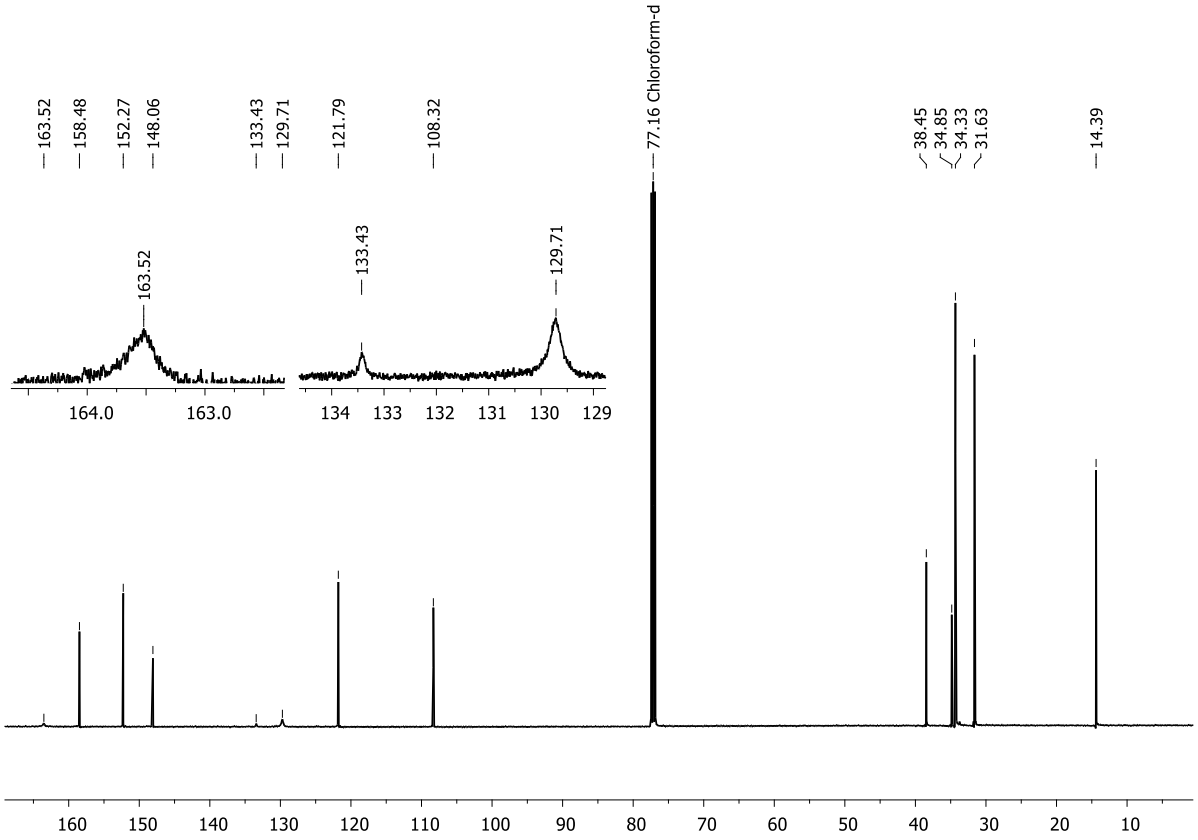

Figure 5.6.68. $^{13}C\{^{1}H\}$ NMR spectrum of **4b**$^{\mathbf{MeMes*}}$ (126 MHz, in $CDCl_3$).

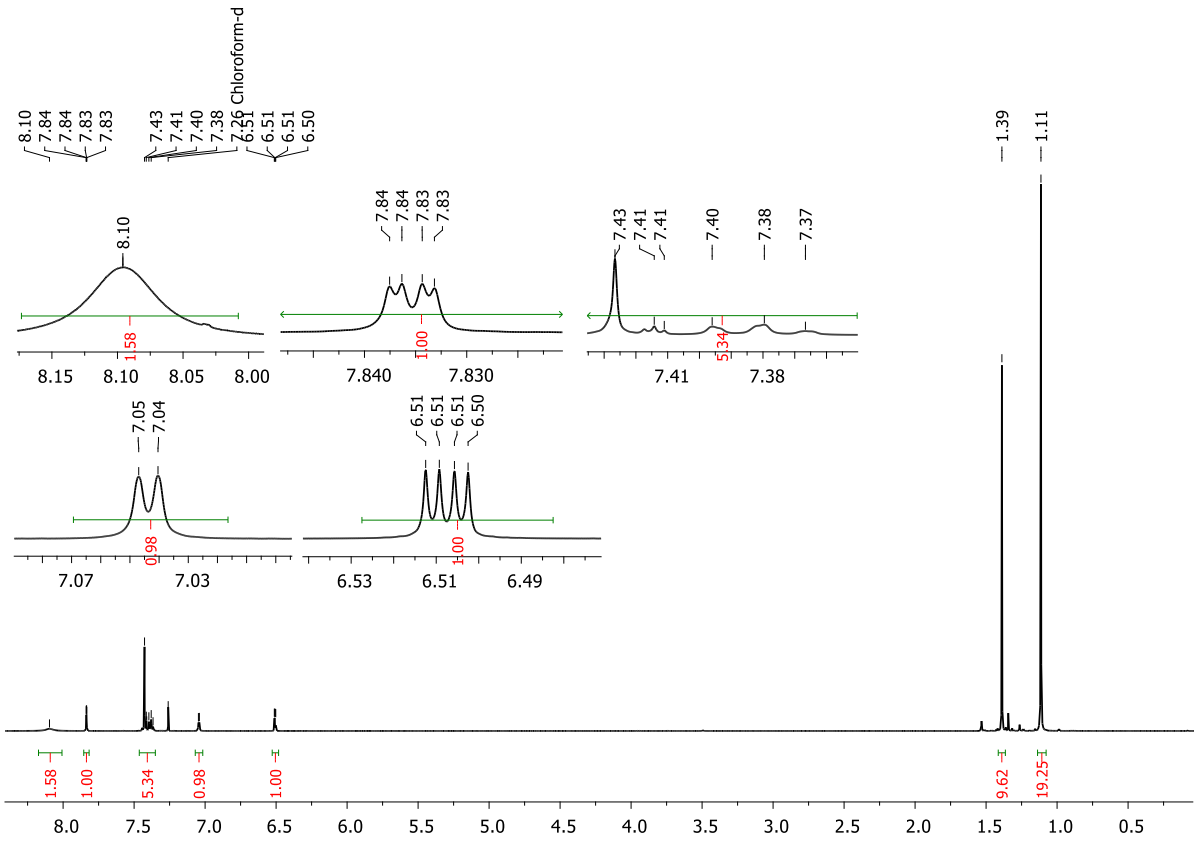

Figure 5.6.69. ^{1}H NMR spectrum of **4bc**$^{\mathbf{Mes*}}$ (500 MHz, in $CDCl_3$).

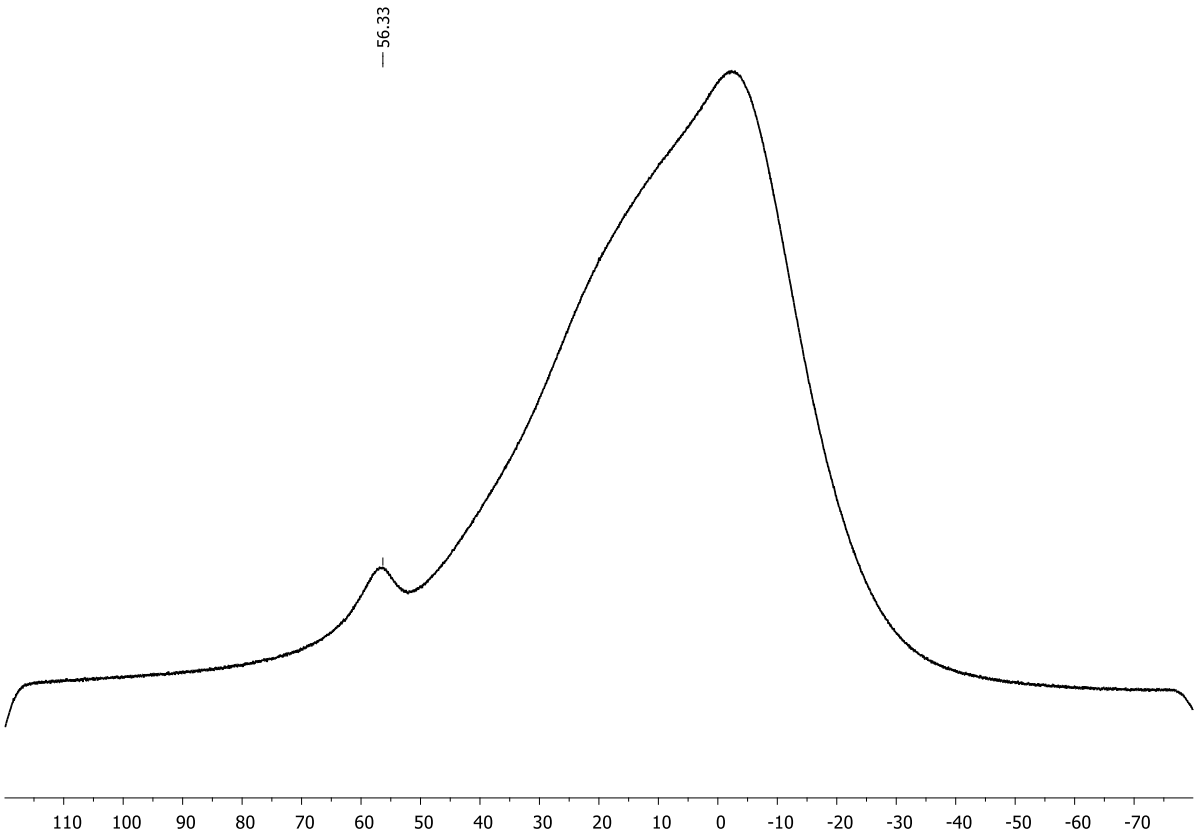

Figure 5.6.70. $^{11}B\{^{1}H\}$ NMR spectrum of **4bc^{Mes*}** (160 MHz, in $CDCl_3$).

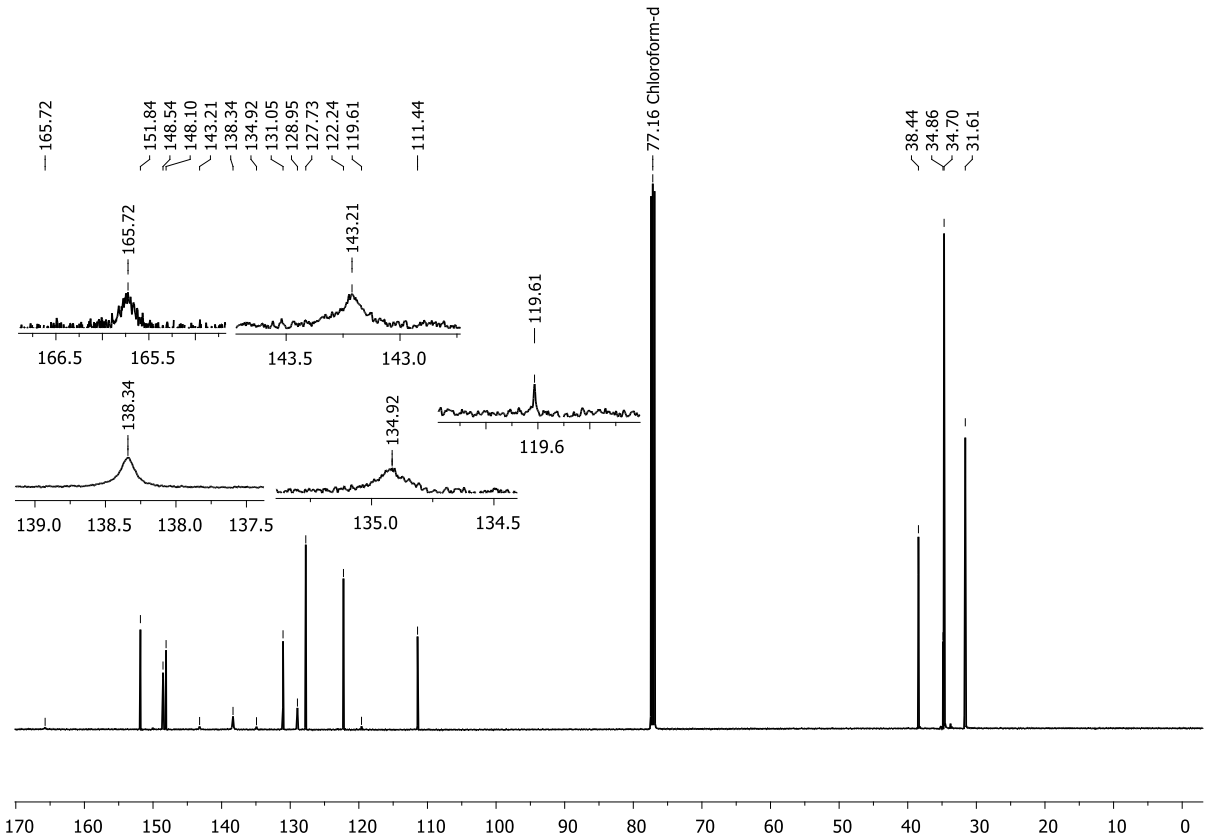

Figure 5.6.71. $^{13}C\{^{1}H\}$ NMR spectrum of **4bc^{Mes*}** (126 MHz, in $CDCl_3$).

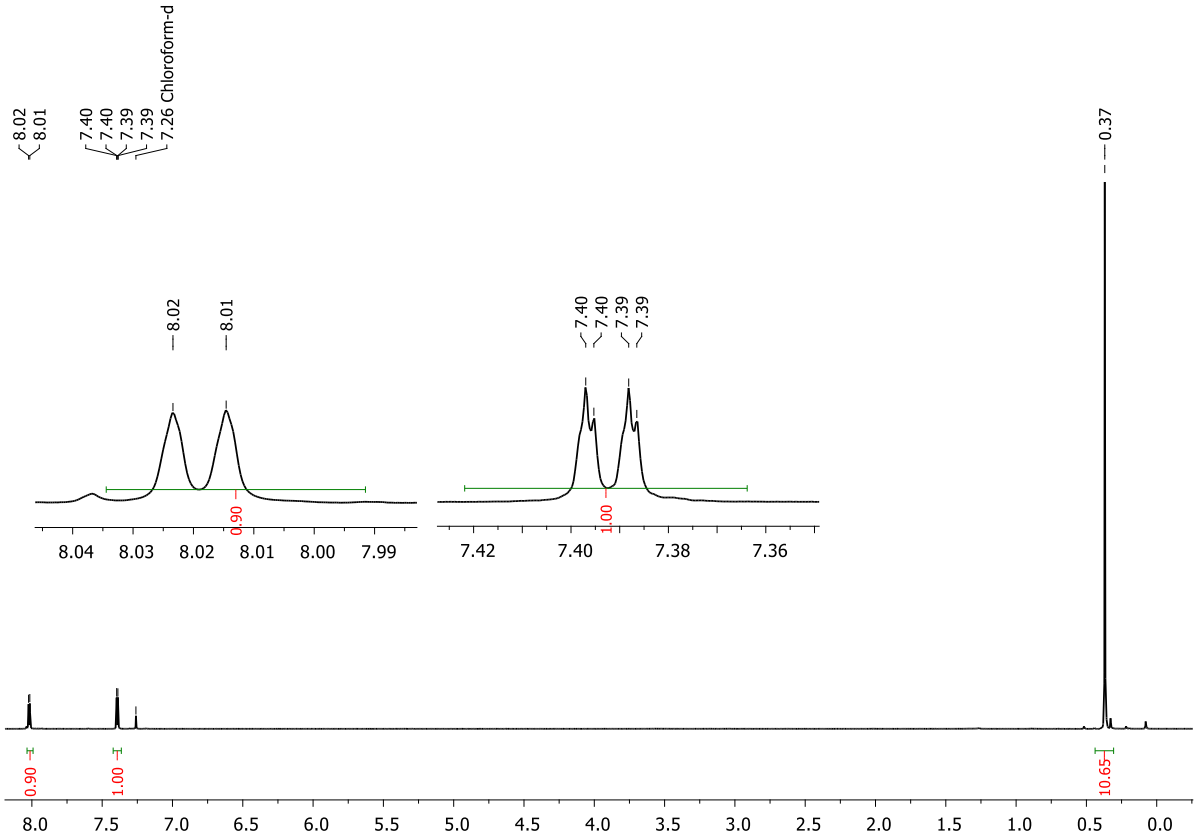

Figure 5.6.72. ^{1}H NMR spectrum of **15a** (400 MHz, in $CDCl_3$).

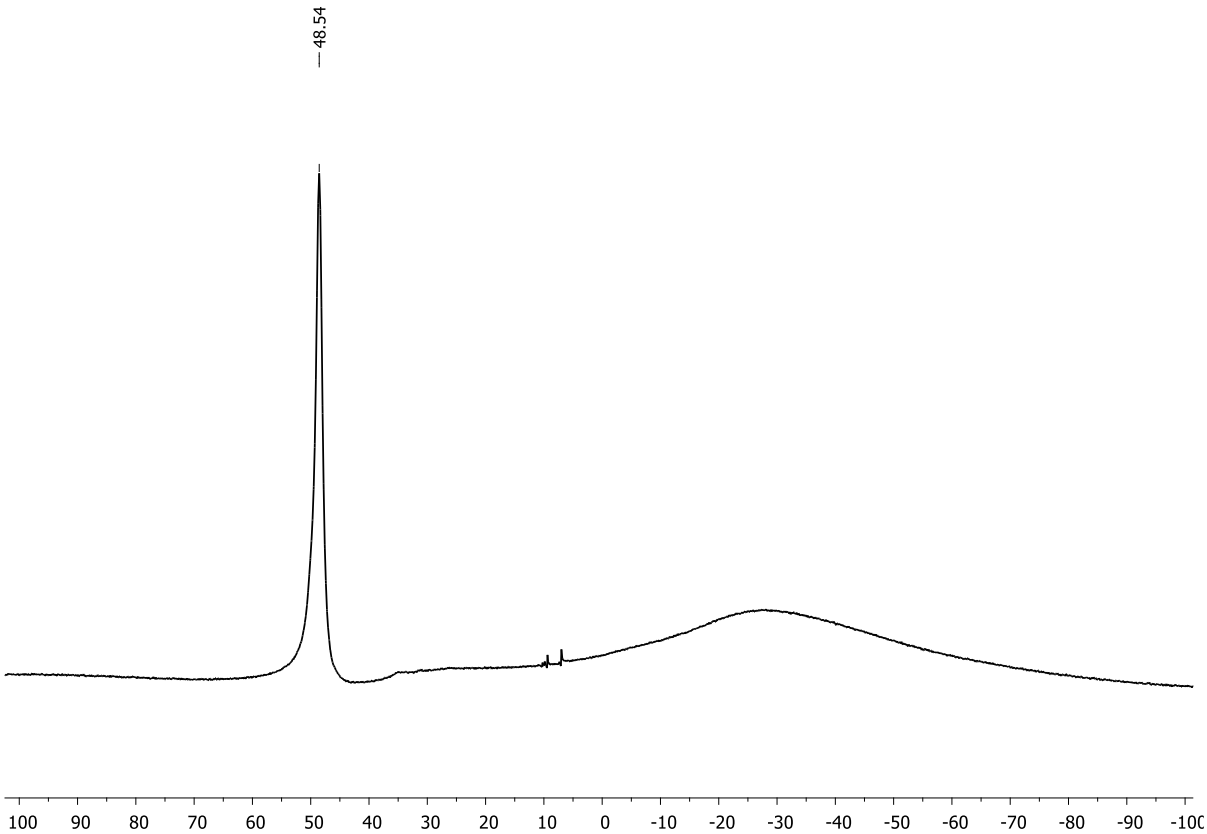

Figure 5.6.73. $^{11}B\{^{1}H\}$ NMR spectrum of **15a** (126 MHz, in $CDCl_3$).

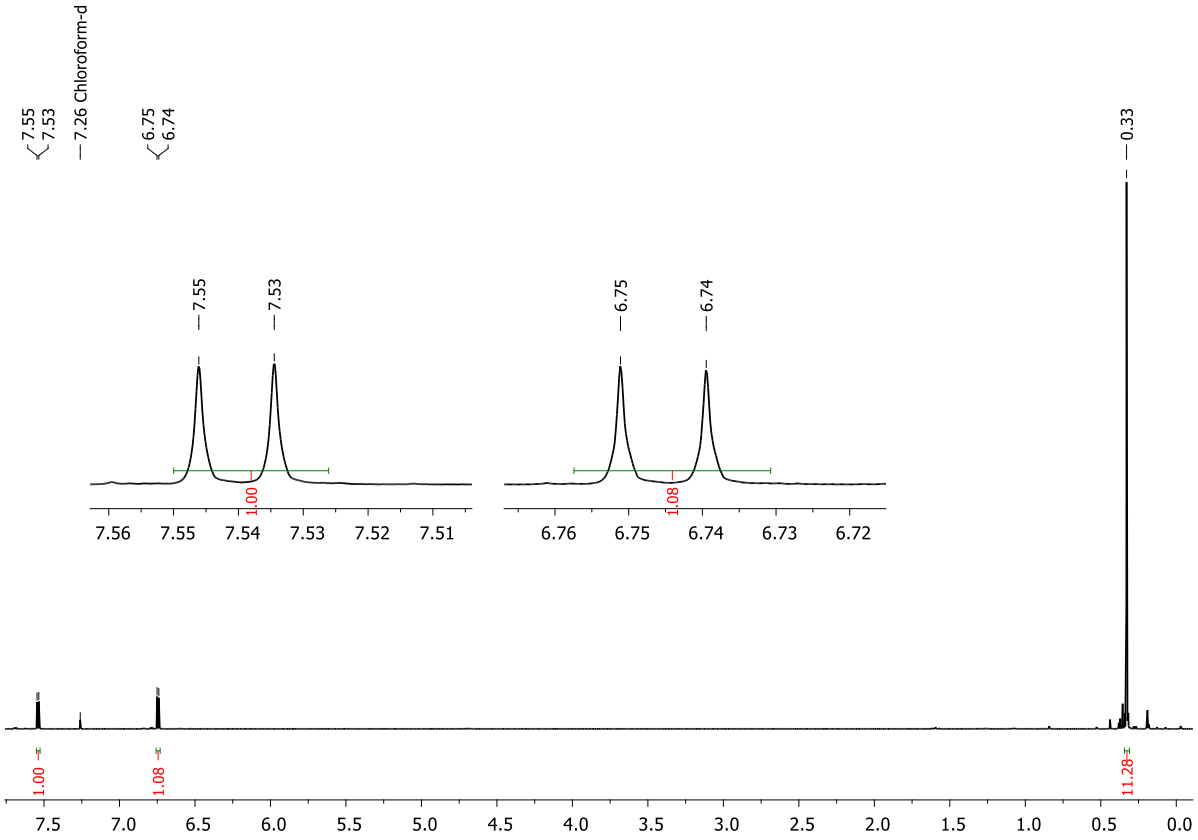

Figure 5.6.74. ^{1}H NMR spectrum of **15b** (300 MHz, in $CDCl_3$).

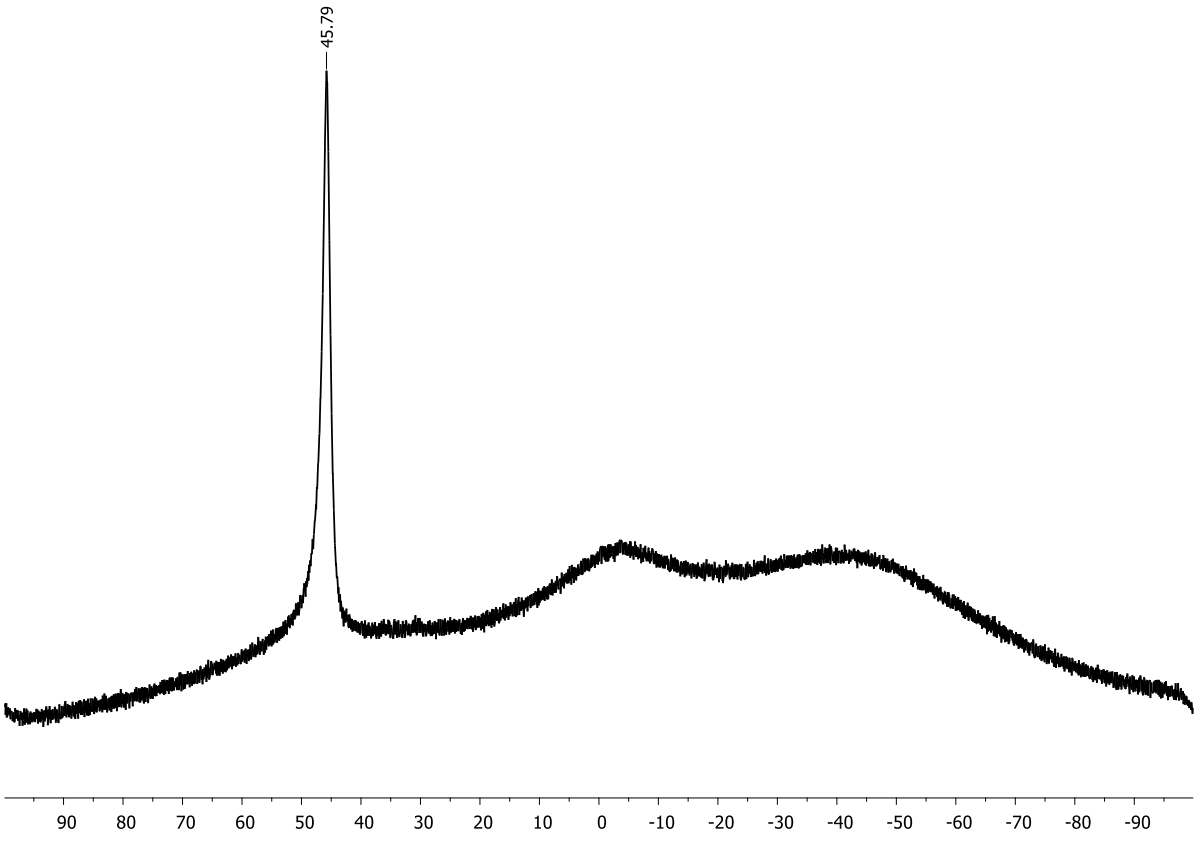

Figure 5.6.75. $^{11}B\{^{1}H\}$ NMR spectrum of **15b** (96 MHz, in $CDCl_3$).

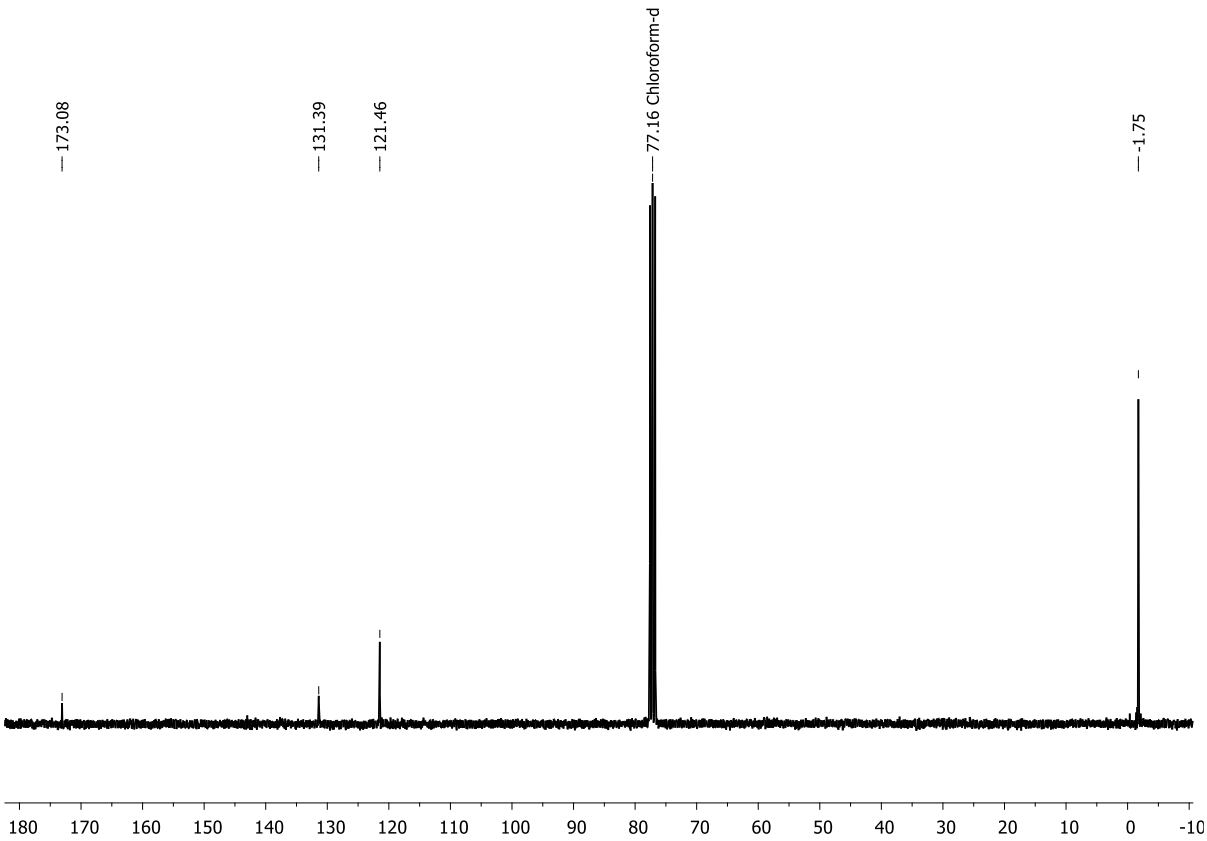

Figure 5.6.76. $^{13}C\{^{1}H\}$ NMR spectrum of **15b** (75 MHz, in $CDCl_3$).

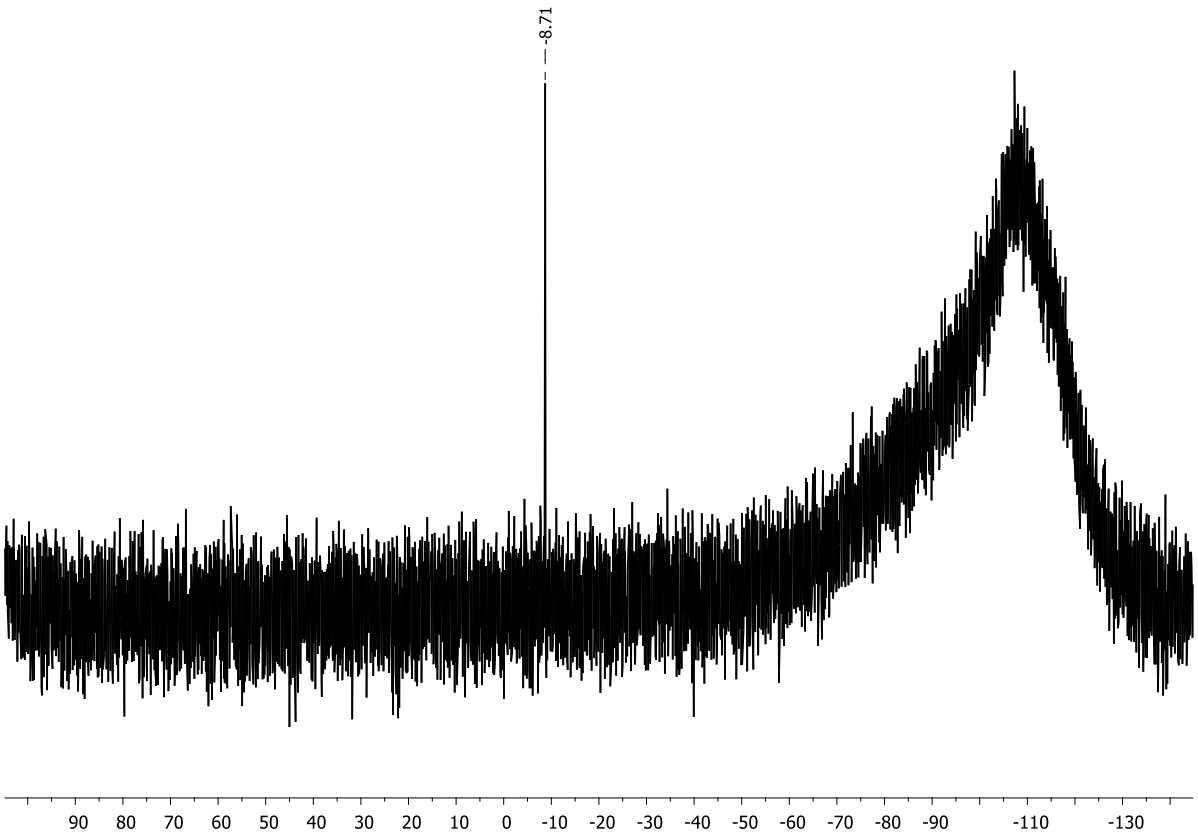

Figure 5.6.77. ^{29}Si NMR spectrum of **15b** (99 MHz, in $CDCl_3$).

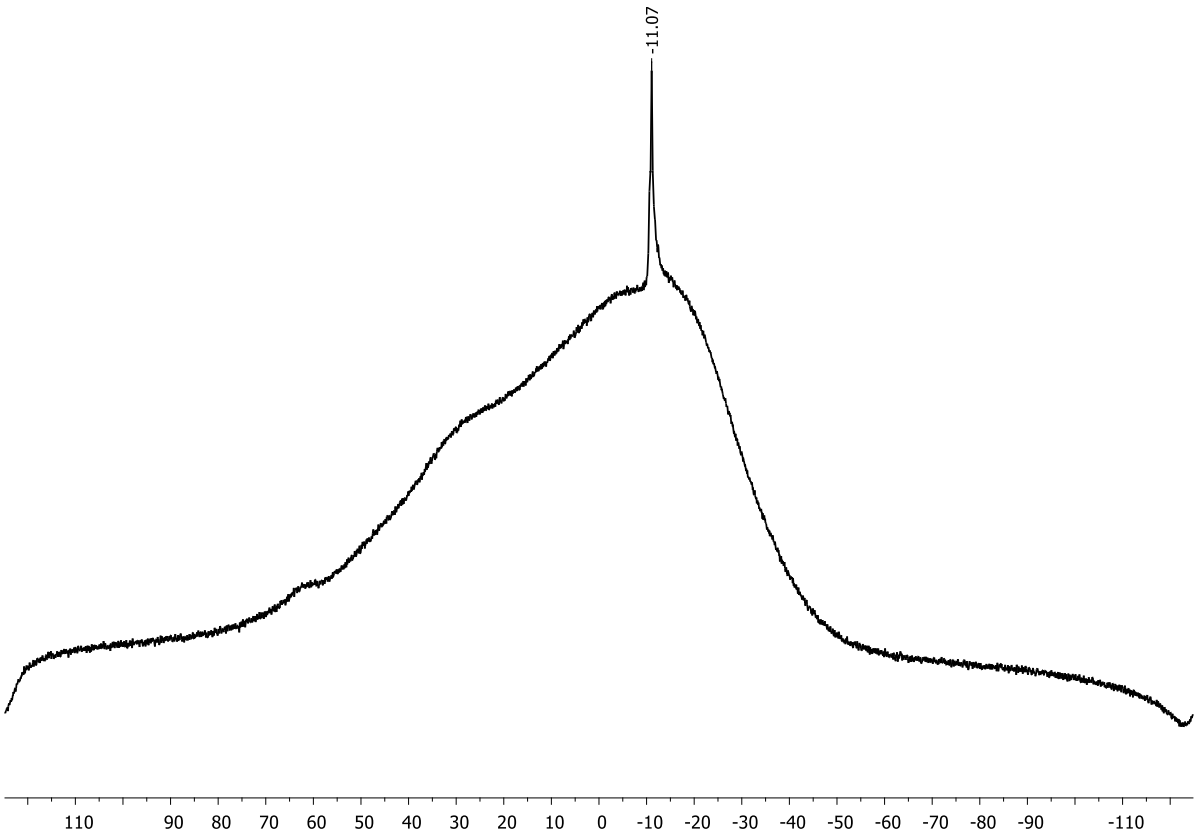

Figure 5.6.78. $^{11}B\{^{1}H\}$ NMR spectrum of a mixture of **2** and two equivalents of TipLi (96 MHz, in C_6D_6).

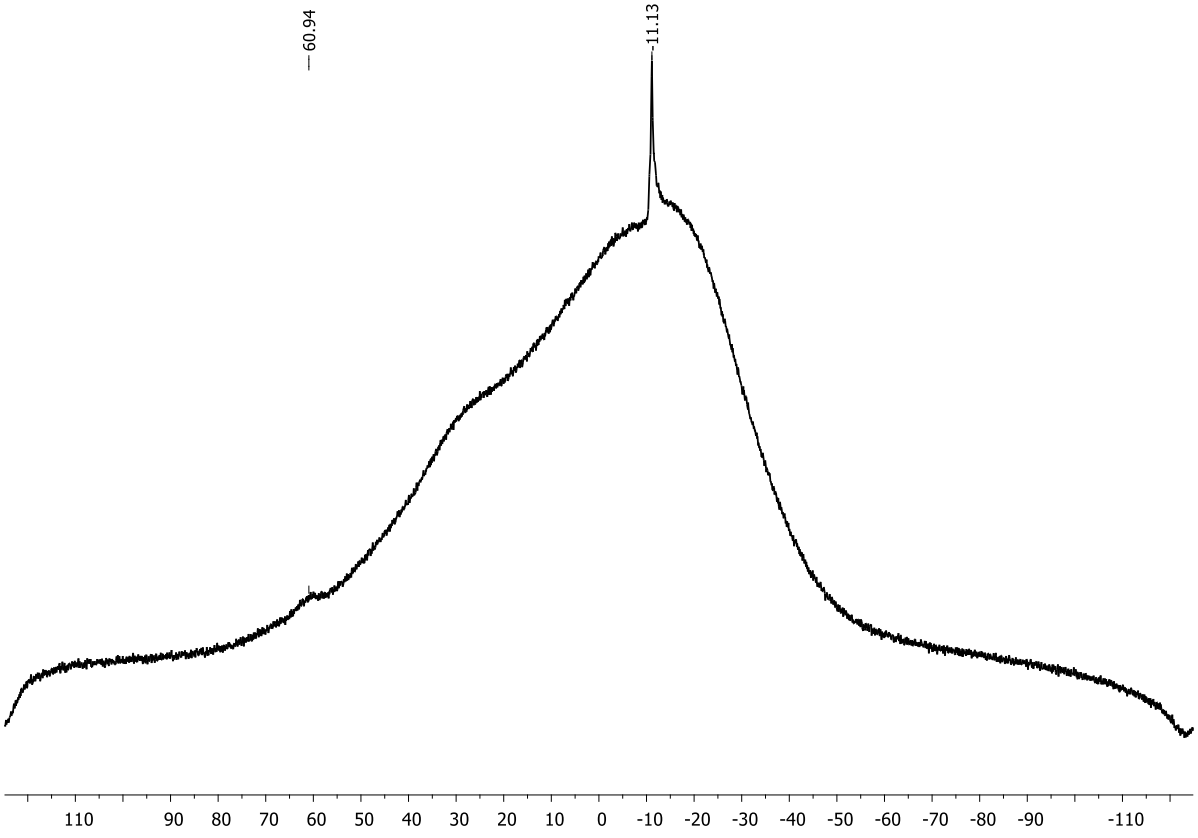

Figure 5.6.79. $^{11}B\{^{1}H\}$ NMR spectrum of a mixture of **12** and two equivalents of TipLi (96 MHz, in C_6D_6).

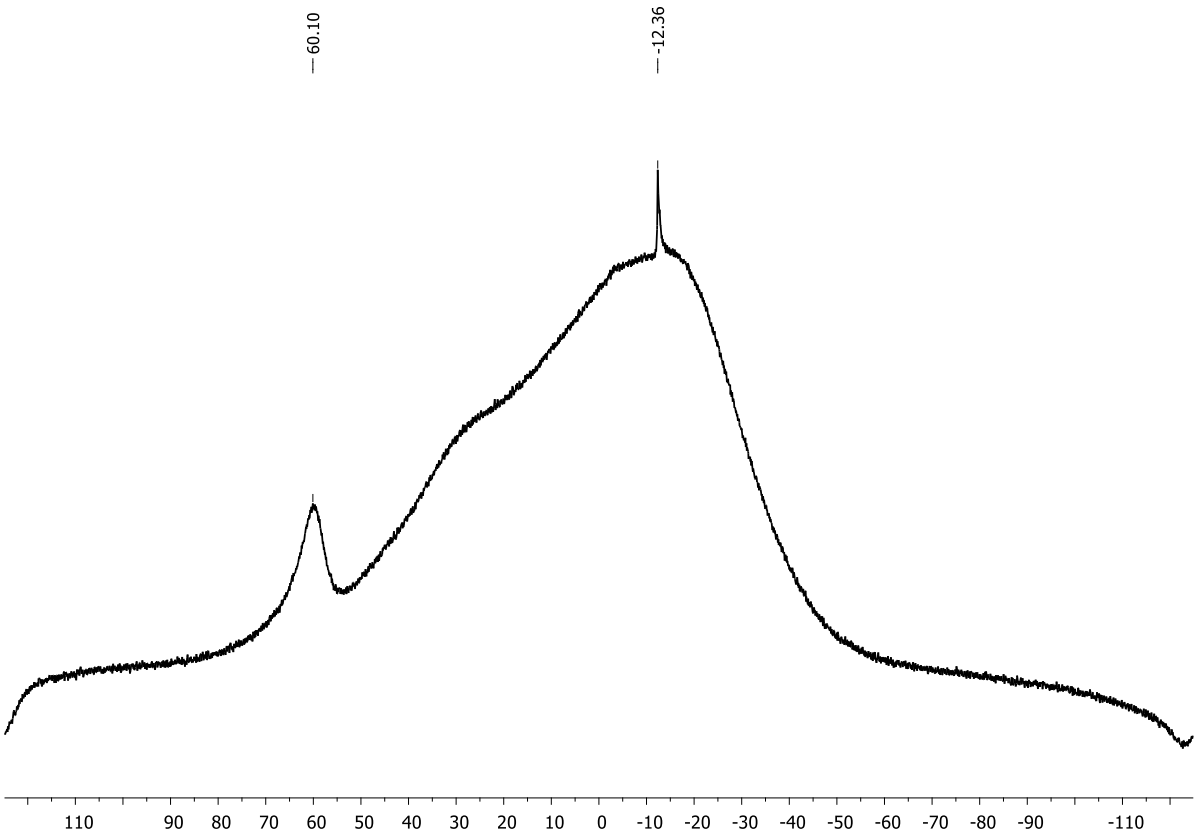

Figure 5.6.80. $^{11}B\{^{1}H\}$ NMR spectrum of a mixture of **12** and two equivalents of Mes*Li (96 MHz, in C_6D_6).

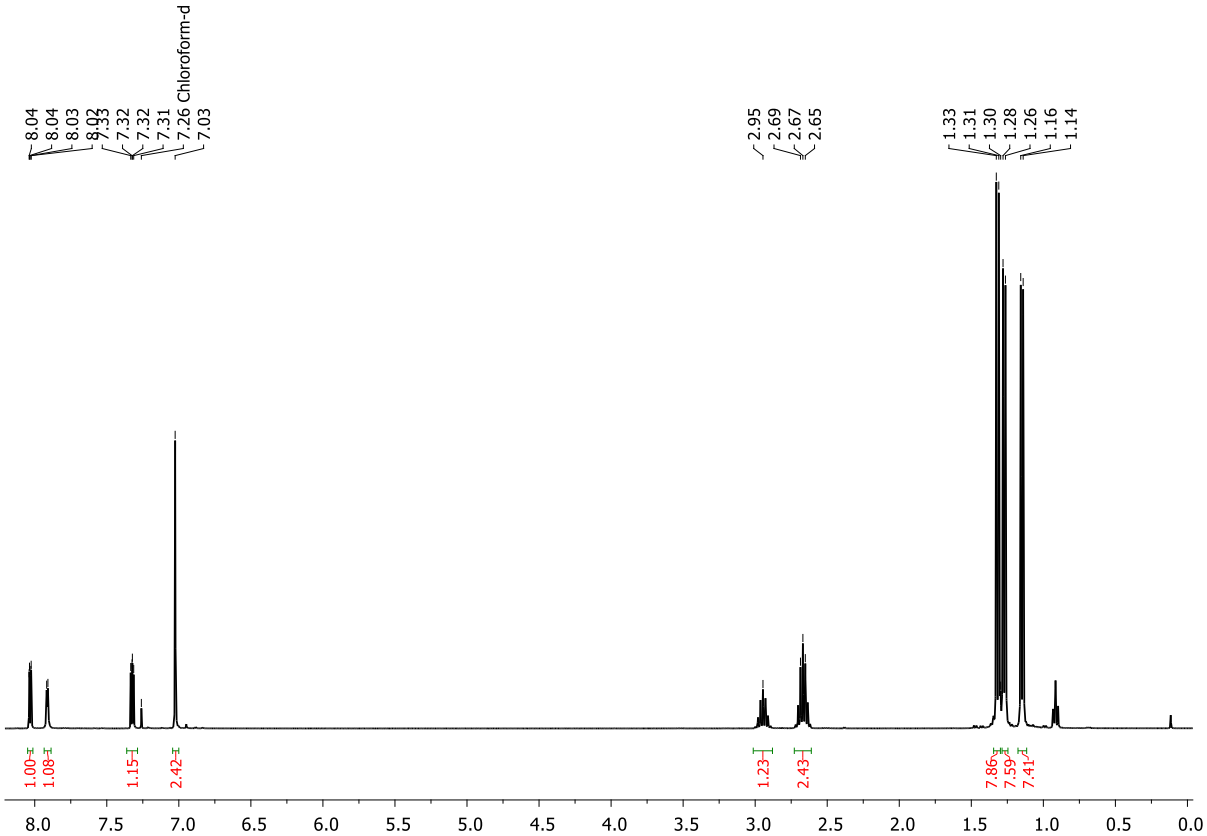

Figure 5.6.81. ^{1}H NMR spectrum of **19a^{Tip}** (400 MHz, in $CDCl_3$).

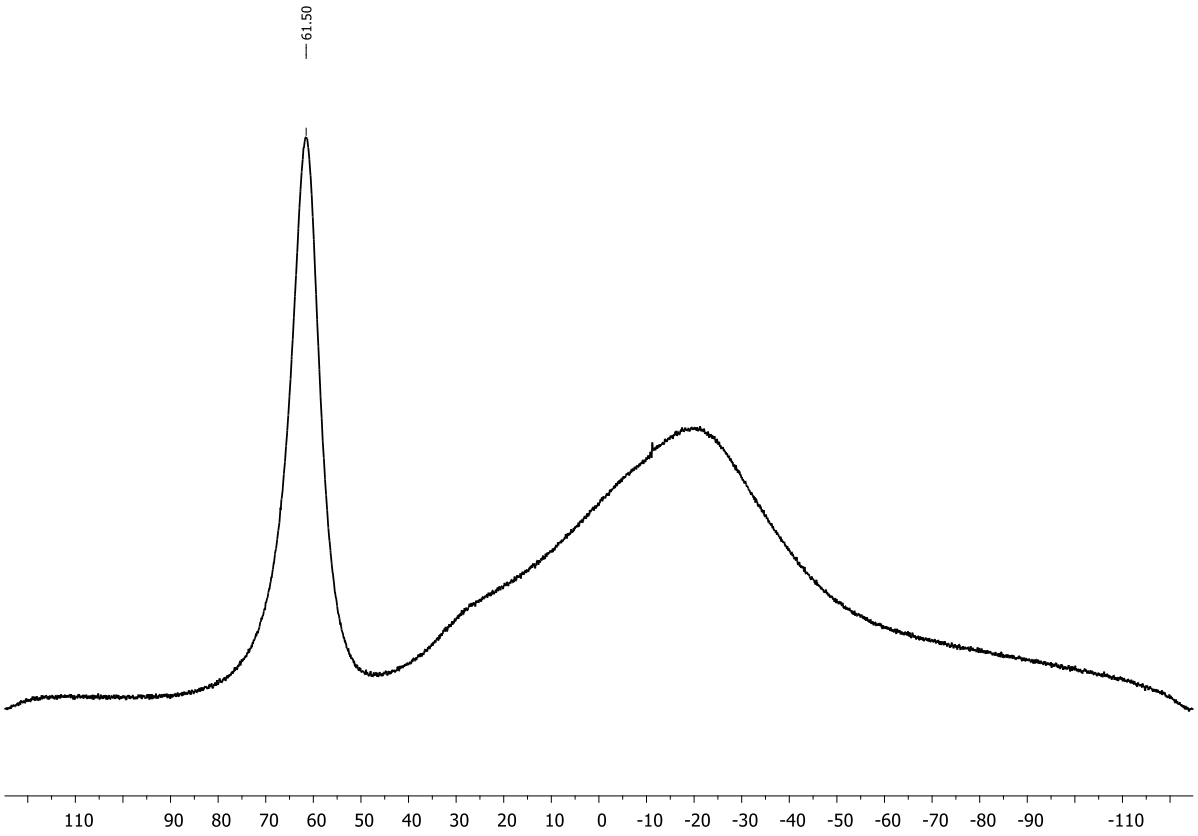

Figure 5.6.82. $^{11}B\{^{1}H\}$ NMR spectrum of **19a^{Tip}** (126 MHz, in $CDCl_3$).

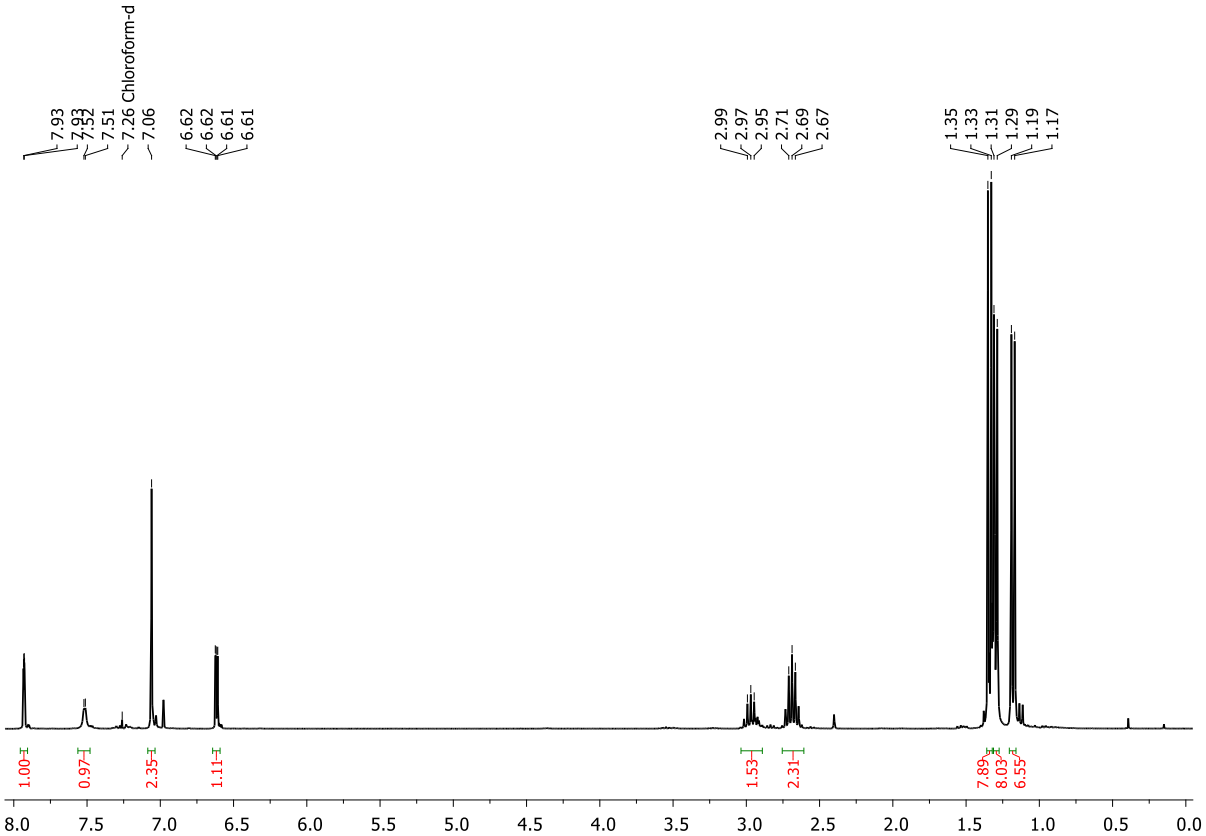

Figure 5.6.83. ^{1}H NMR spectrum of **19b^{Tip}** (500 MHz, in $CDCl_3$).

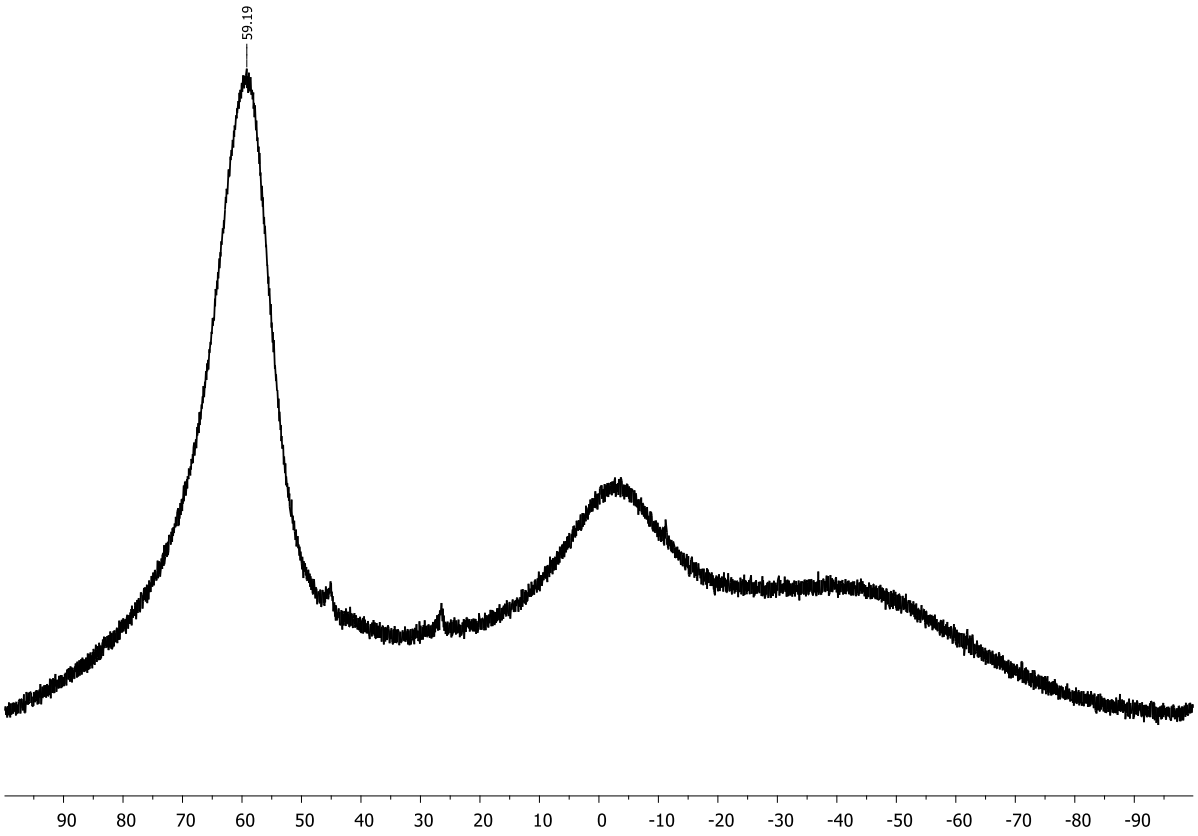

Figure 5.6.84. $^{11}B\{^{1}H\}$ NMR spectrum of **19b^{Tip}** (160 MHz, in $CDCl_3$).

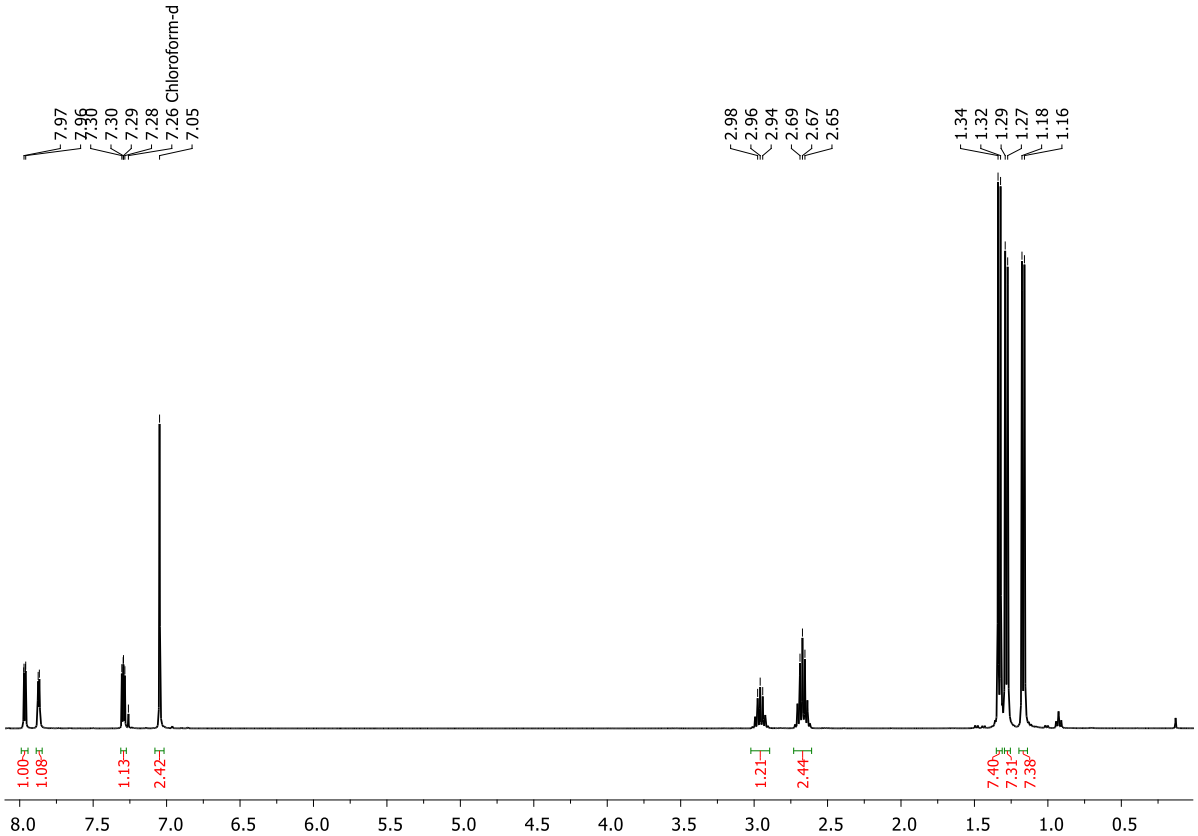

Figure 5.6.85. ^{1}H NMR spectrum of **20a^{Tip}** (400 MHz, in $CDCl_3$).

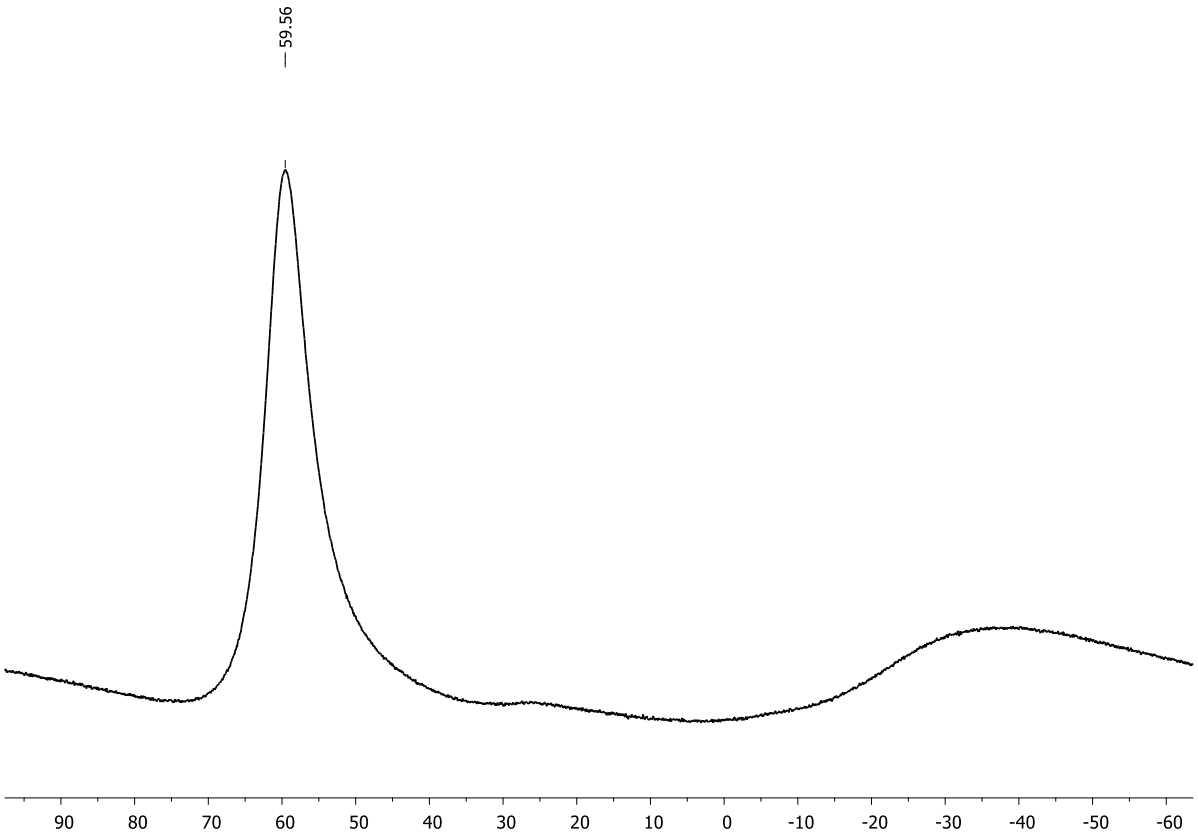

Figure 5.6.86. $^{11}B\{^{1}H\}$ NMR spectrum of **20a^{Tip}** (126 MHz, in $CDCl_3$).

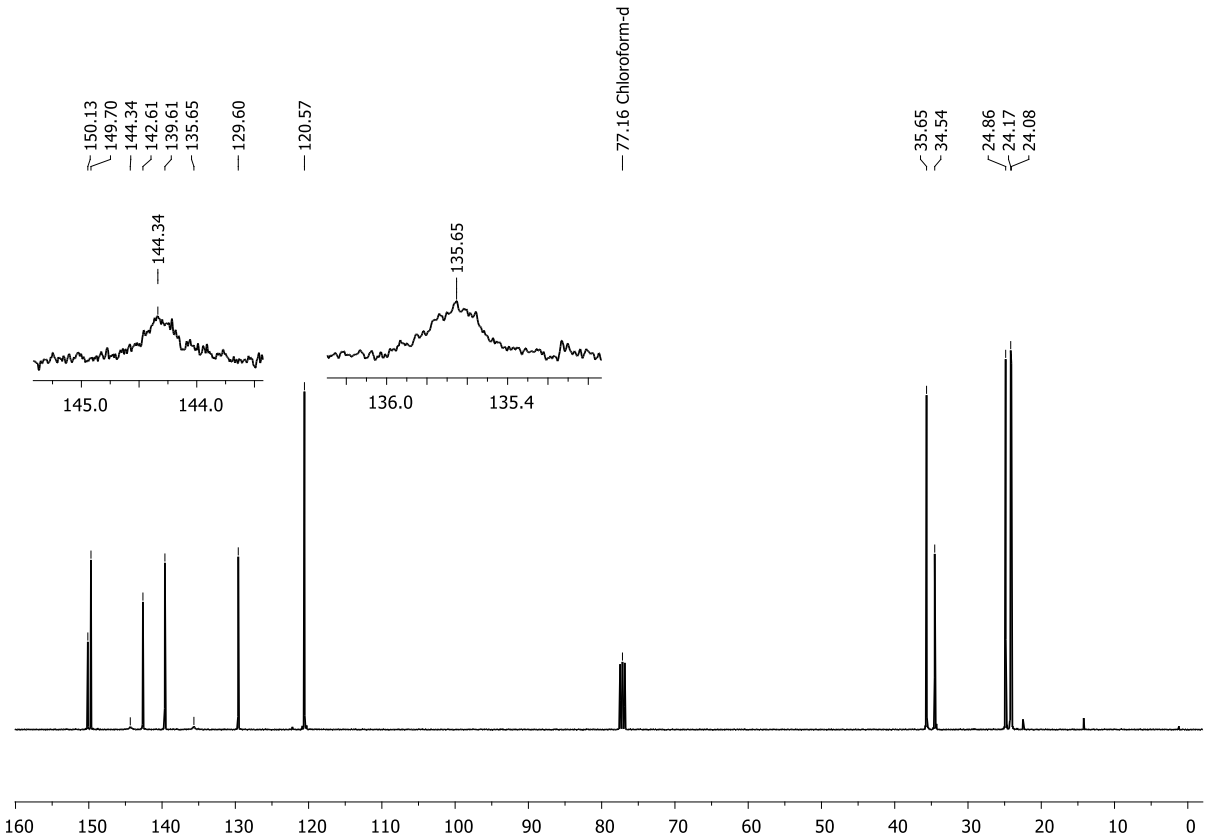

Figure 5.6.87. $^{13}C\{^{1}H\}$ NMR spectrum of **20a^{Tip}** (101 MHz, in $CDCl_3$).

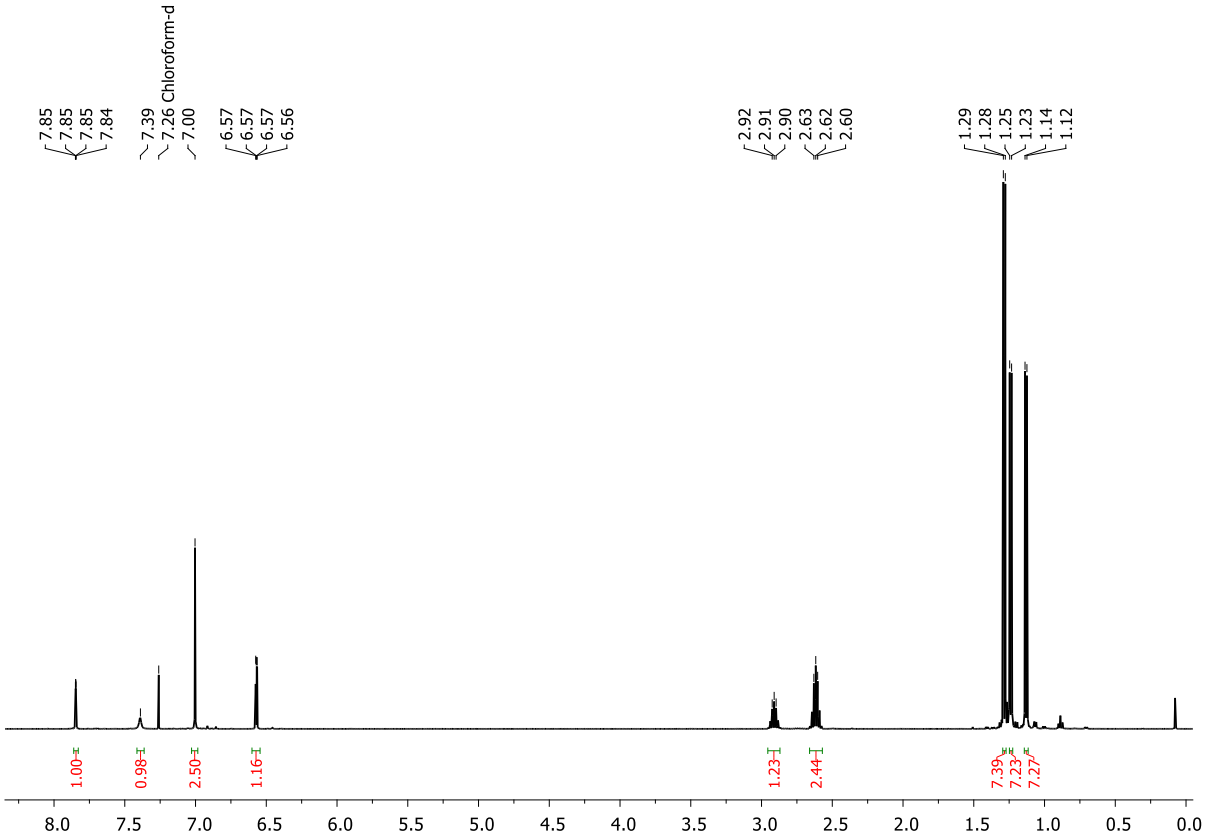

Figure 5.6.88. ^{1}H NMR spectrum of **20b^{Tip}** (500 MHz, in $CDCl_3$).

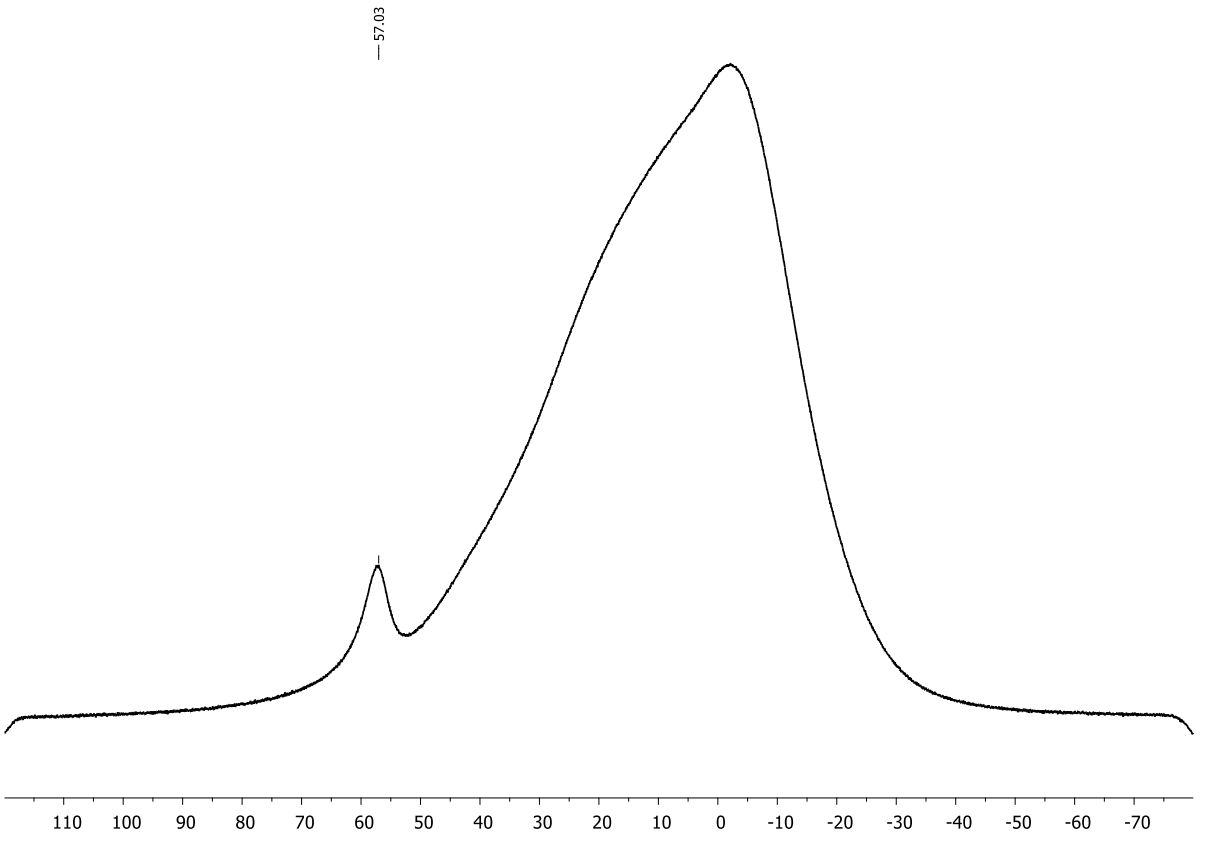

Figure 5.6.89. $^{11}B\{^{1}H\}$ NMR spectrum of **20b^{Tip}** (160 MHz, in $CDCl_3$).

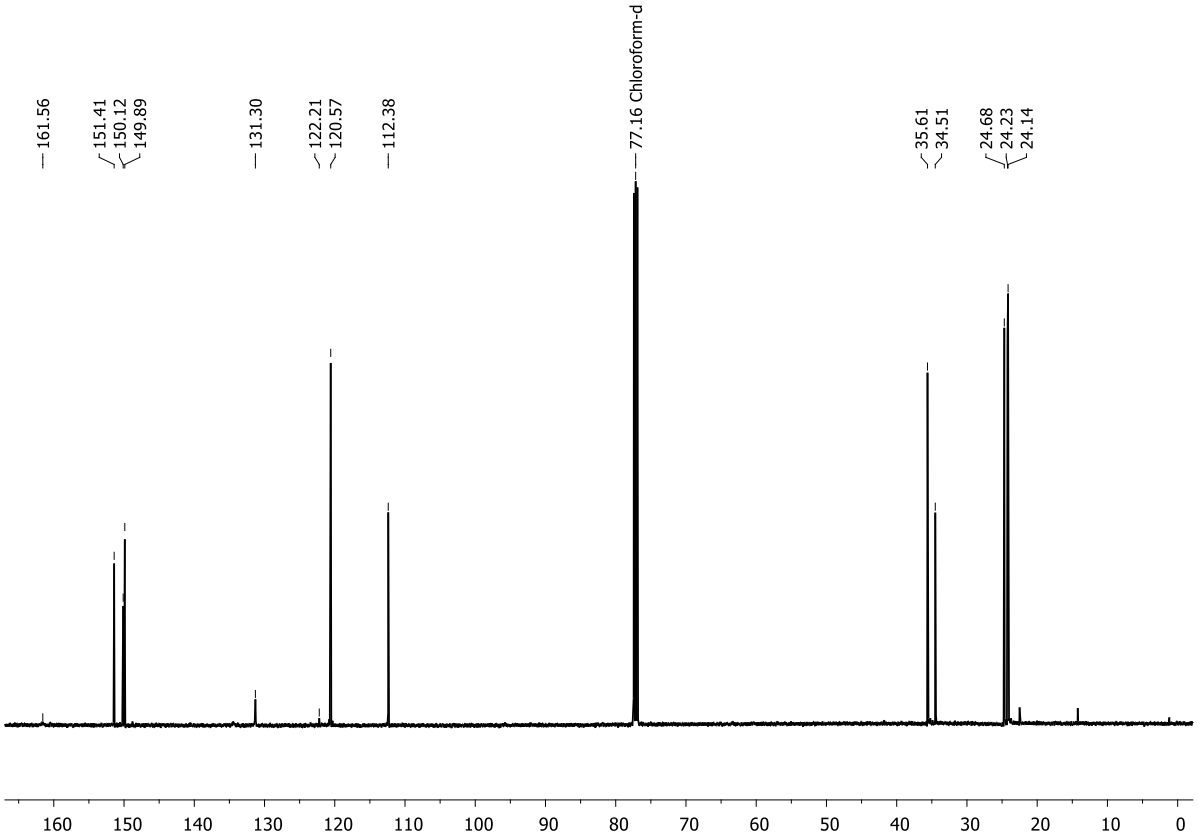

Figure 5.6.90. $^{13}C\{^{1}H\}$ NMR spectrum of **20b^{Tip}** (126 MHz, in $CDCl_3$).

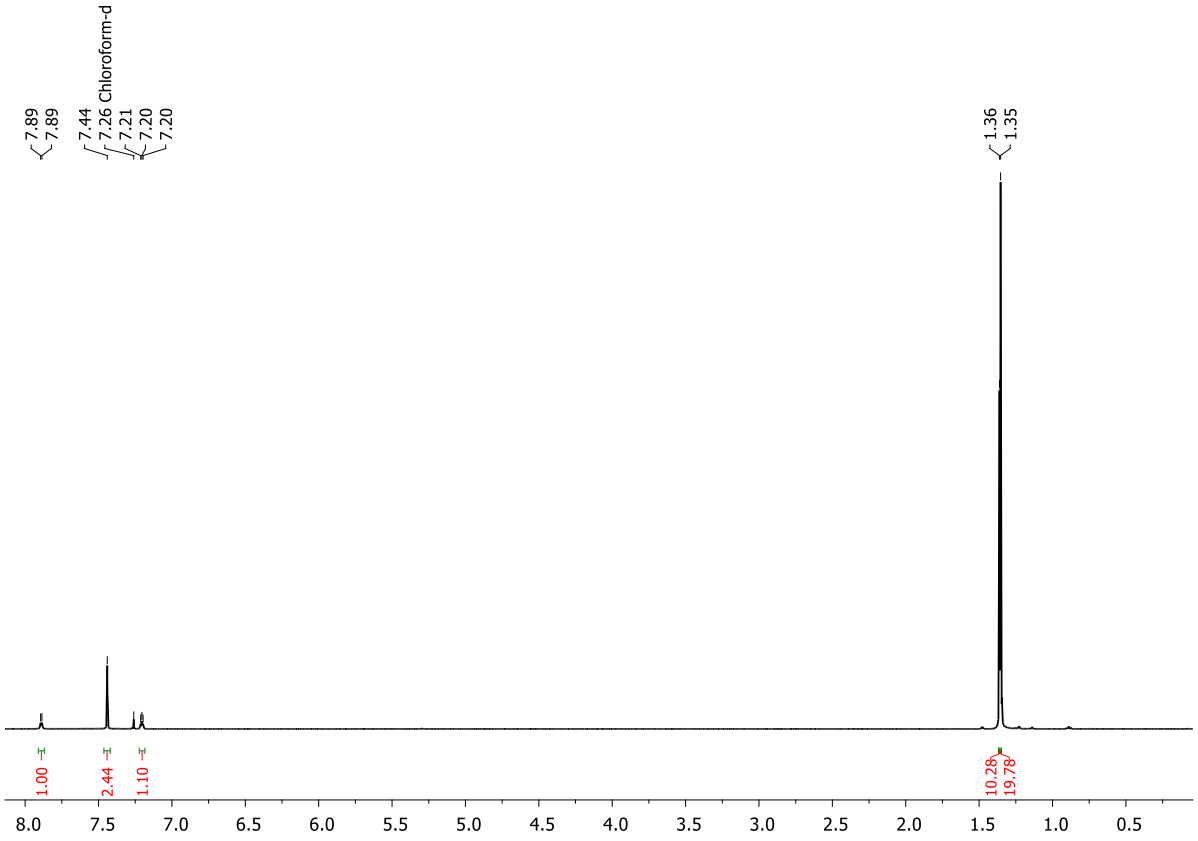

Figure 5.6.91. ^{1}H NMR spectrum of **21a^{Mes*}** (500 MHz, in $CDCl_3$).

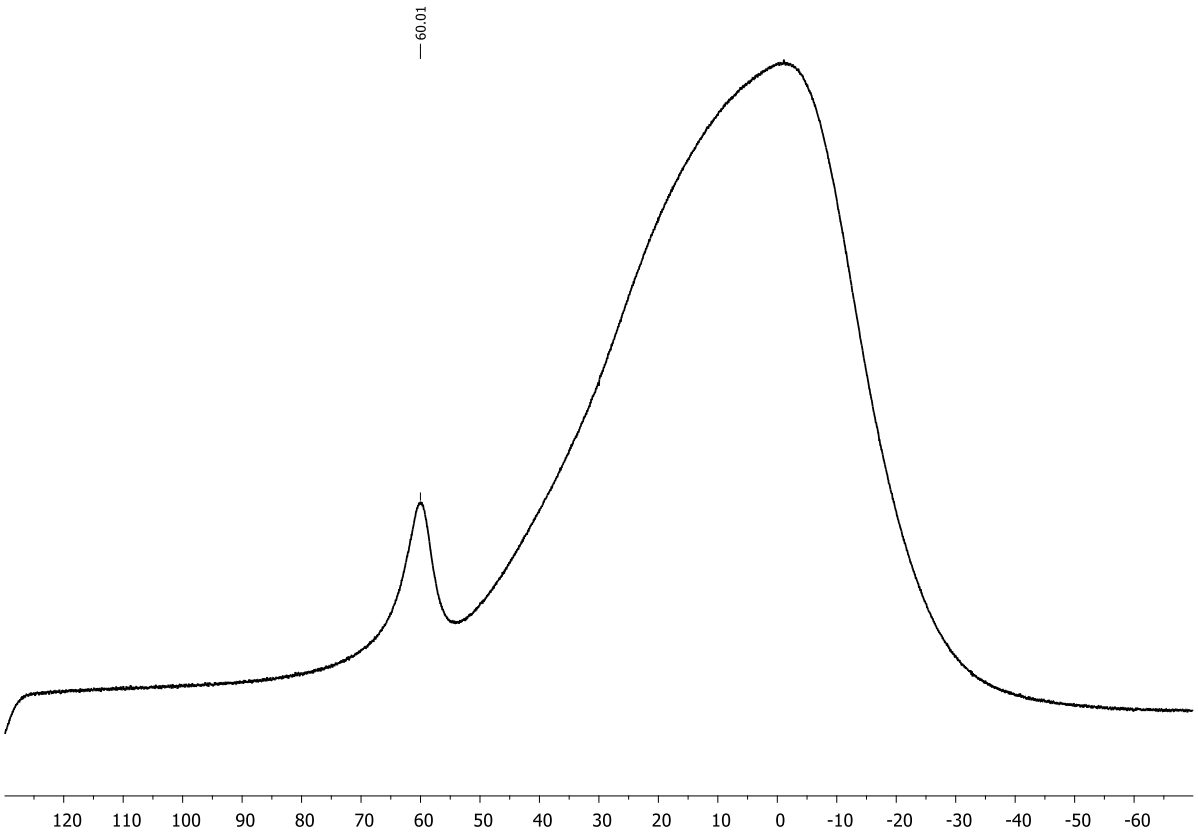

Figure 5.6.92. $^{11}B\{^{1}H\}$ NMR spectrum of **21a^{Mes*}**(160 MHz, in $CDCl_3$).

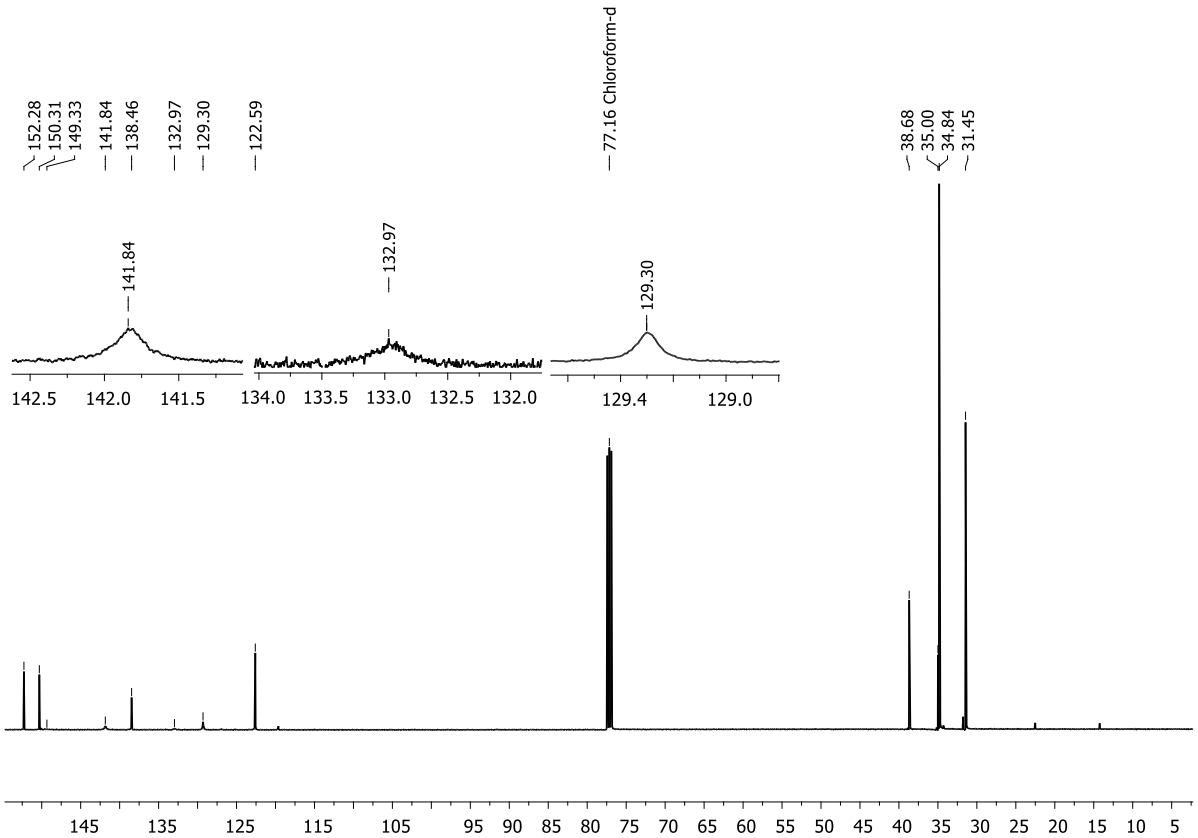

Figure 5.6.93. $^{13}C\{^{1}H\}$ NMR spectrum of **21a^{Mes*}**(126 MHz, in $CDCl_3$).

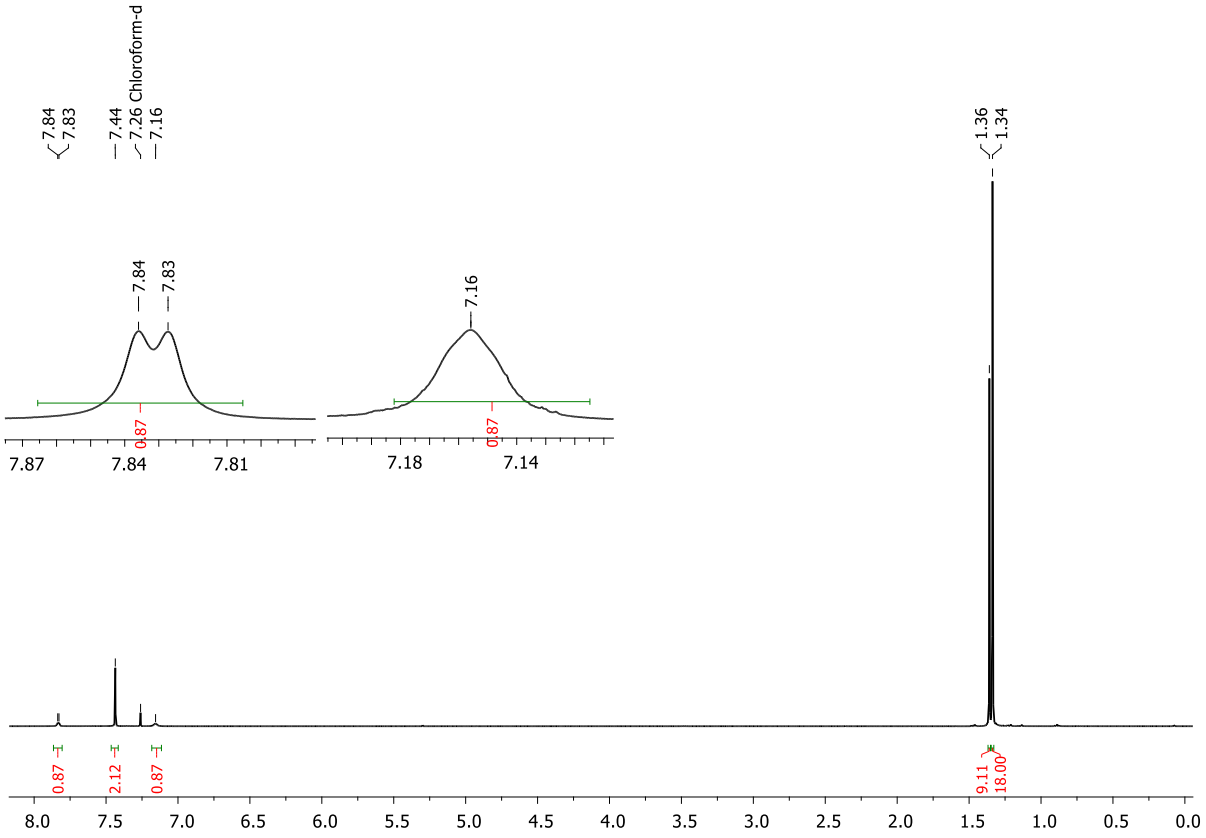

Figure 5.6.94. ^{1}H NMR spectrum of **22a^{Mes*}** (500 MHz, in $CDCl_3$).

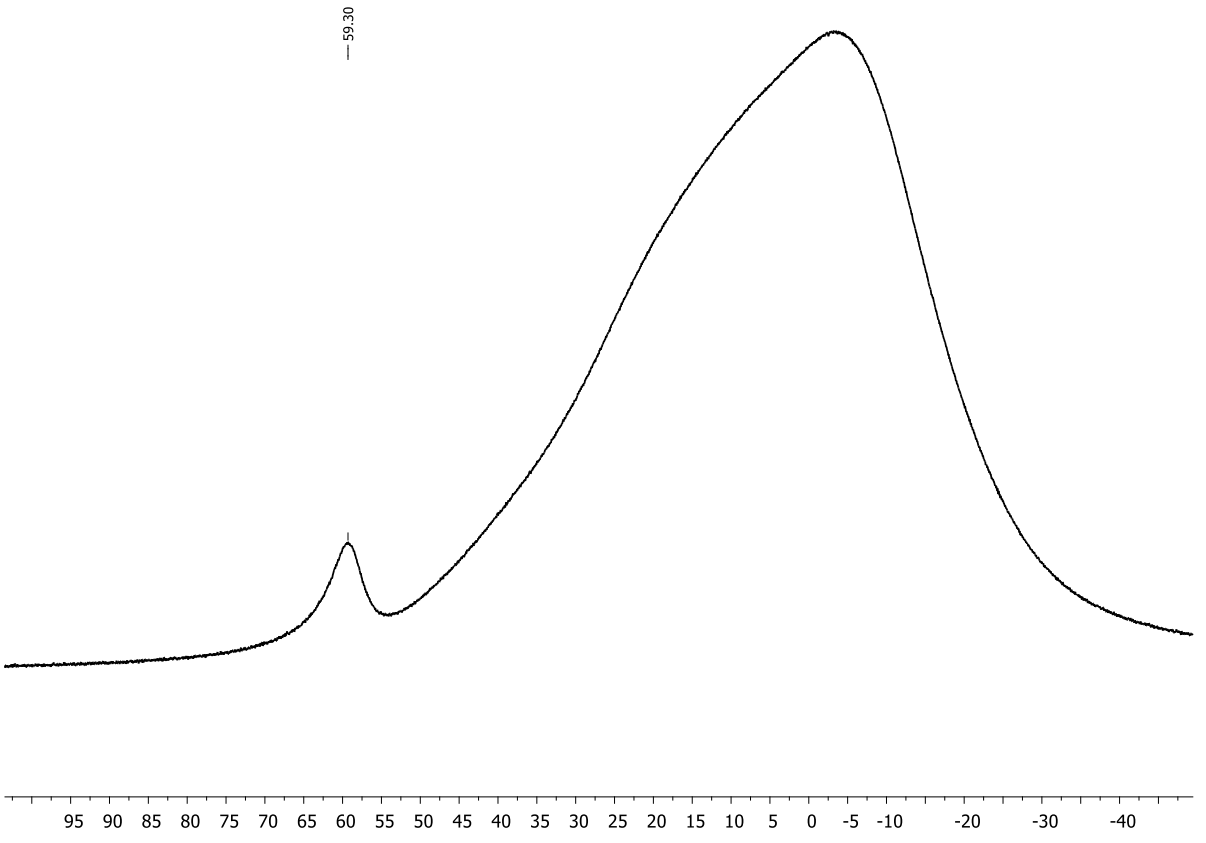

Figure 5.6.95. ^{11}B{^{1}H} NMR spectrum of **22a^{Mes*}** (160 MHz, in $CDCl_3$).

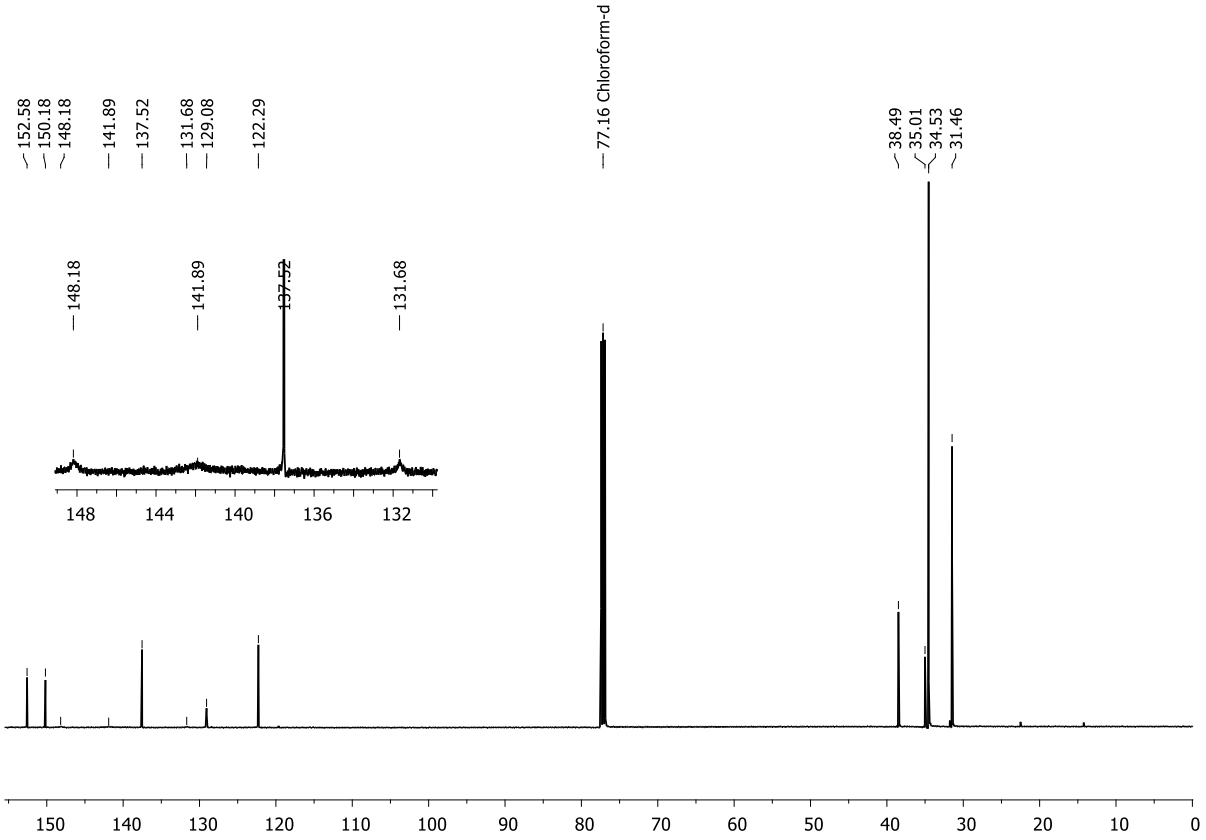

Figure 5.6.96. $^{13}C\{^{1}H\}$ NMR spectrum of **22a^{Mes*}** (126 MHz, in $CDCl_3$).

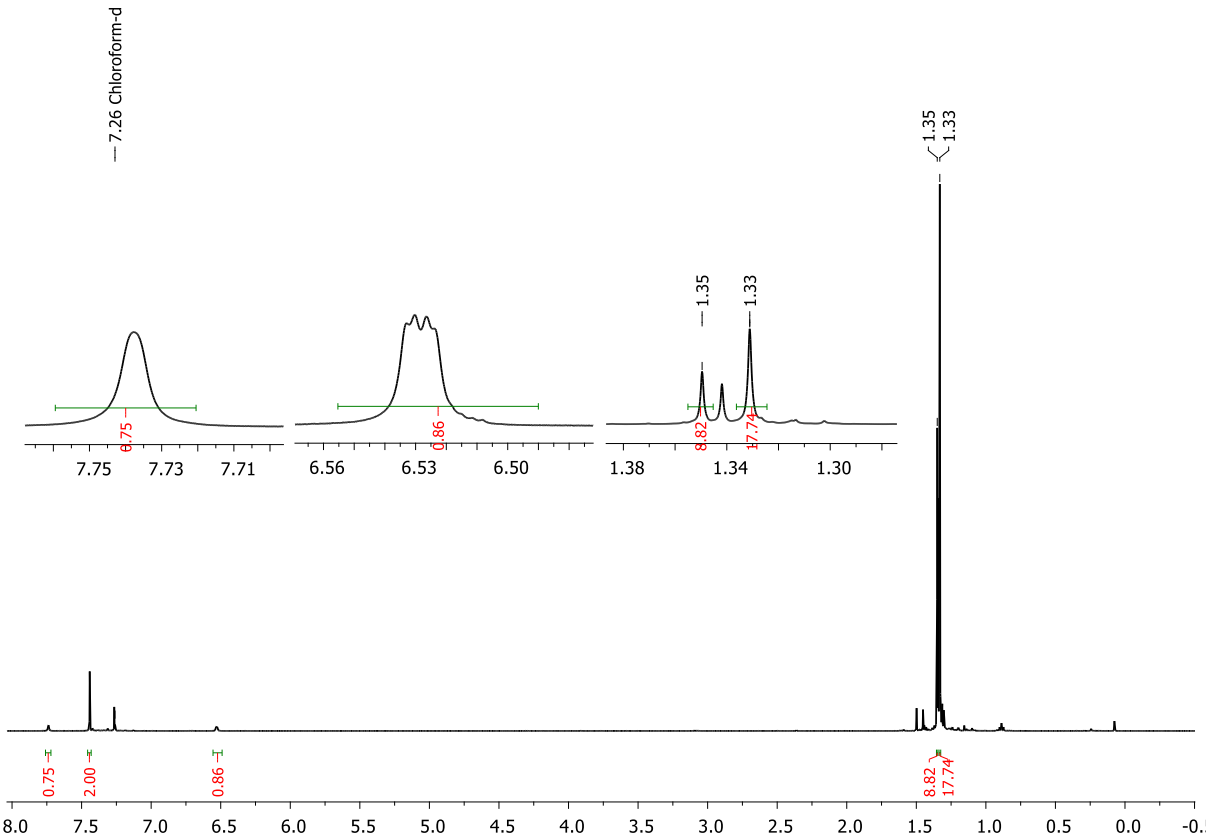

Figure 5.6.97. ^{1}H NMR spectrum of **22b^{Mes*}** (500 MHz, in $CDCl_3$).

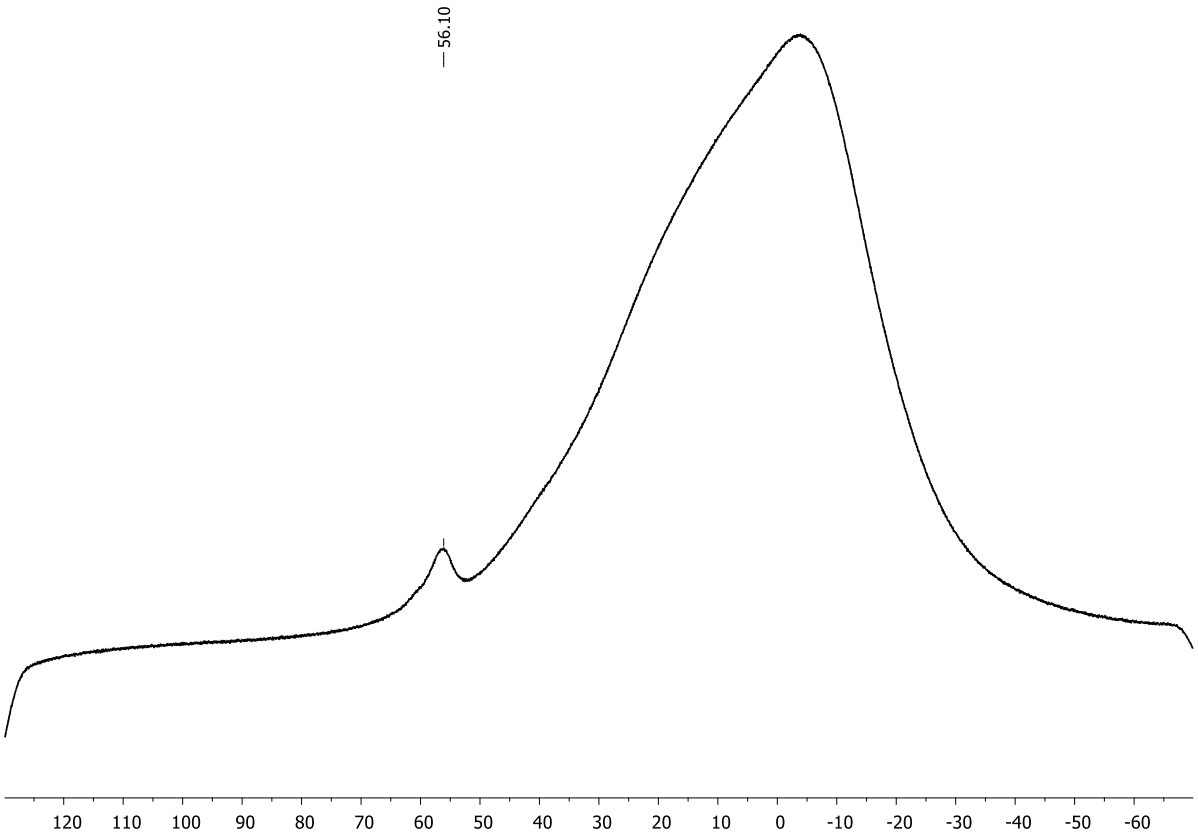

Figure 5.6.98. $^{11}B\{^{1}H\}$ NMR spectrum of **22b^{Mes*}**(160 MHz, in $CDCl_3$).

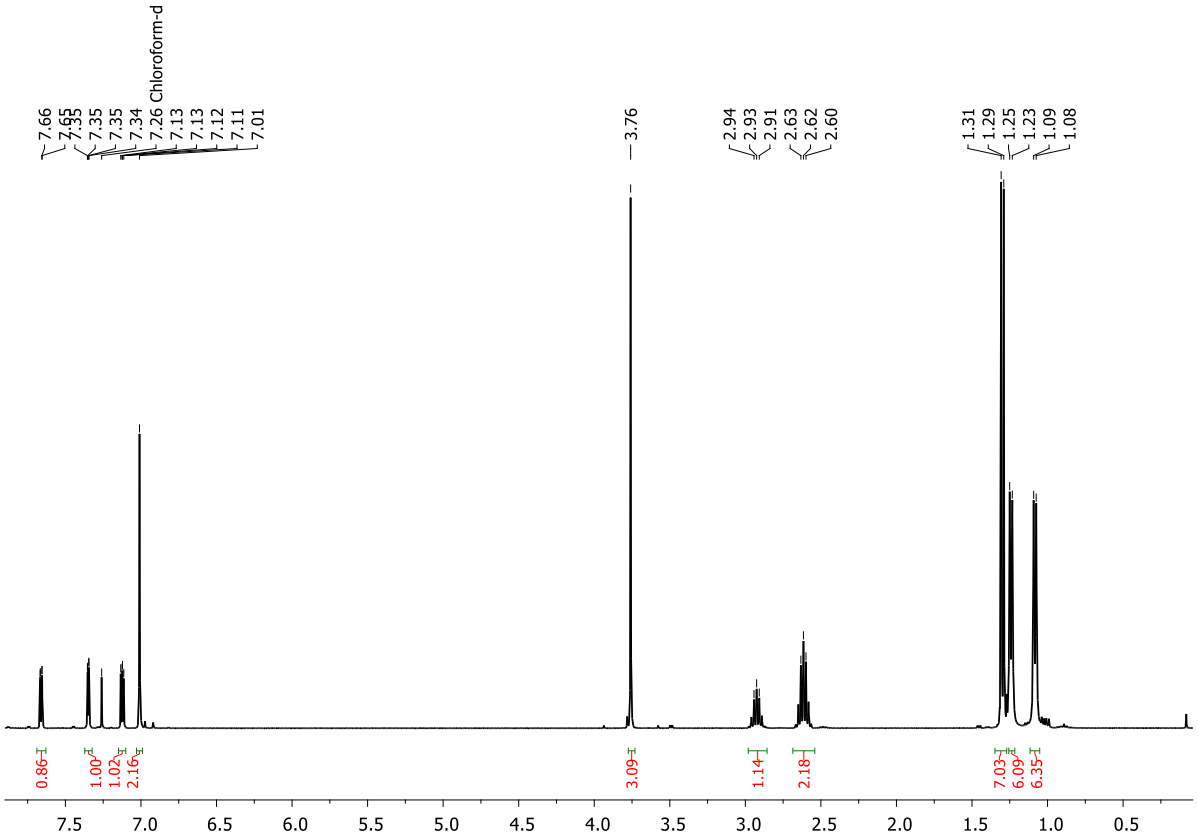

Figure 5.6.99. ^{1}H NMR spectrum of **23a^{Tip}** (500 MHz, in $CDCl_3$).

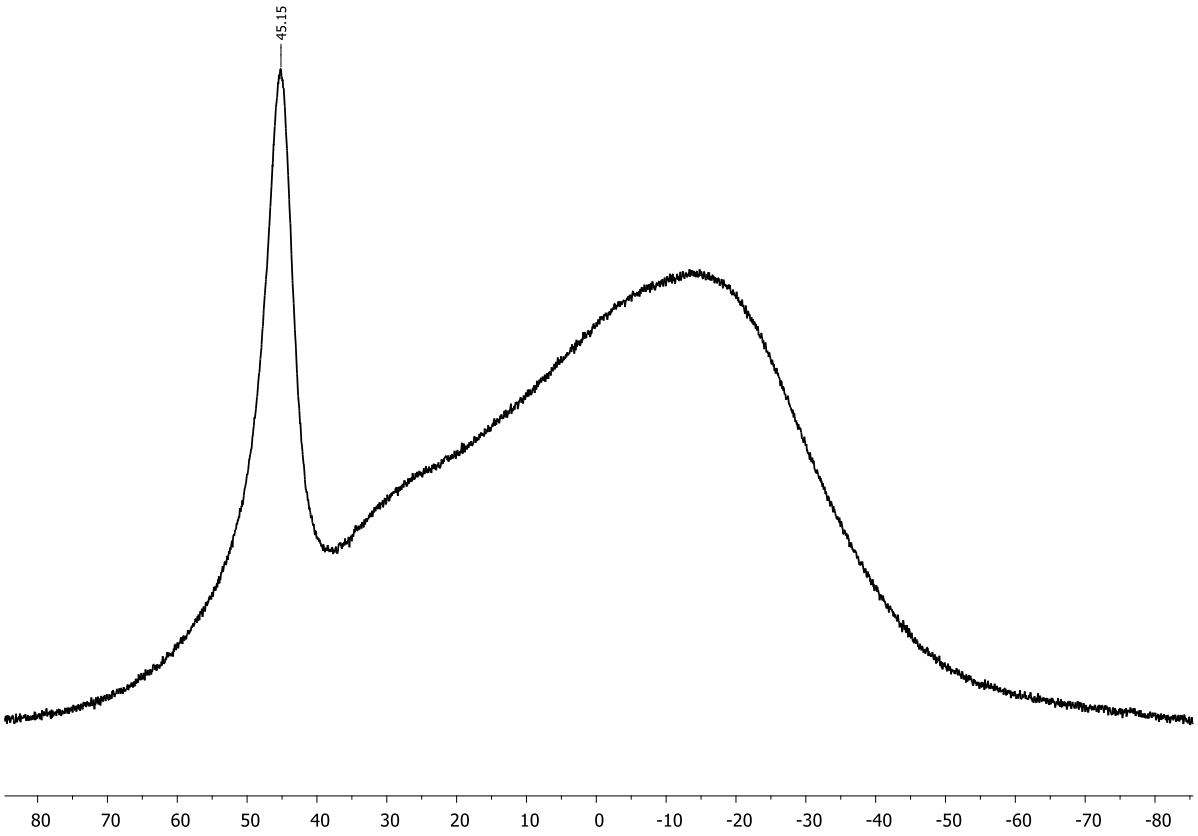

Figure 5.6.100. $^{11}B\{^{1}H\}$ NMR spectrum of **23a^{Tip}** (160 MHz, in $CDCl_3$).

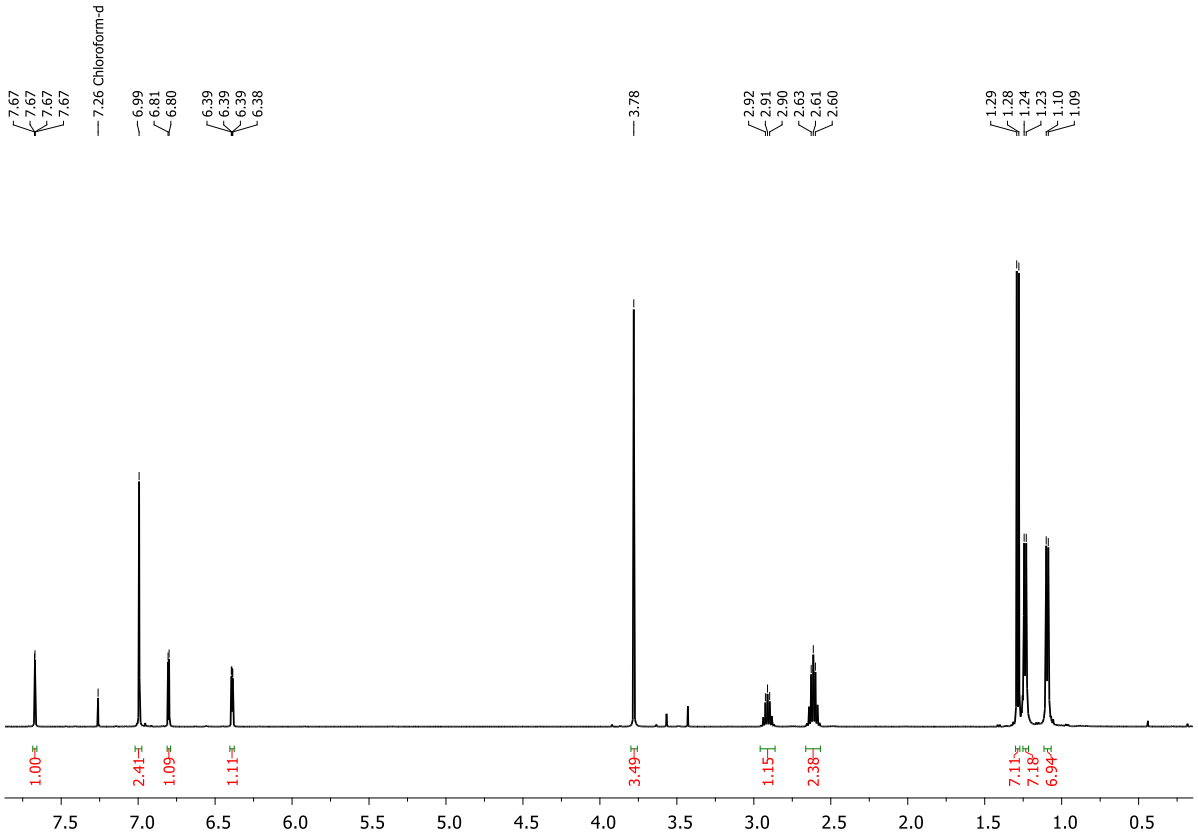

Figure 5.6.101. ^{1}H NMR spectrum of **23b^{Tip}** (500 MHz, in $CDCl_3$).

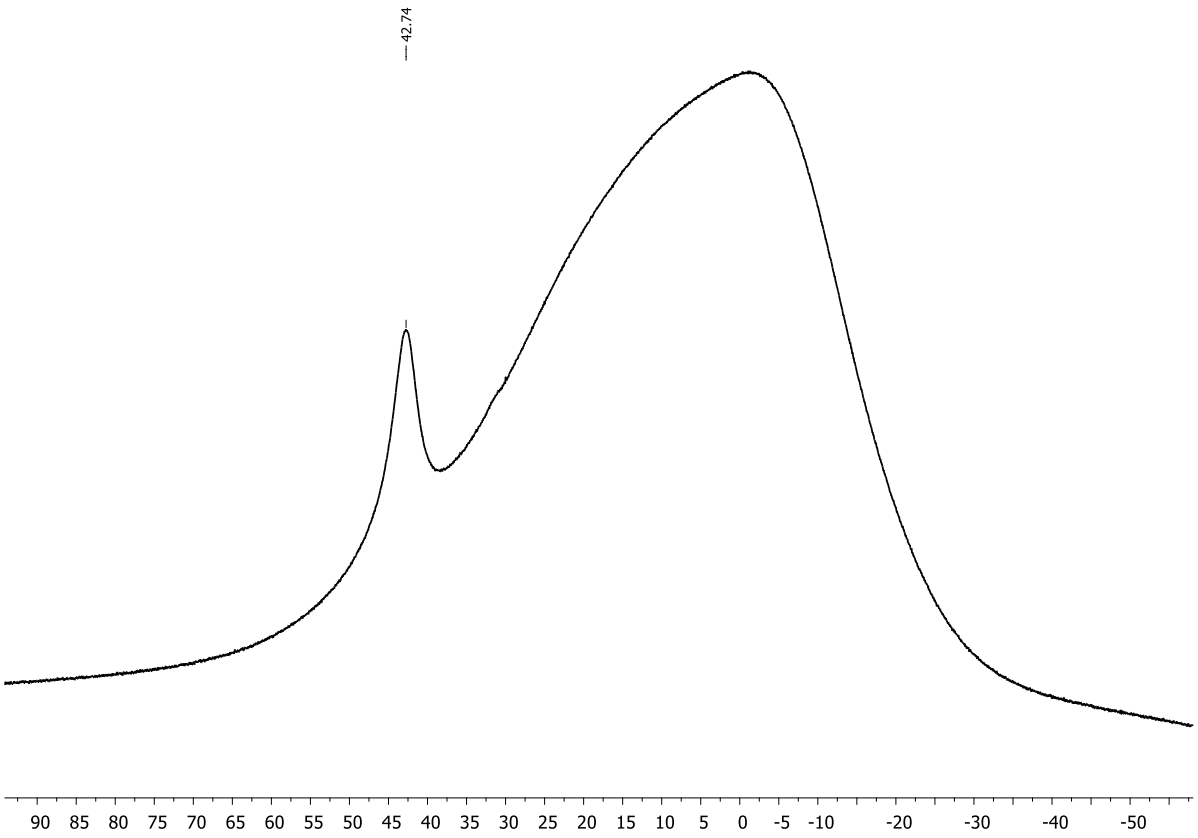

Figure 5.6.102. $^{11}B\{^{1}H\}$ NMR spectrum of **23b^{Tip}** (160 MHz, in $CDCl_3$).

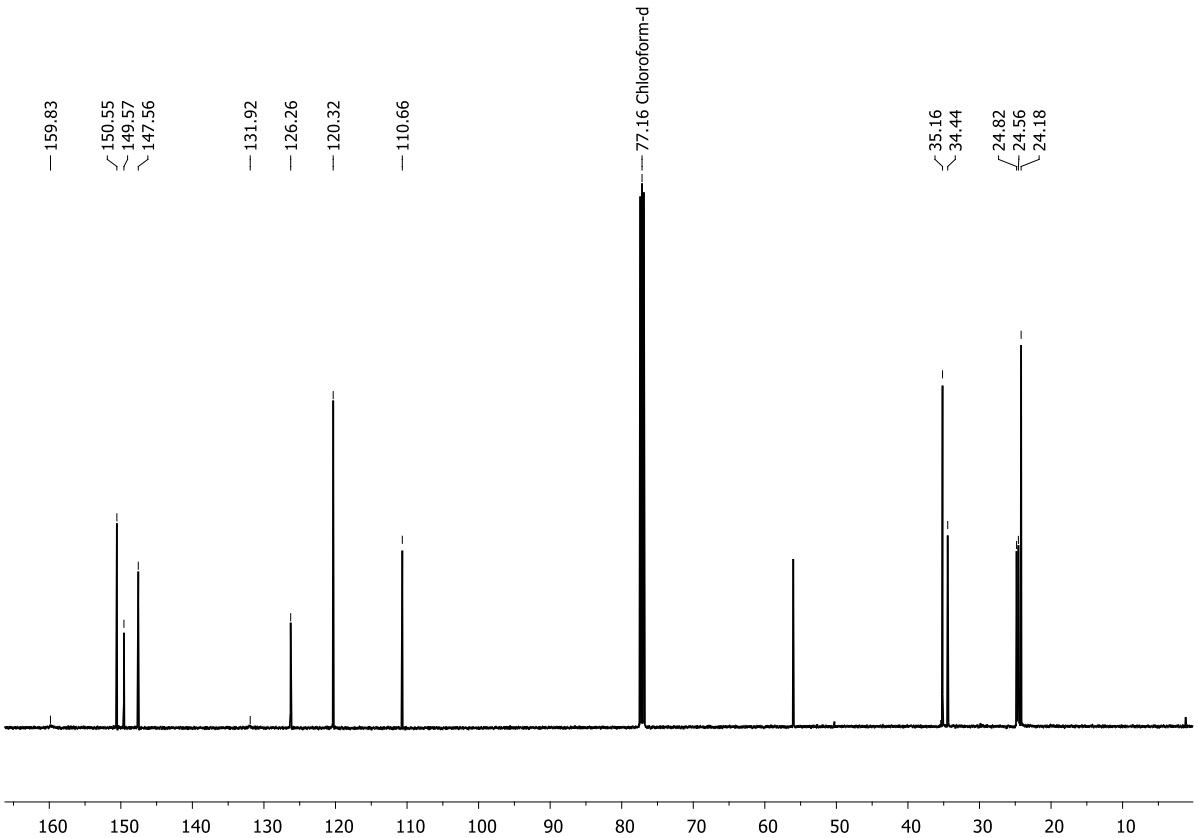

Figure 5.6.103. $^{13}C\{^{1}H\}$ NMR spectrum of **23b^{Tip}** (126 MHz, in $CDCl_3$).

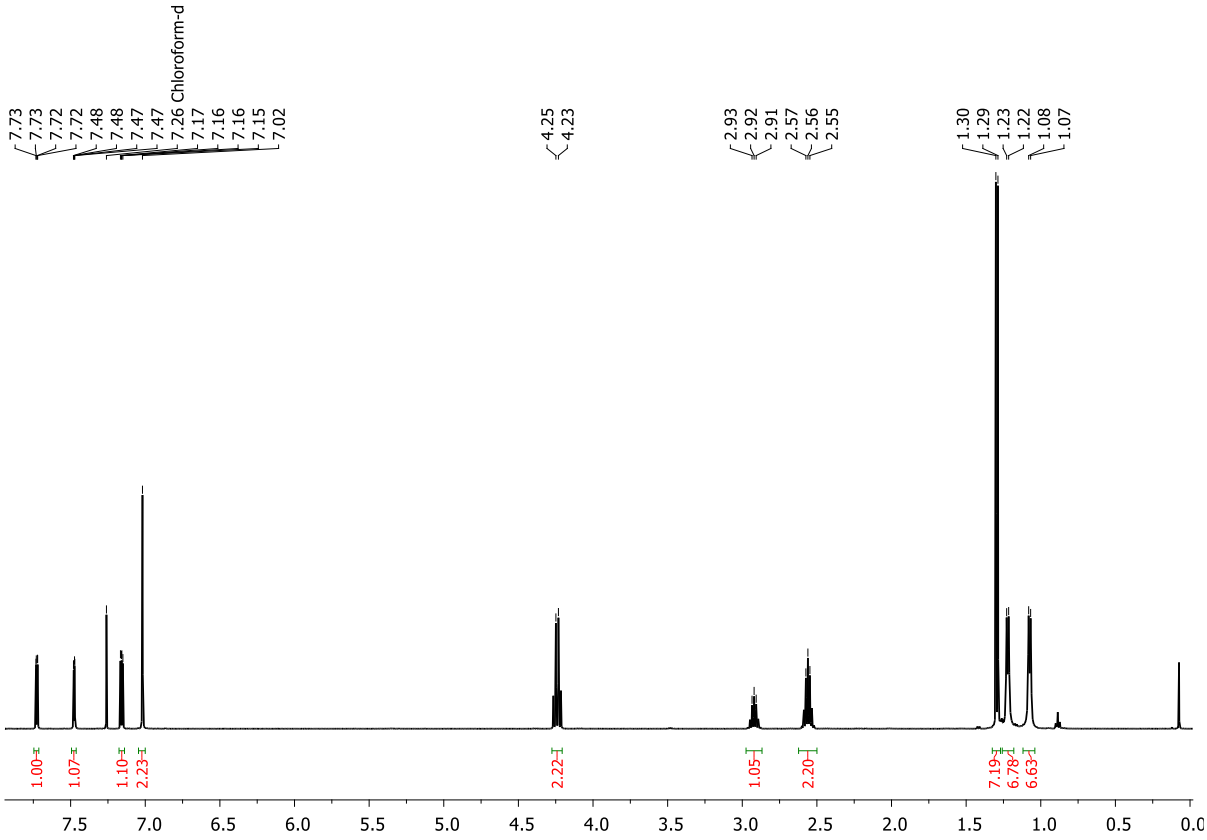

Figure 5.6.104. ^{1}H NMR spectrum of **24a^{Tip}** (500 MHz, in $CDCl_3$).

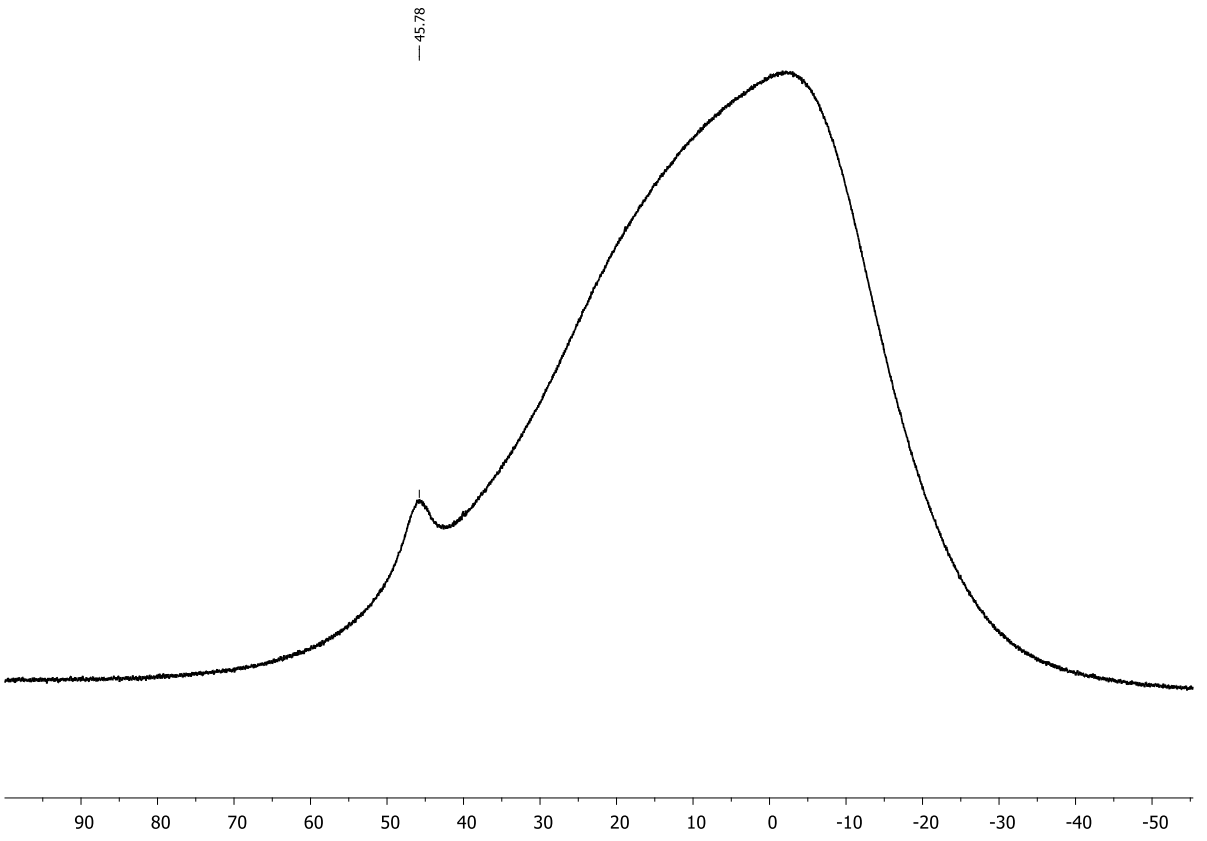

Figure 5.6.105. $^{11}B\{^{1}H\}$ NMR spectrum of **24a^{Tip}** (160 MHz, in $CDCl_3$).

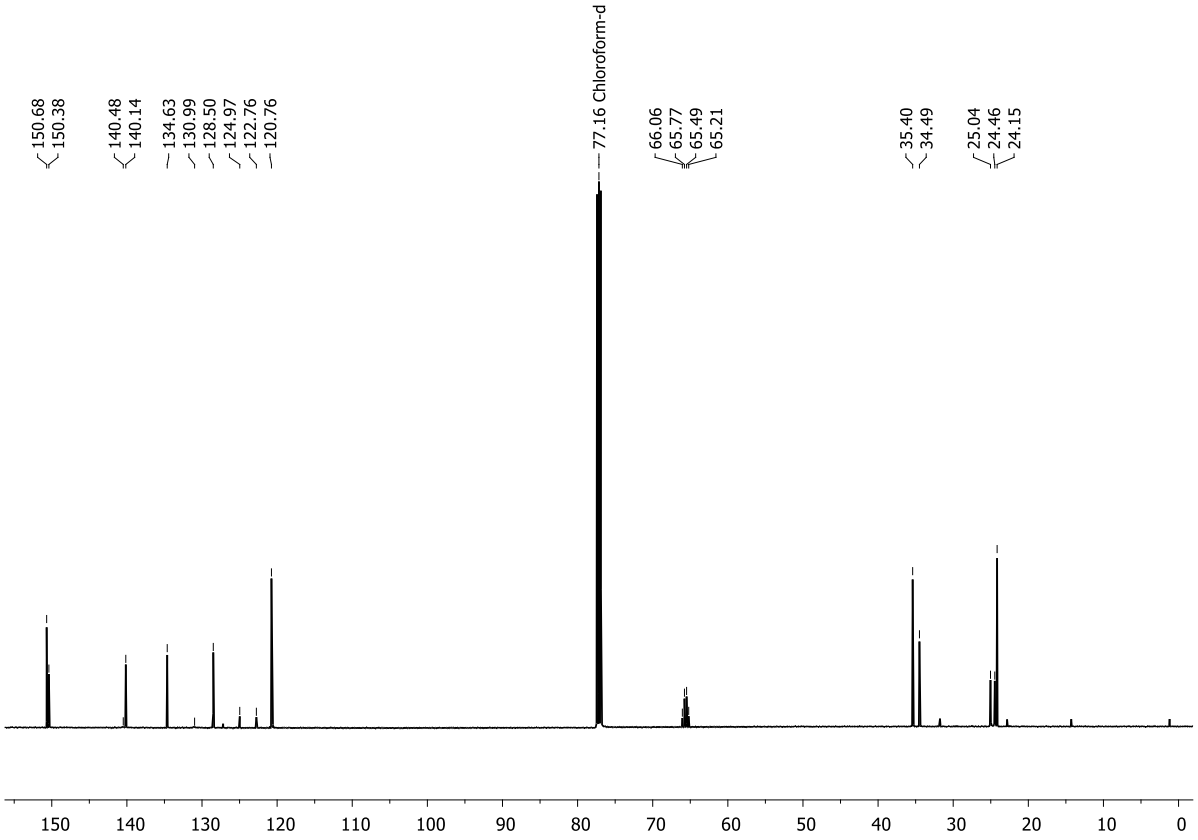

Figure 5.6.106. $^{13}C\{^{1}H\}$ NMR spectrum of **24a^{Tip}** (126 MHz, in $CDCl_3$).

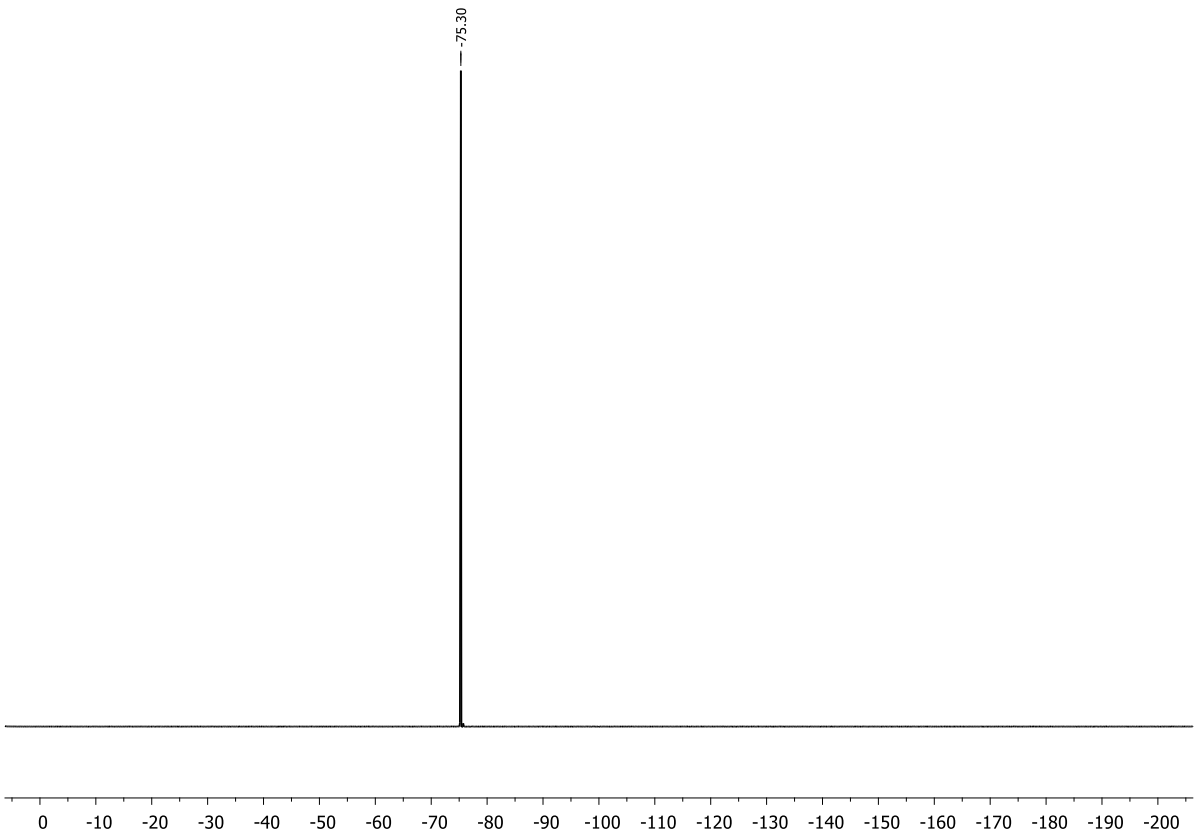

Figure 5.6.107. ^{19}F NMR spectrum of **24a^{Tip}** (471 MHz, in $CDCl_3$).

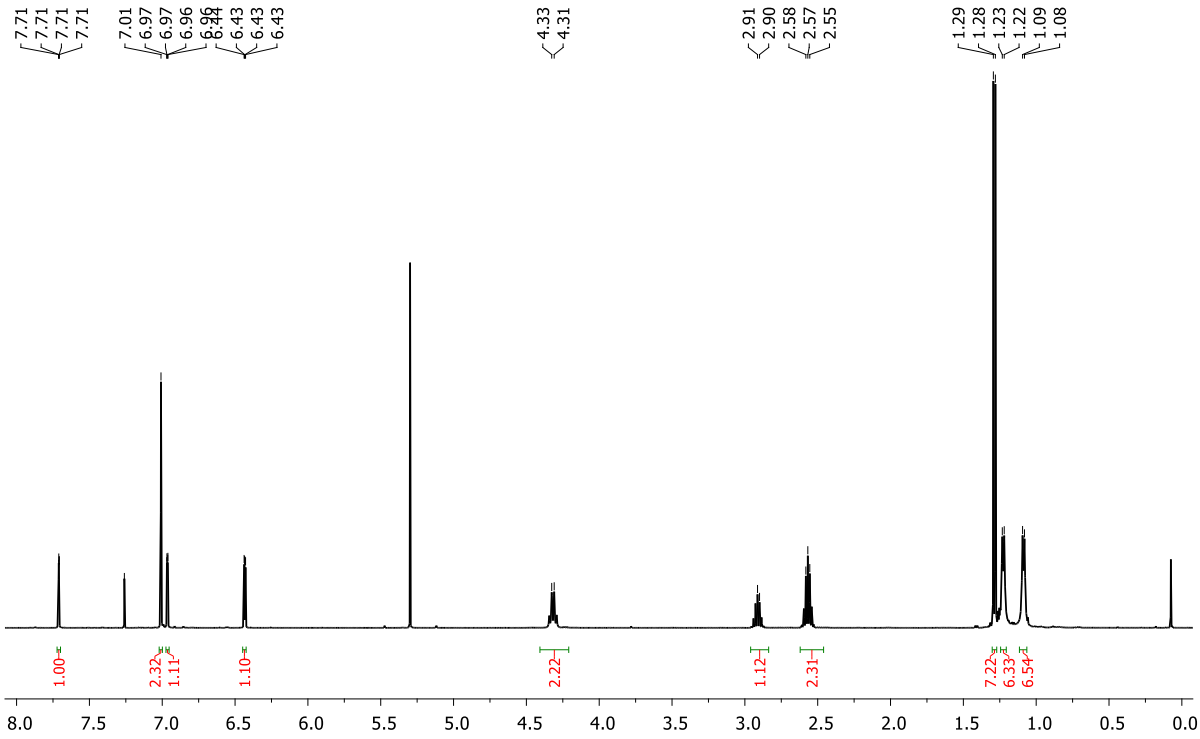

Figure 5.6.108. ^{1}H NMR spectrum of **24b^{Tip}** (500 MHz, in $CDCl_3$).

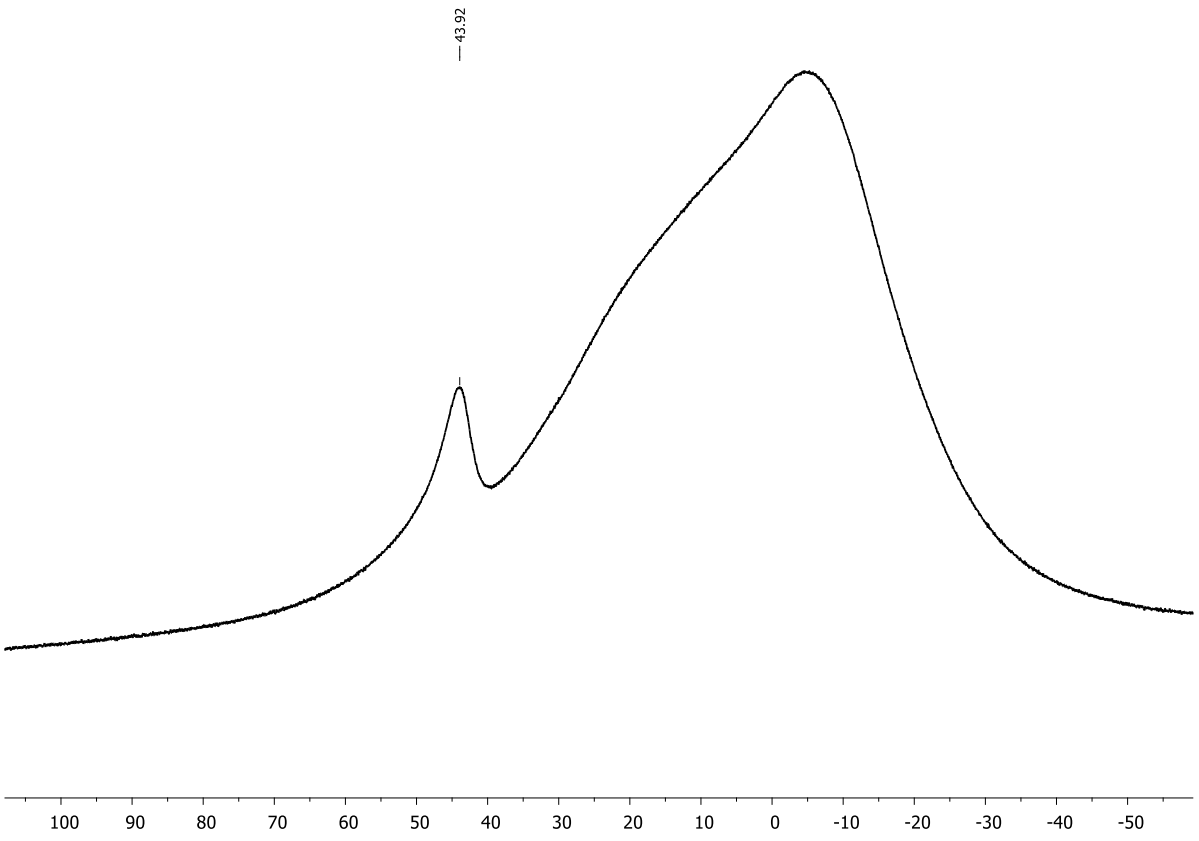

Figure 5.6.109. $^{11}B\{^{1}H\}$ NMR spectrum of **24b^{Tip}** (160 MHz, in $CDCl_3$).

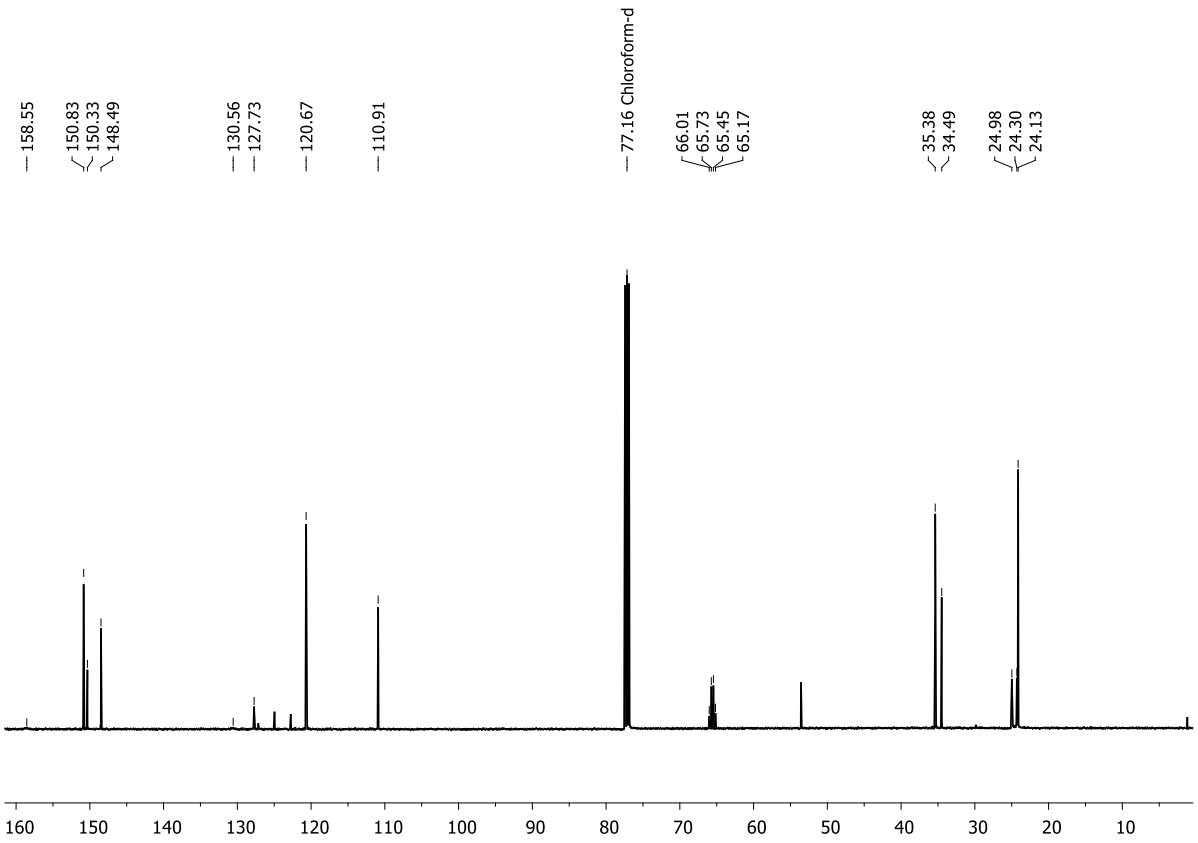

Figure 5.6.110. $^{13}C\{^{1}H\}$ NMR spectrum of **24b^{Tip}** (126 MHz, in $CDCl_3$).

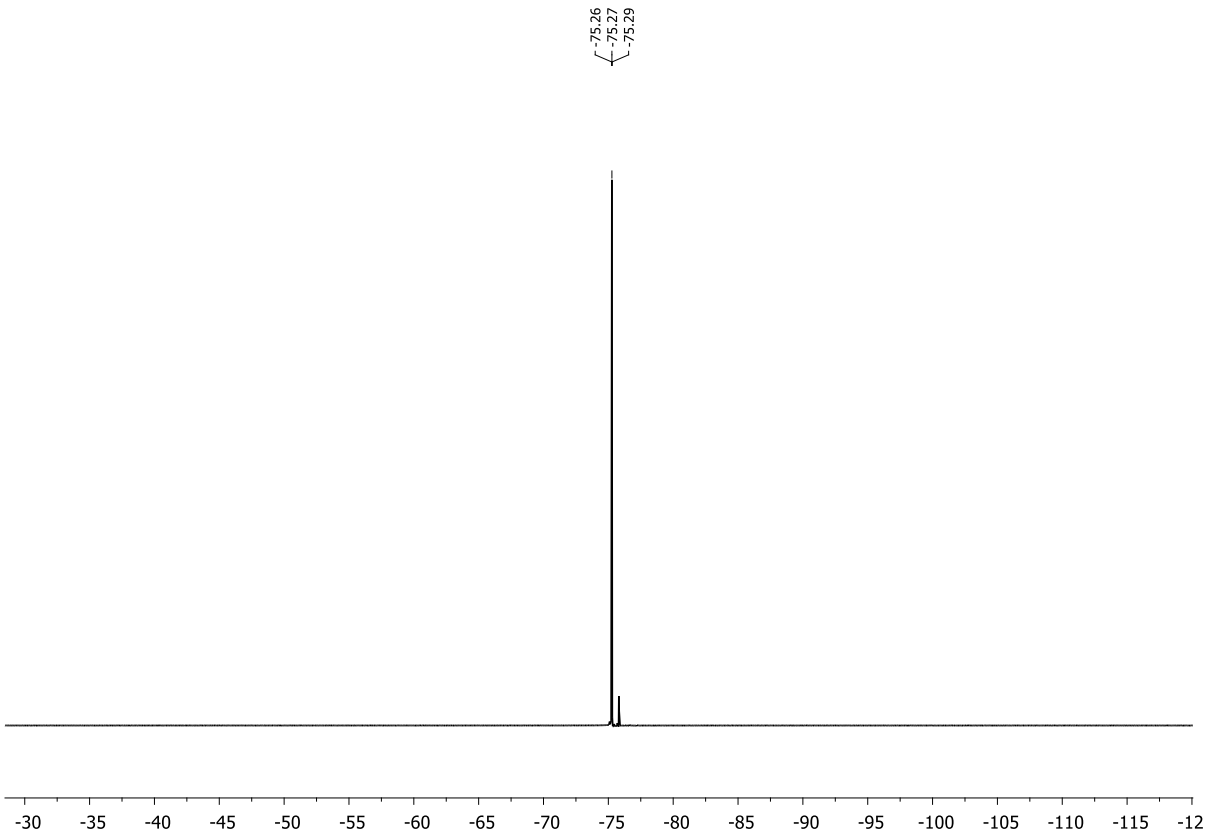

Figure 5.6.111. ^{19}F NMR spectrum of **24b^{Tip}** (471 MHz, in $CDCl_3$).

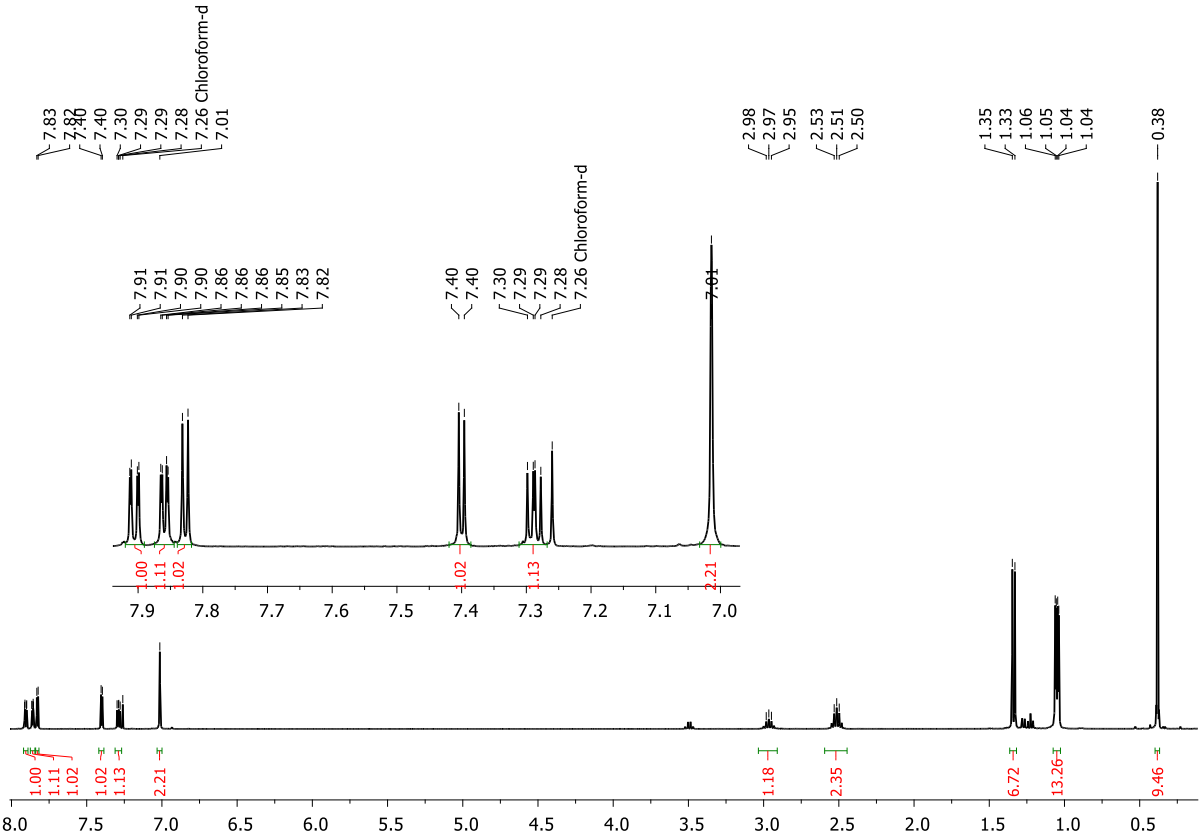

Figure 5.6.112. ^{1}H NMR spectrum of **25a** (400 MHz, in $CDCl_3$).

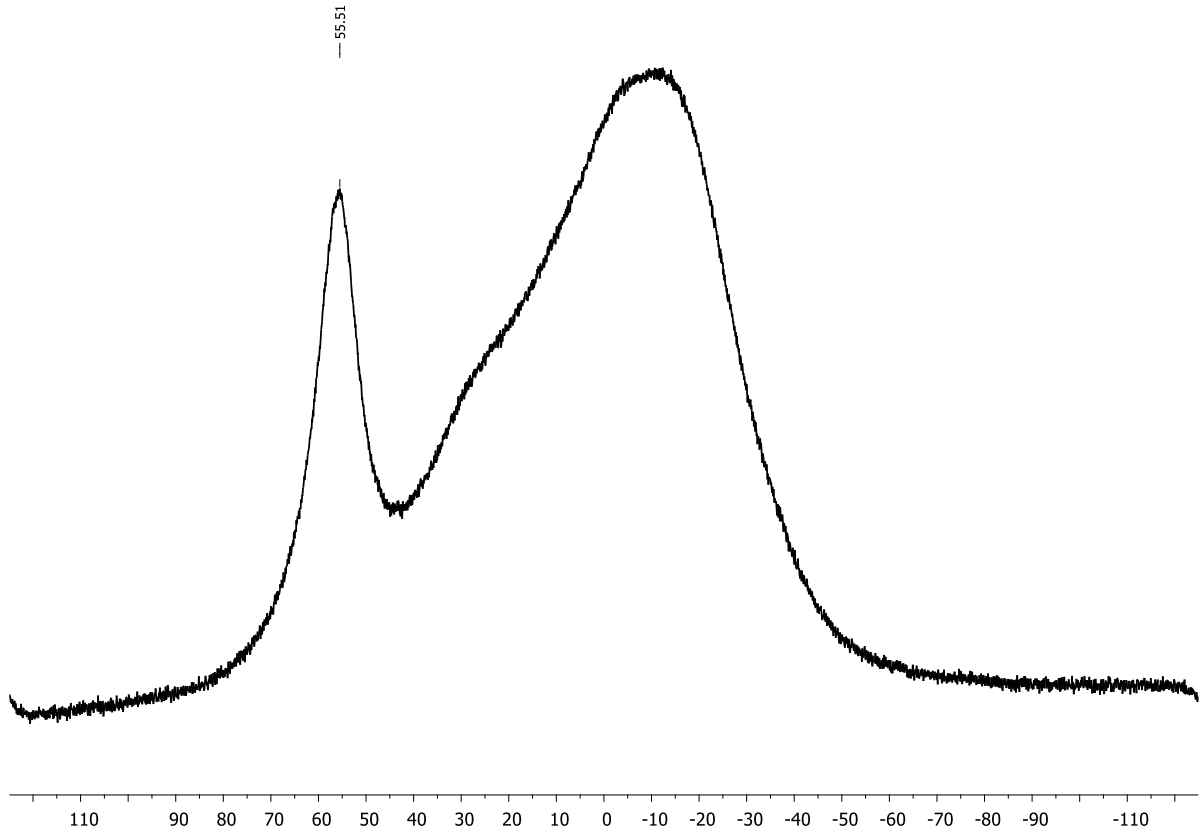

Figure 5.6.113. $^{11}B\{^{1}H\}$ NMR spectrum of **25a** (126 MHz, in $CDCl_3$).

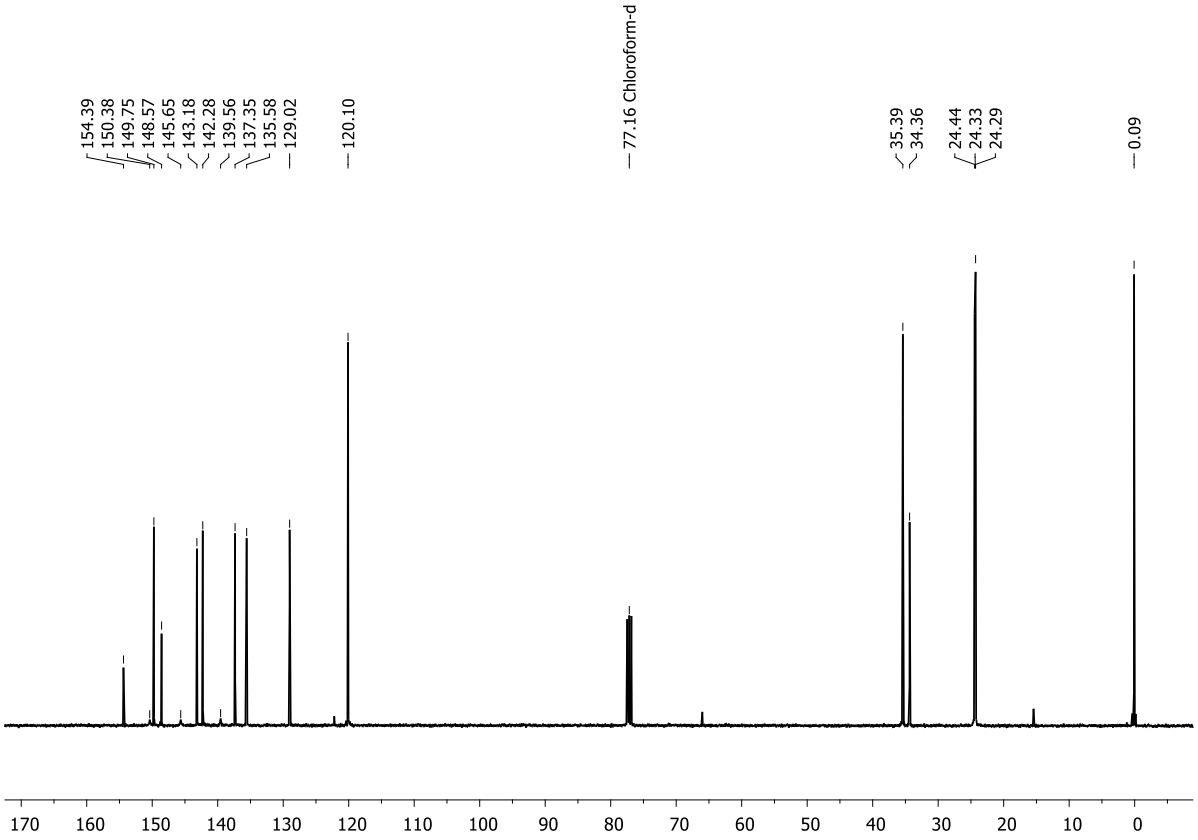

Figure 5.6.114. ^{13}C NMR spectrum of **25a** (101 MHz, in $CDCl_3$).

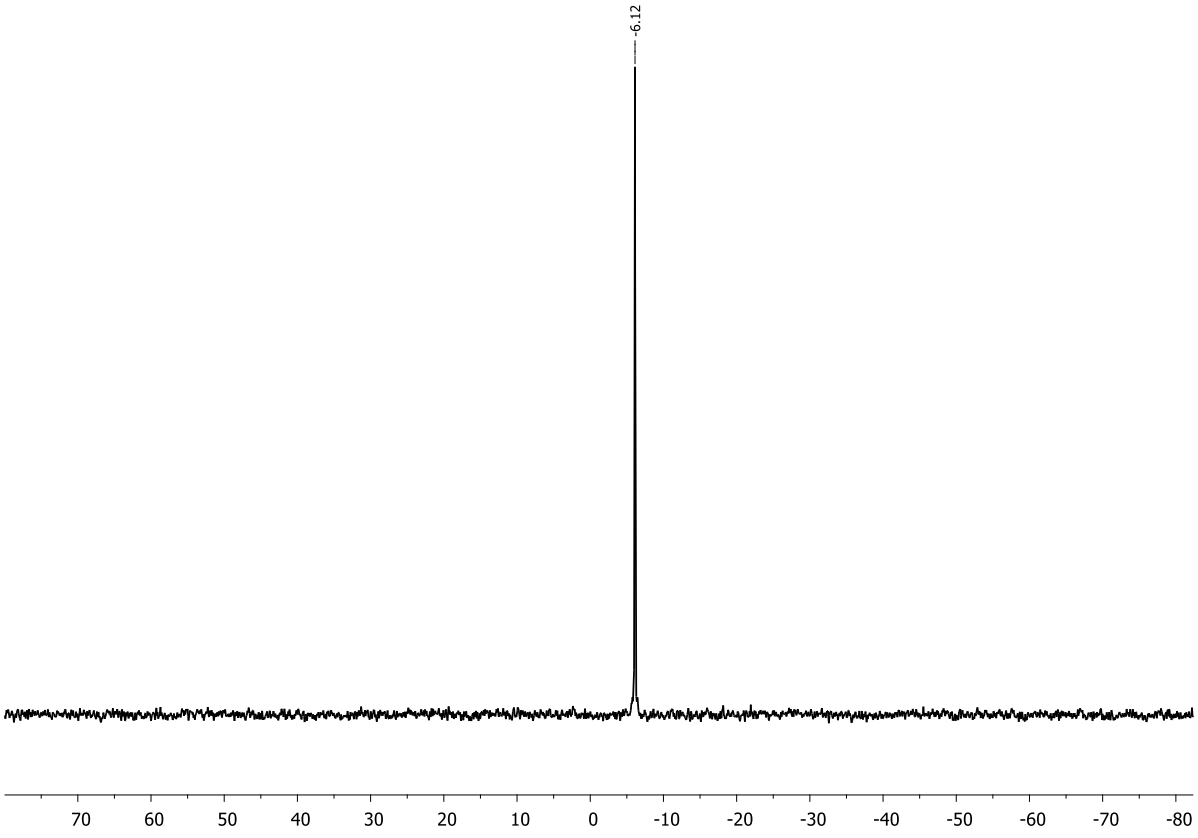

Figure 5.6.115. ^{29}Si NMR spectrum of **25a** (79 MHz, in $CDCl_3$).

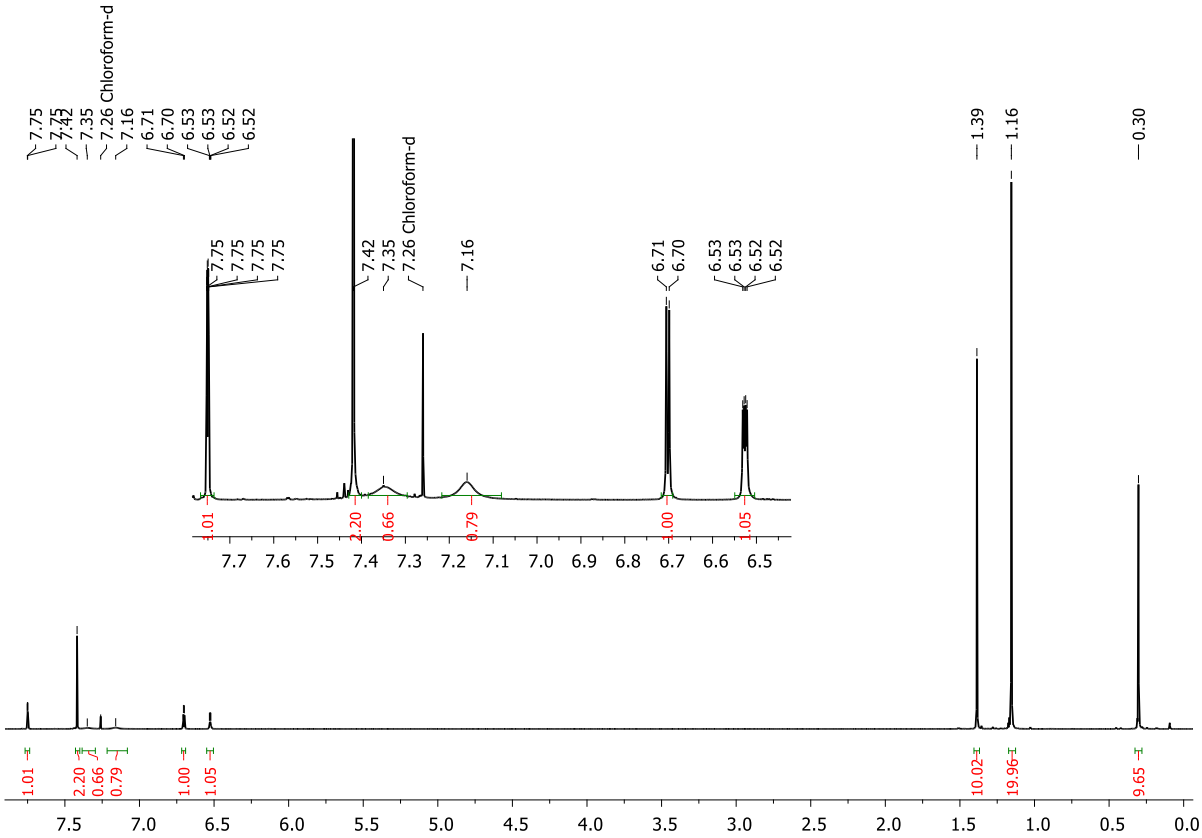

Figure 5.6.116. ^{1}H NMR spectrum of **25b** (500 MHz, in $CDCl_3$).

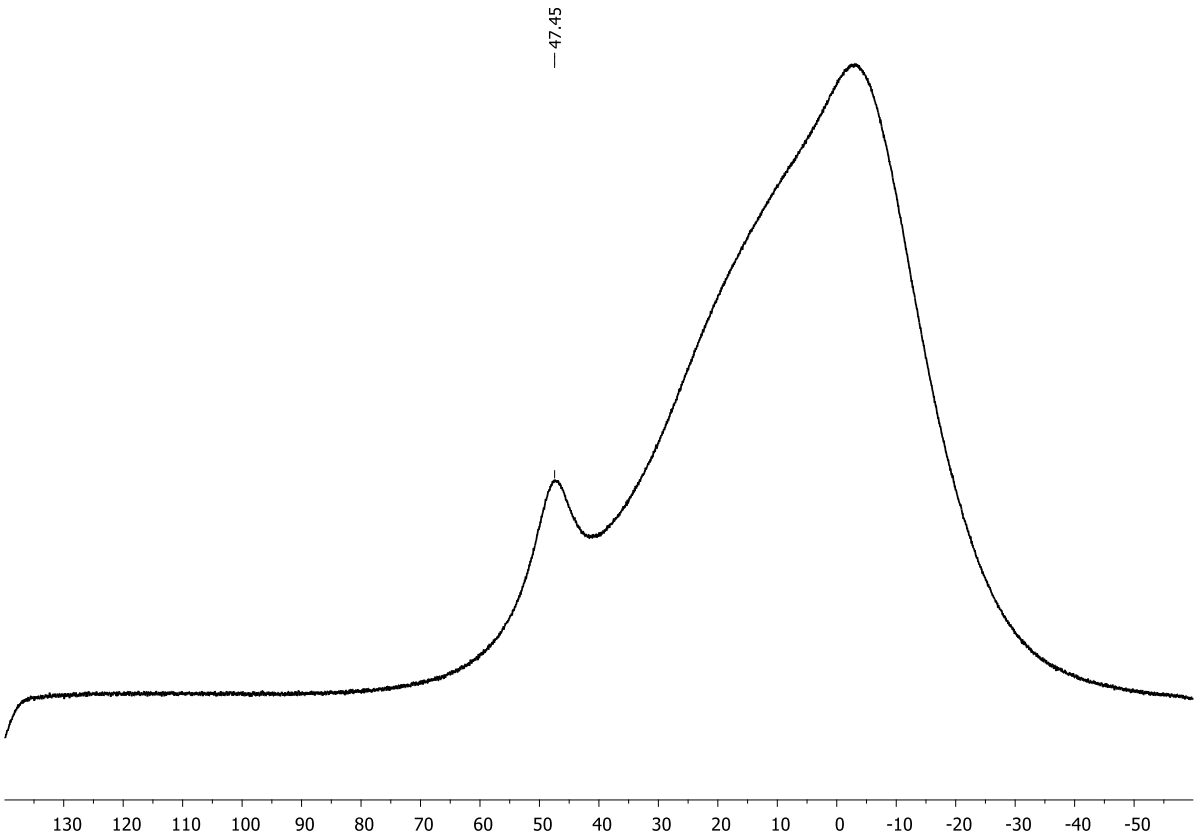

Figure 5.6.117. $^{11}B\{^{1}H\}$ NMR spectrum of **25b** (160 MHz, in $CDCl_3$).

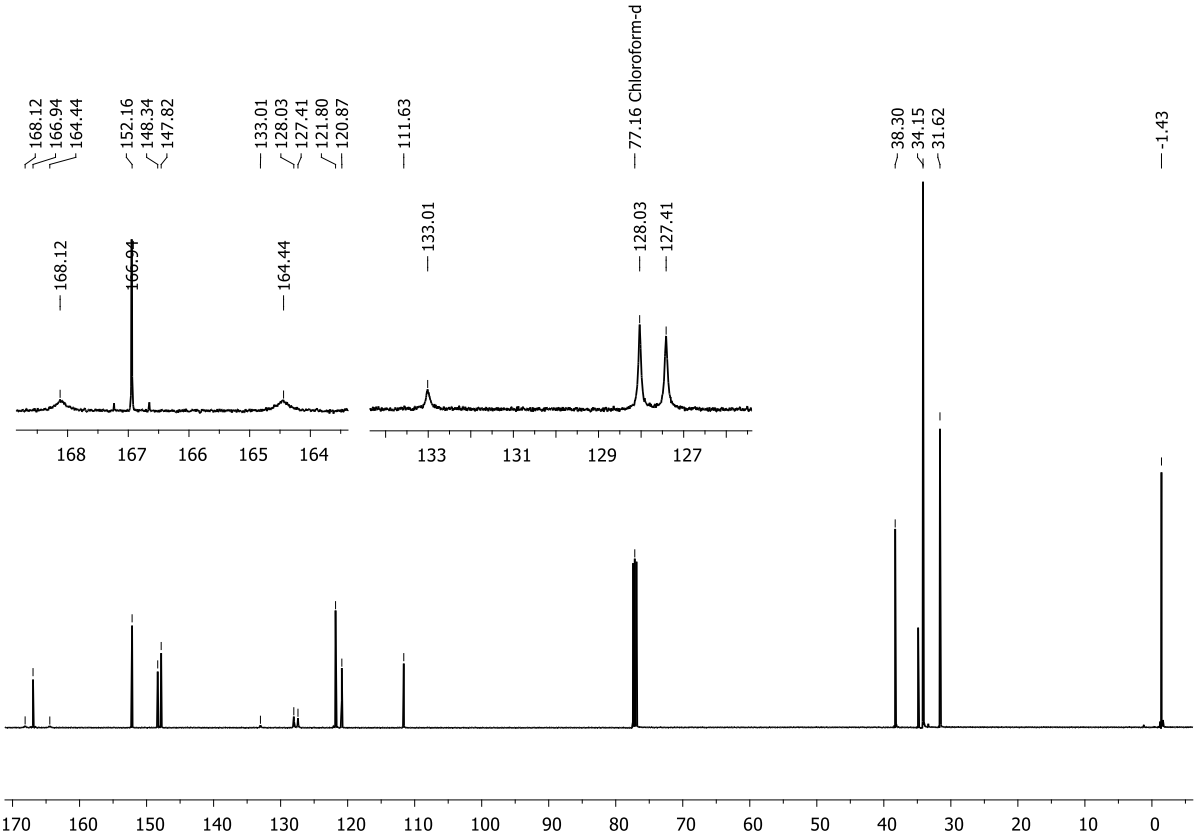

Figure 5.6.118. $^{13}C\{^{1}H\}$ NMR spectrum of **25b** (126 MHz, in $CDCl_3$).

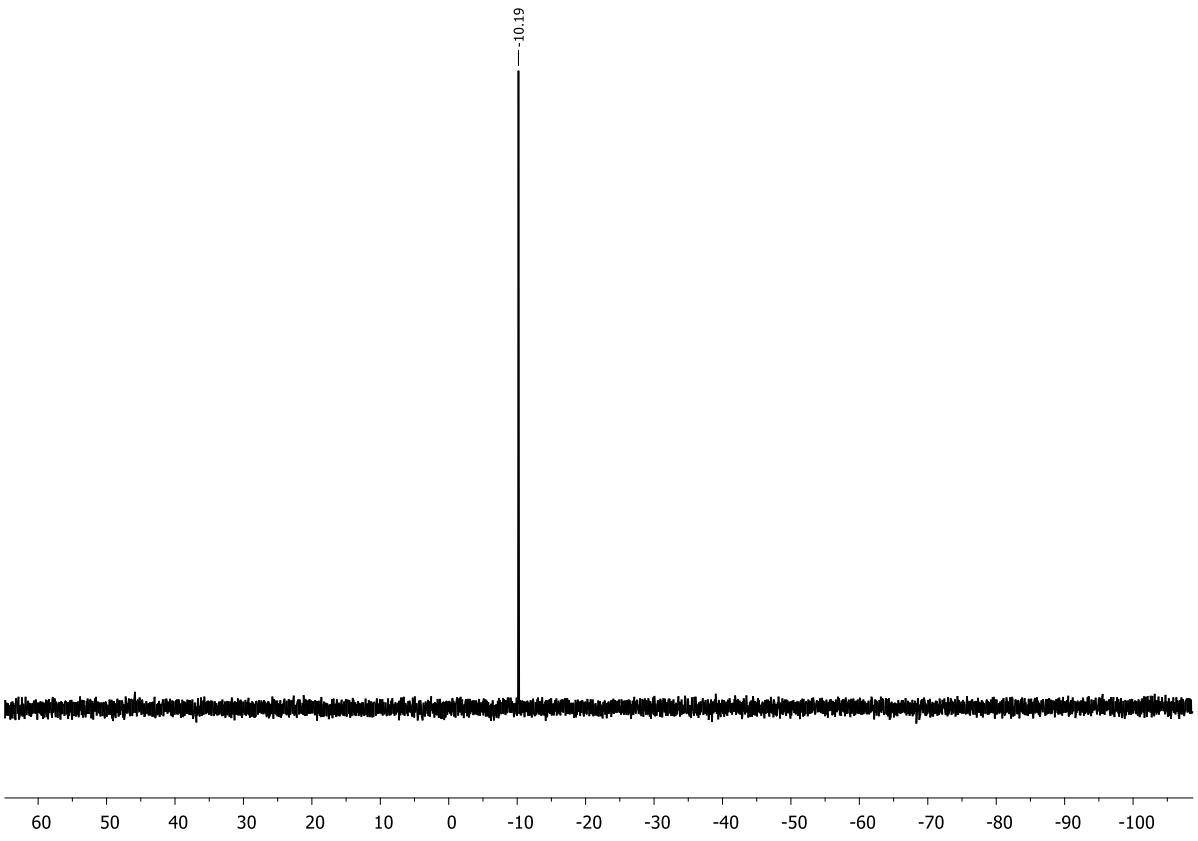

Figure 5.6.119. ^{29}Si NMR spectrum of **25b** (99 MHz, in $CDCl_3$).

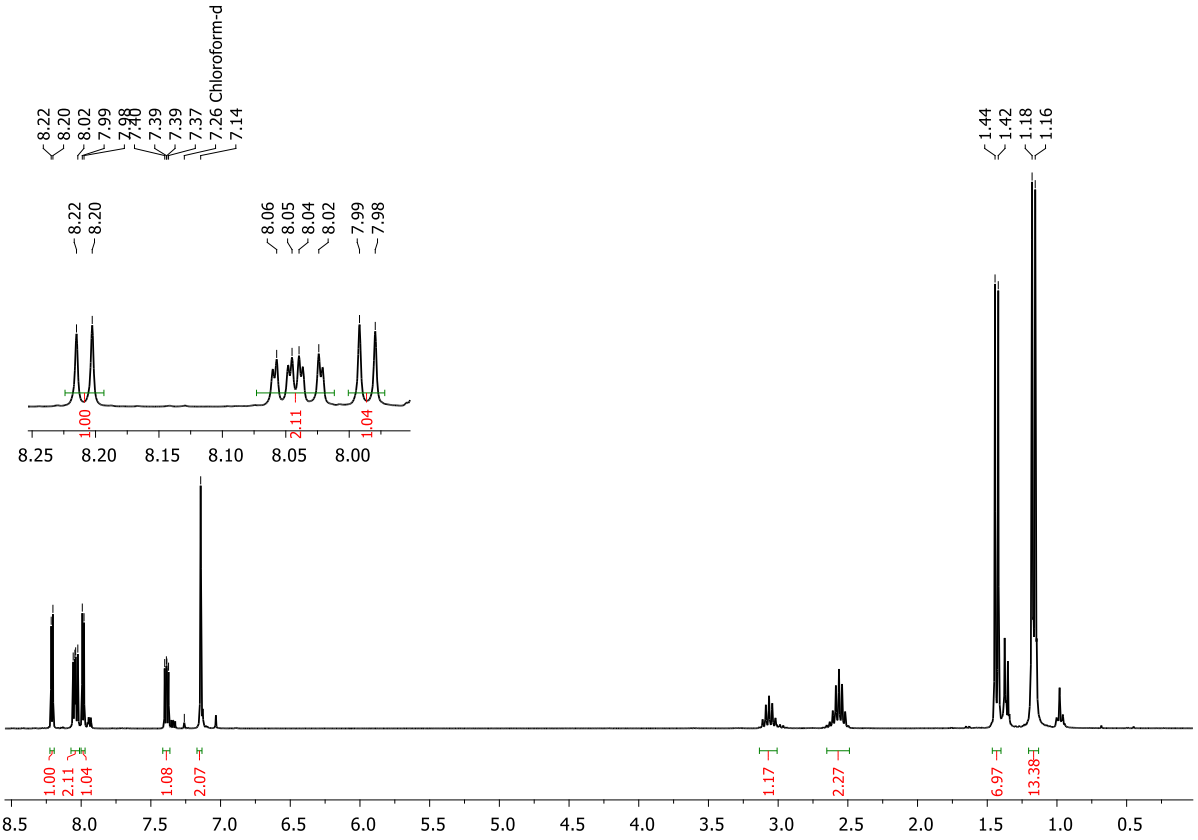

Figure 5.6.120. ^{1}H NMR spectrum of crude **26a** (500 MHz, in $CDCl_3$).

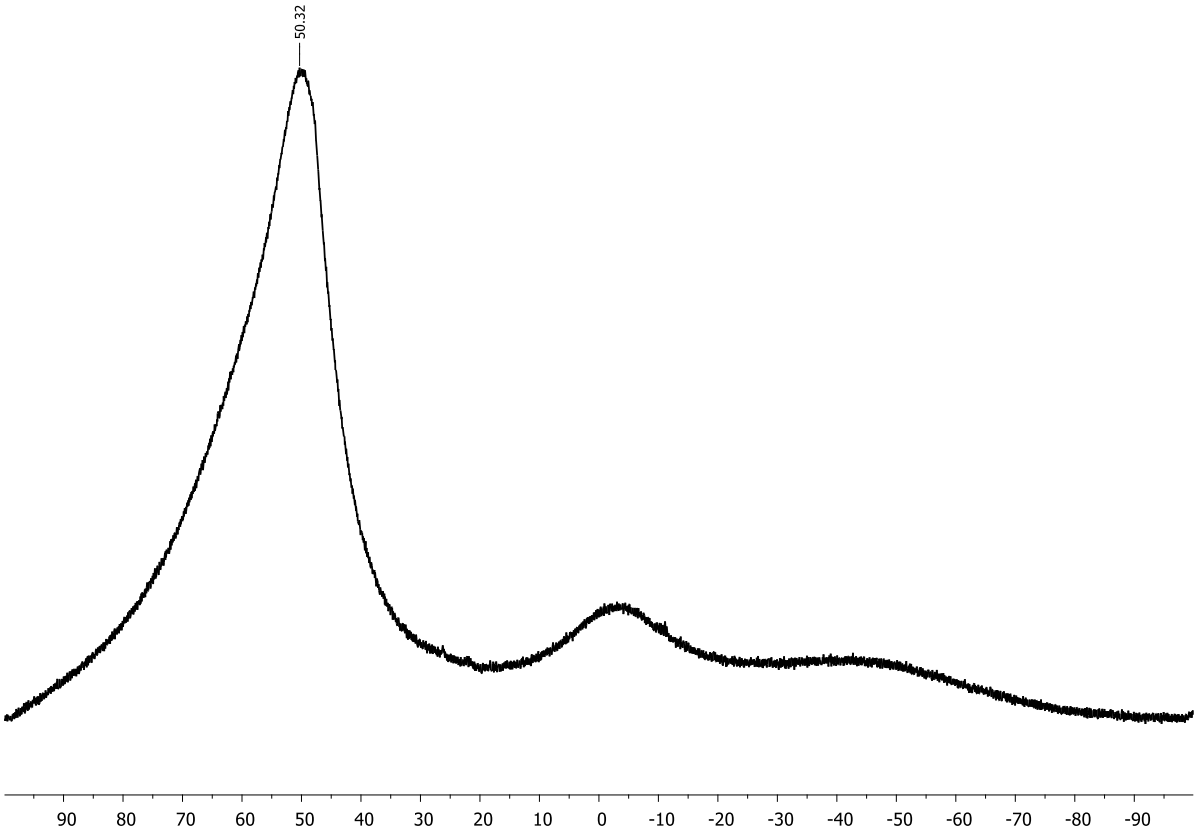

Figure 5.6.121. $^{11}B\{^{1}H\}$ NMR spectrum of **26a** (160 MHz, in $CDCl_3$).

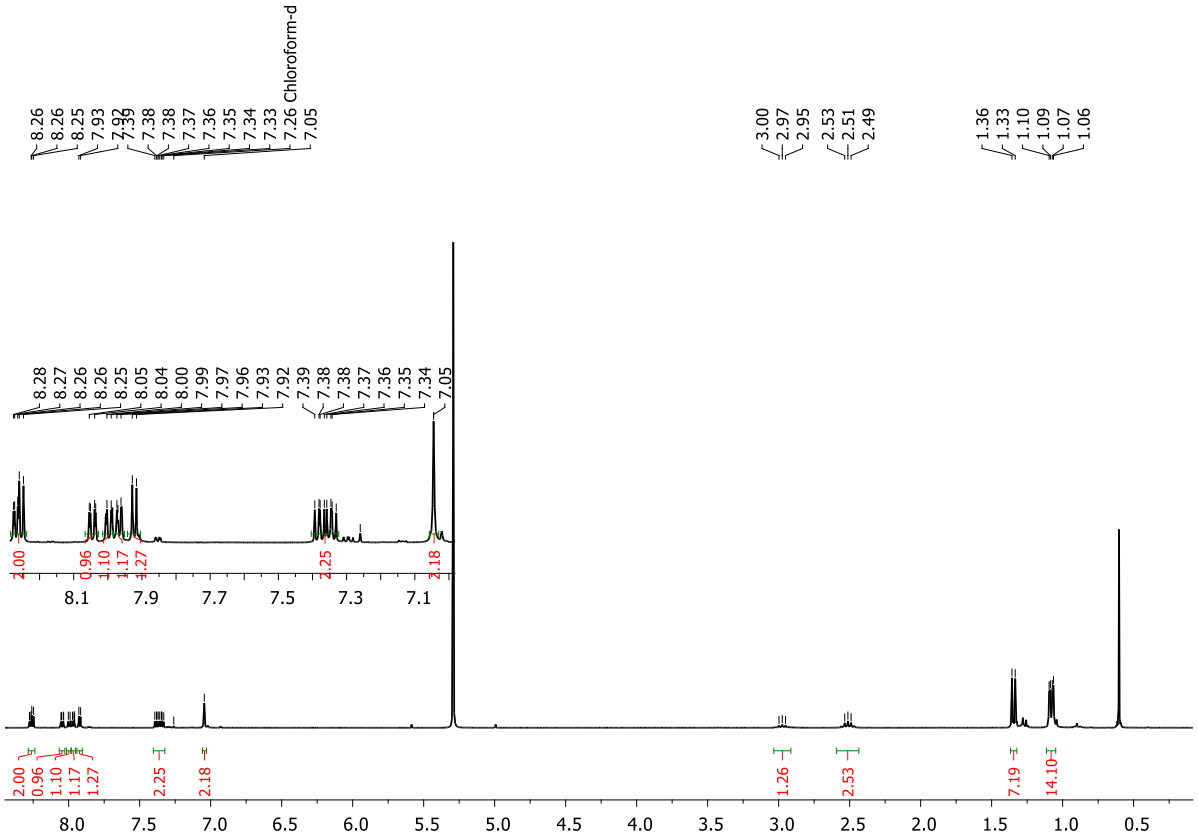

Figure 5.6.122. ^{1}H NMR spectrum of crude **27a** (300 MHz, in $CDCl_3$).

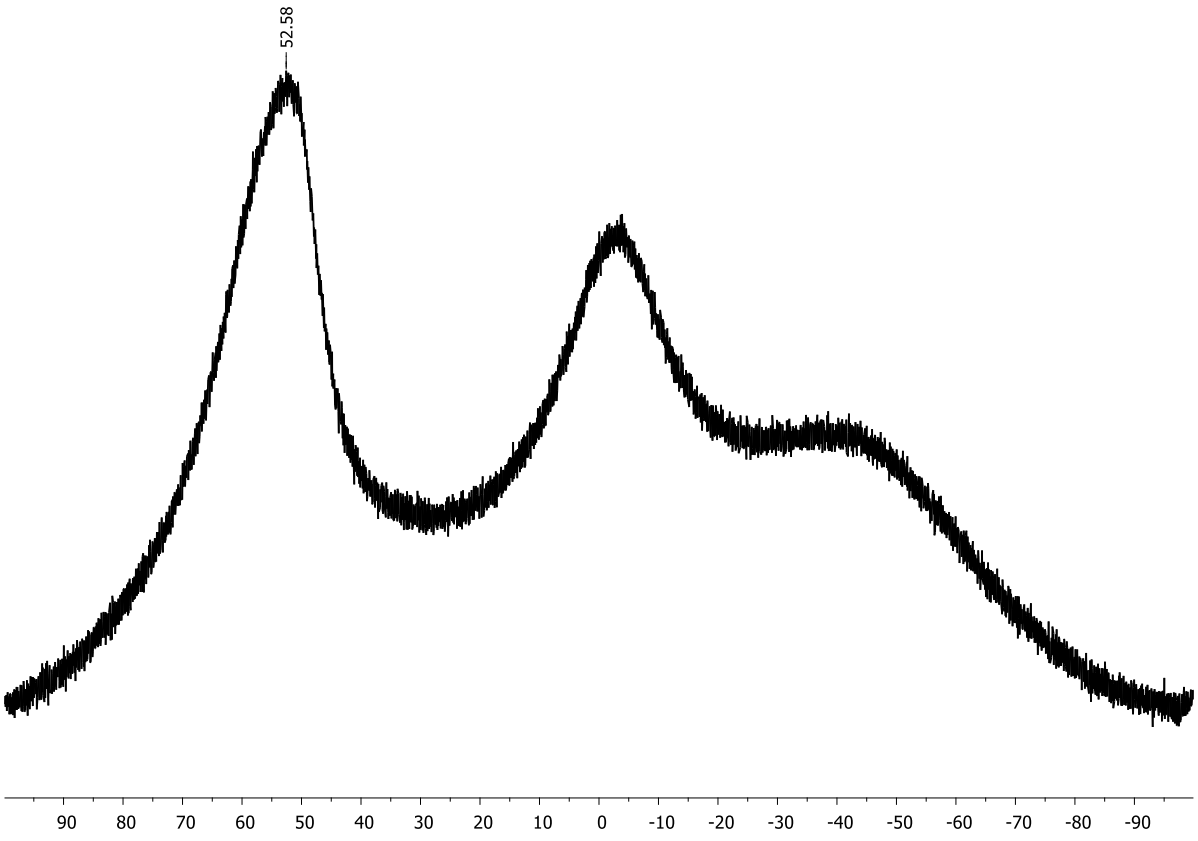

Figure 5.6.123. $^{11}B\{^{1}H\}$ NMR spectrum of crude **27a** (96 MHz, in $CDCl_3$).

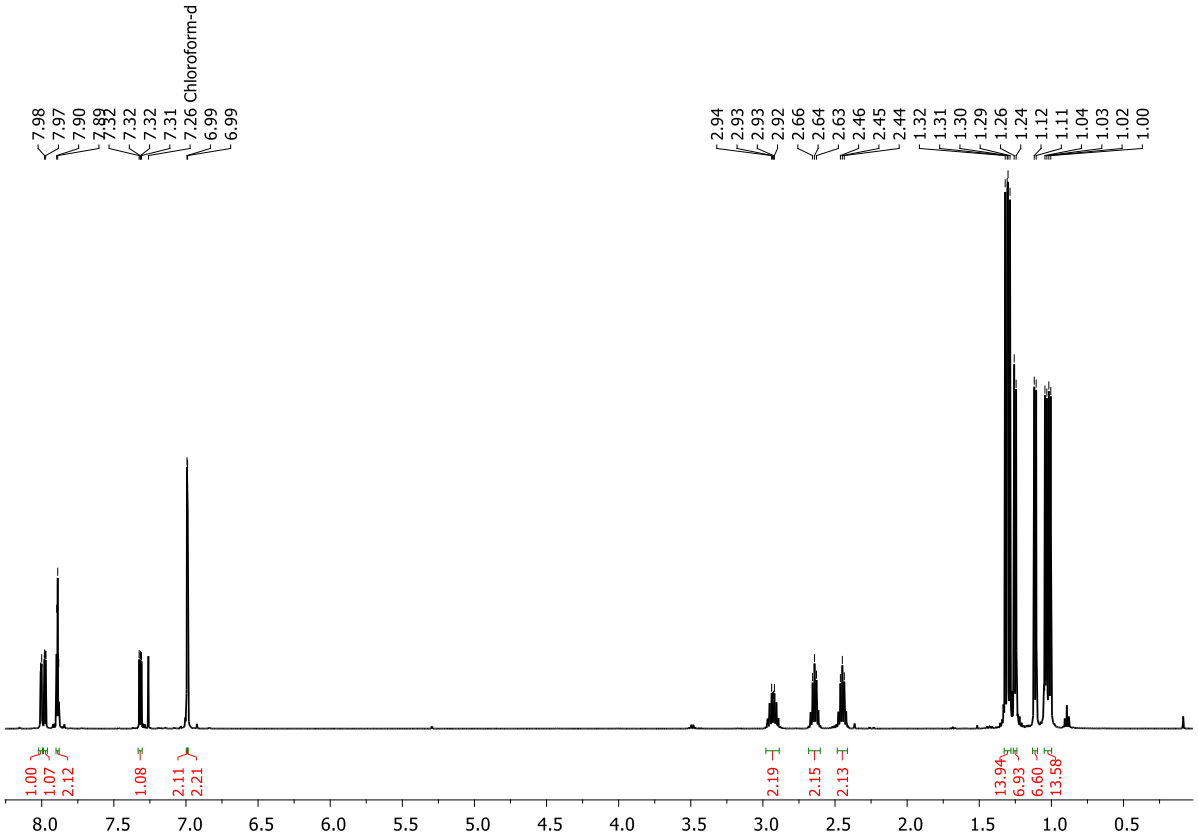

Figure 5.6.124. ^{1}H NMR spectrum of **29a** (500 MHz, in $CDCl_3$).

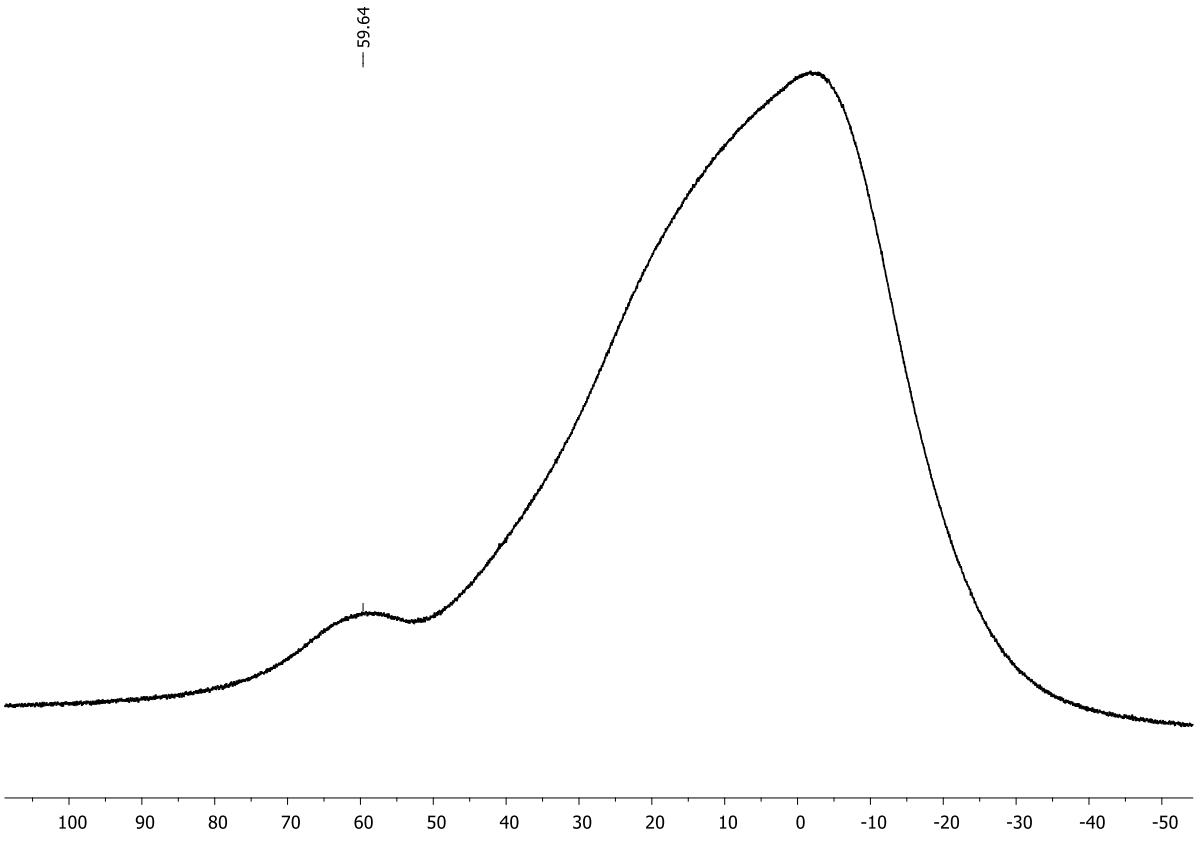

Figure 5.6.125. $^{11}B\{^{1}H\}$ NMR spectrum of **29a** (160 MHz, in $CDCl_3$).

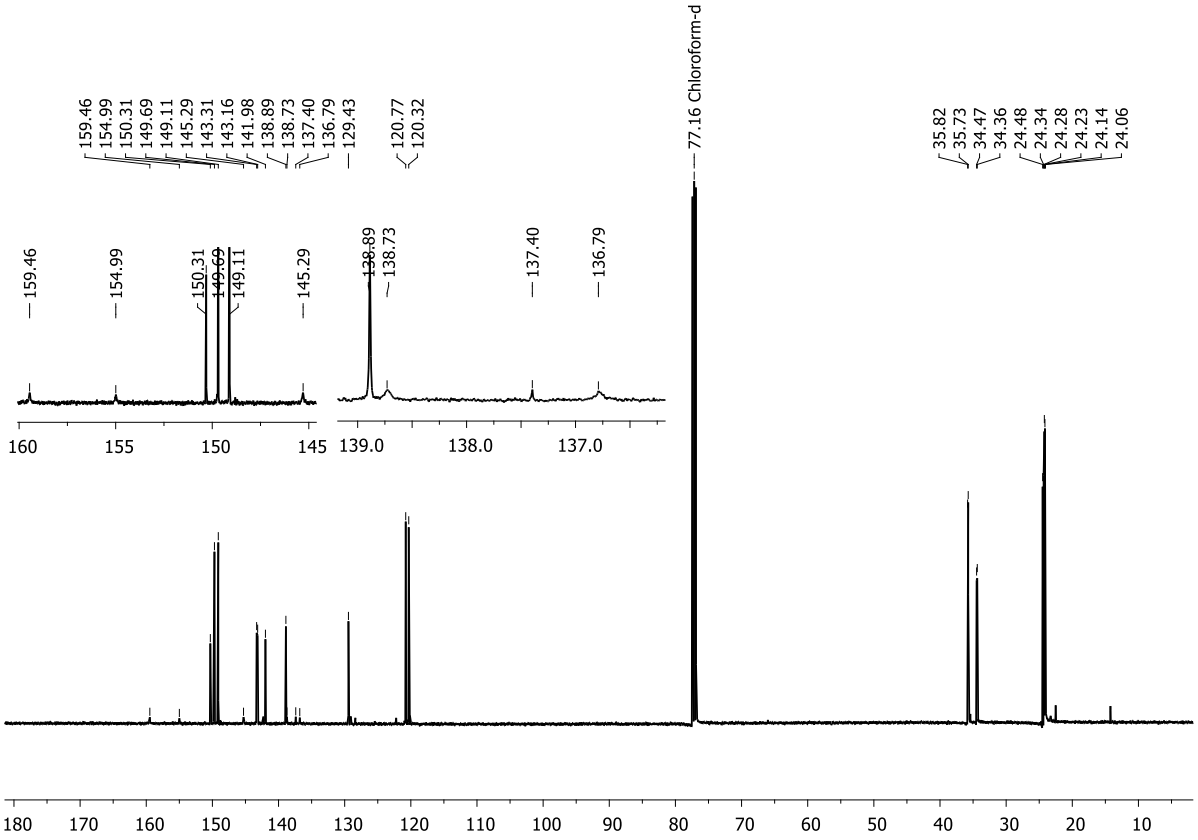

Figure 5.6.126. ^{13}C NMR spectrum of **29a** (126 MHz, in $CDCl_3$).

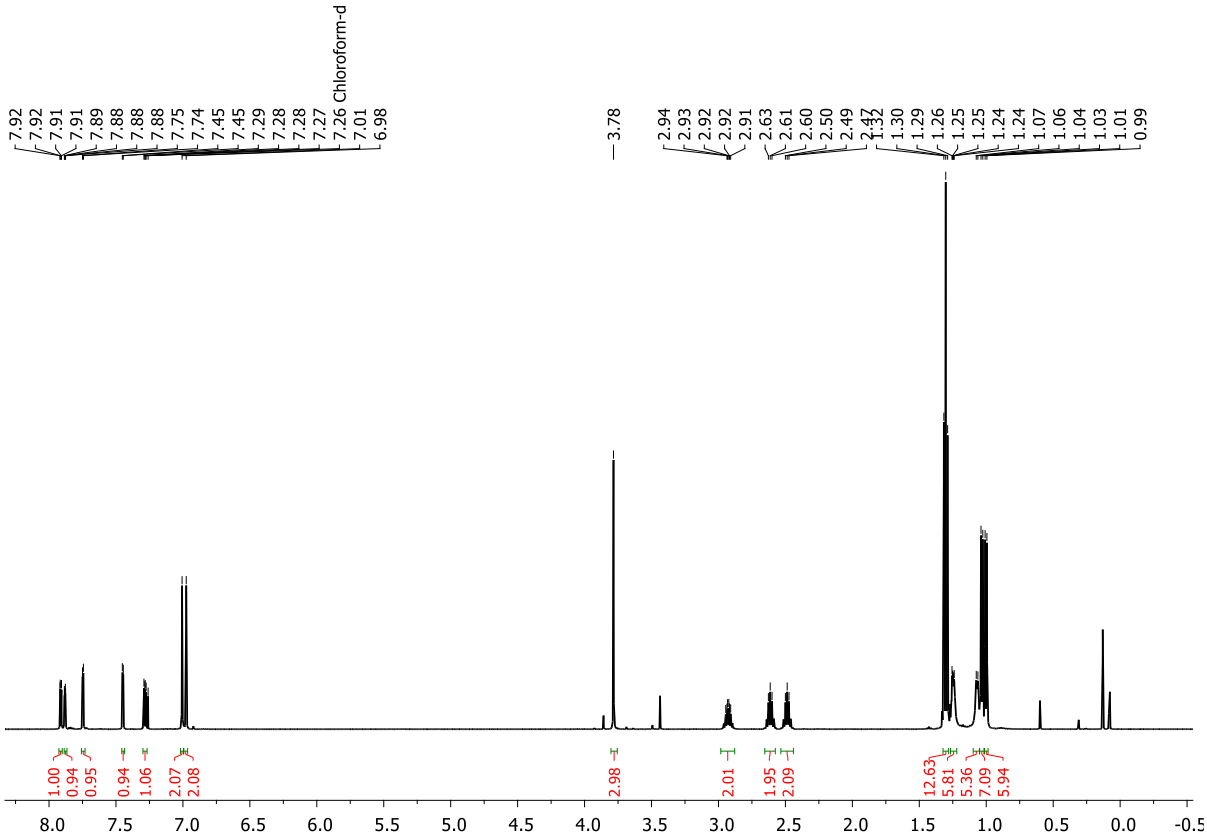

Figure 5.6.127. ^{1}H NMR spectrum of **30a** (500 MHz, in $CDCl_3$).

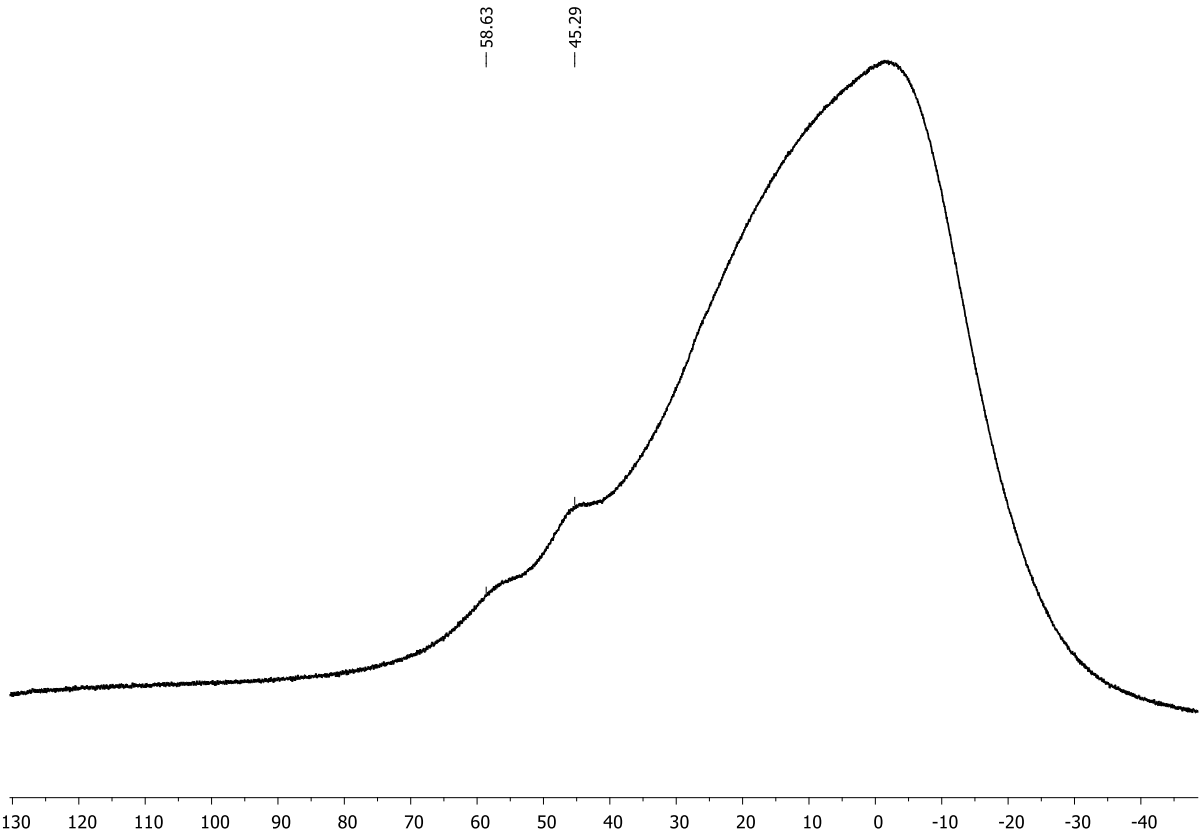

Figure 5.6.128. $^{11}B\{^{1}H\}$ NMR spectrum of **30a** (160 MHz, in $CDCl_3$).

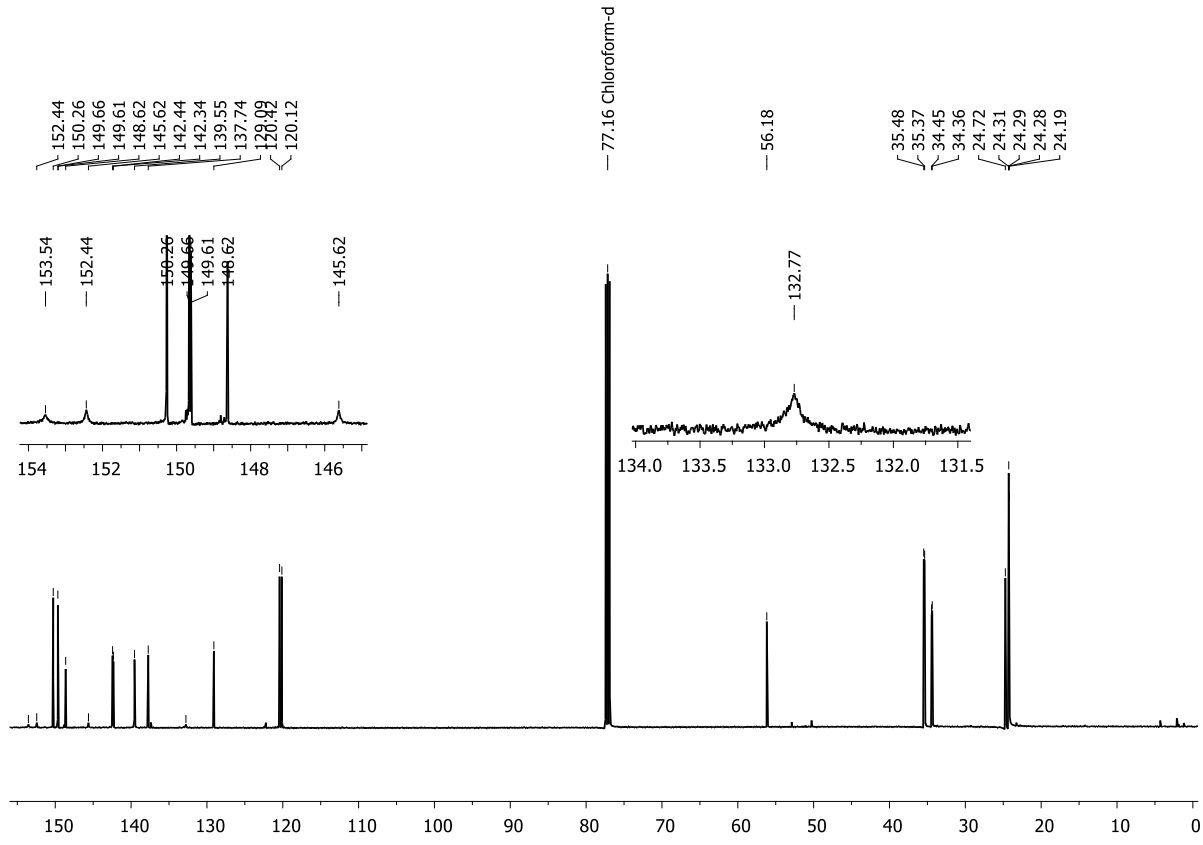

Figure 5.6.129. $^{13}C\{^{1}H\}$ NMR spectrum of **30a** (126 MHz, in $CDCl_3$).

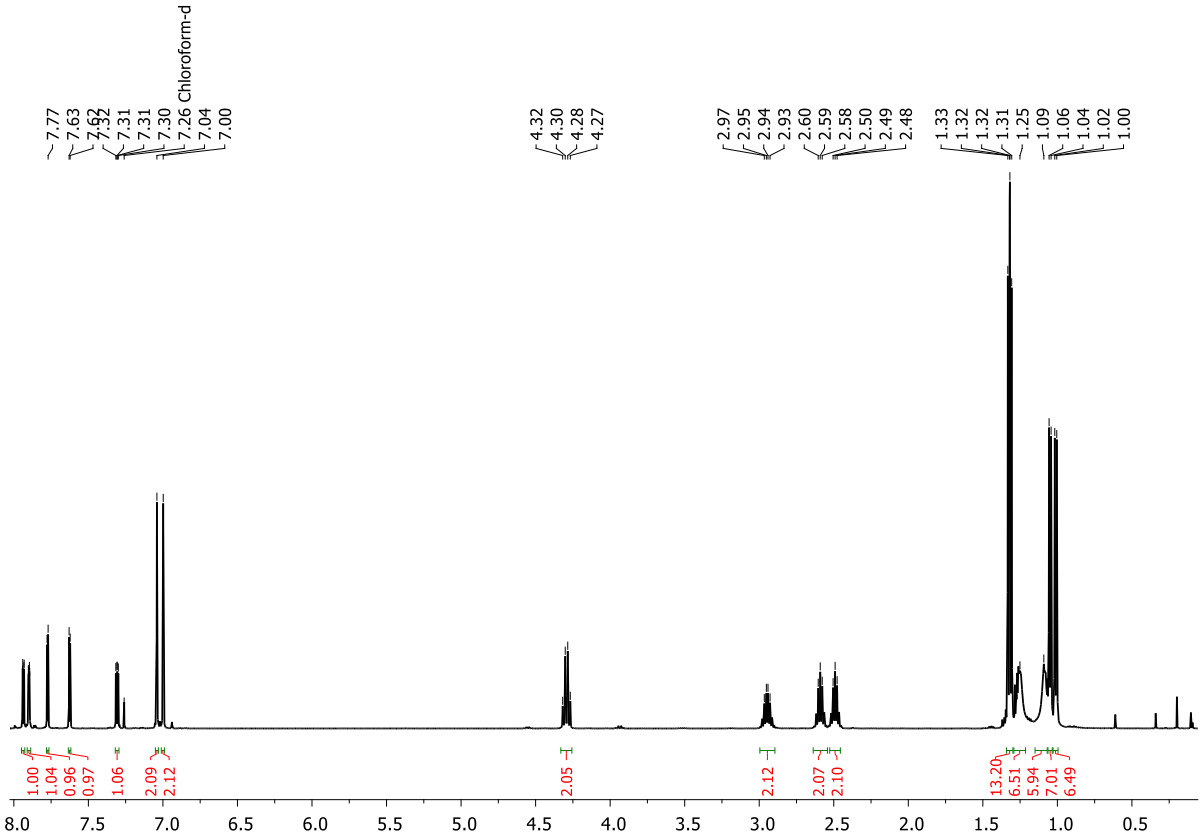

Figure 5.6.130. ^{1}H NMR spectrum of **31a** (500 MHz, in $CDCl_3$).

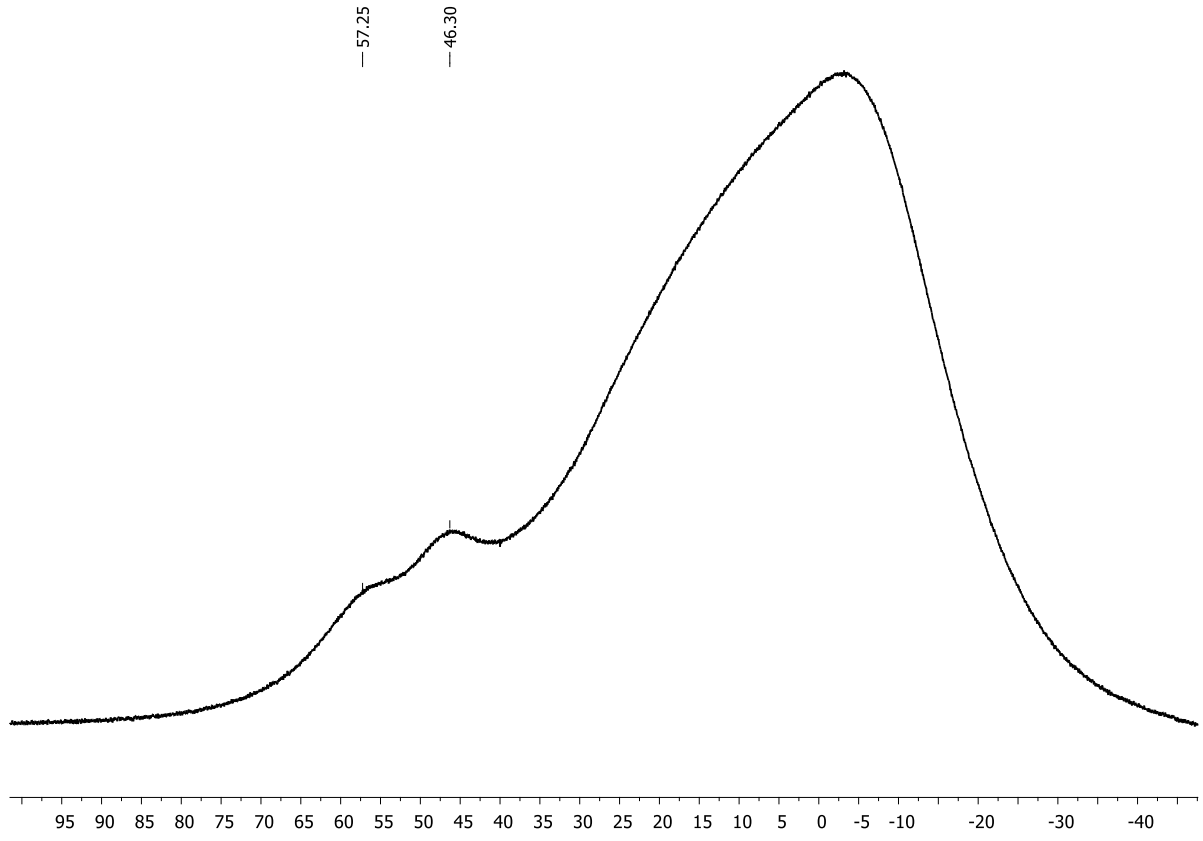

Figure 5.6.131. $^{11}B\{^{1}H\}$ NMR spectrum of **31a** (160 MHz, in $CDCl_3$).

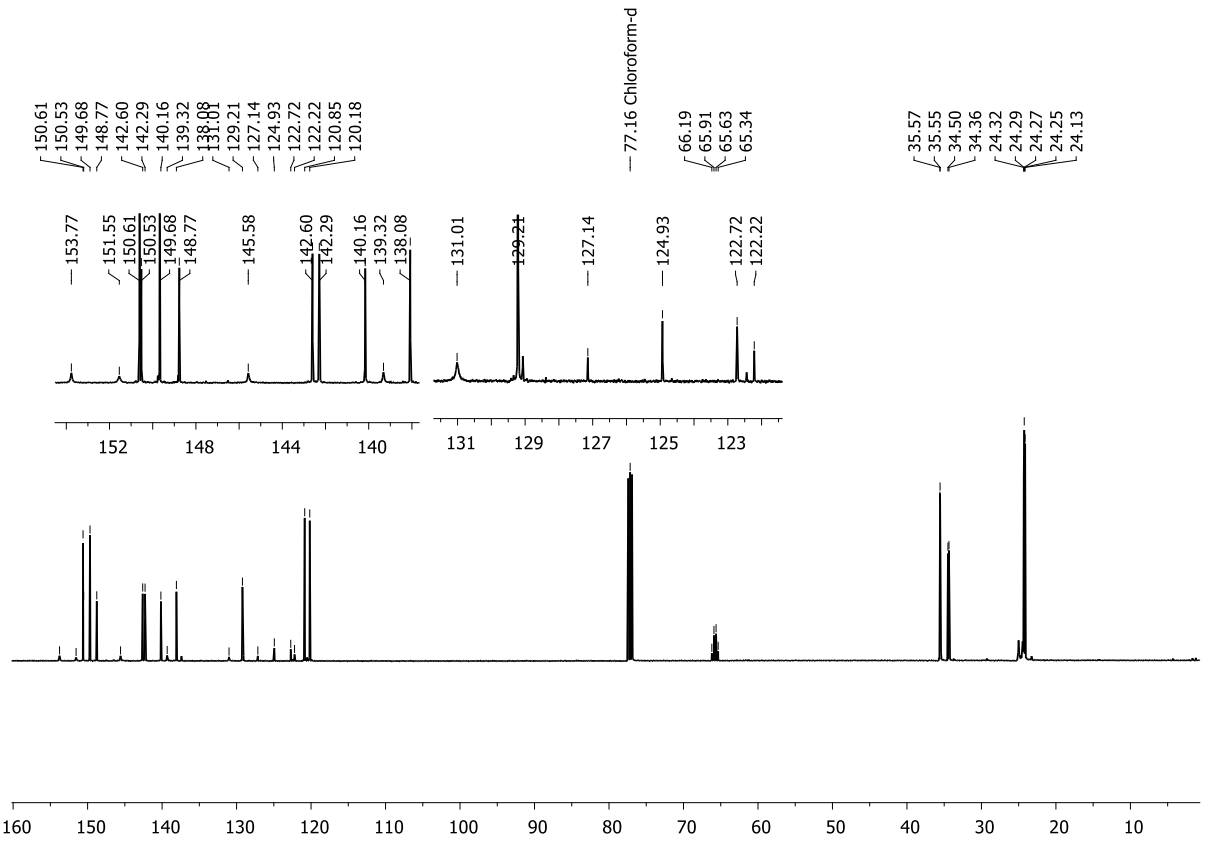

Figure 5.6.132. $^{13}C\{^{1}H\}$ NMR spectrum of **31a** (126 MHz, in $CDCl_3$).

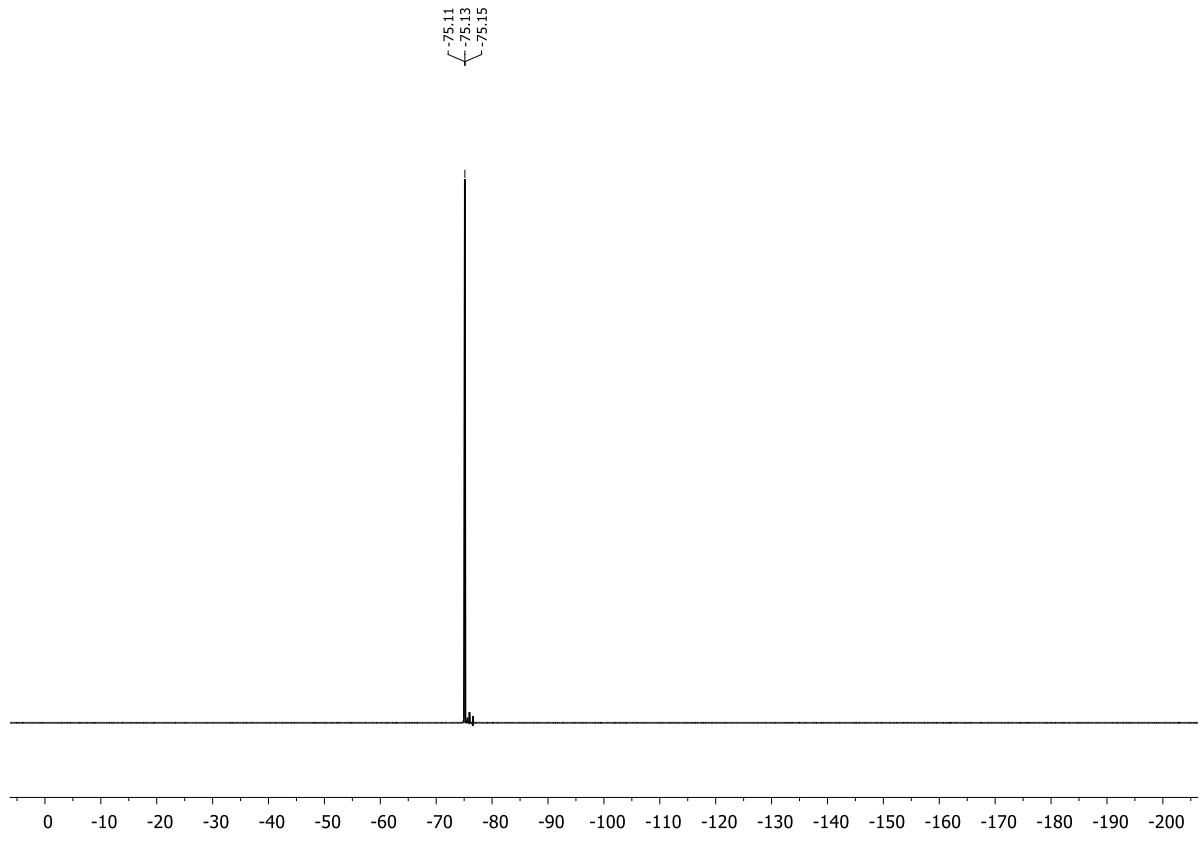

Figure 5.6.133. ^{19}F NMR spectrum of **31a** (471 MHz, in $CDCl_3$).

Mass spectra

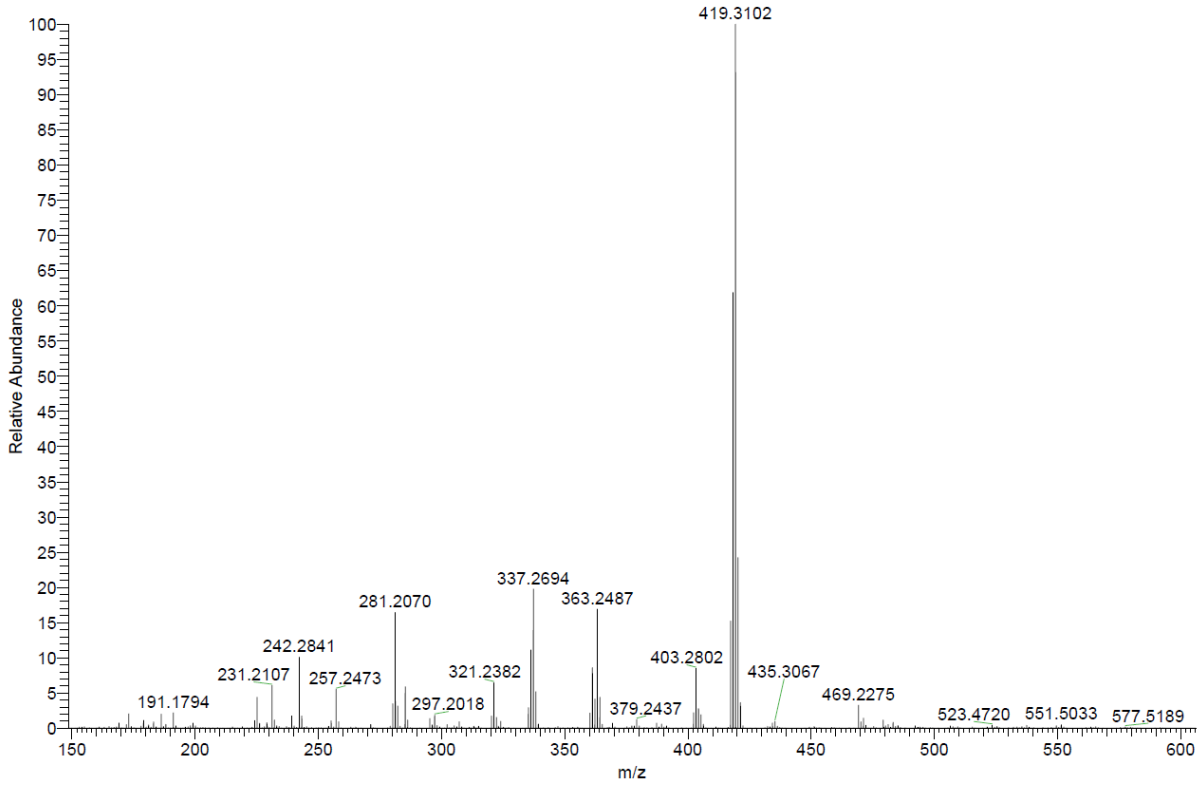

Figure 5.6.134. APCI mass spectrum of **4b**$^{\mathbf{MeMes*}}$.

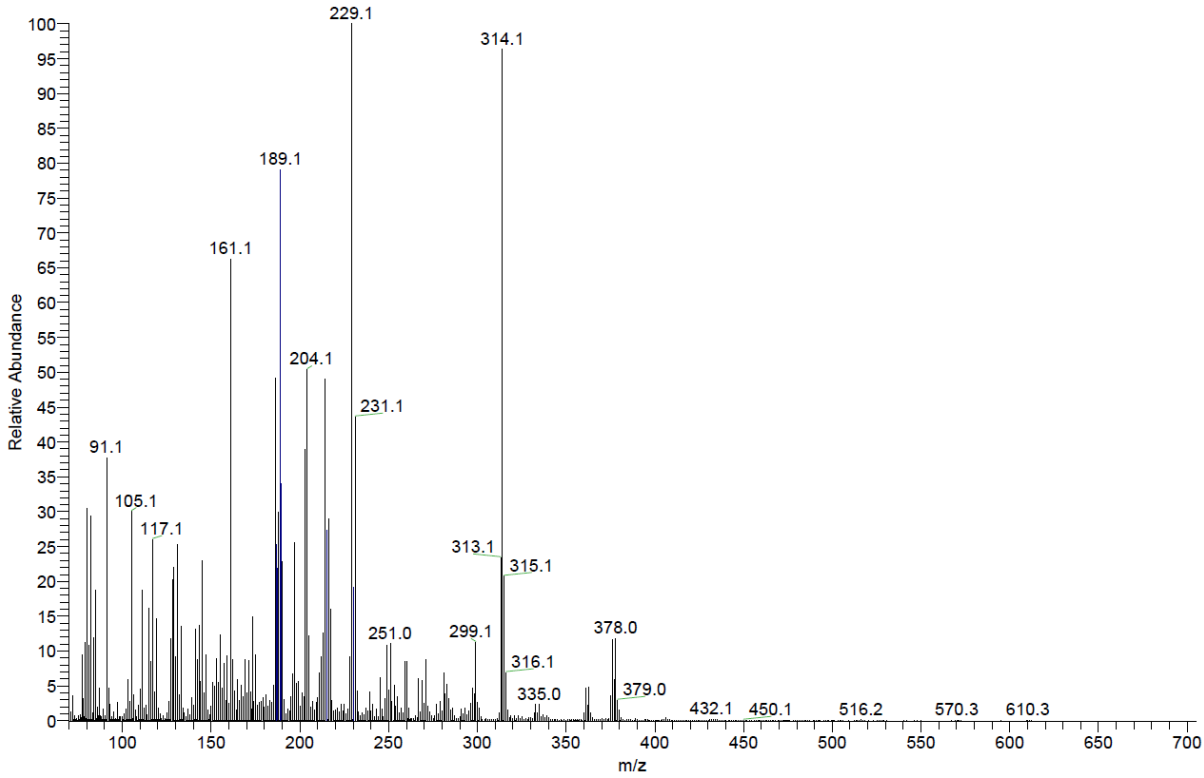

Figure 5.6.135. ESI mass spectrum of **19a**.

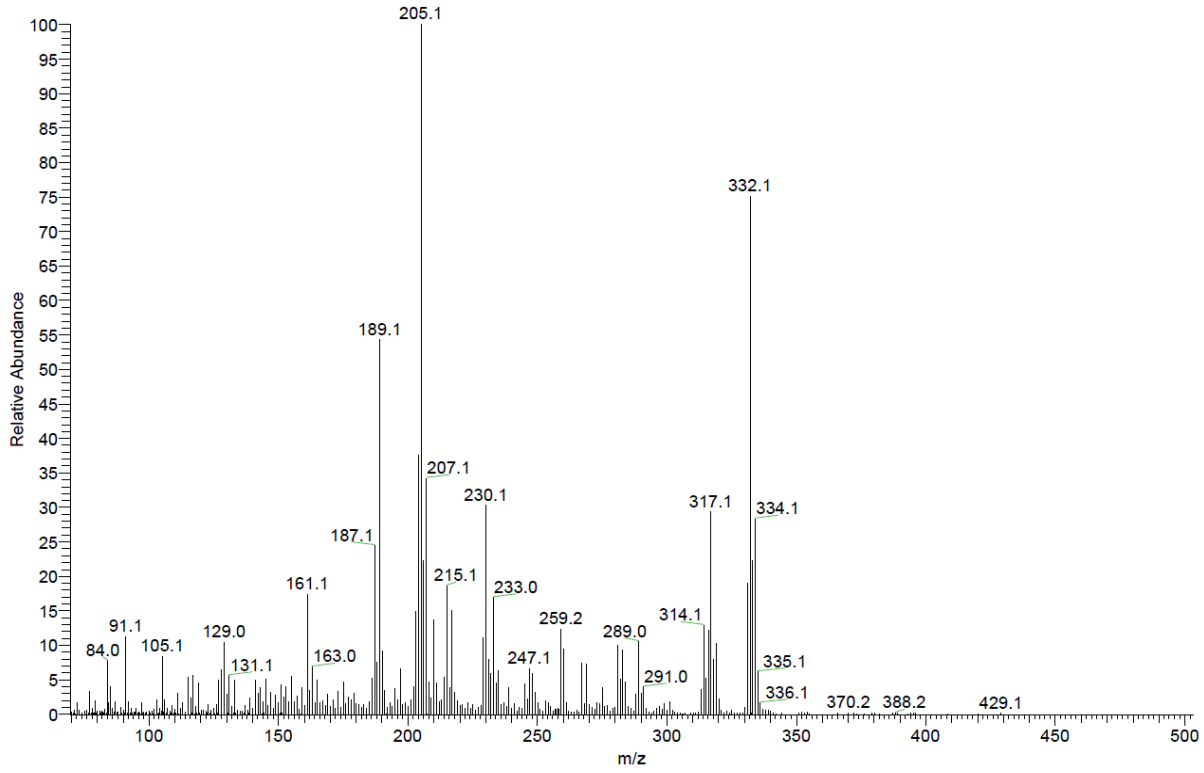

Figure 5.6.136. ESI mass spectrum of **20a**.

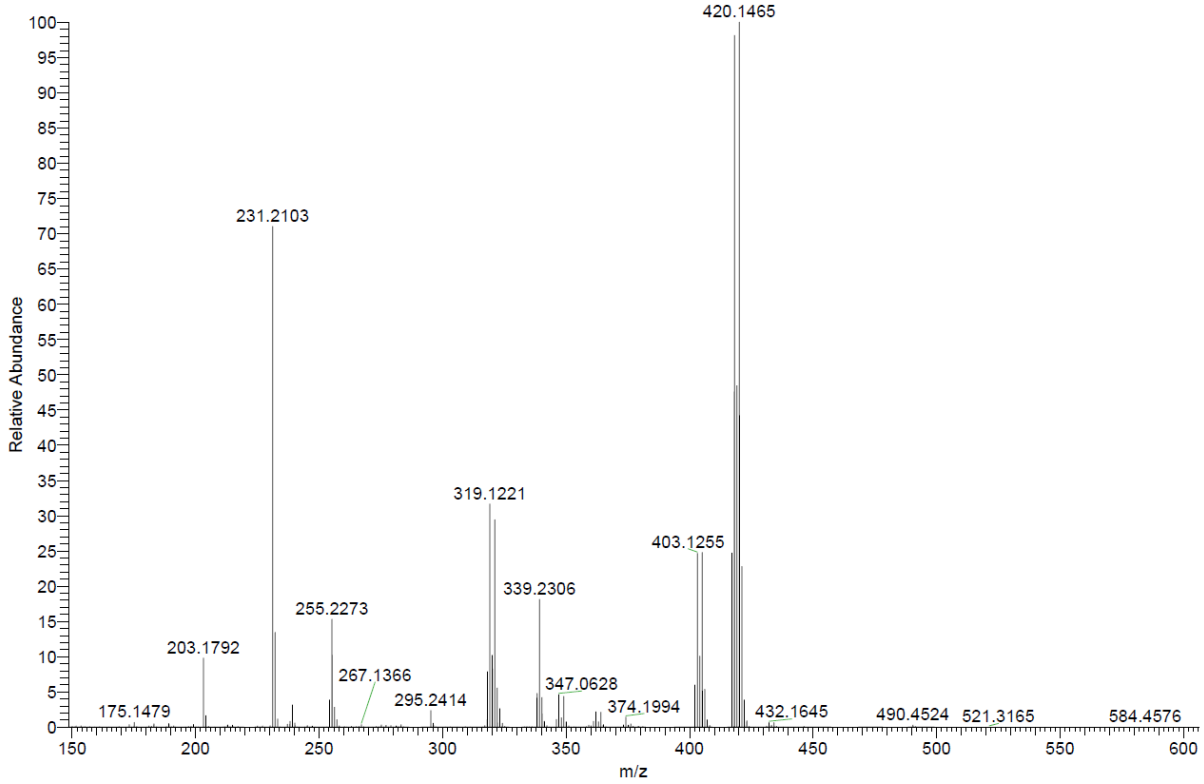

Figure 5.6.137. LIFDI mass spectrum of **21a.**

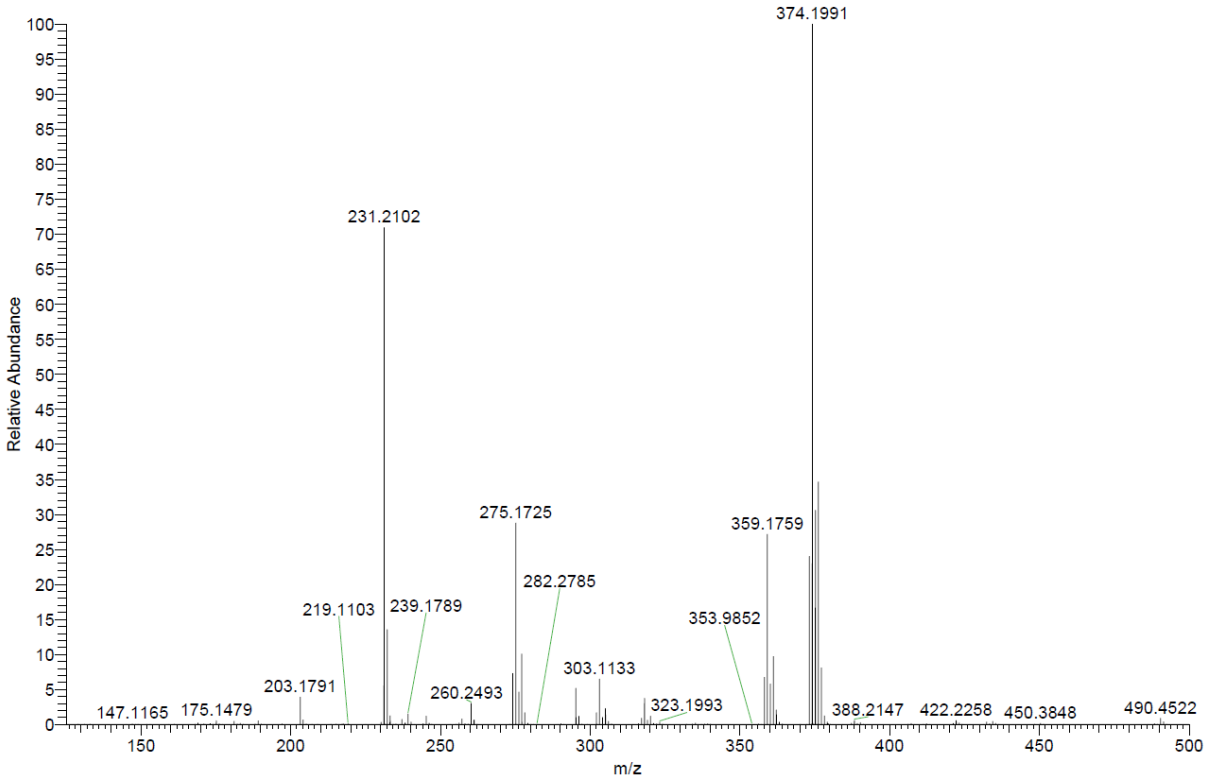

Figure 5.6.138. LIFDI mass spectrum of **22a.**

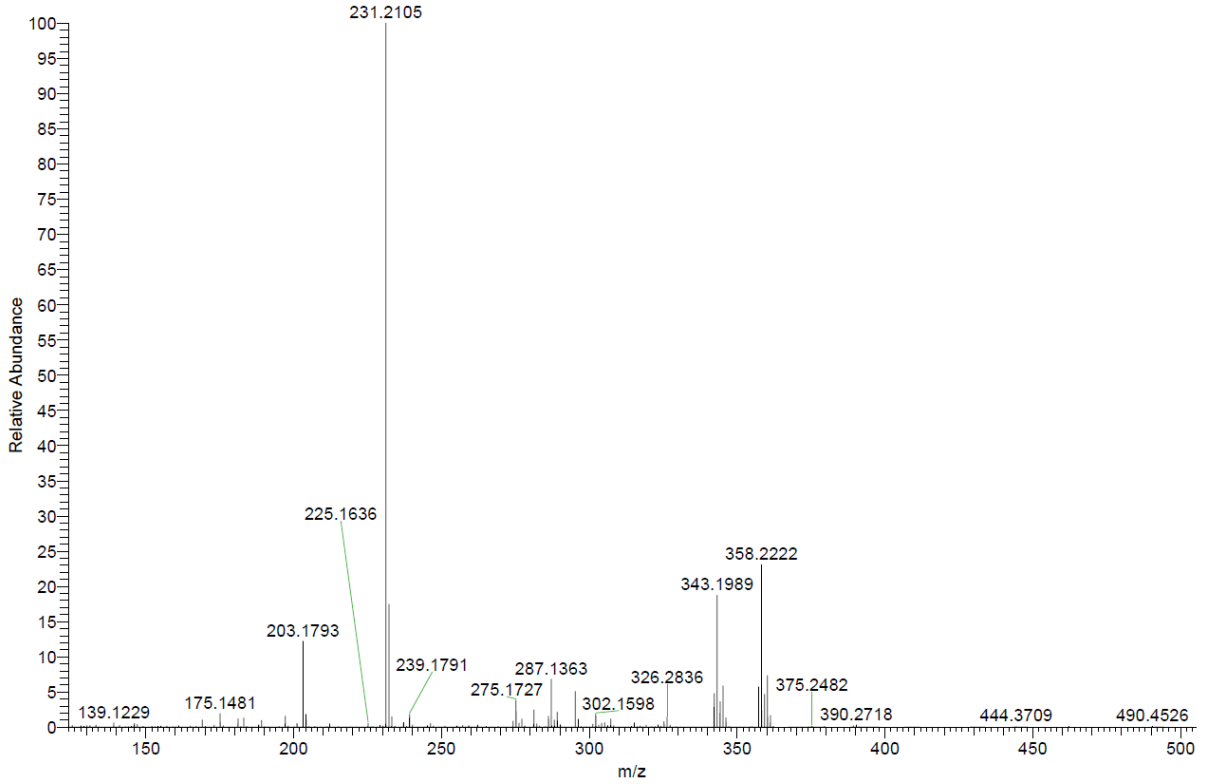

Figure 5.6.139. LIFDI mass spectrum of **22b.**

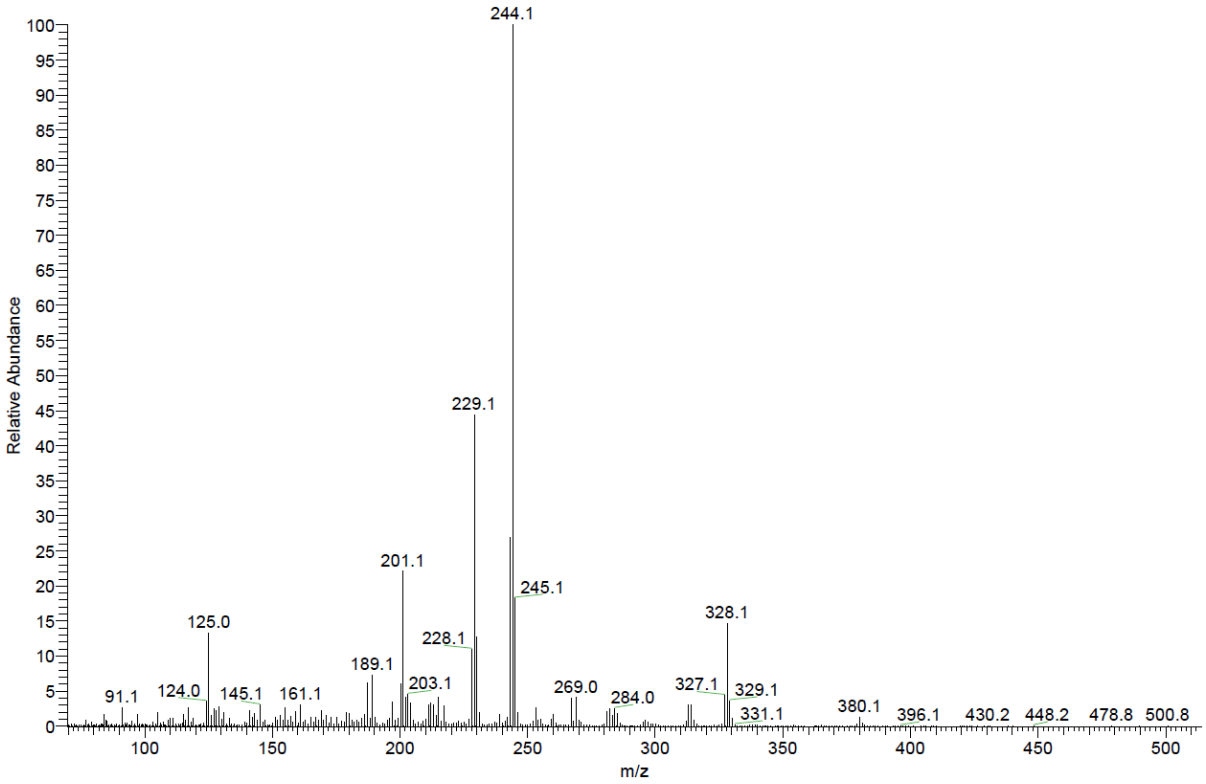

Figure 5.6.140. ESI mass spectrum of **23a**.

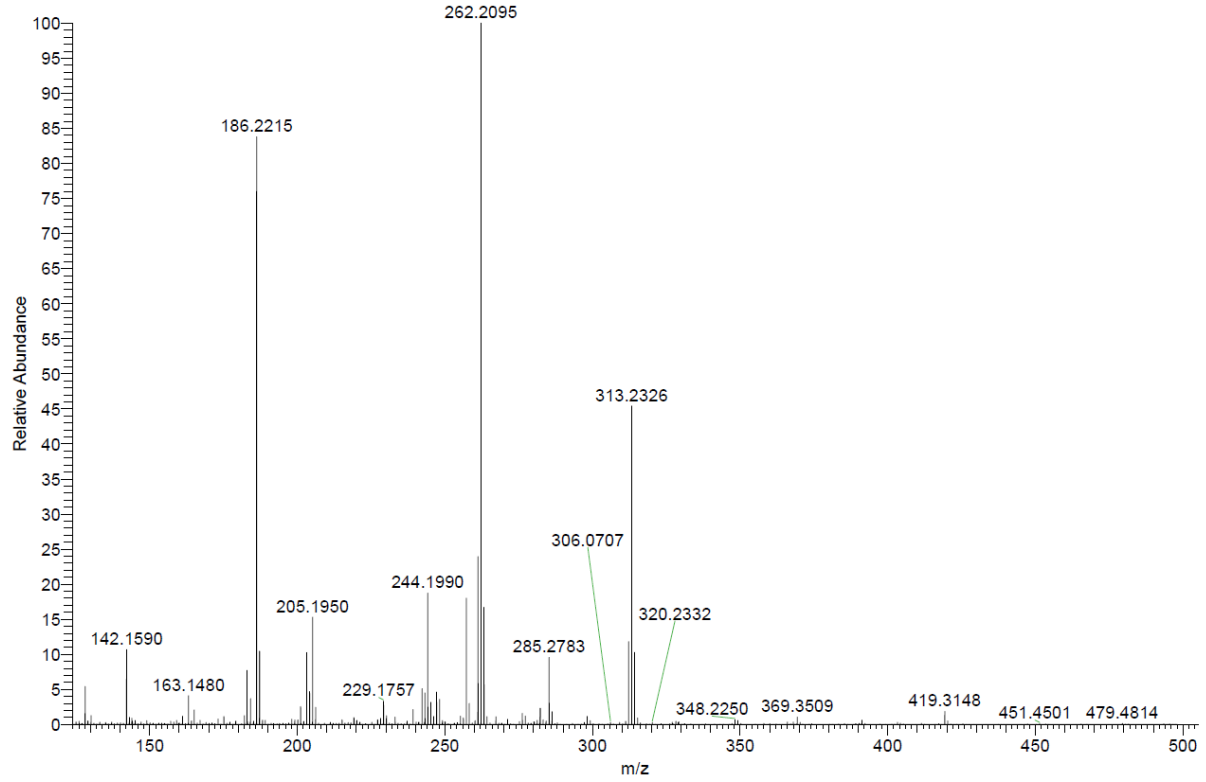

Figure 5.6.141. APCI mass spectrum of **23b**.

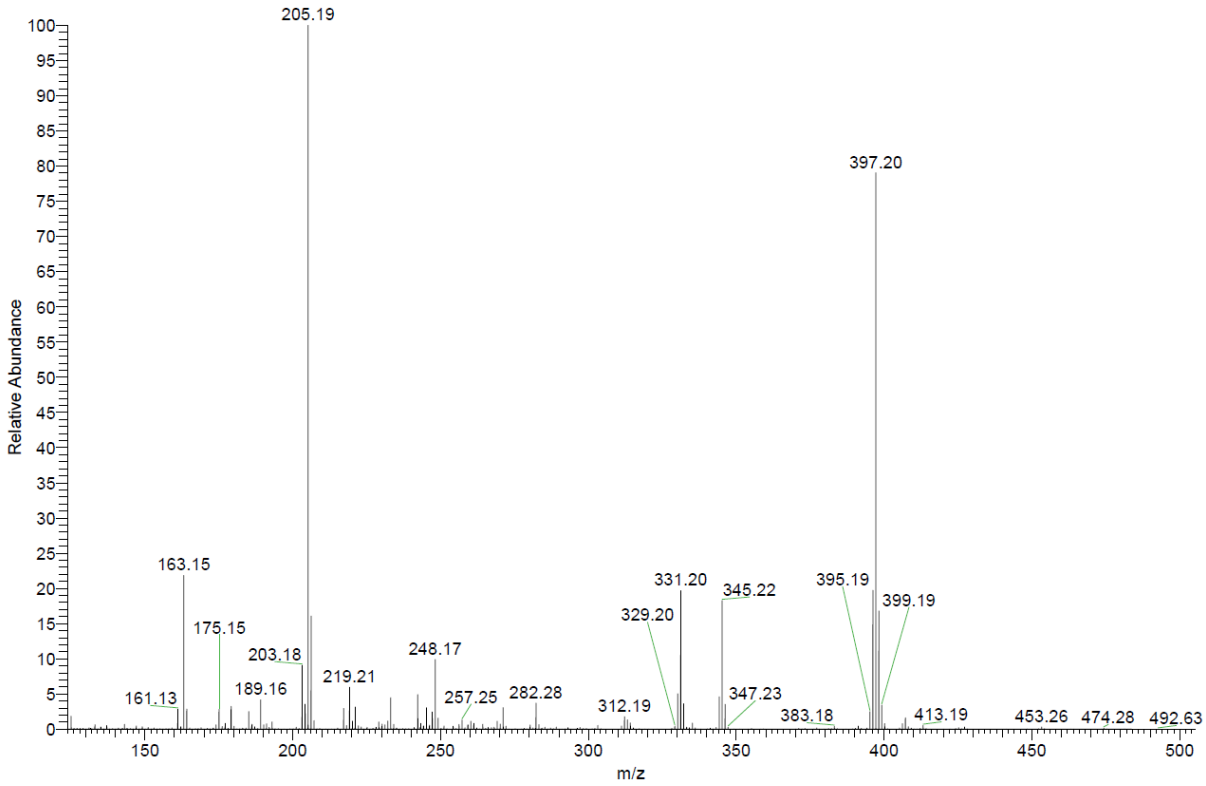

Figure 5.6.142. APCI mass spectrum of **24a**.

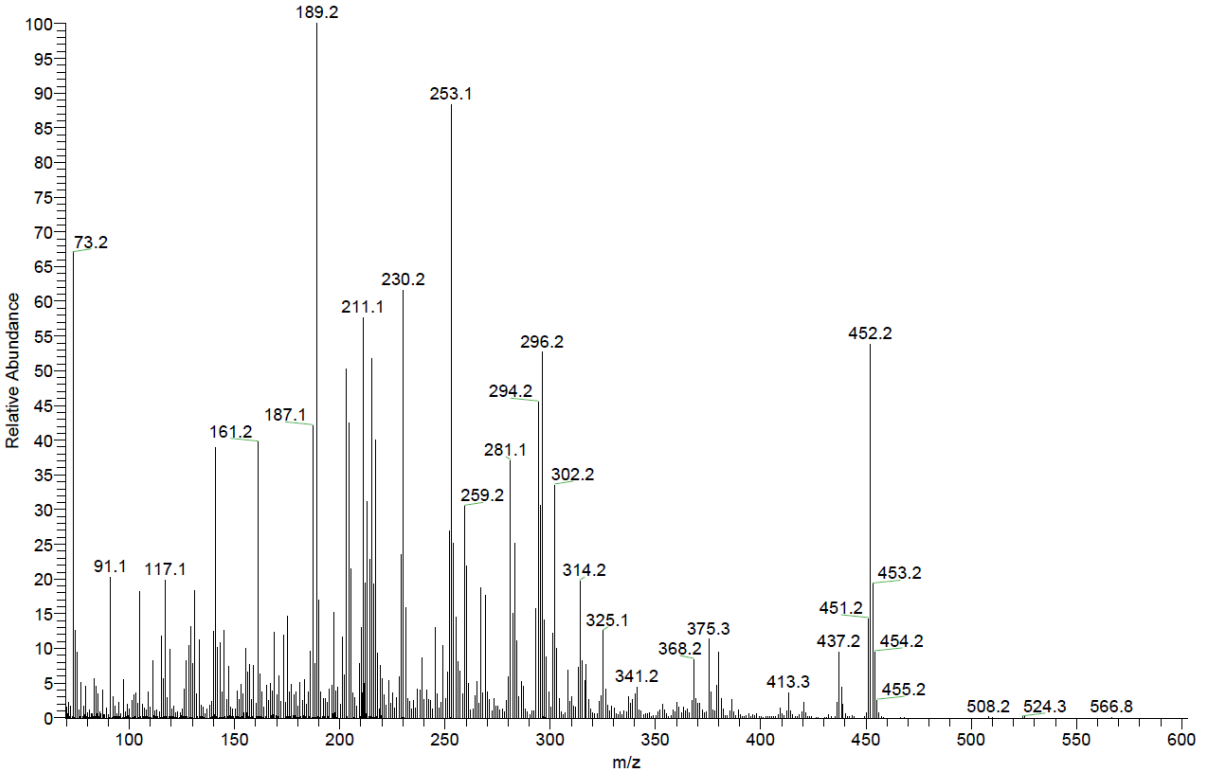

Figure 5.6.143. ESI mass spectrum of **25a**.

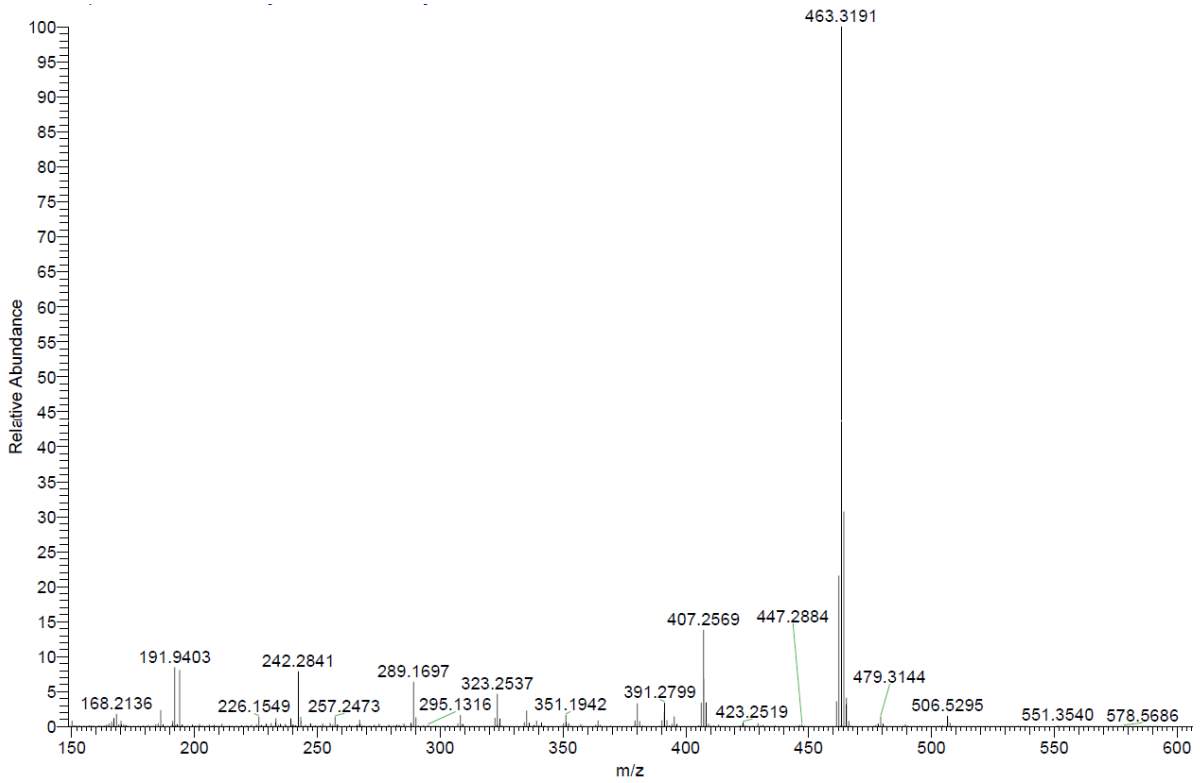

Figure 5.6.144. APCI mass spectrum of **25b**.

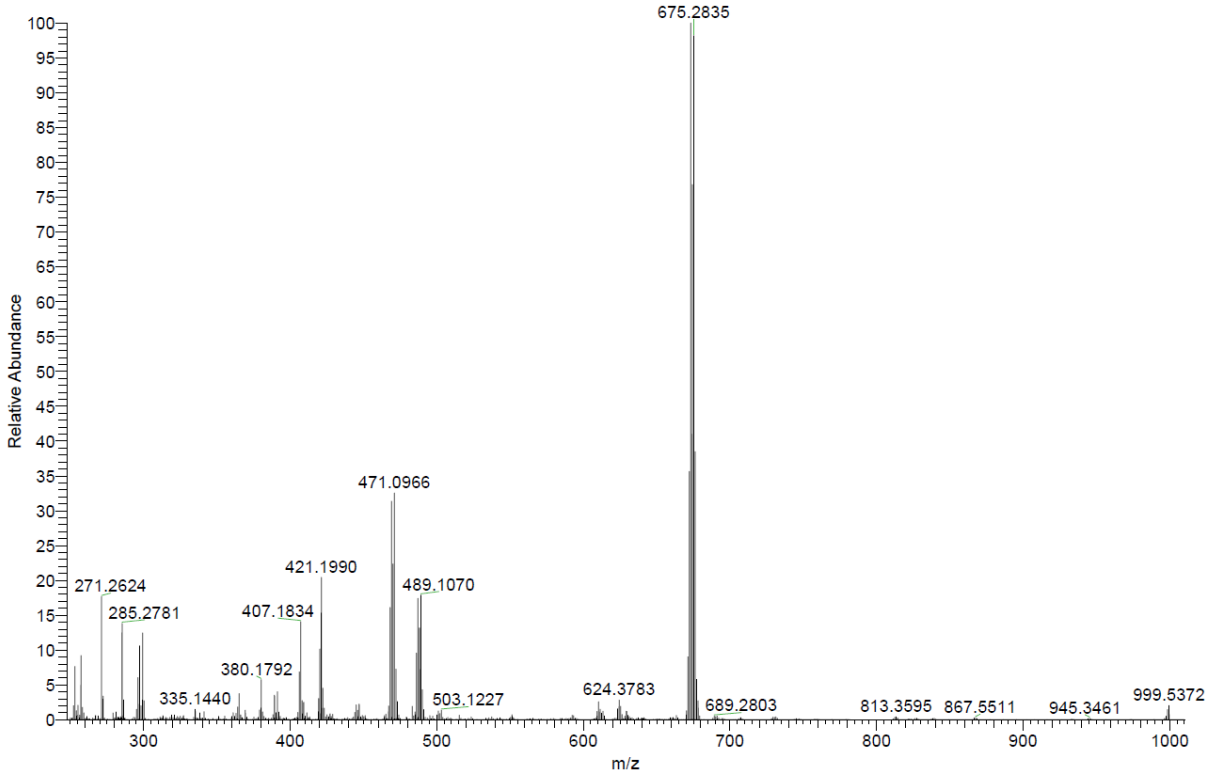

Figure 5.6.145. APCI mass spectrum of **29a**.

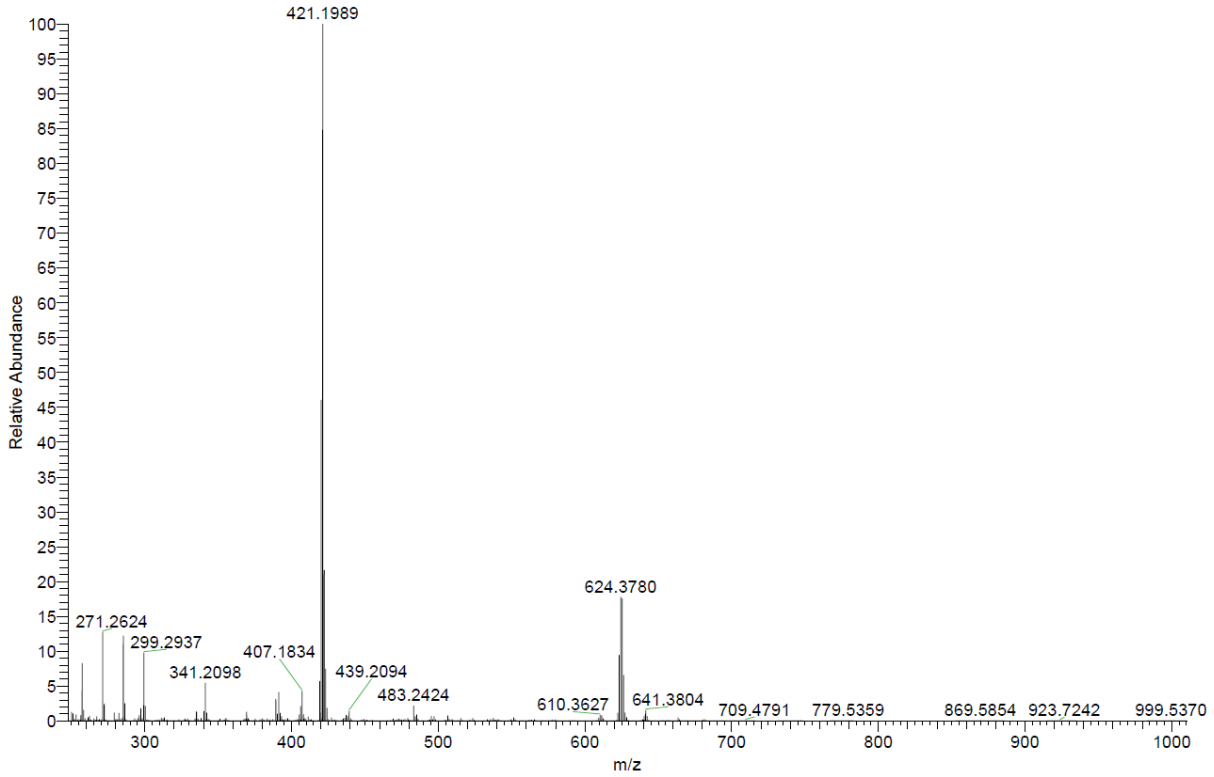

Figure 5.6.146. APCI mass spectrum of **30a**.

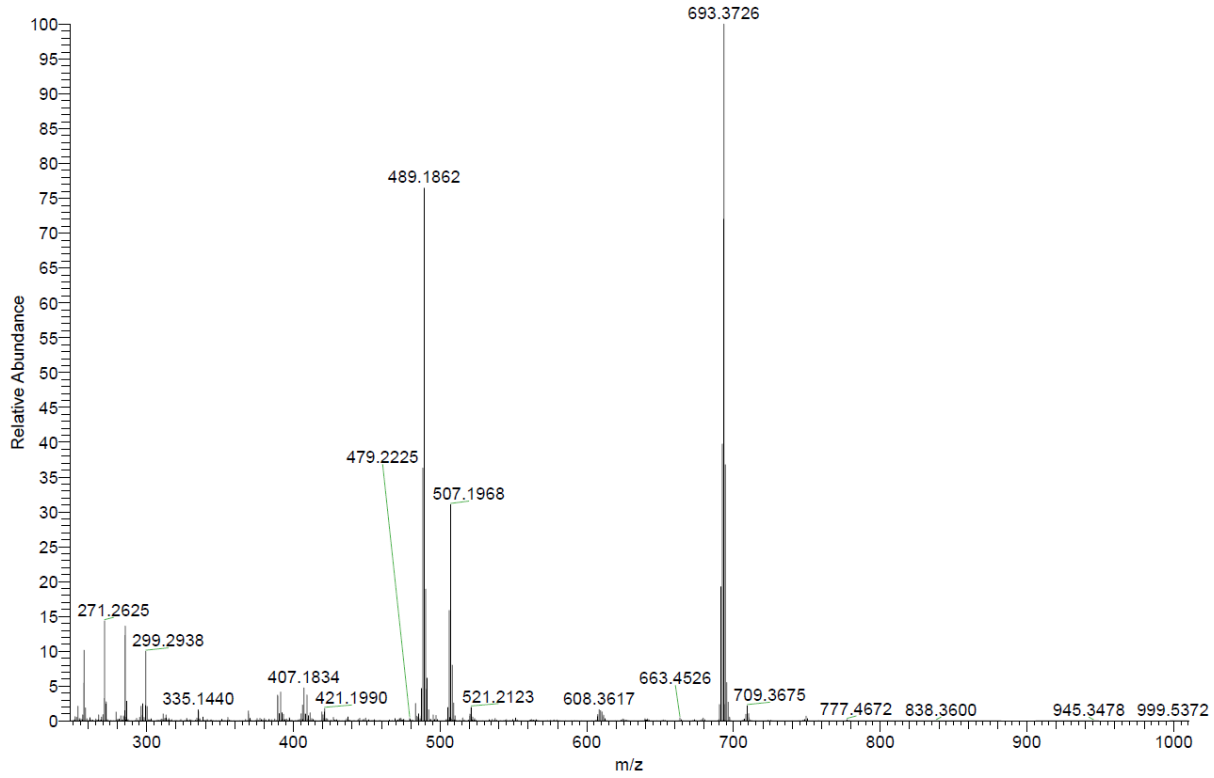

Figure 5.6.147. APCI mass spectrum of **31a**.

Gel permeation chromatography (GPC)

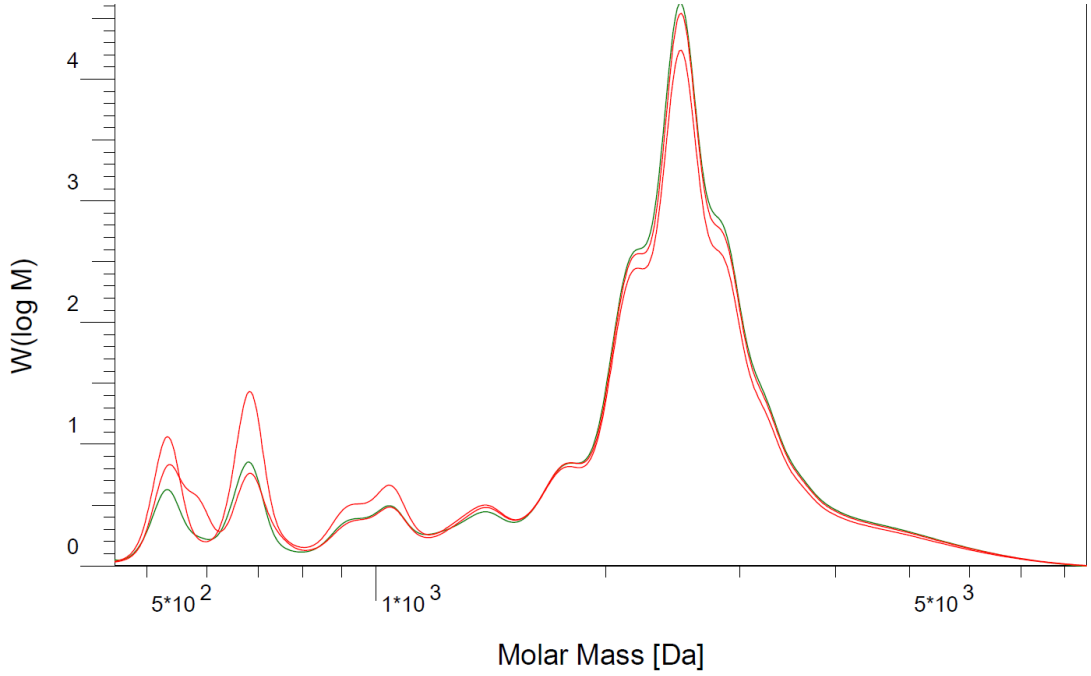

Figure 5.6.148. GPC trace of **17a^{Tip}** obtained after catalytic Si/B exchange polycondensation reaction of **5a** at 40 °C in DCM (*Route I*).

Table 5.6.1: Data of the GPC analysis of **17a^{Tip}** (DCM, 40 °C)

	UV	RI
M_n	1743	1817
M_w	2363	2400
M_z	2851	2861
Mp	2513	2497
PDI	x	x

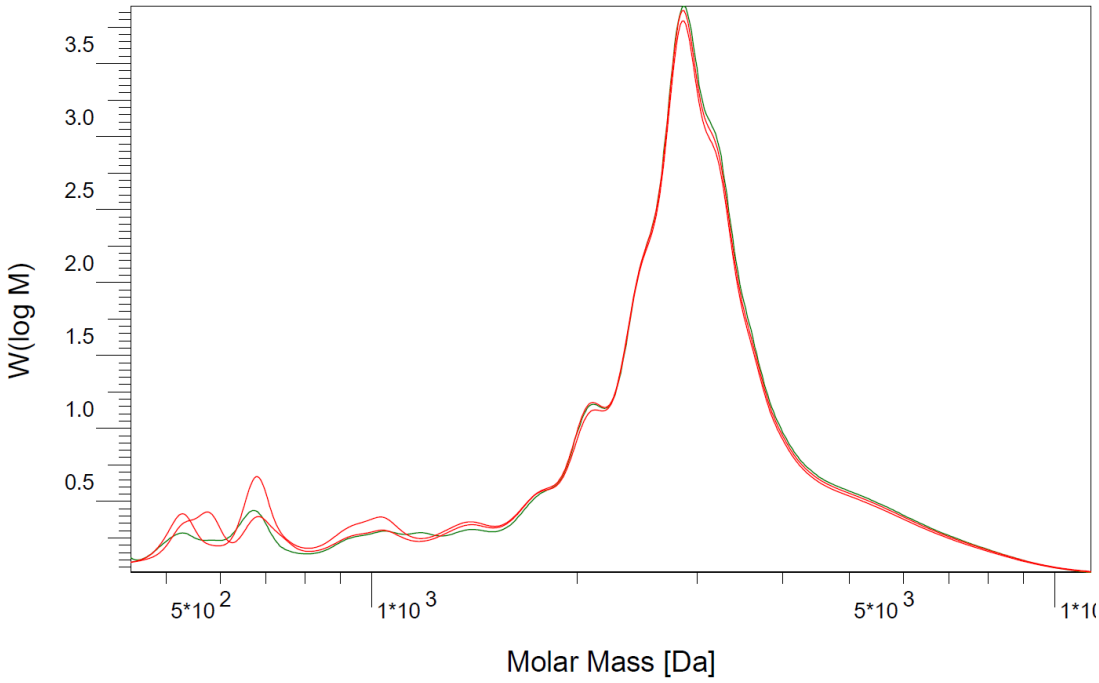

Figure 5.6.149. GPC trace of **17a^{Tip}** obtained after catalytic Si/B exchange polycondensation reaction of **5** at 70 °C in *o*-DCB (*Route I*).

Table 5.6.2. Data of the GPC analysis of **17a^{Tip}** (*o*-DCB, 70 °C).

	UV	RI
M_n	2119	2170
M_w	2951	2983
M_z	3699	3711
Mp	2867	2867
PDI	1.393	1.375

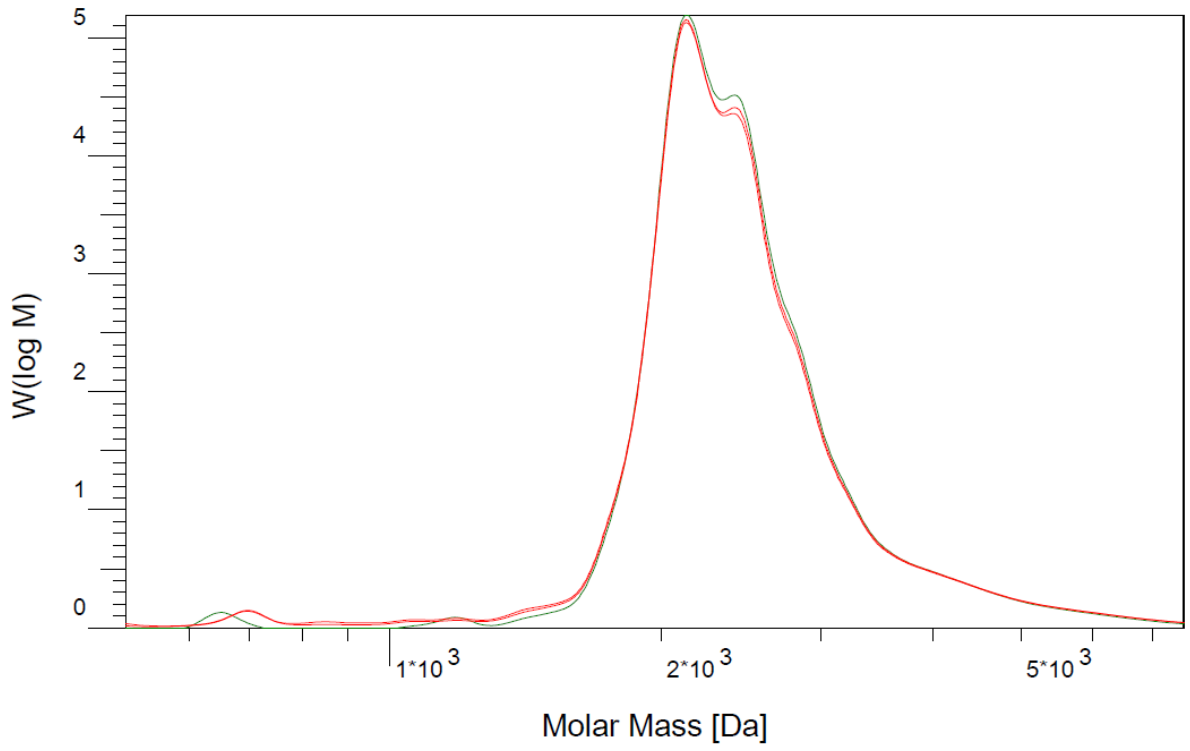

Figure 5.6.150. GPC trace of **17a^{Tip}** obtained after Si/B exchange polycondensation reaction of **15a** at rt in DCM.

Table 5.6.3. Data of the GPC analysis of **17a^{Tip}** (DCM, rt).

	UV	RI
M_n	2316	2359
M_w	2530	2543
M_z	2790	2780
Mp	2129	2129
PDI	1.092	1.078

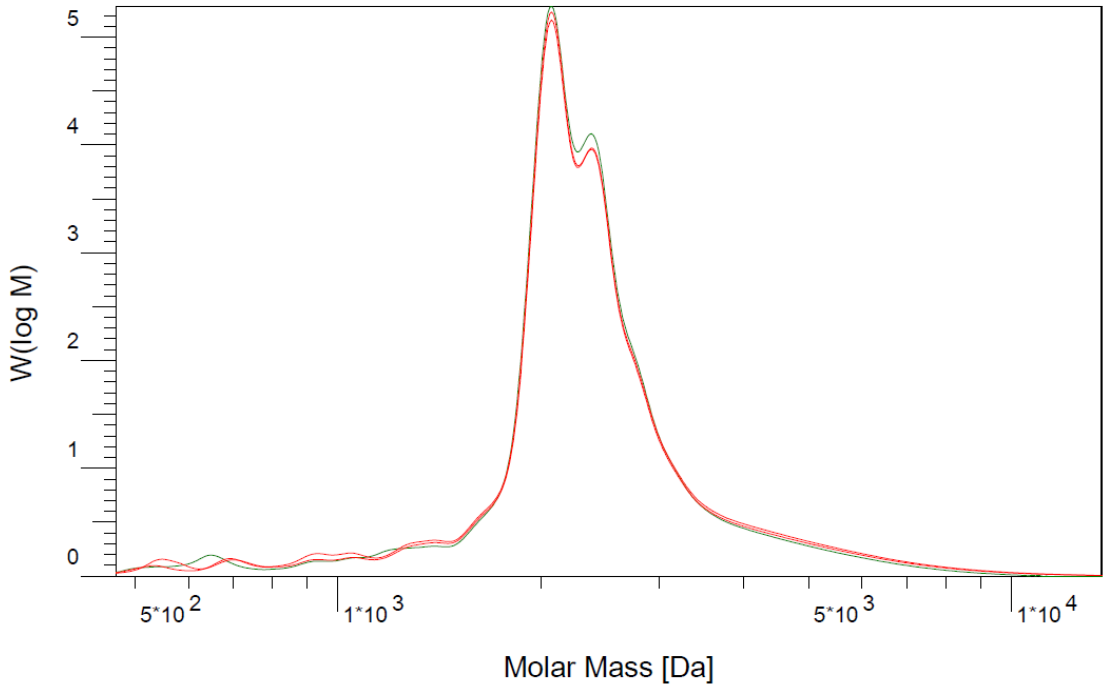

Figure 5.6.151. GPC trace of **34a** obtained via catalytic polycondensation reaction of **5a** via **32a** (*Route A*, arylation in toluene).

Table 5.6.4. Data of the GPC analysis of **34a** (*Route A*, toluene).

	UV	RI
M_n	2145	2125
M_w	2552	2475
M_z	3123	2901
Mp	2075	2074
PDI	1.190	1.165

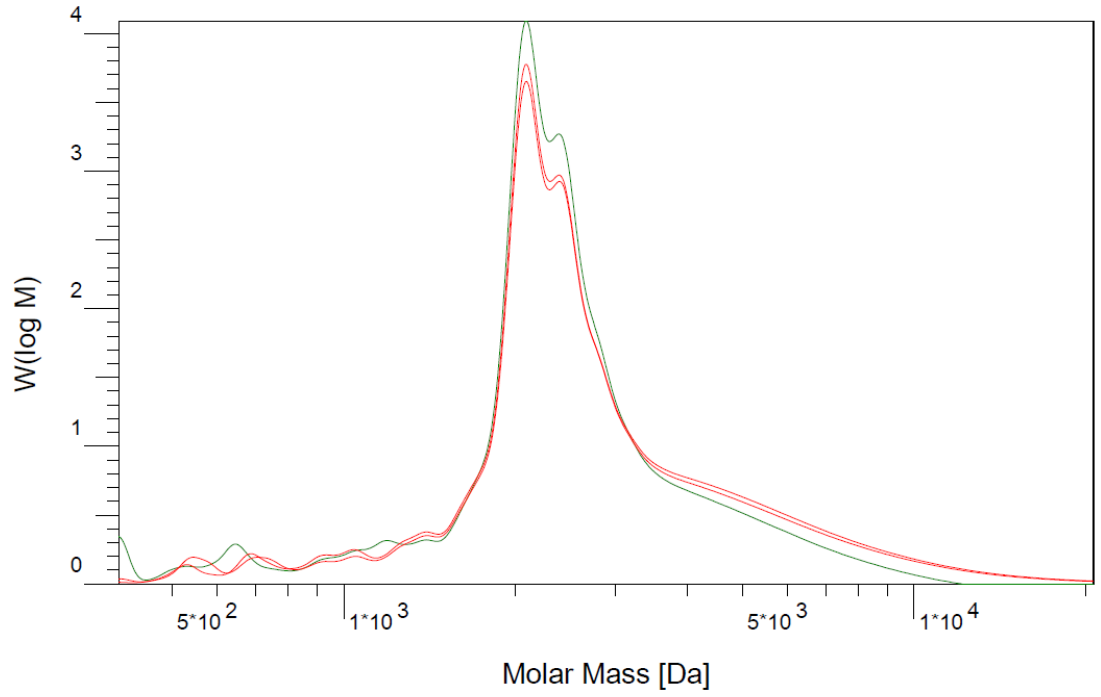

Figure 5.6.152. GPC trace of **34a** obtained via catalytic polycondensation reaction of **5a** via **32a** (*Route A*, arylation in toluene/Et_2O).

Table 5.6.5. Data of the GPC analysis of **34a** (*Route A*, toluene/Et_2O).

	UV	RI
M_n	2280	2078
M_w	3215	2737
M_z	4879	3559
Mp	2095	2095
PDI	1.410	1.317

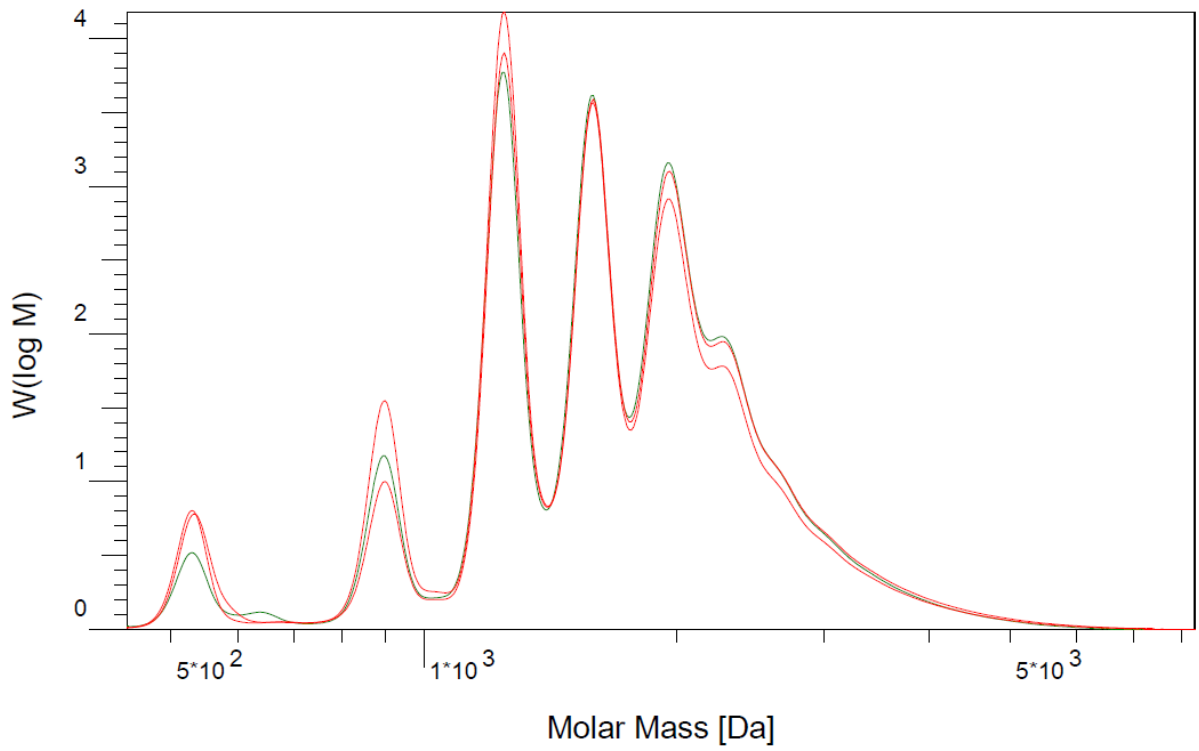

Figure 5.6.153. GPC trace of **34a** obtained via catalytic polycondensation reaction of **15a** via **32a** (*Route A*, arylation in toluene).

Table 5.6.6. Data of the GPC analysis of **34a** (*Route A*, toluene).

	UV	RI
M_n	1514	1530
M_w	1812	1803
M_z	2129	2090
Mp	1248	1248
PDI	1.197	1.178

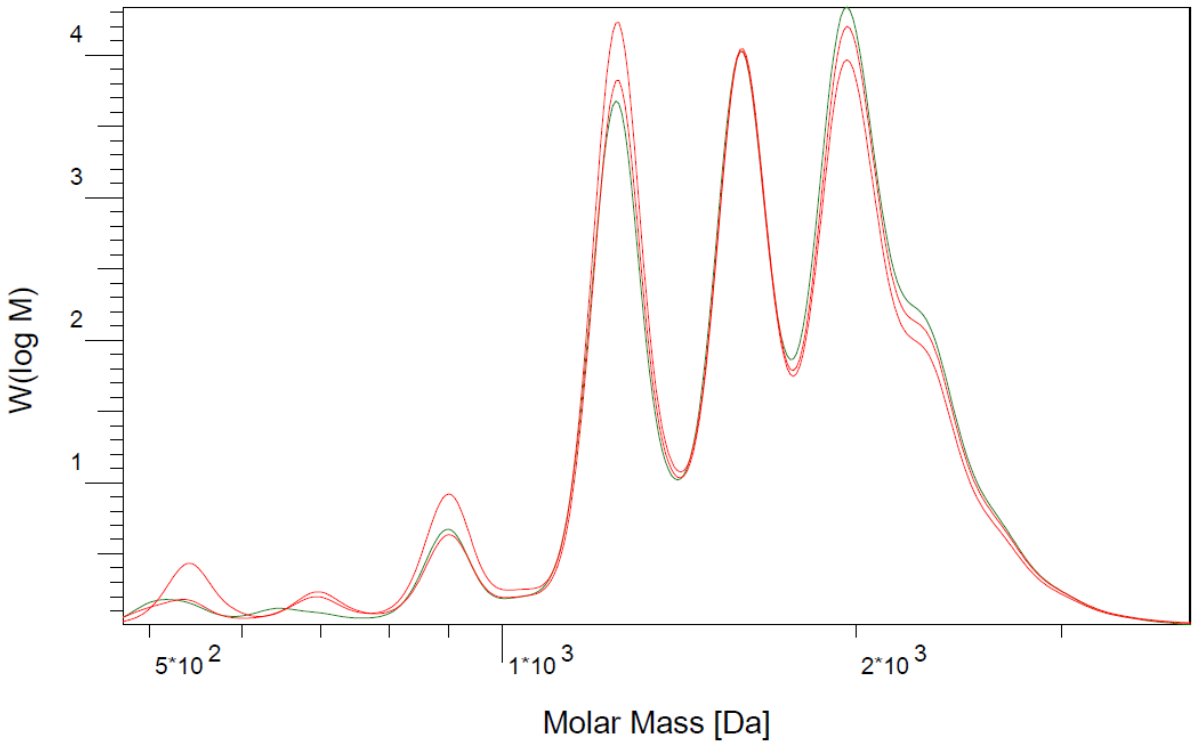

Figure 5.6.154. GPC trace of **17a^{Tip}** obtained via catalytic polycondensation reaction of **15a** and addition of TipMgBr (*Route I*).

Table 5.6.7. Data of the GPC analysis of **17a^{Tip}** (*Route I*, TipMgBr).

	UV	RI
M_n	1524	1567
M_w	1704	1727
M_z	1854	1865
Mp	1996	1966
PDI	1.118	1.102

5.7 Synthetic Routes to Tetrabora- and Diboraporphyrinogens

NMR spectra

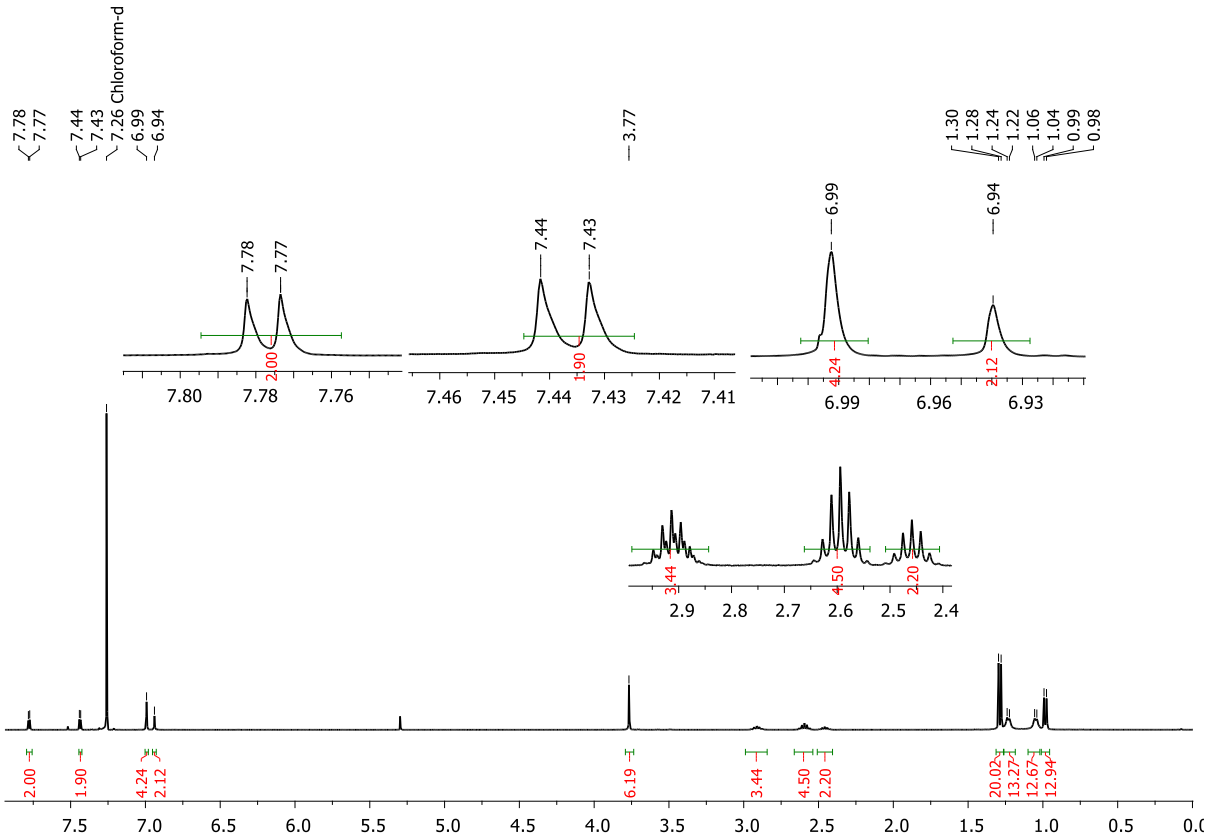

Figure 5.7.1. ^{1}H NMR spectrum of **6b** (400 MHz, in $CDCl_3$).

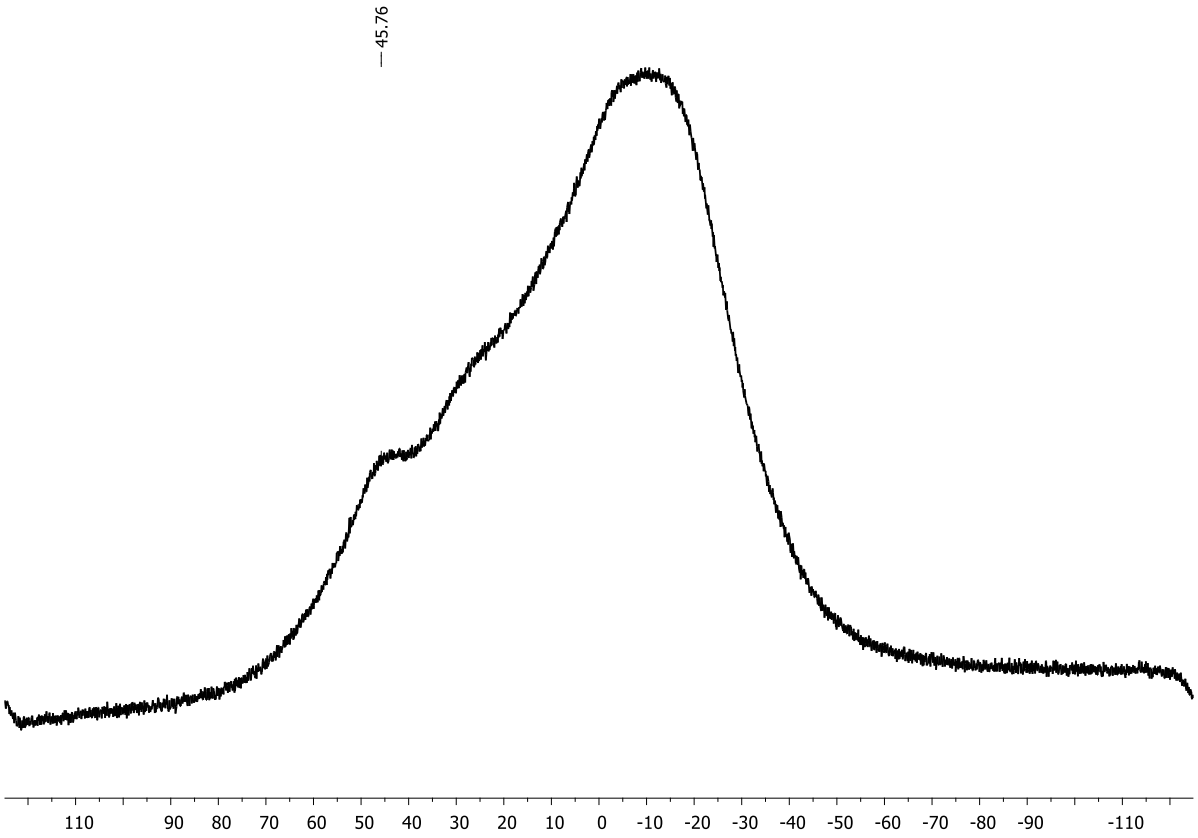

Figure 5.7.2. $^{11}B\{^{1}H\}$ NMR spectrum of **6b** (128 MHz, in $CDCl_3$).

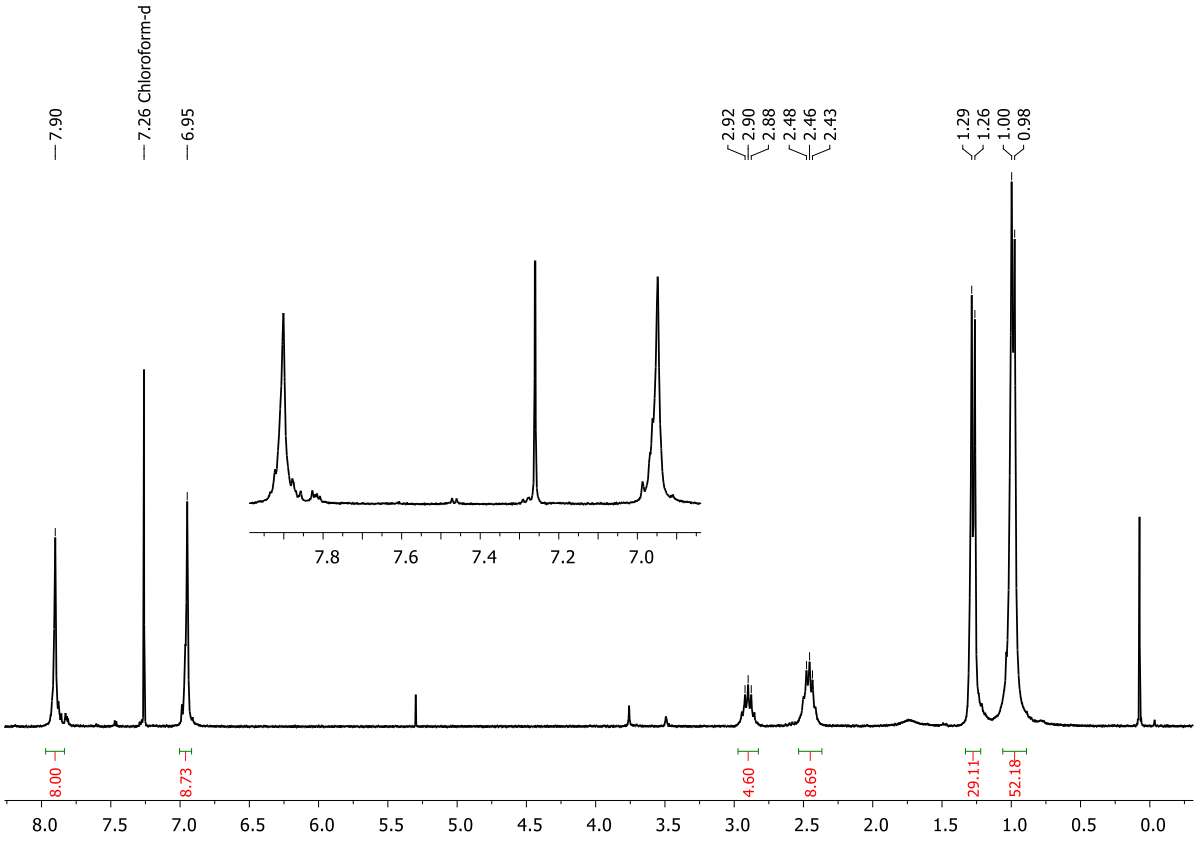

Figure 5.7.3. ^{1}H NMR spectrum of **7b** (300 MHz, in $CDCl_3$).

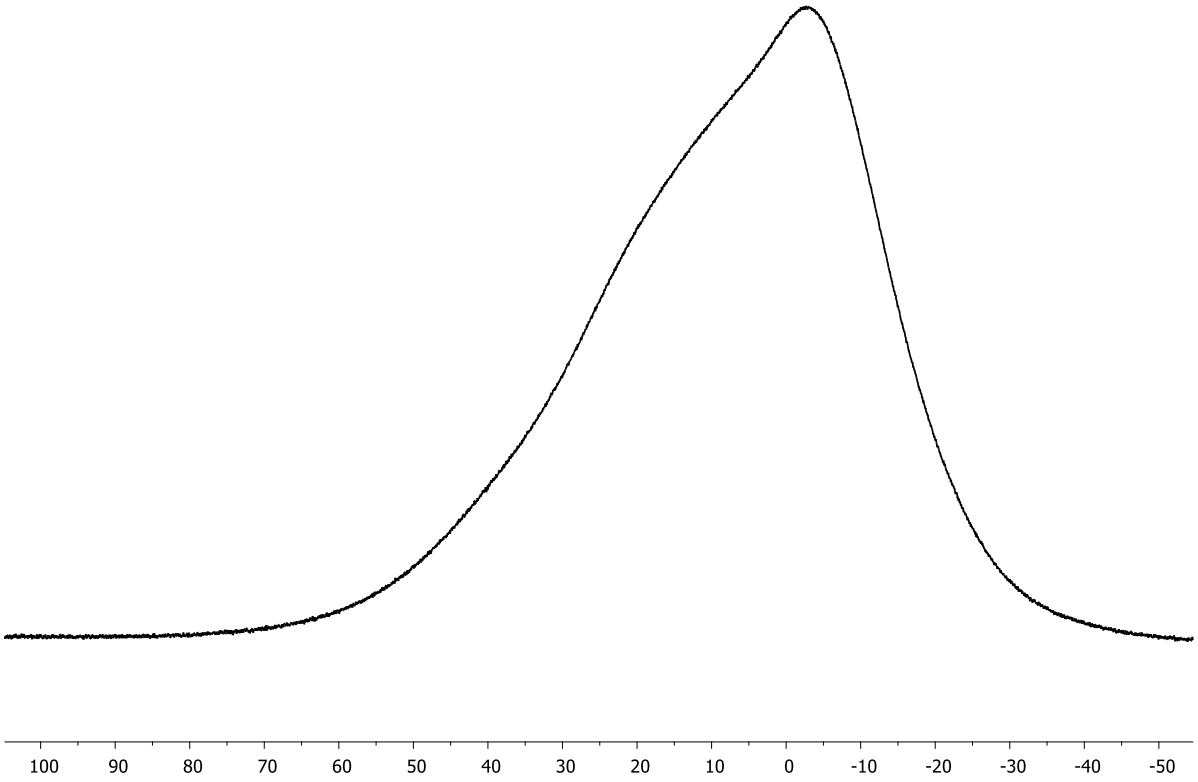

Figure 5.7.4. $^{11}B\{^{1}H\}$ NMR spectrum of **7b** (160 MHz, in $CDCl_3$).

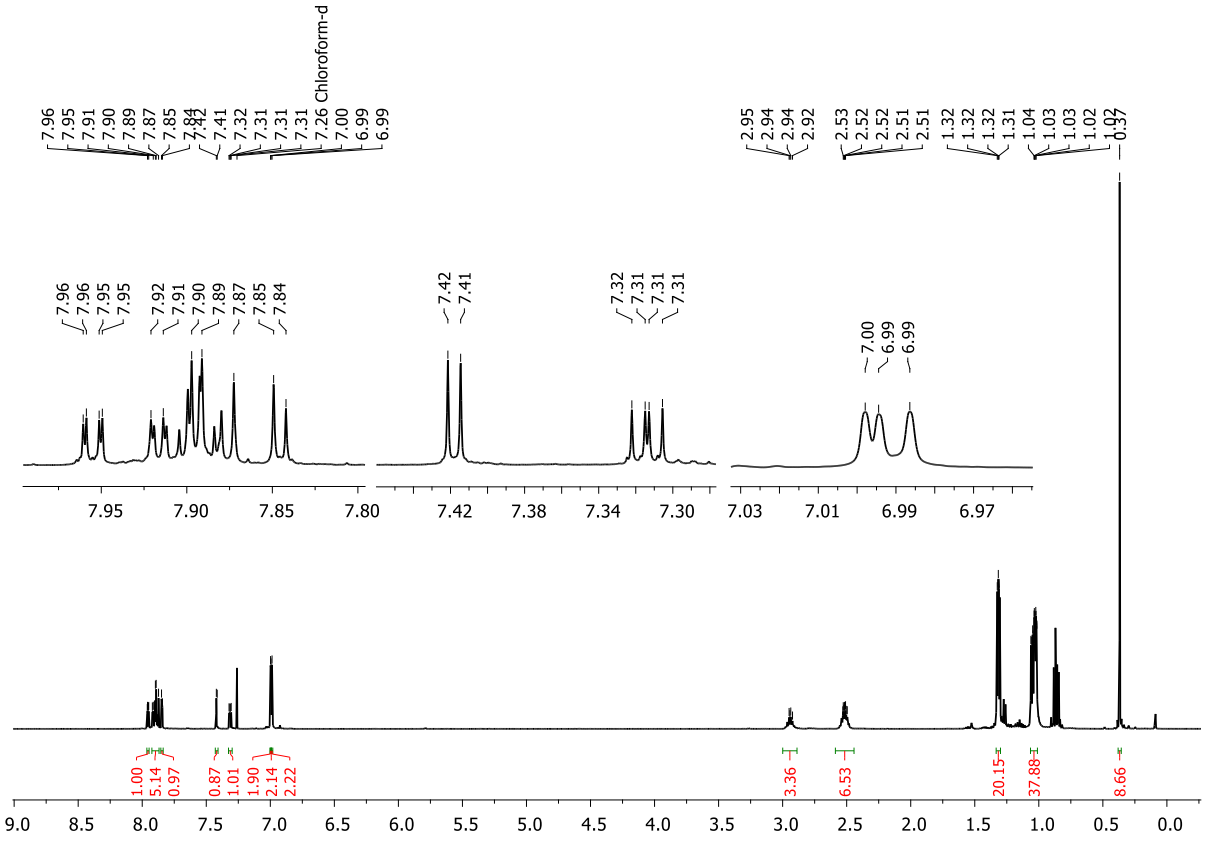

Figure 5.7.5. ^{1}H NMR spectrum of **13a** (500 MHz, in $CDCl_3$).

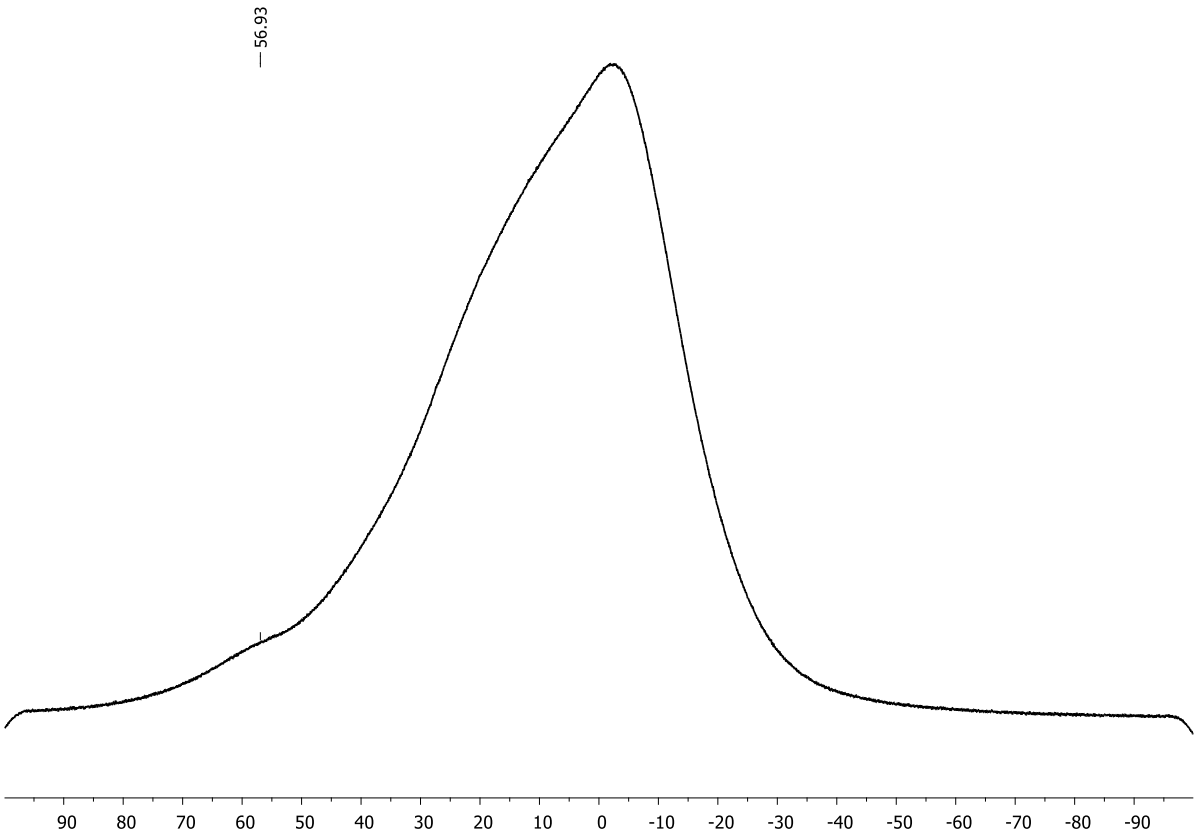

Figure 5.7.6. $^{11}B\{^{1}H\}$ NMR spectrum of **13a** (160 MHz, in $CDCl_3$).

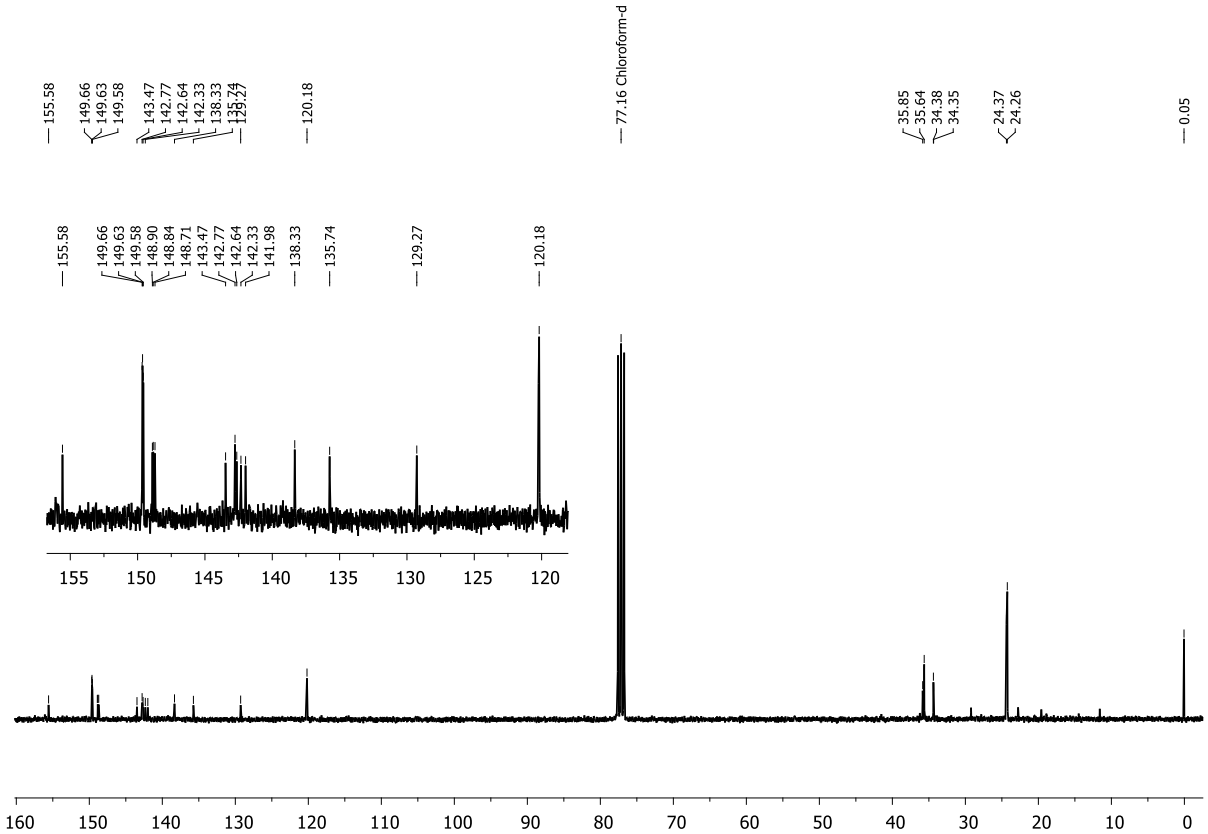

Figure 5.7.7. $^{13}C\{^{1}H\}$ NMR spectrum of **13a** (126 MHz, in $CDCl_3$).

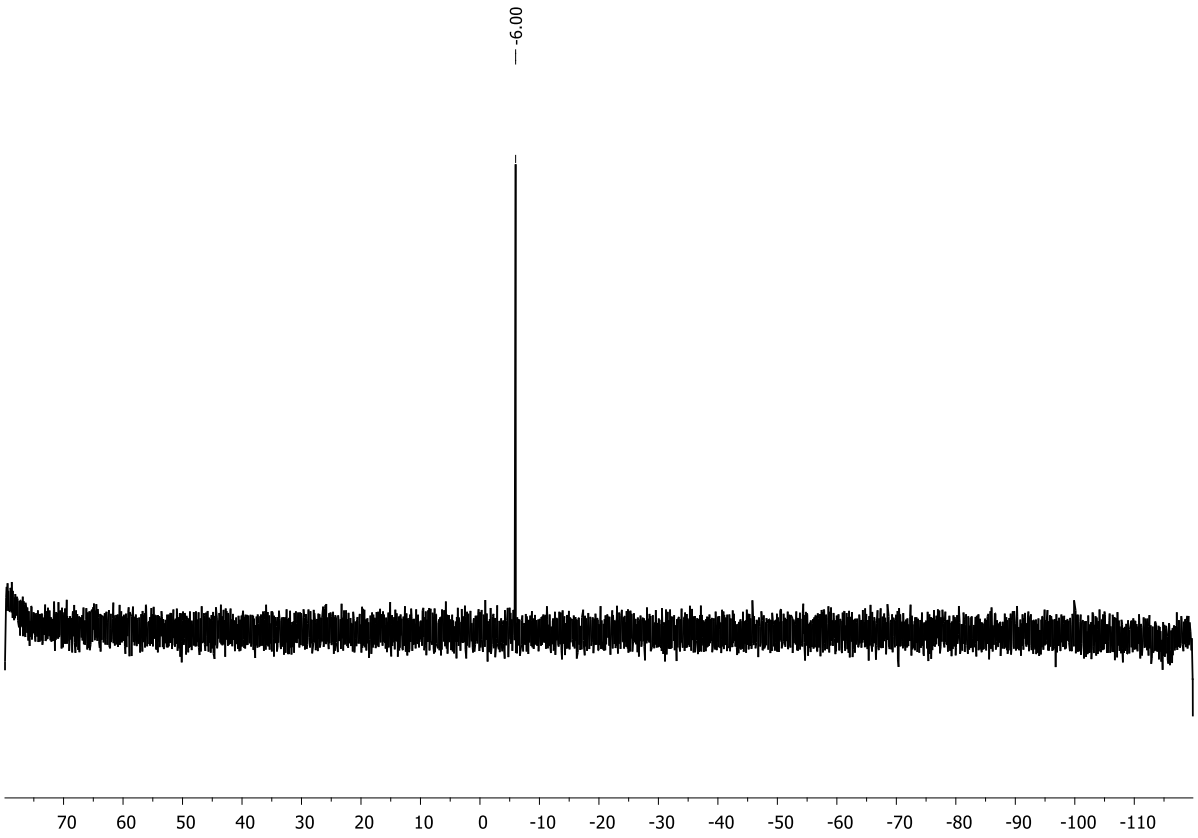

Figure 5.7.8. $^{29}Si\{^{1}H\}$ NMR spectrum of **13a** (99 MHz, in $CDCl_3$).

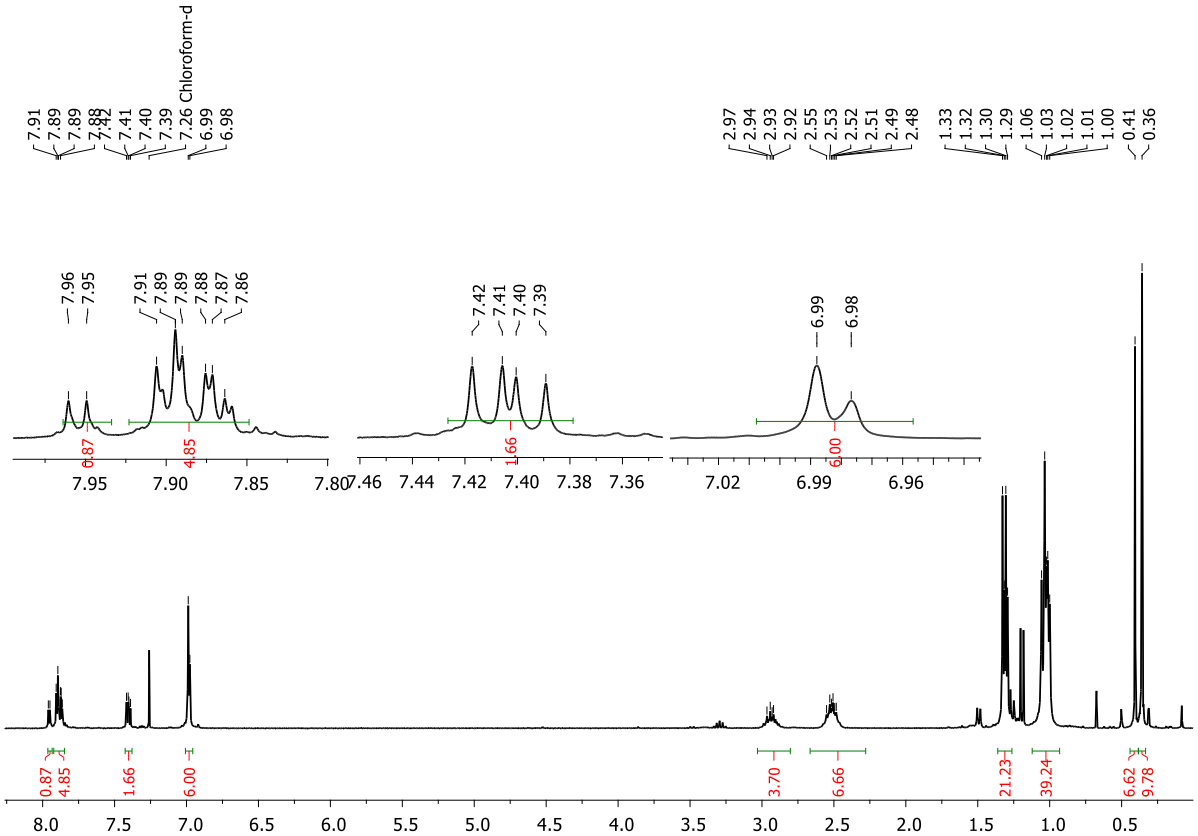

Figure 5.7.9. ^{1}H NMR spectrum of **14a** (300 MHz, in $CDCl_3$).

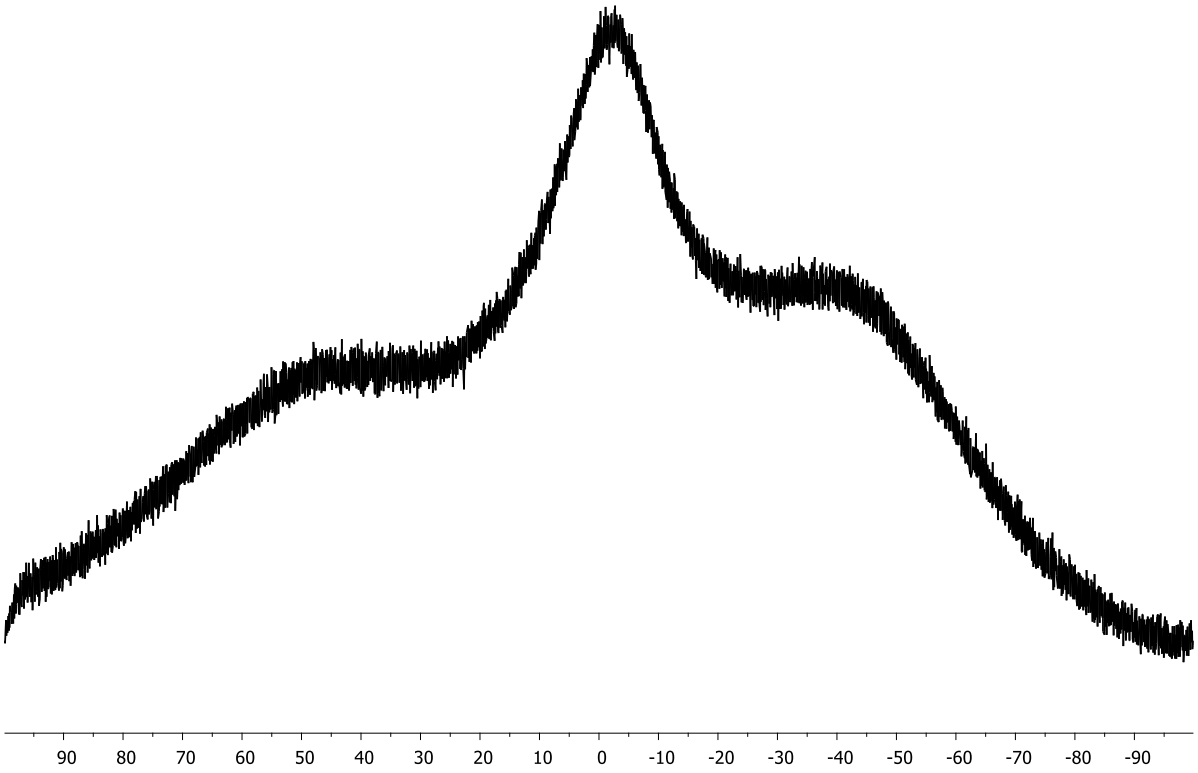

Figure 5.7.10. $^{11}B\{^{1}H\}$ NMR spectrum of **14a** (96 MHz, in $CDCl_3$).

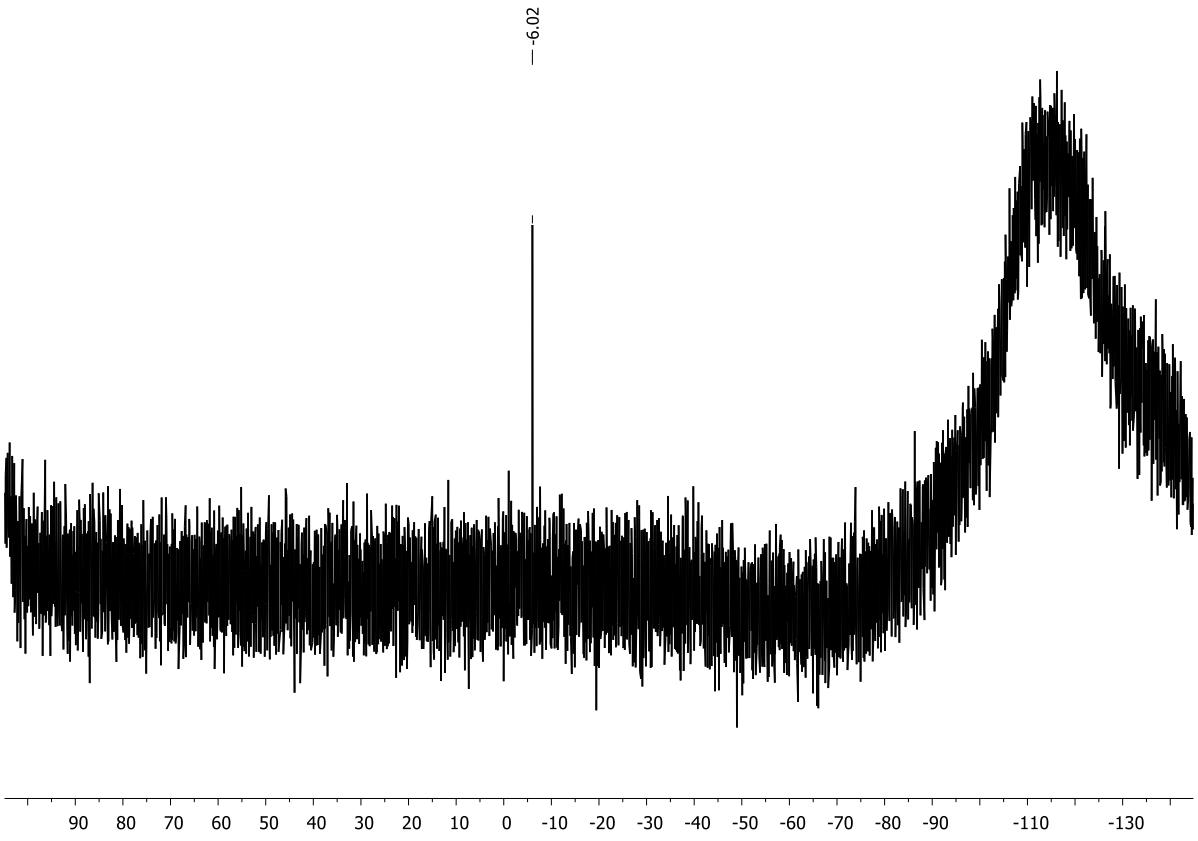

Figure 5.7.11. ^{29}Si NMR spectrum of **14a** (60 MHz, in $CDCl_3$).

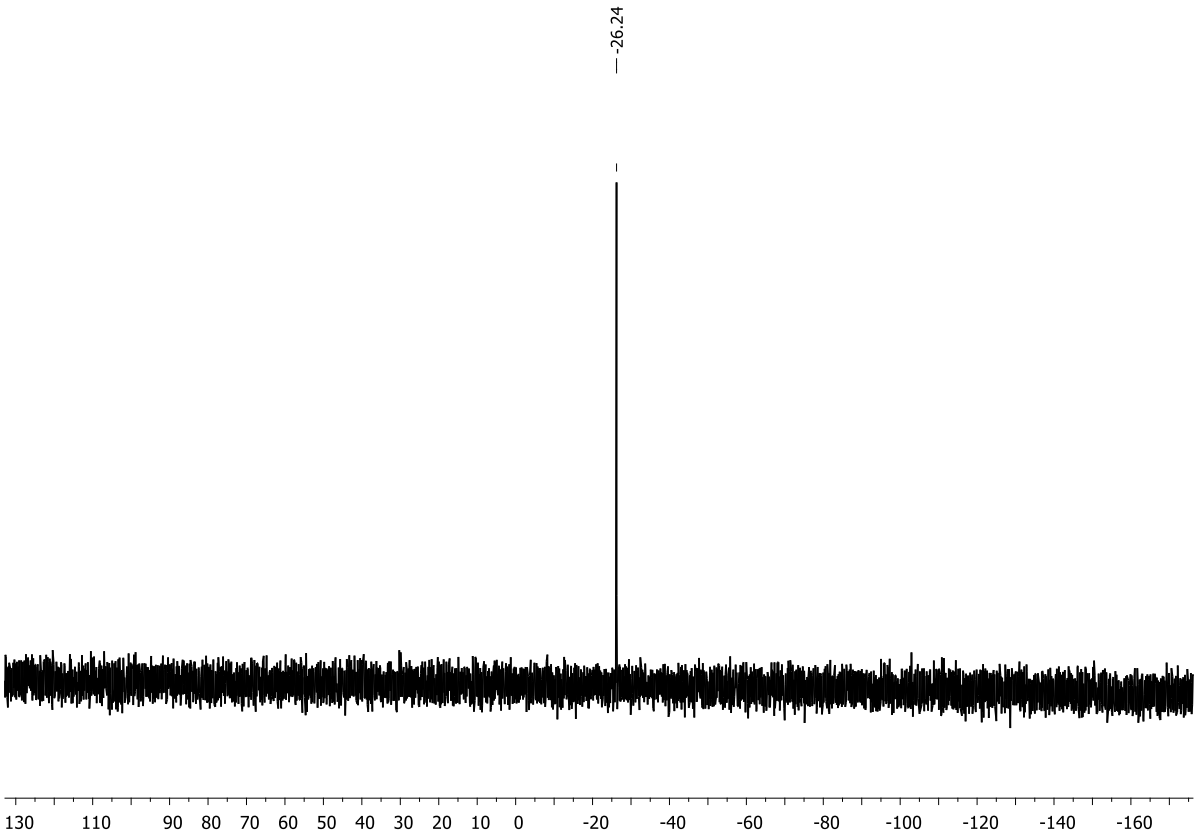

Figure 5.7.12. ^{119}Sn NMR spectrum of **14a** (112 MHz, in $CDCl_3$).

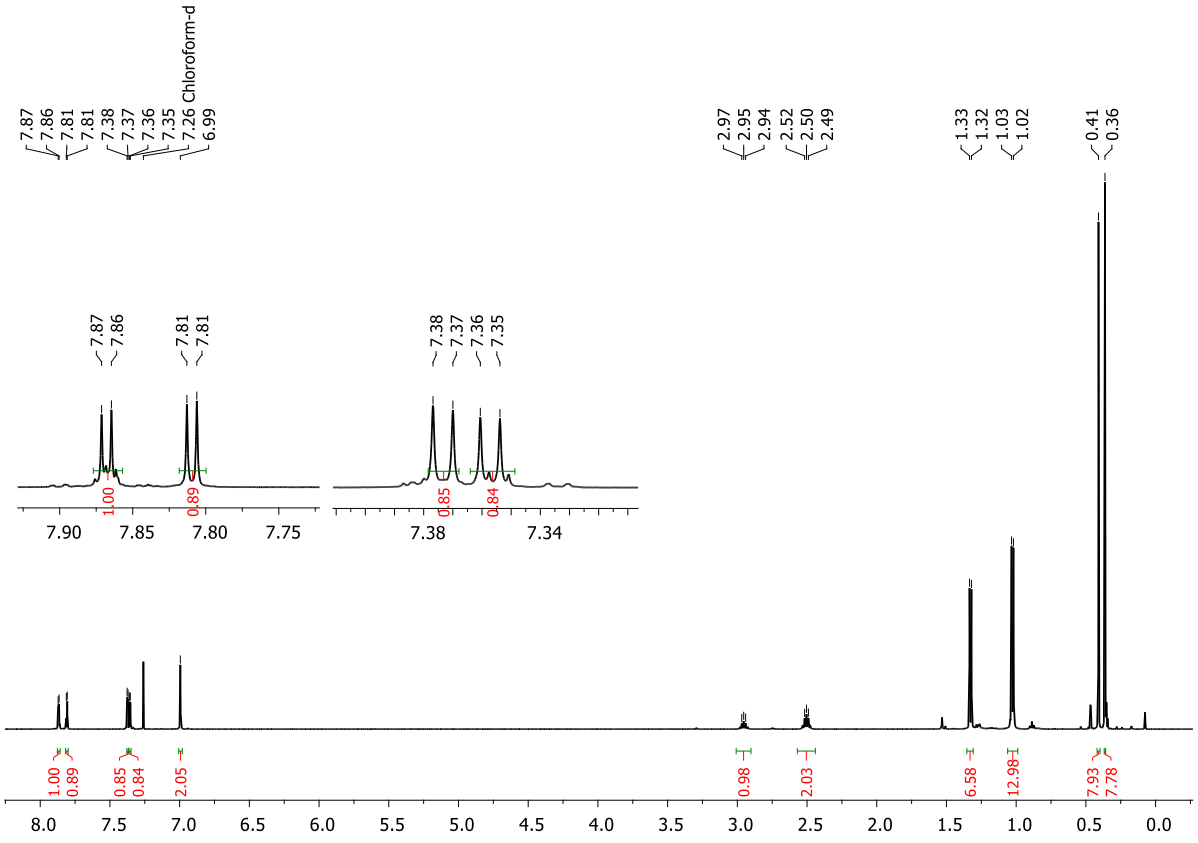

Figure 5.7.13. ^{1}H NMR spectrum of **15a** (500 MHz, in $CDCl_3$).

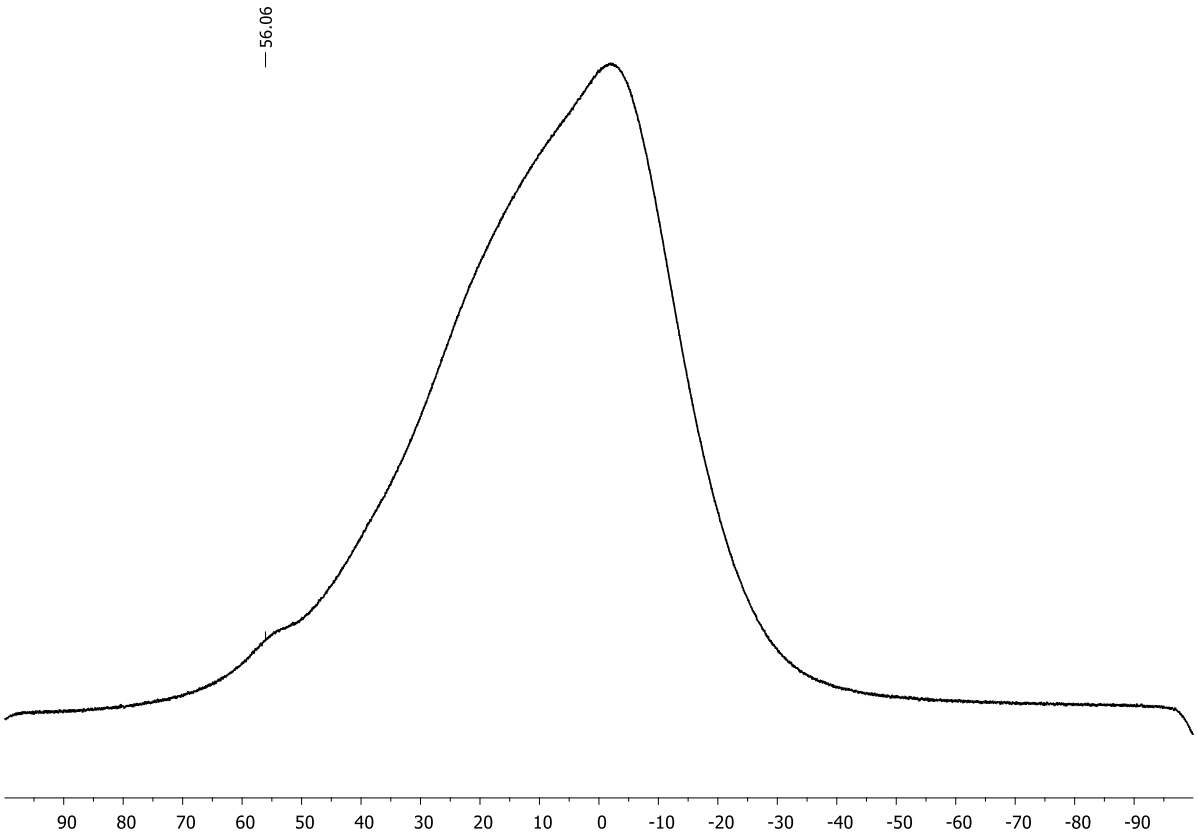

Figure 5.7.14. $^{11}B\{^{1}H\}$ NMR spectrum of **15a** (160 MHz, in $CDCl_3$).

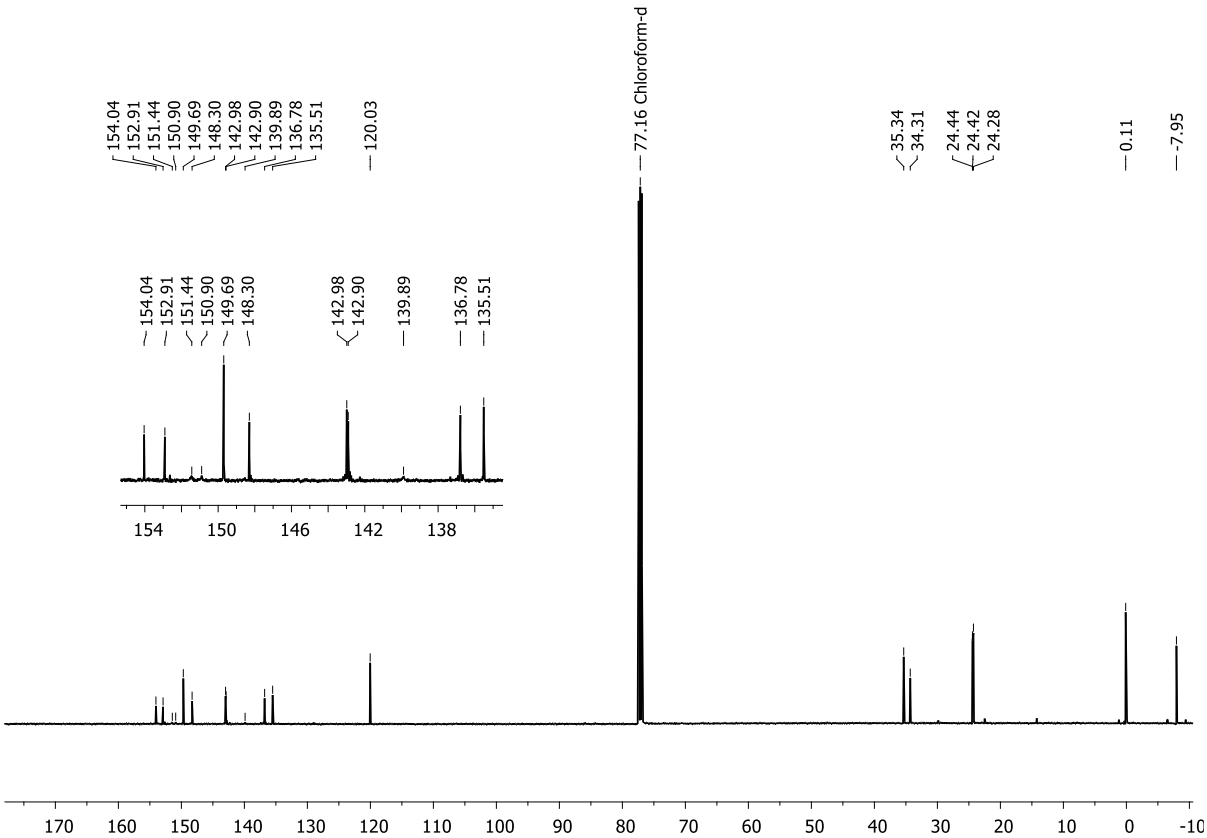

Figure 5.7.15. $^{13}C\{^{1}H\}$ NMR spectrum of **15a** (126 MHz, in $CDCl_3$).

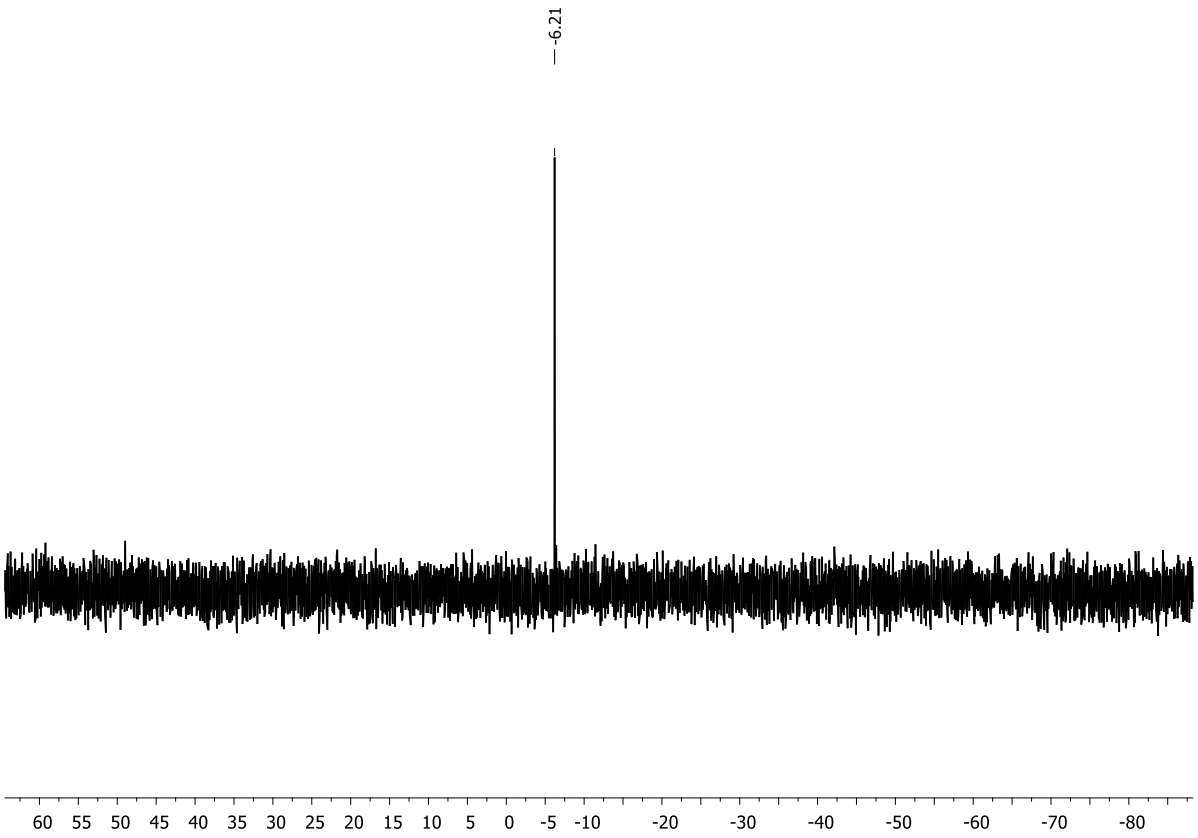

Figure 5.7.16. $^{29}Si\{^{1}H\}$ NMR spectrum of **15a** (99 MHz, in $CDCl_3$).

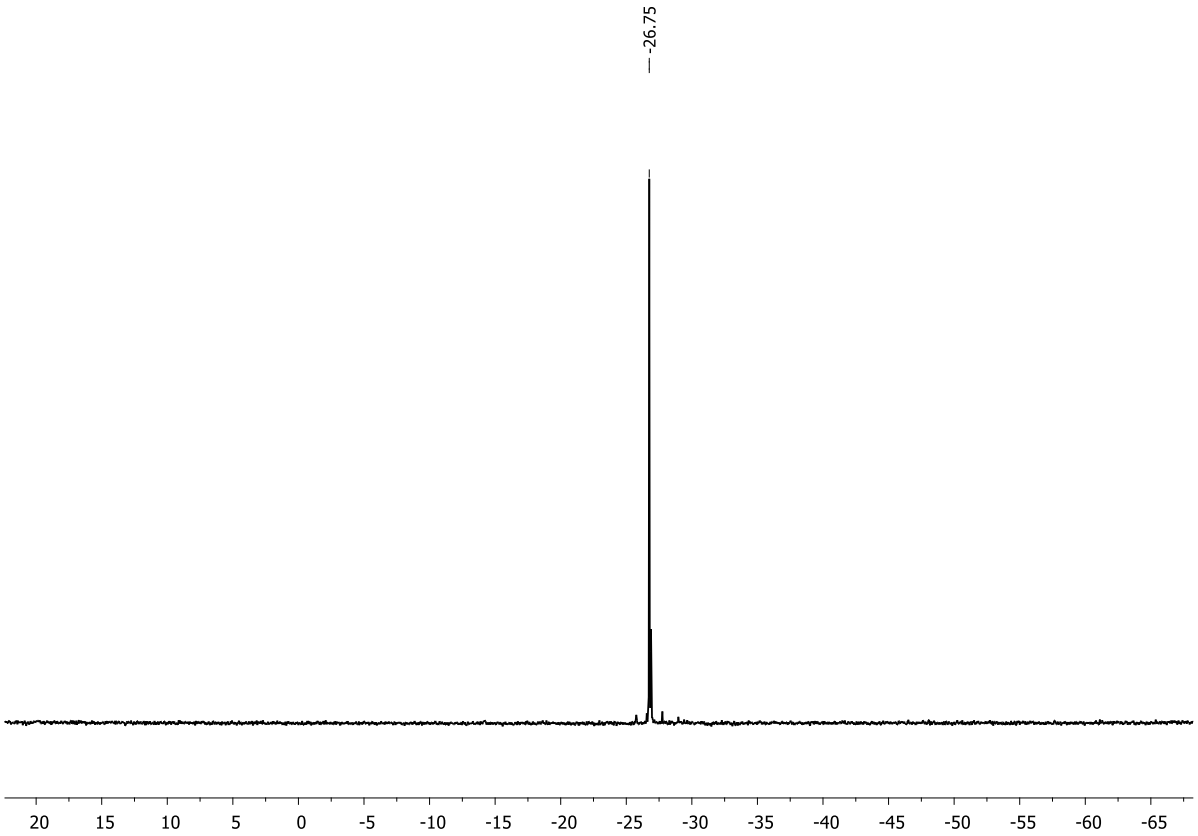

Figure 5.7.17. $^{119}Sn\{^{1}H\}$ NMR spectrum of **15a** (187 MHz, in $CDCl_3$).

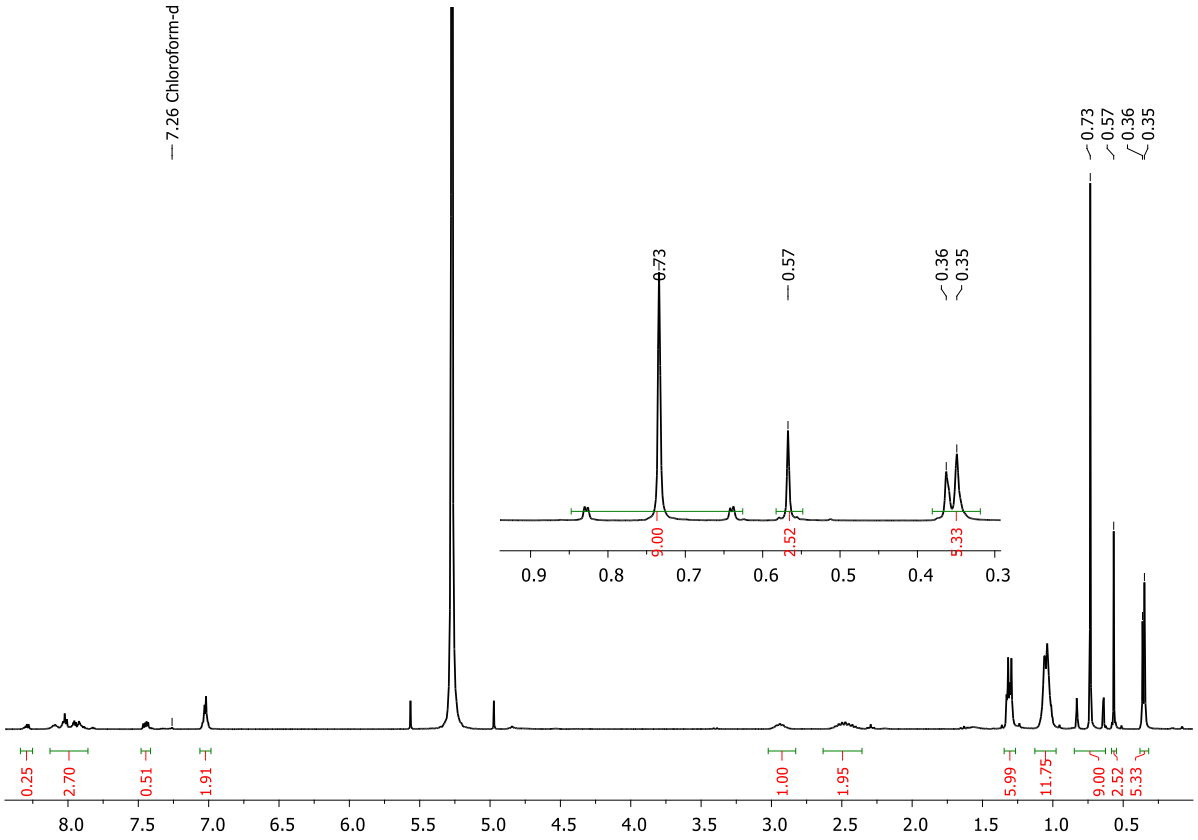

Figure 5.7.18. ^{1}H NMR spectrum of crude **16a** after stirring for 30 minutes (300 MHz, in $CDCl_3$).

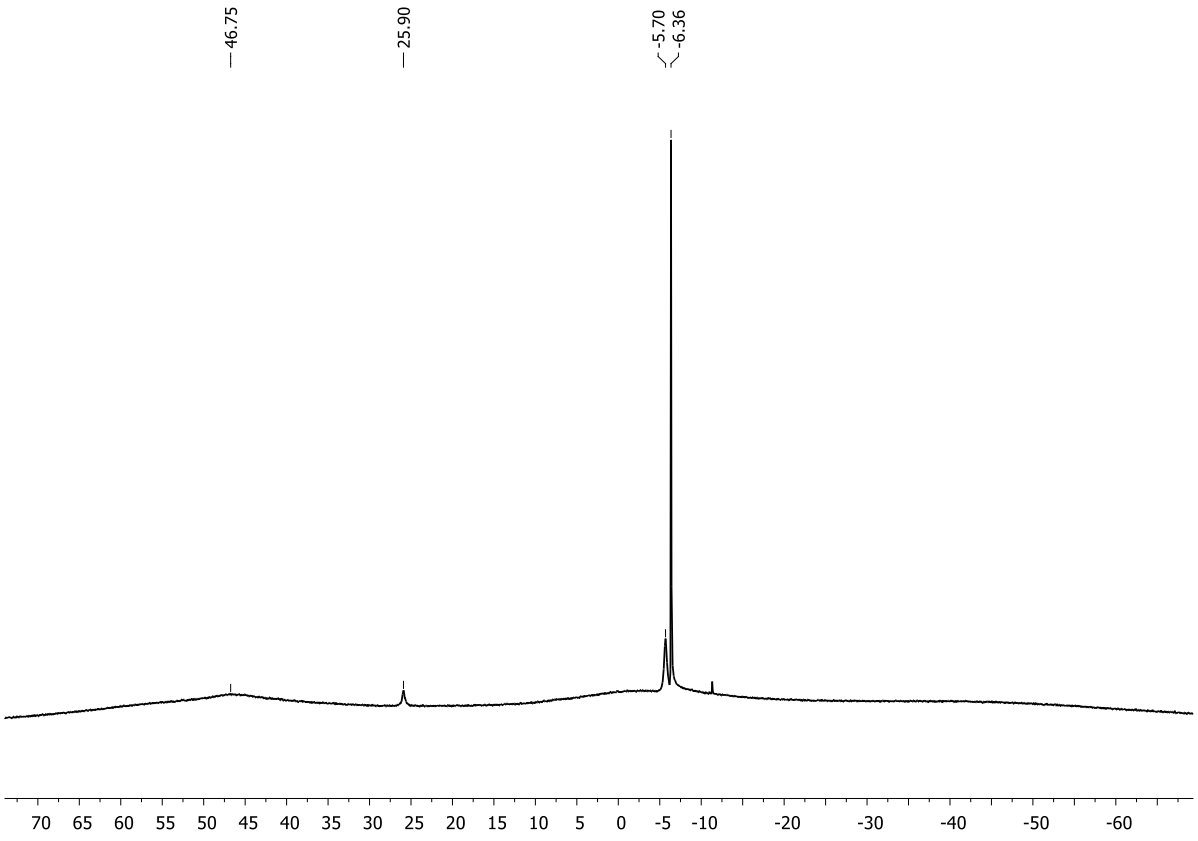

Figure 5.7.19. $^{11}B\{^{1}H\}$ NMR spectrum of crude **16a** after stirring for 30 minutes (96 MHz, in $CDCl_3$).

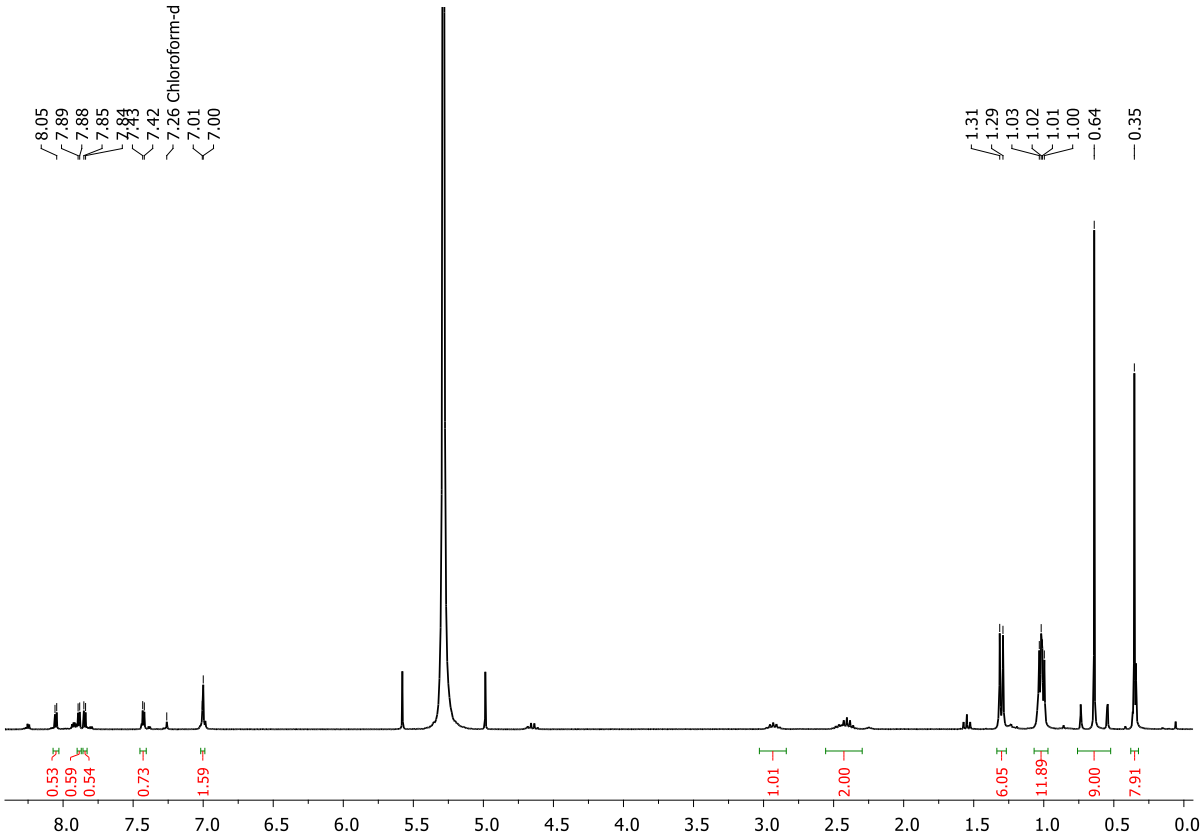

Figure 5.7.20. ^{1}H NMR spectrum of crude **17a** after stirring for 30 minutes (300 MHz, in $CDCl_3$).

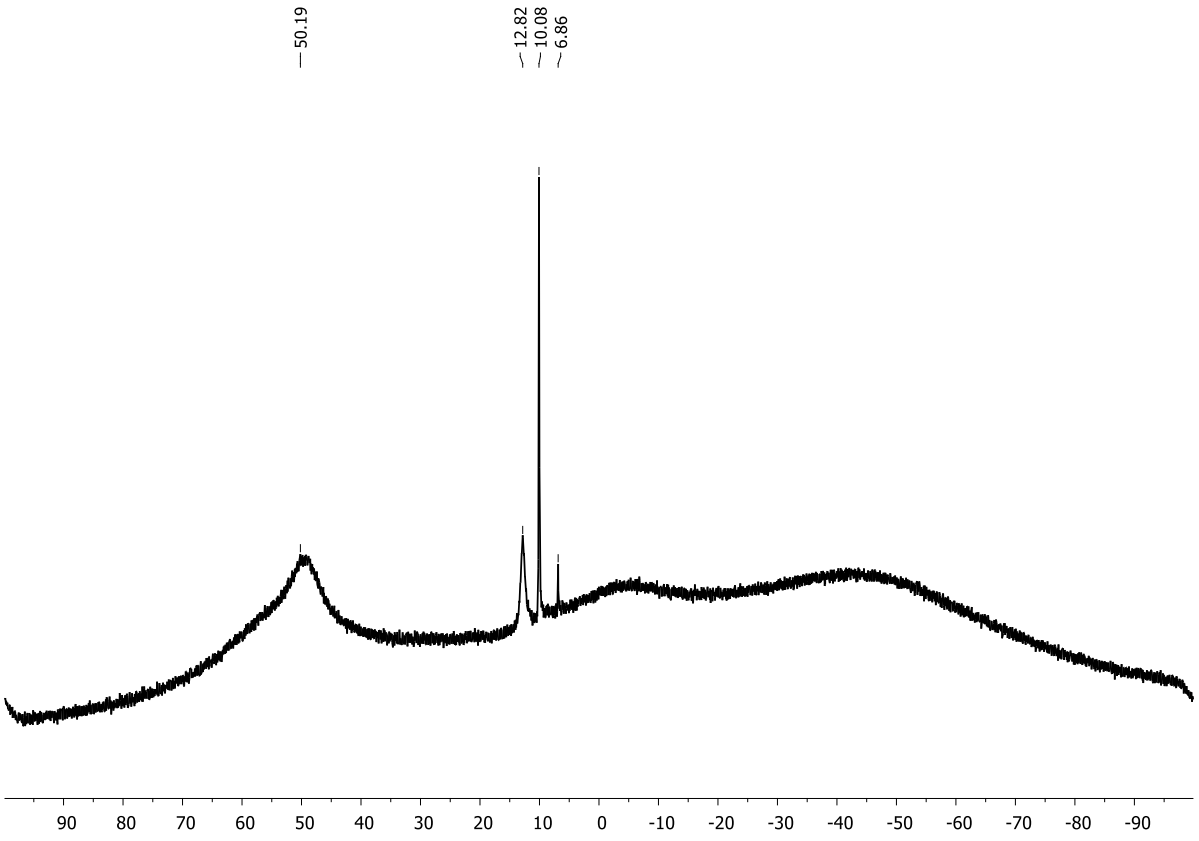

Figure 5.7.21. $^{11}B\{^{1}H\}$ NMR of crude **17a** after stirring for 30 minutes (96 MHz, in $CDCl_3$).

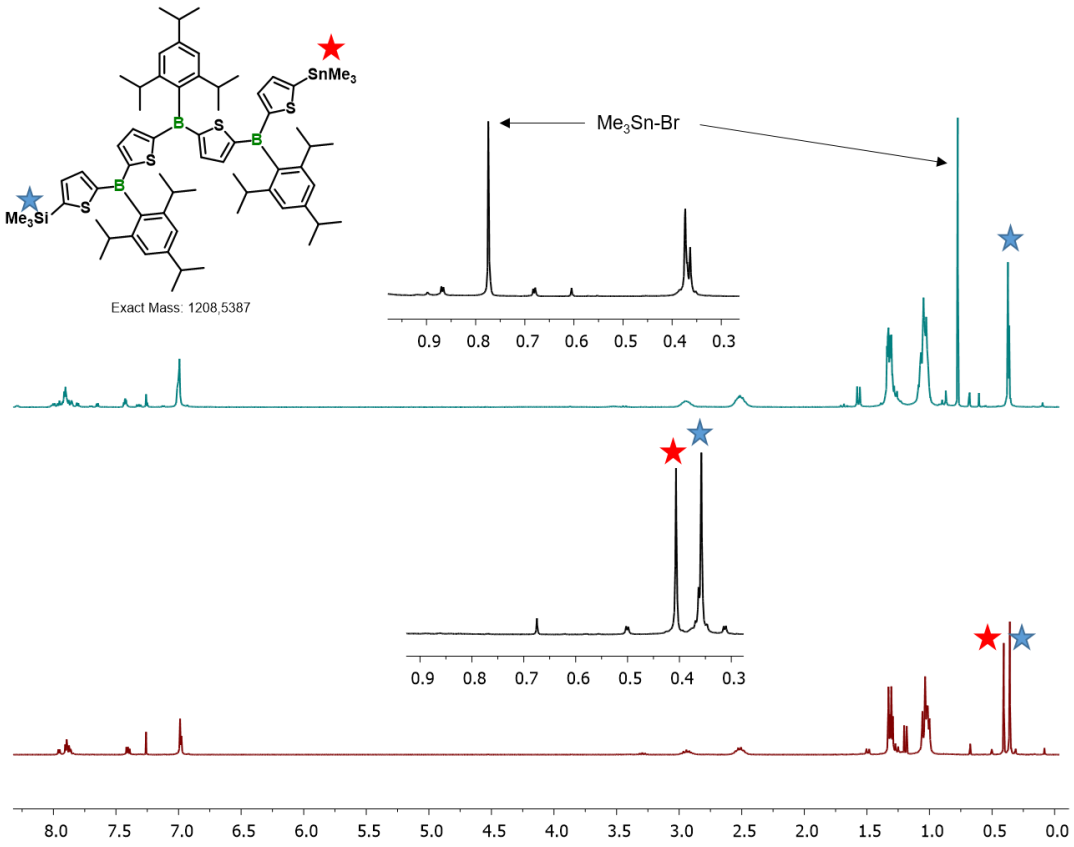

Figure 5.7.22. ^{1}H NMR spectra of **14a** (red) and of crude **18a** (turquoise) after addition to BBr_3 and stirring overnight (300 MHz, in $CDCl_3$).

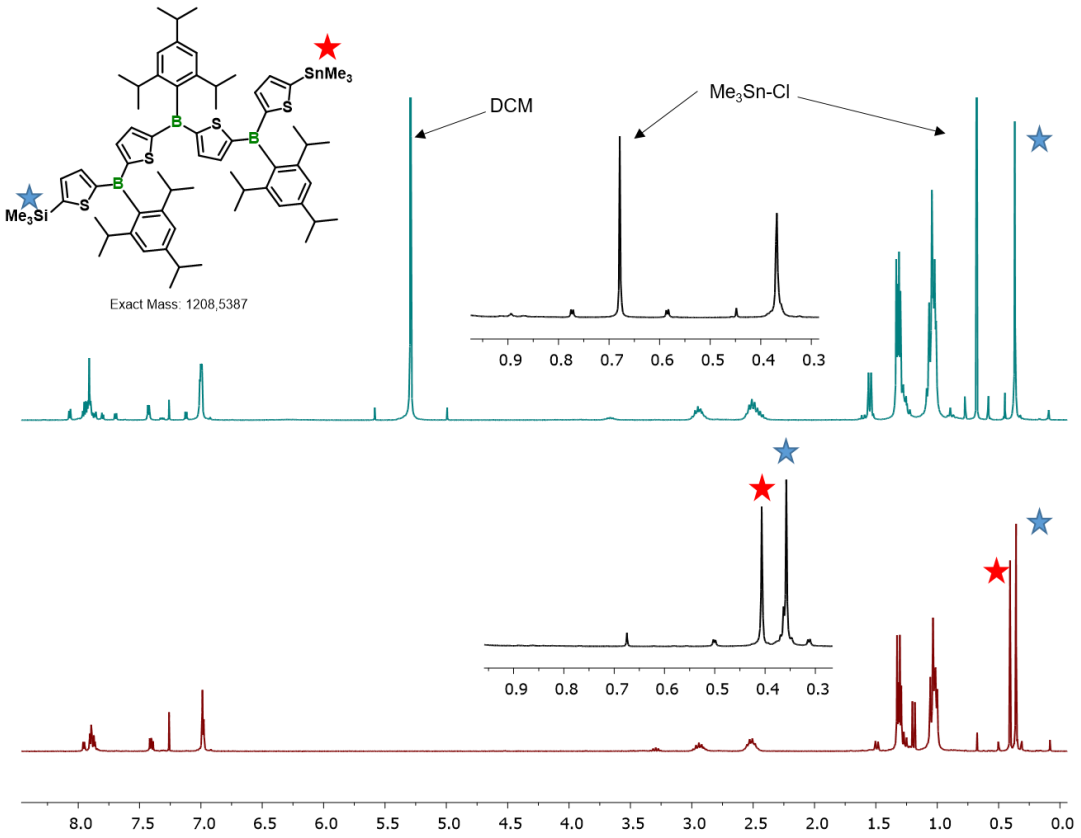

Figure 5.7.23. ^{1}H NMR spectra of **14a** (red) and of crude **19a** (turquoise) after addition to BCl_3 and stirring overnight (300 MHz, in $CDCl_3$).

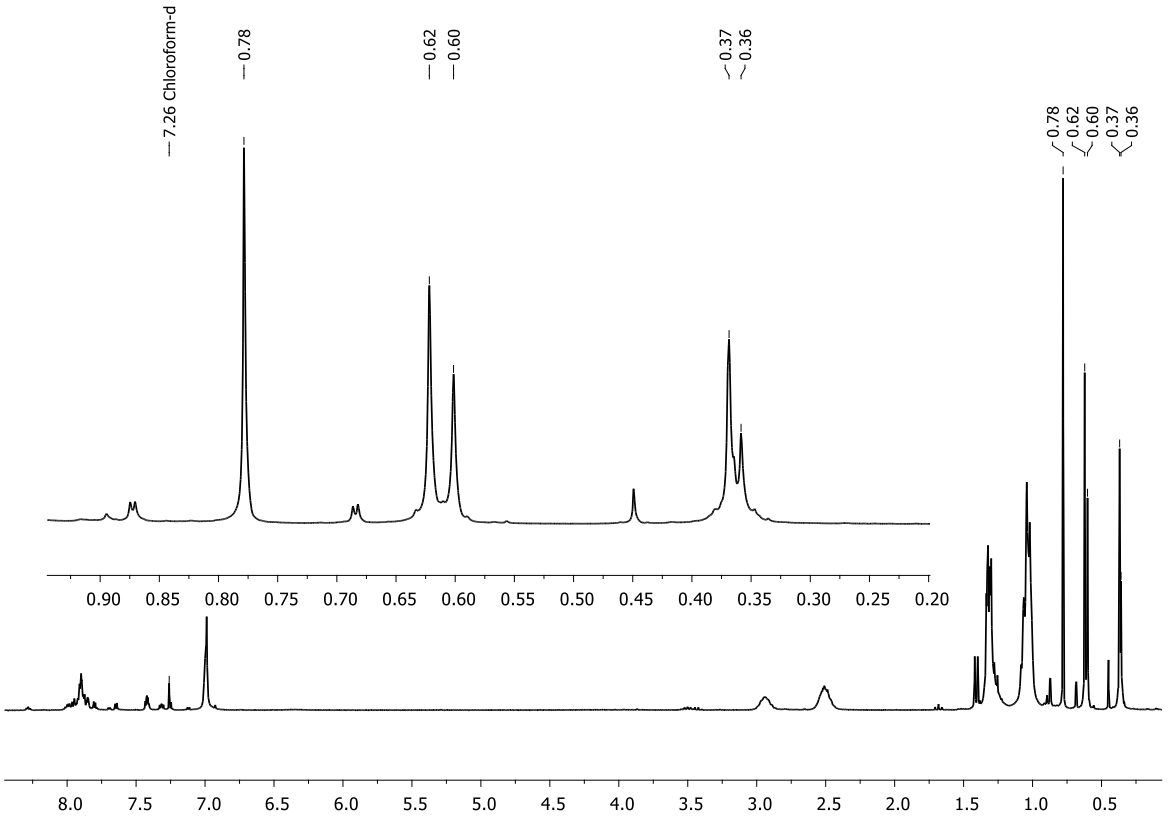

Figure 5.7.24. ^{1}H NMR spectrum of attempted synthesis to **20a** after 5 d and after addition of 50 mol% of catalyst in total (300 MHz, in $CDCl_3$).

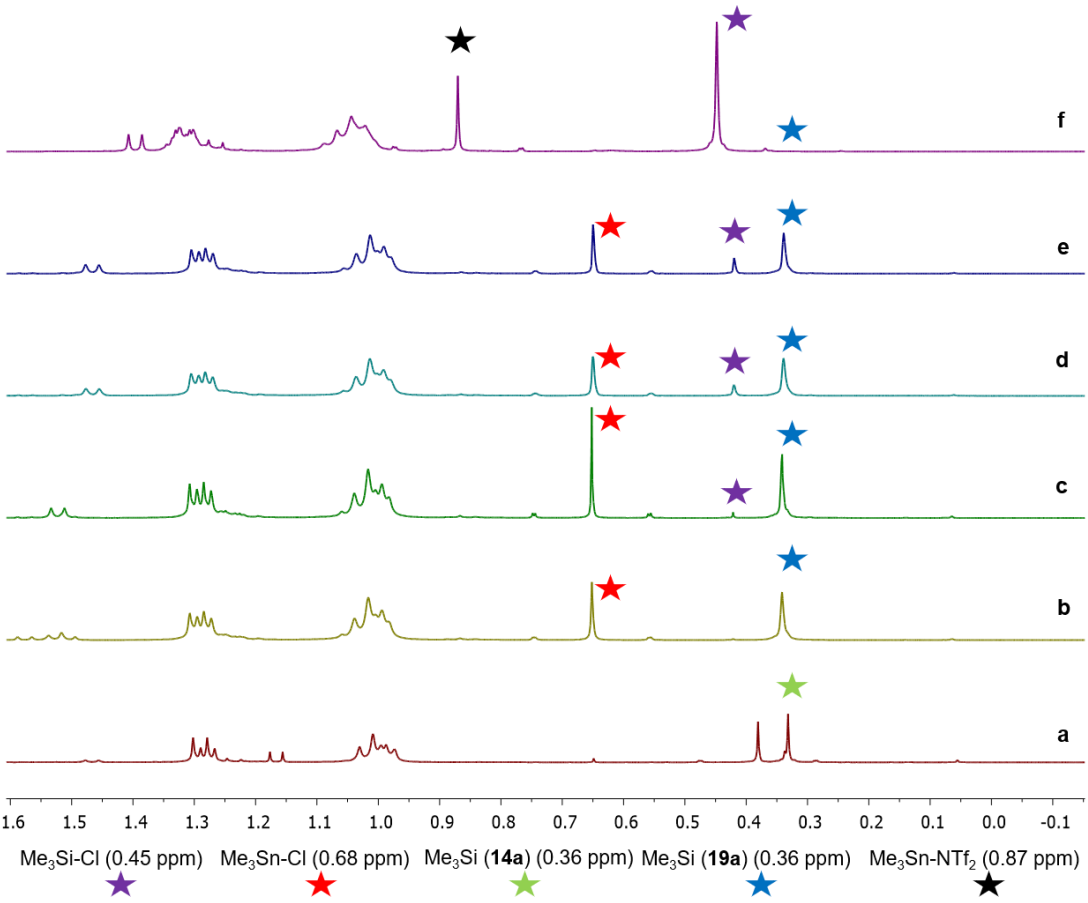

Figure 5.7.25. ^{1}H NMR spectra (300 MHz, in $CDCl_3$) recorded during attempted synthesis to **21a**. (a) ^{1}H NMR spectrum of compound **14a**, (b) after addition of BCl_3 solution and stirring for 30 minutes, (c) after stirring for 25 h, (d) after addition of catalytic amount of Me_3Si-NTf_2 (10 mol%), (e) after stirring for 25 h after the catalyst had been added, (f) after addition of another 40 mol% cat and stirring for total 5 days. Stars: Chemical shifts of silylated (purple) and stannylated (red) condensation products, silyl group of **14a** (green) and **19a** (blue) and forming Me_3Sn-NTf_2 (black).

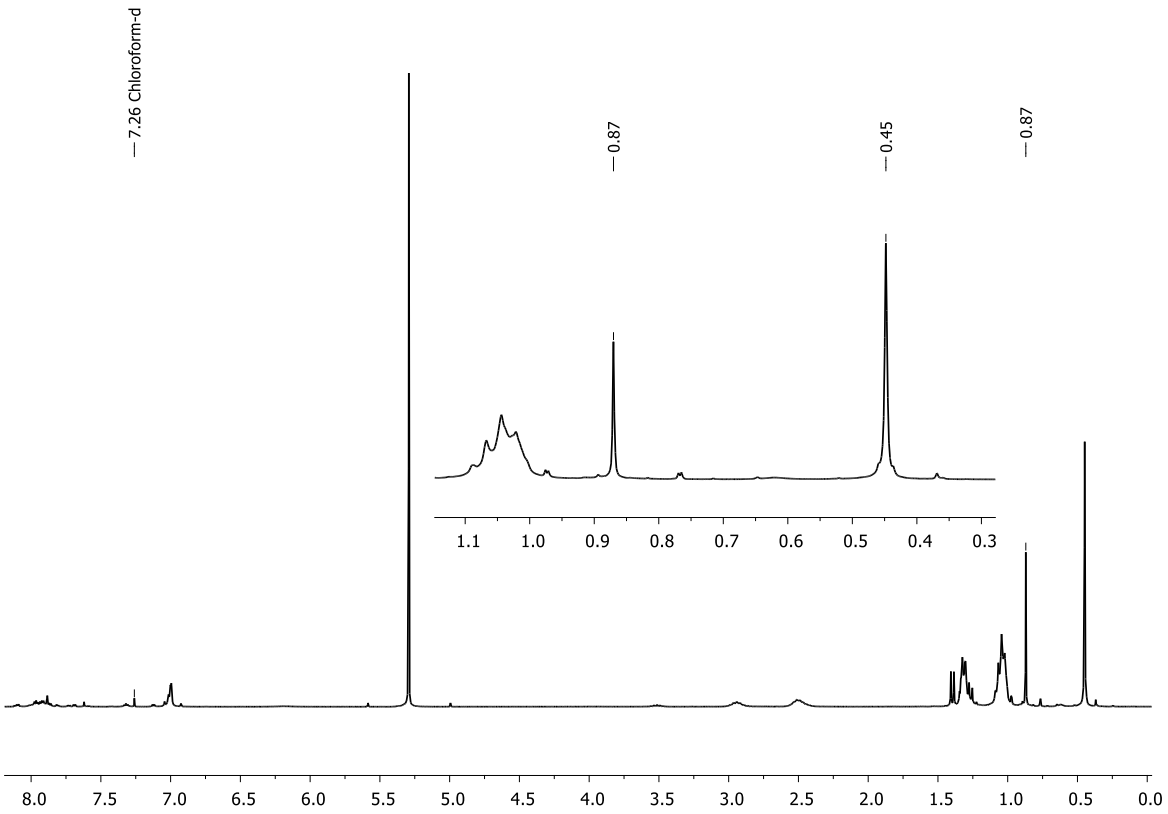

Figure 5.7.26. ^{1}H NMR spectrum of attempted synthesis to **21a** after 5 d and after addition of 50 mol% of catalyst in total (300 MHz, in $CDCl_3$).

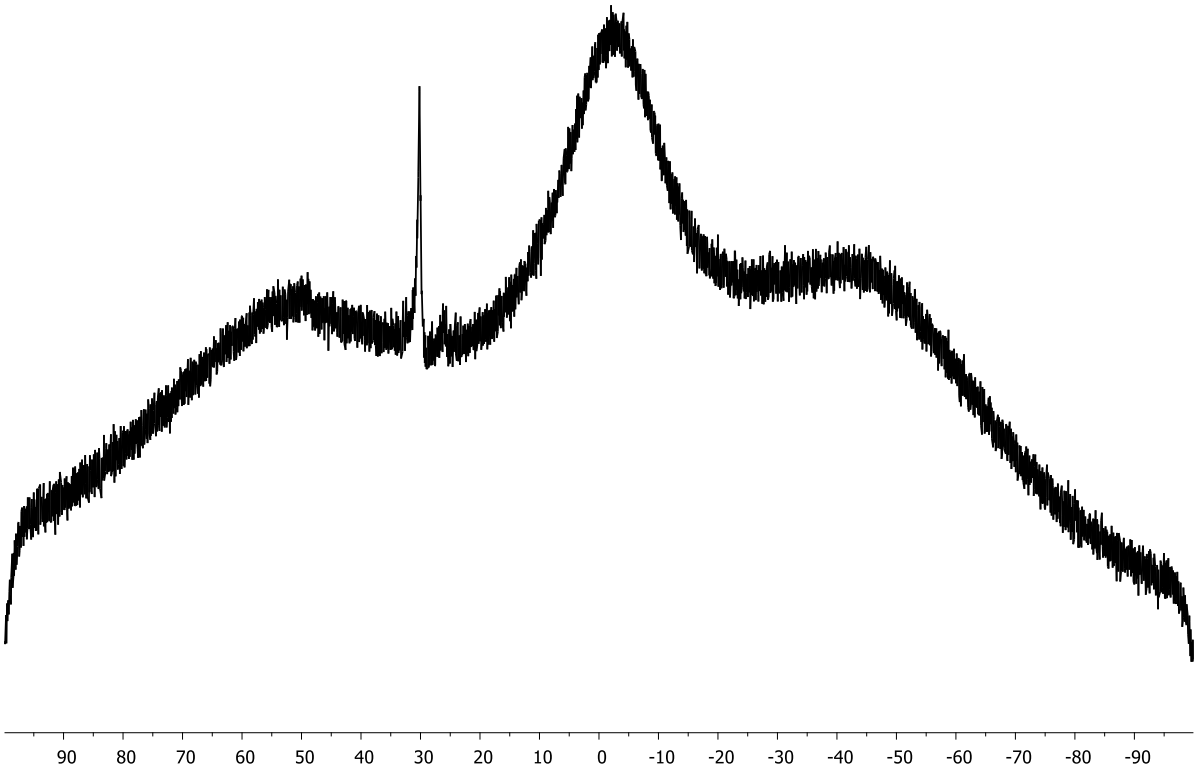

Figure 5.7.27. ^{11}B{^{1}H} NMR of attempted synthesis to **21a** after 5 d and after addition of 50 mol% of catalyst in total (300 MHz, in $CDCl_3$).

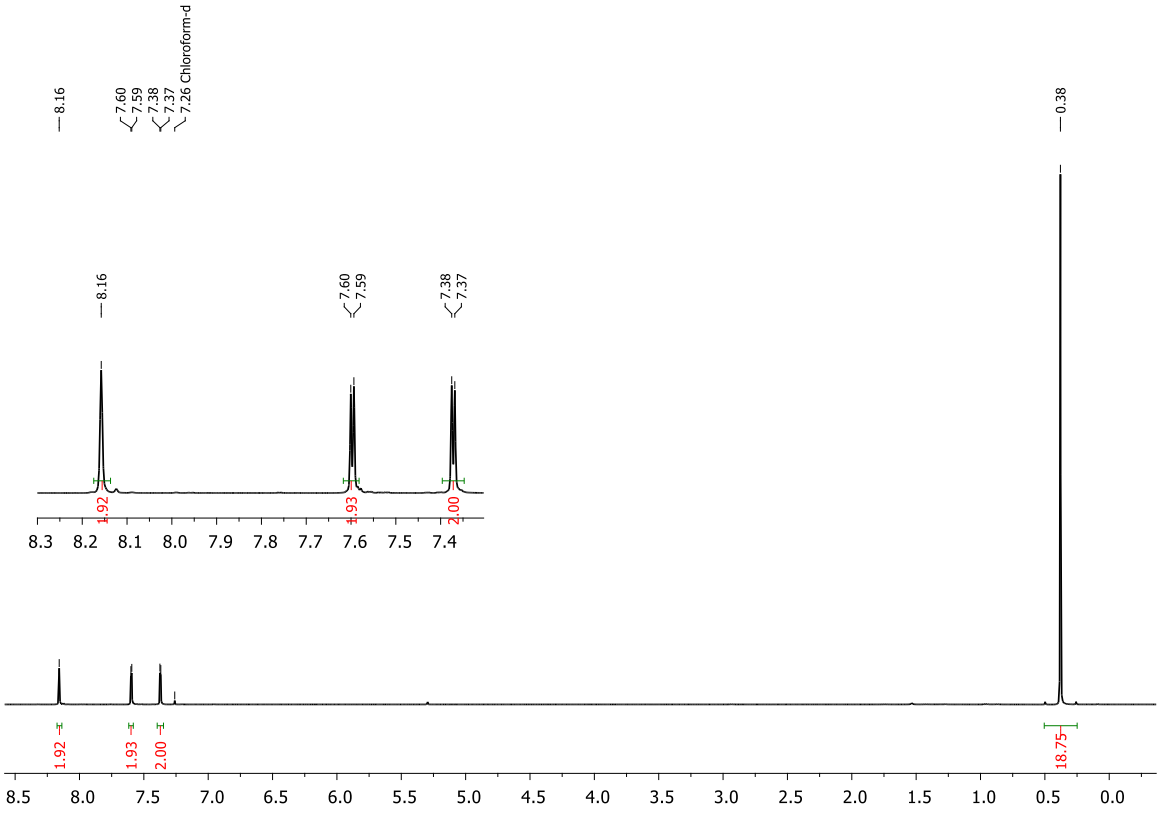

Figure 5.7.28. ^{1}H NMR spectrum of **3c** (500 MHz, in $CDCl_3$).

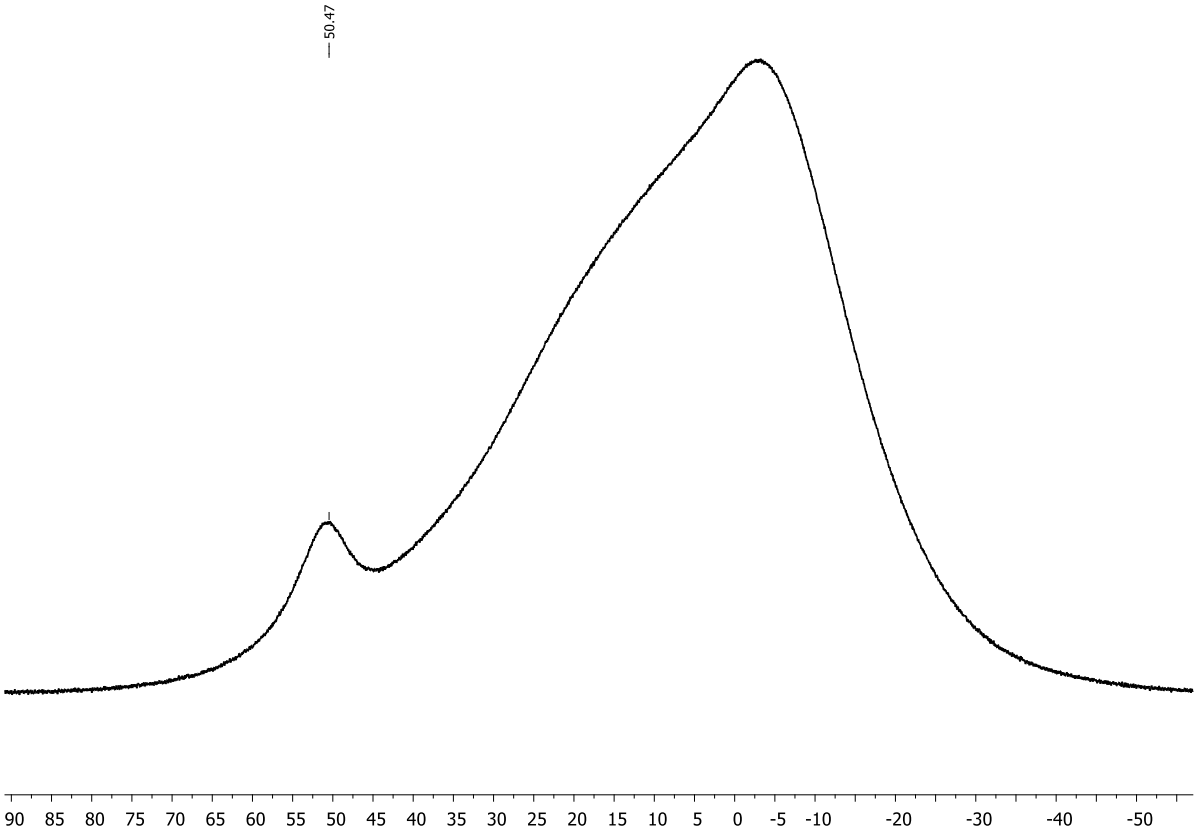

Figure 5.7.29. $^{11}B\{^{1}H\}$ NMR spectrum of **3c** (160 MHz, in $CDCl_3$).

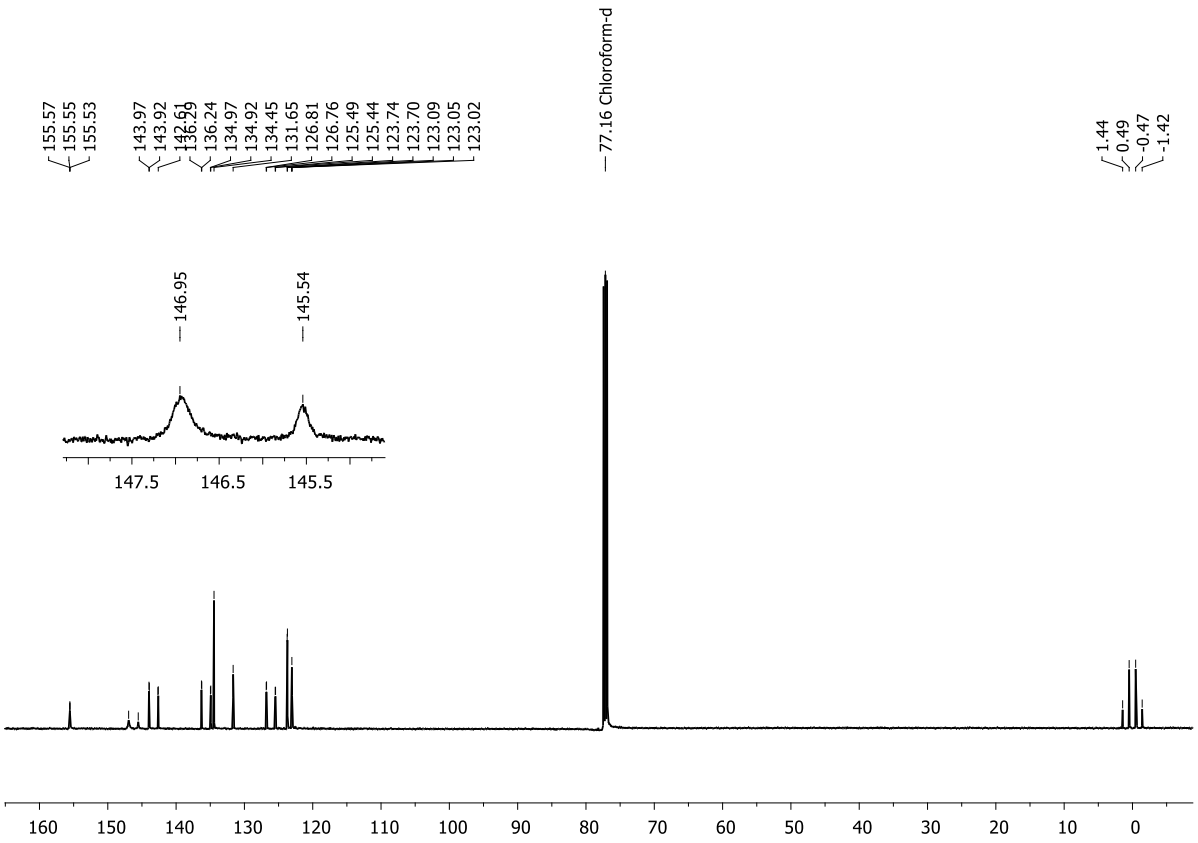

Figure 5.7.30. $^{13}C\{^{1}H\}$ NMR spectrum of **3c** (126 MHz, in $CDCl_3$).

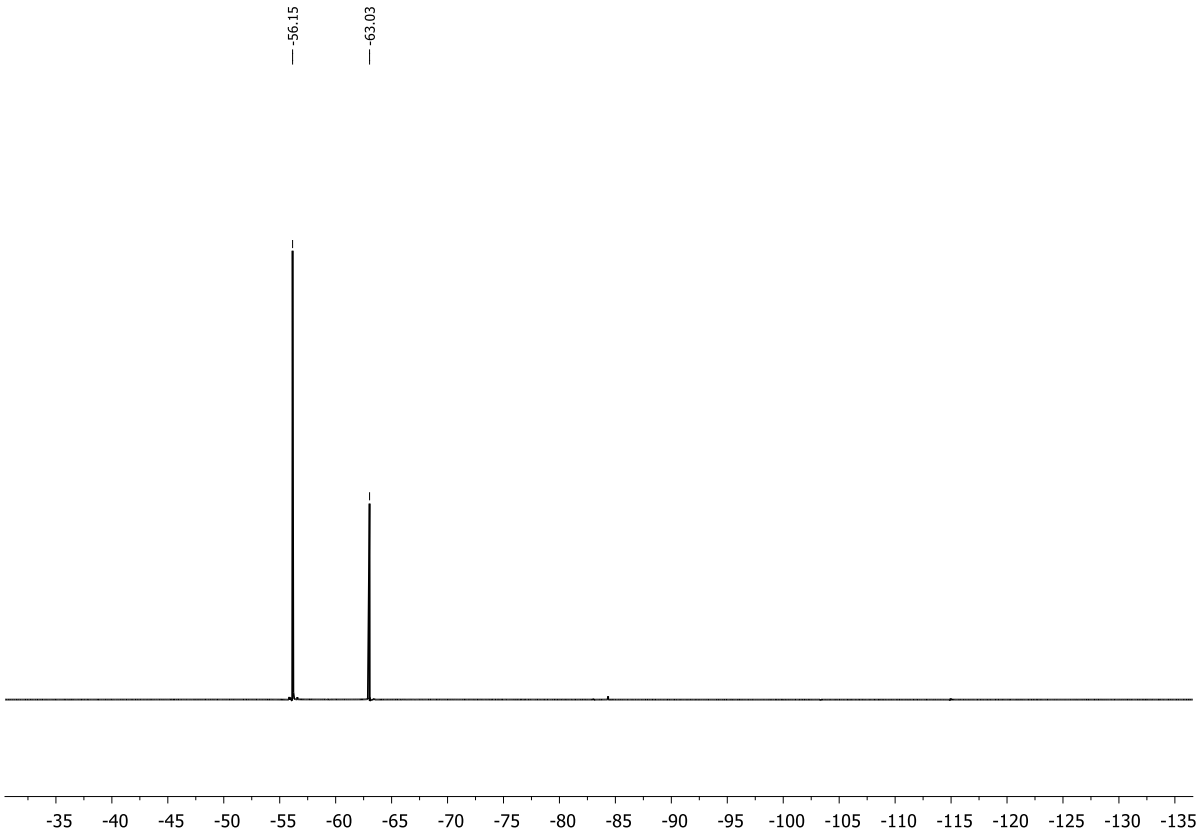

Figure 5.7.31. $^{19}F\{^{1}H\}$ NMR spectrum of **3c** (471 MHz, in $CDCl_3$).

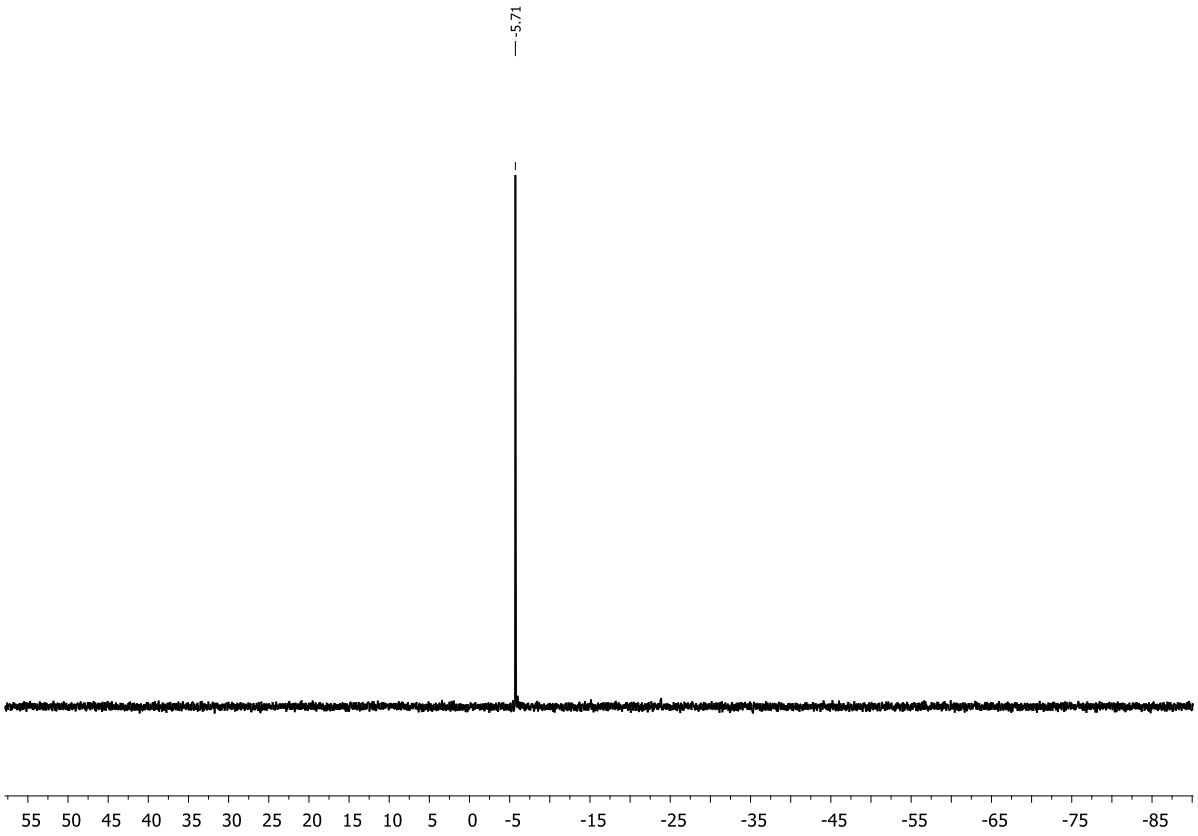

Figure 5.7.32. $^{29}Si\{^{1}H\}$ NMR spectrum of **3c** (99 MHz, in $CDCl_3$).

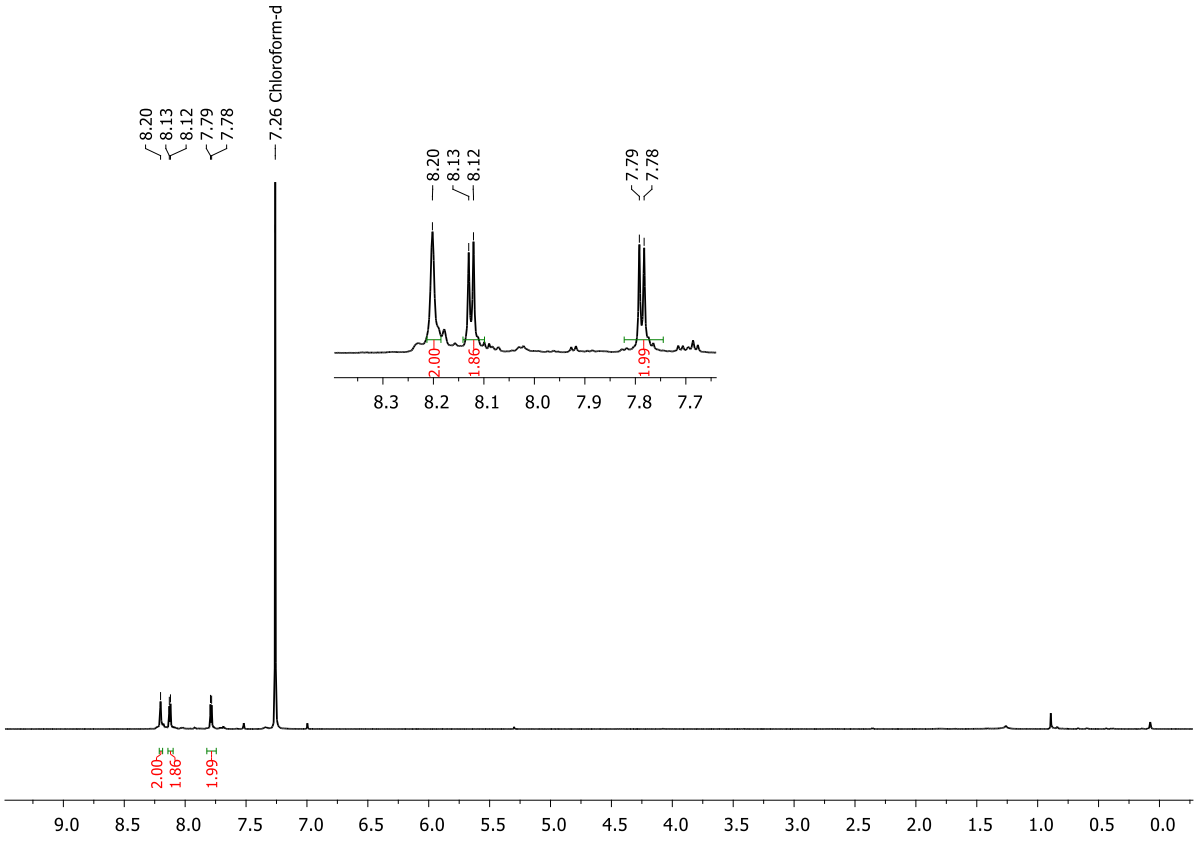

Figure 5.7.33. ^{1}H NMR spectrum of **4c** (400 MHz, in $CDCl_3$).

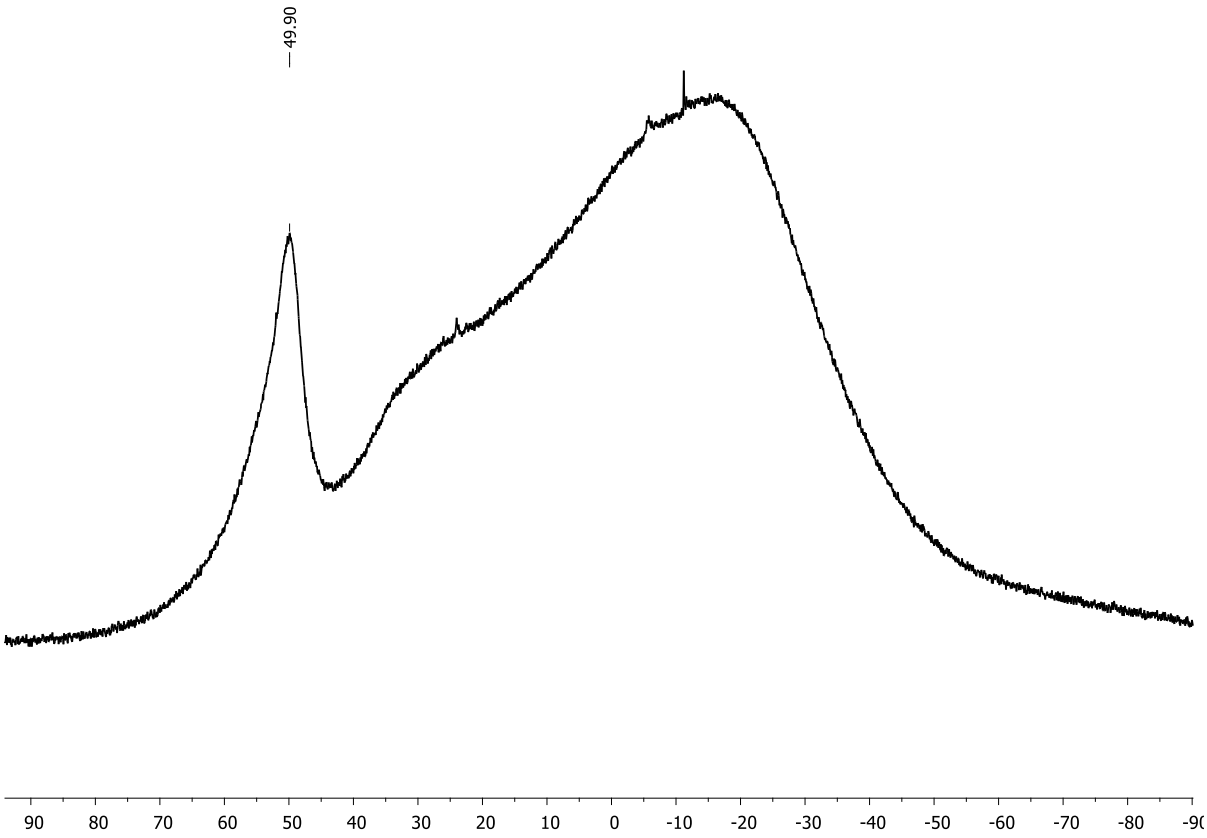

Figure 5.7.34. $^{11}B\{^{1}H\}$ NMR spectrum of **4c** (128 MHz, in $CDCl_3$).

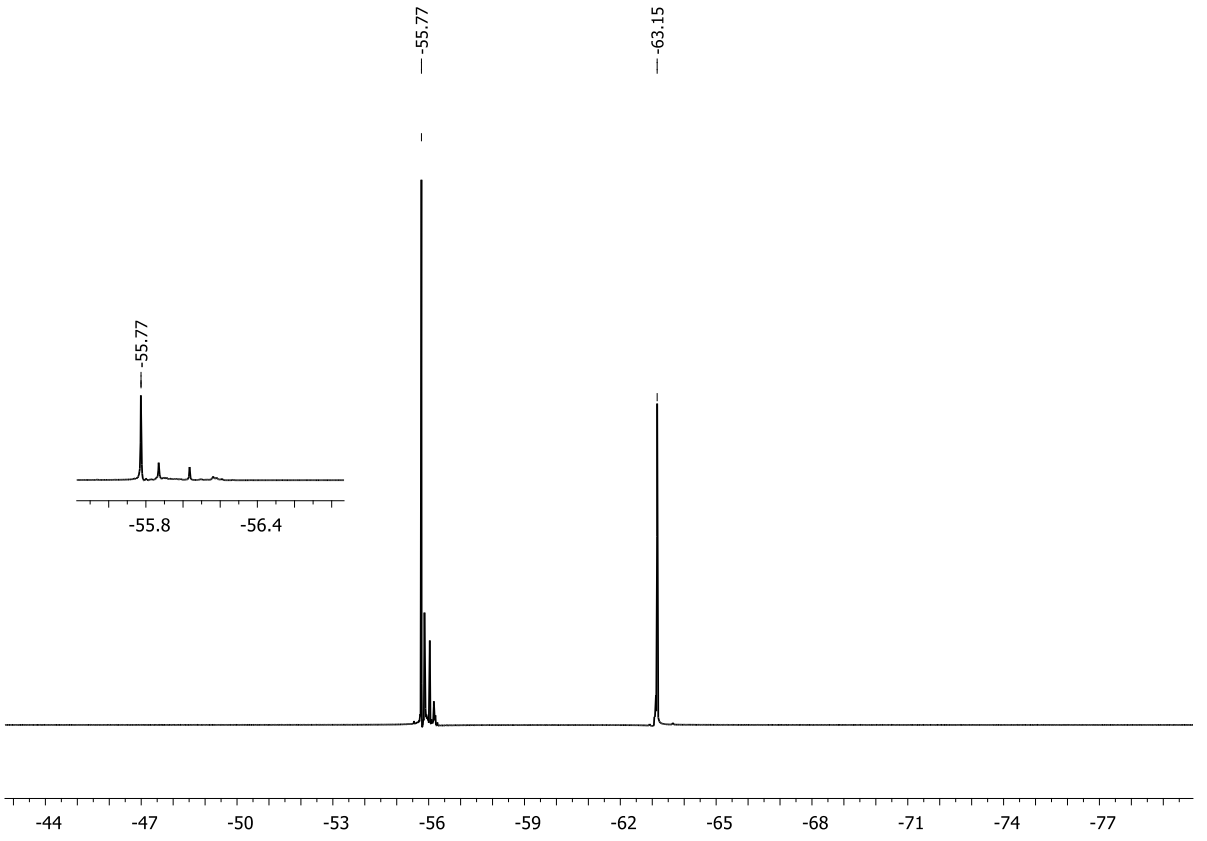

Figure 5.7.35. $^{19}F\{^{1}H\}$ NMR spectrum of **4c** (377 MHz, in $CDCl_3$).

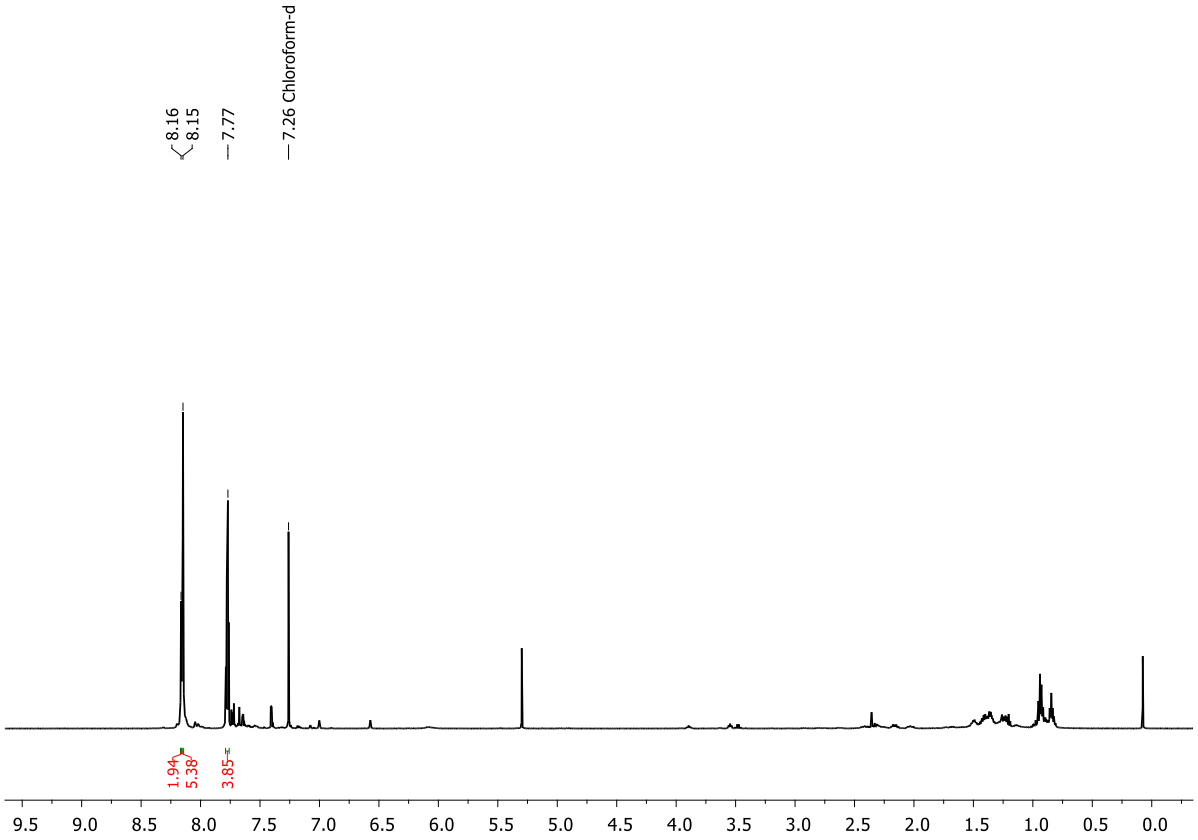

Figure 5.7.36. ^{1}H NMR spectrum of crude **5c** (500 MHz, in $CDCl_3$).

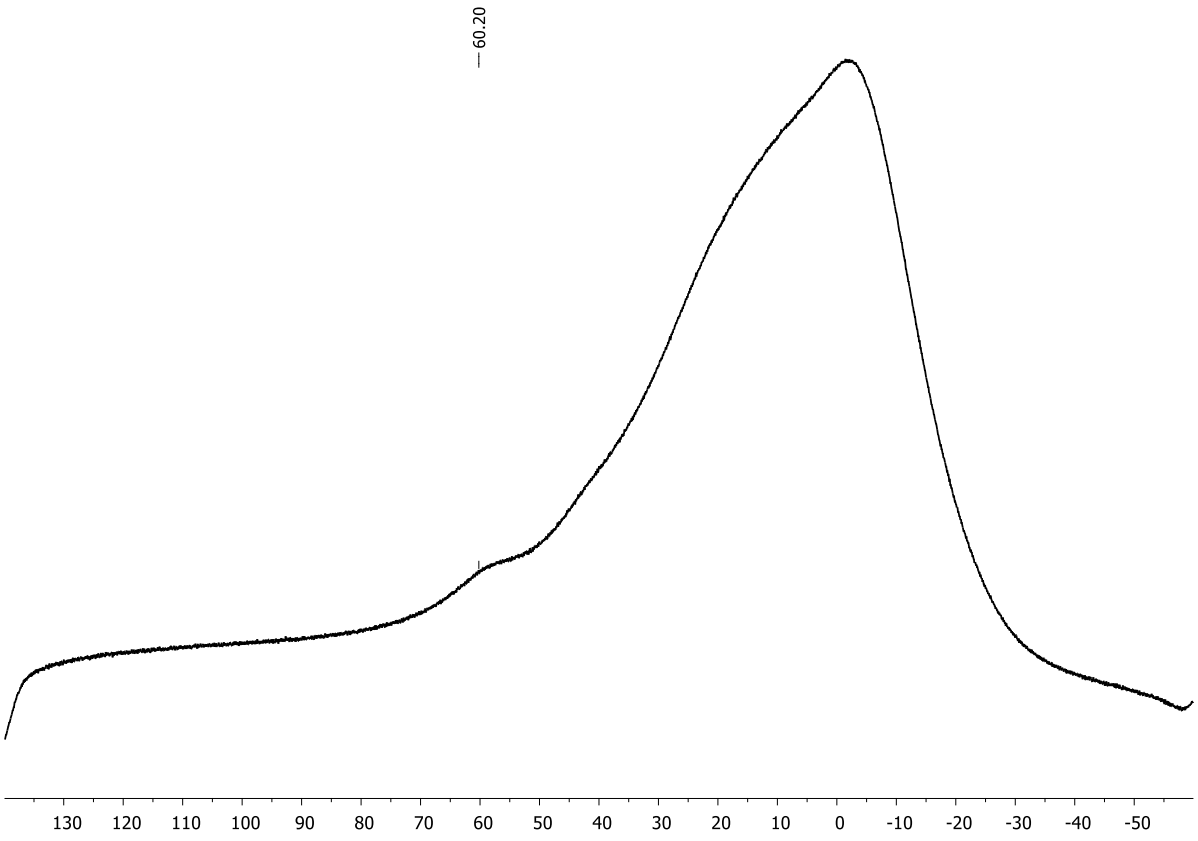

Figure 5.7.37. $^{11}B\{^{1}H\}$ NMR spectrum of crude **5c** (160 MHz, in $CDCl_3$).

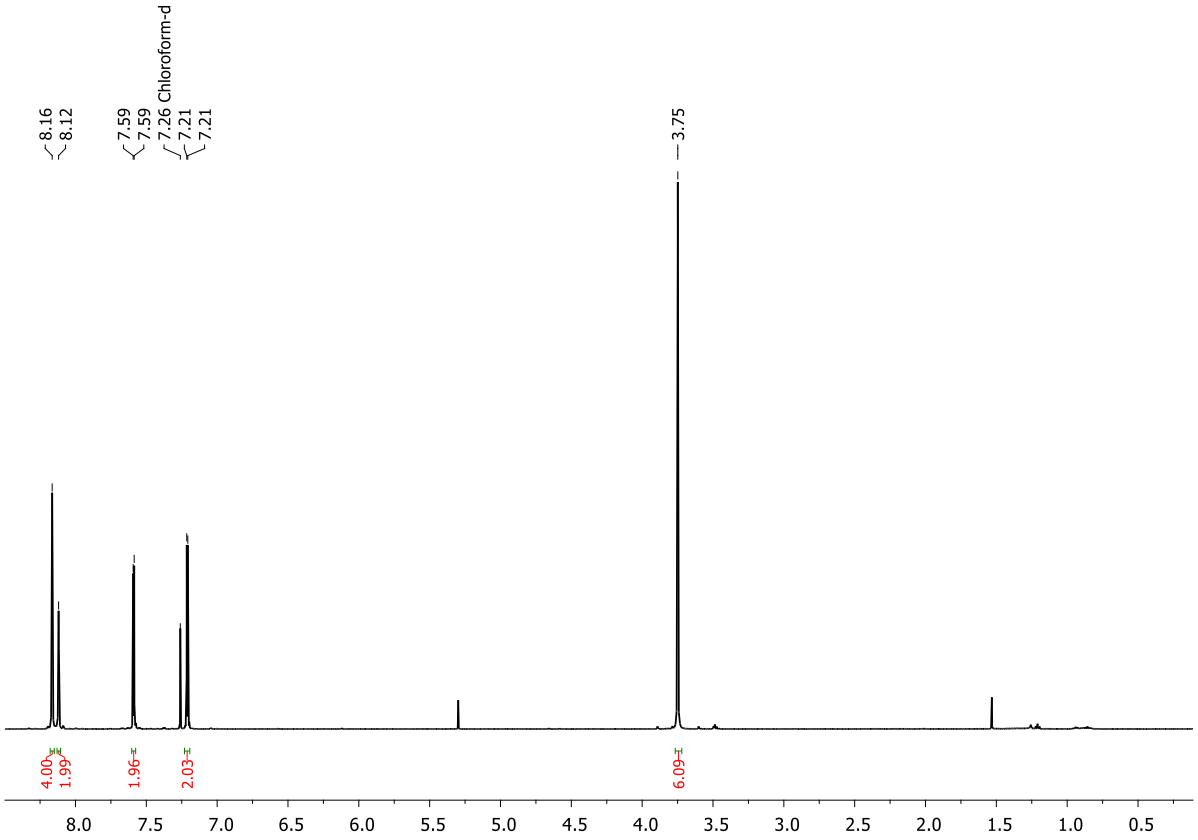

Figure 5.7.38. ^{1}H NMR spectrum of **6c** (500 MHz, in $CDCl_3$).

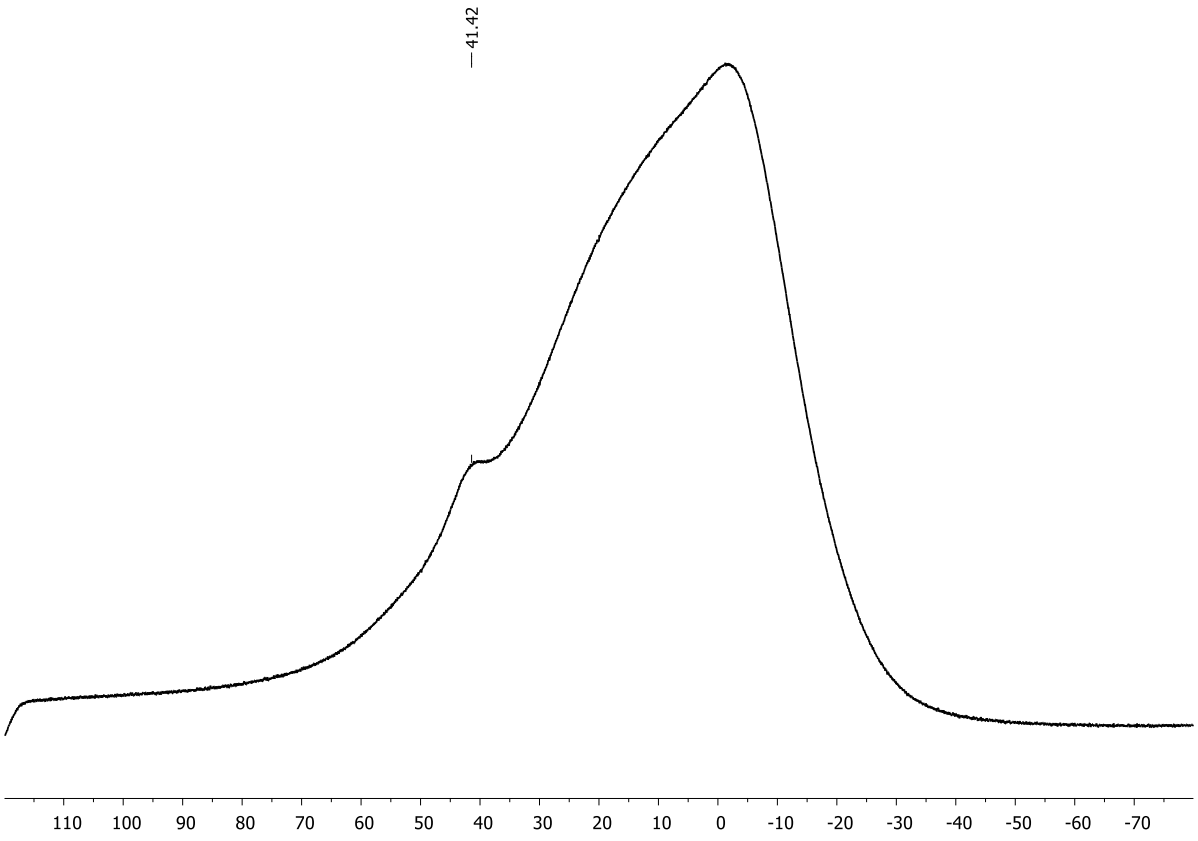

Figure 5.7.39. $^{11}B\{^{1}H\}$ NMR spectrum **6c** (160 MHz, in $CDCl_3$).

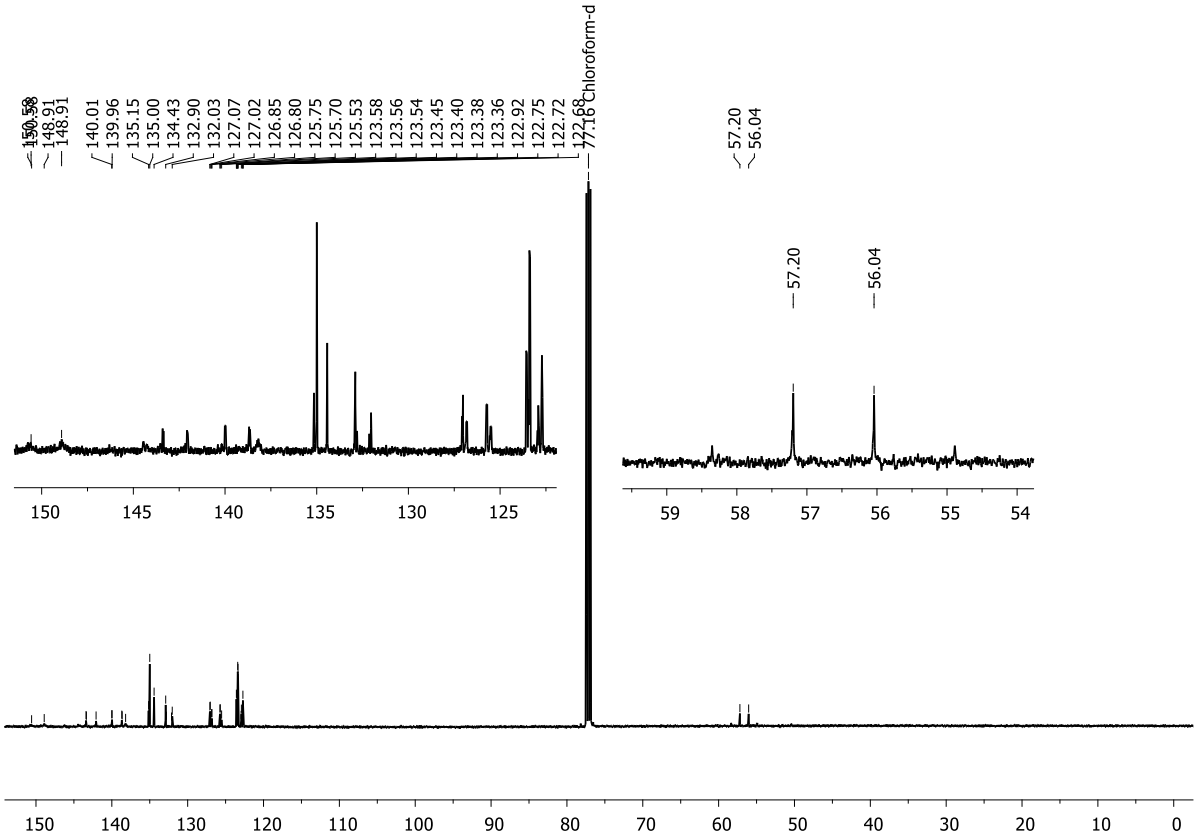

Figure 5.7.40. $^{13}C\{^{1}H\}$ NMR spectrum of **6c** (126 MHz, in $CDCl_3$).

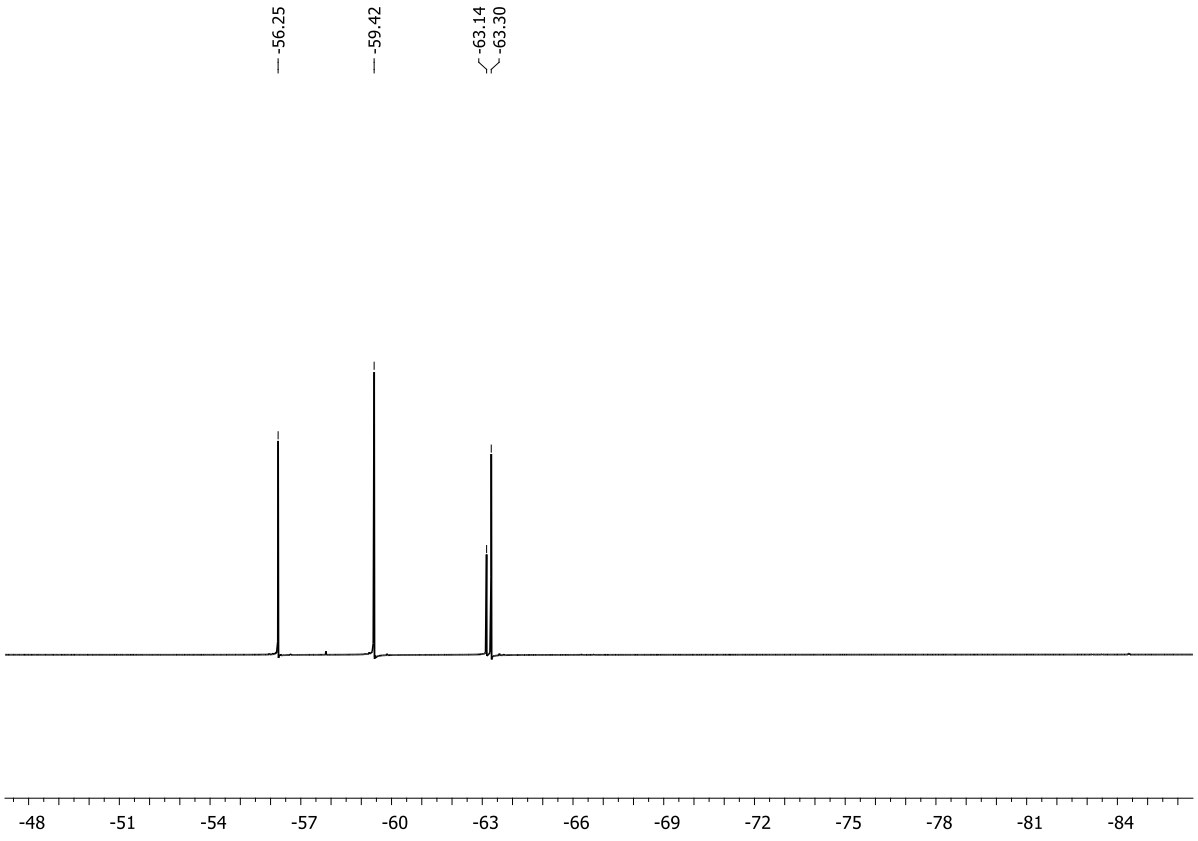

Figure 5.7.41. $^{19}F\{^{1}H\}$ NMR spectrum of **6c** (471 MHz, in $CDCl_3$).

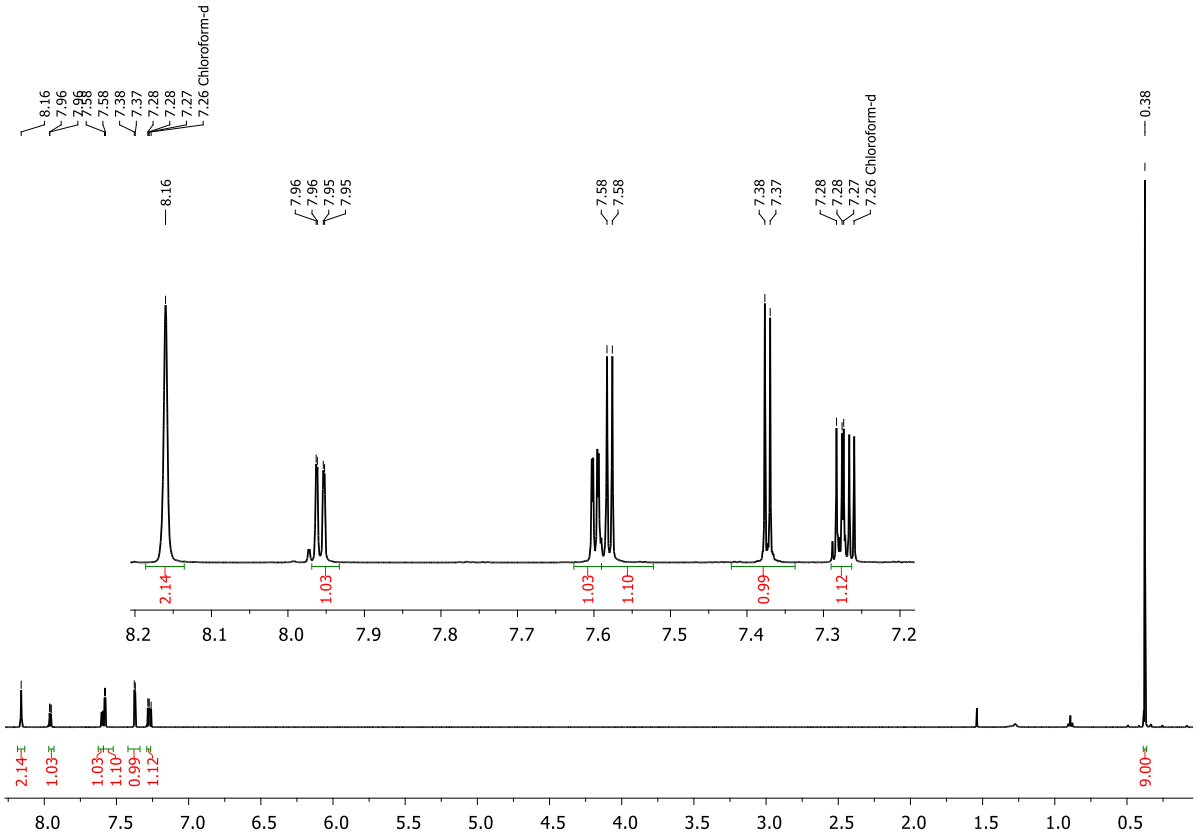

Figure 5.7.42. ^{1}H NMR spectrum of **8b** (500 MHz, in $CDCl_3$).

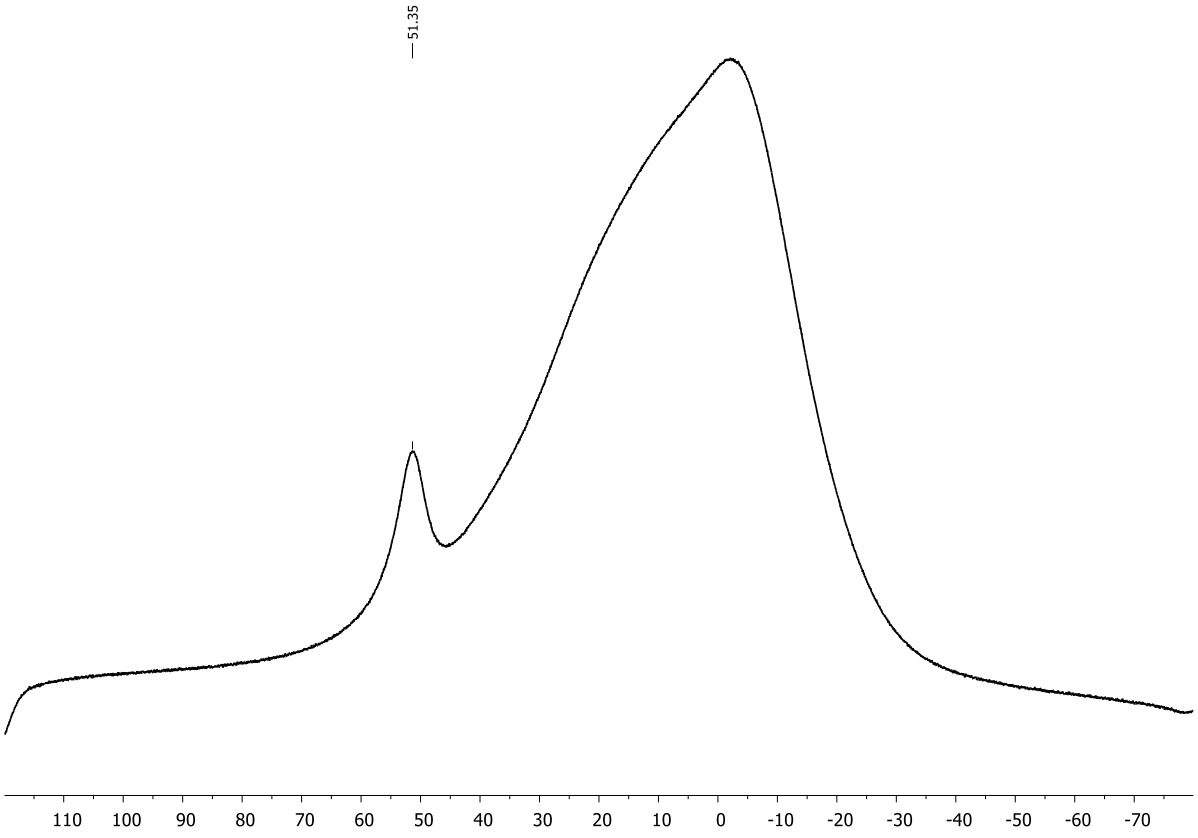

Figure 5.7.43. $^{11}B\{^{1}H\}$ NMR spectrum of **8b** (160 MHz, in $CDCl_3$).

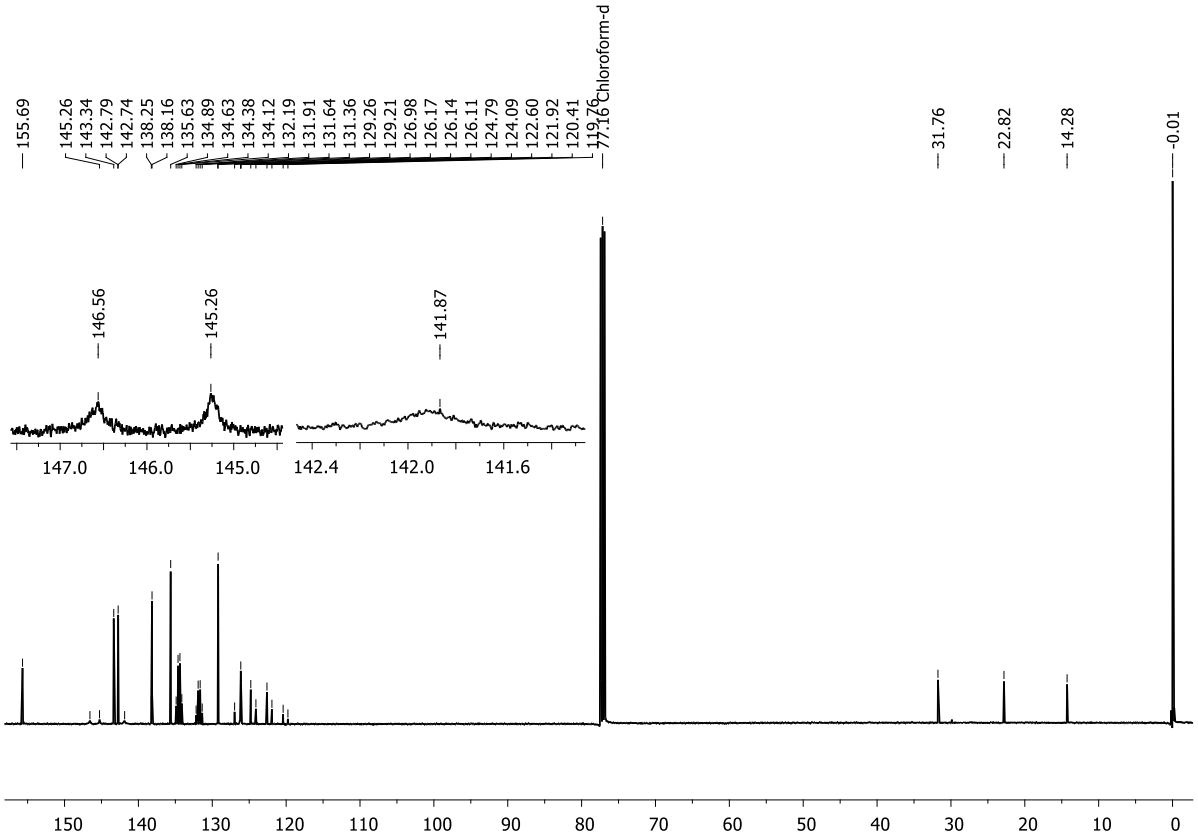

Figure 5.7.44. $^{13}C\{^{1}H\}$ NMR spectrum of **8b** (126 MHz, in $CDCl_3$).

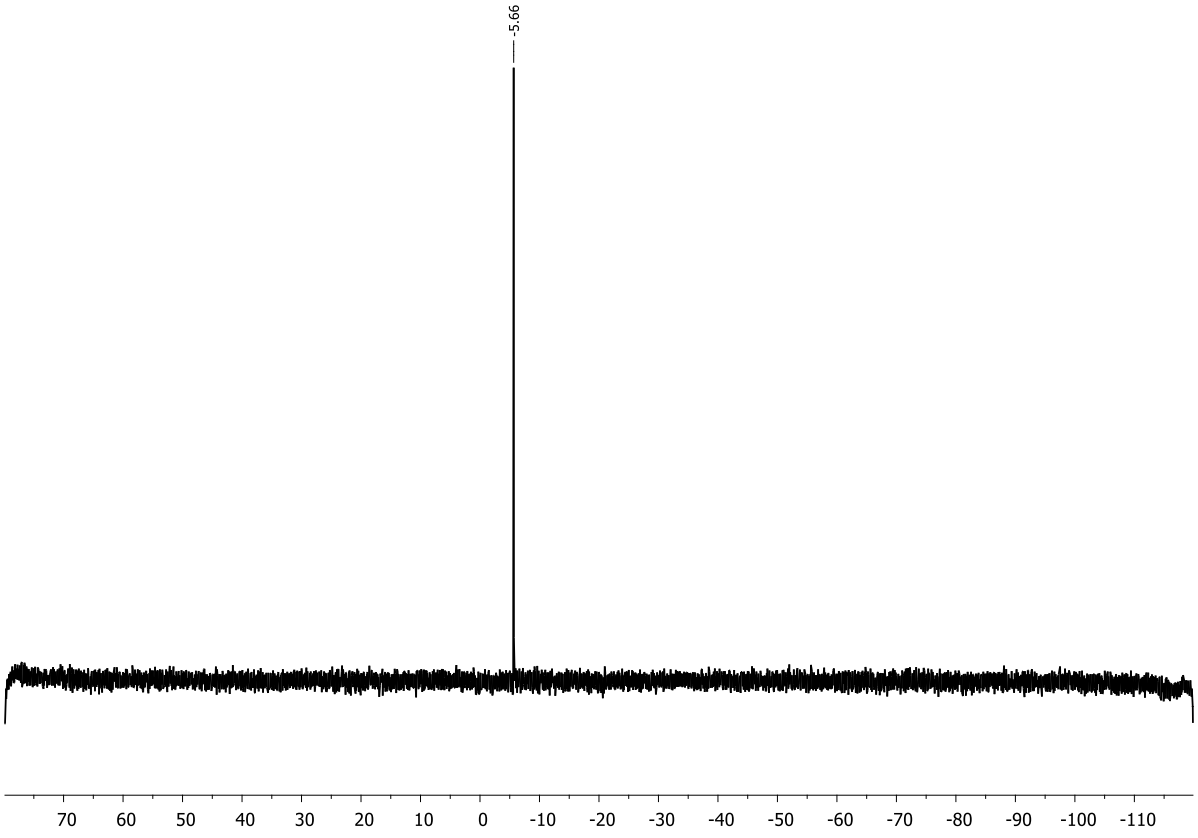

Figure 5.7.45. $^{29}Si\{^{1}H\}$ NMR spectrum of **8b** (99 MHz, in $CDCl_3$).

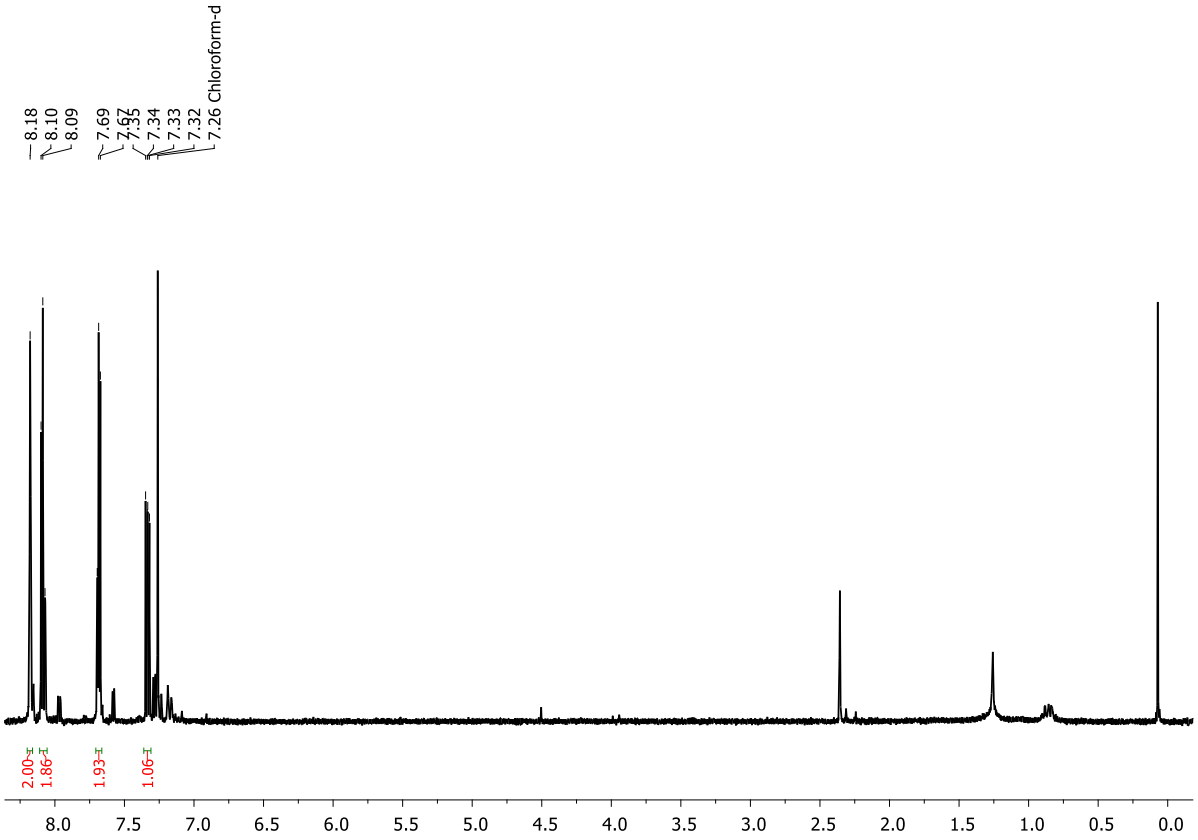

Figure 5.7.46. ^{1}H NMR spectrum of **9b** (300 MHz, in $CDCl_3$).

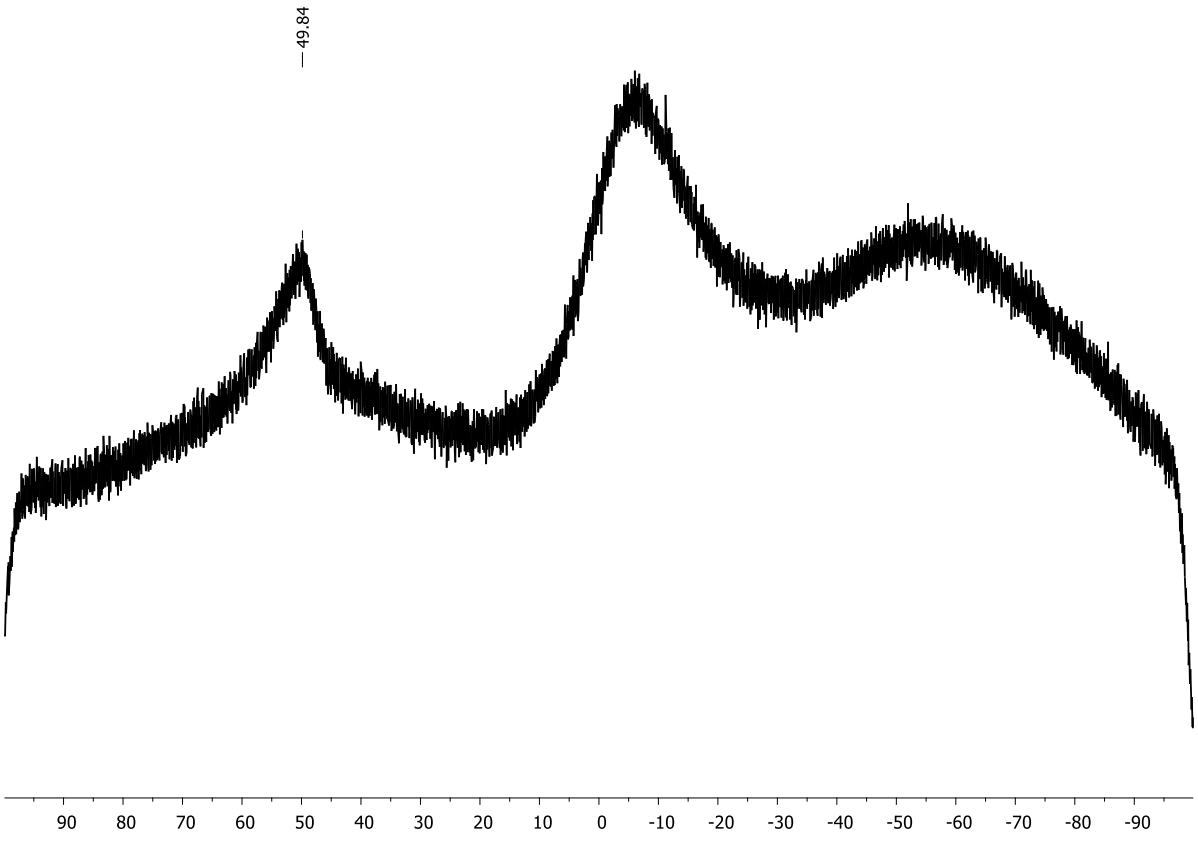

Figure 5.7.47. $^{11}B\{^{1}H\}$ NMR spectrum of **9b** (96 MHz, in $CDCl_3$).

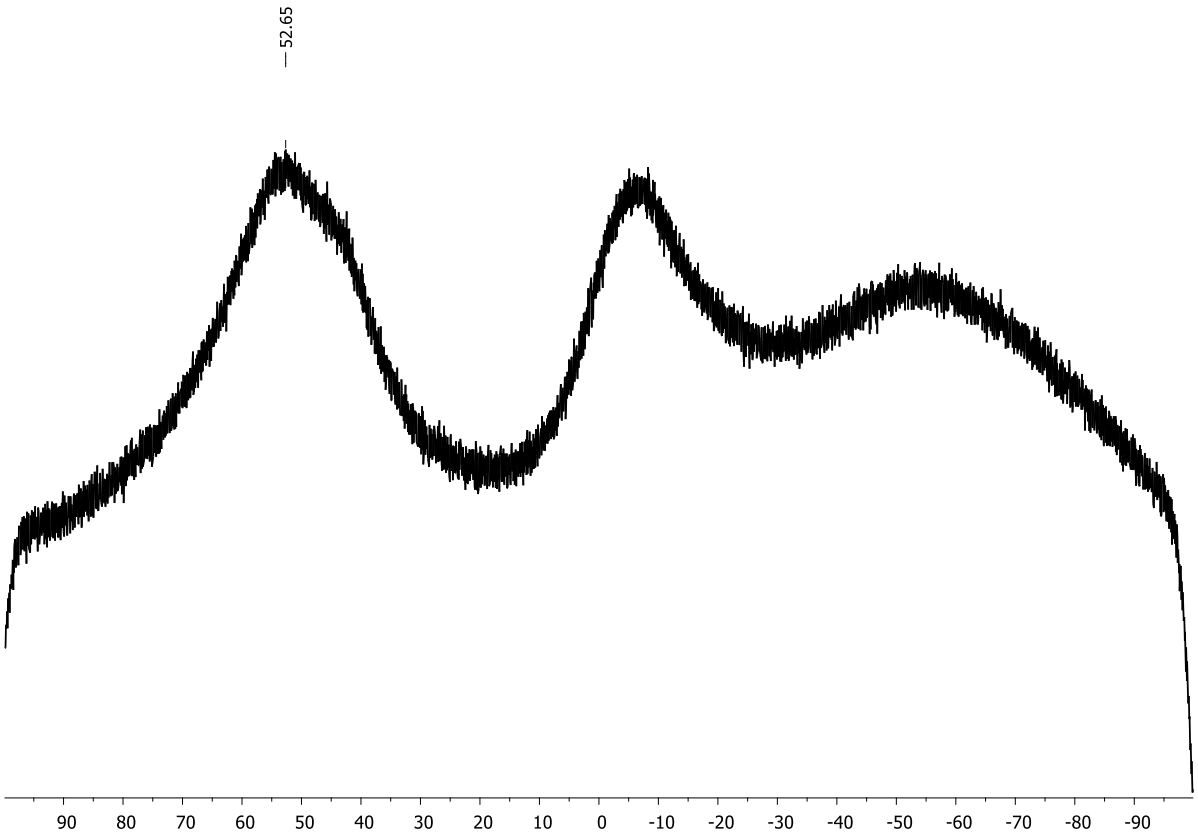

Figure 5.7.48. $^{11}B\{^{1}H\}$ NMR spectrum of **10b** (96 MHz, in $CDCl_3$).

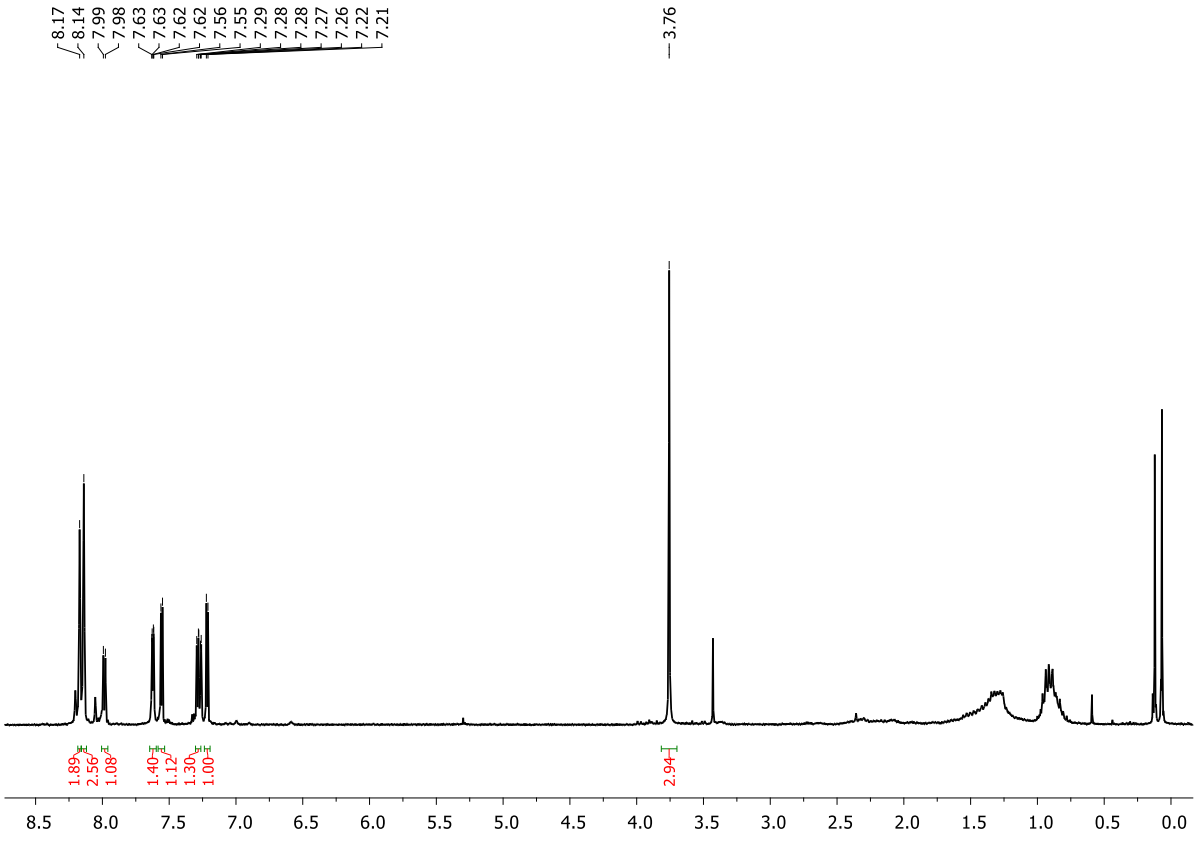

Figure 5.7.49. ^{1}H NMR spectrum of **11b** (300 MHz, in $CDCl_3$).

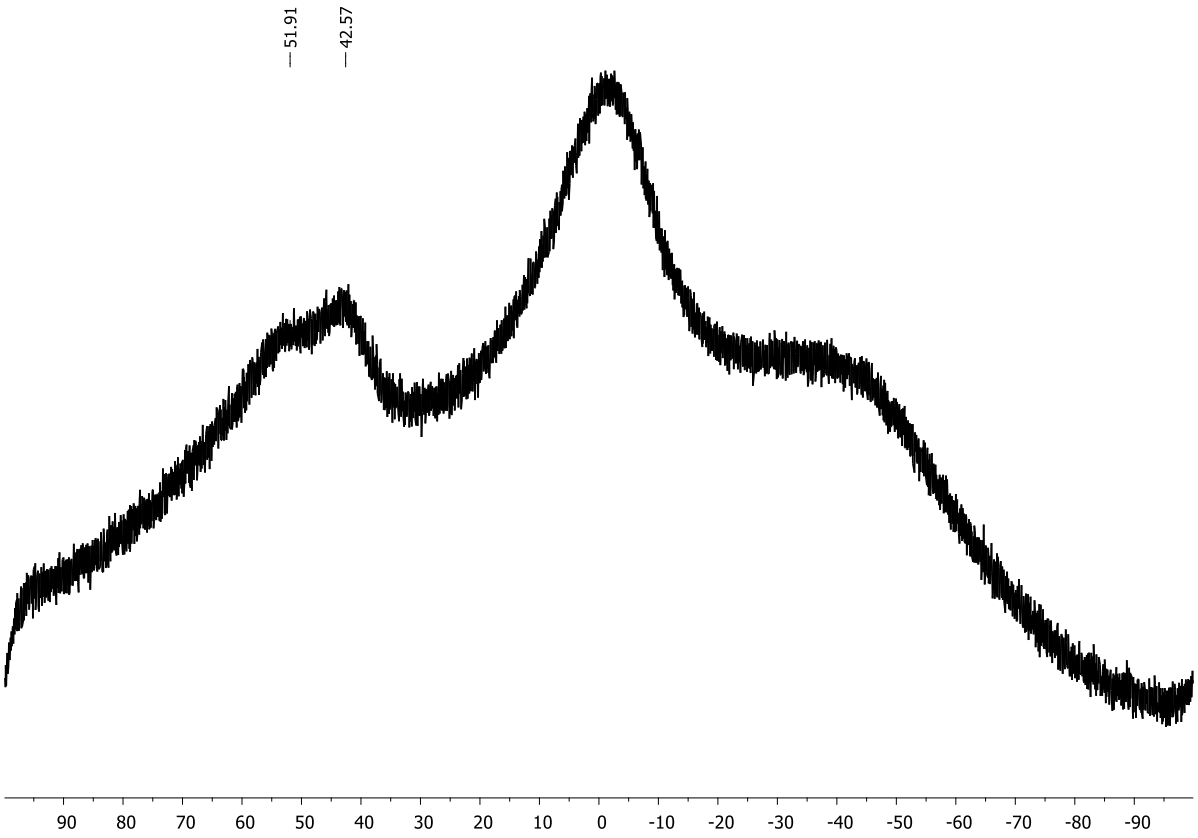

Figure 5.7.50. $^{11}B\{^{1}H\}$ NMR spectrum of **11b** (96 MHz, in $CDCl_3$).

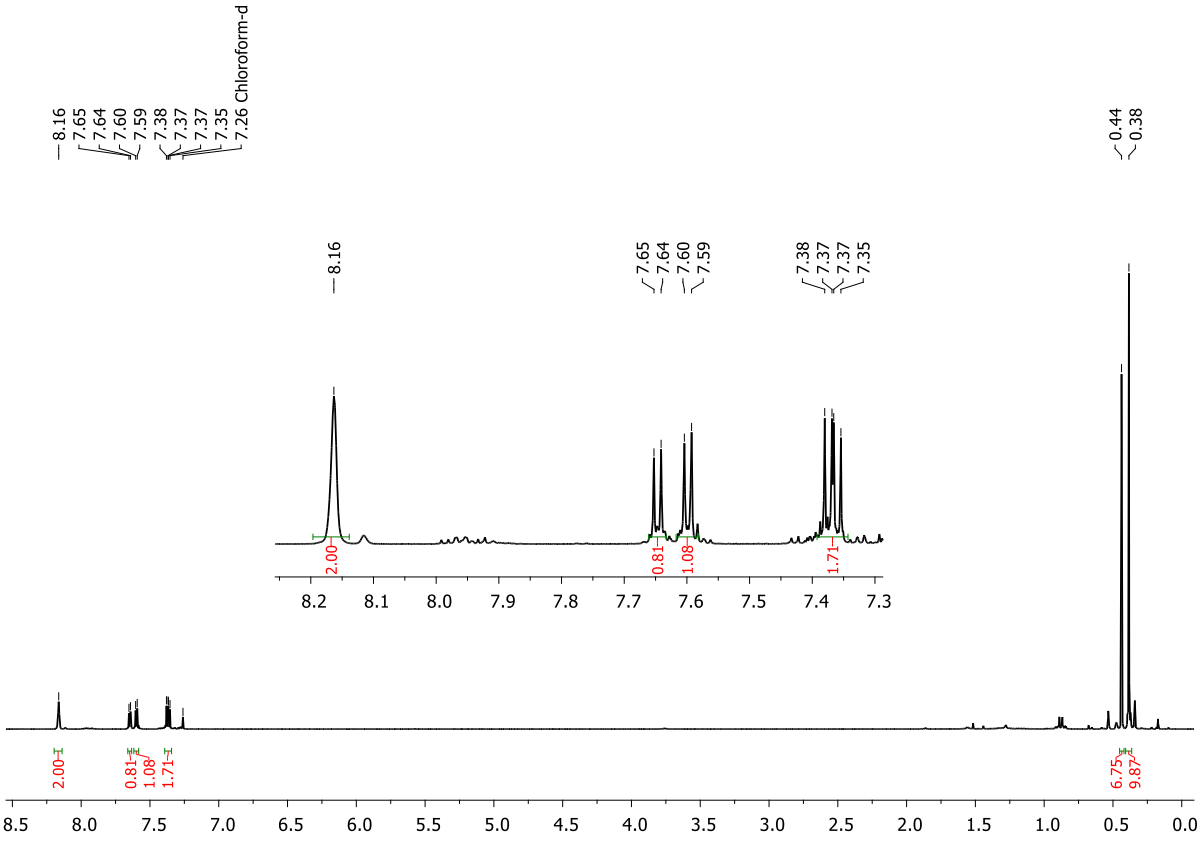

Figure 5.7.51. ^{1}H NMR spectrum of **22** (300 MHz, in $CDCl_3$).

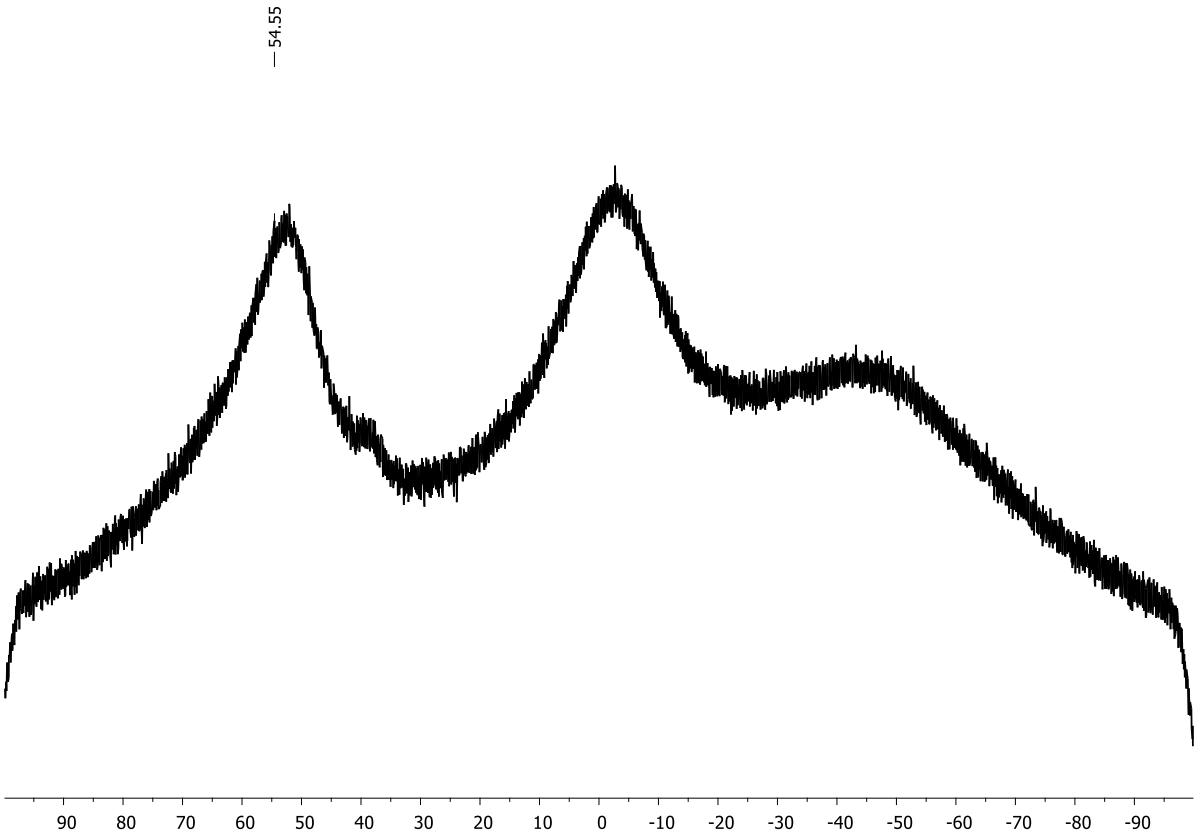

Figure 5.7.52. $^{11}B\{^{1}H\}$ NMR spectrum of **22** (96 MHz, in $CDCl_3$).

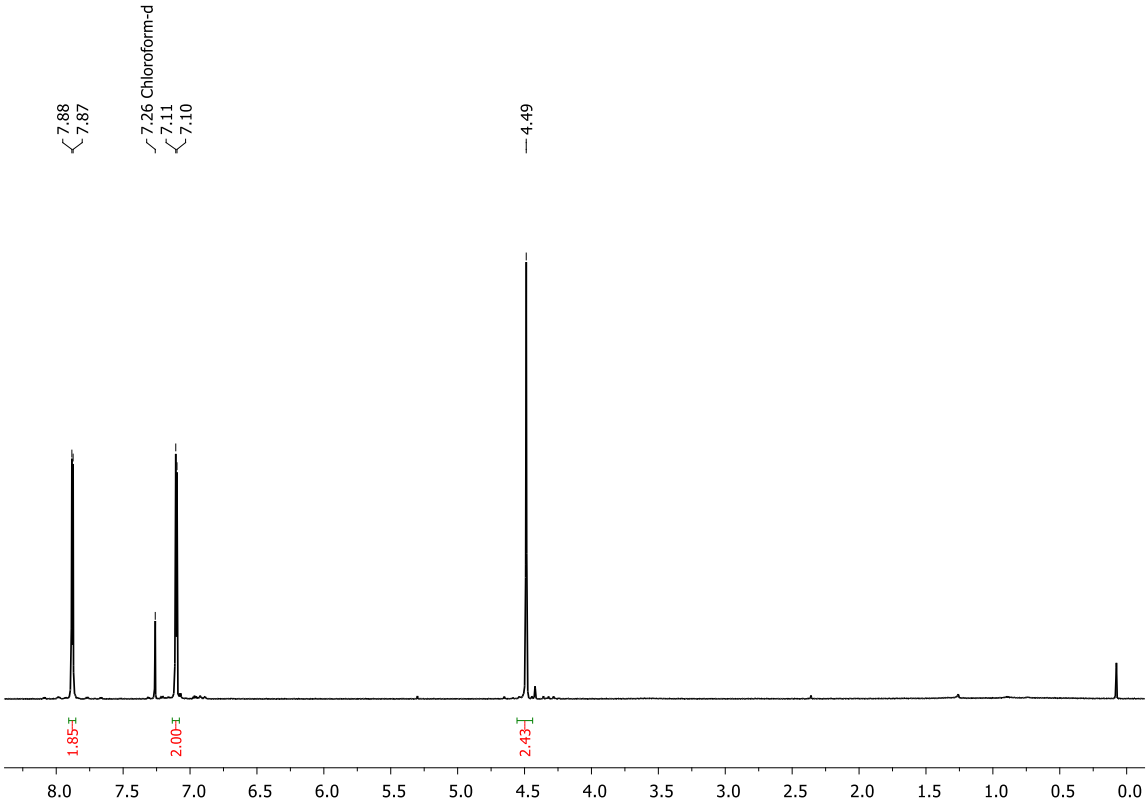

Figure 5.7.53. ^{1}H NMR spectrum of **29a** (400 MHz, in $CDCl_3$).

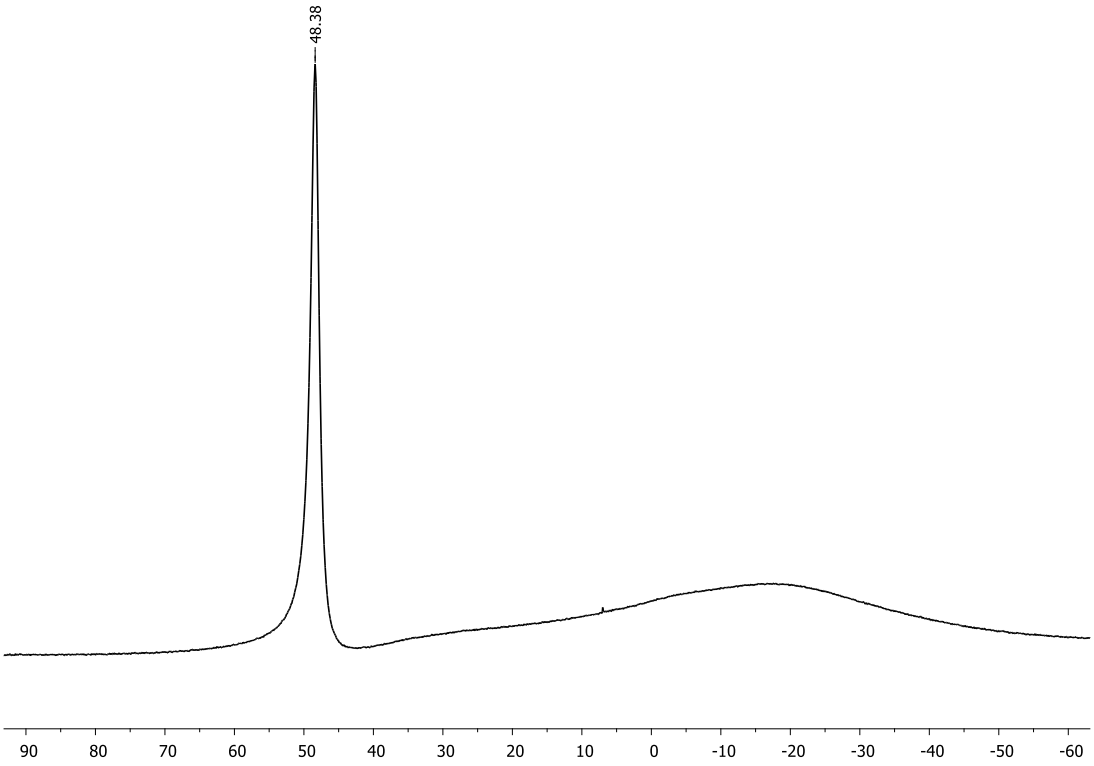

Figure 5.7.54. $^{11}B\{^{1}H\}$ NMR spectrum of **29a** (128 MHz, in $CDCl_3$).

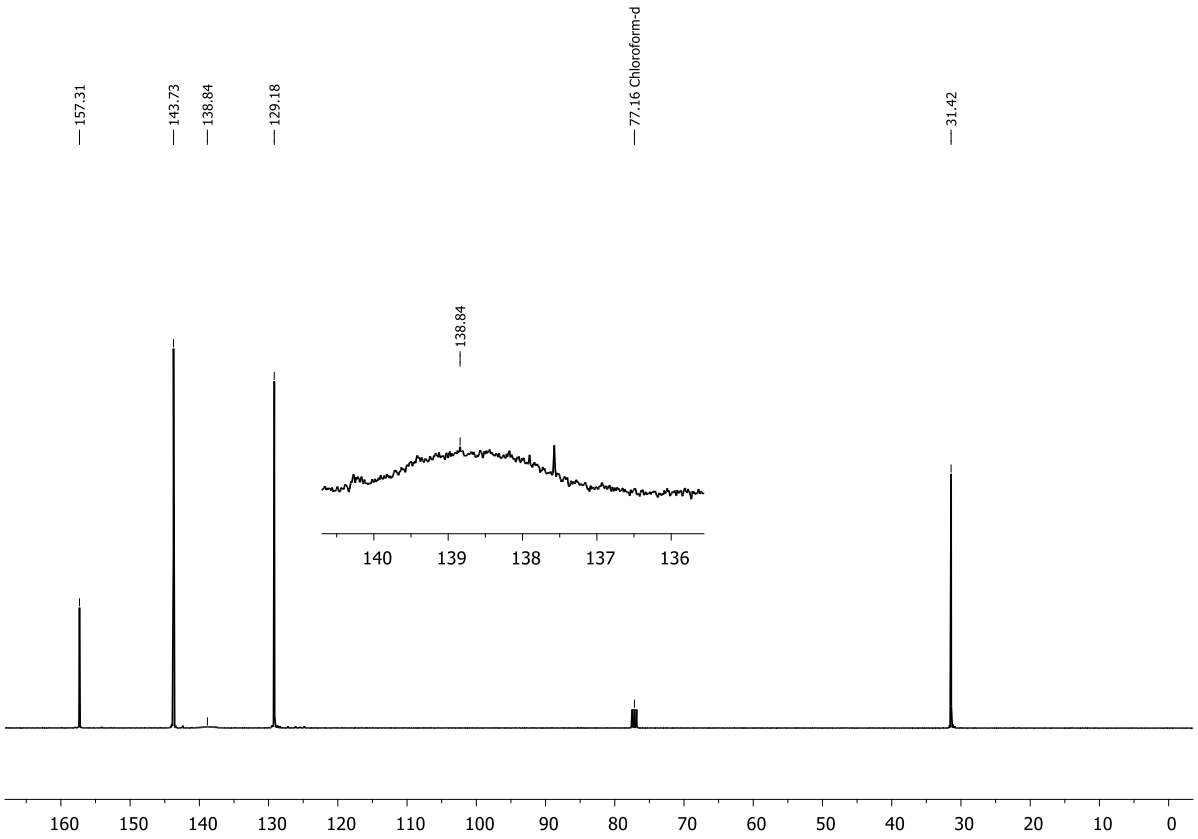

Figure 5.7.55. $^{13}C\{^{1}H\}$ NMR spectrum of **29a** (101 MHz, in $CDCl_3$).

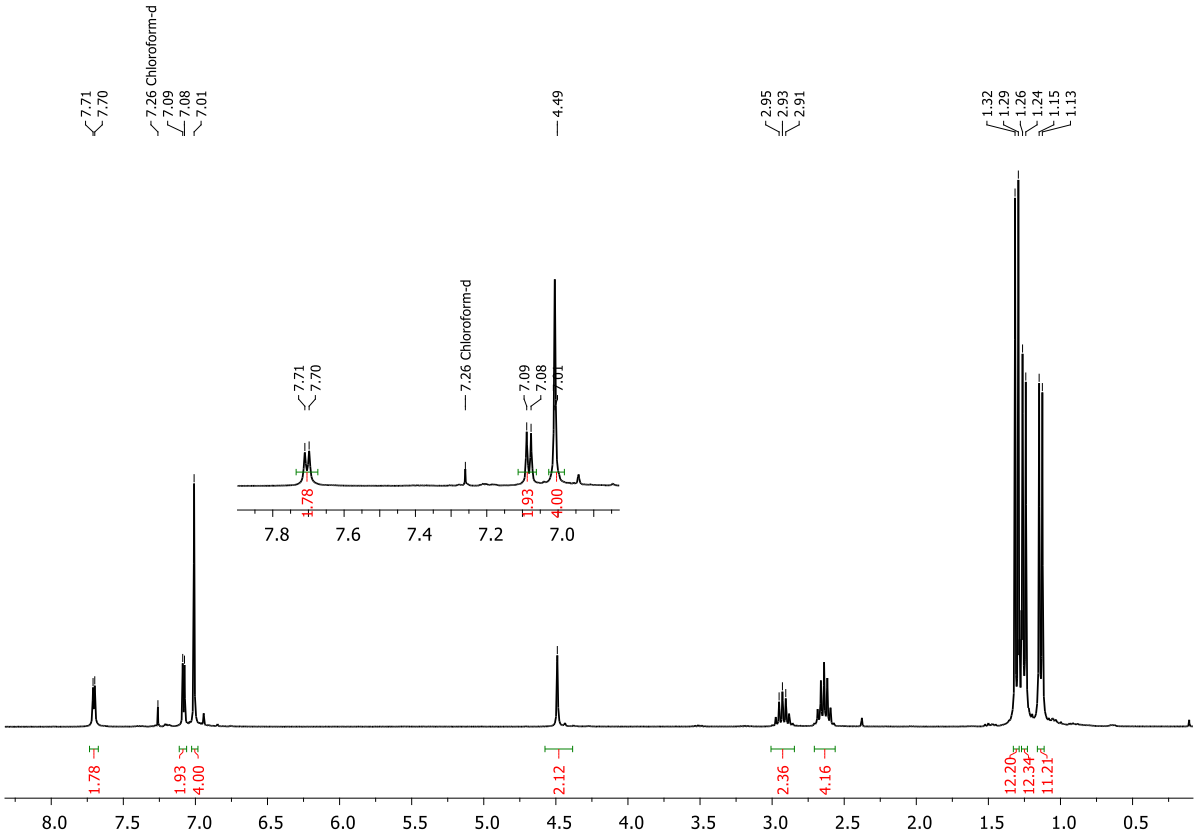

Figure 5.7.56. ^{1}H NMR spectrum of **30a** (300 MHz, in $CDCl_3$).

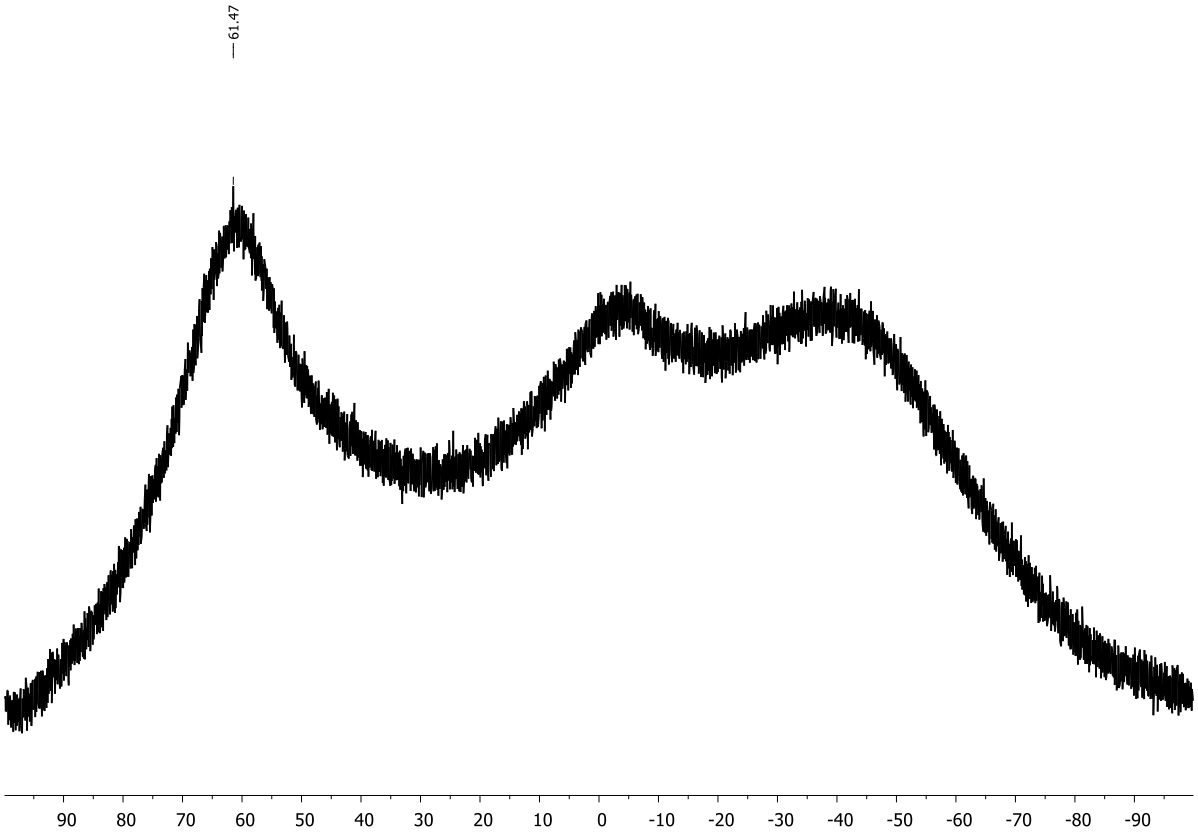

Figure 5.7.57. $^{11}B\{^{1}H\}$ NMR spectrum of **30a** (96 MHz, in $CDCl_3$).

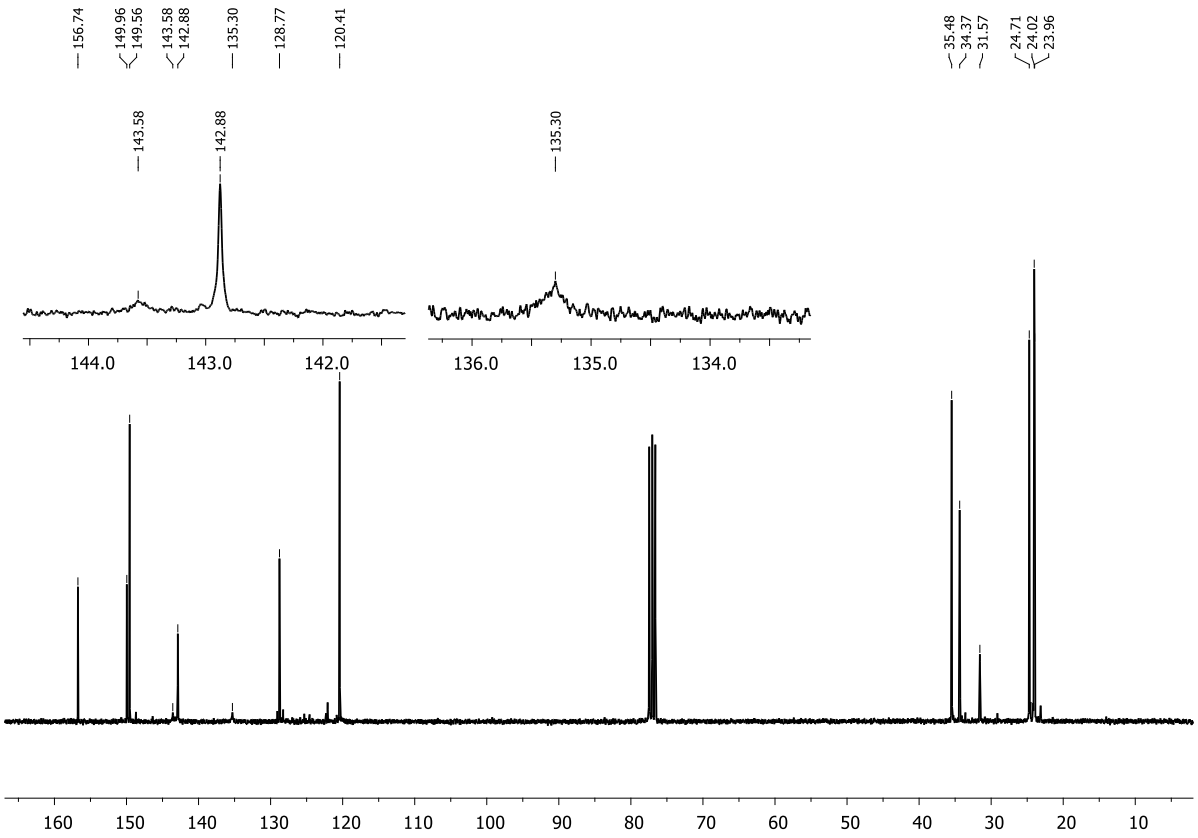

Figure 5.7.58. $^{13}C\{^{1}H\}$ NMR spectrum of **30a** (75 MHz, in $CDCl_3$).

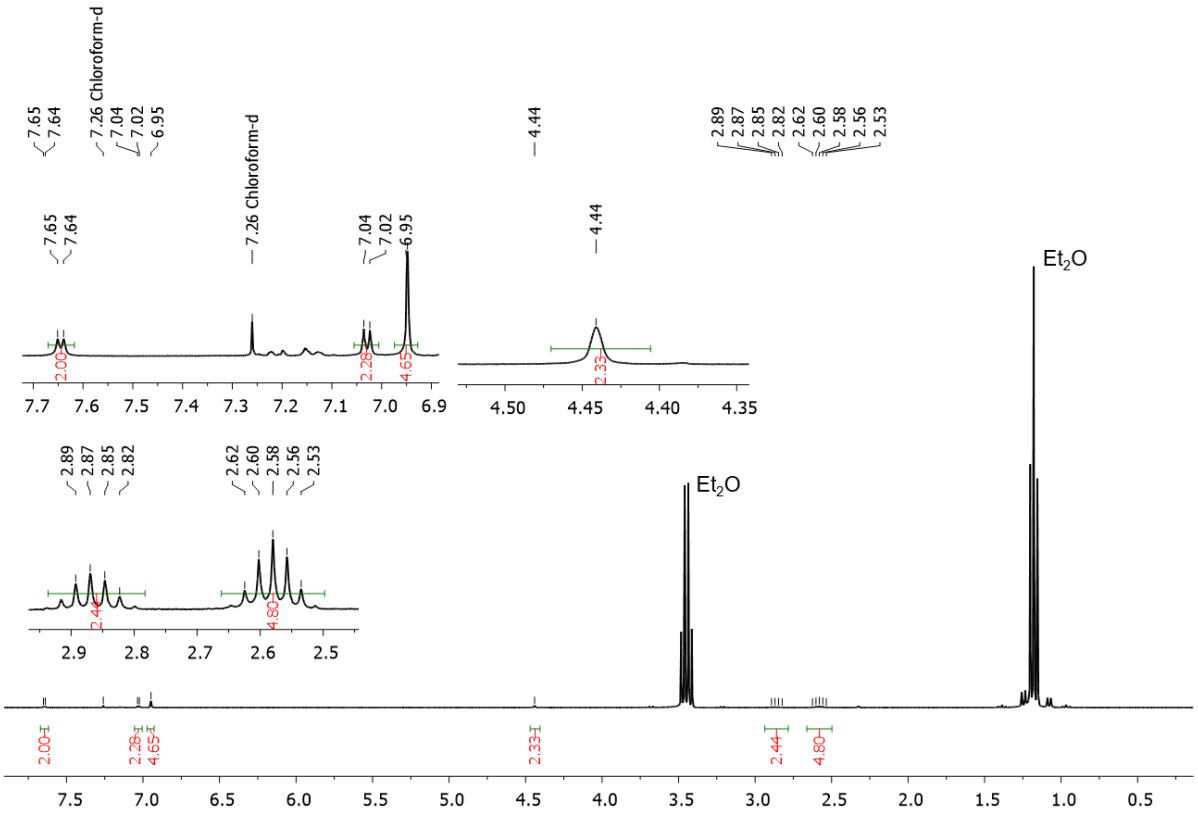

Figure 5.7.59. ^{1}H NMR spectrum of **30a** after addition of diethylether (300 MHz, in $CDCl_3$).

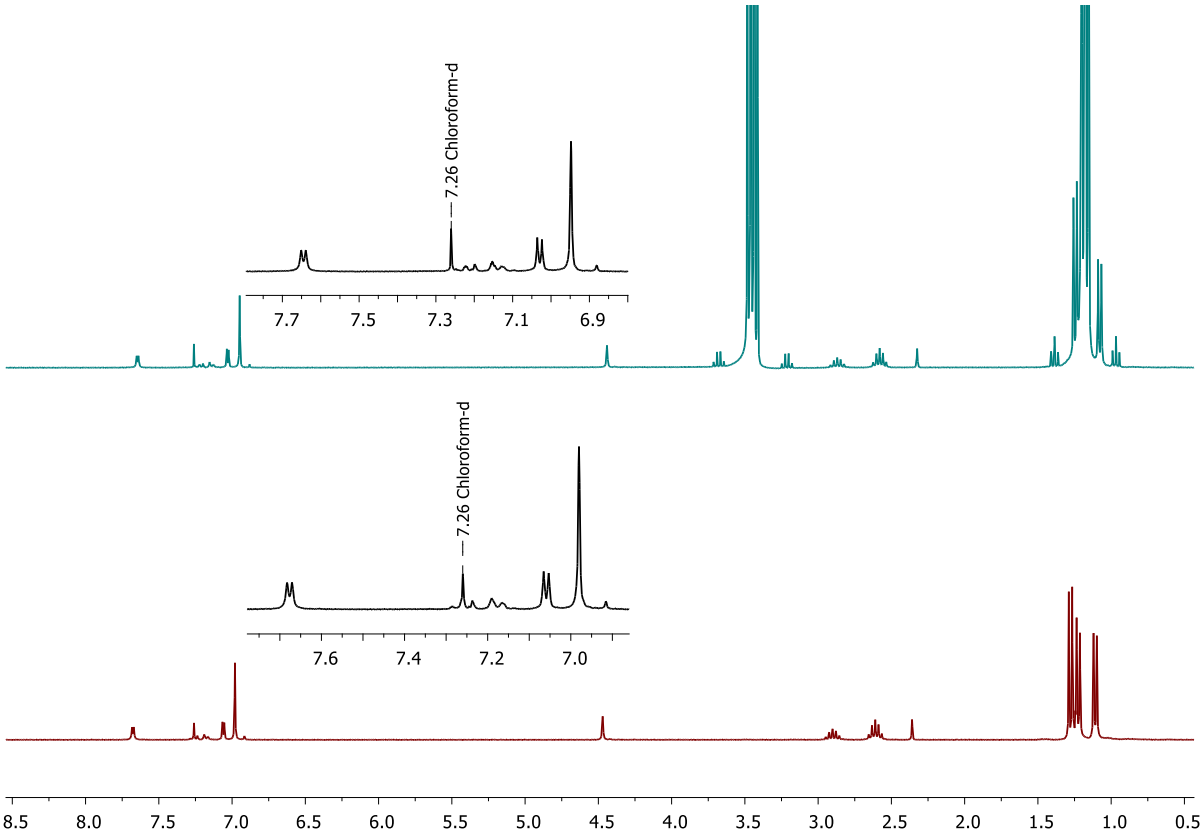

Figure 5.7.60. ^{1}H NMR spectra of **30a** before (red) and after addition (red) of diethylether (300 MHz, in $CDCl_3$).

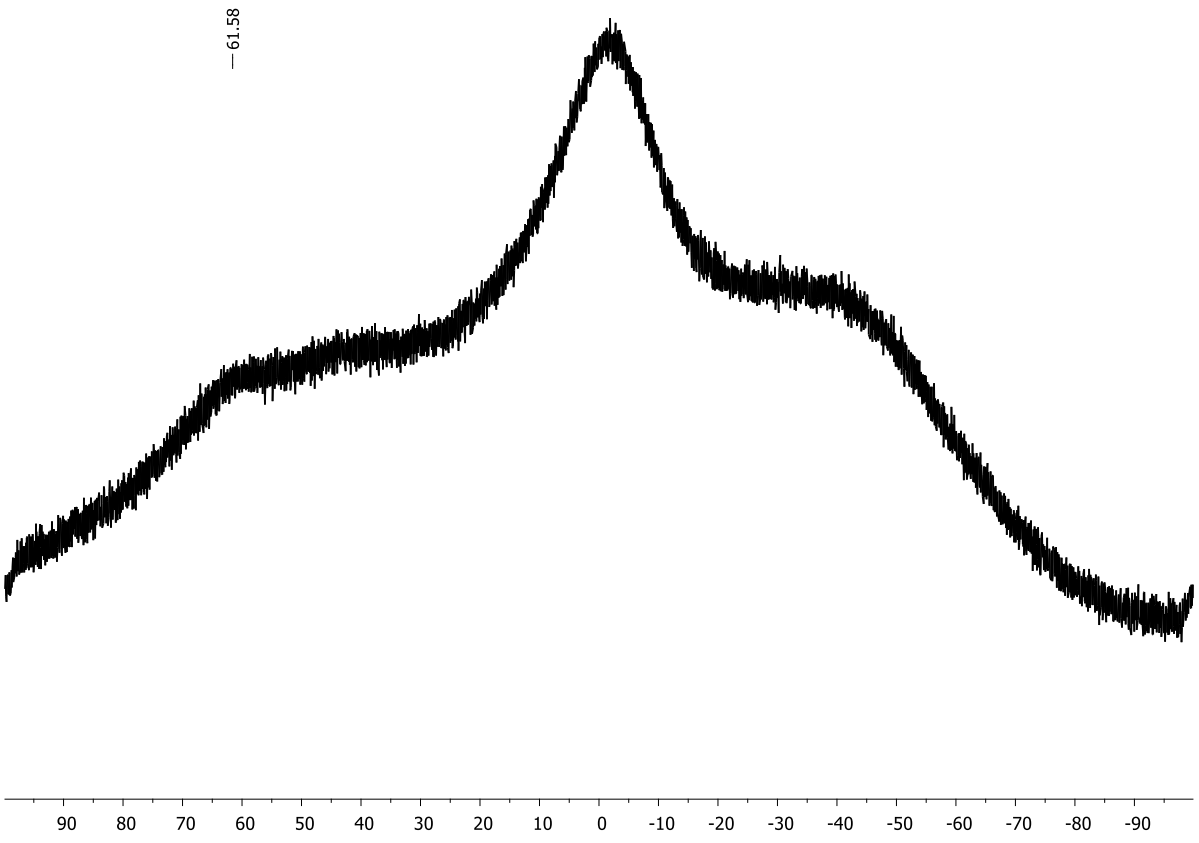

Figure 5.7.61. $^{11}B\{^{1}H\}$ NMR spectrum of **30a** after addition of diethylether (96 MHz, in $CDCl_3$).

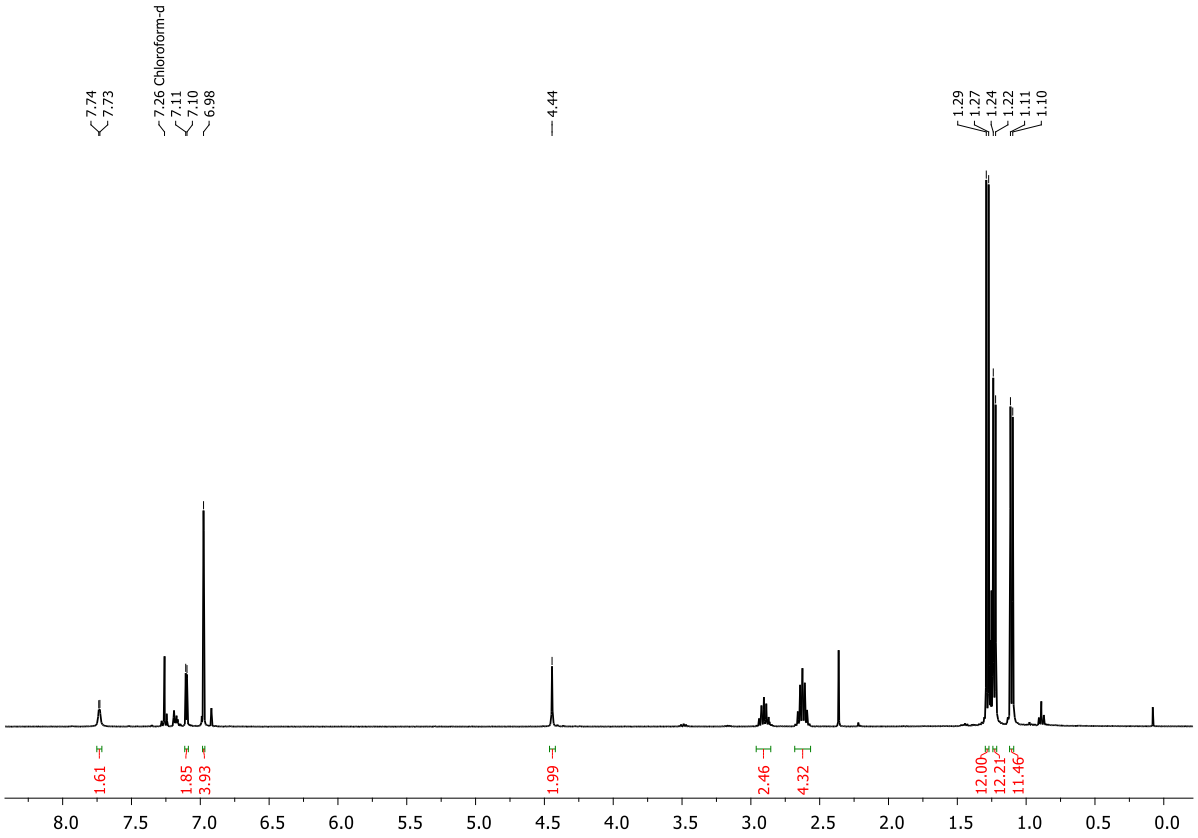

Figure 5.7.62. ^{1}H NMR spectrum of **30b** (400 MHz, in $CDCl_3$).

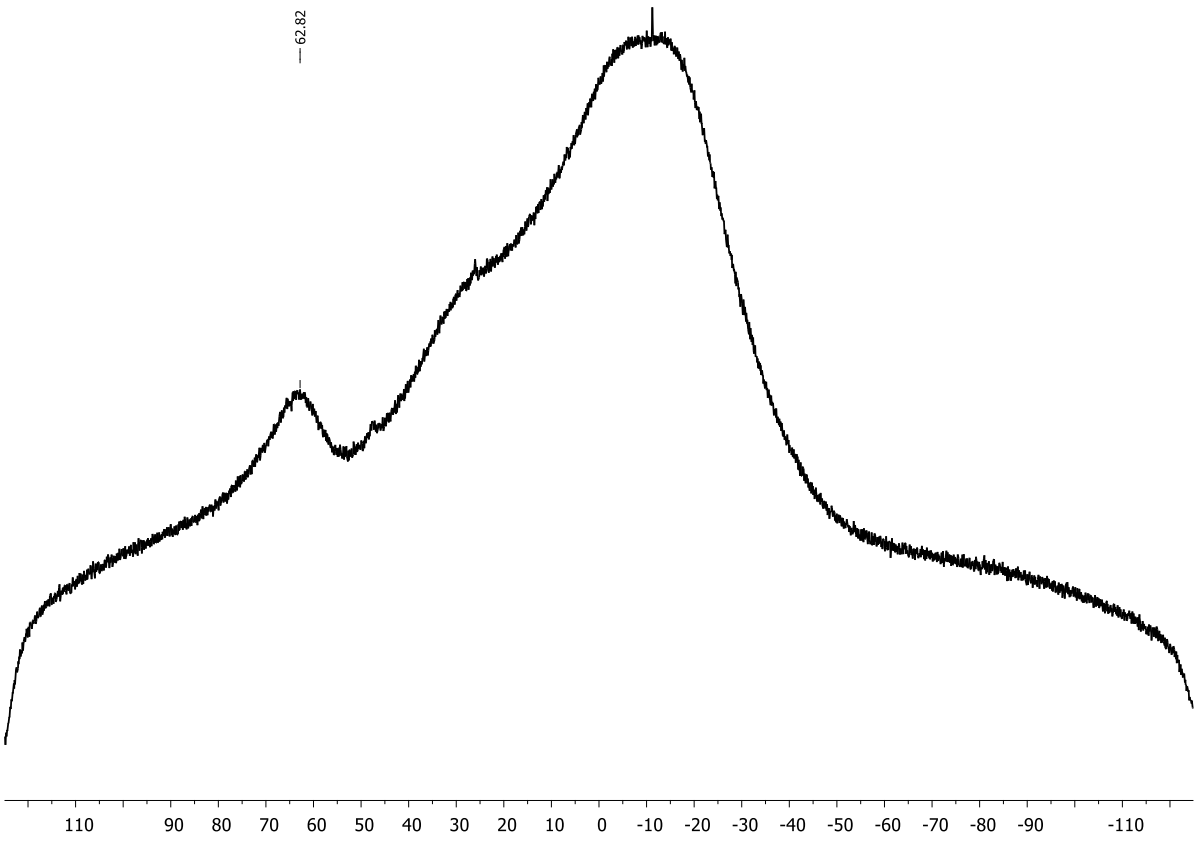

Figure 5.7.63. $^{11}B\{^{1}H\}$ NMR spectrum of **30b** (128 MHz, in $CDCl_3$).

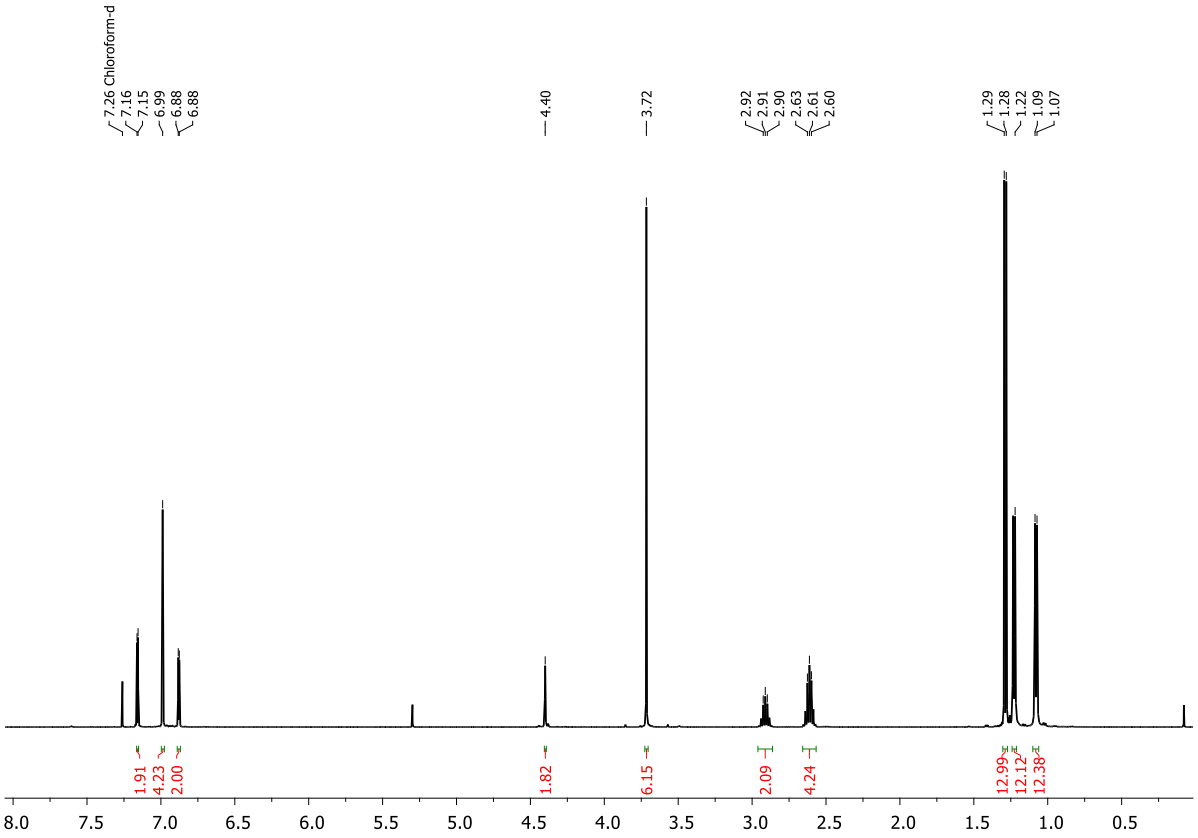

Figure 5.7.64. ^{1}H NMR spectrum of **31a** (500 MHz, in $CDCl_3$).

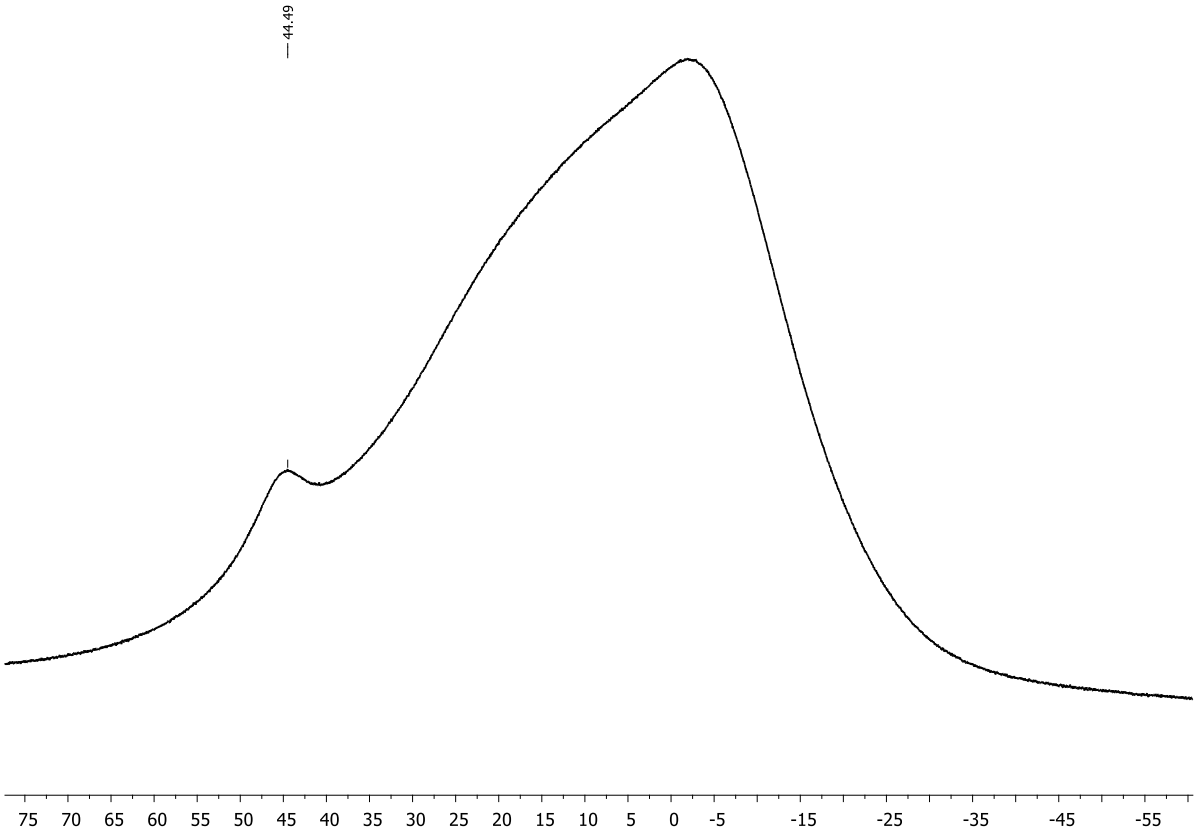

Figure 5.7.65. $^{11}B\{^{1}H\}$ NMR spectrum of **31a** (160 MHz, in $CDCl_3$).

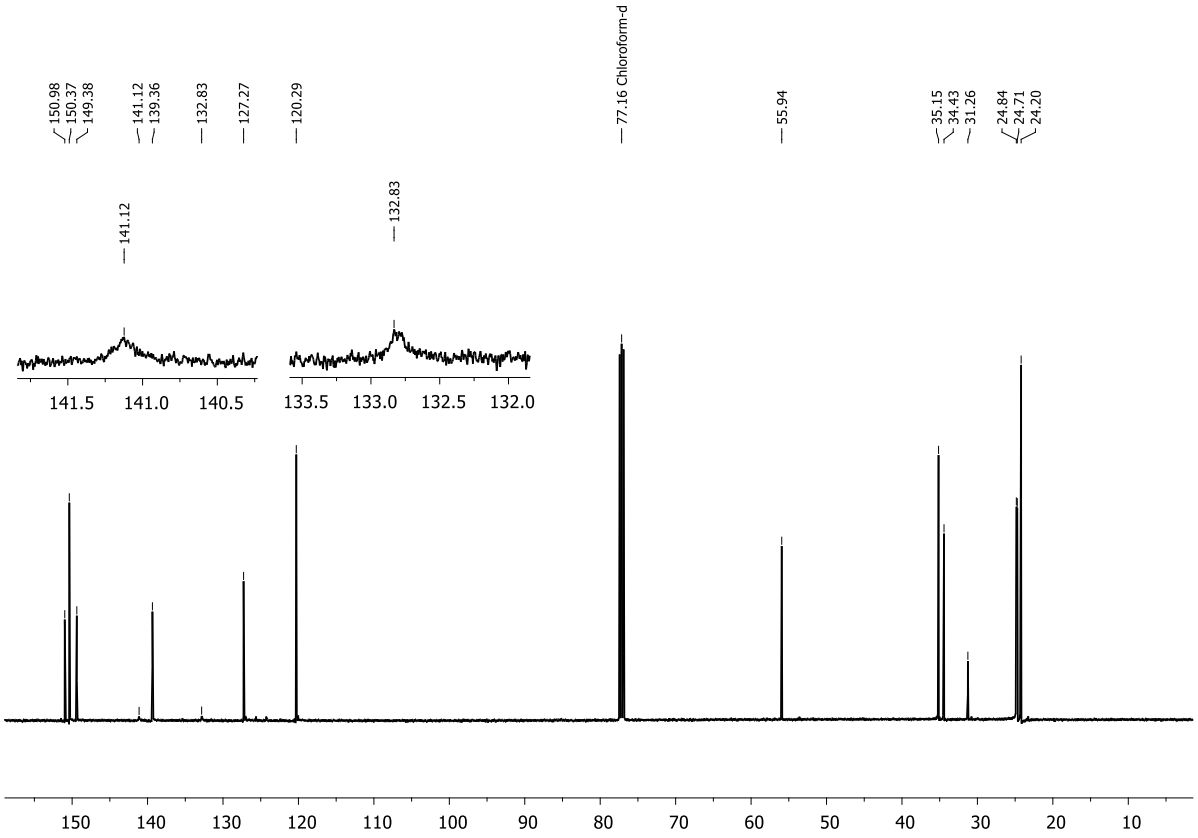

Figure 5.7.66. $^{13}C\{^{1}H\}$ NMR spectrum of **31a** (126 MHz, in $CDCl_3$).

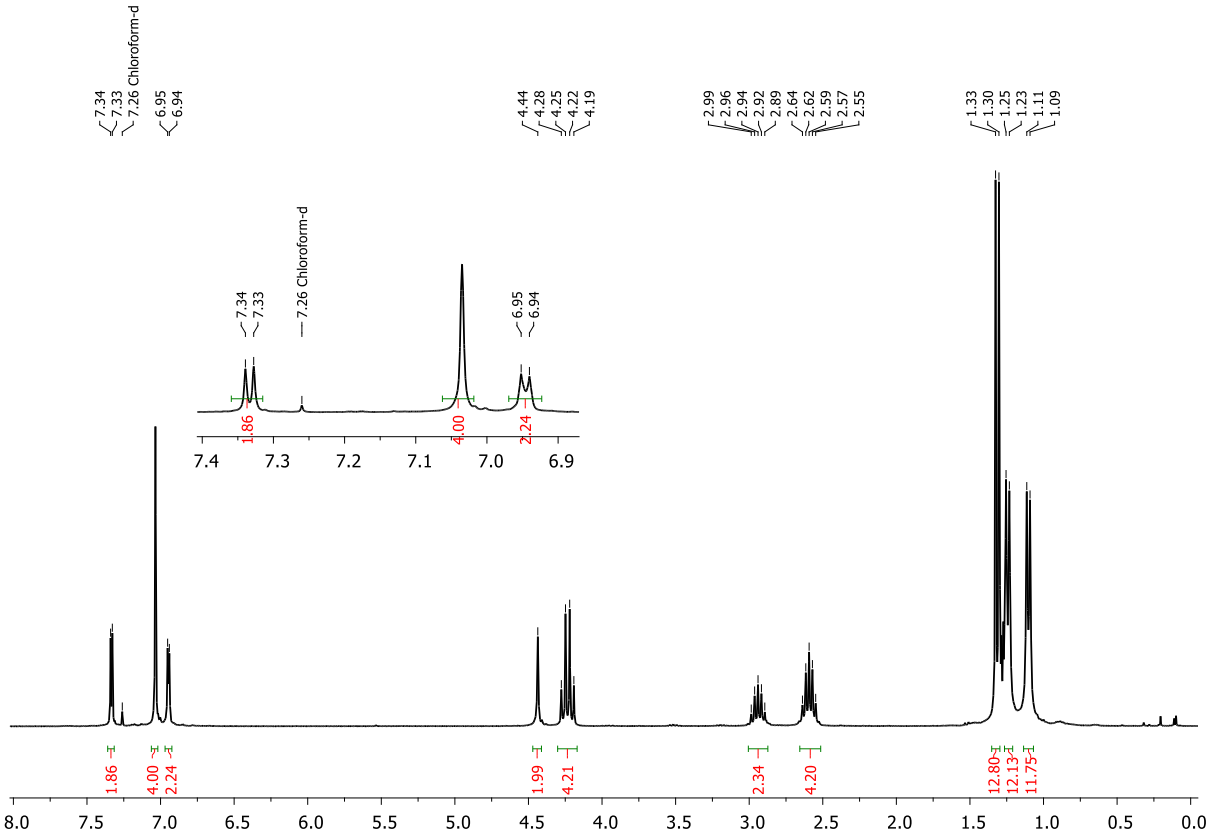

Figure 5.7.67. ^{1}H NMR spectrum of **31b** (300 MHz, in $CDCl_3$).

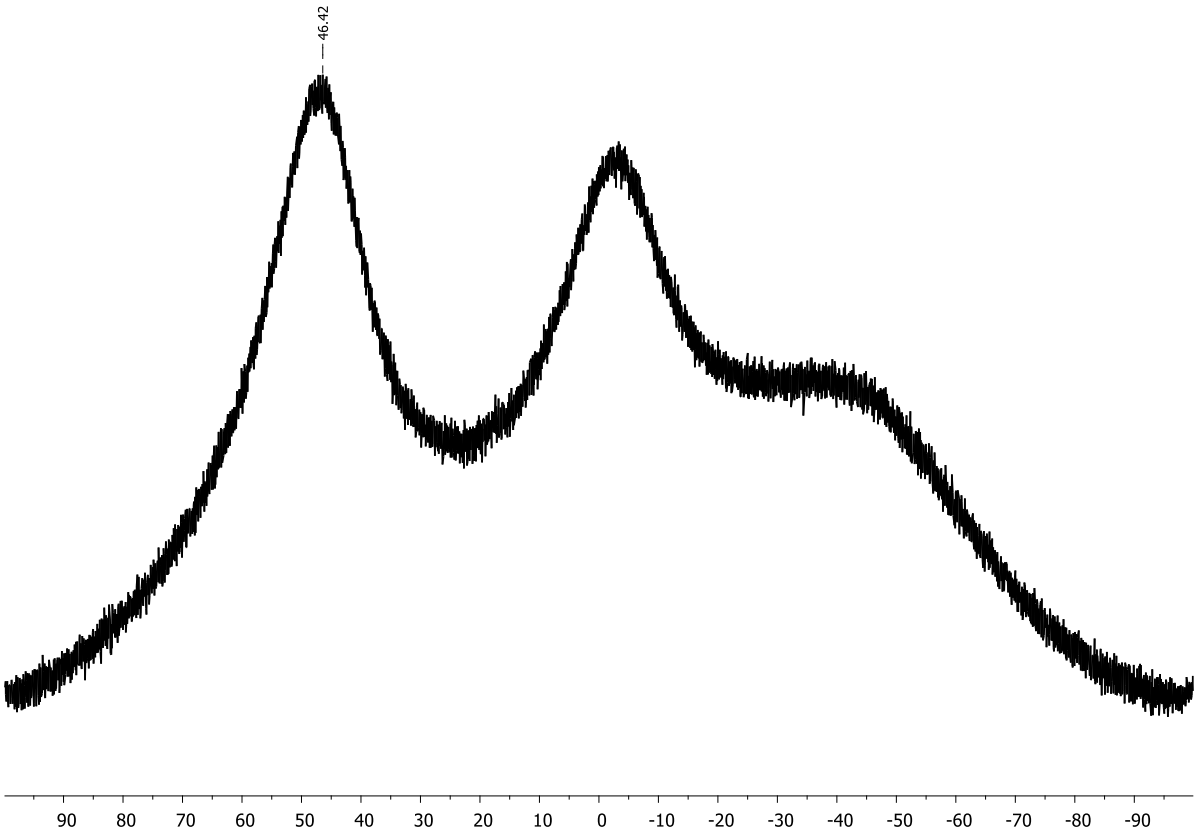

Figure 5.7.68. $^{11}B\{^{1}H\}$ NMR spectrum of **31b** (96 MHz, in $CDCl_3$).

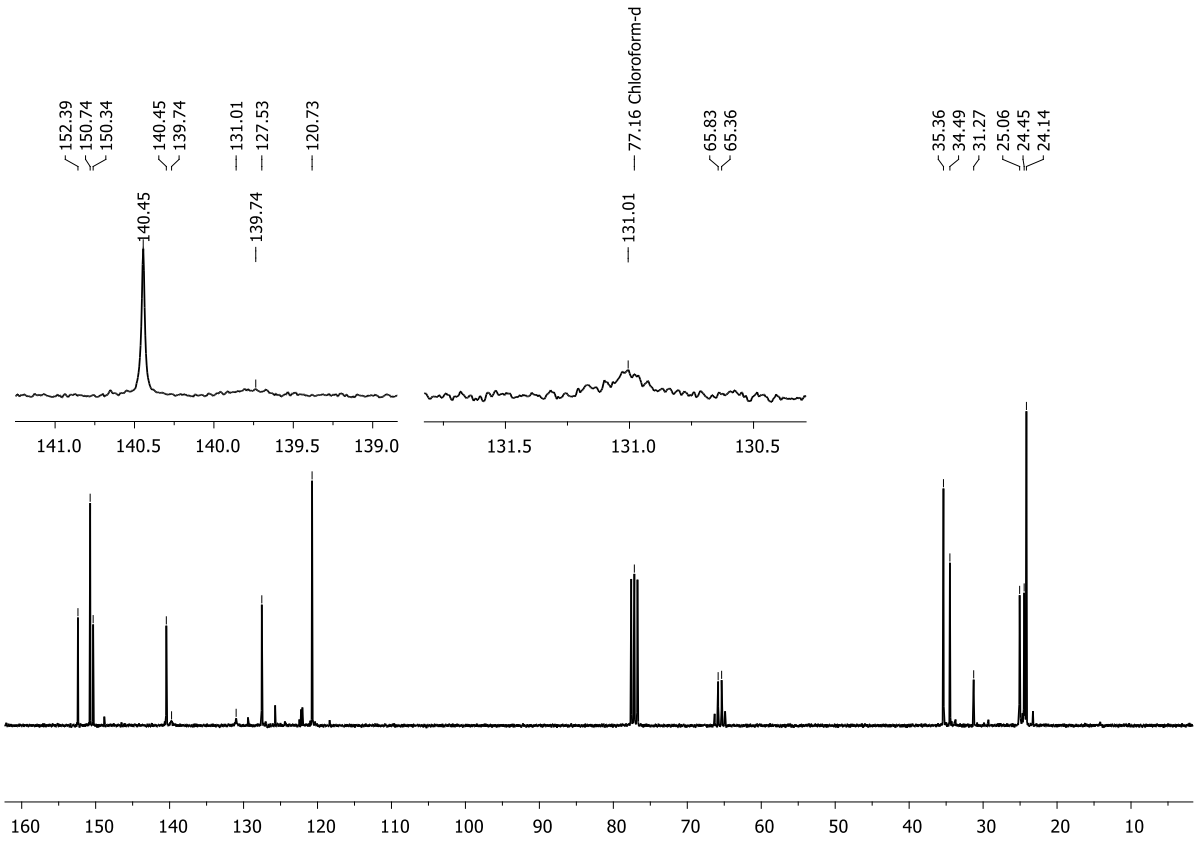

Figure 5.7.69. $^{13}C\{^{1}H\}$ NMR spectrum of **31b** (75 MHz, in $CDCl_3$).

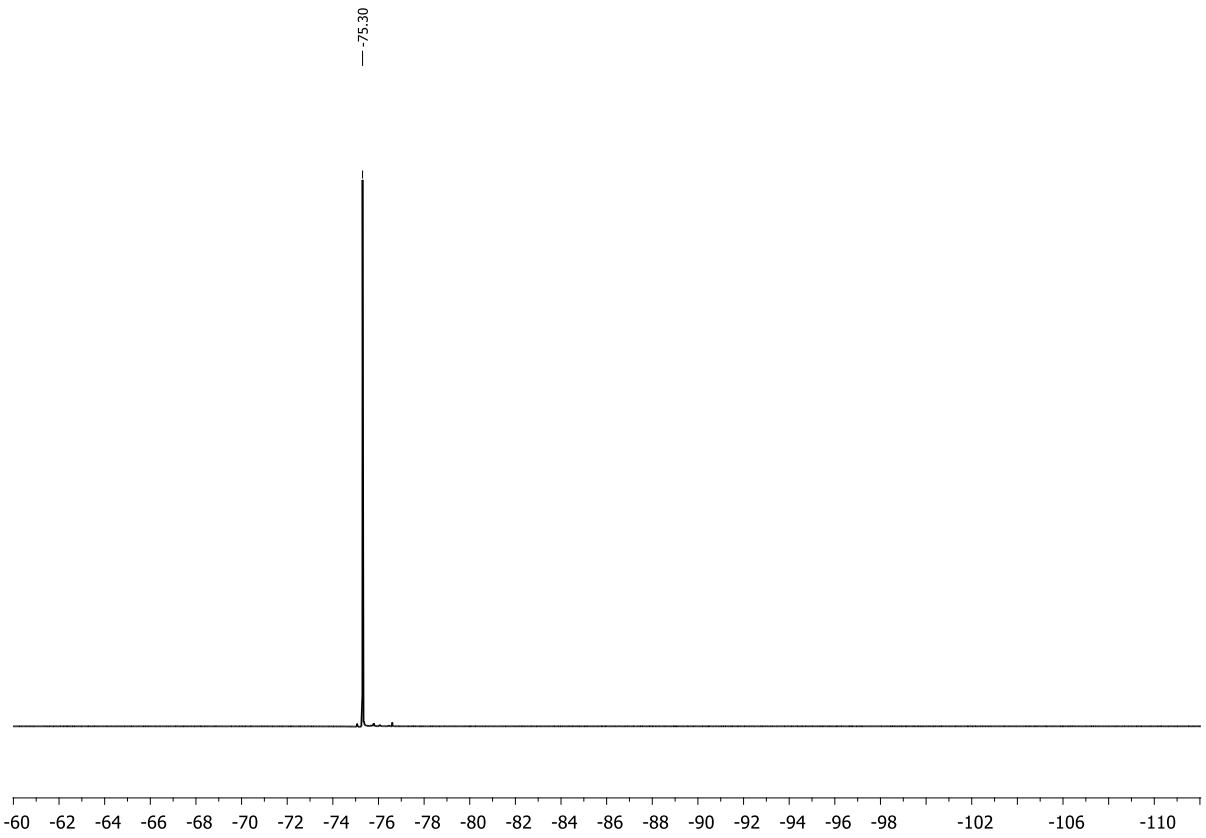

Figure 5.7.70. $^{19}F\{^{1}H\}$ NMR spectrum of **31b** (377 MHz, in $CDCl_3$).

Mass spectrometry

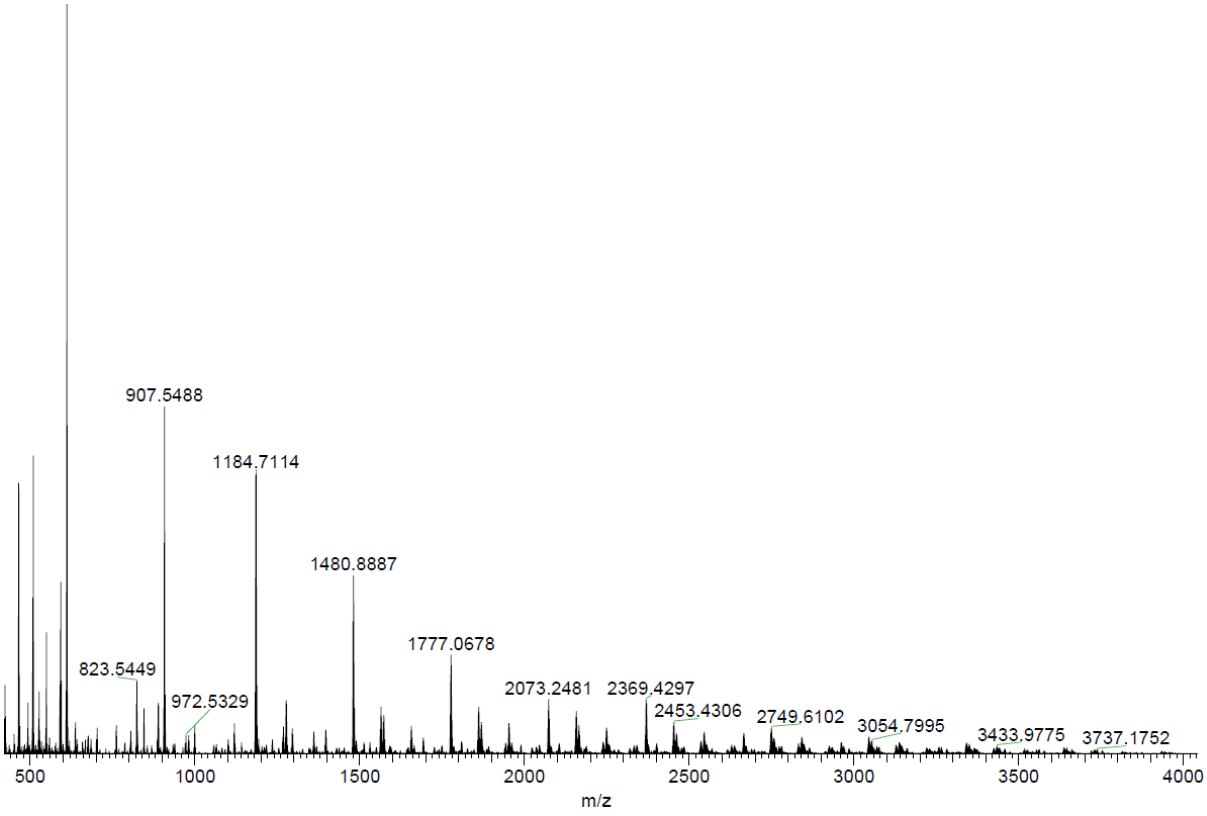

Figure 5.7.71. LIFDI mass spectrum of **7b.**

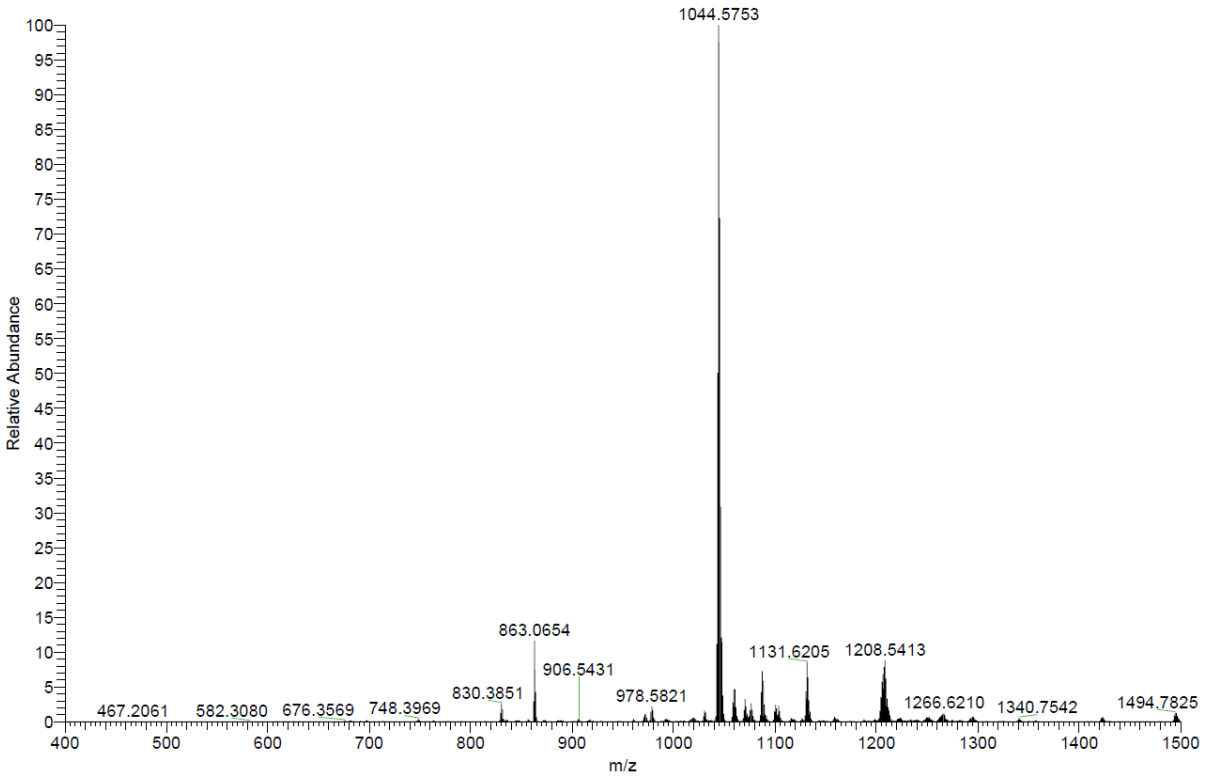

Figure 5.7.72. APCI mass spectrum of **13a.**

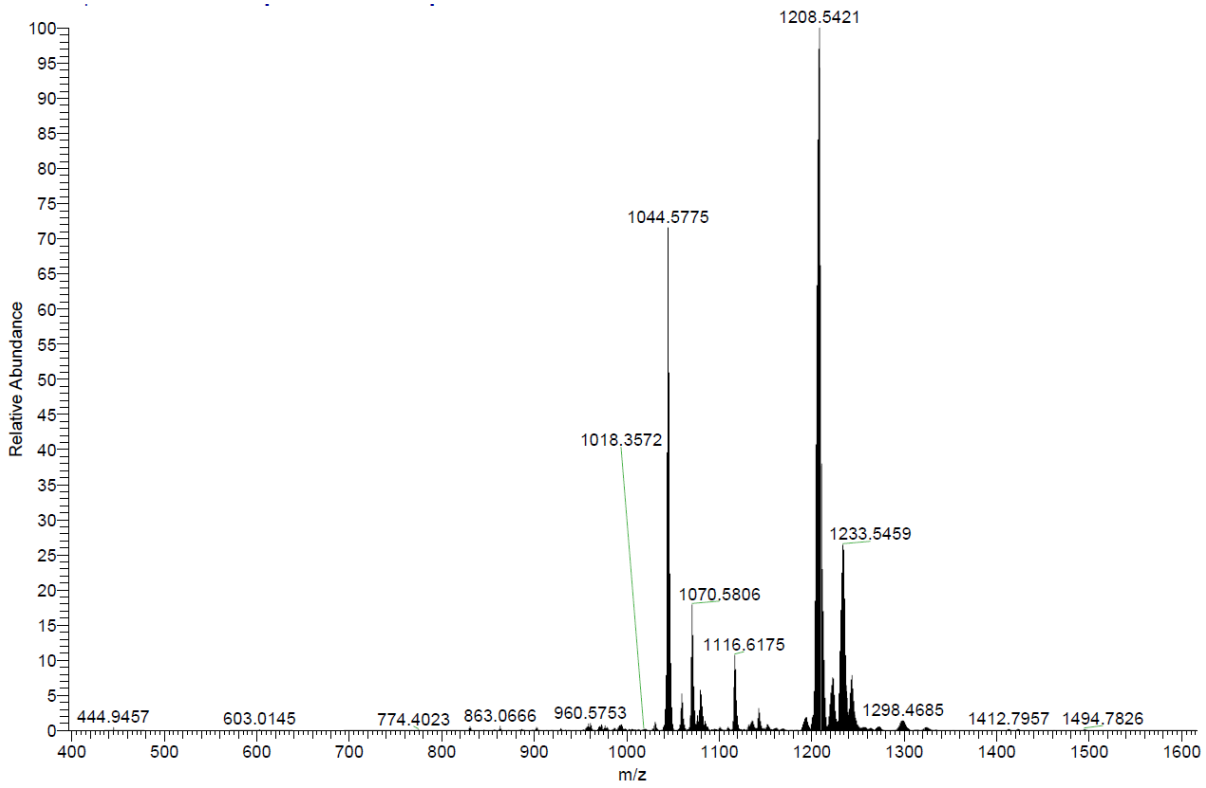

Figure 5.7.73. APCI mass spectrum of **14a.**

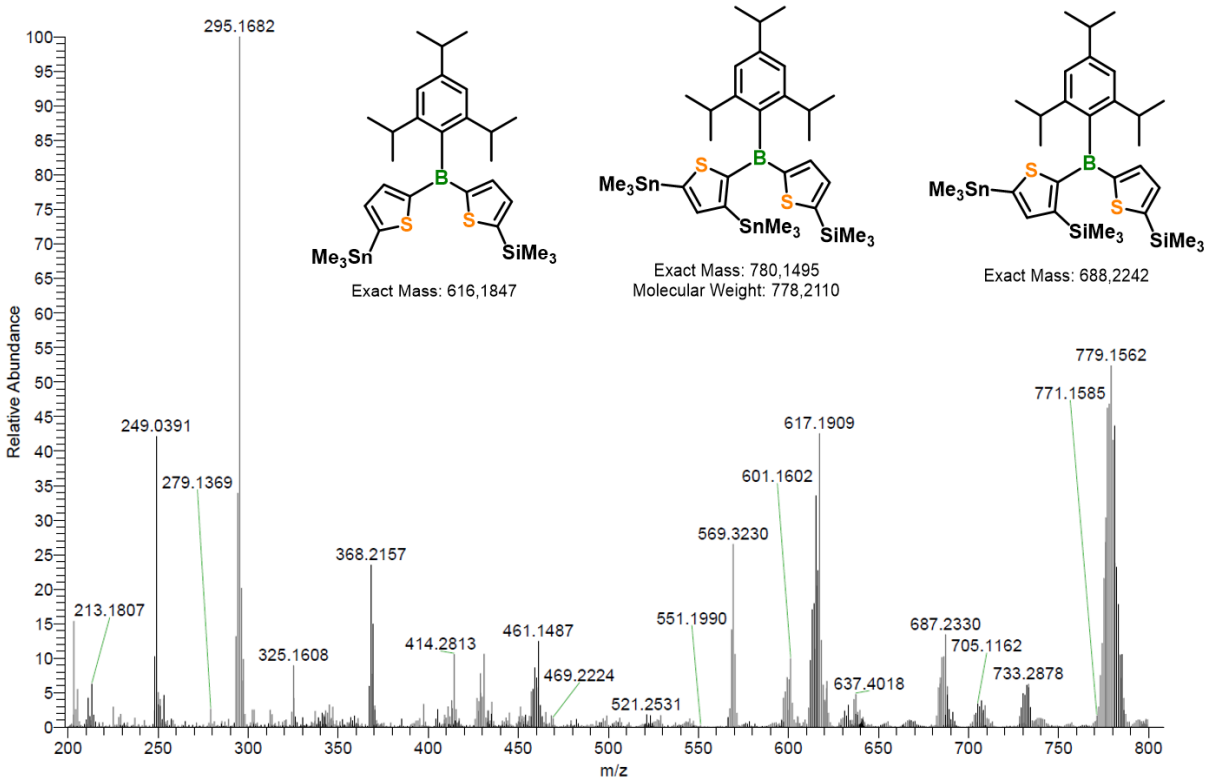

Figure 5.7.74. APCI mass spectrum of **15a.**

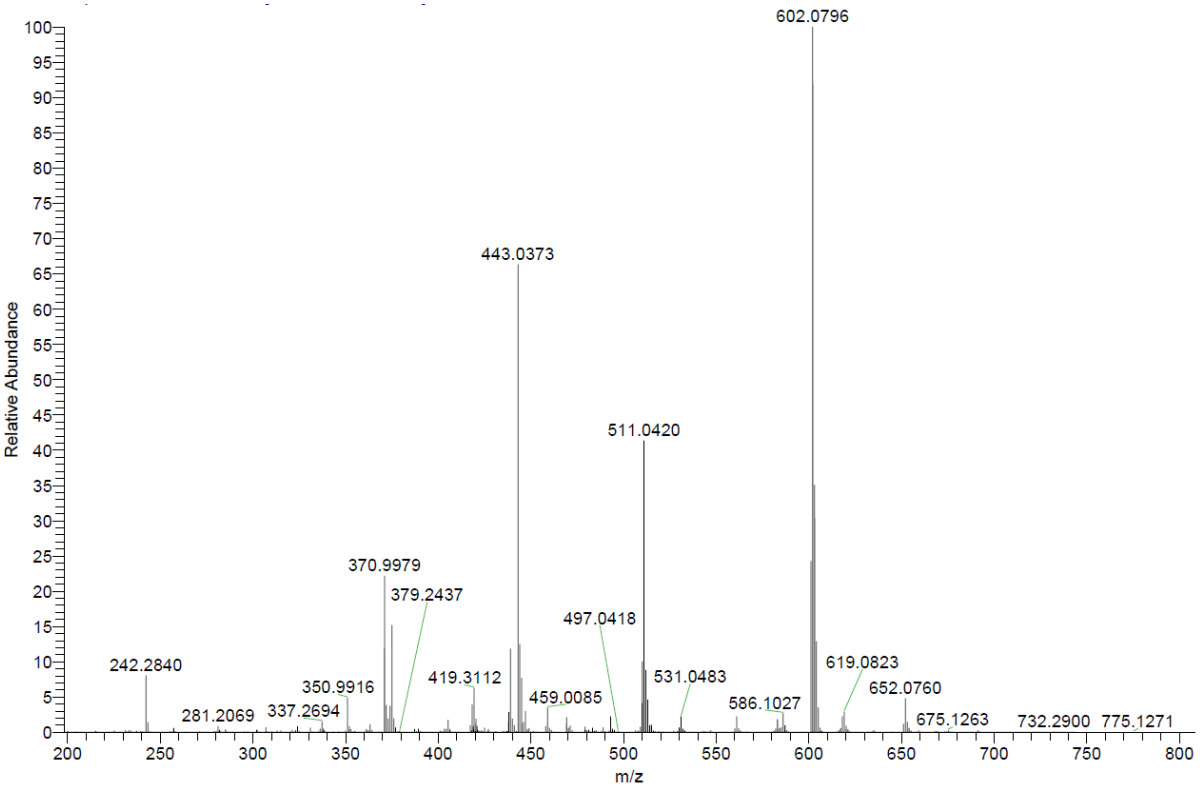

Figure 5.7.75. APCI mass spectrum of **3c.**

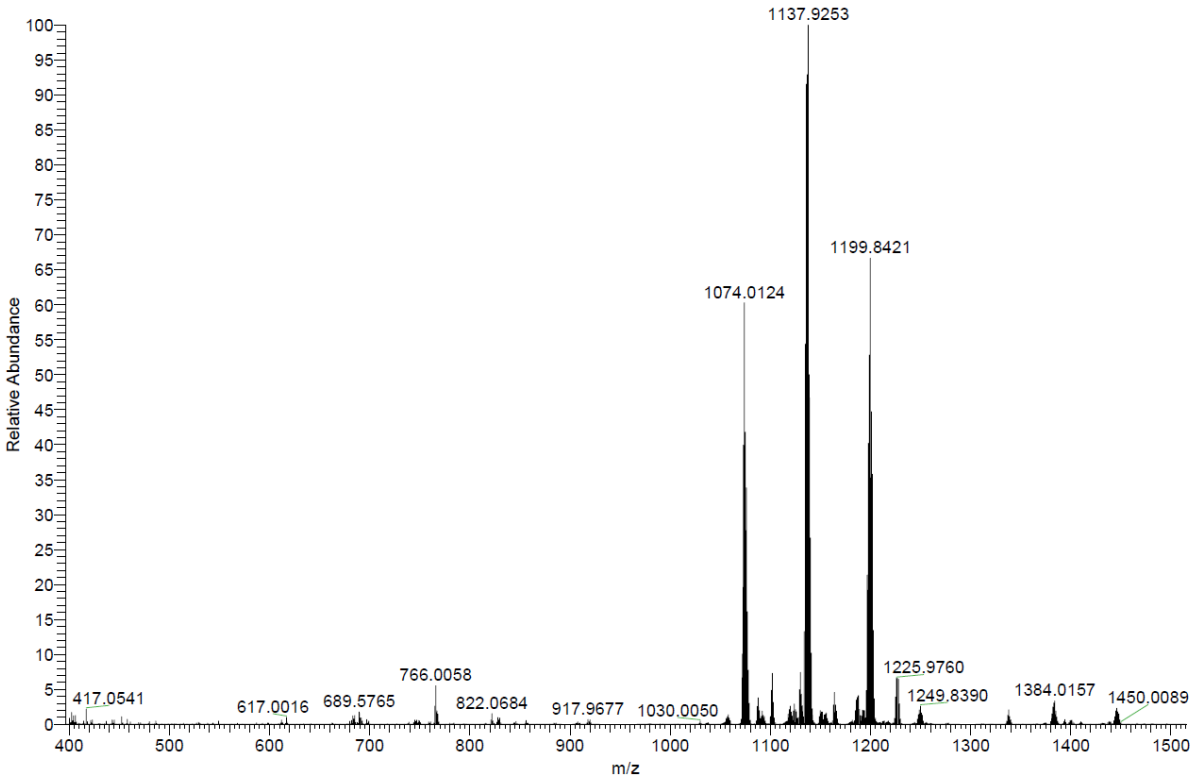

Figure 5.7.76. APCI mass spectrum of **5c.**

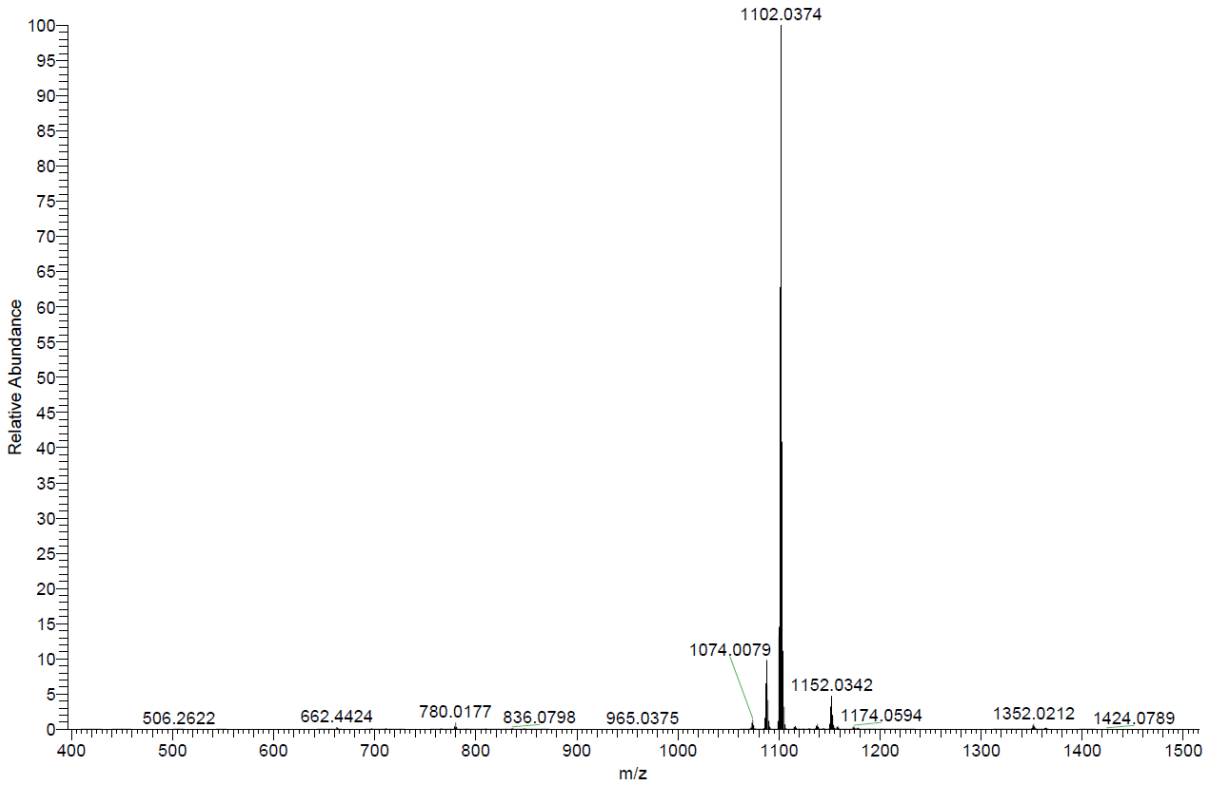

Figure 5.7.77. LIFDI mass spectrum of **6c.**

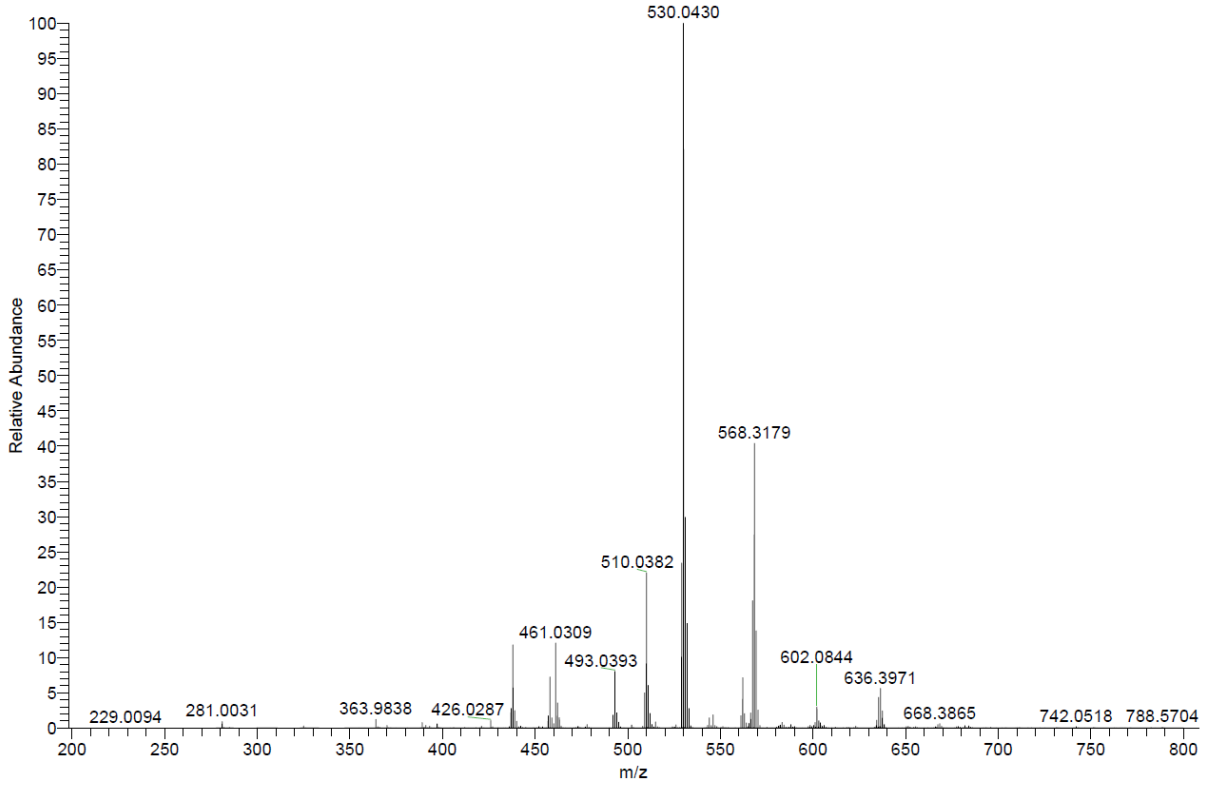

Figure 5.7.78. APCI mass spectrum of **8b.**

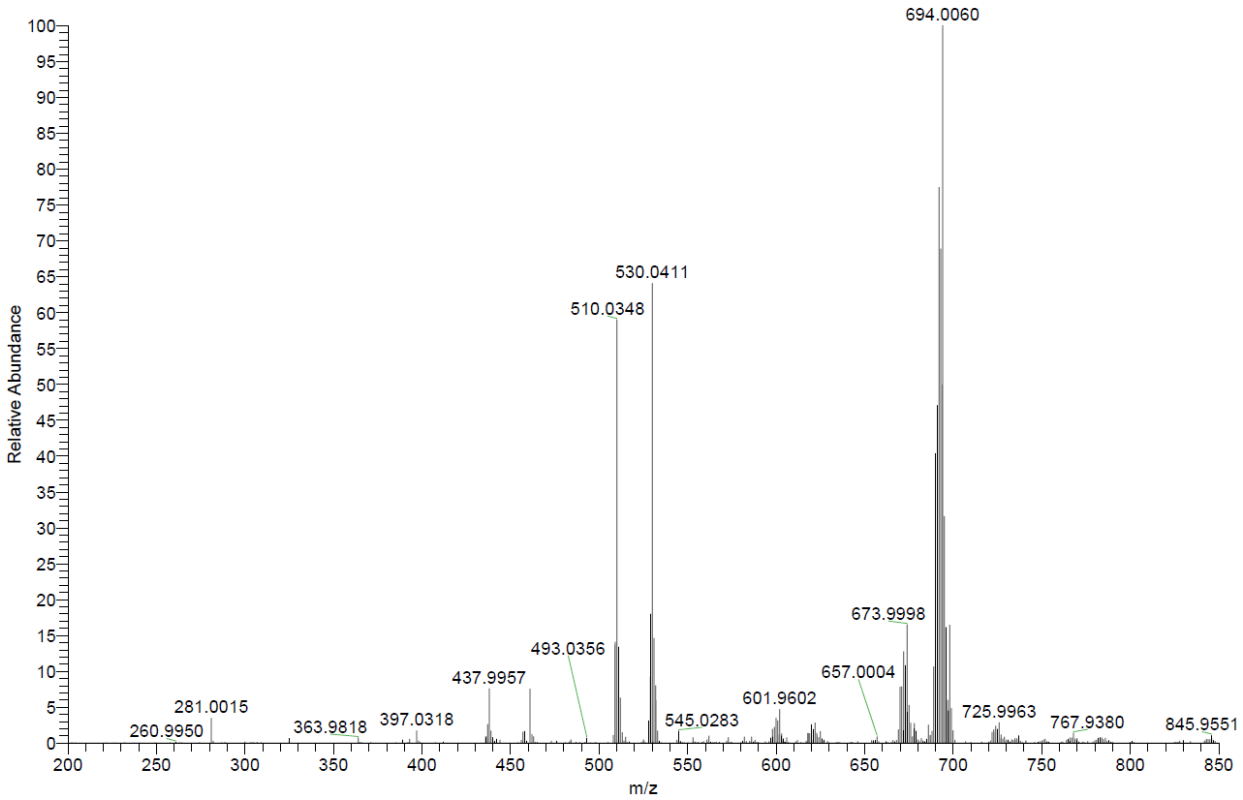

Figure 5.7.79. APCI mass spectrum of **22.**

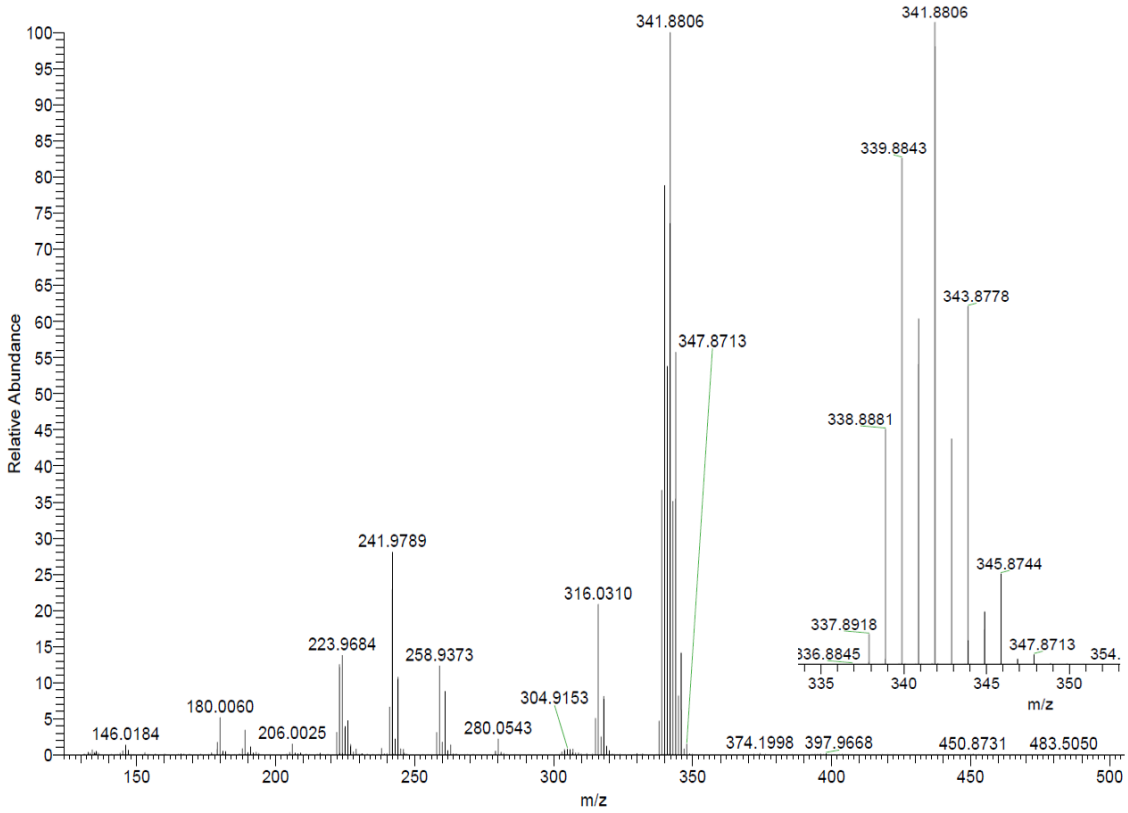

Figure 5.7.80. LIFDI mass spectrum of **29a**.

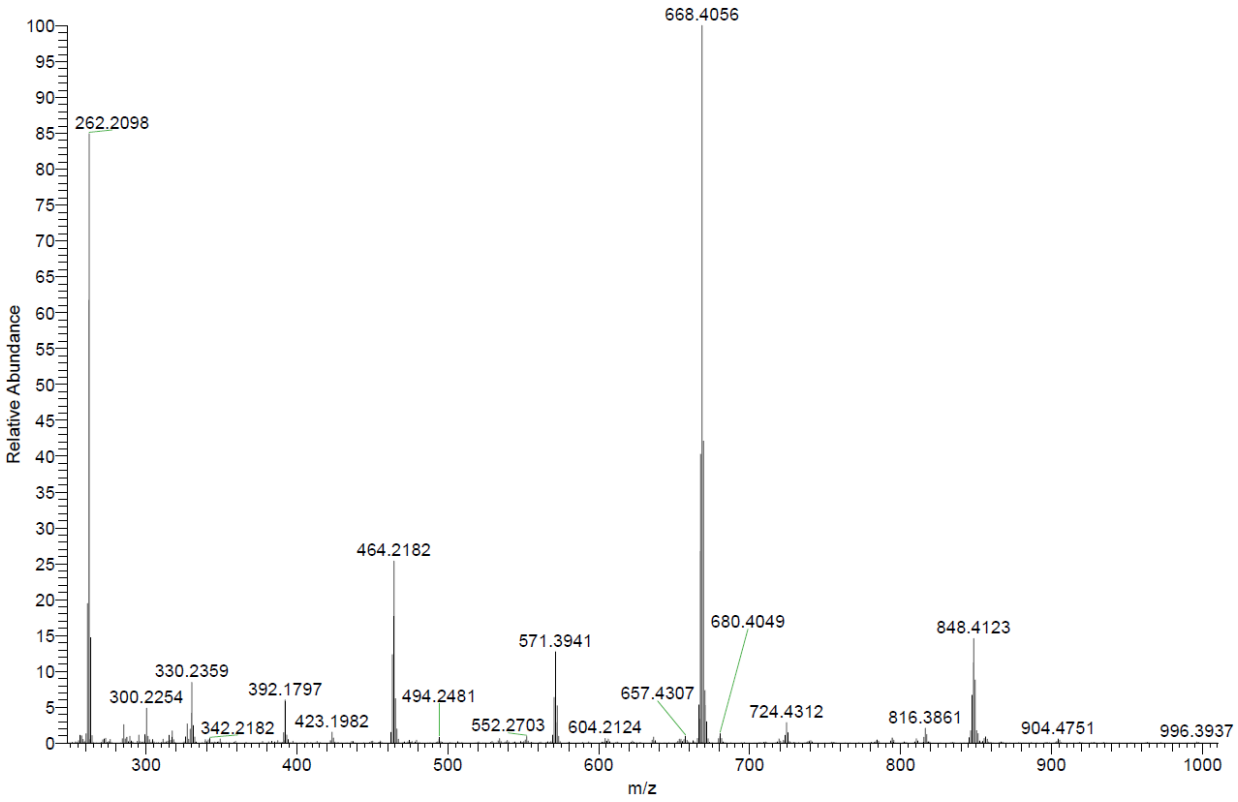

Figure 5.7.81. LIFDI mass spectrum of **31a**.

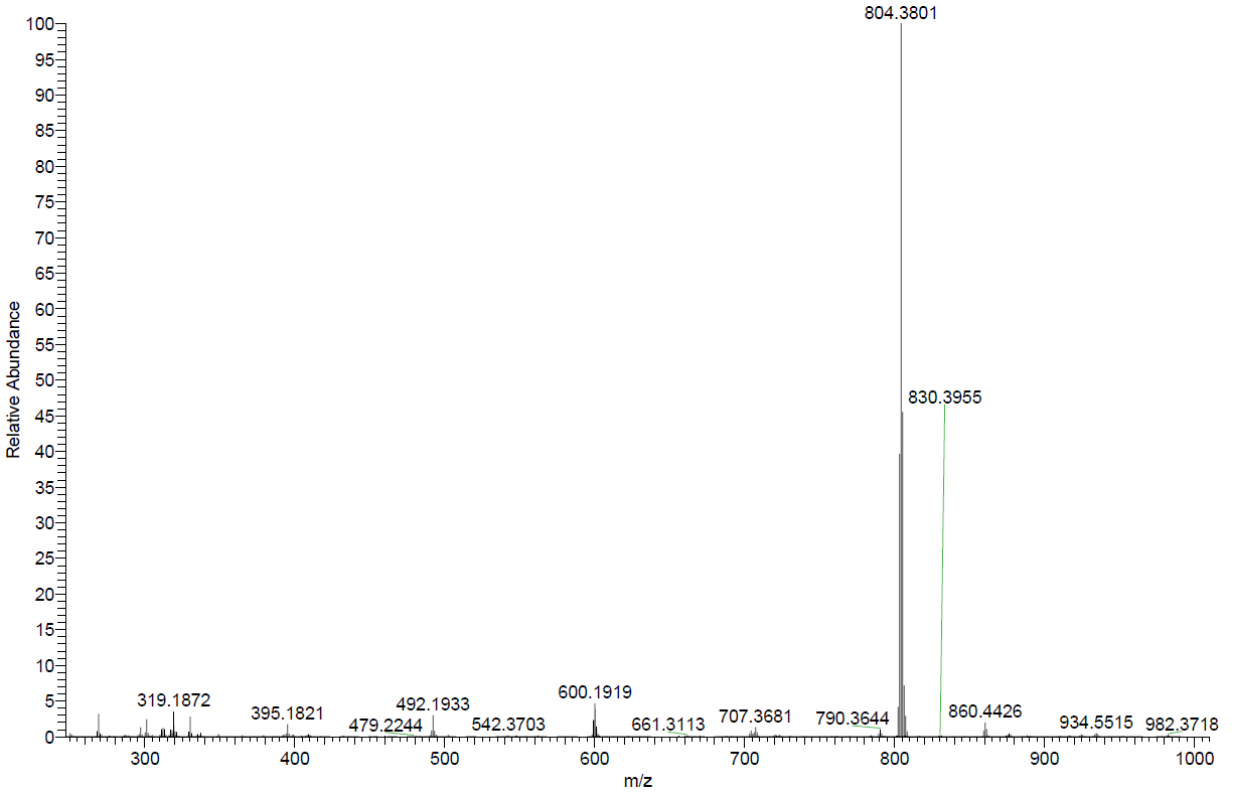

Figure 5.7.82. LIFDI mass spectrum of **31b**.

UV-Vis spectroscopy

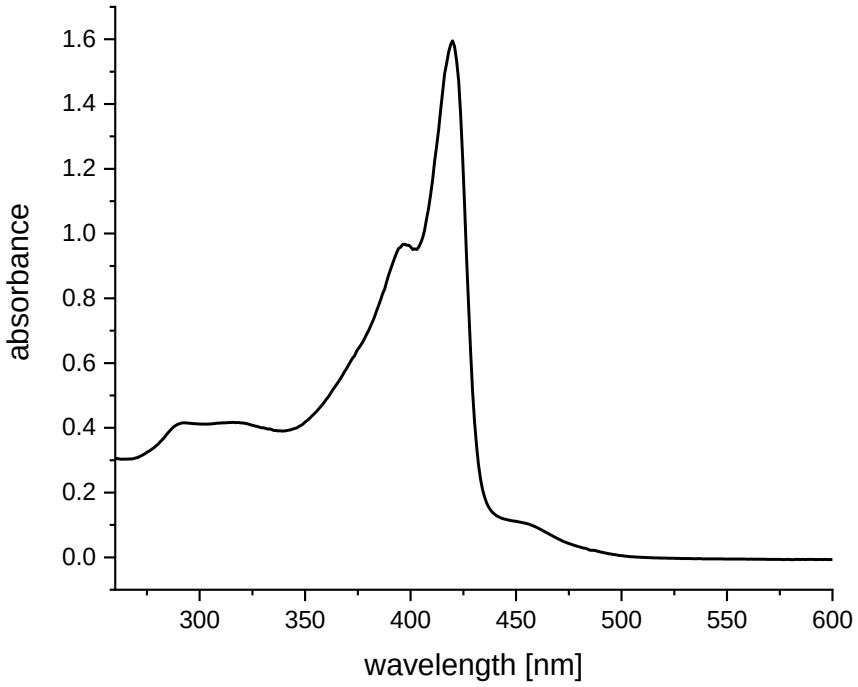

Figure 5.7.83. UV-vis spectrum of **7b** in THF under inert conditions.

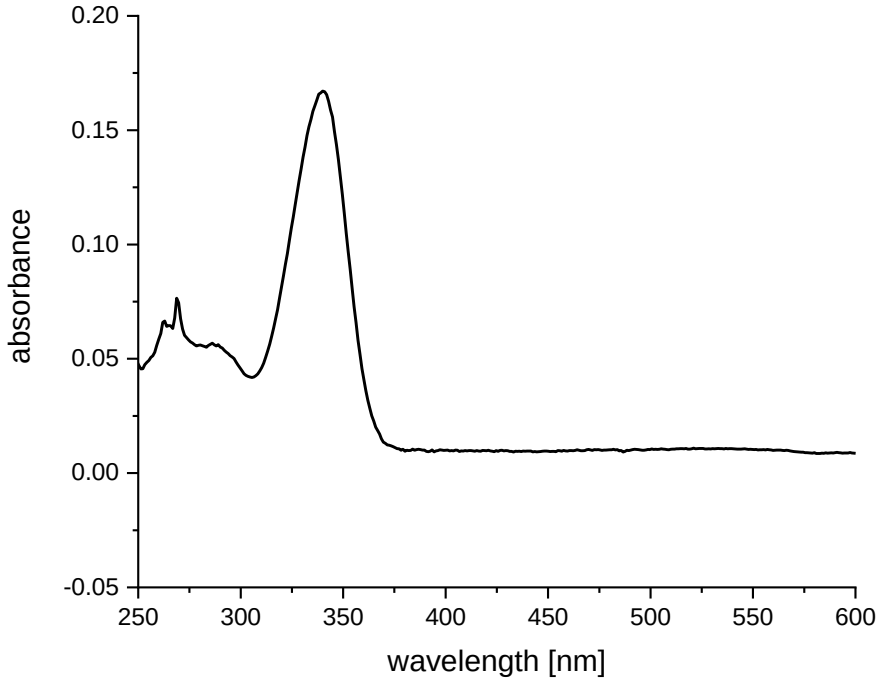

Figure 5.7.84. UV-vis spectrum of **3c** in THF under inert conditions.

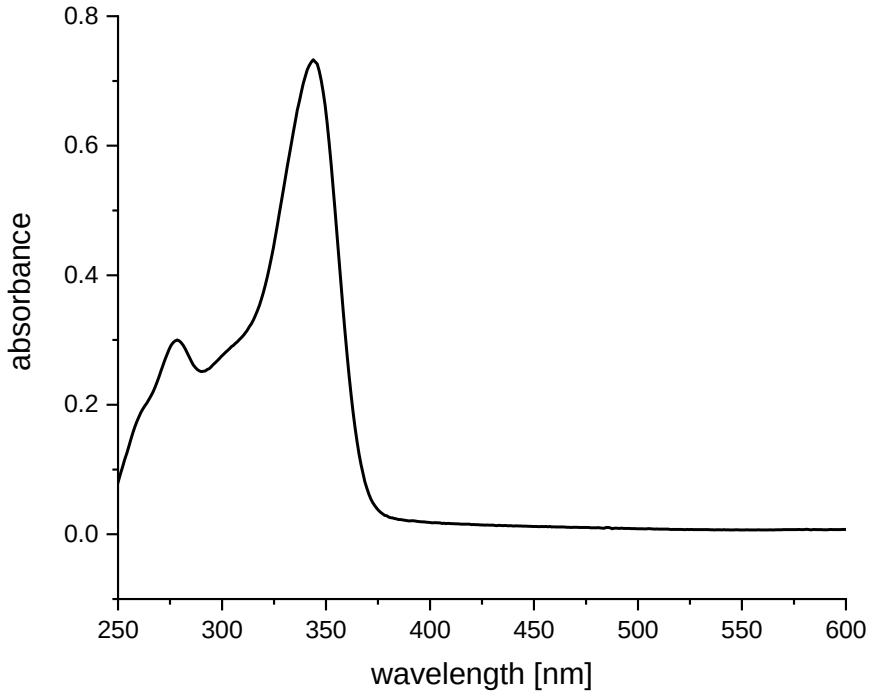

Figure 5.7.85. UV-vis spectrum of **3c** in THF under inert conditions.

Fluorescence spectroscopy

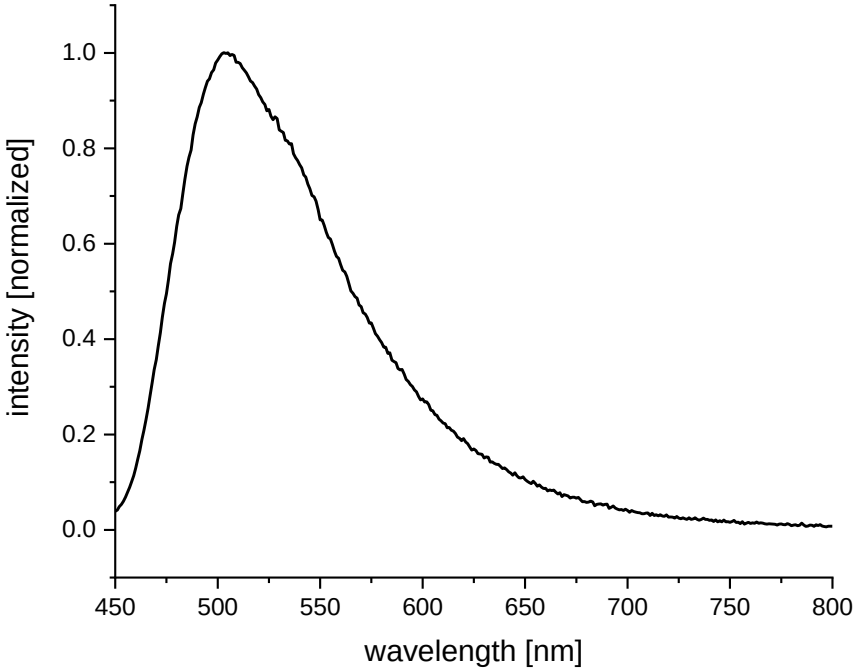

Figure 5.7.86. Fluorescence spectrum of **7b (**in THF λ_{ex} = 420 nm) under inert conditions.

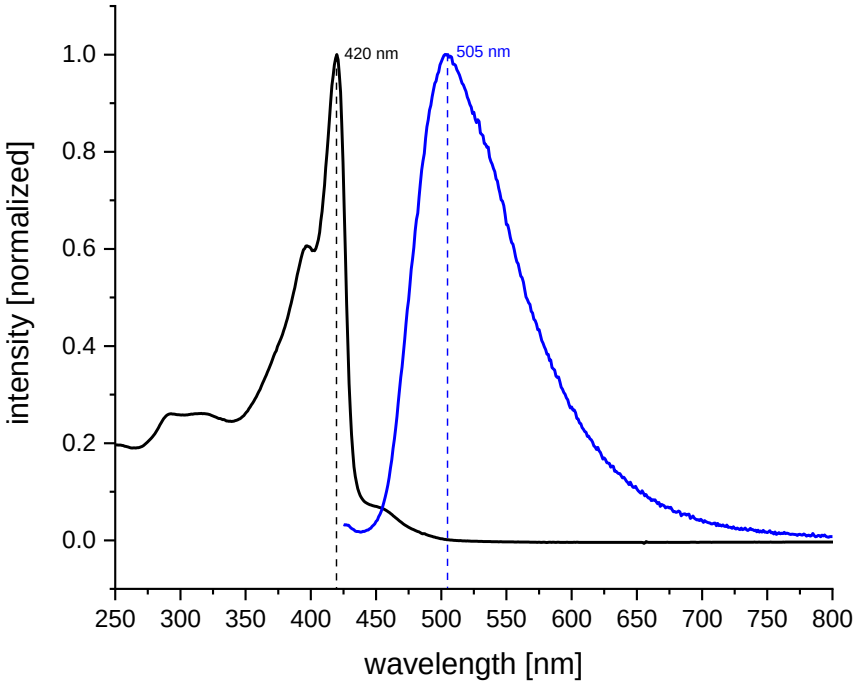

Figure 5.7.87. Overlay of UV-vis (black) and fluorescence (blue, λ_{ex} = 420 nm) of **7b** in THF under inert conditons.

Cyclo Voltammetry

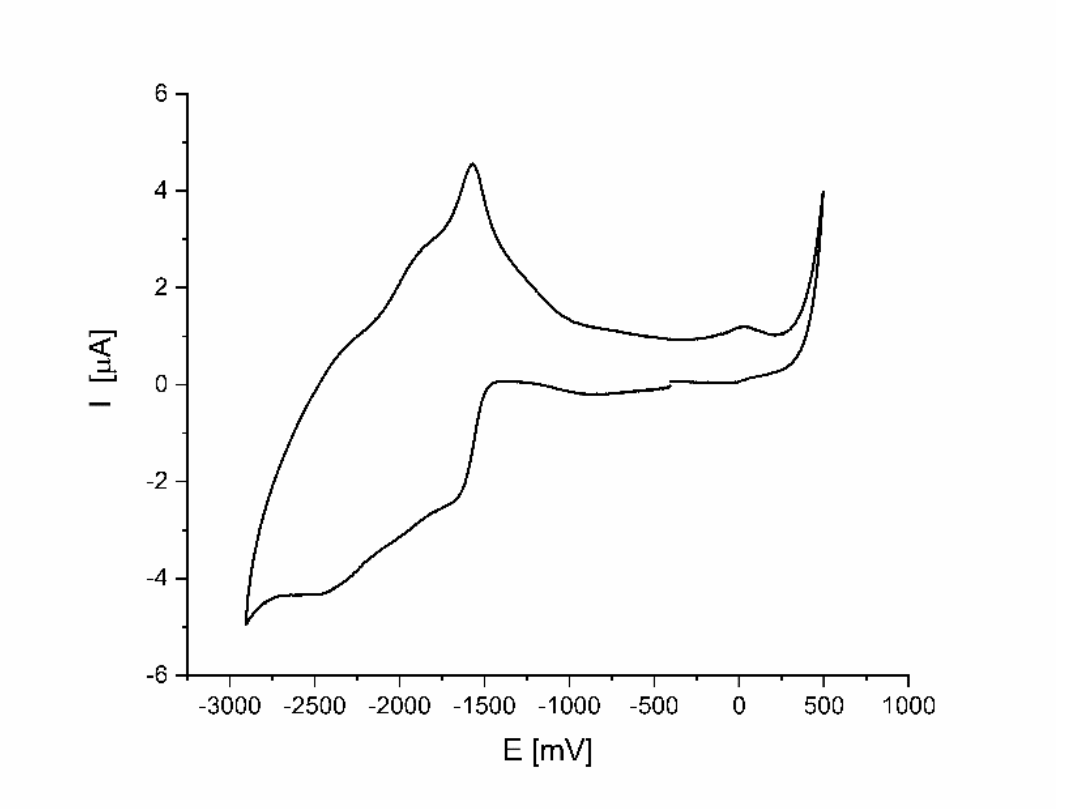

Figure 5.7.88. Cyclic voltammogram of **7b** (in THF).

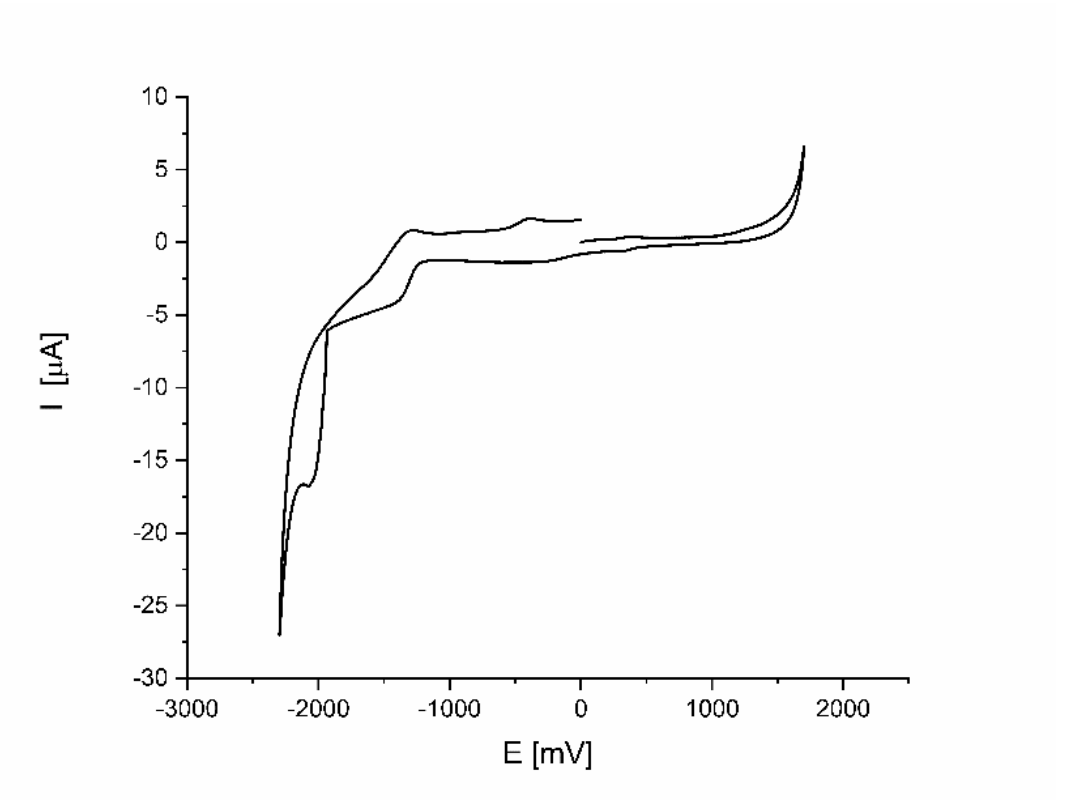

Figure 5.7.89. Cyclic voltammogram of **7b** (in DCM).

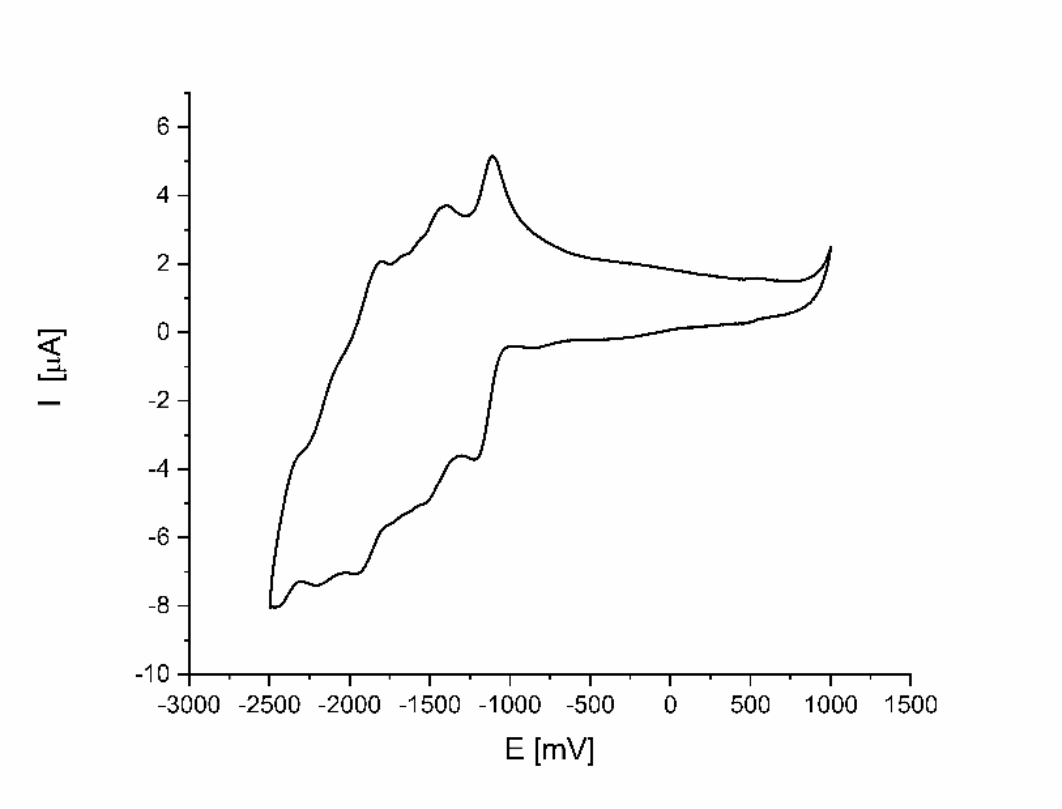

Figure 5.7.90. Cyclic voltammogram of linear oligomeric side product **O** (in DCM).

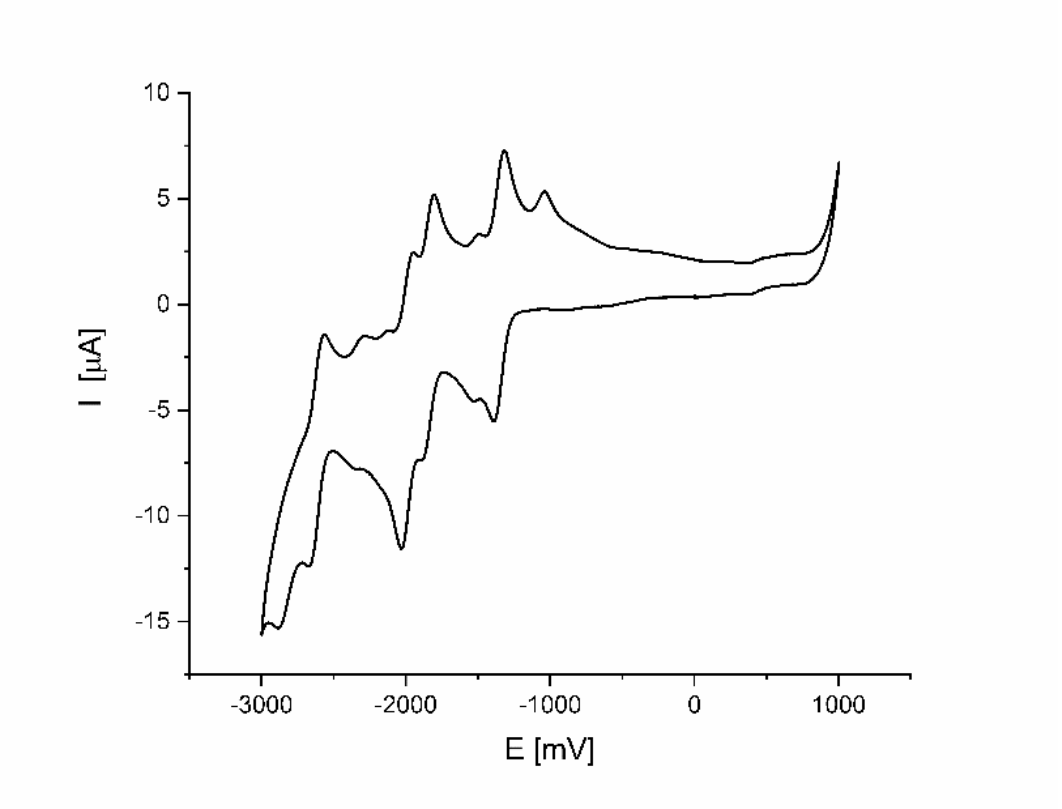

Figure 5.7.91. Cyclic voltammogram of trimeric species **T** (in DCM).

Gel Permeations Chromatography

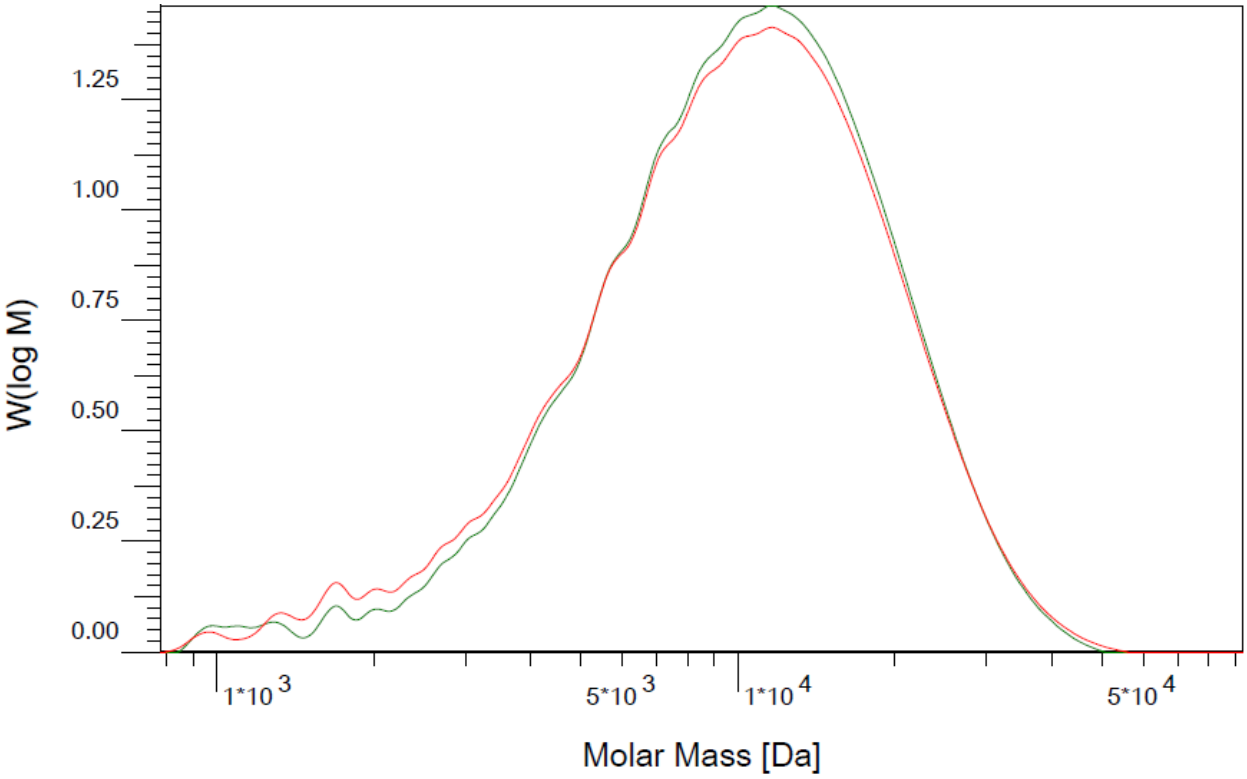

Figure 5.7.92. GPC traces of **7b**.

Table 5.7.1. Data of the GPC analysis of **7b.**

	I1: RID 1, RI Signal	I1: VWD 1, Signal A	
Mn :	7.6077e3	7.2753e3	g/mol
Mw :	1.1864e4	1.1725e4	g/mol
Mz :	1.6185e4	1.6375e4	g/mol
Mv :	0.000000	0.000000	g/mol
D :	1.5595e0	1.6116e0	
[n]:	0.000000	0.000000	ml/g
Vp :	2.3095e1	2.3095e1	ml
Mp :	1.1753e4	1.1754e4	g/mol
FI :	7.7083e0	5.2010e2	ml*V
< 780	0.00	0.00	
w% :	100.00	100.00	
> 93226	0.00	0.00	

Julius-Maximilians-
UNIVERSITÄT
WÜRZBURG

Fakultät für
CHEMIE UND
PHARMAZIE

Erklärung zur Autorenschaft

Borazine-based inorganic—organic hybrid cyclomatrix microspheres by silicon/boron exchange precipitation polycondensation,
N. A. Riensch, A. Deniz, S. Kühl, L. Müller, A. Adams, A. Pich*, H. Helten* *Polym. Chem.* **2017**, *8*, 5264—5268

Detaillierte Darstellung der Anteile an der Veröffentlichung (in %)
Angabe Autoren/innen (ggf. Haupt- / Ko- / korrespondierende/r Autor/in) mit Vorname Nachname (Initialen)

Hauptautor: Nicolas Riensch (NR), Ayse Deniz (AD), Sebastian Kühl (SK), L. Müller (LM), A. Adams (AA), korrespondierender Autor: Andrij Pich (AP), Holger Helten (HH)

Autor	NR	AD	SK	LM	AA	AP	HH					∑ in Prozent
Idee/-entwicklung/Konzept						9%	9%					18.0%
Synthesen	20%			5%								25.0%
Analytik	4%	5%	5%		5%							19.0%
												0%
												0%
Verfassen der Veröffentlichung	4.2%					4.2%	8.3%					16.7%
Korrektur der Veröffentlichung	1.8%					1.8%	3.6%					7.2%
Koordination der Veröffentlichung						7.1%	7.1%					14.3%
Summe	30%	5%	5%	5%	5%	22.1%	28%					100%

Julius-Maximilians-
UNIVERSITÄT
WÜRZBURG

Fakultät für
CHEMIE UND
PHARMAZIE

Erklärung zur Autorenschaft

Difuryl(supermesityl)borane: a versatile building block for extended π-conjugated materials,
N. A. Riensch, L. Fritze, T. Schindler, M. Kremer, H. Helten, Dalton transactions 2018, 47, 10399 – 10403.

Detaillierte Darstellung der Anteile an der Veröffentlichung (in %)
Angabe Autoren/innen (ggf. Haupt- / Ko- / korrespondierende/r Autor/in) mit Vorname Nachname (Initialen)

Hauptautor: Nicolas Riensch (NR), Hauptautor: Lars Fritze (LF), Tobias Schindler (TS), Marius Kremer (MK), korrespondierender Autor: Holger Helten (HH)

Autor	NR	LF	TS	MK	HH							∑ in Prozent
Idee/-entwicklung/Konzept	2,1%	2,1%			12,5%							16,7%
Synthesen	16,2%	16,2%										32,3%
Analysen	11,5%	11,5%	1%	1%								25,0%
Rechnungen					1%							1%
												0%
												0%
Verfassen der Veröffentlichung	3,3%	3,3%			10,1%							16,7%
Korrektur der Veröffentlichung	1,4%	1,4%			1,4%							4,2%
Koordination der Veröffentlichung					4,2%							4,2%
Summe	34,5%	34,5%	1%	1%	29,2%							100%

Julius-Maximilians-
UNIVERSITÄT
WÜRZBURG

Fakultät für
CHEMIE UND
PHARMAZIE

Erklärung zur Autorenschaft

Catalytic Si/B Exchange Condensation: A Green B–C Coupling Method That Provides Access to Monodisperse (Het)arylborane 'Trimers',
L. Fritze, N. A. Riensch, H. Helten, Synthesis 2019, 51, 399 – 406.

Detaillierte Darstellung der Anteile an der Veröffentlichung (in %)
Angabe Autoren/innen (ggf. Haupt- / Ko- / korrespondierende/r Autor/in) mit Vorname Nachname (Initialen)

Hauptautor: Lars Fritze (LF), Hauptautor: Nicolas Riensch (NR), korrespondierender Autor: Holger Helten (HH)

Autor	LF	NR	HH									∑ in Prozent
Idee/-entwicklung/Konzept	2,1%	2,1%	12,5%									16,7%
Synthesen	16,7%	16,7%										33,3%
Analysen	12,5%	12,5%										25,0%
												0%
												0%
												0%
Verfassen der Veröffentlichung	3,3%	3,3%	10,1%									16,7%
Korrektur der Veröffentlichung	1,4%	1,4%	1,4%									4,2%
Koordination der Veröffentlichung			4,2%									4,2%
Summe	36%	36%	28%									100%

Julius-Maximilians-
UNIVERSITÄT
WÜRZBURG

Fakultät für
CHEMIE UND
PHARMAZIE

Erklärung zur Autorenschaft

Bifuran-bridged bisboranes: highly luminescent B-doped oligohetarenes,
N. A. Riensch, M. Fest, L. Fritze, A. Helbig, I. Krummenacher, H. Braunschweig, H. Helten, New J. Chem. 2020

Detaillierte Darstellung der Anteile an der Veröffentlichung (in %)
Angabe Autoren/innen (ggf. Haupt- / Ko- / korrespondierende/r Autor/in) mit Vorname Nachname (Initialen)

Hauptautor: Nicolas Riensch (NR), Maximilian Fest (MF), Lars Fritze (LF), A. Helbig (AH), I. Krummenacher (IK), korrespondierender Autor: Holger Braunschweig (HB), Holger Helten (HH)

Autor	NR	MF	LF	AH	IK	HB	HH					∑ in Prozent
Idee/-entwicklung/Konzept	6%						14%					20.0%
Synthesen	8%	12%										20.0%
Analytik	18%		1%		1%							20.0%
Rechnungen				2%								2%
												0%
												0%
Verfassen der Veröffentlichung	4.2%						12.5%					16.7%
Korrektur der Veröffentlichung	1.8%					1.8%	3.6%					7.2%
Koordination der Veröffentlichung							14.3%					14.3%
Summe	38%	12%	1%	2%	1%	1.8%	44.4%					100%

Julius-Maximilians-
UNIVERSITÄT
WÜRZBURG

Fakultät für
CHEMIE UND
PHARMAZIE

Erklärung zur Autorenschaft

Conjugated Bis(triarylboranes) with Disconnected Conjugation,
N. A. Riensch, L. Swoboda, A. Lik, I. Krummenacher, H. Braunschweig, H. Helten, Z. Anorg. Allg. Chem. **2021**

Detaillierte Darstellung der Anteile an der Veröffentlichung (in %)
Angabe Autoren/innen (ggf. Haupt- / Ko- / korrespondierende/r Autor/in) mit Vorname Nachname (Initialen)

Hauptautor: Nicolas Riensch (NR), Lukas Swoboda (LS), Artur Lik (AL), I. Krummenacher (IK), korrespondierender Autor: Holger Braunschweig (HB), Holger Helten (HH)

Autor	NR	LS	AL	IK	HB	HH						∑ in Prozent
Idee/-entwicklung/Konzept	5%					15%						20.0%
Synthesen	20%	4%	1%									25.0%
Analytik	14%			3%								17.0%
												0%
												0%
Verfassen der Veröffentlichung	5.2%					11.5%						16.7%
Korrektur der Veröffentlichung	0.9%	0.9%			1.8%	3.6%						7.2%
Koordination der Veröffentlichung						14.3%						14.3%
Summe	45.1%	4.9%	1%	3%	1.8%	44.4%						100%